



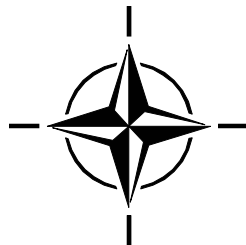
RTO AGARDograph

AG-AVT-039

Unsteady Motions in Combustion Chambers for Propulsion Systems

**(Mouvements instables dans les chambres de
combustion des systèmes de propulsion)**

This AGARDograph was approved by the Propulsion and Energetics Panel (PEP) of NATO's Advisory Group for Aerospace Research and Development (AGARD); subsequently it has been sponsored by the Applied Vehicle Technology Panel (AVT) of NATO's Research and Technology Organisation (RTO).



Published December 2006





RTO AGARDograph

AG-AVT-039

Unsteady Motions in Combustion Chambers for Propulsion Systems

**(Mouvements instables dans les chambres de
combustion des systèmes de propulsion)**

This AGARDograph was approved by the Propulsion and Energetics Panel (PEP) of NATO's Advisory Group for Aerospace Research and Development (AGARD); subsequently it has been sponsored by the Applied Vehicle Technology Panel (AVT) of NATO's Research and Technology Organisation (RTO).

F.E.C. Culick
California Institute of Technology

The Research and Technology Organisation (RTO) of NATO

RTO is the single focus in NATO for Defence Research and Technology activities. Its mission is to conduct and promote co-operative research and information exchange. The objective is to support the development and effective use of national defence research and technology and to meet the military needs of the Alliance, to maintain a technological lead, and to provide advice to NATO and national decision makers. The RTO performs its mission with the support of an extensive network of national experts. It also ensures effective co-ordination with other NATO bodies involved in R&T activities.

RTO reports both to the Military Committee of NATO and to the Conference of National Armament Directors. It comprises a Research and Technology Board (RTB) as the highest level of national representation and the Research and Technology Agency (RTA), a dedicated staff with its headquarters in Neuilly, near Paris, France. In order to facilitate contacts with the military users and other NATO activities, a small part of the RTA staff is located in NATO Headquarters in Brussels. The Brussels staff also co-ordinates RTO's co-operation with nations in Middle and Eastern Europe, to which RTO attaches particular importance especially as working together in the field of research is one of the more promising areas of co-operation.

The total spectrum of R&T activities is covered by the following 7 bodies:

- AVT Applied Vehicle Technology Panel
- HFM Human Factors and Medicine Panel
- IST Information Systems Technology Panel
- NMSG NATO Modelling and Simulation Group
- SAS System Analysis and Studies Panel
- SCI Systems Concepts and Integration Panel
- SET Sensors and Electronics Technology Panel

These bodies are made up of national representatives as well as generally recognised 'world class' scientists. They also provide a communication link to military users and other NATO bodies. RTO's scientific and technological work is carried out by Technical Teams, created for specific activities and with a specific duration. Such Technical Teams can organise workshops, symposia, field trials, lecture series and training courses. An important function of these Technical Teams is to ensure the continuity of the expert networks.

RTO builds upon earlier co-operation in defence research and technology as set-up under the Advisory Group for Aerospace Research and Development (AGARD) and the Defence Research Group (DRG). AGARD and the DRG share common roots in that they were both established at the initiative of Dr Theodore von Kármán, a leading aerospace scientist, who early on recognised the importance of scientific support for the Allied Armed Forces. RTO is capitalising on these common roots in order to provide the Alliance and the NATO nations with a strong scientific and technological basis that will guarantee a solid base for the future.

The content of this publication has been reproduced
directly from material supplied by RTO or the authors.

Published December 2006

Copyright © RTO/NATO 2006
All Rights Reserved

ISBNs 92-837-0059-7 / 978-92-837-0059-3

Single copies of this publication or of a part of it may be made for individual use only. The approval of the RTA Information Management Systems Branch is required for more than one copy to be made or an extract included in another publication. Requests to do so should be sent to the address on the back cover.

Table of Contents

	Page
List of Figures	ix
List of Tables	xx
Foreword	xxi
Avant-propos	xxii
Executive Summary and Synthèse	ES-1
Overview	O-1
Chapter 1 – Combustion Instabilities in Propulsion Systems	1-1
1.1 Introduction	1-2
1.2 Historical Background	1-5
1.2.1 Liquid and Gas-Fueled Rockets	1-7
1.2.2 Combustion Instabilities in Thrust Augmentors	1-13
1.2.3 Combustion Instabilities in Ramjet Engines	1-15
1.2.4 Combustion Instabilities in Gas Turbines	1-17
1.2.5 Combustion Instabilities in Solid Propellant Rocket Motors	1-17
1.3 Mechanisms of Combustion Instabilities	1-22
1.3.1 Mechanisms in Liquid-Fueled Rockets	1-22
1.3.2 Sensitivity of Combustion Processes; Time Lags	1-24
1.3.3 Vortex Shedding and Vortex/Mean Flow Interactions	1-25
1.3.4 Operation Near the Lean Blow-Out Limit	1-27
1.3.5 Mechanisms in Solid-Fueled Rockets	1-28
1.3.6 Combustion Dynamics	1-28
1.4 Physical Characteristics of Combustion Instabilities	1-29
1.5 Linear Behavior	1-33
1.5.1 Gains and Losses of Acoustic Energy; Linear Stability	1-37
1.6 Nonlinear Behavior	1-41
1.6.1 Linear Behavior Interpreted as the Motion of a Simple Oscillator	1-42
1.6.2 Combustion Dynamics and Stability	1-44
1.6.3 Nonlinear Behavior Interpreted as the Motion of a Nonlinear Oscillator	1-45
1.7 Analysis and Numerical Simulations of Combustion Instabilities	1-49
1.8 A Précis of the Book	1-52
Chapter 2 – Combustion Dynamics and Mechanisms of Combustion Instabilities	2-1
2.1 Mechanisms of Instabilities in Solid Propellant Rocket Motors	2-2

2.1.1	Qualitative Interpretation of the Basic Mechanism	2-3
2.1.2	Early Historical Background Leading to the QSHOD Model	2-6
2.2	Analysis of the QSHOD Model	2-18
2.2.1	Estimates of Some Characteristic Lengths and Times	2-19
2.2.2	Calculation of the Response Function	2-22
2.2.3	Measurements of the Response Function; Comparison of Experimental Results and the QSHOD Model	2-30
2.2.4	The Zel'dovich-Novozhilov (Z-N) Model	2-34
2.2.5	Revisions and Extensions of the QSHOD Model	2-35
2.2.6	Some Results for a Special Extension of the QSHOD Model	2-36
2.2.7	Some Results for the Combustion Response Function	2-39
2.2.8	The Combustion Response and Possible Sensitivity of Global Dynamics to Velocity Coupling	2-40
2.2.9	Generation of Vorticity and Vortex Shedding	2-44
2.2.10	Distributed Combustion	2-51
2.3	Mechanisms of Combustion Instabilities in Liquid-Fueled Systems	2-52
2.3.1	Atomization, Droplet Vaporization and Burning	2-52
2.3.2	Interpretation with a Time Lag	2-55
2.3.3	Convective Waves	2-59
2.3.4	Vortex Shedding from Rearward-Facing Steps	2-62
2.3.5	A Model for Vortex Shedding and Excitation of Acoustic Waves	2-70
2.4	Further Remarks on Particular Forms of Liquid-Fueled Systems	2-72
2.4.1	Combustion Instabilities in Liquid Rockets	2-73
2.4.2	Application of the Time Lag Model to Gas and Liquid Rockets	2-75
2.4.3	Pogo Instabilities	2-79
2.4.4	Combustion Instabilities in Thrust Augmentors	2-80
2.4.5	Combustion Instabilities in Ramjet Engines	2-86
2.4.6	Unsteady Behavior of the Inlet/Diffuser	2-87
2.4.7	The Time Lag Model Applied to Combustion Instabilities in Ramjet Engines	2-90
2.5	Dynamics of Flames and Flame Sheets as a Mechanism	2-91
2.6	Fluctuations of Mixture Ratio as a Mechanism	2-92
2.7	The Rijke Tube: Simplest Example of Thermoacoustic Instabilities	2-94
2.7.1	The Electrically Driven Rijke Tube	2-95
2.7.2	Mean Field in the Rijke Tube	2-101
2.7.3	Acoustic Field in the Rijke Tube	2-102
2.7.4	Acoustic Field and Stability by Matching Waves	2-103
2.7.5	Stability Analyzed by a Method of Spatial Averaging	2-106
2.7.6	Nonlinear Behavior due to Rectification	2-110
2.7.7	A Simple Analysis of the Flame-Driven Rijke Tube	2-111

Chapter 3 – Equations for Unsteady Motions in Combustion Chambers 3-1

3.1	Modes of Wave Motion in a Compressible Medium	3-1
3.2	Equations of Motion in a Reacting Flow	3-2
3.3	Two-Parameter Expansion of the Equations of Motion	3-4
3.3.1	Expansion in Mean and Fluctuating Values	3-5
3.3.2	Equations for the Mean Flow	3-7

3.3.3	Systems of Equations for the Fluctuations	3-8
3.4	Nonlinear Wave Equations for the Pressure Field	3-11

Chapter 4 – Modal Expansion and Spatial Averaging; An Iterative Method of Solution **4-1**

4.1	Application of a Green's Function for Steady Waves	4-2
4.1.1	Approximate Solution by Iteration	4-6
4.2	An Alternative Derivation of the First Order Formula	4-7
4.3	Approximate Solution for Unsteady Nonlinear Motions	4-8
4.4	An Alternative Application of Spatial Averaging: The Method of Least Residuals	4-11
4.5	Application of Time-Averaging	4-13
4.6	The Procedure for Iterative Solution to the Oscillator Equations	4-17
4.6.1	Iteration on the Mach Number of the Mean Flow	4-18
4.6.2	Zeroth and First Order Solutions for the Eigenvalues and Basis Functions	4-20

Chapter 5 – Some Fundamentals of Acoustics **5-1**

5.1	The Linearized Equations of Motion; The Velocity Potential	5-1
5.1.1	The Velocity Potential	5-4
5.2	Elementary Solutions to the Linear Wave Equation	5-5
5.2.1	Plane Waves	5-5
5.2.2	Spherical Waves	5-8
5.2.3	Cylindrical Waves	5-10
5.3	An Estimate of the Influence of Internal Heat Conduction on the Propagation of Acoustic Waves	5-10
5.4	Energy and Intensity Associated with Acoustic Waves	5-13
5.5	The Growth or Decay Constant	5-16
5.6	Boundary Conditions: Reflections from a Surface	5-17
5.6.1	Reflections of Plane Waves at a Surface	5-18
5.7	Wave Propagation in Tubes; Normal Modes	5-20
5.7.1	Waves in Closed Tubes	5-20
5.7.2	Normal Modes for Tubes Having Discontinuities of Cross-Sectional Area	5-22
5.8	Normal Acoustic Modes and Frequencies for a Chamber	5-24
5.8.1	Normal Modes for Rectangular Chambers	5-24
5.8.2	Normal Modes for a Circular Cylindrical Chamber	5-25
5.9	Viscous Losses at an Inert Surface	5-26
5.9.1	Dissipation of Energy Within the Acoustic Boundary Layer	5-27
5.9.2	Another Way of Computing the Decay Constant	5-29
5.9.3	Still Another Way of Computing the Decay Constant	5-31
5.9.4	First Order Correction to the Mode Shape	5-33
5.10	Propagation of Higher Modes in Tubes; Cut-off Frequencies	5-36
5.11	The Impedance Tube	5-37

Chapter 6 – Linear Stability of Combustor Dynamics **6-1**

6.1	Historical Background of Linear Stability	6-1
-----	---	-----

6.2	Zero-Dimensional Instability of a Bulk Mode	6-4
6.3	A Formal Solution to the Problem of Linear Stability	6-13
6.4	An Alternative Calculation of Linear Stability	6-15
6.5	Linear Stability with a Heat Source and Motion of the Boundary	6-16
6.6	Rayleigh's Criterion and Linear Stability	6-18
6.7	Some Results for Linear Stability in Three Dimensions	6-21
6.7.1	Linear Stability of Three-Dimensional Motions	6-22
6.7.2	The Admittance and Response Functions for a Burning Surface	6-27
6.7.3	The First Measurements of the Stability Boundary for a Solid Rocket	6-28
6.8	Stability of Oscillations in a Bulk Mode	6-30
6.9	Linear Stability in the One-Dimensional Approximation	6-32
6.9.1	The One-Dimensional Approximation to 'Flow-Turning'	6-35
6.9.2	The One-Dimensional Approximation to 'Pumping'	6-38
6.9.3	Stability of a Simple <i>T</i> -Burner	6-44
6.10	Combined Three-Dimensional and One-Dimensional Results	6-46
6.11	An Example of Linear Stability for a Solid Rocket	6-48
6.12	Vorticity and Stability in Solid Propellant Rockets	6-52
6.12.1	Generation of Large Vortices; Parietal Vortex Shedding	6-53
6.13	Predictions of Stability Boundaries for Liquid Rockets	6-57
6.14	Contributions to the Growth Constant for Linear Stability	6-58
6.14.1	Mean Flow/Acoustics Interactions	6-58
6.14.2	Attenuation by a Choked Exhaust Nozzle	6-59
6.14.3	Attenuation of Acoustic Energy Due to Condensed Products of Combustion	6-66
6.15	Distributed Combustion	6-72

Chapter 7 – Nonlinear Behavior of Combustor Dynamics 7-1

7.1	Early Works on Nonlinear Combustion Instabilities	7-3
7.2	A Single Nonlinear Mode	7-11
7.3	The Two-Mode Approximation	7-18
7.3.1	Existence of Limit Cycles	7-20
7.3.2	Stability of Limit Cycles	7-20
7.4	Transverse Modes and the Method of Averaging	7-23
7.4.1	Periodic Limit Cycles for Transverse Modes	7-25
7.5	Observations of a Spinning Transverse Mode	7-27
7.6	Remarks on Truncation and Reduced-Order Modeling	7-28
7.7	Application of a Continuation Method	7-29
7.8	Recirculation Zones, Hysteresis and Control of Combustion Instabilities	7-33
7.9	Representing Noise in Analysis of Combustor Dynamics	7-37
7.10	System Identification for Combustor Dynamics with Noise	7-40
7.11	Pulsed Instabilities; Subcritical Bifurcations	7-44
7.11.1	Pulsing Solid Propellant Rockets	7-45
7.12	Dependence of Wall Heat Transfer on the Amplitude of Oscillations	7-52
7.13	One Way to Analyze the Behavior of Pulses	7-54
7.13.1	Some Results for the Propagation of Pulses	7-57
7.14	Spatial Averaging and Dynamical Systems Theory Applied to Pulsed Instabilities	7-60

Chapter 8 – Passive Control of Combustion Instabilities	8-1
8.1 Interpretation of Passive Control	8-1
8.2 Baffles	8-4
8.3 Resonators and Acoustic Liners	8-12
8.4 Damping Due to the Formation and Presence of Particulate Material	8-15
8.5 Dynamics of Injection Systems	8-19
8.6 Passive Control of Vortex Shedding	8-19
Chapter 9 – Feedback Control of Unsteady Motions in Combustors	9-1
9.1 The Idea of Feedback Control First Applied to Combustion Systems	9-6
9.2 Early Laboratory Demonstrations	9-7
9.3 Modal Control for Combustion Systems	9-21
9.3.1 State Feedback Control Based on Spatial Averaging	9-24
9.3.2 Application to Combustion Systems	9-27
9.4 An Example of Practical Application of Feedback Control	9-30
9.5 Briefly on Progress in Practical Feedback Control of Combustor Dynamics	9-37
Chapter 10 – References	10-1
Annex A – Equations of Motion	A-1
A.1 General Equations of Motion	A-1
A.2 Mass, Momentum and Energy Transfer by Diffusion	A-3
A.3 Construction of the Single Fluid Model	A-5
A.3.1 Equation for the Density	A-6
A.3.2 Equation for Momentum	A-7
A.3.3 Equation for Energy	A-7
A.3.4 Equation for the Pressure	A-10
A.4 Muster of Equations	A-10
A.5 Expansions in Mean and Fluctuating Variables	A-12
A.6 Definitions of the Ordering Brackets	A-13
Annex B – The Equations for One-Dimensional Unsteady Motions	B-1
B.1 Equations for Unsteady One-Dimensional Motions	B-3
Annex C – The Acoustic Boundary Layer	C-1
Annex D – Accounting for Waves of Vorticity and Entropy	D-1
Annex E – Accommodating Discontinuities in the Method of Spatial Averaging	E-1
Annex F – Basis Functions Satisfying Homogeneous Boundary Conditions	F-1

Annex G – Nyquist Criterion**G-1**

G.1	The Criterion Stated Without Proof	G-2
G.2	Some General Properties of Polar Plots	G-3
G.3	Construction of Nyquist Contours (Polar Plots)	G-4
G.4	Definition of Encirclement	G-7
G.5	Proof of Nyquist's Criterion	G-8
G.5.1	Principle of the Argument	G-8
G.5.2	Proof of Nyquist's Criterion	G-10
G.6	Examples of Nyquist's Criterion	G-13
G.7	Relative Stability; Gain and Phase Margins	G-15

Annex H – Some Alternative Methods of Approximately Analyzing Nonlinear Behavior**H-1**

List of Figures

Figure		Page
Figure 1.1	Schematic diagram of a combustion system as a feedback amplifier	1-4
Figure 1.2	A chronology of combustion instabilities	1-6
Figure 1.3	Pulses of the injected fuel stream in the F-1 engine	1-8
Figure 1.4	The F-1 engine and the face of the injector showing the fourteen baffles	1-8
Figure 1.5	Injection elements commonly used in liquid rockets	1-9
Figure 1.6	Resurging subsequent to a bomb-induced perturbation	1-10
Figure 1.7	Decaying pressure induced initially by a pulse from a 13.5 grain bomb	1-10
Figure 1.8	Simplified forms of coaxial injectors	1-11
Figure 1.9	Pintle injector in the lunar excursion module (LEM) descent engine of the Apollo vehicle	1-11
Figure 1.10	Cutaway display model of the mixing head of the TRW pintle engine	1-11
Figure 1.11	Decay of pulses injected in the TRW LEM engine	1-12
Figure 1.12	Cutaway drawing of the main injector assembly of the Space Shuttle main engine	1-12
Figure 1.13	The RD-0110 engine	1-13
Figure 1.14	Four RD-0110 engines mounted in the upper stage of the Soyuz vehicle	1-14
Figure 1.15	RD-0110 engine cutaway to show combustible ribs intended to attenuate a tangential mode	1-14
Figure 1.16	Stylized configuration of a liquid-fueled ramjet	1-15
Figure 1.17	The Caltech dump combustor	1-16
Figure 1.18	Waveform and spectrum for an instability in the Caltech dump combustor	1-16
Figure 1.19	Flight test record of pressure in a Minuteman II, stage 3	1-18
Figure 1.20	Frequencies and amplitudes of combustion instabilities in the Minuteman II, stage 3 motor	1-19
Figure 1.21	A sketch of the basic T-burner and two variants	1-20
Figure 1.22	A partial summary of U.S. solid propellant motors (1951–1997) having problems of combustion instabilities	1-21
Figure 1.23	An approximate schematic summary of the important rate processes in a liquid rocket combustor	1-23
Figure 1.24	A simplified diagram for the dynamics of a liquid rocket engine	1-23
Figure 1.25	A sketch showing some of the processes taking place in a coaxial injector	1-24
Figure 1.26	Generation of an acoustic field by vortex shedding	1-26
Figure 1.27	A form of axisymmetric lean premixed combustor	1-28
Figure 1.28	A typical 2-D dump combustor	1-28
Figure 1.29	Transient growths and “limit cycles” of combustion instabilities	1-30
Figure 1.30	Growth of a nonlinear instability in a solid rocket showing the unsteady pressure	1-30

Figure 1.31	A waterfall plot taken during a stable firing	1-31
Figure 1.32	A waterfall plot showing an instability, having fundamental frequency < 200 Hz but with developing components at higher frequencies	1-31
Figure 1.33	A severe pulsed instability in a solid rocket; an example of a subcritical bifurcation	1-32
Figure 1.34	Transient behavior of (a) self-excited linearly unstable motions; (b) forced motions	1-34
Figure 1.35	Qualitative dependence of (a) energy gains and losses; and (b) the frequency response of a combustor	1-36
Figure 1.36	Exponential growth and development of a limit cycle out of a linearly unstable motion	1-38
Figure 1.37	Stability boundaries for a laboratory gas-fueled rocket	1-39
Figure 1.38	Predicted stability boundary for a large solid propellant rocket motor, and the separate contributions to α_d and α_g	1-40
Figure 1.39	A computed limit cycle and its normalized spectrum executed by a single nonlinear acoustic mode in the presence of noise	1-42
Figure 1.40	An example of fitting T-burner data with the model of a simple nonlinear oscillator	1-46
Figure 1.41	Steep-fronted waves observed in a liquid propellant rocket motor	1-47
Figure 1.42	Steep-fronted waves observed in solid propellant rocket motors	1-48
Figure 1.43	A comparison of observed and simulated steep-fronted waves in a solid propellant rocket motor	1-48
Figure 2.1	The four possible mechanisms for combustion instabilities in solid propellant rockets	2-2
Figure 2.2	Sketch of steady combustion of a solid propellant	2-3
Figure 2.3	View of the surface of a burning solid propellant containing aluminum	2-4
Figure 2.4	Representation of the temperature field for a burning solid propellant	2-6
Figure 2.5	Measurements showing the presence of the lowest tangential mode during 'sonant' burning	2-8
Figure 2.6	Mean pressure in a cylindrical motor operating with double-bore propellant	2-10
Figure 2.7	Sketch of the first test device having the form of a T-burner	2-11
Figure 2.8	Adapted from Hart and McClure (1959). Part (a): a sketch of their model of surface combustion; Part (b) a result for the quantity proportional to the real part of the admittance function	2-12
Figure 2.9	The first reported values of the real and imaginary parts of the admittance function for a burning surface	2-17
Figure 2.10	A summary of the instability problems for solid propellant rockets in 1970	2-18
Figure 2.11	A view of the areas of research and their connections in solid propellant rockets	2-20
Figure 2.12	Reference system and matching conditions for the QSHOD Model	2-22
Figure 2.13	Sketch of the model of a solid propellant burning with uniform combustion in the gas phase	2-25
Figure 2.14	Real and imaginary parts of a QSHOD response function computed with equation 2.67: $n_s = 0$, $A = 6.0$, $B = 0.60$	2-29
Figure 2.15	Experimental results for the change of burning rate of two double-base propellants	2-31
Figure 2.16	The real part of the response function vs. the non-dimensional frequency, $a_1 w/r^2$ for A-13 propellant: the solid curve is calculated from the QSHOD formula for the values of A and B shown	2-31

Figure 2.17	The real part of the response function vs. the non-dimensional frequency for A-35 propellant	2-32
Figure 2.18	Real part of the response function measured with T-burners	2-32
Figure 2.19	Spatial definition of the model	2-38
Figure 2.20	QSHOD response function with a time lag	2-39
Figure 2.21	Combustion response, QSHOD model with gas phase dynamics	2-40
Figure 2.22	Effects of activation energy and density on the dynamics of the surface layer	2-41
Figure 2.23	Combustion response function including the dynamics of the surface layer and the gas phase	2-41
Figure 2.24	Results of a simulation with a QSHOD combustion response	2-43
Figure 2.25	Results of a simulation including dynamics of a surface layer	2-43
Figure 2.26	Results of a simulation including a time delay ($\tau = 1.5$)	2-43
Figure 2.27	Results of a simulation including dynamics of a surface layer and the gas phase	2-43
Figure 2.28	Sketches illustrating two primary processes involved in the generation of vorticity	2-45
Figure 2.29	Sketch of an apparatus for demonstrating the excitation of acoustic modes by vortex shedding at a pair of annuli	2-47
Figure 2.30	Vortex shedding from (a) an annular obstacle composed of residual inhibitor material; and (b) an edge of a backward facing step at a transition zone; (c) due to instability of the mean flow near a burning surface (parietal vortex shedding)	2-48
Figure 2.31	Typical flow between the baffles when a pure tone is generated	2-49
Figure 2.32	Experimental results for the excitation of acoustic modes by vortex shedding	2-50
Figure 2.33	Vaporization response according to Heidmann and Wieber	2-54
Figure 2.34	Graphical definition of a simple time lag	2-57
Figure 2.35	Early measurements of the time lag and pressure index in a gas rocket	2-59
Figure 2.36	Sketch of a simple case with a single entropy wave (S) and acoustic pressure waves (P_+ , P_-)	2-60
Figure 2.37	Large-scale coherent structures in a mixing layer at 8 atmospheres in flow past a splitter plate	2-62
Figure 2.38	Photograph of vortices shed in a reacting flow	2-63
Figure 2.39	Flow past a bluff body flameholder under two conditions of flow at approximately the same speed	2-64
Figure 2.40	Development of a vortex during one cycle of a pressure oscillation	2-66
Figure 2.41	Development of a vortex at the interface of two unlike fluids	2-67
Figure 2.42	An elementary model of combustion in vortices as a mechanism for driving acoustic waves	2-67
Figure 2.43	Vortex shedding from a backward-facing step, followed by impingement on an obstacle	2-71
Figure 2.44	Normalized spectra of pressure fluctuations at the step of Figure 2.43 for two mean flow velocities at the dump plane	2-72
Figure 2.45	Coupling between pressure oscillations, structural vibrations and the injection system	2-73
Figure 2.46	Some results of calculations based on the n - τ model	2-75

Figure 2.47	Comparison of calculations and some experimental results interpreted with the $n - \tau$ model	2-75
Figure 2.48	A general representation of stability based on the $n - \tau$ model	2-76
Figure 2.49	Stability boundaries inferred with the $n - \tau$ model applied to a gas-fueled rocket	2-77
Figure 2.50	Experimental results for n and τ , using stable hypergolic propellants and various injectors	2-78
Figure 2.51	Two examples of aircraft gas turbine engines with thrust augmentation	2-80
Figure 2.52	Schematic flight envelope showing typical regions of high- and low-frequency instabilities in thrust augmentors	2-82
Figure 2.53	Sketches of the evolution of the geometry of gas turbine engines	2-82
Figure 2.54	Pratt and Whitney F100-PW-100 Augmented Turbofan Engine	2-83
Figure 2.55	Spectra of pressure oscillations observed in thrust augmentors	2-83
Figure 2.56	Flow in the vicinity of typical flameholders emphasizing the recirculation zones	2-84
Figure 2.57	A flame stabilized on a gutter in a tube	2-85
Figure 2.58	Two simple ramjet configurations using stabilization at abrupt changes of area	2-86
Figure 2.59	Model used for measurements in the inlet to a dump combustor	2-88
Figure 2.60	Comparison of measured and calculated mode shapes in the inlet of a laboratory dump combustor	2-89
Figure 2.61	Simple apparatus for demonstrating a singing flame	2-91
Figure 2.62	Location of the flame shown in Figure 2.61 to maintain a continuous tone, i.e. 'singing'	2-92
Figure 2.63	Concentrations at equilibrium of carbon monoxide and oxides of nitrogen	2-93
Figure 2.64	General behavior as the equivalence ratio is reduced near the lean blowout limit	2-94
Figure 2.65	Sketch of an electrically heated Rijke tube	2-95
Figure 2.66	The effect of tube length and heater location on the generation of oscillations in a Rijke tube	2-97
Figure 2.67	The effect of a second heater on the stability of oscillations	2-98
Figure 2.68	A prediction of a stability limit	2-99
Figure 2.69	A sketch of the horizontal Rijke tube used by Matveev	2-100
Figure 2.70	Comparison of experimental data and calculations for stability boundaries of the Rijke tube	2-101
Figure 2.71	Region of integration for obtaining matching conditions	2-102
Figure 2.72	(a) Illustrating the independence of heat transfer on flow direction; (b) illustrating possible dependence of heat transfer on flow direction due to microscopic properties of the surface	2-111
Figure 2.73	Three sorts of nonlinear behavior due to rectification distinguished by the relative values of the mean and fluctuating components of velocity	2-112
Figure 2.74	A basic flame-driven Rijke tube	2-112
Figure 5.1	Wave motions subsequent to an initial pressure pulse at rest	5-7
Figure 5.2	Reflection of a pressure pulse from a rigid surface	5-7
Figure 5.3	Comparison of spherical and planar waves produced by regions of increased pressure	5-9

Figure 5.4	Generation of spherical, planar and cylindrical waves by point sources	5-10
Figure 5.5	Acoustic energy and intensity	5-14
Figure 5.6	A graph of decibels versus pressure (lbs./in ²)	5-15
Figure 5.7	A graph showing the audible range of hearing for a typical human subject	5-15
Figure 5.8	Reflection of a plane wave	5-19
Figure 5.9	A uniform tube having a single discontinuity	5-22
Figure 5.10	Comparison of experimental and theoretical results for normal frequencies in a T-burner at ambient temperature	5-23
Figure 5.11	Rectangular chamber	5-25
Figure 5.12	Circular cylindrical coordinates	5-26
Figure 5.13	The first six transverse modes in a circular cylinder	5-26
Figure 5.14	Acoustic velocity and temperature distributions for the fundamental mode in a closed tube	5-27
Figure 5.15	Definition of the lateral control surface	5-32
Figure 5.16	The basic impedance tube	5-38
Figure 5.17	Sketch of $ \hat{p} $ when distributed losses are ignored	5-39
Figure 6.1	Basic physical model of a liquid rocket used in the Princeton theoretical work	6-3
Figure 6.2	L^* versus chamber pressure, showing the stability limit for oscillations	6-6
Figure 6.3	Block diagram of the system, adapted from Figure 1 of Coates, Cohen, and Harvill	6-6
Figure 6.4	L^* instability data for two propellants	6-7
Figure 6.5	Two examples of natural cessation of L^* instabilities	6-8
Figure 6.6	Five pressure records of chuffing	6-8
Figure 6.7	Real and Imaginary parts of a simple response function	6-11
Figure 6.8	The L^* -chart for determining the parameters A and B	6-13
Figure 6.9	A tube with distributed heat addition and an oscillating piston to drive waves	6-17
Figure 6.10	The Caltech dump combustor	6-20
Figure 6.11	Experimental confirmation of Rayleigh's Criterion	6-21
Figure 6.12	Geometrical parameters defined by Brownlee and a typical time history of the mean chamber pressure	6-29
Figure 6.13	Stability boundaries for the 010 mode: experimental and theoretical	6-30
Figure 6.14	Dependence of the admittance function on frequency inferred from Brownlee's measurements	6-30
Figure 6.15	Velocity vectors for flow through a permeable boundary	6-36
Figure 6.16	The origin of 'flow-turning': An element of fluid shown (a) at entry normal to a burning or porous surface, and (b) in an intermediate state of the process of acquiring the local axial velocity having mean and acoustic components	6-37
Figure 6.17	Grains used in laboratory motors for which data were taken for unstable oscillations	6-43
Figure 6.18	A comparison of data taken with the motors shown in Figure 6.17 with predictions according to (6.161)	6-43
Figure 6.19	Calculation of the decay of the fundamental mode following a pulse	6-43

Figure 6.20	A <i>T</i> -burner chart for determining the parameters <i>A</i> and <i>B</i>	6-46
Figure 6.21	Growth of unstable motions according to the approximate analysis; and a numerical simulation of the same problem	6-49
Figure 6.22	Spectrum for the calculated waveform shown in Figure 6.21(b)	6-51
Figure 6.23	Effect of truncation in the waveforms	6-52
Figure 6.24	Stylized rendition of azimuthal and streamwise vortices in a solid propellant rocket chamber	6-53
Figure 6.25	Some configurations used in observations of vortex shedding and instabilities	6-54
Figure 6.26	The five two-dimensional configurations of the LP3 test motors	6-55
Figure 6.27	Upper image: flow visualization of parietal vortex shedding, using PLIF with acetone; Lower image: result of numerical calculations	6-56
Figure 6.28	The three kinds of vortex shedding	6-56
Figure 6.29	A sketch of the LP6 test device	6-56
Figure 6.30	Experimental results for a test in the LP6 configuration showing parietal vortex shedding	6-57
Figure 6.31	Idealized axisymmetric and two-dimensional nozzles for calculating admittance functions	6-60
Figure 6.32	Numerical values for the admittance function of a nozzle exposed to isentropic oscillations	6-63
Figure 6.33	Results for the real part of the admittance function for a nozzle	6-63
Figure 6.34	Results for the imaginary part of the admittance function for a nozzle	6-63
Figure 6.35	Comparison of the theoretical and experimental admittance results for nozzle 15-08-2.5, longitudinal modes	6-64
Figure 6.36	Comparison of the theoretical and experimental admittance results for nozzle 45-08-2.5, longitudinal modes	6-65
Figure 6.37	Comparison of the theoretical and experimental admittance results for nozzle 45-16-2.5, longitudinal modes	6-65
Figure 6.38	Attenuation of acoustic waves caused by small particles suspended in a gas	6-69
Figure 6.39	Frequency shift of acoustic oscillation caused by small particles suspended in a gas	6-69
Figure 6.40	Mass distribution of subfractions of the combustion residue of NWC Mix No. 10	6-69
Figure 6.41	A possible explanation of increased growth rate due to distributed combustion of aluminum in a <i>T</i> -burner	6-73
Figure 6.42	General view of the Ariane 5 strap-on booster motor P230	6-74
Figure 6.43	Results for the unsteady pressure measured in a static test firing of the Ariane 5, P230 motor	6-75
Figure 6.44	Shape of the grain used in simulations of two-phase unsteady flow in the Ariane 5, P230 motor	6-76
Figure 7.1	Steepening of a planar compressive wave into a shock wave	7-3
Figure 7.2	Acoustic streaming, a consequence of small viscous effects and nonlinear acoustics	7-4
Figure 7.3	Finite streaming motions in a motor having five slots, giving net counterclockwise circulation	7-5
Figure 7.4	An oscillating shock wave in a closed tube	7-5

Figure 7.5	Closed tube containing heater at its midpoint	7-6
Figure 7.6	Model of a liquid rocket analyzed in the Princeton works	7-7
Figure 7.7	Waveforms observed in a gas rocket	7-8
Figure 7.8	Steepening of a longitudinal wave travelling in a cylindrical chamber; $ p'/p $ vs. x	7-10
Figure 7.9	The envelope of oscillations for the T-burner firing shown in Figure 1.36	7-11
Figure 7.10	Data for the growth and decay periods of the firing shown in Figure 7.9	7-13
Figure 7.11	Nonlinear growth of oscillations for several values of the initial amplitude ratio $A_0=A_m$	7-14
Figure 7.12	Nonlinear decay of oscillations for several values of the initial amplitude ratio $A_0=A_m$	7-14
Figure 7.13	A T-burner firing showing stronger nonlinear behavior during the initial portion of the decay of oscillations	7-15
Figure 7.14	The two cases presented by equation (7.22)	7-16
Figure 7.15	The two cases presented by equation (7.24). Part (b) represents a pulsed (triggered) instability	7-17
Figure 7.16	Energy flow in the two-mode approximation	7-18
Figure 7.17	Regions of stability for two longitudinal modes, time-averaged equations	7-21
Figure 7.18	Effects of truncation for a stable limit cycle: first mode unstable, second mode stable	7-21
Figure 7.19	Effects of truncation for an unstable limit cycle: first mode unstable, second mode stable	7-22
Figure 7.20	Development of a stable limit cycle when the first mode is stable but the second mode is unstable	7-22
Figure 7.21	Amplitudes in two limit cycles involving the first tangential and first radial modes only	7-26
Figure 7.22	An example of limit cycles for three normal modes, 1T/1R/2T	7-26
Figure 7.23	Sketch of the interpretation as a 'detonation' wavefront	7-28
Figure 7.24	The test engine, 20,000 lbf-thrust engine and components	7-28
Figure 7.25	Schematic illustration of the continuation method applied to limit cycles	7-29
Figure 7.26	Two examples of bifurcation	7-30
Figure 7.27	The effects of truncation for a two-mode system: second mode unstable, all other modes stable	7-31
Figure 7.28	Effect of time-averaging for two modes	7-31
Figure 7.29	Solutions with truncation of the time-averaged equations	7-32
Figure 7.30	Maximum amplitude of η_1 in the limit cycle; four modes, comparison of results for the full oscillator and the time-averaged equations	7-32
Figure 7.31	Hysteresis loop for a recirculated zone idealized as a simple chemical reactor	7-34
Figure 7.32	Sketch of a recirculation zone formed by a jet of fuel or oxidizer	7-34
Figure 7.33	Stability boundary and an idealized hysteresis loop for the Caltech dump combustor	7-34
Figure 7.34	(a) Sketch of the dump combustor modified to allow injection of pulses; (b) hysteresis observed in the apparatus shown in (a)	7-35
Figure 7.35	Pressure traces and spectra for the two branches of the hysteresis loop	7-35

Figure 7.36	Time history of a portion of trace	7-36
Figure 7.37	Shadowgraphs of the transition induced by a single pulse initiated at $t = 0$	7-37
Figure 7.38	Pressure trace and spectrum for a simulation with noise; four modes, first mode unstable	7-40
Figure 7.39	Simulated pressure trace with noise; all modes stable	7-42
Figure 7.40	Application of Berg's method: power spectrum of the pressure trace in Figure 7.39 and its reconstruction	7-42
Figure 7.41	Dependence of the peak amplitudes of the power spectra for four modes, on noise power	7-43
Figure 7.42	Reconstructed pressure trace for the transient response excited by a 10% pulse	7-43
Figure 7.43	Values of decay rates (modal attenuation) found with Berg's method with multiplicative (ξ_n) noise	7-44
Figure 7.44	Values of decay rates (modal attenuation) found with the method of pulsing	7-44
Figure 7.45	A pulsed instability initiated in an 80 inch long motor by a small explosive charge	7-46
Figure 7.46	Picture taken with schlieren apparatus midway between the head-end and the nozzle	7-46
Figure 7.47	Stability boundaries for three propellants tested in 80 inch motors and the influence of mean pressure (throat diameter) on stability	7-47
Figure 7.48	Stability boundary for 40 inch rockets, 5 inch diameter showing chamber pressure and burning rate below which pulses of pressure are stable	7-48
Figure 7.49	Response of the head end of a motor ($L = 10$ ft.) to a continuously applied input pressure	7-49
Figure 7.50	Three types of pulsing devices used by Baum, Lovine and Levine	7-50
Figure 7.51	Time evolution of pressure perturbations produced by a pyro pulser	7-50
Figure 7.52	Comparison of measured and predicted pressures at the head end, test PCC4	7-51
Figure 7.53	Response functions for the three propellants used by Baum, Levine and Lovine	7-51
Figure 7.54	Comparison of observed and calculated pulsed instabilities in an aft-finocyl motor	7-51
Figure 7.55	Mean heat transfer coefficient measured in T-burners showing dependence on amplitude of pressure amplitude	7-53
Figure 7.56	Mean heat transfer rates correlated as mean Nusselt number versus mean Reynolds number	7-53
Figure 7.57	Superposition of two pulse trains to represent propagation of a single pulse in a closed tube	7-55
Figure 7.58	Propagation of pulses developed from a stationary initial pulse in a closed tube	7-55
Figure 7.59	Approximations to a rectangular initial pulse by 10, 30, 50 modes	7-58
Figure 7.60	Propagation of a rectangular pulse without losses (10 modes)	7-59
Figure 7.61	Propagation of an evolving cosine wave	7-59
Figure 7.62	Propagation of a rectangular pulse (10 modes)	7-59
Figure 7.63	The function $F(u')$ used in the model having a threshold velocity $u_t > 0$; the value $u_t = 0.02$ is only an example	7-61
Figure 7.64	Maximum amplitude of the first acoustic mode in the limit cycle showing the contribution of nonlinear gasdynamics and combustion	7-62

Figure 7.65	Maximum amplitude of the first acoustic mode in the limit cycle showing a subcritical bifurcation with a turning point only if both nonlinear gasdynamics and nonlinear combustion dynamics are accounted for	7-62
Figure 8.1	Schematic diagram showing qualitatively the conditions under which instabilities exist	8-2
Figure 8.2	Qualitative and stylized interpretation of the possible effect of modifications on the dynamical behavior of a combustion system	8-2
Figure 8.3	Block diagram of the basic system (G, Q) with passive control due to modifications of the chamber dynamics (C_G) and of the combustion dynamics (C_Q)	8-3
Figure 8.4	Simple forms of baffles for solid propellant rockets	8-5
Figure 8.5	Early examples showing consequences of high-frequency oscillations	8-6
Figure 8.6	The importance of baffles in the F-1 engine	8-6
Figure 8.7	Perspective view of a rocket combustion chamber with longitudinal baffles installed on the injector face	8-7
Figure 8.8	An injector with baffles and azimuthal slots	8-7
Figure 8.9	Examples of the arrangement and shapes of baffles fixed to the injector face of a liquid rocket	8-8
Figure 8.10	The pressure fields for the lowest order modes commonly encountered in circular cylindrical combustion chambers	8-8
Figure 8.11	Combustible longitudinal baffles (ribs) in the Russian RD-0110 engine and their substantial effects on the amplitude of oscillations	8-10
Figure 8.12	The combustion chamber with a three-bladed baffle analyzed by Wicker, Yoon and Yang	8-10
Figure 8.13	A model of a rocket chamber and the measured spectrum of tangential modes	8-11
Figure 8.14	Two methods for measuring the damping factor: (a) decay rate, α ; (b) bandwidth	8-11
Figure 8.15	Results for the decay rate of tangential modes in the chamber shown in Figure 8.13(a)	8-11
Figure 8.16	The essential features of an idealized cavity resonator	8-12
Figure 8.17	Convectively cooled thrust chamber fitted with an acoustic liner	8-14
Figure 8.18	Apparatus for measurement of the acoustic properties of a model of a liner with bias flow	8-14
Figure 8.19	Absorption coefficient for a portion of acoustic liner	8-15
Figure 8.20	Scheme of a procedure followed to improve the attenuation of combustion instabilities by increasing the particle damping	8-17
Figure 8.21	Particle size distribution for tactical motor propellant and a conventional aluminized propellant	8-18
Figure 8.22	Comparison of particle size distribution to optimum size for damping in motor	8-18
Figure 8.23	Flow past a bluff body flameholder under two conditions of flow at approximately the same speed	8-19
Figure 8.24	Vortex shedding from a rearward-facing step	8-20
Figure 8.25	Examples of configurations used to study vortex shedding in combustion chambers	8-21
Figure 8.26	Sketch of the origin and elimination of pressure oscillations produced in the chamber by vortex shedding in a solid propellant rocket	8-22

Figure 8.27	'Waterfall' plots of low-frequency oscillations observed in a Minuteman III Stage 3 motor	8-22
Figure 8.28	Cylindrical jet of carbon monoxide into air, initial Reynolds number approximately 30,000 (average speed, 127 ft/s)	8-23
Figure 8.29	Test equipment for studying reacting and non-reacting jet flows in a dump combustor	8-25
Figure 8.30	An example of test results showing the presence of coherent vortices when the acoustic forcing frequency f_F equals the preferred mode frequency f_{pm} , the frequency at the maximum of the response	8-26
Figure 9.1	Block diagram for a system containing passive (C_G and C_Q) and feedback (C_f and C_{fb}) control	9-3
Figure 9.2	General block diagram of a combustion system with passive and active control	9-4
Figure 9.3	A general block diagram for classical and modern control	9-5
Figure 9.4	Schematic of the first proposal for active feedback control of the dynamics in a combustion system	9-6
Figure 9.5	Block diagram for the system shown in Figure 9.4	9-6
Figure 9.6	Feedback control of a Rijke tube by injection of acoustic waves	9-8
Figure 9.7	An early example of control based on Rayleigh's Criterion	9-8
Figure 9.8	The geometry of the rig at Rolls-Royce, Derby, with one set of flow conditions	9-10
Figure 9.9	Cambridge apparatus	9-11
Figure 9.10	Magnitude and phase of the pressure distribution and the transfer function for heat release for one configuration of the test apparatus shown in Figure 9.9(a)	9-12
Figure 9.11	Unsteady motions in the test rig shown in Figure 9.9(a)	9-14
Figure 9.12	The device for mixing secondary fuel and air at the upstream end of the flameholder shown in Figure 9.9	9-14
Figure 9.13	Apparatus used in the first tests of feedback control of combustion at École Centrale and the Technische Universität München. (a) Tubular burner exhibiting oscillations; (b) the configuration with provision for feedback control	9-15
Figure 9.14	Feedback control at École Centrale	9-17
Figure 9.15	GE demonstration of feedback control	9-18
Figure 9.16	A Nyquist diagram recorded by Gulati and Mani for their combustor with their first controller	9-19
Figure 9.17	Schematic of a Rijke tube apparatus (a) and the block diagram (b) for loop shaping design	9-20
Figure 9.18	Open and closed loop power spectra for the Rijke tube shown in Figure 9.17(a)	9-21
Figure 9.19	The general scheme according to the procedures followed here for connecting the physical system (a combustor), physical modeling, mathematical modeling, dynamics and control	9-22
Figure 9.20	A simple block diagram for proportional-integral-derivative (PID)	9-28
Figure 9.21	Block diagram for PID control applied to a linear system; the transfer function $G(s)$ is given by equation Figure 9.52	9-29
Figure 9.22	Simplified sketch of the system analyzed by Fung, Sinha, and Yang	9-29
Figure 9.23	The apparatus and stability diagram for the results with no feedback control reported by Schimmer and Vortmeyer	9-31

Figure 9.24	Feedback control at Technische Universität München	9-32
Figure 9.25	Test results found with the apparatus shown in Figure 9.24	9-33
Figure 9.26	Test apparatus and feedback control with a simple liquid fuel nozzle and the direct drive valve (DDV)	9-34
Figure 9.27	A sketch of a combustor used in the Vx4.3A series Siemens gas turbines and an illustration of the size of the combustor	9-35
Figure 9.28	Simplified sketches of the Siemens Hybrid Burner	9-35
Figure 9.29	Minimum number of four actuators, one sensor and one controller to control a standing second azimuthal mode	9-36
Figure 9.30	Addition of the cylindrical burner outlet (CBO) to the Siemens Hybrid Burner	9-36
Figure C.1	Sketch of the flow in an acoustic boundary layer showing the velocity field at two instants separated by one-half period	C-1
Figure E.1	Three examples of discontinuities in a flow field	E-2
Figure E.2	A discontinuity in a one-dimensional flow	E-2
Figure F.1	The problem defined for determining $p(x, y)$	F-2
Figure G.1	The system $G(s)$ with controller $H(s)$ and negative unity feedback	G-1
Figure G.2	Definition of the Nyquist path excluding poles of HG on the imaginary axis. Examples of poles and zeros within the path are not excluded	G-2
Figure G.3	Indentations around poles on the imaginary axis. Poles and zeros within the contour are suppressed	G-4
Figure G.4	Definitions of positive and negative encirclements	G-8
Figure G.5	Illustrating no encirclement ($N_0 = 0$) and two negative encirclements ($N_0 = -2$) by $f(s)$ when s executes a closed contour encircling the origin	G-9
Figure G.6	Examples showing consistent maintenance of the definition of 'interior' of a path under mapping from the s -plane to the G -plane	G-10
Figure G.7	An example showing two negative encirclements of the origin by the path obtained by mapping the Nyquist contour	G-11
Figure G.8	Mappings of the Nyquist contour in the HG and $1 + HG$ planes	G-11
Figure G.9	Examples of positive and negative encirclements of -1 by mappings of the Nyquist contour	G-12
Figure G.10	Forming the Nyquist plot for $HG = \frac{K}{s(s+p_1)(s+p_2)}$	G-14
Figure G.11	A stable second order system with an integrator	G-15
Figure G.12	The Nyquist plot for the system shown in Figure G.11	G-16
Figure G.13	The Nyquist plot for 'any' HG near $ HG _\pi$, i.e., the magnitude of HG when the phase or \arg of HG is π	G-16
Figure G.14	The Bode plot for the system shown in Figure G.11, $K = 1$	G-18

List of Tables

Table		Page
Table 2.1	Typical Values of Combustion and Physical Properties	2-21
Table 2.2	Principal Characteristics of the MURI Propellants	2-33
Table 5.1	Results for Rightward and Leftward Traveling Sinusoidal Waves	5-16
Table 5.2	Some Formulas for Incident and Reflected Plane Waves	5-19
Table 6.1	Values of the Geometrical, Combustion and Physical Properties	6-50
Table 6.2	Linear Growth Constants and Frequency Shifts	6-51
Table 6.3	Total Values of the Linear Growth Constants and Frequency Shifts	6-51
Table 6.4	Frequencies and Amplitudes of Acoustic Pressures	6-51
Table 6.5	Mass Fractions of NWC Mix No. 10 Residue for Particles Smaller than $43 \mu\text{m}$	6-70
Table 6.6	Parameters Used in the Particle Damping Calculations	6-70
Table 6.7	Damping Coefficients Measured, NWC Mix No. 10, for Particle Sizes Smaller than μm	6-71
Table 6.8	Measured and Calculated Damping Coefficients for NWC Mix and 10	6-71
Table 7.1	Summary of Some Works from Princeton on a Theory of Combustion Instabilities	7-7
Table 7.2	Values of the Linear Parameters	7-41
Table 7.3	Relation Between the Noise Power of Ξ_n and the rms Value of the Simulated Pressure Fluctuation	7-41
Table 8.1	Considerations of Baffles for Application to Solid Propellant Rockets	8-9
Table D.1	Definition of Splitting a Disturbance in the Three Modes of Propagation	D-4
Table D.2	Zeroth Approximation for the Flow Variables in the Three Modes	D-4

Foreword

Propulsion systems, which are one of the priority activities of the Applied Vehicle Technology Panel of NATO's Research and Technology Organisation, are frequently confronted by unexpected and unsteady behaviors known by the generic name of "combustion instabilities". Many solid propellant rockets, liquid propellant engines, ramjets and main or reheat combustors of turbojets have been affected by these types of problems during development. Combustion instabilities were identified at the start of the 1950s as an endemic disease and were then the subject of research aimed at understanding their origins, explaining how they developed and, eventually, predicting their levels. The researchers were very quickly convinced of the difficulty of the problem, which is essentially due to two factors: firstly, the difficulty of taking detailed measurements of the internal flow in engines, because of the extremely severe physical conditions inside them, and secondly, the close coupling between numerous unsteady mechanisms related to fluid mechanics, combustion, two-phase flows, etc. The work done on this subject in the United States has had a profound influence in all Western countries and I had the good fortune, when I was asked to study the question for the French Armament Procurement Agency (DGA), to meet Professors Fred Culick and Ed Price, then later Professor Gary Flandro and other US Navy, US Air Force and NASA specialists. These contacts were determining factors for the direction of French work.

Today, Professor Fred Culick proposes a summary entitled "Unsteady Motion in Combustors for Propulsion Systems" in the form of an AGARDograph. There are very few scientists in the world who have accumulated such in-depth expertise and experience on the subject and the RTO should be grateful to Professor Fred Culick for having put all this acquired knowledge at the service of NATO's technological research. An attentive reading of the document prepared reveals that it is a truly comprehensive survey, in the literal sense of the word. What Professor Fred Culick has done is to put several decades of research into an understandable form, thus endowing the work with a true encyclopaedic nature, both by the variety of situations examined and by the abundance and exhaustiveness of the references used. Due to his great teaching ability, Professor Fred Culick has also been able to conduct a quite weighty mathematical analysis with thoroughness and accuracy and to establish the indispensable link between observations made on engines and predictions arrived at by calculation. Furthermore, if only one of the work's qualities had to be pointed out, I, for my part, would opt for Professor Fred Culick's exceptional ability to give physical meaning to the equations.

I therefore think that the AGARDograph prepared by Professor Fred Culick is bound to become a worldwide reference on the difficult but always topical subject of combustion instabilities.

Dr. Paul KUENTZMANN
ONERA, France
Former PEP/AGARD member
Former AVT/RTO member
RTB member

Avant-propos

Les systèmes propulsifs, qui constituent l'une des priorités des activités de la Commission Applied Vehicle Technology de la Research and Technology Organisation de l'OTAN, sont fréquemment confrontés à des comportements instationnaires imprévus connus sous le nom générique « d'instabilités de combustion ». De nombreux moteurs-fusées à propergol solide, moteurs-fusées à ergols liquides, statoréacteurs, foyers principaux ou de rechauffe de turboréacteurs ont connu ce type de problème en cours de développement. Identifiées au début des années 50 comme une maladie endémique, les instabilités de combustion ont dès lors fait l'objet de recherches pour en comprendre l'origine, en expliquer le développement et, à terme, en prévoir les niveaux. Les chercheurs ont été très tôt convaincus de la difficulté du problème, qui tient pour l'essentiel à deux aspects : d'une part, à la difficulté de réaliser des mesures détaillées de l'écoulement dans les moteurs, en raison des conditions physiques très sévères qui y règnent, et, d'autre part, du fait du couplage étroit de nombreux mécanismes instationnaires relevant de la mécanique des fluides, de la combustion, des écoulements diphasiques, etc. Les travaux conduits sur ce thème aux Etats-Unis ont imprégné tous les pays occidentaux et j'ai eu la chance, lorsque j'ai été chargé d'étudier la question pour la DGA française, de rencontrer les Professeurs Fred Culick et Ed Price, puis ultérieurement le Professeur Gary Frandro et d'autres spécialistes de l'US Navy, de l'US Air Force et de la NASA. Ces contacts ont été déterminants pour orienter les travaux français.

Le Professeur Fred Culick propose aujourd'hui sous la forme d'un AGARDograph une synthèse intitulée « Unsteady Motions in Combustion Chambers for Propulsion Systems ». Il existe très peu de scientifiques au monde qui aient accumulé une expertise et un expérience aussi approfondies sur le sujet et la RTO doit être reconnaissante au Professeur Fred Culick d'avoir mis tout cet acquis au service des recherches technologiques de l'OTAN. Une lecture attentive montre que le document préparé constitue une véritable Somme, au sens littéral du mot. Le Professeur Fred Culick a en effet remis en forme plusieurs décennies de recherche, conférant ainsi à l'ouvrage un caractère véritablement encyclopédique, tant par la variété des situations examinées que par l'abondance et l'exhaustivité des références utilisées. Grâce à un sens pédagogique aigu, le Professeur Fred Culick a également su conduire, avec rigueur et précision, une analyse mathématique assez lourde, et établir la liaison indispensable entre observations réalisées sur moteurs et prévisions de calcul. Si en outre une seule qualité de l'ouvrage devait être mise en exergue, j'opterais pour ma part sur l'exceptionnelle faculté du Professeur Fred Culick à donner un sens physique aux équations.

L'AGARDograph préparé par le Professeur Fred Culick m'apparaît donc devoir devenir l'ouvrage mondial de référence sur le sujet difficile mais toujours d'actualité des instabilités de combustion.

Docteur Paul KUENTZMANN
ONERA, France
Ex membre PEP/AGARD
Ex membre AVT/RTO
Membre RTB

Unsteady Motions in Combustion Chambers for Propulsion Systems

(RTO-AG-AVT-039)

Executive Summary

Combustion instabilities were discovered in the late 1930s as anomalies in firings of solid and liquid rockets. During World War II, experience gradually suggested that certain problems encountered in development and actual use of solid rockets were especially associated with pressure oscillations having relatively high frequencies ranging from a few hundred to several thousand Hertz. Associated problems were structural vibrations; greatly increased surface heat transfer rates; sometimes impaired performance; and, in extreme cases, failure of the combustion system and destruction of vehicles. By the 1950s, forms of combustion instabilities had been identified in all types of rockets, gas turbines, thrust augmentors and ramjets. The problem continues to the present time and will always be found in combustion systems, particularly those intended to provide high performance. Eliminating instabilities therefore becomes an important task in a development program.

This study includes a wide span of material ranging from summaries of practical examples of combustion instabilities to the present status of the field; and results of a method for analysis of the general problem. Following a summary of practical problems in Chapter 1, a lengthy discussion is given in Chapter 2 of the best known mechanisms for oscillations in the various kinds of systems. Chapters 3 and 4 summarize a widely used general method of analyzing general unsteady motions in a combustion chamber, based on expansion in normal modes and spatial averaging of the equations of motion. The result is a formulation focused on the behavior of a set of coupled nonlinear oscillators.

Chapter 5 is a summary of those parts of classical acoustics required to understand linear behavior and the elementary aspects of unsteady behavior in combustors. Chapters 6 and 7 are devoted to the theory of linear and nonlinear behavior respectively, with examples taken from experience with combustion systems. In Chapter 8 the subject of passive control is covered, giving a brief summary of experience, with several examples. The last section of the chapter describes work which has been done on some of the connections between the generation and shedding of large vortices and combustion in dump combustors.

The book ends with Chapter 9, a brief coverage of active control applied to combustors. This subject has important potential applications not yet realized. It is particularly interesting because, in an elementary way, the framework of modern active control fits naturally into the scheme formulated here in Chapters 3 and 4. Eight Appendices to the book contain treatments of special topics referred to in the text.

Mouvements instables dans les chambres de combustion des systèmes de propulsion

(RTO-AG-AVT-039)

Synthèse

A la fin des années 30, on avait découvert des instabilités de combustion, qui constituaient des anomalies dans les tirs de fusées à combustible solide et liquide. Au cours de la Deuxième Guerre Mondiale, l'expérience a progressivement suggéré que certains problèmes rencontrés lors du développement et de l'exploitation des fusées à combustible solide étaient particulièrement associés à des oscillations de pression ayant des fréquences relativement élevées entre quelques centaines et plusieurs milliers de Hertz. Ces problèmes étaient accompagnés de vibrations de structure, de taux de transfert de chaleur de surface largement augmentés, de dégradation des performances dans certains cas et, dans des cas extrêmes de la défaillance du système de combustion et de la destruction des véhicules. Au cours des années 50, des formes d'instabilité de combustion ont été identifiées sur tous les types de fusées, de turbines à gaz, d'augmentateurs de poussée et de stato-réacteurs. Le problème se poursuit à l'heure actuelle et existera toujours sur les systèmes de combustion, en particulier ceux destinés à assurer des performances élevées. C'est pourquoi l'élimination des instabilités est devenue un point important des programmes de développement.

Cette étude recouvre un large éventail de sujets, allant des synthèses d'exemples pratiques d'instabilités de combustion à l'état actuel du domaine et aux résultats d'une méthode d'analyse du problème général. Le Chapitre 1 donne une synthèse des problèmes pratiques, le Chapitre 2 donne une description détaillée des mécanismes les plus connus relatifs aux oscillations sur les différents types de systèmes. Les Chapitres 3 et 4 résument une méthode générale largement utilisée pour l'analyse des mouvements instables généraux dans une chambre de combustion, en fonction de l'expansion en modes normaux et d'une moyenne spatiale des équations de mouvement. Il en résulte une formulation axée sur le comportement d'un ensemble d'oscillateurs non linéaires couplés.

Le Chapitre 5 est un résumé des domaines de l'acoustique classique nécessaires à la compréhension du comportement linéaire et des aspects élémentaires du comportement instable des chambres de combustion. Les Chapitres 6 et 7 sont consacrés à la théorie des comportements linéaires et non linéaires respectivement, avec des exemples tirés de l'expérience sur les systèmes de combustion. Le Chapitre 8 traite le sujet du contrôle passif et donne un bref aperçu de l'expérience, ainsi que différents exemples. La dernière section de ce chapitre décrit le travail réalisé sur certaines liaisons entre la génération et la chute des grands tourbillons et la combustion dans les chambres de combustion largables.

L'ouvrage se termine par le Chapitre 9, qui traite brièvement du contrôle actif appliqué aux chambres de combustion. Ce sujet comporte des applications potentielles importantes qui n'ont pas encore été réalisées. Il est particulièrement intéressant car, de manière élémentaire, le cadre du contrôle actif moderne s'adapte naturellement aux schémas formulés dans les Chapitres 3 et 4. Les huit Annexes de l'ouvrage décrivent le traitement de sujets spéciaux mentionnés dans le texte.

Overview

Phenomena referred to generally as combustion instabilities are fundamentally related to the stability of motions in a combustion chamber. Their existence is normally inferred from observations of well defined oscillations of pressure or structural distortions. Instabilities of combustion processes themselves are rarely contributing factors, the chief exceptions being possible intrinsic instabilities of solid propellants, and the weakening of flame stabilization mechanisms near the lean operating limits of gaseous and liquid fueled systems. Broadly, then, the appearance of a combustion instability is due to a loss of stability of the composite dynamical system comprising the combustion processes and the chamber itself, containing the medium which supports waves associated with the unstable motions.

Combustion instabilities have been found in all types of systems. The reason is simple and fundamental: In a combustor, by design the combustion processes generate high power densities under conditions when the losses of energy are small. Only weak coupling between fluctuations of the combustion power and the flow of the medium is sufficient to produce undesirable fluctuations of pressure and kinetic energy in the flow. Mainly three characteristics of a system influence its dynamical behavior: the physical state in which reactants are introduced (solid, liquid, gas); the geometry of the system; and the specific mechanism causing the instabilities to occur. It is therefore possible to construct a general analytical framework sufficiently comprehensive to capture most, if not all, of the main features of instabilities in any combustion system. One purpose of this book is to describe an approach that has been applied successfully to a broad range of problems arising in laboratory devices and in full-scale systems.

The approach follows a well-travelled path which consists essentially in constructing reduced-order models of dynamical behavior by first applying a method of spatial averaging. Formally the dynamics of the continuous flow system having an infinite number of degrees of freedom is represented by the dynamics of a system of coupled nonlinear oscillators in one-to-one correspondence with the natural acoustic modes of the combustor in question. Long understood from experience in several fields, the idea leads to an analytical framework that is easily applied to laboratory test devices, sub-scale tests and to full-scale combustion systems of all sorts. Representation constructed of acoustic modes is not so restrictive as first appears, neither in respect to the perturbing processes, nor in respect to linearity. So long as the amplitudes are not 'too' great, quite general motions can be synthesized. For realistic applications, the greatest difficulties arise in modeling the dominant physical and chemical processes; and in determining certain material and dynamical properties.

I make no attempt in this work to give a survey of possible methods of analysis; nor do I cover much more than the single method, with major applications. In particular, I do not discuss the many analyses based on solutions to partial differential equations. Considerable experience has demonstrated that relying on the averaged equations is an effective strategy both for understanding physical behavior and for obtaining useful results for practical problems. But I certainly do not claim any sort of universality.

This book ranges over a broad spectrum of topics from the physical foundations, experimental results and mathematical methods, to summary examinations of some experiences with combustion instabilities in

OVERVIEW

operational systems. The text is organized roughly into three main parts. Chapters 1 and 2 cover practical examples of combustion instabilities; their interpretation in elementary terms; and lengthy discussions, in Chapter 2, of the chief mechanisms for instabilities in laboratory and full-scale systems. A substantial part of Chapter 2 is devoted to unsteady combustion in solid propellant rockets. Some may consider that the emphasis is misplaced particularly because there is at the present time much greater concern with instabilities and oscillations in gas turbines, covered cursorily in Chapter 9.

There are good reasons for the space devoted to basic problems arising in solid rockets. Practical considerations forced by combustion instabilities have been present since the late 1930s; with changes of design and propellant systems they continue and will likely always be present. Perhaps the most important reason for such intense theoretical considerations is the fundamental property that a solid rocket, or a test sample of solid propellant, can be fired only once. There is accordingly enormous motivation, always present in planning test programs based on solid propellants, for maximizing the information gained from a single firing. That explains the concern with transient behavior, the periods of growth and decay of oscillations. The rates of change exhibited in the envelopes of oscillatory motion are determined by the averaged influences of all contributing physical processes. To understand those rates and their combined consequence, requires attention to the basic behavior of the system, a central motivation throughout this book.

An interesting peripheral issue in the history of solid rockets is the matter of national security and classification. In the very late 1950s and early 1960s, success was achieved in releasing some material for late publication and in relaxing restrictions on availability of current work. The story of that process is part of the main subject here because official rules may have direct effect on the style certainly, but also on the content and quality of research. Section 2.2 serves partly to make the point in respect to combustion instabilities in solid rockets.

Chapters 3, 4 and 5 form the second part of the book, covering largely theoretical and analytical matters. The conservation equations for a two-phase flow are developed in Annexes A and B. Their approximation by a single fluid model is the basis in Chapter 3 for extracting systems of equations for the averaged and time-dependent motions. The latter are then simplified by expansion in two small parameters, characteristic Mach numbers of the mean and fluctuating flows. Five classes of problems are identified according to the orders of terms retained in the expansion; the classes include classical acoustics, linear stability, and three types of nonlinear problems.

The method of approximate analysis used in this book is developed in Chapter 4. In outline it follows well-known strategies for analyzing dynamical systems: A modal expansion; spatial averaging with suitable weighting functions, chosen here to be the unperturbed acoustic modes; and, as an optional possible tactic for further simplifying the equations, application of time-averaging. The spatially averaged equations, a system of ordinary nonlinear second order equations, are solved by a perturbation-iteration procedure that produces systems of equations for the amplitudes of the modes, having forms systematically defined according to the two-parameter expansion procedures. The procedure is well-founded and has long been used in other fields.

An important property, long known but explicitly emphasized here, is that the results are **not** restricted to irrotational velocity fields. That true property is contrary to a criticism often incorrectly directed to this method, most recently in three papers given in August 2004. If the analysis is applied correctly (albeit additional modeling may be required), it is entirely capable of treating problems in which vorticity is important, always to some approximation. Moreover, also contrary to criticisms attempted several times in the literature, the approximate solution satisfies the correct perturbed boundary conditions, not those set on the basis functions used in the modal expansion. Annex F is included to address this point.

Owing to confusion and mis-interpretation of the points just made, I should be more specific. The following remarks are expanded in Chapter 4. For linear harmonic motions, the first order approximation in

\bar{M}_r , the Mach number of the mean flow, is equation (4.82), which is (4.20) written in different symbols:

$$\hat{p}^{(1)}(\mathbf{r}) = \psi_N(\mathbf{r}) + \sum_{n=0}^{\infty}' \frac{\psi_n(\mathbf{r})}{E_n^2(k^2 - k_n^2)} \left\{ \iiint_V \psi_n(\mathbf{r}_0) \hat{h}(\mathbf{r}_0) dV_0 + \iint_S \psi_n(\mathbf{r}_{0s}) \hat{f}(\mathbf{r}_{0s}) dS_0 \right\} \quad (4.82)$$

The prime on the summation sign signifies that the N^{th} term is missing. This expression represents the actual pressure field perturbed from the N^{th} classical acoustic mode $\psi_N(\mathbf{r})$ by the processes accounted for in the perturbation functions. The corresponding formula for the perturbed Mach number field is (4.85), and the wavenumber of the actual motion is given by (4.19) written for the N^{th} mode:

$$i\bar{p}\bar{a}k\mathbf{M}'^{(1)} = -\nabla\hat{p}^{(1)} - \varepsilon\mu\{[\hat{\mathbf{M}}]\}_1 + \varepsilon\hat{\mathbf{F}}_{10} + \varepsilon\mu\hat{\mathbf{F}}_{11} \quad (4.85)$$

$$k^2 = k_N^2 + \frac{1}{E_N^2} \left\{ \iiint_V \psi_N(\mathbf{r}_0) \hat{h}(\mathbf{r}_0) dV_0 + \iint_S \psi_N(\mathbf{r}_{0s}) \hat{f}(\mathbf{r}_{0s}) dS_0 \right\} \quad (4.19)$$

What has apparently been confusing is the well-known property of this kind of perturbation/iteration procedure that the first order properties of the *actual* N^{th} mode can be calculated if the properties of the N^{th} *unperturbed* mode are known. Thus in the work here, besides the perturbations \hat{h} and \hat{f} , only the wavenumber and mode shape of the N^{th} unperturbed classical acoustic mode are required to calculate the properties, including the wavenumber (4.19), of the actual *perturbed* N^{th} mode. To this level of approximation one does not need to know explicitly, for example, the pressure and velocity fields of the actual modes treated. But nevertheless they are implicit. In particular, the classical unperturbed modes are for irrotational flow but the flows of actual perturbed modes are rotational, deducible, for example, from (4.82) and (4.85). The wavenumber (4.19) is therefore the wavenumber of a rotational wave.

Results for a given problem require the functions $\hat{h}(\mathbf{r})$ and $\hat{f}(\mathbf{r})$. The procedure developed in Chapters 3 and 4 is intended only to provide a framework within which particular forms of h and f are placed; the forms themselves must be worked out as a separate chore for a chosen problem.

A few words about the property that the method really is ‘approximate’ are needed. There are two small parameters measuring smallness in the method: A characteristic average Mach number \bar{M}_r measuring in the first instance the intensity of the mean flow; and a Mach number \mathbf{M}'_r indicative of the amplitude of fluctuations, most clearly the amplitude of acoustic velocity waves. It is the nature of perturbation methods that accuracy—somehow defined by comparison with the ‘true’ results which are normally not known—is lost as the sizes of the small parameters are increased. The way in which accuracy deteriorates is simply not known, not is it investigated here, because the real value of the method often lies less with its accuracy than with the ease with which it may produce results indicative of trends produced by changes in a system.

In Chapter 5, classical acoustics is reviewed, chiefly to summarize those results most relevant to problems of combustion instabilities. Much of the material is well-known and available in many texts, but some special topics are included to give a fairly complete muster of the purely acoustical results most commonly useful in the field of combustion instabilities.

The third part, the remainder of the body of this book, includes subjects common to many engineering fields but covered here with emphasis on applications to combustion systems: linear stability (Chapter 6); nonlinear behavior (Chapter 7); passive control (Chapter 8); and feedback control (Chapter 9). Examples of results and, when possible, comparison of predictions with observations, are scattered throughout those four chapters, to convey a sense of the current state of the field; and to suggest some of the areas where effort is required to achieve continued progress. Chapters 6 and 7 contain much material which is basic to the subject and is covered in some detail. In contrast, Chapters 8 and 9 are mainly descriptive. Chapter 8 is an

OVERVIEW

incomplete survey of the principal methods of passively controlling combustion instabilities, the important measures taken in practice; the last section of the chapter covers a simple example to illustrate the matter for an idealized thrust augmentor. Chapter 9 is an introduction to feedback control of combustion systems. I had intended to cover much more, but owing to constraints on time of preparation, the discussion has been cut short.

Although the idea of trying to manage combustion instabilities by some means of active control was first suggested by W. Bollay in 1951 and investigated in detail by Professor H.S. Tsien in 1952, results in the laboratory and in full-scale systems were not achieved until the past fifteen years or so. Despite the early enthusiasm, and subsequent achievement of a few impressive results, feedback control is still far from routine applications. Chapter 9 is included to provide a sketchy idea of how far the subject has progressed; and some indication of how much remains to be done. I believe that significant basic progress towards routine practical applications in this area awaits clearer basic understanding of the systems to be controlled. The subject merits continued attention, particularly at the fundamental level. There are many opportunities for extended research, not merely directed efforts intended to produce short-term 'pay-offs'. Success will contribute much to practical applications as well as to basic understanding.

There are eight annexes. The first two deal with formation of the equations of motion. Annex A is a fairly detailed and complete derivation of the equations for multi-component reacting flows in which one component is liquid or solid and the remainder are gases. The equations are combined to give the set governing flows of an equivalent mass-averaged fluid. Annex B gives the basis for the one-dimensional approximation, extremely important for practical applications. Annexes C and D cover topics which are important for special problems, but which don't fit well in the body of the text. Annex C establishes the correct formula for viscous attenuation of a planar acoustic wave at a rigid surface by using the one-dimensional approximation. It's remarkable that the result is exact. Equally important, this is the basis for the 'pumping' process accompanying unsteady conversion of solid to gas at a burning surface, a topic treated in Chapter 6. Some general aspects of vorticity and entropy fluctuations are covered in Annex D. It is often useful to model combustion zones as flame sheets; special considerations may arise when that approximation is used with spatial averaging. Examples are treated in Annex E. Annex F is included to help clarify some of the reasons that the approximate method of solution (Chapter 4) works well. The discussion is intended mainly to suggest how it is that the expansion for the acoustic field to first and higher order satisfies the correct perturbed boundary conditions even though the basis functions do not. Annex G is an extended discussion of the Nyquist Criterion, with examples, intended to provide part of the background required for understanding some of the works on feedback control covered or cited in Chapter 9. The last annex, H, is included to call attention to methods related to the method of averaging and used in other fields as approximations to nonlinear behavior.

It perhaps comes as a surprise to many that computational methods, especially computational fluid dynamics (CFD), are given almost no space in this book except for references. There are several reasons, mainly the fact that to the present time CFD has not been part of the mainstream of work on combustion instabilities. That circumstance is probably due partly to the backgrounds of the people working in the field, but largely because until rather recently, CFD would have offered little help for solving practical problems in which combustion instabilities are central. However, as in many fields of engineering, the situation is changing rapidly.

I certainly don't intend to imply that numerical computations of reacting unsteady flows have not been attempted. There are many examples. For instance, some of the earliest efforts are cited in NASA SP-194, "Liquid Rocket Instability" covering work carried out in the 1960s in support of the Apollo Program. In the early 1970s computation of transient unstable oscillations in solid rockets were limited to a few periods by the machines available. Much progress has been made since that time. For both research and practical purposes, constraints remain still but are rapidly becoming less severe. Nevertheless, even when CFD reaches the level

of providing perfect simulations of real problems, we will still confront the problem of understanding. I believe that analysis—especially approximate methods—will always fill that basic need.

The main reason that CFD has otherwise been relatively helpless in this subject is that problems of combustion instabilities involve physical and chemical matters that are still not well understood. Moreover, they exist in practical circumstances which are not readily approximated by models suitable to formulation within CFD. Hence, the methods discussed and developed in this book will likely be useful for a long time to come, in both research and practice.

In the past decade especially, increasingly detailed simulations have appeared, providing ever more faithful approximations to unsteady flows in combustion chambers. Those developments are particularly important in the field of solid propellant rockets for which it is necessary to deal with quite elaborate internal geometries. The significant task remains to incorporate in analysis using CFD both the realistic nonlinear behavior and valid models of unsteady (and eventually nonlinear) combustion dynamics. It seems to me that eventually the most effective ways of formulating predictions and theoretical interpretations of combustion instabilities in practice will rest on combining methods of the sort discussed in this book with computational fluid dynamics, the whole confirmed by experimental results.

Probably at this time the most promising formulation of CFD for unsteady flows in combustors is some form of large eddy simulation (LES). Some quite good results have been obtained for realistic geometries, although the methods are far from complete and are certainly not yet available for routine computations or practical design work. The flow fields computed always have characteristics which apparently can be interpreted as turbulent motions similar to those found in real combustors. How faithfully the actual fields are reproduced remains an open question.

As a practical matter, the methods used in this book fall somewhere between CFD and the semi-empirical methods commonly used in design work, at least in the initial stages. There is often—especially, but not only, in industry—a tendency to avoid practicing analysis, particularly in carefully constructed approximate forms, in favor of more appealing (dazzling?) methods requiring extensive computing resources, which may produce appealing multi-colored pictures. Extraordinarily important for many reasons, CFD in its various forms must be developed as far as possible. But suppose CFD could produce perfect results entirely equivalent to perfect experimental results. For some, that would evidently be a state of Nirvana. But others wonder whether our understanding of physical behavior would be correspondingly expanded. The sorts of results discussed in this book, and the procedures followed to obtain them, help serve the implied purpose.

On the other hand, I have also avoided in this book any calculations involving turbulence. That practice raises a serious question: Are the results computed with no effects of turbulence valid for practical flows which inevitably are highly turbulent? Certain experimental results and measurements carried out for full-scale devices have long suggested that narrowly and tentatively the answer is ‘yes’. On the basis of fundamental considerations by Chu and Kovasznay (1957), discussed briefly in Annex D and Sections 3.1 and 7.9, a somewhat more definitive positive answer is available. For most of the purposes here, it seems that the influences of turbulence can be safely overlooked. (But see Section 7.9.) One must especially be aware of the assumption when experimental and theoretical results for variations in time, or the corresponding spectra, are compared, for it is surely true that eventually the effects of turbulence must be accounted for.

If the preceding is accepted as a reasonable interpretation of the broad development of the subject, a corollary conclusion is that convenient approximations to actual behavior are essential. The ability to capture the essence of a phenomenon in a short statement, or perhaps a formula, is evidence of understanding. Naturally one must always possess as well some understanding of the limitations of approximations if they are to be truly useful. An attractive feature of the methods discussed here is the ease with which one may deduce such “rules of thumb.” Examples are scattered throughout the text.

OVERVIEW

In this book I try to give a fair idea of the historical aspects of combustion instabilities from roughly 1950 to the present. I hope that the foundations of the subject are sufficiently well covered that the essentials of the phenomenon in any type of chemical propulsion system may be understood. Although I have tried to include examples of instabilities in all types of propulsion systems now used, I make no claims of completeness. I realize that for want of space, or to avoid excessive reproduction of readily accessible material, I have excluded many good examples. To the best of my knowledge, I have tried to give proper credit to the principal contributors associated with the various fields. I have included more extensive attributions, as well as wider coverage, of certain parts of the material, in three versions of a short course devoted to the subject (Culick 2000a, 2001, 2002a).

Finally, I must vent a few comments on the problem of financial support by government agencies and others. Not surprisingly, as a subject which so often deals with problems, not desirable attributes, of practical systems, combustion instabilities has traditionally become a 'hot topic' only when there are serious problems in costly systems. Too often, support has been given for short-term quick fixes, and then has been withdrawn when the problems are managed. It is apparently not fertile ground for research program managers who seek to support career-building 'break-throughs'. Steady progress based partly on advances in contributing fields such as instrumentation, measurement techniques and computational resources generally, unfortunately, fails to offer obvious prospects of stardom. My own experience is that the subjects discussed in this book capture much of the basic ideas and materials common to broad areas of applied science and engineering. Consequently, even during periods when there are no particularly pressing practical problems, there is a need and ample justification for a well-grounded research program having rather general applications, and meriting continuous support over many years. Only in this way will there be a (small) community educated as required and having experience in the fields of practical applications covered here.

This book has depended on many works and direct help of others, beginning with my Sc.D. dissertation and my supervisor Professor Morton Finston (1919–1986) who gave me complete freedom in my choice of topic and in details of development, both of the subject and of myself. To him I remain forever grateful. Professor F.E. Marble sponsored my move out of student life at MIT to Caltech and from the beginning to the present has been generous with his advice, critiques and cogent opinions. During the time our careers touched, I benefitted much from friendship with Professor E.E. Zukoski (1927–1995). We collaborated most closely in projects involving the Caltech dump cumbustor; the best example is covered in Section 7.8. Mr. E. W. Price, then at the Naval Ordnance Test Station (1965), first gave me a long-term consulting arrangement, but more importantly, a seemingly endless supply of ideas, problems, and knowledgeable discussions. His personal contributions to the field of solid rocketry and his influence on its development are his unique legacy. Ed's careful reading of Chapter 2, especially Sections 2.1 and 2.2, followed by his lengthy and carefully written comments (initially a mixed review!) happily caused me to make significant changes greatly improving the text. Once again I am sincerely grateful to him for his friendship and help.

Professor M.W. Beckstead was first a co-author with me when he was working at NOTS, and later, when he had joined Hercules, Inc., gave me intellectual and financial support for my first work on nonlinear combustion instabilities, leading eventually to my 1974 paper. He has been a collaborator and co-author for many years. Dr. R. L. Derr was, and still is, a close supporter and friend whose opinion I value second to none. We share more than three decades of good memories ranging from late-night chats to a memorable low-level pass over Death Valley. I first met Professor Gary Flandro when he was a doctoral student at Caltech; we have remained mutual admirers and friends, sharing many interests including aeronautical history and model aircraft. We continue our professional collaboration and friendly competition. Mr. Jay Levine and I first became acquainted in the early 70s when I helped him a little with the basis of some of the first numerical calculations of unsteady motions in solid propellant rockets. Our relationship has always been and remains close and respectful. Mr. Norman Cohen was long a professional friend, but in the past few years, through the Caltech MURI program, we have worked closely and profitably; I have benefitted enormously. Professor

Vigor Yang was wonderful as a student with me, but he soon became a professional colleague, co-author, supporter and personal friend. Our meaningful and satisfying friendship will never cease.

My consulting activities have had considerable influence on the subjects and material covered in this book. Particularly I thank the group in the Michelson Laboratory at the Naval Weapons Center (formerly the Naval Ordnance Test Station, NOTS), China Lake, which over the years has had many names. The three successive leaders of that Division have always been gracious hosts and extremely helpful: Mr. E.W. Price, Dr. R.L. Derr and presently Dr. F.S. Blomshield.

Several of my students have helped me in working out various parts of the subjects covered here. I am fortunate to have had them as friends and co-workers. Especially I thank those whose contributions I have included in this text: Kim Aaron, Elias Awad, Victor Burnley, Joe Humphrey, Giorgio Isella, Craig Jahnke, Sanjay Kumar, Ho-Hoon Lee, Windsor Lin, Kirin Magiawala, Konstantin Matveev, Steve Palm, Guido Poncia, Winston Pun, Claude Seywert, Grant Swenson and Vigor Yang. I have also benefitted greatly from postdocs who have worked with me, including Leonidas Paparizos, Jim Sterling, Craig Jahnke, Tae-Seong Roh, Michael Shusser, and Al Ratner.

From January to June 1992, I had the pleasure of holding the post of Professor Associé at École Centrale, Paris where I gave a series of lectures and benefitted greatly from the hospitality and intellectual atmosphere of the Laboratoire. I am indebted to Prof. Sébastien Candel and his colleagues for their generosity and friendship. While I was preparing the manuscript for this book, Dr. François Vuillot gave me much help with an annotated bibliography of the ONERA work on vortex shedding prior to 2001.

In 1998 Dr. Clas A. Jacobson suggested giving a short course on some of the subjects addressed in this book, at the United Technologies Research Center. He helped me greatly in decisions of organization as well as choices of topics. That course, sponsored by the Department of Energy, was accompanied by the notes published as Culick (2000)a, and helped me organize some of my thoughts.

I owe thanks to a huge number of professional colleagues and friends who are nameless here, yet who appear as authors in the list of references. I have chosen not to list you specifically so as not to risk causing prickly feelings by omissions. You surely know who you are—living in many countries! Be assured that I feel very deeply the gratitude I owe for what I have learned from you and for the many ways in which you have helped me. In particular, I have benefitted greatly from more than ten years' service on the AGARD Propulsion and Energetics Panel; six years' membership of the Sverdrup Advisory Council for AEDC; and from my current participation in the activities of the Technical Advisory Committee for Pratt and Whitney, Inc.

Before this work was published, I circulated a ‘nearly final’ draft to a few of the people listed above. I am grateful for their corrections, helpful comments and encouragement. Especially, Mr. Paul Kuentzmann of ONERA obviously spent much time reading the draft; I am grateful to him for his many comments and thoughtful suggestions. The points of view expressed in the text, and any errors of commission or omission, are of course my responsibility.

Dr. Lawrence Quinn, then (early 1990s) at the Air Force Rocket Propulsion Laboratory, helped me begin some of the background work for the book with a small grant. We did not plan such a stretched-out process! I am grateful to AGARD, the Advisory Group for Aerospace Research and Development, which in 1995 became RTO, the Research and Technology Organization, for their willingness to publish the first version of this book. They were most gracious in agreeing to a period of preparation which became extended due to my health problems.

OVERVIEW

Finally, I thank Mrs. Jamie Campbell who skillfully typed much of the manuscript for this book using L^AT_EX; and I extend a special 'thank you' to Ms. Cecilia Lin who expertly (and happily) created and recreated many figures. I am particularly grateful to Ms. Melinda Kirk who contributed much typing and proofreading, but especially she coordinated preparation of the book and managed to bring it all together. In many ways, she has acted effectively as an editor-in-residence. I am much indebted to her.

CHAPTER □

Combustion Instabilities in Propulsion Systems

Chemical propulsion systems depend fundamentally on the conversion of energy stored in molecular bonds to mechanical energy of a vehicle in motion. The first stage of the process, combustion of oxidizer and fuel, takes place in a vessel open only to admit reactants and to exhaust the hot products. Higher performance is achieved by increasing the rate of energy release per unit volume. For example, the power densities in the F-1 engine for the Apollo vehicle (1960s), and the Space Shuttle main engine (1970s) are respectively 22 gigawatts/m³, and 35 gigawatts/m³. The power densities in solid rockets are much less. For a cylindrical bore, the values are approximately $0.25(r/D)$ gigawatts/m³, where r is the linear burning rate, typically a few centimeters per second, and D is the diameter. Thus the power densities rarely exceed one gigawatt/m³. An afterburner on a high-performance fighter may burn fuel at the rate of 75,000 pounds per hour, generating roughly 450 megawatts for a short period in a volume of perhaps (1 m³), giving power densities around 0.3–0.4 gigawatts/m³.

These are indeed very large power densities. To appreciate *how* large, consider the fact that the average power consumption per person in a developed country is about 4 kilowatts (roughly the same as that for astronauts). In the United States, with approximately 195 million people in 1965, the total power consumption was about 1,000 gigawatts. Hence, for a few minutes, the five F-1 engines in the first stage of the Apollo produced power equivalent to nearly 1% of the entire power consumption of the U.S. at that time — in a *very* small volume. We cannot be surprised that such enormous power densities should be accompanied by relatively small fluctuations whose amplitudes may be merely annoying or possibly unacceptable in the worst cases.

We are concerned in this book with the dynamics of combustion systems quite generally. The motivation for addressing the subject arises from particular problems of combustion instabilities observed in all types of propulsion systems. By “combustion instability” we mean generally an oscillation of the pressure in a combustion chamber, having a fairly well-defined frequency which may be as low as 10–20 Hz or as high as several tens of kilohertz. Typically the instabilities are observed as pressure oscillations growing spontaneously out of the noise during a firing. As a practical matter, combustion instabilities are more likely encountered during development of new combustion systems intended to possess considerable increases of performance in some sense. The present state of theory and experiment has not provided a sufficiently strong foundation to provide a complete basis for prediction. Hence there are only a few guidelines available to help designers avoid combustion instabilities.

Under such conditions, it is extremely important to pay attention to the experience gained in the laboratory as well as in full-scale tests of devices. Moreover, because of the many properties of the behavior common to the various systems, much is to be gained from understanding the characteristics of systems other than the one that may be of immediate concern. It is therefore proper to begin with a survey of some typical examples drawn from many years’ experience. Theory is an indispensable aid to making sense of observational results. Conversely, discussion of various experimental observations is a natural place to introduce many of the basic ideas contained in the theory.

From the beginning of this subject, the central practical question has been: What must be done to eliminate combustion instabilities? Traditionally, the approach taken has been based on passive measures, largely *ad hoc* design changes or notably for solid propellant rockets, favorable changes of propellant composition. During the past few years, considerable effort has been expended on the problem of applying active feedback control to combustion systems. It's an attractive proposition to control or eliminate instabilities with feedback control, particularly because one implication, often made explicit, is that the use of feedback will somehow allow one to get around the difficult problems of understanding the details of the system's behavior. Many laboratory, and several full-scale demonstrations, apparently support that point of view. However, for at least two reasons, serious application of feedback control must be based on understanding the dynamics of the system to be controlled:

- (i) all experience in the field of feedback control generally has demonstrated that the better the controlled plant is understood, the more effective is the control;
- (ii) without understanding, development of a control system for a full-scale device is an *ad hoc* matter, likely to involve expensive development with neither guarantee of success nor assurance that the best possible system has been designed.

Therefore we begin this book with a survey of combustion instabilities observed in various systems. The theoretical framework is constructed to accommodate these observations, but later emerges also as a perfect vehicle for investigating the use of active feedback control (Chapter 9).

1.1. Introduction

For the kinds of propulsion systems normally used, combustion chambers are intended to operate under conditions that are steady or change relatively slowly. The central questions addressed here concern the stability and behavior subsequent to instability of steady states in combustors. If a state is unstable to small disturbances, then an oscillatory motion usually ensues. Such combustion instabilities commonly exhibit well-defined frequencies ranging from 15 Hz or less to many kilohertz. Even at the highest amplitudes observed in practice, the instabilities consume only a small fraction of the available chemical energy. Thus, except in extremely severe instances, the oscillations do not normally affect the mean thrust or steady power produced by the systems. Serious problems may nevertheless arise due to structural vibrations generated by oscillatory pressures within the chamber or by fluctuations of the thrust. In extreme cases, internal surface heat transfer rates may be amplified ten-fold or more, causing excessive erosion of the chamber walls.

An observer usually perceives an unstable motion in a combustion chamber as "self-excited," a consequence of the internal coupling between combustion processes and unsteady motion.¹ Except in cases of large disturbances (e.g. due to passage of a finite mass of solid material through the nozzle), the amplitude of the motion normally seems to grow out of the noise without the intrusion of an external influence. Two fundamental reasons explain the prevalence of instabilities in combustion systems:

- i) an exceedingly small part of the available energy is sufficient to produce unacceptably large unsteady motions;
- ii) the processes tending to attenuate unsteady motions are weak, chiefly because combustion chambers are nearly closed.

Those two characteristics are common to all combustion chambers and imply that the possibility of instabilities occurring during development of a new device must always be recognized and anticipated.

¹An alternative explanation, that observed combustion instabilities are (or may be) motions driven by the noise present in combustors is explored in Section 7.9; see also Figure 1.34.

Treating combustion instabilities is part of the price to be paid for high-performance chemical propulsion systems. It is a corollary of that condition that the problem will never be totally eliminated. Advances in research will strengthen the methods for solution in practical applications, and will provide guidelines to help in the design process.

The fact that only a small part of the total power produced in a combustor is involved in combustion instabilities suggests that their existence and severity may be sensitive to apparently minor changes in the system. That conclusion is confirmed by experience. Moreover, the complicated chemical and flow processes block construction of a complete theory from first principles. It is therefore essential that theoretical work always be closely allied with experimental results, and vice versa. No single analysis will encompass all possible instabilities in the various practical systems. There are nevertheless many features common to all combustion chambers. Indeed, it is one theme of this book that the characteristics shared by propulsion systems in many respects dominate the differences. While it is not possible to predict *accurately* the occurrence or details of instabilities, a framework does exist for understanding their general behavior, and for formulating statements summarizing their chief characteristics. For practical purposes, the theory often serves most successfully when used to analyze, understand, and predict *trends* of behavior, thereby also providing the basis for desirable changes in design. Experimental data are always required to produce quantitative results and their accuracy in turn is limited by uncertainties in the data.

Special problems may be caused by combustion instabilities interacting with the vehicle. Because the frequencies are usually well-defined in broad ranges, resonances with structural modes of the vehicle or with motions of components are common. Perhaps the best known form of this sort of oscillation is the POGO instability in liquid rockets. Strong couplings between chamber pressure oscillations, low-frequency structural vibrations, and the propellant feed system sustain oscillations. The amplitudes may grow to unacceptable limits unless measures are taken to introduce additional damping. A striking example occurred in the Apollo vehicle. The central engine of the cluster of five in the first stage was routinely shut off earlier than the others in order to prevent growth of POGO oscillations to amplitudes such that the astronauts would be unable to read instruments. Comments on the vibrations and the early shut off may be heard in communications recorded during the launch phase of several Apollo missions.

In the U.S., and possibly in other countries, notably Germany and Russia before and during World War II, combustion instabilities were probably first observed in liquid rocket engines. Subsequent to the war, considerable effort was expanded in Russia and in the U.S. to solve the problem, particularly in large engines. Probably the most expensive program was carried out during development of the F-1 engine for the Apollo vehicle in the years 1962–1966, reviewed in a useful report by Oefelein and Yang (1993).

Liquid-fueled air-breathing propulsion systems also commonly suffer combustion instabilities. Axial oscillations in ramjet engines are troublesome because their influence on the shock system in the inlet diffuser can reduce the inlet stability margin. Owing to their high power densities and light construction, thrust augmentors or afterburners are particularly susceptible to structural failures.

For any thrust augmentor or afterburner, conditions can be found under which steady operation is not possible. As a result, the operating envelope is restricted by the requirement that combustion instabilities cannot be tolerated. Due to structural constraints placed on the hardware, combustion instabilities in afterburners are particularly undesirable and are therefore expensive to treat.

In recent years combustion instabilities in the main combustor of gas turbines have become increasingly troublesome. The chief reason is ultimately due to requirements that emission of pollutants, notably oxides of nitrogen, be reduced. A useful strategy, particularly for applications to flight, is reduction of the average temperature at which combustion takes place. Generation of NO by the thermal or 'Zel'dovich' mechanism is then reduced. Lower combustion temperature may be achieved by operating under lean conditions, when

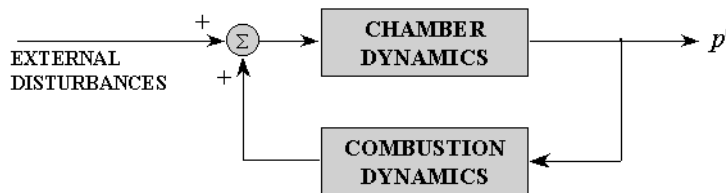


FIGURE 1.1. Schematic diagram of a combustion system as a feedback amplifier.

the flame stabilization processes tend to be unstable. Fluctuations of the flame cause fluctuations of energy release, which in turn may produce fluctuations of pressure, exciting acoustical motions in the chamber.

Finally, almost all solid rockets exhibit instabilities, at least during development, and occasionally motors are approved even with low levels of oscillations. Actual failure of a motor itself is rare in operations, but vibrations of the supporting structure and of the payload must always be considered. To accept the presence of weak instabilities in an operational system one must have sufficient understanding and confidence that the amplitudes will not unexpectedly grow to unacceptable levels. One purpose of this book is to provide the foundation for gaining the necessary understanding.

In the most general sense, a combustion instability may be regarded as an unsteady motion of a dynamical system capable of sustaining oscillations over a broad range of frequencies. The source of energy associated with the motions is ultimately related to the combustion processes, but the term 'combustion instability,' while descriptive, is misleading. In most instances, and always for the practical problems we discuss in this book, the combustion processes themselves are stable: Uncontrolled explosions and other intrinsic chemical instabilities are not an issue. Observations of the gas pressure or of accelerations of the enclosure establish the presence of an instability in a combustion chamber. Excitation and sustenance of oscillations occur because coupling exists between the combustion processes and the gasdynamical motions, both of which may be stable. What is unstable is the entire system comprising the propellants, the propellant supply system, the combustion products that form the medium supporting the unsteady motions, and the containing structure.

If the amplitude of the motions is small, the vibrations within the chamber are often related to classical acoustic behavior possible in the absence of combustion and mean flow. The geometry of the chamber is therefore a dominant influence. Corresponding to classical results, traveling and standing waves are found at frequencies approximated quite well by familiar formulas depending only on the speed of sound and the dimensions of the chamber. If we ignore any particular influences of geometry, we may describe the situation generally in the following way, a view valid for any combustion instability irrespective of the geometry or the type of reactants.

Combustion processes are sensitive to fluctuations of pressure, density, and temperature of the environment. A fluctuation of burning produces local changes in the properties of the flow. Those fluctuations propagate in the medium and join with the global unsteady field in the chamber. Under favorable conditions, the field develops to a state observable as a combustion instability. As illustrated schematically in Figure 1.1, we may view the process abstractly in analogy to a feedback amplifier in which addition of feedback to a stable oscillator can produce oscillations. Here the oscillator is the combustion chamber, or more precisely, the medium within the chamber that supports the unsteady wave motions. Feedback is associated with the influences of the unsteady motions on the combustion processes or on the supply system, which in turn generate fluctuations of the field variables. The dynamical response of the medium converts the local fluctuations to global behavior. In the language of control theory, the field in the chamber is the 'plant,' described by the general equations of motion.

The diagram in Figure 1.1 illustrates the main emphases of this book. Broadly, the subjects covered divide into two categories: those associated with the plant—the fluid mechanics and other physical processes comprising the *combustor dynamics*; and those connected primarily with the feedback path, chiefly combustion processes and their sensitivity to time-dependent changes in the environment, the *combustion dynamics*. The theory we will describe encompasses all types of combustion instabilities in a general framework having the organization suggested by the sketch. External forcing functions are accommodated as shown in the sketch, but the causes associated with the feedback path are far more significant in practice.

Figure 1.1 is motivated by more than a convenient analogy. For practical purposes in combustion systems, we generally wish to eliminate instabilities. Traditionally that has meant designing systems so that small disturbances are stable, or adding some form of energy dissipation to compensate the energy gained from the combustion processes, that is, *passive control*. However, in the past few years interest has grown in the possibility of *active control* of instabilities. If that idea is to be realized successfully, it will be necessary to combine modern control theory with the theory developed in this book. The development of much of control theory rests partly on the use of diagrams having the form of Figure 1.1. It is advantageous to think from the beginning in terms that encourage this merger of traditionally distinct disciplines.

We will return to the subject of control, both active and passive, in the last two chapters of this book. Any method of control is rendered more effective the more firmly it rests on understanding the problem to be solved. Understanding a problem of combustion instabilities always requires a combination of experiment and theory. For many reasons, including intrinsic complexities and inevitable uncertainties in basic information (e.g., material properties, chemical dynamics, turbulent behavior of the flow field, ...), it is impossible to predict from first principles the stability and nonlinear behavior of combustion systems. Hence the purpose of theory is to provide a framework for interpreting observations, both in the laboratory and full-scale devices; to suggest experiments to produce required ancillary data or to improve the empirical base for understanding; to formulate guidelines for designing full-scale systems; and globally to serve, like any good theory, as the vehicle for understanding the fundamental principles governing the physical behavior, thereby having predictive value as well.

All theoretical work in this field has been carried out in response to observational and experimental results. We therefore spend much of the remainder of this introductory chapter on a survey of the characteristics of combustion instabilities observed, and occasionally idealized, in the systems to be analyzed in later chapters.² The general point of view taken throughout the book will then be formulated in heuristic fashion, based on experimental results.

1.2. Historical Background

Some of the consequences and symptoms of combustion instabilities were first observed in the late 1930s and early 1940s, roughly at the same time for liquid and solid propellant rockets, and apparently somewhat earlier in the Soviet Union than in the U.S. With the later development of turbojet engines, high-frequency instabilities were found in thrust augmentors or afterburners in the late 1940s and early 1950s. Although the problem had been encountered in ramjet engines in the 1950s, it became a matter of greater concern in the late 1970s and 1980s. The introduction of compact dump combustors led to the appearance of longitudinal or axial oscillations that interfered with the inlet shock system, causing loss of pressure margin and ‘unstart’ in the most severe cases. Owing to availability, almost all of the data cited here as examples will be derived from liquid rockets, solid rockets and laboratory devices. Figure 1.2 is a qualitative representation of the chronology of combustion instabilities. Due to the accessibility of documentation and the experiences of the author, particular cases cited are mainly those reported in the U.S. We will be mainly concerned in this book

²A few references to papers and books are given in this chapter as guides to the literature. Later chapters contain more complete citations as the topics are treated in greater detail.

COMBUSTION INSTABILITIES IN PROPULSION SYSTEMS

with oscillations in solid rockets; liquid and gas rockets; thrust augmentors or afterburners; ramjets; and, to a lesser extent, gas turbines.

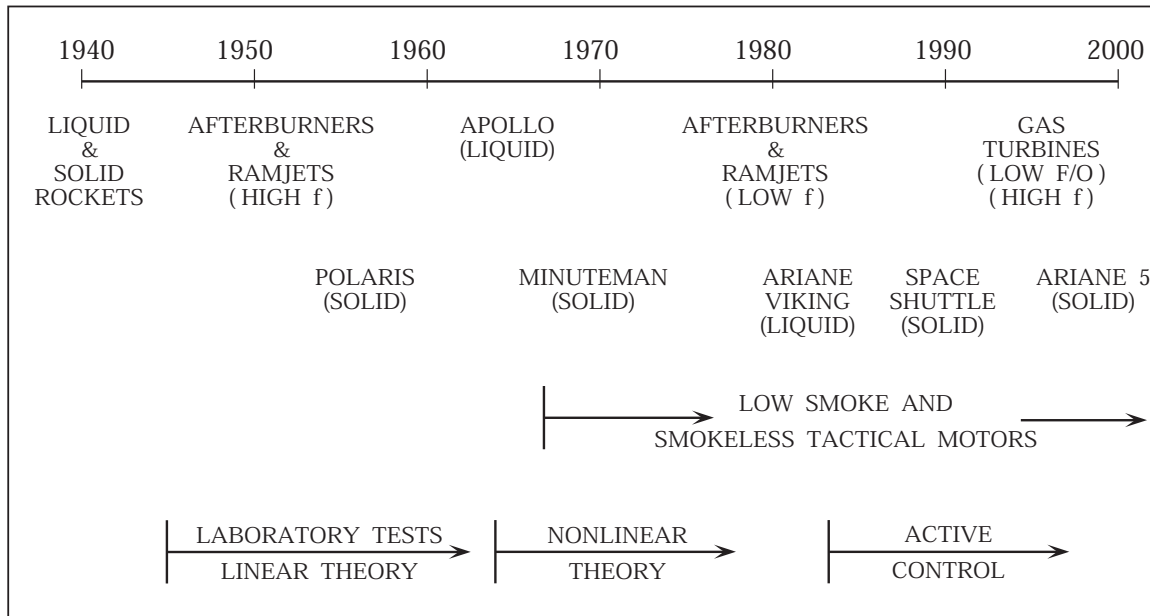


FIGURE 1.2. A chronology of combustion instabilities.

Several reviews of early experiences with combustion instabilities have been prepared for liquid rockets (Ross and Datner 1954) and for solid rockets (Wimpress 1950; Price 1968; Price and Flandro 1992). The details are not important here, but the lessons learned certainly are. Often forgotten is the most important requirement of good high-frequency instrumentation to identify and understand combustion instabilities in full-scale as well as in laboratory systems. Until the early 1940s, transducers and instrumentation for measuring pressure had inadequate dynamic response to give accurate results for unsteady motions. Ross and Datner note that "Prior to 1943, the resolution of Bourdon gauges, photographed at 64 and 128 fps, constituted the principal instrumentation." Recording oscillographs were introduced sometime in 1943, but not until the late 1940s were transducers available with sufficient bandwidth to identify instabilities at higher frequencies (hundreds of hertz and higher).

The situation was even more difficult with solid rockets because of the practical difficulties of installing and cooling pressure transducers. Probably the experience with cooling chamber and nozzle walls helps explain why quantitative results were obtained for instabilities in liquid rockets earlier than for solid rockets (E. W. Price, private communication). Prior to the appearance of high-frequency instrumentation, the existence of oscillations was inferred from such averaged symptoms as excessive erosion of inert surfaces or propellant grains due to increased heat transfer rates; erratic burning appearing as unexpected shifts in the mean pressure; structural vibrations; visible fluctuations in the exhaust plume; and, on some occasions, audible changes in the noise produced during a firing.

Experimental work progressed for several years before various unexplained anomalies in test firings were unambiguously associated with oscillations. By the late 1940s, there was apparently general agreement among researchers in the U.S. and Europe that combustion instabilities were commonly present in rocket motors and that they were somehow related to waves in the gaseous combustion products. In addition to measurements with accelerometers, strain gauges, and pressure transducers, methods for flow visualization soon demonstrated their value, mainly for studies of liquid propellant rockets (Altseimer 1950; Berman and

Logan 1952; and Berman and Scharres 1953). Characteristics of the instabilities as acoustic vibrations, or weak shock waves, were revealed.

It is much more difficult to observe the flow field in a solid rocket motor and during the early years of development, the only results comparable to those for liquid rockets were obtained when excessive chamber pressures caused structural failures. Partially burned grains often showed evidence of increased local burning rates, suggesting (possibly) some sort of influence of the gas flow. The same events also produced indications of unusual heating of the unburned solid propellant, attributed to dissipation of mechanical vibrational energy (Price and Flandro, 1992). Subsequently that interpretation was confirmed by direct measurements (Shuey, H.C. 1970-1975, related to the author by Mr. E.W. Price).

High-frequency or ‘screech’ oscillations were also first encountered in afterburners in the late 1940s; as a result of the experience with rockets and the availability of suitable instrumentation, the vibrations were quickly identified as combustion instabilities. The staff of the Lewis Laboratory (1954) compiled most of the existing data and performed tests to provide a basis for guidelines for design.

Thus by the early 1950s many of the basic characteristics of combustion instabilities had been discovered in both liquid-fueled and solid-fueled systems. Many of the connections with acoustical properties of the systems, including possible generation of shock waves, were recognized qualitatively. Although the frequencies of oscillations found in tests could sometimes be estimated fairly closely with results of classical acoustics, no real theory having useful predictive value existed. During the 1950s and the 1960s the use of sub-scale and laboratory tests grew and became increasingly important as an aid to solving problems of combustion instabilities occurring in the development of new combustion systems of all types.

1.2.1. Liquid and Gas-Fueled Rockets. During the 1960s, the major efforts on combustion instabilities in liquid rockets were motivated by requirements of the Apollo vehicle. Harrje and Reardon (1972) edited a large collection of contributions summarizing the work during that period. Essentially nothing additional was required to treat instabilities in the Space Shuttle main engine, and in the U.S., new programs specifically dealing with liquid rockets did not appear again until the mid 1980s (Fang 1984, 1987; Fang and Jones 1984, 1987; Mitchell, Howell, and Fang 1987; Nguyen 1988; Philippart 1987; Philippart and Moser 1988; Jensen, Dodson, and Trueblood 1988; and Liang, Fisher and Chang 1986, 1987.) Subsequent to a flight failure of an Ariane vehicle due to combustion instability in a first-stage Viking motor, a comprehensive research program was begun in France in 1981 (Souchier *et al.* 1982; Schmitt and Lourme 1982; Habiballah *et al.* 1984, 1985, 1988, 1991; Lourme *et al.* 1983, 1984, 1985, 1986).

The problem of instabilities in liquid rockets received greatest attention in the development of the man-carrying vehicles for flight to the moon. Both the U.S. and the U.S.S.R. expended great effort on the problem. Because virtually all the necessary information is conveniently available, we examine the experience in the U.S., a canonical example. Oefelein and Yang (1992, 1993) have given a good summary of the program; their effort is the basis of the remarks here.

Instabilities in liquid rockets are simpler than in solid rockets, to some extent because the basic internal geometry of the system is simpler. Serious complications are introduced by the flow and mixing of reactants. Practically the only influence that the existence of instabilities had on the configuration of the F-1 was on the form of axial baffles attached to the face of the injector at the head end of the motor; and on the details of the injector which influenced the interactions between the jets of fuel and oxidizer. Once the general form of injector had been chosen—impinging jets of fuel and oxidizer—the number of variables was significantly reduced. Nevertheless, considerable freedom in the details of the injector remained. Consequently, development of the F-1 from October 1962 to September 1966 involved more than 3200 full-scale tests. Approximately 2000 of those tests were conducted as part of Project First, the program carried out to solve the problems arising with combustion instability in the F-1.

During Project First, the global geometry of the chamber and nozzle was not a matter of concern; we shall assume the geometry as given and essentially fixed. Three basic injectors were initially examined, all involving impinging jets. All showed spontaneous instabilities, that is, unacceptable oscillations without any external disturbances. Figure 1.3 shows a typical pressure trace taken at the beginning of the program. Because it was known that baffles were effective for reducing the sort of transverse oscillations observed, a configuration was chosen with thirteen compartments on the injector face, formed by barriers oriented normal to the face of the injector, extending about 7.6 cm. downstream from the injector face. Figure 1.4(b) is a picture of the injector, about one meter in diameter.

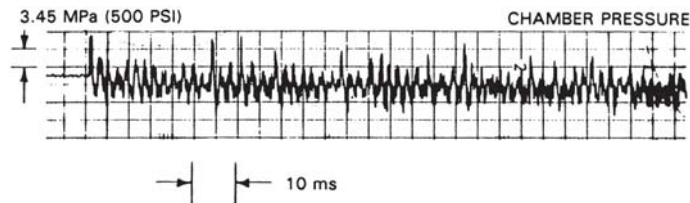


FIGURE 1.3. Pulses of the injected fuel stream in the F-1 engine (Oefelein and Yang 1993).

An informative collection of simplified pictures of the various sorts of injection elements was published by Rocketdyne, Inc. (Jaqua and Ferrenberg 1989), reproduced here in Figure 1.5. The configurations are of course sketched in simplified forms, but one important point is quite clear. If the formation of sheets and clouds of unlike drops depends on impingement of jets or liquid streams, then one expects the process to be sensitive to perturbations, particularly when there is a component of the disturbance normal to the plane of the sheet. Hence the effectiveness of baffles of the sort shown in Figure 1.4(b) is related to the shadowing of the injected streams.

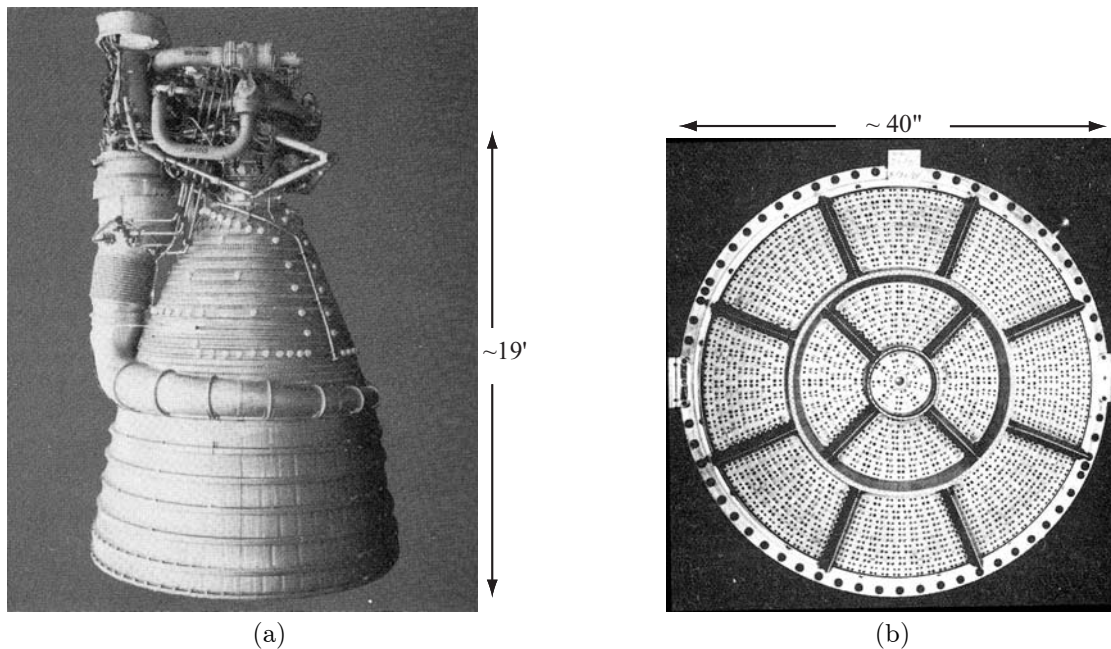


FIGURE 1.4. (a) The F-1 engine and (b) the face of the injector showing the fourteen baffles (Oefelein and Yang 1993).

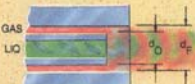
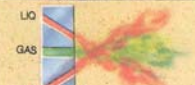
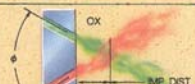
Common Injection Element Configurations			
Element Designation	Element Configuration (Flow Direction)	Characteristics	Engine Application
Concentric Tube	 GAS LOX GAS	<ul style="list-style-type: none"> Very good wall compatibility Very high performance with LOX/H₂ Good stability characteristics with LOX/H₂ Fuel is gas Small annular gap requires care in fabrication and is sensitive to contamination 	<ul style="list-style-type: none"> Shuttle main and preburners J-2 Orbit Transfer Vehicle
Concentric Tube with Liquid Swirl	 GAS LOX GAS RECESS	<ul style="list-style-type: none"> Same as concentric tube except: <ul style="list-style-type: none"> Improved mixing and atomization More complex element Stability characteristics in large engines unknown Possible wall compatibility issue with some designs Gas can also be swirled 	<ul style="list-style-type: none"> R-10
Unlike Pentad (4 on 1)	 LOX GAS LOX	<ul style="list-style-type: none"> Applicable to very high or low mixture or density ratios Good mixing and atomization Difficult to manifold 	<ul style="list-style-type: none"> Experimental
Unlike Doublet (1 on 1)	 OX FUEL IMP. DIST.	<ul style="list-style-type: none"> Good overall mixing and atomization (High Performance) Simple to manifold Subject to blowpart with hypergolic propellants 	<ul style="list-style-type: none"> LEM ascent engine Delta launch vehicle Almost all high response attitude control engines using storable propellants
Unlike Triplet (2 on 1)	 OX FUEL OX	<ul style="list-style-type: none"> Good overall mixing and atomization (High Performance) Symmetric spray pattern Subject to blowpart with hypergolic propellants Fuel can be gas Pattern can be reversed 	<ul style="list-style-type: none"> Agena upper stage Rockwell LEM descent engine design LOX/RP gas generators
Like Doublet (1 on 1)	 OX FUEL OX FUEL	<ul style="list-style-type: none"> Easy to manifold Excellent for chamber wall compatibility Not subject to blowpart Less effective atomization and mixing than unlike impinging elements 	<ul style="list-style-type: none"> Titan I and II first stage Redstone, Jupiter, Thor, Atlas boosters Shuttle OMES H-1, F-1 engines
Showerhead	 OX FUEL	<ul style="list-style-type: none"> Often employed for fuel boundary layer cooling of chamber wall Easy to manifold Poor atomization and mixing (Low Performance) 	<ul style="list-style-type: none"> Aerobee sustainer X-15 Pioneer
Variable Area (Pintle)	 FUEL OX	<ul style="list-style-type: none"> Throttleable over wide range Complex fabrication Lower performance 	<ul style="list-style-type: none"> LEM descent engine Lance sustainer
Splash Plate	 SPLASH PLATE OX FUEL	<ul style="list-style-type: none"> Less sensitive to design tolerances Generally larger elements 	<ul style="list-style-type: none"> Lance booster (early version) Saturn SVB ullage control Apollo CM RCS (SE-6) Gemini SC maneuvering attitude control and reentry engines

FIGURE 1.5. Injection elements commonly used in liquid rockets (Jaqua and Ferrenberg 1989).

The example of the F-1 and experience with reducing the combustion instability forms a basic canonical case. As shown in Figure 1.3, the instability had a frequency of about 440 Hz. and amplitudes greater than the mean chamber pressure in the chamber without baffles, but about 65% of the mean pressure in the chamber with baffles. Hence development proceeded with the baffles in place. Changes in the details of the injector design—such as hole sizes and the angles of impingement of the jets—eventually eliminated resurging. A method of pulsing or ‘bombing’ was then used to assess the stability of an injector, rated according to the damping time of a pulse. The procedure was entirely empirical since no theory existed (and still doesn’t). During this stage, the phenomenon of ‘resurging’ was often observed as an instability, an example is shown in Figure 1.6. However, by November 1965, the engine exhibited acceptable damping times (c. 45 ms or less) following pulse amplitudes of acceptable magnitude. Figure 1.7 shows an example obtained with a flight qualified injector subjected to a 13.5 grain bomb.

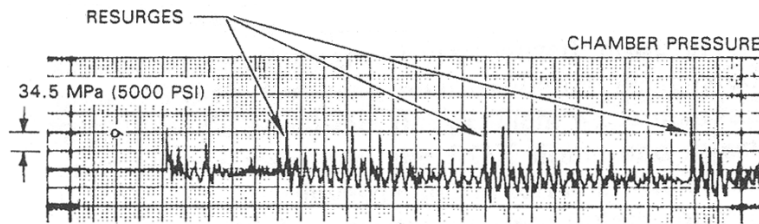


FIGURE 1.6. Resurging subsequent to a bomb-induced perturbation (Oefelein and Yang 1993).

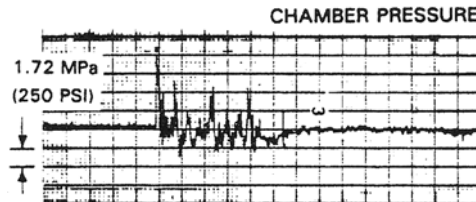


FIGURE 1.7. Decaying pressure induced initially by a pulse from a 13.5 grain bomb (Oefelein and Yang 1993).

There seems little doubt that the mechanisms for the instabilities were understood quite well in broad outline, if not in quantitative detail, for this kind of injector. Stretching downstream from the face of the injector there were three fairly well-defined regions. The first contains the spray fans generated by the injection jets; the next contains fuel drops breaking up and vaporizing; and the last, where only vapor exists, may be characterized by mixture ratio variations in space. Imposition of time-dependent properties, notably pressure and velocity, produces fluctuations of properties which in turn can generate fluctuations of the local burning rate. Thus all three regions can contribute to the tendency to instability.

The F-1 provides an example of an instability in a liquid oxygen (LOX) hydrocarbon (HC) system with injectors based on impinging jets. As the experience suggests, the configuration having jets impinging on one another seems to be quite sensitive to external perturbations. It appears for example, that the jets could be misaligned rather easily, leading possibly to an instability. Hence many designers have favored coaxial injectors, but it is not our purpose here to make a case for any particular kind of injector, which in any case may depend on the propellants in question. Perhaps the most common form of injector in general is based on coaxial flow; examples producing jets with and without swirl are shown in Figure 1.8. Summaries of recent research on coaxial injection elements in the context of combustion instabilities have been given by Hulka and Hutt (1995). They also give a good summary of U.S. experience from the late 1950s to the early 1990s.

An entirely different form of injector was introduced by TRW, Inc. for the lunar descent module of the Apollo vehicle; it was invented by G.W. Elverum at Caltech's Jet Propulsion Laboratory, and later developed at TRW (Elverum *et al.* 1967). The need for a throttleable engine was satisfied by a pintle design, sketched in Figure 1.9. Figure 1.10 is a photograph of a cutaway model of the engine. Thrust could be varied from 1000 to 10,000 pounds by moving the pintle.

The engine gained a deserved reputation for stability. Figure 1.11 shows the decay several pulses in a test of the engine at TRW. As a result of such testing, the engine has been widely viewed as 'absolutely' stable. However it is important to realize that one can state only that the engine is acceptably stable for the fuel and oxidizer used (nitrogen tetroxide and A-50, a 50/50 mixture of hydrazine and unsymmetrical dimethylhydrazine, called UDMH) and for a certain range of operating conditions. Limitations have been shown on more than one occasion, to the embarrassment of test program managers.

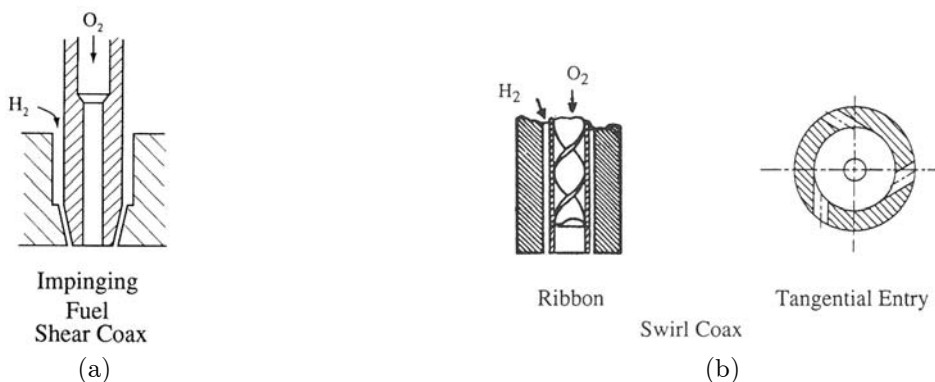


FIGURE 1.8. Simplified forms of coaxial injectors. (a) pure shear coaxial element; (b) coaxial element producing swirl (Hulka and Hutt 1995).

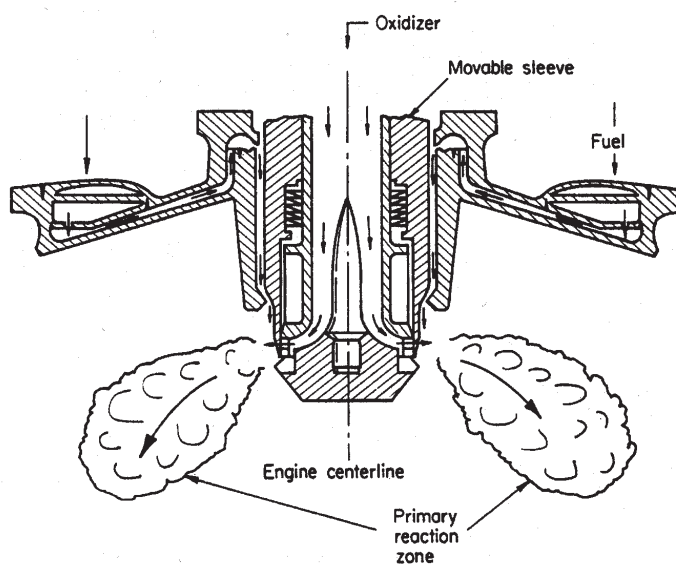


FIGURE 1.9. Pintle injector in the lunar excursion module (LEM) descent engine of the Apollo vehicle (Harrje and Reardon 1972).

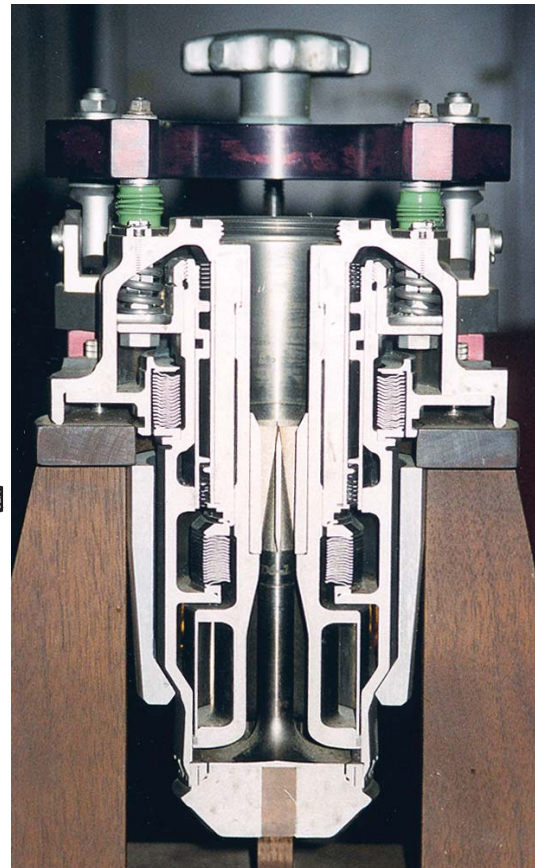


FIGURE 1.10. Cutaway display model of the mixing head of the TRW pintle engine (courtesy of Jack L. Cherne, TRW retired).

Instability problems also arose during development of the Space Shuttle main engine (SSME), which developed 500K pounds of thrust, but the difficulties were overcome. Three SSMEs are used on the Shuttle.

COMBUSTION INSTABILITIES IN PROPULSION SYSTEMS

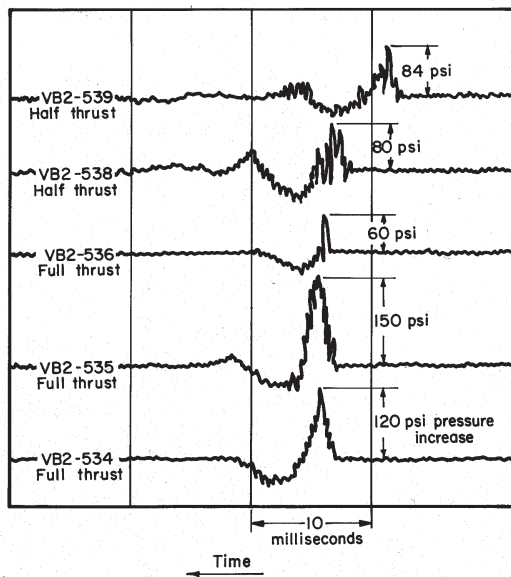


FIGURE 1.11. Decay of pulses injected in the TRW LEM engine (Harrje and Reardon 1972).

Figure 1.12 is a drawing of the engine showing the coaxial elements and the oxidizer elements serving also as baffles.

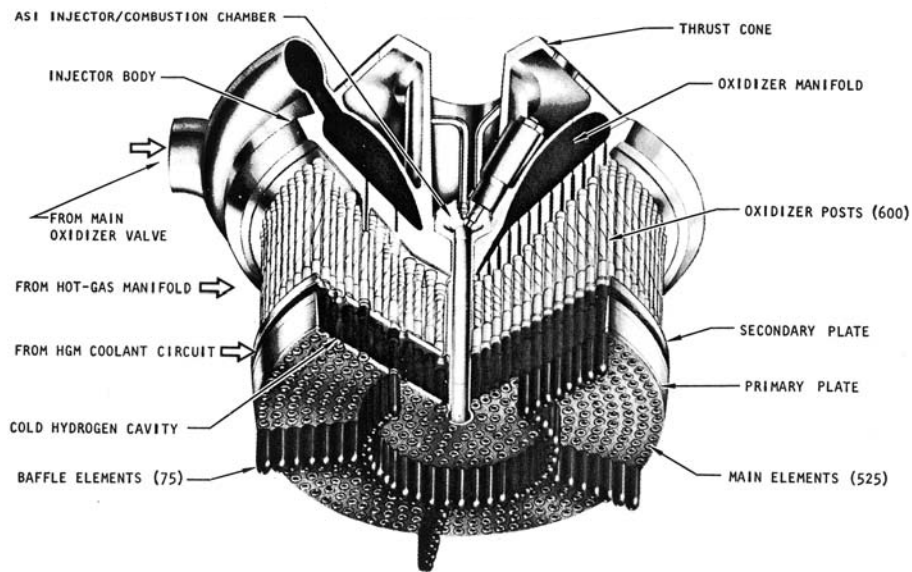


FIGURE 1.12. Cutaway drawing of the main injector assembly of the Space Shuttle main engine (Courtesy of Rocketdyne, Inc.).

Russian experience with combustion instabilities in liquid rockets was not well-known in the West until the 1990s although some publications were available, e.g. Natanzon (1984) which later appeared in English translation. The propulsion community in the U.S. generally did not learn of Russian research concerned

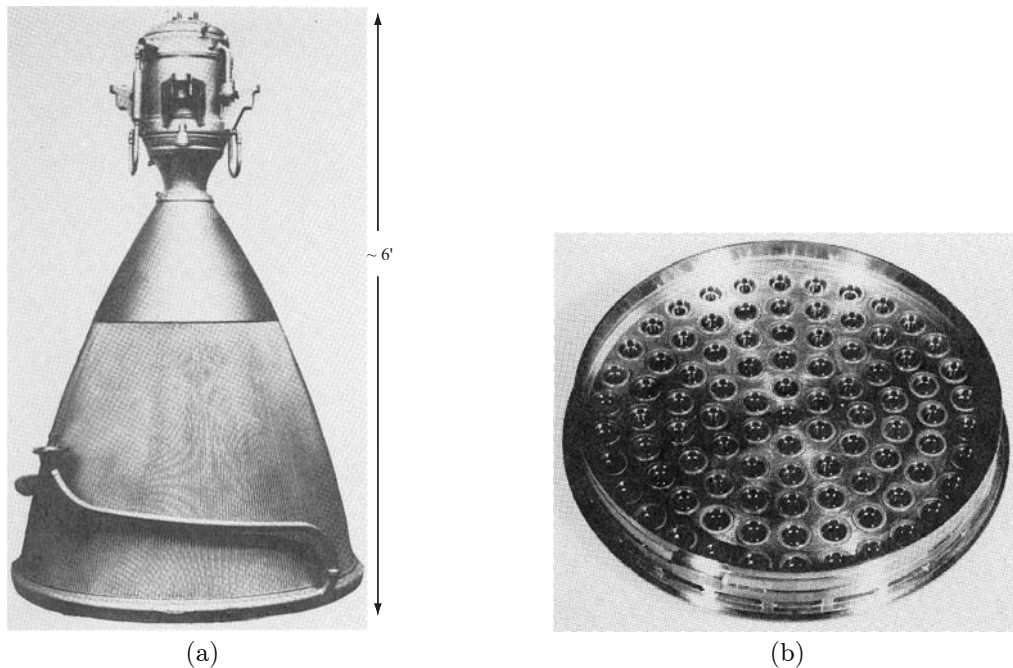


FIGURE 1.13. The RD-0110 engine (a) general view of the basic engine; (b) the injector face (Rubinsky 1995).

with operational rockets until the conference held at Pennsylvania State University in 1993 (“Liquid Rocket Engine Combustion Instability”, 1995). Subsequently an updated English translation of Natanzon’s work appeared (Natanzon 1999). That work offers a good coverage of some fairly recent Russian work as well as a useful summary of many topics basic to the dynamics of liquid rockets. Russian experimental work on instabilities in liquid engines is covered in the book by Dranovsky (2006).

Rubinsky (1995) published what is likely the first thorough account of Russian experience with a problem of combustion instability in a liquid rocket engine, the RD-0110. The system used coaxial injectors (referred to as “bipropellant centrifugal atomizers”) supplying liquid oxygen and a hydrocarbon fuel; the engine produced 67,000 pounds of thrust with a chamber pressure of 1000 psi. Chamber diameter is 7.1 inches, length 10.6 inches and throat diameter 3.3 inches. Figure 1.13 shows the engine and the face of the injector. The engine was used in the Soyuz vehicle with four motors powering the upper stage, Figure 1.14.

Extended development work eventually reduced the instability to a problem occurring once out of about 300 thrust chambers. It was a problem from ignition to 0.1 seconds or so. Installation of longitudinal ribs made of combustible felt solved the problem; Rubinsky (1995) describes the matter in detail. Figure 1.15 shows a chamber with ribs.

1.2.2. Combustion Instabilities in Thrust Augmentors. The situation in respect to instabilities in afterburners³ seems to have changed little in fundamental respects in more than 20 years. Early work

³Increased thrust was obtained from early gas turbines by adding a second combustion chamber downstream of the turbine. The exhaust of the turbine is oxidizer rich, limitations being set on the mixture ratio for combustion (i.e., temperature) according to material properties. All of the flow entering the inlet then passed through both combustors; the second combustor was conventionally called an afterburner. With the development of bypass engines, the ‘afterburner’ received some air which had not passed through the main combustor. Hence the device became known as a ‘thrust augmentor’, referring to its purpose to augment the thrust, without implying the source of air.

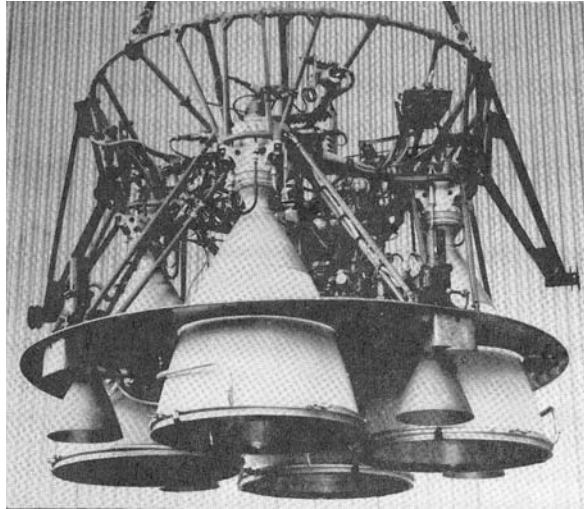


FIGURE 1.14. Four RD-0110 engines mounted in the upper stage of the Soyuz vehicle (Rubinsky 1995).

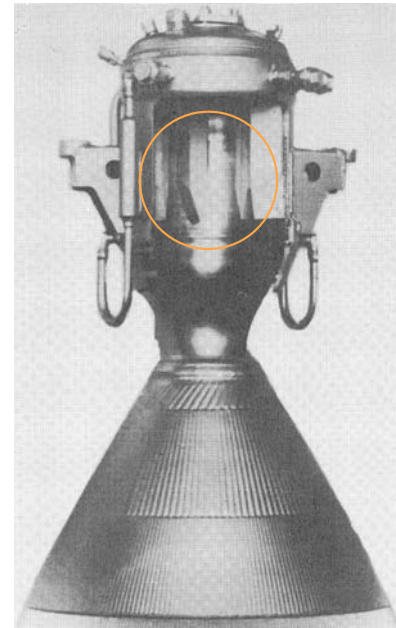


FIGURE 1.15. RD-0110 engine cut-away to show combustible ribs intended to attenuate a tangential mode (Rubinsky 1995).

showed that high-frequency oscillations ('screech') could be treated over fairly broad operating conditions by installing passive suppression devices—usually acoustic liners—and by adjusting the distribution and scheduling of the injected fuel. Problems increased as high-bypass engines were developed because the large annular flow passages allowed waves to propagate upstream to the compressor. As a result, instabilities occurred with longer wavelengths and hence lower frequencies (Bonnell *et al.* 1971; Kenworthy *et al.* 1974; Ernst 1976; Underwood *et al.* 1977; Russell *et al.* 1978). Figure 2.54 is a sketch showing an example of an augmented engine which exhibited low-frequency instabilities. Because considerable effort—and cost—has been spent to try to reduce or eliminate instabilities in augmentors by passive means, the subject will be examined in Chapter 8. See also Section 2.4.4.

Low frequencies are not easily attenuated, so modifications in the supply system and appropriate scheduling of the fuel injection are the main strategies for treating these modes. In any case, it appears that all afterburners are subject to operational constraints set by the need to avoid combustion instabilities. Both because of the operational constraints and because of the high costs incurred during development to give current operating envelopes, combustion instability in afterburners remains an attractive subject of research.

Broadly, then, the inevitable appearance of instabilities has led to a basic general strategy followed generally in the development of new afterburners. To the greatest extent possible, acoustic liners are installed in the lateral boundaries. These are effective for attenuating relatively high frequency oscillations historically called 'screech.' Such vibrations normally involve fluctuations in planes transverse to the axis of the burner, so the liners on the case of the burner work quite well.

Oscillations in the direction of flow are in general much more difficult to eliminate. In fact their presence seems often to set operating limits on the afterburner. Those limitations occur mainly in two regions of the basic operating envelope: at lower Mach numbers and high altitude; and at high Mach number and low

altitude. The limits are found from ground tests of the engine, a significant development cost for a new engine.

In general, current information for instabilities in afterburners is unavailable. The most recent work reported in the open literature deals with possible use of active control mainly to widen the operating envelope. An example of modest success at Rolls-Royce has been reported by Moran *et al.* (2001).

1.2.3. Combustion Instabilities in Ramjet Engines. Instabilities in liquid-fueled ramjet engines are similar in many respects to those in afterburners, an example of the general property that the character of the oscillations is determined largely by the types of propellants used and the geometry of the chamber. In both systems, the steady combustion processes are stabilized behind bluff flameholders. Hence with suitable interpretation, many results of research are applicable to both types of systems. In the late 1970s and 1980s, research programs on combustion instabilities in ramjet engines were initiated by several western countries (see, for example, Hall 1978; Culick 1980; Culick and Rogers 1980; Clarke and Humphrey 1986; Humphrey 1987; Sivasegaram and Whitelaw 1987; Zetterström and Sjöblom 1985; Biron *et al.* 1987; Culick and Schadow 1989). Figure 1.16 is a sketch of a stylized combustor representing the sort of configuration commonly used in liquid-fueled ramjets.

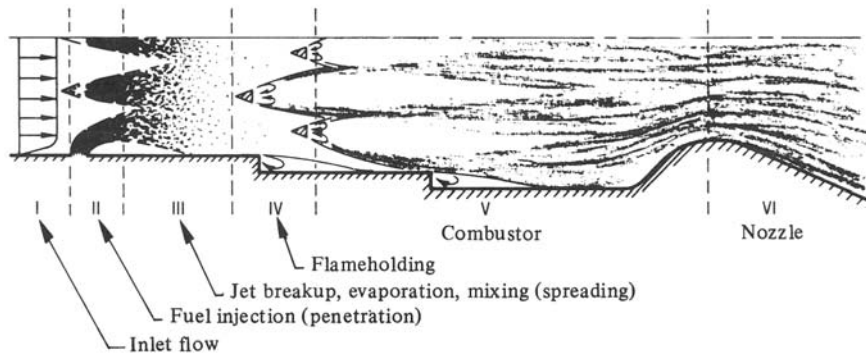


FIGURE 1.16. Stylized configuration of a liquid-fueled ramjet (United Technologies Corp. 1978).

Possibly the most interesting and fundamental result of work during that period was demonstration of the importance of coupling between acoustical motions and large coherent vortex structures shed by a rearward facing step or a flameholder, first emphasized by Byrne (1981, 1983). That phenomenon, with or without combustion processes, arises in many situations and will likely long continue to be the subject of research. Problems associated with generation of unsteady vorticity and vortex shedding arise in all types of combustors. Much effort has been expended in this area, a subject that will arise often in this text.

A typical example is that investigated thoroughly in the dump combustor at Caltech (Smith, 1985; Sterling, 1987; Zsak, 1993; Kendrick, 1995). Figure 1.17 is a sketch of the configuration, in which the flow is subsonic throughout, with premixed gaseous reactants introduced from a plenum chamber and exhausting to the atmosphere. Even for liquid-fueled ramjets, vaporization of the fuel often occurs so rapidly that combustion downstream of the dump plane occurs in a gaseous mixture. The general character of the stability diagram for this geometry has been found in other experimental programs as well: for a given flow rate, the most intense oscillations occur in the vicinity of stoichiometric proportions of the fuel oxidizer.

The waveform and spectrum for the limiting behavior of an unstable oscillation are shown in Figure 1.18. Evidently the spectrum consists of a small number of peaks imbedded in a background of 'noise' spread over the entire frequency range covered. In this respect the motion seems to be dominated by two

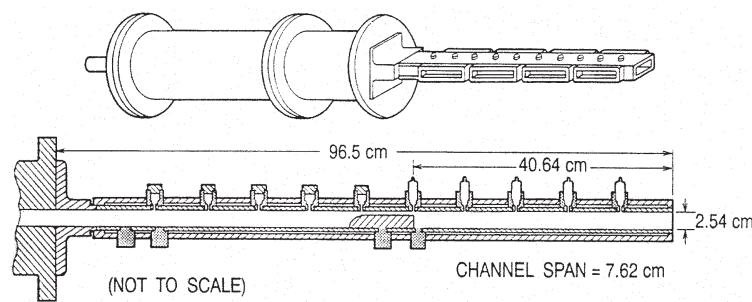


FIGURE 1.17. The Caltech dump combustor.

oscillations having frequencies 530 Hz. and 460 Hz. and subharmonics. Estimates based on the assumption of axial acoustic motions have shown (Sterling 1987; Sterling and Zukoski 1987, 1991; Zsak 1993) that the two oscillations are normal modes of the system. Explanation of the nonlinear mechanism responsible for the sub-harmonics has not been given. It is interesting and significant that the 'noise' exhibited in the spectrum seems to appear as a kind of random modulation of the amplitude of the waveform reproduced in Figure 1.18(a). That interpretation is supported by the approximate analysis of nonlinear acoustics and noise covered here in Chapter 7.

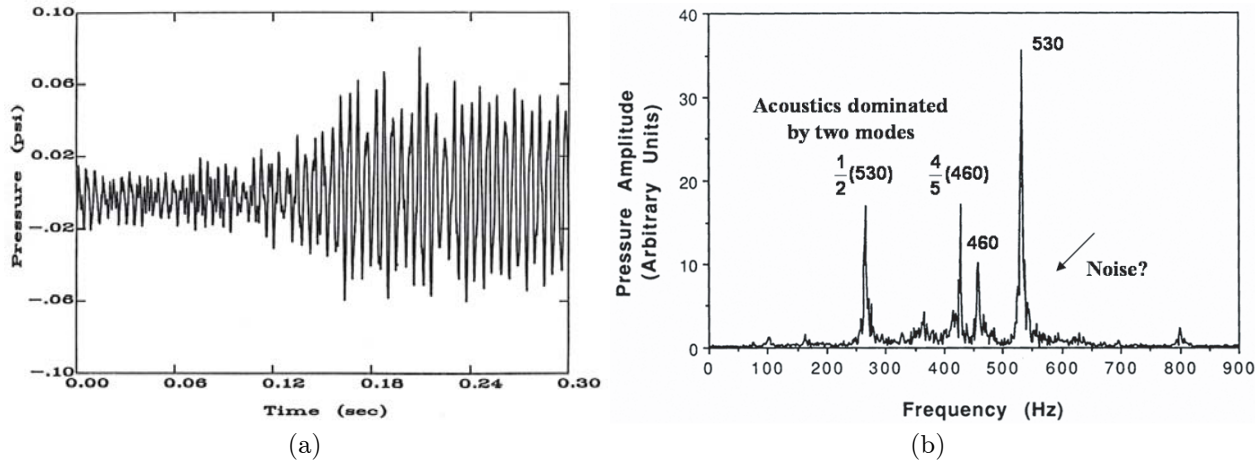


FIGURE 1.18. Waveform and spectrum for an instability in the Caltech dump combustor.

Although this example is special, it does illustrate the chief features of combustion instabilities generally: well-defined organized oscillations within an apparently random field, normally called noise. It is quite common that there are more peaks in the spectra than appear in Figure 1.18(b), and that the frequencies tend to be close to those of the normal acoustics modes of the chamber in question. The quantitative aspects vary widely, but the physical behavior suggested by these results broadly defines the general problem to be addressed by the theory.

The dump combustor has been a favored configuration for laboratory tests having a variety of forms and purposes. We will appeal often to results of such tests. Particularly, the configuration is prone to generate large vortices generated in various forms, a widely studied phenomenon. The dump combustor continues to be a favorite configuration for research as well as applications. Early work by Schadow and his colleagues has been extended by many followers. (Schadow *et al.* 1981, 1983, 1984, 1985, 1987a, b)

1.2.4. Combustion Instabilities in Gas Turbines. Until fairly recently, combustion instabilities in gas turbines had received much less attention than in other systems. We distinguish here main combustors from afterburners which have always exhibited troublesome oscillations. Traditionally, and it is still true, relatively little information has been available about such instabilities in practical systems, for proprietary reasons. However it is probably true for several reasons, mainly relatively large acoustic losses in the combustors, that until fairly recently serious combustion instabilities had been quite rare in gas turbines.

The situation changed with increased emphasis on reducing air pollution. At about the same time, the use of gas turbines for stationary power generation increased. Thus serious concern with any development problems also increased and was not so restricted by proprietary considerations owing to the widespread implications. A strategy for reducing emission of a major pollutant, NO, is to lower the average temperature at which primary combustion occurs, in accordance with the Zel'dovich mechanism for producing NO (Zel'dovich *et al.* 1985). Unfortunately, at lower temperatures achieved by operation at lower local values of fuel/air ratio, the processes stabilizing the flame are less stable and tend to encourage the excitation of oscillations.

As a result, during the past ten–twelve years combustion instabilities have become a serious problem in the development of stationary power generation systems based on combustion, mainly of hydrocarbon fuels. That is not a subject central to this book but the problems are in some cases similar and the methods discussed here are applicable. The subject of combustion instabilities in gas turbines has become important for very practical reasons, but basic problems remain unsolved. Chapter 9 is an abbreviated discussion of instabilities and their active control in gas turbines.

1.2.5. Combustion Instabilities in Solid Propellant Rocket Motors. Instabilities in solid propellant rockets were the first examples discovered, as early as the late 1930s. For reasons which will become clear in this book, unsteady motions in full-scale solid propellant motors and in laboratory devices have probably been the subject of more research than in any other type of system. Accordingly, much of our approach to understanding instabilities in combustion chambers generally can be traced to experiences with solid rockets. An excellent authoritative summary of the research and practical sides of the subject is the short historical article by Price (1992).

Since the late 1950s, serious concern with instabilities in solid propellant motors has been sustained by problems arising in both small (tactical) and large (strategic and large launch systems) rockets. The volume of collected papers compiled and edited by Berle (1960) provides a good view of the state of the field at the end of the 1950s in Western countries. The level of activity remained high and roughly unchanged through the 1960s, due entirely to the demands of the Cold War: The use of solid rocket boosters in systems for launching spacecraft, and for changing trajectories, came later. During the 1950s and 1960s strong emphasis was already placed on sub-scale and laboratory tests, a strategy dictated at least partly by the large costs of full-scale tests. As a result, more is understood about combustion instabilities in solid rockets than for other systems. Moreover, methods and viewpoints developed by the solid rocket community have strongly influenced the approaches to treating combustion instabilities in other systems. The theory developed in this book is an example of that trend.

Many earlier cases exist of combustion instabilities in solid rockets, but a particularly striking example arose in the late 1960s and was documented in the AIAA/ASME Joint Propulsion Meeting in 1971. It was a problem with the third stage of the Minuteman II launch vehicle that initially motivated considerable research activity during the following decade, sponsored largely by the Air Force Rocket Propulsion Laboratory. The causes of three failures in test flights had been traced to the presence of combustion instabilities. Thorough investigation showed that although oscillations had been present throughout the history of the motor, a significant change occurred during production, apparently associated with propellant Lot 10. A record of

the pressure during a flight test is given in Figure 1.19. The broadening of the trace is due to the presence of 'high' frequency oscillations, close to 500 Hz. Figure 1.20 shows the main observable features.

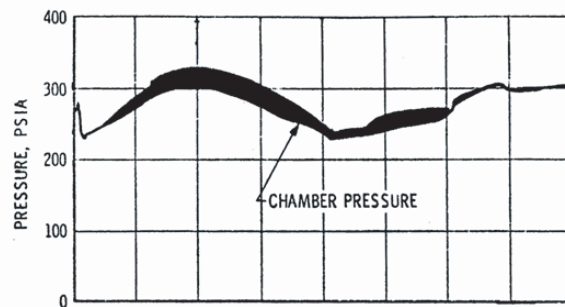


FIGURE 1.19. Flight test record of pressure in a Minuteman II, stage 3.

The oscillations existed during the first fifteen seconds of every firing and always had frequency around 500 Hertz. Whatever had occurred with production Lot 10 caused the maximum amplitudes of oscillations to be unpredictably larger in motors containing propellant from that and subsequent lots. The associated structural vibrations caused failures of a component in the thrust control system.

This example exhibits several characteristics common to many instances of combustion instabilities in solid rockets. In test-to-test comparisons, frequencies are reproducible and amplitudes show only slight variations unless some change occurs in the motor. Any changes must be of two sorts: either geometrical, i.e. the internal shape of the grain; or chemical, consequences of variations in the propellant. Chemical changes, i.e. small variations in the propellant composition, are most likely to affect the dynamics of the combustion processes and indirectly other physical processes in the motor. That is apparently what happened in the Minuteman.

Between production of propellant Lots 9 and 10, the supplier of aluminum particles was changed, because the original production facility was accidentally destroyed. The new aluminum differed in two respects: shapes of the particles, and the proportion of oxide coating on individual particles. Testing during investigation of the instability led to the conclusion that consequent changes in the processes responsible for the production of aluminum oxide products of combustion generated smaller particle sizes of Al_2O_3 . The smaller sizes less effectively attenuated acoustic waves; the net tendency to excite waves therefore increased. As a result, the motors were evidently more unstable and also supported larger amplitudes of oscillation. The second conclusion was purely speculative at the time of the investigation, but can now be demonstrated with the theory covered in this book. Nevertheless, the details explaining why the change in the aluminum supplied led eventually to the significant changes in the combustion products remain unknown.

Subsequent to the Minuteman problem, the Air Force Rocket Propulsion Laboratory supported a substantial program of research on many of the most important problems related to combustion instabilities in solid rockets. Broadly, the intellectual centroid of that program lay closer to the areas of combustor dynamics and combustion dynamics than to the detailed behavior of propellants. The synthesis, chemistry, and kinetics of known and new materials belonged to programs funded by other agencies in the U.S. and in Europe, notably ONERA in France. By far most of the related work in Russia has always been concerned with the characteristics and combustion of propellants, with relatively little attention to the dynamics of combustors.

Investigations and problems of combustion instability in solid rockets have been far more numerous and widespread than for any other system. It is likely an accurate statement that more is generally understood about the problem of oscillations in combustors because of work done to treat the problem in solid rockets.

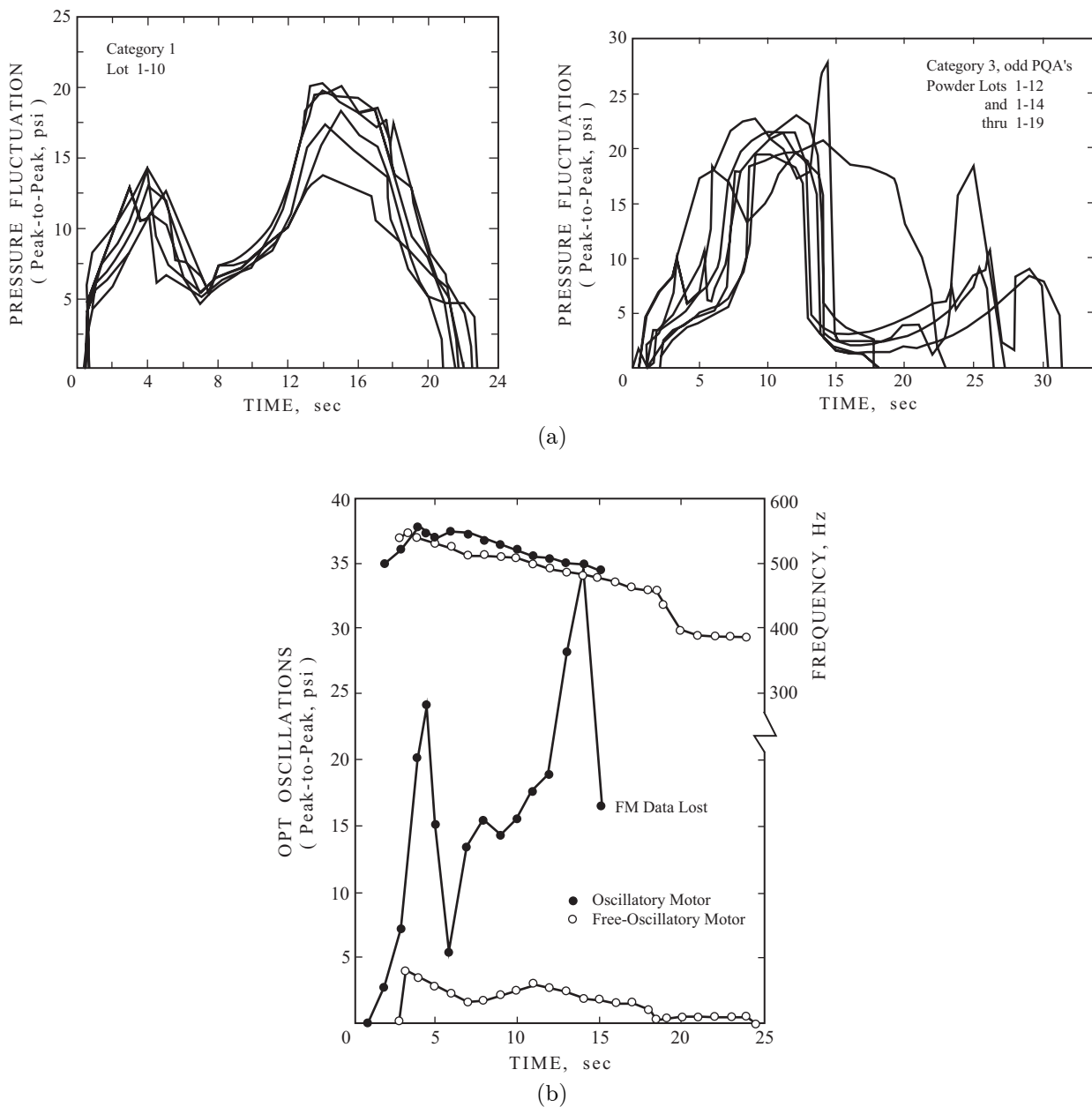


FIGURE 1.20. Frequencies and amplitudes of combustion instabilities in the Minuteman II, stage 3 motor: (a) change of behavior after Lot 1-10 (Fowler and Rosenthal 1971); (b) frequencies and amplitudes measured during static tests (Bergman and Jessen 1971).

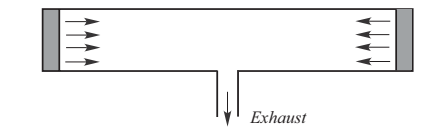
We will mention only a few examples here and refer to others where appropriate in the following text. As Figure 1.2 suggests, much had been accomplished prior to the Minuteman problem. A useful selection of papers was given in a session at the AIAA/ASME Joint Propulsion Meeting, 1971.

In the late 1960s and 1970s there was considerable effort in the U.S. to “solve” the problem of instabilities in solid rockets. Similar research was carried out in Europe, especially in France. Considerable progress

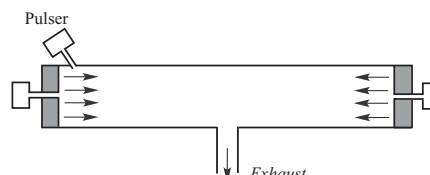
was made, both theoretically—notably the foundation of a method for analyzing nonlinear behavior—and experimentally, especially methods to measure the response function of solid propellants improved at several U.S. companies, at the Naval Air Warfare Center, China Labs (NAWC) and at ONERA in France. But problems of instabilities in motors continued to arise without prediction.

At that time it was known that there remained some difficulties with the theory and serious computational restrictions. That is true as well today although progress continues to be made. The most recent large research program devoted to the subject in the U.S. was the Multidisciplinary University Research Initiative (MURI), “Investigations of Novel Energetic Materials to Stabilize Rocket Motors.” Although the research was primarily concerned with properties and behavior of energetic propellants, some of the work necessarily was devoted to general problems of time-dependent combustion. One conclusion, confirming once again previous work, is that there is no method giving accurate and widely useful results for the propellant response function. An idea of how difficult the problem is may be gained from the fact that at least five methods have been used, several extensively, and none has been found satisfactory for all purposes.

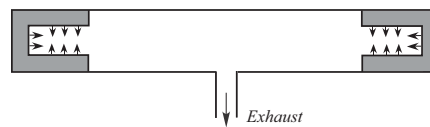
There seems to be general agreement that for most practical purposes the T-burner serves best. This device, sketched in Figure 1.21, in principle gives data for the response of a small flat sample of propellant to a pressure oscillation. Variants have been devised to give results for the response to velocity fluctuations, with only modest success. First discussed by Price and Sofferis (1958), by far most work with the T-burner has been done at NAWC. Price (1992) has given the most authoritative summary of instabilities in solid rockets, including the development of T-burners. The most recent discussions of T-burners have been given by Blomshield *et al.* (1996) and Blomshield (2000).



(a) Basic T-Burner



(b) Pulsed T-Burner



(c) T-Burner with Variable Area Test Samples

FIGURE 1.21. A sketch of the basic T-burner and two variants.

Blomshield (2001) has also compiled a large list of examples of instabilities in operational motors. Figure 1.22 taken from that work is an impressive array of motors that have exhibited instabilities. The examples cover more than 45 years.

No.	Name	Date	App.	Propellant Type	Type				Fix			
					Long	Tang	DC shifts	Pulsed	Prop	Metal	Geo.	Details
1	Sergeant	1951	Sounding	Polysulfide/AP		X						Not fixed
2	RVA-10	1951	TBM	Polysulfide/AP		X						Unknown
3	Sergeant	1957	TBM	Polysulfide/AP		X						Not Fixed
4	Subroc	1961	SAS	Al/Polyurethane	X		X			X		Reduced Al size
5	Iroquois	1960	?	Aluminized	X		X			X		Increased Al%, reduced Size
6	Tartar	1961	SAA	Duel Grain	X		X	X			X	Nozzle moved downstream
7	Tow	1964	STS	Double Base		X	X				X	Added Baffles
8	Genie	1965	ATA	AP/Al/Polyurethane	X					X		Reduced Al size
9	Minuteman	1968	BAL	Double Base/AP/Al	X					X		Changed system, not motor
10	Manpads	1969	SL	AP/Al/HTPB	X		X		X			Lowered Solid Loading
11	ATR	1975	ATA	AP/HTPB		X	X			X		Increased AP size, added catalyst
12	AALM	1975	RES	AP/HTPB				X	X			ZrC containing motors were better
13	MK-12	1975	SAA	AP/Al/HTPB	X	X						Changed system, not motor
14	Slufae	1975	STS	AP/HTPB	X	X					X	Added helmholtz resonator
15	Sidewinder	1977	ATA	AP/HTPB	X		X	X	X			Grain design change, some RDX for AP
16	Maverick	1977	AS	AP/HTPB		X	X			X		Increased AP size, added catalyst, ZrC
17	LCMM	1978	RES	AP/HTPB	X		X				X	Add eroding Nozzle, changed geometry
18	MSM	1978	RES	Double Base/CMDB		X	X				X	Increased port area
19	Harm	1978	AS	AP/HTPB	X						X	No changes required
20	EX-70	1979	SAA	AP/HTPB	X					X	X	Smaller AP, increase nozzle size
21	EX-104	1985	SAA	Duel AP/Al/HTPB	X							No changes required
22	ASROC	1985	SAS	AP/HTPB	X							No changes required
23	Sentry	1985	TBM	AP/Al/HTPB	X		X			X		Program ended, smaller Al
24	LCPM	1988	???	AP/HTPB		X			X			Smaller AP, higher loading
25	SHUTTLE	1990	BOS	AP/Al/PBAN	X							No changed required
26	DBM	1994	SL	AP/Al/HTPB	X		X				X	Grain design change
27	Pathfinder	1996	SPA	AP/Al/HTPB	X					X	X	Increased Al from 2% to 16%
28	NWR	1997	RES	AP/HTPB	X	X	X	X	X	X		Stability additives, geometry, pressure

TBM – Theater Ballistic Missile SAS – Surface Anti-Submarine SAA – Ship Launched Anti-Aircraft STS – Surface to Surface SPA – Space Motor
 ATA – Air-to-Air BAL – Ballistic Missile SL – Surface Launched AS – Air to Surface RES – Research Motor BOS – Space Booster

FIGURE 1.22. A partial summary of U.S. solid propellant motors (1951–1997) having problems of combustion instabilities (Blomshield 2001).

Not covered in the summary just cited is the case which has generated more effort than any other in the recent past—the Ariane 5 Booster. Both the Shuttle and the Ariane 5 booster motors exhibited relatively low level longitudinal oscillations. However, the excursions of pressure in the Ariane 5 have consistently been larger and due to installations of counter-measures, may have cost payload.⁴ The problem has motivated a large amount of very good research and has led to the discovery of a new source of pressure waves called “parietal vortex shedding” discussed further in the following section. Whereas the sort of vortex shedding already mentioned, and commonly found in combustors, occurs at edges, parietal vortex shedding arises when vortices are formed near a boundary through which flow enters a volume. Computations and several tests in laboratory devices of established reality of the phenomenon. It appears, however, that disagreement still exists concerning the importance of parietal vortex shedding in the full-scale Ariane 5.

As the research activities related specifically to solid rockets decreased during the 1980s and new programs began for liquid-fueled systems, the communities, previously quite separate, grew closer together.

⁴As part of the vehicle design—before the first tests—mechanical damping devices were installed between the booster motors and the main vehicle. The problem is particularly bothersome in practice because for odd acoustic modes, there is a large amplification factor (about ten for the Ariane 5) relating fractional thrust oscillations to fractional pressure oscillations. (P. Kuentzmann, private communication.)

For example, prompted by contemporary concern with problems in ramjets, a workshop sponsored by JAN-NAF (Culick 1980) was organized partly with the specific intention to bring together people experienced in the various propulsion systems. During the 1980s there was considerable interchange between the various research communities and since that time, a significant number of people have worked on both solid and liquid-fueled systems. That shift in the sociology of the field has provided the possibility and much of the justification for this book. Events of the past decade have confirmed that the field of combustion instabilities is very usefully approached as a unification of the problems arising in all systems.

In Europe during the 1990s, work on combustion instabilities in solid propellant rockets was motivated largely by low frequency oscillations in the booster motors for the Ariane 5. The most intensive and comprehensive recent work in the U.S. has been carried out in two Multidisciplinary University Research Initiatives (MURI) involving 15 different universities (Culick 2002a, Krier and Hafenrichter 2002). An unusual characteristic of those programs, active for six years beginning in 1995, was the inclusion of coordinated research on all aspects of problems of combustion instabilities in solid propellant rockets, from fundamental chemistry to the internal dynamics of motors. Results of recent works will be covered here in the appropriate places.

1.3. Mechanisms of Combustion Instabilities

The simplest and most convenient characterization of an unstable oscillation is expressed in terms of the mechanical energy of the motion. Linear theory produces the result that the rate of growth of the amplitude is proportional to the fractional rate of change of energy, the sum of kinetic and potential energies. The idea is discussed further in the following section. What matters at this point is that the term 'mechanism' refers to a process that causes transfer of energy to the unsteady motion from some other source. Thus, mechanisms form the substance of the feedback path in Figure 1.1. Generally there are only three sorts of energy sources for unsteady motions in a combustor: the combustion processes; the mean flow, which of course itself is caused by combustion; and a combination of combustion and mean flow simultaneously acting. The distinction is important because the physical explanations of the energy transfer are very different in the three cases.

Just as for steady operation, the chief distinctions among combustion instabilities in different combustors must ultimately be traceable to differences in geometry and the states of the reactants. The root causes, or 'mechanisms', of instabilities are imbedded in that context and are often very difficult to identify with certainty. Possibly the most difficult problem in any particular case is to quantify the mechanism. Solving that problem requires finding an accurate representation of the relevant dynamics.

1.3.1. Mechanisms in Liquid-Fueled Rockets. Combustion instabilities first became a serious problem in liquid rockets and remain a matter of basic concern during development. The chief mechanisms remain those known for many years, associated with the propellant feed system; the injection system; the processes required for conversion from liquid to gas; and combustion dynamics. There seem to be no examples caused primarily by vortex shedding, mean flow/acoustics interactions, or convective waves (of entropy or vorticity).

Figure 1.23 is a broad summary of the main processes taking place in a liquid rocket combustion chamber (Culick and Yang 1993) The listing and categorization serves only as a rough general guide. Particular situations may introduce additional processes.

In order to construct a dynamical model of a combustion chamber, it is necessary to place the processes of Figure 1.23 in space. This is not the occasion to pursue that matter in detail, which must in any case be done for each given design. Figure 1.24, adapted from Bazarov (1979), conveys the general idea. One approach to analyzing linear stability is based on combining the transfer functions according to a diagram like Figure 1.24. Then the problem may be posed in the manner of feedback control theory. Each process

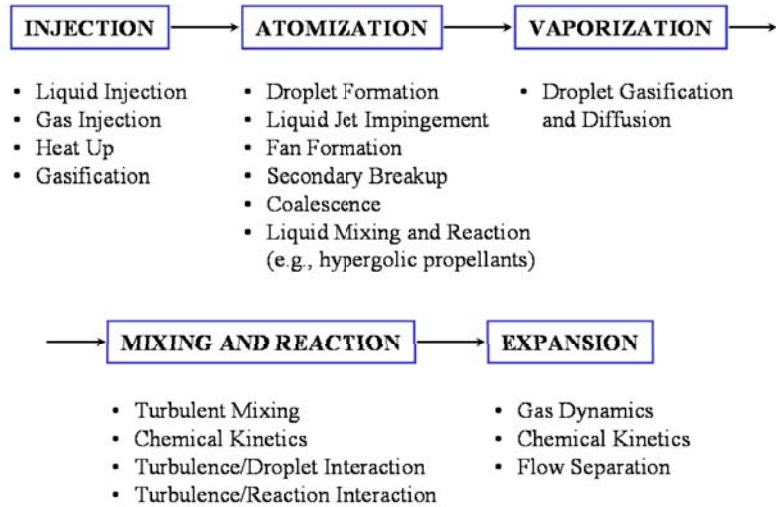


FIGURE 1.23. An approximate schematic summary of the important rate processes in a liquid rocket combustor (Culick and Yang 1993).

suggested or alluded to in Figure 1.23 must then somehow be represented by a transfer function. That may be a difficult and complicated task particularly due to the coupling between the processes.

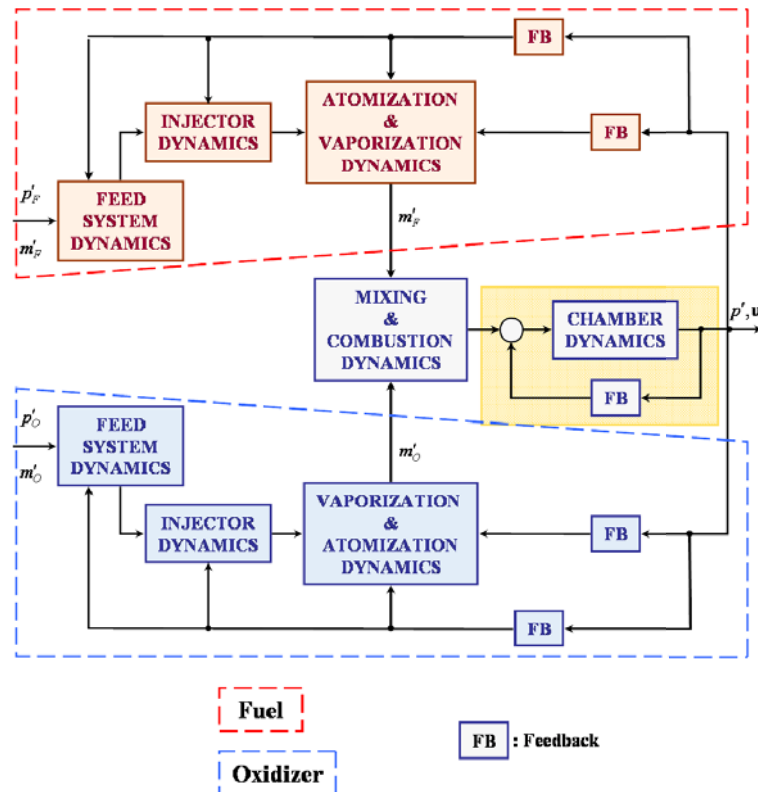


FIGURE 1.24. A simplified diagram for the dynamics of a liquid rocket engine (adapted from Bazarov 1979).

The mechanisms causing instabilities differ in detail, and perhaps grossly, depending on the type of system. Generally there are three types of system depending on the choice of reactants: liquid oxygen/hydrogen (LOX/H) typified by the engines RL-10, J-2, Space Shuttle main engine (SSME), and the Vulcain (European Space Agency); liquid oxygen/hydrocarbon (LOX/HC) of which some examples are the Apollo F-1, the Atlas, and the RD-0110 (Russian); and those systems using storable propellants such as those based on nitrogen tetroxide (N_2O_4) as the oxidizer with fuels commonly hydrazine, monomethylhydrazine (MMH) as in the French Viking motor in the Ariane 1-4, and unsymmetrical dimethylhydrazine (UDMH). The TRW pintle engine which was used in the Lunar Descent Vehicle is perhaps the most famous engine using storable propellants.

For a given choice of reactants, the most significant influence on the instabilities is the injection system. In this context the main classes of injectors are impinging jets; shear and swirl coaxial injectors; showerheads; and impinging sheets. Changes of the geometry may produce a large variety of injectors, many of which are shown in Figure 1.5. Each of these devices exhibits its own mechanism for instability, possibly different in important respects, and subtly dependent on operating conditions. It is not possible to offer generalizations. Figure 1.25 suggests the variety of mechanisms that may arise in a coaxial injector.

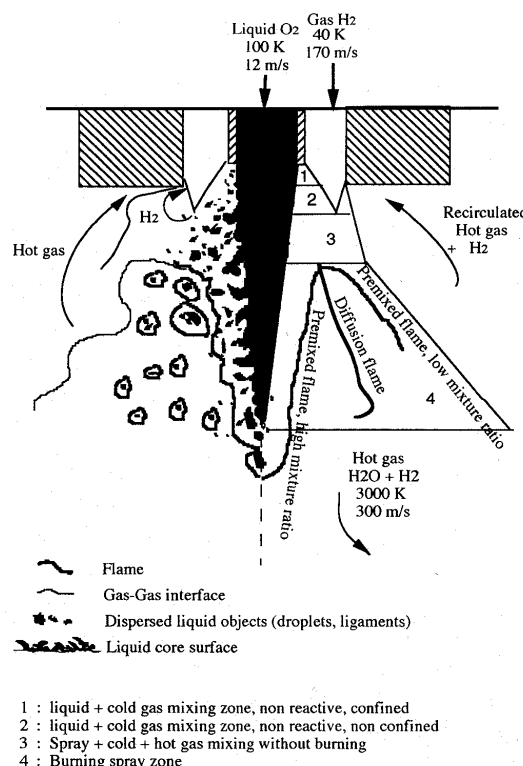


FIGURE 1.25. A sketch showing some of the processes taking place in a coaxial injector (Vingert *et al.* 1993).

1.3.2. Sensitivity of Combustion Processes; Time Lags. Combustion processes are sensitive to the macroscopic flow variables, particularly pressure, temperature and velocity. Even slow changes of those quantities affect the energy released according to rules that can be deduced from the behavior for steady combustion. In general, however, representations of that sort, based on assuming quasi-steady behavior, are inadequate. Combustion instabilities normally occur in frequency ranges such that genuine dynamical

behavior is significant. That is, the transient changes of energy release do not follow precisely in phase with imposed changes of a flow variable such as pressure.

The simplest assumption is that the combustion processes behave as a first order dynamical system characterized by a single time delay or relaxation time. That idea was apparently first suggested by von Karman as a basis for interpreting instabilities discovered in early experiments with liquid propellant rockets at Caltech (Summerfield 1941). That representation, which came to be called the ' $n - \tau$ model' was developed most extensively by Crocco and his students at Princeton during the 1950s and 1960s. Time delays may be due, for example, to processes associated with ignition of reactants. Subsequent to injection as the reactants flow downstream, finite times may be required for vaporization, mixing, and for the kinetics mechanism to reach completions. Both effects may be interpreted as a convective time delay. Under unsteady conditions, the initial state of the reactants, their concentrations, pressure, and velocity, also fluctuate, causing the delay time to be both nonuniform in space and in time. As a result, the rate of energy release downstream in the chamber is also space- and time-dependent, and acts as a source of waves in the combustor.

In the case of liquid-fueled systems, interactions of the injected streams, formation of sheets and break-up into drops are processes sensitive to pressure and particularly velocity fluctuations. Those are purely fluid-mechanical processes impossible to treat analytically and pose extremely difficult problems for numerical simulations. No complete numerical analyses exist and only much simplified models have been used in numerical simulations of combustion instabilities. The dynamics of a combustion system are not likely to be well-represented by an $n - \tau$ model.

If a time-lag model is used, either further modeling and calculations must be carried out, or an assumption must be made for the dependence of the time lag on frequency. It is usual that the time lag is assumed constant. Then the response of the system exhibits unrealistic resonances as the frequency increases. An example is shown later in Figure 2.20 for combustion of a solid propellant. Realistic behavior is found only by taking the lag itself to be a function of frequency. The choice is largely arbitrary unless the physical basis for the model is improved.

Purely gaseous-fueled systems present possibilities for different physical models that also leads to first-order behavior. It is an old idea that even in complicated geometries, combustion in a non-premixed system must occur at least partly in elements of diffusion flames. If the gaseous reactants are premixed then in simple configurations such as tubes, or dump combustors, combustion may occur in large stable flame sheets of the flow is laminar, or in fragments of premixed 'flamelets' when the flow is turbulent. In all of these cases it is reasonable to anticipate that at any given time the rate of energy release is roughly proportional to the area of the flame sheets. Then fluctuations of the velocity or processes responsible for ignition and extinction, will cause fluctuations of the energy release rate. Models of this process lead to an equation representing first order behavior (For example, see Poinsot *et al.* 1988; Candel *et al.* 1992; McManus *et al.* 1993; Dowling 1995; Annaswamy *et al.* 2000).

The approximation of first order behavior fails entirely for the dynamics of burning solid propellants (Culick 1968). Although in good first approximation dominated by unsteady heat transfer in the condensed phase, a diffusive process, the combustion dynamics in this case exhibits behavior closer to that of a second order system. The frequency response of that burning rate tends normally to have a large broad peak centered at a frequency falling well within the range of the frequencies characteristic of the chamber dynamics. Hence there is a clear possibility for a resonance and instability suggested by the diagram in Figure 1.1.

1.3.3. Vortex Shedding and Vortex/Mean Flow Interactions. Generation of oscillations by the average flow is due to causes roughly like those active in wind musical instruments. In all such cases, flow separation is involved, followed by instability of a shear layer and formation of vortices. Direct coupling between the vortices and a local velocity fluctuation associated with an acoustic field is relatively weak; that

is, the rate of energy exchange is in some sense small. However, the interaction between the velocity (or pressure) fluctuation and the initial portion of the shear layer is normally a basic reason that feedback exists between the unsteady field in the volume of the combustor and vortex shedding.

Figure 1.26 conveys the idea of one way in which shed vortices may excite oscillations. The local acoustic velocity field determines the times at which individual vortices are shed at an edge. By some means of coupling, the vortices then act to generate an acoustic field, but with a lag between the shedding and generation processes. The acoustic field so generated is local and the process of filling the chamber is another matter. However, it seems to be generally true that acoustic fields generated by vortex shedding are never as intense as the stronger fields produced by the combustion processes directly.

Byrne (1981, 1983) seems to have been first to suggest that vortex shedding could be responsible for instabilities observed in dump combustors. The idea was developed very actively in the 1980s, both in systems operating at room temperature without combustion (Schadow *et al.* 1981, 1983, 1984, 1985) and in combustors (Schadow *et al.* 1985, 1987a, 1987b).

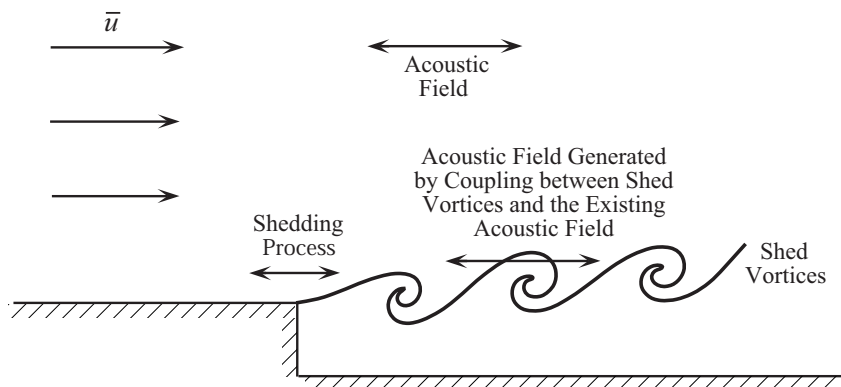


FIGURE 1.26. Generation of an acoustic field by vortex shedding.

Unsteady combustion in vortices was one of the early mechanisms proposed as a cause of combustion instabilities in combustors using bluff body flameholders (Kaskan and Noreen 1955, Marble and Rogers 1956). It was essentially re-discovered in the 1980s during tests of dump combustors (Smith and Zukoski 1985; Daily and Oppenheim 1986; Sterling and Zukoski 1991, for example). Several attempts have been made to quantify the mechanism with analysis (Norton 1983; Karagozian and Marble 1986) and with numerical simulations (Laverdant and Candel 1988; Samaniego and Mantel 1999). Insufficient progress has been made to construct a model suitable for general analysis of combustion instabilities. Thus there is currently no basis for predictions of combustor dynamics excited by this mechanism, although there are recent simplified attempts for special situations by Matveev and Culick (2002, 2003a) and by Matveev (2004). Special cases have been discussed in connection with particular experimental results; see, for example, Sterling 1993 and Sections 2.3.4 and 2.3.5.

It has long been known experimentally that vortices shed in a chamber more effectively generate acoustic waves if they impinge in an obstacle downstream of their origin (Flandro and Jacobs, 1975; Culick and Magiawala, 1979; Nomoto and Culick, 1982; Flandro, 1986). The first practical examples of this phenomenon were found in the solid rocket booster for the Shuttle launch system in the 1970s and the Titan motor (Brown *et al.* 1981, 1985). It was that problem that motivated the works just cited, but since then vortex shedding has been recognized as a mechanism for generating acoustic oscillations in other systems as well, notably the booster motors on the Space Shuttle and on the Ariane 5. A particularly good summary and discussion of the subject has recently been given by Vuillot and Casalis (2002). Owing to their involvement with a problem of pressure oscillations in the Ariane 5 booster motors, the authors focus special attention on a very

different form of vortex shedding. Laboratory tests and numerical simulations have established the existence of a process called ‘parietal vortex shedding’ in which large coherent vortices grow out of the region of shear near a surface through which flow enters the chamber. The flow can either be issuing from a burning solid propellant or may be the flow inward of fluid through a permeable boundary.

It happens that the amplitudes of oscillations in the Ariane motors are significantly greater than those found in the Space Shuttle booster motors. In the latter case, vortices are definitely created by instability of the shear layer formed in flow past an obstacle. The reasons for the difference in amplitudes in the two cases may be due to differences in geometry. One proposal rests on special conditions in the Ariane, possibly encouraging “parietal vortex shedding”, but the problem is not satisfactorily resolved. Parietal vortex shedding involves growth of vortices initiated in the region adjacent to a transpiring surface, such as a burning solid.

1.3.4. Operation Near the Lean Blow-Out Limit. Combustion instabilities have not historically been a serious problem in gas turbine main combustors. Although instabilities have certainly been observed for many years, they have not been persistently troublesome. Due to proprietary considerations almost no detailed results for full-scale machines have been made public, a situation that has recently been changing. In the past few years combustion instabilities have become a serious problem in gas turbines because of the need to operate close to the lean blowout limit of premixed gaseous reactants as part of the strategy to reduce generation of pollutants, notably NO_x .

As the operating condition approaches the lean blowout limit, combustion processes (‘flame dynamics’), including flame stabilization, are more sensitive to fluctuations than under operation at higher mixture (F/O) ratios. The sensitivity extends to flame fronts and zones as well as to the stabilization processes, shear layers and recirculation zones. The latter, associated with injection and stabilization, may possess multiple dynamical states, i.e. special bifurcations and hysteresis.

The dynamical behavior of the premixer and injection devices may contribute to instabilities in various ways. Internal resonances, for example, may be excited by oscillations in the chamber, causing perturbations of the energy released in the combustion processes downstream of the injector. There may also be undesirable coupling between elements of an array of premixers and injectors. Such dynamical behavior may also be turned to advantage to extend the operating range of stable operation. That strategy was successfully pursued on several occasions in the Russian liquid rocket community.

It is likely that fluctuations of the mixture or fuel/oxidizer ratio (F/O) play an important role in the dynamics of gas turbine combustors (Lieuwen *et al.* 2001). If the F/O ratio of the reactants is at all sensitive to conditions in the combustion chamber, there is an obvious feedback path connecting the combustor and combustion dynamics. The possibility has arisen previously in other combustion systems, but at least anecdotal evidence has suggested that serious attention must be paid to fluctuations of mixture ratio as a fundamental mechanism for instabilities in gas turbines.

There is considerable evidence that the ratio of a “convective timescale” and the dominant acoustic period ($1/f$) may be the determining parameters, or at least an important one, governing mixture ratio fluctuations in a given situation. Lieuwen *et al.* (2001) and Cohen *et al.* (2003) have given particularly useful discussions of the matter. Unfortunately the situation is clouded because the first case, shown in Figure 1.27, is a discussion of an axisymmetric configuration and the second, Figure 1.28, is concerned with experiments using a two-dimensional dump combustor. The ratio $\tau_c f$ was around unity or less for the tests with the configuration shown in Figure 1.27, but two or greater for the two-dimensional combustor, Figure 1.28. It seems that explanations of the observed behavior are more convincing when considered separately than when taken together. There is no single reasoning, no matter how lengthy, that explains satisfactorily the observations. The actual case, like the others treated here, is too complicated for such a simple result.

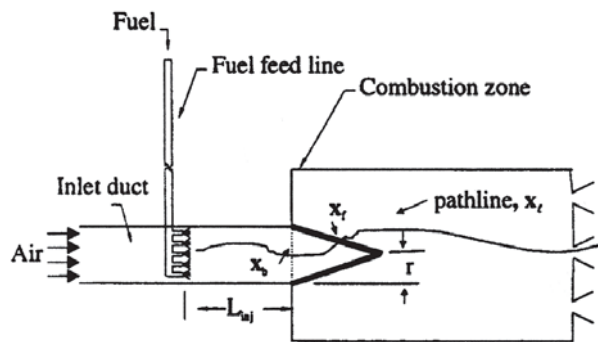


FIGURE 1.27. A form of axisymmetric lean premixed combustor (Lieuwen *et al.* 2001).

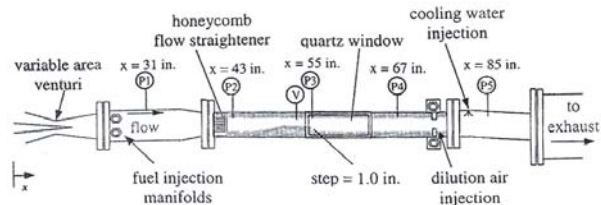


FIGURE 1.28. A typical 2-D dump combustor (Cohen *et al.* 2003).

Much remains to be learned about instabilities in gas turbines, although the subject has been greatly clarified in the past 10–12 years. We will not cover the material thoroughly in this volume, mainly because we are concerned primarily with other types of systems which are of more concern for the applications most significant for aerospace systems. Moreover, the causes of instabilities in gas turbines to a large extent seem to be distinct from those in rockets, afterburners and ramjets. In the most fundamental sense, that conclusion is perhaps illusory. Chapter 9 is devoted to a largely qualitative discussion of some of the recent topics addressed in work on instabilities in gas turbines.

1.3.5. Mechanisms in Solid-Fueled Rockets. No disagreement exists that the predominant mechanisms for instabilities in solid propellant rockets is the sensitivity of burning surfaces to pressure and velocity fluctuations. A large part of Chapter 2 is devoted to the basic essentials, including, in Section 2.2, a detailed derivation of the simplest response of a burning surface to pressure fluctuations. During the past five decades, a great amount of resources has been consumed in an effort to develop methods for measuring the response. Success, however, has been spotty and far short of what is required both for practical and for research purposes. It is an outstanding problem in the field that merits continued work, especially to devise a new method.

Quite a different mechanism also exists, involving the shedding of large vortices and subsequent excitation and interactions with acoustic waves. Vorticity/acoustic coupling is actually a relatively widely recognized mechanism, not only in solid rockets, because its existence does not rest on combustion processes. The importance of vortex shedding in dump combustors, the usual configuration of ramjet engines, has long been established as a major mechanism. Thus, if one is concerned with the possibility that the process is important in a solid propellant motor, attention should be paid to the characteristics of the phenomenon in ramjets. The point is not, of course, that the two sorts of situations are in some sense the 'same' but there are similarities and much may be learned from comparisons of results. No such comparative studies exist.

Partly because a solid propellant rocket cannot be repeatedly tested in the same manner as other systems, more attention has been given combustion instabilities in this kind of combustor than for any other. It is possible, but not likely, that any important mechanisms of instabilities have been overlooked or are unknown. The practical problem, as we will see, is quantifying the contributions well enough to obtain good results.

1.3.6. Combustion Dynamics. Except for instabilities sustained by the purely fluid mechanical mechanism of vortex shedding, all practical cases of combustion instabilities involve combustion dynamics in some form. It is hardly an exaggeration to claim that understanding combustion dynamics is ultimately the most important fundamental problem in the subject of combustion instabilities. Broadly the term refers to the

property possessed by any chemically reacting system that the rate at which energy is released is sensitive, i.e. responds, to the rates of change of pressure, temperature, density and mixture ratio. For solid and liquid propellants, the combustion dynamics is usually more conveniently expressed in terms of the rate of conversion of the condensed phase to gaseous combustion products.

In the limit of small changes (i.e. for linear behavior), dynamical response functions for combustion systems are entirely analogous to transfer functions used in the subject of controls. They are fundamental to analysis of the stability of combustion systems and to application of the principles of feedback control.

Introduction of response functions as general definitions is part of the basis on which combustion instabilities, or, more widely, the dynamics of combustion systems, can be investigated and understood with minimal appeal to the particulars of the combustion dynamics of a specific type of system. However, applications of the theory require close attention to the details of the system at hand. Modeling combustion dynamics on theoretical grounds only carries serious limitations due to the complexities of the systems. Hence experimental methods and, to an increasing extent, numerical simulations are essential to treating combustion instabilities in practical systems.

1.4. Physical Characteristics of Combustion Instabilities

Owing to the difficulty of making direct measurements of the flow field within a combustion chamber, virtually all that is known about combustion instabilities rests on close coordination of experiment and theory. The subject is intrinsically semi-empirical, theoretical work being founded on observational data both from full-scale machines and laboratory devices. Conversely, the theoretical and analytical framework occupies a central position as the vehicle for planning experimental work and for interpreting the results. The chief purposes of this section are to summarize briefly the most important basic characteristics of observed instabilities; and to introduce the way in which those observations motivate the formulation of the theoretical framework.

In tests of full-scale propulsion systems, only three types of data are normally available, obtained from pressure transducers, accelerometers, and strain gauges. Measurements of pressure are most direct but are always limited, and often not possible when the necessary penetration of the enclosure to install instruments is not allowed. Hence the unsteady internal pressure field is often inferred from data taken with accelerometers and strain gauges. In any case, because it is the fundamental variable of the motions, the pressure will serve here as the focus of our discussion.

Figure 1.29 shows examples of pressure records from measurements taken with three different solid propellant rockets. They show many of the features commonly observed for combustion instabilities. The transient records 1.29 (a) and (b) exhibit the exponential growth characteristic of a linear instability. That behavior is most clearly exposed by plotting the logarithm of the peak values versus time, giving a straight line because $p \sim e^{at}$ means $\log p \sim at$. The result is of course not precise because the oscillation is not a pure sinusoidal motion and indeed, the case 1.29(b) shows development of steep fronts, often preceding evolution into approximately triangular waveforms accompanied by an increase in the average burning rate and chamber pressure. In any case, the transient growth usually slows and the oscillation becomes a limit cycle possibly containing several frequencies. Figure 1.29(c) is an example showing behavior often observed for instabilities in solid rockets for which the best measurements of transients have been made.

Figure 1.30 shows details of a test record taken during firing of a full-scale solid rocket. Development of steep waves and higher harmonics are clearly evident. Note also the rise of mean pressure accompanying the appearance of higher harmonics at time D. As shown also in Figures 1.29 (b) and (c), that is not an

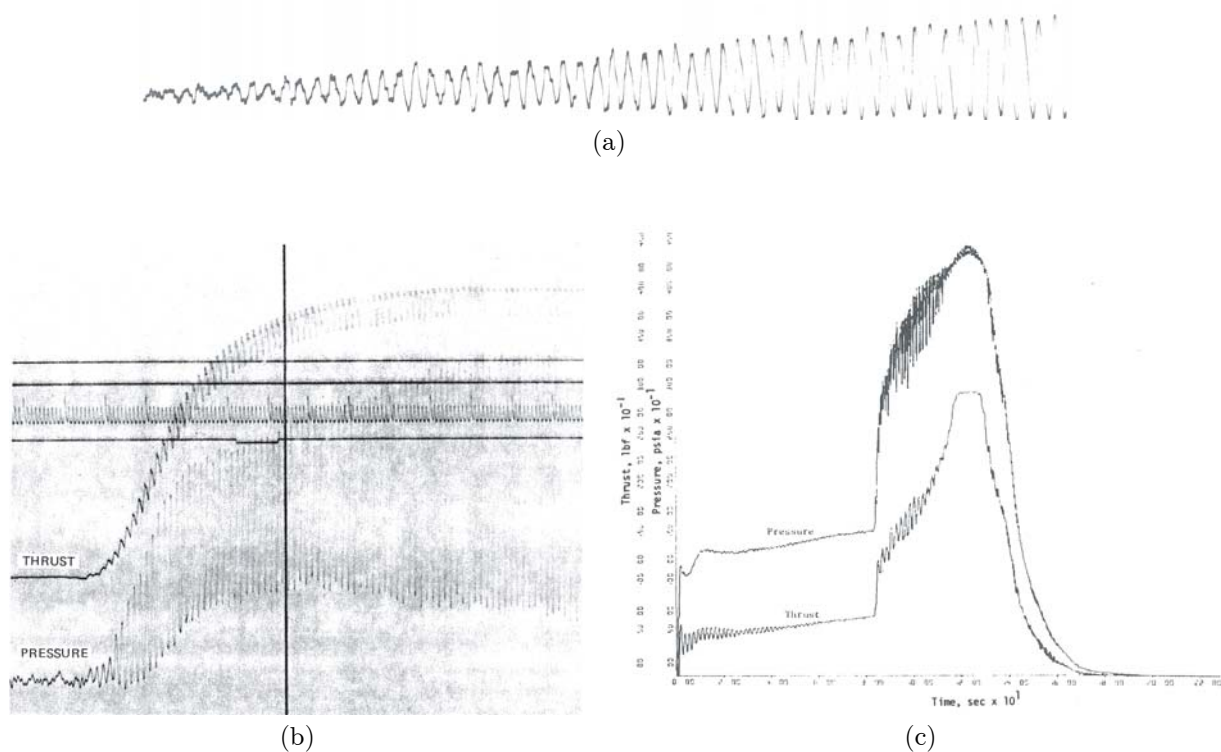


FIGURE 1.29. Transient growths and “limit cycles” of combustion instabilities.

unusual occurrence. In the case giving the records shown in Figure 1.30, the instability was eliminated with a change of the internal configuration, consistent with the ideas pursued in this book.

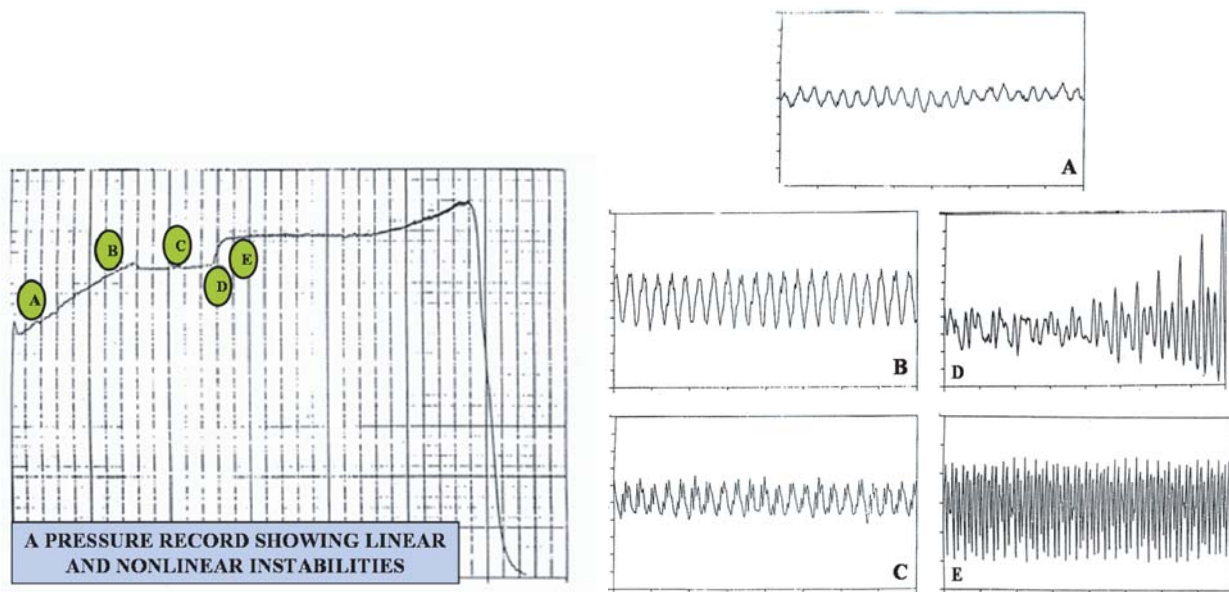


FIGURE 1.30. Growth of a nonlinear instability in a solid rocket showing the unsteady pressure. Note the increased spectral content of the signal as the amplitude increases.

A convenient and quickly informative method of displaying characteristics of an unstable firing is the “waterfall” plot, of which examples are shown in Figures 1.31 and 1.32. Spectra for a sequence of times are plotted on the same axes, the vertical axis serving as the measure of pressure as well as indicating the time intervals at which the spectra are taken. Figure 1.31 is the waterfall plot starting early in the test of a stable motor. A test having an instability, such as that shown in Figure 1.30 is reproduced in Figure 1.32.

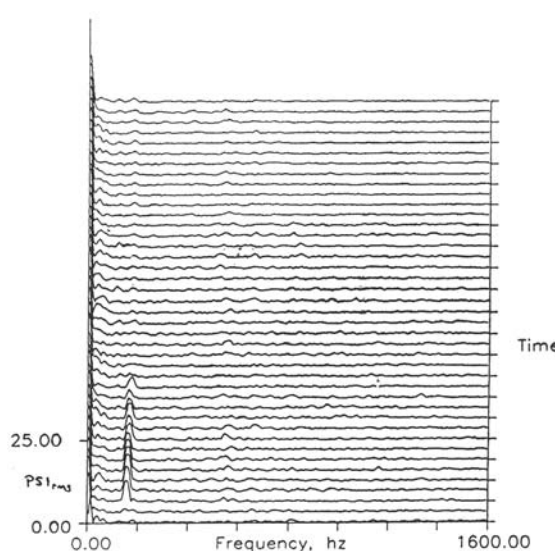


FIGURE 1.31. A waterfall plot taken during a stable firing (Brown 1995).

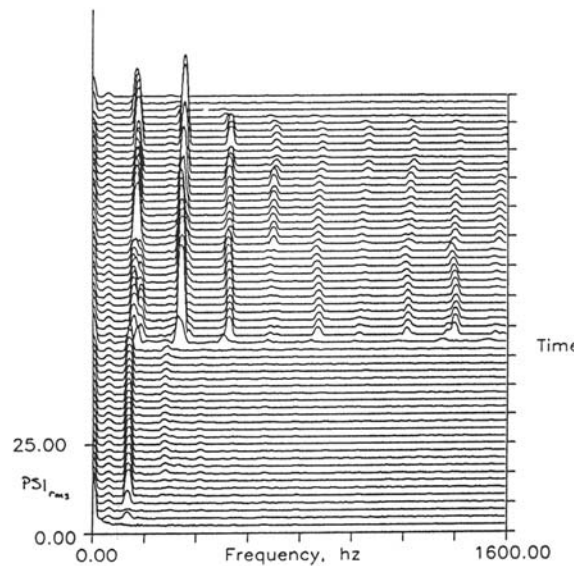


FIGURE 1.32. A waterfall plot showing an instability, having fundamental frequency < 200 Hz but with developing components at higher frequencies (Brown 1995).

The cases chosen here have been examples of fully developed instabilities. The well-defined peaks reflect the clear presence of several frequencies in the waves, the larger amplitudes occurring at the lower frequencies, as commonly happens. A substantial background of broad-band noise is of course always present due to turbulent fluctuations of the flow, noise emission by combustion processes, and possibly other unsteady motions such as flow separation. Some recent laboratory tests have shown that the level of noise depends on the presence and amplitude of combustion instabilities, but the cause is unknown and no such observations exist for full-scale combustors.

Much of this book is devoted to understanding the origins of the behavior illustrated by the examples in Figures 1.3, 1.6, 1.7, 1.29 and 1.30. The classical theory of acoustics has provided the basis for understanding combustion instabilities since early recognition that some unexpected observations could be traced to pressure oscillations. Many basic results of classical acoustics have been applied directly and with remarkable success to problems of instabilities. It is often taken for granted that well-known acoustics formulas should be applicable—their use can in fact be justified on fundamental grounds. However, in the first instance, it is surprising that they work so well, because the medium is far from the ideal uniform quiescent gas assumed in the classical acoustics of resonating chambers.

On the other hand, non-classical behavior is not difficult to find. It has been firmly established with tests using both liquid and solid rockets that instabilities involving “subcritical bifurcations” are common. That is, a combustor may be stable to small disturbances but may exhibit an instability if subjected to a

sufficiently large disturbance. An example of such behavior for a liquid rocket has been cited with Figures 1.6, 1.7 and 1.11. Figure 1.33 shows a typical result found for solid rockets. The subject of subcritical bifurcations is discussed in Section 7.11.

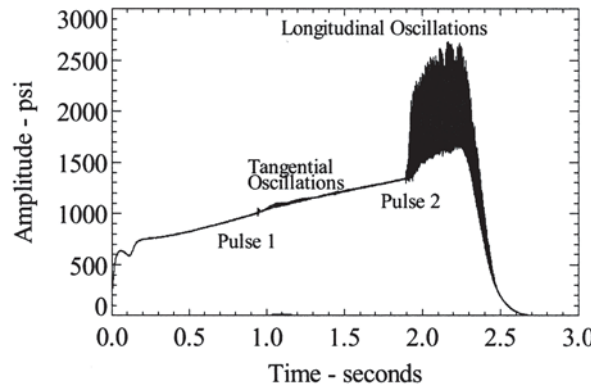


FIGURE 1.33. A severe pulsed instability in a solid rocket; an example of a subcritical bifurcation (Blomshield 2001).

A combustion chamber contains a non-uniform flow of chemically reacting species, often present in condensed as well as gaseous phases, exhausting through a nozzle that is choked in rockets, ramjets, and afterburners. Moreover, the flow is normally turbulent and may include regions of separation. Yet estimates of the frequencies of oscillations computed with acoustics formulas for the natural modes of a closed chamber containing a uniform gas at rest commonly lie within 10–15 percent or less of the frequencies observed for combustion instabilities, if the speed of sound is correctly chosen.

There are three main reasons that the classical view of acoustics is a good first approximation to wave propagation in combustion chamber: (1) the Mach number of the average flow is commonly small, so convective and refractive effects are small; (2) if the exhaust nozzle is choked, incident waves are efficiently reflected, so for small Mach numbers the exit plane appears to be nearly a rigid surface; and (3) in the limit of small amplitude disturbances, it is a fundamental result for compressible flows that any unsteady motion can be decomposed into three independent modes of propagation, of which one is acoustic (Chu and Kovazsnay 1956). The other two modes of motion are vortical disturbances, the dominant component of turbulence, and entropy (or temperature) waves. Hence even in the highly turbulent non-uniform flow usually present in a combustion chamber, acoustic waves behave in good first approximation according to their own simple classical laws. That conclusion has simplified enormously the task of gaining qualitative understanding of instabilities arising in full-scale systems as well as in laboratory devices.

Of course, it is precisely the departures from classical acoustics that define the class of problems we call combustion instabilities. In that sense, this book is concerned chiefly with perturbations of a very old problem, standing waves in an enclosure. That point of view has significant consequences; perhaps the most important is that many of the physical characteristics of combustion instabilities can be described and understood quite well in a familiar context. The remainder of this chapter is largely an elaboration of that conclusion.

The most obvious evidence that combustion instabilities are related to classical acoustic resonances is the common observation that frequencies measured in tests agree fairly well with those computed with classical formulas. Generally, the frequency f of a wave equals its speed of propagation, a , divided by the

wavelength, λ :

$$f = \frac{a}{\lambda} \quad (1.1)$$

On dimensional grounds, or by recalling classical results, we know that the wavelength of a resonance or normal mode of a chamber is proportional to a length, the unobstructed distance characterizing the particular mode in question. Thus the wavelengths of the organ-pipe modes are proportional to the length, L , of the pipe, those of modes of motion in transverse planes of a circular cylindrical chamber are proportional to the diameter, D , and so forth. Hence (1.1) implies

$$\begin{aligned} f \sim \frac{a}{L} & \quad \text{longitudinal modes} \\ f \sim \frac{a}{D} & \quad \text{transverse modes} \end{aligned} \quad (1.2)\text{a,b}$$

There are two basic implications of the conclusion that the formulas (1.2)a,b, with suitable multiplying constants, seem to predict observed frequencies fairly well: evidently the geometry is a dominant influence on the special structure of the instabilities; and we can reasonably define some sort of average speed of sound in the chamber, based on an approximation to the temperature distribution. In practice, estimates of a use the classical formula $a = \sqrt{\gamma RT}$ with T the adiabatic flame temperature for the chemical system in question, and with the properties γ and R calculated according to the composition of the mixture in the chamber. Usually, mass-averaged values, accounting for condensed species, seem to be close to the truth. If large differences of temperature exist in the chamber, as in a flow containing flame fronts, nonuniformities in the speed of sound must be accounted for to obtain good estimates of the frequencies.

Even for more complicated geometries, notably those often used in solid rockets, when the simple formulas (1.2)a,b are not directly applicable, numerical calculations of the classical acoustic motions normally give good approximations to the natural frequencies and pressure distributions. Thus quite generally we can adopt the point of view that combustion instabilities are acoustical motions excited and sustained in the first instance by interactions with combustion processes. That the classical theory works so well for estimating frequencies and distributions of the unsteady motions means that computation of those quantities is not a serious test of a more comprehensive theory. What is required first of a theory of combustion instabilities is a basis for understanding how and why combustion instabilities differ from classical acoustics.

In particular, two global aspects of minor importance in much of classical acoustics, are fundamental to understanding combustion instabilities: transient characteristics and nonlinear behavior. Both are associated with the property that with respect to combustion instabilities, a combustion chamber appears to an observer to be a *self-excited system*: the oscillations appear without the action of externally imposed forces. Combustion processes are the sources of energy which ultimately appear as the thermal and mechanical energy of the fluid motions. If the processes tending to dissipate the energy of a fluctuation in the flow are weaker than those adding energy, then the disturbance is unstable.

1.5. Linear Behavior

When the amplitude of a disturbance is small, the rates of energy gains and losses are usually proportional to the energy itself which in turn is proportional to the square of the amplitude of the disturbance; the responsible processes are said to be linear because the governing differential equations are linear in the flow variables. An unstable disturbance then grows exponentially in time, without limit if all processes remain

linear. Exponential growth of the form $A_0 e^{\alpha t}$, where A_0 is the amplitude of the initial small disturbance, is characteristic of the initial stage of an instability in a self-excited system, sketched in Figure 1.34(a). In contrast, the initial transient in a linear system forced by an invariant external agent grows according to the form $1 - e^{-\beta t}$, shown in Figure 1.34(b). The curve $e^{\alpha t}$ is concave upward and evolves into a constant limiting value for a physical system only if nonlinear processes are active. However, the plot of $1 - e^{-\beta t}$ is concave downward and approaches a limiting value for a linear system because the driving agent supplies only finite power.

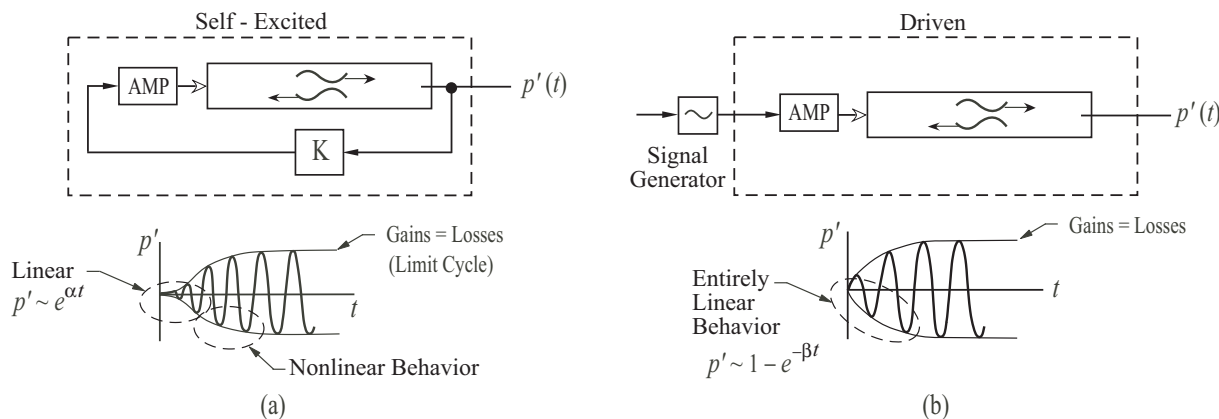


FIGURE 1.34. Transient behavior of (a) self-excited linearly unstable motions; (b) forced motions.

Data of the sort sketched in Figure 1.34 leave no doubt that the unstable motions in combustion chambers are self-excited, having the characteristics shown in Figure 1.34(a). The physical origin of this behavior is the dependence of the energy gains and losses on the motions themselves. For combustion instabilities, the 'system' is the dynamical system whose behavior is measured by the instrument sensing the pressure oscillations. Thus, in view of earlier remarks, the dynamical system is in some sense the system of acoustical motions in the chamber coupled to the mean flow and combustion processes (recall Figure 1.1).

It is a fundamental and extremely important conclusion that by far most combustion instabilities are motions of a self-excited dynamical system. Probably the most significant implication is that in order to understand fully the observed behavior, and how to affect and control it, one must understand the behavior of a nonlinear system. When the motion in a combustion chamber is unstable, except in unusual cases of growth to destruction, the amplitude typically settles down to a finite value: the system then executes a limiting motion, usually a periodic limit cycle. For practical applications, it is desirable to know how the amplitude of the limit cycle depends on the parameters characterizing the system. That information may serve as the basis for changing the characteristics to reduce the amplitude, the goal in practice being zero. In any case, good understanding of the properties of the limit cycle will also provide some appreciation for those variables which dominate the behavior and to which the motions may be most sensitive, a practical matter indeed.

Our global view, then, is that a combustion instability is an oscillatory motion of the gases in the chamber, which can in first approximation be synthesized of one or more modes related to classical acoustic modes. The mode having lowest frequency is a 'bulk' mode in which the pressure is nearly uniform in space but fluctuating in time. Because the pressure gradient is everywhere small, the velocity fluctuations are nearly zero. This mode corresponds to the vibration of a Helmholtz resonator obtained, for example, by blowing over the open end of a bottle. The cause in a combustion chamber may be the burning process itself, or it may be associated with oscillations in the supply of reactants, caused in turn by the variations of pressure in the chamber. In a liquid rocket, structural oscillations of the vehicle or the feed system may also participate, producing the POGO instability (Rubin 1966; Dordain, Lourme, and Estoueig 1974).

Structural vibrations of a solid rocket are not normally influential in that fashion, but an instability of the bulk mode (there is only one bulk mode for a given geometry) has often been a problem in motors designed for use in space vehicles. In those cases, the term L^* -instability has been used because the stability of the mode is predominantly a function of the L^* of the motor and the mean pressure (Sehgal and Strand 1964). The instability is associated with the time lag between fluctuations of the burning rate and of mass flux through the nozzles: That time lag is proportional to the residence time, and hence L^* , for flow in the chamber. L^* -instabilities occur in motors qualified for space flight because they arise in the lower ranges of pressure at which such rockets operate.

Whatever the system, most combustion instabilities involve excitation of the acoustic modes, of which there are an infinite number for any chamber. The values of the frequencies are functions primarily of the geometry and of the speed of sound, the simplest examples being the longitudinal and transverse modes of a circular cylinder, with frequencies behaving according to (1.2)a,b. Which modes are unstable depends on the balance of energy supplied by the exciting mechanisms and extracted by the dissipating processes. We consider here only linear behavior to illustrate the point.

In general the losses and gains of energy are strongly dependent on frequency. For example, the attenuation due to viscous effects typically increases with the square root of the frequency. Other sources of energy loss associated with interactions between the oscillations and the mean flow tend to be weaker functions of frequency. That is the case, for example, for reflections of waves by a choked exhaust nozzle. The gains of energy usually depend in a more complicated way on frequency.

The sources of energy for combustion instabilities, i.e. the mechanisms responsible for their existence, present the most difficult problems in this field. For the present we confine our attention to qualitative features of energy exchange between combustion to unsteady motions. For example, the magnitude of the energy addition due to coupling between acoustic waves and combustion processes for a solid propellant normally rises from some relatively small quasi-steady value at low frequencies, passes through a broad peak, and then decreases to zero at high frequencies. Recent experimental results suggest that flames may exhibit similar behavior (for example, Pun 2001). Energy is transferred to a pressure oscillation having a particular frequency at a rate proportional to the part of the coupling that is in phase with the pressure at that frequency.⁵ Figure 1.35 is a schematic illustration of this sort of behavior.

In Figure 1.35, the gains exceed the losses in the frequency range $f_1 < f < f_2$. Modes having frequencies in that range will therefore be linearly unstable. An important characteristic, typical of combustion chambers generally, is that in the lower ranges of frequency, from zero to somewhat above the maximum frequency of instability, the net energy transfer is a small difference between relatively larger gains and losses. That implies the difficulty, confirmed by many years' experience, of determining the net energy flow accurately. Unavoidable uncertainties in the gains and losses themselves become much more significant when their difference is formed. That is the main reason for the statement made earlier that analysis of combustion instabilities has been useful in practice chiefly for predicting and understanding trends of behavior rather than accurate calculations of the conditions under which a given system is unstable. The ultimate source of all of these difficulties is the fact, cited in Section 1.1, that the motions in question consume and contain only small portions of the total energy available within the system. Hence in both laboratory tests and in operational systems one is confronted with the problem of determining the characteristics of essentially small disturbances imbedded in a complicated dynamic environment.

The best and most complete data illustrating the preceding remarks have been obtained with solid propellant rockets. There are several reasons for that circumstance. First, the ignition period — the time to cause all of the exposed propellant surface to begin burning — is relatively short and the average conditions in

⁵It is possible, due to the behavior of the phase, that in a range of high frequencies the combustion processes may in fact extract energy from the acoustic waves and hence contribute to the losses of energy.

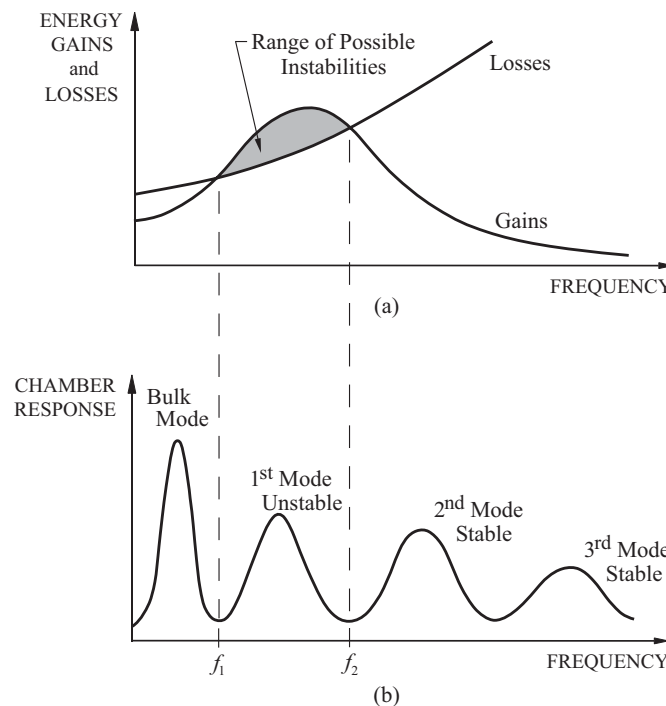


FIGURE 1.35. Qualitative dependence of (a) energy gains and losses; and (b) the frequency response of a combustor.

the chamber quickly reach their intended values. Unless oscillations are severely unstable, and grow rapidly during the ignition transient, there is a good opportunity to observe the exponential growth characteristic of a linear instability. The measurements shown in Figure 1.29 are good examples.

Secondly, it is probably true that more effort has been spent on refining the measurements and predictions of linear stability for solid rockets than for other systems because of the expense and difficulty of carrying out replicated tests. There is no practical routine way of interrupting and resuming firings, and it is the nature of the system that an individual motor can be fired only once. Particularly for large motors used in space launch vehicles, successive firings involve great expense. Development by empirical trial-and-error is costly and there is considerable motivation to work out methods of analysis and design applicable to individual tests.

In contrast, liquid-fueled systems can be fired repeatedly. Trial-and-error has long been a strategy for development of both liquid rockets and air-breathing systems. It seems that attention in that sort of work has generally been focused on modifications to reduce amplitudes (as in 'bombing' tests) rather than on determining the stability of small-amplitude motions. Very little data exists for values of growth constants, and most of those results have been obtained for model or sub-scale laboratory devices. There are examples of stability boundaries inferred from 'bombing' tests of the sort mentioned earlier and theoretical results exist, but there seem to be no investigations comparable to those carried out for solid rockets. A Standard Stability Prediction (SSP) program has been available for solid rockets for 25 years (Lovine *et al.* 1976, Nickerson *et al.* 1983) and is now the subject of a development program (French 2003); no such product in a general form exists for liquid rockets or for other propulsion systems.

We have already noted in Section 1.2 that much progress was achieved in analyzing and understanding combustion instabilities in solid rockets from the late 1960s into the 1980s when there was little work on

liquid rockets. During that period, computing resources, microprocessors, and therefore techniques of data acquisition and processing advanced enormously. Hence by comparison with the situation for solid rockets, the subject of combustion instabilities in liquid-fueled systems, especially liquid rockets, did not benefit as greatly from the general progress of supporting technologies. That situation is changing. Naturally, the problem of instabilities in gas turbines has only relatively recently been subject to widespread attention and therefore has not suffered the same historical deficiencies.

Finally, liquid or gaseous fueled systems are intrinsically more difficult to analyze and understand because of the more complicated chemical processes and coupling with the unsteady flow field. It is true that combustion of a heterogeneous solid propellant containing many ingredients, often including a metal, is very complicated indeed and far from completely understood in general. However, from the point of view of treating combustion instabilities, there is the great advantage that under most conditions, virtually all of the significant combustion processes are completed within a thin zone near the solid propellant itself. Coupling to the unsteady flow field may therefore be represented as a boundary condition. Combustion of liquid fuels is necessarily distributed throughout the volume of the chamber. Making accurate approximations to the spatial dependence is difficult, requiring quite careful treatment of many rate processes, including chemical kinetics and transfer of energy between liquid and gaseous phases. The elementary dynamics of the combustion processes are poorly understood relative to the situation for solid rockets.

1.5.1. Gains and Losses of Acoustic Energy; Linear Stability. It is a general result of the theory of linear systems that if a system is unstable, a small disturbance of an initial state will grow exponentially in time:

$$\text{amplitude of disturbance} \sim e^{\alpha_g t} \quad (1.3)$$

where $\alpha_g > 0$ is called the *growth constant*. If a disturbance is linearly stable, then its amplitude decays exponentially in time, being proportional to $e^{-\alpha_d t}$ and $\alpha_d > 0$ is the *decay constant*. The definition (1.3) implies that for a variable of the motion, say the pressure, having maximum amplitude \hat{p}_0 in one cycle of a linear oscillation:

$$p'(t) = \hat{p}_0 e^{\alpha_g (t-t_0)} \quad (1.4)$$

where \hat{p}_0 is the amplitude at time $t = t_0$. Then if p'_1, p'_2 are the peak amplitudes at time t_1, t_2 ,

$$\frac{\hat{p}_2}{\hat{p}_1} = \frac{p'(t=t_2)}{p'(t=t_1)} = \frac{e^{\alpha_g(t_2-t_0)}}{e^{\alpha_g(t_1-t_0)}} = e^{\alpha_g(t_2-t_1)} \quad (1.5)$$

The logarithm of (1.5) is

$$\log \frac{\hat{p}_2}{\hat{p}_1} = \alpha_g(t_2 - t_1) \quad (1.6)$$

In practice, $t_2 - t_1$ is usually taken equal to the period τ , the time between successive positive (or negative) peaks. Then the logarithm of the ratio \hat{p}_2/\hat{p}_1 for a number of pairs of successive peaks is plotted versus the time t_1 or t_2 at which the first or second peak occurs. The line is straight, having slope α_g . Figure 1.36 shows a good example of both exponential growth and decay of pressure oscillations. The measurements were taken in a small laboratory device, a T-burner.

Whatever the system, the analytical treatment of linear stability is essentially the same. There is really only one problem to solve: find the growth and decay constants, and the frequencies of the modes. Determining the actual mode shapes is part of the general problem, but is often not essential for practical purposes. Typically, both the frequency and the mode shape for small-amplitude motions in a combustion chamber are so little different from their values computed classically as to be indistinguishable by measurement in operating combustors. By “classical” we mean here a computation according to the equations of classical acoustics for the geometry at hand, and with account taken of large gradients in the temperature, which affect the speed of sound. The presence of combustion processes and a mean flow field are not accounted for

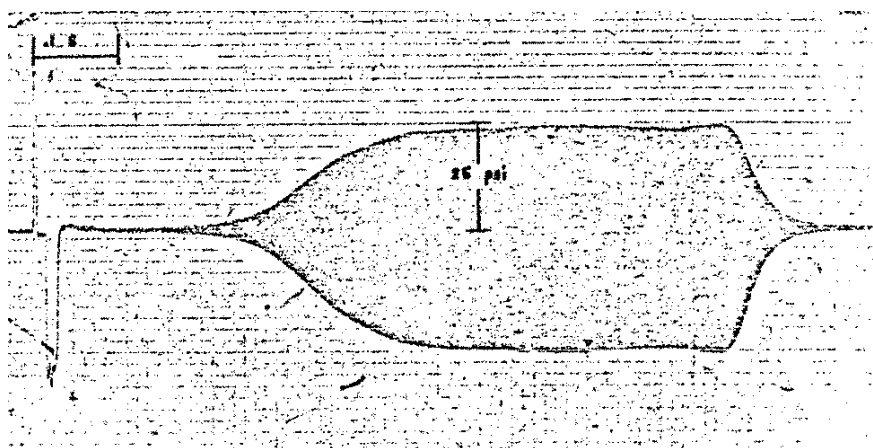


FIGURE 1.36. Exponential growth and development of a limit cycle out of a linearly unstable motion (Perry 1968).

explicitly, but it may be necessary, for satisfactory results, to include a good approximation to the boundary condition applied at the exhaust nozzle, particularly if the average Mach number is not small.

Hence the linear stability problem is really concerned with calculations of the growth and decay constants for the modes corresponding to the classical acoustic resonances. An arbitrary small amplitude motion can, in principle, be synthesized with the results, but that calculation is rarely required for practical applications. Results for the net growth or decay constant have been the central issue in both theoretical and practical work. In combustors, processes causing growth of disturbances and those causing decay act simultaneously. Hence an unstable disturbance is characterized by a net growth constant that can be written $\alpha = \alpha_g - \alpha_d$. Because the problem is linear, the growth constants can quite generally be expressed as a sum of the contributions due to processes accounted for in the formulation, as for example:

$$\alpha := \alpha_g - \alpha_d = (\alpha)_{\text{combustion}} + (\alpha)_{\text{nozzle}} + (\alpha)_{\text{mean flow}} + (\alpha)_{\text{condensed}} + (\alpha)_{\text{structure}} + \dots \quad (1.7)$$

The labels refer to processes of interaction between the acoustic field and combustion, the nozzle, the mean flow, condensed species, the containing structure, Structural interactions comprise not only the vibrations mentioned earlier as a necessary part of the POGO instability, but also quite generally any motions of mechanical components, including propellant. For example, in large solid propellant rockets, motions of the viscoelastic material of the grain may be a significant source of energy losses through internal dissipation (McClure, Hart and Bird 1960a).

The stability boundary—the locus of parameters marking the boundary between unstable ($\alpha > 0$) and stable ($\alpha < 0$) oscillations—is defined by $\alpha = 0$ in (1.7). That statement is a formal statement of the physical condition that the energy gained per cycle should equal the energy lost per cycle:

$$\alpha_g = \alpha_d \quad (1.8)$$

Usually the main source of energy is combustion and in terms of the contributions shown in (1.7), this relation becomes

$$(\alpha)_{\text{combustion}} = -(\alpha)_{\text{nozzle}} - (\alpha)_{\text{mean flow}} - (\alpha)_{\text{condensed}} - (\alpha)_{\text{structure}} \quad (1.9)$$

There are situations in which the acoustic/mean flow interactions may provide a gain of energy. That is, energy is transferred from the average flow to the unsteady motions (as happens, for example, in wind instruments and sirens), but there is no need to consider the matter at this point.

As simple as it appears, equation (1.7) defining α , and its special form (1.8) defining the stability boundary, are basic and extremely important results. There is no evidence, for any propulsion system, contradicting the view that these results are correct representations of actual linear behavior. Difficulties in practice arise either because not all significant processes are accounted for, or, more commonly, insufficient information is available to assign accurately the values of the various individual growth or decay constants.

As examples, Figure 1.37 shows stability boundaries for longitudinal oscillations in a gas-fueled laboratory rocket motor (Crocco, Grey, and Harrje 1960) and Figure 1.38 shows the results of calculations for a large, solid propellant rocket (Beckstead 1974). Those examples illustrate the two uses mentioned above for the formula (1.9). In the case of the gas-fired rocket, the calculations contained two parameters not known from first principles, namely n and τ arising in the time-delay model of the interactions between combustion and the acoustic field. All other parameters defining the geometry and the average flow field were known. The purpose of the work was to compare the calculations with measurements of the stability boundary to infer values of n and τ .

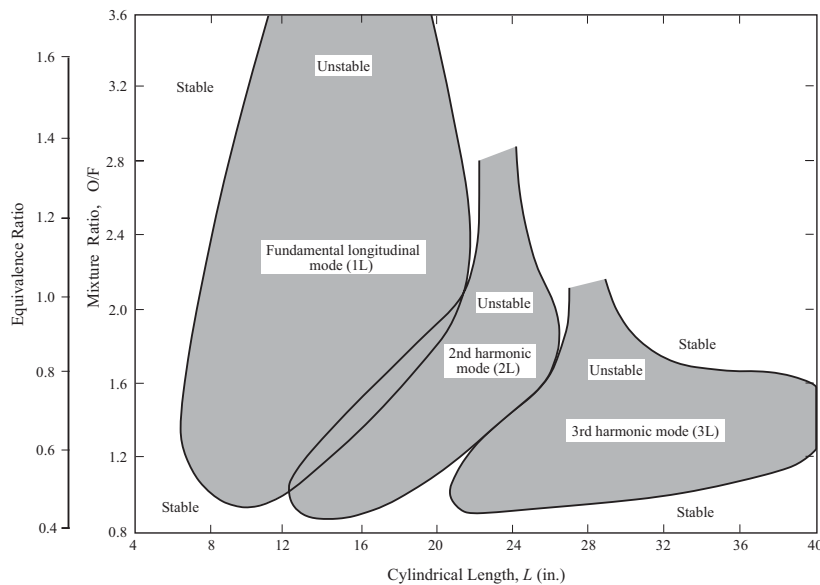


FIGURE 1.37. Stability boundaries for a laboratory gas-fueled rocket (Crocco, Grey, and Harrje 1960).

The purpose of the results reproduced in Figure 1.38 was to predict the stability of a full-scale motor prior to test firing. In that case, all of the parameters appearing in (1.7) must be known. Usually some of the information is available only from ancillary laboratory tests, notably those required to characterize the coupling between propellant combustion and the acoustic field.

Indeed, an important application of the formulas (1.11) and (1.12) is to do exactly that for the laboratory device called the “T-burner”. It is not necessary to restrict attention to the stability boundary if good measurements of the growth constant can be made. Then if all the losses can be computed, one can find the value of the growth constant due to combustion (or, more generally all energy gains) as the difference

$$\alpha_{\text{combustion}} = \alpha - \alpha_{\text{losses}} \quad (1.10)$$

Results for $\alpha_{\text{combustion}}$ can either be adapted for use directly in computing the stability of a motor; or they can be interpreted with models of the combustion processes to obtain better understanding of unsteady combustion. That procedure has been used extensively to assess the combustion dynamics of solid propellants and to investigate trends of behavior with operating conditions and changes of composition.

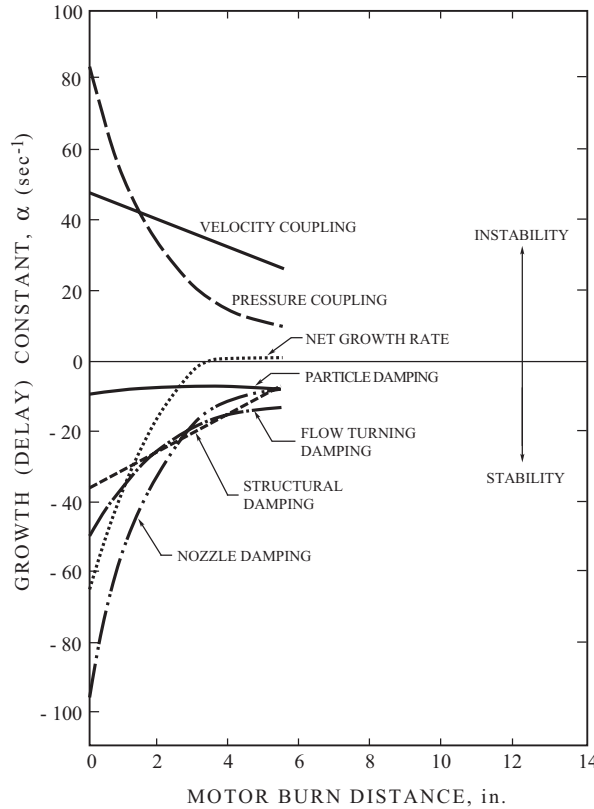


FIGURE 1.38. Predicted stability boundary for a large solid propellant rocket motor, and the separate contributions to α_d and α_g (Beckstead 1974).

The growth constant has a simple interpretation beyond that given by (1.6) as the slope of a semi-logarithmic plot of the peak amplitudes versus time: twice α is the fractional rate of change of time-averaged energy in the classical acoustic field. We will prove the result more rigorously in Chapter 5 but this interpretation is so central to all problems of linear stability that it is useful to have it in hand from the beginning. By the definition of α , both the pressure and velocity oscillations have the time dependence

$$p' \sim e^{\alpha t} \cos \omega t; \quad u' \sim e^{\alpha t} \sin \omega t$$

multiplied by their spatial distributions. The acoustic energy density is the sum of the local kinetic energy, proportional to u'^2 , and potential energy, proportional to p'^2 :

$$\text{K.E.} \sim e^{2\alpha t} \cos^2 \omega t; \quad \text{P.E.} \sim e^{2\alpha t} \sin^2 \omega t$$

If we assume that the period of oscillation, $\tau = 2\pi/\omega$, is much smaller than the decay rate, $1/\alpha$, then the values of these functions averaged over a cycle of the oscillation are proportional to $e^{2\alpha t}$. Hence the acoustic energy density is itself proportional to $e^{2\alpha t}$. Integrating over the total volume of the chamber we find that the total averaged energy $\langle \mathcal{E} \rangle$ in the acoustic field has the form

$$\langle \mathcal{E} \rangle = \langle \mathcal{E}_0 \rangle e^{2\alpha t} \quad (1.11)$$

where $\langle \mathcal{E}_0 \rangle$ is a constant depending on the average flow properties and the geometry. We then find directly from (1.11) the result claimed:

$$2\alpha = \frac{1}{\langle \mathcal{E} \rangle} \frac{d\langle \mathcal{E} \rangle}{dt} \quad (1.12)$$

Another elementary property worth noting is that $1/\alpha$ is the time required for the amplitude of oscillation to decay to $1/e$ of some chosen initial value. Also, the fractional change of the peak value in one cycle of oscillation ($t_2 - t_1 = \tau = 2\pi/\omega$) is

$$|p'_2| - |p'_1| = \delta|p'|_m \sim e^{\alpha t_1} - e^{\alpha t_2} = e^{\alpha t_2} [e^{\alpha(t_1 - t_2)} - 1]$$

where $| \ |_m$ denotes the magnitude of the peak amplitude. We assume as above that the fractional change in one period τ is small so

$$e^{\alpha(t_1 - t_2)} \approx 1 + \alpha(t_1 - t_2) = 1 + \alpha\tau$$

The amplitude itself is approximately proportional to $e^{\alpha t_2}$ or $e^{\alpha t_1}$ and we can write the fractional change as

$$\frac{\delta|p'|_m}{|p'|_m} \approx \alpha\tau = \frac{\alpha}{f} \quad (1.13)$$

where f is the frequency in cycles per second, $f = 1/\tau$. The dimensionless ratio f/α is a convenient measure of the growth or decay of an oscillation. According to the interpretation of $1/\alpha$ noted above, $(1/\alpha)/\tau = f/\alpha$ is the number of cycles required for the maximum amplitudes of oscillation to decay to $1/e$ or grow to e times an initial value.

The ratio α/f must be small for the view taken here to be valid. Intuitively, α must in some sense be proportional to the magnitude of the perturbations of the classical acoustics problem. We will find that the most important measure of the perturbations is a Mach number, \bar{M}_r , characterizing the mean flow; for many significant processes, α/f equals \bar{M}_r times a constant of order unity. Roughly speaking, then, the measured value of α/f is an initial indication of the validity of the view that a combustion instability can be regarded as a motion existing because of relatively weak perturbations of classical acoustics.

1.6. Nonlinear Behavior

It is a fundamental and extremely important conclusion that combustion instabilities are motions of a self-excited nonlinear dynamical system. Probably the most significant implication is that in order to understand fully the observed behavior, and how to affect or control it, one must ultimately understand the behavior of a nonlinear system. When the motion in a combustion chamber is unstable, except in unusual cases of growth to destruction, the amplitude typically settles down to a finite value: the system then executes a limiting motion, usually a periodic limit cycle. For practical applications, it is desirable to know how the amplitude of the limit cycle depends on the parameters characterizing the system. That information may serve as the basis for changing the characteristics to reduce the amplitude, the goal in practice being zero. In any case, good understanding of the properties of the limit cycle will also provide some appreciation for those variables which determine the behavior, and to which the motions may be most sensitive, a practical matter indeed.

Rarely do the motions in a combustion chamber exhibit clear limit oscillations of the sort commonly encountered with simpler mechanical systems. A particularly good example of a limit cycle in a T-burner is shown in Figure 1.36. It appears that combustion devices are subject to influences, probably not easily identified, that prevent constant frequencies and amplitudes in the limit motions. The motions seem not to be limit cycles in the strict sense. However, experience gained in the past few years suggests that the deviations from the well-defined behavior of simpler systems are normally due to secondary influences. There are several possibilities, although not enough is known about the matter to make definite statements. Recent analysis (Burnley, 1996; Burnley and Culick, 1999) has demonstrated that noise, and interactions between random and acoustical motions can cause departures from purely periodic limit cycles appearing very similar to those found in pressure records for operating combustors (Figure 1.39). The random or stochastic motions are likely associated with flow separation, turbulence, and combustion noise.

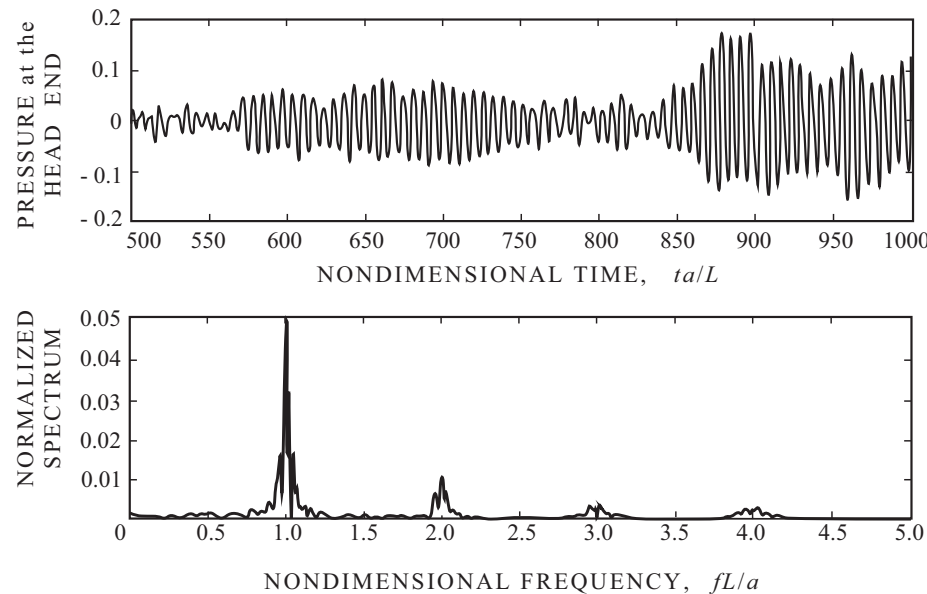


FIGURE 1.39. A computed limit cycle and its normalized spectrum executed by a single nonlinear acoustic mode in the presence of noise (Burnley and Culick 1996).

Probably other causes of departures from strictly periodic limit cycles are associated with the parameters characterizing steady operation of a combustor; and with ‘noise’ or random fluctuation of flow variables. As we have already emphasized, the unsteady motions require only a negligibly small part of the energy supplied by the combustion processes. Relatively minor variations in the combustion field, due, for example, to small fluctuations in the supplies of reactants, may alter the rates of energy transfer to instabilities and hence affect features of a limit cycle. Similarly, adjustments in the mean flow, notably the velocity field and surface heat transfer rates, will directly influence the unsteady field. Laboratory experiments clearly show such phenomena and considerable care is required to achieve reproducible results. In solid propellant rockets, the internal geometry necessarily changes during a firing. That happens on a time scale much longer than periods of unsteady motions, but one obvious result is the decrease of frequencies normally observed in tests. Because there is ample reason to believe that the phenomena just mentioned are not essential to the global nonlinear behavior of combustion instabilities, we ignore them in the following discussion.

1.6.1. Linear Behavior Interpreted as the Motion of a Simple Oscillator. Intuitively we may anticipate that nonlinear behavior may be regarded in first approximation as an extension of the view of linear behavior described in the preceding section, made more precise in the following way. Measurement of a transient pressure oscillation often gives results similar to those shown in Figure 1.34(a). The frequency in each case varies little, remaining close to a value computed classically for a natural resonance of the chamber, and the growth of the peak amplitude during the initial transient period is quite well approximated by the rule for a linear instability, $e^{\alpha t}$. Thus the behavior is scarcely distinguishable from that of a classical linear oscillator with damping, and having a single degree of freedom. The governing equation for the free motions of a simple mass (m)/ spring (k)/ dashpot (r) system is

$$m \frac{d^2x}{dt^2} + r \frac{dx}{dt} + kx = 0 \quad (1.14)$$

It is surely tempting to model a linear combustion instability by identifying the pressure fluctuation, p' , with the displacement x of the mass. Then upon dividing (1.14) by m and tentatively replacing x by p' , we have

$$\frac{d^2p'}{dt^2} + 2\alpha \frac{dp'}{dt} + \omega_0^2 p' = 0 \quad (1.15)$$

where $2\alpha = r/m$ and the undamped natural frequency is $\omega_0 = \sqrt{k/m}$. The familiar solution to (1.15) has the form of the record shown in the lower part of Figure 1.34(a), $p' = \hat{p}_0 e^{\alpha t} \cos \Omega t$ where $\Omega = \omega_0 \sqrt{1 - (\alpha/\omega_0)^2}$ and \hat{p}_0 is the value of p' at $t = 0$.

The preceding remarks suggest the course we should follow to investigate the linear behavior of combustion instabilities, and indeed is the motivation behind the general view described earlier. But this is purely descriptive heuristic reasoning. No basis is given for determining the quantities ‘mass,’ ‘damping coefficient,’ and ‘spring constant’ for the pressure oscillation. The procedure for doing so is developed in Chapter 4; the gist of the matter is the following, a brief description of the method used later to analyze combustion instabilities.

According to the theory of classical acoustics for a sound wave, we may identify both kinetic energy per unit mass, proportional to the square of the acoustic velocity u' , and potential energy per unit mass, proportional to the square of the acoustic pressure p' . The acoustic energy per unit volume is

$$\frac{1}{2} \left(\bar{\rho} u'^2 + \frac{p'^2}{\bar{\rho} \bar{a}^2} \right) \quad (1.16)$$

where $\bar{\rho}$ and \bar{a} are the average density and speed of sound. This expression corresponds to the formula for the energy of a simple oscillator,

$$\frac{1}{2} (m x^2 + k x^2) \quad (1.17)$$

Now consider a stationary wave in a closed chamber. Both the velocity and pressure fluctuations have spatial distributions such that the boundary condition of no velocity normal to a rigid wall is satisfied. Hence the local pressure p' in equation (1.15) must depend on position as well as time. However, the frequency ω_0 depends on the geometry of the entire chamber and according to equation (1.12), we should be able to interpret 2α in equation (1.15) as the fractional rate of change of averaged energy in the entire volume. Therefore, we expect that the parameters m , k , and r implied by the definitions $\alpha = r/2m$ and $\omega_0 = k/m$ must be related to properties of the entire chamber. The approximate analysis used in most of this book is based partly on spatial averaging defined so that the properties ascribed to a particular mode are local values weighted by the spatial distribution of the mode in question, and averaged over the chamber volume.

Locally in the medium, the ‘spring constant’ is supplied by the compressibility of the gas, and the mass participating in the motion is proportional to the density of the undisturbed medium. When the procedure of spatial averaging is applied, both the compressibility and the density are weighted by the appropriate spatial structure of the acoustical motion. As a result, the damping constant and the natural frequency are expressed in terms of global quantities characterizing the fluctuating motion throughout the chamber. We will find rigorously that in the linear limit, an equation of the form (1.15) does apply, but instead of p' itself, the variable is $\eta_n(t)$, the time dependent amplitude of an acoustic mode represented by

$$p'_n = \bar{p} \eta_n(t) \psi_n(\vec{r}) \quad (1.18)$$

where \bar{p} is the mean pressure and $\psi_n(\vec{r})$ is the spatial structure of the classical acoustic mode identified by the index $(\)_n$. Hence the typical equation of motion is

$$\frac{d^2 \eta_n}{dt^2} + 2\alpha_n \frac{d\eta_n}{dt} + \omega_n^2 \eta_n = 0 \quad (1.19)$$

The constants α_n and ω_n contain the influences of all linear processes distinguishing the oscillation in a combustion chamber from the corresponding unperturbed classical motion governed by the equation

$$\frac{d^2 \eta_n}{dt^2} + \omega_{n0}^2 \eta_n = 0 \quad (1.20)$$

if dissipation of energy is ignored. Because damping in a mechanical system causes a frequency shift, the actual frequency is not equal to the unperturbed value, ω_{n0} .

For technical reasons not apparent at this point, it is convenient to regard the linear perturbing process as a force $F_n(\eta_n, \dot{\eta}_n)$ is acting on the ‘oscillator’ and equation (1.19) is written

$$\frac{d^2\eta_n}{dt^2} + \omega_n^2\eta_n = F_n^L(\eta_n, \dot{\eta}_n) \quad (1.21)$$

The superscript $(\quad)^L$ identifies the ‘force’ as linear, and for simplicity ω_{n0}^2 is written ω_n^2 . We will consistently use the symbol ω_n for the unperturbed classical acoustic frequency. If there is no linear coupling between the modes (typically linear coupling is small), the force F_n^L consists of two terms, one representing the damping of the mode and one the frequency shift:

$$F_n^L = -\Delta\omega_n^2\eta_n + 2\alpha_n\dot{\eta}_n \quad (1.22)$$

Equations (1.21) and (1.22) produce (1.19) with ω_n^2 replaced by $\omega_n^2 + \Delta\omega_n^2$.

With the above reasoning we have heuristically constructed equation (1.21) as the fundamental equation for a linear combustion instability corresponding to a classical acoustic mode of the chamber. Its simplicity masks the fact that a great amount of effort is required to determine realistic functions $F_n^L(\eta_n, \dot{\eta}_n)$ applicable to the motions in a combustion chamber. The approximate analysis developed later provides a framework for accommodating all linear processes but does not contain explicit formulas for all of them. Most importantly, there are terms representing interactions between combustion processes and the unsteady motions, but their computation requires modeling the mechanisms that cause combustion instabilities. Some of the purely gasdynamical processes, arising with coupling between mean and fluctuating motions, are given explicitly.

According to classical acoustic theory, a closed chamber of gas at rest has an infinite number of normal or resonant modes. The spatial structures (mode shapes) and resonant frequencies are found as solutions to an eigenvalue problem. A general motion in the chamber, having any spatial structure, can then be represented as a linear superposition of the normal modes. The process of spatial averaging, leading to equation (1.20), amounts to representing any motion as an infinite collection of simple oscillators, one associated with each of the normal modes. That interpretation holds as well for equation (1.21) except that now each mode may suffer attenuation ($\alpha_n < 0$) or excitation ($\alpha_n > 0$). It is this point of view that allows natural extension of the analysis to nonlinear behavior.

1.6.2. Combustion Dynamics and Stability. Determining the linear stability of a system theoretically comes down to computing the value of the constant α , equation (1.21). With the model of an instability as a simple oscillator acted upon by a force dependent on the motion, the governing equation for the amplitude is (1.21). For simplicity, assume only one mode is active and that the driving force is entirely due to fluctuations of the rate of heat \dot{Q}' provided to the flow. This type of motion is commonly called a ‘thermo-acoustic instability.’ In simplest form the equation for the amplitude $\eta_1(t) := \eta(t)$ is

$$\frac{d^2\eta}{dt^2} + \omega_1^2\eta = (\gamma - 1) \int \frac{\partial \dot{Q}'}{\partial t} \psi dV \quad (1.23)$$

where $\psi(\mathbf{r})$ is spatial distribution of the pressure for the mode, the ‘mode shape’, defined so the pressure fluctuation is $p' = \bar{p}\eta\psi(\mathbf{r})$. Derivation of equation (1.23) follows from the procedure worked out in Chapters 3, 4, and 6.

Suppose that the heat release rate is sensitive only to pressure and write its fluctuation as

$$\dot{Q}' = \frac{\dot{Q}'}{p'} p' = R p' = \bar{p} R \eta \psi \quad (1.24)$$

where R is the response function, here having dimensions of inverse time,

$$[R] = \frac{[\text{Energy}/\text{Volume}] \frac{1}{t}}{[\text{Energy}/\text{Volume}]} = t^{-1}$$

Substitution of (1.24) in (1.23) and identification of α by comparison of the result with (1.19) leads to a formula for α :

$$\frac{d^2\eta}{dt^2} + \omega_1^2\eta = \left[(\gamma - 1)\bar{p} \int R\psi^2 dV \right] \frac{d\eta}{dt} = 2\alpha \frac{d\eta}{dt} \quad (1.25)$$

and α is proportional to the response function,

$$\alpha = \frac{\gamma - 1}{2} \bar{p} \int R\psi^2 dV \quad (1.26)$$

The equation governing the amplitude is

$$\frac{d^2\eta}{dt^2} - 2\alpha \frac{d\eta}{dt} + \omega_1^2 = 0 \quad (1.27)$$

with solution

$$\eta(t) = Ae^{\alpha t} \cos(\omega_t t + \phi) \quad (1.28)$$

where A and ϕ are constant and $\omega_t^2 = \omega_1^2 - \alpha^2$. Suppose R is a real constant, i.e. the fluctuation \dot{Q}' of the heat release rate is in phase with the pressure fluctuation p' . If R , and hence α , is positive, the oscillation is driven by the response of the heat release to the pressure fluctuations.

This example is the simplest illustration of the direct connection between oscillations in a combustor and combustion dynamics represented here by a response function. The idea has enormously wide applications in all of the systems discussed in this book.

1.6.3. Nonlinear Behavior Interpreted as the Motion of a Nonlinear Oscillator. In view of the observation that measurements often show development of limit cycles like those shown in Figure 1.40, it is tempting simply to add a nonlinear term to the oscillator equation (1.21) and assume that a combustion instability involves only a single mode. Thus, for example, we could add to the right-hand side a force $F_n^{NL} = c_1\eta_n^2 + c_2\dot{\eta}_n^2 + c_3\eta_n\dot{\eta}_n + c_4|\eta_n| + \dots$ where the constants c_1, \dots may be chosen by fitting the solution to data. Culick (1971) showed that quite good results could be obtained with this approach applied to limited data. Figure 1.40 shows one example. Of course this is a purely *ad hoc* approach and provides no means of computing the coefficients from first principles.

Following the early result shown in Figure 1.40, Jensen and Beckstead (1972) applied that procedure to extensive data taken in laboratory devices intended for measuring the characteristics of unsteady burning of solid propellants. The chief result was that the data could be matched equally well with rather broad ranges of the constants, and no particular kind of nonlinearity seemed to dominate the motions. Consequently, representation with a single mode was not successful. Even though analysis of pressure records for limit cycles often showed relatively small (it seemed) amounts of harmonics of the principle mode, it appeared necessary to account for two modes at least, with coupling due to nonlinear processes.

In other contexts, that conclusion is surely not surprising. The development of a small amplitude compressive disturbance into a shock wave is the oldest and most familiar example in gasdynamics. Steepening of a smooth wave arises primarily from two nonlinear influences: convection of the disturbance by its own motion, and dependence of the speed of sound on the local temperature, itself dependent on the wave motion. A good approximation to the phenomenon is obtained if viscous stresses and heat conduction are ignored. If the disturbance is regarded as a combination of various modes, the flow of energy from modes in the low frequency range to those having higher frequencies is favored by the nonlinear gasdynamic coupling. The rapid growth of the higher-frequency modes having shorter wavelengths produces the steepening, eventually

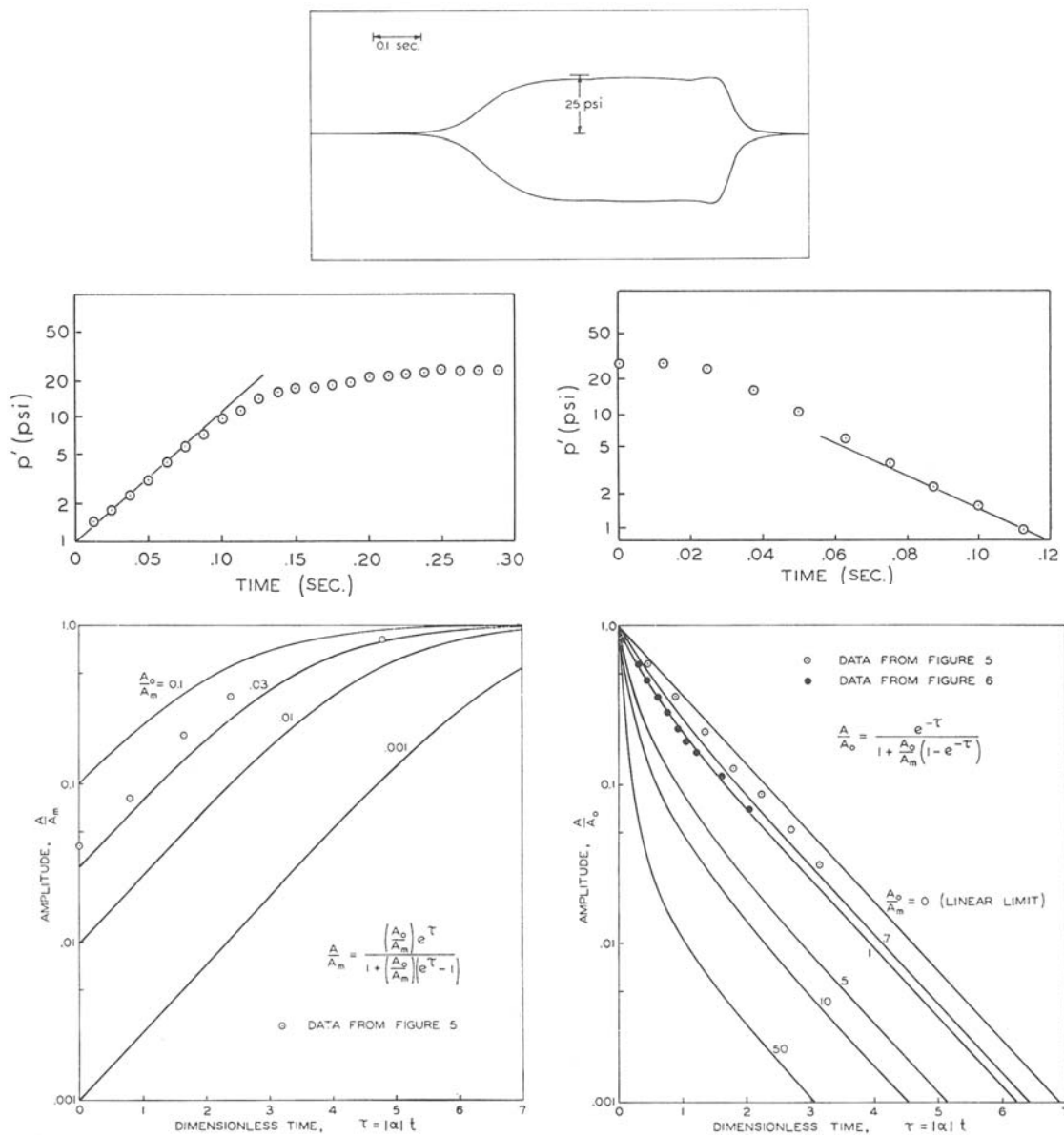


FIGURE 1.40. An example of fitting T-burner data with the model of a simple nonlinear oscillator (Culick 1971).

limited, in real flows, by the actions of various effects, mainly viscous. In a combustion chamber possible consequences of nonlinear combustion processes cannot be ignored. For example, there is much evidence accumulated in recent years that in some small gas-fueled combustors, the combustion processes may dominate the nonlinear behavior (see, for example, Dowling 1997).

In extreme cases of combustion instabilities, particularly in liquid and solid rockets, the approximately sinusoidal motions, substantially systems of stationary waves, may be absent or evolve into a different form. The motions then appear to be weak shock waves, or pulses having measurable width, propagating in the chamber. Instabilities of that type are commonly produced subsequent to excitation by finite pulses. Figure 1.41 shows examples observed in liquid rockets, typically involving motions mainly transverse to the axis.

They were discovered relatively early in the development of liquid rockets (e.g. Ross and Datner 1954) and were identified as ‘spinning’ transverse modes. Their presence is particularly harmful due to the greatly increased surface heat transfer rates causing unacceptable scouring of the chamber walls.

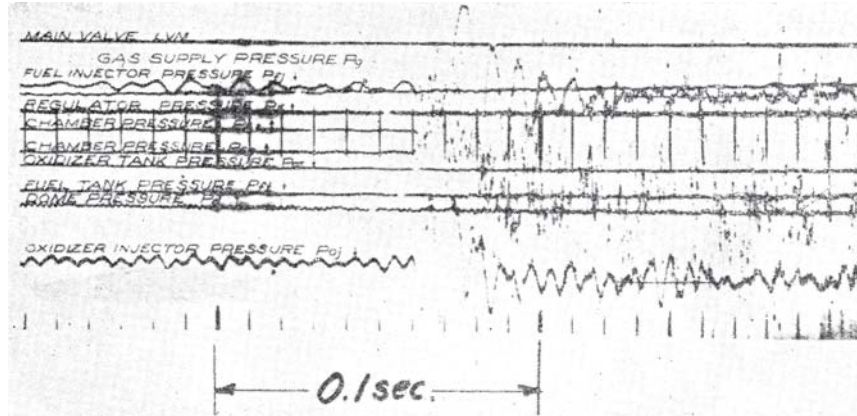


FIGURE 1.41. Steep-fronted waves observed in a liquid propellant rocket motor (Ross and Datner 1954).

The corresponding cases in solid rockets usually are longitudinal motions. They rarely occur in large motors and seem to have been first observed in pulse testing of laboratory motors (Dickenson and Jackson 1963; Brownlee 1960; Brownlee and Marble 1960). An example is reproduced in Figure 1.42 (Brownlee, 1964). Often this sort of instability is accompanied by a substantial increase of the mean pressure, seriously affecting the steady performance of the motors. The primary cause of the pressure rise is evidently the increased burn rate, although precisely why the rate increases is not well understood. More recently, these pulsed instabilities have been the subject of successful comparisons between laboratory test results and numerical simulations (Baum and Levine 1982; Baum, Levine, and Lovine 1988). Figure 1.43 shows an example of their results.

For combustion instabilities, the situation is very different from that for shock waves in a pure gas because the processes governing the transfer of energy from combustion to the gasdynamical motions cannot be ignored and in general depend strongly on frequency. Indeed, it may happen, as seems sometimes to be the case for combustion of solid propellants, that the coupling may cause attenuation of higher frequencies. For that reason, the tendency for steepening by the gasdynamics is partially compensated by the combustion processes, linear or nonlinear. As a result, in a chamber a limit cycle may be formed having very closely the spatial structure and frequency of the unstable mode (commonly, but not always, the fundamental mode) and relatively modest amounts of higher modes. It is that behavior that seems to be important in many combustion problems, explaining in part why the approach taken in the approximate analysis has enjoyed some success. Put another way, relatively small amounts of higher modes, presumed to arise from nonlinear behavior, may in fact represent important action by the nonlinear processes.

Naturally the preceding is a greatly simplified and incomplete description of the events actually taking place in a given combustion chamber. The essential conclusion that nonlinear gasdynamical processes are partly augmented and partly compensated by combustion processes seems to be an important aspect of all combustion instabilities. It appears that the idea was first explicitly recognized in work by Levine and Culick (1972, 1974), showing that realistic limit cycles could be formed with nonlinear gasdynamics and linear combustion processes. Perhaps the most important general implication of those works is that the nonlinear behavior familiar in flows of pure nonreacting gases is not a reliable guide to understanding the nonlinear behavior in combustion chambers.

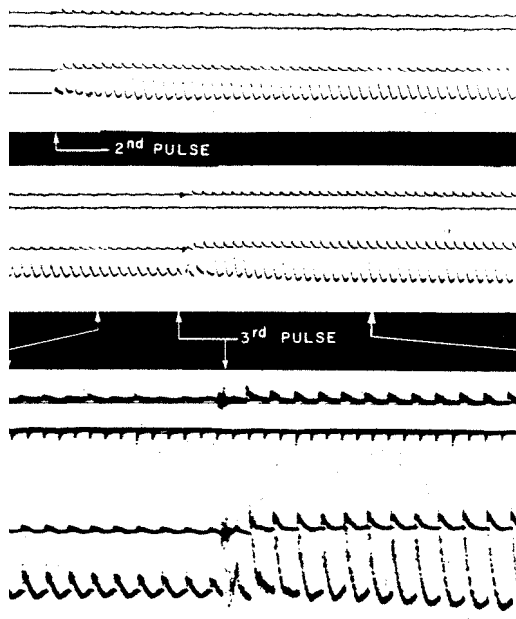


FIGURE 1.42. Steep-fronted waves observed in solid propellant rocket motors (Brownlee 1964).

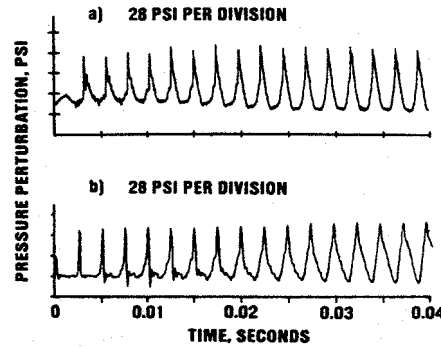


FIGURE 1.43. A comparison of observed and simulated steep-fronted waves in a solid propellant rocket motor. (a) observed; (b) numerical simulation (Baum and Levine 1982).

For nonlinear problems, the governing equations obtained after spatial averaging have the form

$$\frac{d^2\eta_n}{dt^2} + \omega_n^2\eta_n = F_n^L(\eta_n, \dot{\eta}_n) + F_n^{NL}(\eta_i, \dot{\eta}_i) \quad (1.29)$$

where $F_n^{NL}(\eta_i, \dot{\eta}_i)$ is the nonlinear force depending on all amplitudes η_i , including η_n itself. Thus we may regard a combustion instability as the time-evolution of the motions of a collection of nonlinear oscillators, one associated with each of the classical acoustic modes for the chamber. In general the motions of the oscillators may be coupled by linear as well as nonlinear processes, although linear coupling seems rarely to be important. The analytical framework established by the dynamical system (1.29) will serve throughout this book as the primary means for analyzing, predicting, and interpreting combustion instabilities.

Representation of unsteady motions in a combustion by expansion in acoustic modes ('modal expansion') and application of spatial averaging was first accomplished by Culick (1961, 1963) using a Green's function. The work by Jensen and Beckstead cited above motivated extension to nonlinear behavior (Culick 1971 and

1975). Powell (1968) and Zinn and Powell (1970a, 1970b) first used an extension of Galerkin's method to treat nonlinear behavior in liquid rockets; the method was subsequently extended to solid rockets by Zinn and Lores (1972). In practice, application of a method based on modal expansion and spatial averaging is normally useful only if a small number of modes is required. Yet there are a large number of experimental results showing the presence of steep-fronted waves, often sufficiently steep to be interpreted as shock waves. Hence an analysis of the sort followed here would seem to be quite seriously limited unless one is prepared to accommodate a large number of modes. That is, one would expect that wave motions exhibiting rapid temporal changes and large spatial gradients must contain significant amounts of higher modes. However as discussion in this book will show, results have also established that due to fortunate phase relationships, a surprisingly small number of modes serves quite well even to represent many features of waves having steep fronts. The method gives quite a good approximation to both the limiting motions and the transient development of disturbances into weak shock waves.

1.7. Analysis and Numerical Simulations of Combustion Instabilities

In this book, the vehicle for unification is a theoretical/computational framework originating in the late 1960s and early 1970s with treatments of instabilities in liquid rockets (Culick 1961, 1963; Powell 1968; Zinn and Powell 1968; and Powell and Zinn 1971) and in solid rockets (Culick 1971, 1976). Those analyses differed from previous work mainly in their use of a form of spatial averaging, in some instances related to Galerkin's method, to replace the partial differential equations of conservation by a system of ordinary differential equations. The dependent variables are the time-dependent amplitudes of the acoustic modes used as the basis for series expansion of the unsteady pressure. It is the process of spatial averaging over the volume of the chamber that produces a formulation convenient for handling models of widely different geometries and physical processes. Consequently, in return for the approximate nature of the analysis (for example, the series must be truncated to a finite number of terms), one obtains both convenience and a certain generality of applications not normally possible when partial differential equations are used directly. In general form, this approach is applicable to all types of combustors. Different systems are distinguished by different geometries and the forms in which the reactants are supplied (liquid, solid, gas, slurry, ...). Those differences affect chiefly the modeling of the dominant physical processes.

Some analysis of combustion instabilities has customarily accompanied experimental work as an aid to interpreting observations. The paper by Grad (1949) treating instabilities in solid rockets is probably the first entirely theoretical work dealing with small amplitude acoustical motions in a mean flow field with combustion sources. During the 1950s and 1960s, many theoretical works were published on the subject of oscillations in solid rockets (e.g. Bird, McClure, and Hart 1963; Cheng 1954, 1962; Hart and McClure 1959, 1965; Cantrell and Hart 1964; Culick 1966) and in liquid rockets (e.g. Crocco 1952, 1956, 1965; Crocco and Cheng 1956; Reardon 1961; Culick 1961, 1963; Sirignano 1964; Sirignano and Crocco 1964; Zinn 1966, 1968, 1969; Mitchell, Crocco, and Sirignano 1969). It was during that period that the view of a combustion instability as a perturbation of classical acoustics was first extensively developed.

Most of the analyses cited in the previous paragraph were restricted to linear problems (those by Sirignano, Zinn and Mitchell are notable exceptions). Their chief purpose was to compute the stability of small amplitude motions. Indeed, since the earliest works on combustion instabilities, practical and theoretical considerations were directed mainly to the general problem of linear stability: the reasoning is that if the system is stable to small disturbances (e.g. associated with 'noise' always present in a combustion chamber) then undesirable instabilities cannot arise. There is a flaw in that reasoning: The processes in a combustion chamber are nonlinear, so a linearly stable system may in fact be unstable to sufficiently large disturbances. In any case, oscillations in combustors reach limiting amplitudes due to the action of nonlinear processes. Hence understanding nonlinear behavior is the necessary context in which one can determine what changes to the system may reduce the amplitudes. Ultimately, a complete theory, and therefore understanding, must

include nonlinear behavior, a subject covered at considerable length in this book, largely within the context cited in the first paragraph.

Recognition of the practical implications of the deficiencies of a view founded on linear behavior motivated the development of the technique of “bombing” liquid rocket chambers in the 1960s by NASA in its Apollo program (Harrje and Reardon 1972). The idea is to subject an operating combustion chamber to a succession of increasingly large disturbances (generated by small explosive charges) until sustained oscillations are produced. Then the size of the disturbance required to “trigger” the instability is evidently a measure of the relative stability of the chamber.⁶ Another measure is the rate of decay of oscillations subsequent to a pulse injected into a linearly stable system. What constitutes the correct ‘measure’ of relative stability cannot of course be determined from experiments alone, but requires deeper understanding accessible only through theoretical work. This is part of the reason that the nonlinear analyses cited above were carried out; also, an extensive program of numerical calculations was supported (Priem and Hiedmann 1960; Priem and Guentert 1962; Priem and Rice 1968; and other works cited in the summary volume edited by Harrje and Reardon 1972). Owing to the limitations of computing resources at that time, those early numerical calculations involved solutions to quite restricted problems, commonly sectors or annular regions of chambers. It was not possible to compute what are now usually called ‘numerical simulations.’ Moreover, the results were often plagued—and were thus sometimes rendered invalid—by noise in the computations or difficulties with stability of the numerical techniques (for example, see Beltran, Wright, and Breen 1966).

While the intense activities on instabilities in liquid rockets nearly ceased in the early 1970s, work on numerical simulation of combustion instabilities in solid rockets began (Levine and Culick 1972, 1974; Kooker 1974; Baum and Levine 1982). In contrast to the case for liquid rockets, it is a good approximation to ignore chemical processes within the cavity of a solid rocket, an enormous simplification. Combustion occurs largely in a thin layer adjacent to the solid surface and its influences can be accommodated as boundary conditions. Consequently, with the growth of the capabilities of computers, it became possible to carry out more complete computations for the entire unsteady field in a motor. Also during this period appeared one of the earliest attempts to compare results of an approximate analysis with those obtained by numerical simulation for the ‘same’ problem (Culick and Levine 1974), a strategy which has since become generally accepted where it is applicable.

The main idea motivating that work was the following. At that time, the size and speed of available computers did not allow numerical simulations of three-dimensional problems, nor in fact even two-dimensional or axisymmetric cases. Moreover, no numerical calculations had been done of one-dimensional unsteady transient motions in a solid rocket, with realistic models of the combustion dynamics and partial damping. Approximate analysis of the sort mentioned above could be applied, in principle, to instabilities in arbitrary geometries, but owing to the approximations involved, there were no means of determining the accuracy of the results. Experimental data contain sufficiently large uncertainties that comparisons of analytical results with measurements cannot be used to assess accuracy of the analysis. Hence it appeared that the only way to assess the limitations of the approximate analysis must be based on comparison with numerical simulations. It was also important to confirm the validity of the approximate analysis because of its great value for doing theoretical work and for gaining general understanding of unsteady motions in combustion chambers.

That reasoning remains valid today. Despite the enormous advances in computing resources, it is true here as in many fields, that approximate analysis still occupies, and likely always will, a central position. A major reason is its great value in providing understanding. Numerical simulations advanced considerably during the 1980s and important work is currently in progress. Accomplishments for systems containing chemical processes, including combustion of liquid fuels, within the chambers far exceed those possible

⁶A quite different approach based on a statistical assessment of firings of many solid liquid propellant rockets of the same design was developed in Russia in the 1950s and 1960s. The method was unknown in the West, the first reports appearing in an international conference (Yang and Anderson, 1995).

twenty years ago (see, for example, the early papers by Liang, Fisher, and Chang 1986; Liou, Huang, and Hung 1988; Habiballah, Lourme, and Pit 1991; Kailasanath, Gardner, Boris, and Oran 1987a, b; Menon and Jou 1988).

Numerical simulations of flows in solid rockets began more than fifteen years ago to incorporate current ideas and results of turbulence modeling (Dunlop *et al.* 1986; Sabnis, Gibeling and McDonald 1985; Tseng and Yang 1991; Sabnis, Madabhushi, Gibeling and McDonald 1989). The results have compared quite favorably with cold flow experiments carried out using chambers with porous walls. There is no reason to doubt that eventually it will be possible to produce accurate computations of the steady turbulent flow fields in virtually any configuration expected in practical applications. A major step in that direction has been the recent emphasis on use of large eddy simulations (LES).

Remarkable success has also been achieved with computations of unsteady one-dimensional motions in straight cylindrical chambers (e.g. the early results reported by Baum and Levine 1982; Baum, Lovine, and Levine 1988; Tseng and Yang 1991). Particularly notable are the results obtained by Baum, Lovine, and Levine (1988) showing very good agreement with data for highly nonlinear unsteady motions induced in the laboratory by pulses. Although parameters in the representation of the unsteady combustion processes were adjusted as required to produce the good comparison, a minimal conclusion must be that the numerical methods were already quite satisfactory more than fifteen years ago.

Numerical simulation will always suffer some disadvantages already mentioned. In addition, because each simulation is only one case and the problems are nonlinear, it is difficult to generalize the results to gain fundamental understanding. However, the successes of this approach to investigating complicated reacting flows are growing rapidly and the methods are becoming increasingly important for both research and practical application. Historically, we have seen that the three aspects of the subject—experimental, analytical, and numerical simulations—began chronologically in that order. There seems to be no doubt that, as in many other fields of modern engineering, the three will coexist as more-or-less equal partners. We have therefore tried in this book to balance our discussion of methods and results of experiment, analysis, and numerical simulation with much less emphasis on the last. The integration of those activities forms a body of knowledge within which one may understand, interpret and predict physical behavior. For recent results applicable to combustion instabilities in solid propellant rockets, see the notes for a course given at the von Karman Institute (VKI) in 2001.

It is important to realize that experimental information about unsteady motions in combustion chambers is very limited. Commonly only measurements of pressure are available. Accelerometers and strain gauges mounted in a chamber may provide data from which some characteristics of the pressure field can be inferred. Quantitative surveys of the internal flow are virtually unavailable owing to the high temperatures, although optical methods are useful in laboratory work to give qualitative information and, occasionally, useful quantitative data.

As a practical matter we are therefore justified in assuming that only the pressure is available, at most as a function of time and position on the surface of the chamber. That restriction is a fundamental guide to the way in which the theory and methods of analysis for combustion instabilities are developed. Throughout this book we emphasize determining and understanding the unsteady pressure field. The approximate analysis constituting the framework in which we will discuss instabilities is based on the pressure as the primary flow variable. Very little attention will be given to methods of data analysis, an important activity directed chiefly to the problem of inferring quantitative properties of instabilities from pressure records.

1.8. A Précis of the Book

As an introduction to combustion instabilities, we intend to provide a broad foundation sufficiently deep to allow reading the contemporary literature without excessive difficulty, with the exception of modern work on numerical simulations. Many basic topics are simply not included, being assumed as part of the required general background, or outside the intended scope. The general character of the material covered is perhaps closer to applications than to basic research, but the roots in basic subjects are apparent throughout the text.

It is helpful to view the subject as a merging of three kinds of dynamics: chemical dynamics; combustion dynamics; and combustor dynamics; see the review by Culick (2000) which is concerned with solid rockets but some of the ideas apply to combustion systems generally. **Chemical dynamics** is concerned with behavior on a microscopic level and includes, among other topics, properties of elementary reactions (heats of reaction, activation energies, kinetic rate constants, ...); reaction paths and kinetic mechanisms; and products of reactions. **Combustion dynamics** implies the unsteady behavior of reacting systems exposed to variations in the environment, notably pressure, velocity and temperature. The relevant processes occur on a macroscopic scale—i.e. the medium may be regarded as a continuum for most purposes—but the scale is normally much smaller than that of a practical combustion chamber. Two large classes of problems, for example, comprise the dynamical responses of flames and of burning solid propellants.

Combustor dynamics is really the main subject of this book. Indeed, use of the term ‘combustion instabilities’ is dictated more by historical usage than for other reasons. These dynamics evolve on the scale of the combustion chambers in question. It is these dynamics that are observed in tests and that are responsible for the troublesome consequences in practical systems. However, **combustor** dynamics cannot be isolated from **combustion** dynamics, as explained in Section 1.1 and illustrated with Figure 1.1. The dynamics of a combustion chamber is the dynamics of two coupled systems: the medium supporting the motions and the combustion process. Put another way, we are concerned with a general problem of unsteady gasdynamics whose existence depends on the actions of one or more mechanisms almost always⁷ arising from combustion dynamics.

Two characteristics distinguish different combustion chambers: geometry; and the kind of reactants (solids, liquids, gases, slurries, ...). In a formal sense, the details of the geometrical configuration are to a large extent secondary matters, particularly in the theory based on spatial averaging. There are significant quantitative differences among combustion systems arising from geometrical features, but one purpose of this book is to show that the characteristics of combustion instabilities common to all systems are far more significant and form much of the basis for understanding observed phenomena. Not surprisingly, then, the most difficult part of the subject is identifying, understanding and modeling the mechanisms. It is the mechanisms which most significantly differ among combustion systems. That is therefore the subject of Chapter 2. Then Chapter 3, and Annex A, are quite general, being concerned with the equations of motion and their forms most useful for the kinds of problems treated in the remainder of the book.

Much of Chapter 3 covers familiar ground, although the special use of the equations of motion for two-phase flow is perhaps not widely known. The chief result of that chapter is the wave equation for the pressure, constructed specially for treating nonlinear acoustic waves in combustion chambers. A significant distinction from most treatments of acoustics is that careful accounting for a general flow field is crucial matter for subsequent analysis of combustors; non-uniform average flow is an essential feature. In some way all analyses of combustion instabilities have taken advantage of the smallness of characteristic Mach numbers \bar{M}_r and M'_r for the mean and unsteady flows. One strategy for constructing simplified forms of the conservation equations, based on the assumption that \bar{M}_r , M'_r are small, is explained in Chapter 3.

⁷The sole exceptions arise with mechanisms imbedded entirely within fluid mechanics.

A method of spatial averaging is then applied in Chapter 4, to replace the small set of partial differential equations by an infinite set of total differential equations. The procedure requires representation of the flow variables as a synthesis of an infinite set of basis functions. In this work the basis functions are classical acoustic modes for the chamber being studied, but the best choice is still a subject of research. Time-averaging, or the method of two-time scaling may be used to simplify the formal problem further by reducing the second-order equations, produced with spatial averaging, to first order equations. That step is significant for both theoretical and practical purposes.

The remainder of the book is patently parochial, being dominated by the character and results of work by the author, his students and his colleagues for many years. Chapter 5 is a quick review of those parts of acoustics required later. Practically all of the material can be found in several well-known texts, but some special requirements of the applications discussed here justify summarizing familiar material in accessible form. Only those topics are covered that arise in investigations of combustion instabilities.

Chapter 6 covers the basic linear theory of combustion instabilities proper. Probably two technical features most clearly distinguish the subject within the fields of combustion and fluid mechanics. First is the simultaneous presence of a mean flow and unsteady motion, both having relatively low Mach numbers. The second is the requirement that solutions be obtained within a bounded region of space for which the boundary conditions are mixed, ranging from perfectly reflecting to perfectly radiating. For most problems concerning stability of disturbances, experience has established that turbulence seems to play a very small part and can be ignored. Hence the various contributions to linear stability are connected in some way with the presence of an average flow and hence are measured by the characteristic Mach number \bar{M}_r of the steady flow. The principal result is a formula for the wavenumbers of the perturbed acoustic modes, represented in three-dimensions, or within the one-dimensional approximation. For reasons given in Section 1.5, the emphasis in Chapter 6 is on solid rockets, but the general results apply to any type of system.

A broad spectrum of nonlinear behavior is covered in Chapter 7, beginning with examples of the special problems treated with the general analysis worked out in the preceding chapters. A continuation method is discussed in Section 7.7. Based on results obtained so far, this appears to be the most effective means of handling nonlinear combustion instabilities represented by the method of spatial averaging based on expansion in modes. Following a brief discussion of noise, some basic results obtained for pulsed instabilities (subcritical bifurcations) are covered.

The last two chapters are descriptive, discussions of practical methods for controlling combustion instabilities. Chapter 8 is a brief summary of ways to control instabilities passively. The motivations and the explanations for success of the methods rest on the fundamental behavior discussed in earlier chapters. However, in practice the actual problems are usually too involved to be treated analytically. Hence it is important to understand their basis and to obtain results for simple problems which can be solved.

Although it had been suggested more than 30 years earlier, active control became subject to vigorous research in the mid 1980s. But after rather intensive studies by many organizations, since roughly 2002 general interest in the subject has contracted, perhaps owing to the absence of successful applications. There have been many demonstrations that active control works to reduce the amplitudes of combustion instabilities, but no accompanying thorough explanations. Moreover, the power required has caused most cases to be impractical. Chapter 9 is a short coverage of some of the interesting results, including a practical application. Space and time restrictions have limited the present discussion which will be amplified in a later edition. It's a fascinating subject with wonderful possibilities, but achieving success for practical uses is a great deal more difficult and subtle than most people foresaw. The subject has a great future that must be built on basic understanding, which to a large extent is still absent.

It is not the intent of this book to provide only formulas and descriptions of problems. Our emphasis is on understanding the various kinds of combustion instabilities; and on developing and using one reasonably general method for analyzing and treating the phenomena in all types of propulsion systems. Experience over many years has shown that the approach followed here is useful in practice as well as for theoretical work. Familiarity with the basic principles, and with the procedure for their application, will give a sound context for understanding and attacking real problems.

CHAPTER 2

Combustion Dynamics and Mechanisms of Combustion Instabilities

Identifying the primary cause, the *mechanism*, is probably the single most important task in understanding combustion instabilities in full-scale systems. The term ‘mechanism’ refers to that phenomenon or collection of processes forming the chief reason that the instability exists. There may be more than one mechanism, but in any case the ultimate reason for an instability is transfer of energy from the combustion processes, or the mean flow, to unsteady organized motions. Instabilities are commonly observed as nearly periodic oscillations having time-dependent amplitudes. As a practical matter, the chief goal is to reduce the amplitudes to acceptable levels. For that purpose it is essential first to understand the cause, and then to work out the connections with the chamber dynamics. Several of the mechanisms introduced in this chapter will be investigated more thoroughly later in this book.

In the context defined by Figure 1.1, understanding the mechanism of combustion instabilities is equivalent to understanding combustion dynamics. It is essential to keep in mind always that by its very definition, combustion involves chemistry and chemical kinetics within the setting of fluid mechanics. Depending on the mechanism, one or another of those phenomena may dominate. Hence, for example, in some cases involving vortex formation and shedding, we may find that burning is not a central issue. Nevertheless, the presence of the flow field supporting the vortices is itself produced by combustion of reactants. We may therefore justifiably include the phenomenon under the general label ‘combustion dynamics’, although we are stretching the literal meaning of the term. The main topics covered in this chapter relate largely to the feedback path in Figure 1.1.

The last section (2.7) of this chapter has a character different from the preceding material. It is an analysis of a simple example, the Rijke tube, illustrating the use of a time lag or delay to help interpret a mechanism, in this case heat addition from a wire heater. Familiar in other problems as a factor in causing unstable behavior, the idea of a time delay was introduced as the earliest attempt to explain or interpret the presence of combustion instabilities. The idea of delay as the basis for representing the action of a mechanism remains probably the most common approach to interpreting instabilities. However detailed the calculations may be, conclusions based on the presence of a time delay *per se* must not be confused with ‘understanding the mechanism’ of a combustion instability. What is required for proper understanding is knowledge of the physical origin of the delay. Only then may we be in a position to modify the system so as to affect the instability in question.

To be definite, practically all discussions of the consequences of time delays are forced, in the absence of deeper information, to assume some sort of *ad hoc* dependence of the delays on parameters defining the physical characteristics of the system at hand. We assume in Section 2.7 that the time delay is constant. The calculations then serve two purposes: to show explicitly the relation between a delay and linear stability; and to work out simple examples of the general analysis developed in the following chapters. Taking the time delay constant—in particular, independent of frequency—is the usual assumption and places a severe restriction on the results. It is well-known, for example, that the effective time lag for solid propellants is a

strong function of frequency. Assuming otherwise produces misleading if not seriously incorrect results for the dynamical behavior of the system in question.

2.1. Mechanisms of Instabilities in Solid Propellant Rocket Motors

In some respects combustion in a solid propellant rocket chamber appears to present a less complicated situation than those existing in any other types of combustor. The burning processes occur almost entirely within a thin region, normally less than one millimeter thick, adjacent to the propellant surface. Although some residual combustion commonly occurs when the propellant contains aluminum or other metallic additives and may affect unsteady global behavior, there is no unambiguous evidence that combustion within the volume contributes significantly as a basic cause of combustion instabilities. We assume that to be the case, leaving surface combustion and purely fluid mechanical processes as the chief origins of possible mechanisms. Figure 2.1 is a composite sketch of the four mechanisms currently regarded as the chief possible causes of instabilities in solid rockets. Of these, the dynamics of surface combustion is by far the most common.

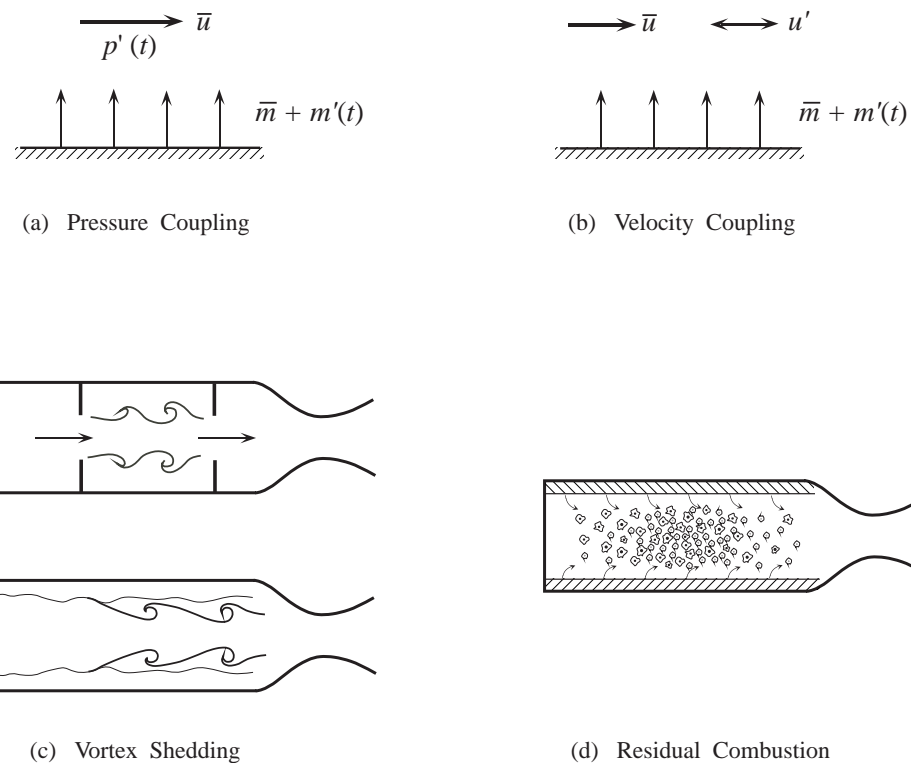


FIGURE 2.1. The four possible mechanisms for combustion instabilities in solid propellant rockets.

Vortex shedding from obstacles—as in the Shuttle solid rocket booster—or vortices produced at the lateral surface ('parietal vortex shedding')—as may be the case in the Ariane 5 solid rocket booster—have been identified as mechanisms only in large motors. Excitation of acoustic waves by vortices is of course a well-known phenomenon in a wide variety of wind musical instruments. The idea that vortices might be responsible for oscillations in a solid propellant rocket seems to have been proposed first by Flandro and Jacobs (1974) but it has received particularly intense attention because of the problem in the Shuttle and, during the past decade or so, in connection with the problem of pressure oscillations in the Ariane 5; a particularly good discussion has been given by Vuillot and Casalis (2002).

The dynamics of residual combustion far from the burning surface—most likely associated with aluminum or other metal fuel additives not completely burned at the surface—remains poorly understood. Although some attention has been given to the process (see Section 6.11), analysis of the dynamics is incomplete. No calculations exist assessing quantitatively the possible contributions of residual combustion to linear stability relative to those of surface combustion.

On the other hand, there is no disagreement that the dynamics of surface combustion is the dominant mechanism causing most combustion instabilities in all types and sizes of solid rockets.

2.1.1. Qualitative Interpretation of the Basic Mechanism. The dependence of the burning rate of a solid propellant on the pressure has long been known as a fundamental characteristic. Experiment and theory for the combustion of gases show that the reaction rates vary strongly with both pressure and temperature. It is therefore not surprising that the burning rate of a solid is sensitive to the impressed temperature and pressure. What is surprising is that the processes in the gas and condensed phases in the vicinity of the burning surface conspire to produce a dynamical response that exhibits significant dependence on frequency. That dependence on frequency is particularly important because the response is noticeably greater over a rather broad frequency range typically including some of the acoustic resonances of combustion chambers. In that range the combustion processes act to amplify pressure fluctuations. That is, some of the energy released in chemical reactions is transformed to mechanical energy of motions in the combustion products. Hence the dynamics in the feedback path, Figure 1.1, not only provide feedback but as well promote an unstable situation. The burning surface exhibits a sort of resonant behavior but without possessing the spring-like (i.e. restoring) forces associated with a resonant oscillating system such as the simple mass/spring oscillator. Hence the phase relations are different in the two cases.

Since the cavity in a solid rocket possesses its own acoustic resonances, we have a system of two coupled oscillators. If it should happen that the resonant frequencies of the two oscillators are close, then conditions clearly favor an instability. That is the situation commonly occurring in solid rockets and is the simplest direct explanation for the widespread occurrences of instabilities in tactical as well as strategic motors (Price 1961, Blomshield, 2000).

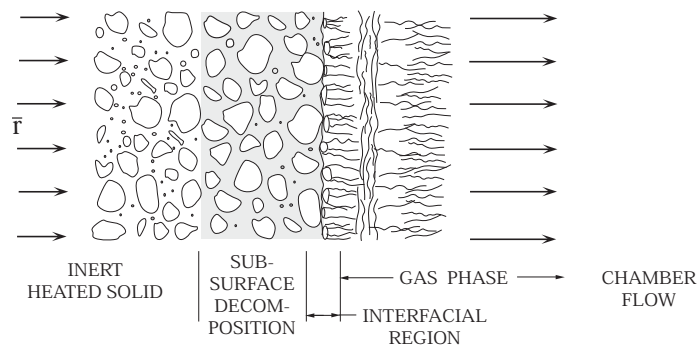


FIGURE 2.2. Sketch of steady combustion of a solid propellant.

The essential features of the combustion processes dominating the behavior just described have long been known. Figure 2.2 is an idealized interpretation showing the main characteristics of a burning composite propellant. The physical character of the materials and the processes involved in their transformation from solid propellant to products of combustion are quite well known. That knowledge has been gained through the efforts of many people and organizations over many years. An excellent summary is the reference volume edited by Davenas (1993). Ultimately it is the fluctuation of the velocity of gases leaving the combustion zone that is the essence of the mechanism. Oscillation of the flow causes the surface to appear locally like

an oscillatory piston or acoustic speaker, a source of acoustic waves. Formally the situation is identical to a planar array of monopoles having zero-average mass flow superposed on the mean flow due to combustion. However, the fluctuation of burning rate is a consequence of fluctuating heat transfer so we can understand the mechanism best by examining the behavior of the temperature profile. In Section 2.2.2 we will treat the propellant as if it were a perfectly homogeneous isotropic material in the condensed phase, and use the one-dimensional approximation throughout, from the cold condensed solid phase to the hot combustion products. Figure 2.3 is one frame from a film of a burning solid taken at the Naval Weapons Center (Price *et al.* 1982), suggesting that any sort of one-dimensional approximation seems unrealistic (See also Price 1984). That is certainly true on the scale of the particle sizes (10s to 100s of microns).

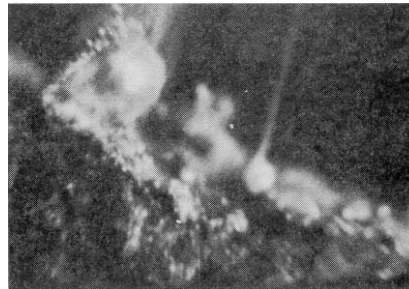


FIGURE 2.3. View of the surface of a burning solid propellant containing aluminum (Price *et al.* 1982).

However, the variations of velocity and pressure in the chamber occur over distances of the order of the chamber dimensions. Hence it is appealing to suppose that for analyzing interactions between the combustion zone and the motions in the chamber, the heterogeneous character propellant can be overlooked in some sense. For example, the linear burning rate of a propellant is measured without special regard for spatial variations on the small scale of compositional inhomogeneities. No instrument is available to do otherwise. That is not to say, of course, that the burn rate and the combustion dynamics do not depend on spatial variations of the condensed material and the gas phase. Rather, we suppose that dependence on such properties as the size distribution of oxidizer particles is accounted for by some sort of averaging procedure. Thus, parameters appearing in the final results, such as A and B in the QSHOD model discussed here, must depend on, for example, an average particle size. No rules exist for the averaging, but recently impressive progress has been made for computed steady burning rates using a “random packing” model (Kochevets, Buckmaster and Jackson 2001). In all of our discussion we adhere to the one-dimensional approximation as far as possible, with no attention paid to the possible errors incurred. In any case it seems a good assumption that if the averaging process is faithful, any errors are likely to be less than uncertainties arising in other parts of the problem, e.g., material properties. We do not address consequences of the statistical nature of the propellant surface which may result in random motions observable as noise in pressure records (e.g., R.L. Glick, Private Communication). Some results for pressure oscillations in the presence of noise are covered in Chapter 7, but possible connections with surface combustion are not investigated.

The mechanism in question here is, broadly speaking, primarily a matter of **combustion** dynamics. It has become customary to represent the mechanism quantitatively as an admittance or response function. We use the latter here, defined generally as the ratio of the fluctuation of the mass flow rate of gases departing the combustion zone, to the imposed fluctuation of either the pressure or the velocity. Thus the response function for pressure fluctuations (commonly referred¹ to as the “response to pressure coupling”) is defined in dimensionless form as R_p ,

$$R_p = \frac{m'/\bar{m}}{p'/\bar{p}} \quad (2.1)$$

¹The term ‘coupling’ in the sense used here is intended to convey the idea that the surface combustion processes are influenced by changes in time of the variable in question, here the pressure. We will be concerned largely with pressure coupling and to a lesser extent with velocity coupling.

where $(\cdot)'$ means fluctuation and $\overline{(\cdot)}$ is an average value. The average value \overline{m} represents the average inflow of mass normal to the surface, due to the propellant burning. In almost all applications, the fluctuations may be approximated as steady sinusoidal oscillations, written as

$$\begin{aligned}\frac{\overline{m}'}{\overline{m}} &= \frac{\hat{m}}{\overline{m}} e^{-i\omega t} \\ \frac{\overline{p}'}{\overline{p}} &= \frac{\hat{p}}{\overline{p}} e^{-i\omega t}\end{aligned}\quad (2.2)a,b$$

and

$$R_p = \frac{\hat{m}/\overline{m}}{\hat{p}/\overline{p}} \quad (2.3)$$

where $(\hat{\cdot})$ denotes the amplitude of the oscillation, including both magnitude and phase. Because generally the oscillations of mass flux rate are not in phase with the pressure oscillations, the function R_p is complex, the real part representing that part of $\overline{m}'/\overline{m}$ that is in phase with the pressure oscillation.

Although the response function for pressure coupling is most commonly used, there is a second response function, that associated with velocity coupling, which under some practical circumstances is far more important. At this point we confine our remarks to the response function for pressure coupling. We return to velocity coupling in a later discussion (Section 2.2.8).

A simple interpretation of the response function explains its importance to combustion instabilities. According to the definition (2.3), a pressure oscillation having amplitude \hat{p}/\overline{p} produces the oscillation \hat{m}/\overline{m} of mass flow into the chamber

$$\frac{\hat{m}}{\overline{m}} = R_p \frac{\hat{p}}{\overline{p}} \quad (2.4)$$

Viewed from the chamber, the boundary appears then to oscillate. The apparent motion is entirely analogous to that of a speaker or piston mounted at the boundary emitting waves into a room. Through a complicated sequence of processes whose details are not germane here, those waves coalesce and combine with the original pressure waves causing the fluctuations of mass flux. Whether or not that merging process augments or subtracts from the existing wave system in the chamber depends on the phase between \hat{m} and \hat{p} . The part of \hat{m} in phase with \hat{p} increases the amplitude of the wave system and is therefore destabilizing. For a particular motor, the tendency for combustion dynamics to drive instabilities is proportional to the integral of R_p over the entire area of burning surface, but weighted by the distribution of fluctuating pressure at the surface. Hence it is clearly essential to know the response function for the propellant used.

All traditional composite propellants using ammonium perchlorate as oxidizer, as well as advanced propellants using higher energy oxidizers and binder, burn in qualitatively similar fashion. The interface between the condensed and gas phases is fairly well defined, may be dry or wet, and may exhibit local dynamical activity owing to the presence of solid particles and responsive collections of liquid pools or drops. The dynamics of the interfacial region is particularly noticeable in microcinematography when the propellant contains aluminum. The metal collects in molten droplets, mobile and ignitable on the surface; those not fully consumed are carried away by the gaseous products of the interface. The high temperature at the surface is sustained by a balance between heat flow away from the interface, required to heat the cool propellant advancing to the surface; energy required to effect the phase changes at and near the interface; and the heat transfer supplied to the interfacial region from the combustion zone in the gas phase. It's a delicate balance, easily disturbed by changes in the chemical processes in the interfacial region, particularly within the subsurface region in the condensed phase. Figure 2.4 is a sketch of the temperature field for two elementary forms of the distribution of combustion. Note that for this figure we imagine that the temperature exists in a spatially averaged sense. Local variations on the scale of oxidizer particles are smeared out in the averaging procedure and explicit effects of inhomogeneities are absent.

The essentials of the behavior represented macroscopically by response functions can be described as a sequence of elementary steps, described here in simplified form with reference to Figure 2.4:

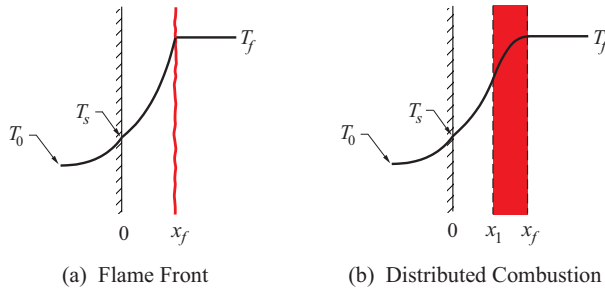


FIGURE 2.4. Representation of the temperature field for a burning solid propellant.

- (i) Suppose that for some reason the rate of reactions in the combustion zone increases—perhaps due to a fluctuation of pressure, or temperature, or to increased local mixing associated with greater intensity of turbulence locally in the chamber.
- (ii) Increased reaction rates produce a rise in the rate of energy release and an increase of temperature of the combustion zone.
- (iii) Due both to radiation and heat conduction, the heat transfer from the combustion zone to the interfacial region increases, having at least two possible consequences: the temperature at the surface is increased; and the rate at which condensed material is converted to gas is also increased.
- (iv) Because the temperature in the interfacial region rises, so also does the heat flow to the subsurface region and further into the solid, tending to cool the interface.
- (v) If there are subsurface reactions, the heat flow will tend to increase their rate, with consequences depending on the associated energy release (or absorption) rate.
- (vi) Exothermic subsurface reactions will act to maintain higher temperature locally, thereby encouraging the conversion of condensed material to gas at the interface, but also tending to increase the heat flow to the cooler solid.
- (vii) The net result may be that if the fluctuation of heat flow, and reduction of temperature, at the interface does not happen too quickly, the enhanced reaction rate assumed in Step (i) may produce a fluctuation of mass flow leaving the surface, that is in phase with the initial perturbation. Hence in this event the entire process is destabilizing in the sense that the initial disturbance has the result that the disturbed mass flow into the chamber tends to augment that initial disturbance.

Whether or not the preceding sequence will be destabilizing depends entirely on details of the processes involved. Notably, if sub-surface reactions are endothermic, then the sequence (v)–(vii) leads to the conclusion that the reactions may cause the propellant combustion to be less sensitive to disturbances.

2.1.2. Early Historical Background Leading to the QSHOD Model. In many important respects, problems of combustion instabilities in solid propellant rockets have raised questions, and forced considerations, which are common to practically all combustion systems. The particulars are of course very different, but a large part of the general behavior among the various devices is surprisingly similar. Much is to be gained from understanding broadly the historical background of combustion instabilities in solid rockets.

The problem was first identified in the Soviet Union and analyzed by Zel'dovich (1942) several years before similar work in other countries. Margolin (1999) has given a brief incomplete account. Further developments were for the most part simply not known in the West until twenty years later. To this day we

have sparse knowledge of the field in the USSR, until the 1990s. We will give here a survey to convey an idea of developments in the U.S., with brief references to progress in Western Europe.

In Chapter 1 we have noted some of the early research in the U.S., sponsored during World War II, principally related to the development of tactical rockets. Perhaps the outstanding example is the 2.75 inch rocket.² Problems with ‘anomalous’ or ‘rough’ burning caused the first uses of resonance rods and other passive ‘fixes’, such as modifications of the internal configuration. Due to the urgency of development, and crude instrumentation, little was accomplished in respect to discovering the source of the problem. The entire program was moved from Caltech to the Mojave Desert before WWII ended, forming part of the newly established Naval Ordnance Test Station (NOTS). E.W. Price, who had started his career at Caltech, expanded his research on combustion instability. His sponsorship of Grad (1949) produced the first work treating the problem of oscillations in a solid rocket as one of acoustics, a fundamental point of view.³

Before Grad’s work, although the notion that the unsteady motions were somehow related to acoustical motions had certainly been discussed, it was only one among several ideas. Grad first worked out a quantitative theory based on the assumption that the pressure fluctuations were ‘self-excited’ and associated initially with small amplitude motions in a compressible medium, the products of combustion. The oscillation then grows if they are unstable, developing into large amplitude motions which were often called ‘sonance’ or ‘sonant burning’, terms which have since been dropped. Grad did not propose a particular mechanism for the unstable motions, but introduced a time lag supposed related to unsteadiness in the rate of decomposition of the propellant in its conversion to gaseous products. The work had some definite results but for several reasons—not least, perhaps, that the community was not yet in a state to make use of the analysis—the approach was not developed until later by others.

In fact, despite continuing practical problems with ‘anomalous burning’, there seem for several reasons to have been no further publications in the open literature until Smith and Sprenger (1952) gave a summary of some of the experimental results obtained at the Aerojet Company.⁴ They reported that ‘high-frequency’ oscillations having large amplitudes were accompanied by large excursions of pressure; the frequencies were close to those of transverse acoustic modes. The general picture was to a considerable extent consistent with that envisioned by Grad, but the paper contains some interesting data taken with laboratory motors. Figure 2.5 is adapted from their Figure 3, showing that the motion was without doubt mainly the first tangential mode of the cylindrical chamber, having frequency proportional to \bar{a}/R where R is the radius of the chamber.

Besides Smith and Sprenger’s contribution clarifying the qualitative nature of combustion instabilities in solid rockets, they offered several important basic general observations about the mechanism. They were first to understand that Rayleigh’s Criterion (or ‘principle’) could be extended to become an “explanation of combustion instability phenomena without conflicting with Rayleigh’s original intentions Interpreting the oscillations during sonance as self-excited, the possible sources of energy and causes of damping must be found, and the mechanism for self-excitation described.” This correct viewpoint seems to have been barely noticed at the time. Their paper ends with a short description of a mechanism primarily related to fluctuations in the rate of reaction and energy release. The importance of the thermal wave in the solid phase was not yet recognized.

Geckler (1954)a,b, also working at the Aerojet Company, gave two summaries of theory and experiment for the combustion of solid propellants, the second one dealing mainly with unsteady problems. He devoted

²The size was set by that of steel pipe readily available during early tests at Caltech. (E.W. Price, Private Communication)

³The analysis had actually been formulated initially by J.K.L. MacDonald of NOTS, who died early in the program; his work was continued by Grad. MacDonald perished in an airplane crash, having taken a seat given up by E.W. Price.

⁴As true for many publications of research solid rockets until the 1990s, many details of the experiments, such as compositions and properties of the propellants used, and geometry of the test device, were not given.

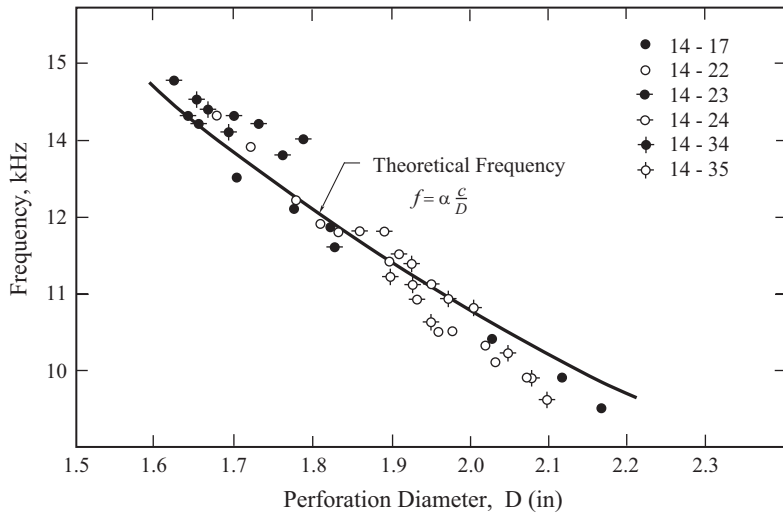


FIGURE 2.5. Measurements showing the presence of the lowest tangential mode during ‘sonant’ burning (Smith and Sprenger 1952).

much of his discussion to the results found by Smith and Sprenger, the remainder consisting of brief summaries of Grad’s model of combustion with a time lag; and Cheng’s analysis which involves a more involved (realistic?) model of the conversion of solid material to gaseous products involving a time lag.

During the early 1950s there was more activity in developing analysis of combustion instabilities in liquid rockets than on the corresponding problems in solid rockets. Crocco and Cheng (1952, 1953) had begun their work on one-dimensional notions that would lead to their monograph in 1956. It was reasonable that some of the same ideas should be applied to solid rockets. (Cheng 1952a,b, 1959, 1960, 1962). The results, however, are not applicable because the mechanism proposed is incorrect.

Cheng’s main idea is that “primary decomposition” causes the solid propellant to generate at a rate $\dot{m}_i(t)$. Then combustion of those gases produced at time t is assumed to take place instantly and completely at the later time $t + \tau$. The instantaneous rate of burning $\dot{m}_b(t)$ is

$$\dot{m}_b(t) = \left(1 - \frac{d\tau}{dt}\right) \dot{m}_i(t - \tau) \quad (2.5)$$

This result is derived as equation (2.88) here, in the context of liquid rockets. Cheng considers briefly and then discards the possibility that the rate of decomposition, \dot{m}_i , depends on the velocity parallel to the surface. As explained later in Section 2.3.2, if the time lag is the period required for completion of unspecified processes in the gas phase, and pressure is the controlling physical variable, then one finds (Cheng’s equation 5 in his 1954a paper):

$$\frac{\dot{m}_b(t)}{\bar{\dot{m}}_b} = \frac{p^{n-s}(t)}{[p(t - \tau)]^{n-s}} \quad (2.6)$$

The decomposition rate is assumed to depend on pressure only, $\dot{m}_i(t) \sim p^n(t)$ (Cheng uses n for s), and n has the same meaning here as in equation (2.90). After linearization of (2.6), Cheng found the result for the fluctuation of the flow velocity normal to a burning surface,

$$\frac{v'/\bar{a}}{\rho'/\bar{p}} = -B\bar{v}_b \quad (2.7)$$

and

$$B = 1 - \gamma n + \gamma(n - s)e^{-i\omega\tau} \quad (2.8)$$

The ratio (2.7) is, within a constant factor, the admittance function for the surface.

We will not cover Cheng's analysis further. His model of the unsteady burning process has long ago been shown to be wrong. It is interesting only as an example of an attempt to take advantage of an idea (the time lag) which became widely used in analysis of combustion instabilities in liquid rockets. Cheng's treatment of the acoustical motions in the chamber added nothing new and in fact fell short of Grad's results in many respects.

During most of the 1950s there were few published papers on unsteady motions in solid rockets (or any rockets for that matter). That meager production of 'open literature' does not give an accurate picture of the work being done by industry and in government laboratories, in the USSR as well as in the West. As the decade progressed, more pressure was exerted in the US to make the problems better known, and to involve researchers other than the small number directly concerned in the development of hardware.⁵ In 1954, Green (1955) wrote a one-page negative critique of Cheng's 1952 work, essentially calling attention to the errors of interpretation of experimental results by Smith and Sprenger, noting particularly that combustion instabilities had been found with 'mesa burning' propellants which have burning rates independent of pressure, for some useful range of pressure. Green's final observation was that limited observations suggested to him that the presence of noise in the appropriate frequency range may precipitate instabilities. It's an idea which has been offered several times since; it has never been shown to be valid. Noise as the origin of substantial oscillations in a combustion chamber is at the present time (2005) being studied in at least one development program.

In the following year, Green (1956) gave a quite good summary of reported observations of instabilities in solid rockets, beginning with early reports by Boys and Schofield (1942) in England, Ferris *et al.* (1945) in the U.S. and the works cited here. Green was evidently concerned largely with "irregular reaction", which meant significant excursions of the mean pressure. He reported no data for oscillations; Figure 2.6 shows an example of some irregular reaction with a composite propellant (composition unspecified).

Green was evidently pre-occupied with his observation that 'irregular reaction' occurred in rockets using propellants having burning rates independent of pressure over substantial ranges. He then reasoned that the basic cause was increasing decomposition rate in the solid phase, with heat transfer due to oscillatory velocity parallel to the surface. Coupling of the temperature and velocity of the gas, near the surface, to the solid material occurs throughout the heat transfer. Consequently the surface temperature of the solid fluctuates, causing variations in the decomposition rate. By implicit assumption, the acoustical motion in the gas phase is supported independently of the decomposition process. It was only a proposal, not supported by a model or calculations.

With his next paper, Green (1958) attempted to work out a quantitative model founded partly on the ideas just summarized. The analysis contains in rudimentary form an idea, the thermal wave, which became part of the description now accepted as the basis for a good first approximation to unsteady combustion of a solid propellant. It's a purely thermal theory, temperature being the sole independent variable. Green's picture for his calculations is the same as Figure 2.4 here; his significant new contribution was inclusion of the thermal wave in the solid material, with no decomposition. Thus Green's calculations rested on solution of the heat conduction equation (2.5) in the solid phase, with no source term. The basic result is a quadratic

⁵Mr. E.W. Price was particularly outspoken and effective in this respect. His efforts were notably influential beginning with the Polaris program. In contrast, the system of classifying information at all levels in the USSR, as the open literature reflects, never relaxed from practices adopted during World War II, continued until the 'fall of the wall'. In the middle 1970s, for example, an academic visitor to Moscow and Novosibirsk, was unable to learn from researchers in the field of combustion of energetic materials that they even knew of anybody working on problems related to solid rockets. That extreme secrecy was mainly a continuation of practices followed in World War II continued until the fall of the wall. The situation was different, for example, in the field of gas lasers; the exchange of information was recognized as an important contribution to progress, practically from the beginnings of the field.

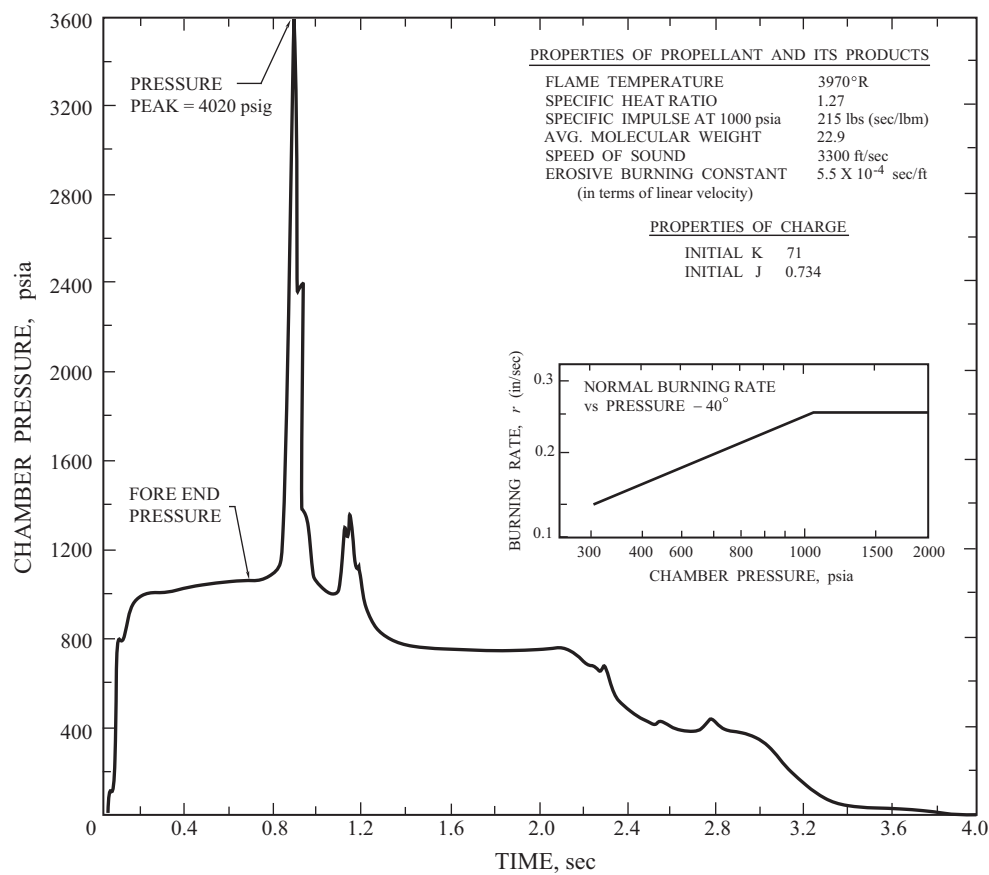


FIGURE 2.6. Mean pressure in a cylindrical motor operating with double-bore propellant (52 inches long, 1 inch initial internal diameter) (Green 1956).

equation for the wavelength of thermal waves, the frequency being set by the oscillatory heat input expressed in terms of a film coefficient.

Because he did not consider the complete problem involving the chamber oscillations—i.e. coupling between motions in the chamber and the thermal waves in the solid was absent—Green was strictly unable to find the conditions for oscillation. He therefore missed the true meaning of his results and tried to force them to produce what he sought, the resonance condition fixing the frequency of oscillations, but without dependence on the properties of the chamber. In doing so he introduced a time lag between the surface temperature and the phase change solid \rightarrow gas at the surface. As a result, the conclusions are of no use and can be ignored.

The same thermal model was used by Nachbar and Green (1959) in an extended discussion of the 'resonant condition' defined by Green (1958). Thus there are no new ideas in the work. Some of their conclusions are at minimum misleading; while the paper is part of the historical background, it offers little of lasting value.

An interesting and significant note appeared in March 1958, a report of the first tests with an early variant of a new device, the T-burner (Price and Sofferis 1958). Their sketch of the burner using a 'full-length charge' is adapted for Figure 2.7. Various grains were used, including the extending parts way into the chamber from the ends. The experimental program at the U.S. Naval Ordnance Test Station

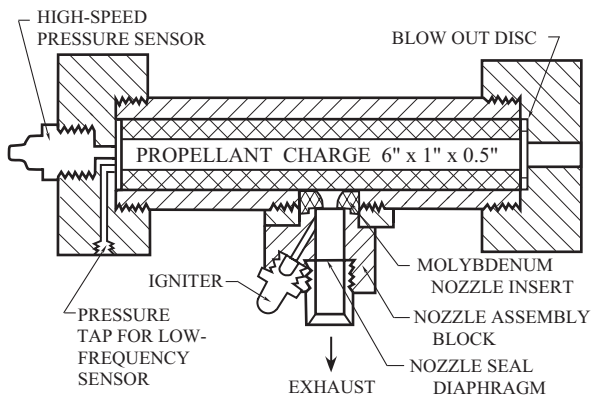


FIGURE 2.7. Sketch of the first test device having the form of a T-burner (adapted from Price and Sofferis 1958).

was especially important for its emphasis on research directed to understanding the basic properties and causes of combustion instabilities in solid rockets, as opposed to performing tests directed primarily to solving a particular problem encountered in a development program. This work was conducted to help clarify the “mechanism of excitation of instability”; and to study the influence of oscillatory behavior on the average burning rate of propellant. Already many tests had established, albeit indirectly, that the burning rate (\bar{r}) increases, sometimes substantially, when the pressure oscillates. The burner shown in Figure 2.7 was specially designed to exhibit unstable longitudinal modes having frequencies comparable with those of tangential modes in motors. Note that the oscillatory velocity would correctly be parallel to the burning surface of the propellant shown in Figure 2.7, so the device provides a good approximation to the motions in a tangential mode. In this sense the work constituted a significant departure from previous experiments by providing a simulation rather than a re-creation of the actual problem.

The bulk of the short paper was devoted to using test results obtained with the new burner to check the truth of five ‘contentions’ identified in the works of Grad; Smith and Sprenger; Cheng; Geckler; and Green. One result concerns the mode excited—longitudinal, in contrast to the tangential modes observed in the works cited. The remaining four were:

- (i) the chamber oscillations were excited by pressure, not velocity oscillations;
- (ii) the noise in the device (lower than in previous equipment) was not a “conspicuous factor in exciting combustion instability”;
- (iii) the average burning rate decreased at low chamber pressures (500–1700 psi) and increased at higher pressures;
- (iv) the average burning rate was apparently unaffected by the low mean gas velocities present in the tests.

Subsequent work in many laboratories have shown that (i), (iii) and (iv) are not generally true. Item (ii) remains not generally settled; it is this author’s belief that while noise modifies some features of instabilities, it is not a fundamental cause or mechanism of instabilities, or of increased amplitudes of modes.

Price (1958) gave a thorough, balanced review of combustion instabilities in solid rockets at the IXth IAF Congress, a short time before a great deal of recent work became publicly available—i.e. was declassified.⁶ It’s a readable qualitative discussion of the field, containing a number of succinct observations still valid. Perhaps

⁶The papers by Grad (1949) and Cheng (1956) seem to be the first works in universities on combustion instabilities. Not until 1960 did Brownlee publish the next account (Brownlee and Marble 1960) of work done at Caltech’s Jet Propulsion Laboratory. At about the same time, Horton completed his Ph.D. thesis at the University of Utah (Horton 1961).

the only real fault with the discussion is a short treatment of the ‘time lag’ assumed to be a crucial item in the excitation process. While the notion of time lag as an important matter in discussions of combustion instabilities in liquid rockets as recently as the late 1980s and 1990s, it was soon rendered obsolete in respect to solid rockets by a well-grounded (albeit approximate) theory of the combustion response function for solid propellants.⁷.

The entire field in the U.S. began to undergo significant changes of emphasis and even, one might argue, direction, with the participation of F.T. McClure and his colleagues at the Johns Hopkins Applied Physics Laboratory, beginning in early 1959. McClure enlisted the cooperation of the leading investigators, almost all of whom were experimentalists working in government or industrial laboratories. Although the Technical Panel on Solid Propellant Instability of Combustion existed for only a bit more than three years, its work had a lasting influence. Its main publication is a useful collection of papers released in 1964, *Technical Panel on Solid Propellant Instability of Combustion—Scientific Papers 1960–1963*. The effectiveness of the Technical Panel was made possible by a decision taken at high levels within the Defense Department to allow open publication of as much information as possible, a decision not to be underrated.

In 1959 Hart and McClure (1959) published the first work by the group at the Applied Physics Laboratory. The work set a tone strongly influenced by the authors’ background as physicists. They tried to extract the main attributes of the phenomena studied, and grounded them in basic principles; often observational details are recognized but gracefully ignored, in seemingly arbitrary fashion, to favor clarification and simplification of the theory at hand. Hart and McClure settled on the interaction (or ”coupling”) between acoustic waves and the burning surface as *the* principal cause of combustion instabilities. Further, they chose to ignore the effects of erosivity in their first approximation to the coupling process. After estimates of characteristic times for gas phase reactions; heat conduction in the solid and gas; mass transfer; and reactions in the solid phase, they formulated a model which is essentially the same as the QSHOD model discussed in Section 2.2. Figure 2.8(a) is an adaptation of Hart and McClure’s sketch of their model; Figure 2.8(b) shows a result for the real part of the admittance function. The details of the analysis have been much simplified in later work (see Section 2.2) and need not be covered here.

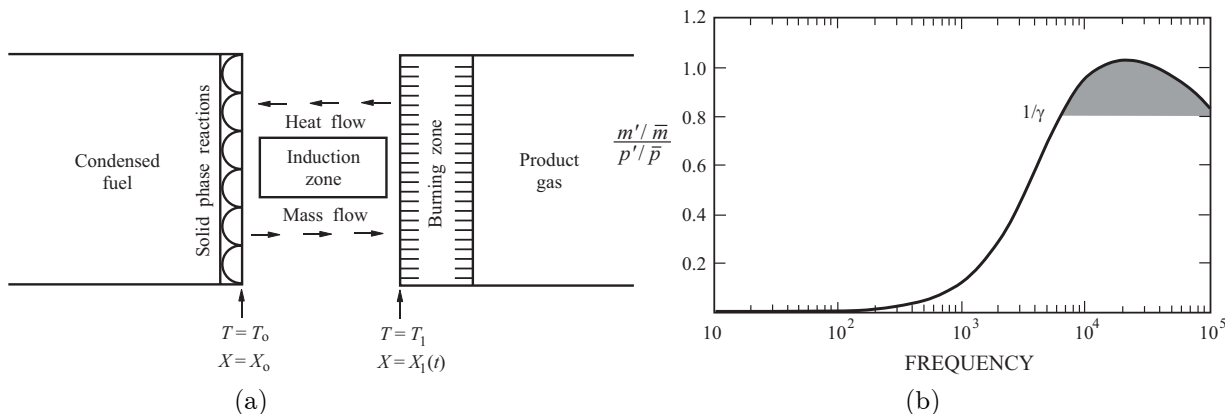


FIGURE 2.8. Adapted from Hart and McClure (1959). Part (a): a sketch of their model of surface combustion; Part (b) a result for the quantity proportional to the real part of the admittance function.

⁷The main shortcoming of a time lag representation is the unknown and important dependence on frequency. Thus the assumption is commonly made that the lag is independent of frequency, a serious error for solid propellants and possibly for liquid propellants as well

In the following year, McClure, Hart and Bird (1960)a began a series of papers dealing with various aspects of combustion instabilities in solid propellant rockets, not all of which had been treated, or even recognized, previously. They treated oscillations in a cylindrical motor with the unsteady combustion processes represented in the manner formulated in the 1959 paper. The principal important new feature, original with this work, was accounting for oscillations of the solid material. Combustion response to pressure oscillations only was accounted for, but in a short section of the paper, the authors examined possible consequences of erosive burning.

It is fairly evident that the normal modes of oscillation in a cavity containing a significant amount of solid material may differ from those in a cavity filled with gas. That result was shown by McClure, Hart and Bird. For applications there are in the first instance two questions to answer: How much material is required to be "significant"?; and What are the actual properties of the material? In other words, roughly, how compressible is the propellant, and how effectively does it dissipate mechanical motions? Subsequent work over the following 10-15 years showed that motions of the solid could be ignored, so far as combustion instabilities are concerned, except in certain large motors. The first question asked above can be answered only for the particular cases one must deal with. Determining material properties under unsteady conditions remains a difficult experimental matter usually carrying large uncertainty.

There are at least two important consequences of unsteady flow parallel to a burning surface: the steady burning rate may be affected, a fairly direct extension of the familiar phenomenon of 'erosive burning'; and there can be a truly time-dependent process affecting unsteady changes in the burning rate, analogous to the unsteady behavior accompanying rapid pressure fluctuations. It is the second type of 'erosive burning' which is of particular interest in the present context for it contains the possibility of coupling acoustic waves to the combustion processes. In their first paper on the possible effects of unsteady erosive burning, Hart, Bird and McClure (1960)a avoided the problem of formulating a theory of the process, but tried to construct a general description which would fit into their structure for computing the acoustics of a chamber. Their beginning point was the linearized representation of the burning rate expressed as the mean flow leaving the surface in the normal direction,

$$m_b(p, v_e; t) = \bar{m}_b(\bar{p}) + \left(\frac{\partial m_b}{\partial p} \right)_0 p' + \left(\frac{\partial m_b}{\partial p_t} \right)_0 \frac{\partial p'}{\partial t} + \left(\frac{\partial m_b}{\partial |\mathbf{u}'|} \right)_0 |\mathbf{u}'| + \left(\frac{\partial m_b}{\partial |\mathbf{u}'|_t} \right)_0 \frac{\partial |\mathbf{u}'|}{\partial t} \quad (2.9)$$

where \mathbf{u}' is the unsteady (acoustic) velocity parallel to the burning surface. In this form, $\left(\frac{\partial m}{\partial |\mathbf{u}'|} \right)_0$ contains the usual erosion constant k for steady burning,

$$\left(\frac{\partial m}{\partial |\mathbf{u}'|} \right)_0 = \bar{m}_0 k \quad (2.10)$$

The terms proportional to p' and $\partial p'/\partial t$ can be re-written using the definition of the admittance function.

We will not consider any further the analysis⁸ by McClure, Hart and Bird, which consists mainly in examining the possible effects of erosion in a cylindrical chamber. Probably the lasting value of the work lies in the formulation of the boundary condition (2.9) which, perhaps in modified forms, has subsequently been used by many others. The manner of incorporating the basic phenomenon of rectification has lasting influence. On the basis of their incomplete calculations, the authors concluded that for reasonably large values of $k|\bar{\mathbf{u}}|$, with $k > 0$, the erosive effect of the mean flow is stabilizing. The real importance of the paper is probably the influence it had, calling the attention of others to the subject. However, the matter of the effects of erosion—any sort—on stability remains to a large extent an unsolved problem.

By 1960 there was no dissension that the simple basic model of the combustion response of a burning solid captured part of the observed behavior, qualitatively at least. To what extent quantitatively could not

⁸It is difficult to follow, contains typographical errors and does not account for all influences of the mean flow, even for a cylindrical chamber.

truly be assessed until more extensive and more accurate data became available. McClure, Hart and Bird (1960) summarized the situation in a page-and-a-half note. In the following year, the same authors (1961) added a few comments concerning the dependence of the propellant response (and, presumably, instabilities) on a few properties: e.g. instabilities are more severe if the rate of heat release is higher, and the chamber pressure is lower. Such conclusions should be regarded with caution, because the actual behavior depends as well on the chamber geometry, flow field and properties of the particular propellant used. The authors also attribute the known result of aluminum to suppress instabilities to its tendency (maybe) to reduce the response function, by affecting surface combustion processes; or to its effect on losses (unspecified) in the system. It would be several years before 'particle damping' would be generally accepted as the dominant process.

Much of the work in the immediate future consisted in working out some of the consequences of ideas introduced in the period c.1959–c.1963. McClure, Bird and Hart (1962) discussed in greater detail their formulation of the influence of erosion on axial modes. Their discussion contains their basic ideas but the development is brief and really doesn't do justice to the importance of the material. It is important to realize that 'erosion' as treated by McClure *et al.*, by Price, and others is really a matter of *kinematics*, not dynamics. Further, despite many speculations and a modest amount of data, which sometimes has questionable relevance, there is no physical theory of the unsteady 'erosion mechanism', now commonly referred to as 'velocity coupling'. Two important features of velocity coupling were recognized in the early 1960s: the kinematic nonlinearity; and the dependence on the magnitude of the sum of the local mean and unsteady gas velocities, causes the coupling of the surface combustion to the gas dynamics to vary with position on the surface. The second property means that any 'response function for velocity coupling' will necessarily depend on position, unlike the case for pressure coupling, for example R_p defined by (2.3). We will discuss velocity coupling further in Section 2.2.8.

The literature in this period was (and to some extent this is still true!) a mixture of classified and unclassified documents. Even if available in principle, the latter may be difficult to locate and obtain. An example is an excellent review by Price (1961) describing the fundamentals of the subject then understood (much of the discussion remains valid) and summarizing in considerable detail virtually all practical examples then known.

The group at APL was quite active in 1960–63, examining several problems which were central to understanding practical aspects of combustion instabilities in solid rockets. With their previous papers cited above, they had constructed a framework which gave the field generally a cohesiveness previously absent, and helped identify the problems that demanded attention. A natural result was the division of processes into 'gains' or 'losses'. Thus two papers, Hart and Cantrell (1963), and Cantrell, McClure and Hart (1963) dealt with an important source, acoustic damping or attenuation. The second was an attempt to compute, by using a variational method, the acoustic losses on the side walls in an end-burning rocket, intended to approximate conditions in some test devices. No further use of the method has been made. While the first of these papers contains some interesting observations, it too has had no lasting consequences.

Extensive observations of unstable tangential modes had first been reported by Brownlee and Marble (1960) and described in detail by Brownlee (1961). That form of instability had been a common problem in tactical solid rockets, but hadn't been subject to interpretation grounded in fundamental ideas until the discussion by Bird, McClure and Hart (1963). The paper is directed mainly to consequences of varying geometrical parameters, all the tests having been done with cylindrical motors. Following their previous work, the authors organize their discussion explicitly around the balance of gains and losses of acoustic energy. At the time, quantitative information was not available for most of the processes; the work is interesting mainly as a measure of the state of the field—there are no specific results. The authors discuss but discard erosive effects except for possible changes in the burning rate. Thus, gains of acoustic energy are ascribed entirely to pressure coupling which could not be assigned a value with confidence.

Of the possible losses—essentially viscous or viscoelastic in the solid or gas—only gas-particle interactions were found to provide (roughly) the correct behavior. The propellant did not contain aluminum and it is questionable (even doubtful) that the combustion products contained the material (1% by mass of 0.5μ particles) postulated to account for the observed stability boundary. Consequently, neither the gains nor the losses seem to have been satisfactorily explained or provided ideas more generally useful. However unsuccessful it was, the paper remains as the first attempt to interpret observed stability boundaries, see Section 6.7.3 for commentary based on later work.

Perhaps motivated partly by the serious lack of certain relevant information, Bird and Hart (1963) gave an interesting survey of the difficulties associated with scaling. The authors recognized that, in a sense, scaling steady combustion instability cannot be done: It is simply not possible to determine the stability of a motor from the stability characteristics of a smaller, geometrically similar model: There are too many processes having diverse dependencies on frequency. Nevertheless, people concerned with problems of stability of small amplitude disturbances in full-scale motors may gain much from understanding the rules governing scaling of the basic processes. It would be a mistake to expect formulation of concise, strict scaling laws such as one finds, for example, in the field of aerodynamics. A fundamental reason is that combustion instabilities necessarily mix time- and space-dependent physical behavior—e.g. wave propagation in complicated geometries—and the physical properties of chemically active solids and gases. Hence useful scaling laws are generally valid only over narrow ranges of the important parameters.

Except for a review, apparently the last paper from APL was essentially an effort by Cantrell and Hart (1964) to derive a formula for the growth constant of unstable oscillations in a general form applicable to any geometry. Although not stated in the account, a motivation was surely increasing concern with combustion instabilities that could not readily be related to the modes of oscillation in a circular cylindrical chamber. The authors' central idea was to begin with the definition of the growth constant as one-half of the time rate-of-change of time-averaged acoustic energy in a chamber,

$$\alpha = \frac{1}{2} \frac{1}{\mathcal{E}} \frac{d\mathcal{E}}{dt} \quad (2.11)$$

The analysis may appear at first acquaintance to be related to the variational method referred to above but it is not. Moreover there is no theoretical connection with the method of least residuals developed by Powell (1971) and Powell and Zinn (1971) or with the spatial averaging first used by Culick (1961) and which were developed to become central to much of this book. The differences arise with definitions of the rates of change of \mathcal{E} in terms of processes at the boundary of the volume treated. We discuss the point in Section 6.9.

Equation 2.11 is a *definition* following from linear theory. Consequently it offers no beginning for extension to nonlinear behavior. Furthermore, because practically no further use is made of the equation of motion, this approach contains no hints for computation of the field variables (\mathbf{u}, T, p) or the terms of their orderly expansion in the Mach number of the mean flow. Thus the value of the work lies mainly with some qualitative discussion of stability in T-burners and cylindrical rockets.

Hart and McClure (1965) brought the program on combustion instability at the Johns Hopkins Applied Physics Laboratory to an end with a review paper covering mainly the state of theory in mid-1965. It's a summary of the field at that time, containing no ideas that had not previously appeared. They devote a short section to comments on nonlinear behavior but, because the APL analytical work seems to be almost irretrievably restricted to linear problems, the discussion does not initiate or suggest novel developments in that direction.

The leadership and significant positive influence exerted by McClure and his colleagues at APL far exceeded the value of their specific technical contributions. Their work on theory gave the field of combustion

instabilities in solid rockets a flavor and a thrust which were new and permanent.⁹ In addition to initiating several lines of analytical work, the APL formulation of the basic acoustics problem greatly encouraged continuation and expansion of the program to measure the response of surface combustion at NOTS under E.W. Price. A thesis (Horton 1961) and three papers (Horton 1961, 1962; and Horton and Price 1961) began the international activity of measuring the admittance function of propellant samples mounted in an 'end-burner', generically called the T-burner.¹⁰ (Figure 1.21.)

In his thesis, Horton (1961) reported the first measurements of an admittance function. Figure 2.9(a) shows his results which were given in his second paper (Horton 1962).¹¹ The picture in Figure 2.9(b) is a record (taken with an 'oscillograph' which no longer exists!) of a particularly good T-burner firing (Horton and Price 1962). Apparently Price had suggested to Horton during the latter's thesis program that the initial (final) periods would ideally show exponential growth (decay), i.e. the envelope of the oscillations has the form $e^{\pm\alpha t}$; and that the information could be used in principle to compute the admittance function for the burning surface. For linear behavior, equation (2.10) applies. For an acoustic field one can write approximately $\varepsilon \sim |p'|^2$ (see Section 5.4) and from the envelope of the pressure trace one can compute

$$\alpha = \frac{1}{|p'|} \frac{d|p'|}{dt} \quad (2.12)$$

Let α_g be the value for the growth period and α_d for the decay. If the losses are the same during the growth and decay, and α_c is due to the combustion driving only, then $\alpha_g = \alpha_c + \alpha_d$, so

$$\alpha_c = \alpha_g - \alpha_d \quad (2.13)$$

Thus with (2.12) and (2.13) one can in principle find α_c . In practice there are serious difficulties obtaining accurate reproducible results, particularly for propellants containing aluminum; see the "T-burner manuals" (Culick 1969, 1974).

It is an interesting aspect of Horton's work that he worked out a simple method for using experimental data to infer both the real *and* the imaginary parts of the response function. That is correctly the information one should obtain from T-burner tests. Owing to experimental difficulties (apparently) it seems that Horton's is the only report for both parts of the response function. See the discussion in Section 6.7.

T-burner tests to characterize fully the dynamics of a propellant over ranges of pressure and frequency are expensive. Moreover, the results generally carry significant experimental errors. Hence the T-burner is best used to detect changes in dynamics, or generally for comparing propellants. Although hopes for improvement may have been held high, the nature of results from T-burner testing has not changed greatly in forty years. Nevertheless, there is still no better test apparatus and for qualitative purposes the T-burner has not been superceded. Indeed, even with the measurement errors always present, no other method has yet been proven more useful for obtaining qualitative data.

After McClure's working group had been established, and more information became publicly available, research on combustion instabilities in solid rockets attracted increasing attention. Brownlee, who had begun work on the problem in Canada, carried out the first systematic measurements of stability boundaries (Brownlee and Marble 1960); Smith (1960) and Shinnar and Dishon (1960) in the same AIAA volume published papers on the response of a burning surface to changes in the environment. While both works treated unsteady temperature profiles in the solid phase, neither emphasized the thermal wave. They could not, therefore, find the very special and important contributions of the thermal wave to the surface admittance function.

⁹For example, the early 1959 and 1960 papers attracted this author's responsive attention at the end of his Ph.D. research program. He subsequently was introduced to the solid rocket community by Mr. W.A. Berl, assistant to Dr. McClure.

¹⁰A center-vented symmetrical burner was first used by Price and Sofferis (1958) but the name T-burner was coined by Dr. H.M. Schuey in honor, it seems, of the piece of plumbing he chose in 1963 to serve as the center vent.

¹¹We should note particularly that Horton inferred both the real and imaginary parts of the admittance function. Most reports of results obtained with T-burners show only the real part.

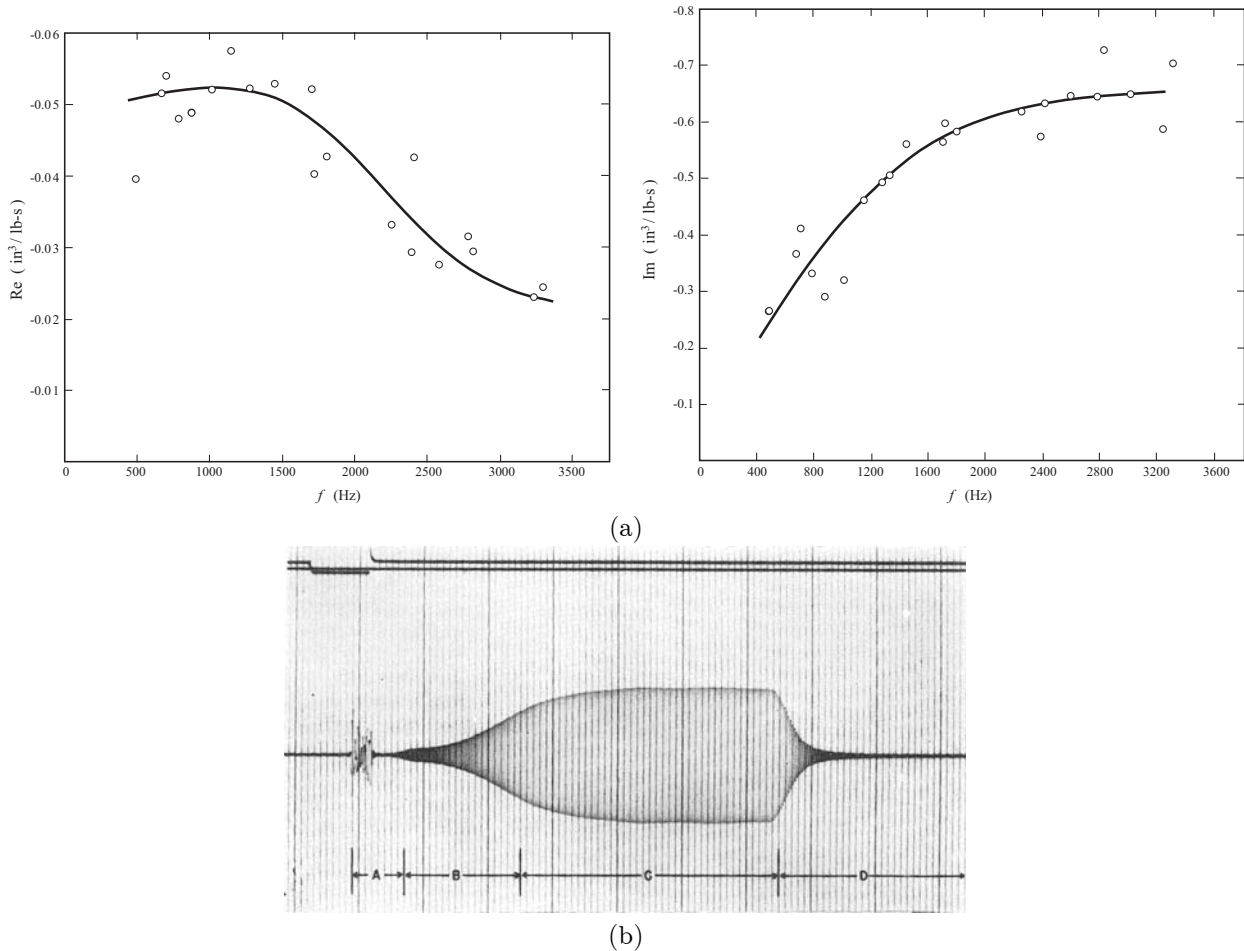


FIGURE 2.9. The first reported values of the real and imaginary parts of the admittance function for a burning surface. (a) experimental results inferred with the real and imaginary parts of equation (5), Horton (1961); (b) pressure record for a T-burner firing (Horton and Price 1962).

In the early 1960s attempts to measure the admittance function were made by more organizations—or perhaps their efforts were finally made public. Watermeier (1961) at the Army Ballistic Research Laboratories reported motion pictures of the burning surface (of a double-base propellant) exposed to the output of a siren. Only qualitative observations were made. Two years later, Watermeier *et al.* (1963) and Strittmater *et al.* (1963) discussed experimental investigations with modified forms of the T-burner, also using double-base propellants. One interesting observation concerned the agglomeration of molten aluminum on the surface, a “probable” cause for reduction of the admittance at low frequencies. Other features of the behavior of molten aluminum in the vicinity of the burning surface were noted, but without quantitative measurements no conclusions can be drawn. Wood (1963) also made measurements in a T-burner with propellant similar to that described by Price and Sofferis. Although he tried to make direct connection between compositional properties and the admittance function defined by McClure *et al.*, Wood’s data and observations were too crude to allow definite conclusions. The work marks a transitional step to more realistic representations involving dynamical thermal behavior of the solid phase.

Denison and Baum (1961) produced a work which not only represented (in retrospect!) the culmination and joining of several ideas but, because it is firmly based on fundamental behavior, has had lasting influence

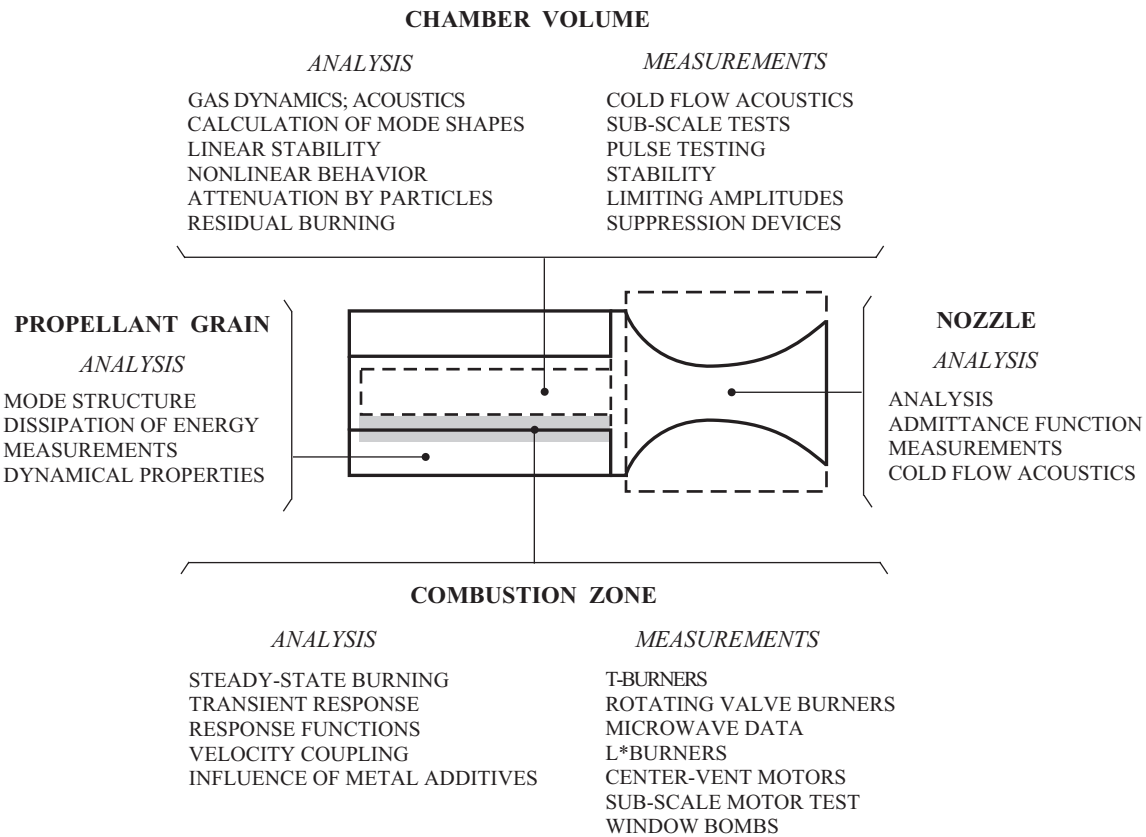


FIGURE 2.10. A summary of the instability problems for solid propellant rockets in 1970 (Culick 1970).

on theoretical treatments of burning. At the time, the paper did not instantly attract widespread attention, but its importance was gradually recognized.¹² When Denison and Baum's analysis appeared, its general applicability was not immediately apparent. In 1968, Culick (1968) showed that at that time ten analyses were equivalent to that of Denison and Baum in the sense that if parameters are given appropriate values in each case, then the response function (2.3) is the same function of frequency. That recognition has had important influence on experimental and theoretical work. Departures from the QSHOD model are important, difficult to treat and are still a subject of research; Sections 2.2.5 to 2.2.8 contain examples.

Figure 2.10 is a complete summary of the various kinds of work proceeding on combustion instabilities in solid propellant rockets, c. 1970.

2.2. Analysis of the QSHOD Model

The model we will analyze here is the simplest possible capturing a dominant contribution to the combustion dynamics. Only unsteady heat transfer in the condensed phase causes true dynamical behavior, i.e. dependence of the response to pressure coupling. That process must in any case be present. This problem

¹²In fact, the model defined by Denison and Baum was in a sense really an unnecessarily detailed special case of that proposed twenty years earlier by Zel'dovich (1942) and developed by Novozhilov (1965). The first was unknown in the West and the second was not recognized properly until the late 1960s. In simplest terms, an imperfect model of the gas phase in Denison and Baum's analysis is replaced by two sorts of experimental data in the Zel'dovich-Novozhilov model.

(model) is therefore the reference always used to assess the possible influences of other dynamical processes, in particular those in the gas phase and decomposition in the condensed phase. The substance of the model is defined by the following assumptions:

- (i) **quasi-steady** behavior of all processes except unsteady conductive heat transfer in the condensed phase;
- (ii) **homogeneous** and constant material properties, non-reacting condensed phase;
- (iii) **one-dimensional** variations in space;
- (iv) conversion of condensed material to the gas phase at an infinitesimally thin interface.

The acronym QSHOD for this model derives from the five bold letters in assumptions (i)–(iii).

During the early years of this subject, from the mid-1950s to the mid-1960s, roughly ten analyses of the response function were published in the Western literature, giving apparently distinct results. Culick (1968) showed that, due to the fact that all of the models were based in the same set of assumptions (i)–(iv), the results were dynamically identical. That is, all had the same dependence on frequency and, with appropriate values for the various parameters involved, give coincident numerical values. Hence the term QSHOD is a useful term referring to a class of models. Differences between the models are associated with different detailed models of the steady processes, notably the flame structure in the gas phase.

A different approach to compute the combustion response was taken by Zel'dovich (1942) in Russia and elaborated in great depth by Novozhilov (1965, 1973, 1996). The result has come to be known as the Z-N model. That representation of the response has certain distinct advantages, most importantly giving convenient connections between the parameters in the response function and quantities characterizing and measurable in steady combustion. The idea is explained briefly in Section 2.2.4. However, an important point often overlooked is that the dynamics contained in the basic Z-N model are the same as those in the flame models treated within the general QSHOD model.

Analysis of the model sketched in Figure 2.1 amounts to quantitative representation of the sequence (i)–(iv). Even in the simplest form described here, the problem is too complicated for a closed form solution. Apart from recent results obtained numerically for the entire region, covering the cold solid to the hot combustion products, the usual procedure familiar in many problems of this sort is based on solutions found for the separate regions defined above; the results are then matched at the interfaces. The solutions and the matching conditions are based on the one-dimensional equations of motion. In the reference frame selected here, the origin is fixed to the average position of the burning surface, and under unsteady conditions all interfaces move, a feature that must be correctly incorporated in the analysis.

2.2.1. Estimates of Some Characteristic Lengths and Times. It is helpful to have a qualitative idea of the sizes of a few important variables. That information provides a context for understanding the physical problem and a basis for making realistic approximations to simplify analyses. One way to view the situation is shown in Figure 2.11, based on Figure 1 of Culick (2000). The four levels of dynamics—chemical dynamics, combustion dynamics, combustor dynamics and motor (engine) dynamics—are each characterized by different lengths and times. A typical size of a rocket, for example, is also the length scale for engine and combustor dynamics, say one meter, to tens of meters. The burning zone for a solid propellant is a millimeter or less. Hence the ratio of those lengths may vary from 10^3 to 10^6 . Chemical dynamics evolve on a scale 10^{-3} to 10^{-6} smaller. Thus it is fairly clear that the details of phenomena associated with the three different scales can, to a very good approximation, be treated separately, although they are ultimately coupled. Averaging of processes on the smaller scale produces consequences that matter on the larger scale. In this book we are concerned largely with unsteady motions on the scale of the device in question. But those motions are commonly driven, e.g., at the boundaries, by forces and energy flow which originate at a smaller scales.

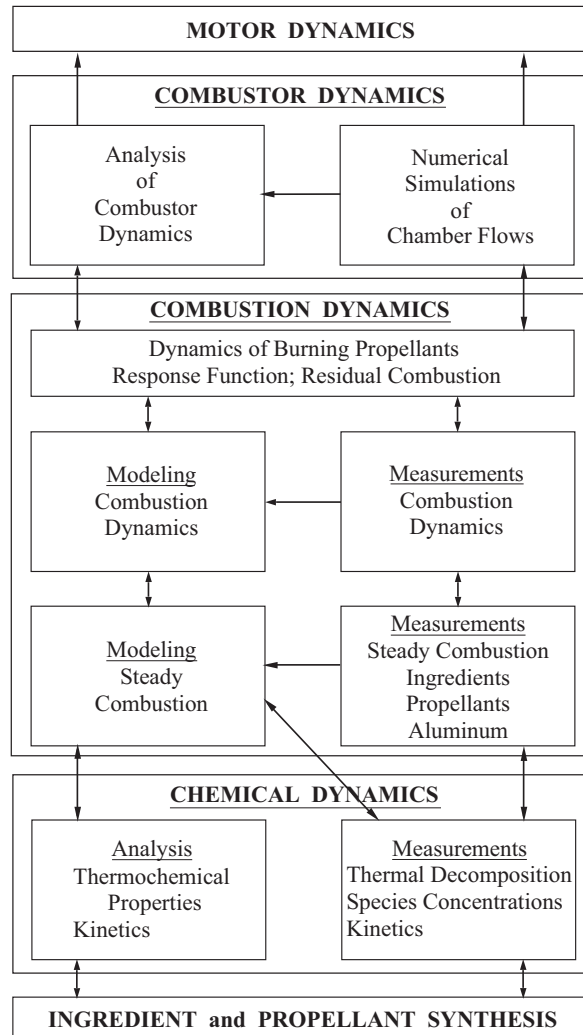


FIGURE 2.11. A view of the areas of research and their connections in solid propellant rockets (Culick 2000).

Often, the *mechanics* of the unsteady motions require descriptions on a much smaller scale. The unsteady response of a burning surface is a good example of that fact. We assume for present purposes that the combustion processes generate a zone like that sketched in Figure 2.2, and make a few estimates of its characteristics. Several discussions of approximate representations exist (e.g. Hart and McClure 1959); we base our remarks on Culick and Dehorter (1969) who computed the burning rate assuming a finite region of uniform combustion. The flame thickness is roughly 0.5μ – 500μ for the thermal conductivity of the gas varying from 2×10^{-5} to 2000×10^{-5} cal/s-cm⁻²K, the pressure less than 900 atmospheres and reasonable values for other parameters (temperatures, heat of reaction, etc.); Table 2.1 is a list of the properties used in the following remarks. We take 250μ as a conservative estimate; as a rough guide, the thicker is a flame, the greater is its tendency to behave dynamically, in contrast to quasi-statically.

Table 2.1 contains values of the properties we need for the following estimates. The characteristic time for the chemical reaction process in the gas phase is the flame thickness divided by the average speed, $\tau_f \sim \delta_f/\bar{u}_g$ where $\delta_f \approx 250\mu$. Thus τ_f is the time for a particle to pass through the flame. We estimate the gas speed from continuity, $\bar{u}_g = \rho_p \bar{r}_b / \bar{\rho}_g$ and taking values from Table 2.1, $\bar{u}_g \sim (1766)(0.01145)/(7.97) \approx 2.5$ m/s.

Then the characteristic time for the steady reaction process is

$$\tau_f \sim \frac{\delta_f}{\bar{u}_g} \sim \frac{250\mu}{2.5 \text{ m/s}} \sim \frac{(250)(10^{-6})}{2.5 \text{ m/s}} \text{ m} \sim 10^{-4} \quad (2.14)$$

for a rather thick flame zone, $250\mu \equiv 0.25 \text{ mm}$.

The period of an oscillation is the reciprocal of the frequency, $\tau_a = 1/f = 2\pi/\omega_a$. For the chemical activity in the gas phase to be treated as ‘quasi-static’, chemical changes must be fast relative to the acoustic period, which implies

$$\frac{\tau_f}{\tau_a} \ll 1 \quad (\text{quasi-static chemical reaction}) \quad (2.15)$$

With the estimate just quoted, $10^{-4}f_a$ should be small for quasi-static reactions. This implies $f_a < 10,000 \text{ Hz}$. We conclude that while the chemistry in a solid propellant flame can probably be assumed to respond quasi-statically over a useful frequency range, something less than 10,000 Hz, the approximation should probably be examined more closely for higher frequencies.

TABLE 2.1. Typical Values of Combustion and Physical Properties.

mean pressure	$\bar{p} = 1.06 \times 10^7 \text{ Pa}$
linear burning rate	$\bar{r}_b = 0.0078[\bar{p}/(3.0 \times 10^6)]^{0.3} = 0.01145 \text{ m/s}$
chamber temperature	$\bar{T} = 3539 \text{ K}$
Prandtl number	$Pr = 0.8$
thermal conductivity of combustion gases	$\lambda_g = 0.0838 \text{ J/K-m-s}$
thermal conductivity of solid propellant	$\lambda_p = 0.126 \text{ J/K-m-s}$
thermal diffusivity of gases	$\kappa_g = 3.97 \times 10^{-4} \text{ m}^2/\text{s}$
thermal diffusivity of propellant	$\kappa_p = 1.0 \times 10^{-7} \text{ m}^2/\text{s}$
specific heat of gas	$C_p = 2020 \text{ J/kg K}$
specific heat of condensed material	$C = 0.68C_p$
propellant density	$\rho_p = 1,766 \text{ kg/m}^3$
gas density	$\bar{\rho}_g = 7.97 \text{ kg/m}^3$
γ (gas only)	$\gamma = 1.23$
gas constant	$R = (\gamma - 1)C_p/\gamma = 377.72 \text{ J/kg K}$
speed of sound	$\bar{a} = \sqrt{\gamma R \bar{T}} = 1282 \text{ m/s}$
speed of combustion products at the burning surface	$\bar{v}_b = (\rho_p/\rho)\bar{r}_b = 1.86 \text{ m/s}$
Mach number at the burning surface	$\bar{M}_b = 0.00173$

For much of our needs, some sort of thermal theory serves quite well to describe both steady and unsteady behavior of a burning propellant surface. The governing equation is then the energy equation which will have a different form in each of the regions (solid, interfacial, gas, ...). An important question is: How quickly does the flow respond to changes of conditions? A very fast response of the flow means that the distribution of temperature in a region will be the same as it would be in steady state for the same boundary (or end) conditions and values of energy sources. If, on the other hand, the state of the flow is not instantaneously responsive, the temperature differs significantly from its steady form due to the presence of waves. A measure of the departure from the ‘quasi-steady’ form is the ratio of the net flow of energy, into a fluid element, by heat conduction to the rate of change of energy in the element,

$$N_c = \frac{\partial}{\partial x} \left(\lambda_g \frac{\partial T}{\partial x} \right) \Bigg/ \bar{\rho} C_v \frac{\partial T}{\partial t} \quad (2.16)$$

where x is measured normal to the burning surface, in the direction of greatest variations.

Suppose (cf. Figure 2.13) that the temperature changes by ΔT in distance Δx and time Δt so we can estimate N_c as

$$N_c = \frac{\lambda_g \Delta T}{(\Delta x)^2} \Bigg/ \frac{\bar{\rho} C_v \Delta T}{\Delta t} = \frac{\lambda_g \Delta t}{\bar{\rho}_g C_v (\Delta x)^2} \quad (2.17)$$

where $\bar{\rho}$ is a representative density (gas or solid), C_v is the specific heat and Δx , Δt are the intervals of space and time in question. For a wave motion, the period $\tau = 1/f$ is a measure of the characteristic time. Spatial variations occur over the flame thickness, $\Delta x \sim \delta_f$, so

$$N_c = \frac{\lambda_g}{\bar{\rho}_g C_v \delta_f^2 f} = \frac{\kappa_g}{\delta_f^2 f} \quad (2.18)$$

where κ_g is the thermal diffusivity. For N_c large, the rate of heat transfer to a layer dominates the rate of change of energy within the layer having thickness δ_f ; then the term $\bar{\rho} C_v \partial T / \partial t$ can be neglected in the energy equation and the temperature field changes in quasi-static fashion. For the properties given in Table 2.1,

$$N_c = \frac{3.97 \times 10^{-4}}{(250 \times 10^{-6})^2 f} = \frac{6352}{f} \quad (2.19)$$

According to this result, the assumption of quasi-static behavior is not valid for frequencies above, say 1000–1500 Hz, perhaps higher. In any case, the analysis is so much simpler when this assumption is made, that it must be used in the initial stage, as a ‘first try’.

2.2.2. Calculation of the Response Function. The following remarks are based on the review cited above, Culick (1968). Since that time much work has been done to determine the consequences of relaxing the assumptions on which the following analysis (the QSHOD model) is based. We will later examine some of those ideas. In this section we assume that the combustion proceeds as transformation of a condensed phase at a single flat surface adjacent to the gas phase, requiring that solutions be matched at only one interface. We choose a reference system with origin ($x = 0$) fixed¹³ to the average position of the interface. Hence the cold unreacted solid material progresses inward from the left. Figure 2.12 shows this definition and the matching conditions that must be satisfied at the interface. Note that the velocity \dot{x}_s of the interface appears explicitly in these conditions and is to be determined as part of the solution to the complete problem.

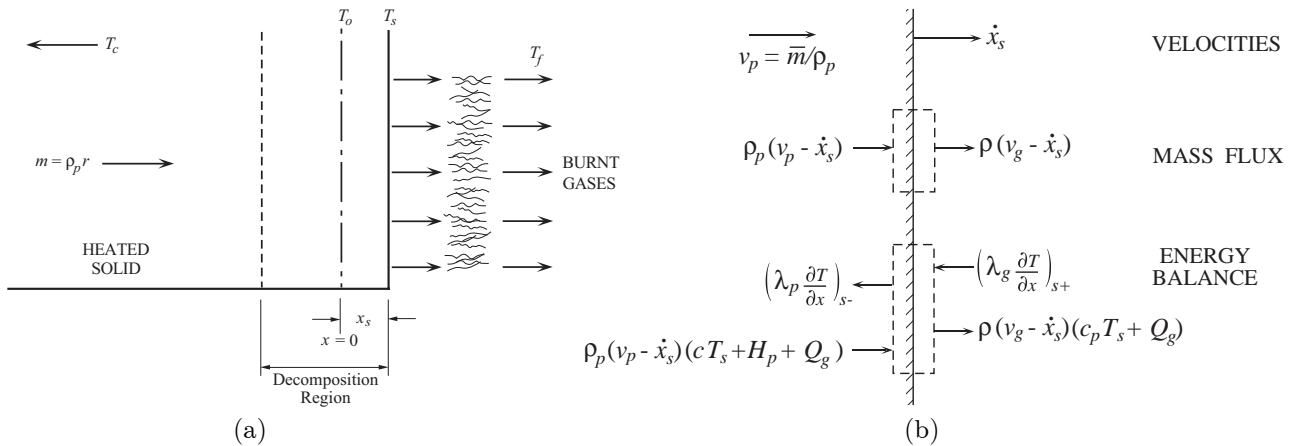


FIGURE 2.12. (a) reference system and (b) matching conditions for the QSHOD Model.

For the simple model used here, the analysis involves only three steps: solution for the temperature field in the solid phase; solution for the temperature field in the gas phase; and matching the two solutions at the interface. Because the temperature field is central to the analysis, the final results should correctly be

¹³Alternatively, the reference frame may be fixed to the instantaneous position of the surface; it is therefore not an inertial frame for the unsteady problem. For the linear problem, it is easy to show the equivalence of the results obtained with the two choices of reference systems. If more than three regions are treated—e.g., when an additional decomposition zone is included in the condensed phase—it may be more convenient to take $x_s = 0$ for the reference frame, and account for the motions of all interfaces relative to that plane, which is the time-averaged location of the solid-gas interface.

regarded as a thermal theory of steady and unsteady combustion of a solid propellant. No diffusive processes are accounted for and the pressure is uniform throughout the region considered: changes of the momentum of the flow do not enter the problem.

(a) *Solid Phase.* The energy equation for the temperature in the solid phase assumed to have uniform and constant properties, is

$$\lambda_p \frac{\partial^2 T}{\partial x^2} - \bar{m}c \frac{\partial T}{\partial x} - \rho_p c \frac{\partial T}{\partial t} = -\dot{Q}_d \quad (2.20)$$

where $\bar{(\)}$ means time-averaged value; $(\)_p$ denotes propellant; c is the specific heat of the solid; $\bar{m} = \rho_p \bar{r}$ is the average mass flux in the reference system defined in Figure 2.12; and \dot{Q}_d is the rate at which energy is released per unit volume due to decomposition of the solid ($\dot{Q}_d > 0$ for exothermic decomposition). We assume $\dot{Q}_d = 0$ here, an assumption to be relaxed in Sections 2.2.5 and 2.2.6. It is convenient to use the dimensionless variables

$$\xi_p = \frac{\bar{r}}{\kappa_p} x; \quad \tau = \frac{T}{\bar{T}_s} \quad (2.21)$$

where values at the interface are identified by subscript s and $\kappa_p = \lambda_p / \rho_p c$ is the thermal diffusivity of the propellant. Equation (2.20) becomes

$$\frac{\partial^2 \tau}{\partial \xi_p^2} - \frac{\partial \tau}{\partial \xi_p} - \frac{\lambda_p \rho_p}{\bar{m}^2 c} \frac{\partial \tau}{\partial t} = 0 \quad (2.22)$$

Solution to (2.22) with the time derivative dropped gives the formula for the normalized mean temperature

$$\bar{\tau} = \bar{\tau}_c + (1 - \bar{\tau}_c) e^{\xi_p} \quad (2.23)$$

satisfying the conditions $\bar{\tau} = \bar{\tau}_s = 1$ at the surface and $\bar{\tau}_c = \bar{T}_c / \bar{T}_s$ far upstream ($\bar{T} = \bar{T}_c$) in the cold propellant.

For harmonic motions, set $\tau = \bar{\tau} + \tau'$ and¹⁴ $\tau' = \hat{\tau} e^{-i\omega t}$, $\hat{\tau}$ being the amplitude, a complex function of position in the solid material. Substitution in (2.22) leads to the equation for $\hat{\tau}(\xi_p)$, easily solved to give

$$\tau' = \hat{\tau}_0 e^{\lambda \xi_p} e^{-i\omega t} \quad (2.24)$$

where λ satisfies the relation

$$\lambda(\lambda - 1) = -i\Omega \quad (2.25)$$

and Ω is the important dimensionless frequency,

$$\Omega = \frac{\lambda_p \rho_p}{\bar{m}^2 c} \omega = \frac{\kappa_p}{\bar{r}^2} \omega \quad (2.26)$$

For the numbers given in Table 2.1, $\Omega \approx 20f$. In order that $\tau' \rightarrow 0$ for $x \rightarrow -\infty$, the solution of (2.25) with positive real part must be used; $\lambda = \lambda_r - i\lambda_i$ and

$$\begin{aligned} \lambda_r &= \frac{1}{2} \left\{ 1 + \frac{1}{\sqrt{2}} \left[(1 + 16\Omega^2)^{1/2} + 1 \right]^{1/2} \right\} \\ \lambda_i &= \frac{1}{2\sqrt{2}} \left[(1 + 16\Omega^2)^{1/2} - 1 \right] \end{aligned} \quad (2.27)a,b$$

Due to the choice of reference system, $\hat{\tau}_0$ in (2.24) is the fluctuation of temperature at the average position of the interface ($\xi_p = 0$). However, matching conditions at the interface requires values and derivatives of the temperature at the interface itself, having position x_s and velocity \dot{x}_s . Values at the interface are calculated

¹⁴Note that consistently throughout this book we use the negative exponential, $\exp(-i\omega t)$. In some of the literature the positive exponential is used, so care must be taken when making comparisons of results.

with Taylor series expansions about $x = 0$; only the first order terms are retained for the linear problem, and on the solid side of the interface¹⁵:

$$\begin{aligned}\bar{T}_s(x_s) &= \bar{T}(0) + x_s \left(\frac{d\bar{T}}{dx} \right)_{0-} ; \quad \left(\frac{d\bar{T}}{dx} \right)_{s-} = \left(\frac{d\bar{T}}{dx} \right)_{0-} + x_s \left(\frac{d^2\bar{T}}{dx^2} \right)_{0-} \\ T'_s(x_s) &= T'_{0-}(0) + x_s \left(\frac{\partial\bar{T}}{\partial x} \right)_{0-} ; \quad \left(\frac{\partial T'}{\partial x} \right)_{s-} = \left(\frac{\partial T'}{\partial x} \right)_{0-} + x_s \left(\frac{\partial^2 T'}{\partial x^2} \right)_{0-}\end{aligned}\quad (2.28)$$

Hence the required results for the upstream side of the interface cannot be completed until the interfacial region is analyzed.

(b) Interfacial Region. Three relations govern the behavior at the interface: conservation of mass and energy, and the law for conversion of solid to gas. The first two are established by considering a small control volume placed about the true burning surface, as sketched in Figure 2.12. The volume is then collapsed to give ‘jump’ conditions associated with the total unsteady mass and energy transfer in the upstream ($s-$) and downstream ($s+$) sides of the interface:

$$\begin{aligned}\frac{\rho_p \dot{x}_s}{\bar{m}} &= - \left[1 - \frac{\bar{\rho}_{gs}}{\rho_{ps}} \right] \frac{m'_s}{\bar{m}} \approx - \frac{m'_s}{\bar{m}} \\ \left[\lambda_g \frac{\partial T}{\partial x} \right]_{s+} &= \left[\lambda_p \frac{\partial T}{\partial x} \right]_{s-} + \bar{m} \left[1 - \frac{\bar{\rho}_p \dot{x}_s}{\bar{m}} \right] (L_s)\end{aligned}\quad (2.29)a,b$$

The mean gas density $\bar{\rho}$ near the surface is much smaller than the density of the condensed phase, for cases of current interest, so the term $\bar{\rho}/\rho_p \ll 1$ will hereafter be dropped. For an exothermic surface reaction, the change $L_s = h_{s+} - h_{s-}$ of the thermal enthalpy is positive and may be viewed as a ‘latent heat’. The heat fluxes $[\lambda_p \partial T / \partial x]_{s-}$ and $[\lambda_g \partial T / \partial x]_{s+}$ are respectively flows of heat *from* the interface to the condensed phase and *to* the interface *from* the gas phase; note that (2.29)b has not yet been split into mean and fluctuating parts.

An Arrhenius law has commonly been assumed for the conversion of solid to gas, giving the total surface mass flux

$$m_s = B p^{n_s} e^{-E_s/R_0 T_s} \quad (2.30)$$

To first order in small quantities, the perturbed form of (2.30) is

$$\frac{m'_s}{\bar{m}} = E e^{i\omega\tau_1} \tau'_s + n_s e^{i\omega\tau_2} \frac{p'}{\bar{p}} \quad (2.31)$$

where $E = E_s/R_0 T_s$ is the dimensionless activation energy for the surface reaction. Time delays or lags τ_1 and τ_2 are included in (2.31), but presently there is no way to compute them; hence they will largely be ignored here except for some results given in Section 2.2.6.

For steady combustion, the energy balance (2.29)b, with (2.23) substituted for $d\bar{T}/dx$, becomes

$$\left(\lambda_g \frac{d\bar{T}}{dx} \right)_{s+} = \bar{m} [c (\bar{T}_s - T_c) + L_s] \quad (2.32)$$

The linear unsteady part of (2.29)b is

$$\left(\lambda_g \frac{\partial T}{\partial x} \right)'_{s+} = \left(\lambda_p \frac{\partial T}{\partial x} \right)'_{s-} + m'_s \bar{L}_s + \bar{m} (c_p - c) T'_s \quad (2.33)$$

¹⁵The temperature is continuous at the interface, but on $x = 0$, the fluctuations T'_{0-} and T'_{0+} computed from the solutions for the solid and gas phase need not be continuous.

Combination of (2.23) and (2.24) and the appropriate parts of (2.28) gives the formula for the heat transfer into the condensed phase from the interface:

$$\left(\lambda_p \frac{\partial T}{\partial x} \right)'_{s-} = \overline{mc} \left[\lambda T'_s + \frac{1}{\lambda} (\overline{T}_s - T_c) \frac{m'_s}{\overline{m}} \right] \quad (2.34)$$

In this result, the approximation in (2.29)a has been used. Substitution of (2.34) in (2.33) leads to the boundary condition to be set on the unsteady heat transfer at the downstream side of the interface:

$$\left(\lambda_g \frac{\partial T}{\partial x} \right)'_{s+} = \overline{mc} \left[\lambda T'_s + \left(\frac{c_p}{c} - 1 \right) T'_s + \left\{ \frac{1}{\lambda} (\overline{T}_s - T_c) + \frac{L_s}{c} \right\} \frac{m'_s}{\overline{m}} \right] \quad (2.35)$$

This result contains two assumptions:

- (i) $\overline{\rho}_g / \overline{\rho}_p \ll 1$ ($x = x_s$)
- (ii) nonreacting condensed phase having constant and uniform properties

Normally, the first assumption is reasonable. However, the second is restrictive, possibly seriously so according to some analyses; see Section 2.2.5. The important point is that (2.35) explicitly contains the transient behavior (the dynamics) associated with unsteady heat transfer in a benign solid material. If no further dynamics is attributed to the processes at the interface or in the gas phase, then the response function found with this analysis reflects only the dynamics of unsteady heat transfer in the single homogeneous condensed phase. That is the basic QSHOD result. Hence it is apparent that the form of the dependence of the response function in frequency *will necessarily in this case be independent of the model chosen for the quasi-static behavior of the gas phase*. The details of the model selected will affect *only* the particular values of parameters appearing in the formula for the response function. The conclusion is true for the basic Z-N model as well as for all flame models assumed to behave quasi-statically.

(c) *Gas Phase.* To complete the analysis, it is best at this stage to choose the simplest possible model for the gas phase. We assume that the thermal conductivity is uniform in the gas phase and that the combustion processes (i.e. the rate of energy release per unit volume) are also uniform in a region beginning some distance from the interface and extending downstream, ending at a location that is, by definition, the edge of the flame zone. This is a useful model containing two simple limits: uniform combustion beginning at the interface; and a flame sheet, obtained by letting the thickness of the combustion zone become infinitesimally thin. Figure 2.13 is a sketch of the model. Analysis of the model for steady burning was given by Culick (1969) with the following results.

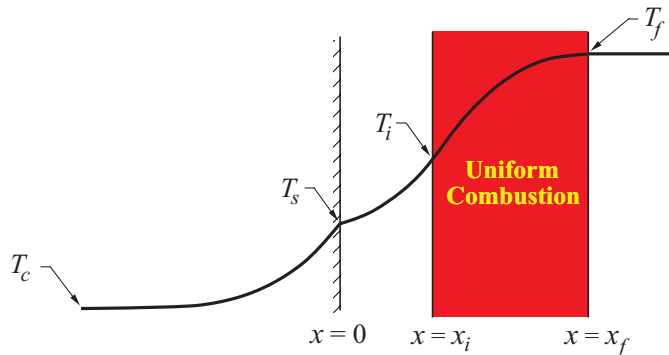


FIGURE 2.13. Sketch of the model of a solid propellant burning with uniform combustion in the gas phase.

The governing equation for this thermal theory is

$$mc_p \frac{d\bar{T}}{dx} - \frac{d}{dx} \left(\lambda_g \frac{d\bar{T}}{dx} \right) = \rho_g Q_f \dot{\epsilon} \quad (2.36)$$

where Q_f is the energy released per unit mass of reactant mixture (assumed to be constant), ρ_g is the local gas density and $\dot{\epsilon}$ is the local rate of reaction. At the downstream edge of the combustion zone, the boundary conditions are

$$\bar{T} = \bar{T}_f ; \quad \frac{d\bar{T}}{dx} = 0 \quad (x = x_f) \quad (2.37)a,b$$

where \bar{T}_f is the adiabatic flame temperature. On the interface,

$$\bar{T} = \bar{T}_s \quad (2.38)$$

and the energy balance at the interface gives

$$\left(\lambda_g \frac{d\bar{T}}{dx} \right)_{s+} = m [c (\bar{T}_s - T_c) + L_s] \quad (2.39)$$

For steady combustion, consideration of the energy flow across the gas phase gives

$$\left(\lambda_g \frac{d\bar{T}}{dx} \right)_{s+} = \bar{m} [Q_f - c_p (\bar{T}_f - \bar{T}_s)] \quad (2.40)$$

On the other hand, integration of (2.36) across the combustion zone, and application of the boundary conditions (2.37)a,b and (2.38) leads to

$$\left(\lambda_g \frac{d\bar{T}}{dx} \right)_{s+} = \int_0^\infty \rho_g Q_f \dot{\epsilon} dx - mc_p (\bar{T}_f - \bar{T}_s) \quad (2.41)$$

Because Q_f is constant, comparison of (2.40) and (2.41) leads to the requirement on the overall reaction rate

$$\int_0^\infty \rho_g \dot{\epsilon} dx = m \quad (2.42)$$

We assume λ_g constant (an assumption that is easily relaxed) and transform from x to the dimensionless variable ζ :

$$\zeta = \frac{mc_p}{\lambda_g} x \quad (2.43)$$

The energy equation (2.36) becomes

$$-\zeta^2 \frac{d^2 \bar{T}}{d\zeta^2} = \Lambda^2 \quad (2.44)$$

where the eigenvalue Λ^2 is

$$\Lambda^2 = \frac{\lambda_g Q_f \bar{w}}{m^2 c_p^2 \bar{T}_s} \quad (2.45)$$

and

$$w = \rho_g \dot{\epsilon} \quad (2.46)$$

Generally, of course, $\dot{\epsilon}$ and hence w and therefore Λ^2 are dependent at least on temperature, so Λ^2 is implicitly a function of ζ . However, we assume Λ^2 independent of ζ , defining the condition of uniform combustion.

Then with ζ_i the value of ζ at the beginning of the combustion zone (where ignition is assumed to occur) and ζ_f the value at the downstream edge of the flame, the first integral of (2.44) gives

$$\left(\frac{d\bar{T}}{d\zeta} \right)_{s+} = \left(\frac{\zeta_f - \zeta_i}{\zeta_f \zeta_i} \right) \Lambda^2 \quad (2.47)$$

Thus

$$\left(\lambda_g \frac{d\bar{T}}{dx} \right)_{s+} = \frac{\lambda_g Q_f}{c_p} \left(\frac{1}{\zeta_i} - \frac{1}{\zeta_f} \right) \frac{w}{m} \quad (2.48)$$

For $\zeta_f \gg \zeta_i$, and in the limit of combustion beginning at the solid/gas interface so $\zeta_i = 1$,

$$\left(\lambda_g \frac{d\bar{T}}{dx} \right)_{s+} = \frac{\lambda_g Q_f}{c_p} \frac{w}{m} \quad (2.49)$$

The assumption of quasi-steady behavior implies that the fluctuation of heat transfer at the surface is given simply by the linearized form of (2.49):

$$\left(\lambda_g \frac{dT}{dx} \right)_{s+}' = \bar{m} c_p \bar{T}_s \Lambda^2 \left(\frac{w'}{\bar{w}} - \frac{m'}{\bar{m}} \right) \quad (2.50)$$

We also find as the linearized form of (2.40):

$$\left(\lambda_g \frac{dT}{dx} \right)_{s+}' = m' [Q_f - c_p (\bar{T}_f - \bar{T}_s)] - \bar{m} c_p (T_f' - T_s') \quad (2.51)$$

This equation gives a formula for the fluctuation of flame temperature,

$$T_f' = T_s' + \frac{m'}{\bar{m}} \left[\frac{Q_f}{c_p} - (\bar{T}_f - \bar{T}_s) \right] - \frac{1}{\bar{m} c_p} \left(\lambda_g \frac{dT}{dx} \right)_{s+}' \quad (2.52)$$

Substitution of (2.50) for the last term gives the formula for computing T_f' when the combustion is uniform. In general, T_f' is not equal to the local fluctuation of temperature due to acoustical motions in the gas phase, the difference appearing the temperature fluctuation associated with an entropy wave carried by the mean flow departing the combustion zone.

By letting $\zeta_i \rightarrow \zeta_f$, the corresponding results can be obtained for a flame sheet; see Culick (1969; 2002). We will consider here only the case of a combustion zone having finite thickness; the response functions found for the two cases differ only in small details.

To progress further, we must specify the form of $w = \rho_g \dot{\epsilon}$; the reaction rate per unit volume. For the quasi-steady part of the processes, we assume that the mass flow provided by the surface is well-approximated by the Arrhenius law (2.30) and its fluctuation is (2.31) with zero time delays,

$$\frac{m'}{\bar{m}} = E \frac{T_s'}{\bar{T}_s} + n_s \frac{p'}{\bar{p}} \quad (2.53)$$

Due to the assumption of quasi-steady behavior, this formula represents the fluctuation of mass flow throughout the gas phase.

Finally, we need an explicit form for w as a function of the flow variables. To construct a consistent formula for the reaction rate in the gas phase, we equate the two results for heat transfer to the interface during steady burning: (2.39), the energy balance for steady combustion, generally valid at the interface; and (2.49) found for the special case of steady uniform combustion. For quasi-steady behavior in the gas phase, we replace average by instantaneous values of the temperatures, giving the expression for w :

$$w = \frac{c_p}{\lambda_g Q_f} m^2 [c(T_s - T_c) + L_s] \quad (2.54)$$

We assume that the right-hand side can be written as a function of pressure only by approximating the pyrolysis law $m = a(T_s)p^n$ as

$$m = ap^n = b(T_s - T_c)^s p^{n_s} \quad (2.55)$$

so

$$T_s - T_c = \left(\frac{a}{b} p^{n-n_s} \right)^{\frac{1}{s}} \quad (2.56)$$

Then (2.54) becomes

$$w = \frac{c_p}{\lambda_g Q_f} (ap^n)^2 \left[c \left(\frac{a}{b} p^{n-n_s} \right)^{\frac{1}{s}} + L_s \right] \quad (2.57)$$

The fluctuation w' of the reaction rate is then

$$\frac{w'}{\bar{w}} = \frac{\left(1 - \frac{T_c}{\bar{T}_s} \right)}{\Lambda^2} \frac{c}{c_p} w \frac{p'}{\bar{p}} \quad (2.58)$$

where Λ^2 is given by (2.45) written for the steady problem,

$$\Lambda^2 = \frac{\lambda_g Q_f \bar{w}}{\bar{m}^2 c_p^2 \bar{T}_s} \quad (2.59)$$

and

$$\begin{aligned} \bar{w} &= \left[2(1 + H) + \frac{c_p}{c} \frac{1 - \frac{n_s}{n}}{c} \right] \\ H &= -\frac{L_s}{c(\bar{T}_s - T_c)} \end{aligned} \quad (2.60)a,b$$

Instead of the calculations leading from (2.49) to (2.58) one could as well simply assume $w' \sim p'$. The only purpose of these remarks is to give an example of relating fluctuations of the reaction rate to the pressure for a well-defined model of combustion in the gas phase.

(d) Construction of the Response Function. We find the formula for the response function in the following way:

- (i) Substitute the pyrolysis law (2.53) in (2.35) which combines the interfacial conditions for energy and mass transfer:

$$\frac{1}{\bar{m}c\bar{T}_s} \left(\lambda_g \frac{\partial T}{\partial x} \right)'_{s+} = \left(\lambda + \frac{A}{\lambda} \right) \frac{\bar{T}'_s}{\bar{T}_s} + \left(\frac{c_p}{c} - 1 + \frac{LA}{1 - \frac{T_c}{\bar{T}_s}} \right) \frac{\bar{T}'_s}{\bar{T}_s} + n_s \left(L + \frac{1 - \frac{T_c}{\bar{T}_s}}{\lambda} \right) \frac{p'}{\bar{p}} \quad (2.61)$$

where

$$\begin{aligned} L &= \frac{L_s}{c\bar{T}_s} \\ A &= \left(1 - \frac{T_c}{\bar{T}_s} \right) \left(\alpha_s + \frac{E_s}{R_0 \bar{T}_s} \right) \end{aligned} \quad (2.62)a,b$$

- (ii) Substitute the reaction rate (2.58) into the expression (2.50) for the heat loss from the gas phase to the interface:

$$\frac{1}{\bar{m}c\bar{T}_s} \left(\lambda_g \frac{\partial T}{\partial x} \right)'_{st} = \left(1 - \frac{T_c}{\bar{T}_s} \right) w \frac{p'}{\bar{p}} - \frac{c_p}{c} \Lambda^2 \frac{m'}{\bar{m}} \quad (2.63)$$

- (iii) Equate (2.61) and (2.63) and use the pyrolysis law (2.53) to eliminate T'_s/\bar{T}_s ; this step leaves an equation which can be rearranged to give the ratio defined to be the response function for pressure coupling:

$$R_p = \frac{m'/\bar{m}}{p'/\bar{p}} = \frac{(AW + \frac{c_p}{c}n_s) + n_s(\lambda - 1)}{\lambda + \frac{A}{\lambda} + \left[\frac{c_p}{c}E\Lambda^2 - HA + \frac{c_p}{c} - 1 \right]} \quad (2.64)$$

- (iv) Write (2.64) in the form

$$R_p = \frac{c_1 + n_s(\lambda - 1)}{\lambda + \frac{A}{\lambda} + c_2} \quad (2.65)$$

For the assumed steady burning rate law, $m = ap^n$, the fluctuation can be written for quasi-steady (infinitely slow) changes of pressure and hence burn rate:

$$R_p = \frac{m'/\bar{m}}{p'/\bar{p}} = n \quad (2.66)$$

Thus in the limit of zero frequency ($\lambda = 1$), the right-hand side of (2.65) must equal n , giving the condition

$$\frac{c_1}{1 + A + c_2} = n$$

Define B and A with

$$c_1 = nB$$

and

$$c_2 = B - (1 + A)$$

Hence (2.65) becomes

$$R_p = \frac{nB + n_s(\lambda - 1)}{\lambda + \frac{A}{\lambda} - (1 + A) + B} \quad (2.67)$$

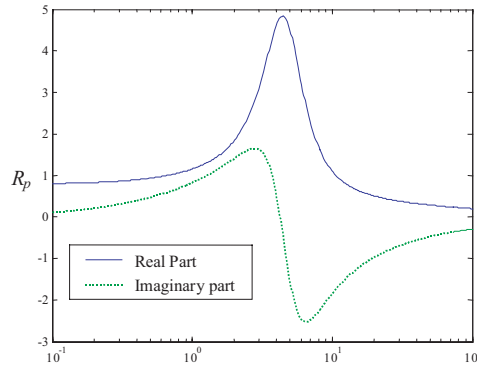


FIGURE 2.14. Real and imaginary parts of a QSHOD response function computed with equation 2.67: $n_s = 0$, $A = 6.0$, $B = 0.60$.

Figure 2.14 shows typical results for the real and imaginary parts of this formulas when $n_s = 0$. Experimental results given in the following section have long established that the QSHOD model captures a major contribution to the dynamical behavior, due to unsteady heat transfer in the condensed phase. Thus it is important to understand the preceding analysis. However, even with the large experimental errors associated with all current experimental methods, it seems there is little doubt that other dynamical processes cannot be ignored for many propellants, especially in the range of frequencies above that where the broad peak of the real part of R_p appears.

An important reason for retaining pressure dependence in the pyrolysis law for the transformation solid→gas (cf. equation 2.30) is that $R_p \neq 0$ if $n_s \neq 0$ even though $n = 0$, so the steady burning rate is independent of pressure. The experimentally observed presence of pressure coupling for ‘mesa’ propellants has long been an ill-explained feature of unsteady surface combustion still not well understood. More generally, n should be taken as a function of pressure, a behavior reported in several of the references cited but not covered here. See especially reports by the group at NWC (later NWAC).

A second deficiency of the QSHOD model of surface combustion response is that it contains no dependence of the mean burning rate on oscillatory pressure. This effect had been reported already in some of the earliest works on oscillations in solid rockets (for some measurements see Crump and Price 1961 and Eisel 1964). Figure 2.15 shows two examples. The observed changes of mean burning rate and mean pressure with oscillatory conditions in a chamber is indeed a complicated and by no means well-understood matter. In a motor, the oscillatory pressures and velocity (‘velocity coupling’) may both affect the mean burning rate and pressure in ways which are quite likely to depend on the distributions of those quantities along the burning surface. Consequently, the internal configuration of the propellant grain may be a significant factor. Thus it is evident that a single response function defined for oscillatory pressures is only part of the story.

2.2.3. Measurements of the Response Function; Comparison of Experimental Results and the QSHOD Model. For more than forty years, measurement of the response function has been the most important basic task in research on combustion instabilities in solid rockets. That problem still exists. Without accurate data, the truth of theoretical results cannot be assessed; predictions and interpretations of instabilities in motors are uncertain; and the ability to screen propellants for optional behavior is seriously compromised. Unfortunately, no entirely satisfactory method exists for accurate measurements of the combustion response over practical range of operating conditions, irrespective of cost. Two recent final reports of extended programs (Culick (editor), 2002, Caltech MURI; and Krier and Hafenrichter (editors), 2002, UIUC MURI) have led to this conclusion after five years’ investigation of the five main existing methods:

- (i) T-burner
- (ii) ultrasonic apparatus
- (iii) laser recoil method
- (iv) magnetohydrodynamic method
- (v) microwave technique

A sixth method based on using a burner (e.g., an L^* burner) in which bulk oscillations are excited, was not investigated, partly because it is intrinsically limited to relatively low frequencies.

It is not our purpose here to review these methods; see the two MURI reports, Cauty (1999), and references contained in those works for discussions of all but the last method. The microwave technique was introduced in the 1970s (Strand *et al.* 1974, 1980) and has been continually improved, but the accuracy of the data remains inadequate, particularly for metallized propellants for which the method is useless under some conditions. The last work with the device was done in the late 1990s by a group in Russia and reported by Zarko (1998).

(a) Examples of Early Data. The ultimate question for modeling and theory is: how good is the agreement between predicted and measured values? It appears that the first extensive comparison for this purpose were carried out many years ago (Beckstead and Culick, 1971) soon after the recognition that all the available models/analyses were equivalent to the QSHOD (A,B) model. With only two parameters available to adjust the theoretical results to fit data, the task of comparing theory and experiment became manageable. At that time, only T-burner and limited L^* -burner data were available. Figures 2.16 and 2.17 show two results.

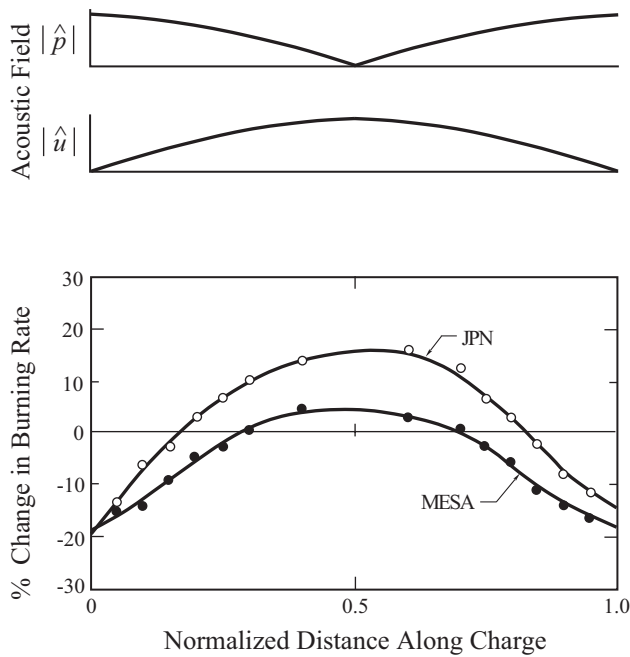


FIGURE 2.15. Experimental results for the change of burning rate of two double-base propellants (Crump and Price 1961).

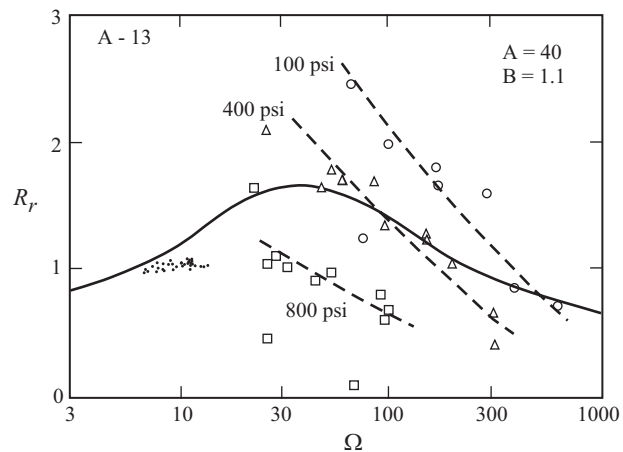


FIGURE 2.16. The real part of the response function vs. the non-dimensional frequency, $\alpha_t \omega / r^2$ for A-13 propellant: the solid curve is calculated from the QSHOD formula for the values of A and B shown; the dashed curves represent the T-burner data at the indicated pressures (Beckstead and Culick 1971).

One purpose of the report by Beckstead and Culick was to combine the formula for the QSHOD response function with results obtained from analyses of the T-burner and the L*-burner to obtain formulas for the parameters A and B in terms of measurable quantities. The main conclusion was that unique values of A and B could not be obtained for a given propellant tested at a chosen value of operating pressure. Consequently, large differences existed between the data and curves of the sort shown in Figure 2.16 and 2.17.

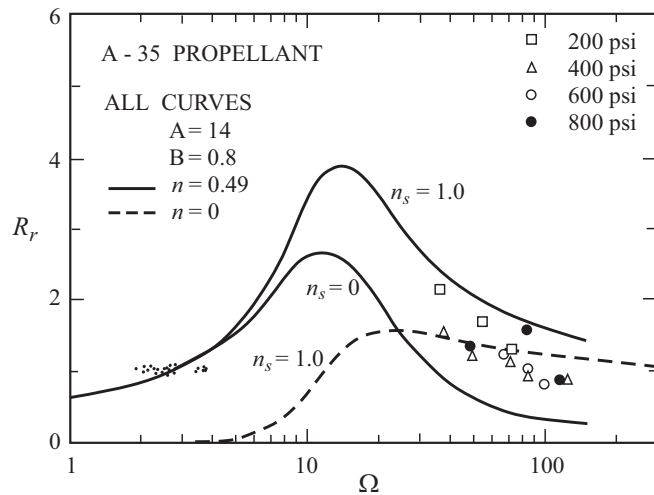


FIGURE 2.17. The real part of the response function vs. the non-dimensional frequency for A-35 propellant; the curves were calculated from the QSHOD formula (Beckstead and Culick 1971).

Since that time, many examples of using the A, B model to fit data have been given. Most, if not all, approach the matter as a two-parameter (A and B) curve fitted to data for the real part of the response function only. Strictly, that tactic is incorrect and could produce misleading results. The proper approach requires that the two-parameter representation be used to fit *simultaneously* the real and imaginary parts of the response function. There are also cases in which investigators have failed to respect the distinction between the response function $R_p \sim m'/p'$ and the admittance function $A_p \sim u'/p'$ defined for velocity fluctuations. That error arises due to failure to recognize which quantity a particular method actually measures. For example, T-burners give R_p directly, but the magnetohydrodynamic method provides data for A_p because it measures the unsteady velocity of the combustion products near the burning surface.

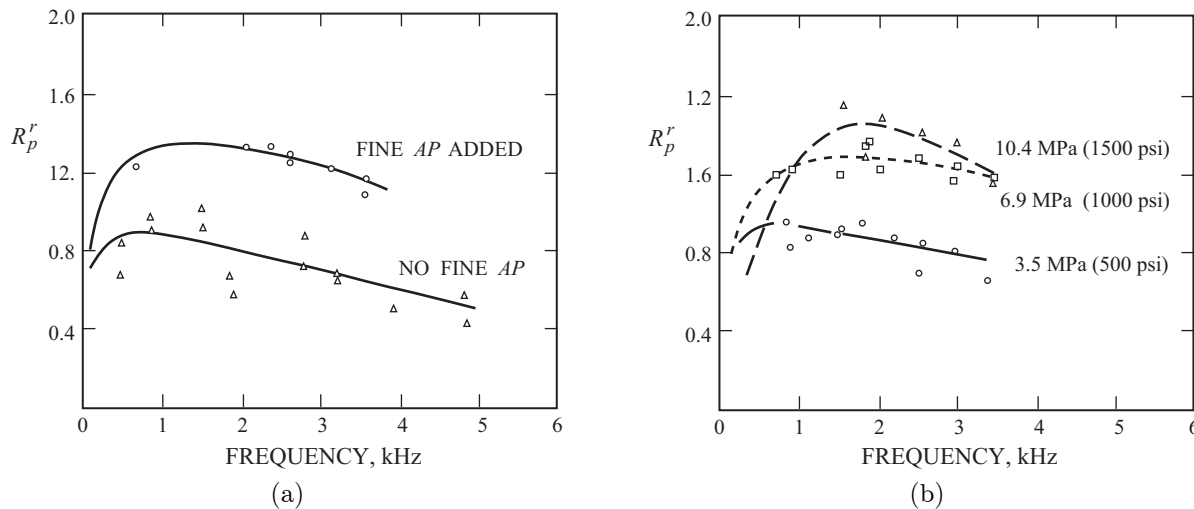


FIGURE 2.18. Real part of the response function measured with T-burners (Price 1984).

The apparent reduction of the real part of the response function when the mean pressure is reduced, more clearly shown by the latter data plotted in Figure 2.16, seems to be a common trend. Fifteen years later,

Price (1984) reported similar results plotted in Figure 2.18. Although the pressure dependence of the surface reaction ($n_s \neq 0$) does seem to explain some of the trend, there still is no incontrovertible explanation. It's just one of many incomplete topics on the subject.

Without attention paid to those points, any comparisons between data and a model are suspect. Even accounting for those common deficiencies, there is no doubt that the QSHOD model cannot and does not accurately represent the dynamics of actual propellants. One would anticipate without experimental results that the assumption of quasi-steady behavior in the gas phase must fail at high frequencies, commonly believed to be around 1000 Hertz and higher. Moreover, observations of steady combustion have shown that important decomposition processes take place in the sub-surface zone near the interface of most propellants. Hence at least two improvements of the QSHOD model should be made.

(b) Some Results from the MURI Program. During the past 40–45 years an immense amount of data has been collected for the combustion dynamics of solid propellants. Some are accessible; much is not. It is inappropriate here to try to give a thorough survey; it seems best in this limited space to quote a few results from the most recent publications, covering work carried out in the period 1996–2001 in the Caltech and UIUC MURI programs cited above. The research spanned the broadest possible range of activities from basic propellant chemistry and synthesis to motor dynamics. Work in the research groups included a complete range of experimental methods; modeling; theory and analysis; and numerical simulations, all for both steady and unsteady combustion of propellants.

Three classes of propellants were tested, to determine their burning rate laws and their dynamical behavior. Table 2.2 summarizes the main characteristics distinguishing the propellants in the three groups referred to as Phase I, Phase II and Phase III. Further details and the chief motivations for selecting those propellants are included in Attachment A of the Caltech MURI Final Report. All propellants were provided to all research groups measuring response functions.

TABLE 2.2. Principal Characteristics of the MURI Propellants.

	Manufacturer	Oxidizers	Binders	Remarks
PHASE I	Thiokol, Inc.	AP	HTPB	<ul style="list-style-type: none"> plateau and biplateau propellants 11 formulations including reduced smoke and smokeless
PHASE IIA	Thiokol, Inc.	AP	BAMMO/AMMO with GAP	<ul style="list-style-type: none"> two formulations reduced smoke and smokeless
PHASE IIB	CSD, Inc.	AP/HMX	HTPB/GAP	<ul style="list-style-type: none"> five aluminized formulations, one with some AP replaced by HMX and one with GAP replacing HTPB AP size distributions varied
PHASE III	Alliant Techsystems, Inc.	AP	Nitrato-type energetic binders	<ul style="list-style-type: none"> seven formulations including four aluminized and three smokeless

2.2.4. The Zel'dovich-Novozhilov (Z-N) Model. Zel'dovich (1942) was first to consider true combustion dynamics for solid propellants. He was concerned with problems of transient burning—i.e. what happens to combustion of a propellant when the impressed pressure is changed rapidly—but not explicitly with the response function. Novozhilov (1965) later used Zel'dovich's basic ideas to find a formula for the response of a burning propellant to sinusoidal oscillations of pressure. The result has exactly the same dependence on frequency as the QSHOD model, i.e. it is identical with the formula obtained by Denison and Baum (1961) four years earlier.

The basic Z-N model incorporates quasi-steady behavior of the burning in a clever and instructive fashion. Moreover, the parameters—there are, of course, two corresponding to A and B in the QSHOD model—are so defined as to be assigned values from measurements of steady combustion of the propellant in question. Hence there is no need to become enmeshed in the details of modeling the combustion processes in the gas phase. If the measurements could be done accurately, it would be possible to obtain good predictions of the combustion response for propellants, subject of course to all the assumptions built into the QSHOD model. Unfortunately, the required quantities are difficult to measure accurately. Confirmation of the results still requires measurements of both the real and imaginary parts of the response function and comparison with the predictions of the model.

The condensed phase and interfacial region are treated as described in Section 2.2 for the QSHOD model. Instead of detailed analysis of the gas phase, that is, construction of a “flame model”, the assumption of quasi-steady behavior is applied by using relations among the properties of steady combustion, the burning rate and the surface temperature as functions of the initial temperature of the cold propellant and the operating pressure:

$$\begin{aligned} m &= m(T_c, p) \\ T_s &= T_s(T_c, p) \end{aligned} \quad (2.68)a,b$$

The assumption is also made that these functions are known sufficiently accurately that their derivatives can also be formed, introducing the four parameters

$$\begin{aligned} \nu &= \left(\frac{\partial \ln \bar{m}}{\partial \ln \bar{p}} \right)_{T_c} \\ \mu &= \frac{1}{\bar{T}_s - T_c} \left(\frac{\partial \bar{T}_s}{\partial \ln \bar{p}} \right)_{T_c} \\ k &= (\bar{T}_s - T_c) \left(\frac{\partial \ln \bar{m}}{\partial T_c} \right)_{\bar{p}} \\ r_{ZN} &= \left(\frac{\partial \bar{T}_s}{\partial T_c} \right)_{\bar{p}} \end{aligned} \quad (2.69)a,b,c,d$$

Subscript *ZN* is attached to *r* to distinguish it from the linear burning rate. It is not apparent from the remarks here why the four parameters (2.69)a–d are significant in this theory; see the works of Novozhilov (1965 and later).

Recall that in Section 2.2 the sole reason for analyzing a model of combustion in the gas phase was to produce a formula for the heat feedback, $\lambda_g(\partial T / \partial x)_{s+}$, to the interface. That is the central problem here as well: to find the heat feedback from considerations of steady combustion and assume (the quasi-steady approximation) that the form of the result holds under unsteady conditions. The trick is to work out the relation between the feedback and the properties of steady combustion. It is in that process that the parameters (2.69)a–d appear.

The formula for the response function corresponding to (2.67) is usually written (e.g., Cozzi, DeLuca and Novozhilov 1999)

$$R_p = \frac{\nu + \delta(\lambda - 1)}{r_{ZN}(\lambda - 1) + k \left(\frac{1}{\lambda} - 1 \right) + 1} \quad (2.70)$$

where

$$\delta = \nu r_{ZN} - \mu k \quad (2.71)$$

Comparison of (2.67) and (2.70) gives the formulas connecting the parameters in the two formulations:

$$A = \frac{k}{r_{ZN}}, \quad B = \frac{1}{k}, \quad n = \nu, \quad n_s = \frac{\delta}{r_{ZN}} \quad (2.72)$$

Much emphasis has been placed in the Russian literature on the “boundary of intrinsic stability,” the locus of values of (A,B), or (k, r_{ZN}) for which the denominator of (2.70) vanishes¹⁶. Under those conditions, the propellant burn rate suffers a finite perturbation in the limit of a vanishingly small change of pressure. Hence, from measured values of ν and r_{ZN} , one can infer how close an actual propellant is to that stability boundary.

With these models, the opportunity exists to use experimental results to determine how accurately the QSHOD approximations capture the combustion dynamics of solid propellants:

- (i) infer ν, μ, k, r_{ZN} from tests of steady combustion;
- (ii) measure the real and imaginary parts of R_p ;
- (iii) compute R_p from (2.67) or (2.70) and compare with (ii)

There seem to be no published reports of results for this procedure, although some results exist for predictions related to the boundary of intrinsic stability.

Novozhilov and his co-workers have investigated many other detailed aspects of the combustion dynamics. However, experimental data to confirm the theoretical results either don’t exist or are too sparse to allow definite conclusions. Hence despite the value of those results, we will not discuss them here.

2.2.5. Revisions and Extensions of the QSHOD Model. As we have already noted in Section 2.2.3, even with the large uncertainties accompanying the experimental results obtained with current methods, it is clear that the QSHOD model does not capture some important dynamical processes. Considerable effort has been devoted to improving the model, with a certain amount of success, but unfortunately the deficiencies in the experimental procedures still prevent definitive identification of the most significant contributions. Thus there is only weak justification for developing three-dimensional models of the processes for practical purposes. It seems that much is still to be gained by investigating extensions of the QSHOD model.

Attention has been given to all three of the regions sketched in Figure 2.12. It is important to recognize that simply changing the model for steady combustion—for example including a finite zone of decomposition in the solid phase—will *not* change the form of the QSHOD result. To affect the frequency dependence of the response function, any additional spatial zones or processes must also contain new dynamics (see, for example, Culick 1969). One cause of ‘new dynamics’ is spatial non-uniformity of material properties when conductive heat transfer is the dominant unsteady process. Here we attend mainly to contributions from different processes which conceivably change the dynamics.

¹⁶This condition is analogous to the way in which instabilities are defined for a classical control system by finding the poles of the appropriate transfer function

(a) Additional Dynamics in the Condensed Phase. It seems that three types of processes have been considered as modifications of the basic model of the condensed phase discussed in Section 2.2.2:

- (i) temperature-dependent thermal properties;
- (ii) phase transitions; and
- (iii) decomposition zones.

Louwers and Gadiot (1999) have reported results for numerical calculations based on a model of HNF. Melting at some interface within the condensed phase is accounted for, as well as energy released by sub-surface reactions. Combustion in the gas phase is also treated numerically. The computed response functions show that the new processes may increase the values of $R_p^{(r)}$ by as much as 10–30% and more in the frequency range above the peak. The peak value is unchanged.

Brewster and his students at the University of Illinois have produced a number of interesting works treating additional dynamics related to chemical processes in the condensed phase and at the interface (Zebrowski and Brewster, 1996; Brewster and Son, 1995). Much attention was given to this matter in the MURI Programs (Culick 2002, Krier and Hafenrichter 2002). Gusachenko, Zarko and Rychkov (1999) have investigated the effects of melting in the response function, finding quite significant consequences. Lower melting temperatures and larger energy absorption in the melt layer increase the magnitude of the response function.

Cozzi, DeLuca and Novozhilov (1999) worked out an extension of the Z-N method to account for phase transition at an infinitesimally thin interface in the condensed phase. The analysis includes new dynamics by allowing different properties of the thermal waves on the two sides of the interface. Additional heat release is allowed only at the interface of the transition and with conversion of condensed material to gaseous products. They found that the response function is increased by exothermic reaction at the internal interface and by reduced temperature of the phase transition.

(b) Additional Dynamics in the Gas Phase. DeLuca (1990; 1992) has given thorough reviews of the various models proposed for the gas phase. Most, however, involve no dynamics, so there are no effects on the dependence of the response function on frequency. An example of truly dynamical effects is covered in the next section, with references to previous works.

2.2.6. Some Results for a Special Extension of the QSHOD Model. The results summarized in this and the following section have been reported in a Ph.D. Thesis (Isella, 2001) and in four publications (Culick, Isella and Seywert, 1998; Isella and Culick, 2000a; 2000b; 2002). A purpose of the works was to address in a small way some of the questions raised in our discussion of prior results. Chiefly two general problems have been addressed in those works:

- (1) develop a simple general analysis of the combustion dynamics of a solid propellant that will conveniently accommodate models of the relevant chemical and physical processes, especially those in the interfacial region; and
- (2) investigate the influences of small changes in the combustion response function on observable features of the combustor dynamics, particularly properties of limit cycles.

Both of those problems were chosen to determine answers to the question: what properties of a solid propellant are responsible for the often observed sensitivity of the dynamics of a solid rocket to apparently small (sometimes not well-known) changes in the composition of the propellant. The main conclusions are:

- (i) small changes in the composition and thermodynamic properties of a propellant have significant consequences for dynamical behavior due to pressure coupling **only** if the propellant is burning near its intrinsic instability boundary; and
- (ii) on the contrary, the dynamics due to velocity coupling may be much more sensitive to small compositional changes.

We do not compare with experimental results, and some of the behavior found may be unrealistic. Our purpose is partly to demonstrate by some examples the sort of behavior one can obtain by altering the basic QSHOD model. It seems that this strategy is an effective means of exploring possibilities in a quantitative fashion. The very important task of establishing which processes are important (and under what condition) has for the most part not been accomplished.

If the conclusions are true, then future work in the area of combustion instabilities must include intensive attention to modeling and measuring the combustion dynamics—i.e. the response function—associated with velocity coupling. In any case, there are several reasons arising with observed behavior of combustion instabilities in solid rockets that velocity coupling should receive more attention than planned.

(a) The Model Framework. One important purpose of the work cited above was to construct a framework within which it would be possible easily to investigate the consequences of various processes participating in the combustion of a solid. Representation of the combustion dynamics must be in a form required for analyzing the global dynamics (Section 3.3). The simplest approach is an extension of the well-known one-dimensional analysis producing the QSHOD response function for pressure coupling (Culick 1968; Beckstead *et al.* 1969; T'ien 1972; among many works). Others have followed a similar tack (e.g., Louwers and Gadiot 1999). The main novel aspects of the work described here are inclusion simultaneously of surface physical dynamics (e.g., due to mobility of liquid or solid particles); dynamics, rather than quasi-steady behavior, of the gas phase; and an elementary representation of velocity coupling. The behavior we find (calculate) may not be realistic in all cases. Our main purpose is to show one way in which the QSHOD model can be used is the initial approximation in a procedure to examine possible consequences of departures from the simplest model.

On the submillimeter scale, a burning solid is heterogeneous both in the region adjacent to the interface and in the gas phase where much of the conversion to products takes place. The flow field in the chamber, in particular the unsteady acoustic field, has spatial variations normally of the order of centimeters and larger. The dynamics of the combustion processes at the surface are formally accommodated as a boundary condition, a response function of some sort, in the analytical framework for the global dynamics. Hence the vast difference in characteristic scales is accommodated, in principle, by spatially averaging the combustion dynamics. The averaging is done over a surface in some sense far from the interface so far as the propellant combustion is concerned, but practically at the interface so far as the field within the chamber is concerned. In that way, the results of solution to the “inner” problem of combustion dynamics in the surface region are used as the boundary conditions for solution to the “outer” problem of the unsteady flow field in the chamber.

We are not concerned here with the matter of spatial averaging: We assume it can be done, although it may not necessarily be an easy or obvious process. It's an important part of the general problem. Therefore we proceed from the beginning with a one-dimensional analysis. The spatial framework for the model is shown in Figure 2.19.

The strategy of the analysis is not novel and has been used in many previous works: Solve the relevant equations, or postulate a model, governing the behavior in each of the three regions: solid phase; surface layer; and gas phase, including the region called ‘combustion zone’ in Figure 2.19. A major purpose of the analysis has been to determine the quantitative effects of the dynamics in the surface layer and gas phase

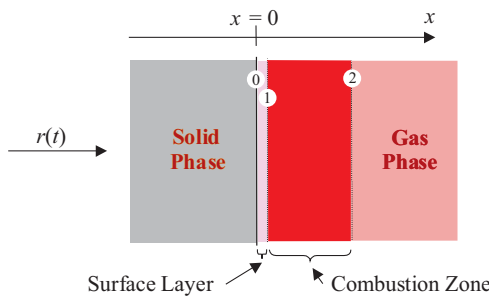


FIGURE 2.19. Spatial definition of the model.

on the response function found from the QSHOD model. Hence throughout the work we assume the same model for the solid phase: The basic dynamics is due to unsteady heat transfer in a homogeneous material having uniform and constant properties.

Separate solutions or representations are obtained for each of the three regions. Unspecified constants or functions are then eliminated by satisfying boundary conditions and applying matching conditions at the two interfaces. Initially the authors intended to find such a form for the general behavior that different models for the surface layer and gas phase could easily be substituted and their consequences assessed. That goal has not been realized and probably is unattainable in a simple form. Results require detailed numerical calculations before interesting information is obtained.

(b) Models of the Surface Layer. An important motivation this work was the idea that because the dynamics of the gas phase are fast (owing to the relatively low material density), then the dynamics of the surface region should have greater effect on the combustion response function in the range of lower frequencies covering the resonances of many practical rockets. Two models of the region have been examined in the analysis:

- (i) first order dynamics represented by a constant time lag; and
- (ii) unsteady heat transfer, with material properties different from those in the solid phase.

The idea of using a time lag is of course an old one, having been used by Grad (1949) in the first analysis of combustion instabilities in solid propellant rockets, and later by Cheng (1954)a,b as part of the Princeton group's extensive investigations (a sort of technical love affair) of time lag representations of unsteady combustion. The result (Isella 2001) for the fluctuation of mass flux is

$$\frac{m'/\bar{m}}{p'/\bar{p}} = R_p \frac{e^{-i\Omega t}}{\sqrt{1 + (\Omega t)^2}} \quad (2.73)$$

where R_p is the response function found in the QSHOD theory. Thus R_p has the familiar two-parameter (A,B) representation. The dimensionless frequency is Ω , eq. (2.26) τ is the dimensionless time lag, equal to the physical time lag divided by κ_p/\bar{r}^2 . Figure 2.20 shows a typical result ($A = 14$; $B = 0.85$; $\tau = 1.5$). The graphs illustrate clearly a basic problem with a time lag theory: if the time lag is assumed constant (i.e. independent of frequency) the response (in this case the real part) possesses an oscillatory behavior with period increasing with frequency. Such behavior has never been observed in experimental results and is a consequence of an incorrect assumption, namely that the time lag is constant.

It is true that any response function for linear behavior can be written in a form showing a time lag, but in general the time lag varies with frequency (Culick, 1968). If the physical model is sufficiently detailed,

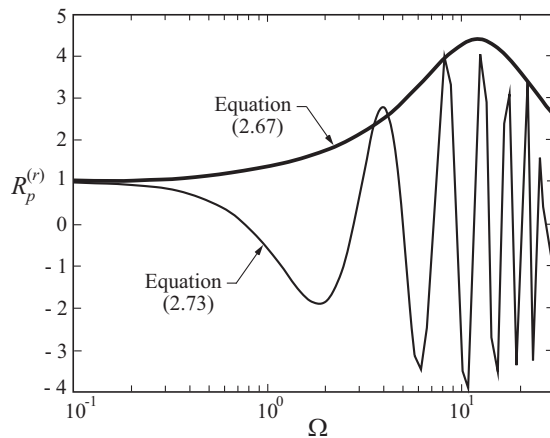


FIGURE 2.20. QSHOD response function with a time lag: thick line: QSHOD theory with $n_s = 0, A = 14, B = 0.85$; thin line: QSHOD model including a surface layer having first order (time lag) dynamics.

the dependence of τ on frequency is found as part of the solution. In particular, the QSHOD theory gives $\tau(\Omega)$ such that the amplitude of the response function decays smoothly for frequencies higher than that at which the single peak occurs.

The second model for the surface is the only one considered for the results discussed here. It is based on a simple representation of the dynamical behavior making use of the same solution as that for the homogeneous solid phase, with two differences:

- (i) the uniform and constant properties are different from those of the condensed solid material;
- (ii) the solution is forced to satisfy matching conditions of continuous temperature and heat transfer at the interfaces with the condensed phase and the gas phase.

(c) Models of the Gas Phase. In the following analysis, all combustion processes are assumed to occur in the gas phase; upstream, only phase changes are accounted for, assumed to take place at the interfaces. We assume distributed combustion of a simplified form, a single one-step reaction as previous treatments have used (T'ien, 1972; Huang and Micci, 1990; Lazmi and Clavin, 1992). Solutions must then be found numerically for the steady and linear unsteady temperature distributions, and subsequently matched to the solution for the surface layer. For details, consult Isella (2001) and other references cited there and at the beginning of this section.

2.2.7. Some Results for the Combustion Response Function. Many experimental results exist suggesting that the responses of actual propellants tend often to be higher than that predicted by the QSHOD model for some ranges of high frequencies; and possibly the existence of peaks in addition to that associated with unsteady heat transfer in the condensed phase. Initially the strongest motivation for much work on the response function has been the need to determine in simple and relatively crude fashion what processes might have greatest effect on the values of the pressure-coupled response at frequencies greater than that at which the peak magnitude occurs. Roughly what that means is finding one or more processes having 'resonant behavior' or characteristic times in the appropriate range. Unfortunately the analysis is sufficiently complicated that it has not been possible yet to deduce any explicit 'rules of thumb.' Therefore, we present here a few plots of computed results to illustrate the behavior. What we find may not be realistic.

A purpose here is to illustrate what one may learn with a simple procedure. The basic or reference response function computed from the simple QSHOD model is that shown in Figure 2.14. Influences of dynamics in the surface layer and gas phase will be shown relative to that reference. Because of the immediate availability of the results we extract details from the thesis prepared by Isella (2001). We will not compare the results with observed behavior. The purpose here is only to show possible indications of deviations from the basic QSHOD model, due to several well-defined processes.

(a) Influence of Gas Phase Dynamics. Figure 2.21 is the result when only the dynamics in the gas phase is added to the QSHOD model. The results are similar to those found by T'ien (1972) and Lazmi and Clavin (1992), not a surprising conclusion. As expected, the dynamics of the gas phase introduce a single additional peak in the real part of the response function ($\sim m'/p'$). Due to the density fluctuation $p'(m'/\bar{m} = \rho'/\bar{p} + v'/\bar{v})$, the real part of the admittance function ($\sim v'/\bar{v}$) shows a negative depression where the real part of the response function R_p has a rise.

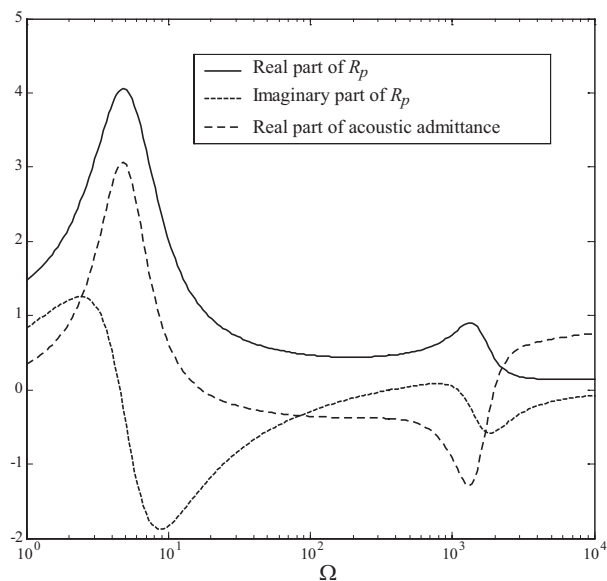


FIGURE 2.21. Combustion response, QSHOD model with gas phase dynamics (Isella 2001; Isella and Culick 2000).

(b) Combined Influences of the Dynamics of the Surface Layer and the Gas Phase. The dynamics of the surface layer itself are the same as those of the condensed phase, but with different values of the defining parameters. Figure 2.22 illustrates the effects of changing the surface activation energy and the material density on a function characterizing the response of heat transfer in the layer. The shape of this function differs from that (Figure 2.14) of the basic response function because it is affected by the dependence of several flow variables on frequency.

Finally, Figure 2.23 shows the result for one example of the response function with the dynamics of both the surface layer and the gas phase accounted for. Evidently for the conditions examined here the dynamics of the gas phase has a greater effect on the response, in the higher frequency range, than does the surface layer.

2.2.8. The Combustion Response and Possible Sensitivity of Global Dynamics to Velocity Coupling. A fundamental problem for practical applications concerns connections between the unsteady motions taking place in a motor and the features of the combustion processes responsible for that behavior.

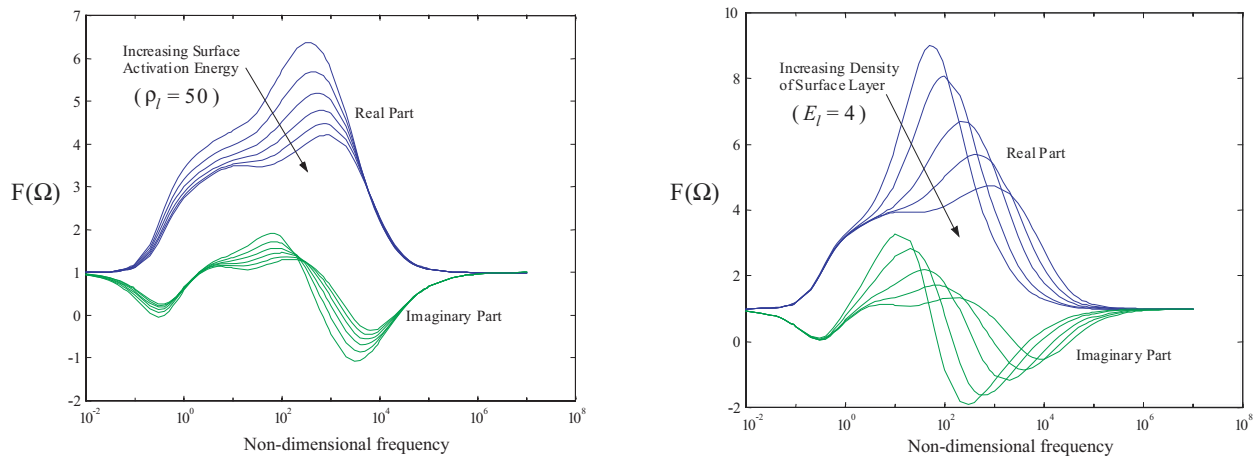


FIGURE 2.22. Effects of activation energy and density on the dynamics of the surface layer (Isella 2001; Isella and Culick 2000).

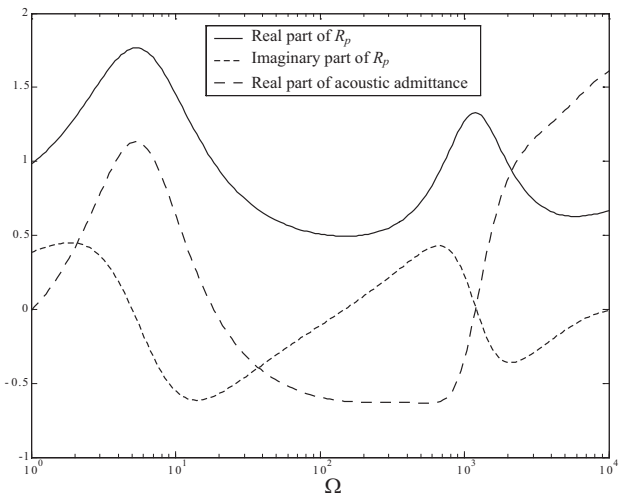


FIGURE 2.23. Combustion response function including the dynamics of the surface layer and the gas phase (Isella 2001; Isella and Culick 2000).

This is far from a solved problem, but we are able to make some tentative observations in respect to both linear and nonlinear characteristics that have already been observed or might be expected.

We will often use the term *global dynamics* to mean the dynamical behavior of the system in question, a combustion chamber, its source of energy and, in some cases, peripheral equipment. Thus we intend the term to have a general meaning, but generally we really mean global dynamics as indicated by the evolution of the unsteady pressure. Recall that the pressure is the one variable we always have available, and it is often the only variable measured. In this section we are examining only computed results interpreted as far as possible in respect to physical behavior. Hence we have at our disposal not only the amplitude of the entire motion, but the amplitude of harmonics as well.¹⁷

¹⁷The phases of the motion are also available but we will not consider them here.

In certain respects, the behavior discussed in this section is well beyond the preparation provided so far. We will be examining, without clarifying the basis, certain consequences of the dependence of nonlinear behavior on linear behavior. The main indicator is the amplitude of the limit cycle, or the amplitudes of the modal components of limit cycles. It happens, as we will see in Chapter 7, that the nonlinear gasdynamics do not introduce physical parameters other than the properties of the gas. Thus when the linear parameters—the growth rate and phase for each mode—are changed, those changes are reflected directly in the limit cycle. In other words, the amplitudes in the limit cycle serve as a diagnostic revealing the consequences of changes in the linear processes. Put another way, we evidently have a means of investigating the consequences for the global dynamics of modifying the linear behavior of the system

The idea of somehow connecting linear and nonlinear behavior is of course not new, and is widely applied in other fields. For example, without having a nonlinear theory as a basis for quantitative reasoning, early discussions by Price, McClure and others used observations as the basis for discussing the subjects treated here. We will not review experimental results. Levine and Culick (1972, 1974) appealed to both numerical calculations and an early form of the analysis developed here in Chapters 3 and 4 to investigate some properties of limit cycles with modest success. The approach was greatly extended by Levine and Baum (1984, 1985) who produced substantial results. They obtained the first quantitative theoretical results for subcritical bifurcations (pulsed instabilities) in solid propellant rockets. To obtain those results they needed a nonlinear response function, explained in Section 7.11. Burnley (1996) and Burnley and Culick (1997) confirmed a conclusion reached by Levine and Baum (1983) that a requirement for the subcritical bifurcation seemed to be that the response should contain both velocity coupling and a threshold velocity (Section 7.11). The question of what behavior of the response function is necessary remains open. Experimental results support the results qualitatively, but there seems to be little possibility at the present time of making firm quantitative connections with theory.

Currently an unsolved problem is the occasionally observed apparent sensitivity of the global behavior to relatively small changes of propellant composition (see remarks (i) and (ii) in the introductory part of Section 2.2.6). We assume that small changes of composition likely have relatively small effects on the magnitude and phase of the response function. Therefore, we are really investigating the effects of small changes in the response function on the observable global dynamics. The main (but tentative) conclusion is that the sensitivity of the dynamics to changes in the response associated with velocity coupling may be significantly greater than that for the response due to pressure coupling. The implications for directions in future research are substantial.

Isella (2001) and Isella and Culick (2000) have reported the main results. Here we will only cite a couple of examples. The idea is to use the framework described in Section 3.2 below to compute the growth and limiting amplitudes for limit cycles. Essentially a modest parameter study has been done, the response function itself (i.e. the combustion dynamics) being the parameter. Following the presentation first introduced by Culick, Isella and Seywert (1998), it is helpful to display the response function as a function of frequency, and the amplitudes of the modes forming a limit cycle, as two parts of the same figure, such as Figure 2.24 prepared as a typical case for the QSHOD response function. The vertical lines in the upper parts of the figures identify the non-dimensional frequencies. For these calculations the model chamber is cylindrical, 0.6 m long, 0.025 m in diameter, operated at a chamber mean pressure equal to 1.06×10^7 Pa. It is the same motor considered previously by Culick and Yang (1992).

Figures 2.24–2.27 show results obtained for the same motor and basic combustion response but including, respectively, surface layer dynamics; a time delay; and dynamics of both a surface layer and gas phase, all according to the analysis described above.

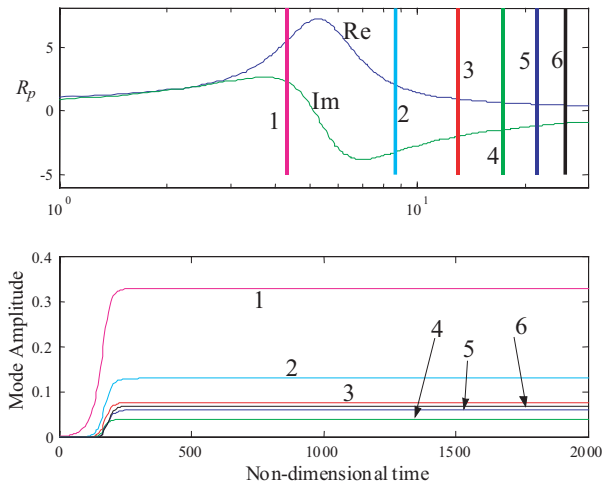


FIGURE 2.24. Results of a simulation with a QSHOD combustion response (pressure coupling: $A = 8.0$, $B = 0.6$, $n = 0.8$) (Isella 2001).

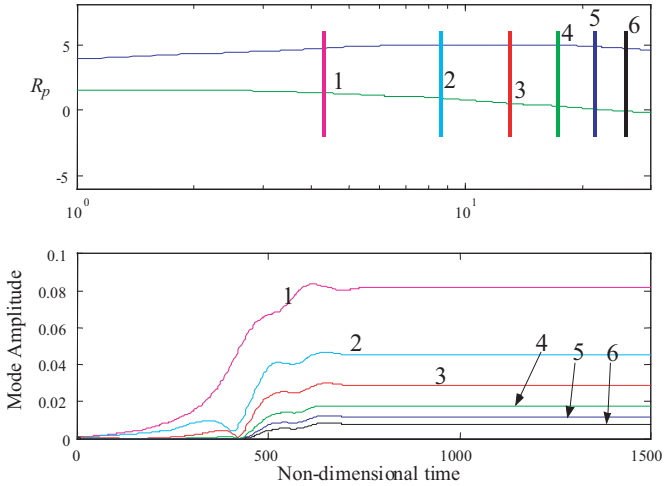


FIGURE 2.25. Results of a simulation including dynamics of a surface layer (Isella 2001).

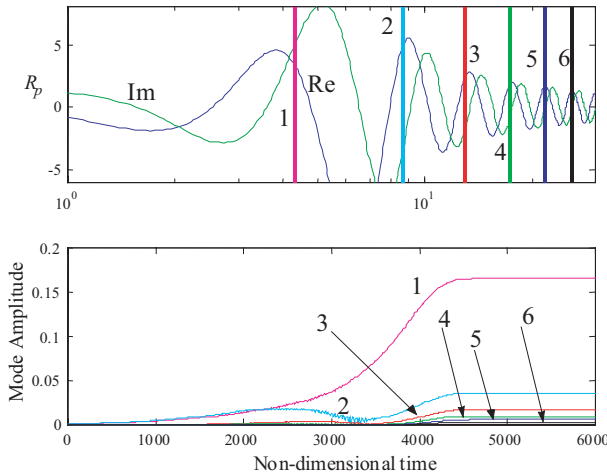


FIGURE 2.26. Results of a simulation including a time delay ($\tau = 1.5$) (Isella 2001).

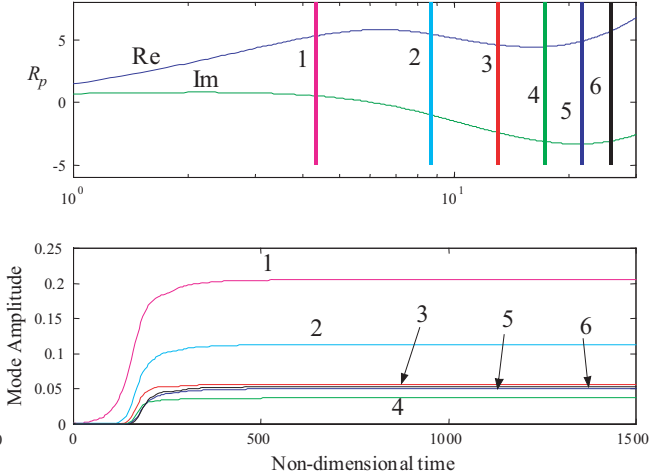


FIGURE 2.27. Results of a simulation including dynamics of a surface layer and the gas phase (Isella 2001).

Owing to the significantly different dynamics added to the basic QSHOD model, the three examples illustrated in Figures 2.26–2.27 show quite different response functions—all, it must be emphasized, representing responses due to pressure coupling. The question here concerns indirectly the sensitivity of the response function to changes of composition (not the qualitative dynamics) and consequently the sensitivity of the global chamber dynamics.

In general, models based on pressure coupling do not seem to show dramatic sensitivity of the combustor dynamics to small changes of composition. That result motivates investigation of similar problems with a simple model of the response due to velocity coupling. The idea is based on the model introduced by Levine and Baum (1988). This work is discussed at greater length in Section 7.11.1.

Some recent work done on the dependence of the global dynamics on the functional form of the equations used in the analysis by Ananthkrishnan *et al.* (2002, 2004) seems to show that the absolute value of the velocity itself, as it appears in a simple model of velocity coupling, is sufficient to produce a subcritical bifurcation (pitchfork) followed by a fold (saddle-node bifurcation). Those ideas are developed further in Chapter 7; the point is that a subcritical bifurcation, followed by a fold or turning point, provides conditions under which pulsed or triggered nonlinear instabilities may exist. Although we have not yet firmly established the point, it seems that with the QSHOD basic model, the dynamics of a chamber seems to be much more sensitive to velocity changes than pressure changes. The conclusion is apparently related to the way in which the global dynamics depends on the unsteady velocity and the phases established among the components of the motion. That is not a startling result in view of the different forms of the combustion terms provided by velocity coupling, in contrast to pressure coupling, in the modal equations.

2.2.9. Generation of Vorticity and Vortex Shedding. There are two phenomena of rotational flow that have significant influences on the stability and behavior of unsteady motions in solid propellant rockets:

- (1) generation of unsteady vorticity at burning surfaces; and
- (2) coupling between acoustical motions and large vortices shed at obstacles or growing out of the region adjacent to the lateral burning surface.

Both of these phenomena have motivated much interesting work that has flourished particularly in the past 10–12 years. Significant effort has been expended, mainly in the U.S. and France, on theory, analysis, numerical simulations and experiments. The reasons for the strong interests are different for the two processes. Both affect stability, but unlike the generation of distributed vorticity, shedding of large vortices has been unambiguously identified as a mechanism in several large rockets, notably the Shuttle SRM, versions of the Titan motor, and the Ariane 5 booster motors. Accordingly, several large research programs have been devoted to understanding the connections between vortex shedding and acoustic field. Blomshield and Mathes (1993) have given the most thorough discussion of the problem existing in the Shuttle motors. Much information exists in internal reports of continuing observations of Shuttle motors in flight, but little has been done to determine how the oscillations might be reduced.

In contrast, the corresponding problem in the Ariane 5 has been the subject of a great deal of work in France. See Vuillot and Casalis (2002) and several other papers in the course “Internal Aerodynamics in Solid Rocket Propulsion” given at the von Karman Institute (2002). The reason for the intensive concern has been the necessity to install vibration dampers between the solid boosters and the main vehicle. As a result, the payload has been reduced by a significant amount, apparently as much as two hundred kilograms.

(a) Generation of Vorticity. The generation of vorticity at a burning surface is special to solid rockets. It occurs whenever there is a variation of pressure fluctuation, and hence a fluctuating velocity, in the direction tangential to a surface from which there is average mass flow normal to surface into the chamber. The vorticity is created because the velocity inward is perpendicular to the surface—the ‘no-slip’ boundary condition. Imposition of a tangential velocity fluctuation, due to the non-uniform pressure along the surface, on the average inward flow constitutes an inviscid mechanism of vorticity generation. Moreover, conservation of mass in the region close to the surface causes a periodic pumping action normal to the surface. Both the vorticity generation and the pumping exist at the expense of work done by the impressed acoustic field and therefore must involve exchange of energy with the acoustic field in the chamber. Sketches of the two processes are shown in Figure 2.28.

An oversimplified and incomplete interpretation of the phenomenon due to the no-slip boundary condition is that the incoming average flow normal to the surface gains some kinetic energy because it must acquire

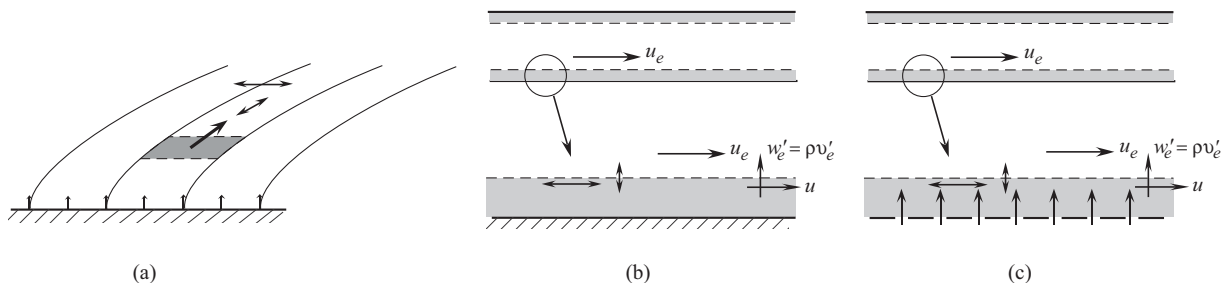


FIGURE 2.28. Sketches illustrating two primary processes involved in the generation of vorticity. (a) flow-turning; (b) 'pumping action': oscillatory motion parallel to the boundary, in the boundary layer, induces oscillatory motion normal to an impermeable wall; (c) similar to (b) with mean flow through the wall.

the oscillatory motion parallel to the surface. Thus there is effectively a "turning" of the flow in the direction of its passage out the nozzle. In a rocket chamber, for example a cylinder, both the average and unsteady velocities must become parallel to the axis of the chamber as the flow approaches the axis. The inelastic acceleration of the mass flow causes a loss that is the unsteady counterpart of the loss accompanying mass injection into a duct flow. This "flow-turning loss" was, not surprisingly, discovered in analysis of unsteady one-dimensional flow with mass injection at the lateral surface (Culick 1973). However, the connection with vorticity generation was not mentioned. It was Flandro (1995) who clarified the phenomenon in terms of the unsteady production of vorticity, emphasizing the central importance of the no-slip boundary condition. Flandro carried out the first rigorous formal analysis of the problem, work that has since prompted a stream of calculations on the basic problem at hand, as well as variations (among them are Majdalani, 1999; Kassoy, 1999; Majdalani, Flandro and Roh, 2000; Malhotra, 2004).

At least five processes must be considered to assess completely the net effect of distributed vorticity on the stability of acoustical motions in a combustion chamber:

- (i) the generation process, Figure 2.28(a);
- (ii) the 'pumping action', Figure 2.28(c);
- (iii) interaction of the vorticity with the acoustic field in the chamber;
- (iv) interaction of the vorticity with the exhaust nozzle; and
- (v) interactions between the generated vorticity waves and turbulence in the chamber.

In practice, the matter of stability in the context of combustion instabilities always means stability of pressure oscillations. It is often helpful to interpret stability in terms of growth or decay of acoustic energy, but care must be exercised: Because the problem *in toto* is very complicated, even in the limit of linear behavior it is easy to obtain misleading, or incorrect, results. The presence of the mean flow and the various paths of energy transfer make intuitive construction of an equation for the time evolution of acoustic energy a delicate task. To ensure accurate theoretical results, the formalism developed here in Chapters 3–7 seems to offer the best method; see, for example, Flandro (1995) and Section 6.9.

The 'flow-turning' contribution identified in the simple one-dimensional approximation by Culick (1972, 1973) was later shown by Flandro (1995) to be, surprisingly, exactly correct. Interpretation of the process, a loss of energy for the acoustic field, in terms of generation of vorticity cannot be accomplished within the one-dimensional approximation. It was somewhat misleading that Culick vaguely related the flow-turning loss to viscous processes associated, at least partly, with flow in the acoustic boundary layer, a speculation that misses the mark. That proposition led to calculations of corrections to the classical theory of the acoustic boundary layer (Flandro 1974, Vuillot and Kuentzmann 1986) which have been superceded by the

more recent works by Flandro (1995)a,b; Majdalani and Van Moorhem (1997) and Majdalani (2000) treat essentially the same problem but contain some errors of understanding.

Unfortunately, the pumping action associated with the generation of vorticity was missed by Culick in his one-dimensional analysis.¹⁸ Pumping in this context refers to a fluctuating velocity induced normal to the surface if the acoustic velocity tangential to the surface is not uniform, a direct consequence of continuity. This motion makes the surface appear as an effective oscillating piston tending, if the phase of the motion is suitable, to drive waves in the chamber. Flandro (1995) has shown that for a cylindrical chamber with uniform flow entering along the entire boundary, the net effect of the generation of vorticity and the pumping is zero for purely longitudinal acoustic modes. Whether or not this energy gain is accounted for is the origin of a controversy centered in the ‘true’ value of the flow turning, i.e. whether it is a loss, a gain, or has no net effect. At this point, the correct answer seems to be that there is no net effect for a cylindrical chamber, but the amount of loss or gain must be calculated separately for each geometry.

There is no question that the processes (i) and (ii) in the list given above are always present. Whatever may be the net effect on stability, due to these two contributions only, nevertheless waves of vorticity are generated at the surface and are carried by the average flow into the chamber. Subsequent interactions with the acoustic field in the chamber may cause energy transfer to or from the acoustic field—there seems to be presently no basis for giving a definite answer.

If the distributed vorticity survives passage to the nozzle, interactions with the non-uniform flow have no direct effect on the stability of acoustic waves. Any energy transferred between the vorticity waves and the mean flow has no consequences for the acoustic field. Thus, process (iv) will not contribute to stability. However, it is conceivable that those interactions may be accompanied by generation of pressure waves. The necessary analysis has not been carried out to determine whether the effect is stabilizing or de-stabilizing. Crocco and Sirignano (1964) have given the most thorough treatment of the influences of supercritical nozzles on stability including vorticity. No work has been done to clarify the case when the vorticity is that produced in flow turning. Culick (1961, 1963) had earlier reported a few results for the behavior of three-dimensional waves incident upon a choked exhaust nozzle, but he did not include vorticity.

On the other hand, the waves of vorticity must interact with the turbulence field necessarily present, process (v). It seems most likely that as a result the vorticity is destroyed. If the destruction occurs close to the burning surface, then the processes (iii) and (iv) become almost irrelevant to stability. We need account only for the processes of generation and pumping. At the present state of analysis and understanding, this seems to be the best resolution of the matter. Thus, for stability of longitudinal motions in a cylindrical chamber, the net effect of flow-turning is zero, as Flandro has reasoned. Contrary conclusions have been reached by others, partly supported by appeal to experimental results, which usually contain substantial uncertainties. The preceding reasoning rests entirely on the equations of motion.

We discuss further the theoretical basis for the preceding remarks in Chapters 6 and 7. Our conclusion here is that generation of vorticity at a burning surface is a mechanism for combustion instabilities but its influence on attenuation or amplification is often small, much smaller, for example, than the damping due to a choked nozzle. Calculations must be done for the particular grain geometry in question—there is no simple generalization that can be formulated.

(b) *Shedding of Large Scale Vortices.* So far as practical consequences are concerned, the production of large vortices in motors has been far more significant than has the generation of vorticity discussed above. The latter is present in all solid rockets, and contributes always to linear stability, although the

¹⁸In the same paper, Culick treated the phenomenon of ‘pumping’ as an interpretation of the way in which an acoustic boundary layer on an impermeable surface attenuates waves. However, he overlooked the analogous process for a permeable surface. The calculations for the acoustic boundary layer are given here in Annex D. See Section 6.9 for the correct one-dimensional analysis.

true quantitative value remains controversial. On the other hand, while the prediction and influences of vortex shedding may contain uncertainties, it is fair to say that the general characteristics are well-known and settled. Moreover, vortex shedding has been identified unambiguously as the mechanism for oscillation observed in several large motors including the Space Shuttle SRM, the Titan IV SRMU and the Ariane 5 SRM. Note that the mechanism has apparently not been active in small operational motors.¹⁹

The main reason for that conclusion seems to be the required special near-coincidence between the frequency of shedding and the frequency of an acoustic mode. Laboratory tests demonstrated that basic feature (Magiawala and Culick 1979; Nomoto and Culick 1982; Aaron and Culick 1984). Satisfaction of the condition requires suitable combinations of geometry, mean flow speed, thickness of shear layer at the origin of the vortex shedding and acoustic frequency which depends mainly on the speed of sound and length of chamber. Nevertheless, only a simple apparatus, sketched in Figure 2.29, is required to demonstrate the phenomenon.

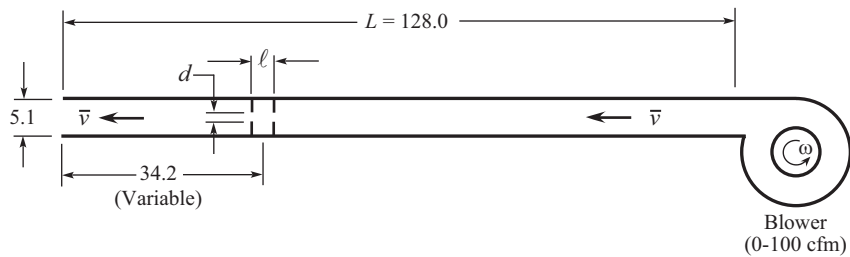


FIGURE 2.29. Sketch of an apparatus for demonstrating the excitation of acoustic modes by vortex shedding at a pair of annuli. All dimensions in centimeters (adapted from Culick and Magiawala 1979).

Three forms of vortex shedding have been unambiguously identified as mechanisms for exciting pressure (acoustic) oscillations in motors, illustrated in Figure 2.30: shedding from obstacles, usually annular rungs of restrictors or inhibiting material (Flandro, 1986; Vuillot, 1995); shedding from backward-facing steps and edges existing due to the geometry of the grain (Flandro, 1986 and Vuillot, 1995); and parietal vortex shedding in which vortices are created as a consequence of instabilities of the mean velocity profile in the vicinity of a burning surface (Casalis and Vuillot, 2002). The first two forms of vortices arise from unstable shear layers so one may state that generally the presence of vortex shedding as a mechanism is due to an instability of the average flow profile.

That conclusion suggests the obvious advice for avoiding this cause of pressure oscillations: Design the grain to exclude all possibilities for unstable velocity profiles. Thus there must be no obstacles, backward facing steps or edges, and the flow along burning surfaces must nowhere reach critical conditions for local instability. In practice those constraints may be too severe to be satisfied entirely. The design problem will then come down to producing a configuration in which the strength of the vortices, and their coupling to the acoustic field, will be minimal even though not necessarily nonexistent.

Suppose, then, that one or more instabilities of the mean flow exist in a chamber. Is it necessarily so that the vortices that may develop will excite and support unacceptable pressure oscillations? No, because we are concerned here once again with a case of coupled oscillatory systems: The system of pressure waves filling the chamber, and the array of vortices periodically shed from some relatively small region. The two

¹⁹The cases of vortex shedding from obstacles and from backward-facing steps have been unambiguously identified in full-scale combustors. So far as the author is aware, parietal vortex shedding, in contrast to shedding from obstacles, has not been shown definitely to exist in full-scale devices although it has been unquestionably identified in laboratory tests (Avalon *et al.* 2000; Vuillot and Casalis 2002). The Ariane 5 is the most likely candidate, but the case still remains open to question; direct observation has not been accomplished.

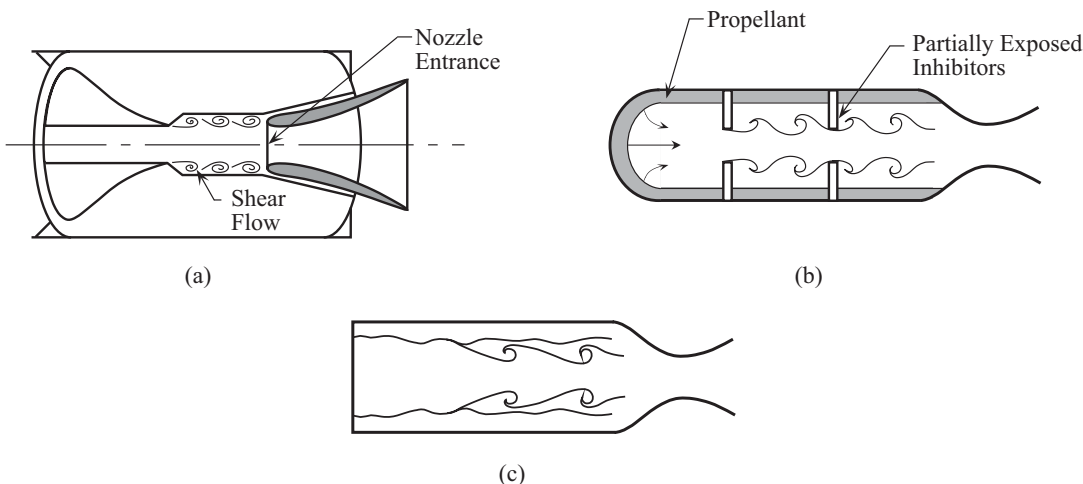


FIGURE 2.30. Vortex shedding from (a) an annular obstacle composed of residual inhibitor material; and (b) an edge of a backward facing step at a transition zone; (c) due to instability of the mean flow near a burning surface (parietal vortex shedding). Parts (a) and (b) from (Flandro 1986); Part (c) from Vuillot and Casalis (2002).

systems are coupled. The vortices, by some process such as that discussed below, may transfer a portion of their energy to the pressure waves; and the pressure waves—or their associated velocity oscillations—have strong influence on the initiation of the vortices by triggering, and, by frequency locking, on instabilities of the mean flow.

That behavior has long been known (e.g., see Rockwell and Naudascher 1979 and Naudascher and Rockwell 1980), implying that the oscillations found in rocket motors require near-coincidence between the shedding frequency and the frequency of an acoustic mode of the chamber. The truth of that conclusion for configurations appropriate to solid rockets seems first to have been demonstrated with the simple laboratory tests cited above. Satisfaction of the condition requires appropriate combinations of geometry; mean flow speed; suitable properties in the region of mean flow where the instability originates; and the acoustic frequency, which depends mainly on the speed of sound and a characteristic dimension, usually the length of the chamber. Sufficient data have been taken for the problem to construct useful scaling laws, ‘rules of thumb’ for design; see the references cited.

The appearance of vortex shedding in the Titan motors caused formation of a very useful program of extensive tests carried out in a subscale cold-flow model of the motor (Dunlap and Brown 1981; Brown *et al.* 1981, 1985). Those tests produced extensive data for the internal flow fields, eventually including results that formed part of the basis for the theoretical work on unsteady vorticity cited in the preceding section.

In 1986, Flandro reported his elaboration and extension of the analysis he had carried out with Jacobs twelve years earlier. The work brought together previous ideas of instability of a shear layer as the initiation of a shear wave; growth and roll-up of the wave into a vortex; propagation of the vortex at a speed something less than that of the average flow; and impingement of the vortices on a solid surface, producing a pulse of pressure that can excite and sustain acoustic waves in the chamber. An acoustic pulse will propagate upstream to the region of the shear instability, possibly to initiate another disturbance to be amplified within the layer, later to develop into another vortex, etc., etc. The process will continue, becoming periodic when the frequency of the vortex shedding is nearly equal to the acoustic frequency. In that work, Flandro also fitted his results in the general analysis of linear instabilities covered here in Chapter 6.

When that behavior occurs in a rocket, toroidal vortices are shed from the inner edge of an annular obstruction, as in the Shuttle and Titan motors, or from edges such as those at the transition from longitudinal slots to the main cylindrical chamber (Figure 2.30(b)). The acoustic frequency is determined mainly by the length of the chamber, while the vortex shedding frequency is influenced by the local geometry and average flow. The local geometry determines the growth of the shear layer and in particular its momentum thickness, a fundamental parameter defining the conditions for instability. Flandro's analysis—an adaptation of earlier work by Michalke (1965)—and experimental results, have confirmed that the vortex shedding is characterized by the value of the Strouhal number, St , at which the growth rate of an unstable disturbance is maximum. The Strouhal number is defined as the product of shedding frequency f_s , times a characteristic length δ , divided by a characteristic speed U , so the shedding frequency is given by the formula

$$f_s = St \frac{U}{\delta} \quad (2.74)$$

where St has some value roughly constant and set by the geometry. The frequencies of the acoustic modes are only weakly dependent on the mean flow of the Mach number so small but do depend strongly on the geometry. For a chamber having length L and closed at both ends²⁰, the longitudinal modes have frequencies given by

$$f_a = \ell \pi \frac{a}{L} \quad (2.75)$$

where a is the speed of sound and $\ell = 1, 2, \dots$ identifies the mode.

The results reported by Nomoto and Culick (1982) confirm the truth of the preceding ideas for a simple laboratory apparatus consisting of two annuli fitted in a tube, separated by some distance ℓ and having a mean flow in the axial direction. Figure 2.31 is a photo of the flow in the vicinity of the two baffles. Figure 2.32 shows some results with lines drawn according to (2.74) and (2.75) and data points indicating the occurrences of oscillations without regard to amplitude. For the conditions of the experiment, significant oscillations were excited only in regions in which (2.74) and (2.75) are simultaneously satisfied. Note that the separate diagonal lines for shedding frequency given by (2.74) represent cases in which there are 1, 2, 3, ... vortices existing between the annuli at any given time. This interpretation of the shedding frequency was first given by Rossiter (1966).

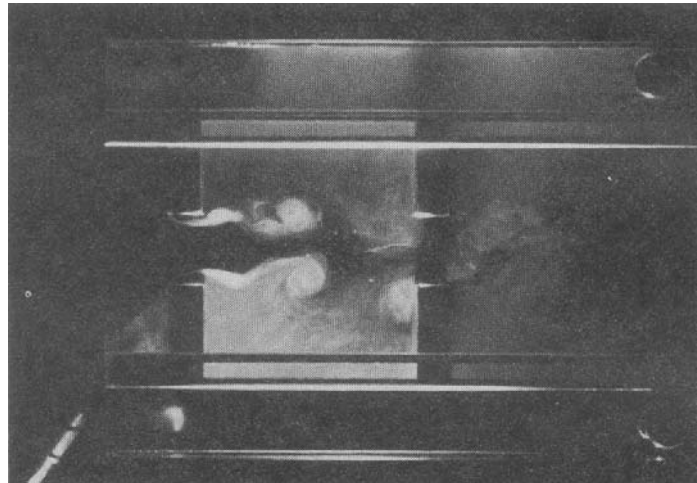


FIGURE 2.31. Typical flow between the baffles when a pure tone is generated (Nomoto and Culick 1982).

²⁰A rocket physically closed at one end and exhausting through a choked nozzle appears to acoustic waves as if it is approximately closed at both ends.

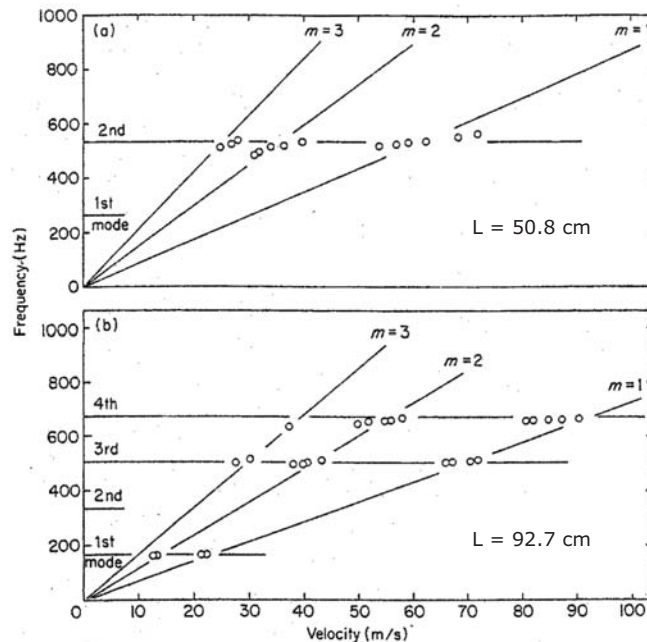


FIGURE 2.32. Experimental results for the excitation of acoustic modes by vortex shedding (Nomoto and Culick 1982). Open circles identify conditions when significant oscillations were observed. The length of the chambers from inlet to exhaust.

A potentially important implication of Figure 2.32 is that the dependence of the observed frequency of oscillation may not have an obvious—or simple—dependence on the length and mean flow speed during the firing of a solid rocket. In fact, as several researchers have noted (see, e.g., Vuillot 1995) the following reasoning shows that the shift of frequency with time is a good basis for distinguishing vortex shedding as the mechanism for oscillations. However, in practice, unambiguous distinction between this form of vortex shedding and parietal vortex shedding as the primary cause of observed oscillations may not be easy (Vuillot and Casalis, 2002).

Instabilities sustained by feedback involving combustion dynamics almost always show dependence on geometry closely given by the formulas of classical acoustics: $f_a \sim 1/L$. Thus, if there is little or no propellant cast at the head end, the longitudinal frequency is nearly constant in time. Or, if, as usually is the case for large motors, there are slots and fins at the head end, the effective length of the chamber tends to increase during a firing and hence the frequency of oscillation decreases.

However, according to the results given in Figure 2.32, because the mean velocity may increase during a burn as more propellant is exposed, the frequency of vortex shedding may increase. Coupling between the process of vortex shedding and the acoustic modes occurs over a broad range of frequency. It is possible (and has been observed) that the frequency suffers discrete changes, corresponding to transition between groups of data points shown in Figure 2.32; that is, the state of the oscillating system shifts because the number of shed vortices present between the shedding and impingement points changes.

The potentially important and very interesting second cause of vortex shedding was discovered several years ago by Vuillot and his colleagues at ONERA while investigating the mechanism for unstable oscillations observed in the Ariane 5 solid rocket boosters. Subscale firings of motors showed that large vortices were initiated, grew, and were shed from the region near the burning surface. (Vuillot *et al.* 1993; Trainneau *et al.* 1997). Hence the phenomenon was called “parietal vortex shedding” by Lupoglazoff and Vuillot (1996).

In an exemplary systematic research program, the group at ONERA have established most of the characteristics of parietal vortex shedding relevant to practical applications. Some issues of scale apparently remain, but very good agreement has been found between subscale hot firings; subscale tests with flow visualization (Avalon *et al.* 2000); and numerical analyses of stability and vortex shedding. LeBreton *et al.* (1999) have given a good review of the subject, including some results for the effects of residual combustion which in this situation may not be negligible. Moreover, there is strong evidence of significant interaction between shedding from obstacles and parietal vortex shedding. The strength and significance of those interactions must clearly depend on the geometry and (changing) flow conditions in the chamber.

Possibly the most important aspect of this subject is weak understanding of nonlinear behavior. Apparently only Aaron (1985) has attempted a simple explanation, with only modest success. No simple explanation exists for the amplitudes of oscillations that can be generated by coupling with the shedding of large vortices. According to LeBreton *et al.* (1999) parietal vortex shedding produces, in their examples, larger amplitudes of oscillation than does shedding from an annulus (inhibitor ring in a segmented rocket). It would clearly be a significant aid to design and development if a rule of thumb could be constructed to place an upper limit to the amplitudes of oscillation caused by vortex shedding. Because the mechanism involves conversion of mechanical energy of the near flow to acoustic energy, it is likely that the maximum possible amplitudes must be much smaller than those that can be generated by coupling between acoustics and combustion dynamics. However, even when the amplitudes are well below values causing damage to the motor, the associated levels of oscillatory vibrations may be unacceptable to the payload.

2.2.10. Distributed Combustion. Combustion of the major components of a solid propellant—the primary oxidizer and the binder in the case of composite solids—normally takes place to completion near the burning surface. Thus the term ‘distributed combustion’ refers to combustion of particles as they are carried into the volume of the chamber. In particular, almost all attention has been directed to residual combustion of aluminum for which there is much photographic evidence. Steady combustion of aluminum particles has long been and continues to be a subject of research owing to its vital importance to the efficiency and performance of motors, and in the formation of slag, a general term referring to condensed material.

Relatively little notice has been taken of the possible influences of residual combustion on the stability of motors. Probably the main reason for this lack of interest is the general view that the existence of combustion instabilities in motors can be satisfactorily explained by other mechanisms, notably the dynamics of surface combustion and vortex shedding. It appears that the dynamics of aluminum combustion within the volume of the chamber must provide at most a small contribution to stability. There are at least two reasons for this conclusion: the available data contain uncertainties too large to allow identification of the influences of unsteady aluminum combustion; and any destabilizing tendencies of the particles are roughly compensated by the attenuation of unsteady motions due to the presence of particles. The second effect is known to be significant if the particles are inert and have suitable sizes for the frequencies of the instability in question.

Several works (Marble and Wooten 1970; Dupays and Vuillot 1998) have treated the effects of condensation and vaporization of non-burning particles, on attenuation of acoustic waves. Whether the attenuation is increased or decreased depends on many factors, including the sizes of particles and the rates at which the particles gain or lose mass. When, for example, a particle is vaporizing, it seems that in the presence of an acoustic wave, the phenomenon of ‘flow turning’ discussed in the preceding section should cause increased attenuation for a given particle size and frequency. However, while the analysis by Wooten (1966) supports that conclusion, recent work by Dupays (2000) suggests that the result is not always true. Moreover, suggestions have been made by investigators of combustion instabilities in ramjets (Sirignano *et al.* 1986) and in liquid rockets (Grenda, Vanketaswaram and Merkl 1995) that the process of vaporization of liquid drops is destabilizing. Those conclusions may be misleading, due to implied direct connections between the vaporization and burning rates. It may in fact be the case that the destabilization found in practice is due to combustion rather than vaporization *per se*.

Owing to the necessary connection between vaporization and combustion of particles, the problem of residual combustion presents certain difficulties of distinguishing what process is really responsible for attenuation or driving of waves. The most extensive experimental work on the problem in the U.S. has been done by Beckstead and his students (Beckstead, Richards and Brewster 1987; Raun and Beckstead 1993; Raun *et al.* 1993; Brooks and Beckstead 1995).

One of the most compelling reasons for investigating the matter was the discovery of anomalous (and still not completely understood) results obtained with a device called the ‘velocity-coupled T-burner’. In this configuration, large areas of propellant are mounted in the lateral boundary to emphasize the interactions between surface combustion and velocity fluctuations parallel to the surface. For reasons not discussed here, Beckstead concluded that residual combustion was possibly a reason that unusually large values of the response function were found. The idea was based partly on the suspicion that the tangential velocity disturbances can strip incompletely burned aluminum from the surface. Subsequently, with both calculations and further experiments (Raun and Beckstead 1993), Beckstead has strengthened his case that the effects of unsteady residual combustion should not be dismissed out-of-hand. It is worth noting the conclusion by Brooks and Beckstead (1995) that the greatest effect of residual combustion (of aluminum) on stability is indirect, due to its effect on the mean temperature profile.

More recent work on distributed combustion has been carried out in France, motivated by the problem of oscillations in the Ariane 5 motor discussed in Section 2.2.6. The program devoted first to non-reacting two-phase flow and later to reacting flow began, apparently, with the dissertation by Dupays (1996). The most recent discussion of the work seems to be the review articles prepared by Dupays *et al.* (2002), but a broader view of the matter is presented in the excellent article by Fabignon *et al.* (2003). Aluminum combustion is discussed, not at great length, in the context of acoustic oscillations driven by vortex shedding with the Ariane 5. A main conclusion must be given close attention: Relatively small drops amplify oscillations, but large drops (diameters 125μ , burning to 60μ) attenuate the motions. It appears that little further work has been accomplished to investigate the reasons for this result which clearly has important practical implications. Simulations of unsteady two-phase flow in the Ariane 5 P230 booster motor have also been described by Lupoglazoff *et al.* (2000). See Section 6.11. It’s an important topic. The subject of the effects of interactions between particles and gas seemed at one time to be quite well in hand. That view changed with recognition that at the temperature of flows in solid rockets residual combustion distributed in a chamber is likely significant under some realistic conditions. How significant, and how widespread the conditions are, has not been defined. It’s an interesting subject that should be better understood.

2.3. Mechanisms of Combustion Instabilities in Liquid-Fueled Systems

Apart from differences in geometry, the primary distinctions between different propulsion systems are due to the internal physical processes. Some are independent of geometry, but others—such as flow separation—are not. In this and the following sections, we discuss the four oldest and main ideas that have been proposed for explaining combustion instabilities in liquid-fueled systems: processes associated with droplet formation and burning; interpretation with a time lag; convective waves; and vortex shedding and combustion. The ideas are not new and much of the material covered was developed during the period 1950–1990. Relatively little has been accomplished in general since that time, although in the past decade much has been done to improve the level of detail. While all have been prompted by experimental results, they differ greatly in the extent to which they have been developed.

2.3.1. Atomization, Droplet Vaporization and Burning. Some years after the time lag model had been developed, work at the NASA Research Center (Priem and Guentert 1962 and Priem 1965) showed that the stability of a liquid rocket motor could be controlled by varying the characteristics of the vaporization process. The conclusion followed from the results of numerical solutions to the equations for nonlinear

unsteady motions in a chamber. Source terms were approximated with models of the atomization, vaporization and burning. Variations of characteristic parameters showed that atomization and vaporization were the dominant rate processes determining the stability limits. That conclusion led to a series of studies particularly emphasizing vaporization.

Because of the difficulty of extracting precise conclusions from numerical analyses, Heidmann and Wieber (1966a, 1966b) devised a method for assessing the vaporization process alone. A droplet is injected axially in a steady flow. An acoustic field is superposed having the spatial distribution of the lowest first tangential mode for a cylindrical chamber, $\sin \theta J_1(\kappa_{11}r)$. The motion and vaporization rate of the droplet is calculated throughout its history. By superposing the results for an array of injected drops, assumed not to interact with one another, one may find the local fluctuation of vaporization rate throughout the chamber. That is the mass source term w'_l in the continuity equation for the gas phase (see Annex A).

Heidmann and Wieber (1966a) defined a “response factor”, N , to interpret their results:

$$N = \sum \frac{w'_l/\bar{w}_l}{p'/\bar{p}} \quad (2.76)$$

where \sum here denotes the sum over all droplets in the volume considered. They gave results for N as a function of various parameters. Typically, N shows a peak of about 0.6–0.9 in a frequency range 0.04–0.1 Hertz. Results obtained for *n*-heptane over fairly wide flow conditions were correlated with a dimensionless parameter containing droplet size, chamber pressure, gas velocity and a dimensionless amplitude of the oscillation.

In a later work, Heidmann and Wieber (1966b) used a restricted form of Rayleigh’s Criterion and a simpler linear analysis to produce essentially the same conclusions. The new definition of the response factor was

$$N = \sum \frac{\int_0^{2\pi/w} \frac{\hat{w}_l^{(r)}}{\bar{w}_l} \frac{\hat{p}}{\bar{p}} dt}{\int_0^{2\pi/w} \left(\frac{\hat{p}}{\bar{p}} \right)^2 dt} \quad (2.77)$$

These analyses amount to detailed examination of a particular process contributing to the time lag discussed Section 2.3.2. Substitution of the real part of (2.94) in (2.77) gives

$$N = n(1 - \cos \omega \tau) \quad (2.78)$$

Heidmann and Wieber found that their numerical results could be approximated quite well in the range $\tau_v \omega < 1$ by the values

$$\begin{aligned} n &= 0.21 \\ \tau &= 4.5\tau_v \end{aligned} \quad (2.79)$$

where τ_v is the mean droplet lifetime. This comparison is shown in Figure 2.33 taken from Heidmann and Wieber (1966).

Note that the function (2.79) oscillates and therefore becomes a poor approximation for $\omega \tau_v > 1$, as show by the solid line in Figure 2.33. The vaporization rates seem physically reasonable for the conditions shown, so one must conclude that the time lag model fails at higher frequencies. Subsequently, Tong and Sirignano (1986a, 1986b, 1987) re-examined the problem of unsteady vaporization. With their more detailed model including the effects of unsteady heat transfer in the gas phase, they concluded that their vaporization rates are much higher than those found by Heidmann and Wieber.

More strongly, Tong and Sirignano proposed that unsteady droplet vaporization is a potential mechanism for driving combustion instabilities. Heidmann and Wieber had earlier noted that the response factor they

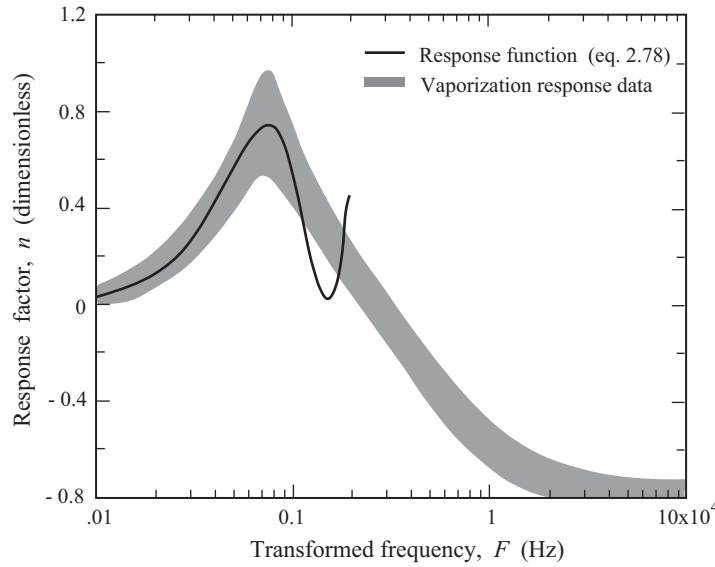


FIGURE 2.33. Vaporization response according to Heidmann and Wieber (1966).

calculated for the vaporization process was less than that calculated for the nozzle losses. Thus, although vaporization itself did add energy to the acoustic field according to their analysis, the effect was too small to be a mechanism for instabilities. Tong and Sirignano concluded that their results show sufficient energy transfer from the vaporizing droplets to the acoustic field to qualify as a mechanism in actual systems²¹. Their conclusion is based solely on the $p - v$ work done by the process of vaporization and does not include any energy release due to combustion. The proposal is evidently wrong, for the following reasons reached by reasoning from at least two points of view.

First, we must emphasize that none of the preceding conclusions involved combustion: The assertion is that coupling between pure vaporization and the acoustic field produces net flow of energy to the oscillations in the gas. The contrary conclusion was reached by Marble and Wooten(1970) and Marble (1969), that both condensing and vaporizing droplets attenuate acoustical motions. In Section 2.2.10 we noted that recent work at ONERA showed that a more complete analysis accounting for condensation and vaporization in greater detail leads to slightly different conclusions.

The reason for the opposite conclusion seems to be that not all interactions between the droplets and the acoustic field are accounted for in the calculations by Heidmann and Wieber, and by Tong and Sirignano. Their conclusions were based on using Rayleigh's Criterion, but only one term was considered. They argued that by analogy with Rayleigh's original statement concerning fluctuations of heat addition, the same criterion should apply to mass addition. Therefore, as in equation (2.77), only the integral involving w'_l was computed; a positive value indicates the possibility for driving the acoustic field. However, the derivation given later will show that the correct form of the criterion involves several contributions. Considering only those associated with the conversion of liquid to gas, the result can be found (Culick, 1988, Section 2.5)

$$\Delta\epsilon_n = \frac{\omega_n^2}{\bar{p}E_n^2} \int dV \int_t^{t+\tau_n} \left[(\bar{\gamma} - 1) \left\{ \delta Q'_l + (\bar{h}_l - \bar{e}) w'_l + \left(h'_l - e' - \frac{p'}{\bar{\rho}_g} \right) \bar{w}_l \right\} + \bar{\gamma} \left(\delta \vec{F}'_l + \bar{w}_l \delta \vec{u}'_l \right) \cdot \vec{u}'_n \right] dt \quad (2.80)$$

²¹Later application of this work to ramjet combustors is discussed briefly in Section 2.4.5

There is indeed a term proportional to the integral of $w'_l p'$, but it is multiplied by $(\bar{h}_l - \bar{e})$ which contains the heat of vaporization. There are also significant amounts of energy transfer associated with the terms involving $\delta Q'_l + \delta F'_l$ which for non-vaporizing drops represent the attenuation of sound waves. Those effects are included in the work by Marble and Wooten: Their results show that the accompanying energy losses dominate, so that in fact if combustion is ignored, vaporizing droplets cause damping, not driving, of unsteady gas motions.

We must emphasize that the conflicting results, and the conclusion that vaporization is not a mechanism for driving combustion instabilities, rests on proper computation of the energy transfer. In the earlier work, an incorrect or, rather, incomplete form of Rayleigh's Criterion was used. It is certainly true that the process represented by $w'_l p'$ alone does cause driving if the fluctuation of mass release has a component in phase with the pressure fluctuation, but that is only part of the story.

Priem (1988) has used Heidmann and Wieber's model of vaporization, combined with the model worked out by Feiler and Heidmann (1967) for a gaseous fuel, to study combustion instabilities in the LOX/methane system. He bases his conclusions concerning stability boundaries on numerical results for the combustion responses, of which that for liquid oxygen is computed with equation (2.77) and the method described above; and on corresponding results found for the losses associated with the exhaust nozzle and baffles. His results seem to compare fairly well with some experimental work. The reason that this could be so—even though vaporization causes net energy losses if all contributions are accounted for—is that the energy released by combustion, immediately following vaporization, is the dominant factor. That is, in equation (2.79) the terms involving energy transfer are larger than those representing losses. Comparison with experimental results seems always to involve multiplicative factors which are determined to provide best fit to data, or are absent in normalized forms. Then when good agreement was found, it seems that it is largely the qualitative behavior that is being checked. The method is dated and no longer useful.

Despite the heavy emphasis, in many works, on vaporization as the rate controlling process, it is generally recognized that other processes contribute and in some situations may be dominant. The injection process itself may be affected under unsteady conditions due to the varying streams, impact of jets, and atomization all are sensitive to unsteady flow fields. Those problems are extremely complicated, difficult to describe in a fashion suitable for use in a general analysis, and are very much dependent on details of the hardware. Thus the work has largely been experimental with some effort to correlate results in a form useful for design (e.g., Levine 1965; Sotter, Woodward and Clayton 1969; Webber 1972; Webber and Hoffman 1972). The time-lag model has been used essentially as a means of correlating all of those processes without concern for details (Reardon, Crocco and Harrje 1964; Reardon, McBride and Smith 1966). Summaries of experimental results obtained prior to 1971 may be found in the reference volume edited by Harrje and Reardon (1972).

Of work in the 1980s, the most fundamental and detailed was that carried out at ONERA as a result of problems due to combustion instabilities in the Viking motor. Special effort was made to understand the unsteady behavior of the injectors used in that engine. The intentions of the research program were described by Souchier, Lemoine and Dorville (1982); and by Lourme and Schmitt (1983). Considerable effort has since been expended to characterize the steady and unsteady behavior as the basis for analyzing instabilities in the engine (Lourme, Schmitt and Brault 1984; Lecourt, Foucaud and Kuentzmann 1986; Lourme 1986; Lecourt and Foucaud 1987). The results range from detailed measurements of the spray (droplet size and velocity distributions) to the more global unsteady response of the injector, using a device adapted from a method developed for solid propellant rockets.

2.3.2. Interpretation With a Time Lag. Owing to the enormous complications associated with analysis of the time-dependent behavior of liquid-fueled systems, representation of the dynamics with a time lag was introduced early in theoretical work. The basic idea is simple, and quite general, related to the familiar experience that a forced oscillating system will gain energy if the force has a component in phase

with the velocity of the point of application. Stability of dynamical systems characterized in some sense by a phase or time lag had been studied prior to the concern with combustion instabilities (for example, see Callender *et al.* 1936 and Minorsky 1942). In 1941, Summerfield (1951) had observed low frequency “chugging” during firings of a liquid rocket. Discussion with von Karman led to the idea of a time lag as a possible explanation. Gunder and Friant (1950) independently introduced a time lag in their analysis of chugging, but it was Summerfield’s paper and subsequent work at Princeton by Crocco that established the time lag theory in the firm widely used.

The essential idea in all applications of the time lag is that a finite interval—the lag—exists between the time when an element of propellant enters the chamber and the time when it burns and releases its chemical energy. Such a time lag must exist in steady operation, and, since combustion is distributed throughout the chamber, there is no unique value. Evidently a complete analysis of injection and subsequent processes could then be interpreted in terms of multiple time lags; results exist only for approximate analyses.

Now suppose that at time t the pressure in the chamber suddenly decreases, causing an increase in the flow of propellant through the injector. The increased mass burns at some later time $t + \tau$, where τ is the time lag. If the pressure is increasing when the added mass burns, the energy released will tend to encourage the pressure increase, a destabilizing tendency. This elementary process is easily interpreted with Rayleigh’s Criterion. Assume that the pressure varies sinusoidally,

$$p' = \hat{p} \sin \omega t \quad (2.81)$$

and that the energy occurs later with constant time lag τ ,

$$Q' = \hat{Q} \sin \omega(t - \tau) \quad (2.82)$$

Integration of the product $p'Q'$ over one period $2\pi/\omega$ gives

$$\int_t^{t+2\pi/\omega} p'Q' dt' = \hat{p}\hat{Q} \int_t^{t+2\pi/\omega} \sin \omega t' \sin(\omega t' - \omega\tau) dt' = \hat{p}\hat{Q} \frac{\pi}{\omega} \cos \omega\tau \quad (2.83)$$

Thus, according to Rayleigh’s Criterion (Section 6.6), we expect that net energy is added to the oscillation if $\cos \omega\tau$ is positive, so the time lag must lie in the ranges

$$0 < \tau \frac{\pi}{2\omega}, \quad \frac{3\pi}{2\omega} < \tau < \frac{5\pi}{2\omega}, \quad \dots \text{etc.} \quad (2.84)$$

Suppose that the system is unstable and the τ lies in the range $3\pi/2\omega < \tau < 5\pi/2\omega$. Then the strategy for fixing the problem is based on modifying the system so that τ is either increased or decreased, placing its value outside the range for instability.

Because the processes subsequent to injection are surely dependent on the flow variables, pressure, temperature, velocity, . . . , it is unrealistic to assume that the time-lag is constant. The most widely used form of the representation with a time lag are dominated by its dependence on pressure. Figure 2.34, taken from Dipprey (1972), is a sketch illustrating the behavior for a sinusoidal pressure oscillation imposed on the system. The total time delay to burning is supposed, in this case, to be composed of two parts due to the propellant feed system and the combustion delay (injection, atomization, vaporization, mixing, and chemical kinetics). It is the second part that is sensitive to the flow conditions in the chamber.

Let m denote the mass flow (mass/sec.) of propellant. At this point we are not concerned with details and we need not distinguish between fuel and oxidizer. The arguments based on the idea of a time lag are directed mainly to constructing a representation of the mass source term w_ℓ (mass/vol.-sec.) in the equation for conservation of mass. Thus the result is intended to express the rate of conversion of liquid to gas in a volume element of the chamber. There is no consideration of combustion processes in detail; the usual assumption is that combustion occurs instantaneously, a view that determines how the time lag model ought to be incorporated in the equations.

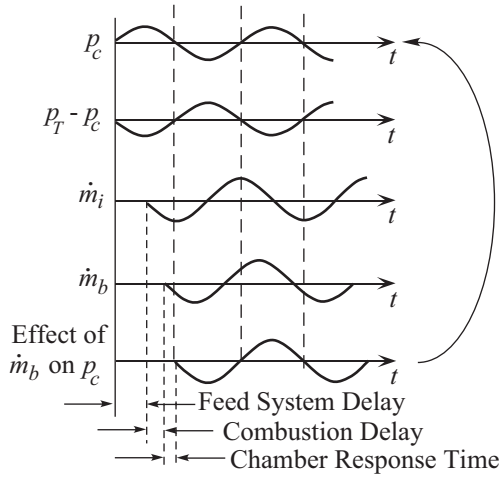


FIGURE 2.34. Graphical definition of a simple time lag (Dipprey 1972).

Let (\vec{r}, dV) denote the volume element at position \vec{r} in the chamber and let (t, dt) denote the small time interval dt at time t . The idea is that the amount of liquid $w_l dV dt$ converted to gas in the element (\vec{r}, dV) in the interval (t, dt) was injected as $\delta\dot{m}(t - \tau)d(t - \tau)$ at the time $t - \tau$ in the interval $d(t - \tau)$. Hence by conservation of mass,

$$w_l dV dt = \delta\dot{m}_i(t - \tau)d(t - \tau) \quad (2.85)$$

According to earlier remarks, the time lag is supposed to be variable, and can be written as the sum of average and fluctuating values, $\tau = \bar{\tau} + \tau'$. In steady-state operation, (2.85) is

$$\bar{w}_l dV dt = \delta\dot{m}_i(t - \bar{\tau}) = \delta\dot{m}_i(t - \bar{\tau})dt \quad (2.86)$$

Expanding $\delta\dot{m}(t - \tau)$ in Taylor series for use in (2.85) we have

$$\delta\dot{m}_i(t - \tau) = \delta\dot{m}_i(t - \bar{\tau}) + \tau' \left[\frac{d}{dt} \delta\dot{m}_i \right]_{t-\tau} + \dots \quad (2.87)$$

The second term is non-zero if the injected mass flow is not constant. There are many situations (notably for low frequency instabilities) for which variations are important. But for instabilities at high frequencies, variations of the propellant flow are generally not important. Hence we ignore the second term in (2.87) and substitute (2.86) in (2.85) to find

$$w_l(\vec{r}, t) = \bar{w}_l \left(1 - \frac{d\tau}{dt} \right) \quad (2.88)$$

The variations of the local conversion of liquid to gas depend in this simple fashion on the time-dependence of the time lag. Note that τ may in general depend on position: The reasoning here is quite widely applicable.

The difficult problem is of course to predict τ — in fact it has never been done. Crocco introduced the idea that the time lag is the period required for the processes leading to vaporization to be completed. He assumed that this integrated effect can be represented by an integral over the time lag of some function f of the variables affecting the processes

$$\int_{t-\tau}^t f \{p, T, \vec{u}, \vec{u}_l, \dots\} dt' = E \quad (2.89)$$

The constant E is supposed to be a measure of the level to which the integrated effects must reach in order for vaporization to occur. Almost all applications of the time lag model rest on the assumption that the time

lag is sensitive only to the pressure. The function f may then be expanded to first order about its value at the mean pressure,

$$f(p) = f(\bar{p}) + p' \frac{df}{dp} = f(\bar{p}) \left[1 + p' \frac{1}{f(\bar{p})} \frac{df}{dp} \right]$$

If $f = cp^n$ then $df/dp = ncp^{n-1}$ and $(df/dp)/f(p) = n/p$. The *interaction index* n is defined as

$$n = \frac{\bar{p}}{f(\bar{p})} \frac{df}{dp} \quad (2.90)$$

and $f(p)$ is approximated as

$$f(p) = f(\bar{p}) \left[1 + n \frac{p'}{\bar{p}} \right] \quad (2.91)$$

This form is now used in approximate evaluation of (2.89).

First differentiate (2.89) with $f(p) = f\{p(t)\}$ to find

$$f\{p(t)\} - \left(1 - \frac{d\tau}{dt} \right) f\{p(t - \tau)\} = 0$$

Substitution of (2.91) gives

$$1 - \frac{d\tau}{dt} = \frac{1 + n \frac{p'(t)}{\bar{p}}}{1 + n \frac{p'(t - \tau)}{\bar{p}}} \approx 1 + n \left[\frac{p'(t)}{\bar{p}} - \frac{p'(t - \tau)}{\bar{p}} \right] \quad (2.92)$$

Set $w_l = \bar{w}_l + w'_l$ in (2.88) and substitute (2.92) to find the basic result of the time lag theory:

$$w'_l = \bar{w}_l n \left[\frac{p'(t)}{\bar{p}} - \frac{p'(t - \tau)}{\bar{p}} \right] \quad (2.93)$$

For analyzing linear stability, $p' = \bar{p}e^{-i\bar{\alpha}kt}\psi(\vec{r})$ and $w'_l = \hat{w}_l e^{-i\bar{\omega}t}$, so

$$\hat{w}_l = \bar{w}_l n (1 - e^{-i\bar{\omega}\tau}) \quad (2.94)$$

where the usual approximation has been made, $\alpha\tau \ll \omega\tau$ in the exponent.

Equation (2.94) is a two-parameter representation of the conversion of liquid to gas. The two parameters, the time lag τ and the interaction or pressure index n , are unknown *a priori*. All work with the time lag theory requires experimental measurements to determine their values. The general idea is simple. After substituting (2.94) in the linearized conservation equations, solution is found for the stability boundary ($\alpha = 0$) with n and τ as parameters. Experimental data for the stability boundary are used to determine n and τ . The approximate range of values for τ had been reasoned, e.g., by Crocco and Cheng (1956). Crocco, Grey and Harrje (1960) were first to obtain sufficient data to confirm the value of this approach. Figure 2.35 reproduces some of their results for the time lag and interaction index inferred from tests with two injectors. The data were taken for the stability boundary of the fundamental longitudinal mode and show the strong dependence on fuel/oxidizer ratio.

Obviously, there are many limitations within the analysis itself. The analysis leading to (2.94) is entirely phenomenological; the final result containing two parameters only is an enormous simplification of the real situation, but there is no way to assess the imperfections. The formula (2.93) can be extended to include, for example, dependence on velocity fluctuations (Reardon, Crocco, and Harrje 1964). Because the values of all parameters must be found from experimental data, the difficulties become prohibitive.

The time lag model (it is, after all, not really a theory) is based on an appealing physical argument but no processes are treated explicitly. Probably the most serious deficiency is that no detailed treatment is given of combustion, which is ultimately the source of the energy driving all combustion instabilities. Nevertheless, the model has been the basis for some success in treating instabilities in liquid rockets, primarily as the basis

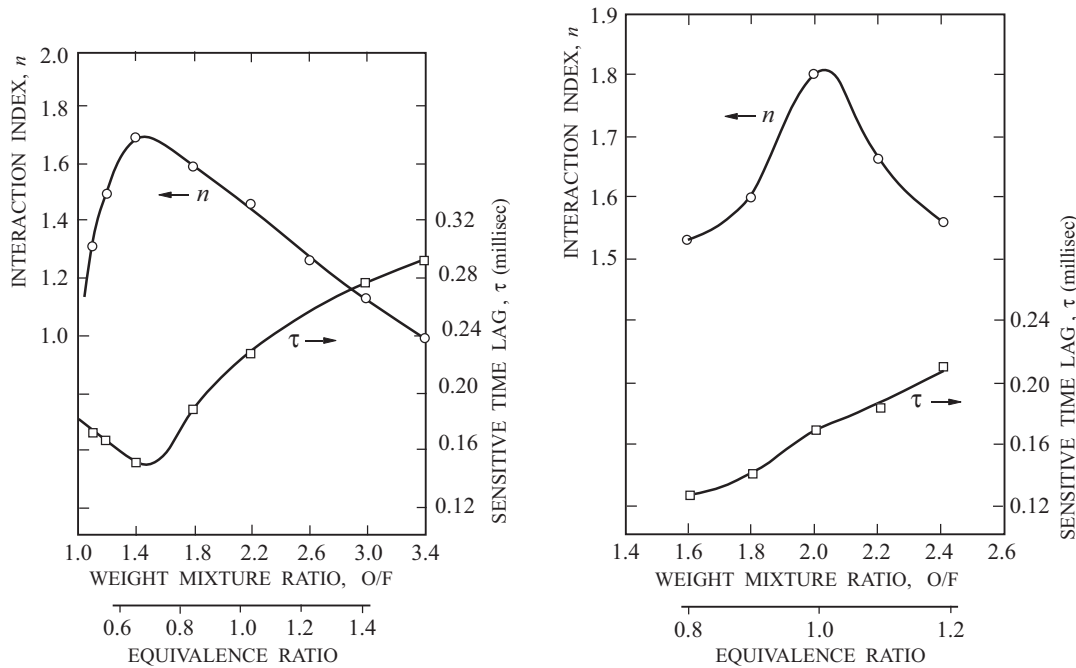


FIGURE 2.35. Early measurements of the time lag and pressure index in a gas rocket (Crocco, Grey and Harrje, 1960).

for correlating data. The two-parameter representation provides a convenient framework for detecting trends with design changes. Its illumination of basic physical processes and its predictive value are very limited indeed.

2.3.3. Convective Waves. Following work by Kovasznay (1953), Chu and Kovasznay (1957) showed one way of decomposing general small disturbances of a viscous compressible fluid into three classes: acoustic, viscous, and entropy waves. Acoustic waves carry no entropy changes, while viscous and entropy waves have no accompanying pressure fluctuations. The direct effects of viscous stresses and heat conduction on combustion instabilities are generally negligible except in the vicinity of surfaces. That entropy fluctuations evidently have second order effects on the acoustic waves is implied by the formal analysis covered in Chapter 3.

However, both viscous effects and non-uniform entropy may affect the acoustic field indirectly through processes at the boundaries. First we examine here the possible influences of entropy fluctuations. These fall within the general class of convective waves, that is, disturbances that are carried with the mean flow: their propagation speed is the average flow speed. Entropy fluctuations are associated with the portion of temperature fluctuations not related isentropically to the pressure fluctuation, such as non-uniformities of temperature due, for example, to combustion of a mixture having non-uniformities in the fuel/oxidizer ratio. In general, an entropy wave may be regarded as a non-uniformity of temperature carried with the mean flow.

As shown by Chu (1953) pressure waves incident upon a plane flame will cause generation of entropy waves carried downstream in the flow of combustion products. Thus one should expect that when combustion instabilities occur, there must be ample opportunity for the production of entropy fluctuations. That process has negligible effect directly on stability (the coupling between acoustic and entropy waves is second order within the volume) but there has long been interest in the possible consequences of entropy waves for the following reason.

When an entropy wave is incident upon the exhaust nozzle, it must pass through a region containing large gradients of mean flow properties. A fluid element must retain its value of entropy and for this condition to be satisfied, the pressure and density fluctuations cannot be related by the familiar isentropic relation, $\delta p \sim \gamma \delta \rho$. As a result, within the nozzle, pressure changes are produced that will generate an acoustic wave that will propagate upstream. Thus, an entropy wave incident upon an exhaust nozzle can produce an acoustic wave in the chamber, augmenting the acoustic field due to other sources.

An artificial elementary example will illustrate the proposition. Consider a chamber admitting uniform constant mean flow at the head end, say through a choked porous plate; the flow exhausts through a choked nozzle (Figure 2.36). Suppose that at the head end a heater is placed, arranged so that its temperature can be varied periodically, with frequency ω . This action produces a continuous temperature or entropy

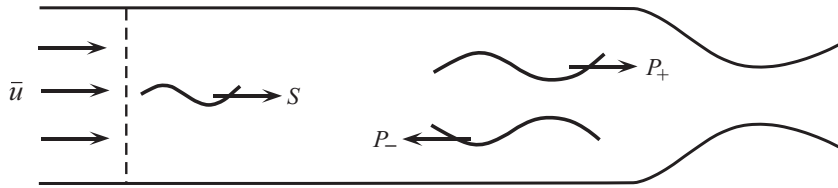


FIGURE 2.36. Sketch of a simple case with a single entropy wave (S) and acoustic pressure waves (P_+ , P_-).

wave convected with the flow. An experimental realization of this situation has been described by Zukoski and Auerbach (1976). We assume no losses within the flow, so a fluid element retains its entropy; small perturbations s' of the entropy satisfy the equation

$$\frac{\delta s'}{\delta t} + \bar{u} \frac{\delta s'}{\delta z} = 0 \quad (2.95)$$

If S is the amplitude of the fluctuation at the heater ($z = 0$), the solution for s' is

$$s' = S e^{-i\omega(t - \frac{z}{\bar{a}})} \quad (2.96)$$

To simplify the calculations, assume that the flow speed is vanishingly small so that we may ignore its effect on acoustic waves. Then the acoustic pressure and velocity fields can be expressed as sums of rightward and leftward traveling plane waves:

$$\begin{aligned} p' &= [P_+ e^{ikz} + P_- e^{-ikz}] e^{-i\omega t} \\ u' &= [U_+ e^{ikz} + U_- e^{-ikz}] e^{-i\omega t} \end{aligned} \quad (2.97a,b)$$

As usual, the complex wavenumber is $k = (\omega - i\alpha)/\bar{a}$. The acoustic pressure and velocity must in this problem satisfy the classical acoustic momentum equation with no sources:

$$\bar{\rho} \frac{\partial u'}{\partial t} + \frac{\partial p'}{\partial z} = 0 \quad (2.98)$$

Separate substitution of the forms for the rightward and leftward traveling waves shows that U_{\pm} , P_{\pm} are related by

$$\bar{\rho} a U_+ = P_+ ; \quad \bar{\rho} a U_- = -P_- \quad (2.99)$$

Assume that the head end acts as a perfect reflector for the acoustic waves, so

$$u' = 0; \quad \frac{\partial p'}{\partial z} = 0 \quad (z = 0) \quad (2.100a,b)$$

In a real case (e.g., if the heater were actually a flame) the pressure fluctuations would cause fluctuations of entropy at the head end. To represent this effect, set s' proportional to p' at $z = 0$:

$$s' = A_0 p' \quad (z = 0) \quad (2.101)$$

Tsien (1952), Crocco (1953) and Crocco and Cheng (1956) have shown that the boundary condition at the nozzle entrance may be written in the form

$$p' + \overline{\rho a} A_1 u' + A_2 s' = 0 \quad (z = L) \quad (2.102)$$

We may now show that the problem formulated here admits solutions representing steady acoustic oscillations in the chamber, whose stability depends on the values of the coefficients A_0, A_1, A_2 . We eliminate the unknown amplitudes S, P_+, P_- and obtain a characteristic equation for the complex wavenumber k , by satisfying the boundary conditions (2.99)-(2.102). Substitute equations (2.97)a,b and (2.99) into (2.100)a,b to find

$$P_+ - P_- = 0 \quad (2.103)$$

With (2.96) and (2.97)a, the condition (2.98) is satisfied if

$$S = A_0(P_+ + P_-) \quad (2.104)$$

Finally, substitution of (2.96), (2.97)a,b and (2.104) in (2.102) gives

$$[(1 + A_1)e^{ikL} + A_0 A_2 e^{i\frac{\alpha}{\overline{a}}L}]P_+ + [(1 + A_1)e^{-ikL} + A_0 A_2 e^{i(\frac{\alpha}{\overline{a}})L}]P_- = 0 \quad (2.105)$$

With $P_- = P_+$ from (2.103) we have the characteristic equation

$$e^{i2kL} = \frac{-1}{(1 + A_1)}[1 - A_1 + 2A_0 A_2 e^{i(k + \frac{\alpha}{\overline{a}})L}] \quad (2.106)$$

Generally A_0, A_1, A_2 are complex numbers. The real and imaginary parts of (2.106) provide transcendental equations for the real and imaginary parts ($\omega/\overline{a}, \overline{\alpha}/\overline{a}$) of k . The solutions are unstable if $\alpha > 0$, corresponding to self-excited waves. Note that in the limiting case of no entropy fluctuations ($A_0 = 0$) and a rigid wall ($A_1 \rightarrow \infty$) at $z = L$, (2.106) reduces to $e^{i2kL} = +1$ or $\cos 2kL = 1$ and $\sin 2kL = 0$. Then $k = n\pi/L$ and the allowable wavelengths are $\lambda = 2\pi/k = 2L/n$, the correct values for a tube closed at both ends.

This example suggests the possibility for producing instabilities if entropy waves are generated and *if* those waves interact with the boundary in such a way as to produce acoustic disturbances. It is in fact a genuine possibility that has been considered both in laboratory tests and as an explanation of instabilities observed in actual engines. The difficulties in applying this idea are largely associated with treating the processes responsible for causing the entropy waves.

In a combustion chamber, possible sources of entropy fluctuations may be distributed throughout the chamber. Burning of non-uniform regions of fuel/oxidizer ratio and interactions of pressure distributions with combustion zones are important causes, both producing non-isentropic temperature fluctuations. Thus in general the property that in inviscid flow free of sources an element of fluid has constant entropy, is inadequate. A proper description of entropy waves should be placed in the broader context accounting also for convective waves of vorticity was worked out first by Chu and Kovasznay (1957). We cannot provide a complete discussion here, but for later purposes it is helpful to have at hand the more general equation governing entropy fluctuations.

Combination of the first law of thermodynamics for a perfect gas and the definition $ds = dq/T$, valid if the heat transfer dq is not too abrupt, gives

$$ds = C_v \frac{dT}{T} - \frac{p}{\rho_g} \frac{d\rho_g}{\rho_g}$$

Now introduce the perfect gas law to eliminate the temperature change. Writing the result for motion following a fluid element we have

$$\frac{1}{C_v} \frac{Ds}{Dt} = \frac{1}{\rho} \frac{Dp}{Dt} - \frac{\gamma}{\rho_g} \frac{D\rho_g}{Dt} \quad (2.107)$$

where $D/Dt = \partial/\partial t + \vec{u}_g \cdot \nabla$ is the convective derivative. From the calculations in Annex A, we find the equation for entropy,

$$\frac{1}{C_v} \frac{Ds}{Dt} = \frac{1}{\rho} \frac{R}{C_v} \left[Q + \delta Q_l + \nabla \mathbf{q} + \Phi + \delta \mathbf{u}_l \cdot \mathbf{F}_l + \frac{p}{\rho_g} \nabla \cdot (\rho_l \delta \mathbf{u}_l) \right. \\ \left. + \left\{ (h_l - e) + \frac{1}{2} (\delta \mathbf{u}_l)^2 \right\} w_l \right] \quad (2.108)$$

The right-hand side contains all sources of entropy changes including viscous effects, combustion and conversion of liquid to gas.

Equation (2.108) completes the set of equations required for complete analysis of combustion instabilities including entropy waves. See also Annex A and Chapter 3. The equations governing vorticity waves are obtained by splitting the velocity field into two parts: the acoustic field which is irrotational, and the rotational vorticity field which, if treated in all generality, includes turbulence as well as large vortex structures and shear waves.

2.3.4. Vortex Shedding from Rearward-Facing Steps. The presence of unplanned swirling, spinning or vortex motions in propulsion systems has long been recognized as a serious problem. They fall broadly into two classes: those with angular momentum directed along the axis, usually (if the rocket itself isn't spinning) related to standing or spinning transverse acoustic modes of the chamber; and those having angular momentum mainly perpendicular to the axis, associated with vortex shedding from bluff bodies or rearward-facing steps.

Motions identified as forms of transverse or tangential modes do not normally qualify as mechanisms: they are themselves the combustion instability. Male, Kerslake and Tischler (1954) gave an early summary of severe transverse oscillations ("screaming" at 10 kHz) and noted what has always been a serious consequence: greatly increased surface heat transfer.

Here we are concerned with vortex motions growing out of unstable shear layers. Those vortices, now commonly called "large coherent structures" (Brown and Roshko 1974) are convected downstream at approximately the average speed of the two streams forming the shear layer. Figure 2.37 shows an example of the observations made by Brown and Roshko for cold flow at relatively low Reynolds number. In propulsion systems, the shear layers in question are generally formed in flow past bluff body flameholders (in thrust augmentors) or past rearward-facing steps (in ramjet engines).

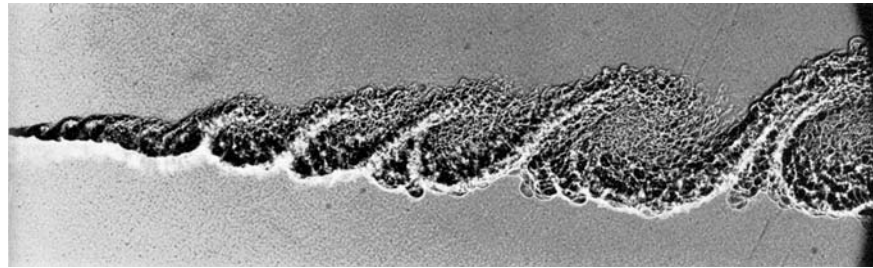


FIGURE 2.37. Large-scale coherent structures in a mixing layer at 8 atmospheres in flow past a splitter plate: upper stream ($v_1 = 10$ m/s) is He; lower stream is N₂, with $\rho_2 v_2^2 = \rho_1 v_1^2$. (Brown and Roshko 1974).

Observations of vortex shedding from flameholders, and recognition of the importance of this process as a possible mechanism for combustion instabilities were first independently reported by Kaskan and Noreen (1955), Rogers (1954) and Rogers and Marble (1956). Both experiments used premixed gaseous fuel and air

flowing past a flameholder in a rectangular channel. However, the particular mechanisms proposed were very different. Figures 2.38 and 2.39 taken respectively from Kaskan and Noreen (1955) and Rogers and Marble (1956) clearly show the vortex shedding. Particularly Figure 2.39 shows a good example of the influence of flow conditions on vortex shedding from a two-dimensional bluff body with combustion; in this case the bluff body was a two-dimensional wedge. At approximately constant speed, when the equivalence ratio in the premixed flow past the lip of the wedge was increased from about 0.75 to around 0.90 continuous vortex shedding began, and high-frequency acoustic oscillations were sustained in the channel. The oscillations were transverse to the axis of the channel.

Particularly noteworthy—and important—is the reasoning by Rogers and Marble for the presence of the oscillations. They give an appealing argument based on the idea that delayed pulses of combustion, producing pulses of pressure, occur periodically with the shed vortices. A vortex formed and shed from the lip of the flameholder entrains fuel mixture from the free stream. A short period of time passes during which the fresh (cold) gas mixes with hot combustion products entrained from the recirculation zone behind the flameholder. At the end of the ignition delay, the mixture in the vortex burns vigorously, generating a pulse of pressure which is supposed to reinforce the pressure oscillation in the chamber. For steady oscillations to be sustained, this process must evidently occur at the same frequency as that of the wave motion. For the tests typified by those shown in Figure 2.39, the ignition delay, according to results given by Zukoski and Marble (1954), was about 0.00028 seconds, suggesting a frequency around 3600 Hz. The observed oscillations (Figure 2.39) had frequencies in the range 3600–3900 Hz.

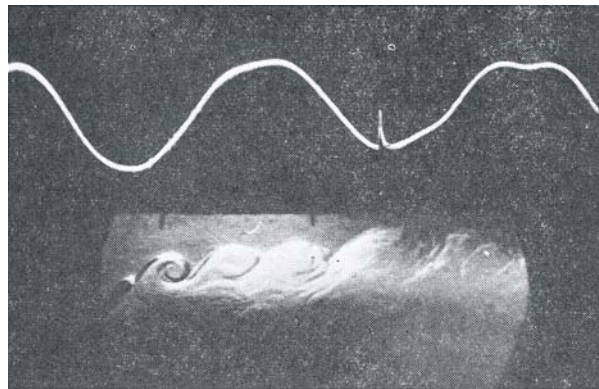


FIGURE 2.38. Photograph of vortices shed in a reacting flow (Kaskan and Noreen 1955).

Motivated partly by earlier observations of Blackshear (1953) and Putnam and Dennis (1953), Kaskan and Noreen proposed a different mechanism, speculating that stretching of the flame front accompanying roll-up in the vortex causes a pressure disturbance. Periodic disturbances generated by vortex shedding may then sustain either transverse or longitudinal acoustic fields. (They observed both in their tests, but transverse waves were most common.) As a quantitative basis for interpreting their results they modified a theoretical relation derived by Chu (1953) for plane flames. Although they had modest success comparing their reasoning with their data, Kaskan and Noreen did not provide a complete explanation of the closed-loop process required to generate self-excited oscillations. This mechanism has subsequently received much notice as a possible cause for combustion instabilities after the idea was revived in the 1980s in connection with work on ramjet combustion. More recently, several groups have used the idea of changing flame to represent a possible mechanism in problems of active control; for example see Section 2.5.

During the past twenty years, the idea that vortex shedding is a dominant factor in mechanisms for many combustion instabilities in liquid-fueled systems has gained growing support. Practically all of the work has been motivated by problems of longitudinal oscillations in ramjet engines. Even though the frequencies are

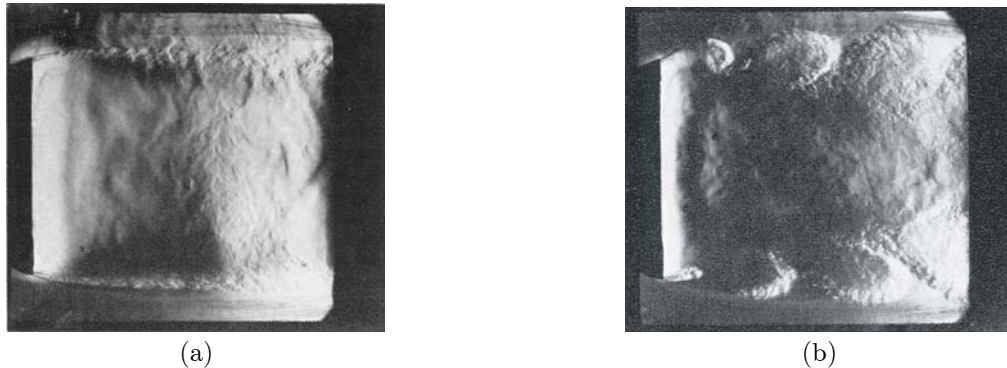


FIGURE 2.39. Flow past a bluff body flameholder under two conditions of flow at approximately the same speed. (a) low equivalence ratio, $\phi \lesssim 0.75$, no oscillations; (b) high equivalence ratio $\phi \gtrsim 0.90$, acoustic oscillations in the channel (Rogers and Marble 1956).

substantially lower than those of the oscillations treated by Rogers and Marble, the essentials of the idea seem to hold true.

The problem of longitudinal oscillations in ramjet engines was found quite early in their development although the direct connection with instabilities in combustors was not immediately clear (Conners 1950). Longitudinal oscillations in small ramjet engines was apparently first recognized by Hall (1978). Rogers (1980a, 1980b) gave thorough summaries of the available experimental work. Those reports marked the beginning of widespread attention and work which continued until the early 1990s. In particular, Rogers' investigation served as the basis for an early analysis of the problem by Culick and Rogers (1983); that work did not include a satisfactory mechanism. Vortex shedding as a possible mechanism for causing the longitudinal modes in a ramjet engine seems to have been discussed first at a JANNAF workshop in 1979 (Culick 1980). Byrne (1981, 1983) gave the first detailed discussion of the mechanism. His 1983 paper is a very nice description of the problem and touches on several problems understood only later, in particular with work at the Naval Weapons Center. Apparently unaware of the earlier work by Rogers and Marble on transverse oscillations, Byrne based his argument on established results for cold jet flows. He used known results for the stability of shear layers and jets, vortex shedding and vortex merging to argue that the frequencies of those processes taking place under the conditions occurring in ramjet engines are in the range of frequencies of the oscillation actually observed. He supported his conclusions by good comparisons of his estimated frequencies with data taken by others for both coaxial and side-dump configurations. Waugh *et al.* 1983 showed modest success in their Appendix B correlating amplitudes of instabilities with Strouhal number.

Since the early 1980s a great deal of attention has been given to the role of vortex shedding in dump combustors, both in cold flow and in laboratory combustion tests (e.g., Keller *et al.* 1982; Smith and Zukoski 1985; Biron *et al.* 1986; Schadow 2001; Sterling and Zukoski 1987; Poinsot *et al.* 1987a,b; Yu *et al.* 1987a,b). There is little doubt now that indeed the coupling between shed vortices and the acoustic field is the dominant mechanism in dump combustors. That coupling may or may not be accompanied by energy release due to combustion. The extent to which the same mechanism is active in contemporary thrust augmentors is less well-established but there is good reason to believe that it is often the main cause.

Extensive experimental work on vortex shedding in shear layers and jets at room temperature has provided a fairly complete picture of the formation of vortices; vortex pairing; and the general features of the flow without heat addition (see Schadow *et al.* 1987b for a brief review of the literature relevant to problems in ramjet engines). Tests in various configurations, including those appropriate to ramjets (e.g., Flandro *et al.* 1972; Culick and Magiawala 1979; Dunlap and Brown 1981; Brown *et al.* 1981, 1983; Schadow *et al.* 1987,

1989; Schadow and Gutmark 1992; Schadow 2001) established the ability of shed vortices to drive acoustic resonances over a broad range of flow conditions. See Section 8.6 for further discussion of experimental work on vortex shedding with no combustion. The works cited above have extended that conclusion to flows with large heat addition accompanying combustion under circumstances simulating those found in actual ramjet engines. We will discuss those results further in Section 8.6.

The obvious qualitative importance of combustion in large vortices has prompted several analytical investigations of the process. Broadly the idea is that the shear layer is formed at the edge of a bluff body, the high speed stream consisting of an unburnt mixture of reactants; the low speed stream is composed largely of hot combustion products forming the recirculation zone behind the body. As Smith and Zukoski (1985) and Sterling and Zukoski (1987) have shown, the shear layer exhibits widely varying degrees of stability depending on the operating conditions. We are concerned here with cases when the layer is highly unstable, a situation encouraged by the action of the acoustic velocity forcing oscillations of the layer at the lip. Large vortices may then rapidly form, entraining unburnt mixture on one side of an interface, with the combustion products on the other side. A flame is initiated at the interface and the question to be answered is: how does the rate of combustion, and therefore heat release, vary as the vortex rolls up and propagates downstream?

Marble (1984) treated an idealized case of a diffusion flame initiated along a horizontal plane when simultaneously the velocity field of a line vortex is imposed along an axis in the interface. Elements of flame initially in the interface are caused to execute circular motions and are stretched by the vortex field, causing an increase in the rate at which reactants are consumed. The expanding core contains combustion products but as the vortex roll-up continues, the rate of consumption always remains greater than that for flame in the flat interface having the same length as that in the rolled-up vortex. Karagozian and Marble (1986) carried out a similar analysis accounting for the influence of stretching along the axis of the vortex. They found that, following a transient period during which the core grows to its asymptotic form, the augmented consumption rate is unaffected by axial stretching. In those cases the rate of heat release reached a constant value monotonically: there is no distinguished period of pulsed combustion as required for the mechanism for instability described above.

Subsequently, Laverdant and Candel (1987a,b; 1988) analyzed both diffusion and premixed flames in the presence of vortex motion with finite chemical kinetics. Their analysis is entirely numerical giving good agreement with the results obtained by Karagozian and Marble (1986) and Karagozian and Manda (1990) for a vortex pair.

Norton (1983) also analyzed the influence of finite chemical kinetics in the problem posed and solved by Marble (1984) who had assumed infinite reaction rates. Under some conditions, the heat release rate shows a modest peak in time. However, neither his results, nor those of Laverdant and Candel, suggest the sort of time delay to pulsed combustion one might like to see to complete the picture.

No work has been accomplished to determine whether or not the augmented reaction rates found in the analyses are sufficient to explain the mechanism of instabilities driven by vortex combustion. On the other hand, the experimental results reported by Smith and Zukoski (1985), Sterling and Zukoski (1987), and Yu *et al.* (1987)a,b show vividly and beyond doubt that unsteady combustion associated with vortex motions is a vigorous source indeed. Figure 2.40 is a sequence of photographs taken by Smith and Zukoski during one cycle of a high amplitude oscillation. They propose the following mechanism. A vortex is initiated at the edge of the step at a time determined partly by the local acoustic velocity. The vortex propagates downstream, releasing energy at a rate that seems to reach maximum when the vortex impinges on the wall. In order for impingement to occur at a favorable time during the acoustic oscillation, the propagation rate and hence strength of the vortex must increase with frequency. Because the vortex strength depends on the magnitude of velocity fluctuation initiating the motion at the lip, it is necessary that the steady amplitude of the acoustic field increase with frequency. That behavior is observed. Moreover, numerical calculations

by Hendricks (1986) have shown quite similar behavior for the unsteady flow induced by an abrupt change of velocity past a rearward-facing step. Figure 2.41 is a sketch taken from Hendricks' work showing the development of a vortex calculated for those conditions.

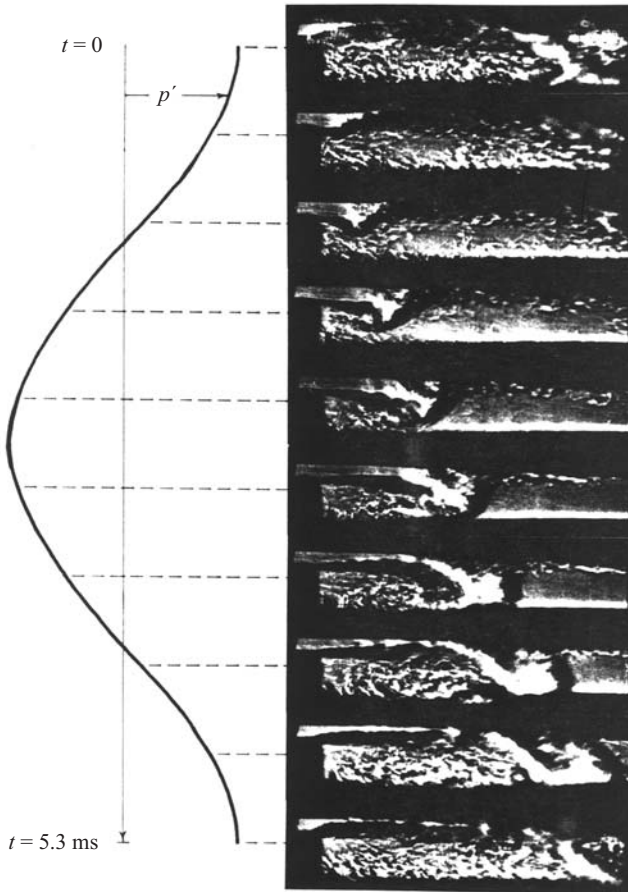


FIGURE 2.40. Development of a vortex during one cycle of a pressure oscillation (Smith and Zukoski 1985).

The essential ideas of vortex combustion as a mechanism for driving instabilities can be incorporated in the approximate analysis developed here. There is ample experimental evidence that large vortices in cold flow can sustain resonances in a duct; Flandro (1986) has shown one means of handling the process analytically, based on direct fluid mechanical coupling between vortical and acoustic motions. See also Aaron (1984) and Aaron and Culick (1985) for an elementary model of coupling associated with impingement of a vortex on an obstacle. Tests with combustors have shown, however, that the amplitudes of oscillation are substantially greater when burning occurs. That result is most likely due to the unsteady energy release. We therefore assume that this is the main source of the driving.

Hence in the forcing function F_n^L , equation (1.21), we retain only the term containing Q' , giving equation (1.23) written now for the time-dependent amplitude of the n^{th} mode:

$$\frac{d^2\eta_n}{dt^2} + \omega_n^2\eta_n = \frac{\gamma - 1}{\bar{p}E_n^2} \int \psi_n \frac{\partial Q'}{\partial t} dV \quad (2.109)$$

A formula for Q' must be constructed to account for the trajectory of the vortex and its associated rate of energy release along the trajectory. To illustrate with a simple example, we consider excitation of longitudinal

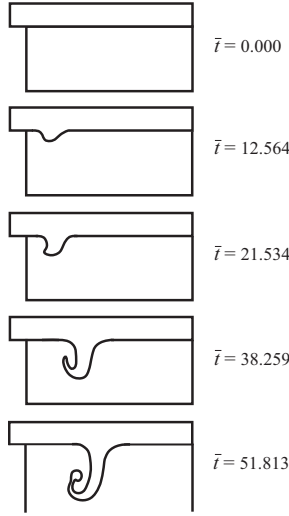


FIGURE 2.41. Development of a vortex at the interface of two unlike fluids (Hendricks 1986).

modes and assume that the vortex travels parallel to the axis. Within the one-dimensional approximation, that implies averaging the presence of the vortex over planes transverse to the axis. The situation is sketched in Figure 2.42. The origin $z = 0$ is at the step, which is not the location of a pressure anti-node. In fact, we must allow the acoustic velocity to be non-zero at the beginning of the shear layer at $z = 0$, so the mode shape is

$$\psi_n(z) = \cos(k_n z + \phi) \quad (2.110)$$

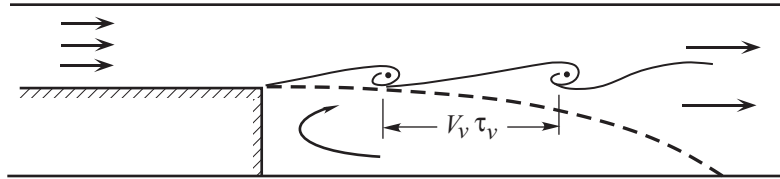


FIGURE 2.42. An elementary model of combustion in vortices as a mechanism for driving acoustic waves.

The values of k_n and ϕ can be set by imposing a boundary condition at $z = l$ and choosing some location $z < 0$ for a pressure anti-node. For example, if pressure anti-nodes occur at $z = -\delta L_0$ and $z = L + \delta L_1$, the two conditions must be satisfied

$$\begin{aligned} \sin(-k_n \delta L_0 + \phi) &= 0 \\ \sin[k_n(L + \delta L_1) + \phi] &= 0 \end{aligned} \quad (2.111)$$

from which k_n and ϕ can be determined. For the purposes here, the particular values of k_n and ϕ are immaterial. With (2.110), the acoustic pressure and velocity are

$$\begin{aligned} p' &= \bar{p} \eta_n(t) \cos(k_n z + \phi) \\ u' &= \frac{\dot{\eta}_n}{\bar{\gamma} k_n} \sin(k_n z + \phi) \end{aligned} \quad (2.112)a,b$$

For simplicity, assume that the vortices propagate with constant speed v_v and are launched periodically with period τ_v at the times $t = 0, \tau_v, 2\tau_v, \dots$. Assume further that these are point vortices releasing energy

at the rate $q(t)$ each. Hence the energy release associated with a train of shed vortices can be represented by δ -functions moving with speed v_v , multiplying the energy release:

$$\begin{aligned} Q'(z_1 t) &= q_1(t) \delta[z - v_v t] + q_2(t) q[z - v_v(t - \tau_v)] + q_3(t) \delta[z - v_v(t - 2\tau_v)] + \dots \\ &= \sum_{j=0}^{\infty} q_j(t) \delta[z - v_v(t - j\tau_v)] \end{aligned} \quad (2.113)$$

In accordance with the behavior reported by Smith and Zukoski we should relate the strength of each vortex and, therefore by assumption its energy release, to the velocity fluctuation causing its birth. For simplicity we ignore the influence of the mean flow speed and set q_j proportional to the acoustic velocity at the step and at the time when the vortex is launched. Hence, we assume

$$q_j(t) = \bar{q}_j(t) u'(0, j\tau_v) = -\bar{q}_j(t) \frac{\dot{\eta}_n(j\tau_v)}{\bar{\gamma} k_n} \sin \phi \quad (2.114)$$

where $q(t)$ is supposed to be common to all vortices. With (2.114) for $q_j(t)$, differentiate (2.113):

$$\frac{\partial Q'}{\partial t} = - \sum_{j=0}^{\infty} \frac{\dot{\eta}_n(j\tau_v)}{\bar{\gamma} k_n} \sin \phi \left\{ \dot{\bar{q}}_j \delta[z - v_v(t - j\tau_v)] - \bar{q}_j v_v \delta[z - v_v(t - j\tau_v)] \right\} \quad (2.115)$$

Now substitute (2.110) and (2.115) in the integral on the right-hand side of (2.107), with $dV = S_c dz$ where S_c is the cross-section area of the chamber:

$$\int \psi_n \frac{\partial Q'}{\partial t} dV = S_c \int_0^L \cos(k_n z + \phi) \sum_{j=0}^{\infty} \frac{\dot{\eta}_n(j\tau_v)}{\bar{\gamma} k_n} \sin \phi \left\{ \dot{\bar{q}}_j \delta[z - v_v(t - j\tau_v)] - \bar{q}_j v_v \delta[z - v_v(t - j\tau_v)] \right\} dz$$

Use the properties

$$\int \delta(x - a) f(x) dx = f(a); \quad \int \delta'(x - a) f(x) dx = -f'(a)$$

to find:

$$\begin{aligned} \int \psi_n \frac{\partial Q'}{\partial t} dV &= - S_c \sum_{j=0}^{\infty} \xi_{nj} \left\{ \dot{\bar{q}}_j(t) \cos[k_n v_v(t - j\tau_v)] \right. \\ &\quad \left. + \bar{q}_j(t) k_n v_v \sin[k_n v_v(t - j\tau_v)] \right\} \end{aligned} \quad (2.116)$$

with

$$\xi_{nj} = \frac{\dot{\eta}_n(j\tau_v)}{\bar{\gamma} k_n} \sin \phi \quad (2.117)$$

Thus we have an expression for the right-hand side of (2.107) representing the forcing due to a train of burning vortices, launched at $t = 0, \tau_v, 2\tau_v, \dots$ from the lip of the step at $z = 0$. This model has been the starting point for two analyses by Matveev and Culick, 2002b and 2003a; the following section is a summary of the work.

By far most attention has been directed to vortex shedding as the most likely mechanism for combustion instabilities in ramjet engines, although recently more attention has been paid to the phenomenon in gas turbines. In addition to extensive experimental work related to those ideas, much has been done, both with laboratory tests and analysis, to clarify the acoustical characteristics of the modes of oscillation. Much more is known, and understood, about vortex shedding and its role as a mechanism for causing combustion instabilities chiefly because that phenomenon is easily identified in experiments and is commonly encountered. Although vortex shedding is arguably the dominant feature causing instabilities in dump combustors—and might therefore be termed the most important mechanism—it cannot be separated completely from convective waves. Furthermore, neither mechanism can be understood apart from the acoustics of the chamber

in which they occur; the type of mode that is unstable always provides some clues about the mechanism. For convenience here we nevertheless treat the phenomena separately. One distinction between the two mechanisms that seems to be true, is that if direct coupling between large vortices and the acoustics field dominates, the frequencies of oscillations tend to be close to those of classical resonances. If convective waves are involved, the frequencies may be quite different, as shown with the elementary example in Section 2.3.3.

As we discussed above, the earliest ideas based on vortex shedding were developed in the 1950s to explain the occurrence of high frequency transverse or tangential waves in afterburners. Periodic combustion of reactants entrained in large vortex structures served as sources of acoustic energy. If properly phased, the sources may supply energy to an acoustic mode of the chamber. The fluctuations of velocity associated with the mode initiate vortex shedding, completing the cycle.

Roughly two decades later vortex shedding was again proposed as a possible mechanism for instabilities in solid rockets, but periodic combustion was not part of the argument (Flandro and Jacobs 1975; Culick and Magiawala 1979). Laboratory tests in cold flow established the result that if vortices shed from a step or corner impinge on an obstacle downstream, there is sufficient coupling with unsteady motions to excite the sustain standing acoustic modes in a duct (Culick and Magiawala 1979; Dunlap and Brown 1981; Dunlap *et al.* 1981; Nomoto and Culick 1982; Aaron and Culick 1985). In all those cases, longitudinal modes were driven. Large “vortex-like” structures were observed in some flow visualization work on dump combustors at AFWAL sometime in the late 1970s [Private communication, F.D. Stull].

Since 1980, a large number of experimental works have established both by visualization and quantitative measurements that vortex shedding is a distinctive feature of dump combustors. (Schadow *et al.* 1985, 1987b; Smith and Zukoski 1985; Brown *et al.* 1985; Biron *et al.* 1986; Sterling and Zukoski 1987; Poinsot *et al.* 1987; Yu *et al.* 1987; Davis and Strahle 1987). All of those tests were performed either in cold flow or with premixed gaseous reactants. The most extensive summary of the subject has been given by Schadow *et al.* (1987b) who included also references to related work not discussed here.

The work by Schadow and co-workers at the Naval Weapons Center (e.g., see the summary by Schadow and Gutmark 1992) is particularly noteworthy for its systematic progression from tests in cold flow to experiments in dump combustors with burning, as well as for studies of vortex combustion in diffusion flames. Their program used at least four different experimental facilities and involved both forced and self-excited oscillations. They also performed limited tests in a water tunnel to show the formation of large vortices in their configuration. Overall, the work at NWC established the existence of vortex shedding at the frequencies of instabilities in realistic coaxial configurations. Moreover, they showed that combustion processes drive oscillations to much higher amplitudes than found in the cold flow tests. We should emphasize that for the cases cited earlier, of oscillations driven by vortex shedding in solid rocket motors, the vortices were formed in essentially non-reacting combustion products. The amplitudes of such instabilities have always been relatively small (<5% of mean pressure). Thus it seems true, as found also in the work by others cited above, that truly large amplitude oscillations require the presence of combustion processes and the conversion of heat released to mechanical energy.

Hegde *et al.* (1986, 1987) and Reuter *et al.* (1988) studied oscillations in a duct driven by a flame sheet, in a situation similar to that devised by Kaskan and Noreen (1955) and by Dowling and co-workers at Cambridge for afterburners (Figure 2.57). In the Georgia Tech tests by Hegde *et al.*, the flame (or flames) is stabilized on one or two wires spanning a duct. Under broad conditions, the flame is unstable and vortices grow in the sheet. Interactions with the flow field are sufficiently strong to excite acoustic waves in the duct. The authors proposed that fluctuations of the flame surface area—and hence of the reaction rate are responsible. They gave data based on emitted radiation, showing that the oscillations of surface area are in phase with the pressure variations. By Rayleigh’s Criterion (Section 6.6) for heat addition, it follows that

the heat addition encourages growth of acoustic waves, a result established also by Sterling and Zukoski (1987) for a dump combustor.

Although most experimental work related to vortex shedding in ramjets has been done with coaxial configurations, the phenomenon has also been found in side-dump combustors. Stull *et al.* (1983) reported early work with that geometry and Nosseir and Behar (1986) have examined similar cases in a small scale. More extensive results with full-scale hardware were discussed by Zetterström and Sjöblom (1986) who investigated a configuration having two or four inlets. Visualization in a water tunnel revealed the presence of vortex shedding. Instabilities in the operating engines were avoided by modifying the fuel injection systems in such a fashion as to minimize combustion within the vortices. That's an important practical result clearly supporting the general picture of vortex shedding as a dominant mechanism.

2.3.5. A Model for Vortex Shedding and Excitation of Acoustic Waves. Despite the widespread recognition of vortex shedding as an important mechanism for the excitation of oscillations in dump combustors, there is no analysis that captures the main features of the process. Since the early observation and interpretations by Kaskan and Noreen (1955) and by Rogers and Marble (1956) there have been a number of experimental works, especially motivated by problems with ramjets in the 1980s and 1990s. There are few theoretical works and they have produced only modest success. The basic ideas are probably understood correctly, but until they have been successfully developed into a predictive theory, one cannot be sure. In this section we summarize one recent attempt to construct a quantitative description of the basic process, based on the model sketched in Figure 2.42.

Expressed in simplest terms, the central idea in most, if not all, treatments of the excitation of acoustic waves by vortex shedding and combustion is simply stated. Vortices are periodically generated, at a backward-facing step in the present case, propagate downstream with little or no burning, and at some later time undergo vigorous combustion, releasing "pulses" of energy. The energy added in a small volume is accompanied by a rapid rise of pressure locally, which is available to augment the pressure in the flow. Whether a sequence of such pulses will in fact cause a wave, or a mode of oscillation, to be sustained is a matter to be worked out by available methods for solving problems of acoustics with sources in a finite volume, a combustor. The simplest governing equation for the process is (2.109), with a damping term included to agree with Matveev and Culick (2003):

$$\frac{d^2\eta_n}{dt^2} + 2\zeta_n\omega_n \frac{d\eta_n}{dt} + \omega_n^2\eta_n = \frac{\gamma-1}{\bar{p}E_n^2} \int \psi_n \frac{\partial \dot{Q}}{\partial t} dt \quad (2.118)$$

The unsteady motions are treated as one-dimensional, but small deviations can be accommodated in $\psi_n(x)$. That is a relatively minor deviation here. We are primarily concerned with the action of periodic burning in vortices which are small compared with characteristic dimensions of the enclosing volume or chamber. A basic assumption is that the burning occurs instantaneously and releases an amount of energy that is proportional to the circulation Γ_j of the j^{th} vortex. Passing to the limit of point vortices, we use the expression for \dot{Q} ,

$$\dot{Q} = \beta \sum \Gamma_j \delta(x - x_j) \delta(t - t_j) \quad (2.119)$$

where β is a constant to be given a value later. To be definite, we suppose that instantaneous burning occurs when a vortex strikes a wall or obstacle, Figure 2.43, or after an induction time as described by Rogers and Marble (1956).

A shed vortex moves with the total flow velocity at the instantaneous position of the vortex. For the case shown in Figure 2.42 a vortex located close to the boundary between the recirculation zone and the primary flow moves with a speed \dot{x}_j which may be approximated as

$$\dot{x}_j(t) = \alpha \bar{u}(x_j) + u'(x_j, t) \quad (2.120)$$

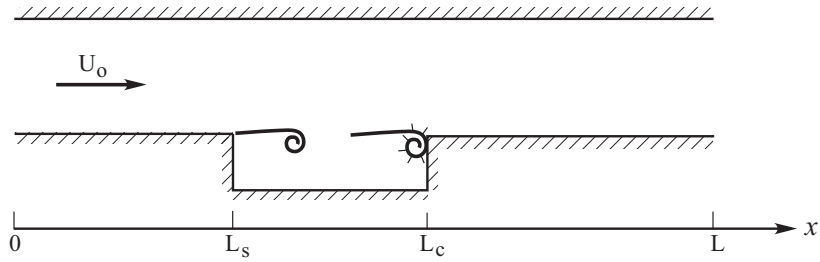


FIGURE 2.43. Vortex shedding from a backward-facing step, followed by impingement on an obstacle.

where α usually lies in the range 0.5 – 0.6 (Dotson *et al.* 1997) for segmented rocket motors. With (2.120) substituted in (2.119), the equation governing η_n in the time interval (t_{j-1}, t_{j+1}) is

$$\ddot{\eta}_n + 2\zeta_n\omega_n\dot{\eta}_n + \omega_n^2\eta_n = c\psi_n(x_j)\Gamma_j\delta(t - t_j) \quad (2.121)$$

Following Andronov *et al.* (1987), (2.121) gives the usual result for the motion of an oscillator in the interval (t_{j-1}, t_{j+1}) except at the instant t_j when the jump conditions are satisfied:²²

$$\begin{aligned} \eta_n(t_j+) - \eta_n(t_j-) &= c\psi_n(x_j)\Lambda_j \\ \dot{\eta}_n(t_j+) - \dot{\eta}_n(t_j-) &= 0 \end{aligned} \quad (2.122)a,b$$

The relation (2.122)b means that the velocity is instantaneously unchanged while the amplitude η_n changes discontinuously by the amount $c\psi_n(x_j)\Lambda_j$ at the instant t_j . Such behavior is characterized as that of a “kicked” oscillator.

The time at which a vortex separates from the step, and its strength are modeled following the idea introduced by Clements (1973). A vortex is formed from the vorticity contained within the thickness of the boundary layer shed from the step. With a relatively simple argument the result for the circulation of a shed vortex is

$$\Gamma = \frac{\bar{u}D}{2St} \quad (2.123)$$

where D is a characteristic dimension roughly equal to the momentum thickness of the boundary layer and St is the Strouhal number for vortex shedding at frequency f_s : $St = \frac{\bar{u}}{f_s D}$. The formula (2.123) has the interpretation that a vortex detaches from a step when its circulation reaches the “critical” value given by the right-hand side of (2.123). Matveev and Culick propose that a vortex is shed in unsteady flow when its circulation reaches the value given by (2.123) with \bar{u} replaced by the instantaneous velocity $\bar{u} + u$:

$$\Gamma(t) = \frac{u(t)D}{2St} \quad (2.124)$$

The Strouhal number is assumed to have the same value in steady and unsteady flow. This formula shows fairly good agreement with experimental results for vortex shedding from a rising in oscillatory flow (Castro 1997). However, the result has been only weakly tested; perhaps most seriously, data is available only for isothermal flows.²³

The model was used by Matveev to calculate a two-dimensional case, Figure 2.43, representative of the experimental results reported by Smith (1985), Sterling (1987), Smith and Zukoski (1985), and Sterling and Zukoski (1991). The damping coefficient was set according to information provided by Sterling and Zukoski,

$$\zeta_n = \frac{1}{2\pi} \left(0.135 \frac{\omega_n}{\omega_1} + 0.015 \sqrt{\frac{\omega_1}{\omega_n}} \right) \quad (2.125)$$

²²Damping is neglected ($\zeta_n = 0$) for derivation of these conditions.

²³Schadow and Gutmark (1992) have discussed vortex shedding for various geometries in isothermal and reacting flows.

in which end losses are represented by the first term and the second term accounts for the attenuation due to acoustic boundary layers. As identified by Smith, five acoustic modes were accounted for, having frequencies (in Hertz) 180, 229, 385, 470, and 590. Values for the various parameters in the model, and reasons for the choices, are given by Matveev and Culick (2002)b, (2003)a and by Matveev (2004). With (2.121), (2.122)a,b and (2.124), the unsteady pressure field may be estimated. Figure 2.44 shows some results.

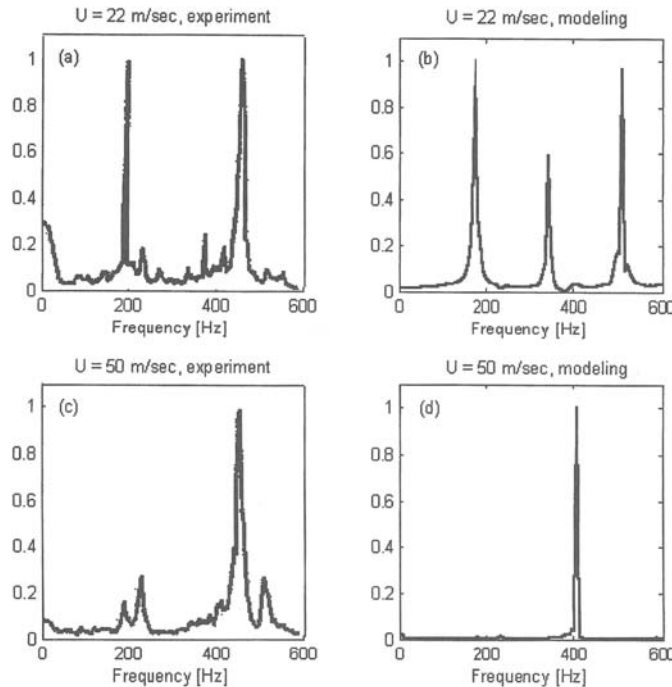


FIGURE 2.44. Normalized spectra of pressure fluctuations at the step of Figure 2.43 for two mean flow velocities at the dump plane. (a), (c) experimental results (Smith 1985); (b), (d) results from the kicked oscillator model.

In its present state, the ‘kicked oscillator’ model has no practical value except as a view or interpretation of a mechanism for oscillations in a combustor. The analysis we have briefly and incompletely described is suggestive and has wider possibilities than discussed here. This example illustrates the relative ease with which results can be obtained without tedious integration of the partial differential equations governing ‘exact’ solutions.

2.4. Further Remarks on Particular Forms of Liquid-Fueled Systems

Most of the discussion in Section 2.3 was concerned with matters common to all types of liquid-fueled systems. Much of the work was in fact carried out in the U.S. originally for liquid fueled rockets, the strongest motivation being applications to engines intended for the Apollo vehicle. Some of the ideas and methods developed for liquid rockets have subsequently been modified or extended for analysis of combustion instabilities in augmentors and ramjets. Moreover, there are special problems peculiar to the different systems themselves. We therefore examine now those particular matters.

2.4.1. Combustion Instabilities in Liquid Rockets. Little work was done outside the USSR on the problem of instabilities in liquid rockets during the 1970s. With the flight failure of an Ariane vehicle due to combustion instability in a first stage Viking motor, a comprehensive research program was initiated in France in 1981. Most of the available reports of that work have already been referred to and little more needs to be added here.

Within the present context, the most important parts of the French work are the experimental and analytical efforts to characterize the liquid spray; and the extensive numerical simulations of unsteady motions, incorporating the results obtained for the propellant sprays. The problem causing the failure involved coupling between the pressure oscillations in the chamber and structural vibrations of the injector which is placed in the lateral boundary as sketched in Figure 2.45 taken from Souchier, Lemoine and Dorville (1982). Figure 2.45(b) shows the computed distortion of the injector plane. As a result, the fuel and oxidizer jets were shaken, causing (apparently) perturbations of the distribution and phase of the energy release, thereby closing the loop and making possible self-excited motions.

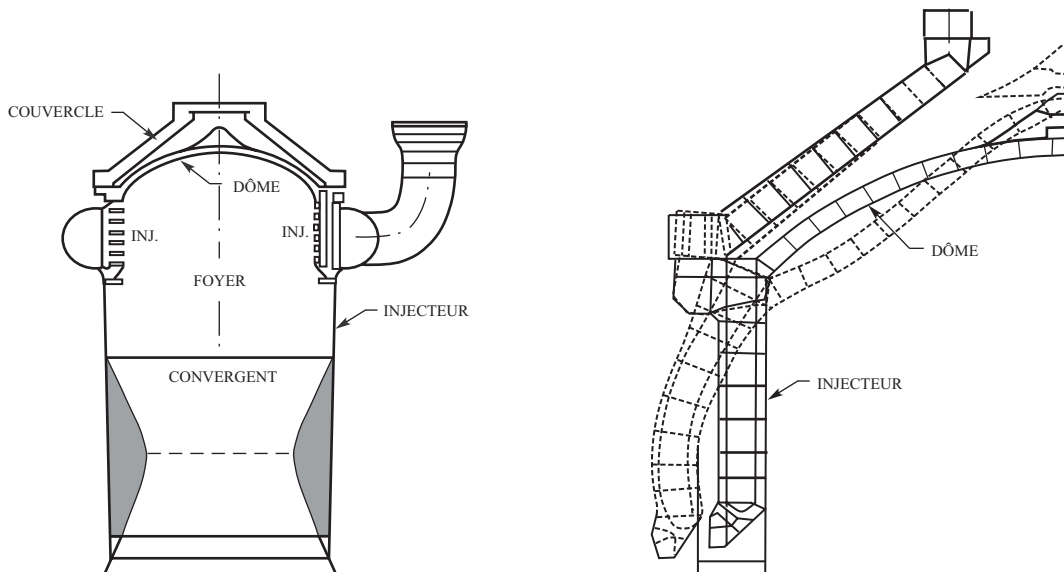


FIGURE 2.45. Coupling between pressure oscillations, structural vibrations and the injection system (based on drawings appearing in Souchier, Lemoine and Dorville 1982).

Such effects on the injection processes have long been known to be a possible cause of instabilities (Levine 1965; Harrje and Reardon 1972) but they have yet to be well-characterized.²⁴ They are likely to be particularly important in cases when the amplitudes of motion are large. It is quite possible that the forms of the representation of the unsteady sources of mass and energy are strongly dependent on the amplitudes of motion as well as on the hardware design. Such behavior is far outside any successes of the time lag model and is likely to remain so. Careful experimental work is essential to clarify the situation.

During the mid-1980s, serious interest in developing new liquid-fueled rockets grew in the U.S., primarily for use in proposed heavy lift launch vehicles. Because of their high densities and good performance, liquid oxygen and hydrocarbon fuels were considered as propellants. In particular, methane was selected by the NASA Lewis Research Center as the favored fuel. As a result, studies of combustion instabilities were carried out at the Aerojet TechSystems Company and at the Rocketdyne Division of Rockwell International.

²⁴The more recent work by Bazarov, cited briefly in Section 8.5, has done much to correct this situation.

Rocketdyne designed and fabricated two engines, for the Lewis Research Center (LeRC) and for the Marshall Space Flight Center (MSFC). Both used LOX/methane and had identical thrust chambers but different injectors. The MSFC engine had an acoustic resonator; the LeRC engine had no damping device. A small number of firings directed to determining stability characteristics were completed (Jensen, Dodson and Trueblood 1988; Philippart and Moser 1988).

A computer program for analysis of instabilities was developed from an earlier program, IFAR. (Fang 1984, 1987; Fang and Jones 1987; Mitchell, Howell and Fang 1987; Nguyen 1988). The program IFAR (Injector Face Acoustic Resonator) had been in existence for some years; the time lag model was used to represent the combustion process. That program was revised and modified for application to both rectangular and axisymmetric chambers to become HIFI (High Frequency Intrinsic Stability) (Nguyen 1988).

With all other variables and parameters specified, the values of n and τ are calculated on the stability boundary. Then to predict whether the engine is stable or not, the values of n and τ must be determined. Traditionally this has been done with correlations for injectors using hydrocarbon fuels, so as part of their work the group at Aerojet performed sub-scale tests and carried out analysis of the injector response (Muss and Pieper 1987; Nguyen and Muss 1987). The analysis and tests were intended to provide correlations of n and τ for the injector with those on the stability boundary calculated with the analyses cited above.

Aerojet carried out a program combining analysis, sub-scale tests using both rectangular and axisymmetric chambers prior to full-scale firings. The chief purpose was to provide as certain as possible basis for confidently predicting the stability of the large engines, thereby reducing development costs. This program was described by Muss and Pieper (1988).

Philippart (1987) and Philippart and Moser (1988) reported comparisons of predictions of the sort mentioned above, with firings of the two Rocketdyne engines. One operating condition was examined for which the LeRC engine was stable and the MSFC engine was unstable. Three calculations of the stability boundary in the $n - \tau$ plane were done, using the program IFAR, HIFI and a modified from (NDORC) of Mitchell and Eckert's (1979) MODULE. Figure 2.46, taken from Philippart and Moser, shows the results obtained with HIFI for the two engines. Results obtained with the other two programs differ in details that are unimportant here. Also shown as filled regions are estimates of the 'combustor response' (i.e. the values of n and τ) based on correlations for LOX/hydrogen injectors. Apparently the predictions of the three codes agreed fairly well. However, there are uncertainties owing to differences between the codes; a significant distinction is that IFAR and HIFI assume that combustion is concentrated in a transverse plane, while MODULE is written for distributed combustion. Comparison with the test data is ambiguous and must be viewed as estimates because the true characteristics of the injectors are unknown.

Jensen, Dodson and Trueblood (1988) gave an early progress report in their tests with the LeRC engine. They measured growth rates and, using the MODULE program, inferred the necessary values of n and τ . Two examples are shown in Figure 2.47. The striking result is that the values of the interaction index are found to be considerably greater than those computed by Philippart and Moser and those provided by previous correlations of data. It is impossible at this point to determine the cause for these differences. The existence of such significant differences probably betrays the absence of a fundamental basis and understanding of any *ad hoc* approach based on a time lag 'model'.

Also at Rocketdyne some interesting work to analyze the characteristics of sprays vaporizing and burning under steady conditions was reported by Liang *et al.* (1986, 1987a,b,c). The calculations were done for various injector types placed in chambers, with provision for computing the internal flow field. When extended to cover transient motions, this work seemed to be potentially an important contribution to analysis of combustion instabilities but it seems that the potential was not realized. Indeed, it appears that among the

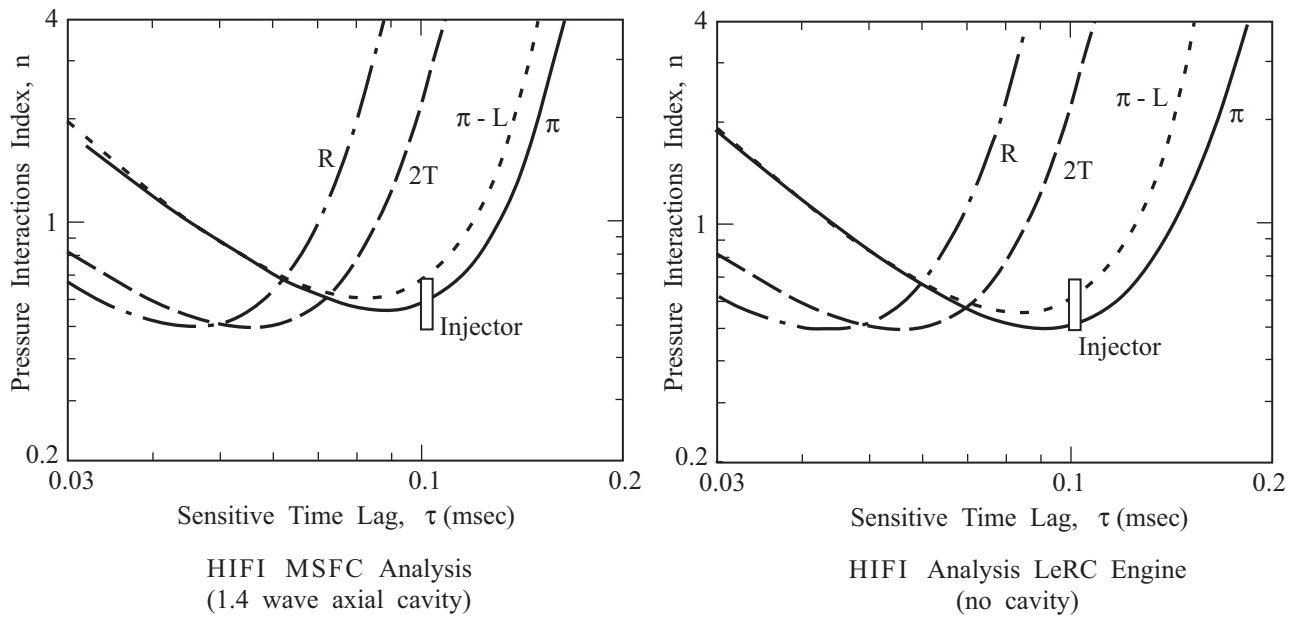


FIGURE 2.46. Some results of calculations based on the n - τ model (Philippart and Moser 1988).

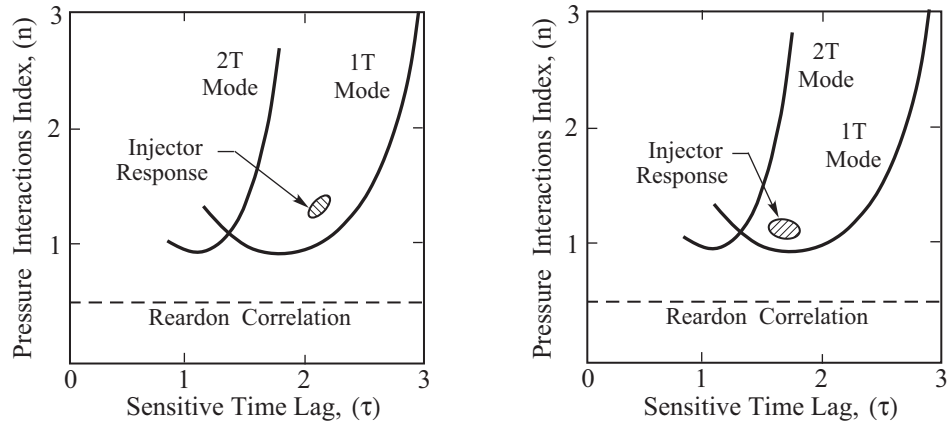


FIGURE 2.47. Comparison of calculations and some experimental results interpreted with the n - τ model (Jensen, Dodson and Trueblood 1988).

most important outstanding problems in the subject are the production of the liquid drops; unsteady spray combustion; and incorporation of the results in a complete formation allowing realistic numerical simulations.

2.4.2. Application of the Time Lag Model to Gas and Liquid Rockets. By 'time lag model' we mean here the most common form, expressed by equation (2.94) for the unsteady conversion of liquid to gas. Crocco and Cheng (1956) examined various elaborations, including spatial variations of the sensitive time lag, but here we shall assume τ to be uniform everywhere and the same for all elements of injected propellant. Also we will not distinguish between oxidizer and fuel. Both assumptions have been adopted in almost all applications, a notable exception being an analysis of chugging in which two time lags were introduced (Szuch and Wenzel 1968).

Although some analysis has been done of nonlinear behavior with the time lag model (see Chapter 7 for work by Sirignano and Crocco 1964; Mitchell, Crocco and Sirignano 1969; and Mitchell and Crocco 1969) by far most results, and all applications, have been worked out for linear behavior. To illustrate here, we appeal to the approximate analysis described later. Although differences in detail will arise, the results will contain all the essential ideas discussed in previous works.

Broadly, the central idea is to use the formula for the growth constant, α , *evaluated on the stability boundary*, so $\alpha = 0$. Those terms containing ω will of course depend on the interaction index, n , and the time lag, τ . If we assume that all other contributions to the formula are known, then the condition $\alpha = 0$ provides a relation between n and τ that must, within the approximations used, hold on the stability boundary.

There is no need to work out details here; see Chapter 6. The equation defining α will take the form

$$\alpha = C_1 \int \psi_n \hat{w}_l^{(r)} dV - C_2$$

where C_1, C_2 are constants. The constant C_2 contains the various effects of liquid/gas interactions, the nozzle, mean flow/acoustics interactions and damping devices. Now with \hat{w}_l given by (2.94), its real part is $n(1 - \cos \omega \tau)$, and for $\alpha = 0$, the last equation gives

$$n(1 - \cos \omega \tau) = \frac{C_1}{C_2 \int \bar{w}_l \psi_n^2 dV} = G_R \quad (2.126)$$

The function G_R is supposed to be known, with value depending on the various parameters (geometrical, etc...) defining the system. Then equation (2.126) is the relation between n and τ referred to above.

Figure 2.48 shows the unstable regions defined by equation (2.126). This is a reproduction of Figure 4.2.2a, p. 180, in an article prepared by Crocco (Harrje and Reardon 1972). The calculations carried out by Crocco were quite different from those summarized here, but the result has the same form, another illustration of the fact that there is, in a deep sense, only one ‘linear stability problem’. Differences in detail among analyses arise only because representations of processes, and therefore characteristic parameters, may differ.

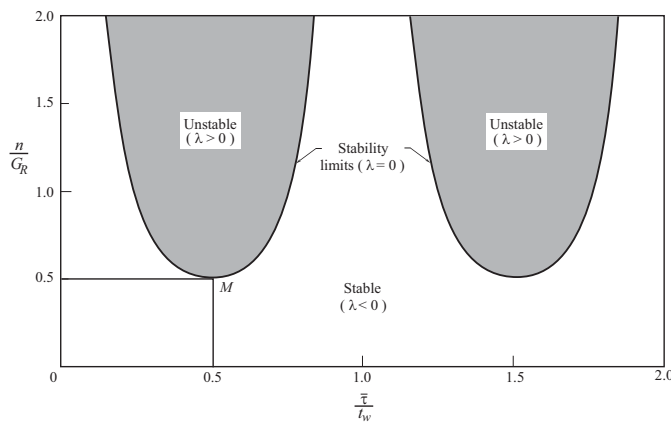


FIGURE 2.48. A general representation of stability based on the $n - \tau$ model (Crocco, Figure 4.2.2a in Harrje and Reardon 1972).

In this normalized form, Figure 2.48 is a kind of universal chart for the $n - \tau$ model. The multiple regions appear because of the factor $1 - \cos \omega \tau$ in (2.126) and correspond to the multiple peaks in the response, noted

in respect to Figure 2.33. They are usually not physically realistic and are another reflection of limitations of the elementary time lag model. A formulation of the $n - \tau$ model showing only a single peak was reported by Crocco (1966) but will not be discussed here.

For applications, equation (2.126) and Figure 2.48 have always been unfolded to give plots of n and τ versus some characteristic parameter, such as the fuel/oxidizer ratio as in Figure 2.48 above; or in some cases the stability boundaries have been presented in terms of system variables, with n and τ parameters along the curves.

An example of the latter is reproduced in Figure 2.49 taken from Crocco, Grey and Harrje (1960). The preparation of this figure, and other quantitative results for n and τ , rests on extensive experimental work. In all cases the strategy is the same: the stability boundary, marking the transition between stable and unstable small amplitude waves, is located experimentally, as a function of the variables defining the instabilities. Then the theoretical relation (2.126) is used to compute the required values of n and τ along the boundary.

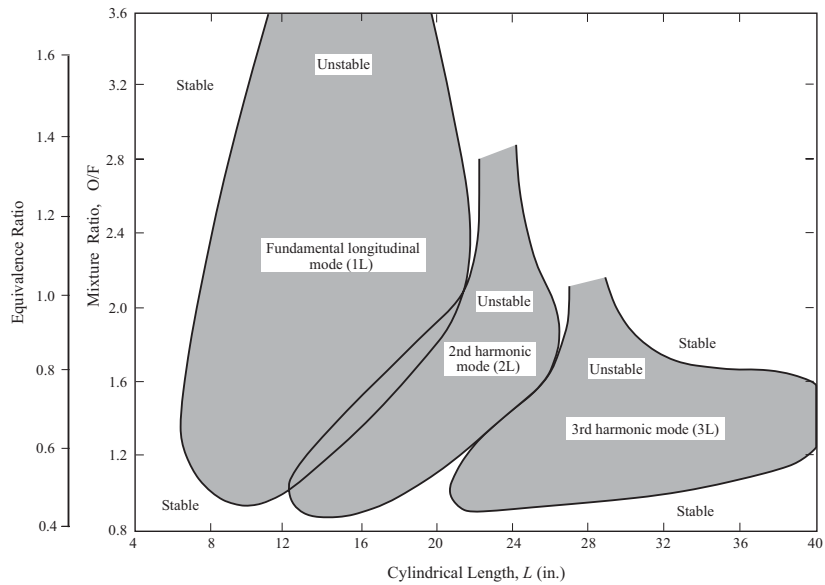


FIGURE 2.49. Stability boundaries inferred with the $n - \tau$ model applied to a gas-fueled rocket (Crocco, Grey and Harrje 1960).

That procedure has been used successfully to interpret longitudinal modes (Crocco, Grey and Harrje 1960) and transverse modes (Crocco, Harrje and Reardon 1962 and Reardon, Crocco and Harrje 1964). By applying the method to large numbers of tests, extensive correlations have been worked out for the interaction index and time lag as functions of geometric variables, injector design, propellant types and operating conditions. A brief summary has been given by Reardon in Harrje and Reardon (1972), pp. 277–286. Figure 2.50 is an example of results for n and τ determined from tests for storable hypergolic propellants, with various types of injectors.

Having values of n and τ , one is now presumably in a position to return to the theoretical result for the growth constant and apply the results to designing new systems. An obvious shortcoming is that the data correlations can be assumed valid only for the systems actually tested. How far the results can be extrapolated cannot be known with any confidence. Nevertheless, this semi-empirical approach has been apparently used successfully both as a framework for correlating data and as an aid to design. It is essential

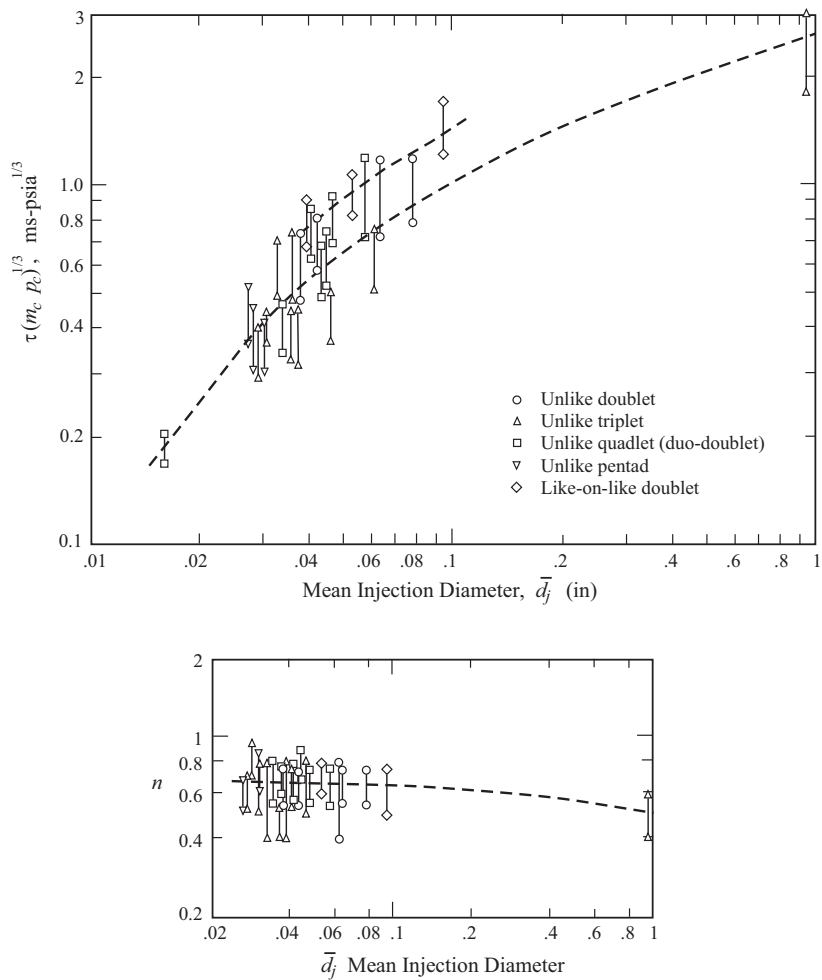


FIGURE 2.50. Experimental results for n and τ , using stable hypergolic propellants and various injectors (Reardon, Figures 6.33 e and f in Harrje and Reardon 1972).

in this procedure that the same theoretical result for the growth constant be used for correlating the data and for subsequent predictions. Otherwise, inconsistent and meaningless results will be obtained.

Although the ideas leading to the definitions of n and τ are appealing, the time lag model should be regarded truly as a framework for correlating data and not as a theory explaining fundamental mechanisms of combustion instabilities. With a different two-parameter representation of the unsteady process, the left-hand side of (2.126) might have a different functional form, but the formula could be used in the same fashion to interpret stability boundaries. Only the forms of the correlations would be changed.

We must also note that because only the single formula for the growth constant (2.126) has been used, the method described above uses one equation to determine two unknowns (n, τ). Thus in practice, some difficulties may arise in obtaining consistent results. That trouble is avoided if, more correctly, both the real and imaginary parts of the complex wavenumber are used. In that event, measured values of the frequency are used and since (2.90) contains the imaginary part of the unsteady mass source (2.94), the two equations

for the frequency and growth constant have the form

$$\omega = \omega_n + C_3 \int \psi_n \hat{w}_l^{(i)} dV - C_4$$

$$\alpha = C_1 \int \psi_n \hat{w}_l^{(r)} dV - C_2$$

Hence with (2.94)

$$n \sin \omega \tau = \frac{\omega - \omega_n + C_4}{C_3 \int \psi_n^2 \bar{w}_l dV} \quad (2.127)a,b$$

$$n(1 - \cos \omega \tau) = \frac{C_2}{C_3 \int \psi_n^2 \bar{w}_l dV}$$

The left-hand sides could equally be regarded, within a multiplier, as the real and imaginary parts of the mass source,

$$\hat{w}_l^{(r)} = \bar{w}_l n(1 - \cos \omega \tau) \quad (2.128)a,b$$

$$\hat{w}_l^{(i)} = \bar{w}_l n \sin \omega \tau$$

and correlations could be done with $\frac{\hat{w}_l^{(r)}}{\hat{w}_l} = \hat{w}_r = n(1 - \cos \omega \tau)$ and $\frac{\hat{w}_l^{(i)}}{\hat{w}_l} = \hat{w}_i = n \sin \omega \tau$ instead of (n, τ) . Thus, even though the heuristic argument leading to \hat{w}_l in the form (2.128)a,b is based on a time lag associated with motions of the propellant (a Lagrangian view), the end result is equivalent to a purely Eulerian representation of local combustion process. The time lag associated with motions in space can be reinterpreted as a phase lag in time at a fixed location in space.

The formulas (2.128)a,b have been deduced from the approximate analysis discussed in Section 2.3.2 and therefore have a particularly simple form. Although it is true that a linear analysis will always produce two formulas, for the real and imaginary parts of complex wavenumber, the forms may be wildly different in detail, depending in the method of solution. Crocco, Grey and Harrje (1960) solved their differential equations directly, a method used later by Crocco, Harrje and Reardon (1962) and Reardon, Crocco and Harrje (1964) to study transverse modes.

The time lag models of the combustion process have been used also in analysis of nonlinear behavior, both for longitudinal oscillations (Sirignano and Crocco 1964; Mitchell, Crocco and Sirignano 1969; Crocco and Mitchell 1969) and for transverse oscillations (Zinn 1966; Zinn and Savell 1968). In those and other works discussed in Chapter 7, either n and τ are assigned values; or the unsteady behavior is studied as a function of n and τ quite analogous to the handling of linear problems. Thus, sufficient experimental data had been gained to support the time lag model that it could be used in a general fashion for theoretical work. However, remarks above emphasize that this practice really amounts to using any combustion response having real and imaginary parts related to n and τ by equations (2.128)a,b. Expressing results and interpreting behavior in terms of n and τ carries no uniqueness.

2.4.3. Pogo Instabilities. The problem of low frequency POGO instabilities is well-documented and understood. Due to the POGO instability in the Apollo vehicle, it is also probably the best known among people otherwise not familiar with combustion instabilities.

Low frequency instabilities ('chugging') arise due to coupling between the fluid dynamics in the combustion chamber, and the propellant supply system. They are perhaps the first sort of combustion instability definitely identified and analyzed for liquid rockets (see the remarks at the beginning of Section 2.3.2). POGO instabilities involve the further complication of coupling between the propulsion system and the structure of the vehicle. The low frequency structural vibrations are the origin of the name, by analogy with the motions of a POGO stick.

During the 1960s, the POGO instability received much attention as a serious problem in several vehicles including the Thor, Atlas, and Titan vehicles. Rubin (1966) has given a clear brief summary, including particular emphasis on pump cavitation and wave propagation in the propellant feed lines. Those are matters often overlooked by those concerned with motions in the combustion chamber. Yet they provide significant contributions to time lags in the system and are crucial items in treating POGO instabilities.

More recent work in France was reported by Dordain, Lourme and Estoueig (1974) for the Europa II and Diamant B vehicles; and by Ordonneau (1986) for the Ariane.

2.4.4. Combustion Instabilities in Thrust Augmentors. Augmentors or, as earlier forms are called, ‘afterburners,’²⁵ have a long history and offer the most varied examples of passive control applied to propulsion systems. The main reasons for this special ranking are basic and simply expressed. First, the geometry is typically ideal for the excitation and sustenance of acoustic oscillations. Figure 2.51 shows two examples of widely used engines; both are turbofans with augmentors. In all designs the injection of fuel takes place at the upstream end of the device. Although the boundary condition does not cause a velocity fluctuation to vanish there, the value is relatively low and the pressure fluctuation can be relatively large. Thus, the product $u'p'$ is likely to have a significantly non-zero positive real part, representing acoustic energy flowing into the region.

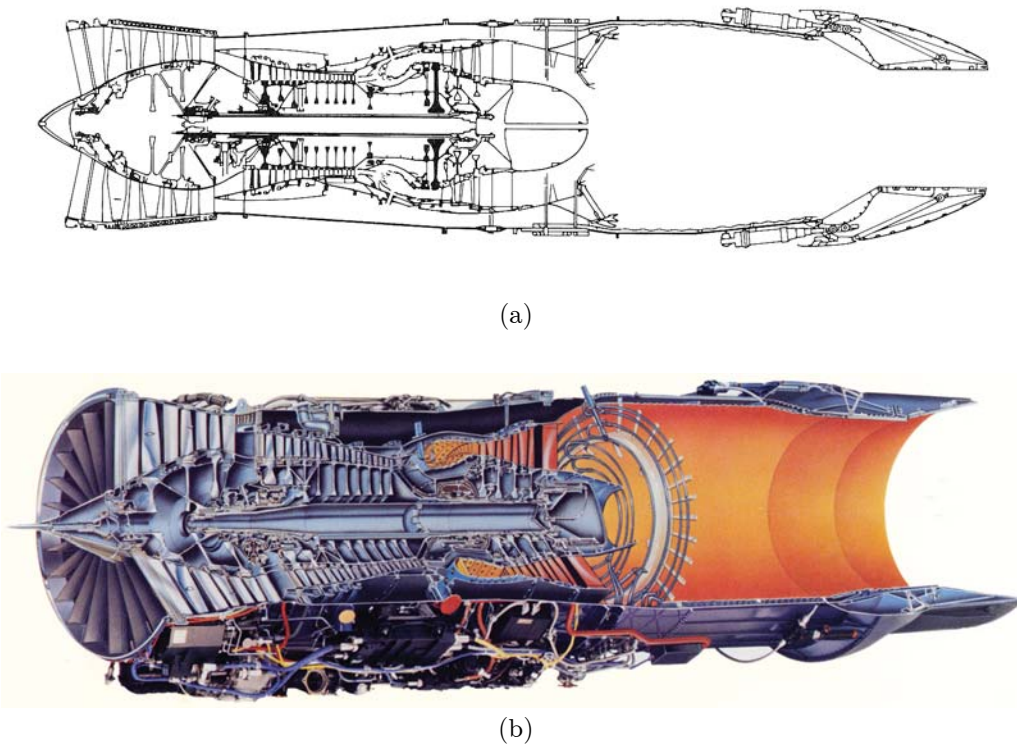


FIGURE 2.51. Two examples of aircraft gas turbine engines with thrust augmentation (a) General Electric F110 engine (taken from *Jane's All The World's Aircraft*, 1988–1989); (b) Pratt and Whitney F100 engine (taken from Pratt and Whitney advertising material).

²⁵The main difference between augmentors and afterburners is that the entire flow in the latter passes through the turbine and therefore the afterburners. To simplify writing, we will use the term ‘augmentor’ to mean afterburner as well.

Second, fuel is usually introduced through radial vanes, perhaps with circumferential supply tubes as well. Those parts, whatever the configuration, are obstructions to the flow, and are sources of vortex shedding, a potential cause of acoustic oscillations. Third, the conditions for instabilities in flow may be enhanced by a bypass design in which the cold outer flow and the hot core from an unstable cylindrical shear layer between them.

Finally, it is apparent from Figure 2.51 that the system has low losses. Thus it has long been standard practice to incorporate acoustic liners as integral parts of thrust augmentors. That is, they are part of a design and not added later when a problem arises. It is virtually guaranteed that as the operational envelope of any augmentor is expanded, problems with oscillations will be found.

Since high frequency or ‘screech’ instabilities were first encountered as a serious problem in the late 1940s and early 1950s, liners have been developed largely by trial and error to act as passive control devices designed to suppress the oscillations. The staff of the Lewis Laboratory²⁶ (1954) compiled most of the existing data and performed some tests to provide a basis for general guidelines for design; Harp *et al.* (1954) reported the results of extensive tests, also at Lewis Laboratory. Of the methods investigated to solve the problem, including baffles and vanes as well as adjusting the distribution of injectors, perforated liners worked best. Groups at Pratt and Whitney Aircraft and the United Aircraft Research Laboratory had already tried Helmholtz resonators and in 1953 demonstrated the first successful use of perforated liners in a full-scale afterburner on a J57. The physical basis for the success of liners is explained in Chapter 8.

Despite several attempts to develop analytical methods and a more quantitative basis for design, treatment of combustion instabilities in thrust augmentors has remained almost entirely an empirical matter. Kenworthy, Woltmann and Corley (1974) reported the results of an experimental program devoted to studying screech instabilities in three different designs of augmentors. The report also contains analysis used to correlate data and to provide some guidance for design of acoustic liners. This seems to be the last reported work on high frequency instabilities in full-scale augmentors; the mechanisms remain obscure. Chamberlain (1983) gave the most recent status report: it seems that little has changed over several decades in respect to augmentors shown in Figure 2.51.

Perforated liners effectively attenuate the high frequency oscillations related to radial and tangential acoustic nodes. Low frequency instabilities, often called ‘rumble’, tend to be more troublesome. Liners are ineffective at low frequencies and the problem of rumble is solved or reduced in practice by careful control and coordination of the distribution of injected fuel and the nozzle opening. It’s a costly process to develop the system, inevitably requiring several designs of the injection system and flameholders, and expensive full-scale tests in altitude simulation test facilities.

The problem of combustion instabilities in thrust augmentors is arguably more difficult than that in liquid rockets for at least two reasons: the processes involved in flame stabilizations are sensitive to pressure and velocity fluctuations; and the device is usually required to perform over a wider range of operating conditions. The first explains the importance of injector and flameholder design. As a result of the second, the high and low frequency instabilities are typically found in different regions of the flight envelope. Figure 2.52, reproduced from the excellent summary of early work by Bonnell, Marshall and Rieche (1971) illustrates the point.

Instabilities in the lower frequency range became increasingly troublesome with the development of turbofan engines, a consequence of the geometry (see Figure 2.53 taken from Bonnell, Marshall and Rieche (1971) and Figure 2.54 taken from Zukoski (1985)). In the pure turbojet, the fluctuations may propagate upstream past the turbine disk but the turbine generally seems to act as a good reflector. In fan engines, it is common that the entire length of the fan duct participates in the oscillations, reducing the frequencies

²⁶Now the NASA Glenn Research Center.

sometimes as low as 50 Hz. See Nicholson and Radcliffe (1953) for an early report of very low frequency oscillations; observations in turbofans have been discussed by Bonnell, Marshall and Rieche (1971); Mach (1971); Ernst (1976); Underwood *et al.* (1977); and Cullom and Johnsen (1979). Figure 2.55 reproduces power spectral densities taken from turbofan augmentors [Bonnell, Marshall and Rieche (1971)]. Because of the rotating parts, spectra of the acoustic field in gas turbine engines tend to exhibit a greater variety of discrete oscillations than do those for liquid rockets. The peaks at the higher frequencies in Figure 2.55(b) are 'screech' modes.

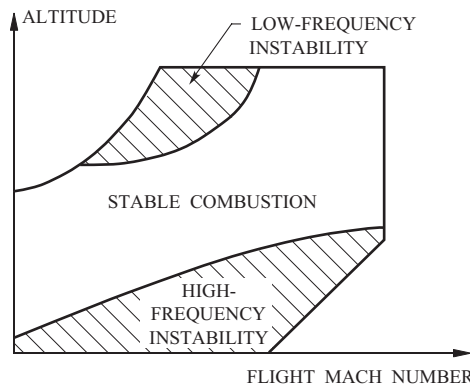


FIGURE 2.52. Schematic flight envelope showing typical regions of high- and low-frequency instabilities in thrust augmentors (Bonnell, Marshall and Rieche 1971).

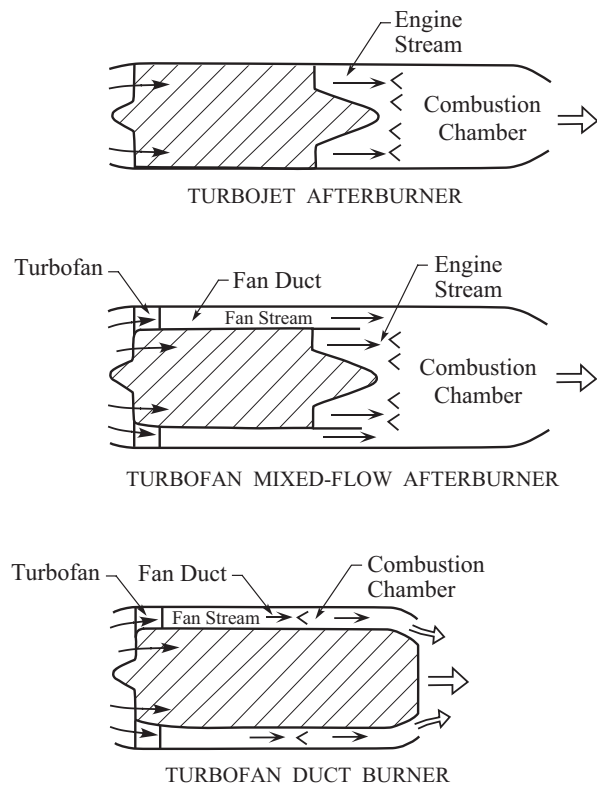


FIGURE 2.53. Sketches of the evolution of the geometry of gas turbine engines (Bonnell, Marshall and Rieche 1971).

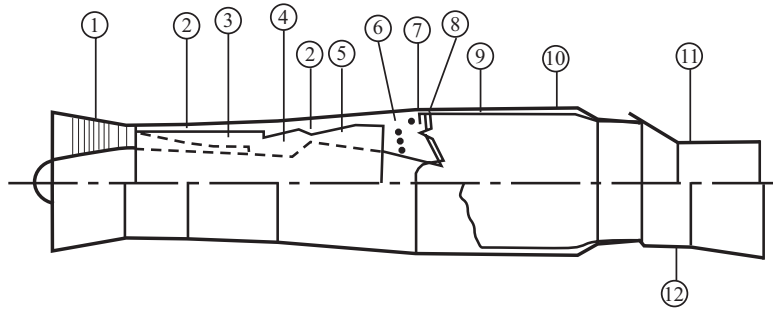


FIGURE 2.54. Pratt and Whitney F100-PW-100 Augmented Turbofan Engine. (1) three stage fan; (2) bypass air duct; core engine compressor(3), burner(4), and turbine(5); (6) fuel injectors for core engine gas stream; (7) fuel injectors for bypass air stream; (8) flame stabilizer for afterburner; (9) perforated afterburner liner; (10) afterburner case; nozzle closed to minimum area (11) and opened to maximum area(12). (Zukoski 1985, Figure 21.0.2).

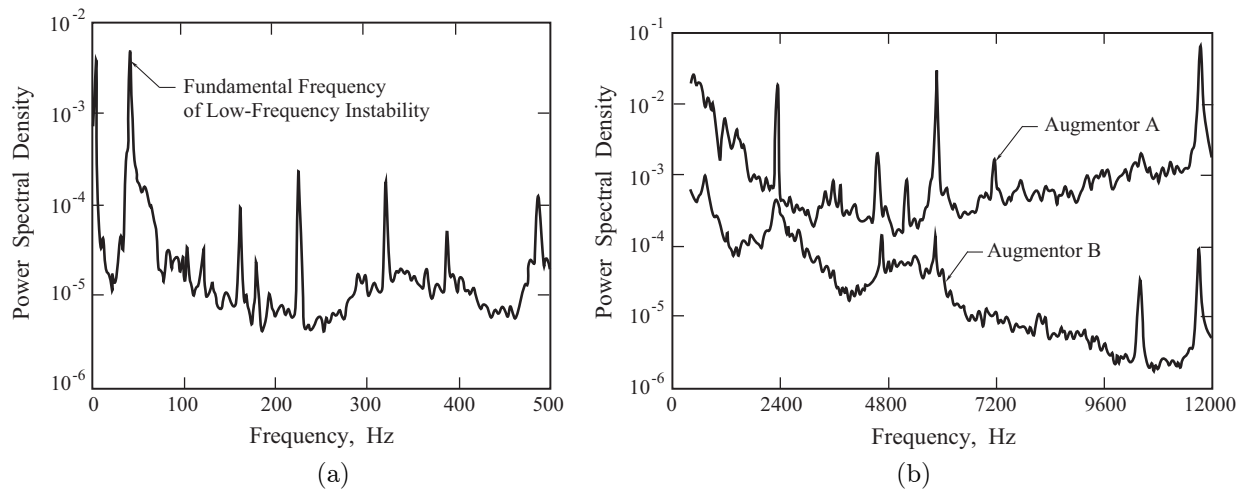


FIGURE 2.55. Spectra of pressure oscillations observed in thrust augmentors. (a) low-frequency range ('rumble'); (b) high-frequency range ('screech'). (Bonnell, Marshall and Rieche 1971).

The combustion processes in an augmentor differ in several fundamental respects from those in a liquid rocket. Only fuel is injected as liquid; the oxidizer is unburnt oxygen in the fuel-lean flows from the bypass and the core engine. There are no impinging fuel and oxidizer liquid stream, but the formation of drops and vaporization of the fuel must obviously occur. Normally, it is intended that the fuel drops should be entirely vaporized prior to ignition in the core flow so burning occurs in the fuel/air gaseous mixture. Because the flame propagation speed is less than the flow speed, a continuous source of ignition is required, normally supplied by the wake of a bluff body, the flameholder. Clearly, the performance of such a system depends not only on the flow conditions and physical properties of the fuel but also very strongly on the geometry of the injectors and flameholders. In the cooler bypass flow, vaporization is not completed upstream and liquid impinges on the flameholders; then liquid may be torn off the flameholder by the high speed of gas stream, or the liquid layer vaporizes. Zukoski (1985) has provided a thorough and readable discussion of the combustion processes in afterburners. Figure 2.56 taken from his article, illustrates the general features of the flow in the vicinity of various flameholders.

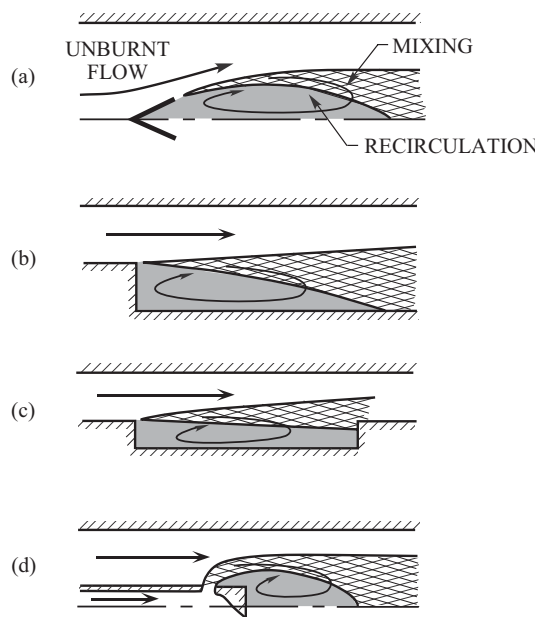


FIGURE 2.56. Flow in the vicinity of typical flameholders emphasizing the recirculation zones (Zukoski 1985).

According to the preceding remarks, it appears unlikely that vaporization of the fuel droplets is a dominant mechanism for combustion instabilities in augmentors. Nevertheless it is certainly quite possible that interaction of the acoustic field with the injection system could produce fluctuations of the fuel flow and hence subsequent fluctuations of fuel/oxidizer ratio and heat release in combustion. The process might be modeled most simply in terms of a time lag but there seems to be no treatment of this sort in the published literature.

One would suspect that processes associated with the flameholder may dominate. That view is generally supported by practical experience with the strong effects of flameholder design on instabilities. We have discussed in Section 2.3.4 the mechanism based on vortex shedding and combustion suggested by Rogers and Marble (1956). Their argument is persuasive and there has never been evidence disproving that process as a possible mechanism of screech. Similar ideas also can be applied to describe a possible 'rumble,' a low frequency instability (see Section 8.6). Theoretical developments and the necessary laboratory tests have not been carried far enough to incorporate the proposal in an analysis suitable for general design work with arbitrary geometries.

Russell, Brant, Ernst, and Underwood (1978), worked out a one-dimensional analysis of instabilities in augmentors; the work is also discussed by Underwood *et al.* (1977). Broadly the analysis represents the acoustic field as a synthesis of up and downstream traveling acoustic waves, and entropy waves, as in the example discussed earlier here in Section 2.2.3. The unsteady heat sources are derived as models of mixing and combustion in the wakes of the flameholders. Bypass and core flows are treated separately and superposed in parallel. It's a linear analysis; the equations for the time-dependent variables are solved by applying the Laplace transform. Conditions for stability are determined by applying the Nyquist criterion. It is difficult to understand all details of the analysis from the available (abbreviated) description. Although some success was evidently achieved with this work, it seems not to have been widely applied. Moreover, the results are mainly in a computer program which has not furthered general understanding of the problem although it may have been useful in treating particular cases.

Over a period of several years Dix and Smith and co-workers developed an analysis based on the formulation published by Culick (1963) for liquid rockets. See Dix and Smith (1971) and references cited there for a description of the work. Although that sort of approach should be useful in treating augmentors, that analysis has also not been widely applied. It is important to note that while their linear analysis is correct, Dix and Smith committed some basic errors in trying to extend their calculations to nonlinear behavior. The results they have reported for the influences of the amplitudes of oscillations are wrong.

A different course of recent work in instabilities in augmentors was reported by Dowling and Bloxsidge (1984); Langhorne (1988) and Bloxsidge, Dowling, Hooper and Langhorne (1988) at Cambridge University. Laboratory experiments were done in a configuration intended, roughly, to represent a longitudinal segment of an augmentor (Figure 2.57). A flame stabilized on a single vee gutter in a duct supplied with premixed gaseous reactants entering through a choked nozzle. With modifications that may have significant influences on the unsteady behavior, this has long been a common configuration (Kaskan and Noreen 1954; Hegde *et al.* 1986, 1987, 1988; Reuter *et al.* 1988). The work by Kaskan and Noreen has already been described briefly (see Figure 2.38). They worked with a flame stabilized on a vee gutter whereas Hegde and co-workers at Georgia Tech used one or two wires to stabilize the burning, although their work has presumably been directed to applications in ramjet engines.

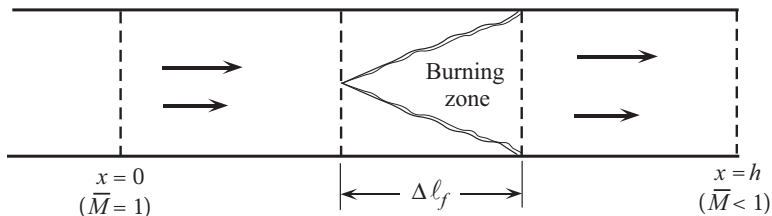


FIGURE 2.57. A flame stabilized on a gutter in a tube (Langhorne 1988).

All of these works are concerned in some broad sense with flames and flame instabilities. The instabilities are often ultimately manifested as vortices, so the mechanism for the instabilities discussed here could be classified as vortex shedding and combustion, as discussed in Section 2.3.5. Another similarity among these works is the use of electromagnetic radiation to identify the heat released by combustion products.

Langhorne (1988) concludes that for the device shown in Figure 2.57, two types of coupling exist between the burning processes and pressure oscillations. The transition between the two occurred in a narrow range of stoichiometric ratio around 0.65. For $\phi < 0.65$ a convective wave of entropy or spots of high temperature appeared to propagate well downstream of the flameholder. With increasing ϕ , that convective aspect seemed to have been confined to a short length and in the remainder of the duct the heat release (as measured by radiation from C_2 and C) seemed to be in phase with the pressure oscillation. No results of flow visualization are available to confirm the behavior directly, but vortex shedding apparently may be involved.

At least partly as a result of the two kinds of coupling, two frequencies of instability were observed with larger amplitudes produced at higher stoichiometric ratios. Bloxsidge, Dowling, Hooper and Langhorne (1988) have worked out an interesting and useful one-dimensional analysis to interpret their observations.

Certain aspects of the Cambridge results are similar to those reported by Heitor, Taylor, and Whitelaw (1984), Sivasegaram and Whitelaw (1987) and by the Georgia Tech group (Hegde *et al.* 1990). The reasons for the similarities and yet only partial reconciliation of differences are not known; a sufficiently general analysis has not been constructed to accommodate all the results on a common basis. There is little doubt that more than one mechanism may act, one or another dominant under different conditions. Because this

is a relatively well-defined situation, (a premixed flame in a duct) the problem merits further attention both experimentally and theoretically to bring clearer understanding of the behavior.

The work at Cambridge seems to have been partly motivated by the idea of using feedback control of combustion instabilities. In fact the results just described were soon followed by laboratory work at Ecole Centrale (Poinsot *et al.* 1988) concerned also with active control. Those are the beginnings of modern work on active control of combustion instabilities, the subject of Chapter 9.

2.4.5. Combustion Instabilities in Ramjet Engines. Particularly from the late 1970s to the early 1990s, substantially more attention has been paid to combustion instabilities in ramjet engines than can be discussed here. Much progress has been made but several essential problems remain unsolved, mainly associated with the conversion of liquid fuel to gaseous reactants; coupling between combustion processes and the unsteady motions; and the inlet/diffuser.

Sketches of two typical configurations are shown in Figure 2.58. Most contemporary liquid-fueled ramjets are “integral ramjet engines.” The combustion chamber is initially filled with solid propellant that is burnt to boost the vehicle to supersonic speed. Liquid propellant is injected upstream of the region where the flow area abruptly increases at the “dump plane.” Flame stabilization is achieved through continuous ignition by the hot combustion products in the recirculation zone. In some designs additional bluff body flameholders may also be used; and occasionally continuous burning of a pilot light may be required.

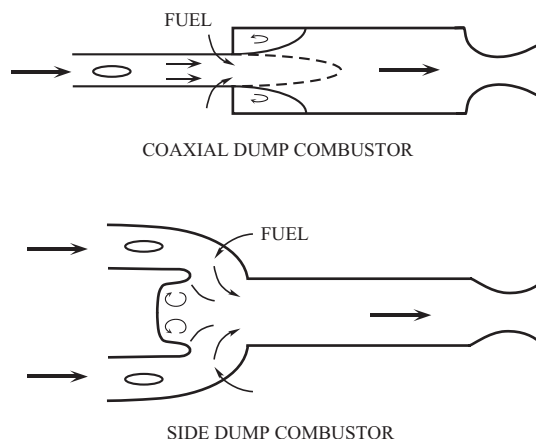


FIGURE 2.58. Two simple ramjet configurations using stabilization at abrupt changes of area.

Zukoski (1985) has given a thorough discussion of steady flame stabilization in thrust augmentors. Much of that material applies with virtually no change to the corresponding problems in ramjet engines. The presence of the rearward-facing step and the sensitivity of shear layers and recirculation zones to fluctuations in the flow are major factors in the problem of combustion instabilities in ramjet engines.

Much of the material we have covered for liquid-fueled rockets and thrust augmentors is relevant as well to ramjet engines. There are, however, several distinguishing features. First, unlike the case for liquid rockets but similar to that for afterburners, spray combustion seems a lesser issue. Although the published evidence is perhaps not wholly conclusive, (see, e.g. Edelman 1981, Edelman *et al.* 1981 and Harsha and Edelman 1982), it appears that in operating engines, the liquid droplets are largely vaporized before the flow reaches the zones of flame stabilization and combustion. Hence the processes in those regions involve mostly gaseous reactants, a great simplification for carrying out research on combustion instabilities; very

little experimental work has been done recently in the coupling between spray combustion and unsteady motions. Laboratory tests have for the most part used gaseous fuels.

That is not to say that transient processes of droplet heating and vaporization are unimportant, for they are surely influential in arranging the distribution of fuel over the plane at the entrance to the combustor. But there is no operational or experimental evidence to support the proposal by Tong and Sirignano (1986a, 1986b, 1987) that the unsteady conversion of liquid to vapor is a potential mechanism for instabilities. This matter has already been discussed in Section 2.3.1 with the conclusion that if all processes *except combustion* are accounted for, the presence of evaporating liquid drops is a stabilizing influence on unsteady motions.²⁷ We will not consider further problems associated with injection, atomization and vaporization. However, it is true that insufficient attention has been paid to the distribution of fuel/oxidizer ratio in the flow. Little is known of the details, either theoretically or experimentally; yet laboratory tests (e.g., Schadow *et al.* 1987b) have shown that the distribution of fuel can have a substantial effect on instabilities, a fact that has long been known qualitatively from experience gained in engine development (Rogers 1980a, 1980b; Grenleski *et al.* 1977). There seems to be no evidence of coupling between oscillations in the flow and the fuel supply system. Thus no oscillations have been observed in ramjets corresponding to 'chugging' or POGO instabilities in liquid rockets.

2.4.6. Unsteady Behavior of the Inlet/Diffuser. So far as combustion instabilities are concerned, the principal feature distinguishing ramjet engines from liquid-fuel rockets and afterburners is the inlet/diffuser. Within the inlet a system of shock waves exists to provide the mass flow and stagnation conditions demanded by the conditions set in the combustion chamber and exhaust nozzle. Under normal operating conditions the shocks are located downstream of the geometric throat in the expanding supersonic flow. The position of the shocks depends chiefly in the stagnation pressure in the combustion chamber; increasing the stagnation pressure causes the shocks to move upstream where the Mach number and therefore loss of stagnation pressure are less. It is this sensitivity of the flow in the inlet to pressure changes downstream that has caused longitudinal oscillations to be such a serious concern in ramjet engines. In the late 1970s (Hall 1978, 1980; Rogers 1980a, 1980b) first qualitative and later limited quantitative relations were established between the amplitudes of pressure oscillations and the loss of dynamic pressure margin.

Since those early works, extensive tests by Sajben and co-workers (Chen, Sajben and Krontil 1979; Sajben, Bogar and Krontil 1984; Bogar, Sajben and Krontil 1983a, 1983b) have shown that the unsteady behavior is greatly more complicated due to flow separation and instability of shear layers. High speed schlieren pictures (see also Schadow *et al.* 1981) have shown large shock oscillations as well as the formation of vortex structures. Although computations based in the one-dimensional approximation to flow in the diffuser (Culick and Rogers 1983; Yang 1984; Yang and Culick 1984, 1985, 1986) are useful and seem to capture some of the dominant features of the behavior, it is quite clear that the true motions can be simulated well only by numerical analysis based on the Navier Stokes equations for two- or three-dimensional flows (Hsieh, Wardlaw and Coakley 1984; Hsieh and Coakley 1987; and references cited there).

There is evidence that under some conditions inlets exhibit self-excited or 'natural' oscillations. Energy is transferred from the mean flow to the fluctuations associated at least partly with separated flow. Although a one-dimensional calculation (Culick and Rogers 1983 and an approximation to some of Sajben's data by Waugh *et al.* 1983, Appendix D) suggests the possibility that the inlet may drive combustion instabilities, there is no firm evidence from tests with combustors that those conclusions hold. Most experimental results strongly suggest that the major source of driving unstable motions is likely associated with processes in the combustion chamber. Nevertheless, because the flow from the inlet is the initial state for flow in the chamber, it is fundamentally important that processes in the inlet be well-understood. In that respect, as we remarked above, perhaps the greatest deficiency is knowledge of the history of the injected fuel and the distribution of liquid droplets and gaseous fuel at the inlet phase.

²⁷This conclusion is not generally true. See the discussion in Section 6.13.

In practice, the first indications of combustion instabilities are almost always fluctuations in recordings of the pressure. If there is only one pressure transducer, one can infer only the amplitude and frequency—best displayed as a power spectral density. While the frequency alone may suggest what modes are involved, the configurations used for ramjet combustors are sufficiently complicated that the modes are not always easily identified. Moreover, in laboratory tests there may be an upstream plenum chamber and other parts of the apparatus that participate in the oscillations. As a general rule, it is essential that measurements of the pressure be taken at several locations in order to provide unambiguous identification of the modes. Sufficient care should be taken that distributions of both the amplitude and relative phase can be determined. This information has also proven extremely useful for confirming the results of analyses.

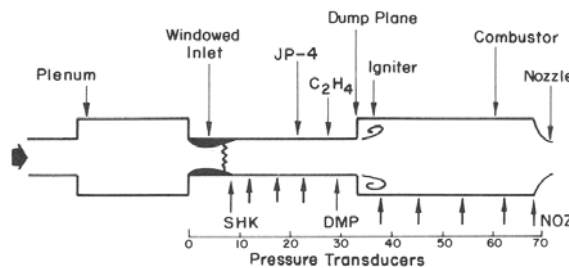


FIGURE 2.59. Model used for measurements in the inlet to a dump combustor (Crump *et al.* 1986).

The most extensive measurements of mode shapes in dump combustors were made at the Naval Weapons Center by Schadow and co-workers. A summary of the results, with references to the previous work, was published by Crump *et al.* (1986). Figure 2.59 shows the geometry of the sub-scale laboratory device; some results of measurements and analysis are reproduced in Figure 2.60. A case in which a bulk mode is excited in the combustion chamber (175 Hz) is shown in Figure 2.60(a); the fundamental wave mode was excited in the chamber excited for the case shown in Figure 2.60(b) (540 Hz). The calculated results were based on a one-dimensional analysis (Yang 1984) in which combustion was ignored and the mean flow was accounted for only in the inlet. The good agreement is further evidence of the point emphasized already that the mode shapes and frequencies for combustion instabilities are often well-approximated by results based on classical acoustics. Here we also find that the one-dimensional approximation works well. For those calculations, the inlet shock was represented with the admittance function computed by Culick and Rogers (1983). It is apparently a good approximation that for these cases, the shock system is highly absorbing: the reflected wave has much smaller amplitude than the upstream-traveling incident wave. That fact, and the presence of the high speed average flow, explains why the relative phase varies linearly in the inlet.

Clark and Humphrey (1986) have also reported fairly good results obtained with a one-dimensional analysis applied to a side-dump configuration. The engine was supplied from a large plenum through inlets that were not always choked. Although the frequencies of oscillation, phase distributions throughout the device, and amplitude distributions within the combustor were predicted well, the amplitude distributions within the inlets diffuser considerably from the measured results. The reasons for the differences are not known. Yang and Culick (1985) later carried out a numerical analysis including vaporization of the liquid fuel and were able to predict quite well both the distribution and level of the pressure field.

A series of tests in a coaxial combustor have been reported by Sivasegaram and Whitelaw (1987), intended to examine the consequences of changing geometric parameters and fuel/air ratio. Data are given for frequencies and sound intensity at one location. Mode shapes were evidently not measured and no results of analysis are cited. It would appear that these data offer an opportunity for a straightforward application of a simple one-dimensional analysis.

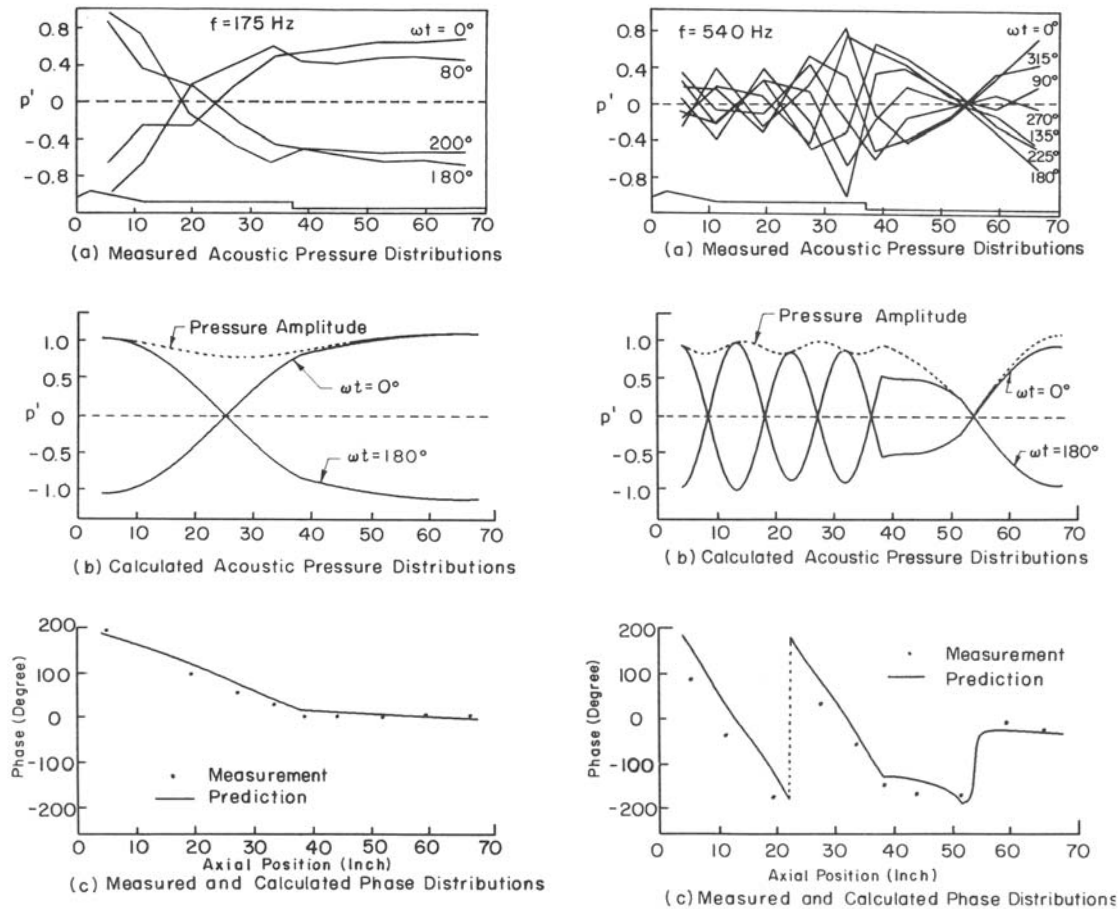


FIGURE 2.60. Comparison of measured and calculated mode shapes in the inlet of a laboratory dump combustor (Crump *et al.* 1986).

The one-dimensional approximation with the average flow accounted for works surprisingly well for rapid estimates of mode shapes and frequencies. It is worthwhile remarking on its application. Few exact solutions exist for arbitrary variations of cross-section area $S_c(z)$, but in the case of ramjet configurations it is generally required to obtain results for piecewise variations. The problem comes down to solving the wave equation

$$\frac{d^2\hat{p}}{dz^2} + k_\ell^2 \hat{p} = -\frac{d\hat{p}}{dz} \frac{1}{S_c} \frac{dS_c}{dz}$$

where dS_c/dz vanishes everywhere except at discontinuities of area where it is infinite.

Hence the general procedure is straightforward to find normal modes of the chamber. In uniform sections, the pressure field is represented by the usual forms, $A_i \cos(k_\ell z + \phi_i)$ or its equivalents, where A_i , ϕ_i are associated with segment i , and k_ℓ is the wavenumber for mode ℓ . These solutions are matched at the discontinuities by requiring continuity of the acoustic pressure and mass flow. Eventually the amplitudes A_i can be found to within a multiplicative constant, and the values of k_ℓ are determined as roots of the characteristic equation.

This sort of analysis has long been known to give satisfactory results if the changes of area are not too large (see Section 5.7.2 and more complete analyses by Culick, Derr, Price 1972; Derr and Mathes 1974).

Simple resonance tests at room temperature have confirmed the calculations, a method that is still useful for investigating the acoustic modes of combustion chambers. For application to actual systems, significant differences between these approximate results and observed values may arise due to uncertainties in the boundary conditions at the inlet and exit planes.

2.4.7. The Time Lag Model Applied to Combustion Instabilities in Ramjet Engines. During the past seven years, Reardon (1981, 1983, 1984, 1985, 1988) has used the time lag model to-correlate and interpret the extensive data taken by Davis (1981). The time lag model is unwieldy (at best) to use if combustion is allowed to be distributed and the time lag is variable. Hence as in many previous applications to liquid rockets, Reardon assumes that the energy release is concentrated in a transverse plane; that the parameters (n, τ) are constant; and that the flow field is one-dimensional. Then the combustion response is given by the part of equation (2.94) depending on frequency; to represent concentrated combustion, the average distribution \bar{w}_l is replaced by δ -function. A modest change in the argument allows one to use this form for the unsteady conversion of liquid to vapor, or for unsteady energy release.

Reardon assumes that the oscillations observed by Davis are bulk modes in the combustor: the pressure is essentially uniform in space and pulsates in time. Hence the mode shape $\psi(\vec{r})$ is approximately constant and one may assume that the total unsteady energy release due to combustion processes in the chamber, E_c , is given by

$$\dot{E}_c = \dot{E}_0 n (1 - e^{-i\omega\tau}) \frac{p'}{\bar{p}}$$

The rate of change of energy in the chamber is the net result of energy released by combustion and the rates at which energy is convected in and out of combustor:

$$\frac{dE}{dt} = \dot{E}_c + \dot{E}_{in} - \dot{E}_{out}$$

This relation is the basis for Reardon's treatment of the experimental results.

As we discussed earlier, in applications of the time lag model to instabilities in liquid rockets, both parameters (n, τ) were determined by matching a theoretical result to experimental results for the stability boundary. The idea then is that those values of (n, τ) can be used to predict the stability characteristics for new (but in some sense similar) designs. In this case, Reardon has chosen to use values of n calculated by Crocco and Cheng (1956) and to compute the time lag independently, using previous results obtained by others. In short, Reardon essentially assumes that the combustion model is known (defined by the two parameters (n, τ) with concentrated combustion) and then uses the relation for the balance of energy in the chamber to correlate data.

Stability of oscillations may be determined by application of the Nyquist criterion after the unsteady energy balance is rewritten by using the Laplace transform. This possibility arises because, as we have briefly described earlier, the problem of self-excited combustion instabilities can be interpreted as a linear system with a negative feedback loop. The stability criterion, expressed with the growth constant α , depends on other processes included in the energy balance. The formal result may therefore be used to test the importance of those processes by comparison with data.

Reardon has used this procedure to study the effects of several processes and geometrical parameters, with mixed results. It seems that this sort of approach suffers from the intrinsic limitation noted earlier: It is really only a method for correlating data and therefore in the first instance has little predictive value without assurance that the models used are accurate. Confidence in the results comes only from good correlations with data over broad ranges of parameters. The results to date do not seem to provide that confidence.

2.5. Dynamics of Flames and Flame Sheets as a Mechanism

Interpreted in the broadest sense, the dynamics of flames includes mechanisms which may be active in any system based on the conversion of energy by combustion processes. Conventionally the term has come to refer only to situations in which the flame or flames are rather well-defined and not spread out in space. What is probably the first example of a “combustion instability” remains virtually a canonical example. In 1777, (that’s only 50 years after Newton’s death!) Byron Higgens (1777) recorded his observations of a “singing flame”, published twenty-five years later in Nicholson’s Journal. The phenomenon has attracted much attention as a curiosity, as a simple informative example of fundamental behavior, and as an elementary guide to understanding the complexities presented by actual combustion systems.

Figure 2.61 is a sketch of Putnam’s apparatus which is easily assembled for observation of a basic singing flame. Two variations are shown, to demonstrate the influence of changing the upstream boundary condition. Figure 2.62 shows some results (Putnam 1945) obtained for the two cases sketched in Figure 2.61. Putnam (1971, pp. 9–16) has given a good brief discussion of Jones’ observations.

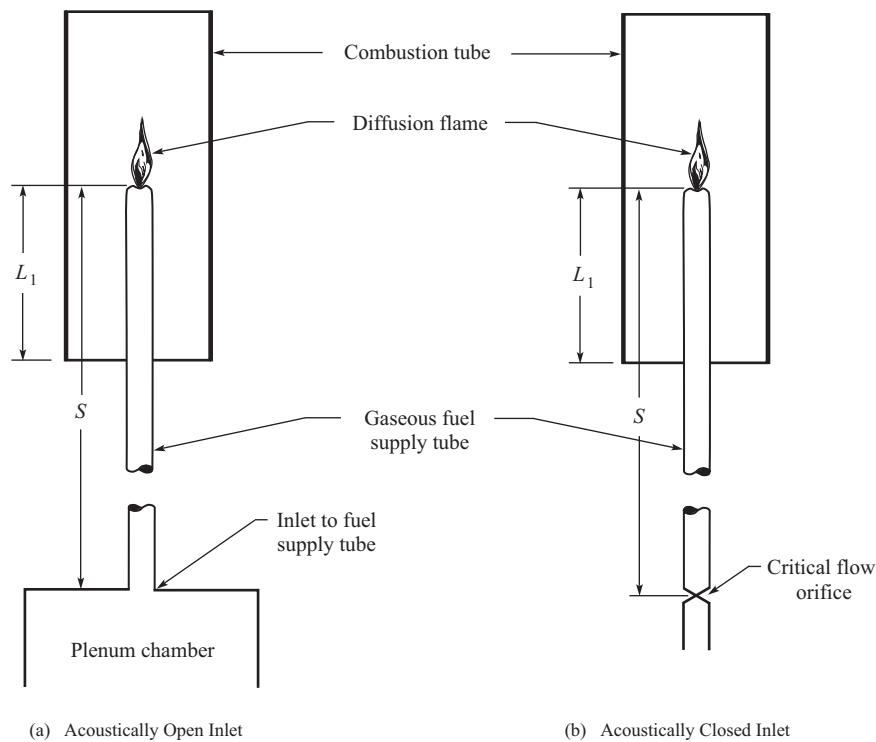


FIGURE 2.61. Simple apparatus for demonstrating a singing flame (Putnam 1971).

The connections between the behavior of the singing flame and results obtained for the Rijke tube (Section 2.7) are fairly evident; they will not be pursued here. These elementary situations are instructive examples of phenomena causing the excitation of acoustic waves by energy released in combustion processes.

Prior to the late 1940s and early 1950s, there was virtually no effort to work out true theories of flames. There were no detailed quantitative representations having predictive value. The idea that at atmospheric pressure most of the chemical reactions in a combustion process take place quickly and in thin regions had long been known, but there were few quantitative consequences. That view, that flames are thin, is at least implicit in practically all of the literature alluded to in the paragraph above. Then, a few years after World

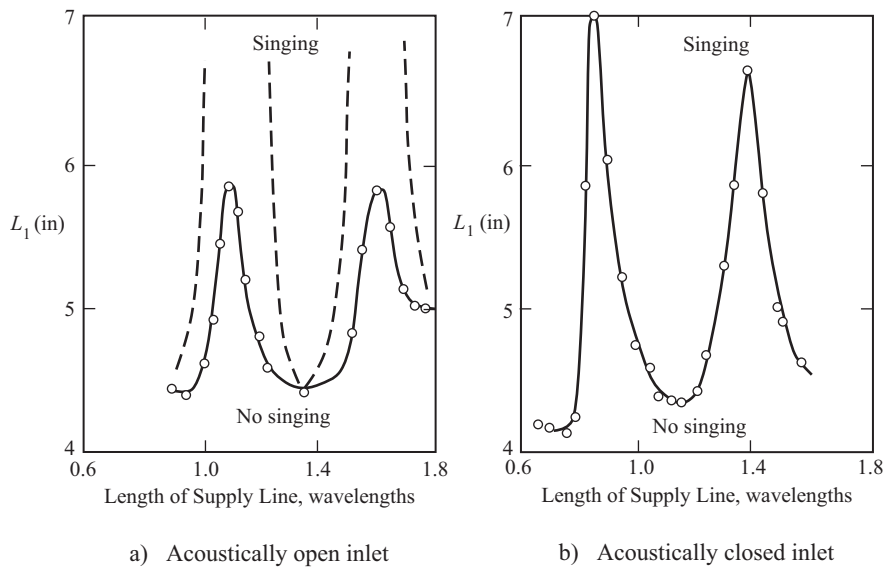


FIGURE 2.62. Location of the flame shown in Figure 2.61 to maintain a continuous tone, i.e. 'singing' (Putnam 1971).

War II, the field of combustion began to develop in the form now understood, most clearly the subject broadly covered by the proceedings of the Combustion Institute. Within that extensive field, the representation of reacting flows with thin flames, or 'flame sheets' became and has remained a useful model developed for many research and practical applications.

Consequently, it was a natural development that unsteady problems of combustion in gaseous systems should be modeled and analyzed with reaction zones treated as flame sheets. A significant increase of activity occurred in the late 1980s with accomplishments at Ecole Centrale, Paris (Poinsot *et al.* 1987) and at Cambridge University (Bloxsidge *et al.* 1988). Those were the first of many works based on variations of similar apparatus at approximately atmospheric pressure. In both programs, the primary goal was successful application of active control to problems of combustion instability. A similar strategy was followed in work at M.I.T. (Annaswamy *et al.* 2000 and Fleifel *et al.* 2000).

All of those works involve models of combustion zones as flame sheets. The analyses are closely tied to investigations of active control and are therefore more appropriately discussed in Chapter 9.

2.6. Fluctuations of Mixture Ratio as a Mechanism

The influence of mixture ratio, or more precisely its fluctuations, in combustion instabilities received little attention until oscillations caused serious problems in the development of combustors for gas turbines. Reduced emissions, perhaps most importantly NO_x , oxides of nitrogen, has been a practical goal for more than fifteen years. Pressure to adopt stronger regulations has increased with time, one consequence being significantly greater investments of people, money and time devoted to research. Many related special topics of research have been, and are investigated; fluctuations of fuel/oxidizer ratio (F/O) hold a special position due to their direct connection with local reaction rates, energy release and therefore potential effects on the presence of combustion instabilities.

An interesting question is: Why do changes in the design, or operation of gas turbines to achieve lower emission of NO_x lead to combustion instabilities? The reason can be explained quite simply. First we should note that there are three main mechanisms for the formation of NO (nitrogen oxide) in combustion of conventional fuels: (1) oxidation of nitrogen contained in the fuel, the principal source of NO in the combustion of coal; (2) production of NO early in flame zones, at a rate faster than that predicted by quasi-equilibrium calculations (called 'prompt' NO); and (3) oxidation of atmospheric nitrogen. It is the last that is the main cause of NO production by gas turbines.

Production of NO is commonly estimated by the 'Zel'dovich mechanism', an approximation to the more accurate mechanism. The approximation by an overall reaction (Zel'dovich *et al.* 1985) is

$$\frac{d[\text{NO}]}{dt} = 1.45 \times 10^{17} \frac{1}{\sqrt{T}} [\text{O}_2]_{eq} [\text{N}_2]_{eq} e^{-\frac{69,460}{T(\text{K})}}$$

The rate of production of nitric oxide is strongly dependent on temperature, the origin of the descriptive label 'thermal NO'. For example, if the temperature is increased by 90°K at 2200°K, the rate doubles. Conversely, the practical implication is that less NO is produced at lower temperatures.

In the interest of reducing pollution by NO (more generally NO_x), combustion should be encouraged at low temperatures. However, at lower temperatures, the rate of production of another pollutant, carbon monoxide, is increased. At high temperatures, the equilibrium of CO_2 and CO is shifted as CO_2 dissociates to form more CO. Thus in practice, the production, or rather the equilibrium concentration of carbon monoxide, is minimum in a range of temperature not too high, not too low. Figure 2.63 shows some results of calculations carried out at the United Technologies Research Center (UTRC). It follows from these results that combustion is most favorably accomplished in a range of moderate temperature.

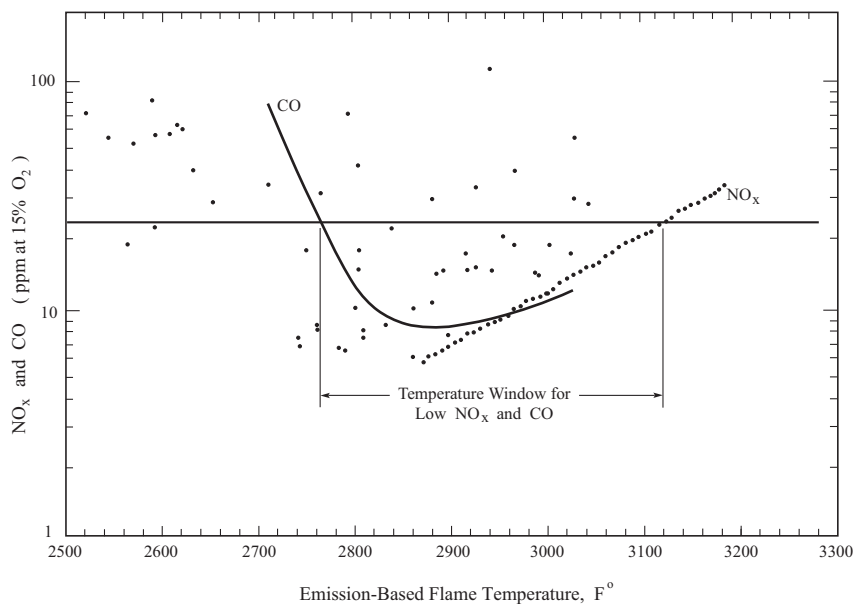


FIGURE 2.63. Concentrations at equilibrium of carbon monoxide and oxides of nitrogen (T. Rosfjord, UTRC; published in AGARD Report 820, Schadow *et al.* 1997).

The combustion temperature is reduced from its normal—i.e., traditionally accepted—value by operating the combustor at lower values of the equivalence or fuel/oxidizer ratio. But as F/O is reduced to give desirably lower levels of NO_x , the combustor operates near the lean blowout limit. Then the combustion zone becomes sensitive to fluctuations and approaches a condition under which it is both statically and dynamically unstable. Flame 'anchoring' and stabilization become insecure and can be lost due to small

disturbances. Local motions of the combustion zone may then couple to the chamber dynamics (acoustic) and grow into a combustion instability. The global consequences of that sequence of events is displayed in Figure 2.64. It is this general behavior that has motivated substantial and widespread research on combustion instabilities during the past decade and more.

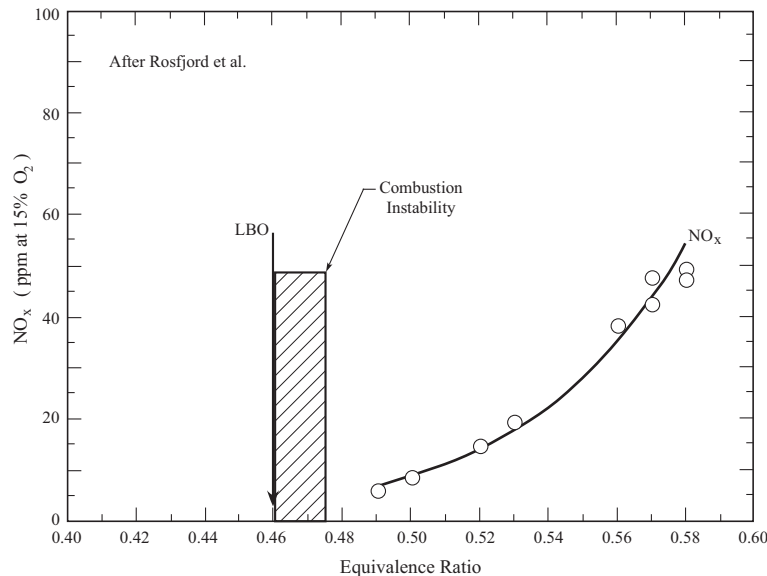


FIGURE 2.64. General behavior as the equivalence ratio is reduced near the lean blowout limit (T. Rosfjord, UTRC; published in AGARD Report 820, Schadow *et al.* 1997).

Eventually the mixture ratio holds a special position as a state variable identifying the change of the operating point of a combustor, as in Figure 2.63. It does not directly follow that F/O is in any sense a ‘mechanism’. On the other hand, because the fuel/oxidizer ratio affects directly such basic properties as energy release (or heat of reaction) and flame speed, it is quite easy to make a convincing case that variations of F/O can certainly produce oscillations. For example, imposing changes in F/O is a convenient means of initiating combustion instabilities in numerical simulations.

Probably the experiments reported by Langhorne (1988) and Langhorne, Dowling and Hooper (1990) were the first works to make explicit use of fuel/oxidizer fluctuations in studies of combustion instabilities. Since then, research on the role and consequences of unsteady variations of mixture ratio has been carried out by several groups; see, for example, reports by Lieuwen and Zinn (1998); Richards, James and Robey (1999); and by Cho and Lieuwen (2003). Those and other works have been motivated mainly by intentions to develop practical methods of active control, for application to problems of combustion instabilities in lean premixed systems as explained above. That is a principal subject of Chapter 9.

2.7. The Rijke Tube: Simplest Example of Thermoacoustic Instabilities

One of the fundamental guiding principles in the field of feedback control is that time delays can cause serious problems with stability and control. We have already mentioned on several occasions the presence of a time delay as a factor in instabilities. It is preferable to view a time delay as a characteristic of the mechanism of an instability rather than a mechanism *per se*. In this section we will treat two physical mechanisms—energy addition from an electrical heater and from a flame sheet—each of which present time delays. In both cases, delays exist between the action of a flow variable (pressure or velocity) and the energy added to the flow. That is, the delays arise in the internal feedback path shown in Figure 1.1.

The role of a time delay is clearly displayed in these special situations. Because heat addition is the root mechanism, the oscillations observed experimentally are often called ‘thermoacoustic instabilities.’ Understanding their behavior is a significant aid to comprehending more complicated instabilities generated by mechanisms quite different in their details.

A second purpose of this section is to introduce the analytical framework developed in the following chapters. The general formalism is quite generally applicable to combustors of any shape operating with any form of reactants, solid, liquid or gaseous. Simple examples share many of the features of the behavior found even in the most complicated applications to operational systems. Consequently, much of general value can be learned from investigating the details of an elementary example.

2.7.1. The Electrically Driven Rijke Tube. Rijke (1859) invented and first studied his device nearly 150 years ago. The experimental results were described and explained by Rayleigh (1878, 1945) as the chief basis for his formulation of the principle that came to be known as Rayleigh’s Criterion (Chu 1956; Zinn 1986; Culick, 1987a, 1992). In recent years the Rijke tube has received much attention because of its potential relations to combustion instabilities generally and for other reasons as well. Raun *et al.* (1993) have published the most complete summary of work with the Rijke tube to 1993. The article contains a virtually complete set of references and useful comments on much of the observed physical behavior, including experimental confirmation of Rayleigh’s Criterion. Still a basic ‘rule of thumb’ in the field of combustion instabilities, Rayleigh’s Criterion is derived here in Chapter 6.

Figure 2.65 is a sketch of the device to be analyzed here, the form of the device originally used. A tube open at both ends is supported vertically and contains an electrically heated grid mounted some distance ℓ_g above the lower end. In the original form of the tube used by Rijke, in place of the grid, a screen is heated by a flame which is subsequently removed. Soon after the flame is removed, a tone of growing intensity is produced. After maintaining a seemingly constant level for some time, the tone decays and ceases as the screen cools. Rijke attributed the sound to periodic heating and expansion of the air rising through the tube, alternating with compression due to cooling by the walls. Twenty years later, partially motivated by his belief that cooling by the walls was too slow to be a controlling process, Rayleigh gave his explanation for the excitation of the tone. He related the cause to the location of the heated screen relative to the form of the acoustic field. It is in that work that we find the succinct statement of conditions under which heat addition will cause oscillations, the famous ‘Rayleigh’s Criterion’ explained in Section 6.6.

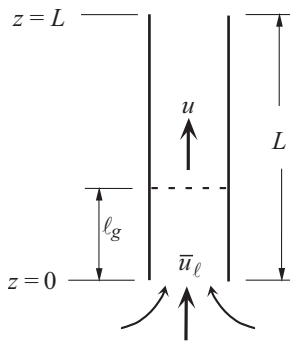


FIGURE 2.65. Sketch of an electrically heated Rijke tube.

Rayleigh’s reasoning was not intended to include explicitly quantitative details of the phenomenon. Another twenty years passed before Pflaum (1909) incorrectly attributed the origin of the sound to friction between the rising current of air and the heater. The idea was essentially an analogy between the tones produced in a Rijke tube and the oscillations excited by wind blowing past electric wires or telephone lines (or a flexible bridge!). Thus the heater served only as the prime mover of the rising air.

In 1937, more than a quarter century after Pflaum's work, Lehmann (1937) carried out experiments with the notable addition of a fine screen above or below the heater. Some of his observations misled him to formulate a 'theory' predicting that the amplitude of oscillation should continually increase with the draft velocity, not having the maximum value shown by experiments. Lehmann's conclusions had no influence, for not until fifteen years later did Neuringer and Hudson (1952) carry out what might be regarded as the first 'modern' discussion of the problem. They assumed that the time-dependent heat transfer depended mainly on the gradient of the local instantaneous velocity. Lehmann's experimental conditions served to define variables of the flow required in the calculations. The results found by Neuringer and Hudson were not extensive, but satisfied the authors that the local velocity gradient contributes crucially, suggesting further that turbulence is likely an important factor. There is little concrete connection between the analysis and observations cited in their discussion.

Carrier (1954) carried out the most detailed analysis of the Rijke tube driven by heat transferred from a heater made of wires or strips of metal. The work was apparently prompted by some experiments carried out by Bailey, who later gave an extended account of tests he performed with a Rijke tube operated with a gas burner (Bailey 1957). The greater part of Carrier's paper is devoted to a careful analysis of the mechanism, unsteady heat transfer from the heater to the gas stream; and to construction of the wave field in the tube. Carrier gave only brief comments regarding comparison with experimental results. The analysis has much instructional value.

Three papers by Merk (1956b, 1957a,b) began with a calculation of one-dimensional motions in flow of premixed combusting gases, and ended with a detailed examination of some possible unstable motions in a Rijke tube. Merk's calculations are linear, for one-dimensional flow and involve use of admittance functions. He eventually uses Carrier's result for the complex transfer function for a metal heater made of thin ribbons. The unsteady heat transfer to the air flow is then proportional to the velocity parallel to the ribbon, with a small phase difference. The physical content of Merk's model of the Rijke tube is essentially the same as Carrier's but his discussion of the observable behavior is much more extensive. He obtained a result for the neutral stability curve given below.

In a short note, Maling (1963) gave what is probably the simplest quantitative analysis of the linear behavior of the Rijke tube. The unsteady pressure is taken to obey the wave equation with a heat source (energy/mass-time) and no explicit effects of mean flow:

$$\frac{\partial^2 p'}{\partial x^2} - \frac{1}{\bar{a}^2} \frac{\partial^2 p'}{\partial t^2} = -\frac{(\gamma - 1)}{\bar{a}^2} \bar{\rho} \frac{\partial \dot{q}}{\partial t} \quad (2.129)$$

The heater is supposed to be an infinitesimally thin screen providing energy at a rate proportional to the velocity. In the notation used here, $p'(x, t) = \hat{p}(x) e^{-i\bar{a}kt}$ and $\dot{q} = F(\bar{u})u'$, so

$$\frac{d^2 \hat{p}}{dx^2} + k^2 \hat{p} = \frac{(\gamma - 1)}{\bar{a}} \bar{\rho} k F(\bar{u}) \hat{u}(x_h - \epsilon) \delta(x - x_h) \quad (2.130)$$

where the heater is located at x_h and ϵ is a small quantity required when the momentum equation is satisfied just upstream of the heater. As in Merk's analysis, Maling used Carrier's results to set $F(\bar{u})$. Limited test results with a three-foot tube and a blower in plenum chamber upstream of the tube established the lower limit speeds for oscillations, 0.84, 0.87, 0.91 m/s with total heater powers equal to 930, 1100, and 1290 Watts. Those can be viewed only as qualitative results because precise behavior is very sensitive to construction imperfections.

The first experiments with a horizontal Rijke tube were done by Friedlander in his thesis work reported by Friedlander, Smith and Powell (1964). Limited tests served only to establish correlations among some variables, mainly the sound pressure level, heater location, tube length and flow velocity which was provided by external means not described. The length of the tube could be adjusted by moving pistons which, while admitting flow, closed the ends. Apparently the observed behavior was consistent with the calculations by Maling. Insufficient details are given in the note to make further use of the report.

Saito (1965) seems to have misunderstood some of the previous work (e.g., he did not fully appreciate the basic nature and generality of Rayleigh's Criterion), and he incorrectly criticized application of Merk's calculations to an electrical heater. The apparatus he used is not described well, and several of his photographs are not clear. His Figures 7 and 8 clearly show that oscillations in his Rijke tube grow out of a linear instability. Unfortunately the work seems not to have fulfilled the author's hope for a new theory, or even for providing the experimental basis for a new theory.

The most extensive experimental results to that time were provided by Marone and Tarakanovskii (1967) using conventional square tubes having various lengths, an electrical heater and a controlled flow of air provided by a fan. Their basic results are reproduced in Figure 2.66. Unfortunately, the velocity V , which appears in the Strouhal number, $St = \omega d/V$, where d is the diameter of the heater, was not given in the paper. The results are therefore qualitative and have limited value. From Figure 2.66(a) it is clear, however, that a longer tube (lower frequency and lower losses/length) has a larger region of oscillation for a given heater power. Figure 2.66(b) shows that for a given tube, the region of oscillations increases with heater power. Marone and Tarakanovskii also give some results obtained when an unheated auxiliary grid was installed. Oscillations at the fundamental frequency could then, under some conditions, be excited by a heater placed in the upper half of the tube. That apparent violation of Rayleigh's Criterion has never been explained. Owing to the incompleteness of the information, a satisfactory explanation probably cannot be worked out with the given data alone.

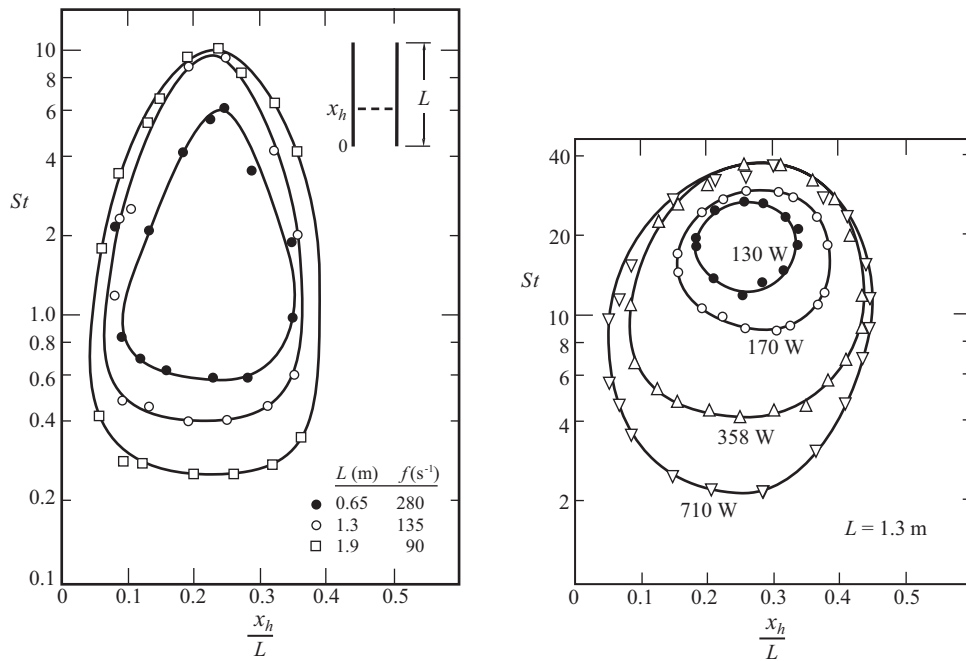


FIGURE 2.66. The effect of tube length and heater location on the generation of oscillations in a Rijke tube, $St = \omega d/V$; (a) heater power input 500W, (b) $L = 1.3$ m (Marone and Tarakanovskii 1967).

In a short note, Marchenko and Timoshenko (1970) later gave incomplete results for some aspects of nonlinear behavior. For example, they found that the ratio of the amplitudes of the second harmonic to that of the fundamental decreased linearly as the heater was moved from 20% to 30% of the tube length. Their data is suggestive but too little to advance understanding.

Collyer and Ayres (1972) briefly explored the generation of harmonics in a Rijke tube by one or two screen heaters appropriately placed in the tube. They reported exciting as many as nine harmonics in a

cold 79 cm tube and eight harmonics when it was 'hot'; the average temperatures were 28°C and 68°C respectively. Apart from a brief comment regarding an explanation for the presence of the second harmonic noted by Marchenko and Timoshenko, the authors merely report their observations without interpretation or explanation. Thus the work adds little to explaining the behavior of the Rijke tube.

Apparently inspired partly by Saito's work a dozen years earlier, and motivated by some fundamental weakness of both the available experimental results and analyses, Kalto and Sajiki (1977) reported quite extensive results for the onset of oscillations, but gave no analysis. Their apparatus was a vertical tube with supporting equipment essentially the same as Saito's. Figure 2.67 shows an example of their results which were always plotted as heater power versus flow rate measured in liters per minute. They show the usual

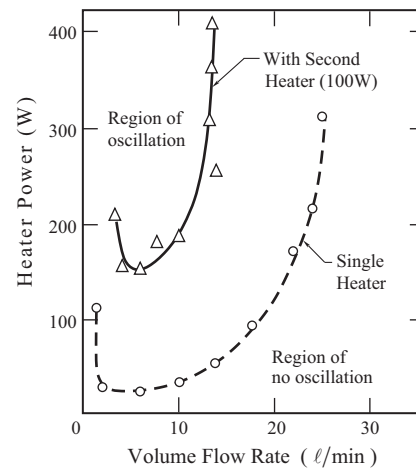


FIGURE 2.67. The effect of a second heater on the stability of oscillations; adapted from Figure 7 of Kalto and Sajiki (1977).

broad region of oscillations with a single heater placed at one-quarter of the tube length from the lower end. A series of tests were carried out with a second heater at one-quarter of the length from the top. The power to the second heater was constant, equal to 100W. When placed at the middle of the tube, the second heater had no effect, a result to be expected on the basis of Rayleigh's Criterion. Kalto and Sajiki examined the consequences of changing other variables, including tube length and form of the heater, which we will not discuss here.

The last of the papers from the University of Tokyo covers results obtained by Madarame (1981) who paid particular attention to the rates at which energy flows to the oscillations. It is unfortunate that the author ignores two hundred years of previous work on the problem: the only citations are the papers by Saito, and Kalto and Sajiki; and the book on boundary layer theory by Schlichting (1968). Madarame reports data for the growth of oscillations and for the limiting amplitude. Some effects, for example, of flow rate and heater power input are given for several lengths of tube. The author found fairly good agreement between observations and a simple analysis for small oscillations and for flow rates which are not high. Madarame speculates that transition to turbulent flow may be responsible for some of the anomalies found.

Probably the first thorough analysis of the stability of small motions in a Rijke tube was worked out by Kwon and Lee (1985). Their best result was the curve of stability limits reproduced here as Figure 2.68. Despite the obviously good agreement, which shows that the calculations contain some truth, the analysis does not constitute a theory of the Rijke tube, nor do Kwon and Lee make such a claim. Only the example shown in Figure 2.68 was given in the paper; the authors note that in other cases they examined, the experimental values of heat input were larger than predicted for large flow rates and smaller for low flow

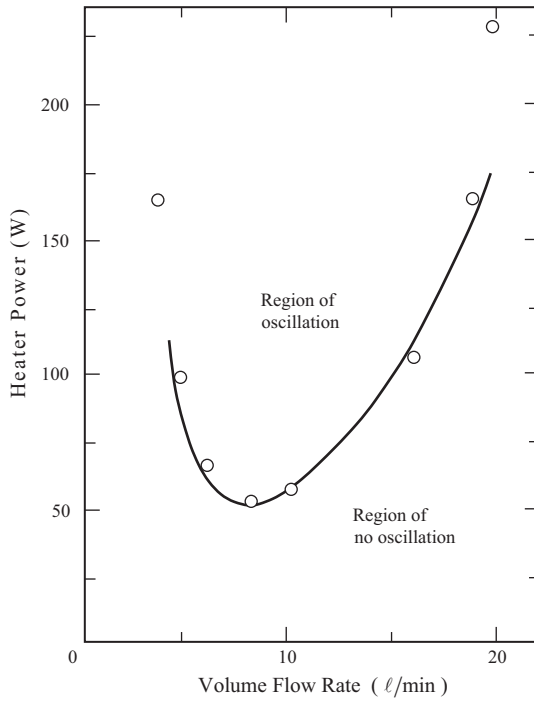


FIGURE 2.68. A prediction of a stability limit (Kwon and Lee 1983) with data reported by Kalto and Sajiki (1977).

rates. Kwon and Lee attribute those differences to a faulty representation of the heat provided by the heater for low flow rates, and to an unaccounted for increase of mean temperature T_m in the tube. In fact, even crude measurements demonstrated that their assumption that T_m is equal to the temperature of the air at the inlet to the tube is simply not valid.

Kwon and Lee define their “stability limit” for oscillations as the condition when the generation of power by the heater and absorbed by the gases exactly equals the acoustic energy dissipated in the tube. Convection of energy at the ends, and radiative losses were estimated to be negligible so the condition for oscillations is equality of the absorption of power and the rate at which acoustic energy is lost due to viscous effects, including heat conduction at the lateral boundary (Appendix C). The rates of generation and dissipation are

$$W_g = \frac{(\gamma - 1)\bar{\rho}_m \bar{a}_m}{4\gamma\bar{p}(\omega\kappa)^{1/2}} EQ_0 |\hat{u}_p|^2 \sin\left(\pi \frac{\ell_g}{L}\right) \quad (2.131)$$

$$W_a = \frac{\pi^2 R \bar{\rho}_m \bar{a}_m}{2\sqrt{2}} \left(\frac{\bar{\nu}_m}{\omega}\right)^{1/2} \left(1 + \frac{\gamma - 1}{\sqrt{Pr}}\right) |\hat{u}_p|^2 \quad (2.132)$$

where $(\quad)_m$ denotes values at the ‘mean temperature’ of the gas flow; $|\hat{u}_p|$ is the magnitude of the peak velocity oscillation; $\bar{\nu}_m$ is the mean kinematic viscosity; Q_0 is the “overall steady heat input to the air from the heater”; and E is an efficiency factor measuring the part of heat release in phase with the pressure. Equating (2.131) and (2.132) leads to the formula for Q_0 :

$$Q_0 = \frac{\sqrt{2}\pi R(\kappa\bar{\nu}_m)^{1/2}\gamma\bar{p}}{E \sin\left(2\pi \frac{\ell_g}{L}\right)} \left(1 + \frac{\gamma - 1}{\sqrt{Pr}}\right) \quad (2.133)$$

The heat input is least when $\sin\left(2\pi\frac{\ell_g}{L}\right) = 1$, or $\ell_g = \frac{L}{4}$, a well-known result. Some additional ancillary calculations are required (see the paper by Kwon and Lee) but the preceding conveys the gist of the matter.

In the greater part of practical cases, the presence of oscillations in combustors is simply not wanted. Hence the main problem is avoiding them in the first place, or suppressing them when they do appear. It seems to be generally true that if an existing combustion system is developed further in the interest of improving its performance in some sense, then unwanted oscillations of pressure will inevitably appear. That is one reason why the Rijke tube has continued to attract attention; it is the simplest system displaying many aspects of general behavior. Given the problem, the practical question arises—how can the oscillations be avoided or suppressed? With an interesting paper, Sreenivasan, Raghu and Chu (1985) used an electrically-driven Rijke tube to introduce the idea and first example of actively controlling acoustic oscillations. Their basic idea was to convert “acoustic to thermal energy so that the acoustic oscillations are quenched and the system is stabilized.”

The apparatus Sreenivasan *et al.* used was a vertical tube with a primary heater mounted in the bottom half and a control heater in the upper half. As part of their study the authors measured the temperature of the air system to be 26°C before the primary heater, 92°C before the control heater and 97° in the exhaust. Thus the temperature rise was about 30% of the initial ambient value, not the small change assumed by Kwon and Lee. As a point we will return to in Chapter Nine, the oscillations in the tube were suppressed by using control heater power roughly 3% of the primary heater power, whereas the acoustic power was approximately 1/100 as much. Active control may be very costly.

Subsequent to the work just described, the Rijke tube has been used either in slightly different forms using various fuels to provide the driving power from combustion (e.g. Putnam and Dennis, 1954, who apparently made the first flame-driven Rijke tube; and Raun and Beckstead, 1993, among many); or as the object to investigate the application of active control. The recent investigation by Matveev (2003) seems to be the latest based on the historically ‘conventional’ form of the electrically powered tube. Matveev and Culick 2002a–d; 2003b,c have discussed the work. Matveev took special care to obtain data having precision as high as possible, a demand that required lengthy tests to reach thermal equilibrium or, better, steady-state. The apparatus was a perfected form of that described by Pun (2001) and sketched in Figure 2.69. Figure 2.70 shows two examples of experimental results and calculations for the stability boundary with two

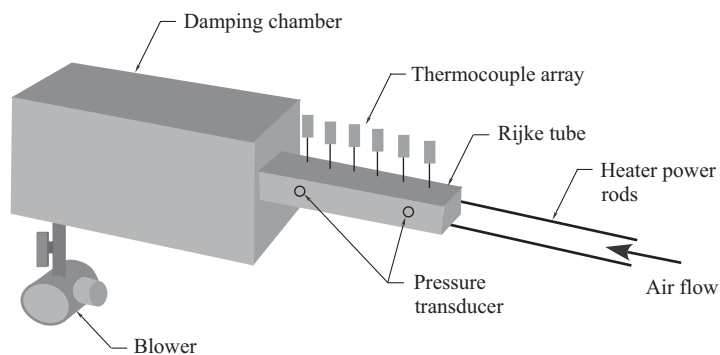


FIGURE 2.69. A sketch of the horizontal Rijke tube used by Matveev (2003).

positions of the heater. The crossed short lines represent experimental error bars; the heavier short vertical lines illustrate the shifts of the computed stability boundary when the impedance of the chamber is assigned an uncertainty of $\pm 20\%$.

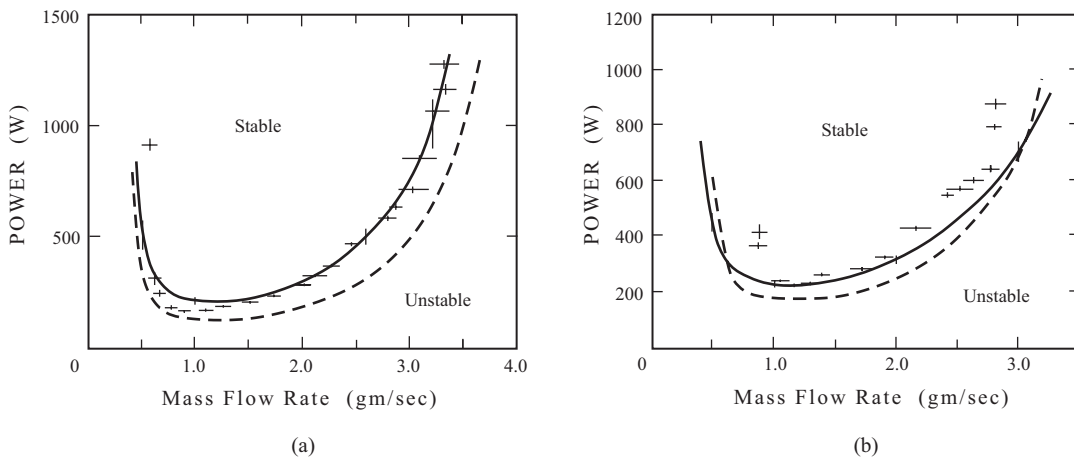


FIGURE 2.70. Comparison of experimental data and calculations for stability boundaries of the Rijke tube in Figure 2.69. Heater position: (a) 1/4 tube length; (b) 1/8 tube length.

These results support the conclusion that we can compute the stability of the electrically driven Rijke tube quite well, but considerable care is required. See Matveev and Culick (2003) for a more detailed discussion. Even in the crudest execution of the experiment, three elementary results are found, implicit in the references cited, if not discussed explicitly:

- (a) If the heater is in the lower half of the tube steady acoustic oscillations can be sustained;
- (b) The frequency of the sound is close to the fundamental frequency $\bar{a}/2L$ of the tube;
- (c) If the tube is tilted, the intensity of sound decreases and is zero when the tube is horizontal.

Correspondingly, three basic questions are raised:

- (i) What determines the frequencies of the observed oscillations?
- (ii) Why does the location of the grid matter?
- (iii) Why does the vertical orientation of the tube affect the oscillations?

All three questions can be answered with linear analysis of the field in the tube and consideration of modest nonlinear behavior of the heat transfer from the heater. The steps in the procedure followed in Section 2.7.2 are in direct correspondence with those followed in the general method.

2.7.2. Mean Field in the Rijke Tube. The hotter gas above the heater rises, inducing a draft in the tube. In steady flow there is an abrupt rise, in the limit a discontinuity, of temperature across the heater. Continuity of mass flow requires²⁸

$$\bar{\rho}_L \bar{u}_L S_c = \bar{\rho}_U \bar{u}_U S_c \quad (2.134)$$

where S_c is the cross-section area. Subscripts $(\)_L$ and $(\)_U$ denote values in the lower and upper regions of the tube; and $(\)$ stands for average value.

We assume that the average flow is uniform above and below the heater, and that the perfect gas law holds with the gas constant having the same value throughout, $p = \rho RT$. In this low speed flow the pressure is approximately uniform except for a negligible change across the heater due to viscous effects (drag and

²⁸Strictly, careful derivation of this relation gives $\bar{\rho} \bar{u} S_c = \text{constant}$. We assume $\bar{\rho} \bar{u} = \bar{\rho} \bar{u}$; see discussion of the equations for the average flow in Chapter 3.

heat transfer). Hence certainly as a good first approximation, we have the simple relation connecting the density and temperature ratios across the heating grid

$$\frac{\bar{\rho}_L}{\bar{\rho}_U} = \frac{\bar{T}_L}{\bar{T}_U} > 1 \quad (2.135)$$

2.7.3. Acoustic Field in the Rijke Tube. The simplest representation of the acoustic field is based on the assumptions that the mean flow has negligible effects on the unsteady field; and that viscous losses at the lateral walls may be ignored. Then the classical acoustic conservation equations for one-dimensional motions apply:

$$\text{Mass} \quad \frac{\partial \rho'}{\partial t} + \frac{\partial \rho'}{\partial x} (\bar{\rho} u') = 0 \quad (2.136)$$

$$\text{Momentum} \quad \frac{\partial u'}{\partial t} + \frac{\partial p'}{\partial x} = 0 \quad (2.137)$$

$$\text{Pressure (Energy)} \quad \frac{\partial p'}{\partial t} + \gamma \bar{p} \frac{\partial u'}{\partial x} = (\gamma - 1) \dot{Q}' \delta(x - \ell_g) \quad (2.138)$$

The effect of the heater is represented by the fluctuation \dot{Q}' of heat exchanged between the grid and the flow, assumed to occur in the infinitesimally thin plane at $x = \ell_g$. These familiar equations are derived in a more general context in Chapters 3–5; see Sections 3.3 and 5.1.

The idea now is to solve (2.136)–(2.138) separately in the regions upstream and downstream of the heater. Because $\dot{Q}' = 0$ outside the heater, the solutions represent freely traveling waves. Then the field in the tube will be found by applying suitable boundary conditions at the ends, and matching conditions at the heater.

The required matching conditions are obtained by integrating the conservation equations over a small region containing the heating grid, Figure 2.71, $(\ell_g - \delta) < x < (\ell_g + \delta)$ and then letting $\delta \rightarrow 0$.

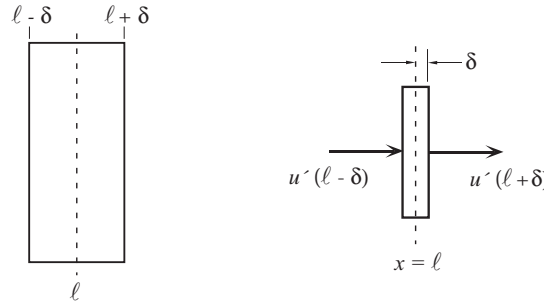


FIGURE 2.71. Region of integration for obtaining matching conditions.

Applying the procedure to the differential equation (2.136) for conservation of mass gives

$$\int_{\ell_g - \delta}^{\ell_g + \delta} \frac{\partial \rho'}{\partial t} dx + \int_{\ell_g - \delta}^{\ell_g + \delta} \frac{\partial}{\partial x} (\bar{\rho} u') dx = 0$$

so for small δ ,

$$(\bar{\rho} u')_{\ell_g + \delta} - (\bar{\rho} u')_{\ell_g - \delta} = 0$$

For $\delta \rightarrow 0$ we have

$$\bar{\rho}_U u'_{\ell_g+} = \bar{\rho}_L u'_{\ell_g-} \quad (2.139)$$

This result is the formal statement that the acoustic mass flux is constant through the heater.

Similarly, the momentum equation (2.137) leads to continuity of the acoustic pressure,

$$p'_{\ell+} = p'_{\ell-} \quad (2.140)$$

Integration of the energy equation (2.138) across the heater introduces the influence of the unsteady heat addition:

$$\int_{\ell_g-\delta}^{\ell_g+\delta} \frac{\partial p'}{\partial t} dx + \int_{\ell_g-\delta}^{\ell_g+\delta} \gamma \bar{p} \frac{\partial u'}{\partial x} dx = (\gamma - 1) \int_{\ell_g-\delta}^{\ell_g+\delta} \dot{Q}'_g \delta(x - \ell) dx$$

For $\delta \rightarrow 0$:

$$\gamma \bar{p} (u'_{\ell_g+} - u'_{\ell_g-}) = (\gamma - 1) \dot{Q}'_g$$

so the discontinuity of the velocity fluctuation is

$$u'_{\ell_g+} = u'_{\ell_g-} + (\gamma - 1) \frac{\dot{Q}'_g}{\gamma \bar{p}} \quad (2.141)$$

Combination of (2.139) and (2.141) gives

$$u'_{\ell_g-} = \frac{1}{\frac{\bar{\rho}_L}{\bar{\rho}_U} - 1} (\gamma - 1) \frac{\dot{Q}'_g}{\gamma \bar{p}} ; \quad u'_{\ell_g+} = \frac{\bar{\rho}_L / \bar{\rho}_U}{\frac{\bar{\rho}_L}{\bar{\rho}_U} - 1} (\gamma - 1) \frac{\dot{Q}'_g}{\gamma \bar{p}} \quad (2.142)a,b$$

There is only one source of energy for the acoustic field in this form of the problem, the heating grid. We will ignore all losses at the ends and lateral boundary of the tube. Depending on the heat transfer between the grid and unsteady motions of the gas, a small amplitude disturbance may grow or decay. That is, we are really concerned at this point with stability of waves in the tube. We examine the matter in two ways: by finding the wave field in the tube subject to appropriate boundary conditions and the matching conditions just derived; and with a method based on spatial averaging. In practice, the chief difference between the two approaches is that the second approach gives the desired result for stability without requiring knowledge of the actual acoustic field.

2.7.4. Acoustic Field and Stability by Matching Waves. The method used in this section has often been applied to problems involving planar waves. Several examples have appeared in the literature of combustion-driven oscillations, e.g., Dowling 1995; Candel 1992, 2001. Here we have only to use the matching conditions derived above to join representations of standing waves on the two sides of the heater. In the regions between the heater and the ends, the linearized momentum and energy equations are

$$\begin{aligned} \bar{\rho} \frac{\partial u'}{\partial t} + \frac{\partial p'}{\partial x} &= 0 \\ \frac{\partial p'}{\partial t} + \gamma \bar{p} \frac{\partial u'}{\partial x} &= 0 \end{aligned} \quad (2.143)a,b$$

The wave equation for the pressure is formed by differentiating (2.123)b with respect to time and replacing $\partial u' / \partial t$ by (2.123)a.

For \bar{p} , $\bar{\rho}$ constant and $\bar{a}^2 = \gamma \bar{p} / \bar{\rho}$, the result is

$$\frac{\partial^2 p'}{\partial t^2} - \bar{a}^2 \frac{\partial^2 p'}{\partial x^2} = 0 \quad (2.144)$$

Solutions of the form $p' \sim e^{\lambda t} e^{\chi x}$ are easily found, appropriate combinations then form representations of standing waves. We ignore radiation of acoustic energy from the ends of the tube, a condition that is enforced by requiring that the pressure fluctuations vanish:

$$\begin{aligned} p'(0; t) &= 0 \\ p'(L; t) &= 0 \end{aligned} \quad (2.145)\text{a,b}$$

It is convenient to use the complex form for the time dependence; a solution to (2.144) for the lower part of the tube, satisfying (2.125)a is

$$p'_L(x; t) = P_L e^{-i\Omega t} \sin(k_L x) \quad (0 \leq x < L) \quad (2.146)$$

where Ω is the complex frequency and k_L is the complex wavenumber:

$$\begin{aligned} \Omega &= \omega + i\alpha \\ k_L &= \Omega/\bar{a}_L = \frac{\omega}{\bar{a}_L} + i\frac{\alpha}{\bar{a}_L} \end{aligned} \quad (2.147)$$

As defined here, α is positive for an unstable wave.

The acoustic momentum equation (2.123)a is satisfied, with (2.146) for the pressure, if the corresponding velocity fluctuation is

$$u'_L(x; t) = -i \frac{P_L}{\bar{\rho}_L \bar{a}_L} e^{-i\Omega t} \cos(k_L x) \quad (0 \leq x < \ell_g) \quad (2.148)$$

Similarly, the solutions in the upper part²⁹ of the tube are

$$\begin{aligned} p'_U(x; t) &= P_U e^{-i\Omega t} \sin k_U(L - x) \\ u'_U(x; t) &= i \frac{P_U}{\bar{\rho}_U \bar{a}_U} e^{-i\Omega t} \cos k_U(L - x) \quad (\ell_g < x \leq L) \end{aligned} \quad (2.149)\text{a,b}$$

With these solutions, application of the conditions (2.140) for continuity of acoustic pressure and (2.141) for the discontinuity of velocity fluctuation gives the two equations relating the unknown amplitudes P_L and P_U :

$$\begin{aligned} P_L \sin(k_L \ell_g) &= P_U \sin k_U(L - \ell_g) \\ P_U \cos k_U(L - \ell_g) &= -P_L \left(\frac{\bar{\rho}_U \bar{a}_U}{\bar{\rho}_L \bar{a}_L} \right) \cos(k_L \ell_g) - i \left(\frac{\bar{\rho}_U \bar{a}_U}{\gamma \bar{p}} \right) (\gamma - 1) \dot{Q}'_g e^{i\Omega t} \end{aligned} \quad (2.150)\text{a,b}$$

The heat exchanged between the grid and the flow likely depends on both the pressure and velocity, but in the absence of experimental and theoretical results, it is reasonable simply to assume that \dot{Q}'_g is proportional to the velocity fluctuation with a time lag. But what velocity fluctuation? As an approximation, we assume that the average value across the heater is a reasonable choice, so

$$\dot{Q}'_g = \frac{Q_u}{2} [u'_L(\ell_g; t - \tau_u) + u'_U(\ell_g; t - \tau_u)] \quad (2.151)$$

Substitution in (2.145)b and rearrangement leads to

$$-\xi P_L \cos(k_L \ell_g) = P_U \cos k_U(L - \ell_g) \quad (2.152)$$

²⁹Note that there is a sign change in $u' L$ because x is replaced by $L - x$. Also, the complex frequency Ω has the same value throughout the tube because we assume ‘steady’ waves—‘steady’ except for slow growth or decay.

where

$$\xi = \frac{\bar{\rho}_U \bar{a}_U}{\bar{\rho}_L \bar{a}_L} \frac{1 + \frac{(\gamma-1)Q_u}{2\gamma\bar{p}} e^{i\Omega\tau_u}}{1 - \frac{(\gamma-1)Q_u}{2\gamma\bar{p}} e^{i\Omega\tau_u}} \quad (2.153)$$

Division of (2.145)a by (2.152) gives the transcendental equation for the complex eigenvalue Ω (recall $k_L = \Omega/\bar{a}_L$ and $k_U = \Omega/\bar{a}_U$):

$$\xi \tan(k_L \ell_g) = -\tan k_U(L - \ell_g) \quad (2.154)$$

The last equation can only be solved numerically in general, but for the case of weak heating, an instructive result is readily obtained by expansion about the limit of no heating. When $Q_0 = 0$ so the gas properties are uniform, $\xi = 1$; after expansion of (2.154) the dependence of ℓ_g drops out and we recover the classical condition setting the wavenumbers in an open-open straight tube:

$$\sin kL = 0$$

and

$$kL = 0, \pi, 2\pi, \dots \ell\pi \quad (2.155)$$

When weak heating is assumed, the wavenumbers differ slightly from (2.155); for the first mode ($\ell = 1$) set³⁰

$$k_L = k_U \approx \frac{1}{L}(\pi + \delta) \quad (2.156)$$

and the problem comes down to determining δ . Then to first order in δ ,

$$\begin{aligned} \tan(k_L \ell_g) &= \tan(\pi + \delta) \frac{\ell_g}{L} \\ \tan k_L(L - \ell_g) &= \tan(\pi + \delta) \left(1 - \frac{\ell_g}{L}\right) \end{aligned} \quad (2.157)a,b$$

It is sufficient for the purposes here to consider the special case $\ell_g/L = 1/4$, when the heating grid is one-quarter of the tube length from the inlet. Experimentally it is well-known that the first mode is excited when the heater is in the lower half of the tube. With $\ell_g/L = 1/4$, substitution of (2.157)a,b in (2.154) gives

$$\xi \tan \frac{1}{4}(\pi + \delta) = -\tan \frac{3}{4}(\pi + \delta) \quad (2.158)$$

where ξ differs from unity by an amount of the order of δ . If we assume $\frac{\bar{\rho}_U \bar{a}_U}{\bar{\rho}_L \bar{a}_L} = 1 + \epsilon$ and set

$$\Delta = \frac{\gamma - 1}{2\bar{p}} Q_u e^{i\Omega\tau_u} \quad (2.159)$$

Then ξ (2.153) becomes

$$\xi = (1 + \epsilon) \frac{1 + \Delta}{1 - \Delta} \cong 1 + (\epsilon + 2\Delta)$$

to first order in small quantities. Also to first order in δ ,

$$\begin{aligned} \tan \frac{1}{4}(\pi + \delta) &\cong \frac{1 + \frac{\delta}{4}}{1 - \frac{\delta}{4}} \cong 1 + \frac{\delta}{2} \\ \tan \frac{3}{4}(\pi + \delta) &\cong \frac{1 - \frac{3}{4}}{-1 - \frac{3}{4}} \cong -\left(1 - \frac{3}{2}\delta\right) \end{aligned}$$

³⁰We ignore the small increase in the speed of sound in the flow through the grid. This affects the frequency slightly and even less the growth or decay constant (time averaging part of the wavenumber).

Substitution of these approximations in (2.158) leads to

$$1 + (\epsilon + 2\Delta) = \frac{1 - \frac{3}{2}\delta}{-1 - \frac{\delta}{2}} \approx 1 - 2\delta$$

and

$$\delta = -\frac{\epsilon}{2} - \Delta = -\left(\frac{\epsilon}{2} + \frac{\gamma - 1}{2\bar{p}}Q_u \cos \Omega\tau_u\right) - i\frac{\gamma - 1}{2\bar{p}}Q_u \sin \Omega\tau_u \quad (2.160)$$

Now by definition, the complex wavenumber and frequency are related by

$$k = \frac{\Omega}{\bar{a}} = \frac{\omega}{\bar{a}} - i\frac{\alpha}{\bar{a}} = \frac{1}{L}(\pi + \delta) ,$$

the second equality following from (2.156). Hence, with (2.160) we find

$$\omega = \pi \frac{\bar{a}}{L} - \frac{1}{2} \left(\epsilon + \frac{\gamma - 1}{\bar{p}}Q_u \cos \Omega\tau_u \right) ; \quad \alpha = \frac{\bar{a}}{L} \frac{\gamma - 1}{2\bar{p}}Q_u \sin \Omega\tau_u$$

But since α is first order in small quantities we must replace Ω , by the unperturbed classical frequency, $\omega \approx \pi \frac{\bar{a}}{L}$, so the first order approximations to the frequency and growth constant are

$$\begin{aligned} \omega &= \pi \frac{\bar{a}}{L} - \frac{1}{2} \left[\left(\frac{\bar{\rho}_U}{\bar{\rho}_L} \frac{\bar{a}_U}{\bar{a}_L} - 1 \right) + \frac{\gamma - 1}{\bar{p}}Q_u \cos \left(\pi \frac{\bar{a}}{L} \tau_u \right) \right] \\ \alpha &= \frac{\bar{a}}{L} \frac{\gamma - 1}{2\bar{p}}Q_u \sin \left(\pi \frac{\bar{a}}{L} \tau_u \right) \end{aligned} \quad (2.161)a,b$$

Because the growth constant α must be positive for the mode to be unstable, we have the simple criterion for instability that the time lag τ_u must be in the range

$$0 < \tau_u < \frac{L}{\bar{a}} \quad (2.162)$$

The period of the fundamental mode is $2\pi/\omega_1 = 2\pi/\bar{a}k = 2L/\bar{a}$. Hence the condition (2.162) requires that for unstable oscillations the heat addition should not lag the velocity oscillation by more than one-half period. Similar results can be obtained for higher modes. For excitation of oscillations, there is also a restriction on the location of the heater, not easily found with the analysis given here. Both restrictions on the temporal and spatial properties of the heater are readily obtained with the method based on spatial averaging.

2.7.5. Stability Analyzed by a Method of Spatial Averaging. The generic character of the mechanism examined in the preceding section is better shown with a special case of the analytical framework developed in Chapters 3 and 4. We use the same example, but initially without the restriction to energy addition at an infinitesimally thin grid. Hence the speed of sound must be treated as a function of position in the tube. However, the mean pressure is constant and uniform, and formation of the wave equation as in the steps leading to (2.144) now gives

$$\frac{\partial^2 p'}{\partial t^2} - \frac{\partial}{\partial x} \left(\bar{a}^2 \frac{\partial p'}{\partial x} \right) = \frac{R}{C_v} \frac{\partial \dot{Q}'}{\partial t}$$

which we write in the form appropriate for small changes in the speed of sound,

$$\frac{\partial^2 p'}{\partial t^2} - \bar{a}_0^2 \frac{\partial^2 p'}{\partial x^2} = \frac{R}{C_v} \frac{\partial \dot{Q}'}{\partial t} - \frac{\partial p'}{\partial x} \frac{d\delta\bar{a}^2}{dx} \quad (2.163)$$

where $\bar{a}^2 = \bar{a}_0^2 + \delta\bar{a}^2$, \bar{a}_0^2 being constant,

$$h = \frac{R}{C_v} \frac{\partial \dot{Q}'}{\partial t} - \frac{\partial p'}{\partial x} \frac{d\delta\bar{a}^2}{dx} \quad (2.164)$$

The boundary conditions set at the ends of the tube are

$$\begin{aligned} p'(0; t) &= 0 \\ p'(L; t) &= 0 \end{aligned} \quad (2.165)a,b$$

We assume always the classical acoustic problem for motions with no perturbations. Here the definition of the unperturbed problem is clear: \dot{Q}' and $d\bar{a}^2/dx$ vanish. Since we are normally interested in determining what effects the perturbations have on the known classical behavior, we concentrate on analyzing the difference between the actual and classical problems. The idea is to construct the spatially averaged weighted difference in the following way.

Let p'_1 denote the pressure in the fundamental mode of classical motion satisfying the homogeneous wave equation and the same boundary conditions as for the actual problem:

$$\frac{\partial^2 p_1}{\partial t^2} - \bar{a}_0^2 \frac{\partial^2 p_1}{\partial x^2} = 0 \quad (2.166)$$

$$\begin{aligned} p_1(0; t) &= 0 \\ p_1(L; t) &= 0 \end{aligned} \quad (2.167)a,b$$

Multiply (2.163) by p_1 , (2.158) by p' , subtract the results and integrate over the volume of the tube to give

$$\int_0^L \left[p_1 \frac{\partial^2 p'}{\partial t^2} - p' \frac{\partial^2 p_1}{\partial t^2} \right] S_c dx - \bar{a}_0^2 \int_0^L \left[p_1 \frac{\partial^2 p'}{\partial x^2} - p' \frac{\partial^2 p_1}{\partial x^2} \right] S_c dx = \int_0^L h S_c dx \quad (2.168)$$

Integrate the second integral by parts and substitute the boundary conditions (2.165)a,b and (2.167)a,b to find

$$\begin{aligned} \int_0^L \left[p_1 \frac{\partial^2 p'}{\partial x^2} - p' \frac{\partial^2 p_1}{\partial x^2} \right] S_c dx &= \int_0^L \left[p_1 \frac{\partial p'}{\partial x} - p' \frac{\partial p_1}{\partial x} \right] S_c dx \\ &\quad - \int_0^L \left[\frac{\partial p_1}{\partial x} \frac{\partial p'}{\partial x} - \frac{\partial p'}{\partial x} \frac{\partial p_1}{\partial x} \right] S_c dx \\ &\quad \left[p_1 \frac{\partial p'}{\partial x} - p' \frac{\partial p_1}{\partial x} \right] S_c dx - 0 \\ &= 0 \end{aligned}$$

From earlier results we take $p'_1 = P_1 \sin \omega_1 t \sin k_1 x$, so in the first integral of (2.168),

$$\frac{\partial^2 p_1}{\partial t^2} = -\omega_1^2 p_1$$

where $\omega_1 = \bar{a}_0 k_1$. We assume that the spatial dependence of the motion is not much affected by the heat addition,³¹ but the amplitude $\eta_1(t)$ varies in time, in a manner to be determined; thus for the actual oscillation we assume the form

$$p' = \bar{p} \eta_1(t) \sin k_1 x \quad (2.169)$$

³¹This is a key step clarified in Chapter 4.

Substituting p_1 and p' in the first integral of (2.168) we have

$$\begin{aligned} \int_0^L \left[p_1 \frac{\partial^2 p'}{\partial t^2} - p' \frac{\partial^2 p_1}{\partial t^2} \right] S_c dx &= \int_0^L \left[P_1 \sin \omega_1 t \sin k_1 x (\bar{p} \ddot{\eta}_1 \sin k_1 x - \omega_1^2 \bar{p} \eta_1 \sin k_1 x) \right] S_c dx \\ &= P_1 \bar{p} \sin \omega_1 t (\ddot{\eta}_1 + \omega_1^2 \eta_1) S_c \int_0^L \sin^2 k_1 x dx \end{aligned}$$

Inserting these results in (2.163) leads to

$$\frac{d^2 \eta_1}{dt^2} + \omega_1^2 \eta_1 = \frac{1}{\bar{p} E_1^2} \int_0^L h \sin k_1 x dx \quad (2.170)$$

and

$$E_1^2 = \int_0^L \sin^2 k_1 x dx = \frac{L}{2} \quad (2.171)$$

With h given by (2.164), equation (2.170) becomes

$$\frac{d^2 \eta_1}{dt^2} + \omega_1^2 \eta_1 = \frac{2(R/C_v)}{\bar{p} L} \int_0^L \sin k_1 x \frac{\partial \dot{Q}'}{\partial t} dx - \frac{2}{\bar{p} L} \int_0^L \frac{\partial p'}{\partial x} \frac{d \bar{a}^2}{dx} dx \quad (2.172)$$

To simplify the calculations we will ignore the change $\delta \bar{a}^2$ in the speed of sound, and for comparison with the results found in the preceding section, we specialize (2.172) to the case of a thin heating region. For some further generality we assume that the fluctuations of heat addition depend on both the local velocity and pressure fluctuations. Hence we add a term to the representation (2.151) to give

$$\dot{Q} = \left\{ \frac{Q_u}{2} [u'_L(\ell_g; t - \tau_u) + u'_U(\ell_g; t - \tau_u)] + Q_p p'(\ell_g; t - \tau_u) \right\} \delta(x - \ell_g) \quad (2.173)$$

It is a great advantage of the method based on spatial averaging that in the right-hand side of (2.172) we can use, as a first approximation,³² the unperturbed classical forms for the pressure and velocity fields. Thus the discontinuity in the velocity fluctuation at the grid is ignored and (2.173) becomes

$$\dot{Q}' = \{Q_u u'(\ell_g; t - \tau_u) + Q_p p'(\ell_g; t - \tau_p)\} \delta(x - \ell_g) \quad (2.174)$$

The unperturbed form for p' is (2.169); the corresponding form for u' is

$$u' \approx \frac{\dot{\eta}_1}{\gamma k_1} \cos k_1 x \quad (2.175)$$

This formula is justified as the zeroth order approximation for the velocity fluctuation because together (2.169) and (2.175) satisfy the unperturbed acoustic momentum equation (2.137) providing $k_1^2 = \omega_1^2 / \bar{a}^2$ and (as zeroth approximation) η_1 satisfies the wave equation without perturbations; substitution in (2.137) gives

$$\bar{p} \frac{\partial}{\partial t} \left(\frac{\dot{\eta}_1}{\gamma k_1} \cos k_1 x \right) + \frac{\partial}{\partial t} (\bar{p} \eta_1 \sin k_1 x) = 0$$

This equation leads to

$$\frac{d^2 \eta_1}{dt^2} + \omega_1^2 \eta_1 = 0 \quad (2.176)$$

where $\omega_1^2 = \bar{a}^2 k_1^2$.

³²The matter of correct systematic approximations, an iterative procedure, is discussed in Chapter 4.

Substitution of (2.162) and (2.175) in (2.174) gives the formula for \dot{Q}' to be used in (2.172):

$$\dot{Q}' = \left\{ \frac{Q_u}{\gamma k_1} \cos k_1 \ell_g \frac{d}{dt} \eta_1(t - \tau_u) + Q_p \bar{p} \sin k_1 x \eta_1(t - \tau_p) \right\} \delta(x - \ell_g) \quad (2.177)$$

Then

$$\frac{\partial \dot{Q}'}{\partial t} = \left\{ -\frac{Q_u \omega_1^2}{\gamma k_1} \cos(k_1 \ell_g) \eta_1(t - \tau_u) + Q_p \bar{p} \sin k_1 x \frac{d}{dt} \eta_1(t - \tau_p) \right\} \delta(x - \ell_g) \quad (2.178)$$

where we have used (2.176) as an approximation in the first term.

Finally, use (2.177) in (2.172) and rearrange the result to give

$$\frac{d^2 \eta_1}{dt^2} - 2 \left[Q_p \frac{R/C_v}{L} \sin^2 k_1 \ell_g \right] \frac{d}{dt} \eta_1(t - \tau_p) + \omega_1^2 \left[\eta_1(t) + Q_u \frac{R/C_v}{\gamma \bar{p} L k_1} \sin 2k_1 \ell_g \eta_1(t - \tau_u) \right] = 0 \quad (2.179)$$

This equation represents the behavior of a linear oscillator with time delays associated with internal feedback. To determine stability, we assume that the amplitude η_1 is a sinusoid with slowly growing or decaying amplitude:

$$\eta_1(t) = C e^{-i\Omega t} \quad (2.180)$$

where C is constant and the complex frequency is

$$\Omega = \omega + i\alpha \quad (2.181)$$

For instability, α must be positive with the sign convention chosen here. Both α and the difference between the actual (ω) and unperturbed (ω_1) frequencies are small: $|\alpha| \ll \omega_1$ and $|\omega - \omega_1| \ll \omega_1$. Substitute (2.180) in (2.179) to find

$$-\Omega^2 - 2A(-i\Omega) e^{i\Omega\tau_p} + \omega_1^2(1 + Be^{i\Omega\tau_u}) = 0 \quad (2.182)$$

where

$$\begin{aligned} A &= Q_p \frac{R/C_v}{L} \sin^2 k_1 \ell_g \\ B &= Q_u \frac{R/C_v}{\gamma \bar{p} L k_1} \sin 2k_1 \ell_g \end{aligned} \quad (2.183)a,b$$

Expanded to show the real and imaginary parts, (2.182) is

$$[-\omega^2 + \omega_1^2(1 + B \cos \omega_1 \tau_u) - 2A \omega_1 \sin \omega_1 \tau_p] + i[-2\alpha \omega_1 = 2A \omega_1 \cos \omega_1 \tau_p + \omega_1^2 B \sin \omega_1 \tau_u] = 0$$

where second order quantities have been ignored.³³ The brackets must vanish separately and we have the approximations for the frequency and growth (or decay) constant.

$$\begin{aligned} \frac{\omega}{\omega_1} &= 1 - \frac{A}{\omega_1} \sin \omega_1 \tau_p + \frac{1}{2} B \cos \omega_1 \tau_u \\ \frac{\alpha}{\omega_1} &= \frac{A}{\omega_1} \cos \omega_1 \tau_p + \frac{1}{2} B \sin \omega_1 \tau_u \end{aligned}$$

With (2.183)a,b, these formulas are

$$\begin{aligned} \frac{\omega}{\omega_1} &= 1 - Q_p \left[\frac{R/C_v}{\omega_1 L} \sin^2 k_1 \ell_g \right] \sin \omega_1 \tau_p + Q_u \left[\frac{R/C_v}{2\gamma \bar{p} L k_1} \sin 2k_1 \ell_g \right] \cos \omega_1 \tau_u \\ \frac{\alpha}{\omega_1} &= Q_p \left[\frac{R/C_v}{\omega_1 L} \sin^2 k_1 \ell_g \right] \cos \omega_1 \tau_p + Q_u \left[\frac{R/C_v}{2\gamma \bar{p} L k_1} \sin 2k_1 \ell_g \right] \sin \omega_1 \tau_u \end{aligned} \quad (2.184)a,b$$

The conditions for instabilities immediately follow from (2.184)b as the conditions under which $\alpha/\omega > 0$. For ‘velocity coupling’, heat addition dependent on velocity fluctuations, the conditions are: $0 < \omega_1 \tau_u < \pi$

³³The perturbations represented by A and B are small, of first order, as are $|\alpha|$ and $|\omega - \omega_1|$.

and $0 < 2k_1\ell_g < \pi$; and for ‘pressure coupling’, the single condition must be satisfied: $-\pi/2 < \omega_1\tau_p < \pi/2$. Hence with $\omega_1 = \pi\frac{\bar{a}}{L}$, we have the conditions for the first mode to be unstable:

$$\text{Pressure Coupling: } -\frac{\tau_1}{4} < \tau_p < \frac{\tau_1}{4} \quad (2.185)$$

$$\text{Velocity Coupling: } \begin{aligned} 0 < \tau_p &< \frac{\tau_1}{2} \\ 0 < \ell_g &< \frac{L}{2} \end{aligned} \quad (2.186)$$

where $\tau_1 = 1/f_1 = 2L/\bar{a}$ is the period of the fundamental mode. There is no restriction on the location of the heater because the pressure fluctuations is in-phase at all points along the tube. The velocity fluctuation suffers a π phase change at the center, so the velocity fluctuations in the upper and lower halves are π out-of-phase.

We are now able to answer two of the three questions posed at the end of Section 2.7.1. To question (i), the answer is that the frequencies are closely those of the classical acoustic modes and hence are determined mainly by the length of the tube and the temperatures distribution axially. According to the calculations just completed, the position of the grid matters because it selects the phase between the acoustic pressure and velocity fluctuations. That conclusion, which answers question (ii), is certainly contained in the results of the method based on matching waves, but is difficult to extract. With the method based on spatial averaging, the conclusion is immediate.

It is particularly to be noted that observations have established that for a Rijke tube excited either by an electrical grid or by a sample of heated gauge, the first mode is excited only if the source of heating is in the lower half of the tube. Hence the results (2.186) demonstrates what is intuitively evident, that convective heat transfer dependent on velocity fluctuations is most probably the basic mechanism. That is likely also true for a tube driven unstable by a flame, but the observational results are too limited to make a definite statement.

2.7.6. Nonlinear Behavior due to Rectification. It seems that the observed dependence of the oscillations on vertical orientation of the Rijke tube is probably due to the need for a draft, an average flow through the tube (question (iii), Section 2.7.1). In this section we use the method of spatial averaging to demonstrate that assertion, but without quantitative results for the amplitudes of oscillation. The starting point is the simplified oscillator equation (2.172) for the first mode and include only the heat source on the right-hand side

$$\frac{d^2\eta_1}{dt^2} + \omega_1^2\eta_1 = 2\frac{R/C_v}{\bar{p}L} \int_0^L \sin k_1 x \frac{\partial \dot{Q}'}{\partial t} dx \quad (2.187)$$

Other than the somewhat vague requirement of ‘smallness’, no restrictions have been placed on \dot{Q}' . In particular, it need not be linear. Two sorts of elementary nonlinear behavior are likely found in practice: rectification, and saturation. The latter refers to an upper limit to the amount or rate of energy supplied to the wave system by whatever processes dominate the mechanism. We will return to some aspects of saturation later in the context of the control and limit cycles. Here we consider rectification associated with convective heat transfer as the only nonlinear process present.³⁴

Convective heat transfer depends mainly on the relative speed of the flow past the surface and less so in the direction. For example, for flow normal to a wire, Figure 2.72(a), the rate of heat transfer should be the same in the two cases. On the other hand, a preferred flow direction for maximum heat transfer rate may be

³⁴In particular we ignore the significant effects of nonlinear gasdynamics, covered in Chapter 7.

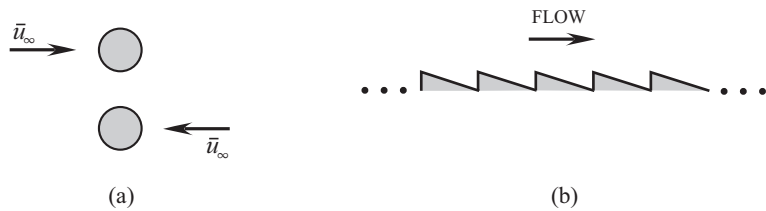


FIGURE 2.72. (a) Illustrating the independence of heat transfer on flow direction; (b) illustrating possible dependence of heat transfer on flow direction due to microscopic properties of the surface.

caused by microscopic characteristics of the surface, one case being shown in Figure 2.72(b). We ignore that type of behavior and assume that the heat transfer depends only on the magnitude of the relative velocity,

$$\dot{Q} = f(|\bar{u}|) \quad (2.188)$$

We also assume for application to the Rijke tube that the flow is always parallel to the axis, having both mean and fluctuating components; the total and average rates are then

$$\dot{Q} = f(|\bar{u} + u'|); \quad \bar{Q} = f(|\bar{u}|) \quad (2.189)$$

Hence the fluctuation is

$$\dot{Q}' = f(|\bar{u} + u'|) - f(|\bar{u}|) \quad (2.190)$$

The simplest possibility, sufficient for the reasoning here, is that \dot{Q} is proportional to $|\bar{u}|$, i.e. $f(|\bar{u}|) = K|\bar{u}|$, and (2.190) becomes

$$\dot{Q}' = K \{ |\bar{u} + u'| - |\bar{u}| \} = K|\bar{u}| \left\{ \left| 1 + \frac{u'}{\bar{u}} \right| - 1 \right\} \quad (2.191)$$

This formula contains three sorts of behavior illustrated in Figure 2.73. To interpret the meanings of Figure 2.73, we assume that the fluctuations of heat transfer is given by (2.191). Hence \dot{Q}' is proportional to the values lying in the heavy lines with lower sketches of the three parts. For small values of the fluctuation, $|u'|/|\bar{u}| < 1$, the heat transfer fluctuates entirely at the frequency of the imposed velocity fluctuation, Part (a). As $|u'|/|\bar{u}|$ increases and is greater than unity, rectification occurs and there are components of heat transfer at other frequencies, including a steady (DC) value, as Part (b) shows. Finally, if there is no average velocity, rectification is complete, as Part (c) indicates, and there is no oscillation of heat transfer at the frequency of the imposed oscillatory flow. The behavior just described seems to offer a likely explanation for the third observation and question (iii) listed at the end of Section 2.7.1. If an operating Rijke tube is tilted from the vertical, the amplitude of the oscillation is reduced, finally disappearing before the tube is horizontal. That is also why an electrically driven tube, conveniently mounted horizontally, must be equipped with a system for forcing air through the tube. It is an important advantage of such an arrangement that one has control over the flow rate (Matveev and Culick, 2002).

2.7.7. A Simple Analysis of the Flame-Driven Rijke Tube. Many laboratory devices for studying thermoacoustic instabilities and their control are essentially straight ducts or tubes with one end closed to permit injection of liquid or gaseous reactions. Combustion takes place downstream, usually anchored by some sort of flameholder. The simplest approximation to the energy addition by combustion is a flat flame (a ‘flame sheet’) perpendicular to the axis, as sketched in Figure 2.74. A configuration of this type is effectively a Rijke tube closed at one end. Hence stability of the system can be investigated with analysis that is chiefly a paraphrase of that covered in Sections 2.7.4 to 2.7.5. First we use the method based on spatial averaging,

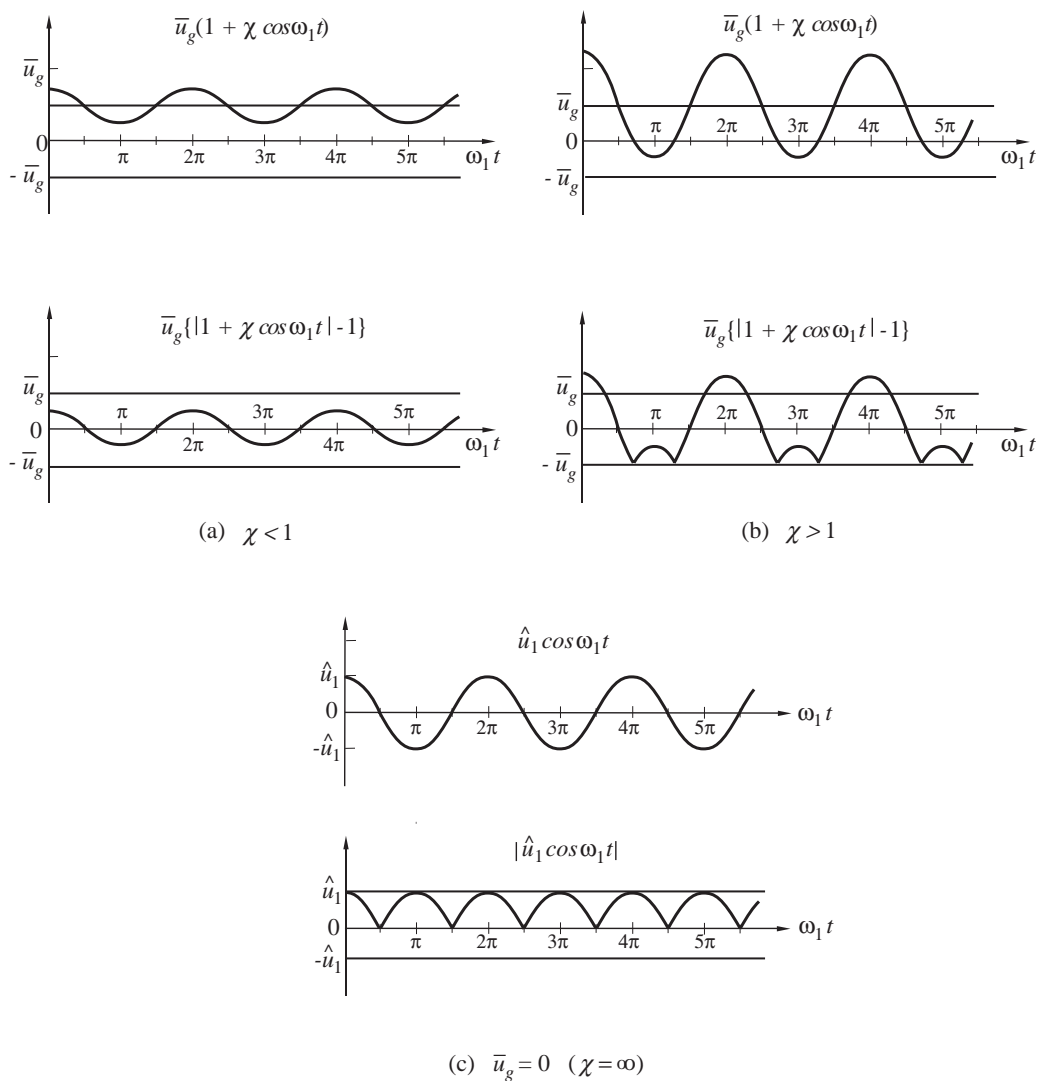


FIGURE 2.73. Three sorts of nonlinear behavior due to rectification distinguished by the relative values of the mean and fluctuating components of velocity: graphs of \dot{Q}'/K , eq. (2.191), with $\chi = \bar{u}/\bar{u}$.

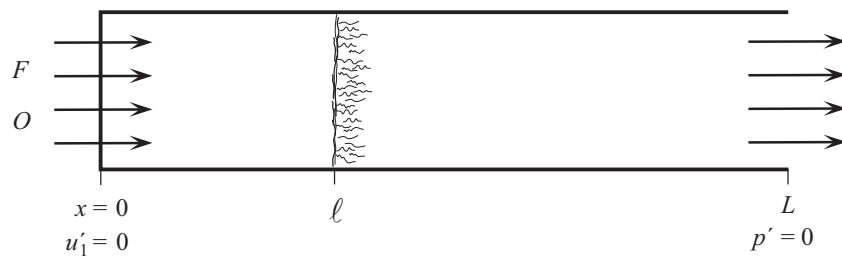


FIGURE 2.74. A basic flame-driven Rijke tube.

beginning again with the oscillator equation (2.170) with only the heat addition accounted for:

$$\frac{d^2\eta_1}{dt^2} + \omega_1^2\eta_1 = \frac{R/C_v}{\bar{p}E_1^2} \int_0^L p_1 \frac{\partial \dot{Q}'}{\partial t} dx \quad (2.192)$$

The modal function p_1 must now be chosen to satisfy the boundary condition of zero velocity normal to the entrance plane at $x = 0$; for the fundamental mode:

$$p_1' = P_1 \sin \omega_1 t \cos k_1 x = p_1 \sin \omega_1 t$$

and

$$k_1 = \frac{\pi}{2L} \quad (2.193)a,b$$

Note that the wavelength, $\lambda_1 = 2\pi/k_1 = 4L$ and the tube is a ‘quarter-wave tube’. The corresponding value of the mode shape for the acoustic velocity is

$$u_1' = -\frac{P_1}{\rho a} \cos \omega_1 t \sin k_1 x \quad (2.194)$$

With p_1 given by (2.149), $E_1^2 = L/2$ and the oscillator equation is

$$\frac{d^2\eta_1}{dt^2} + \omega_1^2\eta_1 = 2\frac{R/C_v}{\bar{p}L} \int_0^L \cos k_1 x \frac{\partial \dot{Q}'}{\partial t} dx \quad (2.195)$$

It is commonly assumed that the fluctuation of energy addition from an infinitesimally thin flat flame is proportional to the velocity fluctuation, with time lag τ_u :

$$\dot{Q}' = Q_0 u'(\ell; t - \tau_u) \delta(x - \ell) \quad (2.196)$$

The question again arises: what velocity should be used? Following reasoning in Section 2.7.5, we ignore the spatial discontinuity due to the heat addition and assume the relation (2.175) for u' , but with the current mode shape $\sin k_1 x$:

$$\begin{aligned} u'(x; t - \tau_u) &= \frac{P_1}{\gamma k_1^2} \frac{d}{dt} \eta(t - \tau_u) \frac{d}{dx} (\cos k_1 x) \\ &= \frac{P_1}{\gamma k_1} \dot{\eta}_1(t - \tau_u) \sin k_1 x \end{aligned} \quad (2.197)$$

The fluctuation of heat addition is

$$\dot{Q}' = -\frac{P_1}{\gamma k_1} \dot{\eta}_1(t - \tau_u) \sin k_1 x \delta(x - \ell) \quad (2.198)$$

which gives to first order in small quantities:

$$\begin{aligned} \frac{\partial \dot{Q}'}{\partial t} &= \frac{P_1}{\gamma k_1} \ddot{\eta}(t - \tau_u) \sin k_1 x \\ &= \frac{P_1 Q_0}{\gamma k_1} \omega_1^2 \eta_1(t - \tau_u) \sin k_1 x \end{aligned} \quad (2.199)$$

Substitution in the oscillator equation (2.194) gives

$$\frac{d^2\eta_1}{dt^2} + \omega_1^2\eta_1 = \kappa \eta_1(t - \tau_u) \quad (2.200)$$

with

$$\kappa = \frac{R}{C_v} \frac{P_1 Q_0}{\gamma \bar{p} L k_1} \omega_1^2 \sin 2k_1 \ell \quad (2.201)$$

Now assume solution of the form

$$\eta_1 = Ne^{\alpha t}e^{-i\omega t} = Ne^{-i\omega t}; \quad \Omega = \omega + i\alpha \quad (2.202)$$

Substitution in (2.200) leads to the complex algebraic equation for α and ω :

$$[-\omega^2 + \omega_1^2 - \kappa \cos \omega_1 \tau_u] + i[-2\alpha\omega + \kappa \sin \omega_1 \tau_u] \quad (2.203)$$

where again we ignore quantities of higher than first order. The real and imaginary parts of (2.203) must vanish, giving to first order:

$$\begin{aligned} \frac{\omega}{\omega_1} &= 1 - \frac{1}{2}\kappa \cos \omega_1 \tau_u \\ \frac{\alpha}{\omega_1} &= -\frac{\kappa}{2\omega_1^2} \sin \omega_1 \tau_u \end{aligned} \quad (2.204)a,b$$

Since $\alpha > 0$ for an instability, and with κ given by (2.201), the fundamental mode is unstable if

$$\sin 2k_1 \ell \sin \omega_1 \tau_u < 0 \quad (2.205)$$

which is satisfied if

$$\begin{aligned} (a) \quad \sin \omega_1 \tau_u &< 0 \quad \text{and} \quad \sin 2k_1 \ell > 0 \\ \text{or} \quad (b) \quad \sin \omega_1 \tau_u &> 0 \quad \text{and} \quad \sin 2k_1 \ell < 0 \end{aligned}$$

In the first case,

$$\begin{aligned} \frac{\pi}{2} &< \omega_1 \tau_u < \frac{3\pi}{2} \\ \text{and} \quad -\frac{\pi}{2} &< 2k_1 \ell < \frac{\pi}{2} \end{aligned}$$

With $k_1 = \pi/2L$ and $\omega_1 = 2\pi f_1 = 2\pi/\tau$ these two inequalities become ($\frac{\ell}{L} < 0$ is excluded):

$$\begin{aligned} \frac{\tau_1}{4} &< \tau_u < \frac{3}{4}\tau_1 \\ 0 &< \frac{\ell}{L} < \frac{1}{2} \end{aligned} \quad (2.206)$$

In the second case (b) above,

$$\begin{aligned} -\frac{\pi}{2} &< \omega_1 \tau_u < \frac{\pi}{2} \\ \frac{\pi}{2} &< 2k_1 \ell < \frac{3\pi}{2} \end{aligned}$$

which become

$$\begin{aligned} -\frac{\tau_1}{4} &< \tau_u < \frac{\tau_1}{4} \\ \frac{1}{2} &< \frac{\ell}{L} < 1 \end{aligned} \quad (2.207)$$

Together, the two cases offer the ranges for the time delay and flame location

$$\begin{aligned} -\frac{\tau_1}{4} &< \tau_u < \frac{3\tau_1}{4} \\ 0 &< \frac{\ell}{L} < 1 \end{aligned} \quad (2.208)a,b$$

The differences between these results for the flame-driven Rijke tube and (2.185) and (2.186) for the electrically-heated case arise entirely because the mode shapes of the fundamental modes differ (a quarter-wave in the present case and a half-wave for the electrically-driven tube).

Solution by matching waves in the manner of Section 2.7.4 produces similar results, but as in that calculation, the restriction on the location of the heating zone, (2.208)b, cannot be obtained (Poinsot and

Veynante 2001; Candel *et al.* 2001). The analyses covered here have shown, even for these simple cases, the ease with which the method based on spatial averaging can be applied. Moreover, matching waves is successful only for problems of longitudinal motions. The analytical framework based on spatial averaging is not only applicable to combustors of any shape, but accommodates any form of reactants—solid, liquid, or gaseous.



CHAPTER □

Equations for Unsteady Motions in Combustion Chambers

The examples described in Chapter 1, and many others, establish a firm basis for interpreting unsteady motions in a combustor in terms of acoustic modes of the chamber. That view has been formalized during the past fifty years and has led to the most widely used methods for interpreting combustor dynamics. In this and the following chapter, we present the foundations of a particularly successful version of methods based on expansion in normal acoustic modes and spatial averaging. We assume familiarity with the basic ideas of classical fluid dynamics and acoustics. Chapter 5 covers the principles and chief results of classical acoustics required as part of the foundation for understanding combustion instabilities. The discussions in Chapters 3 and 4 are quite formal, intended to serve as the basis for a framework within which unsteady motions, especially combustion instabilities, may be treated for all types of combustors. Hence the physical model for which the formalism is developed is quite general.

3.1. Modes of Wave Motion in a Compressible Medium

In this section, the term ‘modes’ refers not to natural motions or resonances of a chamber but means rather a *type* or class of motions in compressible flows generally. The brief discussion here is intended to address the question: How is it possible that apparently coherent, nearly classical acoustic waves exist in chambers containing highly turbulent non-uniform flow? It’s a fundamentally important observation that such is the case. The explanation has been most thoroughly clarified by Chu and Kovasznay (1957), who combined and elaborated some results known for nearly a century. Their conclusions most significant for present purposes may be summarized as follows:

- (i) Any small amplitude (linear) disturbance may be synthesized of three modes of propagation: *entropy waves* or ‘spots’, small regions having temperatures slightly different from the ambient temperature of the flow; *vortical or shear waves* characterized by nonuniform vorticity; and *acoustic waves*.
- (ii) In the linear approximation, *if the flow is uniform*, the three types of waves propagate independently, but may be coupled at boundaries (e.g. nozzles) or in combustion zones.

Entropy and vortical waves having small amplitude propagate (are ‘convected’) in a uniform field with the mean flow speed, but acoustic waves propagate with their own speeds of sound. Moreover, in the linear limit, only acoustic waves carry disturbances of pressure. All three types of waves possess velocity fluctuations. If the medium is non-uniform or the unsteady motions have finite amplitudes, the three modes become coupled. As a result, each of the waves may then carry pressure, temperature and velocity fluctuations. Little extension of the fundamental theory has been accomplished (see Chu and Kovasznay) and what understanding exists has been gained from considerations of particular problems. Some of the consequences of these types of modal coupling arise in the theory developed here, but much remains to be investigated.

Long experience has established the wide applicability of the basic physical model of combustion instabilities as acoustic waves propagating in a non-uniform flow. Vorticity and entropy waves accompany turbulence in a combustor but may also have other origins, such as flow separation, the unsteady behavior

of injection devices, and interactions of the acoustic field with other processes, notably flow injected at the lateral boundaries. Consequently, both the average and time-varying velocity fields in a combustor comprise irrotational and rotational motions. Observational evidence for combustion instabilities suggests that the rotational motions are in some sense often secondary, initially one of the chief guiding principles for the formalism developed in this chapter, but they cannot be ignored. In fact, both steady and unsteady rotational motions participate significantly in combustion instabilities in solid propellant rockets. Several examples of the generation and behavior of vorticity have been intensively studied in the past ten years. We will discuss some of the results in Chapter 6.

The main idea at this point is that in lowest approximation the unsteady field can be expressed as a synthesis of classical acoustic modes having time-varying amplitudes. Then the purpose of the analysis is to work out a means for computing the changes of those amplitudes due to various perturbations. Departures from the simplest classical acoustic behavior arise from the actions of the other physical and chemical processes taking place in a combustion chamber. All of those processes, except basic gasdynamics, are assumed to have relatively weak effects, producing small shifts of the classical acoustic frequencies and, more significantly, small fractional changes of the modal amplitudes during a period of oscillation. Hence there are two small quantities naturally characterizing the procedure: A reference Mach number for the unsteady velocity is a measure of the acoustic amplitudes; and a typical Mach number of the average flow measures perturbations of the classical acoustic behavior. Much of this chapter is concerned with reduction of the general equations of motion by expansion in those two small parameters. In applications of the formalism and interpretation of the results, it is essential to understand and maintain the distinction between the roles of the two parameters. Failure to do so leads to confusion and false conclusions.

Despite the emphasis on the acoustic field, this procedure does *not* exclude the existence of rotational motions. In the expansion procedure they arise from inhomogeneous terms in the equations for the higher order terms. This fundamental point has been missed by several workers in this field and has led at least to misunderstandings and occasionally to misleading or incorrect analyses. The origins of the difficulties will be clarified in later discussions, particularly in Chapter 6, but in view of the considerable confusion about the matter, it is important to begin addressing the matter here. It is not a new idea. Flandro (1967) in his Ph.D. thesis first used the general expansion procedure developed in this chapter to work out a problem involving interactions between acoustic and vorticity fields leading to roll torques in solid propellant rockets. He and others have subsequently investigated other examples of the influences of vorticity on acoustic waves using this approach, occasionally with controversial and sometimes incorrect results. (See, for example, Flandro 1995; Culick *et al.* 1991; Culick 1998; Swenson and Culick 1998; Seywert and Culick, 1998; Flandro and Malhotra 1995; Malhotra, Flandro and Roh 2000; Malhotra and Flandro 2001, 2002; Majdalani and Van Moorhem 1998; Majdalani 2004; Flandro and Majdalani 2003.)

3.2. Equations of Motion in a Reacting Flow

Combustion systems commonly contain condensed phases: liquid fuel or oxidizer, and combustion products including soot and condensed metal oxides. Hence the equations of motion must be written for two or three phases consisting of at least one species each. For investigating the dynamics of combustors, it seems entirely adequate to consider two phases (gas and a condensed phase comprising both liquid and solid particles). The properties of each phase are represented as mass averages of the properties of all member species. For a medium consisting of a multicomponent mixture of reacting gases and, for simplicity, a single condensed phase, it is a straightforward matter to construct a system of equations representing a single fluid. The procedure is explained in Annex A. As a result we can treat combustor dynamics under broad conditions as unsteady motions of a fluid having the mass-averaged properties of the actual medium.¹ The dimensional governing equations are (A.59)–(A.64):

¹We now use C_v , γ , R , ... to stand for the mass-averaged properties represented by boldface symbols in Annex A.

$$\text{Conservation of Mass:} \quad \frac{\partial \rho}{\partial t} + \mathbf{u} \cdot \nabla \rho = -\rho \nabla \cdot \mathbf{u} + \mathcal{W} \quad (3.1)$$

$$\text{Conservation of Momentum:} \quad \rho \left[\frac{\partial \mathbf{u}}{\partial t} + \mathbf{u} \cdot \nabla \mathbf{u} \right] = -\nabla p + \mathbf{F} \quad (3.2)$$

$$\text{Conservation of Energy:} \quad \rho C_v \left[\frac{\partial T}{\partial t} + \mathbf{u} \cdot \nabla T \right] = -p \nabla \cdot \mathbf{u} + \mathcal{Q} \quad (3.3)$$

$$\text{Equation for the Pressure:} \quad \frac{\partial p}{\partial t} + \mathbf{u} \cdot \nabla p = -\gamma p \nabla \cdot \mathbf{u} + \mathcal{P} \quad (3.4)$$

$$\text{Equation for the Entropy:} \quad \rho \frac{Ds}{Dt} = \frac{1}{T} \mathcal{S} \quad (3.5)$$

$$\text{Equation of State:} \quad p = R\rho T \quad (3.6)$$

Definitions of all symbols are given in Annex A.

It is particularly important to realize that the source functions \mathcal{W} , \mathbf{F} , \mathcal{Q} , \mathcal{P} and \mathcal{S} in principle contain all relevant processes in the systems to be analyzed here. They include, for example, the modeling and representations of the actions of actuation mechanisms used for active control. Eventually, the most difficult problems arising in this field are associated with modeling the physical processes dominant in the problems addressed.

For both theoretical and computational purposes it is best to express the equations in dimensionless variables using the reference values:

L : reference length

ρ_r, p_r, T_r, a_r : reference density, pressure, temperature and speed of sound

C_{vr}, C_{pr}, R_r : reference values of C_v, C_p, R

Then define the dimensionless variables represented by \mathbf{M} , and *for simplicity use the same symbols used for dimensional variables*:

$$\begin{aligned} \mathbf{M} = \frac{\mathbf{u}}{a_r}; \quad \frac{\rho}{\rho_r} \rightarrow \rho; \quad \frac{p}{\rho_r a_r^2} \rightarrow p; \quad \frac{T}{T_r} \rightarrow T; \quad \frac{C_v}{C_{pr}} \rightarrow C_v; \quad \frac{C_p}{C_{pr}} \rightarrow C_p; \\ \frac{R}{C_{pr}} \rightarrow R; \quad \frac{a_r}{L} t \rightarrow t; \quad \frac{s}{C_{pr}} \rightarrow s \end{aligned}$$

The dimensionless source functions are

$$\frac{L}{\rho_r a_r} \mathcal{W} \rightarrow \mathcal{W}; \quad \frac{L}{\rho_r a_r^2} \mathbf{F} \rightarrow \mathbf{F}; \quad \frac{L}{\rho_r a_r^3} \mathcal{Q} \rightarrow \mathcal{Q}; \quad \frac{L}{\rho_r a_r} \mathcal{P} \rightarrow \mathcal{P}; \quad \frac{\mathcal{S}}{\rho_r a_r C_{vr}} \rightarrow \mathcal{S}$$

For consistent definitions, $p_r = \rho_r R_r T_r$ and $R_r = C_{pr} = C_{vr}$, so in dimensionless form, the relations $R = C_p - C_v$ and $\gamma = C_p/C_v$ still hold.

Substitution of these definitions in equations (3.1)–(3.6) leads to the set of dimensionless equations for the single fluid model:

$$\text{Mass:} \quad \frac{D\rho}{Dt} = -\rho \nabla \cdot \mathbf{M} + \mathcal{W} \quad (3.7)$$

$$\text{Momentum:} \quad \rho \frac{D\mathbf{M}}{Dt} = -\nabla p + \mathbf{F} \quad (3.8)$$

$$Energy: \quad \rho C_v \frac{DT}{Dt} = -p \nabla \cdot \mathbf{M} + Q \quad (3.9)$$

$$Pressure: \quad \frac{Dp}{Dt} = -\gamma p \nabla \cdot \mathbf{M} + \mathcal{P} \quad (3.10)$$

$$Entropy: \quad \rho \frac{Ds}{Dt} = \frac{1}{T} \mathcal{S} \quad (3.11)$$

$$State: \quad p = \rho RT \quad (3.12)$$

and

$$\frac{D}{Dt} = \frac{\partial}{\partial t} + \mathbf{M} \cdot \nabla \quad (3.13)$$

We emphasize again that the source terms accommodate all relevant physical processes and can be interpreted to include the influences of actuation used in active control.

3.3. Two-Parameter Expansion of the Equations of Motion

The general equations (3.7)–(3.12) are written in the form suggestive of problems that are dominated by fluid mechanical processes, a tactic dictated by the observations described earlier. This point of view is the basis for the approach taken here to construct a general framework within which both practical and theoretical results can be obtained by following systematic procedures.

We are not concerned at this point with simulations or other methods relying essentially on some sort of numerical analysis and large scale computations. The nature of the problems we face suggests perturbation methods of solution. If the source terms \mathcal{W}, \dots were absent from (3.7)–(3.11), the homogeneous equations then represent nonlinear inviscid motions in a compressible fluid: Nonlinear acoustics in a medium without losses. One useful method for investigating such problems is based on expansion of the equations in a small parameter, ε , measuring the amplitude of the motion. Specifically, ε can be taken equal to M'_r , a Mach number characteristic of the fluctuating flow, $\varepsilon = M'_r$.

The problems we are concerned with here are defined essentially by the non-zero functions \mathcal{W}, \dots . Because observed behavior seems to be dominated by features recognizable as ‘acoustical’, those sources which excite and sustain the actual motions must in some sense be small. They should therefore be characterized by at least one additional small parameter. It has become customary to select only one such parameter, $\mu = \bar{M}_r$, a Mach number \bar{M}_r characterizing the mean flow, for the following reasons.²

Any operating combustion chamber contains an average steady flow produced by combustion of the fuel and oxidizer to generate products. The intensity of the flow, partly measurable by the Mach number, is therefore related to the intensity of combustion; both processes can in some sense be characterized by the same quantity, namely the Mach number of the average flow. Thus many of the processes represented in the source functions may be characterized by μ , in the sense that their influences become vanishingly small as $\mu \rightarrow 0$ and are absent when $\mu = 0$.

It is important to understand that the two small parameters ε and μ have different physical origins. Consequently, they also participate differently in the formal perturbation procedures. Familiar nonlinear gas dynamical behavior is, in the present context, governed by the parameter ε ; steepening of compressive waves

²We will use the symbols ε and μ rather than M'_r and \bar{M}_r to simplify writing, and to emphasize the special positions held by the two independent sorts of perturbations.

is a notable example. In the expansion procedure worked out here, the term ‘nonlinear behavior’ refers to the consequences of terms higher order in ε .

On the other hand, the parameter μ characterizes perturbations of the gasdynamics due in the first instance to combustion processes and the mean flow. Terms of higher order in μ , but linear in ε , represent linear processes in this scheme. Failure to recognize this basic distinction between ε and μ can lead to incorrect applications of formal procedures such as the method of time-averaging. Instances of this point will arise as the analysis is developed.

3.3.1. Expansion in Mean and Fluctuating Values. There is no unique procedure for carrying out a two-parameter expansion. We begin here by writing all dependent variables as sums of mean (̄) and fluctuating (̄') parts without regard to ordering:

$$p = \bar{p} + p', \quad \mathbf{M} = \bar{\mathbf{M}} + \mathbf{M}', \dots, \quad \mathcal{W} = \bar{\mathcal{W}}', \quad \mathbf{F} = \bar{\mathbf{F}} + \mathbf{F}', \dots \quad (3.14)$$

We take the fluctuations of the primary flow variables (p' , \mathbf{M}' , ρ' , T' , s') to be all of the same order in the amplitude ε of the unsteady motion. Generally, the source terms are complicated functions of the flow variables and therefore their fluctuations will contain terms of many orders in ε . For example, suppose $\mathcal{W} = kp^3$. Then setting $p = \bar{p} + p'$ and expanding, we have

$$\mathcal{W} = k(\bar{p} + p')^3 = k \left[\bar{p}^3 + 3\bar{p}^2 p' + 3\bar{p}p'^2 + p'^3 \right]$$

Hence we define orders of the fluctuations of the source \mathcal{W} and write

$$\mathcal{W} = \bar{\mathcal{W}} + \mathcal{W}'_1 + \mathcal{W}'_2 + \mathcal{W}'_3 + \mathcal{W}'_4 + \dots$$

where the subscript denotes the order with respect to the amplitude: Here, for the example, $\mathcal{W} = kp^3$ and $\mathcal{W}'_2 = (3k\bar{p})p'^2$. All source functions are expressed in this general fashion, but modeling is required to give explicit formulas.

Most combustors contain flows of relatively low Mach number, say $|\bar{\mathbf{M}}| \lesssim 0.3$ or so. Thus we can assume that for a broad range of circumstances, processes depending on the square of $\bar{\mathbf{M}}$, i.e. of order μ^2 , probably have small influences on the unsteady motions. We therefore neglect all terms of order μ^2 and higher in the equations. As a practical matter, the equations are greatly simplified with this assumption which we adopt throughout this work.

After substituting all variables split into sums of mean and fluctuating values, and collection of terms by orders, we can rewrite (3.7)–(3.13) as

$$\begin{aligned} & \left[\frac{\bar{D}\bar{\rho}}{Dt} + \bar{\rho}\nabla \cdot \bar{\mathbf{M}} + \bar{\mathbf{M}} \cdot \nabla \bar{\rho} - \bar{\mathcal{W}} \right] + \left[\frac{\partial \rho'}{\partial t} + \bar{\rho}\nabla \cdot \mathbf{M}' \right] \\ & + \left[\bar{\mathbf{M}} \cdot \nabla \rho' + \rho' \nabla \cdot \bar{\mathbf{M}} + \mathbf{M}' \cdot \nabla \bar{\rho} + \nabla \cdot (\rho' \mathbf{M}') \right] - \mathcal{W}' = 0 \end{aligned} \quad (3.15)$$

$$\begin{aligned} & \left[\bar{\rho} \frac{\bar{D}\mathbf{M}'}{Dt} + \nabla \bar{p} - \bar{\mathbf{F}} \right] + \left[\bar{\rho} \frac{\partial \bar{\mathbf{M}}}{\partial t} + \nabla p' \right] + \left[\bar{\rho} (\bar{\mathbf{M}} \cdot \nabla \mathbf{M}' + \mathbf{M}' \cdot \nabla \bar{\mathbf{M}}) + \rho' \frac{\bar{D}\bar{\mathbf{M}}}{Dt} \right] \\ & + \left[\rho' \frac{\partial \mathbf{M}'}{\partial t} + \bar{\rho} \mathbf{M}' \cdot \nabla \mathbf{M}' + \rho' (\bar{\mathbf{M}} \cdot \nabla \mathbf{M}' + \mathbf{M}' \cdot \nabla \bar{\mathbf{M}}) \right] + [\rho' \mathbf{M}' \cdot \nabla \mathbf{M}'] - \mathbf{F}' = 0 \end{aligned} \quad (3.16)$$

$$\begin{aligned} & \left[\bar{\rho} C_v \frac{\bar{D}\bar{T}}{Dt} + \bar{p}\nabla \cdot \bar{\mathbf{M}} - \bar{\mathcal{Q}} \right] + C_v \left[\bar{\rho} \frac{\partial T'}{\partial t} + \bar{p}\nabla \cdot \mathbf{M}' \right] + \left[\bar{\rho} C_v (\bar{\mathbf{M}} \cdot \nabla T' + \mathbf{M}' \cdot \nabla \bar{T}) + C_v \rho' \frac{\bar{D}\bar{T}}{Dt} + p' \nabla \cdot \bar{\mathbf{M}} \right] \\ & + \left[C_v \bar{\rho} \frac{\partial T'}{\partial t} + C_v \rho' (\bar{\mathbf{M}} \cdot \nabla T' + \mathbf{M}' \cdot \nabla \bar{T}) + C_v \rho' \mathbf{M}' \cdot \nabla T' + p' \nabla \cdot \mathbf{M}' \right] + [C_v \bar{\rho} \mathbf{M}' \cdot \nabla T'] - \mathcal{Q}' = 0 \end{aligned} \quad (3.17)$$

$$\left[\frac{\bar{D}\bar{p}}{Dt} + \gamma\bar{p}\nabla \cdot \bar{\mathbf{M}} - \bar{p} + \gamma\bar{p}\nabla \cdot \bar{\mathbf{M}} - \bar{P} \right] + \left[\frac{\partial p'}{\partial t} + \gamma\bar{p}\nabla \cdot \mathbf{M}' \right] + [\bar{\mathbf{M}} \cdot \nabla p' + \mathbf{M}' \cdot \nabla \bar{p} + \gamma p' \nabla \cdot \bar{\mathbf{M}}] \quad (3.18)$$

$$+ [\mathbf{M}' \cdot \nabla p' + \gamma p' \nabla \cdot \mathbf{M}'] - \mathcal{P}' = 0$$

$$\left[\bar{\rho}\bar{T}\frac{\bar{D}\bar{s}}{Dt} - \bar{s} \right] + \left[\bar{\rho}\bar{T}\frac{\partial s'}{\partial t} \right] + \left[\bar{\rho}\bar{\mathbf{M}} \cdot \nabla s' + \rho'\bar{T}\frac{\bar{D}\bar{s}}{Dt} + \bar{\rho}\bar{T}\mathbf{M}' \cdot \nabla \bar{s} + \bar{\rho}T'\bar{\mathbf{M}} \cdot \nabla \bar{s} \right]$$

$$+ \left[\rho'\bar{T}\frac{\partial s'}{\partial t} + \rho'T'\frac{\partial D\bar{s}}{\partial t} + \rho'\bar{T}\mathbf{M}' \cdot \nabla \bar{s} + \bar{\rho}T'\mathbf{M}' \cdot \nabla \bar{s} + \bar{\rho}T'\frac{\partial s'}{\partial t} + \bar{\rho}\bar{T}\mathbf{M}' \cdot \nabla \bar{s}' \right] \quad (3.19)$$

$$+ \left[\rho'T'\frac{\partial s'}{\partial t} + (\bar{\rho}T' + \rho'\bar{T})\mathbf{M}' \cdot \nabla s' + \rho'T'(\mathbf{M}' \cdot \nabla \bar{s} + \bar{\mathbf{M}} \cdot \nabla s') \right] + [\rho'T'\mathbf{M}' \cdot \nabla s'] - \bar{s}' = 0$$

$$[\bar{p} - R\bar{\rho}\bar{T}] + [p' - R(\bar{\rho}T' + \rho'\bar{T})] + [-R\rho'T'] = 0 \quad (3.20)$$

where the convective derivative following the mean flow is

$$\frac{\bar{D}}{Dt} = \frac{\partial}{\partial t} + \bar{\mathbf{M}} \cdot \nabla \quad (3.21)$$

As a convenience in writing, it is useful to introduce some symbols defining groups of ordered terms. The set of equations (3.15)–(3.20) then become:

$$\left[\frac{\bar{D}\bar{\rho}}{Dt} + \bar{\rho}\nabla \cdot \bar{\mathbf{M}} - \bar{\mathcal{W}} \right] + \left(\frac{\partial \rho'}{\partial t} + \bar{\rho}\nabla \cdot \mathbf{M}' \right) + \{[\rho]\}_1 + \{\rho\}_2 - \mathcal{W}' = 0 \quad (3.22)$$

$$\left[\bar{\rho}\frac{\bar{D}\bar{\mathbf{M}}}{Dt} + \nabla\bar{p} - \bar{\mathbf{F}} \right] + \left(\bar{\rho}\frac{\partial \mathbf{M}'}{\partial t} + \nabla p' \right) + \{[\mathbf{M}]\}_1 + \{\mathbf{M}\}_2 + \{\mathbf{M}\}_3 + \{[\mathbf{M}]\}_2 - \mathbf{F}' = 0 \quad (3.23)$$

$$\left[\bar{\rho}C_v\frac{\bar{D}\bar{T}}{Dt} + \bar{p}\nabla \cdot \bar{\mathbf{M}} - \bar{\mathcal{Q}} \right] + C_v \left(\bar{\rho}\frac{\partial T'}{\partial t} + \bar{p}\nabla \cdot M' \right) + \{[T]\}_1 + \{T\}_2 + \{T\}_3 + \{[T]\}_2 - \mathcal{Q}' = 0 \quad (3.24)$$

$$\left[\frac{\bar{D}\bar{p}}{Dt} + \gamma\bar{p}\nabla \cdot \bar{\mathbf{M}} - \bar{P} \right] + \left(\bar{\rho}C_v\frac{\partial P'}{\partial t} + \bar{p}\nabla \cdot M' \right) + \{[p]\}_1 + \{p\}_2 - \mathcal{P}' = 0 \quad (3.25)$$

$$\left[\bar{\rho}\bar{T}\frac{\bar{D}\bar{s}}{Dt} - \bar{s} \right] + \left(\bar{\rho}\bar{T}\frac{\partial s'}{\partial t} \right) + \{[s]\}_1 + \{s\}_2 + \{s\}_3 + \{[s]\}_2 + \{s\}_4 - \bar{s}' = 0 \quad (3.26)$$

$$[\bar{p} - R\bar{\rho}\bar{T}] + \{p - R\rho T\}_1 + \{R\rho T\}_2 = 0 \quad (3.27)$$

The definitions of the bracketed terms $\{\rho\}_1, \dots$ etc. are given in Annex A, Section A.6; the subscript $\{\ \}_n$ on the brackets identifies the orders of terms with respect to the fluctuations of flow variables, and the square brackets $[\]$ indicate that the terms are first order in the average Mach number. We have shown here in each equation terms of the highest order fluctuations generated by the purely fluid mechanical contributions plus sources that must be expanded to orders appropriate to particular applications. Only the entropy equation produces terms of fourth order.

Time derivatives of quantities identified with the mean flow are retained to accommodate variations on a time scale long relative to the scale of the fluctuations. This generality is not normally required for treating combustion instabilities and unless otherwise stated, we will assume that all averaged quantities are independent of time.

3.3.2. Equations for the Mean Flow. At this point we have two choices. Commonly the assumption is made that the variables of the mean flow ‘satisfy their own equations’. That implies that the brackets [] vanish identically. With the time derivatives absent, the equations for the mean flow are:

$$\bar{\mathbf{M}} \cdot \nabla \bar{\rho} + \bar{\rho} \nabla \cdot \bar{\mathbf{M}} = \bar{\mathcal{W}} \quad (3.28)$$

$$\bar{\rho} \bar{\mathbf{M}} \cdot \nabla \bar{\mathbf{M}} + \nabla \bar{p} = \bar{\mathcal{F}} \quad (3.29)$$

$$\bar{\rho} C_v \bar{\mathbf{M}} \cdot \nabla \bar{T} + \bar{p} \nabla \cdot \bar{\mathbf{M}} = \bar{\mathcal{Q}} \quad (3.30)$$

$$\bar{\mathbf{M}} \cdot \nabla \bar{p} + \gamma \bar{p} \nabla \cdot \bar{\mathbf{M}} = \bar{\mathcal{P}} \quad (3.31)$$

$$\bar{\rho} \bar{T} \bar{\mathbf{M}} \cdot \nabla \bar{s} = \bar{\mathcal{S}} \quad (3.32)$$

$$\bar{p} = R \bar{\rho} \bar{T} \quad (3.33)$$

This set of equations certainly applies when the average flow is strictly independent of time and there are no fluctuations. The time derivatives cannot be ignored when the flow variables change so slowly that the motion may be considered as ‘quasi-steady’ and fluctuations are still ignorable.

It is possible that when fluctuations are present, interactions among the flow variables cause transfer of mass, momentum and energy between the fluctuating and mean flows, generating time variations of the averaged variables. Then the appropriate equations are obtained by time-averaging (3.22)–(3.27) to give³

$$\frac{\bar{D}\bar{\rho}}{Dt} + \bar{\rho} \nabla \cdot \bar{\mathbf{M}} = \bar{\mathcal{W}} - \overline{\{\bar{\rho}\}}_1 - \overline{\{\bar{\rho}\}}_2 + \bar{\mathcal{W}'} \quad (3.34)$$

$$\bar{\rho} \frac{\bar{D}\bar{\mathbf{M}}}{Dt} + \nabla \bar{p} = \bar{\mathcal{F}} - \overline{\{\bar{\mathbf{M}}\}}_1 - \overline{\{\bar{\mathbf{M}}\}}_2 - \overline{\{\bar{\mathbf{M}}\}}_3 - \overline{\{\bar{\mathbf{M}}\}}_2 + \bar{\mathcal{F}' } \quad (3.35)$$

$$\bar{\rho} C_v \frac{\bar{D}\bar{T}}{Dt} + \bar{p} \nabla \cdot \bar{\mathbf{M}} = \bar{\mathcal{Q}} - \overline{\{\bar{T}\}}_1 - \overline{\{\bar{T}\}}_2 - \overline{\{\bar{T}\}}_3 + \bar{\mathcal{Q}'} \quad (3.36)$$

$$\frac{\bar{D}\bar{p}}{Dt} + \gamma \bar{p} \nabla \cdot \bar{\mathbf{M}} = \bar{\mathcal{P}} - \overline{\{\bar{p}\}}_1 - \overline{\{\bar{p}\}}_2 + \bar{\mathcal{P}'} \quad (3.37)$$

$$\bar{\rho} \bar{T} \frac{\bar{D}\bar{s}}{Dt} = \bar{\mathcal{S}} - \overline{\{\bar{s}\}}_1 - \overline{\{\bar{s}\}}_2 - \overline{\{\bar{s}\}}_3 - \overline{\{\bar{s}\}}_2 - \overline{\{\bar{s}\}}_4 + \bar{\mathcal{S}'} \quad (3.38)$$

$$\bar{p} = \mathbf{R} \bar{\rho} \bar{T} - \overline{\{\bar{\rho}\bar{T}\}}_1 - \overline{\{\bar{\rho}\bar{T}\}}_2 \quad (3.39)$$

³Note that the fluctuations of the source terms denoted by $\mathcal{W}' \dots$ etc., actually contain squares and higher order products of the dependent variables; hence their time averages will generally be non-zero.

If the mean flow is strictly independent of time, then time averages of all first-order brackets, $\overline{\{ \cdot \}}_1$, must vanish. For generality we allow them to be nonzero. There seem to be no analyses in which their variations have been taken into account.

The two sets of equations governing the mean flow in the presence of unsteady motion define two distinct formulations of the general problem. In the first, equations (3.28)–(3.33), computation of the mean flow is uncoupled from that of the unsteady flow. Hence formally we are concerned with the stability and time evolution of disturbances superposed on a given, presumed known, mean flow unaffected by the unsteady motions. That is the setting for all investigations of combustion instabilities founded on the splitting of small flow variables into sums of mean and fluctuating values. This approach excludes, for example, possible influences of oscillations on the mean pressure in the chamber (often called ‘DC shift’), not an unusual occurrence in solid propellant rockets. When they occur, DC shifts of this sort are almost always unacceptable in operational motors. They may be directly affected by the fluctuations, or they may be largely due to changes in the mean burning rate.

In contrast, the set (3.34)–(3.39) is strongly coupled to the fluctuating field. The situation is formally that producing the problem of ‘closure’ in the theory of turbulent flows (see, for example, Tennekes and Lumley, 1972). We will not explore the matter here, but note only that the process of time averaging terms on the right hand sides of the equations introduces functions of the fluctuations that are additional unknowns. Formal analysis then requires that those functions be modeled; perhaps the most familiar example in the theory of turbulence is the introduction of a ‘mixing length’ as part of the representation of stresses associated with turbulent motions. The set (3.34)–(3.39) also can be used to compute ‘DC shifts’ for specified fluctuations of the flow variables. No results have been reported.

Numerical simulations of combustion instabilities do not exhibit the problem of closure if the complete equations are used, avoiding the consequences of the assumption (3.14). Thus, for example, the results obtained by Levine and Baum (1982, 1988) do show time-dependence of the average pressure in examples of instabilities in solid rockets. Another possible cause of that behavior, probably more important in many cases, is nonlinear dependence of the burning rate on the pressure or velocity near the surface of a solid propellant rocket. Within the structure given here, that behavior arises from time-averaged functions of p' , M' , ... contained in the boundary conditions.

We use in this book the formulation assuming complete knowledge of the mean flow, given either by suitable modeling or by solution to the governing equations (3.28)–(3.33). This may in some cases be an important omission. Probably the most important consequence is that the effect of oscillations on burning rate and mean pressure in solid propellant rockets is not covered. See Section 2.1, for example Figure 2.6. This is often, especially in tactical rockets, a significant matter which has been treated by the author only with preliminary calculations in the present scheme. Flandro (private communication) is currently working on this problem.

3.3.3. Systems of Equations for the Fluctuations. The general equations of motion (3.22)–(3.27) and those for the mean flow written in Section 3.3.1 contain a restriction only on the magnitude of the average Mach number. Such generality blocks progress with the analysis and for many applications is unnecessary. The set of equations (3.22)–(3.27) must be simplified to forms that can be solved to give useful results. Many possibilities exist. We follow here a course that previous experience has shown to be particularly fruitful for investigations of combustor dynamics. The choices of approximations and tactics are usually motivated by eventual applications and the type of analysis used.

First we assume that the mean flow is determined by its own system of equations; that is, we avoid the problem of closure and use the first formulation, equations (3.28)–(3.33), discussed in Section 3.3.1. Consequently, the mean flow is taken to be independent of time and the combinations in square brackets [], equations (3.22)–(3.27), vanish identically; we write the equations in the form

$$\frac{\partial \rho'}{\partial t} + \bar{\rho} \nabla \cdot \mathbf{M}' = -\{[\rho]\}_1 - \{\rho\}_2 + \mathcal{W}' \quad (3.40)$$

$$\bar{\rho} \frac{\partial \mathbf{M}'}{\partial t} + \nabla p' = -\{[\mathbf{M}]\}_1 - \{\mathbf{M}\}_2 - \{\mathbf{M}\}_3 - \{[\mathbf{M}]\}_2 + \mathcal{F}' \quad (3.41)$$

$$\bar{\rho} C_v \frac{\partial T'}{\partial t} + \bar{p} \nabla \cdot \mathbf{M}' = -\{[T]\}_1 - \{T\}_2 - \{T\}_3 - \{[T]\}_2 + \mathcal{Q}' \quad (3.42)$$

$$\frac{\partial p'}{\partial t} + \gamma \bar{p} \nabla \cdot \mathbf{M}' = -\{[p]\}_1 - \{p\}_2 + \mathcal{P}' \quad (3.43)$$

$$\bar{\rho} \bar{T} \frac{\partial s'}{\partial t} = -\{[s]\}_1 - \{s\}_2 - \{[s]\}_2 - \{s\}_3 - \{s\}_4 + \mathcal{S}' \quad (3.44)$$

The various brackets are defined in Section A.6 of Annex A. They are formed to contain terms ordered with respect to both the mean Mach number and the amplitude of the fluctuations:

$$\begin{aligned} \{[\]\}_1 &: 1^{st} \text{ order in } \bar{\mathbf{M}}; 1^{st} \text{ order in } \mathbf{M}', O(\mu\varepsilon) \\ \{ \ }_2 &: 0^{th} \text{ order in } \bar{\mathbf{M}}; 2^{nd} \text{ order in } \mathbf{M}', O(\varepsilon^2) \\ \{[\]\}_2 &: 1^{st} \text{ order in } \bar{\mathbf{M}}; 2^{nd} \text{ order in } \mathbf{M}', O(\mu\varepsilon^2) \\ \{ \ }_3 &: 0^{th} \text{ order in } \bar{\mathbf{M}}; 3^{rd} \text{ order in } \mathbf{M}', O(\varepsilon^3) \\ \{ \ }_4 &: 0^{th} \text{ order in } \bar{\mathbf{M}}; 4^{th} \text{ order in } \mathbf{M}', O(\varepsilon^4) \end{aligned} \quad (3.45)$$

No terms have been dropped in passage from the set (3.15)–(3.19) to the set (3.40)–(3.44), but fluctuations of the sources $\mathcal{W}', \dots, \mathcal{S}'$ are not now classified into the various types defined by the brackets (3.45).

We have put the equations in the forms (3.40)–(3.44) to emphasize the point of view that we are considering classes of problems closely related to motions in classical acoustics. If the right hand sides are ignored, (3.40)–(3.44) become the equations for linear acoustics of a uniform non-reacting medium at rest. The perturbations of that limiting class arise from four types of processes:

- (i) interactions of the linear acoustic field with the mean flow, represented by the terms contained in the square brackets within curly brackets, $\{[\]\}_1$;
- (ii) nonlinear interactions between the fluctuations, represented by the curly brackets conveniently referred to as: $\{ \ }_2$, second order acoustics; $\{ \ }_3$, third order acoustics; and $\{ \ }_4$, fourth order acoustics;
- (iii) interactions between the mean flow and nonlinear acoustics to second order, represented by $\{[\]\}_2$;
- (iv) sources associated with combustion processes, represented by the source terms $\mathcal{W}', \mathcal{F}', \mathcal{Q}', \mathcal{P}'$ and \mathcal{S}' .

By selectively retaining one or more of these types of perturbations we define a hierarchy of problems of unsteady motions in combustors. We label these classes of problems O, I, II, III, IV according to the orders

of terms retained in the right hand sides: the left hand sides contain only the terms of order $\varepsilon = \mathbf{M}'_r$, the equations for classical linear acoustics.

O. Classical Acoustics, $(\mu = 0, \varepsilon \rightarrow 0)$

Perturbations to first order in ε are retained on the right-hand sides of (3.40)–(3.44):

$$\begin{aligned}
 \frac{\partial \rho'}{\partial t} + \bar{\rho} \nabla \cdot \mathbf{M}' &= \mathcal{W}' \\
 \bar{\rho} \frac{\partial \mathbf{M}'}{\partial t} + \nabla p' &= \mathbf{F}' \\
 \bar{\rho} C_v \frac{\partial T'}{\partial t} + \bar{p} \nabla \cdot \mathbf{M}' &= \mathcal{Q}' \\
 \frac{\partial p'}{\partial t} + \gamma \bar{p} \nabla \cdot \mathbf{M}' &= \mathcal{P}' \\
 \bar{\rho} \bar{T} \frac{\partial s'}{\partial t} &= \mathcal{S}' \tag{3.46} \text{ a-e}
 \end{aligned}$$

I. Linear Stability, $O(\varepsilon, \mu \varepsilon)$

Retain interactions linear in the average Mach number and in the fluctuations on the right-hand sides:

$$\begin{aligned}
 \frac{\partial \rho'}{\partial t} + \bar{\rho} \nabla \cdot \mathbf{M}' &= -\{[\rho]\}_1 + \mathcal{W}' \\
 \bar{\rho} \frac{\partial \mathbf{M}'}{\partial t} + \nabla p' &= -\{[\mathbf{M}]\}_1 + \mathbf{F}' \\
 \bar{\rho} C_v \frac{\partial T'}{\partial t} + \bar{p} \nabla \cdot \mathbf{M}' &= -\{[T]\}_1 + \mathcal{Q}' \\
 \frac{\partial p'}{\partial t} + \gamma \bar{p} \nabla \cdot \mathbf{M}' &= -\{[p]\}_1 + \mathcal{P}' \\
 \bar{\rho} \bar{T} \frac{\partial s'}{\partial t} &= -\{[s]\}_1 + \mathcal{S}' \tag{3.47} \text{ a-e}
 \end{aligned}$$

II. Second Order Acoustics, $O(\varepsilon, \mu \varepsilon, \varepsilon^2)$

Retain the linear interactions and the nonlinear second order acoustics on the right-hand sides:

$$\begin{aligned}
 \frac{\partial \rho'}{\partial t} + \bar{\rho} \nabla \cdot \mathbf{M}' &= -(\{[\rho]\}_1 + \{\rho\}_2) + \mathcal{W}' \\
 \bar{\rho} \frac{\partial \mathbf{M}'}{\partial t} + \nabla p' &= -(\{[\mathbf{M}]\}_1 + \{\mathbf{M}\}_2) + \mathbf{F}' \\
 \bar{\rho} C_v \frac{\partial T'}{\partial t} + \bar{p} \nabla \cdot \mathbf{M}' &= -(\{[T]\}_1 + \{T\}_2) + \mathcal{Q}' \\
 \frac{\partial p'}{\partial t} + \gamma \bar{p} \nabla \cdot \mathbf{M}' &= -(\{[p]\}_1 + \{p\}_2) + \mathcal{P}' \\
 \bar{\rho} \bar{T} \frac{\partial s'}{\partial t} &= -(\{[s]\}_1 + \{s\}_2) + \mathcal{S}' \tag{3.48} \text{ a-e}
 \end{aligned}$$

III. Third Order Acoustics, $O(\varepsilon, \mu\varepsilon, \varepsilon^2, \varepsilon^3)$

Retain the linear interactions and the nonlinear acoustics up to third order on the right-hand sides:

$$\begin{aligned}
 \frac{\partial \rho'}{\partial t} + \bar{\rho} \nabla \cdot \mathbf{M}' &= -(\{\{\rho\}\}_1 + \{\rho\}_2) + \mathcal{W}' \\
 \bar{\rho} \frac{\partial \mathbf{M}'}{\partial t} + \nabla p' &= -(\{[\mathbf{M}]\}_1 + \{\mathbf{M}\}_2 + \{\mathbf{M}\}_3) + \mathcal{F}' \\
 \bar{\rho} C_v \frac{\partial T'}{\partial t} + \bar{p} \nabla \cdot \mathbf{M}' &= -(\{[T]\}_1 + \{T\}_2 + \{T\}_3) + \mathcal{Q}' \\
 \frac{\partial p'}{\partial t} + \gamma \bar{p} \nabla \cdot \mathbf{M}' &= -(\{[p]\}_1 + \{p\}_2) + \mathcal{P}' \\
 \bar{\rho} \bar{T} \frac{\partial s'}{\partial t} &= -(\{[s]\}_1 + \{s\}_2 + \{s\}_3) + \mathcal{S}' \tag{3.49} \text{ a-e}
 \end{aligned}$$

 IV. Mean Flow/Nonlinear Acoustic Interactions, $O(\varepsilon, \mu\varepsilon, \varepsilon^2, \varepsilon^3, \mu\varepsilon^2)$

Retain all terms on the right-hand sides of (3.40)–(3.44) except $\{s\}_4$ in (3.44). No results have been obtained for this class of problems.

Several other classes of problems possible to define in this context will not be considered here since no results have been reported. There is some indication that problems in class IV may have some important consequences but no theoretical results exist.

In each class of problems, the source terms \mathcal{W}', \dots must be expanded to orders consistent with the orders of the fluid-mechanical perturbations retained.

3.4. Nonlinear Wave Equations for the Pressure Field

Practically all of the subsequent material in this book will be either directly concerned with pressure waves, or with interpretations of behavior related to pressure waves. The presence of unsteady vorticity causes important revisions of such a restricted point of view, as we have already mentioned, but the basic ideas remain in any event. Hence the wave equation for pressure fluctuations occupies a meaningful position in all five classes of problems defined in the preceding section. Its formation follows the same procedure used in classical acoustics.

Define \mathcal{M} and \mathcal{R} to contain all possible terms arising in the sets of equations constructed for the problems O–IV:

$$\bar{\rho} \frac{\partial \mathbf{M}'}{\partial t} + \nabla p' = -\mathcal{M} + \mathcal{F}' \tag{3.50}$$

$$\frac{\partial p'}{\partial t} + \gamma \bar{p} \nabla \cdot \mathbf{M}' = -\mathcal{R} + \mathcal{P}' \tag{3.51}$$

where

$$\begin{aligned}
 \mathcal{M} &= \{[\mathbf{M}]\}_1 + \{\mathbf{M}\}_2 + \{\mathbf{M}\}_3 + \{[\mathbf{M}]\}_2 \\
 \mathcal{R} &= \{[p]\}_1 + \{p\}_2 \tag{3.52} \text{a,b}
 \end{aligned}$$

Differentiate (3.51) with respect to time and substitute (3.50) for $\partial \mathbf{M}' / \partial t$:

$$\frac{\partial^2 p'}{\partial t^2} + \gamma \bar{p} \nabla \cdot \left[-\frac{1}{\bar{\rho}} \nabla p' - \frac{1}{\bar{\rho}} (\mathbf{M} - \mathbf{F}') \right] = -\frac{\partial \mathcal{R}}{\partial t} + \frac{\partial \mathcal{P}'}{\partial t}$$

Rearrange the equation to find

$$\nabla^2 p' - \frac{1}{\bar{a}^2} \frac{\partial^2 p'}{\partial t^2} = h \quad (3.53)$$

with

$$h = -\bar{\rho} \nabla \cdot \left[\frac{1}{\bar{\rho}} (\mathbf{M} - \mathbf{F}') \right] + \frac{1}{\bar{a}^2} \frac{\partial}{\partial t} (\mathcal{R} - \mathcal{P}') + \frac{1}{\bar{\rho}} \nabla \bar{\rho} \cdot \nabla p' \quad (3.54)$$

The boundary condition for the pressure field is found by taking the scalar product of the outward normal, at the chamber boundary, with (3.50):

$$\hat{\mathbf{n}} \cdot \nabla p' = -f \quad (3.55)$$

$$f = \bar{\rho} \frac{\partial \mathbf{M}'}{\partial t} \cdot \hat{\mathbf{n}} + (\mathbf{M} - \mathbf{F}') \cdot \hat{\mathbf{n}} \quad (3.56)$$

Replacing \mathbf{M} and \mathcal{R} by their definitions (3.52)a,b, we have the formulation based on the inhomogeneous nonlinear wave equation and its boundary condition:

$$\begin{aligned} \nabla^2 p' - \frac{1}{\bar{a}^2} \frac{\partial^2 p'}{\partial t^2} &= h \\ \hat{\mathbf{n}} \cdot \nabla p' &= -f \end{aligned} \quad (3.57)\text{a,b}$$

with

$$\begin{aligned} h &= \left[-\bar{\rho} \nabla \cdot \frac{1}{\bar{\rho}} \{[\mathbf{M}]\}_1 + \frac{1}{\bar{a}^2} \frac{\partial \{[p]\}_1}{\partial t} + \frac{1}{\bar{\rho}} \nabla \bar{\rho} \cdot \nabla p' \right] + \left[-\bar{\rho} \nabla \cdot \frac{1}{\bar{\rho}} \{\mathbf{M}\}_2 + \frac{1}{\bar{a}^2} \frac{\partial \{p\}_2}{\partial t} \right] \\ &\quad - \left[\bar{\rho} \nabla \cdot \frac{1}{\bar{\rho}} \{\mathbf{M}\}_3 \right] - \left[\bar{\rho} \nabla \cdot \frac{1}{\bar{\rho}} \{[\mathbf{M}]\}_2 \right] + \left[+\bar{\rho} \nabla \cdot \frac{1}{\bar{\rho}} \mathbf{F}' - \frac{1}{\bar{a}^2} \frac{\partial \mathcal{P}'}{\partial t} \right] \end{aligned} \quad (3.58)$$

$$f = \bar{\rho} \frac{\partial \mathbf{M}'}{\partial t} \cdot \hat{\mathbf{n}} + \hat{\mathbf{n}} \cdot \left[\{[\mathbf{M}]\}_1 + \{\mathbf{M}\}_2 + \{\mathbf{M}\}_3 + \{[\mathbf{M}]\}_2 \right] - \mathbf{F}' \cdot \hat{\mathbf{n}} \quad (3.59)$$

With this formulation, the wave equations and boundary conditions for the classes of problems defined in Section 3.3 are distinguished by the following functions h and f :

O. Classical Acoustics

$$h_O = \bar{\rho} \nabla \cdot \frac{1}{\bar{\rho}} \mathbf{F}' - \frac{1}{\bar{a}^2} \frac{\partial \mathcal{P}'}{\partial t} \quad (3.60)\text{a,b}$$

$$f_O = \bar{\rho} \frac{\partial \mathbf{M}'}{\partial t} \cdot \hat{\mathbf{n}} - \mathbf{F}' \cdot \hat{\mathbf{n}}$$

I. Linear Stability

$$h_I = \left[-\bar{\rho} \nabla \cdot \frac{1}{\bar{\rho}} \{[M]\}_1 + \frac{1}{\bar{a}^2} \frac{\partial \{[p]\}_1}{\partial t} + \frac{1}{\bar{\rho}} \nabla \bar{\rho} \cdot \nabla p' \right] + \left[\bar{\rho} \nabla \cdot \frac{1}{\bar{\rho}} \mathcal{F}' - \frac{1}{\bar{a}^2} \frac{\partial \mathcal{P}'}{\partial t} \right] \quad (3.61)a,b$$

$$f_I = \bar{\rho} \frac{\partial \mathbf{M}'}{\partial t} \cdot \hat{\mathbf{n}} + \hat{\mathbf{n}} \cdot \{[M]\}_1 - \mathcal{F}' \cdot \hat{\mathbf{n}}$$

Allowing \mathcal{F}' and \mathcal{P}' to be non-zero gives the opportunity for representing sources of mass, momentum, and energy both within the volume and at the boundary. The first term in f_I accounts for motion of the boundary.

II. Second Order Acoustics

$$h_{II} = \left[-\bar{\rho} \nabla \cdot \frac{1}{\bar{\rho}} \{[M]\}_1 + \frac{1}{\bar{a}^2} \frac{\partial \{[p]\}_1}{\partial t} + \frac{1}{\bar{\rho}} \nabla \bar{\rho} \cdot \nabla p' \right] + \left[-\bar{\rho} \nabla \cdot \frac{1}{\bar{\rho}} \{M\}_2 + \frac{1}{\bar{a}^2} \frac{\partial \{p\}_2}{\partial t} \right] + \left[\bar{\rho} \nabla \cdot \frac{1}{\bar{\rho}} \mathcal{F}' - \frac{1}{\bar{a}^2} \frac{\partial \mathcal{P}'}{\partial t} \right] \quad (3.62)a,b$$

$$f_{II} = \bar{\rho} \frac{\partial \mathbf{M}'}{\partial t} \cdot \hat{\mathbf{n}} + \hat{\mathbf{n}} \cdot \{[M]\}_1 + \{M\}_2 - \mathcal{F}' \cdot \hat{\mathbf{n}}$$

III. Third Order Acoustics

$$h_{III} = \left[-\bar{\rho} \nabla \cdot \frac{1}{\bar{\rho}} \{[M]\}_1 + \frac{1}{\bar{a}^2} \frac{\partial \{[p]\}_1}{\partial t} + \frac{1}{\bar{\rho}} \nabla \bar{\rho} \cdot \nabla p' \right] + \left[-\bar{\rho} \nabla \cdot \frac{1}{\bar{\rho}} \{M\}_2 + \frac{1}{\bar{a}^2} \frac{\partial \{p\}_2}{\partial t} \right] + \left[-\bar{\rho} \nabla \cdot \frac{1}{\bar{\rho}} \{M\}_3 \right] + \left[\bar{\rho} \nabla \cdot \frac{1}{\bar{\rho}} \mathcal{F}' - \frac{1}{\bar{a}^2} \frac{\partial \mathcal{P}'}{\partial t} \right] \quad (3.63)a,b$$

$$f_{III} = \bar{\rho} \frac{\partial \mathbf{M}'}{\partial t} \cdot \hat{\mathbf{n}} + \hat{\mathbf{n}} \cdot \{[M]\}_1 + \{M\}_2 + \{M\}_3 - \mathcal{F}' \cdot \hat{\mathbf{n}}$$

IV. Mean Flow/Nonlinear Acoustics Interactions

$$h_{IV} = h_{III} - \bar{\rho} \nabla \cdot \frac{1}{\bar{\rho}} \{[M]\}_2 \quad (3.64)a,b$$

$$f_{IV} = f_{III} + \hat{\mathbf{n}} \cdot \frac{1}{\bar{\rho}} \{[M]\}_2$$

With these forms for the functions h and f , the definitions of the classes of problems considered here are complete, giving the basis for the analysis worked out in the remainder of this book. Only problems within classical acoustics can be solved easily. All others require approximations, both in modeling physical processes and in the method of solution. Modeling will be discussed in the contexts of specific applications; a few remarks help clarify the approximate method of solution described in the following chapter.

Remarks:

- (i) The equations derived here are written with the dimensionless variables defined in Section 3.1. This is an important point to recall when results are written in terms of dimensionless variables. Annex D contains the corresponding results in dimensional variables.
- (ii) The classes of problems O–IV defined here are described by inhomogeneous equations that even for linear stability cannot be generally solved in closed form. The chief obstacles to solution arise because the functions h and f contain not only the unknown pressure but also the velocity and temperature. For given functions \mathcal{F}' and \mathcal{P}' , numerical solutions could be obtained for a specified combustor and mean flow field. The results would apply only to the special case considered. To obtain some understanding of general behavior it would be necessary to consider many special cases, a tedious and expensive procedure.
- (iii) Therefore, we choose to work out an approximate method of solution applicable to all classes of problems. Numerical solutions, or ‘simulations’ then serve the important purpose of assessing the validity and accuracy of the approximate results.
- (iv) The approximate method of solution described in the following chapter is based first on spatial averaging, followed by an iteration procedure involving extension of the expansion in two small parameters defined in this chapter. This method has been most widely used and confirmed in applications to combustion instabilities in solid propellant rockets, but it can be applied to problems arising in any type of combustor.
- (v) Instabilities in solid rockets have been particularly helpful in developing the general theory for at least three reasons: 1) the mean flow field, nonuniform and generated by mass addition at the boundary, requires careful attention to processes associated with interactions between the mean flow and unsteady motions; 2) more experimental results for transient behavior have been obtained for solid rockets than for any other combustion system; and 3) although still far from being satisfactorily understood, the dynamics of burning solid propellants is better known than for any other combustion system.
- (vi) The fluctuations of the source terms, \mathcal{W}' , \mathcal{F}' , … \mathcal{S}' will be made explicit as required in particular applications.
- (vii) No assumptions have been made restricting either the average or the time-dependent velocity fields to be irrotational. Moreover, all viscous effects can be accommodated with suitable definitions of the source terms.
- (viii) For reasons explained earlier, the wave equations are written for the pressure which, in lowest approximation, is associated only with acoustic waves. However, on the right-hand sides (i.e., in the functions h and f) the total unsteady velocity appears. Hence by suitable decomposition (see Section 7.9) coupling between, say, vorticity and acoustic waves can be investigated. In particular, this formulation allows calculation of the effects of vorticity on stability (Flandro 1995). However, we must emphasize that the methods and results worked out in the following chapters are intended to be relatively easy to apply. The price of this property is their approximate character.
- (ix) The most significant omission at this stage is accounting for turbulence. In principle, modeling of turbulence could be included in the derivation of the general equations. However, that strategy would bring unnecessary complications and erect serious obstacles to obtaining useful results with minimal effort. For applications to practical situations, the effects of turbulence seem to be definitely secondary. Theoretical justification for ignoring the possible effects of random or statistical fluctuations in the flow is based on the work of Chu and Kovasznay (1957).

CHAPTER 4

Modal Expansion and Spatial Averaging; An Iterative Method of Solution

From the point of view expressed by Figure 1.1, we are concerned in this chapter with representing the combustor dynamics. The procedure, often called ‘modeling’, is based on the equations of motion constructed in the preceding section and hence in principle will contain all relevant physical processes.¹ For the purposes here, all modeling of combustor dynamics and of combustion dynamics—the mechanisms and feedback in Figure 1.1—must be done in the context developed in Chapter 1. Thus we always have in mind the idea of wave motions somehow generated and sustained by interactions between the motions themselves and combustion processes, the latter also including certain aspects of the mean flow within the combustor.

The simplest model of the combustor dynamics is a single stationary wave, a classical acoustic resonance as in an organ pipe, but decaying or growing due to the other processes in the chamber. In practice, the combustion processes and nonlinear gasdynamical effects inevitably lead to the presence of more than one acoustic mode. We need a relatively simple yet accurate means of treating those phenomena for problems of the sort arising in the laboratory and in practice. Modeling in this case begins with construction of a suitable method for solving the nonlinear wave equations derived in Section 3.4. In this context we may regard the analysis of the Rijke tube covered in Section 2.7 as a basic example of the procedure stripped of the formalism covered in this chapter.

The chief purpose of the analysis constructed here is to devise methods capable of producing results useful for prediction and interpretation of unsteady motions in full-scale combustion chambers, as well as for laboratory devices. That intention places serious demands on the methods used for at least two reasons:

- (i) processes that must be modeled are usually complicated and their theoretical representations are necessarily approximate to extents which themselves are difficult to assess; and
- (ii) almost all input data required for quantitative evaluation of theoretical results are characterized by large uncertainties.

In this situation it seems that for applications and, as it will turn out, for theoretical purposes as well, the most useful methods will be based on some sort of spatial averaging. Formal solution of the partial differential equations, even for linear problems, is practically a hopeless task except for very special cases involving simple geometries. Direct numerical simulations (DNS), or numerical solutions to the partial differential equations, are not real alternatives for practical purposes at this time, and alone are not attractive for obtaining basic understanding. However, as we will see later, numerical methods offer the only means for assessing the validity of approximate solutions, and can always be applied to more complicated (realistic?) problems than we can reasonably handle with the analytical methods discussed here. In any event, one should view theory and analysis on the one hand, and numerical simulations on the other, as complementary activities. Recent experiences have shown that careful coordination of the analytical procedures and numerical simulations with experimental observations is the most effective strategy for treating combustion instabilities in actual

¹That seems to be what some people (apparently electrical engineers) mean by the term ‘physics-based modeling.’ What would otherwise be the basis for acceptable modeling of a physical system has not been explained.

combustion systems. With the foundation of basic theory, numerical simulations offer very powerful means for improving understanding.

The greater part of the material on analysis and theory of combustion instabilities in this book is based on a method of spatial averaging. It is important to notice that the elementary example worked out in Section 2.7 already shows the superior results possible with the method of averaging in contrast to an approximate solution not involving averaging. The essential idea is of course not new, the method being nearly identical with similar methods used in other branches of continuum mechanics. There are a few special characteristics associated with applications to combustor that will appear in the course of the following discussion.

4.1. Application of a Green's Function for Steady Waves

The method used later to analyze nonlinear behavior has its origins in an early analysis of linear combustion instabilities in liquid rocket engines (Culick, 1961, 1963). That work was based on solution to problems of steady waves by introducing a Green's function. It is an effective strategy for this application because departures from a known soluble problem are small, due either to perturbations within the volume or at the boundary, all of order μ in the context developed in Chapter 3. Mitchell (1993) has made the most extensive use of Green's functions in this context.

The problem to be solved is defined by the equation derived in Section 3.4,

$$\nabla^2 p' - \frac{1}{\bar{a}^2} \frac{\partial^2 p'}{\partial t^2} = h \quad (4.1)a,b$$

$$\hat{\mathbf{n}} \cdot \nabla p' = -f$$

with \bar{a} constant, and h and f given by (3.61)a,b for linear stability. Because here h and f are assumed linear,² various methods are available to build general solutions by applying the principle of superposition to elementary solutions representing steady waves. Hence we assume that the fluctuating pressure field is a steady wave system within the given chamber, having unknown spatial structure varying harmonically in time:

$$p' = \hat{p} e^{-i\bar{a}kt} \quad (4.2)$$

where k is the complex wavenumber, also initially unknown,

$$k = \frac{1}{\bar{a}}(\omega + i\alpha) \quad (4.3)$$

As defined here, α positive means that the wave has growing amplitude, $p' \sim e^{\alpha t}$. Of course the wave is not strictly stationary, a condition existing only if $\alpha = 0$, certainly true when $h = f = 0$, as in classical acoustics.

Even when h, f are non-zero, it is still possible that $\alpha = 0$, now defining a state of *neutral stability*. In general one must expect $\alpha \neq 0$; it is a basic assumption in all of the analysis covered in this book that α is small compared with ω , so the waves are slowly growing or decaying—they are ‘almost’ stationary, and their spatial structure does not change drastically with time. However, the results obtained are quite robust and seem often to be usable even when α/ω is not small.

In the first instance, the problem here is to determine the spatial distribution \hat{p} and the complex wavenumber k . For steady waves we can write

$$h = \kappa \hat{h} e^{-i\bar{a}kt}; f = \kappa \hat{f} e^{-i\bar{a}kt}$$

²Sections 4.1 and 4.2 cover linear behavior only; Sections 4.3–4.6 include nonlinear behavior.

where again κ is a small parameter³ characterizing the smallness of h and f . Substitution in (4.1)a,b and dropping the common exponential time factor gives

$$\begin{aligned}\nabla^2 \hat{p} + k^2 \hat{p} &= \kappa \hat{h} \\ \hat{\mathbf{n}} \cdot \nabla \hat{p} &= -\kappa \hat{f}\end{aligned}\quad (4.4)a,b$$

This is of course a well-known classical problem thoroughly discussed in many books. Many methods of solution are available for the linear problem. We use here a procedure based on introducing a Green's function discussed, for example, by Morse and Feshbach (1952, Chapter 9). This is an attractive method for several reasons, including:

- (i) Conversion of a differential equation into an integral equation, and the iterative method of solution this suggests, is an effective means for minimizing the consequences of the uncertainties inherent in problems of combustor dynamics;
- (ii) Explicit results can be obtained for real and imaginary parts of the complex wavenumber in forms that are easily interpreted and remarkably convenient both for theoretical work and for applications;
- (iii) The method has motivated a straightforward extension to nonlinear problems, with considerable success. (Chapter 7)

Define a Green's function satisfying the homogeneous boundary condition and the wave equation homogeneous except at the single point where a source is located, having zero spatial extent and infinite strength such that its integral over space is finite. Thus the source is represented by a delta function $\delta(\mathbf{r} - \mathbf{r}_0)$ and $G(\mathbf{r}|\mathbf{r}_0)$ is determined as a solution to the problem

$$\begin{aligned}\nabla^2 G(\mathbf{r}|\mathbf{r}_0) + k^2 G(\mathbf{r}|\mathbf{r}_0) &= \delta(\mathbf{r} - \mathbf{r}_0) \\ \hat{\mathbf{n}} \cdot \nabla G(\mathbf{r}|\mathbf{r}_0) &= 0\end{aligned}\quad (4.5)a,b$$

The notation $\mathbf{r}|\mathbf{r}_0$ as the argument of $G(\mathbf{r}|\mathbf{r}_0)$ represents the interpretation of the Green's function as the wave observed at point \mathbf{r} due to a steady oscillatory point source at \mathbf{r}_0 .

Multiply (4.4)a by $G(\mathbf{r}|\mathbf{r}_0)$, (4.5)a by $\hat{p}(\mathbf{r})$, subtract the results and integrate over volume (in the present case the volume of the chamber) to find

$$\begin{aligned}\iint_V [G(\mathbf{r}|\mathbf{r}_0) \nabla^2 \hat{p}(\mathbf{r}) - \hat{p}(\mathbf{r}) \nabla^2 G(\mathbf{r}|\mathbf{r}_0)] dV + k^2 \iint_V [G(\mathbf{r}|\mathbf{r}_0) \hat{p}(\mathbf{r}) - \hat{p}(\mathbf{r}) G(\mathbf{r}|\mathbf{r}_0)] dV \\ = \kappa \iint_V G(\mathbf{r}|\mathbf{r}_0) \hat{h}(\mathbf{r}) dV - \iint_V \hat{p}(\mathbf{r}) \delta(\mathbf{r} - \mathbf{r}_0) dV\end{aligned}\quad (4.6)$$

Because $G(\mathbf{r}|\mathbf{r}_0)$ and $\hat{p}(\mathbf{r})$ are scalar functions the second integral on the left-hand side vanishes. The first integral is rewritten using a form of Green's theorem, and the basic property of the delta function is applied to the second integral on the right-hand side:

$$\iint_V F(\mathbf{r}) \delta(\mathbf{r} - \mathbf{r}_0) dV = F(\mathbf{r}_0) \quad (\mathbf{r}, \mathbf{r}_0 \text{ in } V) \quad (4.7)$$

Hence (4.6) becomes

$$\iint_S [G(\mathbf{r}|\mathbf{r}_0) \nabla \hat{p}(\mathbf{r}) - \hat{p}(\mathbf{r}) \nabla G(\mathbf{r}|\mathbf{r}_0)] \cdot \hat{\mathbf{n}} dS = \kappa \iint_V G(\mathbf{r}|\mathbf{r}_0) \hat{h}(\mathbf{r}) dV - \hat{p}(\mathbf{r}_0)$$

where $\hat{\mathbf{n}}$ is the outward normal at the surface of the volume V in question.

³Later, κ will be identified with μ introduced in Section 3.3 but it is useful in this discussion to maintain a distinction.

Now apply the boundary conditions (4.4)b and (4.5)b and the last equation can be written in the form

$$\mathbf{p}(\hat{r}_0) = \kappa \left\{ \iiint_V G(\mathbf{r}|\mathbf{r}_0) \hat{h}(\mathbf{r}) dV + \oint_S G(\mathbf{r}_s|\mathbf{r}_0) \hat{f}(\mathbf{r}_s) dS \right\} \quad (4.8)$$

Subscript ()_s means the point \mathbf{r}_s lies on the boundary surface (actually on the inside surface of the boundary). Because the operator for scalar waves is *self-adjoint* (see Morse and Feshbach 1953, Chapter 10), the Green's function possesses the property of symmetry

$$G(\mathbf{r}|\mathbf{r}_0) = G(\mathbf{r}_0|\mathbf{r}) \quad (4.9)$$

This property has the appealing physical interpretation that the wave observed at \mathbf{r} due to a point source at \mathbf{r}_0 has the same amplitude and relative phase as for the wave observed at \mathbf{r}_0 when the point source is located at \mathbf{r} . With (4.9) we can interchange \mathbf{r} and \mathbf{r}_0 in (4.8) to find for the steady field at position \mathbf{r} :

$$\hat{p}(\mathbf{r}) = \kappa \left\{ \iiint_V G(\mathbf{r}|\mathbf{r}_0) \hat{h}(\mathbf{r}_0) dV_0 + \oint_S G(\mathbf{r}|\mathbf{r}_{0s}) \hat{f}(\mathbf{r}_{0s}) dS_0 \right\} \quad (4.10)$$

Equation (4.10) is not an explicit solution for the pressure field, but is rather an integral equation, because the source functions \hat{h} and \hat{f} in general depend on the fluctuating pressure and velocity fields themselves. However, because the sources are assumed to be small perturbations of the classical field having no sources, κ is small and \hat{p} will not differ greatly from a solution to the homogeneous problem defined by $h = f = 0$. The result (4.10) represents the solution to the inhomogeneous problem; the complete solution is (4.10) plus a homogeneous solution. We will take advantage of the smallness of κ to find an approximate explicit solution for \hat{p} by an iterative procedure discussed in Section 4.1.1.

Whatever tactic one may choose to follow, the result (4.10) is of no practical value without having a representation of $G(\mathbf{r}|\mathbf{r}_0)$. The most convenient form of $G(\mathbf{r}|\mathbf{r}_0)$ for our purpose is expansion in eigenfunctions $\psi_n(\mathbf{r})$, here the normal modes of the classical acoustics problem with no sources in the volume and homogeneous boundary conditions; $G(\mathbf{r}|\mathbf{r}_0)$ is therefore expressed as a *modal expansion*,

$$G(\mathbf{r}|\mathbf{r}_0) = \sum_{n=0}^{\infty} A_n \psi_n(\mathbf{r}) \quad (4.11)$$

where the ψ_n satisfy⁴

$$\begin{aligned} \nabla^2 \psi_n + k_n^2 \psi_n &= 0 \\ \hat{\mathbf{n}} \cdot \nabla \psi_n &= 0 \end{aligned} \quad (4.12)a,b$$

and are orthogonal functions,

$$\iiint_V \psi_m(\mathbf{r}) \psi_n(\mathbf{r}) dV = E_n^2 \delta_{mn} \quad (4.13)$$

Substitute (4.11) in (4.5)a, multiply by $\psi_m(\mathbf{r})$ and integrate over the volume to find

$$\iiint_V \psi_m \sum_{n=0}^{\infty} A_n \nabla^2 \psi_n dV + k^2 \iiint_V \psi_m \sum_{n=0}^{\infty} A_n \psi_n dV = \iiint_V \psi_m(\mathbf{r}) \delta(\mathbf{r} - \mathbf{r}_0) dV$$

With (4.7), (4.12) and (4.13), this equation produces the formula for A_n :

$$A_n = \frac{\psi_n(\mathbf{r}_0)}{k_n^2 - k^2} \quad (4.14)$$

⁴Equations (4.12)a,b really are essential to the following general results. They can be altered, e.g. $\hat{\mathbf{n}} \cdot \nabla \psi_n = -g(\mathbf{r})$, but subsequent formulas must be carefully checked.

Thus the expansion (4.11) for $G(\mathbf{r}|\mathbf{r}_0)$ is

$$G(\mathbf{r}|\mathbf{r}_0) = \sum_{n=0}^{\infty} \frac{\psi_n(\mathbf{r})\psi_n(\mathbf{r}_0)}{E_n^2(k^2 - k_n^2)} \quad (4.15)$$

the modal expansion of the Green's function. Substitution of (4.15) in (4.10) leads to the formal modal expansion of the pressure field,⁵

$$\hat{p}(\mathbf{r}) = \kappa \sum_{n=0}^{\infty} \frac{\psi_n(\mathbf{r})}{E_n^2(k^2 - k_n^2)} \left\{ \iiint_V \psi_n(\mathbf{r}_0) \hat{h}(\mathbf{r}_0) dV_0 + \oint_S \psi_n(\mathbf{r}_{0s}) \hat{f}(\mathbf{r}_{0s}) dS_0 \right\} \quad (4.16)$$

Suppose that for κ tending to zero, $\hat{p}(\mathbf{r})$ approaches the unperturbed mode shape ψ_N ; let the corresponding function \hat{p} be denoted \hat{p}_N , so

$$\hat{p} \xrightarrow{\kappa \rightarrow 0} \hat{p}_N = \psi_N \quad (4.17)$$

Now separate the N^{th} term from the sum in (4.16) and write

$$\begin{aligned} \hat{p}(\mathbf{r}) &= \psi_N(\mathbf{r}) \frac{\kappa}{E_N^2(k^2 - k_N^2)} \left\{ \iiint_V \psi_N(\mathbf{r}_0) \hat{h}(\mathbf{r}_0) dV_0 + \oint_S \psi_N(\mathbf{r}_{0s}) \hat{f}(\mathbf{r}_{0s}) dS_0 \right\} \\ &+ \kappa \sum_{n=0}^{\infty}' \frac{\psi_n(\mathbf{r})}{E_n^2(k^2 - k_n^2)} \left\{ \iiint_V \psi_n(\mathbf{r}_0) \hat{h}(\mathbf{r}_0) dV_0 + \oint_S \psi_n(\mathbf{r}_{0s}) \hat{f}(\mathbf{r}_{0s}) dS_0 \right\} \end{aligned} \quad (4.18)$$

where the prime in the summation sign means that the term $n = N$ is missing. The eigenvalues associated with the eigenfunction $\psi_N(\mathbf{r})$ is k_N . This form is consistent with the requirement (4.17) only if the factor multiplying $\psi_N(\mathbf{r})$ is unity, giving the formula for the perturbed wavenumber

$$k^2 = k_N^2 + \frac{\kappa}{E_N^2} \left\{ \iiint_V \psi_N(\mathbf{r}_0) \hat{h}(\mathbf{r}_0) dV_0 + \oint_S \psi_N(\mathbf{r}_{0s}) \hat{f}(\mathbf{r}_{0s}) dS_0 \right\} \quad (4.19)$$

and (4.18) becomes

$$\hat{p}(\mathbf{r}) = \psi_N(\mathbf{r}) + \kappa \sum_{n=0}^{\infty}' \frac{\psi_n(\mathbf{r})}{E_n^2(k^2 - k_n^2)} \left\{ \iiint_V \psi_n(\mathbf{r}_0) \hat{h}(\mathbf{r}_0) dV_0 + \oint_S \psi_n(\mathbf{r}_{0s}) \hat{f}(\mathbf{r}_{0s}) dS_0 \right\} \quad (4.20)$$

Another more direct derivation of (4.19) very useful in later analysis, may be had by first multiplying (4.4) by ψ_N and integrating over the volume:

$$\iiint_V \psi_N \nabla^2 \hat{p} dV + k^2 \iiint_V \psi_N \hat{p} dV = \kappa \iiint_V \psi_N \hat{h} dV$$

Application of Green's theorem to the first integral gives

$$\iiint_V \hat{p} \nabla^2 \psi_N dV + \oint_S [\psi_N \nabla \hat{p} - \hat{p} \nabla \psi_N] \cdot \hat{\mathbf{n}} dS + k^2 \iiint_V \psi_N \hat{p} dV = \iiint_V \psi_N \hat{h} dV$$

⁵The form of (4.16) has been seriously misunderstood by many interested in methods for analyzing and interpreting combustion instabilities. According to (4.12)b, the velocity associated with each of the basis functions must vanish on the surface enclosing the volume considered. Hence the representation (4.16) seems also to imply that the velocity of the actual (perturbed) field must also vanish at the boundary, even with \hat{h} and \hat{f} non-zero. That is, the approximate solution for $p(\mathbf{r}, t)$ and $u(\mathbf{r}, t)$ cannot satisfy the correct (perturbed) boundary conditions. This conclusion is incorrect, following from the implied assumption that as $\mathbf{r} \rightarrow \mathbf{r}_0$ on the boundary, the limit as $\mathbf{r} \rightarrow \mathbf{r}_0$ in the sum (4.16) is equal to the sum of the limits of each of the terms in (4.16). The point is made by example in Annex F; see also Footnote 8 and related remarks at the end of this chapter.

after inserting $\nabla^2\psi_N = -k_N^2\psi_N$ and $\nabla\psi_N \cdot \hat{\mathbf{n}} = 0$, rearrangement gives

$$k^2 = k_N^2 + \frac{\kappa}{\iiint_V \psi_N \hat{p} dV} \left\{ \iiint_V \psi_N(\mathbf{r}) \hat{h}(\mathbf{r}) dV + \iint_S \psi_N(\mathbf{r}_s) \hat{f}(\mathbf{r}_s) dS \right\} \quad (4.21)$$

The integral of $\psi_N \hat{p}$ in the denominator of (4.21) can be evaluated by using (4.20) and is exactly E_N^2 , providing the series in (4.20) converges. Hence (4.21) is identical to (4.19). This simple calculation has shown that (4.18) and (4.20) are consistent.

The preceding calculation contains several basic ideas lying behind much of the analysis used in this book. In summary, the original problem described by the differential equation (4.4)a and its boundary condition (4.4) are converted to an integral equation, in this case (4.10), established by introducing a Green's function. This is not an explicit solution because the functions \hat{h} and \hat{f} generally depend on the dependent variable \hat{p} . However, formulation as an integral equation provides a convenient basis for approximate solution by iteration.

4.1.1. Approximate Solution by Iteration. To apply an iterative procedure, it is necessary first to give the Green's function $G(\mathbf{r}|\mathbf{r}_0)$ explicit form. The natural choice for problems of waves in a chamber is a series expansion in the natural modes of the chamber, a modal expansion, (4.15). For the small parameter κ tending to zero (i.e. all perturbations of the classical acoustics problem are small), a straightforward argument produces the formula (4.19) for the wavenumber and the integral equation (4.20) for $\hat{p}(\mathbf{r})$.

Apparently, equation (4.20) must be solved to give \hat{p} before the wavenumber can be computed with (4.19). We should emphasize that for many practical purposes, it is really k that is required, because its imaginary part determines the linear stability of the system ($\alpha = 0$). The great advantage of this approach may be seen clearly with a simple example. Suppose $\hat{f} = 0$ and $\hat{h} = H(\mathbf{r})\hat{p}$ in (4.4)a,b. Then (4.20) and (4.19) become

$$\hat{p}(\mathbf{r}) = \psi_N(\mathbf{r}) + \kappa \sum_{n=0}^{\infty} \frac{\psi_n(\mathbf{r})}{E_n^2(k^2 - k_n^2)} \iiint_V \psi_n H(\mathbf{r}_0) \hat{p}(\mathbf{r}_0) dV_0 \quad (4.22)$$

$$k^2 = k_N^2 + \frac{\kappa}{E_N^2} \iiint_V \psi_N H(\mathbf{r}_0) \hat{p}(\mathbf{r}_0) dV_0 \quad (4.23)$$

Because κ is assumed to be small, solution by successive approximation, i.e. an iterative procedure, is a natural way to proceed. The initial (zeroth) approximation to the mode shape \hat{p} is (4.22) with $\kappa = 0$, $\hat{p}^{(0)} = \psi_N$. Substitution in (4.23) gives k^2 correct to first order in κ :

$$\begin{aligned} (k^2)^{(1)} &= k_N^2 + \frac{\kappa}{E_N^2} \iiint_V H(\mathbf{r}_0) \psi_N^2 dV_0 \\ &= k_N^2 + \kappa \frac{I_N}{E_N^2} \end{aligned} \quad (4.24)$$

where I_N stands for the integral,

$$I_N = \iiint_V H(\mathbf{r}_0) \psi_N^2 dV_0$$

Calculation of \hat{p} to *first* order in κ requires setting \hat{p} and k^2 to their *zeroth* order values on the right-hand side of (4.22), $\hat{p}^{(0)} = \psi_N$, $(k^2)^{(0)} = k_N^2$:

$$\begin{aligned}\hat{p}^{(1)}(\mathbf{r}) &= \psi_N(\mathbf{r}) + \kappa \sum_{n=0}^{\infty}' \frac{\psi_n(\mathbf{r})}{E_n^2(k_N^2 - k_n^2)} \iiint_V \psi_n H(\mathbf{r}_0) \psi_N dV_0 \\ &= \psi_N + \kappa \sigma_N\end{aligned}$$

and σ_N stands for the series

$$\sigma_N = \sum_{n=0}^{\infty}' \frac{\psi_N}{E_n^2(k_N^2 - k_n^2)} \iiint_V H(\mathbf{r}_0) \psi_N^2(\mathbf{r}_0) dV_0$$

Substitution of this formula for \hat{p} under the integral in (4.23) then gives the second approximation $(k^2)^{(2)}$ to k^2 :

$$\begin{aligned}(k^2)^{(2)} &= k_N^2 + \frac{\kappa}{E_N^2} \iiint_V \psi_N H(\mathbf{r}_0) (\psi_N + \kappa \sigma_N) dV_0 \\ &= (k^2)^{(1)} + \kappa^2 \frac{\kappa}{E_N^2} \iiint_V \psi_N H(\mathbf{r}_0) \sigma_N dV_0\end{aligned}\tag{4.25}$$

A wonderful property of the procedure is already apparent: **Calculation of the wavenumber to some order l in the small parameter requires knowing the modal functions only to order $l - 1$.** That is the basis for the current standard practice of computing linear stability for solid propellant rockets (the “Standard Stability Prediction Program,” Nickerson *et al.* 1984) using the unperturbed acoustic modes computed for the geometry in question.^{6,7}

The “perturbation-iteration” procedure just described is an old and widely used method to obtain solutions to nonlinear as well as linear problems. Often much attention is paid to achieving more accurate solutions by carrying the iterations to higher order in the small parameter. That is a legitimate process providing the equations themselves are valid to the order sought. In Chapter 3 we emphasized the importance of the expansion procedure largely for that reason. If the equations are valid, say, only to second order in the amplitude (ε), there is no need—in fact no justification—to try to find a solution to order ε^3 and higher. Similar remarks apply to the expansion in the average Mach number (μ); see footnote 2 in Chapter 3. The procedure is fully explained in Section 4.6 for the equations derived in Section 3.4.

4.2. An Alternative Derivation of the First Order Formula

The results (4.19) and (4.20) for the complex wavenumber and mode shape can be instructively obtained in a different way. Both formulas provide means for computing the differences $k^2 - k_N^2$ and $\hat{p} - \psi_N$ between the actual (perturbed) quantities and the unperturbed quantities. It is reasonable that those results should somehow follow from comparison of the perturbed ($\kappa \neq 0$) and unperturbed ($\kappa = 0$) problems. The idea is to average the difference between the two problems weighted respectively by the other’s mode shape. That is, subtract \hat{p} times equation (4.12)a from ψ_n times (4.4)a and integrate the result over the volume of the

⁶Failure to respect this basic property of the procedure has rendered useless some discussions of the subject. For example, the lengthy discussion by Van Moorhem (1982) is largely irrelevant to the spatially averaged representation treated here and in earlier works. For reasons different from those offered by Van Moorhem, some of the results in question are incomplete, as discussed in Chapters 6 and 7.

⁷Calculation of the solution, the mode shape to order l , also requires modal functions to order $l - 1$; see Section 4.6.2.

chamber:

$$\iiint_V [\psi_N \nabla^2 \hat{p} - \hat{p} \nabla^2 \psi_N] dV + \iiint_V (k^2 - k_N^2) \psi_N \hat{p} dV_0 = \kappa \iiint_V \psi_N \hat{h} dV$$

Now apply Green's theorem to the first integral, substitute the boundary conditions (4.4)b and (4.12)b and rearrange the result to find (4.21):

$$k^2 = k_N^2 + \frac{\kappa}{\iiint_V \psi_N \hat{p} dV} \left\{ \iiint_V \psi_N(\mathbf{r}) \hat{h}(\mathbf{r}) dV + \iint_S \psi_N(\mathbf{r}_s) \hat{f}(\mathbf{r}_s) dS \right\} \quad (4.26)$$

If k^2 is to be calculated to first order in κ , then \hat{p} must be replaced by its zero order approximation $\hat{p} = \psi_N$. Because the correction to k_N^2 contains the multiplier κ , any contributions of order κ multiplying κ give terms of order κ^2 . Hence to first order, (4.26) of course becomes (4.19).

This approach does not provide a recipe for computing the modal or basis functions to higher order. That does not cause difficulty here because we have the procedure given in the preceding section. We will find later that the simple derivation just given suggests a useful extension to time-dependent nonlinear problems. In that situation there is no result corresponding to (4.20) for computing the mode shapes to higher order. That deficiency is a serious obstacle to further progress with a simplified form of the general procedure, a subject of current research.

4.3. Approximate Solution for Unsteady Nonlinear Motions

The method covered in the preceding two sections, based essentially on the use of Green's functions, was the first application of modal expansions and spatial averaging to combustion instabilities (Culick 1961, 1963). In the early 1970s the procedure was extended to treat nonlinear problems, necessarily involving time-dependence (Culick 1971, 1975). We summarize that approach here; an alternative formulation based on a form of Galerkin's method is discussed in the following section.

We begin with the general problem (4.1)a,b and assume an approximation $\tilde{p}'(\mathbf{r})$ to the pressure field as a truncated expansion in a set of basis functions ψ_m ,

$$\tilde{p}'(\mathbf{r}, t) = \bar{p}_r \sum_{m=1}^M \eta_m(t) \psi_m(\mathbf{r}) \quad (4.27)$$

where for simplicity—not an essential assumption—we take \bar{p}_r to be the average pressure in the chamber, uniform in space and constant in time. In this work we will always take the ψ_m to be acoustic modes defined by the geometry, the distribution of average temperature and suitable boundary conditions.⁸ We would like the right-hand side of (4.27) to become more nearly equal to the actual pressure field in the combustor as more terms are included in the series, so that $\tilde{p}' \equiv p'$ in the limit:

$$p'(\mathbf{r}, t) = \lim_{M \rightarrow \infty} \tilde{p}'(\mathbf{r}; t) = \lim_{M \rightarrow \infty} \bar{p}_r \sum_{m=1}^M \eta_m(t) \psi_m(\mathbf{r}) \quad (4.28)$$

⁸The selection of boundary conditions is part of the art of applying this method. Examples covered later will clarify the point. For the present, it is helpful to think of the ψ_m as classical acoustic modes for a volume having rigid walls and the same shape as the combustion chamber in question. The ψ_m therefore do not satisfy exactly the boundary conditions actually existing in a combustor. Hence the right-hand side of (4.27) is an approximation in three respects: the series is truncated to a finite number of terms; it does not satisfy the correct boundary conditions; and the basis functions are assumed to be solutions to the scalar Helmholtz equation with the homogeneous boundary condition $\hat{\mathbf{n}} \cdot \nabla \psi_n = 0$. The ψ_m alone do not represent solutions with the perturbations taken into account. However, the solution carried out to the next order *does* satisfy the boundary conditions to first order. This important point is discussed in Chapter 10 of Morse and Feshbach (1952). The approximate nature of the modal expansion will be clarified as the analysis proceeds. See also Annex F for an example making the point.

Because the ψ_m do not satisfy the correct boundary conditions, this pointwise property certainly cannot be satisfied at the boundary. It is reasonable, however, to expect convergence in an integral-squared sense; that is, the integral of the square of the difference between the exact solution and (4.27) satisfies

$$\lim_{M \rightarrow \infty} \iiint_V \left[p'(\mathbf{r}, t) - \bar{p}_r \sum_{m=1}^M \eta_m(t) \psi_m(\mathbf{r}) \right]^2 dV = 0 \quad (4.29)$$

We will not prove this properly, but assume its truth.

Convergence in the sense asserted by (4.29) is a common idea arising, for example, in formal treatments of Sturm-Liouville problems; see Hildebrand (1952) for a very readable discussion. The matter of convergence of approximate solutions in the present context is more complicated because one must take into account the fact that the governing equations and their solutions are expanded in the two small parameters μ and ε introduced in Chapter 3. We will also not discuss that problem.

The synthesis of the pressure field expressed by (4.27) does not restrict in any practical fashion the generality of the method. For definitions here we assume that the modal functions satisfy the homogeneous Neumann condition $\hat{\mathbf{n}} \cdot \nabla \psi_n = 0$, but for some applications a different boundary condition, perhaps over only part of the boundary, may serve better. Hence we will assume here that the ψ_n are eigensolutions to the problem (4.12)a,b.

We require that the approximation (4.27) to p' satisfy equation (4.1)a. Multiply (4.12)b written for ψ_N by $\tilde{p}'(\mathbf{r}, t)$, subtract from (4.1)a written for \tilde{p}' multiplied by ψ_N ; then integrate the difference over the volume of the chamber to give

$$\iiint_V [\psi_N \nabla^2 \tilde{p}' - \tilde{p}' \nabla^2 \psi_N] dV - \iiint_V \frac{1}{\bar{a}^2} \frac{\partial^2 \tilde{p}'}{\partial t^2} dV - k_N^2 \iiint_V \tilde{p}' \psi_N dV = \iiint_V \psi_N h dV$$

Apply Green's theorem to the first integral, substitute the boundary conditions and rearrange the result to give

$$\iiint_V \frac{1}{\bar{a}^2} \frac{\partial^2 \tilde{p}'}{\partial t^2} \psi_N dV + k_N^2 \iiint_V \tilde{p}' \psi_N dV = - \left\{ \iiint_V h \psi_N dV + \oint_S f \psi_N dS \right\} \quad (4.30)$$

Now substitute the modal expansion (4.27) in the left-hand side:

$$\frac{\bar{p}_r}{\bar{a}_r^2} \sum_{m=0}^M \ddot{\eta}_m(t) \iiint_V \left(\frac{\bar{a}_r}{\bar{a}} \right)^2 \psi_m \psi_N dV - k_N^2 \bar{p} \sum_{m=0}^M \eta_m \iiint_V \psi_m \psi_N dV = E_N^2 \frac{\bar{p}}{\bar{a}_r^2} F_N \quad (4.31)$$

where

$$F_N = - \frac{\bar{a}^2}{\bar{p} E_N^2} \left\{ \iiint_V h \psi_N dV + \oint_S f \psi_N dS \right\} \quad (4.32)$$

and \bar{a}_r is a constant reference speed of sound. The second sum in (4.31) reduces, due to the orthogonality of the ψ_m , to $\eta_N E_N^2$. Under the first integrals, write

$$\Delta_a = 1 - \left(\frac{\bar{a}_r}{\bar{a}} \right)^2 \quad (4.33)$$

Then the first sum in (4.31) is

$$\sum_{m=0}^M \ddot{\eta}_m(t) \iiint_V (1 - \Delta_a) \psi_m \psi_N dV = E_N^2 \ddot{\eta}_N - \sum_{m=0}^M \ddot{\eta}_m(t) \iiint_V \Delta_a \psi_m \psi_N dV \quad (4.34)$$

With these changes, equation (4.31) becomes

$$\ddot{\eta}_N + \omega_N^2 \eta_N = F_N + \frac{1}{E_N^2} \sum_{m=0}^M \ddot{\eta}_m(t) \iiint_V \Delta_a \psi_m \psi_N dV \quad (4.35)$$

The sum on the right-hand side represents part of the effect of a non-uniform speed of sound in the chamber (if $\Delta_a \neq 0$). To simplify writing we will ignore this term until we consider special problems. For solid rockets it is normally a negligible contribution. If the combustor contains flame sheets, the temperature is piecewise uniform and this term also doesn't appear, but the presence of the discontinuities generates corresponding terms arising from F_N (see Annex E). Thus there are useful situations in which we deal with the system of equations:

$$\ddot{\eta}_N + \omega_N^2 \eta_N = F_N \quad (4.36)$$

This result, a set of coupled nonlinear equations with the forcing function F_N given by (4.32), is the basis for practically all of the analysis and theory discussed in the remainder of this book. A corresponding result is given in Annex B for a purely one-dimensional formulation. In anticipation of later discussions, several general remarks are in order.

- (i) The formulation expressed by (4.36) accommodates all relevant physical processes. In the derivation of the conservation equations in Annex A, only inconsequential approximations (for present purposes) were made, notably the neglect of multi-component diffusion and the representation of the reacting multi-phase medium by a single-fluid model. However, only the basic gasdynamics are known explicitly. All other processes must be modeled in suitable forms.
- (ii) Despite the apparent generality of (4.36), attention must be paid to an assumption implied in the application of Green's theorem in spatial averaging. That is, the functions involved must possess certain properties of continuity within the volume of averaging. The condition is not satisfied, for example, at a flame sheet, where the velocity is discontinuous, an important exception. Annex E introduces the method for handling such cases.
- (iii) The selection of functions for the modal expansion (4.27) is not unique; possible alternatives must always be considered. What works best depends on the nature of the boundary conditions. The closer the boundary is to a rigid reflecting surface, the more effective is the choice $\hat{\mathbf{n}} \cdot \nabla \psi_n = 0$, meaning that the acoustic velocity vanishes on the boundary. Because a combustor must provide for inflow of reactants and exhaust of products, it is simply not possible that the actual enclosure be everywhere rigid and perfectly reflecting. For $\hat{\mathbf{n}} \cdot \nabla \psi_n = 0$ to be a good approximation, as it should be for the modal expansion to serve successfully as a zeroth approximation to the pressure field, the boundary must be 'nearly' reflecting. Choked inlets and outlets satisfy the condition if the Mach number at the chamber side is small (that is, the flow within the volume is consistent with the assumption $\mu \ll 1$). Also, the dynamical response of burning solid propellants is normally such that requiring $\hat{\mathbf{n}} \cdot \nabla \psi_n = 0$ is appropriate. Over a broad useful range of practical conditions, defining the basis functions with (4.12)a,b is therefore a reasonable choice. Exceptions are not rare, however, and care must be exercised. For example, a Rijke tube will contain a heater, or a thin combustion region within the duct. Continuous functions ψ_n may not be good zeroth approximations to the actual behavior discontinuous at the heating zone; moreover, in that case $\psi_n = 0$ at the ends is the proper choice for boundary conditions on the basis functions. More generally, if the temperature field is highly non-uniform, then the zeroth order expansion functions should take that feature into account.
- (iv) An enormous advantage of the result (4.36) is its clear interpretation. A general unsteady motion in a combustor is represented by the time-evolution of a system of coupled nonlinear oscillators in one-to-one correspondence with the unperturbed modes ψ_n . Although the left-hand side of (4.36) describes the motion of a linear oscillator, the forcing function F_N will in general contain terms in η_n representing linear and nonlinear damping, springiness and inertia. Consequently, it is easy to find familiar nonlinear differential equations as special cases of (4.36). Such special results aid

greatly the interpretations of complicated observed behavior in terms of simpler elementary motions. Thus it is important to understand the connections between parameters defining the oscillators, the characteristics of the modes, and the definitions provided in the process of spatial averaging.

- (v) Different problems are distinguished chiefly in two respects: Geometry of the combustor; and the form of the forcing function F_N . The forcing function contains the influences of gasdynamics explicitly, but all other processes must be modeled, either with theory or based on experimental results. The geometry and the boundary conditions determine the modal expansion functions ψ_n and the frequencies ω_n . For complicated geometries, as for many large solid propellant rockets and for most gas turbine combustors, computation of the ψ_n and ω_n has been a time-consuming and expensive process. That situation is gradually changing with the development of more capable software (e.g., French 2003; French and Flandro 2003).
- (vi) The relatively general context in which the oscillator equations (4.36) have been derived does not exclude simpler problems which can either be treated as special cases or constructed without reference to the procedures worked out here. (See, e.g., Section 2.6) However, it is then often more difficult to be certain that all important processes are accounted for or properly ignored.

4.4. An Alternative Application of Spatial Averaging: The Method of Least Residuals

With a series of works beginning in the late 1960s, Professor B.T. Zinn and his students developed and applied a different method based on spatial averaging, an interesting extension of Galerkin's method. See Powell (1970); Powell and Zinn (1969; 1971a,b; 1974); Zinn and Powell (1968; 1970); Lores and Zinn (1973). There are necessarily some similarities with the method discussed in the preceding two sections; in particular the formal results should agree in detail, or at least be reconcilable. There are, however, distinct differences both in the sequence of historical developments and in many important matters of applications.

In respect to the historical developments, the Georgia Tech group was first to apply spatial averaging to analyze nonlinear behavior, in liquid propellant rockets. They were also first to demonstrate several nonlinear phenomena confirmed later in works published by others. Those results are reviewed here in Chapter 7. It was three years after the first Georgia Tech report that Culick independently worked out a much simplified form of the method described in Section 4.2, to explain nonlinear behavior observed in a laboratory device, the T-burner, used to measure the combustion dynamics of solid propellants. At that time, there was practically no communication (or mutual attention) between the liquid and solid rocket communities at the research level, a condition that blocked certain benefits, but which has since been corrected.

Recently, Seywert and Culick (1998) showed that when applied to the same equation, the two methods lead to the same formal result (4.28). To establish that conclusion, we follow the formal procedure discussed by Finlaysen and Scriven (1966) as extended by Powell (1970); Powell and Zinn (1969, 1971a) and Zinn and Powell (1968, 1970) to account for the inhomogeneous boundary conditions. The method is in fact quite general, capable of handling much more elaborate problems than that for which the method covered in Section 4.3 has been worked out. Here we take a direct route to make the main point most clearly. Write the wave equation (4.1) and its boundary condition as

$$\begin{aligned} E(\mathbf{r}, t) &= 0 \\ B(\mathbf{r}, t) &= 0 \end{aligned} \tag{4.37a,b}$$

where

$$\begin{aligned} E(p') &:= \nabla^2 p' - \frac{1}{\bar{a}^2} \frac{\partial^2 p'}{\partial t^2} - h \\ B(p') &:= \hat{\mathbf{n}} \cdot \nabla p' + f \end{aligned} \tag{4.38a,b}$$

The Galerkin method is based on expansion of the dependent variables in a set of basis functions ϕ_n . Here we suppose that there is only the single variable p' in the problem⁹ defined by (4.37). The approximation \tilde{p} expressed as the expansion truncated to M terms is assumed to become equal to the solution p as $M \rightarrow \infty$:

$$\lim_{M \rightarrow \infty} \tilde{p} = \lim_{M \rightarrow \infty} \sum_{m=1}^M a_m \phi_m = p \quad (4.39)$$

At this stage the functions ϕ_n are undefined. The modified Galerkin method consists in spatially averaging, with a weighting function, the governing equation and its boundary condition, both applied to an approximation \tilde{p} , and requiring that the difference vanish:

$$\iiint_V E(\tilde{p}) \phi_N dV - \oint_S B(\tilde{p}) \phi_N dS = 0 \quad (4.40)$$

The spatial weighting function ϕ_N need not be one of the basis functions, but we made that choice to establish the equivalence of the methods without unnecessary complications.

Now substitute the definition (4.36) for E and B :

$$\iiint_V \left(\nabla^2 \tilde{p}' - \frac{1}{\bar{a}^2} \frac{\partial^2 \tilde{p}'}{\partial t^2} \right) \phi_N dV - \oint_S (\hat{\mathbf{n}} \cdot \nabla \tilde{p}' + f) \phi_N dS = 0 \quad (4.41)$$

Apply Green's theorem to the first term to give

$$\iiint_V \nabla^2 \tilde{p}' \phi_N dV = \oint_S (\tilde{p}' \nabla \phi_N - \phi_N \nabla \tilde{p}') \cdot \hat{\mathbf{n}} dS - \iiint_V \tilde{p}' \nabla^2 \phi_N dV$$

and choose $\phi_N \equiv \psi_N$ defined by (4.12):

$$\iiint_V \nabla^2 \tilde{p}' \psi_N dV = - \oint_S \psi_N \nabla \tilde{p}' \cdot \hat{\mathbf{n}} dS + k_N^2 \iiint_V \tilde{p}' \psi_N dV$$

Substitution in (4.41), with $\phi_N \equiv \psi_N$ and some rearrangement leads to the result identical to (4.30):

$$\iiint_V \frac{1}{\bar{a}^2} \frac{\partial^2 \tilde{p}'}{\partial t^2} \psi_N dV + k_N^2 \iiint_V \tilde{p}' \psi_N dV = - \left\{ \iiint_V \psi_N h dV + \oint_S \psi_N f dS \right\} \quad (4.42)$$

Owing to the care taken to recognize the approximation to p' with a truncated expansion, \tilde{p}' appears here in place of p' in (4.30).

The preceding remarks establish the equivalence of the methods only for the case when the equations of motion are written for the fluctuations of the flow variable and then combined to form the wave equation for the pressure. It should be apparent from the discussion in Sections 4.1–4.3 that the method developed there, and used throughout the remainder of this book, is restricted to that formulation. In contrast, the Galerkin method is not constrained to any particular form of the governing equations; of course the problem to be analyzed must lend itself to definition of basis functions. In that sense, the modified Galerkin method is potentially more general than the method discussed in Sections 4.1–4.3 and used throughout this book. However, the method has not been extended beyond the applications investigated by the group at Georgia Tech many years ago and for several reasons seems not to have motivated others to pursue even similar applications. In almost all their work, the Georgia Tech group introduced a form of a potential for the unsteady velocity. Combined with sometimes vague usage of expansion parameters and ordering, that practice renders the method awkward to use and the results difficult to interpret.

⁹The other variables of the flow field must also be expanded, the procedure being the same as that followed in the method based on the results of Section 4.3.

4.5. Application of Time-Averaging

To this point the expansion procedure based on two small parameters has been used only to derive the systems of equations describing successively more difficult classes of problems listed in Section 3.3.2. Later we will see how an iterative method based partly on the expansion reduces those systems of equations to more readily soluble forms. In this section we apply time-averaging to convert the second-order equations (4.36) to first order equations. First, two remarks:

- (i) Use of time-averaging is motivated by the experimental observation that combustion instabilities commonly show slowly varying amplitudes and phases of the modes contributing to the motions. That behavior is a consequence of the relative weakness of the disturbing processes and is therefore measured by the small parameter μ characteristic of the Mach number of the mean flow. It is essential to understand that it is not the amplitudes themselves (i.e. the parameter ε) that matters. Thus the application of time-averaging in the present context is *not* intended to treat nonlinear behavior in μ , but is based on the idea that there is only weak coupling between the mean flow and the unsteady motions, proportional to the Mach number of the average flow. Nonlinear behavior of higher order in ε is a distinct matter, formally unaffected by the time-averaging.
- (ii) Two-time scaling (Kevorkian and Cole, 1996; Cole 1968) is an alternative method to time-averaging. The results obtained are identical up to second order acoustics (Sections 3.3.3(II) and 3.4), a conclusion not proved here but consistent with similar previous works in other fields.

According to the discussion in Section 3.3.3, we can characterize the functions h and f , and hence the forcing function F_N , as sums of terms each of which is of order μ and of zeroth or first order in ε . Thus if we reactivate the ordering parameters μ and ε , the right-hand side of (3.45)b, for example, has the form

$$-\mu\varepsilon \left\{ \{[\mathbf{M}]\}_1 + \frac{\varepsilon}{\mu} \{[\mathbf{M}]\}_2 \right\} + \mathbf{F}'$$

The divergence of these terms eventually appears in h and F_n . Hence we are justified in taking F_n of order μ ; to show this explicitly write (4.36) as

$$\ddot{\eta}_N + \omega_N^2 \eta_N = \mu G_N \quad (4.43)$$

In any event, for μ small, the η_N differ but little from sinusoids so (without approximation) it is reasonable to express $\eta_N(t)$ in the equivalent forms

$$\eta_N(t) = r_N(t) \sin(\omega_N t + \phi_N(t)) = A_N(t) \sin \omega_N t + B_N(t) \cos \omega_N t \quad (4.44)$$

and

$$A_N(t) = r_N \cos \phi_N ; \quad B_N = r_N \sin \phi_N$$

$$r_N = \sqrt{A_N^2 + B_N^2} ; \quad \phi_N = \tan^{-1} \left(\frac{A_N}{B_N} \right) \quad (4.45)$$

One way to proceed follows a physical argument based on examining the time evolution of the energy of the oscillator having amplitude η_N (Culick 1975). The energy \mathcal{E}_N is the sum of kinetic and potential energies,

$$\mathcal{E}_N(t) = \frac{1}{2} \dot{\eta}_N^2 + \frac{1}{2} \omega_N^2 \eta_N^2 \quad (4.46)$$

The time-averaged values of the energy and power input to the oscillator, due to the action of the force μG_N , are

$$\langle \mathcal{E}_N \rangle = \frac{1}{\tau} \int_t^{t+\tau} \mathcal{E}_N dt' ; \quad \langle \mu G_N \dot{\eta}_N \rangle = \frac{1}{\tau} \int_t^{t+\tau} \mu G_N \dot{\eta}_N dt' \quad (4.47)$$

Conservation of energy requires that the time-averaged rate of change of energy equal the time-averaged rate of work done by μG_N on the oscillator:

$$\frac{d}{dt} \langle \mathcal{E}_N \rangle = \mu \langle G_N \dot{\eta}_N \rangle \quad (4.48)$$

From (4.44), the velocity is

$$\dot{\eta}_N = \omega_N r_N \cos(\omega_N t + \phi_N) + [\dot{r}_N \sin(\omega_N t + \phi_N) + \dot{\phi}_N r_N \cos(\omega_N t + \phi_N)] \quad (4.49)$$

Following Krylov and Bogoliubov (1947) we apply the ‘strong’ condition that the velocity is always given by the formula for an oscillator is force-free-motion,

$$\dot{\eta}_N = \omega_N r_N \cos(\omega_N t + \phi_N) \quad (4.50)$$

Hence (4.49) is consistent with this requirement only if

$$\dot{r}_N \sin(\omega_N t + \phi_N) + \dot{\phi}_N r_N \cos(\omega_N t + \phi_N) = 0 \quad (4.51)$$

Now use the definitions (4.44), (4.46) and (4.50) to find

$$\mathcal{E}_N = \frac{1}{2} \omega_N^2 r_N^2 \quad (4.52)a,b$$

$$\mu G_N \dot{\eta}_N = \mu G_N \omega_N r_N \cos(\omega_N t + \phi_N)$$

The statement “slowly varying amplitude and phase” means that the fractional changes of amplitude and phase are small in one cycle of the oscillation and hence during the interval of averaging τ , if τ is at least equal to the period of the fundamental mode:

$$\frac{\tau}{r_N} \frac{dr_N}{dt} \ll 1 ; \quad \frac{\tau}{2\pi} \frac{d\phi_N}{dt} \ll 1 \quad (4.53)$$

These inequalities imply that r_N and ϕ_N may be treated as constants during the averaging carried out in (4.47). To see this, imagine that r_N for example, is expanded in Taylor series for some time t_1 in the interval τ , $t < t_1 < t + \tau$:

$$r_N(t) = r_N(t_1) + (t - t_1) \left(\frac{dr_N}{dt} \right)_{t_1} + \dots$$

For r_N slowly varying, \dot{r}_N doesn't vary much during a period and may be assigned some average value. The increment $t - t_1$ has maximum value τ ; so the second term is negligible according to the first of (4.47). Therefore $r_N(t) \approx r_N(t_1)$ for any t_1 in the interval of averaging and the assertion is proved.

Substitution of (4.52)b in (4.48) then gives

$$\omega_N^2 r_N \frac{dr_N}{dt} = \mu \frac{\omega_N r_N}{\tau} \int_t^{t+\tau} G_N \cos(\omega_N t' + \phi_N) dt'$$

which gives

$$\frac{dr_N}{dt} = \mu \frac{1}{\omega_N \tau} \int_t^{t+\tau} G_N \cos(\omega_N t' + \phi_N) dt' \quad (4.54)$$

Because $r_N(t)$ and $\dot{r}_N(t)$ are nearly constant in the interval $(t, t + \tau)$, this relation implies the equation *before* averaging,

$$\frac{dr_N}{dt} = \frac{\mu}{\omega_N} G_N(t) \cos(\omega_N t + \phi_N) \quad (4.55)$$

The corresponding equation for the phase $\phi_N(t)$ before averaging is found by first rearranging (4.51) to give

$$r_N \frac{d\phi_N}{dt} \cos(\omega_N t + \phi_N) = -\dot{r}_N \sin(\omega_N t + \phi_N)$$

which becomes, after substitution of (4.55),

$$r_N \frac{d\phi_N}{dt} = -\frac{\mu}{\omega_N} G_N(t) \sin(\omega_N t + \phi_N) \quad (4.56)$$

Now time average this equation over the interval τ ; the left-hand side is approximately constant for theorem give above, and the equation for $\phi_N(t)$ is

$$r_N \frac{d\phi_N}{dt} = -\mu \frac{1}{\omega_N \tau} \int_t^{t+\tau} G_N \sin(\omega_N t' + \phi_N) dt' \quad (4.57)$$

With the relations (4.45), equations (4.54) and (4.57) can be converted to equations for A_N and B_N :

$$\frac{dA_N}{dt} = \frac{\mu}{\omega_N \tau} \int_t^{t+\tau} G_N \cos \omega_N t' dt' \quad (4.58)a,b$$

$$\frac{dB_N}{dt} = -\frac{\mu}{\omega_N t} \int_t^{t+\tau} G_N \sin \omega_N t' dt'$$

Whichever pair one chooses to use, (4.54) and (4.57) or (4.55), the general formal problem of solving a system of coupled second order equations (4.43) for the oscillators, has been converted to the simpler approximate formal problem of solving a system of coupled first order equations. The essential basis for that conversion is the removal of the fast oscillatory behavior with the definition (4.44), a transformation made reasonable because the changes of amplitudes and phases take place on a much slower (i.e. longer) time scale than do the oscillations. The presence and role of two time scales is more evident in the following alternative derivation.

From the second equality of (4.44), we find the velocity

$$\dot{\eta}_N = \omega_N [A_N \cos \omega_N t - B_N \sin \omega_N t] + [\dot{A}_N \sin \omega_N t + \dot{B}_N \cos \omega_N t]$$

Now enforce the condition corresponding to (4.51),

$$\dot{A}_N \sin \omega_N t + \dot{B}_N \cos \omega_N t = 0 \quad (4.59)$$

and the velocity is

$$\dot{\eta}_N = \omega_N [A_N \cos \omega_N t - B_N \sin \omega_N t] \quad (4.60)$$

Substitution in (4.43) gives

$$\begin{aligned} \omega_N [\dot{A}_N \cos \omega_N t - \dot{B}_N \sin \omega_N t] + \omega_N^2 [-A_N \sin \omega_N t - B_N \cos \omega_N t] \\ + \omega_N^2 [A_N \sin \omega_N t + B_N \cos \omega_N t] = \mu G_N \end{aligned}$$

and

$$\dot{A}_N \cos \omega_N t - \dot{B}_N \sin \omega_N t = \frac{\mu}{\omega_N} G_N$$

Multiply by $\cos \omega_N t$ and substitute (4.59) for $\dot{B}_N \cos \omega_N t$ to give

$$\dot{A}_N \cos^2 \omega_N t - \sin \omega_N t \left[-\dot{A}_N \sin \omega_N t \right] = \frac{\mu}{\omega_N} G_N \cos \omega_N t$$

so

$$\frac{dA_N}{dt} = \frac{\mu}{\omega_N} G_N \cos \omega_N t \quad (4.61)$$

Similarly,

$$\frac{dB_N}{dt} = -\frac{\mu}{\omega_N} G_N \sin \omega_N t \quad (4.62)$$

Now introduce two time-scales, τ_f the first scale, of the order of the period of the fundamental oscillation (in fact, we might as well set $\tau_f = 2\pi/\omega_1$; and τ_s , the slow scale characterizing transient changes of the amplitudes and phases of the oscillations. Two corresponding dimensionless time variables can be defined, $t_f = t/\tau_f$ and $t_s = t/\tau_s$. Thus we consider the amplitudes and phases to be functions of the slow variable t_s while the forcing functions G_N depend on both t_f and to because they depend on the η_N , ($i = 1, 2, \dots$)

$$\eta_N = A_N(t_s) \sin \left(2\pi \frac{\omega_N}{\omega} t_f \right) + B_N(t_s) \cos \left(2\pi \frac{\omega_N}{\omega_1} t_f \right) \quad (4.63)$$

In terms of the dimensionless time variables, is

$$\frac{1}{\tau_s} \frac{dA_N}{dt_s} = \frac{\mu}{\omega_N} G_N \cos \omega_N t$$

and averaging over the fast variable we have

$$\frac{1}{\tau_s} \int_{t_f}^{t_f + \tau_f} \frac{1}{\tau_s} \frac{dA_N}{dt_s} dt'_f = \frac{\mu}{\omega_N \tau_f} \int_{t_f}^{t_f + \tau_f} G_N \cos \left(2\pi \frac{\omega_N}{\omega_1} t'_f \right) dt'_f$$

On the left-hand side, dA_N/dt'_s is assumed to be sensibly constant in the interval τ_f and we have

$$\frac{1}{\tau_s} \frac{dA_N}{dt'_s} = \frac{\mu}{\omega_N \tau_f} \int_{t_f}^{t_f + \tau_f} G_N(t'_f, t'_s) \cos \left(2\pi \frac{\omega_N}{\omega_1} t'_f \right) dt'_f \quad (4.64)$$

Those parts of G_N depending on t'_s are taken also to be constant and if we now rewrite this equation in terms of dimensional variables, we recover (4.58)a with $\tau = \tau_f = 2\pi/\omega$. Similar calculations will produce again (4.58)a. Note that due to the nonlinear coupling, the amplitude and phases of all modes normally change on roughly the same scale as that for the fundamental mode; thus the single interval of averaging works for all modes.

Krylov and Bogoliubov (1947) discuss procedures for carrying the results of time-averaging to higher order in the small parameter characterizing the expansion. Here, however, the parameter is μ , a Mach number characteristic of the mean flow. Hence, as emphasized in Chapter 3, **extension to higher order in μ is not justified without re-deriving the basic equations to account for higher orders in the mean flow from the beginning.**

With μG_N replaced by F_N , letting $N \rightarrow n$, and $\tau_s t_s = t$, we find the usual forms of the time-averaged equations,

$$\frac{dA_n}{dt} = \frac{1}{\omega_n \tau} \int_t^{t+\tau} F_n \cos \omega_n t' dt' \quad (4.65)a,b$$

$$\frac{dB_n}{dt} = -\frac{1}{\omega_n \tau} \int_t^{t+\tau} F_n \sin \omega_n t' dt'$$

Inserting the definitions of t_s and t_f in (4.63), and replacing N by n , we have the expression for $\eta_n(t)$:

$$\eta_n(t) = A_n(t) \sin(\omega_n t) + B_n(t) \cos(\omega_n t) \quad (4.66)$$

In Chapter 7 we will use a continuation method to assess the ranges of parameters and other conditions for which the first order equations give accurate results when compared with solutions to the complete oscillator equations. In the development of the theoretical matters described in this book, the sets of first order equations, (4.65)a,b, have been central. They remain extremely useful both for theoretical work and for applications.

4.6. The Procedure for Iterative Solution to the Oscillator Equations

The oscillator equations (4.35) and (4.36) are not yet in a form that can be readily solved because the functions F_N , defined by (4.32) contain not only p' but also the dependent variables ρ' , T' and \mathbf{u}' in the functions h and f . With the two-parameter expansion as the basis, the iteration procedure provides a means for expressing F_N in terms of p' only to first order in ε . Thus eventually the oscillator equations become a system soluble for the modal amplitudes $\eta_N(t)$. There are of course approximations required, but the orders of their effects can always be estimated in terms of the parameters ε and μ . To appreciate how the procedure is constructed, it is helpful always to keep in mind the correspondence between the smallness of ε and μ , and the distortions they represent of the unperturbed classical acoustic field.

There are two classes of distortions or perturbations: Those represented by higher orders of ε , arising as nonlinear effects of finite amplitudes,¹⁰ classified generally as energy transfer between modes; and those measured by μ , consequences of interactions, hence energy transfer, between the steady and unsteady fields. Each of those types of perturbations may be identified within the volume in question and at the boundary. Quite generally, then, we must take into account perturbations of the classical acoustic field, associated with three kinds of energy transfer: Linear transfer between the mean and fluctuating motions; nonlinear transfer between modes, or mode coupling, independent of the average flow field; and nonlinear energy transfer between the mean flow and fluctuating fields. Those three kinds of energy transfer characterize, respectively, the Problems I; II; III; and IV defined in Section 3.3. The way in which we view and accommodate those perturbations determines our choice of basis functions ψ_N used in the modal expansion¹¹ (4.27). In this work we are not accounting for nonlinear energy transfer between the mean flow and fluctuating fields; i.e. those contributions represented by terms $O(\mu \varepsilon^2)$, are ignored as in Section 3.4.

¹⁰Recall that in this work, nonlinear behavior is measured in terms of the amplitude ε of the unsteady motions. It is intrinsic to their derivation (Chapter 3) that the governing equations are linear in μ , i.e. in the Mach number of the mean flow. Hence, with those equations, expansions and solutions cannot legitimately be carried further than first order in μ . The procedures developed here can be carried formally to higher order in ε .

¹¹The expansion is not adequate for treating Problem IV defined in Section 3.3. In that case the basis functions must include distortions of order μ .

4.6.1. Iteration on the Mach Number of the Mean Flow. To simplify the discussion here we assume that the functions h and f contain only four sorts of terms: small, roughly of order ε , but not strictly ordered because they are independent of the fluctuating field; linear in the fluctuations, and hence of order ε ; bilinear in the mean flow speed and the fluctuations, and hence of order $\varepsilon\mu$; and nonlinear terms in the fluctuations of order ε^2 and ε^3 . The terms are additive, so the two functions can be written formally by rearranging (3.63)a,b in the form

$$\begin{aligned} h &= \varepsilon(h_{00} + h_{10}) + \varepsilon\mu h_{11} + \varepsilon^2 h_{20} + \varepsilon^3 h_{30} \\ f &= \varepsilon(f_{00} + f_{10}) + \varepsilon\mu f_{11} + \varepsilon^2 f_{20} + \varepsilon^3 f_{30} \end{aligned} \quad (4.67)a,b$$

where h_{00} and f_{00} do not depend on the unsteady field and hence constitute true forcing functions.

The terms h_{10} and f_{10} are linear in the fluctuations and independent of the mean flow speed. They can be immediately combined with the wave operator on the left-hand side of the oscillator equations, showing that they represent attenuation and frequency shifts of classical acoustic modes. A particularly clear and important example is the viscous acoustic boundary layer on a rigid impermeable wall discussed in Annex C and Section 5.9.

Almost all of the processes responsible for linear instabilities in a combustion system are contained in the functions h_{11} and f_{11} with possible contributions from h_{10} and f_{10} . At this stage, it is not clear what phenomena might be represented by the quadratic and cubic nonlinearities not included here. Detailed investigations are required to address the question.

The special reason for retaining those terms shown in (4.67)a,b is the following. Within the ordering procedure followed here, only the unperturbed classical modes ψ_n are required to generate explicit equations for the modal amplitudes with the oscillator equations (4.36). To see the problem, substitute (4.67)a in the right-hand side of the wave equation (4.1)a for p' :

$$\nabla^2 p' - \frac{1}{\bar{a}^2} \frac{\partial^2 p'}{\partial t^2} = \varepsilon(h_{00} + h_{10}) + \varepsilon\mu h_{11} + \varepsilon^2 h_{20} + \varepsilon^3 h_{30} \quad (4.68)$$

The functions h_0 , h_{10} , h_{11} , ... are found by identification with (3.58) and the definitions of the brackets given in Section A.6. While h_{11} , h_{20} and h_{30} can be found explicitly with those formulas, h_{00} and h_{10} arise from \mathcal{F}' and \mathcal{P}' and are determined by the models of processes other than the fluid mechanics covered by the compressible Euler equations. The acoustic boundary layer, for example, contributes to h_{10} and f_{10} ; see Section 6.5 for another example.

In the iterative procedure, the parameter μ defines the iterations so that nonlinear behavior governed by ε is present at each stage to the order selected. The zeroth approximation is the classical acoustic field given by the modal expansions with time dependent amplitudes:

$$\begin{aligned} p'_O &= \bar{p} \sum_0^M \eta_m(t) \psi_m(\mathbf{r}) \\ \mathbf{u}'_O &= \bar{a}^2 \sum_0^M \frac{\dot{\eta}_m(t)}{\gamma k_m^2} \nabla \psi_m(\mathbf{r}) \end{aligned} \quad (4.69)a,b$$

The expansion for the velocity field has been chosen so that term by term the expansions satisfy the classical acoustic momentum equation free of perturbations

$$\bar{\rho} \frac{\partial \mathbf{u}'_O}{\partial t} + \nabla p'_O = 0 \quad (4.70)$$

Correspondingly, the values of density and temperature fluctuations are set by the adiabatic relations,

$$\frac{\rho}{\bar{\rho}} = \left(\frac{p}{\bar{p}} \right)^{1/\gamma}, \quad \frac{T}{\bar{T}} = \left(\frac{p}{\bar{p}} \right)^{\frac{\gamma-1}{\gamma}}$$

Set $p = \bar{p} + p'$, $\rho = \bar{\rho} + \rho'$, $T = \bar{T} + T'$ and expand to find to second order

$$\frac{\rho'_O}{\bar{\rho}} = \frac{1}{\gamma} \frac{p'_O}{\bar{p}} - \frac{\gamma-1}{2\gamma^2} \left(\frac{p'_O}{\bar{p}} \right)^2 \quad (4.71)\text{a,b}$$

$$\frac{T'_O}{\bar{T}} = \frac{\gamma-1}{\gamma} \frac{p'_O}{\bar{p}} - \frac{\gamma-1}{2\gamma^2} \left(\frac{p'_O}{\bar{p}} \right)^2$$

Then the equation for the first approximation, $p'^{(1)}$, to p' is found by setting the fluctuations of flow variables in h equal to their classical values and retaining only terms of appropriate order. To see how this works, begin with (2.78)a,b. Define the function \mathcal{G}

$$\mathcal{G} = \bar{\rho} \nabla \cdot \frac{1}{\bar{\rho}} \mathbf{F}'_{III} - \frac{1}{\bar{a}^2} \frac{\partial \mathcal{P}'_{III}}{\partial t} \quad (4.72)$$

The form of \mathcal{G} is unspecified, but we assume that the processes represented lead to terms of all orders retained in the problem at hand. Then with the ordering parameters shown and the acoustic approximations (4.69)a,b substituted for all fluctuations, indicated by the subscript $(\)_O$, (3.63)a,b give¹²

$$\begin{aligned} h := h_{III} &= \varepsilon [g_{00} + g_{10}]_O + \varepsilon \mu \left[-\bar{\rho} \nabla \cdot \frac{1}{\bar{\rho}} \{[\mathbf{M}]\}_1 + \frac{1}{\bar{a}^2} \frac{\partial \{[p]\}_1}{\partial t} + \frac{1}{\bar{\rho}} \nabla \bar{\rho} \cdot \nabla p' + g_{11} \right]_O \\ &+ \varepsilon^2 \left[-\bar{\rho} \nabla \cdot \frac{1}{\bar{\rho}} \{\mathbf{M}\}_2 + \frac{1}{\bar{a}^2} \frac{\partial \{p\}_2}{\partial t} + g_{20} \right]_O \\ &+ \varepsilon^3 \left[-\bar{\rho} \nabla \cdot \frac{1}{\bar{\rho}} \{\mathbf{M}\}_3 + g_{30} \right]_O \end{aligned} \quad (4.73)$$

$$\begin{aligned} f := f_{III} &= \varepsilon \left[\bar{\rho} \left(\frac{\partial \mathbf{M}'}{\partial t} \right)_{10} - (\mathbf{F}')_{10} \right]_O \cdot \hat{n} + \varepsilon \mu \left[\bar{\rho} \left(\frac{\partial \mathbf{M}'}{\partial t} \right)_{11} + \{[\mathbf{M}]\}_1 - (\mathbf{F}')_{11} \right]_O \cdot \hat{n} \\ &+ \varepsilon^2 \left[\bar{\rho} \left(\frac{\partial \mathbf{M}'}{\partial t} \right)_{20} + \{\mathbf{M}\}_2 - (\mathbf{F}')_{20} \right]_O + \varepsilon^3 \left[\bar{\rho} \left(\frac{\partial \mathbf{M}'}{\partial t} \right)_{30} + \{\mathbf{M}\}_3 - (\mathbf{F}')_{30} \right]_O \end{aligned} \quad (4.74)$$

Substitution of 4.73 and 4.74 into the oscillator equations (4.36),

$$\ddot{\eta}_N + \omega_N^2 \eta_N = -\frac{\bar{a}_r^2}{\bar{\rho}_r E_N^2} \left\{ \iiint_V h_{III} \psi_N dV + \iint_S f_{III} \psi_N dS \right\} \quad (4.75)$$

produces the equations for the amplitudes of the unperturbed modes.

Because the basis functions ψ_m satisfy the boundary conditions for the unperturbed problem, $p'_O(r, t)$ given by (4.69)a, also does not satisfy the actual boundary conditions—it is the zeroth approximation. It is the first order approximation to the pressure field that satisfies the correct boundary conditions, which are first order in μ . Similarly, the unsteady velocity to zeroth order is given by the expansion (4.69)b and not only doesn't satisfy the actual boundary conditions but is clearly an irrotational field, $\nabla \times u'_O = 0$.

¹²Second and third order terms are shown for completeness in (4.73) and (4.74); they will not be needed until the discussion of nonlinear behavior in Chapter 7.

4.6.2. Zeroth and First Order Solutions for the Eigenvalues and Basis Functions. On several occasions, researchers in this field, and users of results, have seriously misunderstood the meaning of the preceding procedure. Its purpose is to give the **first order** (in μ) results for the time-evolution of modal amplitudes (which to zeroth order are constant in the scheme outlined here) and the **first order** (in μ) formulas for the eigenvalues of steady oscillations when the perturbations are accounted for in **first order** (in ε) i.e. linear stability. The complex eigenvalues for steady waves are found by setting¹³

$$\eta_N = \hat{\eta}_N e^{-i\bar{a}kt}$$

$$h = \hat{h} e^{-i\bar{a}kt} \quad (4.76)\text{a,b}$$

$$f = \hat{f} e^{-i\bar{a}kt}$$

Substitution in (4.75) gives

$$\hat{\eta}_N (-\bar{a}^2 k^2 + \omega_N^2) = -\frac{\bar{a}^2}{\bar{p}E_N^2} \left\{ \iiint_V \hat{h} \psi_N dV + \oint_S \hat{f} \psi_N dS \right\} \quad (4.77)$$

Equation (4.77) is useful only if h and f are linear in the fluctuations, for then every term has $e^{-i\bar{a}kt}$ as a factor. Hence from (4.67)a,b only the terms h_{10} , h_{11} , f_{10} and f_{11} can be retained. The formula (4.77) for the eigenvalues of the perturbed (actual) problem to first order is

$$\begin{aligned} (\bar{a}k)^2 = \omega_N^2 + \frac{\bar{a}^2}{\bar{p}E_N^2} \left\{ \varepsilon \left[\iiint_V \hat{h}_{10} \psi_N dV + \oint_S \hat{f}_{10} \psi_N dS \right] \right. \\ \left. + \varepsilon \mu \left[\iiint_V \hat{h}_{11} \psi_N dV + \oint_S \hat{f}_{11} \psi_N dS \right] \right\} \end{aligned} \quad (4.78)$$

This is essentially the result used widely for examining the linear stability of combustion chambers, the subject of Chapter 6.

Now the question is—how can the eigenfunctions, the mode shapes, corresponding to (4.78) be computed. In fact the first order modes have never been computed and are not required if one is satisfied with perturbations to the order carried in (4.78). We return to (4.68) written now for steady waves, with the exponential time dependence; so $p' = \hat{p} e^{-i\bar{a}kt}, \dots$. We also drop the terms h_{00} , h_{20} and h_{30} , giving the equation for \hat{p} :

$$\nabla^2 \hat{p}^{(1)} + k^2 \hat{p}^{(1)} = \varepsilon \hat{h}_{10} + \varepsilon \mu \hat{h}_{11} \quad (4.79)$$

Continuing the iteration procedure, the eigenfunction of zeroth order, ψ_n and its gradient $\nabla \psi_n$ are substituted in the right-hand side wherever p' and \mathbf{u}' appear. Hence (4.79) becomes an inhomogeneous equation with the right-hand side given, say $\mathcal{H}(\mathbf{r})$:

$$\nabla^2 \hat{p}^{(1)} + k^2 \hat{p}^{(1)} = \mathcal{H} \quad (4.80)$$

with

$$\mathcal{H} = \varepsilon \hat{h}_{10} + \varepsilon \mu \hat{h}_{11} \quad (4.81)$$

¹³Here $\bar{a}k$ is the complex frequency in the actual motion, i.e. containing perturbations to first order from the basis (modal) functions.

This equation is most conveniently solved using the Green's function defined in Section 4.1, leading to the solution (4.20), here having the form

$$\hat{p}^{(1)}(\mathbf{r}) = \psi_N(\mathbf{r}) + \sum_{n=0}^{\infty} \frac{\psi_n(\mathbf{r})}{E_n^2(k^2 - k_n^2)} \left\{ \iiint_V \psi_n \mathcal{H} dV + \iint_S \psi_n \mathcal{F}_n dS \right\} \quad (4.82)$$

where \mathcal{F}_n is the boundary condition extracted from (4.67)b consistent with the manner in which (4.67)a was handled,

$$\mathcal{F}_n = \varepsilon \hat{f}_{10} + \varepsilon \mu \hat{f}_{11} \quad (4.83)$$

Although (4.82) seems to satisfy the same boundary conditions as the classical mode shape—because each term contains ψ_n —that is not the case. The reason has to do with the behavior of the infinite series representing the Green's function, equation (4.15). Near the boundary, the function behaves as a delta-function and (4.82) does satisfy the correct boundary condition. The result is not proved here; a good discussion of the matter may be found in Morse and Feshbach (1952). See Annex F for a simpler example.

Finally, the velocity field must be computed to first order by using the linear form of the momentum equation (3.47)b:

$$\bar{\rho} \frac{\partial \mathbf{M}'}{\partial t} + \nabla p' = -\{[\mathbf{M}]\}_1 + \mathbf{F}' \quad (4.84)$$

Again the zeroth order acoustic values are substituted in the right-hand side, and for steady waves, with the mode shape for the pressure given by (4.82), we have for steady waves

$$i\bar{\rho}ak\mathbf{M}'^{(1)} = -\nabla \hat{p}^{(1)} - \varepsilon \mu \{[\hat{\mathbf{M}}]\}_1 + \varepsilon \hat{\mathbf{F}}_{10} + \varepsilon \mu \hat{\mathbf{F}}_{11} \quad (4.85)$$

It is particularly important to notice that **this first order field is in general not irrotational**, possibly the most commonly misunderstood result of the entire procedure developed here. Even though the basis functions used in the zeroth order modal expansion expressed an irrotational field, the field computed to first order may be rotational. Put another way, the approximate procedure proposed and advocated here really does have the potential for handling approximately a wide variety of realistic problems with minimal difficulty. The unspecified function \mathbf{F}' is key in that respect. One has virtually complete freedom in choosing that function. Especially, \mathbf{F}' can be constructed so that \mathbf{M}' satisfies a given boundary condition. For example, one may require that the velocity should be normal to the boundary when there is incoming flow, generally accepted to be the case for a burning solid propellant (Flandro 1995a). This matter will be discussed further in Section 6.9, where some aspects of the 'flow-turning problem' are examined.



CHAPTER □

Some Fundamentals of Acoustics

According to the experiences related in Chapter 1, combustion instabilities may be regarded as unsteady motions closely approximated as classical acoustical motions with perturbations due ultimately to combustion processes. That view, initially an empirical conclusion, motivated the general form of the analytical framework constructed in Chapter 4. Relatively little knowledge of classical acoustics is required to understand and apply that construction formally.

However, interpretation of the details of observed behavior, and effective use of the theory to develop accurate representations of actual motions in combustors require firm understanding of the fundamentals of acoustics. The purpose of this chapter is to provide a condensed discussion of the basic parts of the subject most relevant to the main subject of this book. We therefore ignore those processes distinguishing combustion chambers from other acoustical systems, and restrict attention to the Problem O defined in Sections 3.3.3 and 3.4.

5.1. The Linearized Equations of Motion; The Velocity Potential

We will be concerned here with unsteady motions in a pure non-reacting gas at rest. The governing equations are (3.46) for Problem O, Classical Acoustics, leading to the corresponding wave equation and its boundary condition, equations (3.52) with h_O and f_O given by (3.60)a,b for constant average density $\bar{\rho}$ and written with dimensional variables:

$$\begin{aligned} \nabla^2 p' - \frac{1}{\bar{a}^2} \frac{\partial^2 p'}{\partial t^2} &= \nabla \cdot \mathbf{F}' - \frac{1}{\bar{a}^2} \frac{\partial \mathcal{P}'}{\partial t} \\ \hat{\mathbf{n}} \cdot \nabla p' &= -\bar{\rho} \frac{\partial \mathbf{u}'}{\partial t} \cdot \hat{\mathbf{n}} - \mathbf{F}' \cdot \hat{\mathbf{n}} \end{aligned} \quad (5.1)a,b$$

In the absence of condensed material, the definitions (A.34) and (A.58) of the unperturbed functions \mathbf{F} and \mathcal{P} are:

$$\mathbf{F} = \nabla \cdot \overleftrightarrow{\tau}_v + \mathbf{m}_e - \mathbf{u} w_e \quad (5.2)$$

$$\mathcal{P} = \frac{R}{C_v} \left[\overleftrightarrow{\tau}_v \cdot \nabla \cdot \mathbf{u} - \nabla \cdot \mathbf{q} - Q_e \right] + RT w_e \quad (5.3)$$

where

$\overleftrightarrow{\tau}_v$: viscous stress tensor (force/area)

\mathbf{q} : rate of conductive heat transfer (energy/area-s)

\mathbf{m}_e : rate of momentum addition by external sources (mass-velocity/volume-s)

w_e : rate of mass addition by external sources (mass/volume-s)

Q_e : rate of energy addition by external sources (energy/volume-s)

Thus the function \mathbf{F} contains all processes causing changes of momentum of the gas, except for that due to internal pressure differences; and \mathcal{P} represents all sources of energy addition except that due to internal work by the pressure, accounted for by the term $p \nabla \cdot \mathbf{u}$ in equation (A.47). The linearized forms of the

source terms will be constructed as required for specific problems. For most of this chapter we will treat only problems for which h_O and f_O vanish, giving the simplest equations for classical acoustics,

$$\begin{aligned}\nabla^2 p' - \frac{1}{a^2} \frac{\partial^2 p'}{\partial t^2} &= 0 \\ \hat{\mathbf{n}} \cdot \nabla p' &= 0\end{aligned}\quad (5.4)a,b$$

With no sources in the volume or on the boundary, motions exist only for initial value problems in which the pressure and its time derivative are specified at some initial time, t_0 .

In this case, the wave equation is used to describe freely propagating waves following an initial disturbance or, when the boundary condition (5.4)b is enforced, the normal modes for a volume enclosed by a rigid boundary. The condition $\hat{\mathbf{n}} \cdot \nabla p' = 0$ means that the velocity normal to the boundary is zero, because the acoustic velocity is computed from the acoustic momentum (3.46)b written in dimensional form with $\mathcal{F} = 0$:

$$\bar{\rho} \frac{\partial \mathbf{u}'}{\partial t} = -\nabla p' \quad (5.5)$$

so

$$\hat{\mathbf{n}} \cdot \nabla p' = \bar{\rho} \frac{\partial}{\partial t} (\hat{\mathbf{n}} \cdot \mathbf{u}')$$

from which

$$\frac{\partial}{\partial t} (\hat{\mathbf{n}} \cdot \mathbf{u}') = -\frac{1}{\bar{\rho}} \hat{\mathbf{n}} \cdot \nabla p' = 0 \quad (5.6)$$

Hence $\hat{\mathbf{n}} \cdot \mathbf{u}' = 0$ always

We have just derived the equations for classical acoustics by specializing the general equations of unsteady motion. It is also useful to arrive at the same conclusion in a slightly different way, beginning with the equations for inviscid motion in a homogeneous medium:

$$\text{Conservation of Mass:} \quad \frac{\partial \rho}{\partial t} + \nabla \cdot (\rho \mathbf{u}) = 0 \quad (5.7)$$

$$\text{Conservation of Momentum:} \quad \rho \frac{\partial \mathbf{u}}{\partial t} + \rho \mathbf{u} \cdot \nabla \mathbf{u} + \nabla p = 0 \quad (5.8)$$

$$\text{Conservation of Energy:} \quad \rho \frac{\partial}{\partial t} \left(e + \frac{1}{2} u^2 \right) + \rho \mathbf{u} \cdot \nabla \left(e + \frac{1}{2} u^2 \right) + \nabla \cdot (p \mathbf{u}) = 0 \quad (5.9)$$

$$\text{Equation of State:} \quad p = \rho R T \quad (5.10)$$

Remove the kinetic energy from the energy equation by subtracting $\mathbf{u} \cdot \nabla \mathbf{u}$ (momentum equation) to give

$$\rho \frac{De}{Dt} + p \nabla \cdot \mathbf{u} = 0 \quad (5.11)$$

where $\frac{De}{Dt} = \frac{\partial e}{\partial t} + \mathbf{u} \cdot \nabla e$. Because all irreversible processes have been ignored the entropy of a fluid element remains constant, $\frac{Ds}{Dt} = 0$, a result that follows directly by substituting the mass and energy equations in the thermodynamic definition of the entropy of an element:

$$\rho \frac{Ds}{Dt} = \rho \frac{De}{Dt} - \frac{p}{\rho} \frac{D\rho}{Dt} = -p \nabla \cdot \mathbf{u} + \frac{p}{\rho} (\rho \nabla \cdot \mathbf{u}) = 0 \quad (5.12)$$

Taking the density to be a function of pressure and entropy, we can write for an isentropic process

$$d\rho = \left(\frac{\partial \rho}{\partial s} \right)_p ds + \left(\frac{\partial \rho}{\partial p} \right)_s dp = \left(\frac{\partial \rho}{\partial p} \right)_s dp = \frac{1}{a^2} dp \quad (5.13)$$

where

$$a^2 = \left(\frac{\partial \rho}{\partial p} \right)_s \quad (5.14)$$

will turn out to be the speed of propagation of small disturbances, the 'speed of sound'. With this definition, we can rewrite the continuity equation (5.7) for the pressure:

$$\frac{\partial p}{\partial t} + \rho a^2 \nabla \cdot \mathbf{u} + \mathbf{u} \cdot \nabla p = 0 \quad (5.15)$$

This result is quite general: in particular, its derivation did not involve using the special characteristics of a perfect gas.

Alternatively, we may derive this equation for the special case of a perfect gas for which $de = C_v(T)dT$ and the equation of state is (5.10). Add T times (5.7) to C_v^{-1} times (5.11) with $de = C_vdT$; then use (5.10) to find

$$\frac{\partial p}{\partial t} + \left(1 + \frac{R}{C_v} \right) p \nabla \cdot \mathbf{u} + \mathbf{u} \cdot \nabla p = 0 \quad (5.16)$$

But $R = C_p - C_v$, so $R/C_v = \gamma - 1$ for a perfect gas. Comparison of (5.14) and (5.15) gives the formula for the speed of sound in a perfect gas:

$$a^2 = \sqrt{\frac{\gamma p}{\rho}} = \sqrt{\gamma RT} \quad (5.17)$$

For an isentropic process of a perfect gas, equation (5.13) can be integrated,

$$d\rho = a^2 dp = \frac{\rho}{\gamma p} dp$$

which gives

$$p = p_0 \left(\frac{\rho}{\rho_0} \right)^\gamma \quad (5.18)$$

where ρ_0, p_0 are constant reference values.

We may now eliminate the density from the momentum equation (5.8) to find

$$\frac{\partial \mathbf{u}}{\partial t} + \mathbf{u} \cdot \nabla \mathbf{u} + \frac{1}{\rho_0} \left(\frac{p_0}{p} \right)^{1/2} \nabla p = 0 \quad (5.19)$$

Finally, we obtain the wave equation for the pressure by differentiating (5.16) with respect to time and substituting (5.19) and $a^2 = \gamma p/\rho$:

$$\frac{\partial^2 p}{\partial t^2} - a_0^2 \frac{p}{p_0} \nabla \cdot \left[\frac{\nabla p}{(p/p_0)^{1/\gamma}} \right] = \gamma p \nabla \cdot (\mathbf{u} \cdot \nabla \mathbf{u}) - \gamma \frac{\partial p}{\partial t} \nabla \cdot \mathbf{u} - \frac{\partial}{\partial t} (\mathbf{u} \cdot \nabla p) \quad (5.20)$$

The boundary condition is defined by taking the component of (5.19) normal to the boundary:

$$\hat{\mathbf{n}} \cdot \nabla p = - \left(\frac{p}{p_0} \right)^{1/2} \rho_0 \left[\hat{\mathbf{n}} \cdot \frac{\partial \mathbf{u}}{\partial t} + \hat{\mathbf{n}} \cdot \nabla (\mathbf{u} \cdot \nabla \mathbf{u}) \right] \quad (5.21)$$

Equation (5.20) and its boundary condition are easily linearized by assuming that the gas is at rest and that the fluctuations are all of the same order. To second order in the fluctuations we find

$$\begin{aligned} \frac{\partial^2 p'}{\partial t^2} - a_0^2 \nabla^2 p' &= \left\{ p_0 \nabla \cdot (\mathbf{u}' \cdot \nabla \mathbf{u}') - \gamma \frac{\partial p'}{\partial t} \nabla \cdot \mathbf{u}' - \frac{\partial}{\partial t} (\mathbf{u}' \cdot \nabla p') \right\} \\ &\quad + \rho_0 \left\{ (\gamma - 1) \left(\frac{p'}{p_0} \right) \nabla^2 \left(\frac{p'}{p_0} \right) - \left(\nabla \frac{p'}{p_0} \right)^2 \right\} \end{aligned} \quad (5.22)$$

$$\hat{\mathbf{n}} \cdot \nabla p' = -\rho_0 \frac{\partial \mathbf{u}'}{\partial t} \cdot \hat{\mathbf{n}} - \rho_0 \left\{ \frac{1}{\gamma} \left(\frac{p'}{p_0} \right) \frac{\partial \mathbf{u}'}{\partial t} \cdot \hat{\mathbf{n}} + \hat{\mathbf{n}} \cdot (\mathbf{u}' \cdot \nabla \mathbf{u}') \right\} \quad (5.23)$$

Equations (5.4)a,b are recovered when the second order terms are neglected and $\mathbf{u}' \cdot \hat{\mathbf{n}} = 0$.

5.1.1. The Velocity Potential. It is often convenient to introduce scalar and vector potentials Φ and \mathbf{A} from which the velocity is found by differentiation (Bachelor, 1967):

$$\mathbf{u} = -\nabla\Phi + \nabla \times \mathbf{A}$$

With this representation, the dilatation and curl (rotation) of the velocity field are separated:

$$\nabla \cdot \mathbf{u}' = -\nabla^2\Phi; \quad \nabla \times \mathbf{u}' = \nabla \times \nabla \times \mathbf{A} \quad (5.24)$$

In general, both potentials are required if the mean velocity is non-zero or sources are present in the flow. The boundary conditions may also induce non-zero rotational flow. Here only the scalar potential is required for small amplitude motions because in that limit, the classical acoustic momentum is (5.5); taking the curl with uniform average density gives

$$\bar{\rho} \frac{\partial}{\partial t} (\nabla \times \mathbf{u}') = -\nabla \times (\nabla p') = 0$$

Hence if $\nabla \times \mathbf{u}' = 0$ initially, it remains so and we can take $\mathbf{A} = 0$.

The acoustic equations for momentum, (3.46)b and (3.46)d in dimensional variables with $\mathbf{F}' = \mathbf{P}' = 0$ are

$$\begin{aligned} \frac{\partial \mathbf{u}'}{\partial t} + \frac{1}{\bar{\rho}} \nabla p' &= 0 \\ \frac{\partial p'}{\partial t} + \gamma \bar{\rho} \nabla \cdot \mathbf{u}' &= 0 \end{aligned} \quad (5.25)a,b$$

Differentiate the first with respect to time and insert the second to give the wave equation for the velocity fluctuation,

$$\frac{\partial^2 \mathbf{u}'}{\partial t^2} - \bar{a}^2 \nabla^2 \mathbf{u} = 0 \quad (5.26)$$

Now substitute $\mathbf{u}' = -\nabla\Phi$ to give

$$\nabla \left[\frac{\partial^2 \Phi}{\partial t^2} - \bar{a}^2 \nabla^2 \Phi \right] = 0$$

which is satisfied if the terms in brackets are a function of time only, so

$$\frac{\partial^2 \Phi}{\partial t^2} - \bar{a}^2 \nabla^2 \Phi = f(t) \quad (5.27)$$

The right-hand side represents a source field for the potential, uniform over all space. We may absorb $f(t)$ by defining a new potential $\Phi_1 = \Phi + \int^t dt' \int^{t'} f(t_1) dt_1$ and relabel $\Phi_1 \rightarrow \Phi$ to find¹ the wave equation for Φ :

$$\frac{\partial^2 \Phi}{\partial t^2} - \bar{a}^2 \nabla^2 \Phi = 0 \quad (5.28)$$

¹ Alternatively, one can reason that when the velocity is found by taking the gradient of $\Phi + \int \int f$, the term in f contributes nothing and hence can be simply dropped. The desired solution is unaffected by setting $f = 0$.

When the velocity potential is used, the acoustic velocity is calculated with $\mathbf{A} = 0$

$$\mathbf{u}' = -\nabla\Phi \quad (5.29)$$

The acoustic pressure is found by setting $\mathbf{u}' = -\nabla\Phi$ in the momentum equation (5.25)a, giving

$$\nabla \left(-\frac{\partial\Phi}{\partial t} + \frac{1}{\bar{\rho}} p' \right) = 0$$

This solution is satisfied if the terms in parentheses are a function of t only, $g(t)$, so

$$p' = \bar{\rho} \left(\frac{\partial\Phi}{\partial t} + g(t) \right) \quad (5.30)$$

As above, we may define a new potential $\Phi(t) + \int^t g(t')dt' = \Phi_1(t)$ and hence absorb $g(t)$ so we may redefine $\Phi_1 \rightarrow \Phi$ and

$$p' = \bar{\rho} \frac{\partial\Phi}{\partial t} \quad (5.31)$$

The conditions under which the acoustic field can be completely described by a velocity potential alone are precise and, so far as problems involving combustion are concerned, very restrictive. Any analysis or theory based on the velocity potential alone must also include demonstration that the vector potential can be ignored, i.e. set equal to a constant or zero. In general, the presence of a non-uniform mean flow field and various kinds of sources in the problems we are concerned with in this work, require that the velocity field be derived from both scalar and vector potentials. Use of the unsteady pressure as the primary flow variable provides a simpler approach for many purposes, but, as we will find later, apparently possesses unavoidable fundamental limitations.

5.2. Elementary Solutions to the Linear Wave Equation

The basic property of linear problems is that the principle of superposition applies. Solutions for complicated problems can often be constructed by superposing elementary solutions. Probably the most serious practical difficulty in the use of most methods of solution arises with the need to find solutions for volumes and boundaries not being simple shapes. Hence the basic solutions discussed briefly in this section are rarely usable directly. However, with their simplicity comes the opportunity to understand certain properties of wave motions generally.

5.2.1. Plane Waves. Choose x to be the direction of propagation. Hence the wave fronts, or planes of constant phase, are normal to the x-axis. The wave equation is

$$\frac{\partial^2 p'}{\partial t^2} - \bar{a}^2 \frac{\partial^2 p'}{\partial x^2} = 0 \quad (5.32)$$

which can be factored in the form when \bar{a} is constant,

$$\left(\frac{\partial}{\partial t} + \bar{a} \frac{\partial}{\partial x} \right) \left(\frac{\partial}{\partial t} - \bar{a} \frac{\partial}{\partial x} \right) p' = 0 \quad (5.33)$$

A general solution has the form

$$p'(x; t) = f(x + \bar{a}t) + g(x - \bar{a}t) \quad (5.34)$$

where:

$f(x + \bar{a}t)$ represents a wave traveling to the *left*

$g(x - \bar{a}t)$ represents a wave traveling to the *right*

The density follows from the linear relation for small amplitude isentropic motions,

$$\rho' = \frac{\bar{p} p'}{\gamma \bar{p}} = \frac{1}{\bar{a}^2} [f(x + \bar{a}t) + g(x - \bar{a}t)] \quad (5.35)$$

and the velocity follows upon integration of the linear momentum equation:

$$\frac{\partial u'}{\partial x} = -\frac{1}{\gamma \bar{p}} \frac{\partial p'}{\partial x} = \frac{\bar{a}}{\gamma \bar{p}^2} [f'(x + \bar{a}t) - g'(x - \bar{a}t)] \quad (5.36)$$

Hence

$$u' = -\frac{\bar{a}}{\gamma \bar{p}} [f(x + \bar{a}t) + g(x - \bar{a}t)] \quad (5.37)$$

The important relations follow from comparison of (5.34) and (5.37):

$$\begin{aligned} \text{For a wave traveling to the right: } u' &= \frac{p'}{\bar{\rho} \bar{a}} \\ \text{For a wave traveling to the left: } u' &= -\frac{p'}{\bar{\rho} \bar{a}} \end{aligned} \quad (5.38)\text{a,b}$$

Interpretation of these formulas is easily established by considering a compressive wave, an abrupt increase of pressure. If the front travels to the right into a gas at rest, u' is positive, i.e. to the right. Due to the acceleration of gas by the rising pressure, the motion of the gas is in the same direction as the progression of the front. Thus, a compressive disturbance traveling to the left is followed by leftward motion of the gas. Similarly, (5.38) show that an expansion or rarefaction disturbance produces motion of the gas opposite to that of the wave.

The initial value problem illustrates well the use of the general solution (5.34).

Problem: Find the subsequent motion given the initial conditions on the distribution of pressure and its rate of change:

$$\begin{aligned} p'(x; 0) &= P(x) \\ \frac{\partial p'}{\partial t}(x; 0) &= Q(x) \quad (t = 0) \end{aligned} \quad (5.39)\text{a,b}$$

Solution to the problem means finding the functions $f(x + \bar{a}t)$ and $g(x - \bar{a}t)$ by applying (5.39) to (5.34) to give

$$\begin{aligned} f(x) + g(x) &= P(x) \\ \bar{a} [f'(x) - g'(x)] &= Q(x) \end{aligned} \quad (5.40)$$

Simple manipulation (see, for example, Sneddon 1957) leads to

$$p'(x; t) = \frac{1}{2} [P(x + \bar{a}t) + P(x - \bar{a}t)] + \frac{1}{2\bar{a}} \int_{x - \bar{a}t}^{x + \bar{a}t} Q(\xi) d\xi \quad (5.41)$$

This result is a general solution to the initial value problem. As an illustration, consider an initial stationary pulse of pressure, so $\partial p / \partial t = 0$, Figure 5.1. Because of the pressure differences on both edges, for $t > 0$, the pulse splits into two pulses traveling to the left and right, each having amplitude equal to half the initial amplitude. Both the pressure and velocity disturbances are non-zero within the pulses and zero outside.

For applications to waves in a chamber, the ability to satisfy boundary conditions is essential. The solution (5.34), for example, can be used to represent incidence and reflection from a planar surface bounding a semi-infinite space and an initial rectangular pulse, Figure 5.2. Now the initial condition is (5.39) with

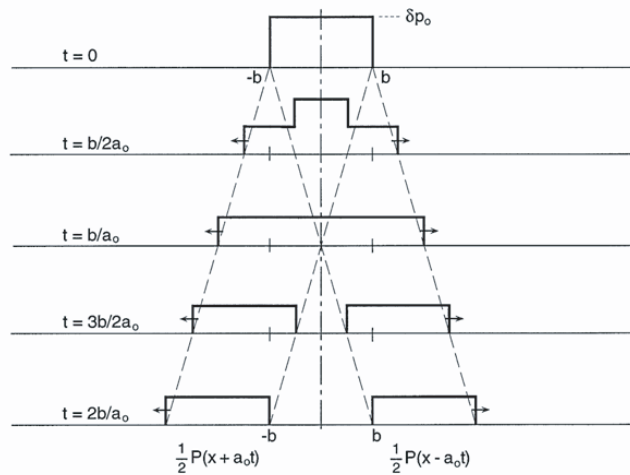


FIGURE 5.1. Wave motions subsequent to an initial pressure pulse at rest.

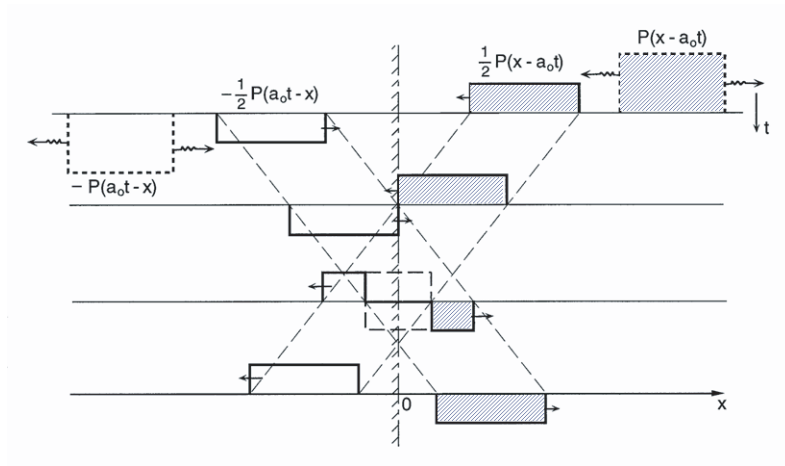


FIGURE 5.2. Reflection of a pressure pulse from a rigid surface.

$Q = 0$ and $P(x; 0)$ representing a rectangular pulse located some distance to the right of the surface at $x = 0$. The solution (5.41) must satisfy the boundary condition at $x = 0$ for all times:

$$\begin{aligned} p'(0; t) &= 0 \\ \frac{\partial p'}{\partial t}(0; t) &= 0 \quad (x = 0; t \geq 0) \end{aligned} \tag{5.42}$$

Note that the ‘surface’ here is not a physically rigid surface but has been chosen as a convenience to require that the pressure disturbance always vanish there. The solution (see Sneddon 1957) is

$$p'(x; t) = \begin{cases} \frac{1}{2} [P(x + \bar{a}t) + P(x - \bar{a}t)] & x \geq \bar{a}t \\ \frac{1}{2} [P(x + \bar{a}t) - P(x - \bar{a}t)] & x \leq \bar{a}t \end{cases} \tag{5.43}$$

This result represents the wave system arising, the splitting of the initial pulse and its image system in the space to the left of $x = 0$. Thus the formalism has led to a special case of the method of images. The behavior of pulses in a combustor is a practical application of this method.

5.2.2. Spherical Waves. Although it is often helpful to regard processes generating pressure waves as distributions of point sources, we will rarely use this point of view explicitly, because we will usually deal directly with continuous distributions (the functions h introduced Section 3.4). Nevertheless it is important to understand the fundamental differences between elementary planar and spherical waves. The wave equation for spherical waves is (5.4)a written in spherical coordinates with no dependence on the polar and azimuthal angles (e.g. see Sneddon 1957, Landau and Lifschitz 1959, and many other standard references):

$$\frac{\partial^2 p'}{\partial t^2} - \bar{a}^2 \frac{1}{r^2} \left(r^2 \frac{\partial p'}{\partial r} \right) = 0 \quad (5.44)$$

This equation is transformed to the equation for planar waves by writing p' as

$$p'(r; t) = \frac{1}{r} \psi(r; t) \quad (5.45)$$

Then (5.44) becomes

$$\frac{\partial^2 \psi}{\partial t^2} - \bar{a}^2 \frac{\partial^2 \psi}{\partial r^2} = 0 \quad (5.46)$$

Hence a general solution for the pressure has the form

$$p'(r; t) = \frac{1}{r} [F(\bar{a}t + r) + G(\bar{a}t - r)] \quad (5.47)$$

where:

$F(\bar{a}t + r)$ represents an inward traveling wave

$G(\bar{a}t - r)$ represents an outward traveling wave

Corresponding to the initial value problem solved in the preceding section, we seek a solution subject to the initial conditions:

$$\begin{aligned} p'(r; 0) &= V(r) \\ \frac{\partial p'}{\partial t}(r; 0) &= W(r) \quad (t = 0, \text{ all } r) \end{aligned} \quad (5.48)$$

We required p' to be finite at the origin, $r = 0$, so

$$\begin{aligned} [p'(r; t)]_{r \rightarrow 0} &= \lim_{r \rightarrow 0} \frac{1}{r} [F(\bar{a}t + r) + G(\bar{a}t - r)] < \infty \\ &= \lim_{r \rightarrow 0} \frac{1}{r} [F(\bar{a}t) + G(\bar{a}t)] < \infty \end{aligned}$$

This condition is satisfied only if

$$G(\xi) = -F(\xi)$$

and the general solution takes the form

$$p'(r; t) = \frac{1}{r} [F(\bar{a}t + r) + F(\bar{a}t - r)] \quad (5.49)$$

To satisfy the initial conditions (5.48) the function $F(\xi)$ must satisfy the two equations

$$\begin{aligned} F(\xi) - F(-\xi) &= \xi V(\xi) \\ F'(\xi) - F'(-\xi) &= \frac{1}{\bar{a}} \xi W(\xi) \end{aligned} \quad (5.50)a,b$$

If the medium is initially at rest everywhere, then $W = 0$. Corresponding to (5.43), the solution for spherical waves is

$$p'(r; t) = \frac{1}{2r} \begin{cases} (\bar{a}t + r)V(\bar{a}t + r) - (\bar{a}t - r)V(\bar{a}t - r) & (r < \bar{a}t) \\ (\bar{a}t + r)V(\bar{a}t + r) + (r - \bar{a}t)V(r - \bar{a}t) & (r > \bar{a}t) \end{cases} \quad (5.51)$$

For example, suppose that a small spherical region of radius r_0 about the origin has uniform increased pressure δp initially, so

$$V(\xi) = \begin{cases} \delta p & 0 < \xi \leq r_0 \\ 0 & r_0 < \xi \end{cases}$$

Then (5.51) gives

$$p'(r; t) = \frac{1}{2r}(\bar{a}t - r) \times \begin{cases} \delta p & 0 < (\bar{a}t - r) \leq r_0 \\ 0 & (\bar{a}t - r) < \xi \end{cases} \quad (5.52)$$

$$p'(r; t) = -\frac{1}{2r}(r - \bar{a}t) \times \begin{cases} \delta p & 0 < (r - \bar{a}t) \leq r_0 \\ 0 & (r - \bar{a}t) < \xi \end{cases}$$

In Figure 5.3 this result is compared with the corresponding result for the rightward traveling wave generated by an initially pressurized region at the origin. The spherical wave propagating outward consists of a triangular compressive wave followed immediately by a triangular rarefaction wave. The rarefaction is generated by reflection at the origin of the compressive wave propagating inward from the initially pressurized region. That inward traveling wave is the counterpart of the leftward traveling wave not shown here, for the planar case. Upon reflection at the origin, the compressive wave becomes a rarefaction wave, as for the reflection of planar waves illustrated in Figure 5.2.

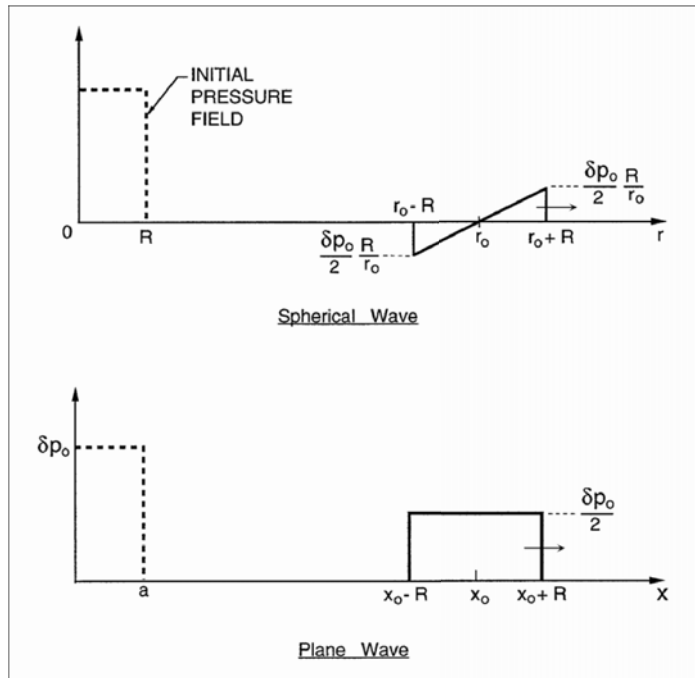


FIGURE 5.3. Comparison of spherical and planar waves produced by regions of increased pressure.

5.2.3. Cylindrical Waves. Cylindrical waves possess a special peculiarity: They always have a wake. The reason can be seen from Figure 5.4 showing the way in which spherical, planar and cylindrical waves are produced by point sources. The solid concentric circles represent wavefronts generated by sequences of infinitesimally short pulses. A single point source generates purely circular fronts in three-dimensions. An infinite flat sheet of uniformly and continuously distributed point sources emitting in phase produces planar waves.

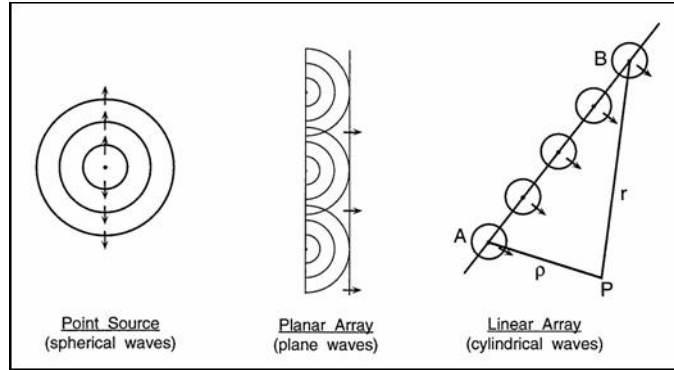


FIGURE 5.4. Generation of spherical, planar and cylindrical waves by point sources.

Cylindrical waves are generated by an infinite linear array of point sources. When an observation is made, the first disturbance observed is that emitted by the closest point on the line. But no matter where the observer is located, signals arrive at all times, the later signals arriving from sources further away in the line. The pressure at an observation point is computed by superposing the signals from the entire linear array:

$$p'(\rho; t) = \int_{-\infty}^{\infty} \frac{G(\bar{a}t - r)}{r} dz \quad (5.53)$$

where ρ , r , and z are defined in the sketch. With $r^2 = \rho^2 + z^2$ and setting $\xi = \bar{a}t - r$, $d\xi = -dr$, the integral can be rewritten to give

$$p'(\rho, t) = 2 \int_{-\infty}^{\infty} \frac{G(\xi) d\xi}{\sqrt{(\xi - \bar{a}t)^2 + \rho^2}} \quad (5.54)$$

For large t ,

$$p'(\rho, t \rightarrow \infty) \rightarrow \frac{1}{\bar{a}t} \int_{\xi_0}^{\xi_0 - \bar{a}t} G(\xi) d\xi \quad (\xi_0 < \xi < \xi_0 + \delta\xi) \quad (5.55)$$

Hence the observed signal for a cylindrical wave can never be discrete: there is always a 'wake'. Morse and Feshbach (1952) and Morse and Ingard (1968) give extended discussions, including solutions to the wave equation for cylindrical waves.

5.3. An Estimate of the Influence of Internal Heat Conduction on the Propagation of Acoustic Waves

Acoustic waves impress gradients of velocity and temperature on the medium, therefore inducing viscous stresses and heat conduction. Those processes necessarily cause dissipation of mechanical energy, the waves

decay in space and time, and the entropy of the medium increases. However, for many purposes and over broad ranges of conditions we may neglect those dissipative influences. The purpose of this section is to discuss one simple way to estimate the effects of heat conduction on steady sinusoidal waves. The effects of internal viscous stresses may be treated in similar fashion.

With Fick's law for heat conduction, the linearized term $\nabla \cdot \mathbf{q}'$ in (5.3) is

$$\nabla \cdot \mathbf{q}' = \nabla \cdot (-\lambda \nabla T')$$

For one-dimensional motions along the x-axis, and constant coefficient of heat conduction, λ_c , we have

$$\nabla \cdot \mathbf{q}' = -\lambda_c \frac{\partial^2 T'}{\partial x^2} \quad (5.56)$$

The linearized form of the energy equation 3.41 is therefore

$$\bar{\rho} C_v \frac{\partial T'}{\partial t} + \bar{p} \frac{\partial u'}{\partial x} = \lambda_c \frac{\partial^2 u'}{\partial t^2} \quad (5.57)$$

With \mathcal{W}' , $\mathbf{F}' = 0$ and in dimensional form, the acoustic continuity and momentum equations (3.40) and (3.41) for one-dimensional motions in a source-free medium at rest are:

$$\begin{aligned} \frac{\partial \rho'}{\partial t} + \bar{\rho} \frac{\partial u'}{\partial x} &= 0 \\ \bar{\rho} \frac{\partial u'}{\partial t} + \frac{\partial p'}{\partial x} &= 0 \end{aligned} \quad (5.58)a,b$$

Substitute (5.58) in (5.57) to give

$$\bar{\rho} C_v \frac{\partial T'}{\partial t} - \lambda_c \frac{\partial^2 T'}{\partial x^2} - \frac{\bar{p}}{\bar{\rho}} \frac{\partial \rho'}{\partial x} = 0 \quad (5.59)$$

Because energy is dissipated, the motions are not isentropic so we cannot assume $p' \sim \rho'$. However we can eliminate the pressure as a dependent variable by taking it as a function of density and temperature, and writing

$$p' = \left(\frac{\partial p}{\partial \rho} \right)_T \rho' + \left(\frac{\partial p}{\partial T} \right)_\rho T' \quad (5.60)$$

Now combine (5.58)a with (5.60) to form a second equation in the density and temperature fluctuations:

$$\frac{\partial^2 \rho'}{\partial t^2} - \left(\frac{\partial p}{\partial \rho} \right)_T \frac{\partial^2 \rho'}{\partial x^2} - \left(\frac{\partial p}{\partial T} \right)_\rho \frac{\partial^2 T'}{\partial x^2} = 0 \quad (5.61)$$

To illustrate the point, it is simplest to consider the case of sinusoidal traveling waves, for which the fluctuations are²

$$\rho' = \hat{\rho} e^{i(kx - \omega t)} ; \quad T' = \hat{T} e^{i(kx - \omega t)} \quad (5.62)$$

and k is the wavenumber. In general, k and ω are complex quantities. Substitution in (5.59) and (5.61) gives the pair of simultaneous algebraic equations

$$\begin{aligned} \left[i\omega + \frac{\lambda_c}{\bar{\rho} C_v} k^2 \right] \hat{T} - i \left[\frac{\bar{p}}{\bar{\rho}^2 C_v} k^2 \right] \hat{\rho} &= 0 \\ \left[k^2 \left(\frac{\partial p}{\partial T} \right)_{\bar{\rho}} \right] \hat{T} - \left[\omega^2 - k^2 \left(\frac{\partial p}{\partial \rho} \right)_{\bar{T}} \right] \hat{\rho} &= 0 \end{aligned} \quad (5.63)$$

²We will consistently use $e^{-i\omega t}$ for harmonic time dependence. Thus sinusoidal wave traveling to the right, in the positive x-direction, will have the form $e^{i(kx - \omega t)}$, a function of $kx - \omega t = k(x - \bar{a}t)$, as suggested by (5.34).

Non-trivial solutions exist for \hat{T} and $\hat{\rho}$ only if the determinant of coefficients vanishes, giving the dispersion relation

$$i \left\{ k^2 \left[\left(\frac{\partial p}{\partial \rho} \right)_{\bar{T}} + \frac{\bar{p}}{\bar{\rho}^2 C_v} \left(\frac{\partial p}{\partial T} \right)_{\bar{\rho}} \right] - \omega^2 \right\} + \frac{\lambda_c}{\bar{\rho} C_v} \frac{k^2}{\omega} \left\{ k^2 \left(\frac{\partial p}{\partial \rho} \right)_{\bar{T}} - \omega^2 \right\} = 0 \quad (5.64)$$

To interpret this result, imagine that plane waves traveling according to (5.62) are generated by an oscillating boundary perpendicular to the x -axis, at $x = 0$. Therefore we take the frequency ω to be real and given. Solution to (5.64) will give the real and imaginary parts of k^2 and hence of k , say $k = k_r + ik_i$. Then the spatial part of the exponentials in (5.63) become

$$e^{ikx} = e^{ik_r x} e^{-k_i x}$$

Consequently, k_i^{-1} is the characteristic length for propagation in space: the amplitude of the traveling wave is reduced to $1/e$ of its initial value after traveling a distance $x = k_i$. Planes of constant phase travel with the speed of sound, the ‘phase velocity’ in this case, and the real part of k is related to the frequency and wavelength λ by:

$$k_r = \frac{\bar{a}}{\omega} = \frac{2\pi}{\lambda} \quad (5.65)$$

If heat conduction is ignored, $\lambda_c = 0$ and, because ω is real, so also is the wavenumber,

$$k = \omega \left[\left(\frac{\partial p}{\partial \rho} \right)_{\bar{T}} + \frac{\bar{p}}{\bar{\rho}^2 C_v} \left(\frac{\partial p}{\partial T} \right)_{\bar{\rho}} \right]^{-1/2} \quad (5.66)$$

Thus the waves travel with unchanging amplitude and wavelength.

Rather than examine the behavior when heat conduction is not ignored, let us determine the conditions under which its influence is negligibly small. We can estimate the conditions by requiring that the term representing heat conduction on the right-hand side of (5.57) should be much smaller than, say, the first term on the left-hand side:

$$\lambda_c \frac{\partial^2 \hat{T}'}{\partial x^2} \ll \bar{\rho} C_v \frac{\partial T'}{\partial t}$$

or, with (5.62),

$$|\lambda_c (-k^2) \hat{T}| \ll |\bar{\rho} C_v (i\omega) \hat{T}|$$

Hence we require

$$\left(\frac{\lambda_c}{\bar{\rho} C_v} \right) \frac{|k|^2}{\omega} \ll 1 \quad (5.67)$$

If this condition is satisfied, then the real part of (5.64) is negligibly small, holds, and the speed of sound is

$$\bar{a} = \frac{\omega}{k} = \left(\frac{\partial p}{\partial \rho} \right)_{\bar{T}} + \frac{\bar{p}}{\bar{\rho}^2 C_v} \left(\frac{\partial p}{\partial T} \right)_{\bar{\rho}} \quad \left(\frac{\lambda_c}{\bar{\rho} C_v} \frac{|k|^2}{\omega} \rightarrow 0 \right) \quad (5.68)$$

Thermodynamics for a two-state system gives the result

$$\left(\frac{\partial p}{\partial \rho} \right)_{\bar{s}} = \left(\frac{\partial p}{\partial \rho} \right)_{\bar{T}} + \left(\frac{\partial p}{\partial T} \right)_{\bar{\rho}} \left(\frac{\partial T}{\partial \rho} \right)_{\bar{s}} = \left(\frac{\partial p}{\partial \rho} \right)_{\bar{T}} + \frac{\bar{p}}{\bar{\rho} C_v} \left(\frac{\partial p}{\partial T} \right)_{\bar{\rho}}$$

so

$$\bar{a} = \sqrt{\left(\frac{\partial p}{\partial \rho} \right)_{\bar{s}}} = \sqrt{\gamma R \bar{T}} \left(\frac{\lambda_c}{\bar{\rho} C_v} \frac{|k|^2}{\omega} \rightarrow 0 \right) \quad (5.69)$$

for negligible internal heat conduction and isentropic flow.

For the inverse limit when $\frac{\lambda_c}{\bar{\rho}C_v} \frac{|k|^2}{\omega}$ is indefinitely large, (5.64) gives

$$\bar{a} = \frac{\omega}{k} = \sqrt{\left(\frac{\partial p}{\partial \rho}\right)_{\bar{T}}} = \sqrt{\gamma R \bar{T}} \quad \left(\frac{\bar{\rho}C_v}{\lambda_c} \frac{\omega}{|k|} \rightarrow 0\right) \quad (5.70)$$

for a perfect gas. This is the limit for infinitely fast internal heat conduction, so the process of sound propagation is isothermal.

To be specific, consider sound waves in air at ambient conditions:

$$\begin{aligned} \lambda_c &= 0.73 \times 10^4 & \frac{\text{cal}}{\text{g}^{-\circ}\text{K}} & \bar{a} = 3 \times 10^4 & \frac{\text{cm}}{\text{s}} \\ \bar{\rho} &= 1.2 \times 10^{-2} & \frac{\text{g}}{\text{cm}^3} & C_v = 0.17 & \frac{\text{cal}}{\text{g}^{-\circ}\text{K}} \end{aligned}$$

Hence

$$\left(\frac{\lambda_c}{\bar{\rho}C_v}\right) \frac{|k|^2}{\omega} = \frac{\lambda_c}{\bar{\rho}C_v \bar{a}^2} \omega = 4 \times 10^{-10} \omega$$

which is less than .01 for $\omega < 25 \times 10^6 \text{ s}^{-1}$. This result confirms, and explains, the familiar fact that acoustic waves in the audio range $10\text{--}20,000 \text{ s}^{-1}$ propagate isentropically under everyday circumstances. The influences of viscous stresses can be estimated in a similar manner.

This conclusion also holds for combustion chambers if the amplitudes of waves are not too large. It is a great simplification that we will ignore internal viscous stresses and heat conduction in practically all problems of combustion instabilities. However, if the waves grow to large amplitudes ('large' must be characterized in the particular problem at hand) then the losses—referred to as 'shock losses'—due to viscous stresses and heat conduction may not be negligible. For problems of combustion instabilities, those circumstances are more likely to arise in combustors having higher densities of energy release, notably liquid and solid rockets.

5.4. Energy and Intensity Associated with Acoustic Waves

In this section we establish definitions of energy density and the intensity—i.e. the flow of energy—for classical acoustic waves. The definitions are only approximate under the more complicated conditions existing in a combustor but the general ideas remain.

Following Landau and Lifschitz (1959) we return to the basic energy equation (5.9) for inviscid flow. The idea is to establish a connection between the rate of change of something (the energy) within a volume and the flow of something (the intensity) through the closed boundary of that volume. Integrate the energy equation over a volume fixed in space; and apply Gauss' theorem to the terms on the right-hand side:

$$\begin{aligned} \frac{\partial}{\partial t} \int \rho \left(e + \frac{u^2}{2} \right) dV &= - \int \nabla \cdot \left[\rho \mathbf{u} \left(e + \frac{u^2}{2} \right) \right] dV - \int \nabla \cdot (\rho \mathbf{u}) dV \\ &= - \oint \left(e + \frac{u^2}{2} \right) \rho \mathbf{u} \cdot d\mathbf{S} - \oint \rho \mathbf{u} \cdot d\mathbf{S} \end{aligned}$$

This relation must be written to second order in the isentropic fluctuations; for example,

$$\begin{aligned} \rho e &= \bar{\rho} \bar{e} + \rho' \left[\frac{\partial}{\partial \rho} (\rho e) \right]_{\bar{\rho}} + \frac{1}{2} \rho'^2 \left[\frac{\partial^2 (\rho e)}{\partial \rho^2} \right]_{\bar{\rho}} + \dots \\ &= \bar{\rho} \bar{e} + \rho' \bar{k} + \frac{1}{2} \frac{\rho'^2}{\bar{\rho} \bar{a}^2} + \dots \end{aligned}$$

SOME FUNDAMENTALS OF ACOUSTICS

Eventually the result is

$$\frac{\partial}{\partial t} \int \varepsilon dV = - \oint \varepsilon \mathbf{u} \cdot d\mathbf{S} - \oint p' \mathbf{u}' \cdot d\mathbf{S} \quad (5.71)$$

where

$$\varepsilon = \frac{1}{2} \frac{p'^2}{\bar{\rho} a^2} + \frac{1}{2} \bar{\rho} \mathbf{u}'^2 \quad (5.72)$$

is the *acoustic energy per unit volume* and $p' \mathbf{u}'$ is the *intensity*, the flux of acoustic energy through an area normal to the direction of propagation (energy/area-s).

The first term on the right-hand side of (5.71) is third order in the fluctuations and must be dropped. Hence we have the important result interpreted in Figure 5.5.

$$\frac{\partial \varepsilon}{\partial t} + \nabla \cdot (p' \mathbf{u}') = 0 \quad (5.73)$$

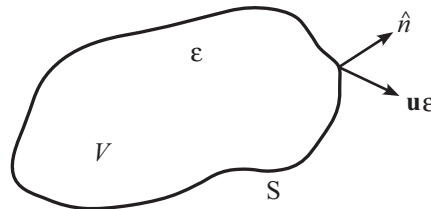


FIGURE 5.5. Acoustic energy and intensity.

Table 5.1 summarizes the basic properties of plane sinusoidal waves. Brackets $\langle \rangle$ denote time averages over some interval τ ; for any scalar function ψ , its time average is

$$\langle \psi \rangle = \frac{1}{\tau} \int_t^{t+\tau} \psi dt'$$

The dimensions of intensity are energy/sec.-area. Physical devices, such as piezoelectric microphones, can be built to measure intensity directly: the output, in volts, say, is proportional to the intensity of a wave incident upon the sensitive element. But the response of the human ear is not linear with intensity; the output (i.e., what one “hears”) is more closely proportional to the logarithm of intensity. That is, what seems to be a doubling of “loudness” corresponds to a ten-fold increase of intensity. To avoid use of large numbers, it has therefore become the practice to use a logarithmic scale for expressing acoustic energies and intensities.

A sound wave is one decibel more intense if its intensity is increased by $\sqrt[10]{10}$. The difference of level for two sound waves, in decibels, is defined to be

$$dB = 10 \log_{10} \left(\frac{I_2}{I_1} \right) \quad (\text{difference in level}) \quad (5.74)$$

It is conventional to choose as an absolute basis the intensity of a wave which is barely audible at 1000 Hz. The rms amplitude of such a wave is

$$dB = 10 \log_{10} \left(\frac{I}{I_0} \right) \quad (\text{level})$$

where

$$I_0 = \frac{(2 \times 10^{-4})^2}{\rho_0 a_0} .$$

Thus,

$$\text{dB} = 20 \log \frac{p_{\text{rms}}}{2 \times 10^{-4}} = 74 + 20 \log_{p_{\text{rms}}} \quad (5.75)$$

With the numbers given above, the relation between dB and pressure is shown in Figure 5.6.

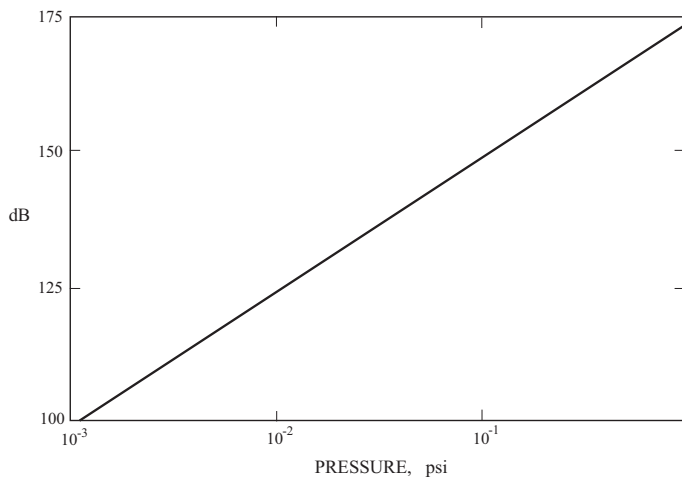


FIGURE 5.6. A graph of decibels versus pressure (lbs./in²).

Finally it is interesting to see the frequency response for the human ear, sketched below.

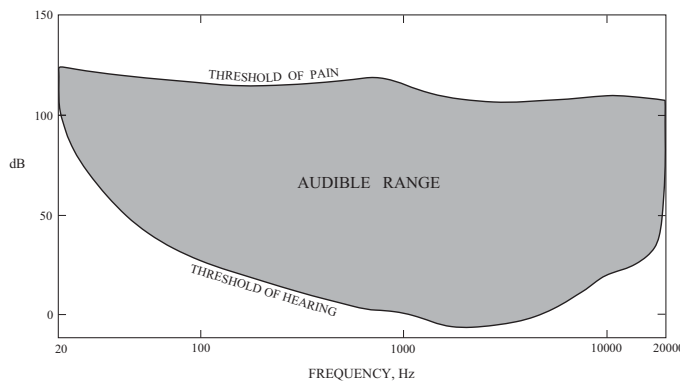


FIGURE 5.7. A graph showing the audible range of hearing for a typical human subject (adapted from Morse 1948).

Note that $1 \text{ dyne/cm}^2 = 74 \text{ dB}$ and one atmosphere is 10^6 dynes/cm^2 . From these two figures it is clear that any steady wave which can be heard without pain has a sufficiently small amplitude that linearization of the equations of motion is reasonable.

TABLE 5.1. Results for Rightward and Leftward Traveling Sinusoidal Waves.

Wave to Right	Wave to Left
$p'_+ = \hat{p}_+ e^{-i(\omega t - kx)}$	$p'_- = \hat{p}_- e^{-i(\omega t + kx)}$
$u'_+ = \hat{p}_+ e^{-i(\omega t - kx)}$	$u'_- = \hat{u}_- e^{-i(\omega t + kx)}$
$\hat{u}_+ = \frac{\hat{p}_+}{\rho_0 a_0}$	$\hat{u}_- = -\frac{\hat{p}_-}{\rho_0 a_0}$
$\varepsilon_+ = \frac{p'^2_+}{\rho_0 a_0}$	$\varepsilon_- = \frac{p'^2_-}{\rho_0 a_0}$
$l_+ = p'_+ u'_+ = \frac{p'^2_+}{\rho_0 a_0}$	$l_- = p'_- u'_- = -\frac{p'^2_-}{\rho_0 a_0^2}$
$\langle (\quad) \rangle = \frac{1}{\tau} \int_t^{t+\tau} (\quad) dt'$	
$\langle p'^2_+ \rangle = \frac{1}{2} \hat{p}_+^2$	$\langle p'^2_- \rangle = \frac{1}{2} \hat{p}_-^2$
$\langle \varepsilon_+ \rangle = \frac{\hat{p}_+^2}{2\rho_0 a_0^2}$	$\langle \varepsilon_- \rangle = \frac{\hat{p}_-^2}{2\rho_0 a_0^2}$
$\langle l_+ \rangle = \frac{\hat{p}_+^2}{2\rho_0 a_0}$	$\langle l_- \rangle = \frac{p_-^2}{2\rho_0 a_0}$
More generally: $p' = \hat{p} e^{-i(\omega t + \varphi)}$; $\bar{u}' = \hat{\mathbf{u}} e^{-i(\omega t + \psi)}$	
$\langle \varepsilon \rangle = \frac{1}{4} \left[\frac{ \hat{p} ^2}{\rho_0 a_0^2} + \rho_0 \hat{u} ^2 \right] = \frac{1}{4} (p'^* p' + \rho_0 \mathbf{u}' \cdot \mathbf{u}'^*)$	
$\langle l \rangle = \frac{1}{2} \hat{p} \hat{\mathbf{u}} \cos(\varphi + \psi) = \frac{1}{4} (p'^* \mathbf{u}' + p' \mathbf{u}'^*)$	
where $(\quad)^*$ denotes complex conjugate.	

5.5. The Growth or Decay Constant

In practice, due to natural dissipative processes, freely propagating waves and oscillations in a chamber will decay in space and time if there is no external source or energy. If there is an internal source of energy, waves may be unstable, having amplitudes increasing in time. The basic measure of the growth or decay of waves is the constant appearing in the exponent describing the sinusoidal spatial and temporal dependence of small amplitude waves, the definitions (5.62). For ‘standing’ or ‘stationary’ waves in a chamber, the wavelength, and hence wavenumber, is real and constant, but the frequency is complex:

$$\omega \rightarrow \omega + i\alpha \quad (5.76)$$

and the variables of the motion have the behavior in time

$$e^{-i(\omega+i\alpha)t} \equiv e^{-i\omega t} e^{\alpha t} \quad (5.77)$$

For the definition (5.76), $\alpha < 0$ means that the waves decay.

Normally in practice, $|\frac{\alpha}{\omega}| \ll 1$, implying that the fractional change of amplitude is small in one cycle of the oscillation. Thus when time averaging is carried out over one or a few cycles, $e^{\alpha t}$ may be taken as constant, and the average energy density computed with (5.72) and (5.73), is

$$\langle \varepsilon \rangle = e^{2\alpha t} \frac{1}{4} \left[\frac{|\hat{p}|^2}{\bar{\rho} \bar{a}^2} + \bar{\rho} |\hat{u}|^2 \right] \quad (5.78)$$

Hence we have the important interpretations which serve as the basis for measuring values of α :

$$\begin{aligned} \alpha &= \frac{1}{|\hat{p}|} \frac{d|\hat{p}|}{dt} \\ \alpha &= \frac{1}{2\langle \varepsilon \rangle} \frac{d\langle \varepsilon \rangle}{dt} \end{aligned} \quad (5.79)a,b$$

The sign of α is a matter of definition and has no fundamental significance. Thus, if the time dependence is taken to be $e^{i(\omega+i\alpha)t}$ then $\alpha < 0$ means that waves are amplified.

The formulas (5.79)a,b define local values of the growth constant. It is often more meaningful to know the value for the entire volume of the system in question, found by using $\int \langle \varepsilon \rangle dV$ rather than $\langle \varepsilon \rangle$:

$$\alpha = \frac{1}{2 \int \langle \varepsilon \rangle dV} \frac{d}{dt} \int \langle \varepsilon \rangle dV \quad (5.80)$$

5.6. Boundary Conditions: Reflections from a Surface

In the absence of other sources, the linearized boundary condition on the pressure at a surface is the first term of (5.1), here in dimensional form:

$$\hat{\mathbf{n}} \cdot \nabla p' = -\bar{\rho} \frac{\partial \mathbf{u}'}{\partial t} \cdot \hat{\mathbf{n}} \quad (5.81)$$

The acoustic surface impedance z_a is defined by

$$\mathbf{u}' \cdot \hat{\mathbf{n}} = \frac{1}{z_a} p' \quad (5.82)$$

and the acoustic surface admittance y_a is the reciprocal of the admittance:

$$y_a = \frac{1}{z_a} \quad (5.83)$$

Then for harmonic motions, $p' = \hat{p}e^{-i\omega t}$, we can rewrite (5.81) as

$$\hat{\mathbf{n}} \cdot \nabla p' = -i \frac{\bar{\rho}\omega}{z_a} p' = -i \bar{\rho}\omega y_a p' \quad (5.84)$$

The units of impedance are (pressure/velocity) \equiv (density \times velocity). Hence for the medium, the product $\bar{\rho}\bar{a}$ is called the characteristic impedance, having value 42 g/cm²-s. for air at standard conditions. Dimensionless forms are defined as:

$$\begin{aligned} \text{acoustic impedance ratio:} \quad \zeta_a &= \frac{z_a}{\bar{\rho}\bar{a}} \\ \text{acoustic admittance ratio:} \quad \eta_a &= \frac{1}{\zeta_a} \end{aligned} \quad (5.85)$$

In general, impedance functions are complex; the real and imaginary parts are called:

$$\begin{aligned} Re(z_a) : & \text{ acoustic resistance} \\ Im(z_a) : & \text{ acoustic reactance} \end{aligned} \quad (5.86)$$

From (5.82) and (5.83), the surface admittance is

$$y_a = \frac{\mathbf{u}' \cdot \hat{\mathbf{n}}}{p'}$$

and the dimensionless surface admittance ratio is

$$\eta_a = \bar{\rho} \bar{a} y_a = \frac{\bar{\rho} \bar{a}^2}{\bar{p}} \frac{\mathbf{M}' \cdot \hat{\mathbf{n}}}{p'/\bar{p}} = \gamma \frac{M'_n}{p'/\bar{p}} \quad (5.87)$$

where M'_n is the fluctuation of the Mach number normal to the surface.

If the surface is impermeable, the velocity at the surface is the velocity of the surface itself. However, if the surface is permeable, or, as for a burning propellant, mass departs the surface, then the impedance and admittance functions are defined in terms of the local velocity fluctuations presented³ to the acoustic field, no matter what their origin.

Quite generally then, the admittance function represents the physical response of processes at the surface. It is of course an assumption that in response to an impressed pressure fluctuation, the fluctuation of velocity normal to the surface is proportional to the pressure change. Alternative definitions of quantities representing the acoustic boundary condition at a surface will arise when we consider special situations.

5.6.1. Reflections of Plane Waves at a Surface. Confinement of waves in a chamber to form modes necessarily involves reflections at the boundary surfaces. In solid propellant rockets the processes causing reflection are complicated, being responsible not only for confining the waves but also are the dominant means for transferring energy to the oscillating field in the chamber. Even at inert surfaces, more than the simple process of reflection is involved. Viscous stresses and heat conduction in the region adjacent to a surface cause dissipation of energy, discussed in Section 5.9.

Here we assume that all activity at the surface can be represented by a complex impedance or admittance function. The calculation follows that discussed by Morse and Ingard (1968). We consider reflection of a planar wave, Figure 5.8, allowing for the possibility of unequal angles of incidence and reflection; for simplicity we assume that there is no transmitted wave. The incident wave travels in the direction defined by the unit vector $\hat{\mathbf{k}}_i$ and the wavenumber vector is

$$\mathbf{k} = \frac{2\pi}{\lambda} \hat{\mathbf{k}} \quad (5.88)$$

We can represent the acoustic pressure and velocity in this plane wave by

$$\begin{aligned} p'(\mathbf{r}; t) &= g_i(\mathbf{k}_i \cdot \mathbf{r} - \omega t) \\ \mathbf{u}'(\mathbf{r}; t) &= \frac{\hat{k}_r}{\bar{\rho} \bar{a}} g_i(\mathbf{k}_i \cdot \mathbf{r} - \omega t) \end{aligned} \quad (5.89)a,b$$

Similar formulas hold for the reflected wave with \mathbf{k}_i replaced by \mathbf{k}_r lying in the direction defined by the unit vector $\hat{\mathbf{k}}_r$. The representations are therefore those shown in Table 5.2

Because the frequency is the same for the incident and reflected waves, so are the magnitude of the wavenumber:

$$|\mathbf{k}_i| = \frac{\omega}{\bar{a}} = |\mathbf{k}_r| = k \quad (5.90)$$

³For burning propellants, care must be taken with definition of the surface at which the boundary condition is imposed. Usually the velocity at the 'edge' of the combustion zone in the gas phase is the most convenient choice. Thus the admittance presented to the acoustic field is not precisely that at the burning surface itself.

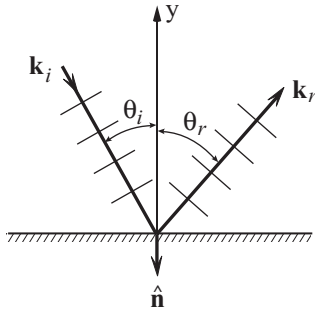


FIGURE 5.8. Reflection of a plane wave.

TABLE 5.2. Some Formulas for Incident and Reflected Plane Waves.

Incident Wave	Reflected Wave
$p'_i = g_i(\xi_i)$	$p'_r = g_r(\xi_r)$
$\mathbf{u}'_i = \hat{\mathbf{k}}_i \frac{1}{\rho a} g_i(\xi_i)$	$\mathbf{u}'_r = \hat{\mathbf{k}}_r \frac{1}{\rho a} g_r(\xi_r)$
$\xi_i = \mathbf{k}_i \cdot \mathbf{r} - \omega t$	$\xi_r = \mathbf{k}_r \cdot \mathbf{r} - \omega t$
$= k(x \sin \theta_i - y \cos \theta_i) - \omega t$	$= k(x \sin \theta_r - y \cos \theta_r) - \omega t$

Reflection is assumed to occur at $y = 0$. By definition of z_a , the surface impedance, with the normal velocity outward from the surface equal to $u'_y = \mathbf{u}' \cdot \hat{\mathbf{j}} = -\mathbf{u}' \cdot \hat{\mathbf{n}}$ where $\hat{\mathbf{n}}$ is the unit outward normal vector:

$$z_a = \left(\frac{p'}{u'_y} \right)_{y=0} = \bar{\rho} \bar{a} \frac{g_i(kx \sin \theta_i - \cot) + g_r(kx \sin \theta_r - \cot)}{\cos \theta_i g_i(kx \sin \theta_i - \cot) - \cos \theta_r g_r(kx \sin \theta_r - \cot)} \quad (5.91)$$

In general z_a is variable along the surface. Suppose that in fact z_a is constant, independent of x . That can be true if

$$\begin{aligned} \theta_i &= \theta_r = \theta \\ g_r(\xi) &= \beta g_i(\xi) \end{aligned} \quad (5.92)$$

Then (5.91) becomes

$$z_a \cos \theta = \bar{\rho} \bar{a} \frac{1 + \beta}{1 - \beta} \quad (5.93)$$

and the complex reflection coefficient β is related to the surface impedance by

$$\beta = \frac{z_a \cos \theta - \bar{\rho} \bar{a}}{z_a \cos \theta + \bar{\rho} \bar{a}} \quad (5.94)$$

This result is special because no transmitted wave has been accounted for. For example, if $z_a = \bar{\rho} \bar{a}$ —perfect impedance matching exists at the interface—(5.93) gives $\beta = 0$ when $\theta = 0$, so there is no reflected wave. That is true in one sense because in physical terms $z_a = \bar{\rho} \bar{a}$ means that the same gas exists in both sides of the interface. Thus we are simply describing wave propagation in a continuous medium. On the other hand,

the physical picture treated here accommodates no transmitted wave, which means that when there is no reflection, processes must exist at the interface providing perfect absorption.

Now suppose $\theta \neq 0$ but $z_a = \bar{\rho}\bar{a}$. Then (5.93) gives β non-zero, i.e. partial absorption, and some of the incident wave is reflected.

5.7. Wave Propagation in Tubes; Normal Modes

The simplest form of combustor is a straight tube, having generally non-uniform cross section and not necessarily axisymmetric. Although the changes of cross section may be abrupt—even discontinuous—experience has shown that good results may be obtained by assuming that the velocity fluctuations are uniform at every section and parallel to the axis: the flow is treated as one-dimensional. The governing equations are given in Annex B, equations (B.2)–(B.4) with no sources:

$$\text{Conservation of mass:} \quad \frac{\partial \rho'}{\partial t} + \frac{1}{S_c} \frac{\partial}{\partial x} (\bar{\rho}u' S_c) = 0 \quad (5.95)$$

$$\text{Conservation of momentum:} \quad \bar{\rho} \frac{\partial u'}{\partial t} + \frac{\partial p'}{\partial x} = 0 \quad (5.96)$$

$$\text{Conservation of energy:} \quad \bar{\rho} C_v \frac{\partial T'}{\partial t} + \bar{p} \frac{1}{S_c} \frac{\partial}{\partial x} (u' S_c) = 0 \quad (5.97)$$

The wave equation for the pressure is:

$$\frac{1}{S_c} \frac{\partial}{\partial x} \left(S_c \frac{\partial p'}{\partial x} \right) - \frac{1}{\bar{a}^2} \frac{\partial^2 p'}{\partial t^2} = 0 \quad (5.98)$$

5.7.1. Waves in Closed Tubes.

(a) Normal Modes for a Tube Closed at Both Ends.

Results for a tube closed at both ends not only contain many ideas basic to general oscillations in chambers, but also are widely useful for practical applications. For a tube closed by rigid walls, the boundary conditions at the ends are that the velocity must vanish. The momentum equation (5.96) then states that acceleration and therefore the pressure gradient must vanish at the ends for all time:

$$\frac{\partial p'}{\partial x} = 0 \quad (x = 0, L ; \text{ all } t) \quad (5.99)$$

General linear motions within the tube can be constructed as superpositions of *normal modes* defined in general by two properties:

- i) sinusoidal variations in time
- ii) the motion at any point bears always a fixed phase relative to that at any other point in the volume

Those conditions imply here that the pressure can be expressed as

$$p'(x; t) = \hat{p}(x) e^{-i\bar{a}kt} \quad (5.100)$$

where k is the complex wavenumber, related in general to the complex frequency by the formula

$$\bar{a}k = \omega + i\alpha \quad (5.101)$$

Because there are no dissipative processes in this problem, $\alpha = 0$ so the wavenumber is real. Substitution of (5.100) in (5.98) with S_c independent of x gives

$$\frac{d^2\hat{p}}{dx^2} + k^2\hat{p} = 0 \quad (5.102)$$

A solution to (5.102) satisfying (5.99) at $x = 0$ is $\hat{p} = A \cos kx$. To satisfy the condition at $x = L$, $\cos kL = 0$. Then k can assume only certain values k_l , called *characteristic* or *eigen* values:⁴

$$k_l = l \frac{\pi}{L} \quad (l = 0, 1, 2, \dots) \quad (5.103)$$

Corresponding to each k_l is a *characteristic function*, or *eigenfunction*,

$$\frac{\hat{p}_l}{\bar{p}} = A_l \cos(k_l x) \quad (5.104)$$

For the problems we treat in this book, the motions represented by the k_l , \hat{p}_l , and \hat{u}_l are usually called *normal modes*, $\bar{a}k_l = \omega_l$ being the *normal* or *modal frequency*, and \hat{p}_l , \hat{u}_l are the *mode shapes* of pressure and velocity. All of these terms are used for two- and three-dimensional motions as well.

A normal mode is characterized by its frequency and the spatial distributions, or ‘shapes’ of all dependent variables. The mode shape for the velocity is derived from the mode shape (5.104) by integrating the acoustic momentum equation (5.96) written for \hat{u}_l :

$$-i\bar{a}k_l \hat{u}_l = -\frac{1}{\bar{\rho}} \frac{d\hat{p}_l}{dx} = \frac{k_l}{\bar{\rho}} \bar{p} A_l \sin k_l x$$

Thus

$$\hat{u}_l = i \frac{\bar{p}}{\bar{\rho}a} A_l \sin k_l x \quad (5.105)$$

or, written as the Mach number of the mode,

$$\hat{M}_l = i \frac{1}{\gamma} A_l \sin k_l x \quad (5.106)$$

(b) Normal Modes for a Tube Open at Both Ends.

In this case, the pressure is assumed fixed at the ends, for example because the tube is immersed in a large reservoir having constant pressure, and $p' = 0$. For isentropic motions, $\frac{\rho'}{\bar{\rho}} = \frac{1}{\gamma} \frac{p'}{\bar{p}}$ so $\rho' = \frac{1}{\bar{a}^2} p'$ and the continuity equation (5.95) is

$$\frac{\partial p'}{\partial t} + \frac{\bar{a}^2}{\bar{\rho}} \frac{\partial u'}{\partial x} = 0 \quad (5.107)$$

Hence if p' is fixed, the velocity gradient must vanish at the ends. Set $p' = A e^{-i\bar{a}t} \sin kx$ and substitute in (5.107)

$$i \frac{\bar{a}}{\bar{\rho}} k A e^{-i\bar{a}t} \sin kx = \frac{\bar{a}^2}{\bar{\rho}} \frac{\partial u'}{\partial x}$$

⁴Only for $l \geq 1$ do we find wave modes. For $l = 0$, a qualitatively different mode exists for which the pressure is uniform in the volume but pulsates at a frequency well below that for the fundamental wave mode. The velocity is practically zero and the oscillator is sustained by some sort of external action. A prosaic example is the low frequency sound one can create by blowing across the narrow opening at the neck of a bottle. In this case the mode is called the *Helmholtz mode* and the bottle is behaving as a *Helmholtz resonator*. Corresponding very low frequency modes have been observed in both liquid and solid rockets.

The left-hand side vanishes (and hence $\partial u'/\partial x = 0$) at $x = 0$ for any k , but at $x = L$, we must have $\sin k_l L = 0$. Hence $k_l = (2l + 1)\frac{\pi}{L}$ and the normal mode shape and frequency are

$$\frac{\hat{p}_l}{\bar{p}} = A_l \sin(k_l x) \quad ; \quad k_l = l \frac{\pi}{L} \quad (l = 1, 2, \dots) \quad (5.108)$$

and the mode shape for the velocity is

$$\frac{\hat{u}_l}{\bar{a}} = \hat{M}_l = i \frac{1}{\gamma} A_l \cos k_l x \quad (5.109)$$

(c) Normal Modes for a Tube Closed at One End and Open at the Other.

Reasoning similar to the above leads in this case to the normal modes when the tube is closed at $x = 0$:

$$\begin{aligned} \frac{\hat{p}_l}{\bar{p}} &= A_l \cos(k_l x) \quad ; \quad \left(k_l = (2l + 1) \frac{\pi}{2L} \right) \quad (l = 1, 2, \dots) \\ \frac{\hat{u}_l}{\bar{a}} &= -i \frac{1}{\gamma} A_l \sin(k_l x) \end{aligned}$$

5.7.2. Normal Modes for Tubes Having Discontinuities of Cross-Sectional Area. Combustors having discontinuous area distributions are commonly used in solid propellant rockets and in various laboratory devices. Consider the example sketched in Figure 5.9. The boundary conditions at the ends are:

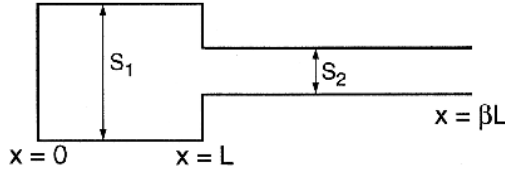


FIGURE 5.9. A uniform tube having a single discontinuity.

$$\begin{aligned} x = 0 : \quad \frac{d\hat{p}}{dx} &= 0 \\ x = \beta L : \quad \hat{p} &= 0 \end{aligned} \quad (5.110)a,b$$

Possible solutions in the regions to the left and right of the discontinuity are:

$$\begin{aligned} \frac{\hat{p}}{\bar{p}} &= A \cos kx \quad (0 \leq x \leq L) \\ \frac{\hat{p}}{\bar{p}} &= B \sin k(\beta L - x) \quad (L < x \leq \beta L) \end{aligned} \quad (5.111)a,b$$

Note that $k = \omega/\bar{a}$ is the same throughout the tube because the motion occurs everywhere at the same frequency.

Completing the problem comes down to determining the conditions for matching the solutions. Two are required:

i) **continuity of pressure:**

$$\lim_{\epsilon \rightarrow 0} [\hat{p}(L - \epsilon) - \hat{p}(L + \epsilon)] = 0$$

which gives

$$A \cos kL = B \sin(\beta - 1)kL \quad (5.112)$$

ii) **continuity of acoustic mass flow:**

Integrate the wave equation (for harmonic motions) across the discontinuity,

$$\int_{L-\epsilon}^{L+\epsilon} \left[\frac{d}{dx} \left(S_c \frac{d\hat{p}}{dx} \right) + k^2 S_c \hat{p} \right] dx = 0$$

Because \hat{p} is continuous, this relation becomes

$$\lim_{\epsilon \rightarrow 0} \left[\left(S_c \frac{d\hat{p}}{dx} \right)_{L+\epsilon} - \left(\frac{d\hat{p}}{dx} \right)_{L-\epsilon} \right] = 0$$

Thus, with $\bar{\rho}$ constant and $\frac{d\hat{p}}{dx} \sim \hat{u}$:

$$(\bar{\rho} S_c \hat{u})_{L+\epsilon} - (\bar{\rho} S_c \hat{u})_{L-\epsilon} \quad (5.113)$$

After substituting the waveforms (5.111)a,b, and using (5.112) we find the transcendental equation for the modal wavenumbers:

$$\frac{S_1}{S_2} \tan k_l L = \cot k_l (\beta - 1) L \quad (5.114)$$

This method of solving a problem with discontinuities is only approximate: a practical question is: how large are the errors? To gain some idea of the errors incurred, tests at ambient temperature ('cold flow tests') were carried out by Derr, Mathis and Brown (1974) for the geometry of a T-burner used for measuring the combustion response of burning solid propellants. Results are shown in Figure 5.10. The measured values of both the frequencies and the mode shapes are surprisingly well-predicted by this theory. The principal reason is that the influence of a discontinuity is confined to a relatively small region near the change of area, but the characteristics of the normal modes depend on the motion in the entire volume.

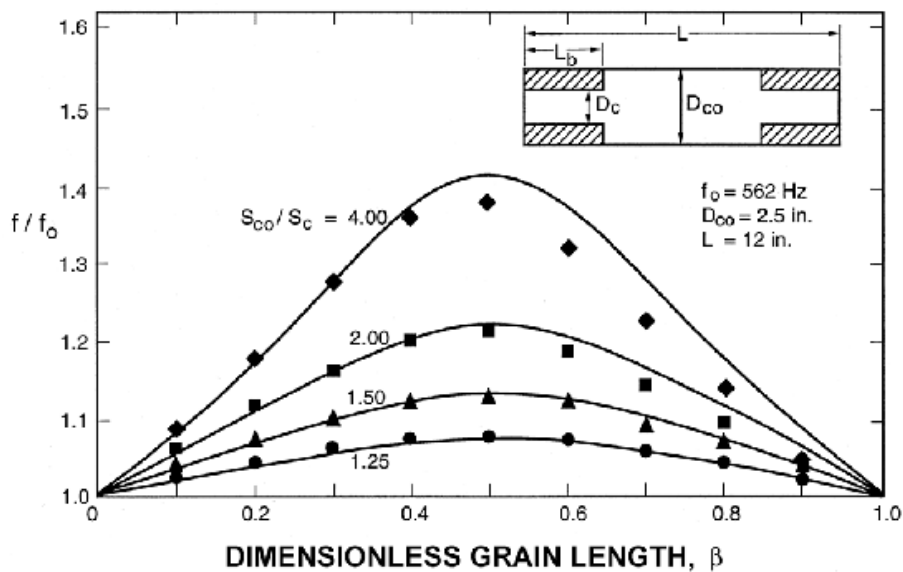


FIGURE 5.10. Comparison of experimental and theoretical results for normal frequencies in a T-burner at ambient temperature. (Derr, Mathis and Brown, 1974).

5.8. Normal Acoustic Modes and Frequencies for a Chamber

We now consider a volume of any shape enclosed by a rigid boundary and containing a uniform gas at rest. Unsteady small amplitude motions therefore satisfy the linear wave equation (5.4)a and its boundary condition (5.4)b requiring that the velocity normal to the boundary vanish at all times. By this definition given in Section 5.7.1, normal modes are solutions to this problem, which oscillate sinusoidally in time and have fixed phase relations throughout the volume. We assume the form⁵ $p' = \psi e^{-i\bar{a}kt}$. The formal problem is to find ψ satisfying the scalar wave equation, also called the Helmholtz wave equation, with vanishing normal gradient at the surface:

$$\begin{aligned}\nabla^2\psi + k^2\psi &= 0 \\ \hat{\mathbf{n}} \cdot \nabla\psi &= 0\end{aligned}\tag{5.115}a,b$$

There are many well-written books covering this problem and its solution, for example Hildebrand (1952); Morse and Feshbach (1952); Morse and Ingard (1968); Matthews and Walker (1964); and Jeffries and Jeffries (1946). The simplest approach is based on the method of separation of variables, applicable for closed form solutions in thirteen coordinate systems; see, e.g., Morse and Feshbach (1952). In practical applications to combustors of these exact solutions, only rectangular and circular cylindrical chambers are important. Otherwise, apart from special cases such as that treated in Section 5.7.2, the normal modes and frequencies must be found by numerical methods.

5.8.1. Normal Modes for Rectangular Chambers. The wave equation in Cartesian coordinates is

$$\frac{\partial^2\psi}{\partial x^2} + \frac{\partial^2\psi}{\partial y^2} + \frac{\partial^2\psi}{\partial z^2} + k^2\psi = 0$$

and $\hat{\mathbf{n}} \cdot \nabla\psi$ must vanish on the six flat surfaces each perpendicular to a coordinate axis, Figure 5.11. Applying the method of separation of variables leads to a solution having the form

$$\psi = A \cos(k_x x) \cos(k_y y) \cos(k_z z)\tag{5.116}$$

and

$$k^2 = k_x^2 + k_y^2 + k_z^2\tag{5.117}$$

The boundary conditions must be satisfied:

$$\begin{aligned}\frac{\partial\psi}{\partial x} &= 0 & \text{on} & \quad x = 0, L \\ \frac{\partial\psi}{\partial y} &= 0 & \text{on} & \quad y = -\frac{a}{2}, \frac{a}{2} \\ \frac{\partial\psi}{\partial z} &= 0 & \text{on} & \quad z = -\frac{b}{2}, \frac{b}{2}\end{aligned}\tag{5.118}a,b,c$$

Reasoning similar to that given in Section 5.7.1 leads to the values of the wavenumbers

$$\begin{aligned}k_x &= l \frac{\pi}{L} \\ k_y &= m \frac{\pi}{b} \\ k_z &= n \frac{\pi}{c}\end{aligned}\tag{5.119}a,b,c$$

⁵Consistent with the general character of this problem, we replace \hat{p} by ψ , introducing a common notation for normal modes. The velocity potential Φ satisfies the same pair of equations (5.115)a,b, a result reflected by equation (5.31) which for sinusoidal motions means that p' and Φ are proportional: $p' = i\bar{a}k\bar{\rho}\Phi$.

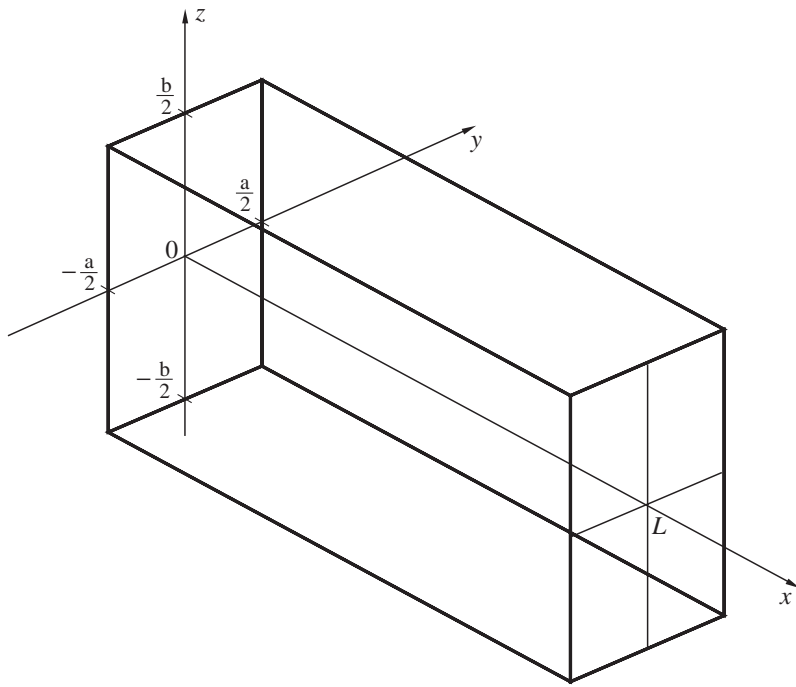


FIGURE 5.11. Rectangular chamber.

and the mode shapes are

$$\psi_{lmn} = A_{lmn} \cos\left(l \frac{\pi}{L} x\right) \cos m \frac{\pi}{a} \left(y + \frac{a}{2}\right) \cos n \frac{\pi}{b} \left(z + \frac{b}{2}\right) \quad (5.120)$$

The distributions of pressure therefore have the same form in all directions; of course the components (5.119)a,b,c of the wave number can assume any of the allowed values, and the frequency is given by (5.117), $\omega = \bar{a}k$.

5.8.2. Normal Modes for a Circular Cylindrical Chamber. Let x be the polar axis (Figure 5.12) and the wave equation in circular cylindrical coordinates is

$$\frac{1}{r} \frac{\partial}{\partial r} \left(r \frac{\partial \psi}{\partial r} \right) + \frac{1}{r^2} \frac{\partial^2 \psi}{\partial \theta^2} + \frac{\partial^2 \psi}{\partial x^2} + k^2 \psi = 0 \quad (5.121)$$

The boundary condition requires that $\hat{\mathbf{n}} \cdot \nabla \psi$ vanish at the ends and on the lateral boundary:

$$\begin{aligned} \frac{\partial \psi}{\partial x} &= 0 & x = 0, L \\ \frac{\partial \psi}{\partial r} &= 0 & r = R \end{aligned} \quad (5.122)$$

Application of the method of separation of variables leads to a solution of the form

$$\psi(r, x, \theta; t) = A \begin{Bmatrix} \cos n\theta \\ \sin n\theta \end{Bmatrix} \cos k_l x J_m \left(\kappa_{mn} \frac{r}{R} \right) \quad (5.123)$$

To satisfy the boundary conditions, the values of k_l are integral multiples of π/L as above and the κ_{mn} are the roots of the derivative of the Bessel function:

$$\frac{dJ_m(\kappa_{mn})}{dr} = 0 \quad (5.124)$$

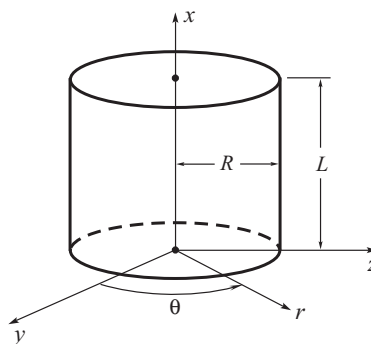


FIGURE 5.12. Circular cylindrical coordinates.

Figure 5.13 shows the lowest six modes in the transverse planes, and the identifying values of n and m . More extended results are given in standard texts and collections of special functions, for example Jahnke and Emde (1938).

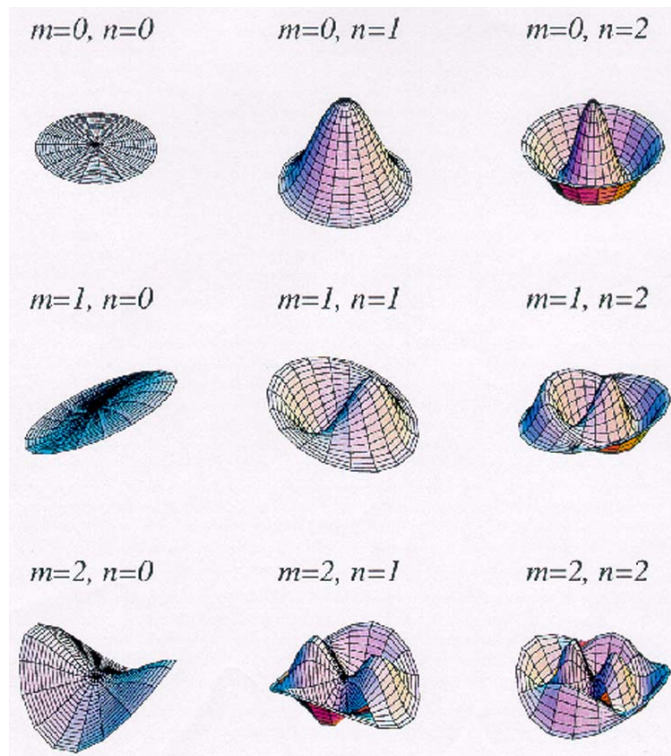


FIGURE 5.13. The first six transverse modes in a circular cylinder.

5.9. Viscous Losses at an Inert Surface

Dissipation of energy at inert surfaces is often a significant contribution to the losses of acoustic energy in a combustion chamber. The problem of computing the losses offers a particularly good opportunity to

illustrate different points of view. We will compute the losses in three different ways, all directly dependent on characteristics of the acoustic boundary layer. To simplify the analysis we assume that the average temperature is uniform throughout, having the value \bar{T}_e . Solutions for the velocity and temperature distributions within the acoustic boundary layer are derived in Annex C, equations (C.14)a,b with the time dependence included:

$$\begin{aligned} u'(x, y; t) &= \hat{u}_e(x) [1 - e^{-\lambda y}] e^{-i\omega t} \\ T'(x, y; t) &= \hat{T}_e(x) [1 - e^{-\lambda \sqrt{Pr} y}] e^{-i\omega t} \end{aligned} \quad (5.125)a,b$$

Note that the local values of the velocity and temperature impressed on the layer are shown explicitly to be functions of position along the surface. The idea is that the solution for the boundary layer flow applies locally, but variations are induced along the surface by the distributions of velocity $\hat{u}_e(x)$ and temperature $\hat{T}_e(x)$ in the external flow. The simplest example is a cylindrical tube closed at both ends, Figure 5.14. Shaded regions indicate the acoustic boundary layers.

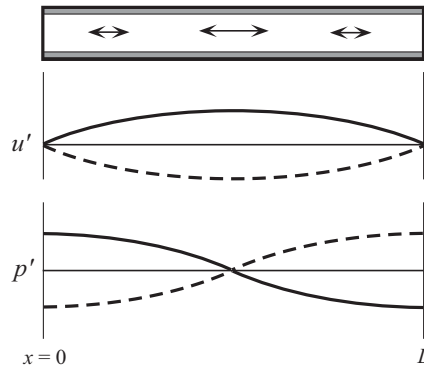


FIGURE 5.14. Acoustic velocity and temperature distributions for the fundamental mode in a closed tube.

5.9.1. Dissipation of Energy Within the Acoustic Boundary Layer. The theory of the acoustic boundary layer predicts a result, confirmed by experimental observations, that the influences of viscous stresses are confined to a thin layer having thickness δ . That is, $\delta/R_t \ll 1$ in the range of audio frequencies and for tubes having radius R_t greater than a centimeter or so. With the formula (C.6), the ambient properties of air given after equation (5.70), and $Pr = C_p\mu/\lambda_c = 0.73$ for air

$$\frac{\delta}{R_t} = \frac{1}{R_t} \sqrt{\frac{2v}{\omega}} = \frac{1}{R_t \sqrt{f}} \sqrt{\frac{v}{\pi}} \approx \frac{2}{R_t \sqrt{f}} \quad (5.126)$$

If $f = 9\text{Hz}$, $\delta/R_t \sim .06/R_t$, where R_t is in centimeters, and the assertion is proved.

Consequently, we can treat the acoustic boundary layer on the lateral boundary of a circular cylinder as if it were locally on a flat surface and the results of Annex C apply directly. We find the total rate of energy dissipation in the tube by integrating the energy dissipation over the acoustic boundary layer, i.e. over $y > 0$. Because the layer is thin and the non-uniformities of the flow properties decay exponentially in y , we integrate over all y from zero to infinity. Application of the formula (C.19) for the rate of entropy

production in this flow gives⁶ (per unit volume)

$$\frac{ds}{dt} = \frac{1}{\bar{T}_e} \left[\mu \left(\frac{d\hat{u}}{dy} \right)^2 + \frac{\lambda_c}{\bar{T}_e^2} \left(\frac{d\hat{T}}{dy} \right)^2 \right]$$

Then the rate of energy dissipation per unit volume is

$$\frac{de}{dt} = -\bar{T}_e \frac{ds}{dt} = -\mu \left(\frac{d\hat{u}}{dy} \right)^2 + \frac{\lambda_c}{\bar{T}_e^2} \left(\frac{d\hat{T}}{dy} \right)^2 \quad (5.127)$$

where either the real or the imaginary parts of \hat{u} and \hat{T} must be used. The time-averaged energy dissipation per unit area of surface is therefore the time average of the integral of (5.127) over the entire acoustic boundary layer:

$$\frac{1}{2\pi} \int_0^{2\pi} dt \int_0^\infty \left[\mu \left(\frac{d\hat{u}}{dy} \right)^2 + \frac{\lambda_c}{\bar{T}_e^2} \left(\frac{d\hat{T}}{dy} \right)^2 \right] dy \quad (5.128)$$

This formula gives

$$\begin{aligned} & \text{time-averaged energy} \\ & \text{loss per unit surface area} \quad \langle \dot{e} \rangle = -\frac{1}{2\gamma\bar{p}} \frac{\sqrt{\omega\nu}}{2} \left[\left| \frac{\hat{u}_e}{\bar{a}} \right|_m^2 + \frac{\gamma-1}{\sqrt{Pr}} \left| \frac{\hat{p}}{\bar{p}} \right|_m^2 \right] \end{aligned} \quad (5.129)$$

where $| \cdot |_m$ means the maximum value in the oscillation and $\nu = \mu/\bar{\rho}$ is the kinematic viscosity.

Suppose that a standing wave is sustained in a tube, like the one sketched in Figure 5.14, by a speaker or piston. If the source of waves is suddenly cut off, the amplitude of the standing wave system will decay exponentially in time according to the discussion in Section 5.5, the decay constant being given by the formula 5.80:

$$\alpha = \frac{1}{2 \int \langle \varepsilon \rangle dV} \frac{d}{dt} \int \langle \varepsilon \rangle dV \quad (5.130)$$

and $\int \langle \varepsilon \rangle dV$ is the total time-averaged energy in the tube. Here energy losses at the ends are ignored and compute $\frac{d}{dt} \int \langle \varepsilon \rangle dV$ as the integral of $\langle \dot{e} \rangle$, the formula (5.129) over the lateral area of the tube with

$$\begin{aligned} \hat{p}_e & \equiv A_l \cos(k_l x) \\ \hat{u}_e & = \frac{A_l}{\bar{\rho}\bar{a}} \sin(k_l z) \\ \langle \varepsilon_l \rangle & = \frac{A_l^2}{4\bar{\rho}\bar{a}^2} (\pi R_t^2 L) \end{aligned} \quad (5.131)\text{a,b,c}$$

The time-averaged total energy is computed with 5.78 and the total time-average rate of dissipation is

$$\frac{d}{dt} \int \langle \varepsilon \rangle dV = -\frac{1}{2\gamma\bar{p}} \sqrt{\frac{\omega\nu}{2}} \left[1 + \frac{\gamma-1}{\sqrt{Pr}} \right] A_l^2 (\pi R_t^2 L) \quad (5.132)$$

Hence we find

$$\alpha = -\frac{1}{R_t} \sqrt{\frac{\omega\nu}{2}} \left[1 + \frac{\gamma-1}{\sqrt{Pr}} \right] \quad (5.133)$$

Early measurements by several groups, e.g. Henderson and Donnelly (1962), gave a result roughly 8–10% higher than that predicted by (5.133). That was a puzzling situation for about fifteen years. The analysis for laminar flow—i.e. for sufficiently low amplitudes of the motion—should, one has reason to expect, be

⁶For purposes of estimation, it is sufficiently accurate to take the value of ν for combustion products to be the same as air at standard conditions, $\nu \approx 0.2 \text{ cm}^2/\text{s}$, and to assume that the average temperature has everywhere its ambient value, \bar{T}_e .

more accurate than that. Yet the experiments seem to have been done carefully and with good precision. Eventually, however, it turned out that the experiments must be carried out with extreme care indeed. With superb work exemplifying how carefully measurements must be made to obtain accurate results for acoustic losses, Quinn, Colclough and Chandler (1976) determined α with an error of 0.069%(!) compared with (5.133).

This example has wide implications in the field of combustion instabilities. Experiments designed to confirm theoretical and analytical results must be carefully carried out with the greatest possible precision; also, uncertainties in the results should be reported, a practice too often ignored. That requirement is a direct consequence of the fact that acoustical motions, despite their 'loudness' to human ears, contain relatively small amounts of energy and therefore are sensitive to small changes in the system containing them.

5.9.2. Another Way of Computing the Decay Constant. The second method of computing the decay constant due to losses in the acoustic boundary layer is based on the method of spatial averaging. We begin with the dimensional forms of the linearized equations including viscous stresses and heat conduction, (5.1)–(5.3) but no external sources and mean flow and with the velocity zero at the boundary:

$$\begin{aligned} \nabla^2 p' - \frac{1}{\bar{a}^2} \frac{\partial^2 p'}{\partial t^2} &= \nabla \cdot \mathbf{F}' - \frac{1}{\bar{a}^2} \frac{\partial \mathcal{P}'}{\partial t} \\ \hat{\mathbf{n}} \cdot \nabla p' &= -\mathbf{F}' \cdot \hat{\mathbf{n}} \end{aligned} \quad (5.134)a,b$$

and

$$\begin{aligned} \mathbf{F}' &= \nabla \cdot \hat{\boldsymbol{\tau}}'_v \\ \mathcal{P}' &= -\frac{R}{C_v} \nabla \cdot \mathbf{q}' \end{aligned}$$

For harmonic motions with complex wave number $k = (\omega + i\alpha)/\bar{a}$, (5.134)a,b are

$$\begin{aligned} \nabla^2 \hat{p} + k^2 \hat{p} &= \hat{h} \\ \hat{\mathbf{n}} \cdot \nabla \hat{p} &= -\hat{f} \end{aligned} \quad (5.135)a,b$$

where

$$\begin{aligned} \hat{h} &= \nabla \cdot \hat{\mathbf{F}} - \frac{ik}{\bar{a}} \frac{R}{C_v} \nabla \cdot \hat{\mathbf{q}} \\ \hat{f} &= -\hat{\mathbf{n}} \cdot \hat{\mathbf{F}} \end{aligned} \quad (5.136)a,b$$

The procedure described in Section 4.1 leads to the formula for the complex wavenumber for the n^{th} mode,

$$k^2 = k_n^2 + \frac{1}{\int \psi_n^2 dV} \left\{ \int \hat{h} \psi_n dV + \iint \hat{f} \psi_n dS \right\} \quad (5.137)$$

where the volume integrals extend over the entire volume of the tube and the surface integral is computed only over the lateral boundary because losses at the end are ignored. For the viscous effects in the boundary layer,

$$\begin{aligned} \hat{\mathbf{F}} &= \nabla \cdot \hat{\boldsymbol{\tau}}_v = \left(\mu \frac{d^2 \hat{u}_x}{dy^2} \right) \hat{\mathbf{i}} \\ \nabla \cdot \hat{\mathbf{q}} &= \frac{d \hat{q}_y}{dy} = -\lambda_c \frac{d^2 \hat{T}}{dy^2} \end{aligned} \quad (5.138)a,b$$

Substitution in the bracketed terms on the right-hand side of (5.137) with μ and λ_c constant gives:

$$\begin{aligned}
 \int \hat{h}\psi_n dV + \oint \hat{f}\psi_n dS &\equiv \int (\nabla \cdot \hat{\mathbf{F}}) \psi_n dV - \frac{ik}{\bar{a}} \frac{R_t}{C_v} \int (\nabla \cdot \hat{\mathbf{q}}) \psi_n dV \\
 &\quad - \oint (\hat{\mathbf{n}} \cdot \hat{\mathbf{F}}) \psi_n dS \\
 &= -\frac{ik}{\bar{a}} \frac{R_t}{C_v} \int (\nabla \cdot \hat{\mathbf{q}}) \psi_n dV - \int \hat{\mathbf{F}} \cdot \nabla \psi_n dV \\
 &= -\frac{ik}{\bar{a}} \frac{R_t}{C_v} \lambda_c \int \frac{d^2 \hat{T}}{dy^2} \psi_n dV - \mu \int \frac{d^2 u_x}{dy^2} \frac{d\psi_n}{dx} dV
 \end{aligned} \tag{5.139}$$

Because the viscous effects are significant only near the wall we can take the incremental element of volume to be $dV = dy dS$ and write the integrals for $\psi_n \equiv \psi_l(x)$ a purely longitudinal mode shape:

$$\begin{aligned}
 \int \frac{d^2 \hat{T}}{dy^2} \psi_n dV &\equiv \oint \psi_l dS \int_0^\infty \frac{d^2 \hat{T}}{dy^2} dy = \oint \psi_l \left(\frac{d\hat{T}}{dy} \right)_0 dS \\
 \int \frac{d^2 \hat{u}}{dy^2} \frac{d\psi_l}{dx} dV &\equiv \oint \frac{d\psi_l}{dx} dS \int_0^y \frac{d^2 \hat{u}}{dy^2} dy = - \oint \frac{d\psi_l}{dx} \left(\frac{d\hat{u}}{dy} \right)_0 dS
 \end{aligned}$$

The derivatives $d\hat{T}/dy$ and $d\hat{u}/dy$ are significant only within the thin acoustic boundary layer and become negligible at the outer edge, y/δ large. Now use the results (C.14)a,b to evaluate the derivatives at the surface:

$$\begin{aligned}
 \left(\frac{d\hat{T}}{dy} \right)_0 &= \lambda \sqrt{Pr} \hat{T}_e & \left(\frac{d\hat{u}}{dy} \right)_0 &= \lambda \hat{u}_e \\
 &= \lambda \sqrt{Pr} \bar{T} \left(\frac{\gamma - 1}{\gamma} \right) \frac{\hat{p}_e}{\bar{p}} & &= \lambda \frac{i}{\bar{\rho}\omega} \frac{d\bar{p}_e}{dx}
 \end{aligned}$$

Inserting these results in (5.139) gives

$$\begin{aligned}
 \int \hat{h}\psi_l dV + \oint \hat{f}\psi_l dS &\equiv \left(\frac{ik}{\bar{a}} \frac{R_t}{C_v} \lambda_c \right) \left[\lambda \sqrt{Pr} \bar{T} \left(\frac{\gamma - 1}{\gamma} \right) \oint \psi_l \frac{\hat{p}_e}{\bar{p}} dS \right] \\
 &\quad + \mu \left[\frac{i\lambda \bar{p}}{\bar{\rho}\omega} \oint \frac{d}{dx} \left(\frac{\hat{p}_e}{\bar{p}} \right) \frac{d\psi_l}{dx} dS \right]
 \end{aligned} \tag{5.140}$$

where dS is the increment of the lateral surface, $dS = (2\pi R_t)dx$.

The mode shapes for the acoustic pressure in a closed-closed uniform tube is (5.104). As the wave decays, its shape is very little different from the normal mode shape at the same (or nearly) the frequency. Hence we can replace \hat{p}_e by $\psi_l = \bar{p}_e A_l \cos k_l x$, and we have the two integrals

$$\begin{aligned}
 \oint \frac{\hat{p}_e}{\bar{p}} \psi_l dS &= q_t A_l \int_0^L \cos^2(k_l x) dx = \pi R_t L A_l \\
 \oint \frac{d}{dx} \left(\frac{\hat{p}_e}{\bar{p}} \right) \frac{d\psi_l}{dx} dS &= q_t A_l k_l^2 \int_0^L \sin(k_l x) dx = \pi R_t L A_l
 \end{aligned} \tag{5.141}a,b$$

In (5.140), the values of k and ω are nearly⁷ those for the normal mode; replacing $k \rightarrow k_l$, $\omega \rightarrow \omega_l$ and substituting (D.14)a-d in (5.140), we eventually find

$$\int \hat{h}\psi_l dV + \iint \hat{f}\psi_l dS = \frac{k_l \bar{p}}{\bar{a}^2} (1 - i) \left(\frac{1}{2} q_t L A_l \right) \left(1 + \frac{\gamma - 1}{\sqrt{P_r}} \right) \quad (5.142)$$

With $\int \psi_l^2 dV = \frac{1}{2}(\pi R_t^2 L)$, (5.137) becomes

$$\begin{aligned} k^2 &= k_l^2 + \frac{1}{\bar{p} A_l \int \psi_l^2 dV} \left\{ \int \hat{h}\psi_l dV + \iint \hat{f}\psi_l dS \right\} \\ &= k_l^2 + \frac{1}{\frac{\bar{p} A_l}{2} (\pi R_t^2 L)} \left\{ \frac{k_l \bar{p}}{\bar{a}^2} (1 - i) (\pi R_t^2 L A_l) \sqrt{\frac{\nu \omega}{2}} \left(1 + \frac{\gamma - 1}{\sqrt{P_r}} \right) \right\} \\ &= k_l^2 + (1 - i) \frac{k_l \bar{p}}{\bar{a}^2} \left(\frac{2}{R_t} \right) \sqrt{\frac{\nu \omega}{2}} \left(1 + \frac{\gamma - 1}{\sqrt{P_r}} \right) \end{aligned} \quad (5.143)$$

The left-hand side is

$$k^2 = \frac{1}{\bar{a}^2} (\omega + i\alpha)^2 = \left(\frac{\omega}{a} \right)^2 - i \left(\frac{2\alpha\omega}{a} \right) - \left(\frac{\alpha}{a} \right)^2$$

Because $\alpha \ll \omega$, (5.143) is approximately

$$\left(\frac{\omega}{a} \right)^2 - i \left(\frac{2\alpha\omega}{a} \right) = k_l^2 + (1 - i) \frac{k_l \bar{p}}{\bar{a}^2} \left(\frac{2}{R_t} \right) \sqrt{\frac{\nu \omega}{2}} \left(1 + \frac{\gamma - 1}{\sqrt{P_r}} \right)$$

of which the imaginary part is

$$\alpha = -\frac{1}{R_t} \sqrt{\frac{\nu \omega}{2}} \left(1 + \frac{\gamma - 1}{\sqrt{P_r}} \right) \quad (5.144)$$

which is exactly (5.133).

5.9.3. Still Another Way of Computing the Decay Constant. A third method for computing the decay constant is instructive for several reasons. First it is a good illustration of the usefulness and at least for the problem considered here, accuracy of the one-dimensional approximation. Second, it illustrates an important consequence of the conservation of mass that has other applications. And third, related to the second, the analysis answers a fundamental question about the problem at hand: how does it happen that dissipation of energy taking place in the thin acoustic boundary layer is communicated to the waves outside the boundary layer? That is, the wave fronts remain very nearly planar in transverse sections, yet the amplitude decays in time due to processes confined to the thin layer near the wall. If the wave fronts (loci of constant phase) did not remain planar, the frequency would change with time, behavior not observed.

We base the analysis on the equations for unsteady one-dimensional flow constructed in Annex B. For the problem at hand, we imagine striking a control surface at the edge of the acoustic boundary layer, represented by the dashed line in Figure 5.15. The unsteady flow field within the acoustic boundary layer, the shaded region, is given by the results found in Annex C, repeated above as equations (5.125)a,b. Within the volume outside the boundary layer, a steady planar acoustic field exists, sustained by the motion of one end, for example. The velocity of the piston face need not be large and we may approximate the acoustic field by a classical resonant mode. Thus in (5.125)a,b we set the frequency equal to ω_l and $\hat{\mathbf{u}}_e(v)$ is given by (5.105). As explained in Annex C, the flow within the boundary layer is reasonably taken to be incompressible and the equation for conservation of mass is

$$\frac{\partial \hat{u}_e}{\partial x} + \frac{\partial v_e}{\partial y} = 0 \quad (5.145)$$

⁷These characterizations ‘not very different’ and ‘nearly’ can be rendered more rigorous in the context of the procedure explained in Chapters 3 and 4. The point here is that including deviations of order \bar{M}_r from k_l introduces corrections of order \bar{M}_r^2 which must be ignored for reasons explained in the places cited.

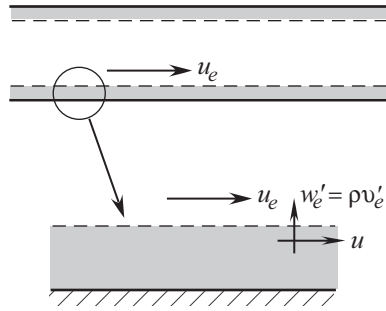


FIGURE 5.15. Definition of the lateral control surface.

Consequently, a velocity normal to the wall is induced within the acoustic boundary layer because the external velocity has non-zero gradient parallel to the wall. Chester (1964) has given the formula for v'_e for the linearized boundary layer theory used here:

$$v'_e(x, t) = \sqrt{\frac{\nu}{\pi}} \left(1 + \frac{\gamma - 1}{\sqrt{Pr}} \right) \int_0^{\infty} \frac{\partial}{\partial x} u'_e(x, t - \tau) \frac{d\tau}{\sqrt{\tau}} \quad (5.146)$$

For the standing acoustic wave, the l^{th} acoustic mode, from (5.105) we have

$$\frac{\partial u'_e}{\partial x} = e^{-i\omega_l t} \frac{d\hat{u}_l}{dx} = i\bar{a}k_l \frac{A_l}{\gamma} \cos k_l x e^{-i\omega_l t} \quad (5.147)$$

Substitution in (5.146) leads to the formula for v'_e :

$$\begin{aligned} v'_e &= i \frac{\omega_l}{\gamma} A_l \sqrt{\frac{\nu}{\pi}} \left(1 + \frac{\gamma - 1}{\sqrt{Pr}} \right) \cos k_l x \int_0^{\infty} \frac{e^{-i\omega_l(t-\tau)}}{\sqrt{\tau}} d\tau \\ &= i \frac{\omega_l}{\gamma} A_l \sqrt{\frac{\nu}{\pi}} \left(1 + \frac{\gamma - 1}{\sqrt{Pr}} \right) \cos k_l x \frac{e^{-i\omega_l t}}{\sqrt{\omega_l}} d\tau \int_0^{\infty} \frac{e^{-i\xi}}{\sqrt{\xi}} d\xi \\ &= \frac{(-1 + i)}{\gamma} A_l \sqrt{\frac{\nu \omega_l}{2}} \left(1 + \frac{\gamma - 1}{\sqrt{Pr}} \right) \cos k_l x e^{-i\omega_l t} = \hat{v}_e e^{-i\omega_l t} \end{aligned} \quad (5.148)$$

We will need the real part of the spatial dependence:

$$\hat{v}_e^{(r)} = -\frac{1}{\gamma} A_l \sqrt{\frac{\nu \omega_l}{2}} \left(1 + \frac{\gamma - 1}{\sqrt{Pr}} \right) \cos k_l x \quad (5.149)$$

Now we focus attention on the acoustic field within the control surface shown in Figure 5.15. All influences of the boundary layer are contained in the velocity by v'_e representing oscillatory pumping of fluid through the surface. Hence we have a simple one-dimensional flow with distributed periodic sources of mass momentum and energy at the boundary. There is, of course, no net flow through the boundary, the time average of (5.148) being zero.

We begin with equations (B.3) and (B.5) written for constant cross-section area and no sources within the volume. The linearized forms are

$$\begin{aligned} \bar{\rho} \frac{\partial u'}{\partial t} + \frac{\partial p'}{\partial x} &= \mathcal{F}'_{1s} \\ \frac{\partial p'}{\partial t} + \gamma \bar{p} \frac{\partial u'}{\partial x} &= \mathcal{P}'_{1s} \end{aligned} \quad (5.150)a,b$$

where \mathcal{F}'_{1s} and \mathcal{P}'_{1s} are given by (B.14) and (B.16). With mean velocity zero and pure gas, those definitions become

$$\begin{aligned}\mathcal{F}'_{1s} &= 0 \\ \mathcal{P}'_{1s} &= \frac{R}{C_v} \frac{1}{S_c} (\bar{h}_{0s} - \bar{e}_0 + C_v \bar{T}) \int (m_s^g)' dq\end{aligned}\quad (5.151)a,b$$

The stagnation and ambient average temperatures are uniform and equal everywhere, so

$$\bar{h}_{0s} - \bar{e}_0 + C_v \bar{T} = (C_p - C_v + C_v) \bar{T} = C_p \bar{T} \quad (5.152)$$

With no average flow inward,

$$(m_s^g)' = \bar{\rho} v_e' \quad (5.153)$$

where v_e' is given here by (5.148). Hence (5.151)b is

$$\mathcal{P}'_{1s} = \frac{\bar{a}^2}{S_c} \int \bar{\rho} v_e' dq \quad (5.154)$$

After combining (5.150)a,b in the usual way to form the wave equation, and substituting (5.152) and (5.154), we have

$$\frac{\partial^2 p'}{\partial x^2} - \frac{1}{\bar{a}^2} \frac{\partial^2 p'}{\partial t^2} = -\frac{1}{S_c} \frac{\partial}{\partial t} \int \bar{\rho} v_e' dq$$

For v_e' uniform on the perimeter of a transverse plane, the integral on the right-hand side becomes $\bar{\rho} v_e' (2\pi R_t)$ and the last equation is

$$\frac{\partial^2 p'}{\partial x^2} - \frac{1}{\bar{a}^2} \frac{\partial^2 p'}{\partial t^2} = -\frac{2}{R_t} \bar{\rho} \frac{\partial v_e}{\partial t} \quad (5.155)$$

Owing to the perturbation caused by the fluctuating mass flow at the boundary, the natural modes of the chamber have frequencies ω slightly different from ω_l , the classical values. Set $p' \approx p'_l = \bar{\rho} A_l \cos k_l x$ and $v_e' = \hat{v}_e e^{-i\omega t}$ in (5.155), giving

$$\begin{aligned}\bar{\rho} A_l \cos(k_l x) (-k_l^2 + k^2) &= -\frac{2}{R_t} \bar{\rho} (-i\omega \hat{v}_e) \\ &\approx i \frac{2\omega_l \bar{\rho}}{R_t \gamma} \frac{(-1+i)}{\gamma} A_l \sqrt{\frac{\nu \omega_l}{2}} \left(1 + \frac{\gamma-1}{\sqrt{Pr}} \right) \cos k_l x\end{aligned}$$

Rearrangement leads to the formula for the complex wavenumber

$$k^2 = k_l^2 + (1-i) \frac{2\omega_l \bar{\rho}}{\bar{\rho} R_t \gamma} \sqrt{\frac{\nu \omega_l}{2}} \left(1 + \frac{\gamma-1}{\sqrt{Pr}} \right) \quad (5.156)$$

The real part again gives the formula (5.133).

5.9.4. First Order Correction to the Mode Shape. In the model analyzed here, the essential idea is that the influence of the acoustic boundary layer is exerted on the bulk flow by the motions induced normal to the wall. A force of interaction is generated tangential to the wall, having the proper phase to attenuate the waves in the tube. That process must alter the mode shape to a form consistent with the first order correction to the acoustic eigenvalue. One way to determine the distortion is to compute the first order correction to the zeroth order basis function by following the procedure described in Chapter 4. An alternative approach is based directly on the differential equation for the pressure subject to the boundary condition set by the radial ‘pumping’ velocity (5.149). The mass source term is the density times (5.149) and the boundary condition on the radial gradient of the pressure mode shape is

$$\hat{\mathbf{n}} \cdot \nabla \hat{p} = -i\omega \rho_0 \hat{\mathbf{u}} \cdot \hat{\mathbf{n}} = i\omega \rho_0 \hat{v} = i\omega \frac{R_c}{2} \hat{w} \quad (5.157)$$

where \hat{v} is given by (5.149). After substitution for \hat{v} , this relation gives the explicit form

$$\frac{d\hat{p}}{dr} = (1 - i)k^{3/2}\beta\hat{p} \quad (5.158)$$

where

$$\beta = \frac{1}{2}\sqrt{\frac{2\nu}{a_0}} \left[1 + \frac{\gamma - 1}{\sqrt{Pr}} \right] \quad (5.159)$$

For axisymmetric motions in a circular cylindrical tube, the scalar wave equation for the pressure is

$$\frac{1}{r}\frac{\partial}{\partial r} \left(r\frac{\partial \hat{p}}{\partial r} \right) + \frac{\partial^2 \hat{p}}{\partial x^2} + k^2\hat{p} = 0 \quad (5.160)$$

with solution

$$\hat{p} = \sum_{n=1}^{\infty} \sum_{m=1}^{\infty} A_{nm} \cos k_n x J_0(v_m r) \quad (5.161)$$

where

$$v_m^2 = k^2 - k_n^2 \quad (5.162)$$

The boundary condition (5.160) sets the permissible values of v_m and hence the wavenumber k :

$$\left[\frac{d}{dr} J_0(v_m r) \right]_{r=R_c} = (1 - i)k^{3/2}\beta J_0(v_m R_c) \quad (5.163)$$

There are an infinite number of the v_m , so that, for example, for the first longitudinal mode, the pressure field is

$$\hat{p} = \cos \left(\frac{\pi}{L} x \right) \sum_{m=1}^{\infty} A_m J_0(v_m r) \quad (5.164)$$

For simplicity here, only the first term will be treated; $v_m = v_1$ and in (5.163) the function $J_0(v_1 R_c)$ appears.

Now one expects that the corrections will be small, so k should not be very different from k_n , and the expansion can be used

$$J_0(v_1 r) \approx 1 - \frac{1}{4}(v_1 r)^2 \quad (v_1 \rightarrow 0) \quad (5.165)$$

Thus,

$$\left[\frac{d}{dr} J_0(v_1 r) \right]_{r=R_c} \approx -\frac{1}{2}v_1^2 R_c$$

and (5.163) is approximately

$$-\frac{1}{2}v_1^2 R_c = (1 - i)k^{3/2}\beta \left[1 - \frac{1}{4}(v_1 R_c)^2 \right]$$

If the second order term on the right-hand side is ignored, substitution of (5.162) gives

$$-\frac{1}{2}R_c(k^2 - k_1^2) = (1 - i)k^{3/2}\beta$$

so

$$v_1^2 = (k^2 - k_1^2) \approx -\frac{2}{R_c}(1 - i)k^{3/2}\beta \quad (5.166)$$

Again write $k = (\omega - i\alpha)/a_0$ with $\alpha \ll \omega$ on the left-hand side; because the second term on the right-hand side represents a small correction, set $k = \omega/a_0$. Equation (5.166) therefore gives approximately

$$\left(\frac{\omega}{a_0} \right)^2 - 2i\frac{\alpha\omega}{a_0^2} = \left(\frac{\omega_1}{a_0} \right)^2 - \frac{2}{R_c}(1 - i) \left(\frac{\omega}{a_0} \right)^{3/2}\beta \quad (5.167)$$

from which the imaginary part is easily shown to be exactly 5.144 again.

But now the first term of (5.164), with (5.165) and (5.166), gives a formula for the distorted one-dimensional (planar) pressure field:

$$\hat{p} \approx \cos \frac{\pi x}{L} J_0(v_1 r) \approx \cos \frac{\pi x}{L} \left[1 - \frac{1}{4}(k^2 - k_1^2)r^2 \right]$$

It is easy to show, using the definition (5.159) of β , that (5.166) is

$$(k^2 - k_1^2) = \frac{2\omega}{a_0^2} (1 - i) \alpha_0 \quad (5.168)$$

where α_0 now stands for the attenuation coefficient (5.144) computed for purely one-dimensional waves, the real part of (5.167). Because $(1 - i)^2 = -2i$, the distorted pressure field can be written

$$\hat{p} \approx \cos \frac{\pi x}{L} \left[1 + i \left(\frac{\omega \alpha_0}{a_0^2} \right)^2 r^2 \right] \quad (5.169)$$

This pressure field is now to be used in the expression for $\hat{w} = 2\frac{\rho_0 \hat{v}}{R_c}$, with $r = R_c$ (because the pressure in that formula is the pressure impressed on the boundary layer):

$$\hat{w} = -(1 + i) \frac{2\alpha_0}{a_0^2} \cos \frac{\pi x}{L} \left[1 + i \left(\frac{\omega \alpha_0}{a_0^2} \right)^2 R_c^2 \right] \quad (5.170)$$

Finally, use this new result for the source term in the solution for the wavenumber associated with the one-dimensional problem:

$$k^2 = k_1^2 - \frac{2\omega \alpha_0}{a_0^2} (1 - i) \left[1 + i \left(\frac{\omega \alpha_0}{a_0^2} \right)^2 R_c^2 \right] \quad (5.171)$$

The real and imaginary parts are

$$\left(\frac{\omega}{a_0} \right)^2 = \left(\frac{\omega_1}{a_0} \right)^2 \left\{ 1 - (1 + \zeta) \frac{2\alpha_0}{\omega} \right\} \quad (5.172)$$

$$\alpha = -(1 - \zeta) \alpha_0 \quad (5.173)$$

where

$$\zeta = \left(\frac{\omega \alpha_0}{a_0^2} R_c^2 \right)^2 \quad (5.174)$$

Thus, as anticipated, the distortion of the plane wavefronts produces a reduction in the value of the attenuation constant, which is in the right direction to give better agreement with experimental results. For $R_c = 5$ cm and $f = 500$ Hz,

$$\zeta = \left[\frac{(2\pi)(500)}{9 \times 10^8} (25) \right]^2 \cong 7.8 \times 10^{-9} a_0^2$$

and for $\alpha_0 = 20 \text{ sec}^{-1}$, $\zeta \approx 30 \times 10^{-7}$. The correction is therefore very small and cannot explain the discrepancy between the predicted and observed values. Although only the first term in the series (5.164) has been retained, it is unlikely that the last conclusion would be changed upon including further terms in the series.

The preceding calculation illustrates two points: it is an example of determining the effect of a boundary layer in its external driving flow, here a standing plane wave; and the result supports the idea that the zeroth order basic functions really are close approximations, over most of the chamber, to the actual mode

shapes. In this case, the small differences occur in a thin zone at the lateral boundary. The corrected mode shape calculated here satisfies the actual boundary condition to first order. However, the zeroth order mode shape *not* satisfying the correct boundary condition nevertheless yields the exact result for the first order eigenvalue (the decay constant) when used in the perturbation-iteration procedure constructed in Chapter 4.

5.10. Propagation of Higher Modes in Tubes; Cut-off Frequencies

In Section 5.7 we constructed the normal longitudinal modes for tubes of finite length. For the cases considered, the wavefronts are planar and the flow properties are always uniform over all transverse sections. The pressure, for example, at a chosen location undergoes a perfect sinusoidal oscillation in time, having maximum amplitude in time and bearing a fixed phase with respect to the pressure at any other location. Those properties define such a normal mode as a stationary or standing wave.

A stationary wave may be regarded as the superposition or synthesis of two traveling waves progressing in opposite directions. We may interpret that result in two ways: 1) the waves are confined to the tube and suffer reflection at the ends, suffering a 180 degree phase change up each reflection and reversing its direction of travel; or 2) two waves each infinitely long and traveling in opposite directions interfere destructively at the locations of the ends of the tube so as to maintain the correct boundary conditions. The second interpretation corresponds to the case for reflection of pulses worked out in Section 5.2.1 and illustrated in Figure 5.2.

Either of those two interpretations suggest a question regarding propagation of plane waves in a tube. What if, because of some sort of disturbance, the wave fronts are distorted? That is, suppose that the wave fronts, while still perfectly plane, suffer some distortion so that the distribution of the flow properties are not uniform in transverse sections. How then is propagation of that wave affected? Any such distortion can be synthesized of two-dimensional normal modes in transverse planes superposed on a traveling wave. Hence we assume the form for pressure wave traveling in the positive x-direction:

$$p'(x, y, z; t) = A \cos(k_y y) \cos(k_z z) e^{i(k_x x - \omega t)} \quad (5.175)$$

The frequency is unspecified, $\omega = \bar{a}k$. This wave must satisfy the wave equation

$$\frac{\partial^2 p'}{\partial x^2} + \frac{\partial^2 p'}{\partial y^2} + \frac{\partial^2 p'}{\partial z^2} - \frac{1}{\bar{a}^2} \frac{\partial^2 p'}{\partial t^2} = 0$$

Substitution of (5.175) produces the relation among the wavenumbers

$$-k_x^2 - k_y^2 - k_z^2 + k^2 = 0$$

and

$$k_x = \sqrt{k^2 - (k_y^2 + k_z^2)} \quad (5.176)$$

must be positive and real for propagation in the positive x-direction. The formulas (5.119)a,b,c give the two transverse wavenumbers and (5.175) is

$$k_x = \sqrt{\left(\frac{\omega}{\bar{a}}\right)^2 - \left[\left(\frac{m\pi}{b}\right)^2 + \left(\frac{n\pi}{b}\right)^2\right]} \quad (5.177)$$

Consequently, if k_x is to be real, the frequency of the wave must be larger than a critical value ω_c :

$$\omega > \omega_c \quad (5.178)$$

with

$$\omega_c = \bar{a} \sqrt{\left(\frac{m\pi}{b}\right)^2 + \left(\frac{n\pi}{b}\right)^2} \quad (5.179)$$

The frequency ω_c is called a “cutoff frequency” for the following reason. Substitute (5.176) in (5.144):

$$p' = \hat{p}(y, z) e^{i(\frac{1}{a} \sqrt{\omega^2 - \omega_c^2} x - \omega t)} \quad (5.180)$$

If $\omega < \omega_c$, the exponential factor can be written

$$e^{-\beta x} e^{i\omega t} \quad (5.181)$$

where the attenuation constant β is

$$\beta = \frac{1}{a} \sqrt{\omega_c^2 - \omega^2} \quad (\omega < \omega_c) \quad (5.182)$$

Two main conclusions follow from this calculation:

- i) If $m = n = 0$, the waves are purely planar longitudinal (or axial) and $\omega_c = 0$. That is, waves having any frequency will propagate freely, with no attenuation, and can form standing waves in a tube of finite length, closed or open.
- ii) If $m, n \neq 0$, the cut off frequency is finite and only waves having frequency greater than the cut off frequency will propagate freely and under suitable conditions will form standing waves. Traveling waves having the transverse structure specified by the given values of m and n will decay exponentially in space, with attenuation constant β given by (5.150)a,b.

In practice, the existence of the phenomenon of ‘cutoff’ may arise if a chamber has slots or passages extending outward. Suppose that the chamber possesses a normal mode having relatively low frequency and a shape such that the amplitude of the pressure varies over the opening of the smaller passage. Then that mode tends to force generation of waves having spatial structure in the cross section of the passage. Therefore the cutoff frequency for oscillations in the passage is finite. If the frequency of the chamber mode is less than that cutoff frequency, the excited waves will have amplitude decaying with distance into the passage. Consequently, a pressure transducer placed at the far end of the passage will register a pressure amplitude much less than that existing in the chamber at that location. If data are obtained only with that transducer, then a misleading impression is obtained for the oscillating pressure in the main chamber. To interpret the data correctly, it is clearly necessary to understand well both the nature of the possible structure of the chamber modes and the phenomenon of cutoff frequency.

The decay of waves as they travel down a tube seems a strange result in view of the fact that no dissipative processes have been accounted for. Resolution of this paradoxical result can be reached by examining reflection and interference of waves traveling in directions not parallel to the axis of the tube. Off-axis propagation is associated with the non-uniform structure of the higher order modes and the reflections occur because of the boundary conditions set on the lateral surfaces. Morse and Ingard (1968) supply the details of this interpretation.

5.11. The Impedance Tube

Perhaps the simplest yet most widely useful acoustical instrument is the impedance tube, known for over one hundred years. Its true origin seems to have been lost. We follow Morse’s analysis (Morse 1948), but the most efficient and effective method for obtaining data is probably that worked out by Baum (1980); the references must be consulted for thorough discussions.

Figure 5.16 shows the essential features of the basic impedance tube. At one end is mounted the test sample of which the impedance or admittance function is to be measured. The other end is fitted with a piston or equivalent apparatus (e.g. a loudspeaker) whose frequency can be controlled. Measurements are taken when the frequency is constant. The piston then causes (‘radiates’) waves having amplitude p_- to the

left. If there are no distributed losses along the tube or its walls, a wave has constant amplitude and phase between the piston and a thin region of transition at the face of the sample. In that thin region waves are generated and propagate both to the left and the right.

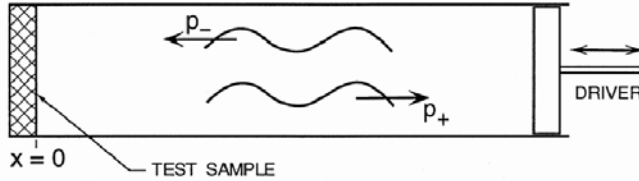


FIGURE 5.16. The basic impedance tube.

When the system has reached a steady state of oscillation, the region outside the transition zone contains a standing wave. The standing wave is the superposition of a wave \hat{p}_- propagating to the left from the piston, and a wave \hat{p}_+ propagating to the right, the net result of reflections from the sample and the transition region. The phase and amplitude of the wave \hat{p}_+ are different from those of wave \hat{p}_- due to the action of the test sample. We assume there is no mean flow, so with no distributed losses (or gains) of energy along the tube, the steady waves are represented by the two amplitudes of pressure and velocity:

$$\begin{aligned} \hat{p}_- &= Ae^{-ikx} & (a) & \hat{u}_- = -\frac{A}{\rho_0 a_0} e^{-ikx} & (b) \\ \hat{p}_+ &= Be^{ikx} & (c) & \hat{u}_+ = -\frac{B}{\rho_0 a_0} e^{ikx} & (d) \end{aligned} \quad (5.183)a-d$$

where k is a real wavenumber.

The total pressure and velocity oscillations are

$$\begin{aligned} \hat{p} &= Ae^{-ikx} + Be^{ikx} = A \left[e^{-ikx} + \frac{B}{A} e^{ikx} \right] \\ \hat{u} &= -\frac{A}{\rho_0 a_0} e^{-ikx} + \frac{B}{\rho_0 a_0} e^{ikx} = -\frac{A}{\rho_0 a_0} \left[e^{-ikx} - \frac{B}{A} e^{ikx} \right] \end{aligned} \quad (5.184)a,b$$

Define

$$\psi = \pi\alpha_0 + i\pi\beta_0 \quad (5.185)$$

and

$$B = -Ae^{2\psi} \quad (5.186)$$

so (5.184)a,b become

$$\begin{aligned} \hat{p} &= A \left[e^{-ikx} - e^{ikx+2\psi} \right] \\ \hat{u} &= -\frac{A}{\rho_0 a_0} \left[e^{-ikx} + e^{ikx+2\psi} \right] \end{aligned} \quad (5.187)a,b$$

On the face of the test sample at $x = 0$, the impedance is

$$z = \left[\frac{\hat{p}}{-\hat{u}} \right]_{x=0} = \rho_0 a_0 \frac{1 - e^{2\psi}}{1 + e^{2\psi}} \quad (5.188)$$

Thus the phase ψ is related to the impedance by

$$e^{2\psi} = \frac{1 - z/\rho_0 a_0}{1 + z/\rho_0 a_0} \quad (5.189)$$

Values of ψ may be inferred from measurements of the envelope of the modal structure along the axis of the impedance tube; (5.187)a becomes

$$\hat{p}(x) = -Ae^{\psi} [e^{ikx+\psi} - e^{-ikx-\psi}] = -2Ae^{\psi} \sin k(\psi + ikx)$$

Write

$$\psi + ikx = \pi(\alpha + i\beta) \quad (5.190)$$

with

$$\alpha = \alpha_0 \quad \text{and} \quad \beta = \beta_0 + \frac{2x}{\lambda} \quad (5.191)$$

The magnitude of the pressure oscillation in the standing wave is

$$|\hat{p}| = 2A|e^{\psi}| |\sin k\pi(\alpha + i\beta)| = 2Ae^{\pi\alpha} \sqrt{\cosh^2 \pi\alpha - \cos^2 \pi\beta} \quad (5.192)$$

Within this idealized picture of the pressure field, one needs only the maxima and minima of $|\hat{p}|$:

$$\begin{aligned} \text{Maxima: } |\hat{p}|_{max} &= 2Ae^{\pi\alpha} \cosh \pi\alpha \quad @ \quad \beta_0 + 2\frac{x}{\lambda} = \pm\frac{1}{2}, \pm\frac{3}{2}, \dots \\ \text{Minima: } |\hat{p}|_{min} &= 2Ae^{\pi\alpha} \sqrt{\cosh \pi\alpha - 1} \quad @ \quad \beta_0 + 2\frac{x}{\lambda} = \pm 1, \pm 2, \dots \end{aligned} \quad (5.193)\text{a,b}$$

A sketch of $|\hat{p}|$ is given in Figure 5.17

The real part of ψ , $\alpha \equiv \alpha_0$, may be found from the ratio of the maxima and minima,

$$\frac{|\hat{p}|_{max}}{|\hat{p}|_{min}} = \coth \pi\alpha \quad (5.194)$$

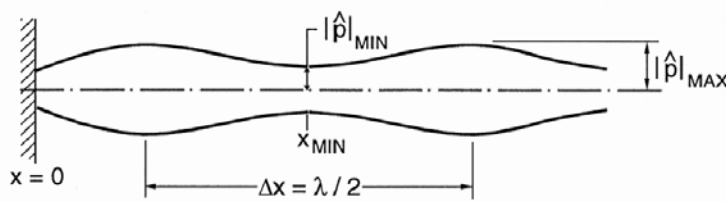


FIGURE 5.17. Sketch of $|\hat{p}|$ when distributed losses are ignored.

Values of β , and hence the imaginary part of ψ , are related to the locations of the maxima and minima. From (5.193)b, the first minimum occurs at $\beta_0 + \frac{2}{\lambda}x_{min} = 1$ which gives

$$\beta_0 = 1 - \frac{2}{\lambda}x_{min} \quad (5.195)$$

According to these results for the idealized impedance tube having no losses except at the test sample, only three measurements ($|\hat{p}|_{max}$, $|\hat{p}|_{min}$, x_{min}) are required to give ψ and hence the impedance at one frequency. In practice, use of the impedance tube is considerably more complicated. Even when the sample presents a well-defined surface to the acoustic field, the distributed losses cannot be ignored. Procedures for taking them into account are well-known in the field; the experimental methods required to handle them may become fairly involved. Baum (1980) has given a good discussion of the method he devised, perhaps the most effective available.⁸

The impedance tube remains the best apparatus for determining the impedance function of an inert surface. Efforts to adapt the method for measuring the impedance (or admittance) function of active surfaces

⁸This statement is based solely on the author's experience with his students, many years ago.

SOME FUNDAMENTALS OF ACOUSTICS

have not led to results useful for routine applications. The best example is probably Baum's effort to measure the admittance of a burning surface. Offering prospects of overcoming rather serious shortcomings of the T-burner and other devices prospects, the impedance tube posed its own problems which have not been overcome (Baum 1980). A short survey of applications of the impedance tube to measure the admittances of gaseous injectors has been given in the article by Brown, Culick and Zinn included in the collection edited by Boggs and Zinn (1978).

CHAPTER 6

Linear Stability of Combustor Dynamics

All problems of unsteady motion in combustion systems can be divided into the two classes: linearized and nonlinear. From the earliest discoveries of their transient behavior until the late 1950s, ‘combustion instabilities’ implied small amplitude unsteady (and unwanted) motions growing out of a condition of linear instability. Even with the expanding awareness that the nonlinear properties must be understood as well, linear behavior always remained an essential part of understanding all aspects of combustion instabilities, including the consequences of nonlinear processes.

The literature of linear combustion instabilities contains many papers dealing with special problems. There seems often to be a tendency to regard the results as somehow disconnected. However, apparent differences arise chiefly from the differences in the processes accounted for and in the choices of models for those processes. So long as the problems are dominated by oscillating behavior in combustors, probably most, if not practically all, of the results can be obtained in equivalent forms by suitable applications of the methods explained here. That statement is not as outrageous as it may seem, following as it does from the generality of the expansion procedures and the method of averaging covered in Chapter 4.

6.1. Historical Background of Linear Stability¹

Among the earliest interpretations of combustion instabilities was the idea of unstable disturbances having small amplitude. That idea lies behind the characterization of small oscillations and is commonly assumed to explain the initial stage, and hence the origin, of an oscillation in a combustion chamber. In fact it is a widely observed motion in solid rockets, but the cases in other systems are often not so clearly defined. The latter are often regarded as ‘nonlinear’ in some sense. Of the wide range of possible behavior, linear motions are most easily and rigorously described, and form the context within which the greater part of understanding combustion instabilities has been developed. We will examine some important aspects of nonlinear behavior in Chapter 7.

Although there were earlier considerations of oscillations in solid propellant rockets, the first analysis of a combustion instability seems to be that worked out by Grad (1949). At the suggestion of E.W. Price (private communication), Grad considered the problem of unsteady motions in a solid propellant rocket. Although he did not ignore the average flow entirely, he managed to avoid treating the details of the velocity field within the chamber away from the burning surface. He used an approximation to the mean flow based on a separate analysis. Eventually Grad worked out simple formulas for perturbations of the wavenumber. However, the calculations are difficult to follow and, so far as this writer knows, the results have never been checked against observations. A natural result of the analysis is that high frequency oscillations are possible. Grad closed his paper with the footnote that “high frequency oscillations have actually been observed recently in experiments performed at Inyokern, California.” That place was the Naval Ordnance Test Station (NOTS) which became the Naval Weapons Center (NWC) and is now the Naval Air Warfare Center (NAWC). Researchers at China

¹ A more thorough account of early developments of linear stability is given in Chapter 2.

Lake have had remarkable influence on the fields of steady and unsteady combustion of solid propellants continuously since the beginnings during World War II.

Grad's analysis and interpretation of his results were largely ignored, perhaps because combustion instabilities in such a well-developed form did not constitute a pressing problem and because accurate data were lacking. Moreover, when troublesome instabilities were encountered in solid rockets, they were eliminated or reduced by making changes in the system.² The situation changed markedly in the late 1950s. Apparently the development of large motors was the main stimulus. The need to develop theoretical, computational, and experimental methods then became clear. In the U.S. a very substantial effort grew, widespread but well-coordinated. A particularly important outgrowth of the coordination was the organization that in 1963 became JANAF and subsequently the JANNAF (Joint Army/Navy/NASA/Air Force) Sub-Committee. Apparently the initial efforts in JANAF were largely exerted by the solid rocket community, which we will tend to first here.

In the period covering the late 1950s to the middle 1960s, the special *ad hoc* group, "The Technical Panel on Solid Propellant Instability of Combustion", accomplished much in urging and coordinating research on instabilities in solid rockets. A useful collection of papers "Scientific Papers 1960–1963" produced by the panel gives a quite complete coverage of work by the group which included participants from Canada and Europe. The titles of the papers correctly suggest that they truly covered the field and set the agenda for much of the research carried out in the following decades.

The dominant group in theoretical developments during this period was that at the Johns Hopkins Applied Physics (JHU) Laboratory, mainly McClure, Hart, Bird and Cantrell. Although they treated unsteady erosive burning (McClure, Bird and Hart 1960b and McClure, Hart and Bird 1962), their results were not extensive; the subject has still not advanced very far. That is practically the only nonlinear subject that they treated deeply enough to obtain results, limited though they were. Thus, almost all the theoretical work dealt with linear stability. One of their most important accomplishments—which may not seem so impressive now—was to gain universal recognition of the admittance function of a burning surface as possibly the most important quantity to know accurately as an essential part of the basis for determining the stability of a motor. That is a consequence of the thorough fashion in which the JHU group formulated the general problem. In fact, that approach to the overall problem had considerable impact on the development of the theoretical aspects as well as on the general understanding of the field.

A large boost was given activity in the field of instabilities in solid propellant rockets. when a problem arose with the ballistic missile Minuteman II, an instability in the third stage (see Section 1.3). From its first use in the late 1950s (Price and Sofferis 1958) the T-burner had become generally accepted as the test device for giving data on the admittance or response function for a burning surface. The Minuteman problem led to a great deal of effort based on the device in the late 1960s and in the 1970s. Many important research programs devoted to the T-burner and to other subjects were sponsored by the Air Force Rocket Propulsion Laboratory (AFRPL).³ Simultaneously, work on all aspects of instabilities in solid rockets was actively pursued at the Naval Weapons Center, China Lake. It was during this period that work was begun to develop 'standard stability prediction' programs.

²E.W. Price (1992) has given the best historical account of oscillatory combustion in solid propellant rockets in the U.S. from the beginning (c. 1948) to 1991. Apparently no comparable document exists for experiences in other countries although there are scattered brief descriptions.

³The author is particularly indebted to AFRPL for supporting programs under which the method of nonlinear analysis described in this book was largely developed. Much of the work, especially in the early stages, was accomplished at Hercules, Inc. where the author served as consultant to a group headed by Dr. Merrill Beckstead. The methods were initiated largely under the sponsorship of the Air Force and the Navy, especially with the encouragement and support of E.W. Price.

The growth of understanding and theory of instabilities in liquid propellant rockets followed a path virtually independent of the work on solid propellant rockets in the U.S.⁴ After the early experimental work reported by Gunder and Friant (1950), discussed also by Yachter (1950), and by Summerfield (1950) who first used a time lag following the suggestion of von Karman, Crocco (1951a, b) developed the idea of the time lag for low-frequency oscillations. ‘Low’ means here that the propagation of disturbances within the chamber was ignored. Higher frequency instabilities, those which are close to normal acoustic modes of the chamber being studied, were then investigated by Crocco and Cheng (1956). They treated only one-dimensional motions in that work.

In his second paper referenced above, Crocco (1951b) essentially formulated the problem subsequently analyzed at great length by the Princeton group, the last published paper on the subject apparently being that by Zinn (1968). Figure 6.1 is a sketch of the situation. During the nearly two decades of work, the method of analyzing the unsteady flow field changed considerably but the prescription of the unsteady injection processes remained virtually unaltered, taking only two or three different forms. Because the injection of mass is restricted to the planar interface at the head end, the ‘injector plane’, the influx of material imposes a boundary condition on the flow of gases within the chamber. That condition is quite simply related to the velocity or mass flux which, following Crocco, is expressed in terms of the time lag. The reasoning has been summarized in Section 2.3.2, leading to a formula (2.88) for the source of mass w_ℓ containing two unknown quantities, the time lag τ and the ‘pressure index’ n :

$$w_\ell = \bar{w}_\ell \left(1 - \frac{d\tau}{dt} \right) \quad (6.1)$$

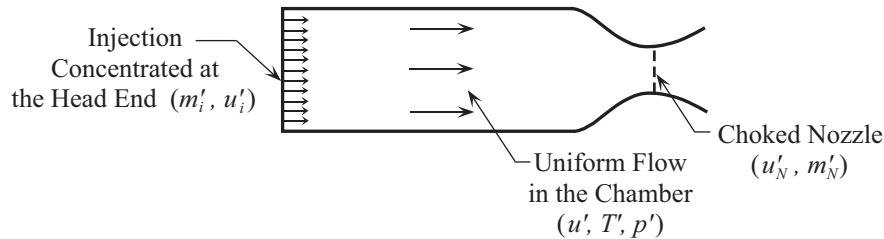


FIGURE 6.1. Basic physical model of a liquid rocket used in the Princeton theoretical work (1950–1968).

As explained in Section 2.3.2, this formula is used for the fluctuation of the mass source in the equation for conservation of mass. When the equations are linearized and written in terms of complex quantities, the real and imaginary parts of the equations effectively serve as two formal conditions determining n and τ as functions of the other variables in the problem.

The first extended theoretical account of linearized combustion instabilities was given in the book by Crocco and Cheng (1956) partly covered in previous papers by the authors. For the most part, the work is really a lengthy discussion and analysis of the linearized formulation of the situation sketched in Figure 6.1. Because the governing equations are not spatially averaged, for simplicity only one-dimensional problems are treated. The text contains an informative extended discussion of the time lag formulation and its linearized form. Appendix B of the book is a calculation of the admittance for a choked nozzle, an elaboration of the works by Tsien (1952) and Crocco (1953).

⁴I have been unable to locate any survey reports from the USSR during this or earlier times. See Natanzon (1999) for brief mention of early work on instabilities in the Soviet Union, and for a good summary of the principal Russian work available, including nonlinear analysis and experimental work. The recent book by Dranovsky (2006) covers test methods and results very thoroughly, but contains no theory dealing with fundamental dynamical processes.

In 1961 Culick (1961, 1963) worked out the first analysis of combustion instabilities using a Green's function and spatial averaging; the analysis was carried out for liquid rockets. That formulation allowed easy handling of linear three-dimensional problems, requiring calculation of the corresponding admittance function for the nozzle. More complete results for the admittance were later reported by Crocco and Sirignano (1967). Three-dimensional oscillations with the approximations shown in Figure 6.1 were analyzed by Scala (1955); Reardon (1961); Crocco, Reardon, and Harrje (1962); and Reardon, Crocco and Harrje (1963). The latter two papers contain limited experimental results.

Probably the greatest motivation for working so diligently to develop theory and prediction methods for solid rockets is the intrinsic limitation of single, short firing times. Thus, much effort has traditionally been devoted to transient behavior, particularly the growth of the amplitude during an unstable firing. The situation is quite different for liquid rockets, and especially for airbreathing systems that present opportunities for relatively long controllable test runs. It is perhaps, therefore, understandable that less attention has been paid to certain details of transient behavior in liquid-fueled systems.⁵ An exception to that practice was the early work by Crocco and co-workers, developed especially in the book written with Cheng. The text was devoted almost entirely to linear unstable motions including transients, and had much useful influence in the subject of instabilities in liquid rockets.⁶ Subsequently there were many papers published on linear instabilities in various systems.

In the 1980s there was renewed strong interest, both in the U.S. and in Europe, in small vehicles using dump combustors as the basic internal configuration for ramjets. As a result, active research programs were conducted to examine theoretical and experimental problems flowing largely from this simple configuration. The kinds of problems considered were, however, somewhat different from most of those traditionally studied as they were presented for solid and liquid rockets. Probably the most significant difference was that largely nonlinear motions were important,⁷ in respects not previously encountered in rocket engines. This characteristic had the far-reaching consequence that computational fluid dynamics became an essential part of progress. One of the first analyses using CFD was the interesting work by Jou and Menon (1986, 1990). Now CFD is widely used to study internal flows, although its practical use is only in early development. The subject is mentioned only briefly in this book.

Despite the rapid growth, broad applications, and truly fundamental importance of numerical methods for internal flows, the approximate literal analysis of internal flows remains an extremely important basis for understanding and designing propulsion systems. Together, this and the following chapter cover the most important practical aspects of the analytical method developed in this book. All results obtained are based on application of the method of spatial averaging.

6.2. Zero-Dimensional Instability of a Bulk Mode

Oscillations characterized by nearly uniform amplitude and phase in a chamber have arisen in practically every type of combustion system. Because the pressure oscillation is nearly independent of position, the velocity fluctuation is approximately zero. These oscillations occur at relatively low frequencies and are often caused by processes confined to the surface of the chamber, or to openings permitting flow. The most familiar related example is the sound produced when one blows past the opening of a bottle. In that case, the term 'Helmholtz mode' is often used to identify the origin of the tone; in discussions of combustion systems, one often finds the descriptive name 'bulk mode', and for solid propellant rockets the special name

⁵I believe that relatively less attention to the fine points of true transient behavior, while no doubt motivated by practical concerns, is responsible for a tendency to acquire less understanding of the behavior of disturbances in liquid-fueled systems.

⁶As a personal note, the author is forever indebted to Professor Crocco, for that work motivated his thesis work (Culick 1960).

⁷An exception enjoying several useful applications was the elementary linear analysis by Culick and Rogers (1981), which included a simple analysis of the choked inlet duct to determine its admittance function.

‘ L^* instability’ is applied. It is the last we treat here in some detail, although in simplified form, to introduce some of the basic ideas of computing linear instability.

Akiba and Tanno (1959) adapted the analysis by Crocco and Cheng (1956, Chapter 2) of a low frequency instability in liquid rockets⁸ to the corresponding problem in solid rockets. The main difference between applications to the two classes of systems is in the models used for unsteady combustion. In the limit of linear behavior there are really no basic distinctions, another example of the practical value to be gained from studying systems other than that of immediate concern.

Although Akiba and Tanno apparently had no concern with particular problems in motors, Sehgal and Strand (1964) worked at the Jet Propulsion Laboratory (later officially named JPL) and were involved with development of motors for space vehicles. Because of operations at low pressures requiring lower structure weights, L^* instability became an important problem. The first published concern with the behavior, particularly its connection to intermittent extinction, was documented by Anderson, Strehlow, and Strand (1963). While the subsequent analysis by Sehgal and Strand differed only in certain details from Akiba and Tanno’s, their lasting contribution was the first comparison of theory and experiment, shown here in Figure 6.2. The two theoretical lines arise from details of the analysis which produces two intersections of curves defined in the specification of the boundary of the stable and unstable regions of operations. No reason was given that one of the theoretical curves is favored by the experimental results. The definitions of the dimensionless critical time constant $(\tau_n)_{cr}$ and characteristic chamber length L^* are

$$(\tau_n)_{cr} = \tau_{cr} \frac{\bar{r}^2}{4\kappa} \quad (6.2)$$

$$L^* = \frac{4\kappa c_D R T_f (\tau_n)_{cr}}{a^2} \bar{p}_c^{-2n} \quad (6.3)$$

where κ is the thermal diffusivity; c_D is the discharge coefficient; T_f is the flame temperature; and a is the constant in the linear burning rate law. Equation (6.3) therefore predicts quite well the behavior $L^* \sim p^{-2n}$ shown in Figure 6.2, prepared using the properties of the propellant tested, JPL-534.

The two analyses just mentioned differed mainly in their representations of unsteady burning of a solid propellant. Akiba and Tanno drew on Green’s model (See Section 2.1.2), while Sehgal and Strand worked out their own analysis of the combustion response, an incomplete⁹ form of Denison and Baum’s earlier approximate theory (Section 2.2.2). Both treatments followed Tsien’s lead in application of a form of Nyquist’s theorem (Annex G and Chapter Nine) to study the stability of the system. Tsien used a modification of the theorem suggested by Satche (1949) to handle an exponential necessarily accompanying introduction of a (constant) time lag in the combustion process.¹⁰ Although neither treatment required a time lag in the same way followed by Tsien, both used Satche’s modification of Nyquist’s theorem. That is an unnecessary complication as Beckstead, Ryan, and Baer (1966) and the next paper by Coates, Cohen and Harvill (1967) implicitly showed.

Following previous authors, Coates *et al.* began their analysis with the transfer function G_m for the motor

$$\frac{\delta m_0}{\delta m_i} = G_m = \frac{G_c}{1 - G_p G_c} \quad (6.4)$$

which follows directly from the block diagram drawn in Figure 6.3.

⁸The discussion by Crocco and Cheng is an extension and elaboration of the original paper by Tsien (1953), based on essentially the same ideas. Tsien also proposed possible use of feedback control; see Chapter Nine.

⁹One consequence of the incompleteness is failure to reach the correct limit for zero frequency; see equation (12) and accompanying comment, in Coates *et al.* (1967).

¹⁰The analyses by Tsien; Crocco and Cheng; Akiba and Tanno; and by Sehgal and Strand were based on Laplace transforms, applied, naturally, to linear problems. Hence the presence of a constant time lag τ in the coupling between, for example, the heat or mass sources, and the pressure fluctuations, produces exponentials, $e^{-s\tau}$, in the characteristic equation.

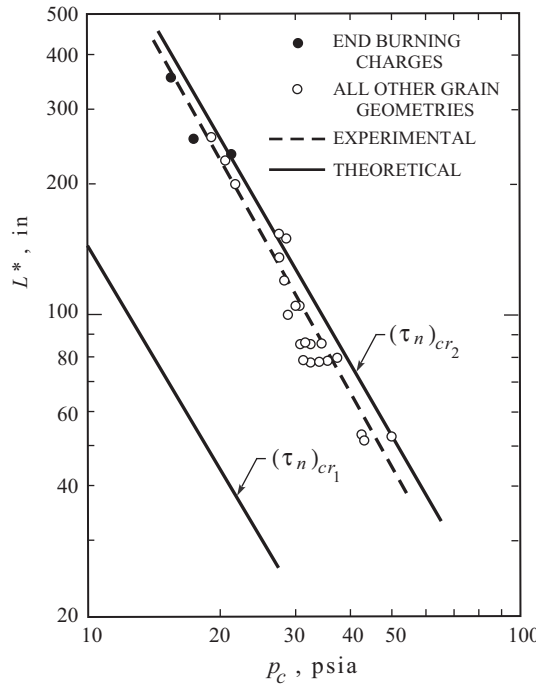


FIGURE 6.2. L^* versus chamber pressure, showing the stability limit for oscillations (Sehgal and Strand 1964).

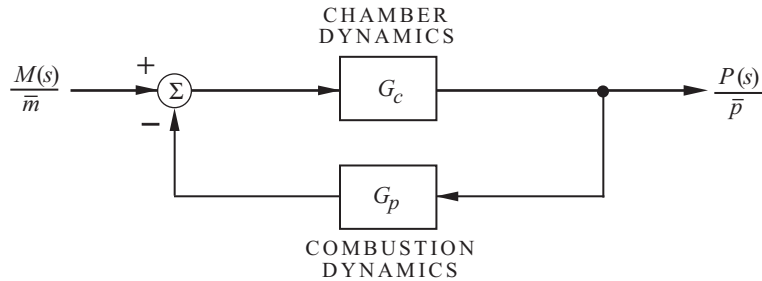


FIGURE 6.3. Block diagram of the system, adapted from Figure 1 of Coates, Cohen, and Harvill (1967).

The transfer function G_p for the combustion dynamics is given by Denison and Baum's result, (2.67) here; G_c is the transfer function for the chamber dynamics. For the model of the L^* burner used in the works cited, and explained in the next section, the equation for the unsteady chamber pressure is,

$$\tau_c \frac{d}{dt} \left(\frac{p'}{\bar{p}} \right) + \frac{p'}{\bar{p}} = \frac{m'}{\bar{m}}. \quad (6.5)$$

The Laplace transform is

$$(1 + s\tau_c) \frac{P(s)}{\bar{p}} = \frac{M(s)}{\bar{m}} \quad (6.6)$$

so

$$G_c = \frac{1}{1 + s\tau_c}. \quad (6.7)$$

Denison and Baum's result, (2.67), gives G_p , completing the basis for the calculation discussed by Coates, Cohen, and Harvill. Figure 6.4 reproduces two results the authors found in support of their calculations. The solid lines are computed from this result

$$\frac{1}{L^*} = \frac{1}{\kappa \Gamma^2 c^*} \frac{\bar{r}^2}{(\tau_n)_{cr}} \quad (6.8)$$

where $(\tau_n)_{cr} = (\tau_c \bar{r}^2 / \kappa)_{cr}$. Beckstead (1965) obtained the data for Utah TF propellant.

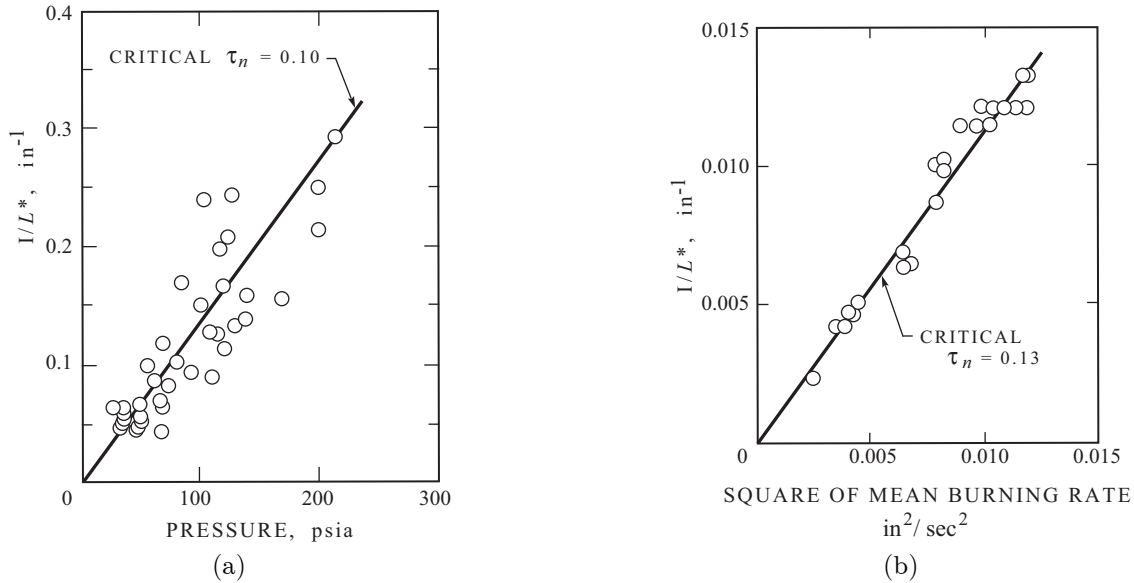


FIGURE 6.4. L^* instability data for two propellants (a) Utah TF (University of Utah) and (b) JPL-534 (Jet Propulsion Laboratory) (Coates, Cohen, and Harvill 1967).

Besides having very low frequencies and nearly uniform but sinusoidal (i.e., pulsating) pressure fields when oscillations are excited, instabilities of the bulk mode often lead to intermittent unsteady behavior commonly referred to as 'chuffing.' Figure 6.5 shows both types of behavior leading to extinction of combustion. Identifying the stability boundary unambiguously, given that loss of stability does not necessarily mean growth of an oscillation out of noise, presents problems under these conditions. The difficulties are both experimental and interpretive, treated at some length in the references. We will not discuss the subject here except to note that whatever the precursor behavior, the limit of stability seems to define a sufficiently narrow band of values, L^* and pressure or burning rate, that a line is a reasonable approximation, Figures 6.2 and 6.4. Put simply, it makes sense to speak of the ' L^* stability limit.'

Chuffing was not a new phenomenon, discovered quite early as one aspect of L^* instability. The earliest written record seems to have been prepared by Crawford *et al.* (1945) although earlier informal reports have been suggested on several occasions. Some early British experiences were discussed by Huffington (1954). An indication of the problem's practical persistence is conveyed by the session on "Nonacoustic Combustion Instability" included in the AIAA Solid Propellant Rocket Conference, January 1964. Eisel *et al.* (1964) reported results of tests with an L^* burner and a very long 'acoustic' burner having adjustable length as long as sixty (!) feet. Several records of chuffing at low frequency instabilities from the paper by Yount and Angelus (1964) are reproduced in Figure 6.6 showing well the intermittent behavior sometimes observed.

Oberg (1968) addressed the problem displayed by Figure 6.5 which had led to the idea of 'nonacoustic' instabilities in contrast to 'acoustic' instabilities of the sort described in Chapter One. It was his correct contention that 'acoustic' and 'nonacoustic' instabilities are in fact closely related. Of those working in the

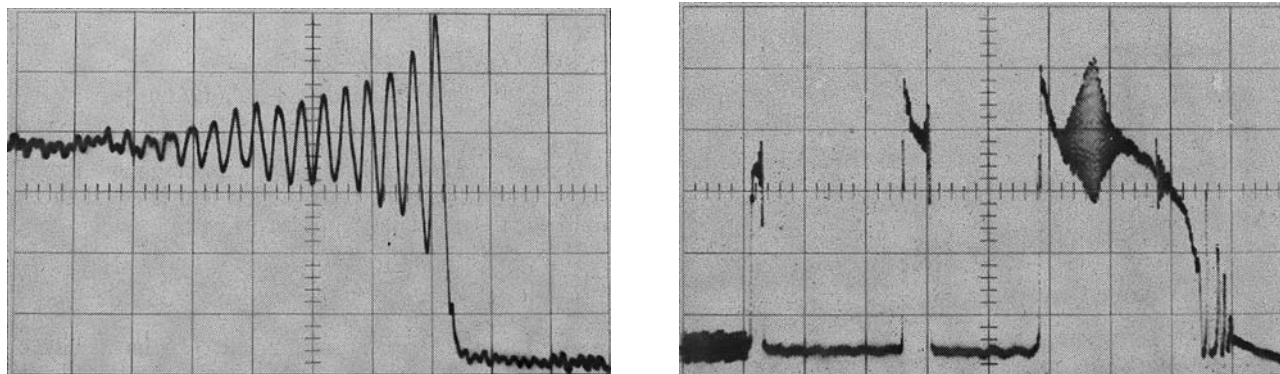


FIGURE 6.5. Two examples of natural cessation of L^* instabilities (a), growth of oscillations ending in extinction; (b) chuffing, leaking to extinction (Beckstead, Ryan, and Baer, 1966).

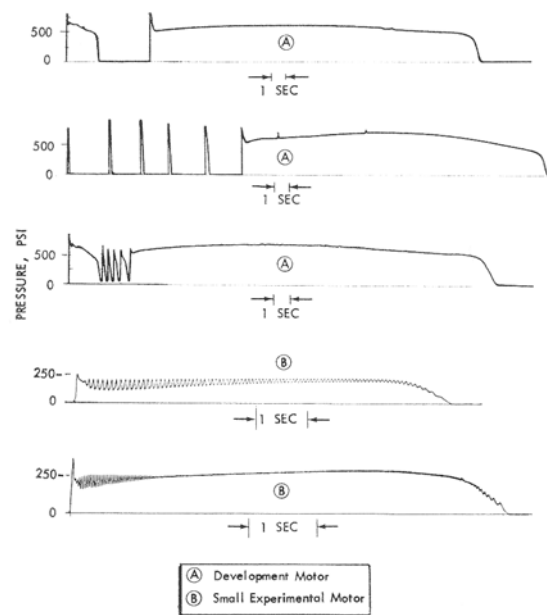


FIGURE 6.6. Five pressure records of chuffing (A) and low frequency instabilities (B) (Yount and Angelus 1964).

field, he was first to recognize that an L^* instability is the limit, as the frequency tends to zero, of the wave or acoustical modes. Oberg showed the result explicitly for longitudinal motions; Culick (1968) subsequently proved that the conclusion holds generally, with a calculation repeated here in Section 6.6.

A straightforward description of the bulk mode or L^* instability is based on the assumption that the frequency is so low that all processes respond essentially instantaneously. This requires that the travel time of a small disturbance in the chamber, and in the nozzle, be much less than the period of the oscillation. The pressure then remains sensibly uniform throughout and pulsates in time.

With this assumption, all variations in space are ignored, and in particular the conservation of momentum need not be considered. Mainly one is concerned with the conservation of mass. Let S_b be the area of burning surface S_t the area of the nozzle throat, V the volume, and c^* the usual characteristic velocity. The total

mass of gas in the volume is ρV at any instant; its rate of change must equal the difference between the rate at which mass enters, and the rate at which it leaves,

$$\frac{d}{dt}(\rho V) = mS_b - S_t \frac{p}{c^*} \quad (6.9)$$

where $m = \rho_s r$ is the mass flux at the burning surface. The relation defining c^* as the ratio of $S_t p$ to the total mass flux out the nozzle $c^* = S_t p / m = \sqrt{RT/\Gamma}$, with $\Gamma^2 = \gamma \left(\frac{2}{\gamma+1} \right)^{\frac{\gamma+1}{\gamma-1}}$ is strictly valid only in steady flow (Altman *et al.* 1960). Its use here is justified by the assumption that the transit time of a fluid element through the nozzle is much less than the period of oscillation. This is sometimes referred to as the “zero-length” approximation to the time-dependent behavior of a nozzle. Note that (6.9) applies to any geometry; it is not restricted to end burners.

We assume that the thermodynamic state of the gases is uniform in the chamber, and that combustion occurs only in a thin zone near the propellant surface; residual combustion is ignored. Further, it is assumed that the gases can be described by the equation of state for a perfect gas, $p = \rho RT$. Thus we have two equations in three variables (p, ρ, T) because the mass flux from the surface m is assumed to be a function of pressure only. The principle of conservation of energy provides a third relation, but it will be handled shortly in a simplified manner.

Now we form a linearized problem in familiar fashion by writing $p = \bar{p} + p'$... etc. and by ignoring squares and higher order terms. Then the linearized equation of state is

$$\frac{p'}{\bar{p}} = \frac{\rho'}{\bar{\rho}} + \frac{T'}{\bar{T}} \quad (6.10)$$

Similarly, equation (6.9) can be expanded as follows:

$$\bar{\rho}V \frac{d}{dt} \left(\frac{\rho'}{\bar{\rho}} - \frac{T'}{\bar{T}} \right) = (\bar{m}S_b) \frac{m'}{\bar{m}} - \frac{S_t \bar{p}}{\bar{c}^*} \left(\frac{p'}{\bar{p}} - \frac{c^{*\prime}}{\bar{c}^*} \right) \quad (6.11)$$

Because $c^* \sim \sqrt{T}$, $c^{*\prime}/\bar{c}^* = T'/2\bar{T}$ and the last equation can be written

$$\frac{\bar{\rho}V}{S_t \bar{p}} \bar{c}^* \frac{d}{dt} \left(\frac{p'}{\bar{p}} \right) = \left[\frac{\bar{m}S_b}{\frac{S_t \bar{p}}{c^*}} \right] \frac{m'}{\bar{m}} - \frac{p'}{\bar{p}} + \frac{\bar{\rho}V \bar{c}^*}{S_t \bar{p}} \frac{d}{dt} \left(\frac{T'}{\bar{T}} \right) + \frac{1}{2} \frac{T'}{\bar{T}} \quad (6.12)$$

In steady flow, conservation of mass requires

$$\bar{m}_b S_b = S_t \bar{p} / \bar{c}^* \quad (6.13)$$

and with the equation of state, we find the characteristic time τ_c ,

$$\frac{\bar{\rho}V \bar{c}^*}{S_t \bar{p}} = \frac{V}{S_t} \frac{\bar{c}^*}{R \bar{T}} = \frac{L^* \bar{c}^*}{R \bar{T}} = \tau_c \quad (6.14)$$

where the conventional definition of L^* is

$$L^* = V/S_t \quad (6.15)$$

Thus the equation for the pressure fluctuation is

$$\tau_c \frac{d}{dt} \left(\frac{p'}{\bar{p}} \right) = \frac{m'}{\bar{m}} - \frac{p'}{\bar{p}} + \left[\tau_c \frac{d}{dt} \left(\frac{T'}{\bar{T}} \right) + \frac{1}{2} \frac{T'}{\bar{T}} \right] \quad (6.16)$$

To simplify the discussion further, consider the extreme case in which the oscillations are so slow, and mixing is so thorough, that the temperature is not only uniform in the chamber but also constant, so $T' = 0$. Then the last equation is

$$\tau_c \frac{d}{dt} \left(\frac{p'}{\bar{p}} \right) = \frac{m'}{\bar{m}} - \frac{p'}{\bar{p}} \quad (6.17)$$

With $m = \rho_s r, m'/\bar{m} = r'/\bar{r}$, and if the burning always responded instantaneously to a change of pressure, $r \sim p^n$, one could write

$$\frac{r'}{\bar{r}} = n \frac{p'}{\bar{p}} \quad (6.18)$$

and (6.17) would become

$$\tau_c \frac{d}{dt} \left(\frac{p'}{\bar{p}} \right) = (n - 1) \frac{p'}{\bar{p}} \quad (6.19)$$

The solution to this equation is immediate:

$$\frac{p'}{\bar{p}} = \left(\frac{p'}{\bar{p}} \right)_0 e^{\left(\frac{n-1}{\tau_c} \right) t} \quad (6.20)$$

where $(p'/\bar{p})_0$ is the fluctuation at $t = 0$. Thus, if $n > 1$, a small disturbance will grow without limit. This is well-known behavior: motors using propellants with n close to unity are very sensitive to small changes in pressure and if n is positive, the system is unstable. That is the first criterion established for stability if combustion in a solid¹¹ propellant rocket, found by Malina (Karman and Malina, 1940).

The relation (6.18) is valid only in the limit of very low frequencies. In general, the burning rate of a propellant exposed to a sinusoidal pressure oscillation will vary sinusoidally also, but not in phase with the pressure, as shown in Section 2.2.2, equation (2.66), for the simplest realistic case. That behavior is represented by the response function R_b ,

$$\frac{m'}{\bar{m}} = R_p \frac{p'}{\bar{p}} = [R_p^{(r)} + iR_p^{(i)}] \frac{p'}{\bar{p}} \quad (6.21)$$

The response function is a complex function of frequency, and can be written as

$$R_p = R_p^{(r)} + iR_p^{(i)} = |R_p|(\cos \phi + i \sin \phi) \quad (6.22)$$

For harmonic motions,

$$\begin{aligned} \frac{p'}{\bar{p}} &= Pe^{-i(\omega+i\alpha)t} \\ &= Pe^{\alpha t} e^{-i\omega t} \end{aligned} \quad (6.23)$$

If the growth constant α is positive, then the oscillation is unstable and grows exponentially in time. In all problems of linear stability, the principal task is to compute the growth constant. Substitution of (6.21) and (6.23) into (6.17) leads to

$$\tau_c(\alpha + i\omega)P = [R_p^{(r)} + iR_p^{(i)}]P - P \quad (6.24)$$

The amplitude P is a common factor, and the real and imaginary parts of (6.20) give the two equations

$$\text{Real Part} \quad \alpha\tau_c = R_p^{(r)} - 1 \quad (6.25)$$

$$\text{Imaginary Part} \quad \omega\tau_c = R_p^{(i)} \quad (6.26)$$

The response function is a fundamental quantity in all problems of combustion instability in solid propellant rockets. It is a dynamical property of the propellant, summarizing all the linear behavior for unsteady-burning. There is presently no way to calculate the response function for a real propellant. As we have emphasized in Chapter 2, the most important current experimental problem is its measurement.

¹¹With only minor changes of definitions and interpretation, the same result follows for liquid or gaseous propellant rockets.

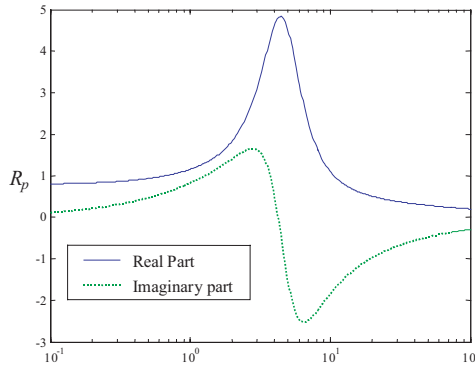


FIGURE 6.7. Real and Imaginary parts of a simple response function (see the same result, Figure 2.14).

Equation (6.25) shows that a sinusoidal oscillation is unstable if the real part of the response function is greater than unity. The frequency of an unstable oscillation is then given by (6.26); obviously $R_p^{(i)}$ must be positive for this relation to make sense.

There have been many attempts to compute the response function. Many of these actually produce the same result,¹² discussed in Section 2.2. The main feature is that the response function depends on two parameters (called A and B) and is a function of the dimensionless frequency

$$\Omega = \frac{\omega\kappa}{\bar{r}^2} \quad (6.27)$$

where κ is the thermal diffusivity of the propellant. The real and imaginary parts of R_b have the form shown in Figure 6.7, a repeat of Figure 2.14. In this case, according to (6.26), a bulk-mode instability can occur only for frequencies such that the dimensionless frequency is below the value Ω_0 at which $R_p^{(i)}$ passes through zero. Let Ω^* be the value of Ω at which $R_b^{(r)} = 1$, so $\alpha = 0$. Then a sinusoidal fluctuation is unstable if Ω lies in the range

$$\Omega^* < \Omega < \Omega_p. \quad (6.28)$$

Equation (6.26) becomes

$$\left(\frac{\bar{r}^2}{\kappa}\right) \frac{\omega\kappa}{\bar{r}^2} \tau_c \equiv \frac{\bar{r}^2}{\kappa} \Omega \tau_c = R_p^{(i)} \quad (6.29)$$

On the stability boundary, when $\Omega = \Omega^*$,

$$\bar{r}^2 \tau_c = \frac{\kappa}{\Omega^*} R_p^{(i)}(\Omega^*) \quad (6.30)$$

With $\bar{r} = a\bar{p}^n$, and $\tau_c = L^* \bar{c}^* / R\bar{T}$, this relation gives

$$L^* = \left[\frac{\kappa R\bar{T}}{\bar{c}^* a^2} \frac{R_p^{(i)}(\Omega^*)}{\Omega^*} \right] \frac{1}{\bar{p}^{2n}} \quad (6.31)$$

The group in brackets is almost independent of pressure, so equation (6.31) gives the result that on the stability boundary, $L^* \sim \bar{p}^{-2n}$. This result has been verified by experimental results such as those given in Figure 6.2 and 6.4.

¹²In the past 10–15 years, efforts have been reported to formulate more realistic forms. The broad characteristics and roles of the real and imaginary parts of the response function remain. That's a useful mnemonic aid. See, however, Section 6.9.3.

For $\alpha \neq 0$, (6.26) again gives (6.31), but with $\Omega > \Omega^*$; dividing the two results one finds

$$\frac{(L^*)_{\alpha>0}}{(L^*)_{\alpha=0}} = \left[\frac{R_b^{(i)}(\Omega)}{R_b^{(i)}(\Omega^*)} \right] \left(\frac{\Omega^*}{\Omega} \right) \quad (6.32)$$

The right-hand side is less than unity, so the unstable region in the plot L^* versus \bar{p} lies below the stability boundary as shown in Figure 6.2.

Equations (6.25) and (6.26) for steady sinusoidal motions follow from the simple model of the combustion dynamics used as the basis of equation (6.17) for general (but linear) time-dependent behavior. Experimental results first confirmed that the picture was correct. For practical applications, and especially as part of the effort to determine the transient behavior of burning propellants at higher frequencies, there was much interest in obtaining firm results for the response function over broad frequency ranges. A reasonable beginning is to determine the extent to which L^* instability may be used to distinguish quantitative differences among propellants.

To do so requires correlating data with the complex equation (6.24) which produces the two real equations (6.25) and (6.26). The two equations allow determination of two parameters. It is a lucky result that Denison and Baum's results (2.66) contains only two parameters, A and B . Then the question is—can A and B be determined from experiments, uniquely for each propellant? Put another way, will the parameters A and B define the dynamical behavior of solid propellants? To answer the question, we must determine how well this theory explains observed behavior.

It is easy to solve (6.25) and (6.26) for A and B to find

$$A = \Omega \frac{\beta_1 h_2 + \beta_2 h_1}{\alpha_1 \beta_2 - \alpha_2 \beta_1} \quad (6.33)$$

$$B = -\frac{\alpha_1 h_2 + \alpha_2 h_1}{\beta_1 h_2 + \beta_2 h_1} \quad (6.34)$$

where $h_1 = 1 + \alpha \tau_c$, $h_2 = \omega \tau_c$ and

$$\begin{aligned} \alpha_1 &= h_2(1 - \lambda_r) + h_1 \lambda_i \\ \alpha_2 &= h_1(1 - \lambda_r) - h_2 \lambda_i \\ \beta_1 &= (h_2 - n)\lambda_r - h_1 \lambda_i \\ \beta_2 &= (h_2 - n)\lambda_i + h_1 \lambda_r \end{aligned} \quad (6.35)a,b,c,d$$

function λ of dimensionless frequency was defined by equation (2.26)a,b;

$$\begin{aligned} \lambda_r &= \frac{1}{2} \left\{ 1 + \frac{1}{\sqrt{2}} \left[(1 + 16\Omega^2)^{1/2} + 1 \right]^{1/2} \right\} \\ \lambda_i &= \frac{1}{2\sqrt{2}} \left[(1 + 16\Omega^2)^{1/2} - 1 \right] \end{aligned} \quad (6.36)a,b$$

Equations (6.25) and (6.26) with Denison and Baum's result for R_b , define the two families of curves drawn in Figure 6.7 for $\alpha = 0$, the only condition for which data are available. Acceptable results must have $A > 0$ (by definition of A) and must also lie to the left of the line for intrinsic stability.¹³ Evidently Denison and Baum's result may represent the dynamics of A-35 (A=14, B=0.8) but not those of A-13. Possible reasons for the difference have not yet been explained. The two propellants had the same oxidizer particle size distribution and differed by only 1% in the amounts by mass. A-13 had 24% by mass of PBAN binder; A-35 contained 25% of an estane type of polyurethane binder. One might guess that the difference in dynamical behavior suggested by Figure 6.8 is related to the different binders, but details are lacking.

¹³The term "intrinsic stability" refers to unlimited growth of a disturbance in the burning rate which is dependent only on the dynamics of the propellant and which occurs without an external disturbance.

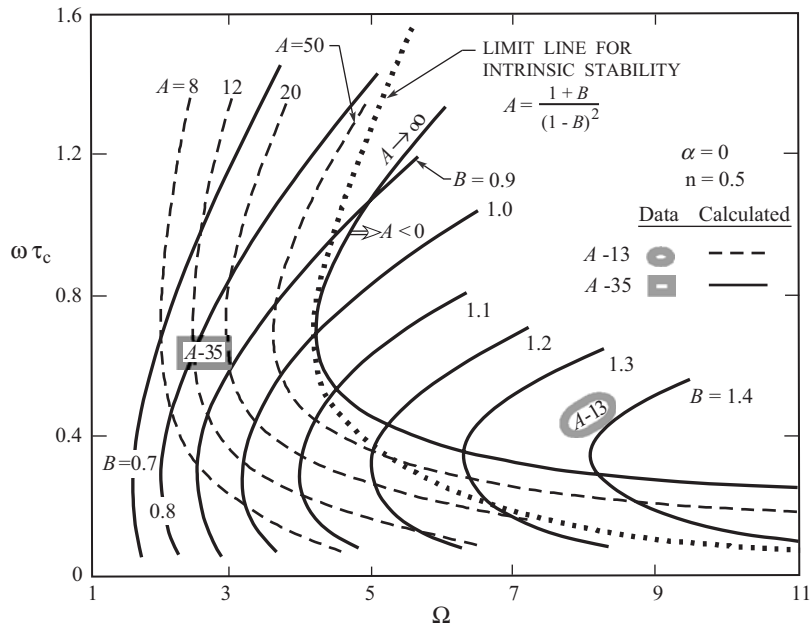


FIGURE 6.8. The L^* -chart for determining the parameters A and B . Data for the propellants A-13 and A-35 lie in the indicated regions. (Beckstead and Culick 1971).

6.3. A Formal Solution to the Problem of Linear Stability

By ‘solution’ we mean here formulas for calculating the amplitudes $\eta_n(t)$ of modes retained in the expansion for the pressure field, $p'(\mathbf{r}, t) = \bar{p}\Sigma\eta_n(t)\psi_n(\mathbf{r})$. The amplitudes satisfy the oscillator wave equations (4.36) with N replaced by n :

$$\frac{d^2\eta_n}{dt^2} + \omega_n^2\eta_n = F_n + F_n^c \quad (n = 1, 2, \dots) \quad (6.37)$$

where F_n^c stands for the generalized ‘force’ associated with the exercise of control; and F_n is the spatial average of that part (sometimes called the “projection” on the basis function ψ_n) of the internal processes affecting the motion of the n^{th} oscillator, given by (4.30):¹⁴

$$F_n = -\frac{\bar{a}^2}{\bar{p}E_n^2} \left\{ \int h\psi_n dV + \iint f\psi_n dS \right\} \quad (n = 1, 2, \dots) \quad (6.38)$$

and

$$E_n^2 = \int \psi_n^2 dV \quad (6.39)$$

Here we will suppress F_n^c because we are concerned only with the internal behavior of the system.¹⁵ In general, the F_n contain contributions associated with the motions of oscillators other than the n^{th} —i.e., the modes are coupled. For analysis of linear stability we are justified in ignoring that coupling, for reasons given by Culick (1997). Each F_n is a linear function of the amplitude and velocity of the oscillator, having

¹⁴In this chapter and subsequently we will often indicate integration over volume by single integral signs, as here, to avoid unnecessary use of $\iint\iint$.

¹⁵The functions \mathcal{F} and \mathcal{P} implicitly contain all effects of control; the generality of subsequent calculations is therefore not reduced by removing F_n^c .

the form

$$F_n = F_n^\eta \eta_n + F_n^{\dot{\eta}} \frac{d\eta_n}{dt} \quad (n = 1, 2, \dots) \quad (6.40)$$

where the F_n^η and $F_n^{\dot{\eta}}$ are constants, depending only on the mode.

With these assumptions, the oscillator equations (6.37) are the uncoupled set

$$\frac{d^2\eta_n}{dt^2} - F_n^{\dot{\eta}} \frac{d\eta_n}{dt} + (\omega_n^2 - F_n^\eta) \eta_n = 0 \quad (n = 1, 2, \dots) \quad (6.41)$$

Because the equations are uncoupled, the normal modes ψ_n for the corresponding classical acoustic problem are also the normal modes for the linear problem of combustor dynamics. The general problem of determining linear stability has therefore come down to the problem of determining the stability of the normal modes. In the usual fashion we assume sinusoidal time dependence with complex frequency Ω ($\Omega \equiv \bar{a}k$ below):

$$\eta_n(t) = \hat{\eta}_n e^{-i\Omega t} \quad (n = 1, 2, \dots) \quad (6.42)$$

Equation (6.41) gives the quadratic equation for Ω_n :

$$\Omega^2 + iF_n^{\dot{\eta}}\Omega - (\omega_n^2 - F_n^\eta) = 0 \quad (6.43)$$

having solution

$$\Omega = -i\frac{1}{2}F_n^{\dot{\eta}} + \omega_n \sqrt{1 - \frac{1}{\omega_n^2} \left[F_n^\eta + \frac{1}{4} (F_n^{\dot{\eta}})^2 \right]} \quad (6.44)$$

where we take the (+) sign on the radical to give a positive real frequency. Hence the amplitudes are

$$\eta_n(t) = e^{\frac{1}{2}F_n^{\dot{\eta}}t} e^{-i\omega_n \sqrt{1-\zeta^2}t} \quad (6.45)$$

with the definition

$$\zeta_n = \frac{1}{\omega_n} \sqrt{F_n^\eta + \frac{1}{4} (F_n^{\dot{\eta}})^2} \quad (6.46)$$

The n^{th} mode is stable of

$$F_n^{\dot{\eta}} < 0 \quad (6.47)$$

That is, the coefficient of $\dot{\eta}_n$ in the expression for F_n must be negative for the n^{th} mode to be stable. That formal condition means that the n^{th} mode has positive damping.

According to the methods of Fourier analysis, an arbitrary disturbance at some initial time (say $t = 0$) in the chamber can be synthesized of the normal modes. The time-evolution of the disturbance is therefore determined by the $\eta_n(t)$. In particular, an arbitrary disturbance in a combustor is stable if (and only if) all of the normal modes are stable and we arrive at the general result for the linear stability of a combustor:

- (i) Write the linearized function for the force acting on the n^{th} oscillator (spatially averaged acoustic mode) in the form

$$F_n = F_n^\eta \eta_n + F_n^{\dot{\eta}} \frac{d\eta_n}{dt}$$

- (ii) Then any initial disturbance in a combustor is stable if and only if all the $F_n^{\dot{\eta}}$ are negative:

$$\text{Linear Stability} \iff F_n^{\dot{\eta}} < 0 \quad (\text{all } n)$$

The preceding calculation, and its conclusion, illustrate further a point first made in Chapter 3: We have found a means of computing the linear stability of a combustor without knowing the actual linear motions themselves. The complex frequency (6.44) is in fact the frequency for the actual linear modes including the influences of all the processes accounted for. But calculation of the F_n^η and $F_n^\dot{\eta}$ with the formula (6.38) requires knowledge only of the **unperturbed** normal modes—their frequencies ω_n and shapes $\psi_n(\mathbf{r})$. The formal statement of this property is that the eigenvalues (Ω_n) to any order in the relevant expansion parameter (here $\bar{M}_r := \mu$ defined in Chapter 3) can be computed knowing the eigenfunctions (ψ_n) only to one less order. The eigenvalues Ω_n are here given to first order in the Mach number of the average flow but only the unperturbed classical eigenfunctions ψ_n are required. This is the basic characteristic of the expansion procedures with spatial averaging that makes the method devised here so useful in practice, as we have emphasized in Chapter 4; examples of this important result are widespread in the field of combustion instabilities generally, but may be found especially in the literature for solid rockets.

6.4. An Alternative Calculation of Linear Stability

An equivalent calculation of the result for linear stability makes direct use of the formula for the wavenumber. Write

$$\eta_n = \hat{\eta}_n e^{-i\bar{a}kt} ; \quad F_n = \hat{F}_n e^{-i\bar{a}kt}$$

and substitute in (6.37) with F_n^c ignored to find $(\bar{a}k)^2 = (\bar{a}k_n)^2 - \hat{F}_n/\hat{\eta}_n$, or

$$(\bar{a}k)^2 = (\bar{a}k_n)^2 - \frac{1}{\hat{\eta}_n} (\hat{F}_n^{(r)} + i\hat{F}_n^{(i)}) \quad (6.48)$$

where $(\)^{(r)}$ and $(\)^{(i)}$ identify real and imaginary parts. With¹⁶ $\bar{a}k = \omega + i\alpha$, this formula is

$$\omega^2 + i(2\alpha\omega) - \alpha^2 = \omega_n^2 - \frac{1}{\hat{\eta}_n} (\hat{F}_n^{(r)} + i\hat{F}_n^{(i)})$$

Because α and \hat{F}_n are first order in the expansion parameter and terms of higher order must be dropped¹⁷, we ignore α^2 with respect to ω^2 . Then the real and imaginary parts of the last equation give

$$\begin{aligned} \omega^2 &= \omega_n^2 - \frac{1}{\hat{\eta}_n} \hat{F}_n^{(r)} \\ \alpha &= -\frac{1}{2\omega_n} \hat{F}_n^{(i)} \end{aligned} \quad (6.49)a,b$$

where ω has been set equal to ω_n in the right-hand sides to ensure that higher order terms are not retained. Now take the square root of the first equation and again drop higher order terms to find

$$\begin{aligned} \omega &= \omega_n - \frac{1}{2\omega_n} \frac{\hat{F}_n^{(r)}}{\hat{\eta}_n} \\ \alpha &= -\frac{1}{2\omega_n} \frac{\hat{F}_n^{(i)}}{\hat{\eta}_n} \end{aligned} \quad (6.50)a,b$$

The system is unstable if $\hat{F}_n^{(i)}$ is negative, so α is positive. This condition is essentially a generalized form of Rayleigh's Criterion discussed further in Section 6.6.

After higher order terms are dropped from (6.44), the real and imaginary parts of $\Omega \equiv \bar{a}k = \omega + i\alpha$ are

$$\begin{aligned} \omega &= \omega_n - \frac{1}{2\omega_n} F_n^\eta \\ \alpha &= -\frac{1}{2} F_n^\dot{\eta} \end{aligned} \quad (6.51)a,b$$

¹⁶Thus $\alpha > 0$ for instability: $e^{-i\bar{a}kt} \equiv e^{-i(\omega+i\alpha)t} = e^{-i\omega t} e^{i\alpha t}$ which grows without limit in time when $\alpha > 0$.

¹⁷Recall remarks in Chapters 3 and 4.

Comparison of (6.50)a,b and (6.51)a,b gives the connections between the two representations of the forcing function:

$$\begin{aligned} F_n^\eta &= \frac{\hat{F}_n^{(r)}}{\hat{\eta}_n} \\ F_n^{\dot{\eta}} &= \frac{1}{\omega_n} \frac{\hat{F}_n^{(i)}}{\hat{\eta}_n} \end{aligned} \quad (6.52)a,b$$

Generally F_n will contain several processes, each of which will depend linearly on η_n and $\frac{d\eta_n}{dt}$, and appears additively in F_n . Hence, formulas corresponding to (6.52)a,b apply to each of the individual processes. They are often useful, if only for checking correctness, in detailed calculations.

6.5. Linear Stability with a Heat Source and Motion of the Boundary

As a first approximation to problems of combustion instabilities it is useful to ignore all processes involving interactions between the unsteady and steady fields, and focus attention on the two generic causes of instabilities: time-dependent energy addition and motions of the boundary. With suitable interpretation the second may represent the influence of unsteady combustion of a solid propellant. Then in dimensional variables the linearized pressure and momentum equations (3.46)d and (3.46)b, and the boundary condition (3.57)b on the pressure fluctuations are

$$\frac{\partial p'}{\partial t} + \gamma \bar{p} \nabla \cdot \mathbf{u}' = \frac{R}{C_v} \dot{Q}' \quad (6.53)$$

$$\bar{\rho} \frac{\partial \mathbf{u}'}{\partial t} + \nabla p' = 0 \quad (6.54)$$

$$\hat{\mathbf{n}} \cdot \nabla p' = -\bar{\rho} \frac{\partial \mathbf{u}'}{\partial t} \cdot \hat{\mathbf{n}} \quad (6.55)$$

Now form the wave equation as in Section 3.4, so the problem is governed by the two equations

$$\begin{aligned} \nabla^2 p' - \frac{1}{\bar{a}^2} \frac{\partial^2 p'}{\partial t^2} &= h \\ \hat{\mathbf{n}} \cdot \nabla p' &= -f \end{aligned} \quad (6.56)a,b$$

where

$$\begin{aligned} h &= -\frac{1}{\bar{a}^2} \frac{R}{C_v} \frac{\partial \dot{Q}'}{\partial t} \\ f &= \bar{\rho} \frac{\partial \mathbf{u}'}{\partial t} \cdot \hat{\mathbf{n}} \end{aligned} \quad (6.57)a,b$$

The expansion procedure and application of spatial averaging leads to the explicit oscillator equations (4.36):

$$\frac{d^2 \eta_n}{dt^2} + \omega_n^2 \eta_n = -\frac{\bar{a}^2}{\bar{p} E_n^2} \left\{ \int \left[-\frac{1}{\bar{a}^2} \frac{R}{C_v} \frac{\partial \dot{Q}'}{\partial t} \right] \psi_n dV + \oint \left[\bar{\rho} \frac{\partial \mathbf{u}'}{\partial t} \cdot \hat{\mathbf{n}} \right] \psi_n dS \right\} \quad (6.58)$$

As a simple example, consider the one-dimensional problem of waves excited in a tube fitted with a piston, Figure 6.9, and with distributed heat addition provided, say, by an electrically heated coil. Only longitudinal modes are considered, and

$$\psi_n = \cos(k_n x) \quad , \quad k_n = n \frac{\pi}{L} \quad , \quad E_n^2 = \frac{1}{2} S_c L \quad (6.59)$$

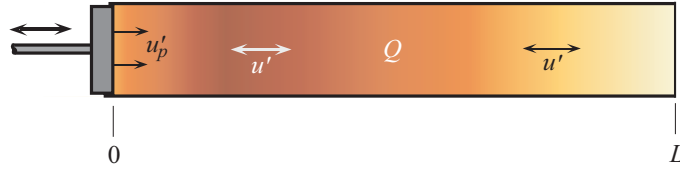


FIGURE 6.9. A tube with distributed heat addition and an oscillating piston to drive waves.

where $S_c = \pi R_c^2$ is the cross-section area of the tube. We ignore any average motion in the tube, and suppose that the average thermodynamic properties are maintained constant and uniform by suitable steady heat losses through the walls of the tube. The heat addition and motion of the piston are sinusoidal, having phases ϕ_Q and ϕ_u with respect to pressure oscillations:

$$\begin{aligned}\dot{Q}' &= |\hat{Q}(x)| e^{-i(\bar{a}kt + \phi_Q)} \\ \mathbf{u}'_p \cdot \hat{\mathbf{n}} &= |\hat{u}_p| e^{-i(\bar{a}kt + \phi_u)}\end{aligned}\quad (6.60)a,b$$

Hence for use in h and f :

$$\begin{aligned}\frac{\partial \dot{Q}'}{\partial t} &= -i\bar{a}k |\hat{Q}(x)| e^{-i(\bar{a}kt + \phi_Q)} \\ \frac{\partial}{\partial t} (\mathbf{u}'_p \cdot \hat{\mathbf{n}}) &= -i\bar{a}k |\hat{u}_p| e^{-i(\bar{a}kt + \phi_u)}\end{aligned}\quad (6.61)a,b$$

With $\eta_n = \hat{\eta}_n e^{-i\bar{a}kt}$, substitution in the oscillator equations (6.58) leads to

$$\begin{aligned}[-(\bar{a}k)^2 + \omega_n^2] \hat{\eta}_n &= -\frac{\bar{a}^2}{\bar{p}E_n^2} \left\{ -\frac{1}{\bar{a}^2} \frac{R}{C_v} (-i\bar{a}k) \int \cos(k_n x) |\hat{Q}(x)| e^{-i\phi_Q} dV \right. \\ &\quad \left. - i\bar{\rho}\bar{a}k \iint \cos(k_n x) |\hat{u}_p| e^{-i\phi_u} dS \right\}\end{aligned}$$

After some rearrangement, and setting $\bar{a}k = \omega + i\alpha$, we find

$$\begin{aligned}(\omega + i\alpha)^2 &= \omega_n^2 + i(\omega + i\alpha) \frac{\bar{a}^2}{\bar{p}(\frac{1}{2}S_c L)} \left\{ \frac{1}{\bar{a}^2} \frac{R}{C_v} S_c \int_0^L \cos(k_n x) \frac{|\hat{Q}(x)|}{\hat{\eta}_n} e^{-i\phi_Q} dx \right. \\ &\quad \left. + \bar{\rho}S_c \frac{|\hat{u}_p|}{\hat{\eta}_n} e^{-i\phi_u} \right\}\end{aligned}$$

Because $|\hat{Q}|$ and $|\hat{u}_p|$ are small perturbations we can write this equation to first order in small quantities:

$$\omega^2 + i(2\alpha\omega) = \omega_n^2 + i\omega_n \frac{2}{\bar{p}L} \left\{ \frac{R}{C_v} \int_0^L \cos(k_n x) \frac{|\hat{Q}(x)|}{\hat{\eta}_n} e^{-i\phi_Q} dx + \bar{\rho}\bar{a}^2 \frac{|\hat{u}_p|}{\hat{\eta}_n} e^{-i\phi_u} dx \right\}$$

Take the real and imaginary parts to find

$$\begin{aligned}\omega^2 &= \omega_n^2 + \frac{2\omega_n}{\bar{p}L} \left\{ \frac{R}{C_v} \int_0^L \cos(k_n x) \frac{|\hat{Q}(x)|}{\hat{\eta}_n} \sin \phi_Q dx + \bar{\rho}\bar{a}^2 \frac{|\hat{u}_p|}{\hat{\eta}_n} \sin \phi_u \right\} \\ \alpha &= \frac{1}{\bar{p}L} \left\{ \frac{R}{C_v} \int_0^L \cos(k_n x) \frac{|\hat{Q}(x)|}{\hat{\eta}_n} \cos \phi_Q dx + \bar{\rho}\bar{a}^2 \frac{|\hat{u}_p|}{\hat{\eta}_n} \cos \phi_u \right\}\end{aligned}\quad (6.62)a,b$$

Internal feedback, and hence a condition for instability, exists if either or both of $|\dot{Q}|$ and $|\hat{u}_p|$ depend on the fluctuating pressure (or velocity). For example, set

$$\begin{aligned} |\dot{Q}| &= q_0 \hat{\eta}_n \psi_n = q_0 \hat{\eta}_n \cos k_n x \\ |\hat{u}_p| &= u_0 \hat{\eta}_n \end{aligned} \quad (6.63)a,b$$

and (6.62)a becomes

$$\omega^2 = \omega_n^2 + 2\omega_n (Aq_0 \sin \phi_q + Bu_0 \sin \phi_u)$$

where

$$A = \frac{1}{2\bar{p}} \frac{R}{C_v} \quad ; \quad B = \frac{\gamma}{L} \quad (6.64)$$

To first order in small quantities we find the results for the frequency and decay or growth constant:

$$\begin{aligned} \omega &= \omega_n + Aq_0 \sin \phi_Q + Bu_0 \sin \phi_u \\ \alpha &= Aq_0 \cos \phi_Q + Bu_0 \cos \phi_u \end{aligned} \quad (6.65)a,b$$

Remarks:

- (i) The n^{th} mode is unstable if $Aq_0 \cos \phi_Q + Bu_0 \cos \phi_u > 0$.
- (ii) If $0 \leq \phi_u \leq \frac{\pi}{2}$ then a necessary condition for instability is $0 \leq \phi_Q \leq \frac{\pi}{2}$.
- (iii) Instability of the n^{th} mode is encouraged if $|\dot{Q}(x)| \cos k_n x$ is larger, i.e., if the heat addition is greater where the mode shape of the pressure takes its largest values, an example of Rayleigh's Criterion.

It is important also to notice that due to the spatial averaging, one cannot distinguish among the ultimate effects of volumetric and surface processes. There is an equivalence of the influences of the various processes, their importance in respect to position within the chamber being dominated by their location relative to the mode shapes. That characteristic has far-reaching consequences in applications to combustion chambers.

6.6. Rayleigh's Criterion and Linear Stability

As part of his research on the excitation of acoustic waves by heat addition¹⁸ in chambers, Lord Rayleigh (1878, 1945) formulated the following explanation for the production of tones in a Rijke tube:

“If heat be periodically communicated to, and abstracted from, a mass of air vibrating (for example) in a cylinder bounded by a piston, the effect produced will depend upon the phase of the vibration at which the transfer of heat takes place. If heat be given to the air at the moment of greatest condensation, or be taken from it at the moment of greatest rarefaction, the vibration is encouraged. On the other hand, if heat be given at the moment of greatest rarefaction, or abstracted at the moment of greatest condensation, the vibration is discouraged.”

That paragraph has become probably the most widely cited ‘explanation’ for the presence of combustion instabilities generally. For easy reference, the explanation has long been referred to as “Rayleigh's Criterion.”

It is important to realize that Rayleigh addressed only the conditions under which unsteady heat addition ‘encourages’ oscillations, i.e., is a destabilizing influence. Other processes, stabilizing or destabilizing, are

¹⁸The literature in the 19th century included many works on ‘singing flames’ which also formed part of the background for Rayleigh's Criterion. It was only in the late 20th century that the close basic connections between the behavior of ‘singing flames’ and the Rijke tube were understood.

neither excluded nor included, and there is certainly no implication that satisfaction of the criterion is either a necessary or a sufficient condition for instability to exist. Several published examples exist of quantitative realizations of the criterion (Putnam and Dennis 1953, Putnam 1971; Chu 1956a; Chu 1956b; Zinn 1986; Culick 1987, 1992). The purpose of this section is to establish a generalized form of Rayleigh's Criterion by using the analysis based on spatial averaging, and to show the equivalence of Rayleigh's Criterion and the principle of linear stability.

The main idea is that a positive change of the time-averaged energy of a modal oscillator in a cycle of oscillation is exactly equivalent to the principle of linear instability, that the growth constant should be positive for a motion to be unstable. To establish the connection we use the oscillator equations,

$$\frac{d^2\eta_n}{dt^2} + \omega_n^2\eta_n = F_n \quad (6.66)$$

The instantaneous energy¹⁹ of the n^{th} oscillator is

$$\varepsilon_n = \frac{1}{2} (\dot{\eta}_n^2 + \omega_n^2\eta_n^2) \quad (6.67)$$

and the change of energy in one cycle is the integral over one period of the rate at which work is done by the force F_n :

$$\Delta\varepsilon_n = \int_t^{t+\tau_n} F_n(t')\dot{\eta}_n(t')dt' \quad (6.68)$$

Under the integral, F_n and $\dot{\eta}_n$ must be real quantities; here we use the real parts of both functions,

$$\begin{aligned} \eta_n &= \hat{\eta}_n e^{-i\bar{a}kt} = |\hat{\eta}_n| e^{-i\bar{a}kt} \\ F_n &= \hat{F}_n e^{-i\bar{a}kt} = |\hat{F}_n| e^{-i(\bar{a}kt+\phi_F)} = |\hat{F}_n| (\cos \phi_F + i \sin \phi_F) e^{-i\bar{a}kt} \end{aligned} \quad (6.69a,b)$$

We measure all phases with respect to the pressure, so $\hat{\eta}_n$ is real and, being the maximum amplitude, is positive. Substitution in the oscillator equations gives

$$k^2 = \frac{1}{\bar{a}^2} \left(\omega_n^2 - \frac{\hat{F}_n}{\hat{\eta}_n} \right)$$

of which the real and imaginary parts are to first order in small quantities:

$$\begin{aligned} \omega^2 &= \omega_n^2 - \operatorname{Re} \left(\frac{\hat{F}_n}{\hat{\eta}_n} \right) = \omega_n^2 - \left| \frac{\hat{F}_n}{\hat{\eta}_n} \right| \cos \phi_F \\ \alpha_n &= \frac{-1}{2\omega_n} \operatorname{Im} \left(\frac{\hat{F}_n}{\hat{\eta}_n} \right) = \frac{-1}{2\omega_n} \left| \frac{\hat{F}_n}{\hat{\eta}_n} \right| \sin \phi_F \end{aligned} \quad (6.70a,b)$$

The oscillator's motion is stable if α_n is *negative* (see Footnote 9), i.e. if the imaginary part of \hat{F}_n is *positive*.

Also for use in (6.68) we have

$$\dot{\eta}_n = -i\bar{a}k|\hat{\eta}_n|e^{-i\bar{a}kt} = \bar{a}k|\hat{\eta}_n|e^{-i(\bar{a}kt+\frac{\pi}{2})} \approx \omega_n|\hat{\eta}_n|e^{-i(\omega_n t+\frac{\pi}{2})}$$

so

$$\operatorname{Re}(\dot{\eta}_n) = \omega_n|\hat{\eta}_n| \cos \left(\omega_n t + \frac{\pi}{2} \right) = -\omega_n|\hat{\eta}_n| \sin \omega_n t \quad (6.71)$$

The real part of F_n is

$$\operatorname{Re}(F_n) = |\hat{F}_n| \cos(\omega_n t + \phi_F) = |\hat{F}_n| \{ \cos \omega_n t \cos \phi_F - \sin \omega_n t \sin \phi_F \} \quad (6.72)$$

¹⁹ ε_n is not the energy of the n^{th} acoustic mode, which is given by the integral of (5.72) over the volume of the chamber.

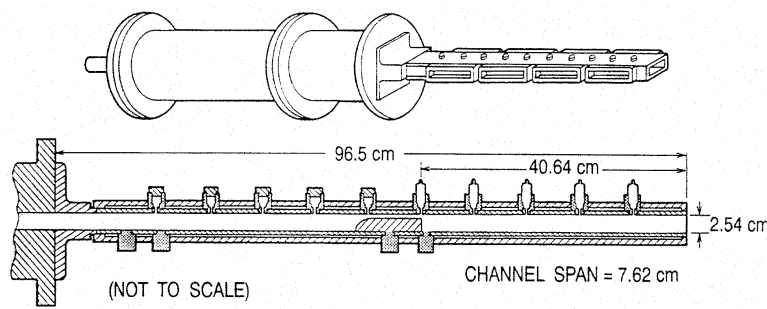


FIGURE 6.10. The Caltech dump combustor.

Hence the right-hand side of (6.68) is

$$\begin{aligned}\Delta\varepsilon_n &= \int_t^{t+\tau_n} Re(F_n)Re(\eta_n)dt' = \omega|\hat{F}_n| \int_t^{t+\tau_n} \left\{ \sin^2 \omega_n t' \sin \phi_F - \frac{1}{2} \sin 2\omega_n t' \cos \phi_F \right\} dt' \\ &= \omega|\hat{F}_n||\hat{\eta}_n| \frac{\tau_n}{2} \sin \phi_F\end{aligned}$$

Substitution of (6.33)b leads to the formula

$$\Delta\varepsilon_n = 2\pi\alpha_n\omega_n|\hat{\eta}_n|^2 \quad (6.73)$$

which establishes the desired connection between Rayleigh's Criterion and linear stability.

Remarks:

- (i) Positive α_n (the system is linearly unstable) implies that the average energy of the oscillator increases, and vice-versa.
- (ii) Rayleigh's original criterion is equivalent to the principle of linear instability **if** only heat exchange is accounted for and is **neither** a necessary **nor** a sufficient condition for existence of a combustion instability.
- (iii) The extended form (6.73) of Rayleigh's Criterion is exactly equivalent to the principle of linear instability, all linear processes being accounted for.

Putnam (1971) has made the most extensive use of Rayleigh's Criterion in practical situations. His book and papers give many examples of applying the Criterion as an aid to making changes of design to avoid oscillations generated by heat release, particularly in power generation and heating systems.

In the past fifteen years many groups have been making direct observations on laboratory systems to check the validity of the Criterion's implications. The key step is based on the assumption that radiation by certain intermediate species in hydrocarbon reactions (CH and OH are the most common identifiers) can be interpreted as a measure of the rate of chemical reactions taking place and hence of the rate at which energy is released. Simultaneous measurements are made of the spatial distribution of radiation in a system, and of the pressure oscillations. The results then allow at least a qualitative assessment of the extent to which the oscillations are being driven by the energy released in the combustion field, or whether other mechanisms may be active and important. It is an important method with many useful applications. However, there are serious matters of interpretation, e.g., due to poorly known rates of collisional de-activation of radiating species. Measurements of time-dependent energy release is an active research topic.

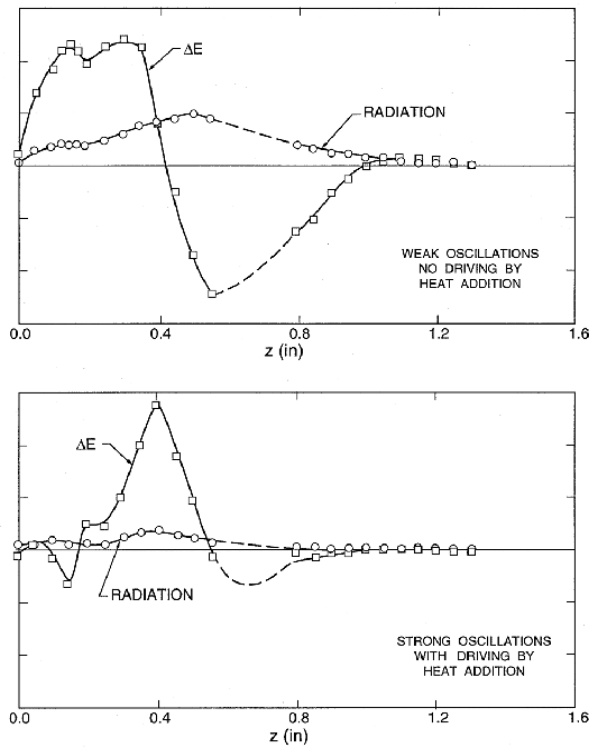


FIGURE 6.11. Experimental confirmation of Rayleigh's Criterion. Data obtained from chemiluminescence of OH (Sterling and Zukoski, 1991).

It seems that the first report of simultaneous measurements of pressure and radiation allowing confirmation of Rayleigh's Criterion appeared in a Ph.D. thesis (Sterling, 1987; Sterling and Zukoski, 1991). Figure 6.10 is a sketch of the dump combustor used as the test device, and Figure 6.11 shows the main result. The integral of ΔE over the volume of the chamber (here the integral over the length is equivalent) is a measure of the severity of oscillations. For the case shown in the lower portion of the figure, the integral of ΔE over the length is clearly positive, consistent with the observed presence of oscillations.

6.7. Some Results for Linear Stability in Three Dimensions

The term 'stability of motions' has several meanings for flows in combustion chambers, including:

- (i) the stability of laminar steady flow when viscous and inertial properties of the medium dominate, leading to formation of large vortices or to turbulence, a field of distributed vorticity if the steady flow is unstable;
- (ii) the stability of shear layers, commonly producing large scale vortex motions when a shear layer is unstable;
- (iii) the stability of laminar flame fronts, responsible for one source of turbulent combustion when fronts are unstable;
- (iv) the stability of small disturbances which, when the compressibility and inertia of the medium dominate the motions, can develop into acoustic waves.

In terms of the modes of motion mentioned in Section 3.1 and discussed further in Section 3.3, the phenomena (i)–(iii) are classified as waves of vorticity and the fourth comprises acoustic waves which, depending on the physical situation, may possess or generate vorticity as well. The perturbations must in some sense be small, as we have stressed with examples we examined in Chapter 2 and already in the present chapter. Even these ‘small’ perturbations produce realistic and useful results. According to remarks we made in connection with the derivation of the formalism in Chapter 3, the results derived there are general; further progress depends on modelling and more explicit calculations.

We discuss in the following section results for motions that are ‘one-dimensional’, an approximation that holds a special position in fluid mechanics generally for two reasons: It is often a surprisingly accurate approximation; and solution to a one-dimensional problem is enormously simpler than its three-dimensional counterpart. This has been a particularly productive approach to analyzing combustion instabilities. While it might seem logical to cover the simpler analysis first, we believe that some of the special aspects of the subject are more readily understood by working out the three-dimensional results first. As ‘special aspects’ we have in mind especially the contributions of ‘flow-turning’ and ‘pumping’ associated with flow at or through lateral surfaces of a combustion chamber. Those phenomena will be treated in a more rigorous fashion using the proper three-dimensional formalism in Sections 6.9 and 6.12 which accommodate vorticity, the true physical origin of both flow-turning and pumping. In his work, Flandro (1995 and later works) has been careful to emphasize this connection.

6.7.1. Linear Stability of Three-Dimensional Motions. The formulas (6.14)a,b are general, restricted only by the approximations used in formulating the analytical framework. Hence the problem of obtaining results specific to any given problem apparently comes down to finding explicit forms for F_n^η and $F_n^{\eta\eta}$, by evaluating the integrals defining F_n , equation (6.38). Section 3.3 and Annex A contain details forming the functions h and f given to second order, defined by (3.62)a,b. Here we need only the linear parts, i.e. terms of order ε and of order $\mu\varepsilon$ in the expansions.

While the use of dimensionless variables is virtually a practical necessary for systematic development of the formal expansions in Chapters 3 and 4, there are certain advantages here in working with primitive dimensional variables. According to the results of Section 6.3, we know everything about linear stability once we know the driving force F_n in the system of oscillator equations. To make the procedure as clear as possible, we repeat some of the results and display some details where it seems helpful. The nonlinear wave equation and its boundary condition are (D.3)a,b:

$$\begin{aligned} \nabla^2 p' - \frac{1}{\bar{a}^2} \frac{\partial^2 p'}{\partial t^2} &= h \\ \hat{\mathbf{n}} \cdot \nabla p' &= -f \end{aligned} \quad (6.74)a,b$$

The linear parts of (D.4)a,b are

$$\begin{aligned} h &= -\bar{\rho} \nabla \cdot \{[\mathbf{u}]\}_1 + \frac{1}{\bar{a}^2} \frac{\partial}{\partial t} \{[p]\}_1 + \nabla \cdot \bar{\mathbf{F}}' - \frac{1}{\bar{a}^2} \frac{\partial \mathcal{P}'}{\partial t} \\ f &= \bar{\rho} \frac{\partial \mathbf{u}'}{\partial t} \cdot \hat{\mathbf{n}} + \bar{\rho} \hat{\mathbf{n}} \cdot \{[\mathbf{u}]\}_1 - \bar{\mathbf{F}}' \cdot \hat{\mathbf{n}} \end{aligned} \quad (6.75)a,b$$

where

$$\begin{aligned} \{[\mathbf{u}]\}_1 &= \bar{\rho} (\bar{\mathbf{u}} \cdot \nabla \mathbf{u}' + \mathbf{u}' \cdot \nabla \bar{\mathbf{u}}) \\ \{[p]\}_1 &= \bar{\mathbf{u}} \cdot \nabla p' + \gamma p' \nabla \cdot \bar{\mathbf{u}} \end{aligned} \quad (6.76)a,b$$

Expansion of the pressure fluctuation in normal modes is the representation we use for the zeroth order approximation to the pressure field,

$$p'(\mathbf{r}, t) = \bar{p} \sum_{m=0}^M \eta_m(t) \psi_m(\mathbf{r}) \quad (6.77)$$

$$\mathbf{u}'(\mathbf{r}, t) = \sum_{m=1}^M \frac{\dot{\eta}_m(t)}{\gamma k_m^2} \nabla \psi_m(\mathbf{r}) \quad (6.78)$$

After spatial averaging has been carried out, the system of oscillator equations is (4.36),

$$\frac{d^2 \eta_n}{dt^2} + \omega_n^2 \eta_n = F_n \quad (6.79)$$

with the definition (4.32)

$$F_n = -\frac{\bar{a}^2}{\bar{p}E_n^2} \left\{ \int h\psi_n dV + \oint f\psi_n dS \right\} \quad (6.80)$$

We write the linear contributions to F_n

$$F_n = -\frac{\bar{a}^2}{\bar{p}E_n^2} \left\{ \bar{\rho}I_1 + \frac{1}{\bar{a}^2}I_2 + \oint \bar{\rho} \frac{\partial \mathbf{u}'}{\partial t} \cdot \hat{\mathbf{n}} \psi_n dS - \int \mathbf{F}' \cdot \nabla \psi_n dV - \frac{1}{\bar{a}^2} \int \frac{\partial \mathcal{P}'}{\partial t} \psi_n dV \right\} \quad (6.81)$$

and from Annex D, equations (D.10)a,b:

$$\begin{aligned} I_1 &= \int (\bar{\mathbf{u}} \cdot \nabla \mathbf{u}' + \mathbf{u}' \cdot \nabla \bar{\mathbf{u}}) \cdot \nabla \psi_n dV \\ I_2 &= \frac{\partial}{\partial t} \int (\gamma p' \nabla \cdot \bar{\mathbf{u}} + \bar{\mathbf{u}} \cdot \nabla p') \psi_n dV \end{aligned} \quad (6.82)a,b$$

With use of two vector identities, I_1 can be re-written

$$I_1 = \int \nabla(\bar{\mathbf{u}} \cdot \mathbf{u}') \cdot \nabla \psi_n dV - \int (\mathbf{u}' \times \nabla \times \bar{\mathbf{u}}) \cdot \nabla \psi_n dV - \int (\bar{\mathbf{u}} \times \nabla \times \mathbf{u}') \cdot \nabla \psi_n dV$$

The first integral can be put in the more convenient form

$$\int \nabla(\bar{\mathbf{u}} \cdot \mathbf{u}') \cdot \nabla \psi_n dV = \oint (\bar{\mathbf{u}} \cdot \mathbf{u}') \nabla \psi_n \cdot \hat{\mathbf{n}} dS - \int (\bar{\mathbf{u}} \cdot \mathbf{u}') \nabla^2 \psi_n dV = k_n^2 \int (\bar{\mathbf{u}} \cdot \mathbf{u}') \psi_n dV$$

because on the boundary surface $\nabla \psi_n$ is everywhere parallel to the surface, so $\nabla \psi_n \cdot \hat{\mathbf{n}} = 0$. Hence I_1 is more simply

$$I_1 = k_n^2 \int (\bar{\mathbf{u}} \cdot \mathbf{u}') \psi_n dV - \int (\mathbf{u}' \times \nabla \times \bar{\mathbf{u}}) \cdot \nabla \psi_n dV - \int (\bar{\mathbf{u}} \times \nabla \times \mathbf{u}') \cdot \nabla \psi_n dV \quad (6.83)$$

and the ‘force’ acting on the n^{th} oscillator is

$$\begin{aligned} F_n &= -\frac{\bar{a}^2}{\bar{p}E_n^2} \left\{ \bar{\rho}k_n^2 \int (\bar{\mathbf{u}} \cdot \mathbf{u}') \psi_n dV - \bar{\rho} \int (\mathbf{u}' \times \nabla \times \bar{\mathbf{u}} + \bar{\mathbf{u}} \times \nabla \times \mathbf{u}') \cdot \nabla \psi_n dV \right. \\ &\quad \left. + \frac{1}{\bar{a}^2} \frac{\partial}{\partial t} \int (\gamma p' \nabla \cdot \bar{\mathbf{u}} + \bar{\mathbf{u}} \cdot \nabla p') \psi_n dV + \bar{\rho} \oint \frac{\partial \mathbf{u}'}{\partial t} \cdot \hat{\mathbf{n}} \psi_n dS \right. \\ &\quad \left. - \int \mathbf{F}' \cdot \nabla \psi_n dV - \frac{1}{\bar{a}^2} \int \frac{\partial \mathcal{P}'}{\partial t} \psi_n dV \right\} \end{aligned} \quad (6.84)$$

This form can be simplified further since within the linear approximation, we take \mathbf{u}' and p' equal to their unperturbed acoustic values in the volume integrals in F_n ²⁰; for harmonic motions the u^{th} terms of (6.77) and (6.78) are

$$\begin{aligned} p' &= \hat{p}e^{-i\bar{a}k_n t} = \bar{p}\hat{\eta}_n \psi_n e^{-i\bar{a}k_n t} \\ \mathbf{u}' &= \hat{\mathbf{u}}e^{-i\bar{a}k_n t} = -i\frac{\bar{a}}{\gamma k_n} \hat{\eta}_n \nabla \psi_n e^{-i\bar{a}k_n t} \end{aligned} \quad (6.85)a,b$$

²⁰In the surface integral, $\partial \mathbf{u}' / \partial t \cdot \hat{\mathbf{n}}$ is a non-zero perturbation because \mathbf{u}' is not given by the classical acoustic value at the surface. For example, this term could represent the influence of motions of a loudspeaker set in a wall. Thus we correctly set $\mathbf{u}' = \hat{\mathbf{u}}e^{-i\bar{a}k_n t}$ and $\hat{\mathbf{u}}$ is left to be specified according to the desired boundary condition.

Then $\mathbf{F}' = \hat{\mathbf{F}} e^{-i\bar{a}kt}$, $\mathcal{P}' = \hat{\mathcal{P}} e^{-i\bar{a}kt}$, $F_n = \hat{F}_n e^{-i\bar{a}kt}$ and 6.84 becomes

$$\begin{aligned}\hat{F}_n = \hat{\eta}_n \frac{\bar{a}^2}{\bar{p}E_n^2} (-i\bar{\rho}\bar{a}k_n) & \left\{ \frac{1}{\gamma} \int (\bar{\mathbf{u}} \cdot \nabla \psi_n) \psi_n dV - \frac{1}{\gamma k_n^2} \int (\nabla \psi_n \times \nabla \times \bar{\mathbf{u}} + \bar{\mathbf{u}} \times \nabla \times \nabla \psi_n) \cdot \nabla \psi_n dV \right. \\ & + \frac{\gamma \bar{p}}{\bar{\rho}\bar{a}^2} \int (\psi_n \nabla \cdot \bar{\mathbf{u}} + \frac{1}{\gamma} \bar{\mathbf{u}} \cdot \nabla \psi_n) \psi_n dV + \oint \frac{\hat{\mathbf{u}}}{\hat{\eta}_n} \cdot \hat{\mathbf{n}} \psi_n dS \Big\} \\ & + \frac{\bar{a}^2}{\bar{p}E_n^2} \left\{ \int \hat{\mathbf{F}} \cdot \nabla \psi_n dV - i \frac{k_n}{\bar{a}} \int \hat{\mathcal{P}} \psi_n dV \right\}\end{aligned}$$

The integrand of the second integral vanishes because the first term in the parentheses is perpendicular to $\nabla \psi_n$ and in the second, $\nabla \times \nabla \psi_n = 0$. From the definition of the speed of sound, $\gamma \bar{p}/\bar{\rho}\bar{a}^2 = 1$ and the amplitude of the force is

$$\begin{aligned}\hat{F}_n = \hat{\eta}_n \frac{\bar{a}^2}{\bar{p}E_n^2} (i\bar{\rho}\bar{a}k_n) & \left\{ \frac{2}{\gamma} \int (\bar{\mathbf{u}} \cdot \nabla \psi_n) \psi_n dV + \int \psi_n^2 \nabla \cdot \bar{\mathbf{u}} dV + \oint \frac{\hat{\mathbf{u}}}{\hat{\eta}_n} \cdot \hat{\mathbf{n}} \psi_n dS \right\} \\ & + \hat{\eta}_n \frac{\bar{a}^2}{\bar{p}E_n^2} \int \left[\frac{\hat{\mathbf{F}}}{\hat{\eta}_n} \cdot \nabla \psi_n - i \frac{k_n}{\bar{a}} \frac{\hat{\mathcal{P}}}{\hat{\eta}_n} \psi_n \right] dV\end{aligned}\quad (6.86)$$

Use the identity

$$(\bar{\mathbf{u}} \cdot \nabla \psi_n) \psi_n = \frac{1}{2} [\nabla \cdot (\bar{\mathbf{u}} \psi_n^2) - \psi_n^2 \nabla \cdot \bar{\mathbf{u}}]$$

and combine terms to write \hat{F}_n in the form

$$\begin{aligned}\hat{F}_n = \hat{\eta}_n \frac{\bar{a}^2}{\bar{p}E_n^2} (i\bar{\rho}\bar{a}k_n) & \left\{ \oint \left[\frac{\hat{\mathbf{u}}}{\hat{\eta}_n} \cdot \hat{\mathbf{n}} + \frac{1}{\gamma} \bar{\mathbf{u}} \cdot \hat{\mathbf{n}} \psi_n \right] \psi_n dS + \frac{\gamma-1}{\gamma} \int \psi_n^2 \nabla \cdot \bar{\mathbf{u}} dV \right\} \\ & + \hat{\eta}_n \frac{\bar{a}^2}{\bar{p}E_n^2} \int \left[\frac{\hat{\mathbf{F}}}{\hat{\eta}_n} \cdot \nabla \psi_n - i \frac{k_n}{\bar{a}} \frac{\hat{\mathcal{P}}}{\hat{\eta}_n} \psi_n \right] dV\end{aligned}\quad (6.87)$$

Four remarks are important:

- (i) The mean flow field may be rotational ($\nabla \times \bar{\mathbf{u}} \neq 0$) and time-averaged sources of mass are accommodated ($\nabla \cdot \bar{\mathbf{u}} \neq 0$).
- (ii) With the iterative procedure discussed in Chapters 3 and 4, the substitutions of classical acoustic mode shapes are required in the right-hand side, except in the surface integral where the correct boundary condition on the velocity must be used:

$$p' = p'_a = \bar{p}\eta_n(t)\psi_n(\mathbf{r}) ; \quad \mathbf{u}' = \mathbf{u}'_a = \frac{1}{\gamma k_n^2} \frac{d\eta_n}{dt} \nabla \psi_n \quad (6.88)$$

- (iii) The calculations in Section 4.6 have shown that to first order in the average Mach number, the unsteady field may also be rotational. However, the greatest influences of rotationality have not been included here. Those are represented by two terms associated with behavior at a burning surface, discussed in Sections 6.9 and 6.12. There are also some important effects associated with vorticity, contained in the terms $I_{\Omega\Omega}$ and $I_{a\Omega}$. They have been dropped from (6.87), but they will be discussed later in Sections 6.12 and 7.4.
- (iv) The processes of ‘pumping’ and ‘flow-turning’ are implied by these results, but are obtained only after considerable further calculations discussed in Sections 6.9 and 6.12. The integrals containing $\hat{\mathbf{F}}$ and $\hat{\mathcal{P}}$ are central in this respect, containing pieces related to production of vorticity. See the last remark in the introduction to this section. It’s true that there is a bit of ‘after-the-fact’ flavor here, but that is within the spirit of the construction of 6.79 and 6.87. These do not, and are not intended to, constitute a ‘theory’ based on first principles. To give \mathbf{F}' and \mathcal{P}' specific forms for particular

processes, requires using special results calculated independently of the apparatus constructed here, namely those found by Flandro (1995)a. The required computations have not been done.

Now we follow the procedure explained in Section 4.1 to find the formula for the complex wavenumber. For linear harmonic motions (6.37) and (6.48) give

$$k^2 - k_n^2 = -\frac{1}{\bar{a}^2} \frac{\hat{F}_n}{\hat{\eta}_n} \quad (6.89)$$

Substitution of (6.87) in (6.89) gives

$$\begin{aligned} k^2 - k_n^2 = -i \frac{k_n}{\bar{a} E_n^2} & \left\{ \iint \left[\frac{\gamma \hat{\mathbf{u}}}{\hat{\eta}_n} \cdot \hat{\mathbf{n}} + \bar{\mathbf{u}} \cdot \hat{\mathbf{n}} \psi_n \right] \psi_n dS + (\gamma - 1) \int \psi_n^2 \nabla \cdot \bar{\mathbf{u}} dV \right\} \\ & - \frac{1}{\bar{p} E_n^2} \int \left[\frac{\hat{\mathcal{F}}}{\hat{\eta}_n} \cdot \nabla \psi_n - i \frac{k_n}{\bar{a}} \frac{\hat{\mathcal{P}}}{\hat{\eta}_n} \psi_n \right] dV \end{aligned} \quad (6.90)$$

This formula is actually quite general due to the functions $\hat{\mathcal{F}}$ and $\hat{\mathcal{P}}$, which have not been assigned specific forms, for reasons examined in Section 6.7; at least two important processes, ‘flow-turning’ and ‘pumping’ are not shown explicitly.

Let the right-hand side be denoted by iK so (6.90) is

$$k^2 - k_n^2 = iK = iK^{(r)} + K^{(i)}$$

Because $k = (\omega + i\alpha)/\bar{a}$ and k_n is real, this equation can be expanded to give

$$\left(\frac{\omega}{\bar{a}} \right)^2 - \left(\frac{\alpha}{\bar{a}} \right)^2 + i \left(2 \frac{\omega \alpha}{\bar{a}^2} \right) - \left(\frac{\omega_n}{\bar{a}} \right)^2 = iK^{(r)} - K^{(i)} \quad (6.91)$$

All parts of the right-hand side of (6.90) written in dimensionless form are of first order in the Mach number of the mean flow. Hence the last equation shows that α^2 is of second order and can be ignored. Similarly, the real part is of the same order, so ω differs from ω_n by terms of first order and

$$\left(\frac{\omega}{\bar{a}} \right)^2 - \left(\frac{\omega_n}{\bar{a}} \right)^2 = \left(\frac{\omega}{\bar{a}} - \frac{\omega_n}{\bar{a}} \right) \left(\frac{\omega}{\bar{a}} + \frac{\omega_n}{\bar{a}} \right) \approx \left(\frac{\omega}{\bar{a}} - \frac{\omega_n}{\bar{a}} \right) \left(2 \frac{\omega_n}{\bar{a}} \right) + 0(\bar{M}_r^2) \quad (6.92)$$

Thus, for use in (6.90), $k^2 - k_n^2 \approx (\omega - \omega_n)(2\omega_n/\bar{a}^2) + i(2\omega_n\alpha/\bar{a}^2)$ so $\omega - \omega_n = \frac{\bar{a}^2}{2\omega_n} K^{(r)}$ and $\alpha = \frac{\bar{a}^2}{2\omega_n} K^{(i)}$. With these approximations, and $K^{(r)}$, $K^{(i)}$ replaced by their explicit forms, (6.91) leads to the formulas for $\omega - \omega_n$ and α :

$$\omega - \omega_n = \frac{1}{2} \frac{\gamma}{E_n^2} \iint \frac{\hat{\mathbf{u}}^{(i)}}{\hat{\eta}_n} \cdot \hat{\mathbf{n}} \psi_n dS - \frac{\bar{a}^2}{2\omega_n \bar{p} E_n^2} \int \left[\frac{\hat{\mathcal{F}}^{(r)}}{\hat{\eta}_n} \cdot \nabla \psi_n + \frac{k_n}{\bar{a}} \frac{\hat{\mathcal{P}}^{(i)}}{\hat{\eta}_n} \psi_n \right] dV \quad (6.93)$$

$$\begin{aligned} \alpha = -\frac{1}{2 E_n^2} & \left\{ \iint \left[\gamma \frac{\hat{\mathbf{u}}^{(r)}}{\hat{\eta}_n} \cdot \hat{\mathbf{n}} \psi_n + (\bar{\mathbf{u}} \cdot \hat{\mathbf{n}}) \psi_n^2 \right] dS + (\gamma - 1) \int \psi_n^2 \nabla \cdot \bar{\mathbf{u}} dV \right\} + \\ & - \frac{\bar{a}^2}{2\omega_n \bar{p} E_n^2} \int \left[\frac{\hat{\mathcal{F}}^{(i)}}{\hat{\eta}_n} \cdot \nabla \psi_n + \frac{k_n}{\bar{a}} \frac{\hat{\mathcal{P}}^{(r)}}{\hat{\eta}_n} \psi_n \right] dV \end{aligned} \quad (6.94)$$

With slight rearrangement, the formulas (6.90), (6.93) and (6.94) have been given as (86)–(88) by Culick and Yang (1992)²¹

²¹Here, with $p' = \hat{p} e^{-i\bar{a}kt}$ and $\bar{a}k = \omega + i\alpha$, $e^{-i\bar{a}kt} = e^{\alpha t} e^{-i\omega t}$, stability requires $\alpha < 0$, i.e. α must be negative.

Both $\omega - \omega_n$ and α are sums of contributions from the various processes accounted for. Most importantly, the formula for the growth constant has the form

$$\begin{aligned}\alpha = & (\alpha)_{\text{combustion}} + (\alpha)_{\text{meanflow/acoustics}} + (\alpha)_{\text{nozzle}} \\ & + (\alpha)_{\text{particles}} + (\alpha)_{\text{injection system}} \\ & + (\alpha)_{\text{inert surfaces}} + \dots\end{aligned}\quad (6.95)$$

By suitable interpretation of the first two integrals in (6.93), the first three pieces of α are given explicitly; the last three are generated by the terms involving $\hat{\mathcal{F}}^{(i)}$ and $\hat{\mathcal{P}}^{(r)}$ and hence cannot be written explicitly at this point.

For most combustion systems, the six contributions shown explicitly seem to cover practically all dynamical behavior, with the exception of two surface contributions mentioned in note (iv) above. Those are fundamentally important in solid rockets; see Section 6.9. Interactions of the oscillations with turbulence may also be significant but that subject remains essentially undeveloped; no results have been reported for the effects of turbulence on instabilities in full-scale systems. Descriptions of some major contributions to (6.95) are given in Section 6.6.

That the growth constant representing the difference between gains and losses of acoustic energy has the form (6.95) for a linear system has long been known (McClure *et al.* 1960). At least implicitly, (6.95) has been a part of all considerations of combustion instabilities. However, extensive data giving good quantitative results for the transient growth of oscillations have been obtained only for solid propellant rockets and related laboratory devices. Despite the widespread attention to the problem in liquid rockets (see, for example, Crocco and Cheng 1956, Crocco 1965 and Harrje and Reardon 1972), including theoretical predictions, and observations of stability boundaries, little experimental data exists for the values of α itself under conditions of true linear instability. The same can be said of other liquid and gas-fueled systems: Emphasis in most treatments has been on the stability boundary where $\alpha = 0$.

When α is negative (i.e., small disturbances decay) its value may be regarded as a measure of the stability margin of the system. During development of the liquid rockets for the Apollo vehicle, an experimental method for assessing the stability margin was worked out, based on measurement of the decay of disturbances following injection of a small explosive charge (Harrje and Reardon 1972, Chapters 9 and 10). There seem to be no reports of efforts to determine the values of the various contributions to the decay constants determined in those tests. The same may be said of the very extensive experimental work carried out in Russia over many years (Dranovsky 2006).

There may be other reasons for those conclusions but the main one seems to be due to an intrinsic difference in the nature of the systems. A liquid or gas-fueled system can be tested repeatedly, so as a practical matter, improvement of the dynamical behavior can be pursued on a trial-and-error basis. Development of the F-1 engine (Oefelein and Yang 1993) is perhaps the outstanding example. The processes responsible for the instabilities are so complicated that theory and experiments directed to understanding the mechanisms in detail would have been expensive, time-consuming and perhaps even impossible to complete successfully with the tools available forty years ago.

In contrast, no solid rocket can be retested without repeating the expensive process of cleaning and preparing the motor case and nozzle; manufacturing propellant; loading the motor; and allowing the material to cure. Moreover, there is likely no control of the firing. Hence, practically from the beginnings of solid rocketry, attention has been paid to time-dependent behavior during tests. When linear stability theory became available, it was natural to develop sufficiently good instrumentation and methods of data processing to obtain accurate values for α and its constituent parts. In recent years, great efforts have been expended on measurement and interpretation of the growth constant for many solid rockets and under many experimental conditions.

The growth constant has a useful quantitative interpretation. With the definition

$$p'(\mathbf{r}, t) = \hat{p}(\mathbf{r})e^{-i\bar{a}kt} = \hat{p}e^{-i(\omega+i\alpha)t} = \hat{p}e^{-i\omega t}e^{\alpha t},$$

we find the ratio of values of two peaks of the oscillation at a fixed location, occurring at times t_1 and $t_2 = t_1 + mT = t_1 + m2\pi/\omega$.

$$\frac{|p'_2|_{\text{peak}}}{|p'_1|_{\text{peak}}} = \left| \frac{e^{-i\omega(t_1+m\frac{2\pi}{\omega})}e^{\alpha t_2}}{e^{-i\omega t_1}e^{\alpha t_1}} \right| = e^{m2\pi\alpha/\omega} \quad (6.96)$$

because $e^{-im2\pi} = \cos m2\pi + i \sin m2\pi = \pm 1$. Hence the peak value is e times larger when $m2\pi\alpha/\omega = 1$, or

$$\frac{\omega}{\alpha} = 2\pi m \text{ or } \frac{f}{\alpha} = m \quad (6.97)$$

Hence, f/α is the number of cycles required for the peak value of the pressure oscillation to increase by e (or decrease by $1/e$ if $\alpha < 0$). This interpretation suggests the potential practical value of measuring transient growths and decay. Normally, many tens or perhaps hundreds of cycles are required for e-folding of the peak values. That is the best and most convincing evidence for the essential assumption on which the analysis is based, that perturbations of the acoustic field are ‘small’, implying α and $\omega - \omega_n$, equations (6.93) and (6.94) are both small compared with ω .

6.7.2. The Admittance and Response Functions for a Burning Surface. The term $\hat{\mathbf{u}} \cdot \hat{\mathbf{n}}$ in the surface integral, equation (6.90), arises from the part $\bar{\rho} \partial \mathbf{u} / \partial t \cdot \hat{\mathbf{n}}$ of f , equation (6.38). Although $\hat{\mathbf{u}} \cdot \hat{\mathbf{n}} = 0$ is required for the basis functions used here, it is allowed to be non-zero in f to account for motion of the surface in the actual problem; in other words, it is a perturbation. In general, the boundary surface is not rigid. At burning surfaces, the unsteady combustion process produces fluctuations of burning rate, and hence velocity, of the order of the average Mach number. A model of the processes involved and calculation of the fluctuations have been discussed in Section 2.2. The response function R_p defined for the fluctuation of mass flux, by the relation (2.4), is given in its simplest form as equation (2.52).

It is a convention in classical acoustics, that has become standard practice in the subject of this book, to replace fluctuations of the velocity at the boundary by admittance functions. The idea is that if a small pressure fluctuation is imposed on a boundary, the surface will move, at a velocity proportional, in first approximation, to the pressure fluctuation. In solid rockets, there are chiefly three classes of boundaries: inert impermeable surfaces; burning surfaces; and areas through which flow may pass, mainly the exhaust nozzle. Most other systems contain only the first and third types.

No exposed surface in a solid rocket chamber is truly inert, but erosion of insulation material is slow compared with combustion rates. Thus, we may consider the material to be inert as a good first approximation. In that case, there is negligible motion of the surface, and the acoustic field is influenced primarily by viscous effects confined to an acoustic boundary layer, treated in the following section.

Burning surfaces and regions of flow through the boundary may be treated together. From the definition of mass flux, $m_b = -\rho_s \mathbf{u} \cdot \hat{\mathbf{n}}$, and with the perfect-gas law, we have

$$-\hat{\mathbf{u}} \cdot \hat{\mathbf{n}} = \frac{\hat{m}_b}{\hat{\rho}_s} - \bar{\mathbf{u}} \cdot \hat{\mathbf{n}} \frac{\Delta \hat{T}_s}{T_s} + \frac{\hat{p}}{\gamma \hat{p}} \bar{\mathbf{u}} \cdot \hat{\mathbf{n}} \quad (6.98)$$

where subscript s denotes the value at the surface. The minus sign appears on $\hat{\mathbf{u}} \cdot \hat{\mathbf{n}}$ because $\hat{\mathbf{n}}$ is positive outward but $\hat{\mathbf{u}}$ and m_b are positive inward (i.e., into the chamber). The quantity $\Delta \hat{T}_s$ represents the difference between the actual temperature change \hat{T}_s and the isentropic temperature fluctuation associated with the

pressure disturbance:

$$\Delta\hat{T}_s = \hat{T}_s - \frac{\gamma-1}{\gamma} \frac{\hat{p}}{\bar{p}} \bar{T}_s \quad (6.99)$$

With $\gamma\bar{p} = \bar{\rho}\bar{a}^2$, and $\hat{p}/\bar{p} = \hat{\eta}_n\psi_n$, (6.98) can be solved for the combination appearing in the first integral of (6.90):

$$\frac{\gamma}{\hat{\eta}_n} (\hat{\mathbf{u}} \cdot \hat{\mathbf{n}}) \psi_n + (\bar{\mathbf{u}} \cdot \hat{\mathbf{n}}) \psi_n^2 \equiv -\gamma \left(\frac{\hat{m}_b}{\bar{\rho}_s} - \bar{\mathbf{u}} \cdot \hat{\mathbf{n}} \frac{\Delta\hat{T}_s}{\bar{T}_s} \right) \frac{\psi_n}{\hat{\eta}_n} \quad (6.100)$$

Analysis of the unsteady response of a burning surface produces most directly results for fluctuations of the mass flux \hat{m}_b , whereas measurements provide directly the combination on the left-hand side of (6.100). Hence, two functions have been introduced in the literature for solid rockets, the response function R_b and the admittance function A_b , defined by the relations

$$\begin{aligned} \frac{\hat{m}_b}{\bar{m}_b} &= R_b \frac{\hat{p}}{\gamma\bar{p}} \\ -\frac{\hat{\mathbf{u}} \cdot \hat{\mathbf{n}}}{\bar{a}} &= A_b \frac{\hat{p}}{\gamma\bar{p}} \end{aligned} \quad (6.101)a,b$$

With these definitions, the combination (6.100) gives

$$\frac{1}{\bar{a}} \left(\gamma \frac{\hat{\mathbf{u}} \cdot \hat{\mathbf{n}}}{\hat{\eta}_n \psi_n} + \bar{\mathbf{u}} \cdot \hat{\mathbf{n}} \right) \equiv -(A_b + \bar{M}_b) \equiv -\bar{M}_b \left(R_b + \gamma \frac{\Delta\hat{T}_s / \bar{T}_s}{\hat{\eta}_n \psi_n} \right) \quad (6.102)$$

where the subscript *b* has been introduced to indicate conditions at the burning surface.

Because the processes at burning surfaces are ultimately the source of the energy for instabilities in solid rockets, the problem of coupling to acoustical motions has received much attention for many years. It is not possible to compute accurate values of the response function for a given propellant. Experimental methods carry considerable uncertainties but have advanced to the point of being effective for comparing propellants, and for assessing trends of behavior accompanying compositional changes. (Section 2.2)

Denison and Baum (1961) first discovered an approximation to the response function now commonly used for correlating data and in computations of stability of solid rockets, Culick (1968)b reviewed the analyses of the response function available in the late 60s. As we have shown in Section 2.2, because of common assumptions of the physical behavior, almost all results have the same form as Denison and Baum's formula,

$$R_b = \frac{nAB}{\lambda + \frac{A}{\lambda} - (1+A) + AB} \quad (6.103)$$

if combustion processes at the surface are insensitive to pressure.

More recently, there have been continuing attempts to improve the representation (6.103), based on test results and incorporating ideas relating to the basic behavior of modern propellants. See, for example, Section 2.2; the final reports of the MURI programs (Culick 2002; Krier and Hofenrichter 2002); and papers by the investigators involved. The representation (6.103) remains the basic result used as a first approximation in studies of the internal dynamics of solid propellant rockets. Deviations from this form (see Chapter 2) are extremely important and continue to be a subject of research in this area.

6.7.3. The First Measurements of the Stability Boundary for a Solid Rocket. Probably the first systematic experimental investigation of the stability boundary for a solid rocket was carried out by Brownlee as his dissertation (Brownlee 1959). A useful summary of some of the results was published by Brownlee and Marble (1960). Brownlee's work fitted into a larger program on unstable burning in solid

rockets carried out at the Jet Propulsion Laboratory (JPL) during the 1950s and 1960s. A companion paper by Landsbaum, Kuby and Spaid (1960) appeared in the same volume with Brownlee and Marble's report. Further aspects of the tests are discussed there, but the topics are not germane to the present discussion.

The portion of the results relevant here were interpreted by Culick (1966) using a form of the theory worked out in this book. Figure 6.12 is a sketch of the cylindrical motors used and a typical pressure trace suggesting how the onset of a linear instability was defined with the data. The boundary was defined to be reached when the mean pressure rose above its predicted value in steady combustion. Stability boundaries for the motors tested are shown in Figure 6.13. Data from 250 firings were used.

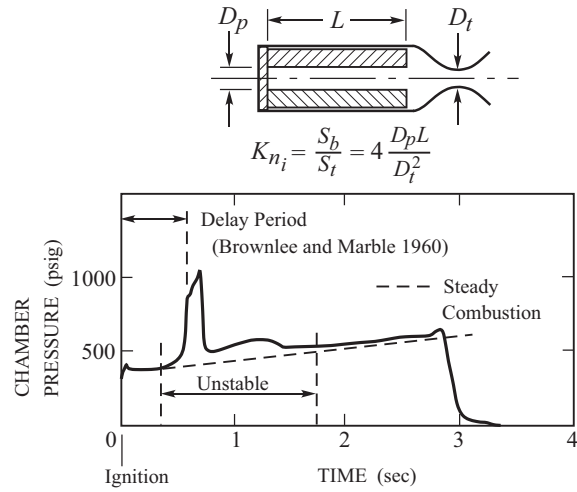


FIGURE 6.12. Geometrical parameters defined by Brownlee and a typical time history of the mean chamber pressure (Brownlee and Marble 1960).

In all tests the instability was dominated by the first tangential $(lmn) := (010)$ mode. More recently, roughly in the last 20–30 years, longitudinal modes have been more commonly unstable. The important difference is that the velocity fluctuation parallel to the axis of the motor is very small when a tangential mode is excited (zero in the classical limit). However, in both cases the fluctuating motion is largely parallel to the surface. The scouring effect—a kind of unsteady erosive burning—is likely the cause of the large increase of the mean pressure appearing in Figure 6.12. This is the mechanism commonly referred to as “velocity coupling.” Stability boundaries are shown in Figure 6.13. Two features are especially striking: The boundaries are nearly straight with positive slope; and the boundaries have slope increasing with the length of the motor.

The reasoning by Culick (1966) led to the conclusion that the stability boundary was determined by the balance of energy loss through the nozzle and energy gain from combustion. After the Mach number at the burning surface has been eliminated in favor of $K_n :=$ area of burning surface/area of the nozzle throat, the power balance leads to

$$K_n = 0.0935 \frac{\Gamma \bar{a}}{\sqrt{\gamma}} \frac{L}{D_p} \left(A_b^{(r)} + m_1^2 \right) \quad (6.104)$$

where $m_1 = 1.84$. At the time (1966) this analysis was carried out, the admittance for the propellant was not known. Therefore the tack was taken to fit the data reasonably well by choosing $A_b^{(r)}$, especially its dependence on the chamber diameter D_p , that is, frequency. Figure 6.14 is a plot of the values of $A_b^{(r)}$ inferred to provide an exact fit for $L = 31''$, requiring $K_n = 2.13L D_p$. The data are for an early composite

propellant tested in a T-burner (Angelus 1960). Then the stability boundaries for other values of L are calculated, with the results shown in Figure 6.13.

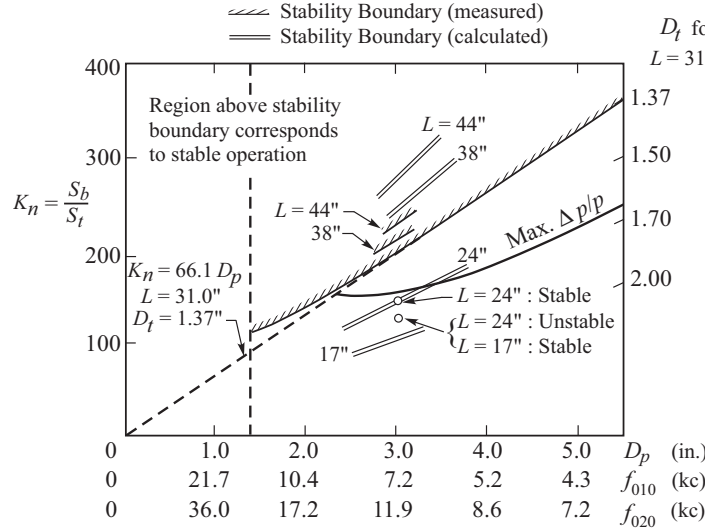


FIGURE 6.13. Stability boundaries for the 010 mode: experimental (measured) (Brownlee and Marble 1960); theoretical (calculated) (Culick 1966).

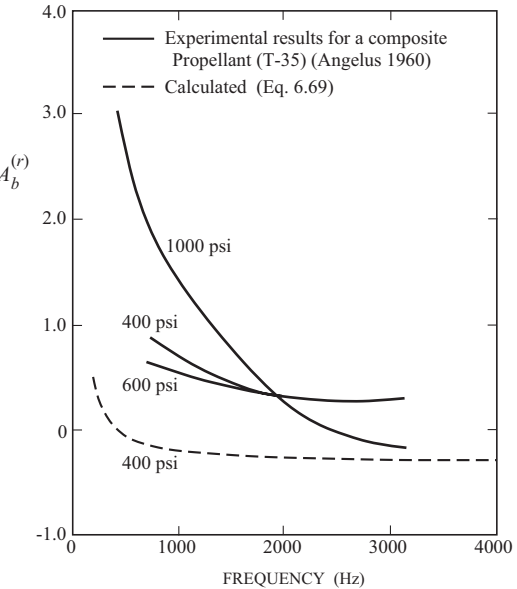


FIGURE 6.14. Dependence of the admittance function on frequency inferred from Brownlee's measurements (Culick 1966).

While these results are useful and seem clearly to contain much truth, they are certainly not free of questions. An important one in particular is raised by the use of the admittance function as the boundary condition for the 010 mode. Because this mode has no velocity component in the direction normal to the burning surface, it is by no means clear that one can even use A_b as it is defined in terms of the normal velocity component. The same difficulty arises for longitudinal modes with burning surfaces not perpendicular to the direction of propagation. This matter has been addressed in development of the theory of longitudinal modes treated within the one-dimensional approximation, discussed in the following section.

A second question concerns the possible influences of 'flow-turning' and other rotational contributions, a matter raised and presently being studied by Flandro and Perry (2006). On the other hand, it is not obvious that the situation here is analogous to that of a longitudinal wave. The difference is that for a longitudinal wave, the unsteady velocity is coplanar (locally) with the mean velocity, whereas for a transverse mode the unsteady and steady velocities are perpendicular. The analysis necessary to settle this question has not been worked out. Flow-turning is discussed in Section 6.12.

6.8. Stability of Oscillations in a Bulk Mode

Most oscillations occurring in combustion chambers are related to wave modes of motion. They can often be interpreted and analyzed as perturbed forms of individual or mixed classical acoustic modes. For many years, oscillations having very low frequencies were regarded as somehow different, but in the context of acoustics generally, that view misses the mark. In fact the oscillations at frequencies below that of the lowest acoustic mode are perturbed forms of the classical acoustic mode having frequency equal to zero, as

explained in Section 6.3. The purpose of this discussion is to show how the result for the bulk mode of a chamber—the L^* -mode in a solid propellant rocket—is extracted quite easily from the results discussed already for wave modes. That this result should be true is fairly clear from the calculations in Section 6.3 because the distribution of burning surface was not required. This point was first made by Culick (1968) in a note generalizing Oberg's 1968 computation.

For the mode in a rocket chamber corresponding to the N^{th} classical acoustic mode, the wavenumber and mode shape for sinusoidal oscillations are given by equations (4.19) and (4.20), with $\kappa = 1$,

$$k^2 = k_N^2 + \frac{1}{E_N^2} \left\{ \iiint_V \psi_N(\mathbf{r}_0) \hat{h}(\mathbf{r}_0) dV_0 + \oint_S \psi_N(\mathbf{r}_{0s}) \hat{f}(\mathbf{r}_{0s}) dS_0 \right\} \quad (6.105)$$

$$\hat{p}(\mathbf{r}) = \psi_N(\mathbf{r}) + \sum_{n=0}^{\infty} \frac{\psi_n(\mathbf{r})}{E_n^2(k^2 - k_n^2)} \left\{ \iiint_V \psi_n(\mathbf{r}_0) \hat{h}(\mathbf{r}_0) dV_0 + \oint_S \psi_n(\mathbf{r}_{0s}) \hat{f}(\mathbf{r}_{0s}) dS_0 \right\} \quad (6.106)$$

The mode ψ_N has the classical shape for the bulk mode, namely $\psi_N = 1$, to which the corresponding value of k_N is $k_N = 0$. Thus $E_N^2 = \iiint_V \psi_N^2 dV = V$ and the two equations are

$$k^2 = \iiint_V \hat{h}(\mathbf{r}_0) dV_0 + \oint_S \hat{f}(\mathbf{r}_{0s}) dS_0 \quad (6.107)$$

$$\hat{p}(\mathbf{r}) = 1 + \sum_{n=0}^{\infty} \frac{\psi_n(\mathbf{r})}{E_n^2(k^2 - k_n^2)} \iiint_V \psi_n(\mathbf{r}_0) \hat{h}(\mathbf{r}_0) dV_0 + \oint_S \psi_n(\mathbf{r}_{0s}) \hat{f}(\mathbf{r}_{0s}) dS_0 \quad (6.108)$$

Equation (6.108) shows that the pressure field differs from a constant value by an amount of order mean flow Mach number. With the formulas (6.75)a,b written for \hat{h} and \hat{f} , there is a common factor k in all terms of (6.107), which can be written

$$k = \frac{i}{V} \oint_S \bar{\mathbf{m}}_0 \cdot \hat{\mathbf{n}} dS_0 + \oint_S A dS_0 \quad (6.109)$$

The first term represents the sum of acoustic energy convection through the boundary, and a contribution of work done on the oscillations due to interaction with the mean flow. Fluctuations at a non-rigid boundary, for which $A \neq 0$, cause work done on or by the surface.

With the definitions of A_b for a burning surface and A_n for a nozzle, the real and imaginary parts of (6.109) are

$$\begin{aligned} \frac{\omega}{\bar{a}} &= \frac{1}{V} \left[S_b A_b^{(i)} - S_n A_n^{(i)} \right] \\ \frac{\alpha}{\bar{a}} &= \frac{1}{V} \left[S_b (A_b^{(r)} + \bar{M}_b) - S_n (M_n + A_n^{(r)}) \right] \end{aligned} \quad (6.110)a,b$$

These equations assume the forms given in Section 6.3 after introducing the definitions of the response function, $R_b = (m'/\bar{m})/(p'/\bar{p})$, and setting the density fluctuation equal to its isentropic value in the relation

$$A_b = \frac{\gamma \bar{p} u'}{\bar{a} p'} = \gamma \bar{M}_b \left[\frac{m'/\bar{m}}{p'/\bar{p}} - \frac{\rho'/\bar{\rho}}{p'/\bar{p}} \right] = \gamma \bar{M}_b \left[R_b - \frac{1}{\gamma} \right] \quad (6.111)$$

Then with the characteristic time $\tau_c = V/\gamma \bar{M}_b S_b \bar{a} = c^* \bar{V}/\bar{a}^2 S_t = c^* L^*/\bar{a}^2$,

$$\begin{aligned} \omega \tau_c &= R_b^{(i)} - \frac{1}{\gamma \bar{M}_b} \left(\frac{S_n}{S_b} \right) A_n^{(i)} \\ \alpha \tau_c &= R_b^{(r)} - \frac{1}{\gamma \bar{M}_b} \left(\frac{S_n}{S_b} \right) (M_n + A_n^{(r)}) \end{aligned} \quad (6.112)a,b$$

which are equivalent to (6.25) and (6.26).

6.9. Linear Stability in the One-Dimensional Approximation

Results corresponding to (6.90), (6.93) and (6.94) can be derived for the case when the one-dimensional approximation is used. The formulas found for the one-dimensional (1-D) case are in the first instance apparently much simpler to use than those found for three-dimensional (3-D) problems. Details of the grain configuration, for example, do not appear. Only the cross section of the port and its variation along the length of the motor must be known. Applications have apparently confirmed that the formula for the growth or decay constant seems to be sufficiently accurate for many purposes, but we will see that positive result is partly illusory.

The foundations of the calculations have been discussed by Culick (1970, 1973, 2001) and Culick and Yang (1992). This formulation is the basis of the Standard Stability Program (SSP) first written by Lovine *et al.* (1976) and in improved form by Nickerson *et al.* (1983). The corrected and improved version including extension to three-dimensional problems is currently under development (French 2004).

When longitudinal or axial acoustic modes are excited in a slender (i.e., L/D not small) solid rocket contain a uniform grain burning only at the lateral boundary, an important basic question arises: How are the waves driven? The difficulty in understanding the mechanism due to combustion processes confined to the boundary arises because the flow from the boundary enters normally to the surface but the mean and unsteady motions in the bulk of the volume are parallel to the surface. Evidently there must be a transition zone, an unsteady layer normally thin, because experimentally, the frequencies of the longitudinal modes are estimated quite closely by the classical formulas for organ pipe oscillations. As an attempt to address part of the question with a relatively simple analysis, Culick (1970, 1973) worked out the consequences of a strictly one-dimensional approximation to the problem; some omissions in that work are corrected here.

In the one-dimensional approximation, the equations to be solved are written for properties averaged over a cross section, with only the axial component of flow accounted for. The inflow of mass, momentum and energy from the combustion zone then appear as sources in the equations of motion. In particular, the inward momentum is assumed to have no axial component at the surface, but must acquire the axial component of the bulk flow at each section of the combustor. It is implied in the analysis that the adjustment occurs instantaneously so no account needs to be taken of any process of memory in the axial direction.

Much discussion, and correction of the original results, has been precipitated exactly because the formulation to treat ‘one-dimensional’ problems is, after all, an approximation. One must be aware that the question always is present: Does the one-dimensional approximation contain imperfect forms of *all* processes present in the *complete* three-dimensional formulation? The query is difficult to answer, partly because in the process of applying the one-dimensional approximation, some viscous effects may also be implied although the coefficient of viscosity does not appear (see, for example, Shapiro 1952). Only comparison of exact and approximate results may give an answer, and even then questions may remain. In this section we cover the procedure and results cited above; in Sections 6.9.1 and 6.9.2 we summarize the current results containing recent corrections.

The procedure for deducing the formula for the wavenumber is the same as that followed in Section 6.7 for three-dimensional problems. Annex B is a summary of the equations derived for the one-dimensional approximation, including source terms denoted by $(\)_s$ which are associated with flow through the lateral boundary. With only linear terms retained, the wave equation, its boundary condition, and the functions h_1 and f_1 are

$$\frac{1}{S_c} \frac{\partial}{\partial x} \left(S_c \frac{\partial p'}{\partial x} \right) - \frac{1}{a^2} \frac{\partial^2 p'}{\partial t^2} = h_1 \quad (6.113)$$

$$\frac{\partial p'}{\partial x} = -f_1 \quad (x = 0, L) \quad (6.114)$$

where

$$h_1 = -\bar{\rho} \frac{1}{S_c} \frac{\partial}{\partial x} \left(S_c \frac{\partial}{\partial x} \bar{u} u' \right) + \frac{\bar{u}}{\bar{a}^2} \frac{\partial^2 p'}{\partial t \partial x} + \frac{\gamma}{\bar{a}^2} \frac{\partial p'}{\partial t} \frac{1}{S_c} \frac{d}{dx} (S_c \bar{u}) + \frac{1}{S_c} \frac{\partial}{\partial x} S_c (\mathcal{F}'_1 + \mathcal{F}'_{1s}) - \frac{1}{\bar{a}^2} \frac{\partial (\mathcal{P}'_1 + \mathcal{P}'_{1s})}{\partial t} \quad (6.115)$$

$$f_1 = \bar{\rho} \frac{\partial u'}{\partial t} + \bar{\rho} \frac{\partial}{\partial x} (\bar{u} u') - (\mathcal{F}'_1 + \mathcal{F}'_{1s}) \quad (6.116)$$

Equations (6.113)–(6.116) correspond to (6.74)a,b and (6.75)a,b. To simplify the formulae, and to emphasize several important points that do not depend on gas/particle interactions, we will assume that the flow contains no particulate matter. Then \mathcal{W}'_1 , \mathcal{F}'_1 and \mathcal{P}'_1 are found as the fluctuations of (B.8), (B.9) and (B.11) without the contributions from particles:

$$\mathcal{F}'_1 = \frac{\partial \tau'_v}{\partial x} + m'_e + m'_D - \sigma'_e \approx 0 \quad (6.117)$$

$$\mathcal{P}'_1 = \frac{R}{C_v} Q'_1 + RT \mathcal{W}'_1 \approx \frac{R}{C_v} Q'_1 \quad (6.118)$$

$$\mathcal{W}'_1 = \mathcal{W}'_e \approx 0 \quad (6.119)$$

Recall that $(\)_e$ identifies external sources and m'_D is the fluctuation of mass associated with diffusional processes; see Annex A for the definition of m_D . With viscous terms ignored, only \mathcal{P}'_1 is non-zero. Finally, the surface terms \mathcal{F}'_{1s} and \mathcal{P}'_{1s} in h_1 and f_1 are found from the definitions (B.20) and B.22) to be

$$\mathcal{F}'_{1s} = \frac{1}{S_c} \left\{ (\bar{u}_s - \bar{u}) \int m'_{sg} dq + (u'_s - u') \int \bar{m}_{sg} dq \right\} \quad (6.120)$$

$$\mathcal{P}'_{1s} = \frac{R}{C_v} \frac{1}{S_c} \left\{ (\bar{h}_{0s} - \bar{e}_0 + C_v \bar{T}) \int m'_{sg} dq + (h'_{0s} - e'_0 + C_v T') \int \bar{m}_{sg} dq \right\} \quad (6.121)$$

Expansion of the zero-order representations of the pressure and velocity fields have the forms corresponding to (6.77),

$$p'(x, t) = \bar{p} \sum_{\ell=1}^{M_1} \eta_{\ell}(t) \psi_{\ell}(x) \quad (6.122)$$

$$u'(x, t) = \sum_{\ell=1}^{M_1} \frac{\eta_{\ell}}{\gamma k_{\ell}^2} \frac{d \psi_{\ell}}{dx} \quad (6.123)$$

where the ψ_{ℓ} are normal modes satisfying the homogeneous equations

$$\frac{1}{S_c} \frac{d}{dx} \left(S_c \frac{d \psi_{\ell}}{dx} \right) + k_{\ell}^2 \psi_{\ell} = 0 \quad (6.124)$$

$$\frac{d \psi_{\ell}}{dx} = 0 \quad (x = 0, L) \quad (6.125)$$

After substitution of (6.122) in (6.113) and spatially averaging the result, we find the system of oscillator equations and the ‘forcing functions’ F_{ℓ} :

$$\frac{d^2 \eta_{\ell}}{dt^2} + \omega_{\ell}^2 \eta_{\ell} = F_{\ell} \quad (6.126)$$

$$F_{\ell} = -\frac{\bar{a}^2}{\bar{p} E_{\ell}^2} \left\{ \int_0^L h_1 \psi_{\ell} S_c dx + [f_1 \psi_{\ell} S_c]_0^L \right\} \quad (6.127)$$

and $E_\ell^2 = \int_0^L \psi_\ell^2 S_c dx$. Equations (6.126) and (6.127) correspond to (6.79) and (6.80).

For harmonic motions, $h_1 = \hat{h}_1 e^{-i\bar{a}kt}$, etc., substitution of (6.127) in (6.126) leads to the formula for the square of the wavenumber,

$$k^2 = k_\ell^2 + \frac{1}{\bar{p}E_\ell^2} \left\{ \int_0^L \frac{\hat{h}_1}{\hat{\eta}_\ell} \psi_\ell S_c dx + \left[\frac{\hat{f}_1}{\hat{\eta}_\ell} \psi_\ell S_c \right]_0^L \right\} \quad (6.128)$$

where (6.115) and (6.116) are now

$$\hat{h}_1 = -\bar{\rho} \frac{1}{S_c} \frac{d}{dx} \left(S_c \frac{d}{dx} \bar{u} \hat{u} \right) - ik \frac{\bar{u}}{\bar{a}} \frac{d\hat{p}}{dx} - i\gamma \frac{k}{\bar{a}} \hat{p} \frac{1}{S_c} \frac{d}{dx} (S_c \bar{u}) + \frac{1}{S_c} \frac{d}{dx} S_c (\hat{\mathcal{F}}_1 + \hat{\mathcal{F}}_{1s}) + i \frac{k}{\bar{a}} (\hat{\mathcal{P}}_1 + \hat{\mathcal{P}}_{1s}) \quad (6.129)$$

$$\hat{f}_1 = -i\bar{\rho}\bar{a}\hat{k}\hat{u} + \bar{\rho} \frac{d}{dx} (\bar{u}\hat{u}) - (\hat{\mathcal{F}}_1 + \hat{\mathcal{F}}_{1s}) \quad (6.130)$$

are the one-dimensional forms of equations (6.75)a,b.

The first three terms of \hat{h}_1 and the first two terms of \hat{f}_1 , correspond exactly to their three-dimensional counterparts in (6.75)a,b; $\mathcal{F}'_1 + \mathcal{F}'_{1s}$ and $\mathcal{P}'_1 + \mathcal{P}'_{1s}$ correspond to \mathcal{F}' and \mathcal{P}' . Thus the special topics which we discuss shortly have to do mainly with \mathcal{F}'_{1s} and \mathcal{P}'_{1s} and parts of \mathcal{F}' and \mathcal{P}' . First we carry through the manipulations equivalent to those beginning with (6.77), but now for one-dimensional problems. Substitution of (6.129) and (6.130) into (6.128) gives

$$\begin{aligned} k^2 - k_\ell^2 &= \frac{1}{\hat{\eta}_\ell \bar{p} E_\ell^2} \left\{ -\bar{\rho} \int_0^L \frac{1}{S_c} \frac{d}{dx} \left(S_c \frac{d}{dx} \bar{u} \hat{u} \right) \psi_\ell S_c dx - ik \int_0^L \frac{\bar{u}}{\bar{a}} \frac{d\hat{p}}{dx} \psi_\ell S_c dx - i\gamma \frac{k}{\bar{a}} \int_0^L \hat{p} \frac{1}{S_c} \frac{d}{dx} (S_c \bar{u}) \psi_\ell S_c dx \right\} \\ &\quad + \frac{1}{\hat{\eta}_\ell \bar{p} E_\ell^2} \left\{ \int_0^L \frac{1}{S_c} \frac{d}{dx} S_c (\hat{\mathcal{F}}_1 + \hat{\mathcal{F}}_{1s}) \psi_\ell S_c dx + i \frac{k}{\bar{a}} \int_0^L (\hat{\mathcal{P}}_1 + \hat{\mathcal{P}}_{1s}) \psi_\ell S_c dx \right\} \\ &\quad + \frac{1}{\hat{\eta}_\ell \bar{p} E_\ell^2} \left\{ -i\bar{\rho}\bar{a}k [\hat{u}\psi_\ell S_c]_0^L + \bar{\rho} \left[\frac{d}{dx} (\bar{u}\hat{u}) \psi_\ell S_c \right]_0^L - [(\hat{\mathcal{F}}_1 + \hat{\mathcal{F}}_{1s}) \psi_\ell S_c]_0^L \right\} \end{aligned} \quad (6.131)$$

The zeroth order forms of \hat{p} and \hat{u} are given by the one-dimensional acoustic formulas,

$$\begin{aligned} (p')_{\substack{\text{zeroth} \\ \text{order}}} &= p'_\ell(x, t) = \hat{p}_\ell(x) e^{-i\bar{a}k_\ell t} = \bar{p} \hat{\eta}_\ell \psi_\ell(x) e^{-i\bar{a}k_\ell t} \\ (u')_{\substack{\text{zeroth} \\ \text{order}}} &= u'_\ell(x, t) = \hat{u}_\ell(x) e^{-i\bar{a}k_\ell t} = -i \frac{\bar{a}}{\gamma k_\ell} \hat{\eta}_\ell \frac{d\psi_\ell}{dx} e^{-i\bar{a}k_\ell t} \end{aligned} \quad (6.132)\text{a,b}$$

Consistent with the general ordering procedure, these formulas are to be used anywhere \hat{p} and \hat{u} are multiplied by $\bar{u}(x)$ or its derivative(s). Thus, only the first term in the last set of brackets in (6.131) contains the perturbed form of \hat{u} (not \hat{u}_ℓ).

Integration by parts and use of equation (6.124) leads to the result

$$\begin{aligned} -\bar{\rho} \int_0^L \frac{1}{S_c} \frac{d}{dx} \left(S_c \frac{d}{dx} \bar{u} \hat{u} \right) \psi_\ell S_c dx &= -\bar{\rho} \left[\psi_\ell S_c \frac{d}{dx} (\bar{u} \hat{u}) \right]_0^L + \bar{\rho} \left[\bar{u} \hat{u} S_c \frac{d\psi_\ell}{dx} \right]_0^L + \bar{\rho} k_\ell^2 \int_0^L \bar{u} \hat{u} \psi_\ell S_c dx \\ &= -\bar{\rho} \left[\psi_\ell S_c \frac{d}{dx} (\bar{u} \hat{u}) \right]_0^L + \bar{\rho} \left[\bar{u} \hat{u} S_c \frac{d\psi_\ell}{dx} \right]_0^L - i \frac{\hat{\eta}_\ell}{\gamma} \bar{\rho} \bar{a} k_\ell \int_0^L \bar{u} \psi_\ell \frac{d\psi_\ell}{dx} S_c dx \end{aligned} \quad (6.133)$$

The second and third terms in the first curly brackets of (6.131) are

$$-ik \int_0^L \frac{\bar{u}}{\bar{a}} \frac{d\hat{p}}{dx} \psi_\ell S_c dx = -i\bar{p}\hat{\eta}_\ell \frac{k_\ell}{\bar{a}} \int_\ell^L \bar{u} \psi_\ell \frac{d\psi_\ell}{dx} S_c dx \quad (6.134)$$

$$-i\gamma \frac{k}{\bar{a}} \int_0^L \hat{p} \frac{1}{S_c} \frac{d}{dx} (S_c \bar{u}) \psi_\ell dx = -i\gamma \bar{p}\hat{\eta}_\ell \frac{k_\ell}{\bar{a}} \int_0^L \psi_\ell^2 \left[\frac{1}{S_c} \frac{d(S_c \bar{u})}{dx} \right] S_c dx \quad (6.135)$$

and the terms in (6.131) containing $(\hat{\mathcal{F}}_1 + \hat{\mathcal{F}}_{1s})$ combine in an obvious fashion. With (6.133)–(6.135), the formula (6.131) can be written

$$\begin{aligned} k^2 - k_\ell^2 &= -i \frac{k_\ell}{\bar{a} E_\ell^2} \left\{ 2 \int_0^L \bar{u} \psi_\ell \frac{d\psi_\ell}{dx} S_c dx + \gamma \int_0^L \psi_\ell^2 \left[\frac{1}{S_c} \frac{d(S_c \bar{u})}{dx} \right] S_c dx \right\} \\ &\quad - \frac{1}{\bar{p} E_\ell^2} \left\{ \int_0^L \left[\left(\frac{\hat{\mathcal{F}}_1 + \hat{\mathcal{F}}_{1s}}{\hat{\eta}_\ell} \right) \frac{d\psi_\ell}{dx} - i \frac{k_\ell}{\bar{a}} \left(\frac{\hat{\mathcal{P}}_1 + \hat{\mathcal{P}}_{1s}}{\hat{\eta}_\ell} \right) \psi_\ell \right] S_c dx \right\} \\ &\quad - i \frac{k_\ell}{\bar{a}} \frac{\gamma}{E_\ell^2} \left[\frac{\hat{u}}{\hat{\eta}_\ell} \psi_\ell S_c \right]_0^L \end{aligned} \quad (6.136)$$

Now we rewrite the terms in the first bracket set to show that (6.136) is exactly the one-dimensional form of (6.90). Integration of the first term by parts gives two terms, one of which is proportional to the last term in brackets and the other is a boundary term:

$$\begin{aligned} 2 \int_0^L \bar{u} \psi_\ell \frac{d\psi_\ell}{dx} S_c dx &= \int_0^L \frac{d}{dx} (S_c \bar{u} \psi_\ell^2) dx - \int_0^L \psi_\ell^2 \left[\frac{1}{S_c} \frac{d}{dx} (S_c \bar{u}) \right] S_c dx \\ &= [S_c \bar{u} \psi_\ell^2]_0^L - \int_0^L \psi_\ell^2 \left[\frac{1}{S_c} \frac{d}{dx} (S_c \bar{u}) \right] S_c dx \end{aligned} \quad (6.137)$$

Substitution of (6.137) in (6.136) and some rearrangement gives

$$\begin{aligned} k^2 &= k_\ell^2 - i \frac{k_\ell}{\bar{a} E_\ell^2} \left\{ \left[\left(\gamma \frac{\hat{u}}{\hat{\eta}_\ell} + \bar{u} \psi_\ell \right) \psi_\ell S_c \right]_0^L + (\gamma - 1) \int_0^L \psi_\ell^2 \left[\frac{1}{S_c} \frac{d}{dx} (S_c \bar{u}) \right] S_c dx \right\} \\ &\quad - \frac{1}{\bar{p} E_\ell^2} \int_0^L \left[\left(\frac{\hat{\mathcal{F}}_1 + \hat{\mathcal{F}}_{1s}}{\hat{\eta}_\ell} \right) \frac{d\psi_\ell}{dx} - i \frac{k_\ell}{\bar{a}} \left(\frac{\hat{\mathcal{P}}_1 + \hat{\mathcal{P}}_{1s}}{\hat{\eta}_\ell} \right) \psi_\ell \right] S_c dx \end{aligned} \quad (6.138)$$

which is (6.90) written from one-dimensional problems. However, the terms containing $\hat{\mathcal{F}}_{1s}$ and $\hat{\mathcal{P}}_{1s}$ are additional here because of the explicit accounting for flow through the lateral boundary.

6.9.1. The One-Dimensional Approximation to ‘Flow-Turning’. The correspondence between the terms in (6.138) and (6.90) is clear. What is especially important are the effects represented by the sources at the lateral boundaries, $\hat{\mathcal{F}}_{1s}$ and $\hat{\mathcal{P}}_{1s}$, found from the formulas (6.120) and (6.121). It is important for interpretation of this result to remember (Annex B) that \mathcal{F}_{1s} represents the source of momentum, and \mathcal{P}_{1s} the pressure source, both associated with the mass source at the boundary. Moreover, the average values

of the sources may be zero (Annex C) or non-zero, as for a burning surface. We treat first the contribution to stability by unsteady momentum addition of flow at the boundary,

$$\int_0^L \frac{\hat{\mathcal{F}}_{1s}}{\hat{\eta}_\ell} \frac{d\psi_\ell}{dx} S_c dx = \int_0^L \frac{1}{S_c} \left[(\bar{u}_s - \bar{u}) \int \frac{\hat{m}_{sg}}{\hat{\eta}_\ell} dq + \left(\frac{\hat{u}_s - \hat{u}}{\hat{\eta}_\ell} \right) \int \bar{m}_{sg} dq \right] \frac{d\psi_\ell}{dx} S_c dx \quad (6.139)$$

Figure 6.15 shows interpretations of the various quantities appearing in (6.139).

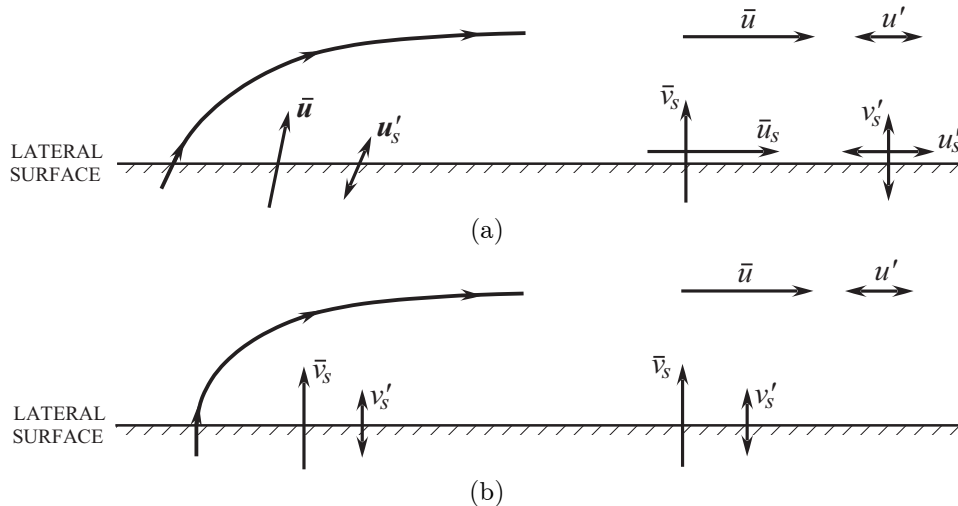


FIGURE 6.15. Velocity vectors for flow through a permeable boundary. (a) non-zero mean flow parallel to the boundary; (b) only normal flow at the boundary.

Observation, for example by use of films, and physical arguments, suggest that the average flow from the surface of a burning solid propellant is always normal to the surface. The situation sketched in Figure 6.15(a) apparently does not exist. Hence we assume $\bar{u}_s = \hat{u}_s = 0$ as shown in Figure 6.15(b); (6.139) is therefore

$$\int_0^L \frac{\hat{\mathcal{F}}_{1s}}{\hat{\eta}_\ell} \frac{d\psi_\ell}{dx} S_c dx = - \int_0^L \frac{1}{S_c} \left[\bar{u} \int \frac{\hat{m}_{sg}}{\hat{\eta}_\ell} dq + \frac{\hat{u}}{\hat{\eta}_\ell} \int \bar{m}_{sg} dq \right] \frac{d\psi_\ell}{dx} S_c dx \quad (6.140)$$

Substitute (6.89)b for \hat{u} and the second term is

$$- \int_0^L \frac{1}{S_c} \frac{\hat{u}}{\hat{\eta}_\ell} \int \bar{m}_{sg} dq \frac{d\psi_\ell}{dx} S_c dx = i \frac{\bar{a}}{\gamma k_\ell} \int_0^L \left(\frac{d\psi_\ell}{dx} \right)^2 \int \bar{m}_{sg} dq dx \quad (6.141)$$

We estimate the first term in (6.140) by assuming \hat{m}_{sg} to be independent of position on the surface; with $q(x)$ the total perimeter of the chamber at position x ,

$$- \int_0^L \frac{1}{S_c} \bar{u} \int \frac{\hat{m}_{sg}}{\hat{\eta}_\ell} dq \frac{d\psi_\ell}{dx} S_c dx = - \frac{\hat{m}_{sg}}{\hat{\eta}_\ell} \int_0^L \bar{u} q \frac{d\psi_\ell}{dx} dx = - \left(\frac{1}{\hat{\eta}_\ell} \frac{\hat{m}_{sg}}{\bar{m}} \right) \bar{m} \int_0^L \bar{u} q \frac{d\psi_\ell}{dx} dx$$

The ratio in parentheses is the response function, of order unity (Chapter 2 equations (2.66) and (2.67), for example). Thus the term depends on the square of the mean velocity and must be ignored. Hence for use

in (6.138), combination of (6.140) and (6.141) gives

$$\frac{1}{\bar{p}E_\ell^2} \int_0^L \frac{\hat{\mathcal{F}}_{1s}}{\hat{\eta}_\ell} \frac{d\psi_\ell}{dx} S_c dx = i \frac{k_\ell}{\bar{\rho}aE_\ell^2} \int_0^L \frac{1}{k_\ell^2} \left(\frac{d\psi_\ell}{dx} \right)^2 \int \bar{m}_{sg} dq dx \quad (6.142)$$

This result is the one-dimensional approximation to ‘flow-turning’. It appeared first in equation (3.9) in Culick (1973), and has since been the motivation for considerable discussion in the literature and in various technical meetings. Always to be kept in mind is perhaps the most interesting aspect of the matter, the contrast with the results of three-dimensional analyses. An especially important property is the accuracy with which behavior that is necessarily three- (or two-) dimensional is approximated by the results of one-dimensional predictions.²²

What has come to be accepted as the ‘flow-turning’ process has the following elementary interpretation for a burning solid propellant exposed to oscillations. We imagine that the solid/gas interface is fixed and that solid material advances to the interface with constant speed. As soon as the solid is transformed to gas, it begins to acquire both steady and oscillatory motion, partly due to viscous forces exerted by gas released earlier, but principally due to the oscillatory pressure. Thus the incoming fluid acquires sufficient unsteady motion to join the flow field existing at some distance from the interface. Figure 6.16 is a simplified interpretation of this process in two dimensions. From the interpretation just given, it is evident that, because work is done on the incoming fluid both to impart the oscillatory motions and to turn the flow as sketched in Figure 6.16, the process of ‘flow-turning’ constitutes a loss. For harmonic motions, oscillations parallel to the surface, the loss is given by (6.142) within the one-dimensional approximation. Twenty years after the approximation was deduced, Flandro (1995) showed rigorously with analysis of a two-dimensional flow that the result (6.142) is exact.

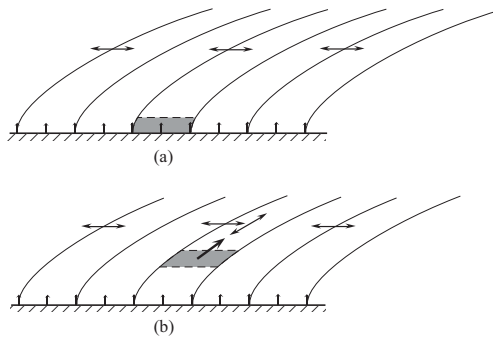


FIGURE 6.16. The origin of ‘flow-turning’: An element of fluid shown (a) at entry normal to a burning or porous surface, and (b) in an intermediate state of the process of acquiring the local axial velocity having mean and acoustic components.

If ‘flow-turning’ is the only contribution to momentum transfer at the lateral surface and there is no momentum addition within the volume ($\mathcal{F}_1 = 0$), the formula (6.138) becomes

$$\begin{aligned} k^2 = k_\ell^2 - i \frac{k_\ell}{\bar{a}E_\ell^2} & \left\{ \left[\left(\gamma \frac{\hat{u}}{\hat{\eta}_\ell} + \bar{u} \psi_\ell \right) \psi_\ell S_c \right]_0^L + (\gamma - 1) \int_0^L \psi_\ell^2 \left[\frac{1}{S_c} \frac{d}{dx} (S_c \bar{u}) \right] S_c dx \right\} \\ & - i \frac{k_\ell}{\bar{\rho}aE_\ell^2} \int_0^L \left[\frac{1}{k_\ell^2} \left(\frac{d\psi_\ell}{dx} \right)^2 \right] \int \bar{m}_{sg} dq dx + i \frac{k_\ell}{\bar{a}} \frac{1}{\bar{p}E_\ell^2} \int_0^L \left(\frac{\hat{\mathcal{P}}_1 + \hat{\mathcal{P}}_{1s}}{\hat{\eta}_\ell} \right) \psi_\ell S_c dx \end{aligned} \quad (6.143)$$

²²We refer to behavior which, in principle at least, is covered by terms involving $\hat{\mathcal{F}}$ and $\hat{\mathcal{P}}$ in (6.90), and correspondingly may arise from $\hat{\mathcal{F}}_1$, $\hat{\mathcal{P}}_1$, $\hat{\mathcal{F}}_{1s}$ and $\hat{\mathcal{P}}_{1s}$ in (6.138).

6.9.2. The One-Dimensional Approximation to ‘Pumping’. There is a second equally important contribution to the unsteady energy transfer accompanying flow through a lateral boundary. This process was mistakenly not included, with ‘flow-turning’, in the general analysis discussed by Culick (1973), although a restricted form was discussed at the end of the same paper (see Annex C). The basic process has acquired the name ‘pumping’, referring to the influence of the flow immediately adjacent to the boundary on the flow past the boundary. It arises because the flow *parallel* to the surface has a time-varying component which varies with position along the boundary. The discussion here concerns largely the one-dimensional counterpart of the two- or three-dimensional process first found and explained by Flandro (1995)a.

Due to conservation of mass, as demonstrated in Section 5.9.3, motion is then induced in the direction *normal* to the boundary. It is that portion of the fluid motion that is called ‘pumping’. For the case of harmonic motions past an impermeable boundary, the fluid velocity accompanying the pumping action is given by equation (5.146). We investigate now the pumping action for the case when flow with average velocity \bar{v}_b passes through the boundary. We assume that there is no fluctuating component of v at the surface: $v'_b = 0$.

Unlike the case for fully three-dimensional calculations, the first integral in (6.143), which has as part of its integrand the one-dimensional form of $\nabla \cdot \bar{u}$, is generally non-zero. The conservation of mass is expressed for one-dimensional flow by equation (B.2) written for steady purely gaseous flow,

$$\bar{u} \frac{d\bar{\rho}}{dx} = -\bar{\rho} \frac{1}{S_c} \frac{d}{dx} (S_c \bar{u}) + \frac{1}{S_c} \int \bar{m}_b dq$$

We take $\bar{\rho}$ to be strictly constant and the continuity equation for steady flow is

$$\frac{1}{S_c} \frac{d}{dx} (S_c \bar{u}) = \frac{1}{\bar{\rho} S_c} \int \bar{m}_b dq \quad (6.144)$$

Let $\bar{m}_b = \bar{m}_{sg}$ for the case here and substitute in (6.143) to give

$$\begin{aligned} k^2 = k_\ell^2 - i \frac{k_\ell}{\bar{a} E_\ell^2} & \left\{ \left[\left(\gamma \frac{\hat{u}}{\hat{\eta}_\ell} + \bar{u} \psi_\ell \right) \psi_\ell S_c \right]_0^L + (\gamma - 1) \int_0^L \psi_\ell^2 \int \frac{\bar{m}_{sg}}{\bar{\rho}} dq dx \right\} \\ & - i \frac{k_\ell}{\bar{a} E_\ell^2} \int_0^L \left[\frac{1}{k_\ell^2} \left(\frac{d\psi_\ell}{dx} \right)^2 \right] \int \frac{\bar{m}_{sg}}{\bar{\rho}} dq dx + i \frac{k_\ell}{\bar{a}} \frac{1}{\bar{p} E_\ell^2} \int_0^L \left(\frac{\hat{\mathcal{P}}_1 + \hat{\mathcal{P}}_{1s}}{\hat{\eta}_\ell} \right) \psi_\ell S_c dx \end{aligned} \quad (6.145)$$

The definition (6.121) for \mathcal{P}'_1 gives the contribution from fluctuations of heat release within the flow,

$$\hat{\mathcal{P}}_1 = \frac{R}{C_v} \hat{Q}_1 = (\gamma - 1) \hat{Q}_1 \quad (6.146)$$

From (6.121) we find the term representing the effect of flow through the lateral boundary,

$$\hat{\mathcal{P}}_{1s} = \frac{R}{C_v} \frac{1}{S_c} \left\{ (\bar{h}_{0s} - \bar{e}_0 + C_v \bar{T}) \int \hat{m}_{sg} dq + (\hat{h}_{0s} - \hat{e}_0 + C_v \hat{T}) \int \bar{m}_{sg} dq \right\} \quad (6.147)$$

After substitution of the appropriate definitions,

$$h_{0s} - e_0 + C_v T := (C_p T_s + \frac{u_s^2}{2}) - (C_v T + \frac{u^2}{2}) + C_v T = C_p \Delta T_s + C_p T + \frac{1}{2} (u_s^2 - u^2)$$

where $\Delta T_s = T_s - T$. Because the kinetic energy is normally negligible in combustion chambers,

$$\frac{R}{C_v} (h_{0s} - e_0 + C_v T) \approx \frac{C_p}{C_v} R T + \frac{C_p}{C_v} R \Delta T = a^2 + \gamma R \Delta T \quad (6.148)$$

Hence (6.147) becomes

$$\hat{\mathcal{P}}_{1s} = \frac{1}{S_c} (\bar{a}^2 + \gamma R \Delta \bar{T}_s) \int \hat{m}_{sg} dq + \frac{1}{S_c} (\gamma R \hat{T} + \gamma R \Delta \hat{T}_s) \int \bar{m}_{sg} dq \quad (6.149)$$

Substitution of (6.146) and (6.149) into (6.145) gives

$$\begin{aligned}
 k^2 = & k_\ell^2 - i \frac{k_\ell}{\bar{a}E_\ell^2} \left\{ \left[\left(\gamma \frac{\hat{u}}{\hat{\eta}_\ell} + \bar{u}\psi_\ell \right) \psi_\ell S_c \right]_0^L + (\gamma - 1) \int_0^L \psi_\ell^2 \int \frac{\bar{m}_{sg}}{\bar{\rho}} dq dx \right\} \\
 & - i \frac{k_\ell}{\bar{a}E_\ell^2} \int_0^L \left[\frac{1}{k_\ell^2} \left(\frac{d\psi_\ell}{dx} \right)^2 \right] \int \bar{m}_{sg} dq dx + i \frac{k_\ell}{\bar{a}} \frac{1}{\bar{p}E_\ell^2} (\gamma - 1) \int_0^L \frac{\hat{Q}_1}{\hat{\eta}_\ell} \psi_\ell S_c dx \\
 & + i \frac{k_\ell}{\bar{a}} \frac{1}{\bar{p}E_\ell^2} \int_0^L \psi_\ell \int \left[(\bar{a}^2 + \gamma R \Delta \bar{T}_s) \frac{\hat{m}_{sg}}{\hat{\eta}_\ell} + \left(\frac{\gamma R \hat{T}}{\hat{\eta}_\ell} + \gamma R \frac{\Delta \hat{T}_s}{\hat{\eta}_\ell} \right) \bar{m}_{sg} \right] dq dx
 \end{aligned} \tag{6.150}$$

Temporarily denote the last integral by P and rewrite the various terms in the following way:

$$\begin{aligned}
 \hat{\eta}_\ell P &= \int_0^L \psi_\ell \int \left[(\bar{a}^2 + \gamma R \Delta \bar{T}_s) \hat{m}_{sg} + \gamma R (\hat{T} + \Delta \hat{T}_s) \bar{m}_{sg} \right] dq dx \\
 &= \bar{\rho} \bar{a}^2 \int_0^L \psi_\ell \int \left(\frac{\hat{m}_{sg}}{\bar{\rho}} + \frac{\Delta \hat{T}_s}{\bar{\rho} \bar{T}} \bar{m}_{sg} \right) dq dx + \gamma R \bar{T} \int_0^L \psi_\ell \frac{\hat{T}}{\bar{T}} \int \bar{m}_{sg} dq dx + \int_0^L \psi_\ell \int (\gamma R \Delta \bar{T}_s) \hat{m}_{sg} dq dx \\
 &= \bar{\rho} \bar{a}^2 \int_0^L \psi_\ell \int \left(\frac{\hat{m}_{sg}}{\bar{\rho}} + \frac{\Delta \hat{T}_s}{\bar{\rho} \bar{T}} \bar{m}_{sg} \right) dq dx + R \bar{T} (\gamma - 1) \hat{\eta}_\ell \int_0^L \psi_\ell^2 \int \bar{m}_{sg} dq dx + \int_0^L \psi_\ell \int (\gamma R \Delta \bar{T}_s) \hat{m}_{sg} dq dx
 \end{aligned}$$

The penultimate term can be written using the relation (6.144) for conservation of mass,

$$\begin{aligned}
 R \bar{T} (\gamma - 1) \int_0^L \psi_\ell^2 \int \bar{m}_{sg} dq dx &= R \bar{\rho} \bar{T} (\gamma - 1) \int_0^L \psi_\ell^2 \int \frac{\bar{m}_{sg}}{\bar{\rho}} dq dx \\
 &= \bar{\rho} (\gamma - 1) \int_0^L \psi_\ell^2 \left[\frac{1}{S_c} \frac{d(S_c \bar{u})}{dx} \right] S_c dx
 \end{aligned}$$

Upon substitution of $\hat{\eta}_\ell P$ in (6.150), this term is cancelled by the second term in curly brackets; k^2 is now given by the sum of terms²³

$$\begin{aligned}
 k^2 = & k_\ell^2 - i \frac{k_\ell}{\bar{a}E_\ell^2} \left[\left(\gamma \frac{\hat{u}}{\hat{\eta}_\ell} + \bar{u}\psi_\ell \right) \psi_\ell S_c \right]_0^L + i \frac{k_\ell}{\bar{a}} \frac{\gamma}{E_\ell^2} \int_0^L \psi_\ell \int \left(\frac{\hat{m}_{sg}}{\bar{\rho}} + \frac{\Delta \hat{T}_s}{\bar{\rho} \bar{T}} \bar{m}_{sg} \right) dq dx \\
 & - i \frac{k_\ell}{\bar{a}E_\ell^2} \int_0^L \left[\frac{1}{k_\ell^2} \left(\frac{d\psi_\ell}{dx} \right)^2 \right] \int \bar{m}_{sg} dq dx + i \frac{k_\ell}{\bar{a}} \frac{(\gamma - 1)}{\bar{p}E_\ell^2} \int_0^L \frac{\hat{Q}_1}{\hat{\eta}_\ell} \psi_\ell S_c dx \\
 & + i \frac{k_\ell}{\bar{a}} \frac{1}{\bar{p}E_\ell^2} \int_0^L \psi_\ell \int (\gamma R \Delta \bar{T}_s) \hat{m}_{sg} dq dx
 \end{aligned} \tag{6.151}$$

When interpreting this result, it is helpful to recall that with $\bar{a}k = \omega + i\alpha$, $e^{-i\bar{a}kt} = e^{-i(\omega+i\alpha)t} = e^{\alpha t - i\omega t}$, so $\alpha < 0$ for decay of waves, i.e., the imaginary part of the right-hand side of (6.151) must be negative for stability.

²³Taking into account differences of definitions (mainly $e^{i\bar{a}kt}$ in earlier work is replaced by $e^{-i\bar{a}kt}$ here, and $p'_\ell = \hat{p}_\ell e^{i\bar{a}k_\ell t}$ is written $p'_\ell = \hat{p}\hat{\eta}_\ell \psi_\ell e^{-i\bar{a}k_\ell t}$) equation (6.151) agrees with equation (3.13) in Culick (1973) written for a flow without particles. The last term in (6.151) was mistakenly dropped from (3.13) in the earlier work.

For practical purposes it is necessary to have the real and imaginary parts of k , corresponding to the formulas (6.93) and (6.94) found for three-dimensional waves. Write (6.151) as

$$k^2 = k_\ell^2 + (A + iB)$$

Then with $\omega - \omega_\ell$ and α small,

$$\begin{aligned}\omega - \omega_\ell &= \frac{\bar{a}^2}{2\omega_\ell} A \\ \alpha &= \frac{\bar{a}^2}{2\omega_\ell} B\end{aligned}$$

Then with $\bar{a}k_\ell/\omega_\ell = 1$, we find for the real and imaginary parts of (6.151),

$$\begin{aligned}\omega &= \omega_\ell - \frac{1}{2E_\ell^2} \left[\left(\gamma \frac{\hat{u}^{(i)}}{\hat{\eta}_\ell} \right) \psi_\ell S_c \right]_0^L - \frac{\gamma}{E_\ell^2} \int_0^L \psi_\ell \int \left(\frac{\hat{m}_{sg}^{(i)}}{\bar{\rho}} + \frac{\Delta \hat{T}_s^{(i)}}{\bar{\rho} \bar{T}} \bar{m}_{sg} \right) dq dx \\ &\quad - \frac{(\gamma - 1)}{2E_\ell^2} \int_0^L \frac{\hat{Q}_1^{(i)}}{\hat{\eta}_\ell} \psi_\ell S_c dx - \frac{1}{2E_\ell^2} \int_0^L \psi_\ell (\gamma R \Delta \bar{T}_s) \hat{m}_{sg}^{(i)} dq dx\end{aligned}\quad (6.152)$$

$$\begin{aligned}\alpha &= - \frac{1}{2E_\ell^2} \left[\left(\gamma \frac{\hat{u}^{(r)}}{\hat{\eta}_\ell} + \bar{u} \psi_\ell \right) \psi_\ell S_c \right]_0^L + \frac{\gamma}{2E_\ell^2} \int_0^L \psi_\ell \int \left(\frac{\hat{m}_{sg}^{(r)}}{\bar{\rho}} + \frac{\Delta \hat{T}_s^{(r)}}{\bar{\rho} \bar{T}} \bar{m}_{sg} \right) dq dx \\ &\quad - \frac{\gamma}{2E_\ell^2} \int_0^L \left[\frac{1}{k_\ell^2} \left(\frac{d\psi_\ell}{dx} \right)^2 \right] \int \bar{m}_{sg} dq dx + \frac{(\gamma - 1)}{2E_\ell^2} \int_0^L \frac{\hat{Q}_1^{(r)}}{\hat{\eta}_\ell} \psi_\ell S_c dx \\ &\quad + \frac{1}{2E_\ell^2} \int_0^L \psi_\ell \int (\gamma R \Delta \bar{T}_s) \hat{m}_{sg}^{(r)} dq dx\end{aligned}\quad (6.153)$$

The terms containing $\Delta \hat{T}_s$ represent the effects of a frequency shift depending on $\Delta \hat{T}_s^{(i)}$, the part of $\Delta \hat{T}_s$ out-of-phase with the pressure oscillation; and attenuation depending on the in-phase part $\Delta \hat{T}_s^{(r)}$ associated with convection inward at the lateral boundary. Fluctuations of the mass flux inward affect the frequency shift and attenuation by carrying flow having an average temperature difference $\Delta \bar{T}_s$, represented by the last term of 6.152 and 6.153.

More significant are the terms identified by * and ** which we will temporarily denote as the contributions $\tilde{\alpha}_{sp}$ and α_{FT} to α :

$$\tilde{\alpha}_{sp} = \frac{\gamma}{2E_\ell^2} \int_0^L \psi_\ell \int \frac{\hat{m}_{sg}^{(r)}}{\bar{\rho}} dq dx \quad (6.154)$$

$$\alpha_{FT} = - \frac{\gamma}{2E_\ell^2} \int_0^L \left[\frac{1}{k_\ell^2} \left(\frac{d\psi_\ell}{dx} \right)^2 \right] \int \bar{m}_{sg} dq dx \quad (6.155)$$

The contribution α_{FT} , generally referred to as the ‘flow-turning’ damping, was discovered by Culick (1973) in his analysis of unsteady one-dimensional oscillations.

In his 1995a paper, Flandro found a second contribution which Culick had not identified²⁴ in his 1973 paper. This difference has directly—or indirectly—been part of the cause for much discussion, occasionally controversy. The difference (with hindsight!) is illusory: The 1973 result, equation (6.153) here, contains the important process called “pumping”²⁵ by Flandro.

In the 1973 work, the mass influx was implicitly taken to represent flow of combustion products from burning solid propellant. That was certainly what the author had in mind. But the quantity m'_{sg} may of course represent flow normal to the lateral boundary due to any cause. For example, in Section 6 of Culick (1973) and here in Annex C, the fluctuation $m' = \bar{\rho}v'$ represents changes associated with the acoustic boundary layer. The time-averaged value \bar{m}' is then zero. For the linear behavior we are dealing with, we may write m'_{sg} as a superposition of various possible contributions. It is sufficient for our purpose to take m'_{sg} as the sum of the fluctuation m'_{sc} due to unsteady combustion; and the unsteadiness m'_{PU} produced by the flow:

$$m'_{sg} = m'_{sc} + m'_{PU} \quad (6.156)$$

Thus for harmonic variations in time, (6.154) becomes a sum,

$$\tilde{\alpha}_{sp} = \alpha_{sc} + \alpha_{PU} = \frac{\gamma}{2E_\ell^2} \int_0^L \psi_\ell \int \left(\frac{\hat{m}_{sc}^{(r)}}{\bar{\rho}} + \frac{\Delta \hat{T}_s^{(r)}}{\bar{\rho} \bar{T}} \bar{m}_{sg} \right) dqdx + \frac{\gamma}{2E_\ell^2} \int_0^L \psi_\ell \int \frac{\hat{m}_{PU}^{(r)}}{\bar{\rho}} dqdx \quad (6.157)$$

In the first form, $\hat{m}_{sc}^{(r)}$ may be replaced, for example, by its formula obtained after introducing the admittance or response function defined in Section 6.7.2. Together, the flow-turning contribution, (6.155), and the second term of (6.157), which is the one-dimensional form of the ‘pumping’ process, form the acoustic interaction at a surface,

$$\alpha_A = \alpha_{FT} + \alpha_{PU} = -\frac{\gamma}{2E_\ell^2} \int_0^L \left[\frac{1}{k_\ell^2} \left(\frac{d\psi_\ell}{dx} \right)^2 \right] \int \bar{m}_{sg} dqdx + \frac{\gamma}{2E_\ell^2} \int_0^L \psi_\ell \int \frac{\hat{m}_{PU}^{(r)}}{\bar{\rho}} dqdx \quad (6.158)$$

This result is the one-dimensional counterpart of (49) in Flandro (1995)b, an identification we indicate here without decoding the various definitions of dimensionless quantities²⁶:

$$\text{FLOW-TURNING} \quad -\frac{\gamma}{2E_\ell^2} \int_0^L \left[\frac{1}{k_\ell^2} \left(\frac{d\psi_\ell}{dx} \right)^2 \right] \int \bar{m}_{sg} dqdx \quad \longleftrightarrow \quad +\frac{1}{2E_m^2} \iint \frac{M_b}{k_m} \tilde{\mathbf{u}}^{(i)} \cdot \nabla p'_m dS_b \quad (6.159)$$

$$\text{PUMPING} \quad \frac{\gamma}{2E_\ell^2} \int_0^L \psi_\ell \int \frac{\hat{m}_{PU}}{\bar{\rho}} dqdx \quad \longleftrightarrow \quad -\frac{1}{2E_m^2} \iint \hat{\mathbf{n}} \cdot \tilde{\mathbf{u}}^{(r)} p'_m dS_b \quad (6.160)$$

As an aid to recognizing that the correspondence noted is indeed true, four remarks are helpful:

- (i) By Flandro’s definition, p'_m does not contain any time dependence.
- (ii) In the right-hand side of (6.159) specialized to one dimension, $\tilde{\mathbf{u}}^{(i)}$ and $\nabla p'_m$ both become proportional to $\frac{d\psi_\ell}{dx}$.
- (iii) The mass flux $\bar{m}_{sg} = \bar{\rho} \bar{u}_{sg} = \bar{\rho} \bar{a} \frac{\bar{u}_{sg}}{\bar{a}} = \bar{\rho} \bar{a} \bar{M}_{sg}$, and \bar{M}_{sg} is the same as M_b , the Mach number of the average flow departing the surface.
- (iv) For the correspondence (6.160), we note that $p'_m \sim \psi_\ell$ and $\hat{\mathbf{n}} \cdot \tilde{\mathbf{u}}^{(r)} \sim \frac{\hat{m}_{PU}}{\bar{\rho}}$. To make equality hold in (6.160), closer attention must be paid to the details.

²⁴An example was treated in Section 6 of Culick’s 1973 paper, but the generality of the process was not recognized; see Annex C.

²⁵It is referred to as “surface pumping” here, denoted $(\)_{sp}$ to distinguish it from subscript $(\)_p$ often used to identify contributions from particulate material.

²⁶Note that $(\)$ denotes the rotational part of velocity, which cannot be distinguished for one-dimensional flow.

Verifying the exact correspondence, which is only implied in (6.159) and (6.160), is not germane here. (See the following section.) The important point is that the one-dimensional approximation does in fact contain both ‘flow-turning’ and ‘pumping’. The physical interpretation of flow-turning, always a mechanism of energy loss for flow inward, has already been described with reference to Figure 6.16. Annex C explains the pumping process which, the preceding remarks show, must occur whether flow issues from the surface, or the surface is impermeable.

Much attention has been given these two processes because they can bring significant contributions to the rate of change of acoustic energy in a combustion chamber. Incorporating the form of the $*$ term in (6.153), written according to this discussion, we have

$$\begin{aligned}
 \alpha = & -\frac{1}{2E_\ell^2} \left[\left(\gamma \frac{\hat{u}^{(r)}}{\hat{\eta}_\ell} + \bar{u}\psi_\ell \right) \psi_\ell S_c \right]_0^L + \frac{\gamma}{2E_\ell^2} \int_0^L \psi_\ell \int \left(\frac{\hat{m}_{sc}^{(r)}}{\bar{\rho}} + \frac{\Delta \hat{T}_s^{(r)}}{\bar{\rho} \bar{T}} \bar{m}_{sg} \right) dq dx \\
 & - \frac{\gamma}{2E_\ell^2} \int_0^L \left[\frac{1}{k_\ell^2} \left(\frac{d\psi_\ell}{dx} \right)^2 \right] \int \bar{m}_{sg} dq dx + \frac{\gamma}{2E_\ell^2} \int_0^L \psi_\ell \int \frac{\hat{m}_{PU}^{(r)}}{\bar{\rho}} dq dx \\
 & + \frac{\gamma - 1}{2E_\ell^2} \int_0^L \frac{\hat{Q}_1^{(r)}}{\hat{\eta}_\ell} \psi_\ell S_c dx + \frac{1}{2E_\ell^2} \int_0^L \psi_\ell \int (\gamma R \Delta \bar{T}_s) \hat{m}_{sg}^{(r)} dq dx
 \end{aligned} \tag{6.161}$$

The terms in the first line contain the principal sources of driving due to combustion at the end of the chamber and on the lateral boundary; and attenuation due to the exhaust nozzle. Flow-turning and pumping are represented by the next two terms. The last line contains the effects of volumetric heat addition and the term representing the effect of unsteady mass addition when the temperature difference $\Delta \bar{T}_s = \bar{T}_s - \bar{T}$ is non-zero.

Flandro (1995)a has given an example showing clearly the effects of flow-turning and pumping in data taken by Harris (1994) for unstable oscillations in the laboratory motors sketched in Figure 6.17. Figure 6.18 shows the result reported by Flandro. The dashed line is the locus representing exact agreement between predicted and measured values of the growth rate. Flandro carried out calculations according to the Standard Stability Program, SSP (Nickerson *et al.* 1983) which did not contain the pumping term; and SSP with the pumping term added, giving points labeled “SSP with Vorticity.” These results seem clearly to show that the pumping term is a positive (‘driving’) contribution improving the agreement between the experimental results and theoretical values. The latter were computed with $\hat{Q}_1^{(r)} = \Delta \bar{T}_s = 0$ and assumed values for the propellant response.

The test program conducted by Harris (1994) produced very useful data carefully reduced. Results for the decay rates shown in Figure 6.18 were obtained by measurements of the waves generated by pulses having amplitudes approximately 1% of the chamber pressure. In the reference cited, results are given for two grain diameters; three grain lengths; four grain configurations; three HTPB/AP propellants; and three chamber pressures. Figure 6.19 shows the decay of the fundamental mode in one test, the raw signal having been processed by a bandpass filter. In this case, the motor had a cylindrical grain, 2.55 inch diameter and 30.6 inches long. The data reported by Harris cover fairly broad conditions and can probably be used for wider checks of theoretical results than carried out to date.

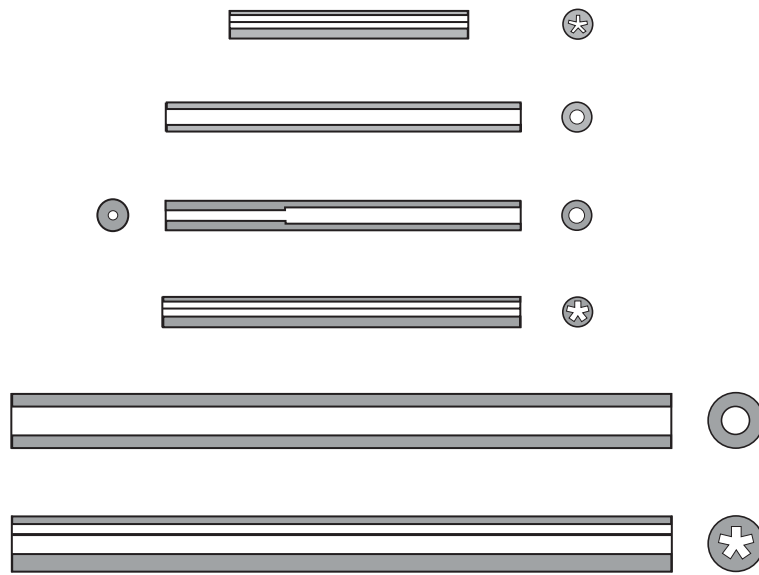


FIGURE 6.17. Grains used in laboratory motors for which data were taken for unstable oscillations (Harris 1994).

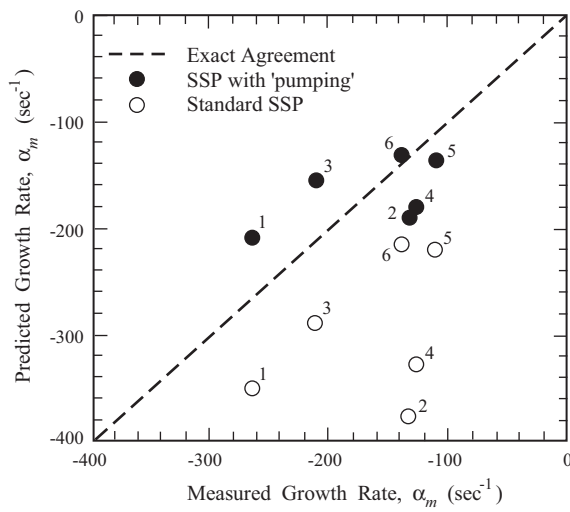


FIGURE 6.18. A comparison of data taken with the motors shown in Figure 6.17 with predictions according to (6.161) with $Q_1 = \Delta \bar{T}_s = \Delta \hat{T}_s^{(r)} = 0$. Accounting for the 'pumping' process gives closer agreement between theory and experiment (Flandro 1995b).

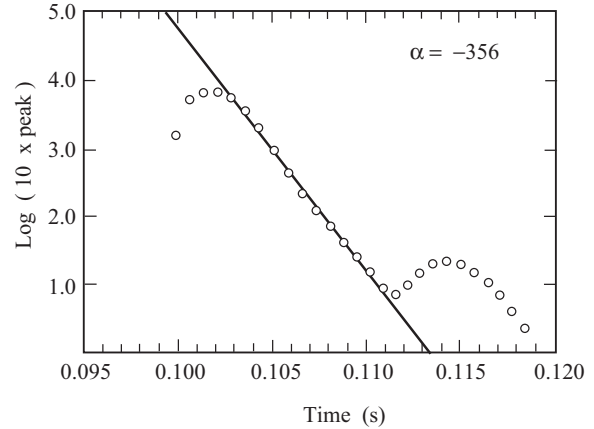


FIGURE 6.19. Calculation of the decay of the fundamental mode following a pulse (Harris 1994).

6.9.3. Stability of a Simple *T*-Burner. Since its invention, the *T*-burner has been widely used a device for measuring the dynamics of a burning solid propellant. For a number of reasons, largely associated with experimental difficulties, it has never fulfilled its great promise. Yet despite the appearance of several other promising methods (see Section 2.2.3), the *T*-burner remains generally the primary means considered for determining—at least qualitatively—the unsteady behavior of a new propellant. Another method may ultimately prove to be superior for a particular application, but first understanding the *T*-burner, how it works, and its practical deficiencies is usually the proper strategy to follow.

Two documents, “the *T*-Burner Manual,” CPIA Publication 191 (1969) and “*T*-Burner Testing of Metallized Solid Propellants,” Air Force Rocket Propulsion Laboratory Report AFRPL-TR-74-28, cover virtually all practices existing in the 1970s. Both volumes incorporated the experiences and contributions of all practitioners in the U.S. Two decades later, extended test programs involving groups in the U.S., France, Canada, and Australia collaborated in test programs based primarily on the “Pulsed *T*-burner,” to refine the methods mainly for treating metallized propellants (Blomshield *et al.* 1991, 1992 and 1997).

In this section, we reproduce the simplest analysis of the *T*-burner, including comparison with early test data, to show some of the difficulties the method presents (Beckstead and Culick, 1971). Unresolved problems still remain. If we ignore the possibility that combustion produces particles in the flow, and we assume that combustion occurs only on the surfaces of discs having the diameter of the tube,²⁷ the square of the wavenumber of longitudinal oscillations is

$$k^2 = k_\ell^2 - 4i \frac{k_\ell}{L} (A_b + \bar{M}_b) + \alpha_\alpha \left(\frac{k_\ell}{\bar{a}} \right) \quad (6.162)$$

where α_α is the decay constant representing all losses in the system during a period of steady oscillations.

With $k^2 = (\omega - i\alpha)^2/\bar{a}^2 \approx (\omega/\bar{a})^2 - i(2\alpha\omega)/\bar{a}^2 \approx (\omega/\bar{a})^2 - i(2\alpha\omega_\ell/\bar{a}^2) \approx (\omega/\bar{a})^2 - i(2\alpha\ell\pi\bar{a}/L)$ and $k_\ell = \ell\pi/L$,

$$\left(\frac{\omega}{\bar{a}} \right)^2 - i(2\alpha\ell\pi) \frac{1}{L\bar{a}} = \left(\frac{\ell\pi}{L} \right)^2 - i \frac{4\ell\pi}{L^2} (A_b + \bar{M}_b) + \alpha_\alpha \left(\frac{k_\ell}{\bar{a}} \right)$$

The real and imaginary parts are

$$\left(\frac{\omega L}{\bar{a}} \right)^2 = (\ell\pi)^2 + 4(\ell\pi)A_b^{(i)} = (\ell\pi)^2 + 4\ell\pi\gamma\bar{M}_b R_b^{(i)} \quad (6.163)$$

$$\frac{\alpha L}{\bar{a}} = 2(A_b^{(r)} + \bar{M}_b) - \alpha_d \frac{L}{\bar{a}} = 2(\gamma\bar{M}_b R_b^{(r)}) - \alpha_d \frac{L}{\bar{a}} \quad (6.164)$$

The admittance function can be replaced by the response function with the definitions given in Section 6.7.2,

$$A_b = \gamma \frac{\bar{p}}{\bar{a}} \frac{\bar{u}}{p'} \left(\frac{m'}{\bar{m}} - \frac{p'}{\bar{p}} \right) = \gamma \bar{M}_b \left(\frac{m'/\bar{m}}{p'/\bar{p}} - \frac{p'/\bar{p}}{p'/\bar{p}} \right) = \gamma \bar{M}_b R_b - \bar{M}_b$$

in which the last equality rests on the approximation that the wave propagation is isentropic. Then (6.163) and (6.164) can be written

$$R_b^{(i)} = \frac{1}{4\gamma\ell\pi\bar{M}_b} \left[\left(\frac{\omega L}{\bar{a}} \right)^2 - (\ell\pi)^2 \right] \quad (6.165)$$

$$R_b^{(r)} = \frac{1}{2\gamma\bar{M}_b} \frac{(\alpha + \alpha_d)L}{\bar{a}} \quad (6.166)$$

²⁷Extension of the analysis to other grain configurations can be accomplished, but attention must be paid to the form of the average flowfield and to the effects of edges of the grains.

According to (6.165) and as observed experimentally, the frequency of oscillation is close to the classical longitudinal value, almost always the fundamental mode ($\ell = 1$), so

$$\left(\frac{\omega L}{\bar{a}}\right)^2 - (\ell\pi)^2 = \left(\frac{\omega L}{\bar{a}} + \ell\pi\right)\left(\frac{\omega L}{\bar{a}} - \ell\pi\right) \approx 2\ell\pi\left(\frac{\omega L}{\bar{a}} - \ell\pi\right)$$

and (6.165) becomes

$$R_b^{(i)} = \frac{1}{2\gamma\bar{M}_b} \left(\frac{\omega L}{\bar{a}} - \ell\pi\right) \quad (6.167)$$

Equations (6.166) and (6.167) correspond to (6.25) and (6.26) for an L^* burner. Hence if we assume the result found by Denison and Baum for the response function, we find the solutions (6.126) and (6.127) for the parameters A and B , but with

$$k_1 = \frac{1}{2\gamma\bar{M}_b} \left(\frac{\omega L}{\bar{a}} - \ell\pi\right); \quad k_2 \frac{1}{2\gamma\bar{M}_b} \frac{(\alpha + \alpha_\alpha)L}{\bar{a}} \quad (6.168)a,b$$

It has been common practice to interpret T -burner data using only equation (6.126), justified with the observation that the frequency of the oscillations has very closely the classical value, $\omega \approx \ell\pi\frac{\bar{a}}{L}$ so equation (6.127) can be ignored. Then, for example, if Denison and Baum's formula is used, correlations of experimental results are carried out with the two parameters A and B . In fact, one should use only one. Just as for data taken with an L^* burner, there are two parameters and two equations. If one equation is dropped then, in some sense, so should one parameter! Otherwise, the fit or no-fit to data cannot be interpreted as truth or falsity of Denison and Baum's result.

On the other hand, strictly one has the basis, equations (6.126) and (6.127), for a two-parameter family corresponding to equations (6.25) and (6.26), and Figure 6.8 for the L^* -burner. Assume that the T -burner oscillates in the lowest mode, the fundamental or first harmonic, and let $\zeta = (2\gamma\bar{M}_b)^{-1}$. Then equations (6.126) and (6.127) are

$$\begin{aligned} R_b^{(r)} &= \zeta(\alpha_d\tau_c + \alpha\tau_c) = \zeta\alpha_t\tau_c \\ R_b^{(i)} &= \zeta\left(\frac{\omega L}{\bar{a}} - \pi\right) = \zeta(\omega\tau_c - \pi) \end{aligned} \quad (6.169)a,b$$

Beckstead and Culick chose to construct the two-parameter A, B family of curves in the $\alpha_t\tau_c, \Omega$ plane rather than the $\omega\tau_c^*, \Omega$ plane used for the L^* burner ($\tau_c^* = L^*c^*/RT$, $\tau_c = L/\bar{a}$). Figure 6.20 shows the result they found, with data taken for A-13 propellant. This interpretation of the dynamical behavior is clearly unsuccessful. The data for a given value of chamber pressure should lie on a vertical line; that is they should be independent of frequency.

The authors tried—unsuccessfully—to rationalize the result. It seems unlikely that the data is so wildly poor as the chart may suggest. The analysis is straightforward and transparent; the viewpoint taken seems to be correct, and unlikely to be deeply flawed in any event. Probably the source of the evident inaccuracy is the special form of the response function. While the Denison and Baum formula captures an important part of the behavior, the two-parameter formula is apparently an over-simplification. Several modifications are discussed briefly in Section 2.2. There seem to be no subsequent efforts to use data in the manner suggested by Beckstead and Culick. However, the approach taken in the present section, and in Section 6.2 with results produced by low frequency burners still appears to be worthwhile.

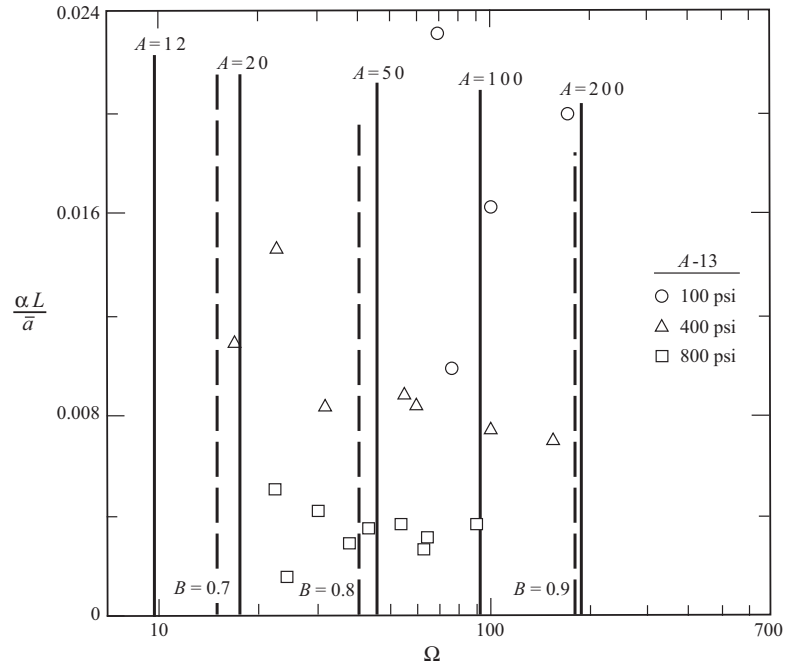


FIGURE 6.20. A T -burner chart for determining the parameters A and B ; data are shown for the propellant A-13 (Beckstead and Culick 1971).

6.10. Combined Three-Dimensional and One-Dimensional Results

There remains a significant gap in the formal treatment of stability. In Section 6.7 we have deduced the formula (6.90) for the wavenumber and (6.94) for the growth or decay rate, of three-dimensional disturbances. Separately in Section 6.9 we have found the approximations (6.151) and (6.161) to the corresponding quantities for one-dimensional motions. For easy comparison, we repeat the results here, preceded by their origins. The reasoning begins with the precise correspondence between (6.90) and (6.138):

3-D Equation (6.90)

$$k^2 - k_n^2 = -i \frac{k_n}{\bar{a} E_n^2} \left\{ \oint \left[\gamma \frac{\hat{\mathbf{u}}}{\eta_n} \cdot \hat{\mathbf{n}} + \bar{\mathbf{u}} \cdot \hat{\mathbf{n}} \psi_n \right] \psi_n dS + (\gamma - 1) \int \psi_n^2 \nabla \cdot \bar{\mathbf{u}} dV \right\} - \frac{1}{\bar{p} E_n^2} \int \left[\hat{\mathcal{F}} \cdot \nabla \psi_n + i \frac{k_n}{\bar{a}} \frac{\hat{\mathcal{P}}}{\hat{\eta}_n} \psi_n \right] dV \quad (6.170)$$

1-D Equation (6.138)

$$k^2 - k_\ell^2 = -i \frac{k_\ell}{\bar{a} E_\ell^2} \left\{ \left[\left(\gamma \frac{\hat{u}}{\eta_\ell} + \bar{u} \psi_\ell \right) \psi_\ell S_c \right]_0^L + (\gamma - 1) \int_0^L \psi_\ell^2 \left[\frac{1}{S_c} \frac{d}{dx} (S_c \bar{u}) \right] S_c dx \right\} - \frac{1}{\bar{p} E_\ell^2} \int_0^L \left[\left(\hat{\mathcal{F}}_1 + \hat{\mathcal{F}}_{1s} \right) + i \frac{k_\ell}{\bar{a}} \left(\hat{\mathcal{P}}_1 + \hat{\mathcal{P}}_{1s} \right) \psi_\ell \right] S_c dx \quad (6.171)$$

As the development in Section 6.9 showed, the term containing $\hat{\mathcal{F}}_{1s}$ leads to the formula for ‘flow-turning’, which is therefore a consequence of momentum transfer between the flow entering at the boundary and the flow in the chamber. Then (6.138) becomes (6.143); if we retain the possibility for momentum addition

within the volume, $\hat{\mathcal{F}}_1$ is non-zero, and (6.138) is

$$\begin{aligned}
 k^2 - k_\ell^2 = & -i \frac{k_\ell}{\bar{a}E_\ell^2} \left\{ \left[\left(\gamma \frac{\hat{u}}{\hat{\eta}_\ell} + \bar{u}\psi_\ell \right) \psi_\ell S_c \right]_0^L + (\gamma - 1) \int_0^L \psi_\ell^2 \left[\frac{1}{S_c} \frac{d}{dx} (S_c \bar{u}) \right] S_c dx \right\} \\
 & - \frac{1}{\bar{p}E_\ell^2} \int \frac{\hat{\mathcal{F}}_1}{\hat{\eta}_\ell} \frac{d\psi_\ell}{dx} S_c dx - i \frac{k_\ell}{\bar{\rho}\bar{a}E_\ell^2} \int_0^L \left[\frac{1}{k_\ell^2} \left(\frac{d\psi_\ell}{dx} \right)^2 \right] \int \bar{m}_{sg} dq dx + i \frac{k_\ell}{\bar{a}} \frac{1}{\bar{p}E_\ell^2} \int_0^L \left(\frac{\hat{\mathcal{P}}_1 + \hat{\mathcal{P}}_{1s}}{\hat{\eta}_\ell} \right) \psi_\ell S_c dx
 \end{aligned} \tag{6.172}$$

This is (6.145) with the addition of the integral containing $\hat{\mathcal{F}}_1$ and (6.144) used in the first integral.

The ‘pumping’ term in k^2 arises from $\hat{\mathcal{P}}_{1s}$ while $\hat{\mathcal{P}}_1$ produced the term containing heat release, equation (6.146). If we do not write $\hat{\mathcal{P}}_1$ as the heat release, and ignore the cancellation noted just before (6.151), equation (6.172) is

$$\begin{aligned}
 k^2 = & k_\ell^2 - i \frac{k_\ell}{\bar{a}E_\ell^2} \left[\left(\gamma \frac{\hat{u}}{\hat{\eta}_\ell} + \bar{u}\psi_\ell \right) \psi_\ell S_c \right]_0^L - \frac{ik_\ell}{\bar{a}E_\ell^2} (\gamma - 1) \int_0^L \psi_\ell^2 \left[\frac{1}{S_c} \frac{d}{dx} (S_c \bar{u}) \right] S_c dx \\
 & - \frac{1}{\bar{p}E_\ell^2} \int_0^L \frac{\hat{\mathcal{F}}_1}{\hat{\eta}_\ell} \frac{d\psi_\ell}{dx} S_c dx + i \frac{k_\ell}{\bar{a}} \frac{1}{\bar{p}E_\ell^2} \int_0^L \frac{\hat{\mathcal{P}}_1}{\hat{\eta}_\ell} \psi_\ell S_c dx - i \frac{k_\ell}{\bar{\rho}\bar{a}E_\ell^2} \int_0^L \left[\frac{1}{k_\ell^2} \left(\frac{d\psi_\ell}{dx} \right)^2 \right] \int \bar{m}_{sg} dq dx \\
 & + i \frac{k_\ell}{\bar{a}} \frac{1}{\bar{p}E_\ell^2} \int_0^L \psi_\ell \int \left[(\bar{a}^2 + \gamma R \Delta \bar{T}_s) \hat{m}_{sg} + \gamma R (\hat{T} + \Delta \hat{T}_s) \bar{m}_{sg} \right] dq dx
 \end{aligned} \tag{6.173}$$

The symbols above the terms in this equation are only for identification according to the following discussion.

With the definition (6.144) for the mass addition in steady flow, the first integral corresponds to the integral $\int \psi_n^2 \nabla \cdot \hat{\mathbf{u}} dV$ and there is precise correspondence between all of (6.170) and (6.173) without the last two integrals. Those two integrals represent, within the approximations used here, the entire difference between the three-dimensional formulation and the one-dimensional ‘approximation.’

‘Approximation’ is set off by quotes because it is a little surprising that the one-dimensional ‘approximation’ possesses *more* information than the three-dimensional formulation. The term in (6.173) containing $\frac{1}{k_\ell^2} \left(\frac{d\psi_\ell}{dx} \right)^2$ is pure imaginary and gives the flow-turning contribution to α ; hence define

$$k_{FT}^2 = -i \frac{k_\ell}{\bar{\rho}\bar{a}E_\ell^2} \int_0^L \left[\frac{1}{k_\ell^2} \left(\frac{d\psi_\ell}{dx} \right)^2 \right] \int \bar{m}_{gs} dq dx \tag{6.174}$$

Write

$$\frac{1}{S_c} \frac{d}{dx} (S_c \bar{u}) = (\nabla \cdot \bar{\mathbf{u}})_1$$

as the one-dimensional divergence of \bar{u} ; the first integral in (6.173) and the integral containing $\gamma R \hat{T}$ in the last line are²⁸

$$k_{is}^2 = -i \frac{k_\ell}{\bar{a}E_\ell^2} (\gamma - 1) \int_0^L \psi_\ell^2 (\nabla \cdot \bar{\mathbf{u}})_1 S_c dx + i \frac{k_\ell}{\bar{a}} \frac{1}{\bar{p}E_\ell^2} \int_0^L \psi_\ell (\gamma R \hat{T}) \bar{m}_{sg} dq dx \tag{6.175}$$

²⁸The flow through the surface corresponding to the second term in (6.175) is accounted for in the boundary conditions in three-dimensions.

The calculation immediately preceding (6.151) showed that these two terms together vanish if we assume that \hat{T} is a consequence of an isentropic motion. This is the one-dimensional counterpart of the statement that $\nabla \cdot \mathbf{u} = 0$ in three dimensions, eliminating the first volume integral in (6.170). There is no surface contribution corresponding to the second term of (6.175) in three dimensions. We therefore ignore these terms in the following discussion, $k_{is}^2 = 0$.

The terms dependent upon $\Delta\bar{T}_s$ and $\Delta\hat{T}_s$ will have values dependent on the thermodynamics of the flow through the surface. Flandro and Majdalani have not considered such processes. Write

$$k_{\Delta T}^2 = i \frac{k_\ell}{\bar{a}} \frac{1}{\bar{p}E_\ell^2} \int_0^L \psi_\ell \int \left[(\gamma R \Delta\bar{T}_s) \bar{m}_{sg} + (\gamma R \Delta\hat{T}_s) \bar{m}_{sg} \right] q dx \quad (6.176)$$

As we defined with (6.156) the sum of fluctuations m'_{sc} due unsteady combustion and m'_{PU} produced by unsteady flow, so $m'_{sg} = m'_{sc} + m'_{PU}$, we can write the remaining term in (6.173) as

$$k_{PU}^2 + k_{sc}^2 = i \frac{k_\ell}{\bar{a}} \frac{1}{\bar{p}E_\ell^2} \int_0^L \psi_\ell \int \bar{a}^2 \hat{m}_{sg} dq dx = i \frac{k_\ell}{\bar{a}} \frac{1}{\bar{p}E_\ell^2} \int_0^L \psi_\ell \int \bar{a}^2 \hat{m}_{PU} dq dx + i \frac{k_\ell}{\bar{a}} \frac{1}{\bar{p}E_\ell^2} \int_0^L \psi_\ell \int \bar{a}^2 \hat{m}_{sc} dq dx \quad (6.177)$$

Finally, let k_{3D}^2 denote those terms in (6.173) which have precise correspondences in the perturbed three-dimensional problem,

$$k_{3D}^2 = -i \frac{k_\ell}{\bar{a}E_\ell^2} \left[\left(\gamma \frac{\bar{u}}{\hat{\eta}_\ell} + \bar{u} \psi_\ell \right) \psi_\ell S_c \right]_0^L - \frac{1}{\bar{p}E_\ell^2} \int_0^L \frac{\hat{\mathcal{F}}_1}{\hat{\eta}_\ell} \frac{d\psi_\ell}{dx} S_c dx + i \frac{k_\ell}{\bar{a}} \frac{1}{\bar{p}E_\ell^2} \int_0^L \frac{\hat{\mathcal{P}}_1}{\hat{\eta}_\ell} \psi_\ell S_c dx \quad (6.178)$$

Substituting (6.174), (6.176), (6.177) and (6.178) into (6.173) with the combination (6.175) dropped, gives

$$k^2 = k_\ell^2 + k_{3D}^2 + k_{FT}^2 + k_{PU}^2 + k_{sc}^2 + k_{\Delta T}^2 \quad (6.179)$$

Equation (6.179) is the most general form obtained to date for the wave number of motions represented by the one-dimensional approximation. By suitable interpretation, according to comparison of (6.170) and (6.172), of the first two terms on the right-hand side, (6.179) also contains the purely three-dimensional formula for which the last four terms on the right-hand side are absent.

Then (6.179) evidently serves as the basis for constructing a formula for three-dimensional wavenumber including flow-turning, pumping, and the unsteady processes generating the wavenumbers k_{sc}^2 and $k_{\Delta T}^2$. The recipe implies replacing k_ℓ^2 by k_n^2 ; calculating k_{3D}^2 with the right-hand side of (6.170); and retaining k_{FT}^2 , k_{PU}^2 , k_{sc}^2 and $k_{\Delta T}^2$ given by their definitions quoted above as surface integrals:

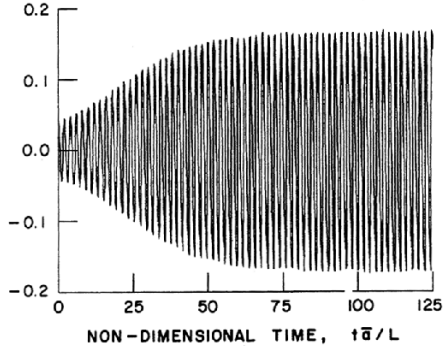
$$k^2 = k_n^2 + k_{3D}^2 + k_{FT}^2 + k_{PU}^2 + k_{sc}^2 + k_{\Delta T}^2 \quad (6.180)$$

No results are available to confirm or deny the truth of this conjecture.

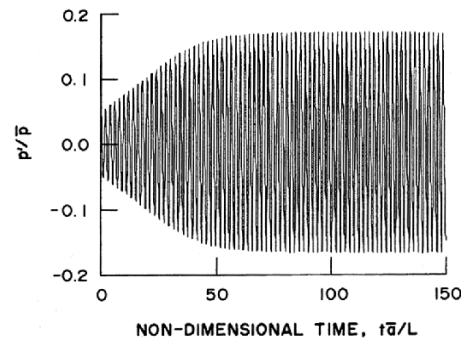
6.11. An Example of Linear Stability for a Solid Rocket

Results for a simple example, a longitudinal mode for a solid propellant rocket, are shown in Figures 6.21–6.23 (Culick and Yang 1992). It is a common problem encountered particularly in the development of tactical motors. The calculations were carried out with linear and nonlinear gasdynamics. The example was first covered by Culick and Yang (1992, pp. 769–774).

Linear contributions from the exhaust nozzle, small particles (inert Al_2O_3) coupling with the mean flow, and unsteady burning were included. The effects of ‘flow-turning’ and ‘pumping’ were not considered. At



(a) approximate analysis



(b) numerical simulation

FIGURE 6.21. Growth of unstable motions according to (a) the approximate analysis; and (b) a numerical simulation of the same problem (Culick and Yang 1992).

the time, the authors did not realize that those contributions in fact sum to zero for this special case, a result that explains the quite good agreement between the approximate and numerical results. That the difference between the two calculations was not much greater was a puzzling conclusion at the time, but now constitutes a marvelous vindication of the one-dimensional approximation. Remarks concerning the effects of ‘flow-turning’ in calculations for a ‘complete’ problem, Culick and Yang (1992), must be ignored. See Section 6.12.

The effects of the exhaust nozzle are represented by the first bracketed terms in (6.161),

$$\begin{aligned}\alpha_{\text{nozzle}} \equiv \alpha_N &= -\frac{1}{2\omega_\ell E_\ell^2} \left(\frac{\bar{\rho} \bar{a}^2}{\gamma \bar{p}} \right) (\bar{a} k_\ell) \left[\left(\frac{\hat{u}^{(r)}}{\gamma \hat{\eta}_\ell} \psi_\ell + \bar{u} \psi_\ell^2 \right) S_c \right]_{z=L} \\ &= -\frac{1}{2E_\ell^2} \left[\left(\gamma \frac{\hat{u}^{(r)}}{\hat{\eta}_\ell} \psi_\ell + \bar{u} \psi_\ell^2 \right) S_c \right]_{z=L}\end{aligned}\quad (6.181)$$

in which $E_\ell^2 = \int_0^L \psi_\ell^2 S_c dz = S_c L / 2$. At $z = L$, $\psi_\ell^2 = \cos^2(k_\ell L) = 1$ for $k_\ell = \ell\pi/L$ and with (6.181) written for $z = L$, so $-(A_b + \bar{M}_b) \rightarrow (A_N + \bar{M}_N)$,

$$\alpha_N = -\frac{\bar{a}}{L} \left(A_N^{(r)} + \bar{M}_N \right) \quad (6.182)$$

For the approximation (6.204) quoted later, valid if the nozzle is ‘short’,

$$A_N^{(r)} + \bar{M}_N = \bar{M}_N \left(\frac{\gamma - 1}{2} + 1 \right) = \bar{M}_N \frac{\gamma + 1}{2} \quad (6.183)$$

and

$$\alpha_N = -\frac{\gamma + 1}{2} \frac{\bar{a}}{L} \bar{M}_N \quad (6.184)$$

Note that, according to the derivations of (6.94) and (6.181), the term \bar{M}_N in (6.182) represents part of the net effects of the acoustics/mean flow interactions.

We will find in Section 6.14.3 that under quite broad realistic conditions in solid rockets, the presence of Al_2O_3 as liquid drops in motors, can be the source of substantial attenuation of oscillations. If all the

particles are spherical and have the same diameter, the attenuation constant is given by (6.152)a below, with X_1 and X_2 represented by the formulas (6.211)a,b:

$$\alpha_\ell = -\frac{1}{2} \frac{C_m}{1+C_m} \left[X_1 + (\gamma - 1) \frac{C}{C_p} X_2 \right] \quad (6.185)$$

where subscript () _{ℓ} stands for 'liquid.'

Least well-known are the contributions from unsteady combustion. For this example, the simplest result was used, the formula (6.103) for Denison and Baum's response function. We use the relation (6.102) and assume $\Delta\hat{T}_s = 0$. The corresponding formula for the contribution of surface combustion to the growth constant is

$$\alpha_e = \frac{\bar{v}_b}{r_c} R_p^{(r)} \quad (6.186)$$

Table 6.1 is a list of the property values required for the calculations of the instability. Calculations were done both with numerical solution to the one-dimensional equations (the method of Baum and Levine 1982) and using the results of the approximate analysis. Figures 6.21–6.23. Table 6.2 contains the linear growth constants and frequency shifts, $\omega - \omega_n = -\theta$, calculated with the results of the approximate analysis. Table 6.3 contains the total values of the growth constants and frequency shifts.

TABLE 6.1. Values of the Geometrical, Combustion and Physical Properties (used in the example discussed in Section 6.7.1).

Geometrical properties:	
length	$L = 0.5969 \text{ m}$
radius of cylindrical port	$r_c = 0.0253 \text{ m}$
throat radius	$r_t = 0.00936 \text{ m}$
Combustion properties:	
mean pressure	$\bar{p} = 1.06 \times 10^7 \text{ Pa}$
linear burning rate	$\bar{r}_b = 0.0078[\bar{p}/(3.0 \times 10^6)]^{0.3} = 0.01145 \text{ m/s}$
parameters in the combustion response	$A = 6.0$
chamber temperature	$\bar{T} = 3539 \text{ K}$
mass particles/mass gas	$C_m = 0.36$
particle diameter	$\sigma = 2 \times 10^{-6} \text{ m}$
Physical properties:	
Prandtl number	$Pr = 0.8$
thermal diffusivity of propellant	$\kappa_p = 1.0 \times 10^{-7} \text{ m}^2/\text{s}$
specific heat of gas	$C_p = 2020 \text{ J/kg K}$
specific heat of condensed material	$C = 0.68C_p$
viscosity	$\mu = 0.8834 \times 10^{-4}(T_c/3485)^{0.66} = 8.925 \times 10^{-5} \text{ kg/m-s}$
particle density	$\rho_s = 4.0 \text{ g/cm}^3 = 4 \times 10^3 \text{ kg/m}^3$
propellant density	$\rho_p = 1,766 \text{ kg/m}^3$
gas density	$\bar{\rho}_g = 7.97 \text{ kg/m}^3$
γ (gas only)	$\gamma = 1.23$
$\bar{\gamma}$ (mixture)	$\bar{\gamma} = [\gamma(1 + C_m C/C_p)]/(1 + C_m \gamma C/C_p) = 1.18$
gas constant	$R = (\gamma - 1)C_p/\gamma = 377.72 \text{ J/kg K}$
speed of sound in gas/ particle mixture	$\bar{a} = \sqrt{(\bar{\gamma}RT_c)/(1 + C_m)} = 1075 \text{ m/s}$
speed of combustion products at the burning surface	$\bar{v}_b = (\rho_p/\rho)\bar{r}_b = 1.86 \text{ m/s}$
Mach number at the burning surface	$\bar{M}_b = 0.00173$

TABLE 6.2. Linear Growth Constants and Frequency Shifts.

Mode	α_c	θ_c	α_N	θ_N	α_P	θ_P
1	288.1	32.2	-160.1	0	-46.6	2.6
2	28.5	80.5	-160.1	0	-184.8	20.5
3	16.7	48.5	-160.1	0	-417.7	69.1
4	13.6	36.0	-160.1	0	-727.4	160.5
5	12.0	29.3	-160.1	0	-1107.5	305.5

TABLE 6.3. Total Values of the Linear Growth Constants and Frequency Shifts.

Mode	α_n	θ_n
1	81.4	34.8
2	-316.4	100.9
3	-561.1	117.6
4	-873.9	196.6
5	-1255.6	334.8

TABLE 6.4. Frequencies and Amplitudes of Acoustic Pressures.

Mode	Frequency, Hz					Amplitude, $ p'/\bar{p} $				
	1	2	3	4	5	1	2	3	4	5
Numerical	926	1824	2698	3595	4491	0.151	0.042	0.0234	0.0203	—
Approximate	895	1785	2683	3571	4449	0.151	0.0478	0.0280	0.0153	0.0188

For direct comparison of the numerical and approximate results, Table 6.4 contains the values of the frequencies and amplitudes computed for the first two modes. A few cycles of the limiting waveforms are plotted in Figure 6.21 showing results for both the approximate and numerical computations: Figure 6.22 is the spectrum for the numerical results.

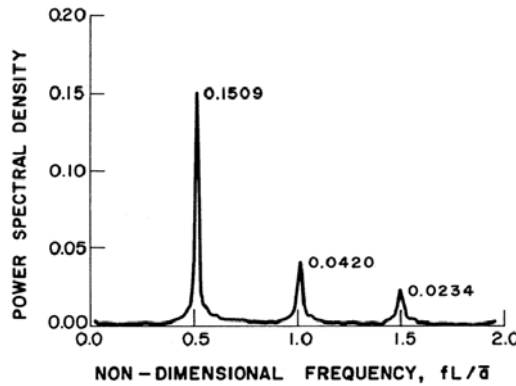


FIGURE 6.22. Spectrum for the calculated waveform shown in Figure 6.21(b) (Culick and Yang 1992).

The approximate analysis produces quite accurate values of the frequencies (within 3%) and the approximate total waveform is reasonably close to the “exact” result except for some rippling due to the absence of higher frequencies. Even so, the amplitudes of the individual modes found with the approximate analysis agree well with those computed with the numerical analysis except for the highest ($n = 5$) mode. The reason for the high value (even larger than that for $n = 4$) is that there is no transfer of energy to higher modes. Because the rate of energy dissipation from the highest mode considered, represented by its attenuation constant, must be such that the total energy loss equals the total rate of energy gain, the amplitude of the highest mode must be such as to satisfy this condition. Even with only two modes accounted for, the frequencies and total waveform are quite well predicted. The frequencies are the same as for the case of five

modes; Figure 6.23 shows the waveforms. However, according to Table 6.4, the approximate amplitudes of the individual modes differ considerably from the exact values. The phases of the two modes in the approximate solution apparently assume values that compensate for the consequences of the inaccurate amplitudes. Figure 6.15a,b

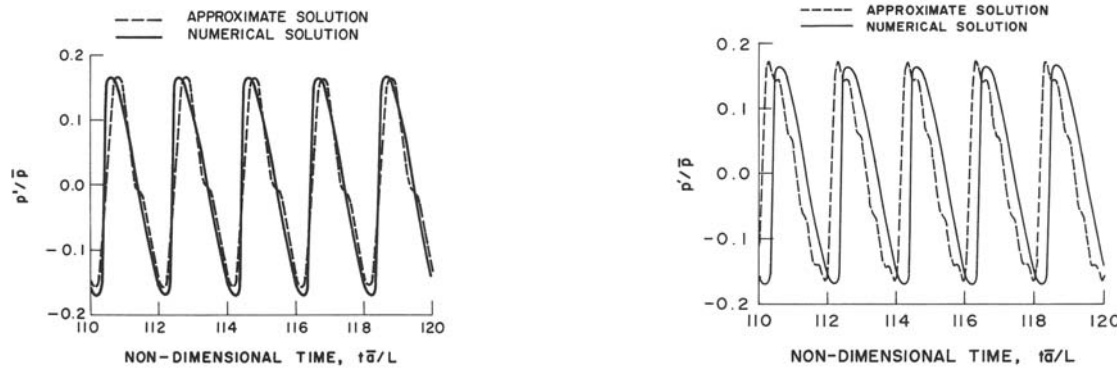


FIGURE 6.23. Effect of truncation in the waveforms (Culick and Yang 1992).

6.12. Vorticity and Stability in Solid Propellant Rockets

Vorticity appears in combustion chambers chiefly on three forms: random motions associated with turbulence; large 'coherent' vortices growing out of unstable shear layers; and waves of vorticity generated by interactions between the acoustic field and a flow entering the chamber through the lateral boundary. In Section 7.6 we regard all random motions together as noise and show how the net pressure may affect the acoustic pressure field. Here we are concerned only with distributed vorticity, either as waves carried by the mean flow or as large vortices.

Probably the first observations of possible consequences of vorticity²⁹ in a combustor are those reported by Boys and Schofield (1942). Some features of recorded pressure histories and of grain erosion caused them to speculate the presence of "... some abnormal flow on oscillation ... as if the gas were swirling with a high velocity." (Quoted by Flandro 1967). Since that time, many examples of scoured lateral boundaries have been reported, both in liquid rockets and in solid rockets, all for laboratory tests or static firings of full-scale motors. Green (1958) reported visual observations of swirling flows in a solid rocket.

By conservation of angular momentum, exhaust of a swirling or vortex flow from a combustor must be accompanied by a roll torque (of the opposite sign) exerted about the axis of symmetry. Substantial roll torques were first observed in flight tests of the Sergeant motor (Flandro 1964). An extreme example occurred in the first flight test of the Scout space probe which failed when the control system was unable to compensate large roll motions (Mayhue 1962).

Swithenbank and Sotter (1963; 1964a,b) were first to attempt a theoretical explanation of the generation of roll torques by adapting an analysis of finite amplitude transverse waves by Maslen and Moore (1956). Partly due to errors in the latter paper, and partly due to some misinterpretations, the results by Swithenbank and Sotter are incomplete. The main idea is that acoustic streaming generated by the transverse waves carries angular momentum causing the roll torque.

²⁹We refer to the effects of streamwise vorticity or vortices. The discussion in Section 6.12.1 and subsequently is concerned primarily with azimuthal vorticity generated by processes associated with nonuniform flow inward at the lateral boundary. The two kinds of vortices are illustrated in Figure 6.24.

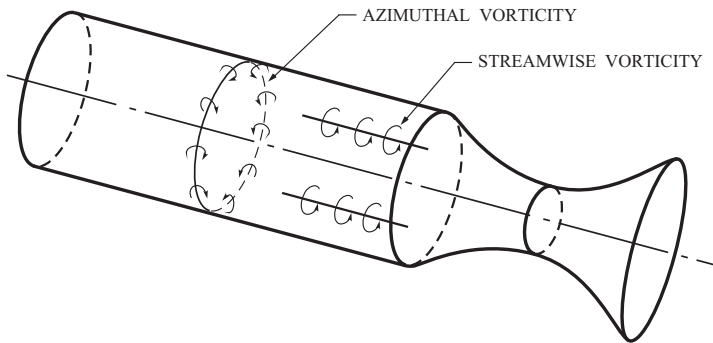


FIGURE 6.24. Stylized rendition of azimuthal and streamwise vortices in a solid propellant rocket chamber.

In a fine piece of work, Flandro (1967) corrected the deficiencies of Swithenbank and Sotter's work and produced what is essentially the correct explanation for the generation of roll torques in solid propellant rockets. That work probably makes unnecessary any further theory of the phenomenon. The details of Flandro's work need not be covered here. Its importance in the present context is that the analysis is the first application of the scheme developed here in Chapters 4 and 5, in which vorticity is explicitly accommodated in a calculation of the acoustic field. The most significant technical point in the analysis is proper satisfaction of the no-slip boundary condition at the boundary. When a tangential or transverse acoustic mode is present, which necessarily has a velocity component parallel to the surface, a second contribution to the velocity is required to cancel the acoustical motion. That second component arises with generation of vorticity convected into the chamber. Eventually, the vorticity combined with a travelling transverse wave mode produces the angular momentum in the flow. The reaction to the loss of that angular momentum appears as a roll torque. Further discussion of the possible flow fields and the connection with acoustic streaming are discussed briefly in Chapter 7.

It's a beautiful model of the problem and successfully explains the observed behavior. Technically, the essential result was making explicit the basic connection between acoustics and vorticity, the vehicle for the connection being the mean flow, and the consequence being generation of angular momentum experienced as a roll torque. The analytical procedure served as a precursor to Flandro's later analysis of waves of vorticity generated in response to the presence of longitudinal acoustic instabilities in solid propellant rockets. (Flandro 1995). That work has several times been misinterpreted and consequently has been unjustifiably and incorrectly criticized.

6.12.1. Generation of Large Vortices; Parietal Vortex Shedding. Oscillations found in large solid rocket motors, developed as boosters for launching spacecraft, have presented problems somewhat different from those discussed in most of this book. The primary examples are the Space Shuttle booster (Mason, Folkman and Behring 1979; Mathes 1980; Blomshield and Mathes 1993); the Titan solid rocket (Alden 1980; Brown *et al.* 1981); and the Ariane 5 MPS P230 (Scippa *et al.* 1994). All these motors have had relatively low-level pressure, and thrust, oscillations at frequencies suggesting that the first longitudinal mode is unstable. Yet estimates based on the ideas developed in Chapters 3 and 4, or similar arguments, led to the conclusion in each case that the longitudinal mode should be unquestionably stable. For example, such a conclusion was reached by Kumar and Culick (1977) before the first test firing of the SRM in the late 1970s. When the motor was fired, vibrations at approximately 15 Hz were detected at levels high enough to cause concern, both in respect to oscillatory accelerations of some structural components and motions of the pilots' cabin. The existing stability analysis could not explain the observation because, as it turned out, a contribution was missing. That missing contribution was due to vortex shedding from inhibitor material exposed at the joints of the segmented motor.

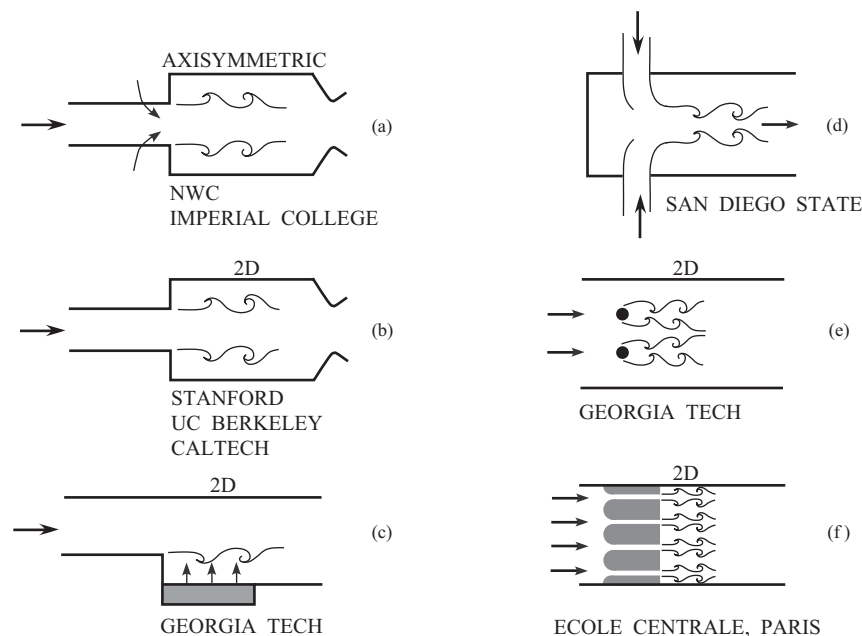


FIGURE 6.25. Some configurations used in observations of vortex shedding and instabilities (adapted from Schadow 2001).

The earlier suggestion by Flandro and Jacobs (1975) that vortex shedding could couple to acoustic modes of the motor was recalled. That prompted the simple laboratory tests by Culick and Magiawala (1979) followed later by the extended work of Nomoto and Culick (1982), and Aaron and Culick (1985). The last contains a simple approximation to the excitation of acoustic waves by the impingement of vortices on an obstruction. Meanwhile the idea was pursued vigorously in the Titan program, with convincing results published by Dunlap and Brown (1981) and Brown *et al.* (1981). At about the same time, Byrne (1981, 1983) suggested vortex shedding in dump combustor configurations as the mechanism for oscillations found in ramjets (Culick 1980; Culick and Rogers 1980). Thus by 1981, vortex shedding had been established as a fundamental mechanism of instabilities in combustion systems.

Subsequently, vortex shedding was found to be even more widespread than previously considered. It was well-established experimentally, especially by the work of Schadow and his colleagues at the Naval Weapons Center, China Lake, to be a potentially significant mechanism for oscillations in laboratory dump combustors; a good summary of the matter was given by Schadow and Gutmark (1992). In his lecture, part of the Short Course “Active Control of Engine Dynamics” held at the von Karman Institute (VKI), Schadow (2001) gave a useful tutorial emphasizing vortex shedding in dump combustors. Figure 6.25 summarizes the main configurations that have been studied; and locations of principal experimental efforts. The Short Course given at the Glenn Research Center (Culick 2001) also includes as Section 9 a summary of the subject, with references. Section 8.6 contains a discussion of vortex shedding and its modification as a means of passive control.

A quite different form of vortex shedding as a driving mechanism for oscillations in a combustor was discovered in series of fine experimental and theoretical works by French investigators motivated by the Ariane 5 problem. Put most succinctly, they found that unlike all previous demonstrations, and (therefore) contrary to general expectations, neither obstacles nor edges are required to generate large vortices in a stream. Lepoglazoff and Vuillot (1996) named the phenomenon “parietal vortex shedding” because the vortices formed in the region close to a wall through which fluid was injected. They discovered the phenomenon experimentally while carrying out a lengthy series of tests devoted broadly to clarifying the coupling between

vortex shedding and acoustic modes. The investigations began in the early 1990s, driven by serious practical considerations. The payload of the Ariane 5 might be reduced (it eventually was) by the mass of devices added to the solid rocket boosters as protection against the oscillatory accelerations. For example, Prévost *et al.* (1996) cited a maximum amplitude of 0.28 bar (14.5 psi) at 20 Hz; the mean chamber pressure is around 50 bar. Oscillations of this magnitude have persisted in the motor and the Ariane 5 has consequently suffered a reduction of payload equal to several hundred pounds.³⁰ Hence the primary goal of the work was evidently elimination of the vortex shedding or the coupling between the vortices and the acoustic modes.

The problem of oscillations produced by the formation of large vortices was apparently encountered quite early in the development of the Ariane 5 (c. 1990 in subscale work and during the first full-scale tests beginning in 1993). It was the subject of serious concern in the early 1990s; the French work was summarized in the informative paper by Vuillot (1995) written just prior to the discovery of parietal vortex shedding, reported by Lupo and Vuillot (1996). A series of tests was carried out in 1/15 scale laboratory motors, named LP3A-E shown in Figure 6.26. The results are reported in several places, but the contribution of Vuillot and Casalis (2002) to the VKI Short Course “Internal Aerodynamics in Solid Rocket Propulsion” (2002) is the best summary.

There was no flow visualization of the hot firings in the LP3 test series. Careful interpretation of the data, and numerical simulation established conclusively that parietal vortex shedding had been shown. Direct confirmation was provided by Avalon *et al.* (2001) using PLIF with acetone. Figure 6.27 reproduces a picture they obtained with the ONERA VECLA³¹ apparatus.

Casalis and coworkers have carried out analyses establishing conclusively the origin of parietal vortex shedding. (Vuillot and Casalis 2002 Part II, and references there to the original work.) As background, recall that vortex shedding from edges or obstacles is initiated by an instability of a shear layer. Parietal vortex shedding occurs because the flow itself is unstable. Figure 6.28 shows some results of numerical simulations for the three cases. The case has been established for the profile in a cylindrical cavity closed at one end having a uniform porous lateral boundary passing a uniform flow (Taylor 1956, Culick 1966b). The analysis shows, as observed, that the vortex shedding begins some distance from the closed end of the cylinder where the profile in question is unstable to small disturbances (Urgutis *et al.* 2000).

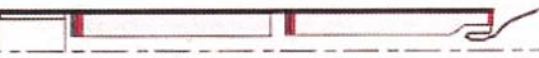
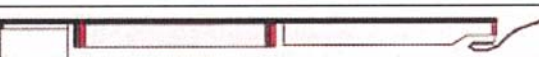
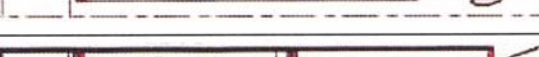
LP3 A		Nominal configuration : mid and aft segments inhibited on their forward ends
LP3 B		Inhibitor rings on both ends of the mid-segment. Aft segment free of inhibitor.
LP3 C		Mid segment inhibitor moved to segment aft end.
LP3 D		Mid and aft segment replaced by a single longer segment
LP3 E		Aft segment free of inhibitor

FIGURE 6.26. The five two-dimensional configurations of the LP3 test motors. Parietal vortex shedding was discovered in model D. (Vuillot *et al.* 1993; Prévost *et al.* 1996).

³⁰The payload of the Space Shuttle also was reduced in the late 1980s, by an even larger amount due to design changes following the loss of the Challenger. In that case, parietal vortex shedding was not an issue.

³¹Veine d'Etude de la Couche Limité Acoustique. The test device operated with air injection through the porous sidewalls, to allow the flow visualization shown in Figure 6.27.

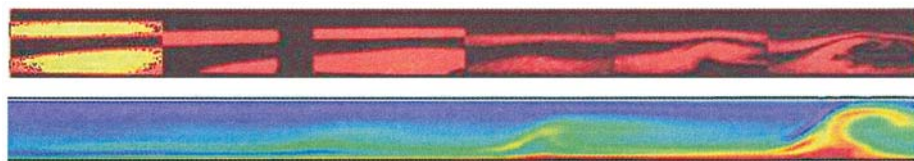


FIGURE 6.27. Upper image: flow visualization of parietal vortex shedding, using PLIF with acetone; Lower image: result of numerical calculations (Avalon *et al.* 2001).

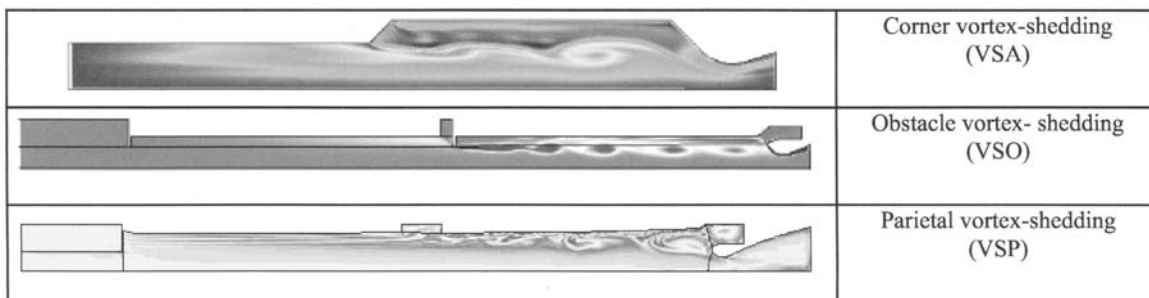


FIGURE 6.28. The three kinds of vortex shedding (Fabignon *et al.* 2003).

Prévost, Godon, and Innegrave (2005) have reported the most recent tests supporting the view that parietal vortex shedding may be a significant contribution to the problem of oscillations in the Ariane 5. Three series of sub-scale tests have been carried out, a total of seventy-six firings in configurations identified as LP6(1/15 scale), LP9(1/35 scale) and LP10(1/35 scale). In the series LP6, the propellant was changed to a non-metallized form during the series. In all tests having no restrictors at the ends of propellant segments, parietal vortex shedding occurred. Figure 6.29 is a drawing of the test device; Figure 6.30 shows typical results.

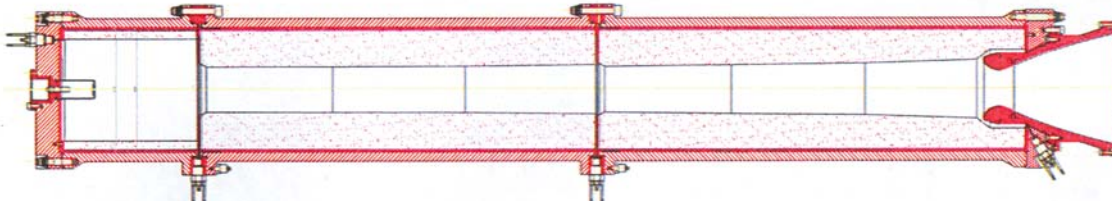


FIGURE 6.29. A sketch of the LP6 test device (Prévost *et al.* 2005).

Test series for the LP9 and LP10 configurations showed the presence of oscillations apparently due to parietal vortex shedding. Accompanying analysis by Chedevergne and Casalis (2005) supports that explanation. No direct confirmation by flow visualization was reported, but that may be an unnecessary step. An interesting comment was made in connection with Figure 17 of the paper by Chedevergne and Casalis, that "...all the instabilities begin at the burnout of the propellant around the submerged nozzle."

The significance of the parietal form of vortex shedding may be great indeed. If this really is the source of the acoustic waves (modes) excited in the Ariane 5 or other large boosters), then there are significant

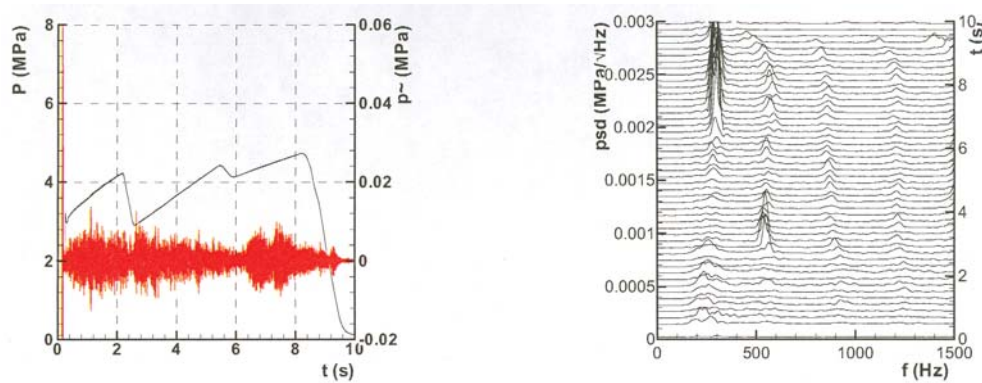


FIGURE 6.30. Experimental results for a test in the LP6 configuration showing parietal vortex shedding (Prévost *et al.* 2005).

implications for design of new motors to avoid the problem. However, despite the extensive and impressive accomplishments by the French research program for the Ariane 5, it seems that available evidence doesn't prove conclusively that familiar vortex shedding originating with an unstable shear layer formed at an edge is eliminated is a (the?) potential cause in the full-scale motor. Direct confirmation is difficult. However, it is not clear at this time that the more familiar formation of vortices at the joints of the segments of the grain can be dismissed as the primary cause, even in the Ariane 5.

6.13. Predictions of Stability Boundaries for Liquid Rockets

Stability boundaries were apparently first treated systematically for liquid rockets, in the early 1950's. In 1956 Crocco and Cheng completed their book treating one-dimensional motions, with the $n - \tau$ representation of the unsteady conversion of liquid to combustion products. That idea, introduced a few years earlier by von Karman and Summerfield (1950) achieved an enormous simplification of the actual processes. Combined with significant approximations to the spatial extent of the unsteady combustion, the model was the basis for much work in the theory of combustion instabilities in liquid rockets. Attempts to extend application of the $n - \tau$ model to solid propellant rockets (Cheng 1954a) and other liquid-fueled systems (e.g., Reardon 1983) seem to have had few useful consequences.

From the early 1950s through the 1980s in the U.S. the $n - \tau$ model dominated the views and practical considerations of unsteady combustion in liquid-fueled systems. First linear behavior and then, beginning in the early 1960s, nonlinear combustion instabilities were investigated. It is important to appreciate that, as discussions in Chapter 2 and in the next chapter show clearly, the geometries of combustion chambers treated in those works were all quite simple variations of a cylindrical chamber with a sonic exhaust nozzle. Thus the basic flow fields in all cases shared nearly the same characteristics, differences arising from the absence or presence of a shock wave and the spatial extent of the combustion processes. The general methods used are cumbersome to apply to distributed combustion. Consequently, most of the analyses were restricted to concentrated combustion. For example a common choice, perhaps a reasonable approximation to combustion of fast burning propellants, was combustion in a plane located at the head end of the chamber. One exception was examination of distributed combustion by Crocco and Cheng (1956; pp. 103ff). The practical difficulties with a formulation based on differential equations become apparent fairly soon.

Probably the apex of the Princeton work on linear stability was reached with Crocco's long paper given at the Tenth Combustion Symposium (1965). Crocco spent at least half of the paper on explicit modeling of

combustion processes and on nonlinear behavior, virtually signaling the conclusion of their research dealing with linear problems.

The way in which stability boundaries were treated with the $n - \tau$ representation has been explained in Section 2.4.2. It is important to realize that apart from estimates, no work seems to have been done to predict values of n and τ , so there really are no true predictions of stability boundaries using the $n - \tau$ model. The usual approach in applications has been based on the assumption that all other contributions to the formula for the growth constant are known. Then setting $\alpha = 0$ gives a relation between n and τ on the stability boundary. Or, if one more correctly uses both the real and imaginary parts of the eigenvalue for wave motions, then there are two relations. These have the forms (2.127)a,b which can, in principle be used to define a stability boundary and the variation of the frequency along the boundary.

However, no true predictions of stability boundaries are available without knowledge of n and τ . Consequently, for applications to a real system, and to obtain some understanding of the way in which its stability may depend on important parameters and operating conditions, experimental data are required. Examples are given in Section 2.4.2; extended discussions may be found in Harrje and Reardon (1972).

Theorists in Russia took a very different approach not married so tightly to a simple representation of the principle mechanism for instabilities in liquid rockets. Natanzon (1984, 1999) has written the best known treatise on instabilities in liquid rockets. The work covers several methods not well-known in the West and includes a summary of some experimental work on hysteresis. Since it is based entirely on differential equations, Natanzon's work has little overlap with the methods covered in this book.

6.14. Contributions to the Growth Constant for Linear Stability

It is one of the great benefits of the linear analysis that the influences of the processes causing or discouraging instabilities are displayed additively. Their relative importance is therefore easily assessed and the basis is given for determining where most effort should be expended to provide good predictions of stability in actual systems. Consequently much expense and effort in the field of combustion instabilities generally has been planned according to the formal organization of the subject suggested by the results (6.94) and (6.161) for the linear growth constant. In this section we will discuss several contributions which are important mainly in solid propellant rockets. The subjects of Section 6.14.1 and 6.14.2 arise in all types of propulsion systems.

6.14.1. Mean Flow/Acoustics Interactions. Of the many processes participating in combustion instabilities those that are purely fluid-mechanical are best known, mainly for two reasons: Their foundations are understood; and usually they can be investigated experimentally with laboratory tests at room temperature. It is a fortunate peculiarity of the fluid mechanics that the formal results are relatively simple to first order in the amplitude and in the mean flow speed. For internal flows, the first order interactions combine in such a way that the net result appears as convection through the boundary, the surface integral containing $(\bar{\mathbf{u}} \cdot \hat{\mathbf{n}})\psi_n$ in (6.87), (6.90) and (6.94).

Thus, to lowest order, the mean flow/acoustics interactions are simple both in form and interpretation. As the manipulations leading to (6.87) show, the surface integral in fact accounts for some contributions occurring in the volume. It is a fortunate accident that for a finite volume, their net contribution turns out to be represented as a surface effect only.

On the other hand, when viscous effects and especially flow separation occur, the situation becomes immeasurably more complicated. For example, all of the phenomena associated with shear layers and vortex

shedding enter the picture. We have discussed them elsewhere in this book. It is best to treat them in the physical contexts where they arise.

6.14.2. Attenuation by a Choked Exhaust Nozzle. Liquid and solid propellant rockets, ramjets and augmentors for gas turbines all exhaust through choked nozzles. In a gas turbine, the combustor supplies the turbine directly and the exit flow from the combustor has traditionally been well below sonic speeds. In modern gas turbines the exit Mach number is larger, approaching unity in some cases. Combustion instabilities have become troublesome in gas turbines in recent years, mainly a consequence of the need to operate at lower fuel/air ratios as part of the strategy to minimize the generation of nitrogen oxides. Otherwise, undesirable oscillations have been relatively infrequent in such systems.

On the basis of those observations—crude but nevertheless valid—one is tempted to offer the generalization that any combustion system possessing a choked exhaust is liable to exhibit combustion instabilities. Is there any reason why such a simple characterization might contain some truth? In fact there is, broadly, a reason: A system having a choked exhaust nozzle in general will have lower acoustic losses than it would if the exhaust flow were not choked. The main purpose of this section is to clarify how this result comes about; and to show how those losses are determined theoretically and experimentally. A useful consequence is that with the solution we discover how to obtain a good estimate for the length of chamber to use for approximate calculation of the frequency of an instability.

The essential idea is quite simple, as sketched in Figure 6.31. An acoustic wave is incident from the left on an axisymmetric sonic nozzle, Figure 6.31(a), or two-dimensional nozzle, Figure 6.31(b). The wave propagates in the direction parallel to the axis of the nozzle but in general has an unspecified distribution of variables in planes normal to the axis. For this analysis we assume the flow upstream of the entrance to the nozzle is uniform. Because we consider only linear behavior, it is consistent with the analysis of motions in the chamber to assume the first-order representation of the incident wave in the radial and azimuthal coordinates,³²

$$\begin{aligned} J_m(\kappa_{mn}r) \cos n\theta & \quad (\text{standing waves}) \\ J_m(\kappa_{mn}r)e^{\pm in\theta} & \quad (\text{travelling or "spinning" waves}) \end{aligned} \quad (6.187)$$

For the two-dimensional case, the incident waves have amplitude independent of y defined in Figure 6.31(b) and dependence on $\cos(k_l x)$ upstream of the nozzle. A source of the steady incident waves is assumed to exist somewhere far to the left (upstream) of the nozzle and is ideal in the sense that it perfectly absorbs any waves travelling after reflection from the nozzle.

A large fraction of the incident waves passes through the nozzle and the remainder is reflected back to the chamber. That is the result of complicated interactions between the waves, the mean flow and the nozzle itself. The last introduces explicit dependence of the reflected waves on the shape of the nozzle. Most available calculations of the nozzle admittance function rest partly on the approximation that the nozzle is slender;³³ that restriction eliminates explicit dependence on the shape, where ‘shape’ means the variation of cross section with position.

Reflection of a portion of the incident waves therefore occurs because the average flow is non-uniform in the streamwise direction. Without the shape of the nozzle appearing in the problem, satisfying any conditions on a lateral boundary is unnecessary—indeed not possible. The form of a wave having structure

³²We use dimensionless coordinates, r standing for r/R and z for z/L where R is the radius of the nozzle at its entrance and L is the length from the entrance to the throat. For the two-dimensional nozzle, R is replaced by $W/2$; see Figure 6.31.

³³‘Slender’ means that the slope of the nozzle boundary, the rate of change of the diameter of the cross section with position, along the axis is small. We will not try to make this statement more precise. See the cited references for somewhat closer estimates.

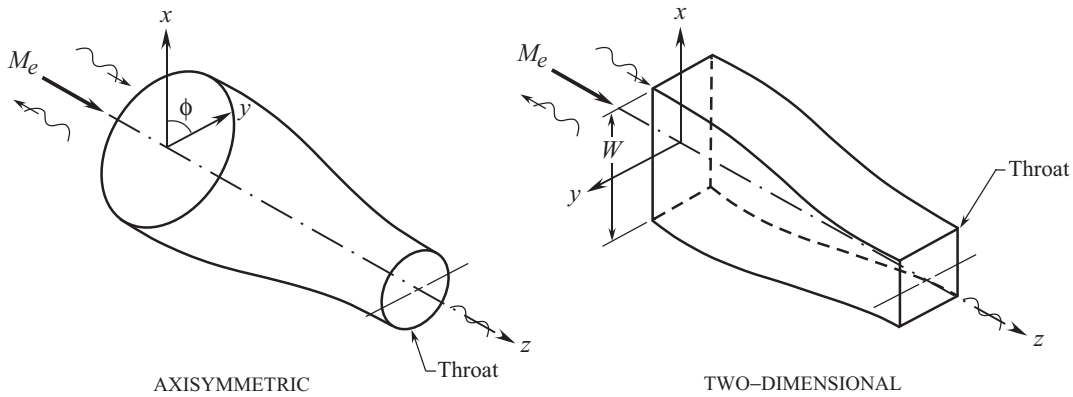


FIGURE 6.31. Idealized axisymmetric and two-dimensional nozzles for calculating admittance functions.

in transverse planes is set by its form at the entrance. As a result of these approximations we have described only qualitatively, determining the wave system produced in the nozzle by its action on the planar incident wave, comes down to finding the variation of one quantity in the flow through the nozzle. Usually that quantity has been chosen to be the density, or the pressure, of the wave system.

In his seminal work, Tsien (1952) assumed that the oscillations in the nozzle are isothermal, an approximation corrected by Crocco (1953). Crocco's analysis of purely longitudinal waves for which the velocity fluctuations are parallel to the axis of the nozzle is included as Appendix B of Crocco and Cheng (1956). That is probably the best place to become acquainted with analysis of the problem; we follow Crocco's analysis with little change. The linearized continuity and momentum equations for one-dimensional unsteady motions can be written

$$\frac{\partial}{\partial t} \left(\frac{\rho'}{\bar{\rho}} \right) + \bar{u} \frac{\partial}{\partial z} \left(\frac{\rho'}{\bar{\rho}} + \frac{u'}{\bar{u}} \right) = 0 \quad (6.188)$$

$$\frac{\partial}{\partial t} \left(\frac{u'}{\bar{u}} \right) + \left(\frac{\rho'}{\bar{\rho}} + 2 \frac{u'}{\bar{u}} \right) \frac{d\bar{u}}{dz} + \bar{u} \frac{\partial}{\partial z} \left(\frac{u'}{\bar{u}} \right) = \frac{p'}{\bar{p}} \frac{d\bar{u}}{dz} + \frac{\bar{p}}{\bar{\rho} \bar{u}} \frac{\partial}{\partial z} \left(\frac{p'}{\bar{p}} \right) \quad (6.189)$$

We assume that the entropy of an element of fluid does not change in passage through the nozzle, so the linearized equation is

$$\left(\frac{\partial}{\partial t} + \bar{u} \frac{\partial}{\partial z} \right) \frac{s'}{C_v} = \left(\frac{\partial}{\partial t} + \bar{u} \frac{\partial}{\partial z} \right) \left(\frac{p'}{\bar{p}} - \gamma \frac{\rho'}{\bar{\rho}} \right) = 0 \quad (6.190)$$

Note that the averaged quantities $\bar{\rho}$, \bar{p} , \bar{u} are all functions of position. They are assumed known from the shape of the nozzle.

The last equation is integrated to give

$$\frac{s'}{C_v} = \frac{p'}{\bar{p}} - \gamma \frac{\rho'}{\bar{\rho}} = F \left(t - \int_{z_e}^z \frac{dz'}{\bar{u}(z')} \right) \quad (6.191)$$

in which the function F is determined by the (presumed known) time dependence of the entropy at z_e , the entrance plane of the nozzle. To make the connection with Crocco's analysis easy to follow, we assume

harmonic time dependence³⁴ and introduce the definitions of $\varphi(z)$, $\sigma(z)$, and $\nu(z)$

$$\frac{p'}{\bar{p}} = \varphi(z)e^{-i\omega t}; \quad \frac{\rho'}{\bar{\rho}(z)} = \sigma(z)e^{-i\omega t}; \quad \frac{u'}{\bar{u}(z)} = \nu(z)e^{-i\omega t} \quad (6.192)$$

Then (6.191) becomes

$$\varphi(z) - \gamma\sigma(z) = \varepsilon e^{i\omega \int_{z_e}^z \frac{dz'}{\bar{u}}} \quad (6.193)$$

where ε is C_V^{-1} times the amplitude of the entropy oscillation.

With (6.192), equations (6.188) and (6.189) are now

$$\bar{u} \frac{d\nu}{dz} + \bar{u} \frac{d\sigma}{dz} - i\omega\sigma = 0 \quad (6.194)$$

$$\bar{u} \frac{d\nu}{dz} + \frac{\bar{a}^2}{\bar{u}} \frac{d\sigma}{dz} + \left(2 \frac{d\bar{u}}{dz} - i\omega\right) \nu - (\gamma - 1) \frac{d\bar{u}}{dz} \sigma = \varepsilon \left(\frac{d\bar{u}}{dz} - i\omega \frac{\bar{a}^2}{\gamma \bar{u}^2} \right) e^{i\omega \int_{z_e}^z \frac{dz'}{\bar{u}}} \quad (6.195)$$

Tsien (1952) first noticed that this pair of equations could be solved to give σ and ν in terms of a known function for the special case in which the mean velocity increases linearly with distance from the entrance plane. To simplify the discussion and results even further we will not account for entropy changes and set $\varepsilon = 0$.

To specify a linear velocity profile, take the slope to be constant, written as

$$\frac{d\bar{u}}{dz} = \frac{\bar{u}}{z} = \frac{\bar{a}_*}{z_*} = \frac{\bar{a}_* - \bar{u}_e}{(z_* - z_e)} \quad (6.196)$$

where $(\)_*$ denotes values at the throat and, as earlier, $(\)_e$ identifies values at the entrance.³⁵ Thus $z_* - z_e$ is the length of the subsonic section of the nozzle. Tsien introduced the new variable ζ ,

$$\zeta = \left(\frac{z}{z_*} \right)^2 = \left(\frac{\bar{u}}{\bar{a}_*} \right)^2 \quad (6.197)$$

The relation between the speed of sound and the Mach number,

$$\frac{T}{T_0} = 1 + \frac{\gamma - 1}{2} M^2$$

may be used to give the formula

$$\left(\frac{\bar{a}}{\bar{a}_*} \right)^2 = \frac{\gamma + 1}{2} - \frac{\gamma - 1}{2} \zeta^2 \quad (6.198)$$

Finally define a dimensionless or “reduced” angular frequency β ,

$$\beta = \frac{z_* \omega}{\bar{a}_*} = \frac{\omega(z_* - z_e)}{\bar{a}_* - \bar{u}_e} \quad (6.199)$$

Substitution of the preceding definitions and combination of (6.194) and (6.195) eventually produces the equation with which σ may be computed:

$$\zeta(1 - \zeta) \frac{d^2\sigma}{d\zeta^2} - \left(2 - \frac{2i\beta}{\gamma + 1} \right) \zeta \frac{d\sigma}{d\zeta} + i\beta \frac{2 - i\beta}{2(\gamma + 1)} \sigma = 0 \quad (6.200)$$

³⁴Recall that we use the convention $e^{-i\omega t}$ whereas Crocco uses $e^{+i\omega t}$.

³⁵Except M_N (not M_e) denotes the Mach number of the flow entering the nozzle.

The point $\zeta = 0$ lies upstream of the entrance to the nozzle, but $\zeta = 1$ is at the throat ($\bar{M} = \bar{M}_* = 1$). Hence we must choose the solution to (6.200) which is non-singular at $\zeta = 1$, known as the hypergeometric series (Morse and Feshbach 1953). Expanded in powers of $1 - \zeta$, the solution is

$$F(a, b, c; 1 - \zeta) = 1 + \frac{ab}{c}(1 - \zeta) + \frac{a(a+1)b(b+1)}{c(c+1)} \frac{(1 - \zeta)^2}{2!} + \dots \quad (6.201)$$

with

$$\begin{aligned} c &= a + b + 1 = 2 \left(1 - \frac{2\beta}{\gamma + 1} \right) \\ ab &= \frac{-i\beta}{\gamma + 1} \left(1 - \frac{1\beta}{2} \right) \end{aligned} \quad (6.202a,b)$$

Crocco and Cheng (1956) noted that the convergence of (6.201) is slow for $1 - z_e$ near one (i.e. when z_e is small, as the case is for small Mach number at the nozzle entrance) and have given alternative representations for z_e small. Thus the problem of calculating the admittance function is solved, subject to the limitations of the analysis discussed above. Using the relation for isentropic flow assumed here, we find the admittance function for a nozzle³⁶

$$A_N = -\frac{(\hat{\mathbf{u}} \cdot \hat{\mathbf{n}})/\bar{a}}{(\hat{p}/\gamma\bar{p})} = \frac{\hat{u}/\bar{a}}{\hat{\rho}/\bar{\rho}} = \bar{M}_N \frac{\nu_e}{\sigma_e} \quad (6.203)$$

where \bar{M}_N stands for the Mach number of the average flow entering the nozzle.

A particularly important limit of (6.201) is that for very slow or “quasi-static” conditions, the value assumed for $\omega \rightarrow 0$ (i.e. $\beta \rightarrow 0$). This condition is equivalent to that existing in a “short” nozzle, that is when the wavelength of the oscillation is long compared with the length of the nozzle. Evidently the same result can therefore be obtained with at least two arguments. Under these conditions, the fluctuation of velocity at the nozzle entrance is in phase with the imposed pressure fluctuation. The admittance function for short nozzles was first obtained by Crocco (1953, p. 52, $\beta = 0$) and subsequently by several others, including Zinn (1972), the result being

$$A_N = \bar{M}_N \frac{\gamma - 1}{2} \quad (6.204)$$

This is of course the value of the nozzle admittance function for β (i.e. $\omega = 0$).

Figure 6.32 shows some results for realistic ranges of β and \bar{M}_N . For example, for a rocket having a nozzle entrance 15 cm long and with $\bar{a} = 1500$ m/s, $\beta = 0.3$ when $\omega = 3000s^{-1}$ ($f \approx 500s^{-1}$). This estimate shows that for practical purposes, since β is quite small, the approximation (6.204) is in fact quite good.

Experimental results have shown that for the conditions supposed, the theory worked out by Tsien and Crocco gives accurate results: The action of a choked exhaust nozzle on small amplitude sinusoidal oscillations may be assumed accurately known. Crocco, Monti and Grey (1961) reported the first test results, in which the velocity was measured with a hot wire. Data were obtained for relatively high values of β because the speed of sound in cold-flow test is much lower than the values in hot firings. Figures 6.33 and 6.34 show that their experimental results seem to agree quite well with the theory described above. However, the authors expressed some reservations since they were forced to apply significant adjustments to the raw data, owing in large part to inaccuracies in the results for the velocity fluctuations.

Bell (1972) has obtained the best data for the nozzle admittance function; his experimental results were included in the papers by Zinn, Bell, Daniel and Smith (1973) and by Bell, Daniel and Zinn (1973). The data were obtained using the method based on an impedance tube as recommended by Culick and

³⁶Sometimes the density replaces the pressure, giving a quantity differing from (6.204) by a factor γ . Then (6.204), for example, becomes $\bar{M}_N(\gamma - 1)/2\gamma$.

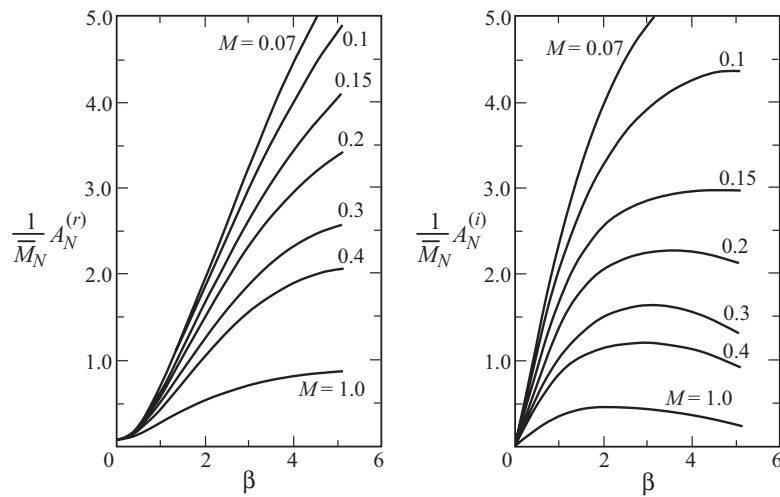


FIGURE 6.32. Numerical values for the admittance function of a nozzle exposed to isentropic oscillations, equation (6.203): (a) real part; (b) imaginary part. (Crocco and Cheng 1956)

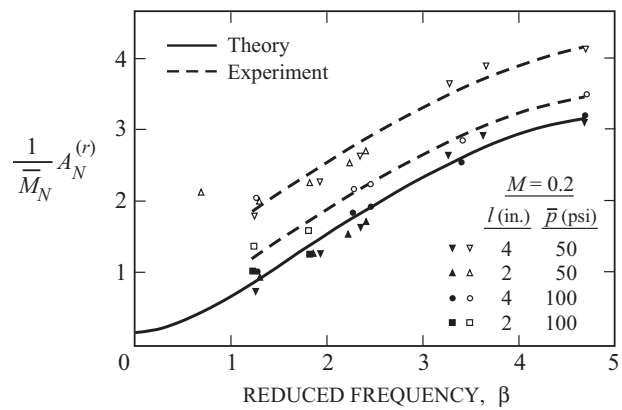


FIGURE 6.33. Results for the real part of the admittance function for a nozzle. Open symbols represent uncorrected data; filled symbols represent the same data corrected for closer agreement with Crocco's theory (Crocco, Monti, and Grey 1961).

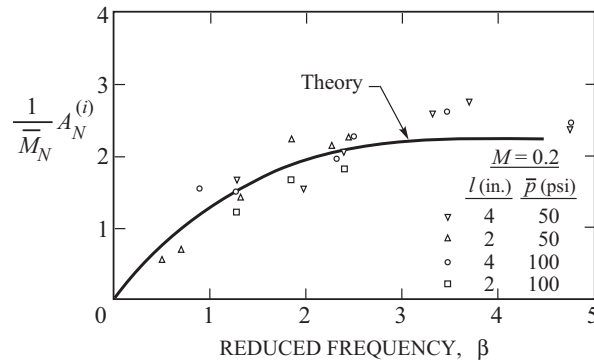


FIGURE 6.34. Results for the imaginary part of the admittance function for a nozzle (Crocco, Monti, and Grey 1961).

Dehority (1969).³⁷ Figures 6.35–6.37 show the experimental results and the predictions according to the theory described by Crocco and Sirignano (1967). The agreement with the theory is clearly quite good.³⁸ Results are shown for purely longitudinal modes, but Bell reported equally good agreement between theory and his data for the lowest longitudinal/tangential modes.³⁹

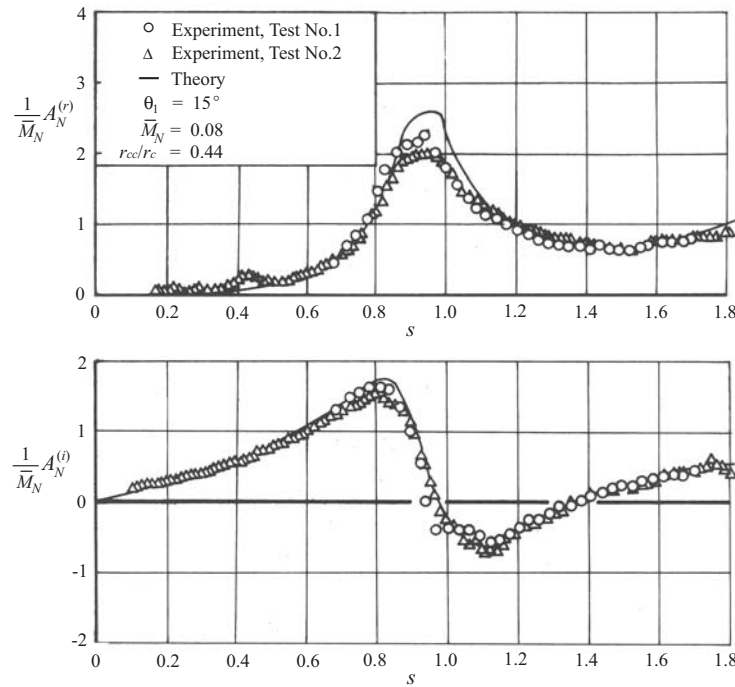


FIGURE 6.35. Comparison of the theoretical and experimental admittance results for nozzle 15-08-2.5, longitudinal modes (Bell 1972).

Some related data were taken in tests at the Naval Weapons Center (at that time the Naval Ordnance Test Station, usually called NOTS), reported by Buffum, Dehority, Slates and Price (1967); see also cited documents by the same authors. Those works are useful for a comparison of three methods of measuring the losses: the decay of pulses produced by small explosive charges; decay of steady oscillations; and properties of the resonance curve. The last seems to have been the best at that time although the results given are not useful for other applications.

³⁷The general features of the method and its most effective realization, including best experimental procedure, have been described by Baum (1980).

³⁸The independent variable is the dimensionless frequency, $s = \frac{\omega r_c}{a}$, where r_c is the radius of the impedance tube; r_{cc} is the radius of the throat of the nozzle.

³⁹Still not firmly established experimentally is the result predicted by the analyses (Culick 1961, Crocco and Sirignano 1967) that under some conditions, tangential modes are amplified by passage through a choked nozzle.

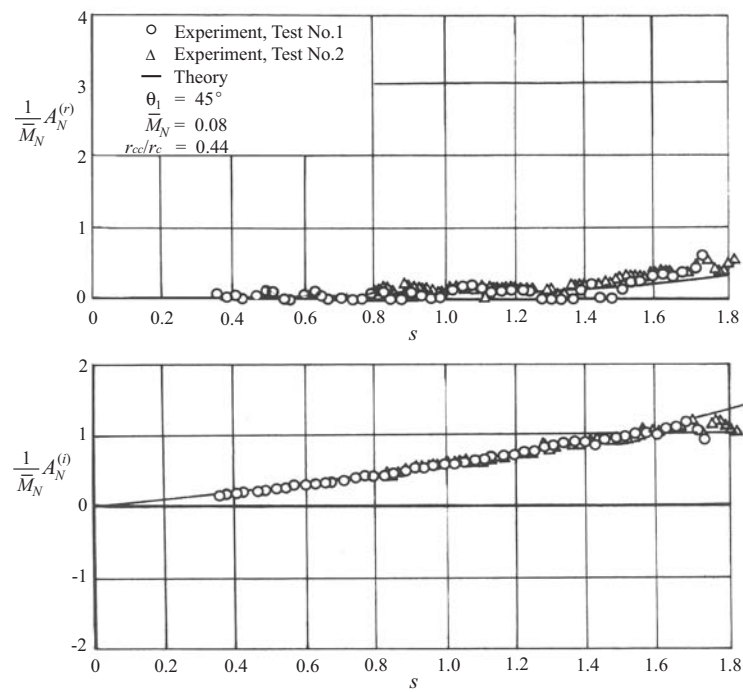


FIGURE 6.36. Comparison of the theoretical and experimental admittance results for nozzle 45-08-2.5, longitudinal modes (Bell 1972).

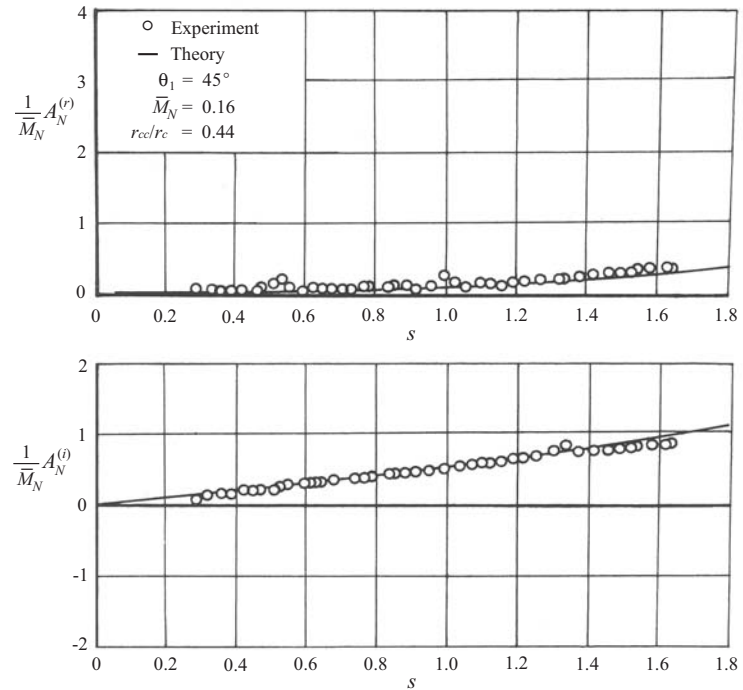


FIGURE 6.37. Comparison of the theoretical and experimental admittance results for nozzle 45-16-2.5, longitudinal modes (Bell 1972).

6.14.3. Attenuation of Acoustic Energy Due to Condensed Products of Combustion. Particularly in solid propellant rockets using metallized propellants, but in other systems as well, some of the combustion products are formed as liquid or solid particles. The viscous interactions between the particles and the gas may, under conditions, provide significant dissipation of energy. In the context of this chapter, that means that the corresponding contribution to α must be taken into account. It is often the case that the Reynolds number based on the particle diameter and the relative gas/particle velocity is outside the range for which Stokes' law—i.e. linear behavior—is a valid approximation. It is then necessary to use a more realistic nonlinear representation of the drag force. However, the linear approximation to attenuation tends in a sense to be conservative, so it is a good basis for an approximation. It is conservative in the sense that the curve of attenuation as a function frequency is broader, for a given particle size, for nonlinear behavior. Thus, over a frequency range centered at $\omega_n\tau = 1$, (Figure 6.38), the linear approximation is an over-estimate of the actual value one might expect would be the actual value.

In this section we discuss a contribution that is well-established as an important factor in the stability of solid propellant rockets, the energy loss and damping of acoustic waves caused by small-amplitude motions of small liquid droplets. By far the most important example is the attenuation of instabilities by liquid droplets of aluminum oxide (Al_2O_3) produced in the combustion of aluminized propellants.⁴⁰ The fact that (due to the high temperatures) the particles are liquid does not explicitly enter the following analysis. Internal motions of the droplet material are not accounted for.

The amount of damping provided by condensed material (liquid or solid) depends principally on three quantities: the mass fraction $C_m = \rho_l/\rho_g$ of condensed material; the size of the particles; and the frequency of the oscillations. Perhaps the most significant practical consequence of the analysis summarized here is the result that, for a given frequency, there is a particle size (diameter) for which the attenuation per particle is maximum. That conclusion has been confirmed in practice and is the basis for one important means of treating instabilities in solid propellant rockets.

Attenuation of sound by suspended particles in a gas was first treated theoretically more than 85 years ago. The modern theory began with the work of Epstein and Carhart (1953). A simplified analysis and experimental confirmation of the results have been provided by Temkin and Dobbins (1966)a,b. The calculations discussed here constitute an alternative method fitting naturally in the approximate analysis. Extensive work by Dehority and Kraeutle (1976) and by Kraeutle *et al.* (1976) has shown that this approach works in practice.

The linear gas/particle interactions arise from equations (A.34) and (A.49) written to first order in the fluctuations:

$$\begin{aligned}\delta\mathbf{F}'_l &= -\bar{\rho}_l \frac{\partial \delta\mathbf{u}'_l}{\partial t} \\ \delta Q'_l &= -\bar{\rho}_l C \frac{\partial \delta T'_l}{\partial t}\end{aligned}\quad (6.205a,b)$$

The parts of \mathcal{F}' and \mathcal{P}' due to these terms only are found from the linearized forms of equations (A.68) and (A.70):

$$\begin{aligned}\mathcal{F}'_l &= \delta\mathbf{F}'_l = -\bar{\rho}_l \frac{\partial \delta\mathbf{u}'_l}{\partial t} \\ \mathcal{P}' &= \frac{R}{C_V} \delta Q'_l = -\bar{\rho}_l R \frac{C}{C_V} \frac{\partial \delta T'_l}{\partial t}\end{aligned}\quad (6.206)a,b$$

⁴⁰The discussion in this section is a slightly revised form of Section IVD of the article by Culick and Yang (1992)

Thus, equations (6.93) and (6.94) give the contributions to the frequency shift and the growth constant:

$$(\omega - \omega_n)_l \equiv \delta\omega_l = \frac{-\bar{a}^2}{2\omega_n \bar{p} E_n^2} \left\{ \frac{k_n}{\bar{a}} \frac{R}{C_V} C \bar{\rho}_l \int \frac{1}{\eta_n} \left(\frac{\partial \delta T'_l}{\partial t} \right)^{(i)} \psi_n dV \right. \\ \left. - \bar{\rho}_l \int \frac{1}{\eta_n} \left(\frac{\partial \delta \mathbf{u}'_l}{\partial t} \right)^{(r)} \cdot \nabla \psi_n dV \right\} \quad (6.207)$$

$$\alpha_l = \frac{-\bar{a}^2}{2\omega_n \bar{p} E_n^2} \left\{ \frac{k_n}{\bar{a}} \frac{R}{C_V} C \bar{\rho}_l \int \frac{1}{\eta_n} \left(\frac{\partial \delta T'_l}{\partial t} \right)^{(r)} \psi_n dV \right. \\ \left. + \bar{\rho}_l \int \frac{1}{\eta_n} \left(\frac{\partial \delta \mathbf{u}'_l}{\partial t} \right)^{(i)} \cdot \nabla \psi_n dV \right\} \quad (6.208)$$

We have assumed, a good approximation in most practical cases, that the mass of particles per unit volume, ρ_l , and the mass fraction are nearly independent of position in the chamber and constant in time.

To find $\delta \mathbf{u}'_l$ and $\delta T'_l$, we treat the motions as locally one-dimensional and solve the problem of single particle motion, $\mathbf{u}'_l(t)$ and $T'_l(t)$ being the velocity and temperature, respectively, of a particle located in a gas having oscillatory velocity $\mathbf{u}'(t)$ and $T'(t)$. Temperature gradients within a particle are ignored. See, for example, Rangel and Sirignano (1989) for a discussion of problems in which this assumption is not made. Moreover, for the following calculations we also ignore the effects of vaporization and combustion of the particles. In the absence of combustion, condensation or vaporization may cause increased attenuation of acoustic waves; the matter is addressed at the end of this section. We assume tentatively that the motions are such that the Reynolds number based on the relative speed, $|\mathbf{u}'_l - \mathbf{u}'|$, is less than unity. The approximation of Stokes' flow then applies, and the equations of motion are

$$\frac{d\mathbf{u}'_l}{dt} = -\frac{18\mu}{\rho_s \sigma^2} (\mathbf{u}'_l - \mathbf{u}') \\ \frac{dT'_l}{dt} = -\frac{12k}{\rho_s C \sigma^2} (T'_l - T)$$

where \mathbf{u}'_l is the velocity in the same direction as \mathbf{u}' , and σ is the particle diameter. These equations can be rewritten as

$$\frac{d\mathbf{u}'_l}{dt} + \frac{1}{\tau_d} \delta \mathbf{u}'_l = -\frac{d\mathbf{u}'}{dt} \\ \frac{dT'_l}{dt} + \frac{1}{\tau_t} \delta T'_l = -\frac{dT'}{dt} \quad (6.208)a,b$$

The relaxation times are

$$\tau_d = -\frac{\rho_s \sigma^2}{18\mu} \\ \tau_t = \left(\frac{3}{2} \frac{C\mu}{k} \right) \tau_d \quad (6.209)a,b$$

With $\mathbf{u}' = (\dot{\eta}_n / \gamma k_n^2) \nabla \psi_n$ and $T' / \bar{T} = (\gamma - 1) \eta_n \psi_n / \gamma$, the steady-state solutions ($t \rightarrow \infty$) to equations (6.208)a,b are

$$\delta \mathbf{u}'_l = X_1 (\eta_n - \tau_d \dot{\eta}_n) \frac{1}{\gamma k_n^2} \nabla \psi_n \\ \delta T'_l = -X_2 \left(\tau_t \eta_n + \frac{\dot{\eta}_n}{\omega_n^2} \right) \frac{\gamma - 1}{\gamma} \bar{T} \psi_n \quad (6.210)a,b$$

Dependence on frequency and particle properties is contained chiefly in the two functions X_1 and X_2 :

$$X_1 = \frac{\omega_n \Omega_d}{1 + \omega_d^2} \quad X_2 = \frac{\omega_n \Omega_t}{1 + \omega_t^2} \quad (6.211)\text{a,b}$$

where $\Omega_d = \omega_n \tau_d$ and $\Omega_t = \omega_n \tau_t$. For use in equations (6.207) and (6.208), the time derivatives of equations (6.210)a,b are required. This produces terms containing $\dot{\eta}_n$ and $\ddot{\eta}_n$. To be consistent, we replace $\dot{\eta}_n$ by $-\omega_n^2 \eta_n$ and, after setting $\eta_n = \hat{\eta}_n e^{i\omega_n t}$, we eventually find the results

$$\begin{aligned} \alpha_l &= -\frac{1}{2} \frac{C_m}{1 + C_m} \left[X_1 \frac{1}{E_n^2} \oint \left(\frac{\nabla \psi_n}{k_n} \right)^2 dV + (\gamma - 1) \frac{C}{C_p} X_2 \right] \\ \delta\omega_l &= \frac{1}{2} \frac{C_m}{1 + C_m} \left[\Omega_d X_1 \frac{1}{E_n^2} \oint \left(\frac{\nabla \psi_n}{k_n} \right)^2 dV + (\gamma - 1) \frac{C}{C_p} \Omega_t X_2 \right] \end{aligned} \quad (6.212)\text{a,b}$$

Equations (6.212)a,b, normalized to the angular frequency ω_n , are plotted in Figures 6.38 and 6.39 for longitudinal oscillations. The independent variable is $\omega_n \tau_d$, 2π times the ratio of the relaxation time for relative motion [see equation (6.137)a] to the period of the motion. According to equation (6.137)a, the dominant influence on the relaxation time is the particle diameter $\tau_d \sim \sigma^2$. For typical solid propellants and operating conditions, the diameters of particles may range from fractions of a micron to tens of microns. The results shown in the figures have been computed for longitudinal oscillations in a chamber of constant cross section, so $\psi_n = \cos k_n z = \cos(\pi n z / L)$. In this case, equations (6.212)a,b reduce to

$$\begin{aligned} \alpha_l &= -\frac{1}{2} \frac{C_m}{1 + C_m} \left[X_1 + (\gamma - 1) \frac{C}{C_p} X_2 \right] \\ \delta\omega_l &= \frac{1}{2} \frac{C_m}{1 + C_m} \left[\Omega_d X_1 + (\gamma - 1) \frac{C}{C_p} \Omega_t X_2 \right] \end{aligned} \quad (6.213)\text{a,b}$$

The most striking feature of the curves in Figure 6.38 is that, for a fixed value of mass loading C_m , the dimensionless attenuation constant has a maximum value. That is, according to the interpretation expressed by equation (6.96), the number of cycles of oscillation required to reduce the amplitude by $1/e$ is minimum. Thus, for a fixed frequency, there is a best value of relaxation time, that is, particle size, for obtaining maximum attenuation. This result has served as a successful practical guide to treating combustion instabilities in motors. Addition of inert particles having appropriate sizes, or altering the propellants in other ways to affect the sizes of particular produced, has reduced the amplitudes of oscillations in actual examples (e.g. Derr *et al.* 1979), discussed in Section 8.4.

If, as usually is the case, there is a distribution of particle sizes, (6.212)a,b become sums over the contributions from different sizes:

$$\begin{aligned} \alpha_\ell &= -\frac{1}{2} \frac{C_m}{1 + C_m} \sum_{s=1}^m K_s \left[x_{1s} + (\gamma - 1) \frac{C}{C_p} x_{2s} \right] \\ \delta\omega_\ell &= \frac{1}{2} \frac{C_m}{1 + C_m} \sum_{s=1}^m K_s \left[\Omega_{ds} x_{1s} + (\gamma - 1) \frac{C}{C_p} \Omega_{ts} x_{2s} \right] \end{aligned} \quad (6.214)\text{a,b}$$

The result (6.145)a was used by Dehority and Kraeutle (1976) to compute the damping for the experimentally determined distribution shown in Figure 6.40. These data were obtained as measured values for the residue produced in a T-burner firing. The process is extremely tedious and time-consuming. Details are given in the reference cited and other works. Table 6.5 is a list of the measured mass fractions used in

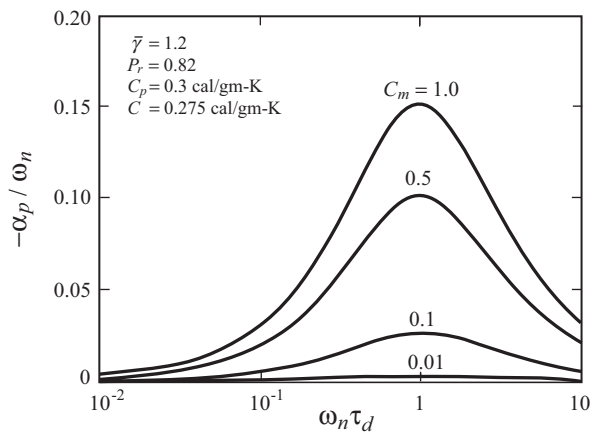


FIGURE 6.38. Attenuation of acoustic waves caused by small particles suspended in a gas (Culick and Yang 1992).

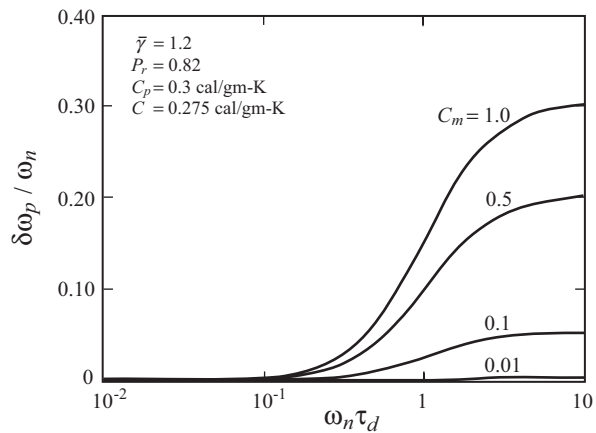


FIGURE 6.39. Frequency shift of acoustic oscillation caused by small particles suspended in a gas (Culick and Yang 1992).

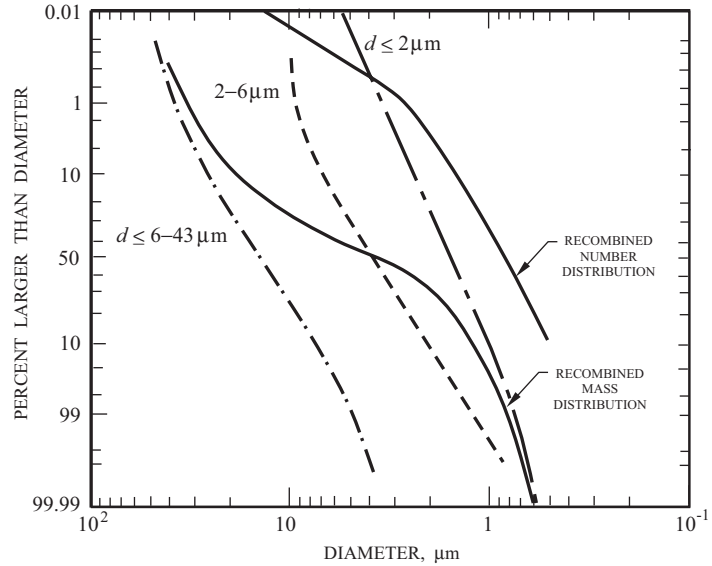


FIGURE 6.40. Mass distribution of subfractions of the combustion residue of NWC Mix No. 10. The total mass distribution was obtained by recombination of the distributions of subfractions. The total number distribution was calculated from the total mass distribution. (Dehorty and Kraeutle 1976).

the preparation of Figure 6.40. The main parameter values used in the calculations of the particle damping are given in Table 6.6.

To check the validity of the theory over a realistic range of frequency, data were used from tests with T-burners of different lengths. The frequencies of the oscillations were about 290Hz, 640Hz and 1920Hz. Table 6.7 is a list of the attenuation coefficients computed for intervals of particle size varying from $0.4 \mu\text{m}$ to $3 \mu\text{m}$.

TABLE 6.5. Mass Fractions of NWC Mix No. 10 Residue for Particles Smaller than $43 \mu\text{m}$.

Diameter, μm	Residue in % of weight	Center of interval, μm	Interval, μm	% residue in interval	Mass fraction in interval
0.5	0.0	0.7	0.4	1.9	0.016891
0.9	1.9	1.1	0.4	9.1	0.080899
1.3	11.0	1.5	0.4	13.0	0.115570
1.7	24.0	1.9	0.4	10.0	0.088900
2.1	34.5	2.3	0.4	6.0	0.053340
2.5	40.3	3.0	0.4	8.7	0.077343
3.5	49.0	4.0	1.0	5.4	0.048006
4.5	54.4	5.0	1.0	4.1	0.036449
5.5	58.5	6.0	1.0	3.1	0.027559
6.5	61.6	7.0	1.0	3.4	0.030226
7.5	65.0	8.0	1.0	3.0	0.026670
8.5	68.0	9.0	1.0	2.5	0.022225
9.5	70.5	10.0	1.0	2.3	0.020447
10.5	73.0	11.0	1.0	2.2	0.019558
11.5	75.3	12.0	1.0	2.1	0.018669
12.5	77.5	13.0	1.0	1.9	0.016891
13.5	79.7	14.0	1.0	1.7	0.015113
14.5	81.8	15.0	1.0	1.4	0.012446
15.5	83.7	16.0	1.0	1.3	0.011557
16.5	85.4	17.0	1.0	1.2	0.010668
17.5	86.8	18.0	1.0	1.1	0.010000
18.5	88.2	19.0	1.0	1.0	0.009223
19.5	89.5	20.0	1.0	0.9	0.008556
20.5	90.7	22.0	3.0	0.7	0.007779
23.5	93.7	25.0	3.0	0.6	0.006223
26.5	96.0	28.0	3.0	0.5	0.005556
29.5	97.5	31.0	3.0	0.4	0.004889
32.5	98.6	34.0	3.0	0.3	0.004223
35.5	99.3	37.0	3.0	0.2	0.003556
38.5	99.7	40.0	3.0	0.2	0.001778
41.5	99.9				

TABLE 6.6. Parameters Used in the Particle Damping Calculations.

C	0.3396 cal/g $^{\circ}\text{C}$
C_m	0.48 (obtained from propellant composition)
Pr	0.75
γ	1.2
ρ_i	3.0 g/cc
μ	0.00065 poise

The final results of this work are given in Table 6.8, the measured and calculated values of the attenuation coefficient for the three frequencies. The close agreement is actually very surprising and is probably fortuitous. Nevertheless, it is really a testimony to two factors: the careful experimental work by Dr. Kraeutle⁴¹ and the apparent accuracy of the approximate theory.

Figure 6.38 shows a strong dependence of the frequency shift on both particle mass loading and on $\omega_n \tau_d$ or, as reasoned earlier, on particle size. The behavior is better understood by recognizing that, in a fixed geometry (here a tube of length L), the wavelength is fixed so that, from the fundamental relation $a = f\lambda = \omega\lambda/2\pi$, a frequency shift is equivalent to a change in the speed of sound:

$$\frac{\delta\omega}{\omega} = \frac{\delta a}{a} \quad (6.215)$$

Note especially in Figure 6.39 that, as $\omega_n \tau_d$ approaches unity, when the attenuation constant is maximum, the change in the speed of sound is not a small perturbation if the particle mass loading is greater than 0.5. The mass loading as a function of aluminum content μ in the solid propellant is given by the formula

$$C_m = \frac{1.89\mu}{1 - 1.89\mu} \quad (6.216)$$

⁴¹Dr. Karl Kraeutle worked at the Naval Air Warfare Center for 40 years and produced many results of fundamental and practical value. He was widely known and highly respected for his dogged and precise experimental work on problems associated with solid propellants and hazardous materials. He suffered a premature death due to cancer in 2003.

TABLE 6.7. Damping Coefficients Measured, NWC Mix No. 10, for Particle Sizes Smaller than μm .

Center of interval, μm	Interval, μm	Damping (sec^{-1}) for interval		
		290Hz	640Hz	1,920Hz
0.7	0.4	-0.01	-0.06	-0.56
1.1	0.4	-0.15	-0.73	-6.59
1.5	0.4	-0.40	-1.94	-17.44
1.9	0.4	-0.49	-2.39	-21.37
2.3	0.4	-0.43	-2.09	-18.53
3.0	1.0	-1.07	-5.14	-43.58
4.0	1.0	-1.17	-5.57	-41.68
5.0	1.0	-1.38	-6.37	-38.61
6.0	1.0	-1.48	-6.51	-30.06
7.0	1.0	-2.16	-8.82	-30.55
8.0	1.0	-2.41	-8.90	-23.64
9.0	1.0	-2.42	-7.95	-16.87
10.0	1.0	-2.80	-8.10	-14.36
11.0	1.0	-2.88	-7.29	-11.26
12.0	1.0	-2.99	-6.63	-9.23
13.0	1.0	-3.14	-6.19	-7.97
14.0	1.0	-3.07	-5.44	-6.62
15.0	1.0	-2.79	-4.51	-5.26
16.0	1.0	-2.46	-3.68	-4.15
17.0	1.0	-1.97	-2.76	-3.04
18.0	1.0	-1.90	-2.51	-2.72
19.0	1.0	-1.68	-2.13	-2.27
20.0	1.0	-1.48	-1.80	-1.89
22.0	3.0	-3.28	-3.78	-3.92
25.0	3.0	-2.09	-2.28	-2.33
28.0	3.0	-1.13	-1.20	-1.21
31.0	3.0	-0.69	-0.72	-0.73
34.0	3.0	-0.35	-0.35	-0.36
37.0	3.0	-0.17	-0.17	-0.17
40.0	3.0	-0.08	-0.08	-0.08

TABLE 6.8. Measured and Calculated Damping Coefficients for NWC Mix and 10.

NWC mix No.	Frequency, Hz	Measured damping (sec^{-1})	Calculated damping (sec^{-1})
10	290.7	-46.1	-48.52
10	640.6	-115.0	-116.09
10	1927.3	-364.2	-367.05

If the propellant contains 15% aluminum ($\mu = 0.15$), $C_m = 0.4$, substantial shifts in the speed of sound occur. That is why this effect of particles was included in the formulation of the conservation equations derived in Annex A and discussed further in Chapter 3. The speed of sound given by equation $\bar{a} = (\gamma RT)^{1/2} = \left[\frac{\gamma}{1+C_m} \left(\frac{p}{\rho_g} \right) \right]^{1/2}$, has the value implied by Figure 6.39 for $\omega_n \tau_d \rightarrow \infty$.

The dependence of the frequency shift on $\omega_n \tau_d$ may be interpreted as follows. According to equation (6.148)a, the relaxation time is proportional to the square of the particle diameter, and so $\omega_n \tau_d \sim \omega_n \sigma^2$. For low frequencies or small particles, $\omega_n \tau_d \rightarrow 0$; according to Figure 6.39, the frequency shift and change in the speed of sound, equation (6.215), vanish. In either case—slow unsteady motions with finite particle sizes or vanishingly small particles exposed to unsteady motions—the viscous losses in the flow about the particles become negligible. Hence, there can be no frequency shift, a result to be expected by analogy with the behavior of the resonant frequency of a classical mass/spring/dashpot system.

On the other hand, if the frequency is high enough, even for small particles, or if the particles are large, the viscous stresses cause substantial motions of the particles. When $\omega_n \tau_d$ is sufficiently small, the particles follow the gas motion very closely. The gas/particle mixture then behaves as a single fluid having density equal to the sum of the mass of gas and condensed material per unit volume, $\rho = \rho_g + \rho_\ell = \rho_g(1 + C_m)$,

but the compressibility is provided by the gas. Hence, the speed of sound assumes the equilibrium value, $\left[\frac{\gamma}{1+C_m} \left(\frac{p}{\rho_g} \right) \right]^{1/2}$ with mass-averaged values for the thermodynamic properties.

The preceding results rest crucially on the assumptions of Stokes' flow and rapid decay of transient motions so that equations (6.208)a,b apply. It is an easy calculation to show that the Reynolds number based on the relative velocity exceeds unity for realistic particle sizes ($1\mu - 10\mu$) even for quite modest amplitudes of oscillation. Hence, it appears that a nonlinear analysis of gas/particle interactions is required to cover conditions arising in practice. However, in all current applications, including the SSP program (Nickerson *et al.* 1983) the linear results are used. Dehority and Kraeutle (1976) based their experimental confirmations on the assumption of linear behavior, and it is likely that nonlinear effects cannot be detected within the experimental uncertainties.

Calculations of the attenuation constant including nonlinear effects have shown that the linear results tend to be conservative. That is, for a fixed frequency, increasing the amplitude of oscillation broadens the curves in Figure 6.38 and moves the peak to slightly larger particle size; the maximum value of the attenuation is practically constant with amplitude. Levine and Culick (1972, 1974) have produced some interesting results for the damping of nonlinear waves but with linear gas/particle interactions. The problem of nonlinear attenuation probably merits careful analysis, but the prospects for experimental verification are not especially promising at this time. Probably the best relevant reference for calculations is Korman and Micheli (1971).

6.15. Distributed Combustion

It may seem somewhat strange to identify 'distributed combustion' as a distinguished topic. All of the systems we have been discussing involve combustion distributed in space. In treatment of liquid rockets one must in fact take care to specify when the burning processes are idealized to be so rapid that they occur in thin sheets, in the limit having no volume. The early works at Princeton described in Sections 6.1 and 7.1 are well-known examples. Distributed combustion has therefore become a term and a subject referring virtually always to solid propellant rockets. The discussion in this chapter has illustrated some advantages of the realistic approximation that combustion is then confined to the boundary. This section is a brief essay on some problems arising with the presence of combustion distributed in space away from the surface.

In the context of an analysis based on spatial averaging, however, there is hardly any difference in the computational difficulties presented by processes concentrated or distributed in space. The important distinctions between combustion in a thin zone and distributed combustion are associated mainly with the modeling required: Attention is forcibly directed to the aspects of the subject where it will produce the greatest benefits.

Combustion processes in virtually all gas- and liquid-fueled systems are spread out in space and are logically referred to as distributed, except when approximated as isolated flame sheets. It is a matter of convention that the term 'distributed combustion' has come to refer to combustion within the volume of a solid rocket, removed from the boundary where most of the conversion solid \longrightarrow products occurs. Moreover, at the usual chamber pressures, if distributed combustion occurs, it probably is primarily the oxidation of aluminum to aluminum oxide. That is the subject of this section.

The principal motivation to study distributed (sometimes referred to as 'residual') combustion has been the burning of aluminum. It's a subject which has received much attention, for several reasons, in connection with the formation of 'slag', relatively large collections or coalescences, of aluminum oxide (liquid Al_2O_3). So far as combustion instabilities are concerned, the central questions are directed to the dynamics. Particularly, do the dominant processes depend on frequency, or are they essentially quasi-static?

Although the idea that combustion of aluminum continues far from the primary burning surface of a metallized solid propellant, it had been considered mainly a matter of steady burning until the late 1970s. For example, in 1977 Geisler (1977) chaired a workshop on aluminum combustion in which the topic of residual combustion, reflected as distributed combustion in a chamber, received considerable attention. General characteristics of aluminum combustion, including behavior far from a propellant burning surface, was at that time a topic of fairly active research (e.g., see Derr *et al.* 1974, Micheli and Schmidt 1977, and a later comprehensive report by Price *et al.* 1982) which is especially interesting for its photographic evidence.

Beckstead (1987) first proposed that unsteady combustion of aluminum might not be negligible in the interpretation of T-burner data. His reasoning was based on unusually large values of the velocity-coupled response function inferred for metallized propellants, as much as ten times the values normally measured for the pressure-coupled response. The velocity-coupled T-burner has test grains on the lateral walls. Hence when a longitudinal mode is unstable, as suggested in Figure 6.41, the velocity fluctuation acts to 'scour' aluminum particles from the test propellant. Then the aluminum burns as it moves with the flow away from burning surface. Any fluctuations in the burning rate of the aluminum may contribute to the instability of waves in the chamber, but should not be attributed to the response of surface combustion.

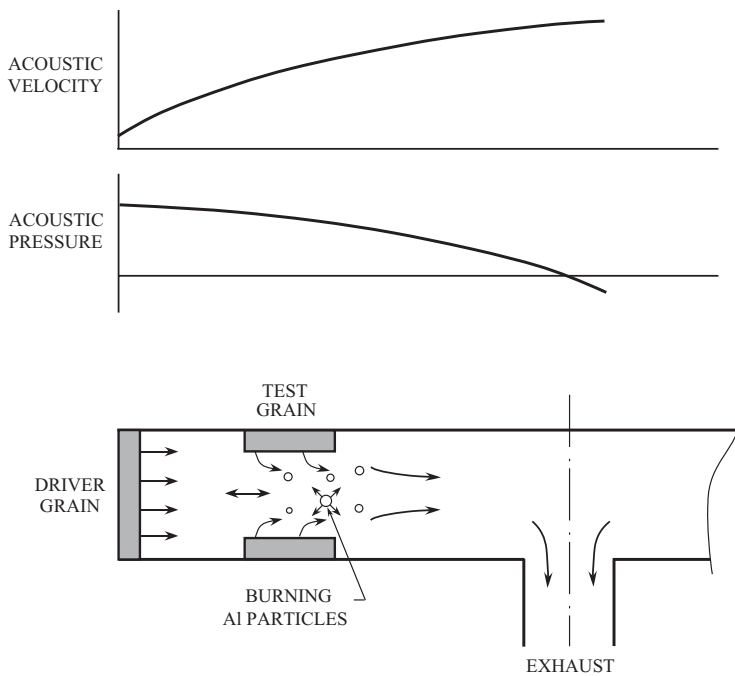


FIGURE 6.41. A possible explanation of increased growth rate due to distributed combustion of aluminum in a T-burner.

Consequently, the distributed combustion of aluminum could conceivably give falsely increased values of the surface response if the traditional interpretation is used. This idea seems not to have been pursued further. There have been other, isolated and brief, speculations concerning the possible importance of distributed combustion of aluminum in laboratory test devices but no incontrovertible evidence is available and the matter remains open.

The term involving combustion in the volume of a chamber is explicit in the general equations developed in Annex A and Chapter 3. Formally, then, it is quite easy in a linear analysis to treat distributed combustion. Beckstead and Brooks (1990) noted that the Standard Stability Program (SSP, Nickerson *et al.* 1984) contains the term, therefore providing a means of investigating the possible effects of distributed combustion on

stability. They had only an elementary model of the combustion processes so the results are probably too over-simplified to be of great value. However, the strategy is correct and merits further development.

Professor Beckstead and his students reported some interesting work based on use of a Rijke tube to investigate combustion of aluminum under unsteady conditions. Measurements of distributed combustion were carried out by Braithwaite *et al.* (1984) and Beckstead *et al.* (1985). Results of experimental work with the Rijke tube were summarized by Finlinson *et al.* (1987) and Raun and Beckstead (1993); a useful general review of Rijke tubes was provided by Raun *et al.* (1993). The main final results of the program are summarized in the paper by Brooks and Beckstead (1995) in which they give a good list of references. Much of the paper is devoted to some aspects of the steady combustion of aluminum and is not of immediate interest here. So far as the unsteady behavior is concerned, perhaps the main conclusion in the present context is that the effects of aluminum combustion on acoustics are indirect, in the words of the authors, "... a significant part of the acoustic growth with the addition of aluminum is due strictly to the change in the gas temperature profile." The effects observed are therefore, apparently, specific to the device. It does not seem possible to draw any conclusions or guidelines generally helpful to understanding the role of aluminum combustion in problems of unsteady combustion in solid propellant rockets.

In contrast to the situation in the U.S., there was a significant effort in France devoted to distributed combustion of aluminum from the mid-1990s to 2002. As true of much of the French work on unsteady behavior in solid propellant rockets in the 1990s and later, motivation was related to significant difficulties associated with an instability of the fundamental longitudinal mode in the Ariane 5 booster motor (P230). The program devoted to two-phase flow in that motor apparently began with the doctoral thesis by Dupays (1996), who remained a central figure in the work until it ended in \sim 2002. Work on distributed combustion was a logical development in the broader program formed to treat problems in the Ariane motor P230.

Early concern with oscillations in the Ariane 5 led to the integrated effort with the broader program ASSM, Aerodynamics of Segmented Solid Motors. The Pressure Oscillations Program (POP) has been devoted to obtaining numerical and experimental results for subscale tests (1/15th scale) of the P230. Much effort has been appended on validating numerical tools for predicting the frequencies and amplitudes of oscillations. Fabignon *et al.* (2003) gave a very informative overview of the principal results for oscillations studied in ASSM and POP. A general view of the three-segment motor in question is shown in Figure 6.42.

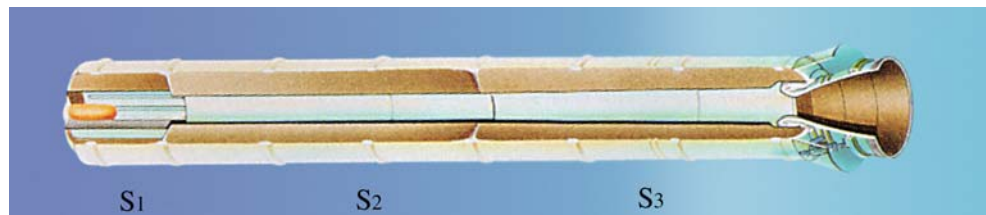


FIGURE 6.42. General view of the Ariane 5 strap-on booster motor P230 (Fabignon *et al.* 2003).

Evidence of a serious problem is reproduced in Figure 6.43, based on measurements taken during static qualification tests of the full-scale motor performed sometime in 1993–1995. The maximum amplitude of the oscillatory pressure is about 0.5% of the mean pressure but the thrust oscillation has maximum amplitude 5% which causes practical problems due to oscillatory accelerations. That is the main reason that the programs ASSM and POP have existed.⁴² Recall that the propellant in the Ariane 5 contains 18% aluminum. Vortex shedding leads to interactions between the vortices and either the internal structural surfaces of the motor, or the mean flow field. There are two potentially troublesome consequences: Acoustic waves may be excited and sustained; and the accompanying fluctuations of thrust are liable to be unacceptably large.

⁴²The greater thrust oscillations, for roughly the same amplitude of pressure oscillations, in the Ariane 5 than in the Shuttle, are due to geometrical and phase relations (Vuillot and Casalis 2002).

Already by the early 1990s, subscale firings of motors related to the P230 configuration had caused concern about the prospects for oscillations in the full-scale motor. The possible amplitudes were of course unknown, but more worrisome for the program, as were the causes. For the range of low frequencies characterizing the first few longitudinal modes, weak pressure and velocity-coupled driving (nearly quasi-steady), combined with the large damping associated with the nozzle and convective flow acoustic losses, to give stable modes according to widely accepted procedures based on the ideas developed in this chapter. However, known experience with the Shuttle SRMs and the Titan had shown that vortex shedding in segmented motors could drive the fundamental mode to relatively low amplitudes. (See discussion in Sections 1.3.3, 2.2.7, and 6.12.1. The process of vortex shedding is not included in the systematic treatment of unsteady motions based on the ideas and equations developed in the framework suggested by classical acoustics.

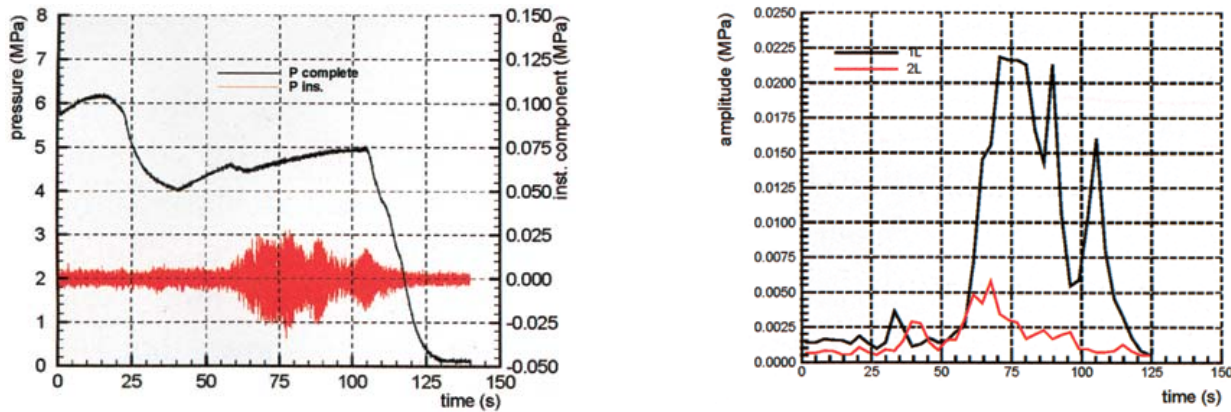


FIGURE 6.43. Results for the unsteady pressure measured in a static test firing of the Ariane 5, P230 motor (Fabignon *et al.* 2003).

We have already discussed the developments beginning with the suggestion by Flandro and Jacobs (1973) followed by the sequence of analytical and experimental works establishing the importance of the process in particular cases (Dunlap and Brown 1981, Dotson *et al.* 1997) and in general (Flandro 1995, Vuillot 1995). Vortex shedding from edges exposed as propellant burned away from inhibitor material installed between segments in the Shuttle SRM was confirmed in the 1980s as the source of low-level oscillations (Blomshield 2001, Blomshield and Mathis 1993). Reproducibly present during a predictable interval of every firing, the oscillations have never become a practical problem.

It was therefore logical to investigate vortex shedding as a possible, if not likely, cause of oscillations in the Ariane 5 booster motor. The first report of this cause was the paper by Scippa, Pascal and Zanier (1994). For the next eight years, researchers at ONERA especially, but at several other organizations in France as well, collaborated in a broadly based program directed to solving the problem of vortex shedding. The immediate motivation of course came from the Ariane 5; the research has, however, been sufficiently general to be of value much more generally. Progress in understanding the phenomenon of vortex shedding, particularly the discovery of parietal vortex shedding, has been discussed in Section 6.12.1.

As noted above, the work was coordinated in the ASSM program which began with definition of two phases (Fabignon *et al.* 2003):

- (1) demonstration of numerical tools to predict instabilities excited and sustained by vortex shedding;
- (2) development of physical models including the propellant combustion response with two-phase flow accounted for.

The second item bears directly on the subject of distributed combustion. A report of results obtained in the first half of the program was published by Dupays *et al.* (2000). Various aspects of two-phase flows, with emphasis on slag accumulation and, relevant here, interactions associated with acoustic oscillations as well as vortex shedding. It was in this work that, based on earlier results obtained by Dupays and Vuillot (1998), the suggestion was made that distributed combustion is potentially an important contribution to instabilities.

Subsequent calculations by Lupoglazoff *et al.* (2000) showed that with distributed combustion accounted for, oscillations in the Ariane 5 boosters seem to be amplified by combustion of small aluminum drops and attenuated by combustion of large drops ($> 125\mu\text{m}$). The situation is in fact more complicated than this simple conclusion suggests. Simulations were carried out for the full-scale P230 motor with a rough approximation to the particle size distribution and combustion. An important factor is interaction between parietal vortex shedding and vortices shed from the vicinity of the joint between segments. Figure 6.44 is a sketch of the grain geometry used in the simulations. It is an interesting example of how far simulations have progressed in treating realistic configurations. Compare Figure 6.44 with the actual shape shown in Figure 6.42; there is little difference. The paper by Lupoglazoff *et al.* is really a progress report, but their conclusion that distributed combustion was essential for successful simulation of unsteady flow in the Ariane 5 must be taken into account in formulating simulations for other large boosters.



FIGURE 6.44. Shape of the grain used in simulations of two-phase unsteady flow in the Ariane 5, P230 motor (Lupoglazoff *et al.* 2000).

CHAPTER 7

Nonlinear Behavior of Combustor Dynamics

It is linear behavior, especially linear stability, that is most easily understood and therefore has dominated discussions of combustion instabilities, particularly for solid propellant rockets. For example, the conclusion that a disturbance is unstable if the gain of energy exceeds the loss of energy in a short time interval, is founded in the first instance on linear ideas, although properly interpreted it is true generally. Because in a combustor there are many species and processes, the situation is extremely complicated. Moreover, unlike the case for linear motions, there are almost no generalizations available for nonlinear behavior to serve as the basis for classifying the results of either experiments or of theory.

The situation is simplified considerably if we restrict our attention to gas dynamics. Nonlinear behavior of disturbances in a compressible medium has long been the subject of research, steady shock waves being the most familiar phenomenon. Although there are many examples of shock waves generated in severe combustion instabilities, usually the motions do not contain shocks, or if they do, the amplitudes are small. In this chapter we examine various consequences of nonlinear gasdynamics within the framework developed in Chapters 3 and 4. Moreover, almost all of our discussion will be limited to second order nonlinear behavior, that is, to analysis in which only terms containing squares of the gasdynamic variables are considered. It appears that this approximation in fact accommodates a surprisingly large part of observed behavior, although not enough has been accomplished to assess the results in a definitive fashion.

While there is a broad spectrum of nonlinear problems that arise in combustion systems, two kinds of behavior have most recently received much of the attention: unsteady flows in solid propellant rockets; and the motions in gas turbine combustors. The first form the main subject of this chapter while the second are particularly common in systems intended for power generation. In the period stretching roughly from the early 1960s into the 1980s, for reasons earlier related, nonlinear behavior in liquid rockets attracted much interest, both in the U.S. (e.g., Sirignano 1964, Crocco 1965, Zinn 1966, Mitchell 1967) and in Russia (Natanzon 1999, where earlier work in Russia is cited and discussed at length). Nonlinear processes act to limit unsteady motions in augmentors. However, despite the work devoted to instabilities in augmentors for gas turbines over many years, relatively little seems to have been established concerning the fundamental character of the instabilities and for the reasons that their amplitudes may—or may not—be limited.

Although we will not discuss nonlinear control of combustion instabilities in this book, the subject is probably more important than the lack of general interest suggests. In fact, little attention has been paid to understanding nonlinear behavior in works on control of combustion instabilities. One justification for that deficiency has been the view that if control of the oscillations works properly, it should stop the growth of the motion before its amplitude reaches a large value. There are several reasons why that reasoning is flawed:

- (i) if the growth rates are unusually large, the control system may not have a sufficiently large bandwidth to be effective;
- (ii) because combustion systems are intrinsically nonlinear, design of a control system based only on linear behavior may produce a control system far from optimal;

- (iii) linear control demands actuation at the frequency of the oscillation to be controlled, while nonlinear control of particular types may be effective at frequencies lower than that of the oscillation being controlled;
- (iv) observed nonlinear behavior contains much information about properties of the system in question and in the interests of understanding should not be ignored.

Limitations of an interpretation based entirely on linear behavior may therefore become especially evident in attempts to control an unstable motion. Existing examples of controlling combustion instabilities have almost totally ignored issues of nonlinear behavior, although such behavior is evident in all experimental work. In no demonstration, either laboratory or full-scale, have the amplitudes of the oscillations been predicted or interpreted either before or after control has been exercised. Hence nothing has been learned about why the initially unstable motions reach the amplitudes they did, or why the control system affected them in the observed way. In fact, few attempts exist to determine quantitatively the stability of motions. Consequently the subject of controlling the dynamics of combustion systems has largely been a matter at best of exercising the principles of control with little attention paid to the characteristics of the systems ('plants') being controlled. It seems that following this strategy is likely not the most fruitful way of achieving meaningful progress. Especially, this is not a sound approach to developing the basis for designing control systems. The current practice in this field is often that feedback control is designed and applied in *ad hoc* fashion for systems already built and exhibiting instabilities.¹

A central concern of a control system designer is construction of a 'reduced order' model of the system. What that really means in the present context is the need to convert the partial differential equations of conservation developed in Chapter 3, to a finite—and probably small—system of ordinary differential equations. The analysis developed in Chapters 3 and 4 accomplishes exactly that purpose. It is not the only approach possible—e.g., although proper orthogonal decomposition has been examined briefly, in the author's experience no useful results have yet been found—but the method of modal expansion and spatial averaging has many favorable properties and has been proven to work well.

Nonlinear behavior is always present and is essential if disturbances are to have finite size in a self-excited unstable system. Thus, any considerations of limiting amplitudes—a practical matter in the treatment of instabilities in actual systems—must account for nonlinear processes. At the present time the subject is in a relatively weak state. The presence of nonlinear behavior is often remarked upon in discussions of observations. But it seems that little of practical value has been accomplished theoretically, and experimental results supporting conclusions reached in theory are almost non-existent. It does seem, however, that potentially useful theoretical results are available and some interesting opportunities exist which have not yet been explored.

The main purposes of this chapter are to examine a few results displaying some aspects of the nonlinear behavior arising from gasdynamics; and to illustrate some consequences of truncating the modal expansion, that is, what might be the consequences of reducing the order of the model. Another important issue we will examine briefly is the application of time-averaging. As the calculations in Chapter 4 showed, the great advantage of time-averaging is that it replaces N second order oscillator equation by $2N$ first order equations. That transformation enormously reduces the cost of obtaining solutions, aids theoretical work, and provides a simplified representation for application of feedback control. But as for truncation, the question arises: How accurate are the results and what are the limits of the validity of time-averaging?

It happens that both important matters of truncation and time-averaging can be investigated by applying a continuation method outlined in Section 7.7. The method has not yet been widely used but offers an efficient means for investigating solutions over wide ranges of parameters. It is a grand recipe for discovering how solutions behave as some defining quantities (such as the number of dependent variables and hence

¹There are some recent exceptions, for example the experiments reported by Liewen *et al.* (2004).

the number of equations) is changed. Moreover, the method has been used to determine the existence of sub-critical bifurcations. It is therefore a promising approach to the practical problem of pulsed instabilities, examined in Section 7.11.

Mainly the nonlinearities due to gasdynamics are treated in this chapter. The results must be viewed with that caveat, particularly because the forms of the nonlinearities are very special, if only because the dominant coupling acts to cause energy to flow from low to high frequency waves, the tendency which produces the familiar steepening of compressive disturbances into shock waves. The results can be applied to other nonlinearities only with care because, in particular, the coupling between modes will differ from the special form provided by gasdynamics.

7.1. Early Works on Nonlinear Combustion Instabilities

It is a classical result established by Riemann (1858) and Rankine (1870) that a planar compressive wave tends to steepen, forming, in the absence of adequate dissipative processes, a shock wave as suggested by the sketch in Figure 7.1. The interpretation of this fundamental behavior rests on the fact that the propagation speed of a disturbance depends on amplitude because it depends on the temperature.² Thus it is mainly the change in the local speed of sound that is the cause of the steepening.

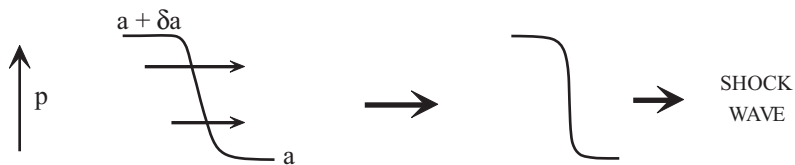


FIGURE 7.1. Steepening of a planar compressive wave into a shock wave.

The process sketched in Figure 7.1 is always active in combustion instabilities. Thus the real question in respect to observed behavior concerns the importance of wave steepening, i.e., is it a dominant process? It is never the only process at work, for in addition to those responsible for an instability (the mechanism) there are necessarily dissipative processes acting. The competition between the steepening and those processes tending to cause decay of a wave, or to modify the steepening process, is the substance of one way to view a combustion stability. This is the simplest and most fundamental basis for interpreting results found with the expansion in normal modes and spatial averaging discussed in Chapters 3 and 4.

Motivated by many observations of transverse waves in liquid and solid rockets, Maslen and Moore (1956) investigated the nonlinear problem in a circular cylinder, without combustion and flow. They were particularly concerned with steepening of transverse waves, and the accompanying change of frequency. At that time (1955) the nonlinear behavior of plane waves was quite well understood, but transverse waves had not been studied. The main difference from longitudinal waves is evident if one considers travelling waves. A wave that travels circumferentially suffers continuous reflections from the boundary. That process may be regarded as a kind of scattering which of course is absent from the case of plane wave propagation and reflection. The tendency for a wave to steepen is evidently softened in the case of transverse waves. This

²The ideal propagation speed of a weak isentropic disturbance is $\sqrt{\gamma RT}$ in an ideal gas, where T stands for the temperature of the medium. However, the local temperature change in an isentropic wave having local pressure δp different from the ambient value is $\delta T = \frac{\gamma-1}{\gamma} T(\delta p/p)$ while $\delta T = 0$ for an isothermal wave. For combustion instabilities, speeds of propagation are more closely given by the values for isentropic processes.

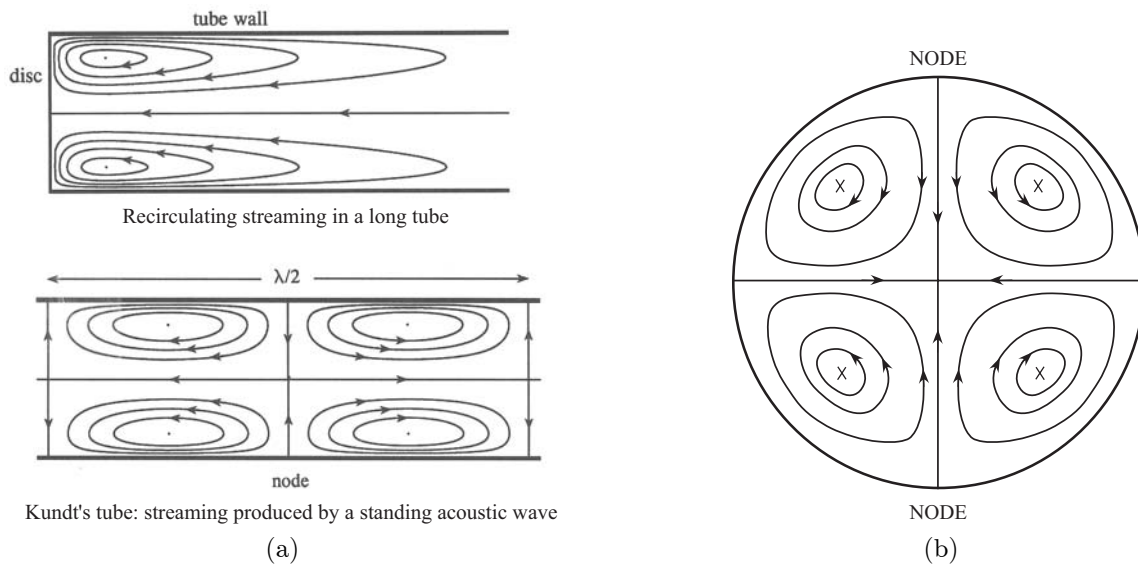


FIGURE 7.2. Acoustic streaming, a consequence of small viscous effects and nonlinear acoustics (a) plane waves (Figures 5.6.6 and 5.6.7 of Howe 1998); (b) transverse standing waves in a cylinder (Maslen and Moore 1956).

result suggests what was shown to be the case by Maslen and Moore, that transverse waves will grow to higher amplitudes without the formation of shocks than will longitudinal waves.³

One consequence of this behavior is a quite natural development of the low order nonlinear phenomenon known as “acoustic streaming,” also shown by Maslen and Moore for transverse waves. For plane wave motion parallel to a wall, a pattern of cellular motions is formed, as sketched in Figure 7.2(a). The confinement provided by the boundary causes the cells to fill the cylinder defining a transverse wave, producing a streaming motion of the form shown in Maslen and Moore’s Figure 6 reproduced as Figure 7.2(b).

Much later, Flandro (1964, 1967) analyzed the problem of unwanted roll torques in solid propellant rocket motors building on the ideas of Maslen and Moore, using the formulation described here in Chapters 3 and 4; recall the remarks in Section 6.12. It’s an interesting and useful analysis illustrating the procedure applied to a serious practical problem arising with a special case of combustion instability. As an example, suppose that transverse travelling waves develop in all cavities in a motor having five slots, as suggested in Figure 7.3. There is therefore an imbalance of rotating motions (an odd number of slots is required) and when the flow exhausts, a roll torque is created. The sign of the roll torque and how it is actually exerted on the motor requires careful attention to the angular momentum involved, as Flandro (1967) has shown.

Before high-speed computers became generally available, the method of characteristics was commonly used as the basis for analysis of several classes of problems involving large amplitude waves. Theoretical work in this vein seems to have originated with the analysis by Betchov (1958) who had no interest in combustion instabilities. He was concerned with oscillations in a closed tube of gas driven by an oscillating piston at one end. When viscous effects are ignored, the small amplitude motion has the familiar linear form, with the velocity given by

$$u = u_p \frac{\sin kx}{\sin kL} \cos \omega t \quad (7.1)$$

³Zinn (private communication) has found errors of details in the work, but Maslen and Moore’s conclusions are broadly unaffected.

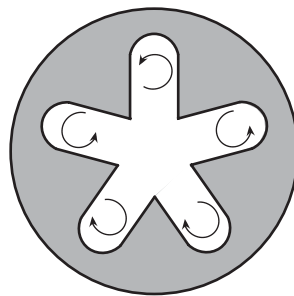


FIGURE 7.3. Finite streaming motions in a motor having five slots, giving net counterclockwise circulation (adapted from Flandro 1964).

where $\omega = kc$ and L is the length of the tube. Evidently the velocity becomes indefinitely large when $kL = \pi$. The effects of viscous friction can be computed within the linear approximation to show that they limit the amplitude. However, if the radius of the pipe is imagined to increase, frictional effects are less important, the amplitude becomes indefinitely large and nonlinear effects become more significant than viscous effects. Thus, especially so when the frequency is near resonance, nonlinear effects are increasingly significant as the amplitude increases. Not surprisingly, this problem, relatively simple and easily formulated, has attracted much attention.

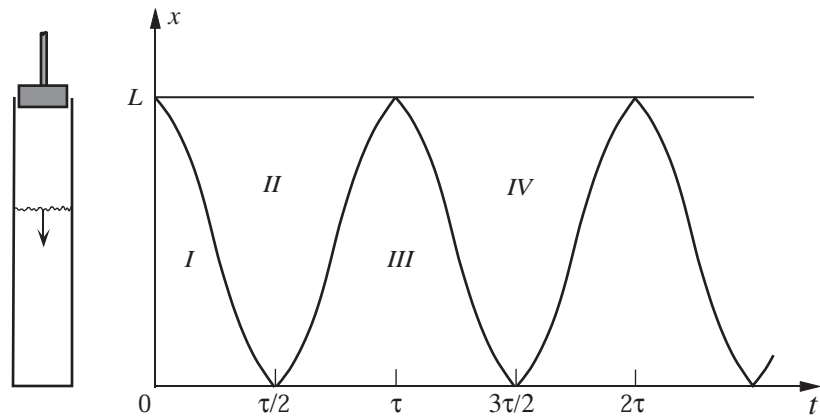


FIGURE 7.4. An oscillating shock wave in a closed tube (Betchov 1958).

On physical grounds, one may anticipate that if the amplitude and frequency of the piston's oscillatory motion are fixed, the motions of the gas will eventually settle down to a periodic form. Moreover, to emphasize the nonlinear effects, one may suppose that the periodic motion consists of a shock travelling back-and-forth in the tube with period τ . Figure 7.4, adapted from Betchov's paper, is an approximation to the flow showing only the shock wave. Betchov analyzed this problem using the method of characteristics as explained by Courant and Friedrichs (1948) and by Shapiro (1953). His discussion of the analysis includes useful comments interpreting the formalism in physical terms.

Chu (1963) and Chu and Ying (1963) analyzed a similar problem which is much more difficult to solve, although it remains quite simple compared to actual problems. A source of waves is contained in the tube, Figure 7.5, but to simplify the analysis, the source has no extent in space and is placed at the midpoint of

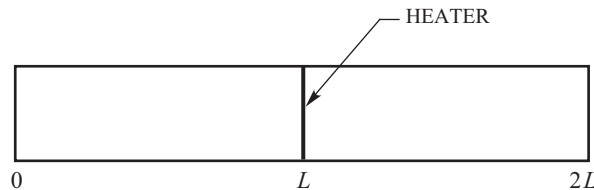


FIGURE 7.5. Closed tube containing heater at its midpoint.

the tube.⁴ There is no flow in the tube but the source emits heat at a rate proportional to the local pressure fluctuation (Chu) or in addition the rate is modulated sinusoidally (Chu and Ying):

$$\text{heat release rate} \sim \begin{cases} \delta p & \text{(Chu)} \\ \delta p \sin \Omega(t + t^0) & \text{(Chu and Ying)} \end{cases} \quad (7.2)$$

Chu solved the problems of the initial growth of a disturbance, and self-sustained periodic oscillations. In both cases the fluid motion is essentially that associated with a single shock wave propagating in the tube and reflecting from the end closures. The calculations were done using a perturbation form of the method of characteristics due to Lin (1954), which in turn was suggested by the method introduced by Lighthill (1949).

The analysis by Chu and Ying was motivated mainly by the motions observed in a Rijke tube (Section 2.7) but also by combustion instabilities. Perhaps the most important aspect of this work is application of Lin's formulation of the method of characteristics to nonlinear problems involving heat addition. Two earlier reports Chu (1955, 1956), are instructive discussions of these problems, but because, as in virtually all of Chu's work, no average fluid motion is accounted for, their applications to combustion instabilities are limited.

An important qualitative change in the Princeton analyses of combustion instabilities occurred in the early 1960s when the first investigations of nonlinear behavior were carried out. Refer to Table 7.1 for a summary of the works in question. Experimental results with gas-fueled rockets had shown the presence of discrete sharp-fronted waves, suggesting a model that could be analyzed using the method of characteristics⁵ as first accomplished by Sirignano (1964a,b) and Sirignano and Crocco (1964). Those papers introduced several phenomena which have since been commonly found in treatments of nonlinear instabilities. Both works are based largely on the thesis by Sirignano (1964) and treat variants of the same basic problem: the motion of a shock wave in a rocket chamber having planar combustion concentrated at the head end and terminating in a choked nozzle, Figure 7.6; or unsteady flow without a shock wave. Besides the presence or absence of a shock wave, a main difference between the two works is the model used for the response of the sheet of combustion to unsteady flow conditions. In both analyses, solutions were discussed for periodic motions, the shock wave neither growing nor decaying. The authors speculate that the driving mechanism could be related to the instability in such a way that it could be investigated by observing and interpreting the waveform. That goal has been re-stated many times since but it remains unattained.

Although he used the time lag (n, τ) model exclusively in his thesis (Sirignano 1964a), Sirignano (1968), and Sirignano and Crocco (1964) represented unsteady mass flux at the head end of the rocket by a somewhat different form not containing a time lag. With steady values denoted by subscript $(\)_0$, Sirignano and Crocco

⁴This problem is a simplified form of that treated in Section 2.7. It is also solved (approximately) by Culick (2002). The second work shows that if a formulation based on spatial averaging is used, it is not necessary to simplify the analysis by supposing the heater to be fixed at the midpoint of the tube.

⁵There is no obvious way to extend to nonlinear instabilities the methods used by Crocco and Cheng (1956) in their analysis of one-dimensional linear instabilities, although the authors briefly discussed some aspects of nonlinear behavior.

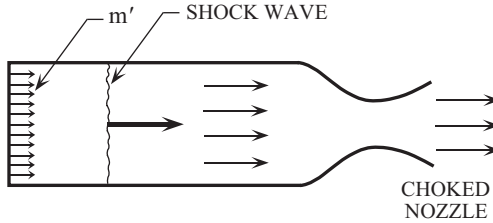


FIGURE 7.6. Model of a liquid rocket analyzed in the Princeton works. The shock wave is sometimes absent.

TABLE 7.1. Summary of Some Works from Princeton on a Theory of Combustion Instabilities.

	Combustion Model	Wave Motion	Type of Mode	Triggering	Method of Analysis
Sirignano (1964a, 1968)	$n, \tau; u'_{inj}$	Continuous Shock Waves	Axial	Inconclusive	Characteristics
Sirignano and Crocco (1964)	n, τ	Continuous Shock Waves	Axial	—	Characteristics
Zinn (1966, 1968)	n, τ	Continuous (Irrational)	Axial	Unstable	Expansion
Mitchell (1967)	n, τ (Distributed)	Continuous Shock Waves	Axial	Inconclusive	Chester (1964)
Mitchell, Crocco and Sirignano (1969)	$n, \tau; u'_{inj}$	Continuous Shock Waves	Axial	Inconclusive	Chester (1964)
Crocco and Mitchell (1969)	n, τ (Distributed)	Continuous Shock Waves	Axial Transverse	Inconclusive	Chester (1964)

Notes:

- (i) Concentrated combustion except where noted.
- (ii) $u'_{inj} \neq 0$ implies $\tau = 0$.
- (iii) Triggering to stable motions may have been found to exist in some cases but the references are unclear on this point.

wrote the velocity deviation from the mean value,

$$\frac{u - u_0}{u_0} = \omega \left(\frac{a - a_0}{a_0} \right) + \delta \left(\frac{a - a_0}{a_0} \right)^2 + O \left(\frac{a - a_0}{a_0} \right) \quad (7.3)$$

and carried their analysis to second order in changes of the speed of sound. They compared their results with some observations reported by Schob, Glassman and Webb (1963) made on a gas-fired rocket. Figure 7.7 shows an example of the waveform for an instability having amplitude $\Delta p/\bar{p} = 0.115$. Note that the secondary peaks in the waveform suggest that the motion could be accurately represented by a superposition of five normal modes. Thus the observations lend support of the general model used in this book. A clear case for comparison is the example cited in Section 6.11, especially Figure 6.22.

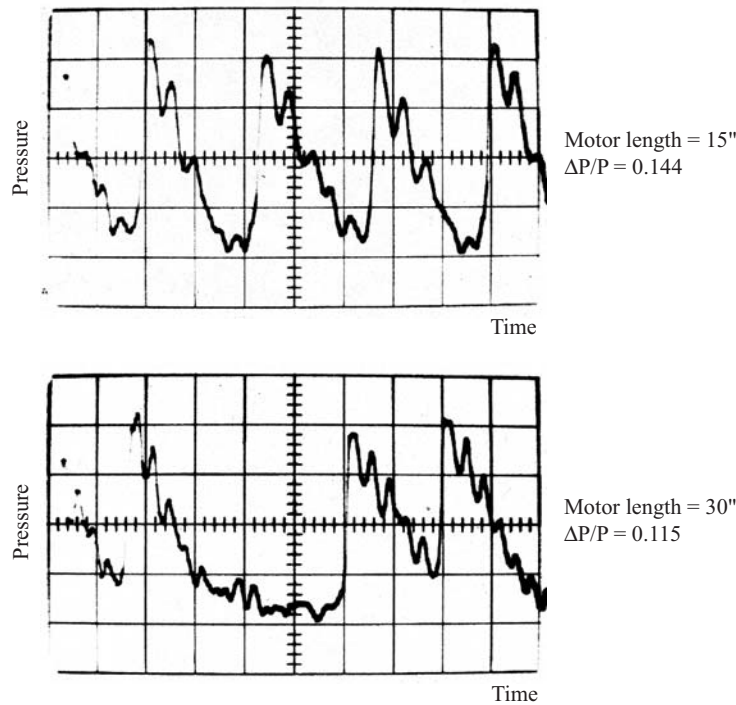


FIGURE 7.7. Waveforms observed in a gas rocket (Schob, Glassman and Webb 1963).

Sirignano (1968) analyzed the same problem using essentially the same computational methods. The main difference between that work and the calculations he did with Crocco, just mentioned, was the expression of the boundary condition at the head end,

$$\frac{\partial}{\partial t} \frac{T'}{\bar{T}} = A \frac{T'}{\bar{T}} + B \frac{p'}{\bar{p}} \quad (7.4)$$

The relation $\partial/\partial t(T'/\bar{T}) \sim A(T'/\bar{T})$ inserts a time lag in the response at the head end, distinguishing this analysis in an important qualitative way.⁶ Numerical values of A and B were set according to the model for a flame response worked out by Krier *et al.* (1968). Then the results represent an approximation to the periodic motion of a shock wave in an end-burning solid propellant rocket. The behavior found is, not surprisingly, similar to that reported by Sirignano and Crocco. The idea that “information about the combustion process can be determined by experimental observation of the nonlinear waveforms” while appealingly suggested by the calculations, seems never to have been realized in practice, for any system. Mitchell, Crocco and Sirignano (1969) also examined essentially the same problem, but used a method similar to that worked out by Chester (1964).

Zinn (1966, 1968) seems to have been first in the U.S. to treat nonlinear motions not entirely in the axial direction.⁷ While still analyzing the same problem shown in Figure 7.6—but, importantly, without a shock wave—he calculated results for a class of three-dimensional unsteady motions. The flow was taken to be irrotational, a restriction which can be serious under certain conditions as noted elsewhere in this book (see Chapters 3 and 4). As for most of the Princeton analyses of combustion instabilities, the $n - \tau$ model was assumed for the unsteady combustion response. Zinn obtained some results which were interpreted to

⁶In his thesis, Sirignano (1964a) had already accounted for a time lag, following earlier work on the linear problem by Crocco in several papers, and by Crocco and Cheng (1956).

⁷See also Zinn and Crocco (1967, 1968) for further details.

represent triggering but their meaning and value are doubtful because the motions were apparently found to be unstable.

First in his thesis and subsequently in collaboration with Crocco and Sirignano, Mitchell (1967) was the last of the Princeton students to analyze the problem sketched in Figure 7.6. He based his analysis on the recent work of Chester (1964) which gives results more simply than a method using characteristics, but cannot be used to study three-dimensional motions. A second advantage of the method, compared with the previous Princeton works, is the possibility of treating continuously distributed combustion. As Table 7.1 shows, Mitchell was able to treat a wider span of nonlinear problems than his predecessors at Princeton. However, his work still suffered from several serious deficiencies, notably the restriction to the $n - \tau$ model of combustion. It is not apparent from the analyses that the combustion model can easily be changed without embarking on a totally fresh analysis.

Mitchell also attempted to obtain results for triggering. However, it appears that his results share some of the same difficulties with the other Princeton works of this period. The most serious problem is that the process called ‘triggering’ does not produce a final state having a finite amplitude. That is, when pulsed, the system initially in a state of steady oscillation makes a transition to a condition in which the amplitude of oscillation grows without limit. Whether this sort of behavior should usefully be called ‘triggering’ is arguable. The definition followed in the present work is the conventional choice that triggering involves a subcritical bifurcation for which the final state is one of steady oscillation.

The theoretical ideas and approach to analyzing combustion instabilities originated by Crocco in the early 1950s dominated the field for many years in the U.S. More than three decades later the time lag was still used by some as the basis for understanding and for developing new liquid rocket engines, as discussion in Section 2.3 has shown. It is probably not an unfair characterization to note that the ideas were applied beyond their level of usefulness; progress in the design of certain aspects of liquid rockets was likely hindered. Alternative approaches were of course proposed (see Harrje and Reardon 1972) but for various reasons they were not developed extensively.

It seems that greater emphasis in the Soviet Union and Russia was placed on fundamental work directed to understanding details of the causes of instabilities. Theoretical, and some experimental, work is described in the book by Natanzon (1999). Much of the Russian experience with testing as part of liquid rocket development has been summarized by Dranovsky (2006). A discussion of those works is outside the intent of this book, but they are primary references and cannot be ignored.

Closer to the topic of the present chapter is the recent paper by French (2004). That report is a summary of progress for a program devoted to software development for predicting nonlinear combustion instabilities in solid propellant rockets. Much of the program is based on methods described in this book. The main purpose of the work is to produce a computer program capable of providing quantitative results for solid propellant rockets having quite general configurations. An example showing the growth of a finite, smooth disturbance into a steep-fronted wave is shown in Figure 7.8. That result shows clearly that the method developed here in Chapters 3–5 applies quite well to waves characterized by large gradients as well as to less abrupt disturbances.

Many computer programs have been written to compute various aspects of combustion instabilities in propulsion systems. In the past ten–fifteen years there has been increasing use of large eddy simulations (LES) to investigate flows in combustion chambers. Especially, applications to unsteady problems in gas turbines have been reported, with increasingly successful simulations of actual results found experimentally. Our purpose here is to examine some results found with the method developed in this book. The approach, based on expansion in modes and spatial averaging, seems to lend itself more effectively to understanding the physical behavior than to accurate simulation of the flows.

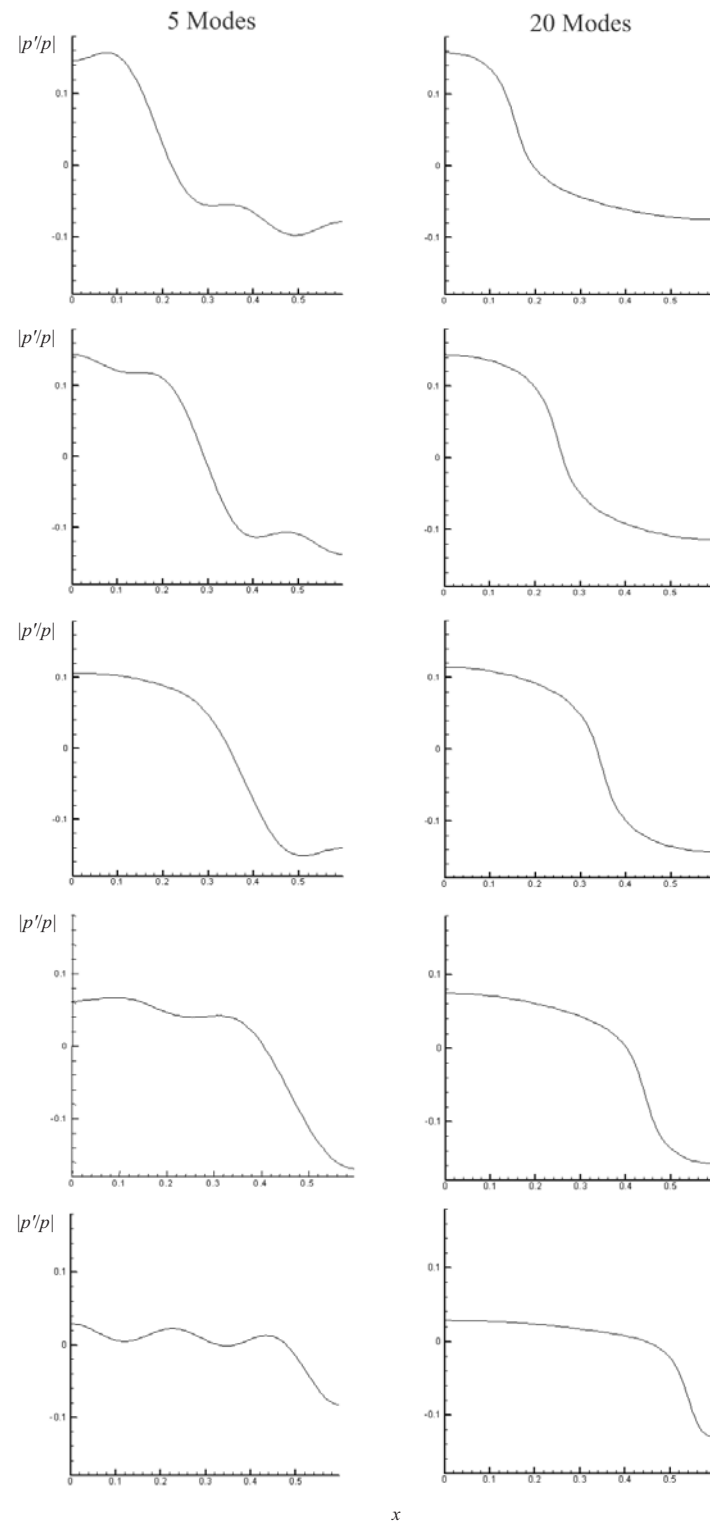


FIGURE 7.8. Steepening of a longitudinal wave travelling in a cylindrical chamber; $|p'/p|$ vs. x (French 2004).

7.2. A Single Nonlinear Mode

Interpretation of nonlinear behavior with a single mode is a sensible first step. For some purposes such a simple representation may be adequate, but experience has demonstrated that description of actual behavior must be based on more general models. The first attempt to treat a combustion instability as a single mode with the point of view taken here was Culick's (1971), an extension of earlier work on linear problems (see Sections 4.1–4.3).

Many observations suggested that point of view, but one of the clearest and most persuasive has been reproduced as Figure 1.36, taken from an oscillograph record (Perry 1970). Figure 7.9 is a drawing of the amplitude measured on Figure 1.36.

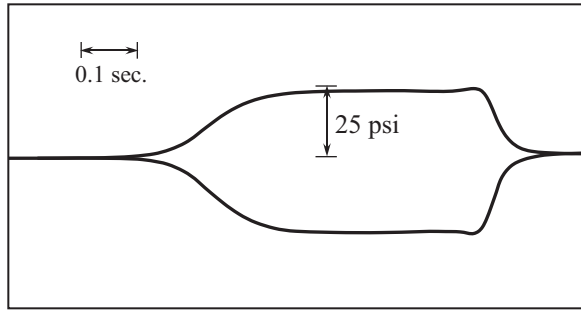


FIGURE 7.9. The envelope of oscillations for the T-burner firing shown in Figure 1.36 (Culick 1971).

The amplitude of the unstable pressure oscillation in a T-burner initially grows exponentially; levels off due to some nonlinear process; executes a limit cycle having approximately constant amplitude; and finally decays exponentially after the driving ceases, due mainly to combustion processes. The idea for a simple model of this motion was that the pressure in the burner always had the spatial distribution of the fundamental mode, $\psi(\mathbf{r})$, but with time-dependent amplitude $\eta(t)$. Thus the basic assumption was made that the pressure could be written in separable form,

$$p(\mathbf{r}, t) = \eta(t)\psi(\mathbf{r}) \quad (7.5)$$

At the time the analysis was done, the full theoretical apparatus developed here in Chapters 3 and 4 was not available. A procedure of spatial averaging was applied, similar to the method discussed in Chapter 4 but in a much simplified form. The most important difference is that nonlinear gasdynamics was not treated. Only the damping processes were ultimately taken to be nonlinear and the wave equation for the amplitude $\eta(t)$ took the form

$$\frac{d^2\eta}{dt^2} + \dot{\eta}f(\eta, \dot{\eta}) + \omega^2\eta = 0 \quad (7.6)$$

It seemed reasonable on physical grounds to assume that $f(\eta, \dot{\eta})$ had a simple form representing possible elementary physical processes,

$$f(\eta, \dot{\eta}) = -2\alpha + \beta_1|\eta| + \beta_2\eta^2 + \gamma_1|\dot{\eta}| + \gamma_2\dot{\eta}^2 \quad (7.7)$$

Moreover, again based on experimental results, the amplitude was approximated by a sinusoid having fixed frequency ω but time-dependent amplitude $A(t)$ and phase $\varphi(t)$ to be determined,

$$\eta(t) = A(t)\sin(\omega t + \varphi(t)) \quad (7.8)$$

Familiar procedures worked out by Krylov and Bogoliubov (1947) and covered here in Section 4.5, then led to first order equations for $A(t)$ and $\varphi(t)$. For $f(\eta, \dot{\eta})$ given by (7.7), those results are

$$-\frac{1}{A} \frac{dA}{dt} = -\alpha + c_1 A + c_2 A^2 \quad (7.9)$$

$$\frac{d\varphi}{dt} = \frac{\gamma_1}{4\pi} A \quad (7.10)$$

where

$$\begin{aligned} c_1 &= \frac{2}{3\pi} (\beta_1 + 2\gamma_1\omega) \\ c_2 &= \frac{1}{8} (\beta_2 + \frac{3\gamma_2}{4}\omega^2) \end{aligned} \quad (7.11)a,b$$

Equation (7.9) can be integrated by first factoring the right-hand side to give

$$\frac{dA}{dt} = -c_2(A - A_1)(A - A_2)A$$

of which the integral is

$$\frac{A}{A_0} \left(\frac{A_0 - A_1}{A - A_1} \right)^{a_1} \left(\frac{A_0 - A_2}{A - A_2} \right)^{a_2} = e^{\alpha t} \quad (7.12)$$

with

$$\begin{aligned} a_1 &= \frac{2\kappa}{(1 + 4\kappa) - \sqrt{(1 + 4\kappa)}} \\ a_2 &= \frac{2\kappa}{(1 + 4\kappa) + \sqrt{(1 + 4\kappa)}} \end{aligned} \quad (7.13)a,b$$

and $\kappa = \alpha c_2 / c_1^2$. The amplitude at $t = 0$ is A_0 .

Very good and promising results were obtained by Culick (1971) with a linear correction to the attenuation coefficient, $\beta_2 = \gamma_2 = c_2 = 0$ so the right-hand side of (7.9) is $-\alpha + c_1 A_1$. Then one finds the simple results

$$\text{growth } (\alpha > 0) \quad \frac{A}{A_m} = \frac{\zeta e^{\frac{|\alpha|}{t}}}{1 + \zeta e^{|\alpha|t}} \quad (7.14)$$

$$\text{decay } (\alpha < 0) \quad \frac{A}{A_m} = \frac{\zeta e^{-\frac{|\alpha|}{t}}}{1 - \zeta e^{-|\alpha|t}} \quad (7.15)$$

with

$$\text{growth} \quad \zeta = \frac{A_0/A_m}{1 - A_0/A_m} \quad (7.16)$$

$$\text{decay} \quad \zeta = \frac{A_0/A_m}{1 + A_0/A_m} \quad (7.17)$$

For the growth of waves, after a long time ($t \rightarrow \infty$), the limiting amplitude is

$$A(t \rightarrow \infty) = \frac{\alpha}{c_1} = \frac{3\pi\alpha}{2|\beta_1 + 2\gamma_1\omega|} = A_m \quad (7.18)$$

Thus the limiting amplitude is independent of the initial amplitude A_0 as it should be if the limit cycle is unique.

The growth or decay rates for the case $\beta_2 = \gamma_2 = 0$, expressed as logarithmic slopes, are

$$\frac{1}{A} \frac{dA}{dt} = \begin{cases} \frac{|\alpha|}{1+\zeta e^{|\alpha|t}} & (\text{growth}) \\ \frac{-|\alpha|}{1-\zeta e^{-|\alpha|t}} & (\text{decay}) \end{cases} \quad (7.19)\text{a,b}$$

which for short and long times become

$$t \rightarrow 0 : \quad \frac{1}{A} \frac{dA}{dt} \rightarrow \begin{cases} \frac{|\alpha|}{1+\zeta} & (\text{growth}) \\ \frac{-|\alpha|}{1-\zeta} & (\text{decay}) \end{cases} \quad (7.20)$$

$$t \rightarrow \infty : \quad \frac{1}{A} \frac{dA}{dt} \rightarrow \begin{cases} 0 & (\text{growth}) \\ -|\alpha| & (\text{decay}) \end{cases} \quad (7.21)$$

Three interesting conclusions follow from (7.18) and (7.19)a,b:

- (i) Both $|A_m|$ and $(d \ln A / dt)_{t \rightarrow 0}$ are proportional to $|\alpha|$; hence the initial growth rate and final amplitude increase together with $|\alpha|$. Because α represents the difference between linear driving and attenuation, increased driving produces both a larger initial growth rate and a larger final amplitude.
- (ii) If the nonlinear damping is increased, the final amplitude is reduced. The initial growth rate is unaffected.
- (iii) For a given $|\alpha|$ (i.e., linear contributions) and amplitude prior to decay, the initial decay rate is greater if the nonlinear coefficient of attenuation (c_1) is increased.

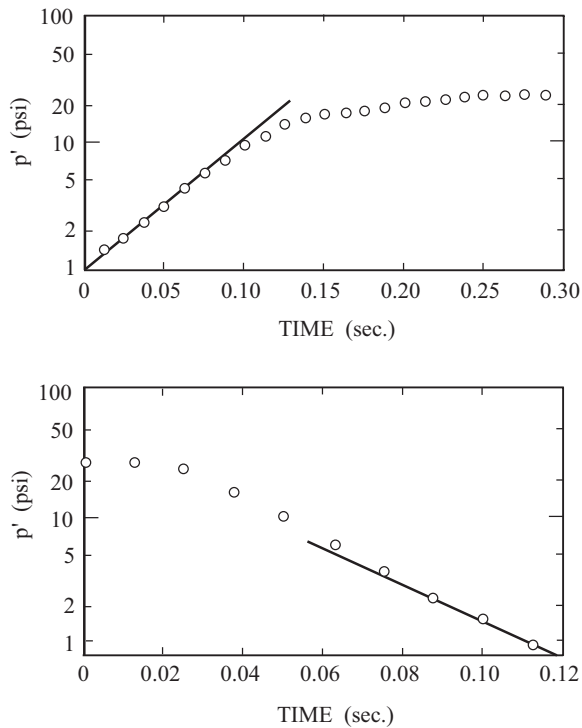


FIGURE 7.10. Data for the growth and decay periods of the firing shown in Figure 7.9.

Test data taken from the firing shown in Figure 7.9 are plotted in semi-logarithmic coordinates, Figure 7.10. The slopes of the lines shown are the values of α_g during the growth period and of α_d during decay. Figures 7.11 and 7.12 are plots of the data taken during the growth and decay periods, in coordinates giving a direct comparison with the simple theory outlined above. Apparently the behavior during both periods is quite well reproduced by this simple theory.

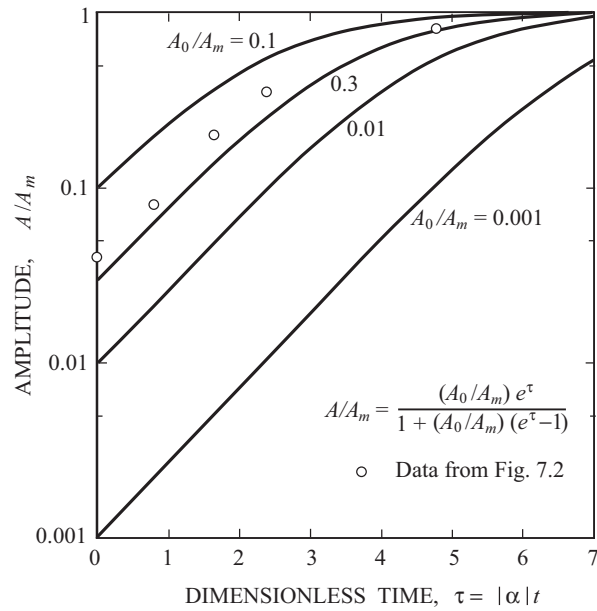


FIGURE 7.11. Nonlinear growth of oscillations for several values of the initial amplitude ratio A_0/A_m (Culick 1971).

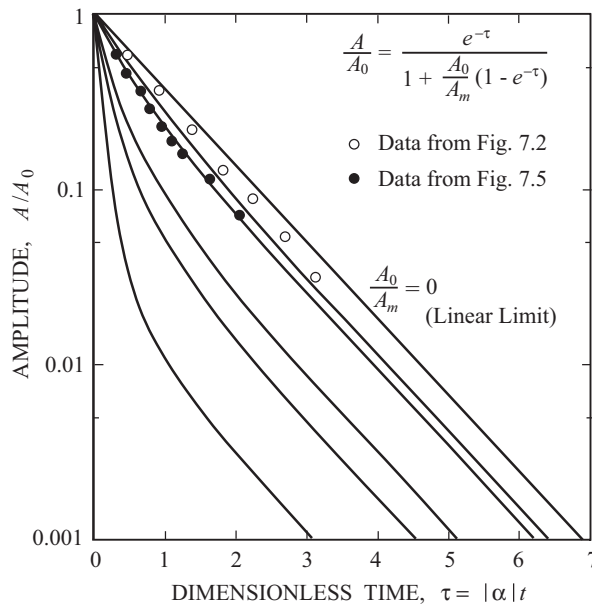


FIGURE 7.12. Nonlinear decay of oscillations for several values of the initial amplitude ratio A_0/A_m (Culick 1971).

In several respects the behavior examined in the preceding example is not a particularly difficult test of the theory worked out here. In the original work, consideration of the relatively low amplitudes present in the test discussed with Figures 7.9 to 7.12 was already recognized as a restriction. A T-burner firing at lower frequency (600 Hz, whereas the frequency of the oscillations in Figure 7.9 was 2800 Hz) exhibited more apparent nonlinear behavior, Figure 7.13. This aspect of the data was discussed in the paper, but a more important matter became clear only as the initial ideas were applied to more cases.

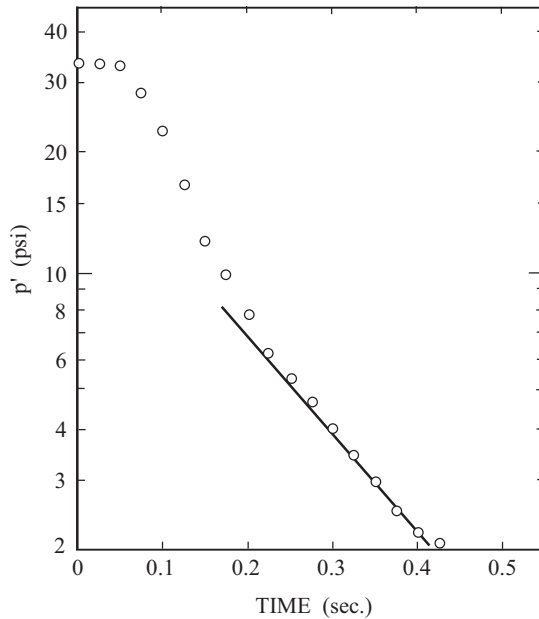


FIGURE 7.13. A T-burner firing showing stronger nonlinear behavior during the initial portion of the decay of oscillations (Culick 1971).

Immediately following the accomplishments just described, a project was begun to analyze available T-burner data to obtain values of the parameters arising with nonlinear behavior. The intent was to discover trends of the values with characteristics such as propellant composition, pressure and frequency; and eventually to attach physical meanings to the results. Considerable data was available so there was ample opportunity for enforcing consistency of the results. Although the initial results were good, a difficulty slowly became clear: A given set of data could equally well be represented by several combinations of the parameters $\beta_1, \gamma_1, \gamma_2, \dots$. Other choices of parameters exhibited the same property. Thus it was apparently not possible to settle on unique values of empirically determined parameters. That approach to understanding nonlinear behavior failed.

As part of the effort required to carry out the failed program, it was necessary—better expressed, the opportunity was provided—to examine spectra of T-burner records. What became particularly apparent was that records which previously had been treated as ‘clean’, that is consisting of single frequencies, in fact often contained noticeable amounts of harmonics. That was the beginning of the author’s research on systems having many degrees of freedom and concern with the importance of harmonics in combustion instabilities. The simplest case is a system having only two degrees of freedom discussed in the next section.

Representation of dynamical behavior with a single degree of freedom is enormously appealing. Not only is understanding greatly aided, but graphical representation is particularly simplified. The classic book by Minorsky (1947) contains many examples of the methods of presenting the behavior of a system. Awad (1983) and Awad and Culick (1986) used the phase plane in their discussion of nonlinear behavior. The procedure was later used by Beckstead (1987) to describe possible mechanisms. However, since the approach

is useful only for a small number of degrees of freedom, its applications are limited and, as the following remarks show, the results can be mortally misleading if the limitations are not respected.

The phase plane is usually defined with a dependent variable (displacement, say) and its rate of change (i.e., velocity) as coordinates. Thus, the equations produced by the method of averaging (Section ____) are directly applicable. As the simplest example, consider again the case treated above. The amplitude of the motion obeys (7.9) which can be written, to second order:

$$\frac{dA}{dt} = 2\alpha A + bA^2 = kA(A_1 - A) \quad (7.22)$$

If this is taken to serve as an approximation to the behavior we are concerned with here, then the second order term, bA^2 , in some sense represents the effects of second order acoustics. The integral of (7.22) is

$$A = \frac{A_1}{1 + \left(\frac{A_1}{A_0} - 1\right) e^{-\alpha t}} \quad (7.23)$$

where A_0 is the initial value of A and $kA_1 = 2\alpha$. We take A to be positive, so two possibilities exist, corresponding to $kA_1 = 2\alpha$ positive or negative. Figure 7.14 shows examples for $\alpha > 0$ ('spontaneous' instability) and $\alpha < 0$ (linear stability).

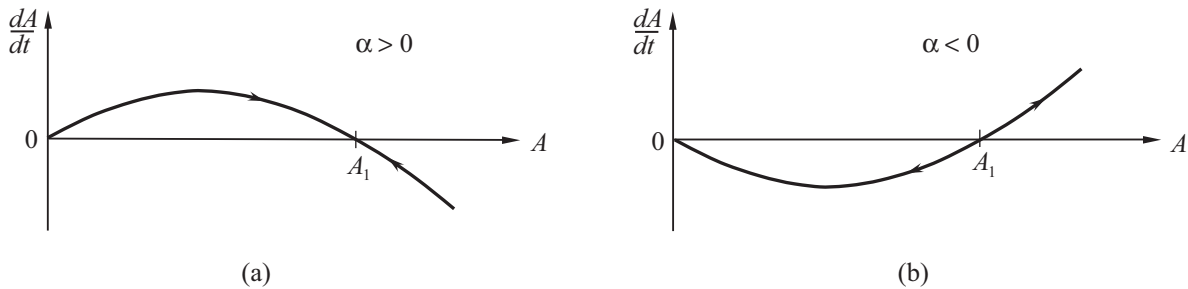


FIGURE 7.14. The two cases presented by equation (7.22).

In the case $\alpha > 0$, Figure (7.14)a, motions having any initial amplitude are unstable and eventually reach the limit amplitude A_1 . This is the same behavior found with the second order acoustics equations accounting for many modes. The approximate model seems to be promising. However, the promise is tarnished for the case $\alpha < 0$, as shown in Figure (7.14)b; if the initial amplitude A is greater than A_1 , the 'limit cycle' grows without limit. This behavior is not found with the complete equations (Chapter 4) for many degrees of freedom discussed in the next section.

In the late 1970s, and later, concern grew with pulsed instabilities in solid rockets. It was logical to determine first what might be predicted by the model for a single mode. The equation for a single mode, now governed by third order acoustics, is

$$\frac{dA}{dt} = kA(A_1 - A)(A_2 - A) \quad (7.24)$$

in which $kA_1 = 2\alpha$ again. A second possible form is

$$\frac{dA}{dt} = kA(A^2 - A_1^2) \quad (7.25)$$

The typical plot of (7.25) looks similar to Figure (7.14) and so is not interesting. Equation (7.24) gives the two possibilities shown in Figure 7.15. For a linearly unstable mode, $\alpha < 0$, Figure 7.15(a), the behavior is similar to that for $A < A_2$. But if the initial amplitude is larger than A_2 , the motion grows without limit. This is contrary to the results of numerical calculation for cases covering many modes.

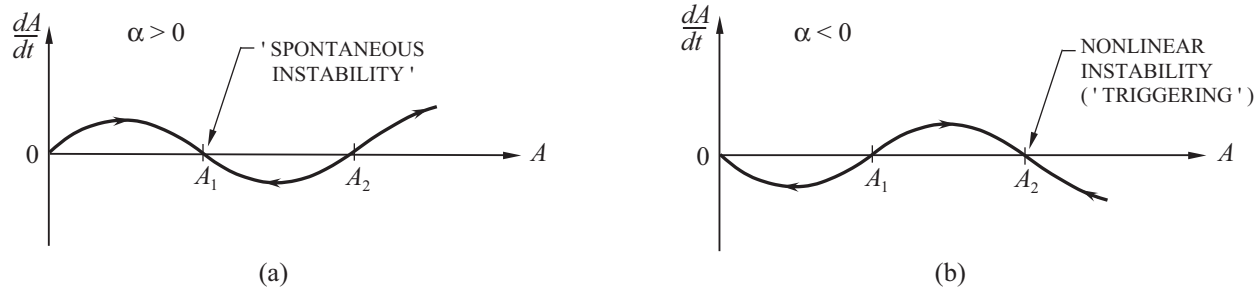


FIGURE 7.15. The two cases presented by equation (7.24). Part (b) represents a pulsed (triggered) instability.

For $\alpha < 0$, if the initial amplitude is less than A_1 , the system ultimately executes a limit cycle having amplitude A_2 . Thus, as shown by Figure 7.15(b), third order acoustics seem to hold the possibility of triggering.

That was an encouraging result, found at a time when interest in determining the condition for triggering, and hence learning how to avoid the phenomenon in practice, was particularly strong. Several analyses were carried out to determine how third order acoustics could be used to explain triggering (Awad 1983; Awad and Culick 1984, 1986; Yang and Culick 1986; Yang, Kim and Culick 1987, 1988, 1990). No cases of triggering were found in many examples worked out for a range of realistic conditions. It is important that those results were obtained for systems containing two or more modes.

The conclusions of several years' effort, reached not on theoretical grounds but purely by trial and error 'numerical experimenting', was that nonlinear acoustics alone did not contain the possibility of triggering to a stable limit cycle. That was an important result (albeit not strictly proved) because it implied that another nonlinear process had to be taken into account. Combustion was the obvious candidate. The matter was far from settled, however, even on practical grounds. Further exploration showed that rather special characteristics of nonlinear combustion are required. Culick, Burnley and Swenson (1995) showed that nonlinear combustion and gasdynamics together could be used to demonstrate the possibility of triggering; Burnley (1996) discussed further details in his dissertation. See also Section 7.14 here. One practical implication is that understanding pulsed instabilities requires more thorough experimental results for nonlinear characteristics—particularly of unsteady combustion—than have been obtained to date.⁸

From the practical point of view, the procedures involved here have not been developed to the level required for convenient application. And with the complications accompanying analysis accounting for two or more degrees of freedom, a simpler approach is desirable. The approximation based on a single degree of freedom is undeniably attractive. Jensen (1972), Beckstead and Jensen (1972) and Beckstead (1987) have pursued this approach, and its application to the behavior of instabilities in solid propellant rockets, further than others working in the field. They have obtained some appealing results and have emphasized several practical aspects. However, their conclusions must be viewed with caution, since they are based on a strictly flawed model having a single degree of freedom.

⁸The results cited here have apparently been obtained largely for solid propellant rockets. However, because of the generality of the procedures developed in Chapters 3 and 4, the discussion and conclusions apply equally well to any combustion system of the form treated.

7.3. The Two-Mode Approximation

This is the simplest class of problems for which nonlinear mode coupling is accommodated. Each mode is characterized by two constants: α (energy gain or loss) and θ (frequency shift). The energy gain or loss may be nonlinear—that is, α could in principle depend on amplitude—but here both α and θ are taken to be constant, characterizing entirely the linear processes. As a result of several works in the past few years, the two-mode approximation is quite well understood (Awad and Culick, 1986; Paparizos and Culick, 1989; Yang and Culick 1990; Jahnke and Culick, 1994; Culick, 1994).

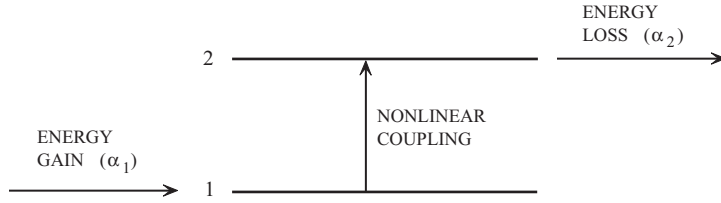


FIGURE 7.16. Energy flow in the two-mode approximation.

Only gasdynamic nonlinearities to second order are accounted for here. Their special structure allows the convenient closed form solutions to the time-averaged equations, first found by Awad (1983). The results provide much basic understanding which is applicable to more complicated nonlinear problems. For example, contrary to one's expectation based on the behavior of shock waves, nonlinear behavior in the present context need not involve large amplitudes, and the pressure oscillation may appear to be a clean sinusoid, free of significant harmonic content. The basic reason is that here the two-mode system both gains and loses energy; each interaction with the environment is necessary. Moreover, both stable and unstable limit cycles exist. In the absence of nonlinear modal coupling, or some other nonlinear process, limit cycles cannot exist.

Truncation of the modal expansion to two modes introduces errors because the flow of energy to higher modes is blocked. The amplitude of the highest mode is therefore greater than the correct value in order to provide the higher linear rate of energy loss required to sustain a limit cycle. The example in Section 6.11 showed this effect.

It's an interesting feature of the two-mode approximation that with linear gains and losses of energy, nonlinear instability (pulsing) to stable limit cycles seems not to exist. Although no rigorous proof exists, experience with many examples has shown that conclusion to be quite generally true for any number of modes if only the acoustic (gasdynamics) nonlinearities are accounted for. 'Triggering' or pulsing to stable limit cycles does occur for special forms of nonlinear energy gain from the environment (i.e., extraction from the mean flow or supply from combustion processes) as the example in Section 7.11 shows. By 'triggering' we mean here pulsing **from** a quiescent initial state or a stable limit cycle, **to** a stable limit cycle. More generally, one can imagine triggering from one stable limit cycle to another.

If we ignore linear mode coupling and account for acoustic nonlinearities to second order, the oscillator equations can be put in the form

$$\frac{d^2\eta_n}{dt^2} + \omega_n^2 \eta_n = \alpha_n \dot{\eta}_n + \theta_n \eta_n - \sum_{i=1}^{\infty} \sum_{j=1}^{\infty} [A_{nij} \dot{\eta}_i \dot{\eta}_j + B_{nij} \eta_i \eta_j] + F_n^{NL} \quad (7.26)$$

where F_n^{NL} represents other nonlinear contributions. The coefficients A_{nij} , B_{nij} are defined as integrals involving the basis functions ψ_{nij} . Hence their values are fixed primarily by the geometry of the chamber in question. See Section 4.5 and Culick (1976) for additional details of the derivation of (7.26). It is a crucially important result that the nonlinear gasdynamic terms involve no cross products $\dot{\eta}_i \eta_j$ and also (not obvious

here) no ‘self-coupling’, terms proportional to $\dot{\eta}_n^2$ or η_n^2 . Those properties seem to be the formal reasons that nonlinear (pulsed) instabilities do not exist if only these nonlinearities are included, particularly when the combustion processes are linear.

Equation (7.26) simplifies considerably for longitudinal modes. Due to orthogonality and special properties of the $\cos k_n z$, the double sum becomes a single sum and (7.26) can be put in the form (Jahnke and Culick 1994):

$$\begin{aligned} \frac{d^2\eta_n}{dt^2} + \omega_n^2\eta_n &= \alpha_n\dot{\eta}_n + \theta_n\eta_n - \sum_{i=1}^{\infty} \left[C_{ni}^{(1)}\dot{\eta}_i\dot{\eta}_{n-i} + D_{ni}^{(1)}\eta_i\eta_{n-i} \right] \\ &\quad - \sum_{i=1}^{\infty} \left[C_{ni}^{(2)}\dot{\eta}_i\dot{\eta}_{n+i} + D_{ni}^{(2)}\eta_i\eta_{n+i} \right] + F_n^{NL} \end{aligned} \quad (7.27)$$

The time-averaged forms of (7.27) are

$$\begin{aligned} \frac{dA_n}{dt} &= \alpha_n A_n + \theta_n B_n + \frac{n\beta}{2} \sum^i [A_i(A_{n-i} - A_{i-n} - A_{i+n}) - B_i(B_{n-i} - B_{i-n} - B_{i+n})] \\ \frac{dB_n}{dt} &= -\theta_n A_n + \alpha_n B_n + \frac{n\beta}{2} \sum^i [A_i(B_{n-i} - B_{i-n} - B_{i+n}) - B_i(A_{n-i} - A_{i-n} - A_{i+n})] \end{aligned} \quad (7.28)a,b$$

where, as in Chapter 3, $\eta_n = A_n \cos \omega_n t + B_n \sin \omega_n t$. For longitudinal modes, the frequencies are all integral multiples of the fundamental, a property that is crucial to the forms of (7.28)a,b. For example, for transverse modes in a cylindrical chamber, the nonlinear terms contain factors representing modulation.

For two modes, the four first order equations are

$$\begin{aligned} \frac{dA_1}{dt} &= \alpha_1 A_1 + \theta_1 B_1 - \beta(A_1 A_2 - B_1 B_2) \\ \frac{dB_1}{dt} &= \alpha_1 B_1 + \theta_1 A_1 + \beta(B_1 A_2 - A_1 B_2) \\ \frac{dA_2}{dt} &= \alpha_2 A_2 + \theta_2 B_2 + \beta(A_1^2 - B_1^2) \\ \frac{dB_2}{dt} &= \alpha_2 B_2 + \theta_2 A_2 + 2\beta B_1 A_1 \end{aligned} \quad (7.29)a,b,c,d$$

The great advantage of this system of equations is that some useful exact results can be found. One way to find them is to change independent variables to the amplitude and phases (r_n, ϕ_n) of the two modes by writing

$$\begin{aligned} \eta_1(t) &= r_1(t) \sin(\omega_1 t + \phi_1) \\ \eta_2(t) &= r_2(t) \sin(2\omega_1 t + \phi_2) \end{aligned}$$

where $r_n = \sqrt{A_n^2 + B_n^2}$. The governing equations for r_1, r_2 and the effective relative phase $\psi = 2\phi_1 - \phi_2$ are

$$\begin{aligned} \frac{dr_1}{dt} &= \alpha_1 r_1 + \beta r_1 r_2 \cos \psi \\ \frac{dr_2}{dt} &= \alpha_2 r_2 + \beta r_1^2 \cos \psi \\ \frac{d\psi}{dt} &= (\theta_1 - 2\theta_2) + \beta(2r_1 - \frac{r_1^2}{2} \sin \psi) \end{aligned} \quad (7.30)a,b,c$$

where

$$\beta = \frac{\theta_2 - 2\theta_1}{2\alpha_1 \alpha_2} \quad (7.31)$$

The problem of linear stability is solved directly:

$$\alpha_1, \alpha_2 < 0 \iff \text{small amplitude motions are stable} \quad (7.32)$$

7.3.1. Existence of Limit Cycles. Nonlinear behavior in general poses two basic questions:

- (i) What are the conditions for existence of limit cycles?
- (ii) What are the conditions that the limit cycles are stable?

Stability of a limit cycle of course is a matter entirely separate from the linear stability of small amplitude motions. We are concerned here with a system executing a steady limit cycle. If the limit cycle is stable, then if slightly disturbed, the motion will eventually return to its initial form.

In this time-averaged formulation, existence of limit cycles corresponds to existence of stationary or equilibrium points of the system (7.30)a,b,c:

$$\frac{dr_1}{dt} = \frac{dr_2}{dt} = \frac{d\psi}{dt} = 0 \iff \text{transcendental algebraic equations}$$

The solutions are

$$\begin{aligned} r_{10} &= \frac{1}{\kappa} \sqrt{-\alpha_1 \alpha_2 (1 + \beta^2)} \\ r_{20} &= \frac{1}{\kappa} \sqrt{\alpha_1^2 (1 + \beta^2)} \\ \psi_o &= \tan^{-1}(-\beta) \end{aligned} \quad (7.33)\text{a,b,c}$$

where

$$\kappa = \frac{\gamma + 1}{8\gamma} \omega_1 \quad (7.34)$$

For r_{10} to be real, $-\alpha_1 \alpha_2$ must be positive, implying that the constants α_1, α_2 must have opposite signs. The physical interpretation is that if the first mode is unstable, for example, ($\alpha > 0$), then the second mode must be stable ($\alpha_2 < 0$): the rate of energy flow into the first mode must equal the rate of loss from the second mode in order that the amplitudes be constant in time. The transfer rate upwards due to coupling must have the same value. Similar reasoning explains the case when the second mode is unstable, requiring that the first mode to be stable.

7.3.2. Stability of Limit Cycles. To determine the stability of limit cycles, the variables are written as $r_i = r_{i0} + r'_i$, $\psi = \psi_o + \psi'$ and substituted in the governing equations (7.29)a,b,c,d. The linearized equations for the disturbances are then solved for the characteristic value λ in the assumed forms $r'_i = r'_{i0} e^{\lambda t}, \dots$. For stability, an initial disturbance must decay. Applying that requirement produces regions of stability in the plane of the parameters $\beta_o = (\theta_2 - 2\theta_1)^2 / (\alpha_2 + 2\alpha_1)^2$ and α_2/α_1 , shown in Figure 7.17.

There is presently no basis for understanding why stable limit cycles occur only for the special ranges of parameters shown in Figure 7.17. However, more elaborate analysis (Jahnke and Culick 1994) has shown that the result that the stability region has boundaries for finite values of α_2 and α_1 is a consequence of time-averaging. That conclusion shows the importance for both practical and theoretical reasons of assessing and quantifying as far as possible the consequences of time-averaging and truncation. Considerable progress has been made in that direction by using a continuation method to solve the systems of oscillator equations. Some results are discussed in Section 7.7.

Here it is useful to examine the details of several special cases. Figure 7.18 shows that if the parameters are chosen so that the operating point lies within the range for stable limit cycles and the first mode is unstable, truncation may have relatively small effects. On the other hand, if the limit cycle is unstable

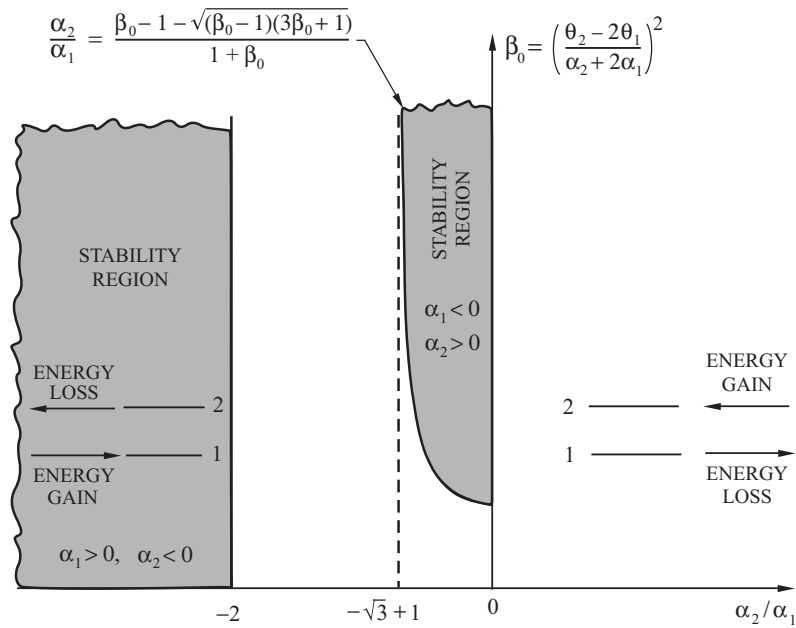


FIGURE 7.17. Regions of stability for two longitudinal modes, time-averaged equations (Awad and Culick 1986).

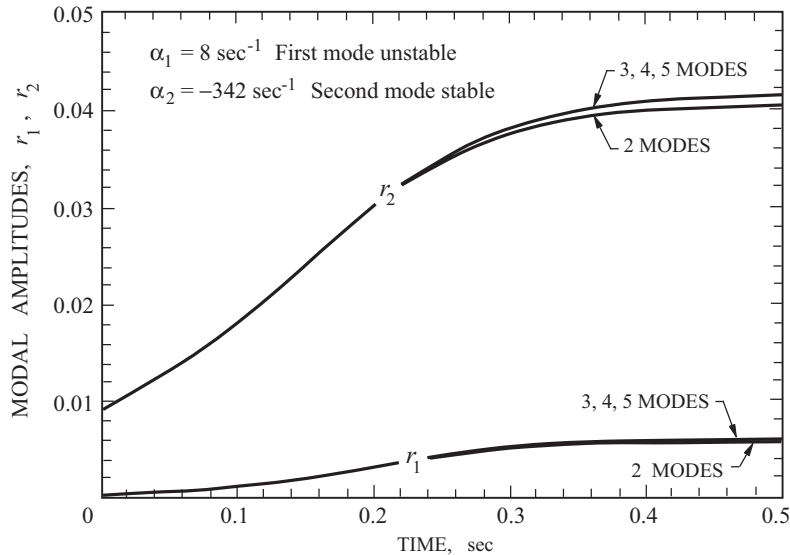


FIGURE 7.18. Effects of truncation for a stable limit cycle: first mode unstable, second mode stable (Paparizos and Culick 1989).

according to the two-mode approximation with an unstable first mode, it may become stable (with the same values of $\alpha_1, \alpha_2, \theta_1, \theta_2$) if higher stable modes are accounted for. That behavior is shown in Figure 7.19

Figure 7.20 is interesting for a quite different reason. In this case the second mode is unstable, and the motion evolves to a stable limit cycle. However, unlike the example in Figure 7.18, the amplitudes do not grow smoothly and monotonically to their values in the limit cycle. Their erratic behavior is due to the

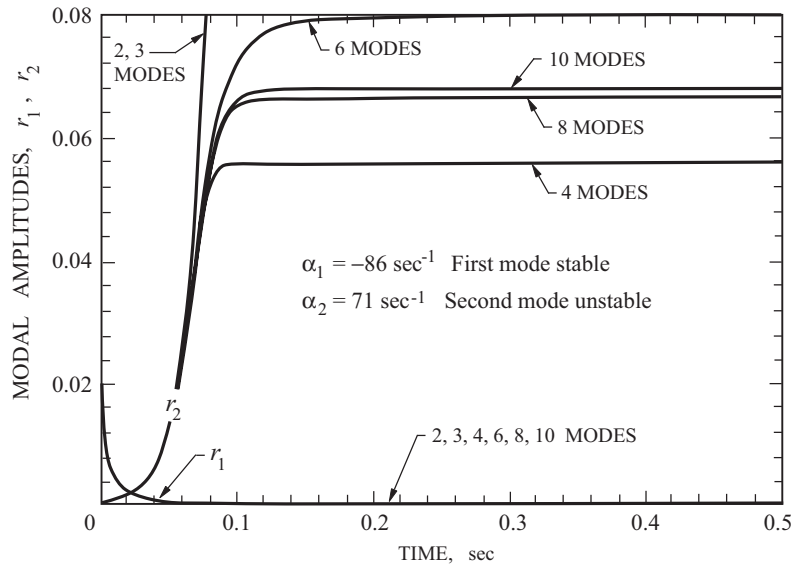


FIGURE 7.19. Effects of truncation for an unstable limit cycle: first mode unstable, second mode stable (Paparizos and Culick 1989).

fact that with the second mode unstable, energy must flow from high frequency to low frequency. That is contrary to the direction of flow imposed naturally by the fluid mechanics (of the steepening of a compressive disturbance into a shock wave). The conflict between the natural action of the nonlinear coupling on the one hand and the flow of energy imposed by energy exchange with the environment causes the amplitudes of the two modes to wander during the transient phase before finally reaching their ultimate values. More special cases are treated in the references. It is an important conclusion that truncation of the time-averaged equations for two modes will give misleading or incorrect results unless the initial state is close to the stability boundary.

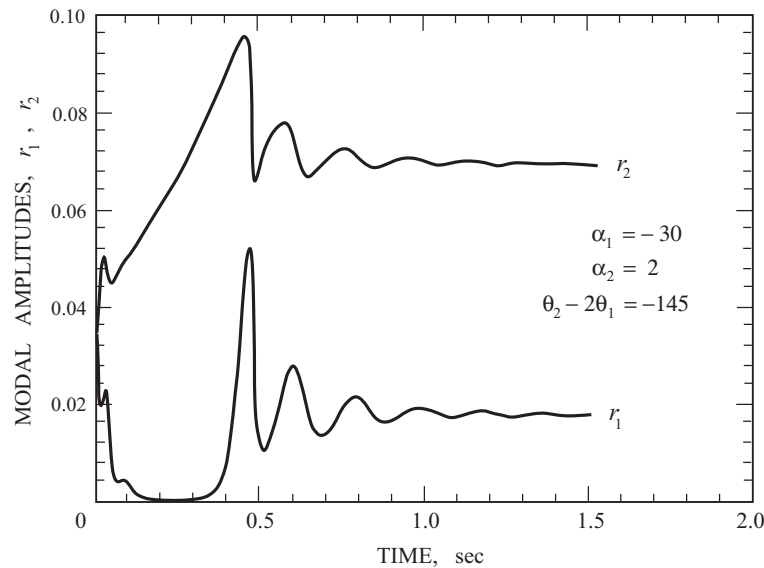


FIGURE 7.20. Development of a stable limit cycle when the first mode is stable but the second mode is unstable (Paparizos and Culick 1989).

7.4. Transverse Modes and the Method of Averaging

The term “transverse modes” refers to motions which are the simplest involving time-dependent velocity not aligned with the center-line of a straight chamber. Apart from a rectangular cross section, which is generally not a practical form for a combustion chamber, the most common geometry is a circular cylinder. Thus the classical unperturbed linear acoustic modes have the familiar separable form (Section 5.8.2), a product of a Bessel function of the radius, a trigonometric function of azimuthal angle, and a trigonometric or hyperbolic function of position along the axis. It has become customary in the field of combustion instabilities to call transverse modes any motion which has the same time variation for all degrees of freedom and the same spatial dependence in planes perpendicular to the axis of the chamber as for classical acoustic modes. We are concerned in this section with the time dependence of such motions. Their spatial forms define normal modes but the time-dependence is not simply trigonometric.

It seems a somewhat remarkable result that relatively simple conditions for existence and stability of transverse modes, in a circular cylinder, can be obtained by following the same approach used to treat purely longitudinal modes. The reason is that the time-averaged equations again have a special structure allowing construction of exact solutions for two modes. Furthermore, some results can be obtained for a special case of three modes as well. What makes these results surprising in a practical sense is that now the natural frequencies do not satisfy the conditions $\omega_n = n\omega$, and the time-averaged equations contain factors representing modulation on the right-hand side.

The set of equations valid for second order acoustics in a circular cylindrical chamber have been given by Yang and Culick (1990),

$$\begin{aligned} \dot{A}_n = & -\frac{1}{2\omega_n} \sum_{i=1}^{\infty} \{ c_{ni} [\cos(\omega_n + \omega_i)t + \cos(\omega_n - \omega_i)t] \\ & + s_{ni} [\sin(\omega_n + \omega_i)t - \sin(\omega_n - \omega_i)t] \} \\ & - \frac{1}{2\omega_n} \sum_{i=1}^{\infty} \sum_{j=1}^{\infty} \{ F_{nij} a_{ij} [\cos(\omega_n + \omega_{ij+})t + \cos(\omega_n - \omega_{ij+})t] \\ & + G_{nij} b_{ij} [\cos(\omega_n + \omega_{ij-})t + \cos(\omega_n - \omega_{ij-})t] \\ & - F_{nij} d_{ij} [\sin(\omega_n + \omega_{ij+})t + \sin(\omega_n - \omega_{ij+})t] \\ & + G_{nij} e_{ij} [\sin(\omega_n + \omega_{ij-})t + \sin(\omega_n - \omega_{ij-})t] \} , \end{aligned} \quad (7.35)$$

$$\begin{aligned} \dot{B}_n = & -\frac{1}{2\omega_n} \sum_{i=1}^{\infty} \{ C_{ni} [\sin(\omega_n + \omega_i)t + \sin(\omega_n - \omega_i)t] \\ & + S_{ni} [-\cos(\omega_n + \omega_i)t + \cos(\omega_n - \omega_i)t] \} \\ & + \frac{1}{2\omega_n} \sum_{i=1}^{\infty} \sum_{j=1}^{\infty} \{ F_{nij} a_{ij} [\sin(\omega_n + \omega_{ij+})t + \sin(\omega_n - \omega_{ij+})t] \\ & + G_{nij} b_{ij} [\sin(\omega_n + \omega_{ij-})t + \sin(\omega_n - \omega_{ij-})t] \\ & - F_{nij} d_{ij} [\cos(\omega_n + \omega_{ij+})t - \cos(\omega_n - \omega_{ij+})t] \\ & + G_{nij} e_{ij} [\cos(\omega_n + \omega_{ij-})t - \cos(\omega_n - \omega_{ij-})t] \} , \end{aligned} \quad (7.36)$$

where

$$\begin{aligned} \omega_{ij+} &= \omega_i + \omega_j; & \omega_{ij-} &= \omega_i - \omega_j; \\ C_{ni} &= \omega_i D_{ni} A_i + E_{ni} B_i; & S_{ni} &= -\omega_i D_{ni} B_i + E_{ni} A_i; \\ F_{nij} &= \omega_i \omega_j A_{nij} - B_{nij}; & G_{nij} &= \omega_i \omega_j A_{nij} + B_{nij}; \end{aligned}$$

$$\begin{aligned} a_{ij} &= \frac{1}{2}(A_i A_j - B_i B_j); & b_{ij} &= \frac{1}{2}(A_i A_j - B_i B_j); \\ d_{ij} &= \frac{1}{2}(A_i B_j - A_j B_i); & e_{ij} &= \frac{1}{2}(A_i B_j - A_j B_i). \end{aligned}$$

We follow the example worked out by Yang and Culick (1990) and consider three transverse modes: the first and second tangential and the first radial, having the following wave numbers and mode shapes:

First Tangential Mode (1T)

$$\kappa_1 R = 1.8412; \psi_1 = \cos \theta J_1(\kappa_1 r), \psi_4 = \sin \theta J_1(\kappa_1 r), \quad (7.37)$$

First Radial Mode (1R)

$$\kappa_2 R = 3.8317; \psi_2 = J_0(\kappa_2 r), \quad (7.38)$$

Second Tangential Mode (2T)

$$\kappa_3 R = 3.0542; \psi_3 = \cos 2\theta J_2(\kappa_3 r), \psi_5 = \sin 2\theta J_2(\kappa_3 r). \quad (7.39)$$

To simplify writing we have defined $\kappa_1 = \kappa_{11}$, $\kappa_2 = \kappa_{01}$, $\kappa_3 = \kappa_{21}$. The inclusion of both azimuthal eigenfunctions for tangential modes of oscillations allows the possibility of either standing or spinning waves, or a combination of both. Only standing modes will be treated here. The corresponding coefficients F_{nij} and G_{nij} , have non-zero values. Self-coupling terms therefore arise only in the equations for the radial mode, while the nonlinear behavior of the tangential modes is mainly determined by cross-coupling. However, the self-coupling terms in the equation for the radial mode drop out after time-averaging and do not affect the results obtained here.

We will treat standing transverse oscillations; only the mode functions ψ_1 , ψ_2 and ψ_3 need to be retained. Moreover, with time-averaging, terms containing oscillations at frequencies greater than half the normal frequencies drop out (see Yang and Culick 1990) and the equations for A_n and B_n become

First Tangential Mode (1T)

$$\begin{aligned} \frac{dA_1}{dt} &= \alpha_1 A_1 + \theta_1 B_1 \\ &+ a_1(A_1 A_2 + B_1 B_2) \cos \Omega_1 t + a_2(A_1 A_3 + B_1 B_3) \cos \Omega_2 t \\ &+ a_1(A_1 B_2 - A_2 B_1) \sin \Omega_1 t + a_2(A_1 B_3 - A_3 B_1) \sin \Omega_2 t, \end{aligned} \quad (7.40)$$

$$\begin{aligned} \frac{dB_1}{dt} &= -\theta_1 A_1 + \alpha_1 B_1 \\ &- a_1(A_1 A_2 + B_1 B_2) \sin \Omega_1 t - a_2(A_1 A_3 + B_1 B_3) \sin \Omega_2 t \\ &+ a_1(A_1 B_2 - A_2 B_1) \cos \Omega_1 t + a_2(A_1 B_3 - A_3 B_1) \cos \Omega_2 t, \end{aligned} \quad (7.41)$$

First Radial Mode (1R)

$$\frac{dA_2}{dt} = \alpha_2 A_2 + \theta_2 B_2 + b_1(A_1^2 - B_1^2) \cos \Omega_1 t - b_1(2A_1 B_1) \sin \Omega_1 t \quad (7.42)$$

$$\frac{dB_2}{dt} = -\theta_2 A_2 + \alpha_2 B_2 + b_1(A_1^2 - B_1^2) \sin \Omega_1 t - b_1(2A_1 B_1) \cos \Omega_1 t, \quad (7.43)$$

Second Tangential Mode (2T)

$$\frac{dA_3}{dt} = \alpha_3 A_3 + \theta_3 B_3 + b_2(A_1^2 - B_1^2) \cos \Omega_2 t - b_2(2A_1 B_1) \sin \Omega_2 t \quad (7.44)$$

$$\frac{dB_3}{dt} = -\theta_3 A_3 + \alpha_3 B_3 + b_2(A_1^2 - B_1^2) \sin \Omega_2 t - b_2(2A_1 B_1) \cos \Omega_2 t, \quad (7.45)$$

where

$$\begin{aligned}
 \alpha_n &= -\frac{D_{nn}}{2}; \quad \theta_n = -\frac{E_{nn}}{2\omega_n}, \quad n = 1, 2, 3; \\
 a_1 &= -\frac{1}{4\omega_1}(G_{112} + G_{121}) = 0.1570\left(\frac{\bar{a}}{R}\right); \\
 a_2 &= -\frac{1}{4\omega_1}(G_{113} + G_{131}) = -0.0521\left(\frac{\bar{a}}{R}\right); \\
 b_1 &= -\frac{1}{4\omega_2}F_{211} = -0.1054\left(\frac{\bar{a}}{R}\right); \\
 b_2 &= -\frac{1}{4\omega_3}F_{311} = 0.1873\left(\frac{\bar{a}}{R}\right); \\
 \Omega_1 &= 2\omega_1 - \omega_2 = -0.1493\left(\frac{\bar{a}}{R}\right); \\
 \Omega_2 &= 2\omega_1 - \omega_3 = 0.6282\left(\frac{\bar{a}}{R}\right)
 \end{aligned}$$

7.4.1. Periodic Limit Cycles for Transverse Modes.

(a) First Tangential and First Radial Modes.

Write $A_n(t)$ and $B_n(t)$ in terms of amplitude and phase, which serve as radial coordinates:

$$A_n(t) = r_n(t) \cos \Phi_n(t) \quad B_n(t) = r_n(t) \sin \Phi_n(t) \quad (7.46)a,b$$

Now substitute (7.46)a,b in (7.40)–(7.43), neglect the second tangential mode, and rearrange the results to give

$$\frac{dr_1}{dt} = \alpha_1 r_1 + a_1 r_1 r_2 \cos(2\Phi_1 - \Phi_2 + \Omega_1 t), \quad (7.47)$$

$$\frac{dr_2}{dt} = \alpha_2 r_2 + b_1 r_1^2 \cos(2\Phi_1 - \Phi_2 + \Omega_1 t), \quad (7.48)$$

$$\frac{d\Phi_1}{dt} = -\theta_1 - a_1 r_2 \sin(2\Phi_1 - \Phi_2 + \Omega_1 t), \quad (7.49)$$

$$\frac{d\Phi_2}{dt} = -\theta_2 - b_1 \frac{r_1^2}{r_2} \sin(2\Phi_1 - \Phi_2 + \Omega_1 t). \quad (7.50)$$

All of these equations have a common time-varying term $2\Phi_1 - \Phi_2 + \Omega_1 t$ in the sinusoidal functions. For convenience, we may combine (7.49) and (7.50) to simplify the analysis. Thus (7.47)–(7.50) reduce to

$$\frac{dr_1}{dt} = \alpha_1 r_1 + a_1 r_1 r_2 \cos X, \quad (7.51)$$

$$\frac{dr_2}{dt} = \alpha_2 r_2 + b_1 r_1^2 \cos X, \quad (7.52)$$

$$\frac{dX}{dt} = -2\theta_1 + \theta_2 + \Omega_1 - \left(2a_1 r_2 + b_1 \frac{r_1^2}{r_2}\right) \sin X, \quad (7.53)$$

where

$$X(t) = 2\Phi_1 - \Phi_2 + \Omega_1 t. \quad (7.54)$$

Figure 7.21 shows two results for different initial conditions. The eventual values of the amplitude are the same in the two cases, an example of the (apparently) general result for these equations that the limit cycle (if it exists) is independent of the initial conditions. The property has not been proved; it holds at most if the

only nonlinear process is given by the fluid mechanics, but seems not to be restricted only to second-order acoustics. Yang, Kim and Culick (1990) demonstrated the same result for third-order acoustics.

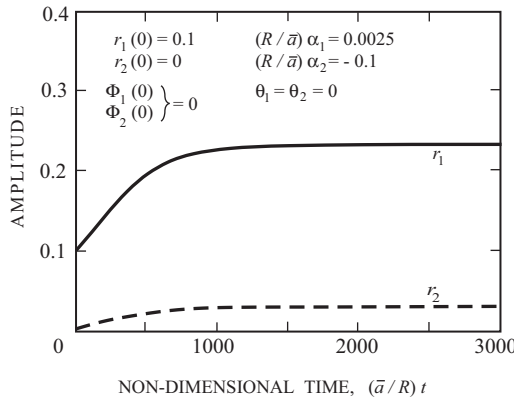
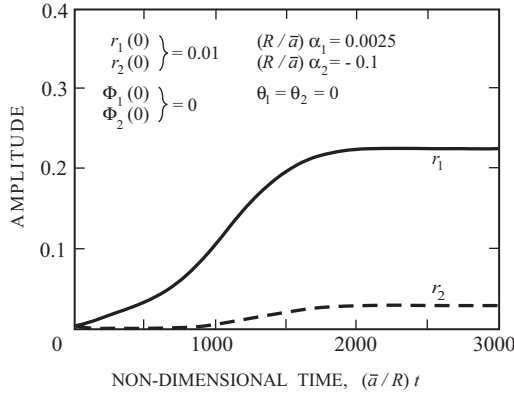


FIGURE 7.21. Amplitudes in two limit cycles involving the first tangential and first radial modes only, based on the time-averaged equations. The two cases are for different initial conditions (Yang and Culick 1990).

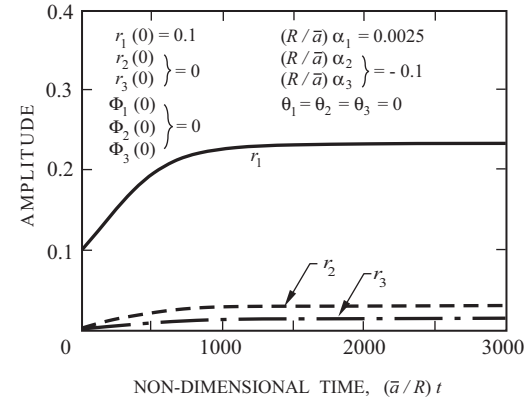
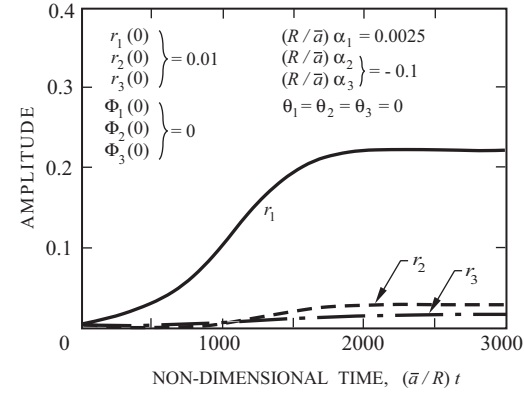


FIGURE 7.22. An example of limit cycles for three normal modes, 1T/1R/2T accounted for; two cases of initial conditions are shown (Yang and Culick 1990).

Although closed form solutions to (7.51)–(7.53) have not been found, a great deal of information can be gained by examining the conditions for periodic limit cycles. The idea is to seek solutions for r_1, r_2, X when they are independent of time, and formulate the conditions that must be satisfied for those solutions to be real. The procedure has been worked out by Yang and Culick (1990) giving $\alpha_1\alpha_2 < 0$, as shown already for two longitudinal modes; the condition must be true according to a physical argument already given. It also follows from the calculations that the amplitudes in the limit cycle are given as

$$\begin{aligned}\eta_{16} &= r_{20} \sin [(\omega_1 + \nu_1)t + \xi_1] \\ \eta_{20} &= r_{20} \sin [2(\omega_1 + \nu_1)t + \xi_2]\end{aligned}\quad (7.55)a,b$$

where ν_i and ξ_i are constants. Thus, the amplitude of the second mode oscillates at twice the frequency of the first mode *in the limit cycle*. This must be true for the limit cycle to be periodic. The result was first established by Powell (1970) and reported by Zinn and Powell (1971) for transverse modes.

The conditions for stability of these limit cycles have also been given by Yang and Culick (1990),

$$\begin{aligned}\alpha_1 + \alpha_2 &< 0 \\ 2\alpha_1 + \alpha_2 &< 0 \\ \alpha_1 \alpha_2 &< 0\end{aligned}\tag{7.56a,b}$$

These conditions and their derivation are given in the reference.

Because of the difference in frequencies of the first radial and second tangential modes, the 1T/1R and 1T/2T limit cycles have quite different characteristics (quantitatively). The matter is discussed in some detail by Yang and Culick (1990) where the relevant energy equations are also considered. The examples of the 1T/1R and 1T/2T limit cycles form a very useful comparison of limit cycles existing with only two modes.

(b) Periodic Limit Cycles for Three Modes.

It came originally as a pleasant surprise that a limit cycle for three modes can be analyzed with the same procedures used for two modes. Much of the detail has been given by Yang and Culick (1990) and will not be repeated here. Only the case 1T/1R/2T has been worked out; it is simply not known *a priori* how cases can be solved in this way. Figure 7.22 shows limit cycles computed for two sets of initial conditions. The amplitudes for long times are evidently independent of initial conditions. In this case the frequencies for $t \rightarrow \infty$ are $\omega_1 + \nu_1$, $2(\omega_1 + \nu_1)$, $2(\omega_1 + \nu_1)$ where ν_1 is constant.

7.5. Observations of a Spinning Transverse Mode

Many years ago there were several reports of observational results for travelling waves interpreted as ‘spinning’ transverse modes. Owing to limitations of the instrumentation, the results depend to some extent on the interpretational powers of the observers. For example, following the early conjecture by Smith and Springer (1953) that the instabilities they had observed appeared to be longitudinal detonation waves, that idea was extended to be the basis for interpreting waves that appeared to rotate about the axis of the chamber (Denisov *et al.* 1962, Krieg 1962, Nicholls and Cullen 1965, Oppenheim and Laderman 1965). The most complete and convincing results were reported by Clayton, Rogero and Sotter (1968) which we summarize here.⁹

Figure 7.23 is a picture of the wave, inferred by Clayton *et al.* from data obtained with pressure transducers installed on the injection face and on the chamber wall. The chamber; one unlike injector element; and the device used for pulsing are shown in Figure 7.24. Fifty-two injection elements were mounted in the injection plane at the head end of motor. The pulsing device is so positioned that it is not surprising that a spinning tangential wave was initiated by the pulsing. Both clockwise and counterclockwise rotations occurred, depending on, among other quantities, the relative circumferential positions of the pulses and the pattern of injection elements. This feature of the experimental situation was only remarked upon in the paper and was not explored further. The authors also noted that in a different but similar engine, the unstable mode appeared without pulsing. No further details were given and the problem seems not to have been treated theoretically (see Footnote 9). In particular, there are presently no results—theoretical or experimental—showing that a spinning mode of the sort reported may be a detonation wave rather than a large amplitude acoustic wave, or shock wave.

⁹Flandro (private communication) renewed the author’s interest with his recent 2004 remark that he is engaged in work on this problem.

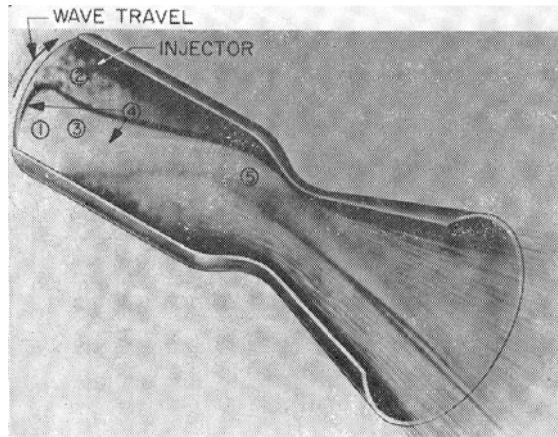


FIGURE 7.23. Sketch of the interpretation as a 'detonation' wavefront. 1 Shock wave rotating within sensitive reaction zone near injector, strong coupling between wave environment, and energy release from reactants. 2 Fresh reactants continuously replenished during wave rotation period. 3 Frontal surface inclined to chamber longitudinal axis and oriented nonradially in planes of chamber cross section. 4 Intersection of wave with chamber boundaries. 5 Possible helical path of burned gas immediately following the wave (Clayton, Rogero and Sotter 1968).

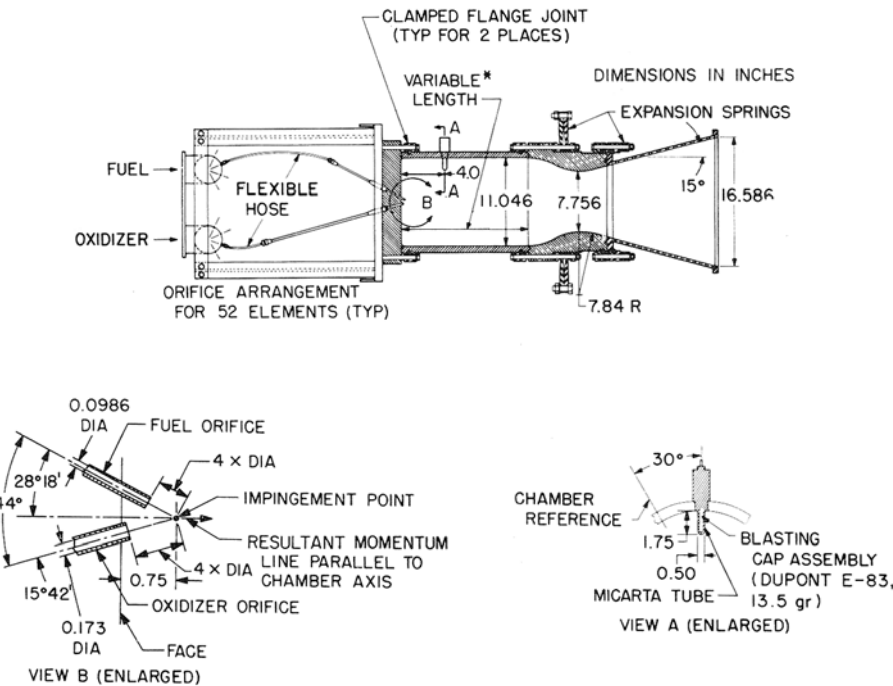


FIGURE 7.24. The test engine, 20,000 lbf-thrust engine and components (Clayton, Rogero and Sotter 1968).

7.6. Remarks on Truncation and Reduced-Order Modeling

As a practical matter, the problem of establishing a reduced-order approximation occupies an extremely important position. In general, the term 'reduced-order' has qualitative implications that the formal description of a physical system is simplified because the governing set of differential equations has a lower order. A

major problem is determining the extent to which the description of the physical system is imperfect: How good is the approximation? In the present context, an (almost) equivalent question is: How many modes must be considered in a given problem to obtain ‘good’ results? We have already seen simple special cases treated with the method of time-averaging; some results are given, for example, in Figures 7.18 and 7.19. Some results for more difficult problems are given in Section 7.7.

Reduced-order modeling has become an active area of concern during the past few years owing to its immediate applications in problems of active control. We will discuss the subject further in Chapter 9.

7.7. Application of a Continuation Method

Much of the work during the past decade at Caltech on chamber dynamics has been directed to understanding the extent to which nonlinear behavior can be explained on the basis of nonlinear gasdynamics. The reasoning is first that we know the model of gasdynamics—the Navier-Stokes equations for compressible flow—so we can do accurate analysis; and second, those features that cannot be explained must be due to other causes so, by elimination we have some guidelines for what we should seek in other processes. Experience has shown that ‘other processes’ in this context most probably means combustion.

To carry out this program with numerical simulations—after all, few exact results exist—would be a formidable task because of the number of characteristic parameters. The parameter space comprises those quantities defining the geometry of a chamber and two parameters (α_n, θ_n) characterizing linear behavior of each mode. The effect required to search the parameter space is much reduced by applying a continuation method. The procedure is an efficient systematic means of locating values of parameters for which the dynamical behavior suffers a qualitative change, i.e., bifurcation points. The simplest—almost trivial—example is the Hopf bifurcation point which arises when, for a stable system, one of the values α_n changes from a negative to a positive value; the system becomes linearly unstable and under suitable conditions the motion develops into a stable limit cycle. In fact, linear instability is not always such a simple matter. We have found cases with special sorts of nonlinear processes for which a Hopf bifurcation may occur when the critical value of α_n is non-zero.

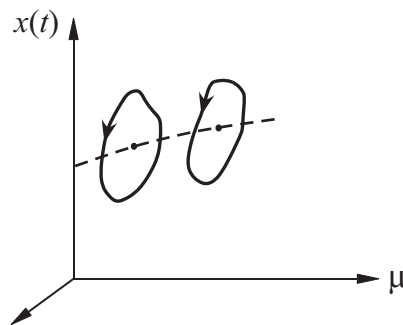


FIGURE 7.25. Schematic illustration of the continuation method applied to limit cycles.

The essential idea of applying a continuation method to limit cycles is illustrated in Figure 7.25 where the variables of the motion are $x(t)$ and μ is the parameter in question, the bifurcation parameter. A continuation method is a computational (numerical) scheme for following, in this case, the changes of a period solution—a limit cycle—as the values of one or more parameters are changed. A picture like Figure 7.25 is impossible to draw for more than three coordinates, so the conventional display of information is a bifurcation diagram in which the amplitude of one variable in the limit cycle is plotted versus the parameters varied as the continuation method is applied. Figure 7.26 shows two examples, a Hopf bifurcation, also called

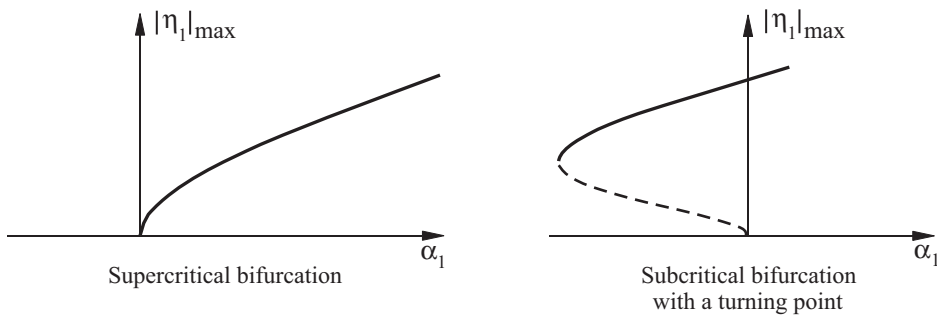


FIGURE 7.26. Two examples of bifurcation.

a *supercritical bifurcation*; and a *subcritical bifurcation* with a turning point. Those are the two types of bifurcation most common in the present context.

A bifurcation diagram is a locus of equilibrium points traced as the bifurcation parameter is changed. As a practical matter, a continuation method is more systematic and cheaper to use than numerical simulations. We have successfully used a continuation method developed by Doedel and colleagues (Doedel *et al.* 1991a,b; Doedel *et al.* 1997) to investigate four classes of problems:

- (i) consequences of time-averaging
- (ii) consequences of truncating the modal expansion
- (iii) influences of the linear parameters (α_n, θ_n) on nonlinear behavior
- (iv) pulsed instabilities (triggering): the conditions for existence of stable limit cycles in a linearly stable system.

The problems (i) and (ii) are central to the matter of constructing reduced-order models. Hence it is important to emphasize that in our view, application of the continuation method to investigate the consequences of time-averaging and truncation is part of the procedure for establishing the validity of reduced order models within the framework of analysis based on modal expansion and spatial averaging.

The continuation method is a powerful means for investigating many nonlinear problems in the classes listed above. Commercial software is available for this purpose. For more extensive discussions see Jahnke and Culick (1994); Burnley (1996); Burnley and Culick (1996); and Ananthkrishnan, Deo and Culick (2002). As an illustration we quote here some results for limit cycles in systems of longitudinal modes when only the gasdynamical nonlinearities are accounted for. We are interested in the consequences of truncation with time-averaging.

In Section 7.3 we cited a few results for the limiting case of two modes described by the four equations found with time-averaging. Figure 7.27 shows the special example of the effect of truncating the series expansion for the time-averaged system: Increasing the number of modes apparently widens the region of stability. In fact, use of the continuation method has established the result that the existence of a region of stability for limit cycles with two modes is due to truncation. When the first mode is unstable, stable limit cycles exist for all values of α_1 , if more than two modes are taken into account. That is true even if the original oscillator equations are used.

Figure 7.28 shows that if time-averaging is not used, there is a turning point in the bifurcation diagram. Moreover, the boundary of stability persists for the time-averaged equations but moves to larger values of α , as the number of modes is increased. Figure 7.29 is the result for the time-averaged equations and Figure 7.30 shows the case of 4 modes computed for the full oscillator equations.

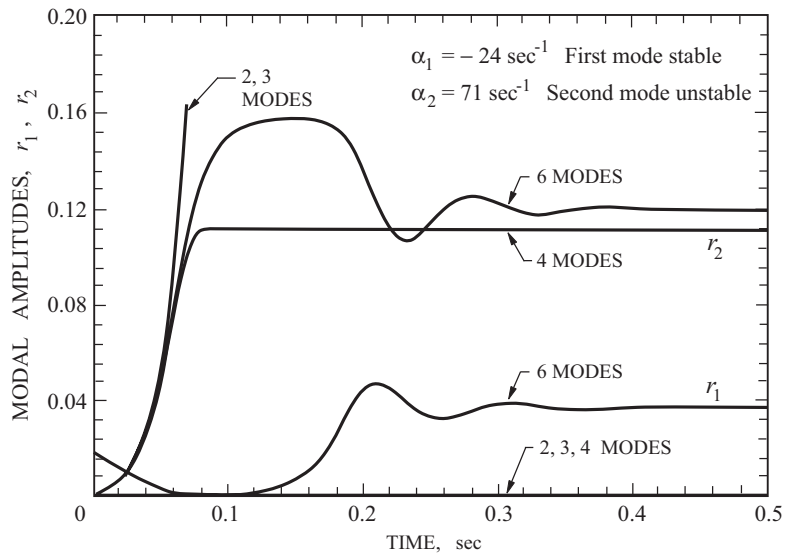


FIGURE 7.27. The effects of truncation for a two-mode system: second mode unstable, all other modes stable (Paparizos and Culick 1989).

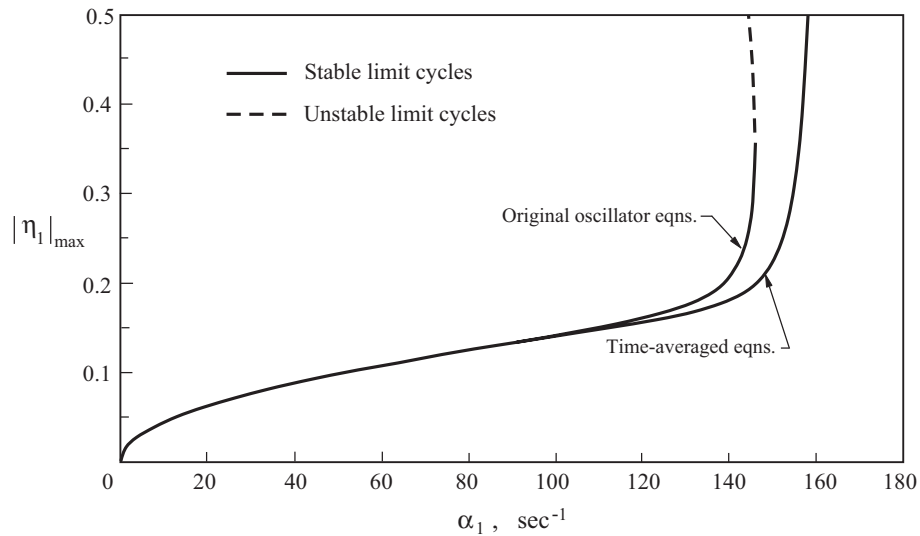


FIGURE 7.28. Effect of time-averaging for two modes (Jahnke and Culick 1994).

It seems true that if the system is only slightly unstable, then the system of time-averaged equations for two-longitudinal modes is a good approximate model for investigating nonlinear behavior. However, if one is generally interested in producing reduced order models, the effects of truncation and time-averaging should be investigated. Applying a continuation method seems to be the best approach for doing so. It is a quick and inexpensive way to learn a great deal about a system.

Ananthkrishnan *et al.* (2005) have given the first analysis addressing the practical question of how many—or perhaps more accurately, how few—modes are required to obtain faithful results. The reasoning is based on properties of the energy transfer between modes, with the full second-order equations used for the formal description of longitudinal modes. Thus, errors accompanying application of time-averaging are absent. The

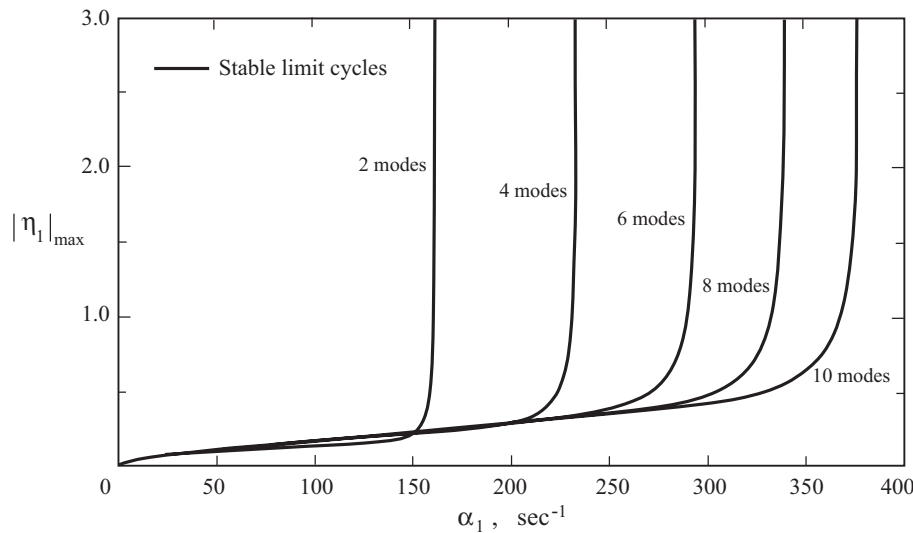


FIGURE 7.29. Solutions with truncation of the time-averaged equations (Jahnke and Culick 1994).

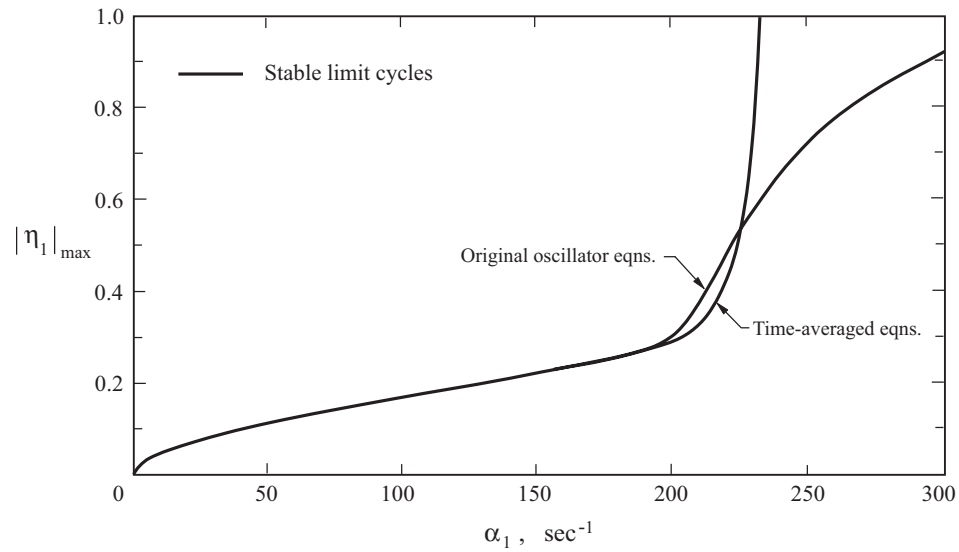


FIGURE 7.30. Maximum amplitude of η_1 in the limit cycle: four modes, comparison of results for the full oscillator and the time-averaged equations (Jahnke and Culick 1994).

view is maintained that the global behavior is dominated by the fluid mechanics represented by the second-order terms in equation (7.27). We emphasize again that the results will be special because the nonlinear terms involve only squares ($\eta_r \eta_s$ and $\dot{\eta}_r \dot{\eta}_s$) and no quadratic terms such as $\eta_r \dot{\eta}_s$. That property alone has much to do with the conclusions reached.

The reasoning is covered thoroughly in the reference and will not be reproduced here. An important conclusion is that for correct qualitative analysis of the motion when the first mode is unstable requires four modes: the unstable mode (mode 1); the coupled mode (mode 2) and energy sinks (modes 3 and 4). If the second mode is linearly unstable, at least the first eight modes must be retained. Reported results by Janke

and Culick (1994), Burnley (1996), and Culick, Burnley and Swenson (1995) support the point. See also the more carefully argued conclusions reached by Ananthkrishnan *et al.* (2005).

A second conclusion of the last work is that theoretical justification can be given to the idea that the second-order gasdynamic nonlinearities alone will not produce subcritical bifurcations, i.e., ‘triggered’ limit cycles. As we have discussed, various works carried out over roughly two decades suggested this result but no substantial proof had been previously found. The paper also contains further investigation of triggering with second-order gasdynamics and nonlinear velocity coupling.

In a general respect, the work reported by Ananthkrishnan *et al.* shows most clearly the usefulness of a continuation method as a tool for investigating and understanding nonlinear behavior.

7.8. Recirculation Zones, Hysteresis and Control of Combustion Instabilities

The existence of hysteresis in the dynamical behavior of combustions is both an interesting phenomenon to investigation and a characteristic that has potentially important practical consequences. It seems that the first evidence for hysteresis in combustors was found by Russian researchers concerned with instabilities in liquid rockets (Natanzon *et al.* 1978, 1992; Natanzon 1999). In that case, Natanzon and his co-workers proposed bifurcation of *steady states* of combustion, and the associated hysteresis, as a possible explanation for the random occurrences of combustion instabilities. The Russian workers were in a special situation affording them the opportunity to make such observations. The large Russian boosters were designed to use many (as many as thirty-three) liquid rocket engines in a single stage. Hence large numbers of nominally identical engines were manufactured and tested for operational use. Sufficient data were obtained that statistical analysis of the behavior could be carried out. A basis therefore existed for identifying random behavior. More information is available in Natanzon’s monograph, including interesting discussions of experimental work. The results are convincing arguments for the basic importance of hysteresis, which may have widespread implications. The idea is the following.

In a liquid rocket many zones of recirculation are created at the injector where jets of liquid fuel and/or oxidizer enter the chamber. As an approximation, one may regard a recirculation zone as a chemical reactor whose behavior is known to be well-characterized by the temperature of the incoming gases entrained from the environment, and the average temperature within the zone. A fairly simple calculation based on consideration of energy and mass flows leads to the results sketched in Figure 7.31. The upper and lower branches of the hysteresis loop represent different branches of stable combustion. Those states have different influences on the state of combustion in the chamber. It was Natanzon’s assertion that the state associated with the lower branch in Figure 7.31 (the cold recirculation zone) is more unstable and prone to lead to combustion instabilities. Which branch is reached depends on the history of the engine, starting from ignition or some other sort of abrupt transient. The final state of a recirculation zone depends on random ‘accidents’ of history. Therefore, random occurrences of combustion instabilities may be observed. Figure 7.32 is a sketch of a possible recirculation zone and adjacent flow of a fuel or oxidizer jet. This model has been used as the basis for numerical calculations supporting Natanzon’s proposal (Natanzon 1999).

In the mid-1980s, research with a dump combustor at Caltech revealed the presence of a different kind of hysteresis of dynamical states of combustion (Smith, 1985; Sterling, 1987). The combustor has been described in Chapter 1, Figure 1.17; Figure 7.32 shows the inlet region and the recirculation zone at a dump plane during steady combustion. The combustor showed combustion instabilities in the neighborhood of the stability boundary defined in the plane of flow rate and equivalence ratio, Figure 7.33(a). Figure 7.33(b) shows an idealized hysteresis loop, observed as dependence of the level of pressure oscillation on equivalent ratio with the total flow rate held constant. This sort of behavior has been observed also in other dump

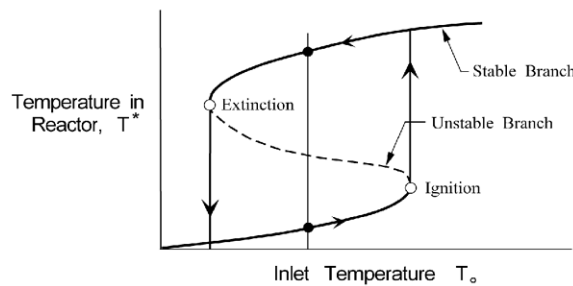


FIGURE 7.31. Hysteresis loop for a recirculated zone idealized as a simple chemical reactor.

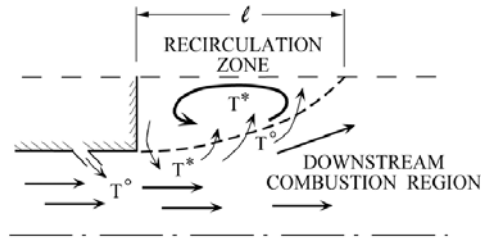
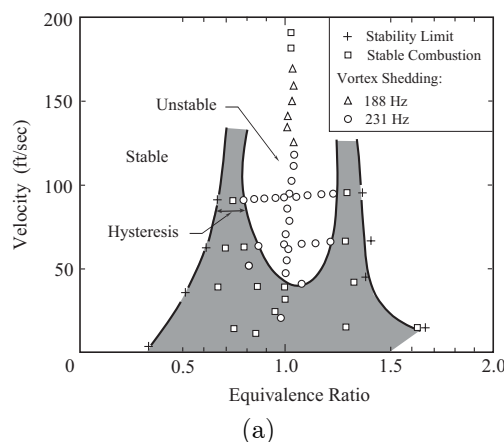


FIGURE 7.32. Sketch of a recirculation zone formed by a jet of fuel or oxidizer (adapted from Natanzon 1999).

combustors as well as in a flame-driven Rijke tube (Seywert, 2001) and in an electrically driven Rijke tube (Matveev, 2002; Matveev and Culick, 2002a,c); see Section 2.7.



(a)

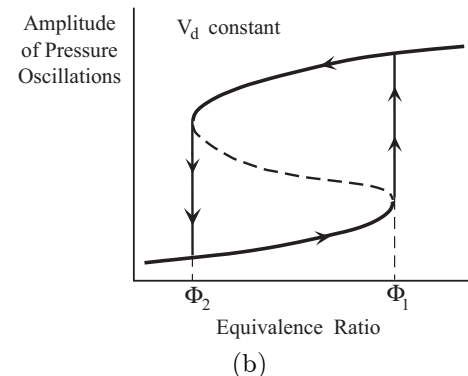


FIGURE 7.33. (a) Stability boundary (Sterling 1987) and (b) an idealized hysteresis loop suggested by the data shown in (a) for the Caltech dump combustor.

Recent experimental works (Knoop *et al.* 1996; Isella *et al.* 1996) have established the physical nature of the hysteresis in this case and have shown how active control can be used to extend the range of steady operation into the hysteretic region. High speed films have confirmed that the upper branch of the loop is associated with shedding of large vortices which, causing periodic combustion of entrained reactants sustain high amplitude pressure oscillations. The lower branch is associated with relatively quiet combustion in a shear layer shed from the lip at the inlet.

Familiar considerations of dynamical behavior suggest that it should be possible to achieve pulsed transitions between the two branches of stable dynamical states. Those processes were demonstrated by Knoop *et al.* and Isella *et al.* by injecting pulses of fuel at the inlet plane. Single pulses of fuel cause transition from the upper to the lower branch. Thus with suitable sensing and actuation it is possible always to maintain the low level of oscillations (effectively 'noise') within the zone where hysteresis exists.

Figure 7.34(a) shows the modified step allowing injection of pulses; Figure 7.34(b) shows an example of the hysteresis observed. Examples of the unsteady pressure found during stable burning and unstable burning, on the lower and upper branches respectively, of the hysteresis loop are reproduced in Figure 7.34(b).

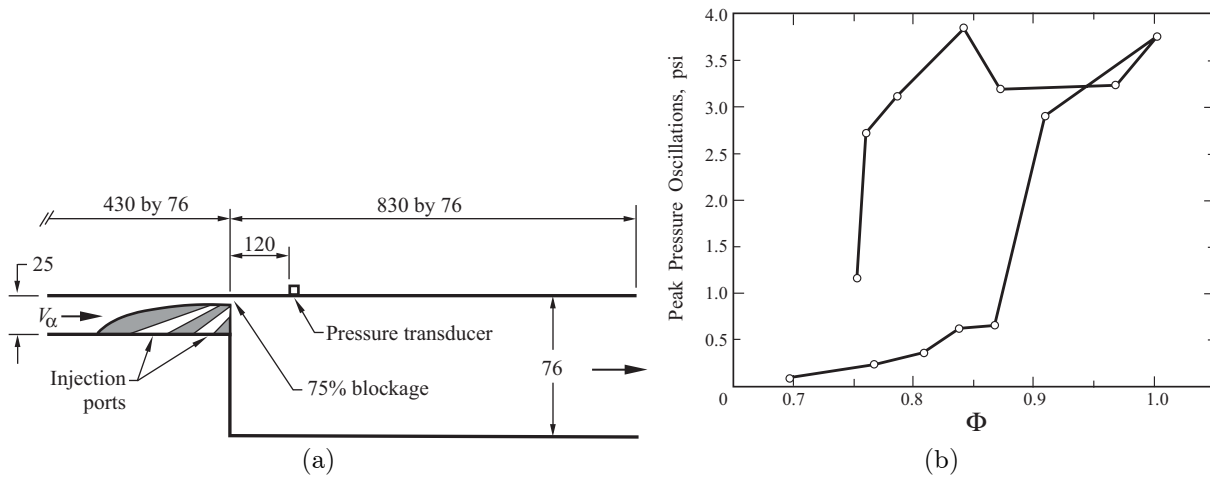


FIGURE 7.34. (a) Sketch of the dump combustor modified to allow injection of pulses; (b) hysteresis observed in the apparatus shown in (a) (Isella, Seywert, Culick and Zukoski 1997).

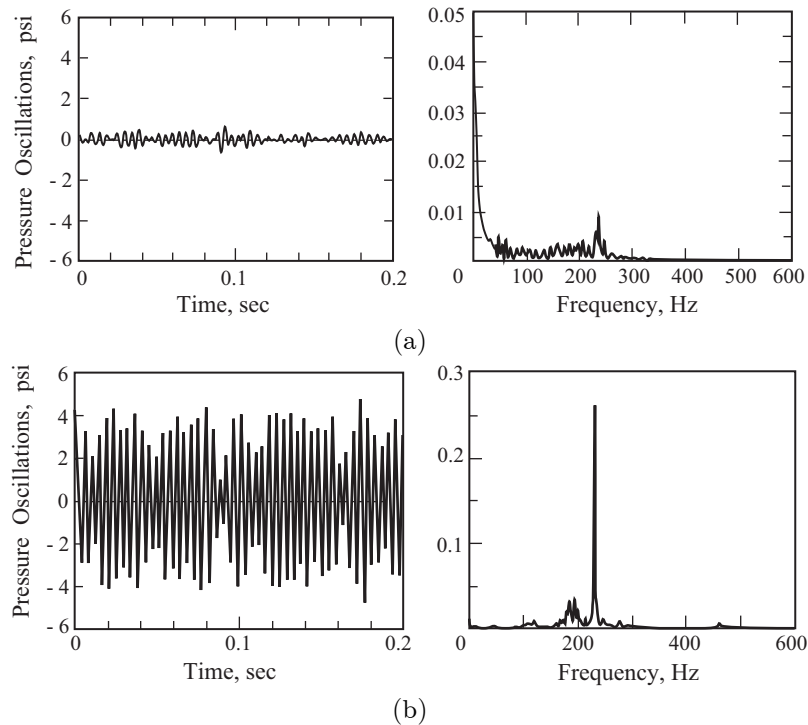


FIGURE 7.35. Pressure traces and spectra for the two branches of the hysteresis loop. (a) stable burning on the lower branch; (b) unstable burning on the upper branch. (Isella, Seywert, Culick, and Zukoski 1999).

The idea motivating the series of tests (carried out as a project in a student laboratory course) was the following theoretical notion. If the combustor were operating in an unsteady state on the upper branch of the hysteresis loop, Figure 7.34(b), then it should be possible, by pulsing, to cause the system to undergo

a transition to the lower branch, hence reducing the amplitude of the oscillations. Originally it seemed necessary that fuel be used, because combustion was assumed to be the origin of the behavior. In the event, it happened that a pulse of nitrogen would also cause a transition, but not always. Thus the behavior, not surprisingly, involves a combination of combustion processes and the fluid mechanics of the separation zone.

Figure 7.36 shows the time history of oscillations in an interval including the introduction of a pulse. The series of circled numbers in part (b) identify times when high speed shadowgraphs were taken of flow immediately downstream of the step. An example of the results is shown in Figure 7.37. The solid lines approximately indicate instantaneous lines of flow. The test results confirmed the authors' guess *a priori* that the origin of the strong oscillations was associated with combustion in a separated region of recirculation at the step. Relatively quiet behavior accompanies combustion in turbulent shear layer.

Further discussion of the effects of pulsing is given in the references, but many details remain unexplained in terms of fundamental causes. For example, the consequences of using a noncombustible injected gas, mentioned above, are similar but not as inevitable as those just described. Interactions of strong acoustic waves, secondary (including pulsed) flows and recirculation zones are likely to be more important to the unsteady behavior of combustors than the present level of understanding may suggest.

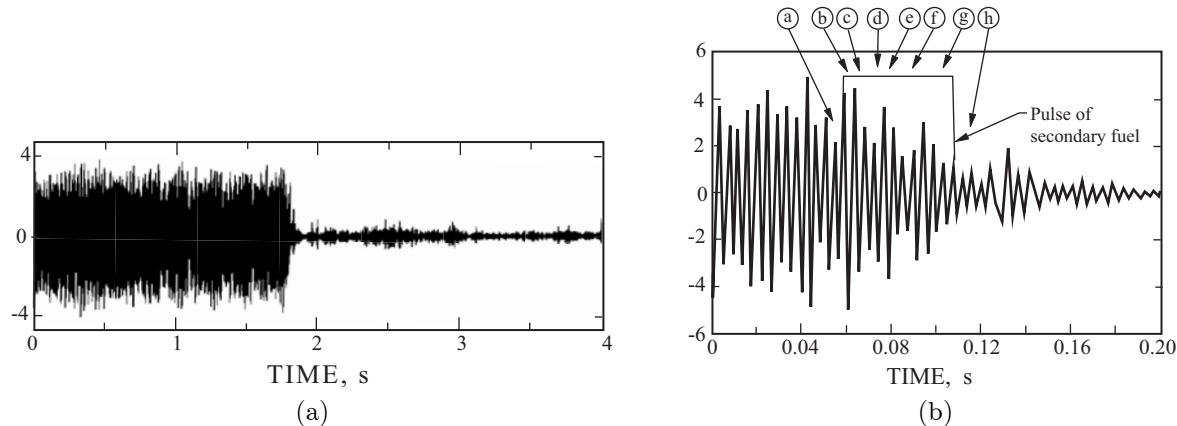


FIGURE 7.36. Time history of a portion of trace. (a) low resolution showing quenching pressure oscillations by a pulse; (b) high resolution showing times of the photographs in Figure 7.37 (Isella, Seywert, Culick and Zukoski 1997).

The behavior shown with a pulsed recirculation zone is a form of nonlinear control. Although it has been demonstrated only for the range of equivalence ratio covering the zone of hysteresis, it is an important demonstration of active control at a frequency far less than the frequency of the oscillations. That is a significant characteristic because if the reduced bandwidth required of the control system, particularly the actuation, is smaller, the demands placed on the equipment are reduced. See Chapter 9 for further comments.

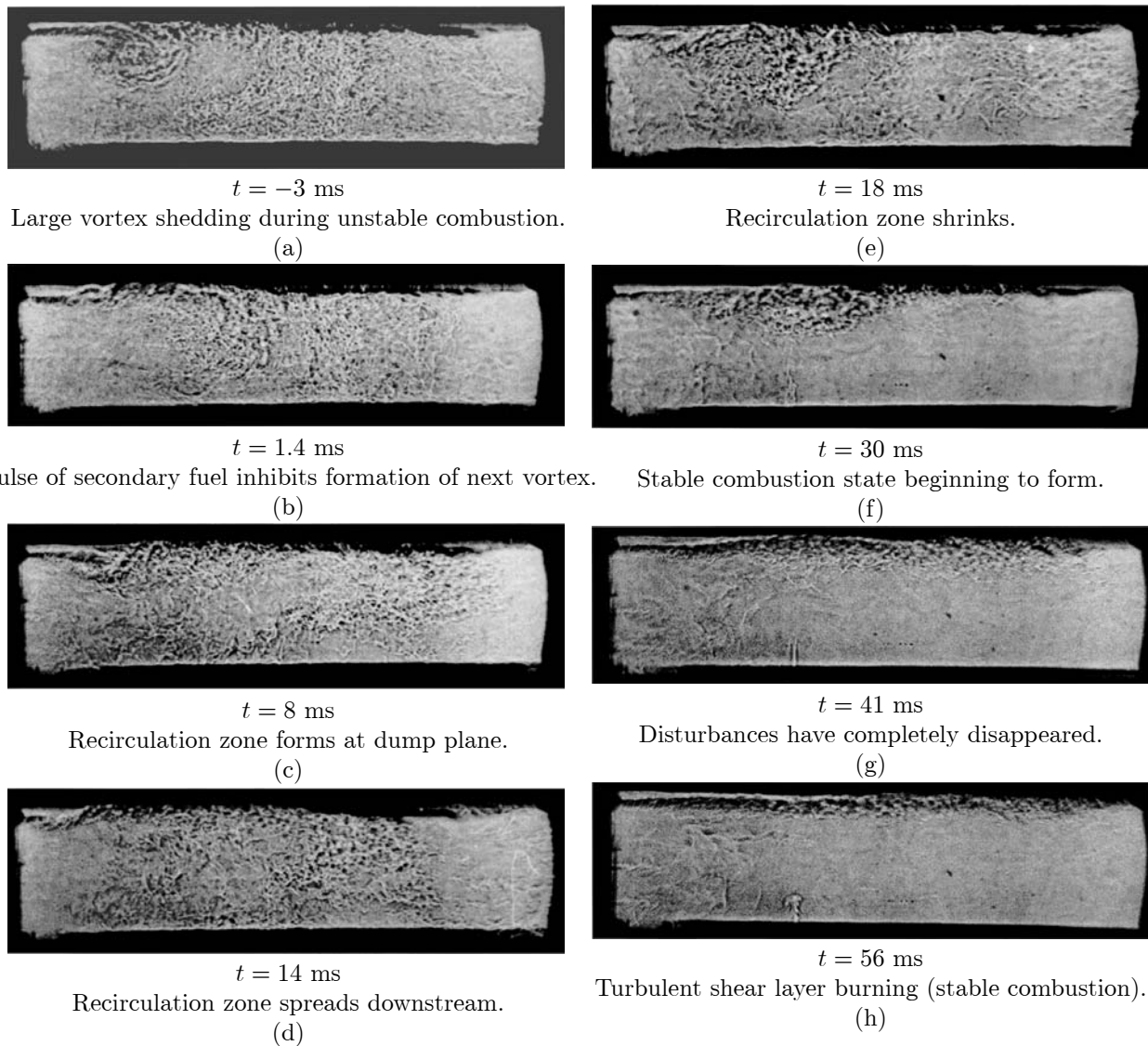


FIGURE 7.37. Shadowgraphs of the transition induced by a single pulse initiated at $t = 0$ (Isella, Seywert, Culick and Zukoski 1997).

7.9. Representing Noise in Analysis of Combustor Dynamics

Generation and emission of noise is a characteristic feature of all combustors. The difference in sound level produced by a burning jet contrasted with an unburning jet, for example, is obvious and convincing evidence of the phenomenon. Combustion noise has long been studied—see, for example, early interest by Lord Rayleigh (1945)—and in the past fifty years, has been through several periods of increased emphasis, followed inevitably by general papers such as those by Strahle (1971, 1978, 1985) convey the vicissitudes of the field. Currently the developments of large numerical simulations (e.g. LES) hold promise for increased understanding. It appears that good experimental results may be more difficult to acquire.

Considerable experience during the past five decades has established the result that combustion noise is a minor part of the noise produced by a gas turbine; see, for example, Cumpsty (1979) and Cumpsty and Marble (1977). Hence, interest in the subject has not been motivated and sustained by practical considerations of noise pollution of the environment. The energy contained in the noise field of a combustor, and the power radiated, do not have serious environmental consequences in the same sense as, for example, jet noise does. Our concern here is relatively narrow, related to possible causes or effects of combustion instabilities, and especially how noise may be included in the framework we have been discussing.

Even a small laboratory combustor radiates considerable noise, generated by turbulent motions (often called ‘combustion noise’) within the chamber. See, for example, the spectrum reproduced earlier as Figure 1.18. The scaling laws are not known, but it is obvious to any bystander that a full-scale combustor of any sort is noisy indeed. Presently it is not well understood how important noise is to the behavior of combustion instabilities or to the application of feedback control. The purpose of this section is to introduce a means for investigating those matters within the framework developed in Chapters 3 and 4.

There are three sorts of problems that will arise:

- (i) formal incorporation of noise (stochastic) sources in the framework of spatially averaged equations for unsteady motions in a combustor;
- (ii) modeling the noise sources;
- (iii) solving the stochastic differential equations.

The first step, as explained in Section 3.1, is to apply the principle of splitting small disturbances into the three basic modes of propagation: acoustic waves, vorticity waves, and entropy waves. All of the discussion so far in this book has been devoted to the acoustic field. Noise is associated with the random motions comprising mainly vorticity but also entropy (or temperature) waves in a combustion chamber. Our concern in the present context is directed chiefly to interactions of those motions with the acoustic field. The formal representation will be relatively simple and intuitively persuasive, but modeling the details remains to be accomplished. Numerical results require assumptions that cannot be justified *a priori*.

Following the principle of splitting, we write the flow variables as sums of the three contributions, one each corresponding to the three modes of motion:

$$\begin{aligned}
 p' &= p'_a + p'_{\Omega} + p'_s \\
 \boldsymbol{\Omega}' &= \boldsymbol{\Omega}'_a + \boldsymbol{\Omega}'_{\Omega} + \boldsymbol{\Omega}'_s \\
 s' &= s'_a + s'_{\Omega} + s'_s \\
 \mathbf{u}' &= \mathbf{u}'_a + \mathbf{u}'_{\Omega} + \mathbf{u}'_s
 \end{aligned} \tag{7.57a,b,c,d}$$

Subscripts $(\)_a$, $(\)_{\Omega}$, $(\)_s$ denote acoustic, vortical and entropic contributions. Once again, the ordering procedure explained in Chapters 3 and 4 allows us to derive meaningful results by considering only the first order components. Hence we assume that only the acoustic waves contain pressure fluctuation; in this linear limit, only the waves of vorticity contain vorticity fluctuations; and only the entropy waves have fluctuations of entropy. The velocity field possesses contributions from all three modes.

The idea then is to substitute the assumed general forms of the variables in the primitive equations of motion expanded to third order in the fluctuations. Then form the nonlinear equation for the pressure and apply spatial averaging. This procedure was first reported by Culick *et al.* (1992) but in revised and corrected form by Burnley (1996) and Burnley and Culick (1999). Eventually one finds the oscillator equations,

$$i\dot{\eta}_n + \omega_n^2 \eta_n = F_n$$

but now F_n contains stochastic sources. The ‘general’ form of F_n is

$$-\frac{\bar{\rho}E_n^2}{\bar{a}^2}F_n = \bar{\rho}I_1 + \frac{1}{\bar{a}^2}I_2 + \bar{\rho}I_3 + \frac{1}{\bar{a}^2}I_4 + \bar{\rho}I_5 + \oint\left[\rho\frac{\partial\mathbf{u}'}{\partial t}\cdot\hat{\mathbf{u}} + \bar{\rho}\frac{\partial\mathbf{u}'}{\partial t}\right]\cdot\hat{\mathbf{n}}\psi_ndS - \int\mathbf{F}'\cdot\nabla\psi_ndV + \frac{1}{\bar{a}^2}\int\frac{\partial\mathcal{P}'}{\partial t}\psi_ndV$$

where

$$I_1 = \int [\bar{\mathbf{u}}\cdot\nabla\mathbf{u}' + \mathbf{u}'\cdot\nabla\bar{\mathbf{u}}]\cdot\nabla\psi_ndV$$

and similar definitions for the remaining integrals I_1 . See Annex D and the references for details.

Then the unsteady velocity field is split according to (7.57)a,b,c,d. Eventually, re-arrangement and application of the assumptions discussed above leads to the result

$$\begin{aligned} \ddot{\eta}_n + \omega_n^2\eta_n &= 2\alpha_n\dot{\eta}_n + 2\omega_n\theta_n\eta_n - \sum_{i=1}^{\infty}\sum_{j=1}^{\infty}[A_{nij}\dot{\eta}_i\dot{\eta}_j + B_{nij}\eta_i\eta_j] \\ &\quad + \sum[\xi_{ni}^v\dot{\eta}_i + \xi_{ni}\eta_i] + \Xi_n + (F_n^{NL})_{other} \end{aligned} \quad (7.58)$$

where the ξ_{ni}^v , ξ_{ni} and Ξ_n are stochastic sources defined as integrals over the vortical and entropic fluctuations of the velocity. See the references cited above for details.

No intensive modeling based on experimental, theoretical or phenomenological grounds has been accomplished. Explicit results have been obtained by approximating the stochastic sources as white noise processes having properties chosen to be realistic, i.e., the results seem to be reasonably consistent with available measurements of actual behavior.

Two types of stochastic influences arise in (7.58):

- (i) ξ_{ni} , ξ_{ni}^v represent stochastic influences on the ‘spring’ or natural frequency of the n^{th} mode and on the damping or growth rate. These are formally referred to as ‘multiplicative noise sources’ because they appear as factors multiplying the dependent variables, the displacement and velocity of the n^{th} oscillator. (Stratonovich 1963)
- (ii) ξ_n represents a stochastic driving source causing excitation of the n^{th} oscillator even in the absence of driving by combustion processes; the Ξ_n are formally called ‘additive noise sources’.

It is evident from the form of (7.58) that the random character of the stochastic sources will appear as random fluctuations imposed on the amplitudes $\eta_n(t)$ of the acoustic modes, exactly the sort of behavior found experimentally. Thus, Fourier synthesis of the pressure field, the modal expansion, continues to serve as a good approximate representation of the deterministic results can be obtained by retaining only a small number of terms.

Results were obtained first for the simplest case of two modes, with noise sources only in the fundamental mode. Nonlinear gasdynamic coupling transfer stochastic behavior to the second mode. Computations have been carried out using a Monte-Carlo method to give probability density functions, with the equations written in the Stratonovich form of stochastic differential equations (Burnley, 1996). Figure 7.38 shows the pressure trace and spectrum for a simulation in which the first mode is unstable.

This method of accounting for noise in a combustor seems to be very promising. However, modeling the noise sources is in a primitive state, and comparisons of results with experimental observations can only be done qualitatively.

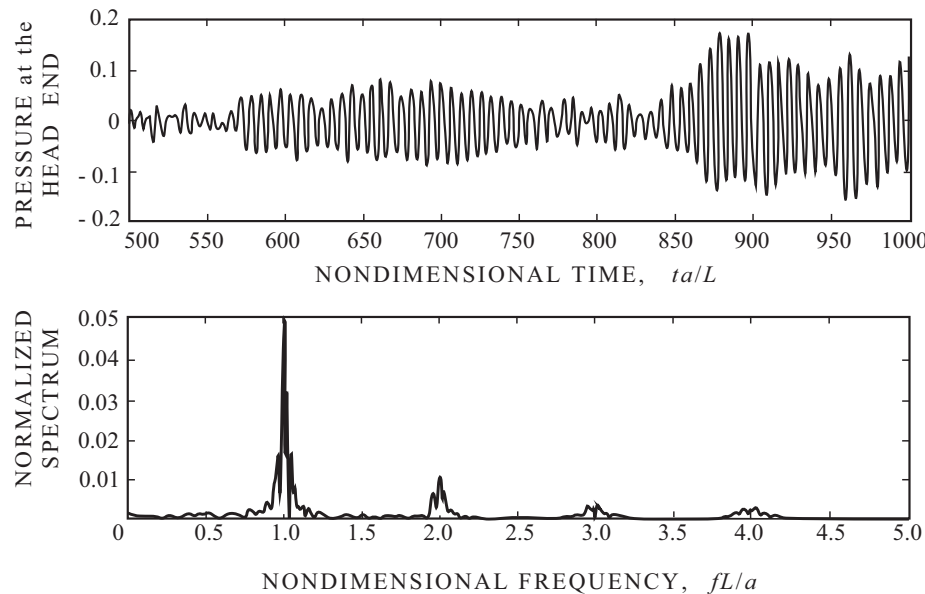


FIGURE 7.38. Pressure trace and spectrum for a simulation with noise; four modes included, first mode unstable (Burnley and Culick 1996).

7.10. System Identification for Combustor Dynamics with Noise

Use of system identification in the field of combustor dynamics seems to have been developed first by Russian groups as part of their development of liquid rocket engines, beginning perhaps as early as the 1950s but certainly in the 1960s (Agarkov *et al.* 1993).

In several papers during the 1980s, Hessler (1979, 1980, 1982); and Duer and Hessler (1984); and more recently Hessler and Glick (1998), have asserted that the oscillations observed as combustion instabilities in solid rocket motors are *driven* rather than *self-excited*. The sources of the driving—i.e., the ‘mechanisms’—are supposed to be either vortex shedding or noise. Hessler and co-workers conclude that the properties of the noise measured in a stable chamber can be used as the basis for infusing properties of the primary mechanism causing instabilities when they arise or more correctly, such data will provide quantitative information about the static stability margins—how close the dominant acoustic modes are to becoming unstable.

The basic idea is sound. When the mechanisms are interpreted as driving forces independent of the acoustic field, and they are assumed to be broad-band, then the acoustic modes are excited to amplitudes related directly to the amount of damping (α_n). Hence the idea is to process noisy records in such a fashion as to extract the values of the linear parameters (α_n, θ_n). The proposed method can be tested using the oscillator equations with some sources derived in the preceding chapter.

Seywert (2001) and Seywert and Culick (1999) have reported results of some numerical simulations carried out to check the idea just described. In particular, the main purpose was to determine the accuracy with which the experimental method would give the linear parameters. The procedure is straightforward. To be definite and to keep the computations within practical bounds, we consider a system of four modes, each containing noise sources which, as explained in Section 7.9, are assumed to be white noise. The amplitudes of the noise (rms values) are selected so that random amplitude fluctuations in the pressure spectrum have values in the ranges experimentally observed (Seywert and Culick).

Three types of problems arise, associated with the three types of noise sources: additive noise, Ξ_n ; and two kinds of multiplicative noise, ξ_n^v which affects mainly the growth and decay rates, and ξ_n which causes random variations of the frequency. In all cases we are concerned here with discovering the ways in which noise affects the result of system identification. The idea is to select values of the α_n , θ_n and carry out numerical simulations. Then the data are processed to give values of the α_n , θ_n which now have mean values and some uncertainties due to the presence of the noise. The questions to be answered are: How close are the mean values to the time values used as inputs? and How large are the uncertainties? These are important practical matters. If the method is effective, then data from hot firings of full-scale combustors could be used to infer the linear parameters characterizing the dynamics represented by several modes. Those parameters identify the poles of the response function of the chamber. Hence a relatively straightforward process would give the information required to proceed with designing a linear control system.

Actually there are two ways to get the information: process pressure records naturally occurring; or process the pressure record following a pulse. The method of pulsing has long been used as means of assessing the stability margin of liquid rockets (Harrje and Reardon, 1972). Both methods have been used for a stable system of four longitudinal modes having the parameters given in Table 7.2; the fundamental frequency is 900 s^{-1} . Figure 7.39 shows a simulated pressure trace and Figure 7.40 shows its power spectrum and construction using Berg's method.¹⁰

TABLE 7.2. Values of the Linear Parameters.

mode	1	2	3	4
$\alpha_n(\text{s}^{-1})$	-50	-375	-584	-889
$\theta_n(\text{s}^{-1})$	12.9	46.8	-29	-131

Without good data for the noise in an actual combustor and no model, we assume white noise sources. Their amplitudes are chosen so that the average (rms) values of the simulated pressure records are reasonable. Table 7.3 shows the relation between the rms value of the system response (p'/\bar{p}) and the noise power of Ξ . The 'noise power' cannot be measured, being the height of the power spectral density of the noise. Figure 7.41 gives a more detailed picture, showing how the amplitudes of the spectra of the four modes increase with noise power.

 TABLE 7.3. Relation Between the Noise Power of Ξ_n and the rms Value of the Simulated Pressure Fluctuation.

Noise Power of Ξ_n	rms Values of p'/\bar{p}
10^1	.005%
10^3	.05%
10^5	.5%

¹⁰Berg's method is a standard method of signal processing, widely available. We have used the software included in the Signal Processing Toolbox, an extension of MATLAB.

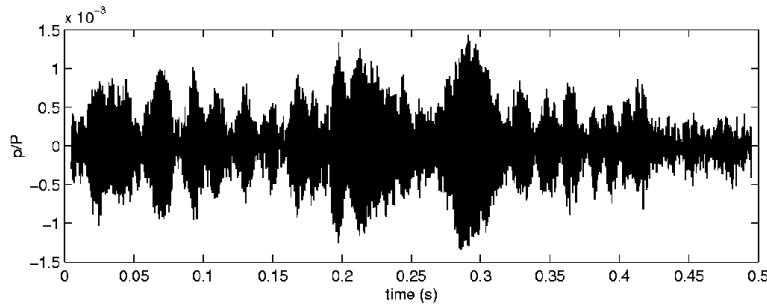


FIGURE 7.39. Simulated pressure trace with noise; all modes stable.

In Figure 7.42, a simulated response to a pulse is fitted by the superposition of four modes:

$$\frac{p'}{\bar{p}} = \sum_{i=1}^4 A_i e^{\alpha_i t} \cos(\omega_i t + \phi_i)$$

The parameters $A_i, \alpha_i, \omega_i, \phi_i$ are fitted using a least squares method.

We use the noise power as a parameter. Figure 7.43 shows an example of the sort of results one finds for multiplicative noise in the modal damping ($\xi_n^v \neq 0; \xi_n = 0; \Xi_n = 0$). The corresponding results of using the pulse method are given in Figure 7.44.

We conclude from these results that substantial errors may accompany system identification in the presence of realistic (we believe) noise. How significant the errors are depends on the particular application at hand and on how small the stability margins are. For a weakly stable system, values of the margins

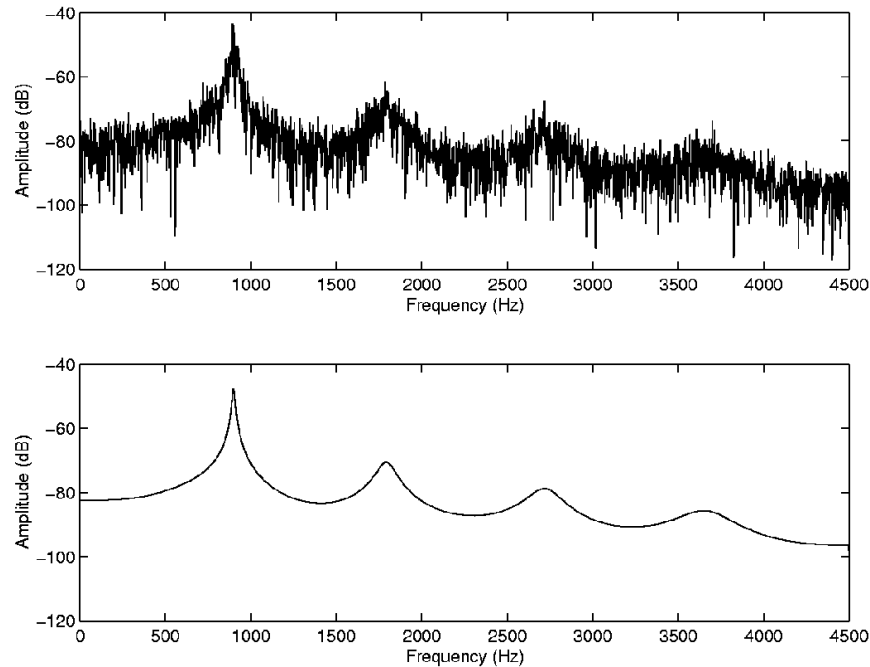


FIGURE 7.40. Application of Berg's method: power spectrum of the pressure trace in Figure 7.39 and its reconstruction.

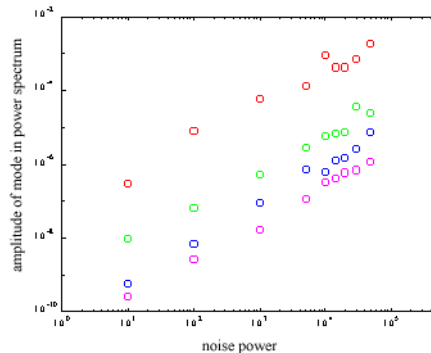


FIGURE 7.41. Dependence of the peak amplitudes of the power spectra for four modes, on noise power.

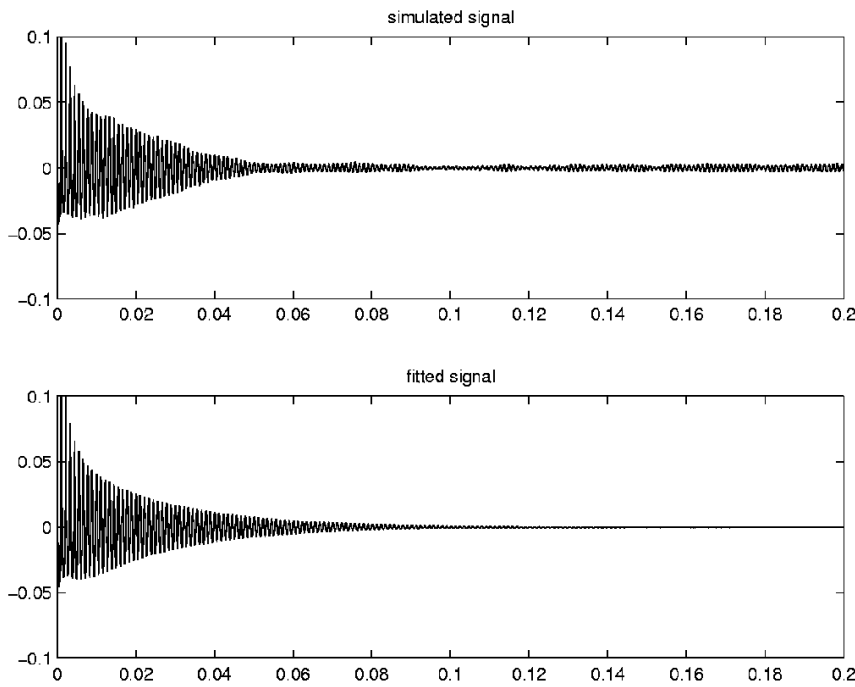
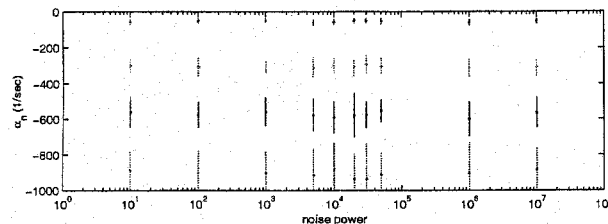


FIGURE 7.42. Reconstructed pressure trace for the transient response excited by a 10% pulse.

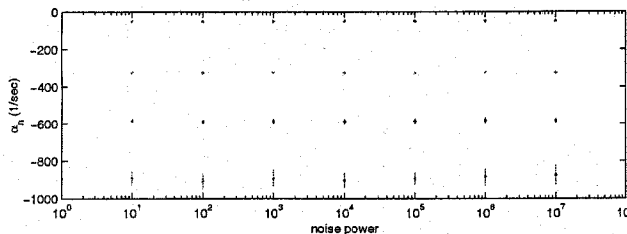
determined in this way are suspect because of the finite uncertainties. The results would therefore not be useful as a basis for representing the combustor's response function.

It should be clear from the nature of the methods described here that the system must be stable (i.e., all modes must be stable) for this application. For example, if data (simulated) for a limit cycle are processed in this fashion, the inferred values of α_n , θ_n have no apparent connection with the correct values.



Noise	α_1	α_2	α_3	α_4
10^1	-57±14	-301±31	-560±84	-886±98
10^2	-51±13	-307±52	-576±75	-903±126
10^3	-47±11	-307±38	-558±78	-901±117
10^4	-56±16	-300±51	-591±88	-883±150
10^5	-59±18	-310±53	-598±95	-914±128
10^6	-53±15	-310±46	-564±84	-905±172
10^7	-59±19	-313±44	-591±83	-887±124
correct	-50	-325	-584	-889

FIGURE 7.43. Values of decay rates (modal attenuation) found with Berg's method with multiplicative (ξ_n) noise.



Noise	α_1	α_2	α_3	α_4
10^1	-50±2	-323±6	-584±9	-889±35
10^2	-50±2	-325±5	-589±8	-908±36
10^3	-50±2	-322±4	-587±10	-891±44
10^4	-50±3	-326±5	-589±8	-902±37
10^5	-49±3	-326±4	-586±12	-895±35
10^6	-50±2	-324±4	-582±15	-886±43
10^7	-49±3	-327±4	-583±11	-877±51
correct	-50	-325	-584	-889

FIGURE 7.44. Values of decay rates (modal attenuation) found with the method of pulsing.

7.11. Pulsed Instabilities; Subcritical Bifurcations

Pulsed instabilities are produced by a process sometimes called 'triggering.' We suppose that the dynamical system, here a combustor, is stable; that is, small disturbances decay to vanishingly small amplitude. It often happens that a real system behaves differently if it is exposed to a finite disturbance. There are three possibilities: the subsequent motion decays; the induced motion grows without limit; or the motion settles into some form having finite maximum size which, if periodic, is called a limit cycle. It is the last case that concerns us in this section. We explicitly exclude from our considerations the possibility that the system may enter an uncontrolled motion. (See Table 7.1 for contrary cases.) Whatever may be the form—i.e., the shape in time—of the initial disturbance, the overall process is generally called 'pulsing.'

Unfortunately, at the time of writing we do not have information about the history or current practice of pulsing in Russia. It has been and still is an important part of the development of Russian rockets. The subject is covered in the monograph by Dranovsky (2006), including results obtained in the early 1990s.

As we have already explained, pulsed instabilities include several practical problems involving the initiation of oscillations. It often happens that an instability is born during or soon after ignition of the device. A rocket, liquid or solid, may suffer a rapid rise of pressure followed by an overshoot of pressure. Oscillations may be a result, the Russian RD-0110 being just one example; see Chapter 1, and the remarks accompanying Figures 1.13–1.15. Sufficiently large pulses to excite instabilities may also be produced by material passing through the nozzle. For example, in large solid rockets, liquid Al_2O_3 exhausted as streamers, originating from the cavity surrounding the inlet to the nozzle, has been observed to produce small disturbances of chamber pressure, a consequence of a temporary reduction of throat area. Inadvertent and undesirable reductions of throat area are always possible. For these reasons, understanding the causes and consequences of finite pulses is an important theoretical and practical matter.

Pulsing without intent to cause instabilities has become a standard means of ranking or rating liquid rocket motors especially. The method has been used less widely for solid rockets. For both solid and liquid

rockets, repeated pulsing with different size pulses forms the basis for assessing the relative stability of a motor. For solid rockets, the time of pulsing during a firing is a second, but not necessarily secondary, variable. The procedure may also be used, for example, to assess the effect of modifications of the design on stability. Presently the status of calculating the unsteady flow is such that it is not possible to predict meaningful results.

In this section we are concerned mainly with the development of waves in a chamber following a pulse. It is not yet possible to predict completely the conditions under which an instability may develop. As an aid to interpreting the behavior, we will use results we have developed in Chapters 3 and 4. However, the available conclusions for the behavior and properties of pulses in a combustion chamber are few and quite limited; much remains to be done before the subject may be considered understood.

7.11.1. Pulsing Solid Propellant Rockets. Dickinsen (1962)¹¹ first reported pulsed instabilities, in a simple solid propellant rocket, a circular cylinder having diameter eight inches and initial port four inches in diameter.¹² Reports of the work in detail were given by Brownlee (1963) and Brownlee and Roberts (1963). Figure 7.45 shows a typical pressure record; see also Figure 1.42. Later, in similar tests, Brownlee and Kimball (1966) were able to use schlieren apparatus to show directly the discrete nature of the waves. An example is reproduced in Figure 7.46. The presence of the longitudinal wave train caused a continual rise of chamber pressure until a safety diaphragm failed. Note that the amplitude of the travelling waves became as large as (approximately) 30% of the mean pressure. Several characteristics distinguished this instability from previous works, such as those at NOTS, China Lake, which were concerned with spontaneous instabilities:

- (i) All of the propellants tested, even with nineteen percent aluminum, would, under appropriate conditions, support pulsed instabilities;
- (ii) The instabilities always involved longitudinal (axial) waves, as shown in Figure 7.47;
- (iii) The instability always produced increases in the mean pressure, the average burning rate, and the thrust, compared with their values in the absence of an instability;
- (iv) At sufficiently high chamber pressure, all the propellants tested would support pulsed instabilities;
- (v) Propellants having higher burn rates at a given pressure could be operated at higher chamber pressures before pulsed instabilities could be produced;
- (vi) Propellants more susceptible to erosive burning also exhibited more severe instabilities in the axial mode.

In a paper covering solid rockets more broadly, Dickinson and Jackson (1963) included Figure 7.47(a), a useful presentation of the stability boundaries for three propellants whose properties were not disclosed. Examples of the sort of data obtained in those tests are reproduced in Figure 7.47(b) showing the shift of the stability boundary with chamber pressure (throat diameter). Like many details of stability behavior, the result shown is likely to be in fact dependent on the propellant used. Thus, generalizing on the basis of results for one propellant should not be done. In a subsequent paper, Roberts and Brownlee (1971) clearly made the point by testing 54 propellants (polybutadiene and polyurethane binders) to show that a stability criterion proposed by Capener, Dickinson and Kier (1967) did not hold generally.

The tests analyzed by Brownlee *et al.* served to clarify one type of instability and established stability boundaries for the propellants tested. Unfortunately, the results contain almost no information in respect to the influence of particular propellant properties. It was also not an intent of the work to investigate the properties of the wave motions or the dependence of the instabilities on the geometry of the combustor.

¹¹The method of pulsing had apparently been in use for two years or so before this first report was made.

¹²The Canadian work described in this section was carried out to support development of the Black Brant sounding rocket. Hence the test conditions don't span the ranges one might prefer, to define the problem completely.

NONLINEAR BEHAVIOR OF COMBUSTOR DYNAMICS

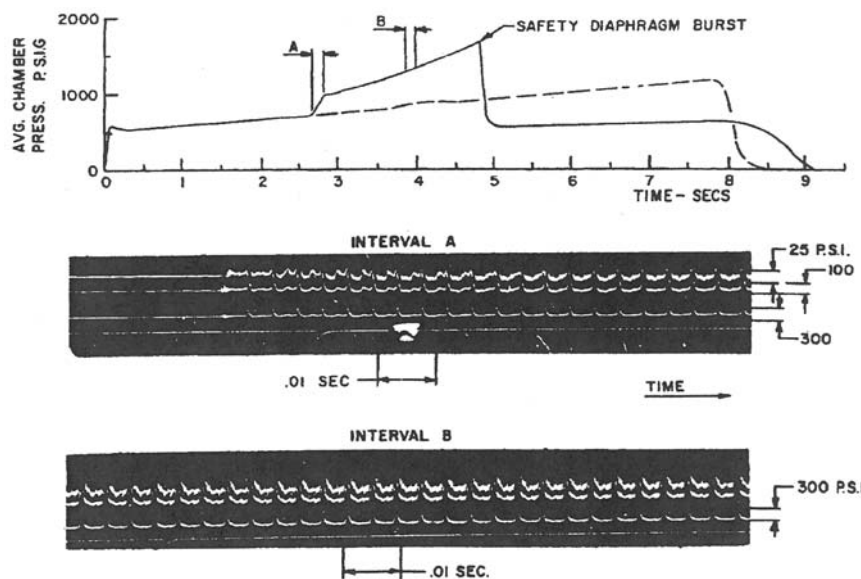


FIGURE 7.45. A pulsed instability initiated in an 80 inch long motor by a small explosive charge (Dickinson 1963; Brownlee and Roberts 1963).

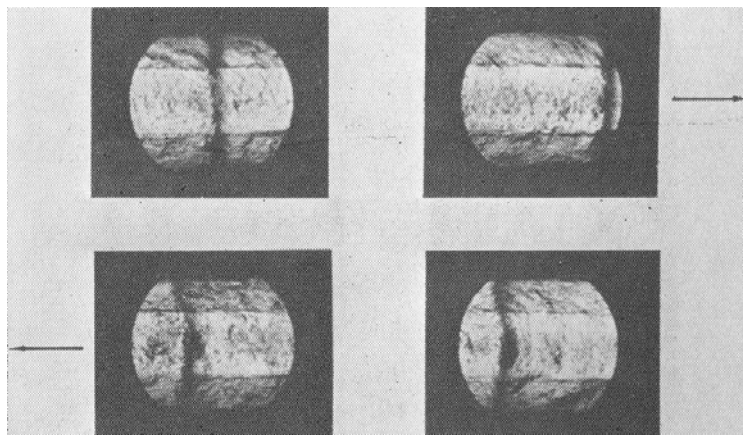


FIGURE 7.46. Picture taken with schlieren apparatus midway between the head-end and the nozzle (Brownlee and Kimbell 1966).

A program carried out at the Stanford Research Institute in the mid and late 1960s was not connected to a development effort and was therefore free to explore more basic questions. The main accomplishments were reported by Capener, Dickinson and Kier (1967); and Marxman and Wooldridge (1968, 1969). Unlike the works described above, these investigations placed considerable emphasis on the influence of propellant composition on the combustion instability leading to large-amplitude axial waves. As in the studies by Brownlee and his colleagues, the instability is 'subcritical' in the sense defined in Figure 7.26; to be initiated, a finite disturbance or pulse is required. Thus the motors, for the propellants used, were intrinsically stable for the range of conditions tested.

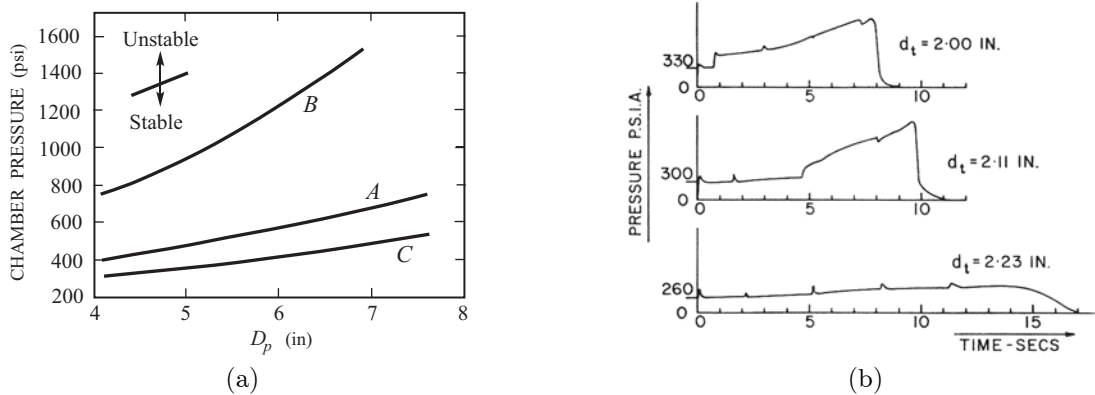


FIGURE 7.47. (a) Stability boundaries for three propellants tested in 80 inch motors and (b) influence of mean pressure (throat diameter) on stability (Dickinson and Jackson 1963).

Although some firings were made with potassium perchlorate, by far most propellants used ammonium perchlorate, the oxidizer used in practice.¹³ The binder was PBAN (polybutadiene, acrylic acid, acrylonitrile) which is no longer favored since higher-energy materials are available. Consequently, as often the case with older propellants, the results may be qualitatively suggestive but certainly not valid quantitatively for modern propellants. Figure 7.48 is a compilation of data for a 40 inch series of tests, practically all using AP/PBAN propellants. The similarity with the results obtained by Brownlee, Roberts *et al.* is clear. As in the earlier work, the pressure/burn rate relation was varied by changing the oxidizer particle size, a particularly attractive feature of ammonium perchlorate. The main purpose of the experiments discussed by Capener *et al.* was to obtain results like those shown in Figure 7.48 for a broad range of practical propellant compositions.

Marxman and Wooldridge (1968) apparently were first to attempt to relate the excitation of the finite-amplitude instability to the dynamical properties of the propellant. At that time the subject of the dynamics of propellant burning was a subject of active research; see Section 2.1 and, for example, the extended review by Culick (1968). In particular, Marxman and Wooldridge (1968) had paid special attention to the influence of surface reactions on the response of a burning surface propellant. Using a linearized representation of the propellant response (see Section 2.1) they found that surface reactions can have substantial effect on the amplitude of the propellant response.¹⁴ So far as the present context is concerned, the importance of this work is the use Marxman and Wooldridge made of it in their interpretation of travelling waves in a solid propellant rocket, the axial-mode instability.

The main idea is that the oscillating wave in the chamber is a weak shock wave presenting to the surface an oscillating pressure. That oscillation of pressure causes the burning rate to oscillate. It is the oscillation of burning rate that sustains the shock in the presence of losses, notably attenuation accompanying partial reflection by the exhaust nozzle. Thus the dynamical burning process, travelling with the shock wave, "acts essentially as an annular piston behind the shock wave, ... similar to the role of exothermic chemical reactions in supporting a detonation wave." This idea was developed by requiring that the frequency of the wave should be close to the value at which the propellant response is maximum; and that the response at this frequency should be at least as large as required to support the shock wave.

¹³For unknown reasons, propellants containing potassium perchlorate were also stable to pulsing. There are practical reasons for not using potassium perchlorate in operational propellants.

¹⁴Marxman and Wooldridge were critical of alternative treatments of surface reactions by Brown *et al.* (1968); Friedly and Peterson (1966)a,b; and Krier *et al.* (1968). The similarities and differences among the analyses lie outside the range of the present discussion.

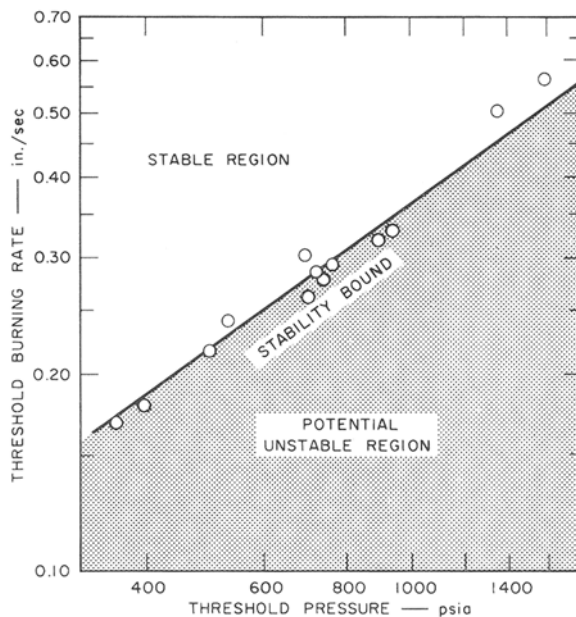


FIGURE 7.48. Stability boundary for 40 inch rockets, 5 inch diameter showing chamber pressure and burning rate below which pulses of pressure are stable (Capener, Dickinson and Kier 1967).

For typical conditions in the experiments examined, the value of the response required was about 1–1.2, ignoring other losses, notably that provided by the nozzle. The response required is reasonable, and overall the model proposed has several appealing features. However, despite the quantitative estimates, the results cannot be used, or extended, for predicting details of the instabilities produced in practice.

With a series of papers¹⁵ in the period 1981–1986, Levine and co-workers have given the most successful and thorough numerical solutions for instabilities with steep-fronted waves in solid-propellant rockets. The success of the work was established by good comparison of the computed results with specially conducted experiments in cold flow as well as motor firings. While the calculations cannot give the fine details of the flow field found with LES simulations, the waveforms produced are remarkably close to those observed, and the consequences of changing physical parameters in the problem are generally explicable and fairly well-understood.¹⁶

In the early 1970s, numerical methods were first applied to instabilities in solid-propellant rockets, independently in two efforts by Levine and Culick (1972, 1974); and by Kooker (1974), reported also by Kooker and Zinn (1973). Particularly to be noted is that Kooker found a form of triggering in his work. Figure 7.49 reproduces one of his results showing a clear qualitative change of the response with amplitude of a continuously applied pressure oscillation. He reported no results for responses to input pulses.

The requirements of the problems taxed computing capabilities to the extent that only a few (c. 20 at most) cycles of an unstable oscillation could be produced with the numerical methods used. There was therefore strong practical motivation for developing approximate methods (Culick 1973a,b; Powell 1970,

¹⁵Levine and Baum (1982, 1983); Baum and Levine (1982, 1986, 1987); Baum, Lovine, and Levine (1983); Baum, Levine, and Lovine (1984); Baum, Levine, Chew and Lovine (1984); Lovine, Baum, and Levine (1985); and Baum, Levine and Lovine (1988).

¹⁶Recall some basic principles governing the behavior of waves in a compressible medium, formulated by Chu and Kovasznay (1957) and summarized briefly in Sections 3.1 and 7.9.

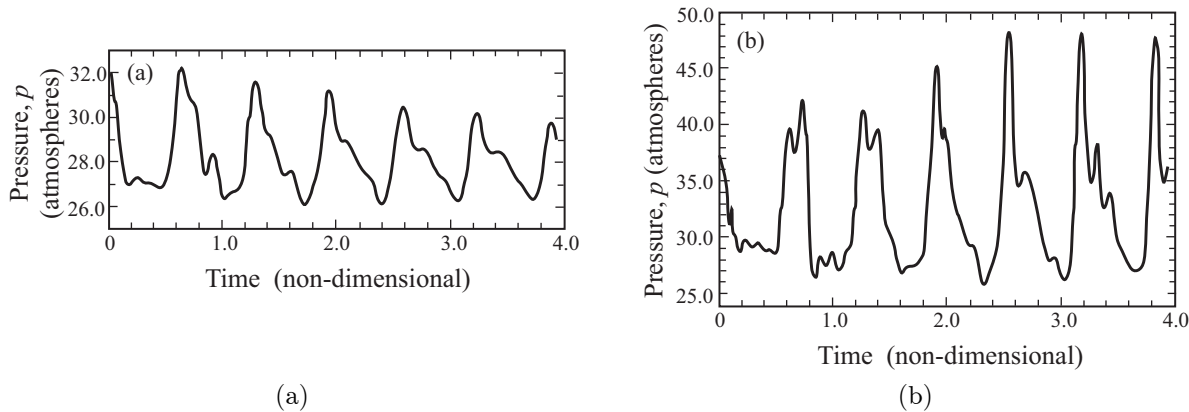


FIGURE 7.49. Response of the head end of a motor ($L = 10$ ft.) to a continuously applied input pressure (Kooker and Zinn 1973).

example). Comparison of exact and approximate methods was a central issue (Culick and Levine 1974) in the early work, but in the period covered by the works of immediate concern here, and for the instabilities treated, the principal matter was reconciliation of the results of numerical calculations with observations.

The works in question (see Footnote 15) form a very instructive example of properly applying numerical methods and modeling to internal flows found in solid propellant rockets, accompanied by specially conducted experimental works. It must be recognized, however, that significant limitations are imposed on possible applications because all combustion processes are confined to the lateral surface of a chamber; and the dynamics of combustion are represented by an extension of the model due to Dennison and Baum (1961), as described here in Section 2.1. Most of the cases treated in the references are for uniform chambers.

In the first paper of the series, Baum and Levine (1982) addressed in detail the problem of computing the development of a standing wave or a pulse into traveling waves. They followed the general strategy worked out by Levine and Culick (1972, 1974) but used a combination of three computational methods, the Lax-Wendroff, hybrid, and artificial compression schemes. It was an important achievement that they were able to treat a shock wave as an abrupt discontinuity “without generating artificial pre- or post-shock oscillations” and without introducing artificial viscosity.

With subsequent publications Levine and Baum (1982, 1983) demonstrated that by taking velocity coupling into account, they were able to obtain results for triggering; shifts of the mean pressure when oscillations are present; and some cases when limit cycles were modulated. They also worked with Levine at Aerojet Tactical Systems to demonstrate the first results comparing numerical computations and oscillations produced by pulsing in cold flow tests (Baum, Levine and Levine 1983). Figure 7.50 shows the three devices used. Figure 7.51 shows the time-evolution of a measured and a predicted pressure perturbation within a chamber containing only the flow from the pulsing unit.

In a paper presented publicly in 1982 but published two years later, Baum, Levine and Levine (1984) essentially combined the main results presented in their previous works and treated sub-critical instabilities in laboratory motors and full-scale motors. The laboratory motor was 48 in. (1.22 m) long with internal case diameter 2.25 in. (5.7 cm); results were reported for three tests having partial grain either eight or nine inches long, and a fourth test having three short grain elements. In all cases quite good agreement was obtained for the observed and calculated time evolutions of sharp fronted wave following pulses. An example is reproduced as Figure 7.52 showing the results for the first and second pulses of the second test

NONLINEAR BEHAVIOR OF COMBUSTOR DYNAMICS

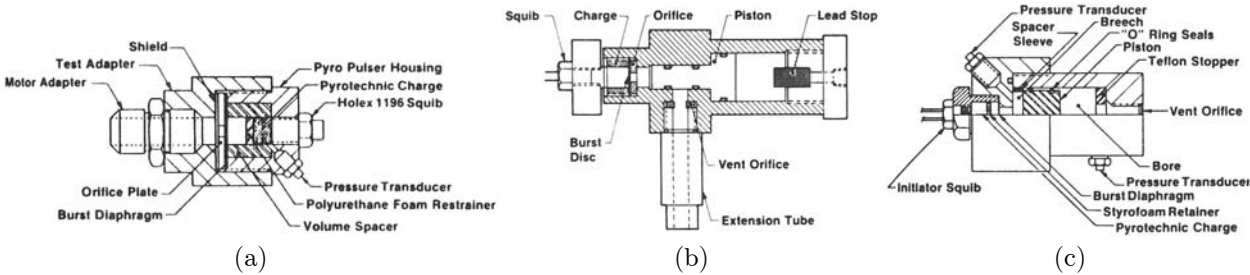


FIGURE 7.50. Three types of pulsing devices used by Baum, Lovine and Levine (1983). (a) pyro pulser; (b) low-brisance pulser; (c) piston pulser.

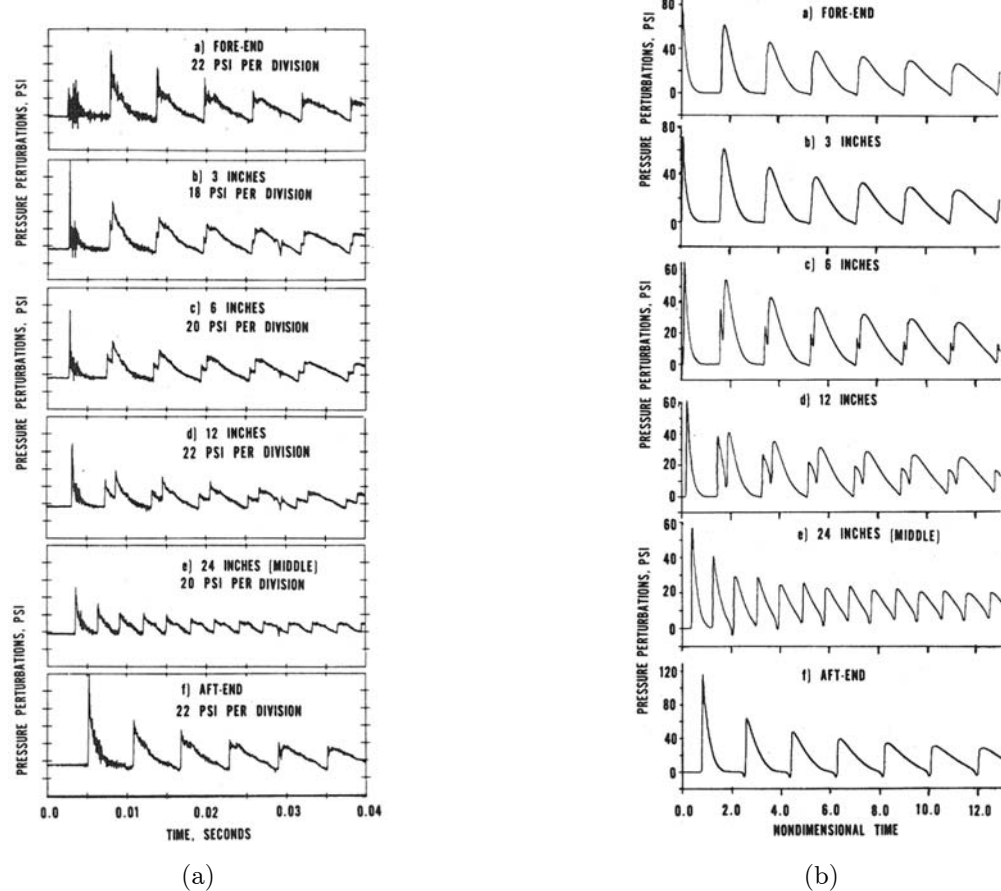


FIGURE 7.51. Time evolution of pressure perturbations produced by a pyro pulser. (a) measured; (b) calculated (Baum, Lovine and Levine 1983).

called PCC4. The wave following the first pulse was stable and decayed before the second pulse was fired 0.23s after the first.¹⁷

There is a significant piece of the problem which is certainly not known well, namely representation of the dynamical characteristics of the propellant combustion. Levine *et al.* chose to use the basic result of

¹⁷Note the horizontal scale in Figure 7.52.

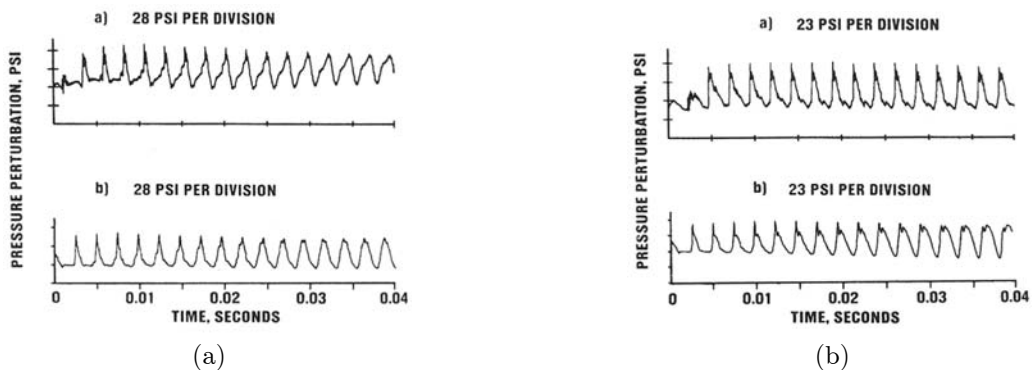


FIGURE 7.52. Comparison of measured and predicted pressures at the head end, test PCC4 (a) first pulse; (b) second pulse (Baum, Levine and Lovine 1984).

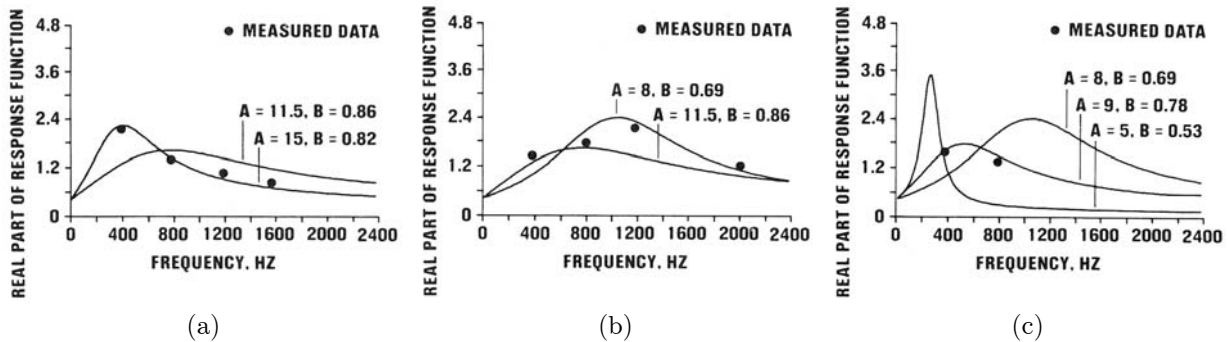


FIGURE 7.53. Response functions for the three propellants used by Baum, Levine and Lovine (1988).

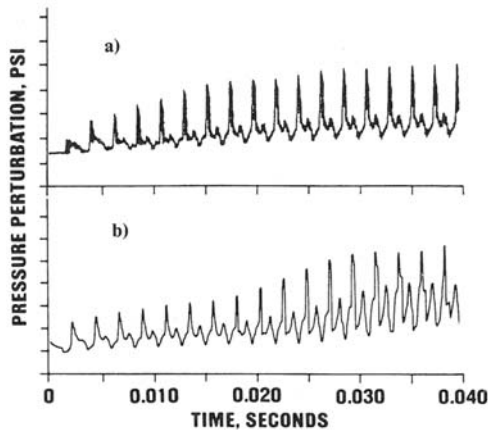


FIGURE 7.54. Comparison of observed and calculated pulsed instabilities in an aft-finocyl motor (a) observed; (b) calculated (Baum, Levine and Lovine 1988).

Dennison and Baum (1961) which forty years later still remains the best starting point. However, to obtain (even qualitatively in some respects) their good results, Levine and Baum found it essential that the surface combustion should be sensitive not only to pressure changes but also to fluctuations of velocity tangential to

the surface, *velocity coupling*. The idea that velocity coupling may be an important aspect of the dynamics of surface combustion is not new, dating back to the late 1950s; see Culick (1970) for a review of early work. In a later paper Baum and Levine (1983) have given a short discussion of their experience with modeling velocity coupling. They eventually chose the form for the fluctuation of mass flux produced by the propellant

$$\dot{m}' = \dot{m}'_{pc} [1 + R_{vc} F'(\bar{u})] \quad (7.59)$$

where $F(u) = |u'|$ represents the dependence on the magnitude of the velocity and \dot{m}'_{pc} is related to the response function R_p for pressure coupling by (2.2). Much of the work by Levine *et al.* to obtain good agreement between their predicted results and observations was spent on adjustments to the parameters in (7.59).

The last paper by Baum, Levine and Lovine (1988) not only gives their final results but also summarizes their approach in general. It is probably the best paper of the series, giving an overall view of the work as well as some new findings. Results are present for eighteen pulsed motor tests in motors 8.38 cm (3.3 in) in diameter, having lengths 0.61 m., 0.91 m. and 1.22 m. (24, 36, 48 in). Three reduced-smoke propellants were tested in four different grain designs: cylinder, fore- and aft-finocyls and “dog-bone”. In all tests three pulses were planned, a pyrotechnic, an ejected sphere, and a pyrotechnic in that order; ten tests were unstable on the second pulse and nine on the first, leading to amplitudes $\Delta p/\bar{p} = 0.1$ to 0.3. Two of the propellants produced “significantly higher wave amplitudes” in the aft-end finocyl configuration. That configuration also produced consistently greater DC shifts of mean pressure than the fore-end finocyl, a behavior that was found also in numerical predictions.

A limited amount of T-burner data, shown in Figure 7.53, was available for the response functions of the propellants used. These results for the parameters A and B were used to fix the response function according to our form (2.67) of Dennison and Baum’s formula. Experience has shown that the values of A and B suggested are quite reasonable; see Section 2.2.3.

The discussion by Baum, Levine and Lovine explains how the values of the various parameters were chosen and fixed for comparison of predicted and observed waveforms. In the paper, six remarkably good comparisons are given. Figure 7.54 shows an example in which a secondary wave grows out of the primary wave. The original reference contains not only further examples but informative discussion and interpretation.

7.12. Dependence of Wall Heat Transfer on the Amplitude of Oscillations

Surface heat transfer is sometimes an important contribution to the loss of acoustic energy for oscillations in chamber. Normally for solid rockets that is not the case, but the T-burner (Figure 2.7) is a special contrary case. The problem of measuring the linear limit of heat transfer under oscillatory conditions has been discussed in Chapter 6 and Annex C. Here we are concerned with the dependence in the amplitude of oscillation, a very significant effect. The most recent work seems to have been reported by Merkli and Thomann (1975) in which oscillations were driven mechanically in a tube containing air. The observed increase of heat transfer rate was shown to be associated with the development of turbulence in part of an oscillatory cycle.

Combustion driven oscillations may reach considerably higher amplitudes than those sustained mechanically. As part of his work with the T-burner, Perry (1970) inferred mean heat transfer rates (\bar{h}) over oscillatory amplitudes from 2 to 60 psi, the average pressure being 300 psig. Results are given in Figure 7.55. The notation $(\bar{\quad})$ indicates an average over the length of the T-burner so the dependence shown can be regarded only as approximate. Data taken for five propellants, presented in dimensionless correlations, Nusselt number versus Reynolds number, are plotted in Figure 7.56. The definitions are used

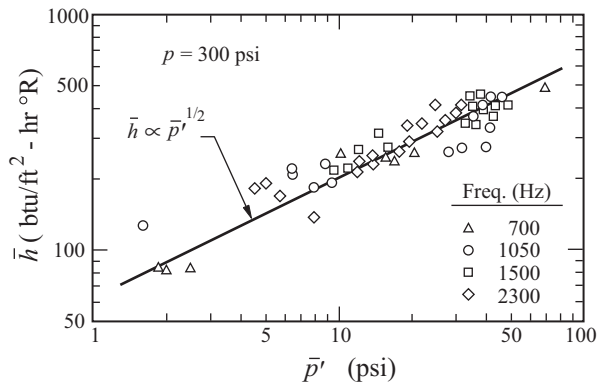


FIGURE 7.55. Mean heat transfer coefficient measured in T-burners showing dependence on amplitude of pressure amplitude (Perry 1970).

$$\bar{N}u = \frac{\bar{h}\delta}{k} \quad (7.60)$$

$$\bar{R}e = \frac{\bar{p}'\delta}{\bar{\mu}\bar{a}} \quad (7.61)$$

where \bar{a} is the average speed of sound, and

$$\delta = \sqrt{\frac{\nu}{\pi f}} \quad (7.62)$$

is the ‘thickness’ of the acoustic boundary layer. The straight line in Figure 7.56 is

$$\bar{N}u = 0.044 \sqrt{\bar{R}e} \quad (7.63)$$

which implies $\bar{h} \propto \sqrt{\bar{p}'} f^{1/4}$. Perry and Culick (1974) note that the data shown in the figures cover a range of maximum velocity fluctuation to mean velocity from near zero to twenty.

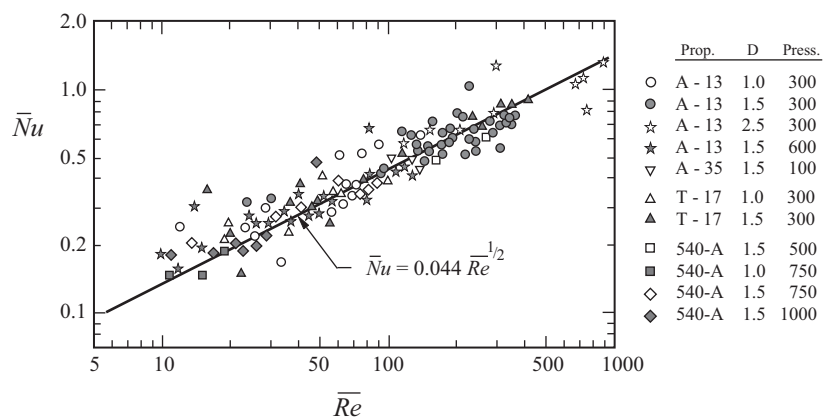


FIGURE 7.56. Mean heat transfer rates correlated as mean Nusselt number versus mean Reynolds number (Perry 1970).

No theory of the behavior shown in Figures 7.55 and 7.56 was given in the original work, or apparently since that time. The quantities defined by (7.60)–(7.62) were chosen as reasonable references and have at best qualitative significance. A brief attempt was made by Perry and Culick (1974) to determine a local

correlation (local heat transfer rate versus local oscillating pressure amplitude) with some reasonable results identical to equation (7.62).

The general problem summarized by the title of this section arises in several practical situations. For example, consequent structural failures in liquid propellant rockets and gas turbine combustors are well-documented. There is a genuine practical need for further clarification of the matter.

7.13. One Way to Analyze the Behavior of Pulses

Levine and Baum achieved remarkably good results using a one-dimensional representation of the wave motions. At least two reasons account for their success in obtaining such close agreement between their computations and observed behavior: careful development and application of the methods to calculate the steep-fronted waves; and close attention to (and modification of) the representation of the unsteady supply of material from the lateral burning surface. The second matter is heavily involved with the problem of velocity-coupling.

It is intrinsic to the works described in the preceding section that the calculations are elaborate and must be entirely done with a computer. In this section we discuss a way of computing the same sorts of problems, which is at best roughly approximate but which offers the possible advantage of investigating some aspects more easily. Although the specific problems discussed in the previous section will not be treated, the possible applications should be clear.

The basis for this calculation has been thoroughly discussed in Chapters 3 and 4. We will use equations (4.64)a,b based on the method of averaging applied to the more general second-order equations (4.36), or (7.5) with $F_n^{NL} = 0$. Since the wave motions that concern us here involve purely longitudinal motions, we assume that they are well-represented by longitudinal modes; the time-averaged equations are therefore (7.28)a,b. A simple example, a square pulse propagating in a quiescent gas contained in a closed tube with no combustion, displays the main idea. As indicated in Figure 7.57, a single pulse within the chamber may be represented as the superposition of two infinitely long trains of pulses, one train moving to the left, and one to the right. At the instant for which the figure is drawn, the pulse A is about to cross the boundary $z = 0$ from left to right, and the pulse B is about to cross from right to left. This represents reflection of a leftward moving pulse at the end, $z = 0$, of the tube. It is easy to deduce from the figure that during reflection the amplitude of the pulse is doubled near the reflecting boundary. Just before reflection, the real pulse within the chamber is represented by pulse B, and after reflection pulse A represents the real pulse. Note that pulses in each of the trains are separated by the distance $2L$, twice the length of the chamber. Hence the wave system comprising the two wave trains has period $2L$. This represents the pulse within the chamber travelling the distance $2L$ for a full cycle.

Under the conditions chosen here, the pressure pulse in the chamber must satisfy the homogeneous wave equation subject to the boundary condition for rigid walls at the ends,

$$\frac{\partial^2 p'}{\partial z^2} - \frac{1}{a^2} \frac{\partial^2 p'}{\partial t^2} = 0 \quad (7.64)$$

$$\frac{\partial p'}{\partial z} = 0 \quad (z = 0, L) \quad (7.65)$$

The general solution of (7.64) may be written as the sum of rightward and leftward moving waves:

$$\frac{p'}{\bar{p}} = f(z - at) + g(z + at) \quad (7.66)$$

Figure 7.58 shows a special case of this solution. The train of pulses moving to the right is represented by $f(z - at)$ and those moving to the left are contained in $g(z + at)$. It is apparent that in order to satisfy the boundary conditions at the ends of the chamber having length L , the wave trains must have period $2L$.

We will be particularly concerned here with the wave motions subsequent to specified initial conditions. Note that the example shown in Figure 7.58 was constructed artificially; it is not immediately obvious what *initial* conditions will produce the wave motion. The simplest initial value problem is that for a pulse initially at rest:

$$(t = 0; \quad 0 \leq z \leq L) \begin{cases} p'(z, 0) = \bar{p}P(z) \\ \frac{\partial p'}{\partial t}(z, 0) = 0 \end{cases} \quad (7.67)$$

For $t > 0$ such a pulse splits into *two* pulses, one moving to the left and one moving to the right. The solution can be represented as the superposition of two pulse trains as sketched in Figure 7.58. For this case the pulses in each of the trains have half the amplitude of the initial pulse.

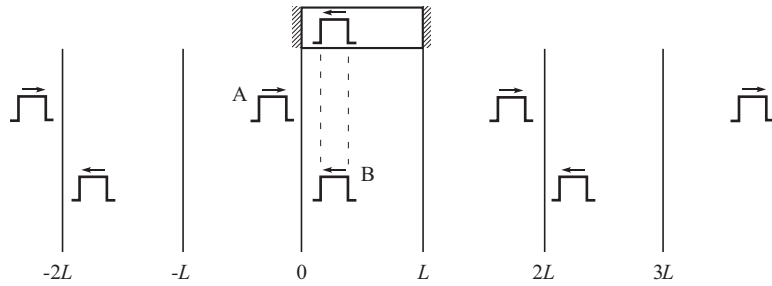


FIGURE 7.57. Superposition of two pulse trains to represent propagation of a single pulse in a closed tube.

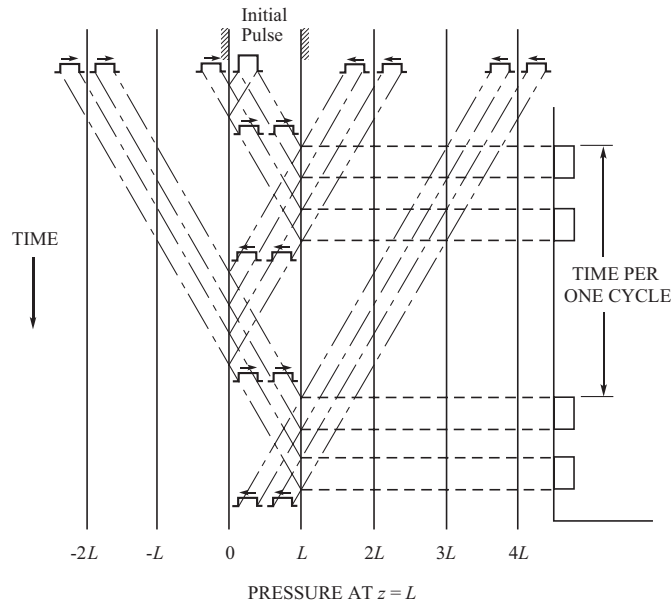


FIGURE 7.58. Propagation of pulses developed from a stationary initial pulse in a closed tube.

Because the initial pulse splits, there are always two pulses in the chamber. Measurement of the pressure at one end produces a signal which is periodic, having period equal to the round trip time for *one* of the pulses. The fundamental frequency of the signal is the fundamental frequency. For example, if a symmetric pulse is introduced at the center of the chamber, then the fundamental frequency of the signal is the frequency of the *second* mode of the chamber.

The case of a single pulse, sketched in Figure 7.57, is the simplest to visualize, and constitutes a special case of the general initial value problem. In order to satisfy the boundary conditions, it is necessary, as Figure 7.57 illustrates, to use wave trains having period twice the length of the chamber. We wish to account for both the initial pulse shape, $P(z)$, and its initial rate of change with time, $Q(z)$; the initial conditions are

$$\frac{p'}{\bar{p}}(z, 0) = P(z) \quad (7.68)$$

$$\frac{\partial}{\partial t} \frac{p'}{\bar{p}}(z, 0) = Q(z) \quad (7.69)$$

Define the function $F(z)$ representing leftward and rightward moving pulse trains required to satisfy the initial shape (7.68):

$$F(z) = \begin{cases} P(z) & 0 \leq z \leq L \\ P(-z) & -L \leq z \leq 0 \end{cases} \quad (7.70)$$

Outside the region $-2L \leq z \leq 2L$, $F(z)$ is periodic, having period $2L$:

$$F(z + 2nL) = F(z) \quad -2L \leq z \leq 2L; \quad n = \pm 1, \pm 2, \dots \quad (7.71)$$

Similarly, a function $G(z)$ is defined to represent pulse trains required to satisfy the initial rate of change of the pressure field

$$G(z) = \begin{cases} Q(z) & 0 \leq z \leq L \\ -Q(-z) & -L \leq z \leq 0 \end{cases} \quad (7.72)$$

$$G(z + 2nL) = G(z) \quad -2L \leq z \leq 2L; \quad n = \pm 1, \pm 2, \dots \quad (7.73)$$

Note that $F(z)$ is an even function and $G(z)$ is an odd function, with respect to the origin $z = 0$.

The pressure field for any $t \geq 0$ is given by the formula

$$\frac{p'}{\bar{p}} = \frac{1}{2} [F(z - at) + F(z + at)] + \frac{1}{2a} \int_{z-at}^{z+at} G(\xi) d\xi \quad (7.74)$$

It is easy to confirm that this formula for p'/\bar{p} satisfies the initial conditions (7.68) and (7.69), and because of the definitions of $F(z)$ and $G(z)$ as periodic functions, the boundary conditions at $z = 0, L$ are satisfied.

Now the connection between the solution (7.74) and the normal modes of the chamber is established by expanding $F(z)$ and $G(z)$ in Fourier series:

$$F(z) = \sum_{n=0}^{\infty} B_n \cos k_n z \quad (7.75)a,b$$

$$G(z) = \sum_{n=0}^{\infty} C_n \cos k_n z$$

The Fourier coefficients are calculated from the formulas

$$\begin{aligned}
 B_0 &= \frac{1}{L} \int_0^L P(z) dz \\
 B_n &= \frac{2}{L} \int_0^L \cos(k_n z) P(z) dz \\
 C_0 &= \frac{1}{L} \int_0^L Q(z) dz \\
 C_n &= \frac{2}{L} \int_0^L \cos(k_n z) Q(z) dz
 \end{aligned} \tag{7.76}a,b,c,d$$

The average values of the pulse and its rate of change are B_0 and C_0 . In calculations we will be concerned only with the evolution of departures from the average values. Substitution of (7.75)a,b into (7.49) leads to the Fourier series for $p'(z, t)$:

$$\begin{aligned}
 \frac{p'}{\bar{p}} &= \frac{1}{2} \sum_{n=0}^{\infty} B_n [\cos k_n(z - at) + \cos k_n(z + at)] \\
 &+ \frac{1}{2} \sum_{n=0}^{\infty} C_n \frac{1}{\omega_n} [\sin(z - at) + \sin k_n(z + at)]
 \end{aligned} \tag{7.77}$$

Because C_n has dimensions of frequency, the factor $\omega_n = ak_n$ makes C_n/ω_n dimensionless.

Expansion of the functions in (7.77) leads to the form

$$\frac{p'}{\bar{p}} = \sum_{n=0}^{\infty} [A_n \sin \omega_n t + B_n \cos \omega_n t] \cos k_n z \tag{7.78}$$

in which A_n has been written from C_n/ω_n . This result is identical with the expansion (4.27), using (4.65) for $\eta_n(t)$. For a pulse which propagates in a passive medium, with unchanging shape, the Fourier coefficients A_n and B_n are constant. For the problems arising in combustion chambers, A_n and B_n vary with time according to equations (4.64)a,b.

Hence we now have a means for analyzing the behavior of an arbitrary pulse in terms of the normal modes of a chamber, and accounting for nonlinear gasdynamics. The procedure may be summarized in the following steps.

- 1) The initial shape and rate of change of the pressure are specified, giving the functions $P(z)$ and $Q(z)$.
- 2) The initial values of B_n and $A_n = C_n/\omega_n$ are calculated from the formulas (7.76)a,b.
- 3) The time evolution is calculated by using the appropriate forms of equations (7.28)a,b.
- 4) The pressure field can then be calculated at any time by using (7.78).

In principle, any problem of one-dimensional pulse propagation can be handled in this way, accounting for linear and nonlinear processes in the medium. Practical difficulties may arise in the treatment of a steep-fronted pulse requiring a large number of modes for a faithful representation.

7.13.1. Some Results for the Propagation of Pulses. We shall consider here only cases of rectangular pulses with the initial pressure not changing in time. Thus $Q(z) = 0$ in (7.69), and the Fourier

coefficients are given by (7.51)a,b. For a pulse having height Δ , and non-zero in the range $L_1 \leq z \leq L_2$, the coefficients are

$$B_0 = \Delta(L_2 - L_1) \quad (7.79)$$

$$B_n = \frac{2\Delta}{n\pi} \left[\sin\left(n\pi \frac{L_2}{L}\right) - \sin\left(n\pi \frac{L_1}{L}\right) \right] \quad (7.80)$$

Figure 7.59 shows the approximations using 10, 20, 30 and 50 modes for a pulse generated at one end of a chamber in the range $.1L \leq z \leq .4L$.

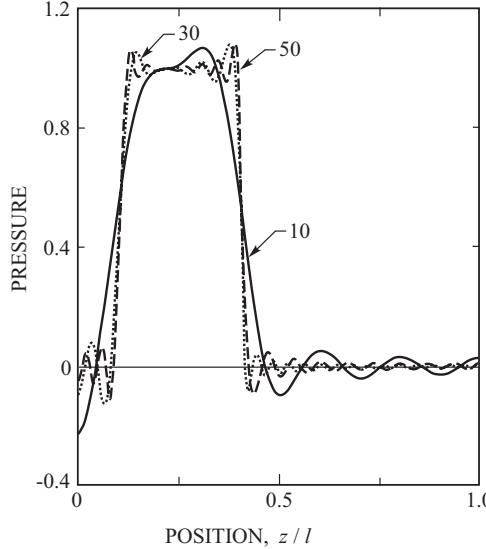


FIGURE 7.59. Approximations to a rectangular initial pulse by 10, 30, 50 modes. Pulse initially in the range $0.1L \leq z \leq 0.4L$.

Equations have been solved here for two cases: $\alpha_n = \theta_n = 0$; and for the values of α_n θ_n chosen to illustrate the propagation of pulses. No results have been obtained for the conditions in a motor. The simplest case is a small amplitude pulse with no losses: $\alpha_n = \theta_n = 0$. Figure 7.60(a) is the pressure at the head end ($z = 0$) for the pulse represented by ten modes, Figure 7.60(b), and $\Delta = 0.006$. Because only ten modes are used, ripples appear in the waveform. The pulse shape in the chamber is shown in Figure 7.60(b) for various times during three cycles. For the small amplitude of this pulse, the second order nonlinearities have no discernible effect on the pulse shape for the short time covered in this figure.

In contrast, the case $\Delta = 0.1$ is a large amplitude pulse, and the influence of nonlinearities appear already in the first cycle. The initial shape is that of Figure 7.60(a). Figure 7.60(a) is the waveform at $z = 0$, and Figure 7.60(b) shows the pulse shape at various times. For comparison, the waveform of a simple cosine, the fundamental mode, is shown in Figure 7.61. Note the steepening into a weak shock after three cycles. The generation of higher harmonics is evident, both in the waveform measured at $z = 0$ and in the shape of the pressure distribution, in the chamber. However, an interesting feature is that the smoothness of the spatial distribution is not reflected in the time history, appearing in Figure 7.61(a). The uneven character of the latter is due to the excitation of higher frequencies whose associated spatial waves combine to form the smoothly steeping solitary wave which propagates as shown in Figure 7.61(b).

One of the interesting and potentially useful features exhibited by pulses in motors is the change of shape due to different rates of decay for the modes. In Figure 7.62, the decay of a small amplitude pulse is shown. For this case, $\alpha_n = -40n$, and $\theta_n = 0$ in equations (7.28)a,b; again the initial pulse shape is the

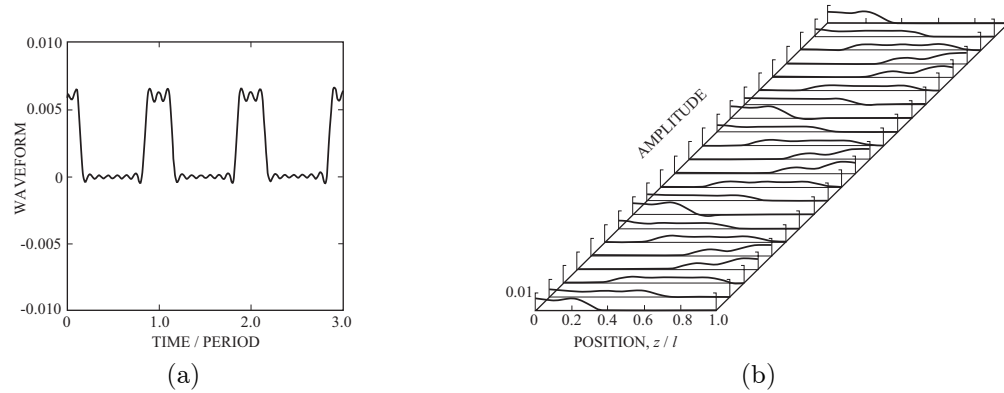


FIGURE 7.60. Propagation of a rectangular pulse without losses (10 modes): $p'(z, 0) = 0.006p_0$; $0 \leq z \leq 0.3L$. (a) Waveform at $z = 0$; (b) pulse shapes for three cycles.

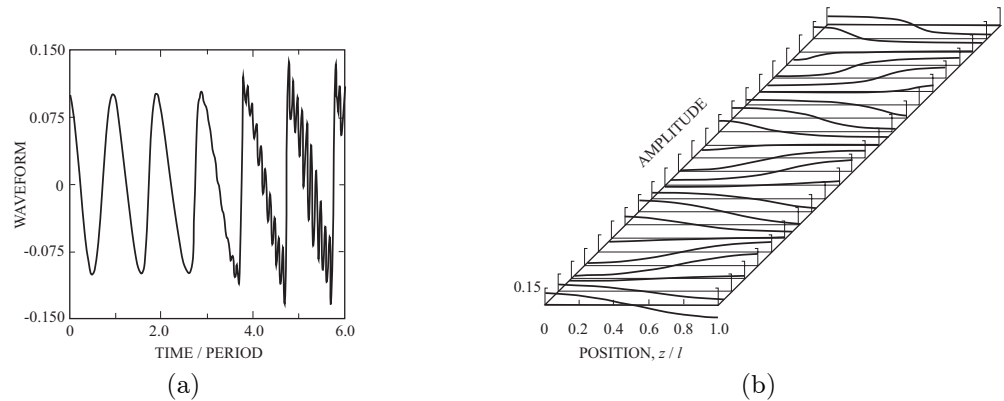


FIGURE 7.61. Propagation of an evolving cosine wave: $p'(0, 0) = 0.01p_0$. (a) Waveform at $z = 0$; (b) pulse shapes for three cycles. Notice the form of the steepened cosine wave shown at the end of the third cycle.

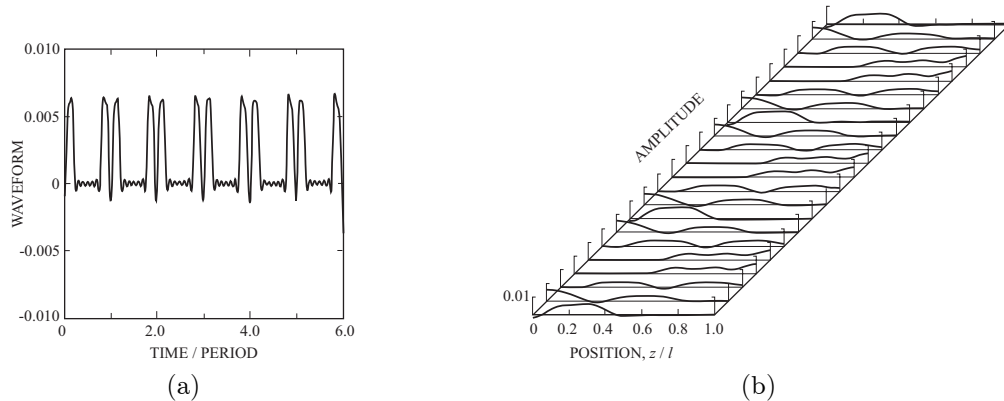


FIGURE 7.62. Propagation of a rectangular pulse (10 modes): $p'(z, 0) = 0.006p_0$; $0.1L \leq z \leq 0.4L$. (a) Waveform at $z = 0$; (b) pulse shapes for three cycles.

approximation for ten modes, Figure 7.62(a). After six cycles there are still substantial amounts of the first five harmonics but the next five are practically absent. The average value of the pulse remains fixed at its initial value, so the pressure fluctuation does not become negative after several cycles.

Finally, in Figure 7.62 the behavior of a rectangular pulse initially displaced from one end is shown. The initial shape is the approximation with ten modes, Figure 7.62(b). This case corresponds to the perfect rectangular pulse sketched in Figure 7.58. The qualitative similarities are obvious.

7.14. Spatial Averaging and Dynamical Systems Theory Applied to Pulsed Instabilities

Attention to the problem of triggering shifted in the 1990s from numerical solutions to use of the method based on spatial averaging as described in Chapters 3 and 4. Although there was no proof, numerous examples had finally led to the conclusion that the equations with linear combustion sources and second order acoustics do not contain triggering. Attempts to find triggering with the equations carried to third order in nonlinear acoustics also failed (Yang, Kim and Culick 1990). The general conclusion was (and is) that the nonlinear acoustics alters the distribution of energy among the modes of oscillation, but since there is no external source of energy, the process cannot support triggering. Therefore, emphasis shifted to the role of the source terms. Due to the conclusion just stated, it is sufficient, at least for the initial work, to consider only second order acoustics. To the present time, third and higher order acoustics have not been considered; there seems to be no need to use an expansion procedure higher than second order.

Earlier work (Yang, Kim and Culick 1990) had shown although the result was not rigorously proven in general, that triggering could occur if either quadratic self-coupling or linear cross-coupling between modes are present. For example, in unpublished work, a model system examined by Awad and Culick (1984) demonstrated the importance of quadratic self-coupling which, however, does not arise in the modal expansion of the purely fluid mechanics contributions ($\rho\vec{u} \cdot \nabla\vec{u}$, etc.). Thus, it appeared again that the resolution of the matter lay with the source terms.

In 1996, Wicker, Green, Kim and Yang (1996) used the time-averaged equations accounting for two modes, to study the conditions under which triggering occurs for five forms of the unsteady burning rate. When \dot{m}'_1 is proportional to p'^2 , u'^2 or $p'u'$ no triggering. The authors found in that case no linear or quadratic self-coupling so the result is consistent with the conclusion cited above. However for \dot{m}'_b proportional to $|\vec{u}'|$ or $p'|\vec{u}'|$. They used the time-averaged equations. An interesting, and probably important, feature of their results was the fact that linear cross-coupling among the acoustic modes and quadratic self-coupling of the fundamental mode were the origin of triggering. A bit unsettling is the conclusion that the “initial phase difference and harmonic content can be just as important as initial composite amplitude in determining the stability of a pulse.” This result suggests a certain kind of sensitivity that may be associated with the use of the time-averaged equations. See Jahnke and Culick (1994) for relevant results dealing with the limitations of the time-averaged equations; they did not, however, examine triggering.

Nearly contemporaneous with the work of Wicker *et al.* were results obtained by Jahnke and Culick (1995) using the continuation method described in Section 7.4. They used two models for nonlinear combustion, that of Levine and Baum (1983), and a slightly simpler one by Greene (1990) in which $\dot{m}'_b \sim |\vec{u}'|$. We will discuss only the first here, for which the fluctuation mass flux departing the burning surface is computed with a slightly more complicated form of (7.59). Assume that the *total* mass flux (not just \dot{m}') is given by (7.59) so the fluctuation is now

$$\begin{aligned}\dot{m}' &= \dot{m} - \bar{\dot{m}} \\ &= (\dot{m}'_{pc} + \bar{\dot{m}}'_{pc}) [1 + R_{vc}|\mathbf{U}'|] - \bar{\dot{m}}'_{pc}\end{aligned}$$

Some rearrangement and introduction of the response function R_b leads to the relation

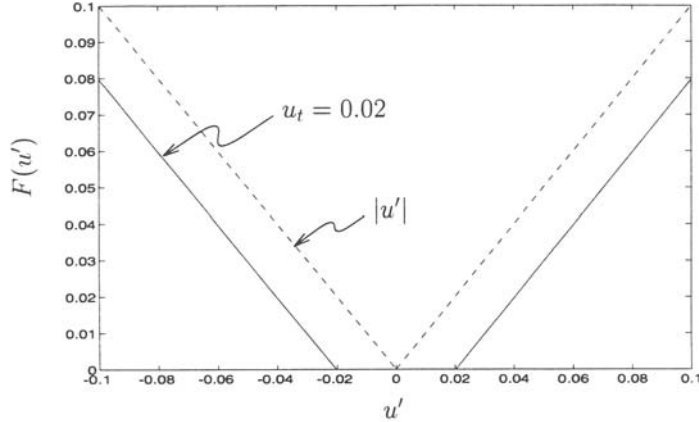


FIGURE 7.63. The function $F(u')$ used in the model having a threshold velocity $u_t > 0$; the value $u_t = 0.02$ is only an example (Burnley 1996).

$$\frac{\dot{m}'}{\bar{m}} = R_b \left(\frac{p'}{\gamma \bar{p}} \right) + R_{vc} R_b \left(\frac{p'}{\gamma \bar{p}} \right) |\mathbf{U}'| + \frac{\dot{m}_{pc}}{\bar{m}} R_{vc} |\mathbf{U}'| \quad (7.81)$$

Substitution into the combustion term of the forcing function () leads to

$$(F_n)_{comb} = \frac{\bar{u}_b}{E_n^2} \left\{ C_1 \iint \frac{\partial}{\partial t} \left(\frac{p'}{\bar{p}} |u'| \right) \psi_n dS + C_2 \iint \frac{\partial |u'|}{\partial t} |u'| \psi_n dS - C_3 \iint \frac{p'}{\bar{p}} \frac{\partial}{\partial t} \left(\frac{p'}{\bar{p}} \right) \psi_n dS \right\} \quad (7.82)$$

where

$$C_1 = R_{vc} R_b, \quad C_2 = \frac{1}{\gamma} R_{vc}, \quad C_3 = \frac{2}{\gamma} (R_b - 1) \quad (7.83)$$

Note that R_{vc} is a constant but R_b is in general a function of frequency, as for example in (2.52). To simplify the calculations in order to understand more easily the qualitative behavior, we set the imaginary part of R_b equal to zero, that is, in (2.40), $R_b = R_b^{(r)}$ given as the real part of (2.52), with $n_s = 0$.

The functions $|u'|$ and $|u' - u_t|$ are shown in Figure 7.63, with $|u' - u_t|$ by definition zero for $u' < u_t$; u_t is called the threshold velocity. Burnley (1996) gave an extended discussion of the consequences of truncation; various simplifications of the combustion model; the threshold velocity; and time-averaging. Results obtained with the second-order equations (7.27) compared with those based on time-averaging have shown that time-averaging must be used with care, for it can lead to misleading results (see Wicker *et al.* 1996, Burnley and Culick 2000 and Wicker and Yang 2000).

A main general conclusion reached by Culick, Burnley and Swenson is that triggering exists only if both nonlinear combustion and nonlinear gasdynamics are included. The point is made most strikingly and clearly with the bifurcation diagram, Figure 7.64.

The role of velocity coupling is clearly important and the results *suggest* that it is important for triggering to occur under practical circumstances, but proof of the point has not been established beyond all doubt. Much remains to be done on this aspect of the problem.

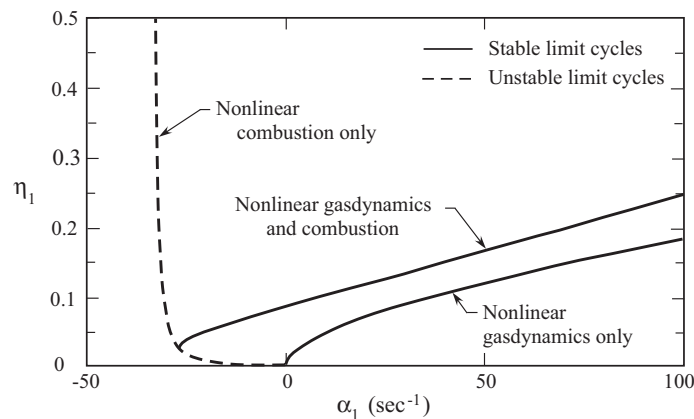


FIGURE 7.64. Maximum amplitude of the first acoustic mode in the limit cycle showing the contribution of nonlinear gasdynamics and combustion (Culick, Burnley and Swenson 1995).

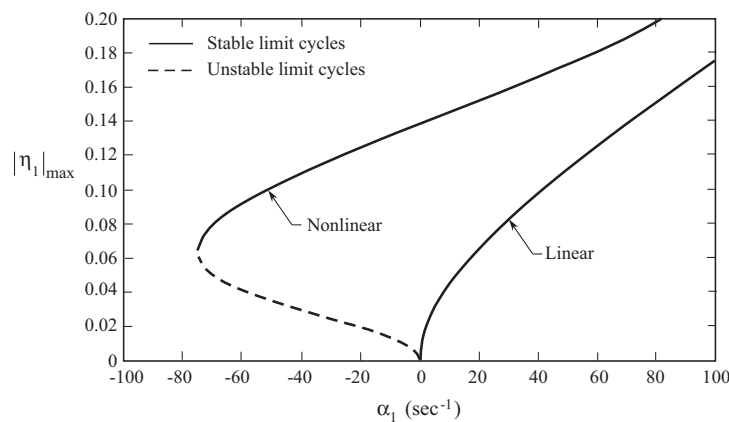


FIGURE 7.65. Maximum amplitude of the first acoustic mode in the limit cycle showing a subcritical bifurcation with a turning point only if both nonlinear gasdynamics and nonlinear combustion dynamics are accounted for (Culick, Burnley and Swenson 1995).

CHAPTER 8

Passive Control of Combustion Instabilities

Treating combustion instabilities in combustors for operational propulsion systems has always been and remains a matter of passive control. Methods of active control, which are discussed in Chapter 9, still (2005) remain largely in the realm of demonstrations although some recent work suggests that more basic problems and approaches are attracting attention. Quite generally, methods of passive control fall into two classes: modifications of the propellant supply system; and changes of the combustor geometry. Both kinds of control (in this context commonly referred to as 'fixes') have been used in all types of propulsion systems.

For solid rockets, two sorts of passive control are routinely applied: changes in the propellant composition; or modifications of the geometry of the propellant grain. It is rarely possible to alter the reactants in liquid fueled systems. Hence passive control in those cases has been exercised largely by adjusting the design of the fuel supply system; or by changing the combustor geometry, often with the addition of baffles, resonators, or acoustic liners. In any case, the basis for using passive control is mainly qualitative and empirical, founded on understanding the basic processes. The discussion in this chapter is descriptive, largely a brief survey of experiences. Wherever possible the physical reasons for successes are given. Our treatment is cursory because much of the material is covered well in easily accessible references.

Further effort has been devoted in the past decade to using computational methods to aid design of passive devices. The approach will clearly become more important as experience grows and the procedures improve. Nevertheless, testing remains the primary basis for developing practical means of passive control.

8.1. Interpretation of Passive Control

How passive control works in a general sense can be explained most simply by appealing to the basic ideas illustrated in Figures 1.1 and 1.9. The essential point is that a combustion system really consists of two dynamical systems: the chamber dynamics and the combustion dynamics. The combustion chamber acts as an amplifier of acoustical motions; the combustion processes provide feedback, giving the possibility for unstable oscillations. Instabilities will occur if the energy gained by unsteady motions in the chamber exceeds the energy lost during a cycle. Passive control consists in modifying or blocking at least one of the factors contributing to the existence of oscillations; or suitably increasing the damping in the system. Figure 8.1 combines the two parts of Figure 1.9 to show schematically the fact that a mode (here the second wave mode) of the chamber dynamics will become unstable if the rate of energy gains exceeds the rate of energy loss in the frequency range covering that mode. Thus there are clearly three possible tactics that may be followed to eliminate, or at least reduce, the instability: decrease the energy gains; increase the energy losses; or shift the frequency response of the chamber so all peaks lie outside the shaded range where the gains exceed the losses. The three possibilities are sketched in Figure 8.2 where the dashed lines indicate the behavior before modification, shown in Figure 8.1.

Note that for Figures 8.2(a) and (b) we assume that the losses are increased sufficiently (Part a) or the gains are reduced sufficiently (Part b) that the losses exceed the gains for all frequencies and the system is completely stable. In 8.2(c), the gains exceed the losses in the frequency range $f_1 < f < f_2$ so the chamber

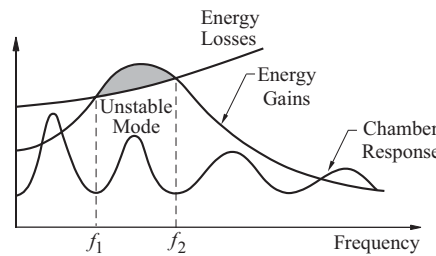


FIGURE 8.1. Schematic diagram showing qualitatively the conditions under which instabilities exist.

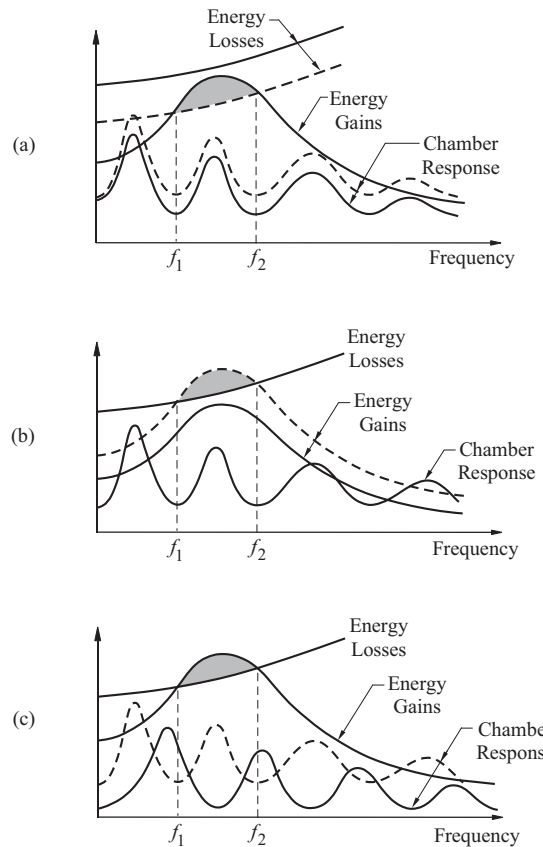


FIGURE 8.2. Qualitative and stylized interpretation of the possible effect of modifications on the dynamical behavior of a combustion system; dashed lines indicate behavior before modifications are made to reduce the tendency for instability. (a) energy losses increased, usually by a small change of the chamber response; (b) energy gains reduced; (c) modified chamber response. Dashed lines indicate conditions prior to modifications.

dynamics may exhibit oscillations. However, since no peak of the response lies in that range, the amplitude of any oscillation will be much reduced from its value existing with the unmodified chamber response. The point is that when purely changes of geometry are made, the system may still show instabilities: The details can be known (approximately) only by carrying out calculations using, for example, the analytical apparatus developed here in Chapters 3–7.

Corresponding to the behavior sketched in Figure 8.2, we can construct block diagrams, modified forms of Figure 1.1. This procedure makes the connection between the subject at hand and the field of feedback control. To illustrate the idea we assume linear behavior and adopt conventions familiar in the theory of feedback control, elaborated further in the following chapter. We assume that the governing equations have been transformed from the time domain to the complex frequency (s) domain by applying the Laplace transform. The various transfer functions are identified by the following symbols:

- $G(s)$: chamber dynamics
- $Q(s)$: combustion dynamics
- $C_G(s)$: modification of the chamber dynamics
- $C_Q(s)$: modification of the combustion dynamics

Then the complete linear dynamical system is represented by the diagram given in Figure 8.3, where F and P represent the Laplace transforms of the external input and pressure respectively.

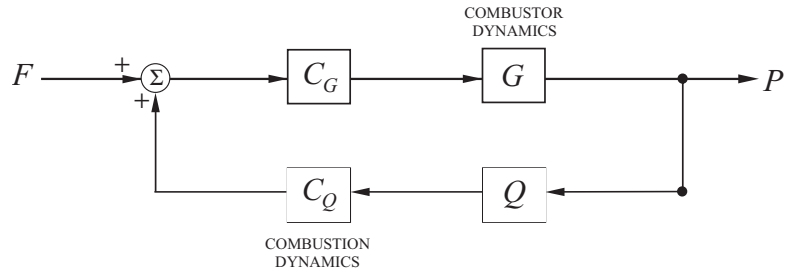


FIGURE 8.3. Block diagram of the basic system (G, Q) with passive control due to modifications of the chamber dynamics (C_G) and of the combustion dynamics (C_Q).

The transfer function for the system can be found directly by noting that the input to C is

$$F + QC_Q P$$

and the output of G is therefore

$$GC_G(F + QC_Q P)$$

But the output of G is P , so

$$P = GC_G(F + QC_Q P)$$

and

$$P = \frac{(GC_G)}{1 - (GC_G)(QC_Q)} F \quad (8.1)$$

Thus the effective transfer functions of the chamber and combustion dynamics are GC_G and QC_Q .

An instability may be interpreted as a motion, i.e. a non-zero value of the pressure (P), that occurs when the external disturbance (F) is vanishingly small. That event arises if the denominator of (8.1) vanishes,

$$(GC_G)(QC_Q) = 1 \quad (8.2)$$

This equation (here the transfer functions are all assumed to be scalars) gives the values s_n of the complex frequency for which instabilities arise. Those values of s_n identify the peaks of the response function sketched in Figures 8.1 and 8.2.

Instabilities in the unmodified system are found for values of s_n given as the roots of (8.2) with $C_G = C_Q = 1$. Hence, if C_G or C_Q both differ from unity, here representing the effects of passive control, then the roots of (8.2) are shifted in the complex plane. The sketches in Figure 8.2 suggest the consequences of

C_G and C_Q differing from unity. As indicated in Figure 8.2(a), the energy losses tend to be related to the response of the chamber for liquid fueled systems. If, for example, viscous or acoustic radiation losses are increased, the peaked portions of the response broadens (the “Q” of each mode is decreased) and the peak values are reduced. Particularly if losses due to particulate matter are significant, as for solid rockets, the connection with the chamber response is relatively weak.

On the other hand, if the combustion processes are affected, for example, by small changes in the injection system of a liquid rocket, and the chamber dynamics are practically unaffected, then the conditions sketched in Figure 8.2(b) are met. It appears that this case arises when the dynamics of the injection system are changed for a fixed design of the chamber. For solid rockets, the gains of energy—commonly referred to as ‘driving’—can be significantly affected by modifications of the propellant.

Finally, if the geometry of the chamber is significantly altered—as, for example by adding baffles—then the frequencies of the natural modes may be shifted, quite possibly with relatively small changes in the energy losses. That case is represented in Figure 8.2(c).

The preceding discussion is intended only as an introduction to some of the principal ideas applicable to passive control and one way to think of the problems. For gas turbine combustors and augmentors especially, real cases become considerably more complicated, involving normally a great deal of testing. Recent articles by Mongia *et al.* (2005), Krebs *et al.* (2005), Richards *et al.* (2005) and Scarinci (2005) contain informative discussions of experiences with problems in full-scale operating engines.

8.2. Baffles

A ‘baffle’ is a structure placed in a combustion chamber in such a fashion as to reduce the amplitude of an unacceptable oscillation. There is no unique way to accomplish the desired result, and there are few well-defined rules for either the shapes or locations of baffles. Ultimately the best arrangement of baffles to effect a desired result is established by testing.

Perhaps the earliest discussion of methods to reduce oscillations appears in Chapter 9 of the book *Internal Ballistics of Solid Fuel Rockets* by Wimpress (1950). Although it appeared in 1950, the book actually covers work done during World War II in the period 1941–1945, and therefore does not include discussion of case-bonded grains which were invented later. Figure 8.4 shows qualitatively three configurations of baffles used in solid propellant rockets. Instrumentation available at that time did not resolve oscillations but large excursions of the average pressure are obvious; examples are shown in Figure 8.5.

Attempts to reduce or eliminate the effects such as those shown in Figure 8.5 formed the earliest uses of passive control. The attempts included inhibiting portions of the grain; changing the internal shape; installing resonance rods; and drilling holes in the grain normal to the flow direction. Resonance rods may be regarded as early forms of baffles more familiar in liquid-fueled systems which we will mainly discuss here.

Figure 8.6 is a convincing example of the effectiveness of an array of baffles installed in the F-1 engine, of which five formed the first stage of the Apollo vehicle. Baffles mounted on the injector face and extending longitudinally formed multiple cavities; the array of twelve cavities is shown. Comparison of the two results reproduced in the figure shows that the unacceptable time-dependent motions generated by a pulse were effectively eliminated. For baffles extending from the injector face in a liquid rocket, the three main geometrical variables are the length and height of the baffles or ‘blades’ as they are referred to; the number of blades; and their orientation. This configuration, also shown in Figure 8.7, became quite common in U.S. liquid rockets: Longitudinal baffles extending from the injector face.

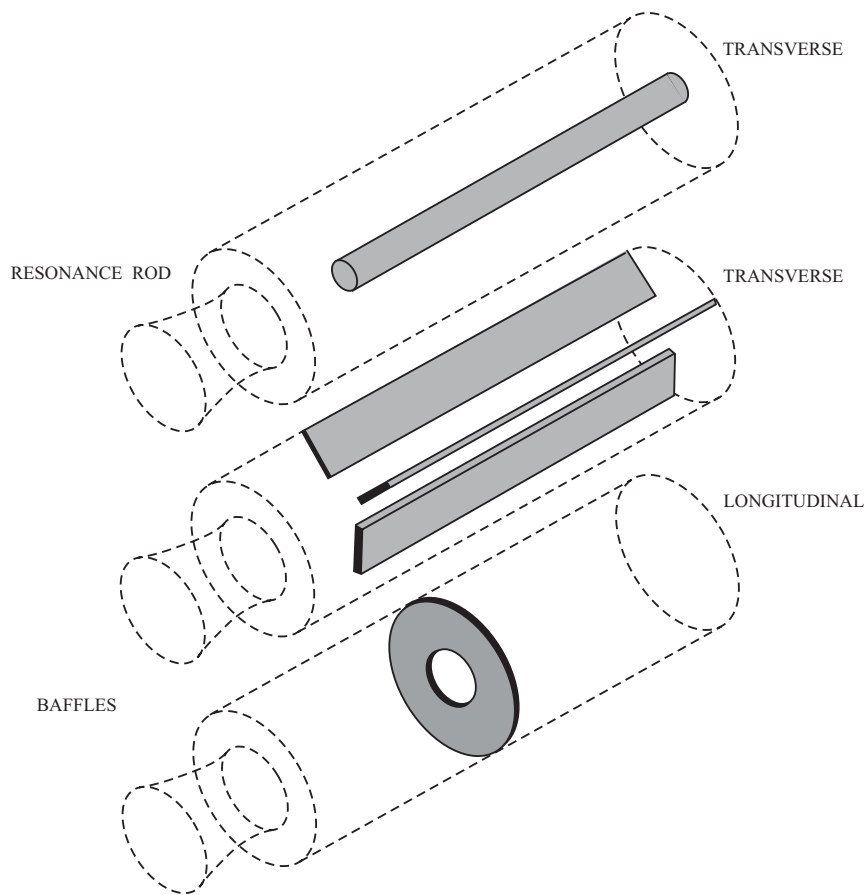


FIGURE 8.4. Simple forms of baffles for solid propellant rockets (Culick 1981).

As shown in Figure 8.8, baffles may be combined with other devices, such as small acoustic cavities. In the example shown, the azimuthal slot along the outer periphery is divided into smaller volumes each of which will contain a mode of oscillation. Because longitudinally a single cavity is closed at one end and open at the other, it supports naturally a quarter wave and is therefore called a 'quarter wave resonator'. If it is to be effective, such a cavity must be 'tuned' to support a quarter wave of the correct frequency. That is, the dimensions must be correctly chosen, a process which is guided to some extent by theory but in practice involves trial and error. The temperature in the cavity is always known poorly and cannot be computed accurately. Thus, determining actual behavior must always await test results.

Chapter 8 of the volume by Harrje and Reardon (1972) contains an extensive discussion of baffles. More detailed considerations of particular applications and of special characteristics are covered in references cited there. Figure 8.9 suggests the wide variety of baffles used in liquid rockets. The configuration chosen in a specific application is motivated, in the first instance, by the characteristics of the mode to be suppressed. Figure 8.10 shows the pressure fields for seven of the lowest transverse modes in a circular cylinder. It is easy to sketch the associated velocity fields. Then a configuration of baffles may be chosen to interrupt the motions, thus preventing formulation of the mode in question, as indicated in Figure 8.9. Oberg, Haymes and Wong (1972) have given a brief summary of devices used to suppress oscillations in solid rockets. Installation of baffles was the authors' preference for relatively low frequencies, the favored orientation being normal to the wave motion. Table 8.1, taken from Oberg, Haymes and Wong, summarizes many practical considerations for baffles and for cavities, covered briefly in Section 8.3.

PASSIVE CONTROL OF COMBUSTION INSTABILITIES

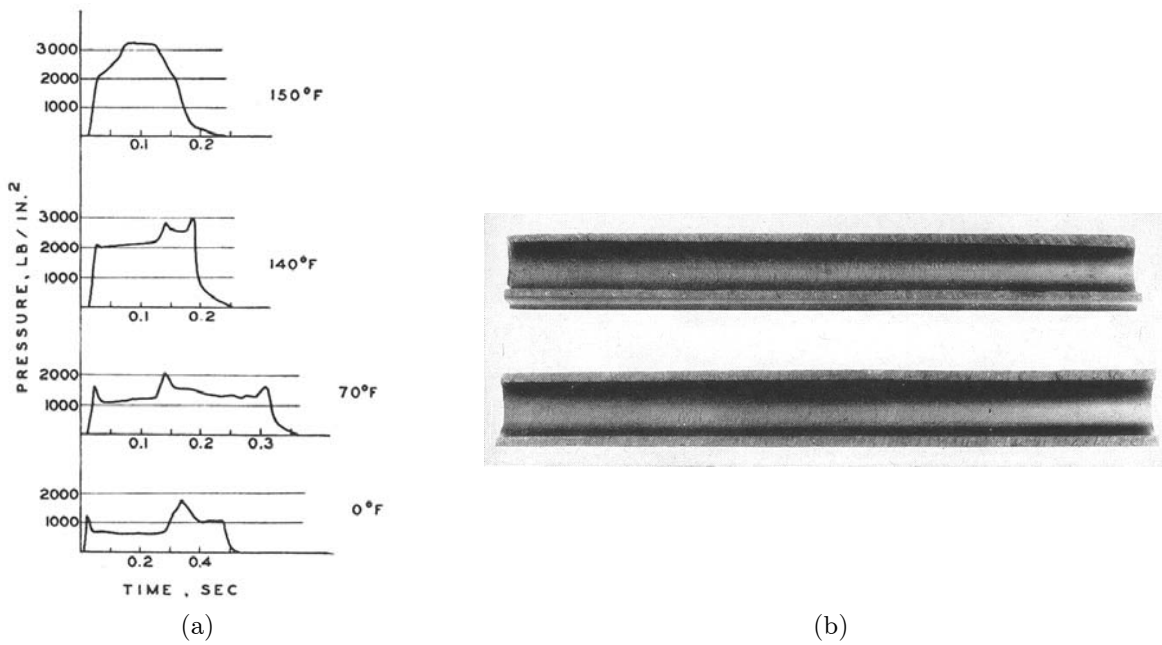


FIGURE 8.5. Early examples showing consequences of high-frequency oscillations. (a) Departures of the mean pressure from design values. (b) Uneven burning of a propellant grain due to oscillations (Wimpress 1950).

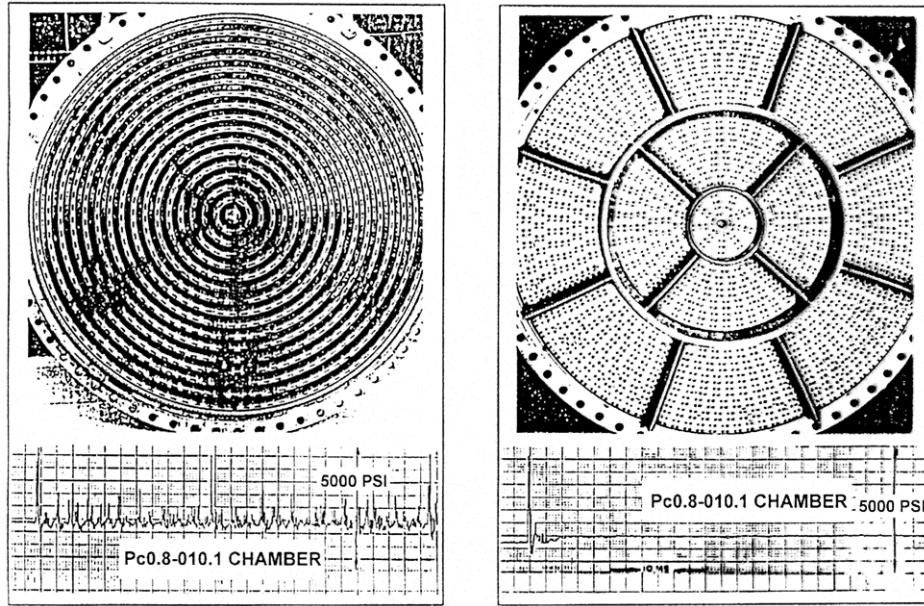


FIGURE 8.6. The importance of baffles in the F-1 engine (Oefelein and Yang 1993).

An unusual application of baffles, of a disposable sort never used in the U.S., is shown in Figure 8.11(a), a photograph of baffles for the Russian RD-0110 liquid-fueled engine (Rubinsky 1995). The instability was a longitudinal mode and as Figure 1.15 shows, the baffles were installed to be oriented with, not normal to,

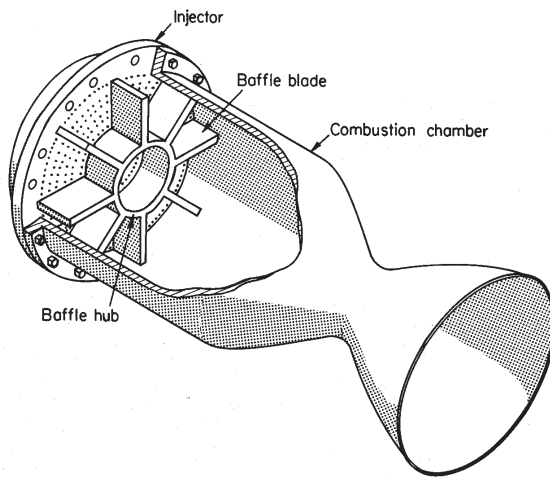


FIGURE 8.7. Perspective view of a rocket combustion chamber with longitudinal baffles installed on the injector face (Harrje and Reardon 1972).

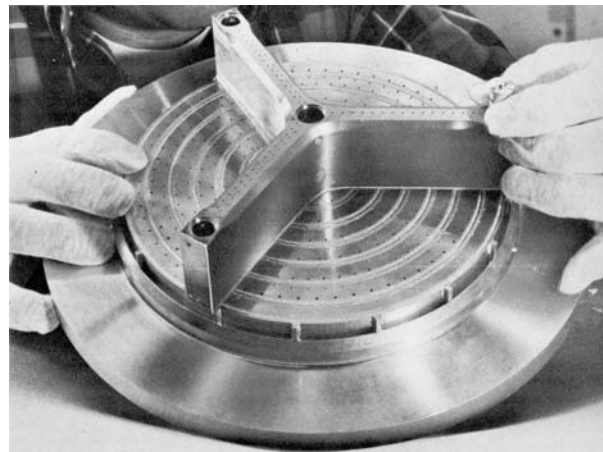


FIGURE 8.8. An injector with baffles and azimuthal slots (Harrje and Reardon 1972).

the wave motion. Moreover, what is unique, the 'ribs' were designed to be consumed very early in a firing and so were fabricated of felt. Figure 8.11(b) shows the very significant reduction of the amplitude of the instability due to the ribs. Evidently in this case the ribs acted practically as pure absorbers, and did not greatly affect the modal shape of the wave motion.

Mitchell and his students have for many years used linear theory to study the effects of various configurations of baffles on the acoustic field without taking account of a mean flow. An accessible discussion of their work appears as the article by Baer and Mitchell (1977). Their accomplishments are summarized as part of the report by Mitchell *et al.* (1987).

The most extensive calculations for a simple configuration, to determine the main nonlinear acoustical effects of baffles appear in the paper by Wicker, Yoon and Yang (1995). A concise survey of work on baffles is included as the introduction. Both linear and nonlinear behavior are covered, based on the formulation summarized here in Chapters 4–7. The details of the analysis are of course conditioned by the configuration treated, which is shown in Figure 8.12. No combustion or flow were taken into account, but the calculations form an example of the approach which can be useful for investigating the properties and effects of baffles. The calculations can be extended to configurations other than that shown in Figure 8.12, but no further results have been reported and there are no experimental data.

It is a straightforward matter to gain an initial idea of how effective a baffle is by making measurements in a model at room temperature. For example, the procedure has been used by Laudien *et al.* (1995) to assess the effectiveness of both resonators and baffles. Figure 8.13(a) shows their experimental arrangement, with the results for the spectrum of modes plotted in Figure 8.13(b). Figure 8.14 suggests the two well-known methods for measuring the damping factor and Figure 8.15 shows measured decay rates per cycle of oscillation for the first five tangential modes of the model shown in Figure 8.13(a). The values for the decay rate measured in this way will not be the same as those applicable under operating conditions at high temperature and with flow. However, as a qualitative indication, room-temperature measurements and observations are extremely useful.

PASSIVE CONTROL OF COMBUSTION INSTABILITIES

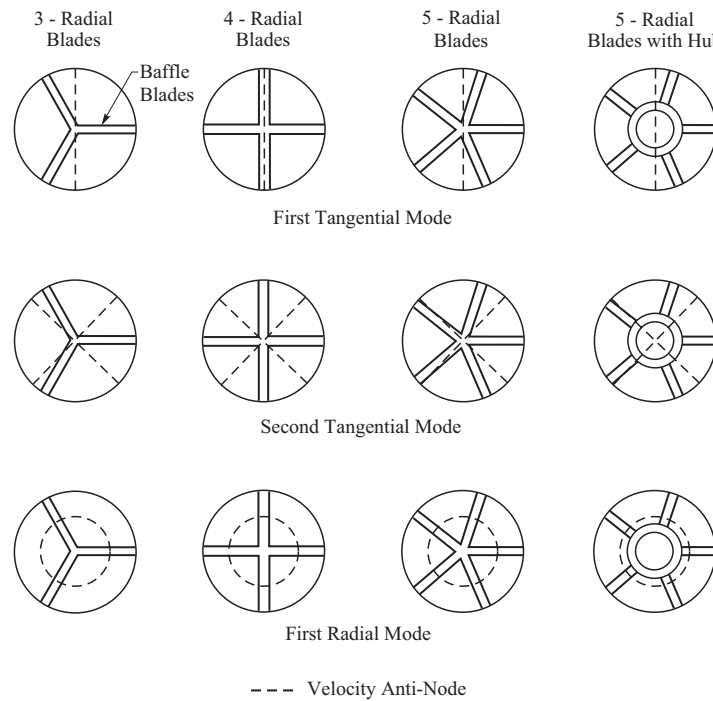


FIGURE 8.9. Examples of the arrangement and shapes of baffles fixed to the injector face of a liquid rocket (Figure 8.2.2d of Harrje and Reardon 1972).

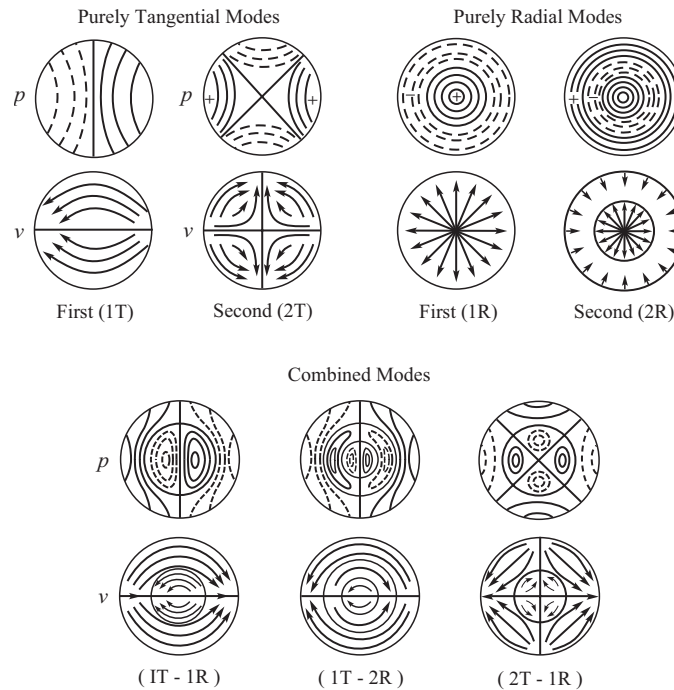


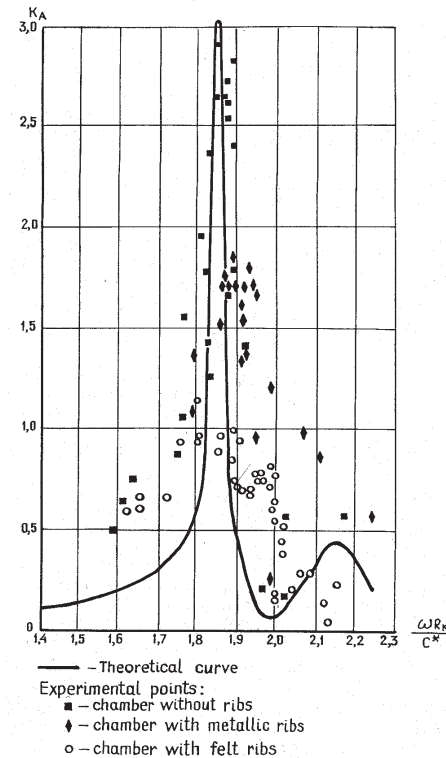
FIGURE 8.10. The pressure fields for the lowest order modes commonly encountered in circular cylindrical combustion chambers (Figure 8.2.2b of Harrje and Reardon 1972).

TABLE 8.1. Considerations of Baffles for Application to Solid Propellant Rockets (Oberg, Haymes and Wong 1972).

Type of Suppression Device	Transversely Oriented Baffles		Longitudinally Oriented Baffles (Rods and Paddles)	Cavities	
	Orifice	Tab(s)		Integral with Igniter	Located in Forward or Aft End of Case
<u>Fabrication of the Device</u> General Materials Used	Insulation/Structure— High pressure molded filled phenolic/epoxy	... same same same same ...
	Structure—Steel Graphite— Titanium or high temp metal	... same same same same ...
Component Fabrication Processes	Insulation/Structure— Cut or machined from sheets or slabs or lay-up/wrap-cure	... same ...	Insulation/Structure— Cut or machined from sheets or slabs or lay-up/wrap-cure plus molded rods	... same same ...
	Structure—Machined, forged, or molded	... same same same same ...
Assembly Fabrication	Integral molding/wrapping of plastic to metal support or mechanical attachment	... same same same same ...
Special Installation Preparations/Procedures	Plastic parts stored in low-humidity condition	... same same same same ...
Quality of Materials and Fabrication Processes	Materials used should be certified and some degree of receiving inspection used. Critical areas should receive rigorous final inspection	... same same same same ...
<u>Motor Adaptations and Installation Requirements</u> Special Case Structural Features Required	Internal tabs or rings may be required to locate and fix the assembly in place. Hard wall insulation may be used	... same ...	Internal frames, rings, or attachment points in domes may be used	Igniter structure attach features may be governed by integral cavity configuration	Integral tabs or ring(s) may be required to fix assembly in place
Special Case Insulation Features Required	Insulation may have to be installed in sections and have special fillets and seals to interface with assembly	... same ...	Cutouts in dome insulation and special fillets may be required	... same same ...
Special Grain Inhibiting Required	Grain may have to be inhibited on one or both sides of orifice assembly. Special sealing at wall interface may be required	... same ...	Secondary support on internal surface of grain may require local surface protection	None	Grain may require end inhibitors depending on configuration
Special Grain Casting/Trimming Procedures	Two grain casts may be necessary with curing, trimming, and inhibiting for each, or perforated baffle coordinated with casting plate	... same ...	None, unless design interferes with grain. If required integrated grain-baffle cast tooling must be so designed	Can be none, or provide for recess or clearance by casting mandrel design or grain trim	Grain may require end cast relief or trim depending on configuration
Special Ignitor or Ignition Features Required	None, unless orifice area causes abnormal ignition response or transient condition	None	Attach structure may be integral with igniter assembly. Heat absorption by device may require igniter tailoring	Can be integral with igniter structure	None



(a)



(b)

FIGURE 8.11. (a) Combustible longitudinal baffles (ribs) in the Russian RD-0110 engine and (b) their substantial effects on the amplitude of oscillations (Rubinsky 1995).

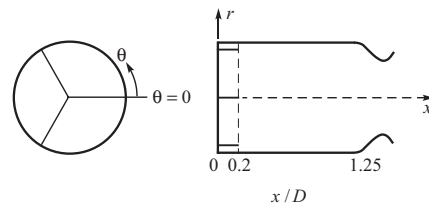


FIGURE 8.12. The combustion chamber with a three-bladed baffle analyzed by Wicker, Yoon and Yang (1995).

An important effect of a baffle is often ‘shadowing’ of the combustion zone from flow disturbances, particularly the fluctuating velocity associated with acoustic waves. This is evidently a major reason for the effectiveness of baffles on the injection face in the F-1 engine, Figure 8.6. However, the secondary flows, including unsteady vortices, make this method virtually impossible to perfect. Not only is the actual flow difficult to compute, but it is also not easily reproduced in the laboratory. There are no experimental results directed explicitly to the matter of shadowing.

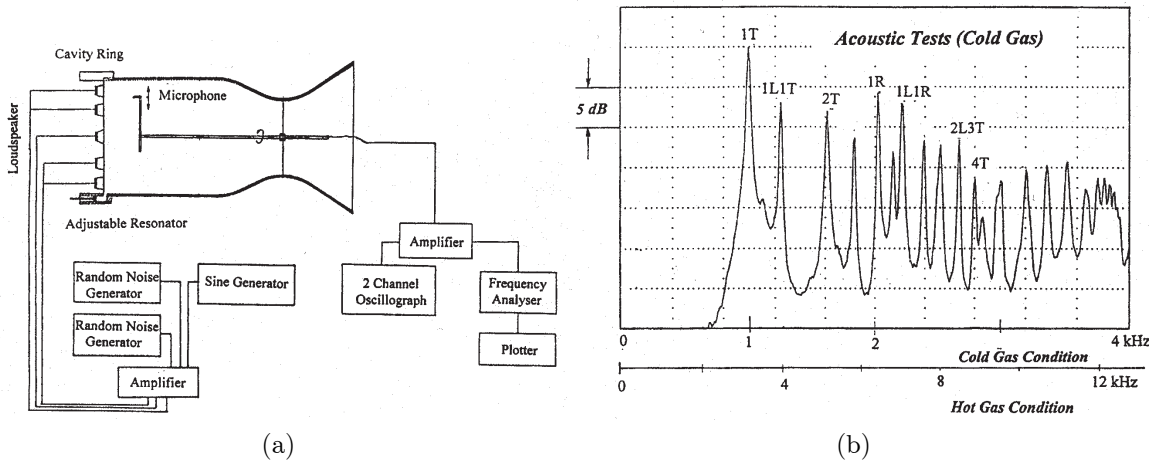


FIGURE 8.13. A model of a rocket chamber and the measured spectrum of tangential modes (Laudien *et al.*, 1995).

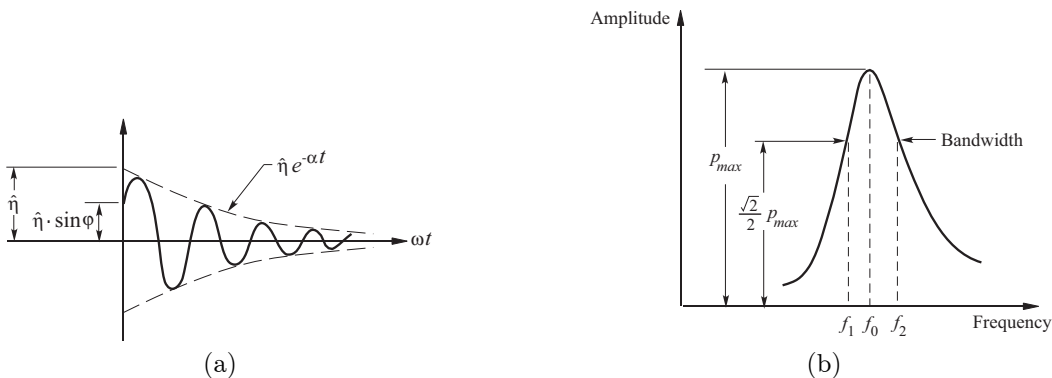


FIGURE 8.14. Two methods for measuring the damping factor: (a) decay rate, α ; (b) bandwidth.

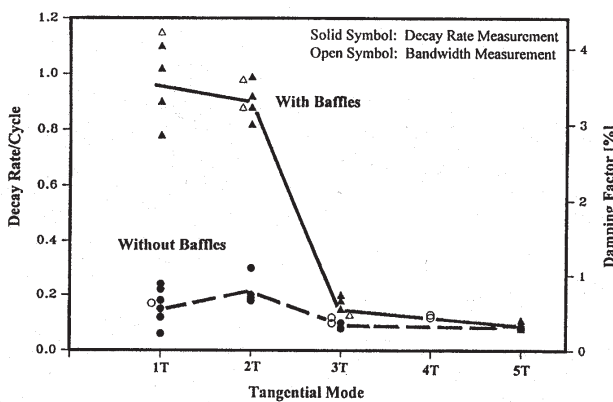


FIGURE 8.15. Results for the decay rate of tangential modes in the chamber shown in Figure 8.13(a) (Laudien *et al.* 1995).

8.3. Resonators and Acoustic Liners

Resonators are the basic elements of acoustic liners which consist of many elements arranged on the surface of a combustor. The most important properties of an acoustic resonator are that it responds to an incident acoustic wave having frequency in a more-or-less narrow range depending on the geometry of the device and the amplitude of the wave; and the wave produced (reflected) in the response, while it necessarily has the same frequency as the incident wave, will be scattered into many directions. Because of the second property, a resonator causes the incident wave to lose energy independently of any viscous effects which add significantly to the losses. It is that energy loss that makes a resonator such an attractive and important tool in practical control of combustion instabilities.

The earliest use of resonators seems to be that reported by Fox (1951), to attenuate oscillations in a ramjet. An array of orifices was cut in the lateral boundary, backed by small cavities, one for each orifice, thus forming an array of resonators. That general idea, known from the beginning of concerns with combustion instabilities, is used at the present time, notably in afterburners, but also in gas turbines and liquid rockets. In fact, for practical purposes, much of the development of resonators and acoustic liners was completed by the 1970's. Representative references include Blackman (1960); Chapter 8 of Harrje and Reardon (1972); Utvik and Blackman (1965); Phillips and Morgan (1967); Phillips (1968); and Phillips, Hannum and Russell (1969). The principal part of the behavior that required special attention was the influence of flow, both through the orifice and parallel to the opening, sometimes referred to as grazing flow. Experiments were often motivated by the need to specify the behavior in terms of a small number of parameters.

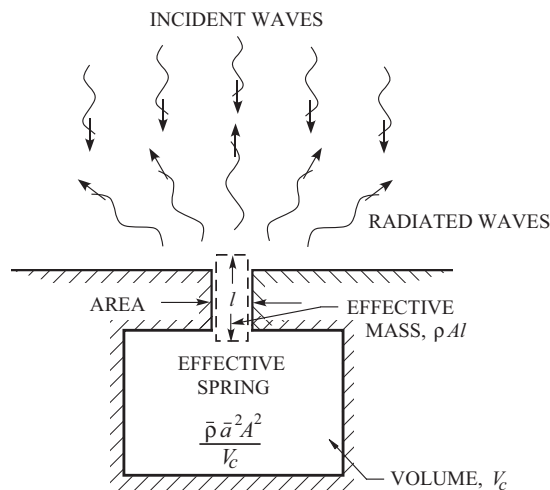


FIGURE 8.16. The essential features of an idealized cavity resonator.

An idealized resonator is sketched in Figure 8.16. The simplest view of the device is that it is a simple mass/spring/dashpot system. A plug of fluid mainly in the neck, but including small amounts from the environment at both ends, is the mass; the springiness is provided mainly by the fluid in the cavity having volume V_c . Damping—identified with the ‘dashpot’—accompanies the motion, being caused partly by viscous forces and partly by radiation of acoustic waves that do not combine with the incident wave. Suppose that the damping force on the plug of fluid is proportional to its velocity. Then with the definitions given in Figure 8.16, the equation of motion of the plug is

$$\bar{\rho}Al \frac{d^2x}{dt^2} + \gamma \frac{dx}{dt} + \frac{\bar{\rho}\bar{a}^2A^2}{V_c}x = A\hat{p} \cos \omega t \quad (8.3)$$

where x is the excursion of the plug from its equilibrium position.

Damping has a small effect on the frequency which we ignore in the interest of simplicity. With $\hat{p} = 0$, we have the equation of motion for an undamped oscillator.

$$\bar{\rho}Al \frac{d^2x}{dt^2} + \frac{\bar{\rho}\bar{a}^2 A^2}{V_c} x = 0 \quad (8.4)$$

The frequency of the undamped, unforced oscillator is

$$\omega = \bar{a} \sqrt{\frac{A}{lV_c}} \quad (8.5)$$

If damping is included, the frequency is reduced by a small amount. The formula (8.5) already shows that using a resonator as a means of affecting low-frequency motions is impractical because the size must be large. For example, suppose the frequency is 100 Hz so $\omega = 200\pi \text{ s}^{-1}$. Take $\bar{a} = 1000 \text{ m/s}$ and (8.5) gives $\sqrt{A/lV_c} = \pi/5$ so $A/lV_c = \pi^2/25 \approx 0.4 \text{ m}^{-2}$. A reasonable hole might have diameter comparable to its thickness: $A/l \sim (\pi l^2/4)/l \sim l$ so $A/lV_c \sim l/V_c \sim 0.4 \text{ m}^{-2}$. and $V_c \sim (0.4/l) \text{ m}^3$. The neck of a resonator is often cut in sheet material (see Figure 8.15) which we may take to be, say, 2 mm thick, or $2 \times 10^{-3} \text{ m}$. Thus $V_c \sim (0.4)/(2 \times 10^{-3}) \sim 20 \text{ m}^3$ which is of course unacceptably large. This result shows why resonators are practical for oscillations in the frequency range of thousands of Hertz, not hundreds. If an application requires attenuation in a moderate range of frequency, then a single or small number of resonators may be used, perhaps in combination with baffles, providing there is sufficient volume available for the cavities. In the range of frequency where resonators are commonly used, they are most commonly used in the form of acoustic liners.

‘Acoustic liner’ is the term used to describe the structure covering all or part of the lateral boundary of a combustor. Figure 8.17 is a good example used on a 15,000-pound thrust rocket motor. Probably the two main problems arising with installation of a liner are tuning so oscillations in the troublesome frequency range are attenuated; and cooling. See Section 8.3.5 of Harrje and Reardon (1972) for a good discussion of the cooling problem and its practical solution for liquid rockets.

It is probably true that acoustic liners are used more widely in gas turbines and their components than in any other application. They are part, for example, of inlet design to reduce the amount of noise radiated forward of transport aircraft. Here we are concerned only with acoustic liners incorporated in rockets and thrust augmentors. It is accepted practice to incorporate a liner as part of the basic design of an augmentor to attenuate screech or relatively high frequency oscillations. Lower frequencies require special measures, such as modifying the distribution of injected fuel, even to the extreme of shutting off some of the injectors. Such problems may determine limits in some parts of the flight envelope.

The problem of cooling is commonly reduced by directing a ‘bias flow’ through the liner. Hughes and Dowling (1990); and Jing and Sun (1998) seem to have reported the last works on the subject. A central question is: In what respects does a bias flow affect the acoustics of the liner? Hughes and Dowling worked out a theory for the absorption coefficient and its dependence on $\kappa a \equiv \omega a/\nu$ where $2a$ is the diameter of the holes and ν is the mean velocity of the bias flow. Both they and Jing and Sun measured the absorption with a form of the impedance tube method (Section 5.11) sketched in Figure 8.18.

A system of holes in a liner supported some distance from a (nearly rigid) wall, with or without a bias flow, has certain resonance and reflection properties which depend on the various geometrical parameters and the bias flow. It is those properties that matter for practical applications. For example, the effective absorption by a liner depends on, among other quantities, the thickness of the liner material and the size and spacing of the holes. In these experiments, the principal parameters are the Mach number of the bias flow, certain geometrical parameters and a ‘resonance parameter’ Q defined by Hughes and Dowling. The resonance parameters are proportional to the square of the wavenumber times the distance d between the

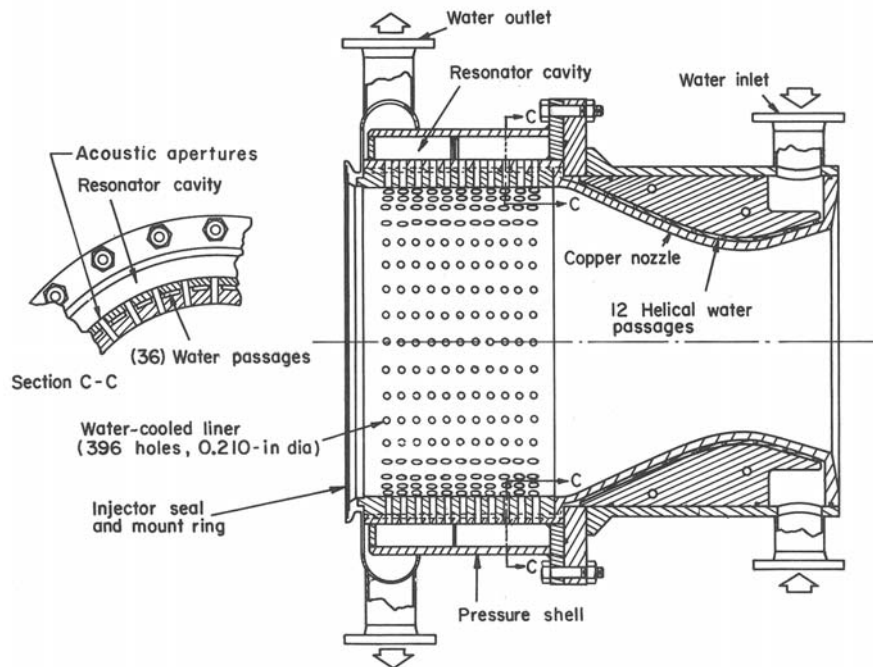


FIGURE 8.17. Convectively cooled thrust chamber fitted with an acoustic liner (Figure 8.3.5b of Harrje and Reardon (1972)).

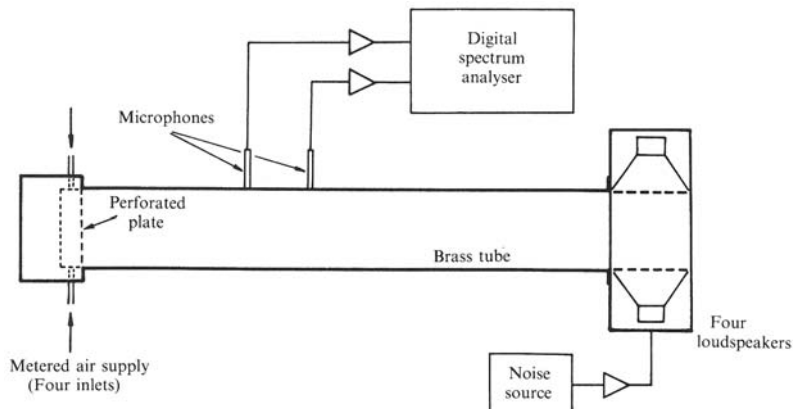


FIGURE 8.18. Apparatus for measurement of the acoustic properties of a model of a liner with bias flow (Hughes and Dowling 1990).

apertures; and proportional to the ratio of the depth l of liner divided by the diameter $2a$ of the holes,

$$Q = (kd \cos \theta)^2 \frac{l}{2a} \quad (8.6)$$

where θ is the angle between the direction of wave propagation and the normal to the wall. Figure 8.19 shows a comparison of the theory worked out by Hughes and Dowling with some data taken by themselves and by Jing and Sun. It appears that the general basis for design of acoustic liners is settled. The difficult matter of mounting liners in the hardware at hand must be solved specially for each case.

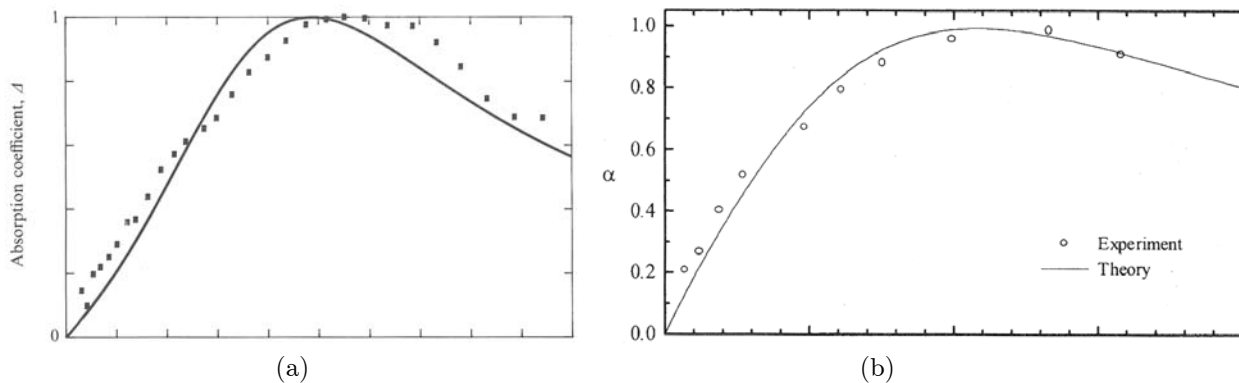


FIGURE 8.19. Absorption coefficient for a portion of acoustic liner (a) from Figure 7 of Hughes and Dowling (1990); (b) from Figure 7 of Jing and Sun (1998).

8.4. Damping Due to the Formation and Presence of Particulate Material

Sometime after aluminum powder (particle sizes $< 100\mu$ usually much less) was introduced as a significant constituent in solid propellants, it became apparent that amplitudes of combustion instabilities were often much reduced. Apparently Neustein and Altman (1958) first proposed that the reason was the dissipation of acoustic energy by viscous interactions between Al_2O_3 particles and the combustion gases induced by oscillatory motions. The idea was based on earlier work done by Epstein and Carhart (1953) which we mentioned in Section 6.14.3. An alternative interpretation, which also has a long history, is based on the idea that condensed-phase reactions may be effective, especially if they are exothermic. Waesche (1999) recently published a note discussing the relative merits (and truths) of these contrasting views. A test program was carried out some years ago using an unspecified, but large (perhaps 25–30), number of small cylindrical laboratory motors 11.5 inches long, having initial port diameters of 5 inches. The motor oscillated in its first tangential mode, having frequency 4800 Hz soon after ignition and 4000 Hz at burnout.

Many tests were run, using several additives as well as aluminum and Al_2O_3 . It is inappropriate here to try to describe the details or to summarize the test program. Waesche's main conclusion was that "heat release near the surface was a significant factor in the effective suppression of instability." Photographs of the combustion zone supported the idea that those additives were most effective that "liberated large amounts of energy." The results suggested that "incorporation of an additive that suppresses oscillations by releasing energy appears to be a more practical method of eliminating combustion instability than one based solely on particle damping."

There is other (publicly unreported) evidence that exothermic reactions in the region where the solid is converted to gas may be responsible for damping or reducing the amplitudes of combustion instabilities; for example, reference 4 of Waesche's note evidently supports the case. An analysis such as a modified form of the sort carried out in Section 2.2.4 could probably be used to confirm the proposal; it seems that the calculations carried out specially for this purpose remain to be done.

Quite a different source of attenuation of oscillations are the responsive motions of particulate matter, the idea introduced by Neustein and Altman. We have given an appropriate analysis of the basic phenomenon, and data confirming the results, in Section 6.14.3. To summarize, the idea is roughly the following. A solid propellant containing aluminum to increase its specific impulse, produces condensed aluminum oxide (Al_2O_3) among its combustion products. For example, a propellant containing 19% aluminum (said to be "heavily aluminized") will produce 42% by mass of aluminum oxide in its products of combustion. As an actual example, the propellant in the Space Shuttle booster motors contains 16% aluminum; the exhaust therefore

consists of roughly 58% gases and 42% liquid. Many small tactical rockets contain comparable amounts of aluminum. The presence of a significant amount of Al_2O_3 has the secondary effect of attenuating unsteady motions. Note that at the usual combustion temperatures ($> 3000^\circ\text{F}$) the Al_2O_3 is liquid and exists in combustion chambers as droplets normally having sizes from the sub-micron range to tens of microns.

The attenuation of sound by particles suspended in a gas has a long history beginning with calculations of the absorption of sound by fog, by Sewall in 1910¹. Epstein (1941) discussed comparison of the experimental results (Knudsen 1931; Laidler and Richardson 1938) with the theory which had been improved by Lamb (1932) and by Epstein himself. Epstein and Carhart (1953) worked out essentially a complete theory for the attenuation of sound by non-interacting spherical particles; both the acoustic field and the motions of the particles are described by linear equations. The formulas derived in Section 6.14.3 are much simplified forms of those given by Epstein and Carhart but, the experimental work by Kraeutle, discussed below, has established that the approximations are apparently quite accurate.

There are several important consequences of having large amounts of condensed material in a gas. We are concerned here only with the two main effects that interactions between the wave motion and the motions of the particles may have: the propagation speed of the waves is reduced; and the energy of the wave motions is dissipated. Figures 6.22 and 6.23 show the approximate results for the frequency shift and attenuation of a sinusoidal wave propagating in a gas containing particles having uniform size and uniformly dispersed. The fractional change in frequency of a wave having fixed wavelength, as for a standing wave in a closed volume, is equal to the fractional change of the speed of sound. From the relation $\bar{a} = f\lambda = \omega\lambda/2\pi$, we have equation (6.103),

$$\frac{\delta f}{f} = \frac{\delta\omega}{\omega} = \frac{\delta\bar{a}}{\bar{a}} \quad (8.7)$$

where here the basic change of the speed of sound is due to a change in the number density of particles. We find $\delta\bar{a}$, or $\delta\omega$, from Figure 6.39. For a propellant containing 15% aluminum ($\mu = 0.15$ in equation 6.216), $C_m = 0.4$, and the reduction in the speed of sound is about $\delta\bar{a} = 0.163\bar{a}$.

The dissipation of energy associated with the presence of particles is another matter that has for some time been recognized as an important means of passively controlling combustion instabilities in solid propellant rockets. Part of the reason for strong practical interest in this behavior is the connection between attenuation, particle size and frequency of oscillation shown in Figure 6.39. What is particularly important is the fortuitous circumstances that the particle sizes produced in most solid rockets are in the range for which the attenuation is greatest for the frequencies of oscillations encountered. Finally, there is a firm basis for performing the calculations necessary to understand the general behavior and, in principle, carry out the required design procedure. The most difficult part of ensuring that the desired conditions are reached in practice, a goal dependent on the physio/chemical conditions which are partly dependent on uncontrollable conditions within the combustion processes.

There are many reports of using purposely altered particle sizes to affect (the intent is to do this favorably) the attenuation of acoustic waves by particle damping. A particularly clear discussion of the matter was given by Derr, Mathes and Crump (1979) which we summarize here. Earlier reports of the background and progress of the work were given by Mathes *et al.* (1978), Kraeutle (1977) and Kraeutle *et al.* (1976). A central motivation for the series of works was to optimize the attenuation of acoustic waves due to small particles ('particle damping') by providing the appropriate size distribution of particles. Because the necessary measurements are carried out in a motor, the information is obtained for the particular operating system in question. We assume here that the properties of the unstable motions, notably the dominant frequency, are known from observation of actual firings. Thus we restrict attention to the particles which we assume are mainly Al_2O_3 produced in the combustion of aluminum in the propellant.

¹Zink (1957), and briefly Zink and Delsasso (1958), have reviewed the history of the subject.

Figure 8.20 is a diagram showing the strategy. If this procedure is to be successful, there are, at this stage, three crucial processes which must be well in hand:

- (i) Collection of particles from motor firings;
 - (ii) Analysis of the size distribution;
 - (iii) Modification of the propellant to effect a favorable in the size distribution.

The details of these three important procedures are outside the scope of this book. We intend here only to indicate what must be done by outlining the special example treated in the reference cited.

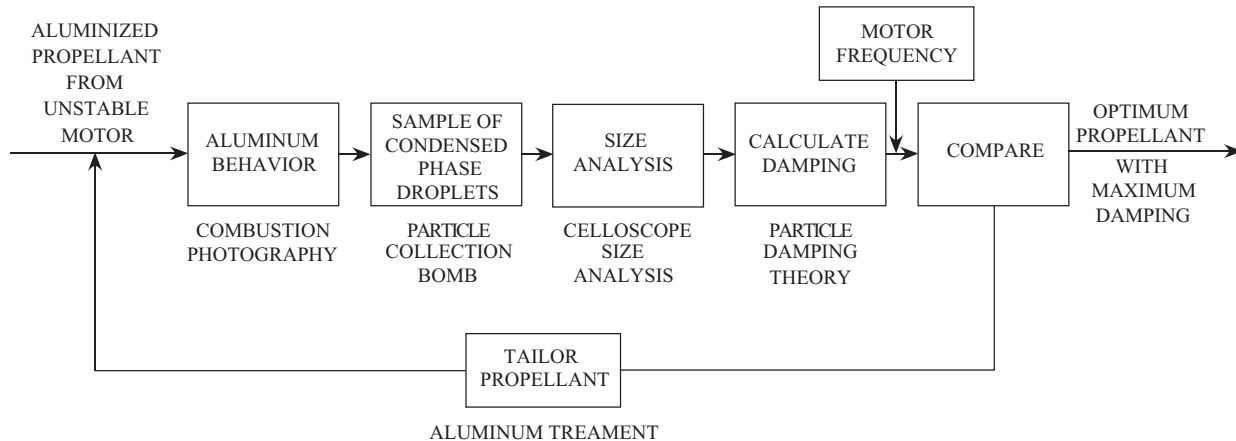


FIGURE 8.20. Scheme of a procedure followed to improve the attenuation of combustion instabilities by increasing the particle damping (Derr, Mathes and Crump 1979).

The example is based on a motor cast with a metallized double-base propellant which showed unacceptable oscillations in the range of frequency 2K to 4K Hz. Samples of the propellant were burned at the motor pressure. Collection of the particles and analysis of the sizes gave the results shown in Figure 8.21 with comparable results from a more 'conventional' motor.² Figure 8.22 is a comparison of the particle damping calculated with the method discussed in Section 6.14.3, for the size distribution shown in Figure 8.21; and the particle damping for two uniform size distributions giving optimum damping respectively at 2 KHz and 4 KHz. Evidently the actual particle size distribution is quite far from the best possible. This result was accepted as the reason that the motor had a problem with oscillations. Correcting the problem required measures not discussed in the reference.

²The configurations of both motors were omitted from the references.

PASSIVE CONTROL OF COMBUSTION INSTABILITIES

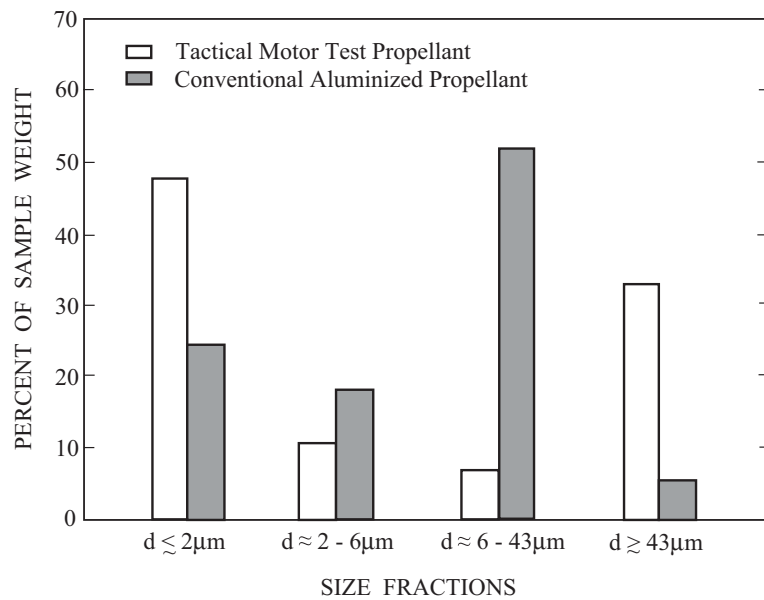


FIGURE 8.21. Particle size distribution for tactical motor propellant and a conventional aluminized propellant (Derr, Mathes and Crump 1979).

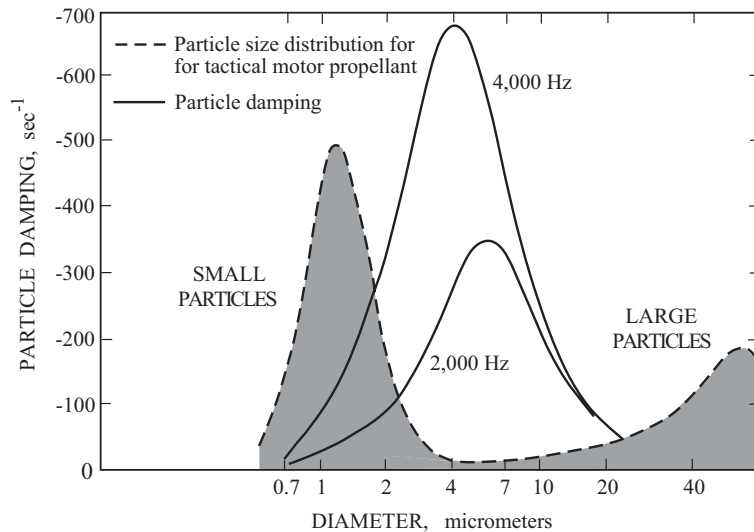


FIGURE 8.22. Comparison of particle size distribution to optimum size for damping in motor (Derr, Mathes and Crump 1979).

8.5. Dynamics of Injection Systems

Liquid-fueled systems offer a special possibility for passively controlling oscillations, based on the dynamics of the injection system. The subject has been discussed briefly with the aid of Figure 1.1 in Section 1.2. Probably the most extensive and effective work, both research and practical applications, has been done by Professor V.G. Bazarov of the Moscow Aviation Institute (for example, much of his work is covered by Bazarov 1979, Bazarov and Lul'ka 1978, Andreyev *et al.* 1991, Bazarov 1995, 1998). The most accessible work in English is Bazarov and Yang 1998 in which some of the ideas are summarized.

Put most simply, the essential idea can be stated in the following way. We view the combustion chamber containing the flow of the combustion reactants and products as a dynamical system. The injection system, the supplied reactants, liquid and gas, and the associated processes form a second, extraordinarily complicated system. Thus we view a liquid- (or gas-) fueled system as consisting of two dynamical systems coupled in some unknown way by the injection and combustion processes. This sort of simplified model is implied by practically all treatments of the time-dependent behavior viewed in this fashion; the consequences are pursued as a means for passive control of the dynamics of the combined system.

Much of the discussion in Bazarov's papers is concerned with the fundamental unsteady processes occurring within injection devices and in the injected flows. A significant theme throughout is the use of those unsteady processes and their coupling to the chamber dynamics to control unsteadiness—in particular combustion instabilities—in a combustion chamber. Consequently, a large part of the experimental work is devoted to the dynamics of the injection processes and how they may be used to affect favorably the dynamics of the combined system. See Figure 1.24 and the accompanying remarks.

8.6. Passive Control of Vortex Shedding

Shedding of large vortices has long been a well-known phenomenon in many contexts. Vortex shedding occurs in combustion chambers particularly in flow past blunt flameholders and rearward-facing steps. Rogers (1954) carried out experiments establishing the importance of the first case and reported the work in Rogers and Marble (1956). We discussed their findings in Section 2.3.4; for convenience, Figure 8.23 is a repetition

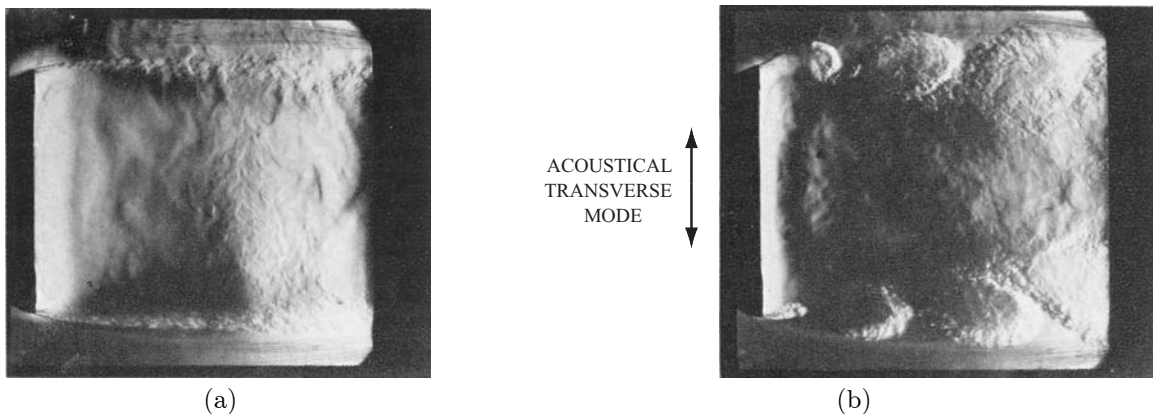


FIGURE 8.23. Flow past a bluff body flameholder under two conditions of flow at approximately the same speed. (a) low equivalence ratio, $\phi < 0.75$, no oscillations; (b) high equivalence ratio $\phi > 0.90$, transverse acoustic oscillations in the channel (Rogers and Marble 1956).

of Figure 2.32 showing the essential qualitative features. Recall that in this case, the shedding supported a transverse mode, the particle motions being normal to the streamwise (longitudinal) direction. The frequency was about 3800–3900 Hz. Pulses of combustion and heat addition associated with the vortices together formed the driving mechanism of the oscillations. The results obtained by Rogers and Marble and by Kaskan and Noreen (1955) were the earliest confirmations of vortex shedding as a mechanism for oscillations in a combustion chamber.

Figure 8.24 shows an example of vortex formation at a two-dimensional rearward-facing step, accompanied by a longitudinal mode of oscillation (Smith and Zukoski 1985). Several frequencies were detected in this case, the highest being 530 Hz; a spectrum is given in Figure 1.18. Many examples of oscillations in dump combustors have been studied in the past twenty years. Figure 8.25 is a summary of configurations used in tests involving vortex shedding, a modified form of a figure prepared by Schadow (2001).

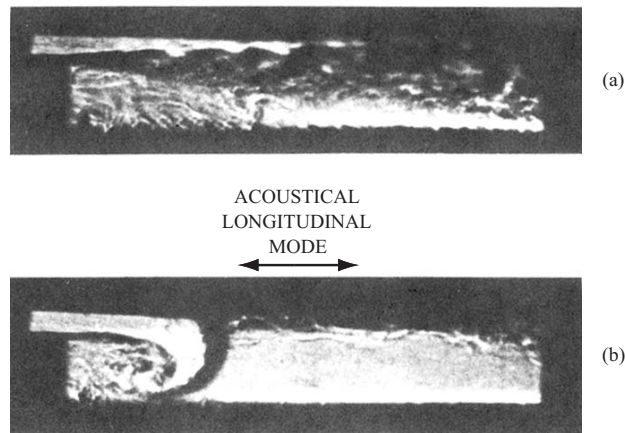


FIGURE 8.24. Vortex shedding from a rearward-facing step. (a) stable flow without vortex shedding; (b) unstable flow with vortex shedding and excitation of longitudinal oscillators (Smith and Zukoski 1985).

Byrne (1981, 1983) was first to propose the idea that vortex shedding in a dump combustor could be the cause of the pressure oscillations observed in tests of full-scale devices (see Section 2.3.4). It is easier to gain understanding of the related but vastly simpler problem of flow in the same configuration without combustion. The most extensive works on this subject have been reported by Schadow, Gutmark and their colleagues (Schadow *et al.* 1985, 1987a,b; 1989; 1990a,b; Gutmark *et al.* 1986, 1989, 1990). Schadow and Gutmark (1992) give a good review of their works, and Schadow (2001) has recently given a concise summary of the same material, covering examples with and without combustion. We draw heavily on those two works for the following discussion.

There is no doubt that the presence of combustion affects the flow in significant fashion. This may be contrasted with the similar problem of vortex shedding at the joints of a segmented solid rocket described in Sections 1.2.5, 2.2.7 and 6.8; combustion is then not part of the problem. In the present case, the same conclusion surely cannot be valid generally. Moreover, it is likely true that as a result of increased mixing, vortices enhance, or, under some circumstances, could conceivably stabilize combustion, even with the penalty of generating oscillations. An important purpose here is first to understand better the relations between vortex shedding and oscillations in the absence of combustion; and subsequently to gain some confidence in the possible applications of passive control. The eventual goal in practice is to reduce the oscillations, and accompanying vibrations, without sacrificing average performance.

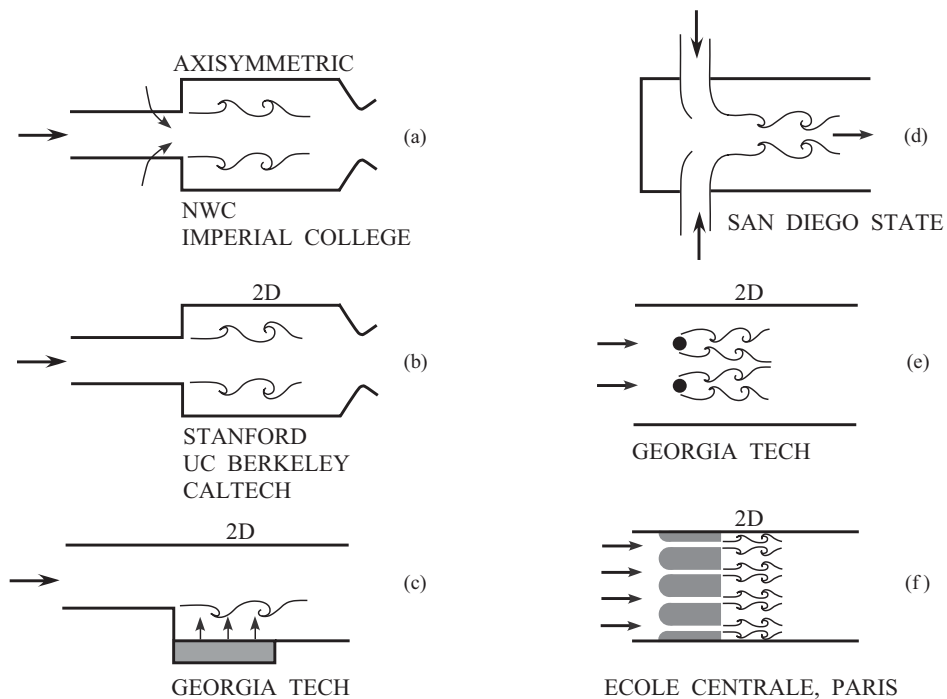


FIGURE 8.25. Examples of configurations used to study vortex shedding in combustion chambers (adapted from Schadow 2001).

The strategy followed to address the problem in dump combustors in a sense has some precedence set by similar problems in solid propellant rockets. As Flandro and Jacobs (1973) first suggested, and Culick and Magiawala (1979) demonstrated with simple apparatus, shed vortices may excite acoustic modes in a chamber if there is close coincidence between the shedding and modal frequencies (see Figure 2.29). For those cases and others related to problems in solid propellant rockets the shedding process is often characterized by a well-defined single frequency. In practice, the “single frequency” has a value which often drifts during a firing, or may suffer abrupt changes. That behavior is quite characteristic and generally has served as the basis for establishing vortex shedding as the determining mechanism. A particularly clear example makes the point.

The Stage 3 motor of the Minuteman III large booster exhibited two types of instability. For the first five seconds or so of a firing, tangential modes were excited in the slots in the forward portion of the grain sketched in Figure 8.26. There were six fins and slots. The fundamental frequency was 800–900 Hz. Then in the interval five to twenty seconds after ignition, a longitudinal mode having frequency 200–400 Hz appeared. As shown in the ‘waterfall’ plot, Figure 8.27(a), the frequency exhibited both gradual and slow increases. The variation with time is obviously very different from that of the first longitudinal mode shown by the solid line.

A program was carried out at the Air Force Rocket Propulsion Laboratory (AFRPL) to test G.F. Flandro’s suggestion that vortex shedding was responsible for the oscillations in the low frequency range. The steps at the downstream ends of the slots were removed as indicated in Figure 8.26. A waterfall plot for a subsequent firing is shown in Figure 8.27(b); the low-frequency oscillations are absent. Both the range of frequency spanned by the motions shown in Figure 8.27(a) and the trends exhibited, demonstrate beyond doubt that the oscillations were associated with vortex shedding from the steps subsequently removed. Small

changes were caused in the tangential modes. It is hard to conceive of a more convincing demonstration of the connection between nonreactive vortex shedding and pressure oscillations.³

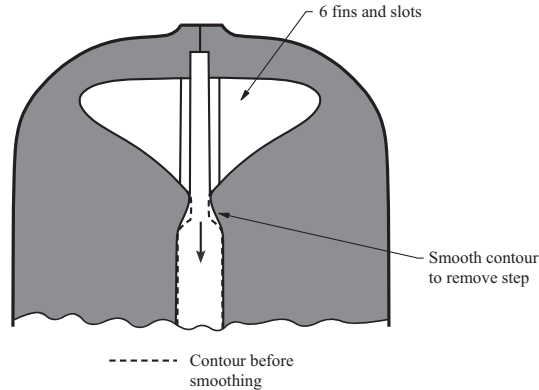


FIGURE 8.26. Sketch of the origin and elimination of pressure oscillations produced in the chamber by vortex shedding in a solid propellant rocket (Flandro *et al.* 1983).

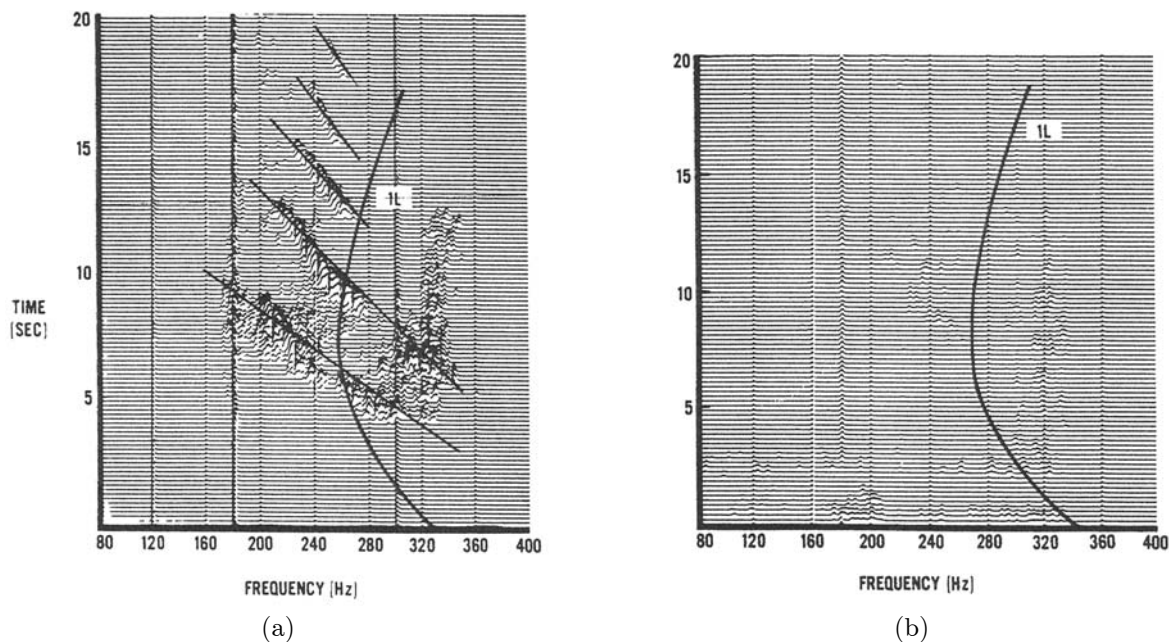


FIGURE 8.27. 'Waterfall' plots of low-frequency oscillations observed in a Minuteman III Stage 3 motor. (a) unstable oscillations produced by large vortices shed at the slots; (b) plot showing the absence of oscillations after modification of the slots (Dawson *et al.* 1981).

The examples we concentrate on here have been thoroughly treated due to concern for the problem of vortex shedding in dump combustors intended for use in ramjets. That problem evolves out of the behavior of unstable motions in the shear layer at the surface of a jet issuing from a circular orifice. Vortices develop near the surface of the jet in roughly three stages, ultimately to influence much of the volume of the jet; the

³Recall that the actual cause of the pressure oscillations is the generation of pressure pulses as the vortices are carried by the flow through the nozzle. The pulses then generate waves that reinforce oscillations in the chamber.

shadowgraph in Figure 8.28 shows the behavior in a three-dimensional jet issuing from a pipe.⁴ Three fairly well-defined stages can be identified:

- (i) initial instability of the shear layer, close to its origin, the most unstable disturbances having frequency f_s (Michalke 1965);
- (ii) growth of small, well-defined vortices merging to form larger vortices having the dominant ‘preferred mode frequency’ f_{pm} near the end of the potential core⁵ (Ho and Huerre 1984);
- (iii) the subsequent behavior and the physical disposition of the ‘train’ of vortices depends on conditions in the flow and environment of the jet.

For the example shown in Figure 8.28, the subsequent behavior referred to consisted in a rapid breakdown of the coherent vortices into a field of turbulence. The behavior in Figure 8.28 is to be contrasted with the sustained form of the shear layer in Figure 8.23(a), for example, which involves combustion in flow past an approximately two-dimensional bluff body.

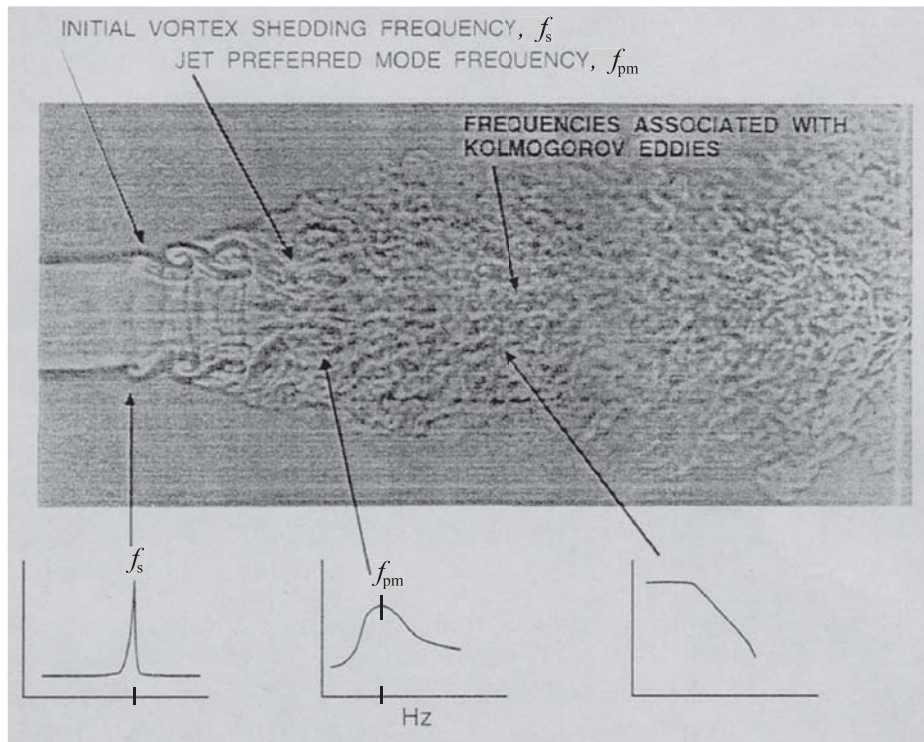


FIGURE 8.28. Cylindrical jet of carbon monoxide into air, initial Reynolds number approximately 30,000 (average speed, 127 ft/s). The photograph is due to F. Landis and A.H. Shapiro, published by Van Dyke (1982). Schadow *et al.* (1987)b added the notes and rough sketches of spectra.

Viewed in a somewhat simplistic form, the problem of passive control addressed experimentally in the works referred to here is essentially the same sort faced by those concerned with acoustic modes excited by vortex shedding in solid propellant rockets discussed in Section 2.2.7. The acoustic oscillations in both cases

⁴The picture was published by Van Dyke (1982), but was attributed to F. Landis and A.H. Shapiro with reference details. Schadow and Gutmark (1989) added the remarks and idealized spectra which have been slightly modified here.

⁵The distinguished frequencies f_s and f_{pm} are denoted f_i and f_j by Schadow and Gutmark following earlier usage; we change notation to avoid confusion with summation indices i and j .

arise because, when an acoustic frequency is approximately coincident with a vortex shedding frequency, a coupling process produces energy transfer from the vortices to the acoustical motions. In neither case are the details of the coupling processes completely known. There is a major difference between the two bodies of work. In those works discussed in this section, much greater emphasis is placed on experimentally exploring the fundamental processes of formation, growth and eventual disposition of the vortices. The main reason is that, unlike the case of solid rockets, there is ample opportunity for lengthy and repeated tests, often with considerable freedom to change the geometry involved.

Investigations of vortex shedding in combustion chambers rest heavily on earlier investigations carried out initially for their own sake, with no particular application intended. Crow and Champagne (1971) had already shown that when the initial portion of the shear layer created by a jet is exposed to acoustic waves there are strong effects on various properties of the flow, including the spreading rate and the strength (size) of shed vortices. Moreover, they found that the forcing was most effective when the frequency of the incident acoustic waves is close to the frequency of the jet's 'preferred mode'.

In 1982, Gutmark and Ho (1982) had shown that an elliptical jet, initially laminar, entrained fluid at many times the rate (up to eight) at which a circular jet does so.⁶ Some possible implications for practical application were later investigated by Schadow *et al.* (1984)b. They found, for example, that due to better mixing they obtained higher combustion temperatures and combustion efficiencies with elliptical supply nozzles in the rig they used. Although they remarked on the presence of large-scale structures, they did not elaborate upon their role.

Schadow *et al.* (1987a,b; 1989) carried out extensive tests with the apparatus shown in Figure 8.29. The lower part of the figure is a sketch of the flow field produced by the jet from the inlet duct and flow through the lateral boundary. The orifice at the entry to the chamber was either circular or (roughly) elliptical having a 3:1 aspect ratio in the early tests (1984) referred to above. For the combustion tests gaseous fuel was injected through the lateral wall of the chamber where N_2 was injected for the non-reacting tests. Variations of this basic design were used in most of the NWC tests. The most extreme geometrical departures involved triangular inlet ducts, with fuel injection either at the faces or at the apexes of the triangle (Schadow *et al.* 1990b) and an inlet with a multi-step dump (Schadow *et al.* 1990a).

The motivation for the changes of geometry was of course the well-established correlation between the formation of large coherent vortices, and pressure oscillations. It is helpful to view the situation in simplified form as the interaction between, or coupling of, two dynamical systems: the acoustic field, and the stream of shed, large-scale vortices. Rather than deal with the coupled problem as it develops with vortex shedding occurring naturally in a dump combustor, it is much better to have control over some of the behavior. The most convenient method is based on exciting the acoustic field independently of the vortex shedding process. In their first report of results, Schadow *et al.* (1984a) showed that the response of the flow into a dump chamber (Figure 8.29) was greatest when the forcing frequency approximately matched the 'most amplified frequency', the latter was either the vortex merging frequency in the initial portion of the shear layer near the dump plane; or the preferred mode frequency, f_{pm} , in the flow at the end of the potential core.

Figure 8.30 shows one example of the response of the system measured with a hot wire placed in the potential core of the jet flow exiting the inlet duct.⁷ Forcing the flow was accomplished with a rotating valve. The oscillations were longitudinal, the frequencies of the largest response being in the range of one hundred to several hundred Hertz, increasing with the average speed of flow through the chamber. Thus, while the reasoning worked out by Rogers and Marble is relevant, it cannot simply be adopted without change because the acoustic modes are so different.

⁶A hint of the reason for this result had been given in the analysis of the behavior of an isolated elliptical vortex by Dhanak and Debernardinis (1981).

⁷Although Figure 8.30 shows test results (redrawn Figure 2 of Schadow *et al.* 1987a), no data points are shown here or in the original work.

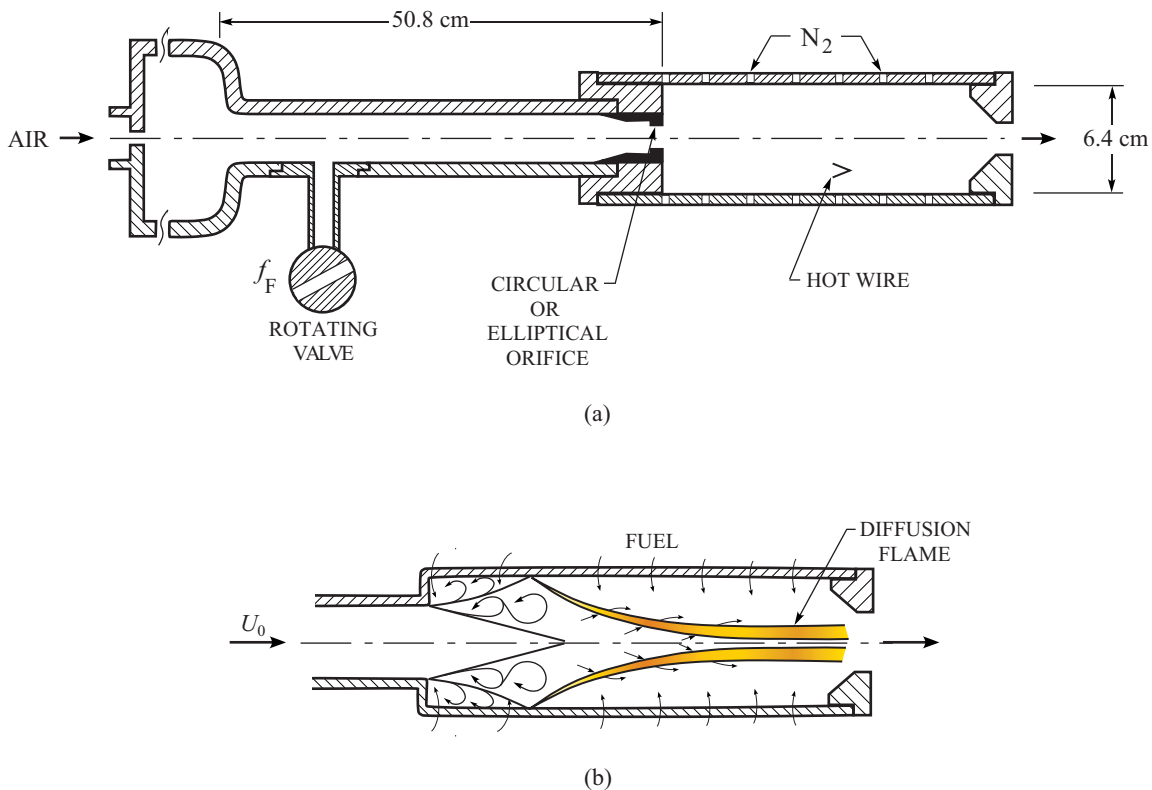


FIGURE 8.29. Test equipment for studying reacting and non-reacting jet flows in a dump combustor. (a) sketch of the complete apparatus; (b) arrangement of the dump configuration for combustion tests (adapted from Schadow *et al.* 1987a).

Without forcing, the response of a hot wire placed as shown in Figure 8.29 is typically like that given by the dotted curve for $U_0 = 71$ m/s in Figure 8.30. The frequency at the peak of the response is called the preferred mode frequency and was identified in the experiments as the ‘vortex shedding frequency’. With reduced average speed, the peak of the response curve shifts to lower frequency and seems to be smaller. With forcing— f_F is non-zero—the hot wire shows a pronounced response at f_F , indicating the presence of velocity waves superposed on the natural responses of the jet. The enhanced response implies that higher velocity at the forcing frequency produced more intense vortices, perhaps larger, but that conclusion does not directly follow from these data. Vortices having dominant frequency f_F will always be driven; the response is greatest when $f_F = f_{pm}$, the preferred mode frequency. According to Schadow and Gutmark, the response is least when $f_F = f_s$, the initial shedding frequency.

Tests of that sort suggest the following behavior in the *absence* of forcing. Consider a configuration that may contain shedding of vortices, as for example the case is with an annulus (or two annuli) in a tube, Figure 2.30. If further the configuration will easily support acoustic resonances—or, put another way, acoustic modes are readily excited—the possibility exists for coincidence between the frequencies of the vortex shedding and the acoustic modes. Figures 2.31 and 2.32 show the apparatus and some results for the case of vortex shedding in a pair of annuli mounted in a tube which has well-defined modes. The conditions identified by the open circle correspond to the cases when the forcing frequency f_F equals the preferred frequency f_{pm} in Figure 8.30.

There is therefore no doubt that quite generally near coincidence of the rate of vortex formation and the frequency of an impressed acoustic field will produce a more intense acoustic field or stronger vortices,

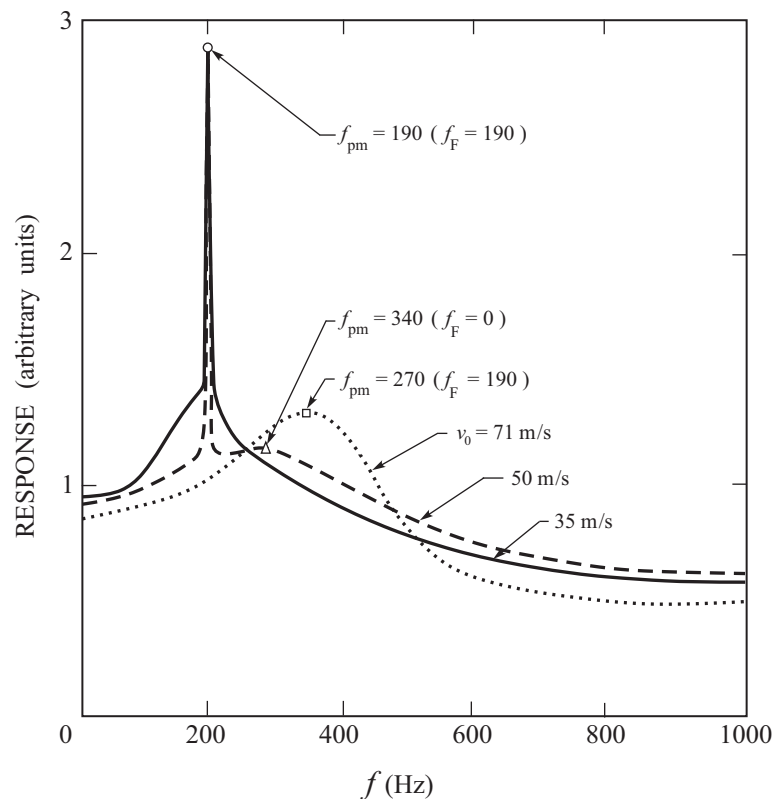


FIGURE 8.30. An example of test results showing the presence of coherent vortices when the acoustic forcing frequency f_F equals the preferred mode frequency f_{pm} , the frequency at the maximum of the response (taken from Schadow *et al.* 1987a). No data points were given in the original figure.

or *both*. The coupled system can extract energy from the average flow field. For successful application of these ideas to combustion chambers, we need to know the extent to which the presence of combustion may affect the fundamental behavior. It appears from available test results that our basic understanding of the shedding of large vortices, and the significance of equality between shedding and acoustic frequencies, are qualitatively unaffected by heat addition and quite large temperature gradients. Essentially that conclusion guided Schadow, Gutmark *et al.* and others in their investigations of methods to eliminate oscillations in dump combustors by passive means.

As the works referred to in Figures 8.23–8.25 have shown, there is virtually an inevitable correlation between the shedding of large vortices and excitation of pressure oscillations in combustion chambers. The significance of resonance between the shedding process and the acoustical vibrations of the chamber has been shown experimentally by a convincing range of tests with and without combustion. Consequently, the possibilities for exercising passive control fall into three classes: eliminate the vortex shedding; suppress the troublesome acoustic modes; or destroy the coupling between the vortex shedding and the acoustics. The last is not likely to be a realistic strategy in practice. We have discussed the problem of suppressing acoustic modes in Sections 8.1–8.3. Thus, elimination of unwanted pressure oscillations in the present case comes down finally to avoiding the cause itself. Taking advantage of the (possible) natural evolution of large vortices shown in Figure 8.28 is likely not a practical measure because physical conditions that must prevail are probably not satisfied in a combustion chamber.

Hence, if vortex shedding is established as the cause of pressure oscillations in a combustor, there seems to be no alternative to destroying the cause. If the necessary re-design of the chamber is not practical, then the only solution may be restricting the performance of the chamber to conditions under which the unacceptable oscillations do not occur.



CHAPTER 9

Feedback Control of Unsteady Motions in Combustors

Persistent problems of combustion instabilities have motivated serious interest in possible application of feedback control to combustion systems. The idea is quite simple; successful practical implementation is another matter and truly successful implementations remain to be found. Although some attention has been given to active control of instabilities in solid propellant rockets, the only reported successes with laboratory and full-scale demonstrations have been accomplished with liquid and gaseous fueled systems.

Feedback control has become a central element in the development of modern automobile and truck engines. Great advances have been made in performance over the entire speed range, and in the reduction of unwanted emissions, notably oxides of nitrogen. The contrasts between, say, a new four-passenger car and a 1923 Ford three-door black Model T are obvious, but no distinctions are more impressive than those defining the engines, hybrid or not. Feedback controls, transparent to the driver, now play a large part in changing the performance—and selling!—of cars. So what about the corresponding improvements already made in the design of the systems that concern us here?

In fact, there have been considerable advances in the performance of gas turbines—notably emissions and fuel consumption—for which feedback control has been a crucial matter. Improved design of mechanical components as well has produced significant changes. But probably the greatest qualitative difference in the combustors of those systems we treat in this book on the one hand, and those of internal combustion engines on the other, is cyclic operation. With intrinsically repetitive, in contrast to continuous, injection and combustion of reactants comes the fundamental variable called ‘timing’. It is likely that property, more than any other, that has allowed the evolution we alluded to above in engines for earthbound vehicles. The systems we discuss here lack that degree of freedom.

With the exception of solid propellant rockets, all practical combustion systems are nevertheless in some sense actively controlled during their operation. What is special about the subject of this chapter is the incorporation of feedback, in other words, closed-loop control. That is, control is exerted on a system in a manner depending on the current or recent state of the system, and in such a fashion as to achieve a desired result. While feedback control may under many circumstances be exerted by an operator—a fine example is the rider on a bicycle—we will be concerned here with control not involving human intervention. Moreover, because the subject of this book is unsteadiness of combustion processes, we restrict attention mainly to the use of control to eliminate unwanted motions. We do not cover, for example, possible use of feedback control in the important problem of lean blowout in gas turbine combustors.

Short of the sort of ‘intelligent’ control systems envisioned here, there have been several efforts in research programs to gain control over self-excited instabilities in order to obtain better data. A device invented at ONERA (Kuentzmann and Nadaud 1975) used a rotating exhaust valve to modulate the flow and impose pressure oscillations on a burning solid propellant. The purpose was to provide a controllable means of measuring the frequency response of a burning surface. Subsequently the method was modified and used with some success at lower frequencies by several groups in the U.S. and England. Another technique for switching oscillations on and off involves a movable baffle described in the reference manual edited by Culick (1974). This technique has been used to produce several growth and decay periods of oscillations during

firings of solid propellant devices lasting less than one minute. Similar results have been obtained with the addition of control resonators, but with much greater difficulty because the temperature in the orifice and cavity of a resonator changes rapidly during a test, causing great problems with tuning. All such methods are motivated largely by the need to gain some measure of control over naturally unstable oscillations in laboratory tests. Here we are more concerned with techniques that have promise for application to full-scale propulsion systems, intended to extend the operating range free of oscillations.

The origin of the main subject of this chapter was a proposal by Bollay (1951), first examined in detail by Tsien (1952), to use a feedback system to control a low-frequency instability in a liquid rocket. No experimental results were obtained. Control of oscillations in a Rijke tube was demonstrated by Dines in a thesis completed at Cambridge University in 1983, the first example of feedback control applied experimentally to a combustion device. That work was soon followed by successful demonstrations by Heckl (1985, 1988, 1990) in her doctoral program at Cambridge. Proposals for other applications have been made—for example, control of behavior near the lean blowout limit of a gas turbine combustor—but owing to the immediacy of the problem, main emphasis has been placed on developing control of combustion instabilities.

Subsequent to the demonstrations at Cambridge, and at École Centrale in Paris, widespread interest rapidly grew, and several significant research programs began. Feedback control¹ of combustion instabilities—or, more generally, of the dynamics of combustion systems—is a subject of current research, although interest (and financial support) seems to have decayed in the recent past. Despite the demonstrated applications, relatively little has been accomplished in respect to understanding fundamental issues. The reason for this state of affairs seems to be that work in this area has been largely in the nature of *ad hoc* efforts. That is, the common situation has been that feedback control has been applied to a combustor already exhibiting instabilities. Adjustments have then been made empirically until best results (i.e. greatest reduction of the amplitudes of oscillations) have been obtained. Then, in only a small number of cases, supporting analysis has been attempted after the fact to explain what happened. No example exists for which the amplitudes of oscillations before and after exercising control have been predicted *a priori*. Comprehensive interpretation of the action of a feedback control system on an operating combustor is non-existent. To correct that state of affairs poses difficult problems because in all cases nonlinear behavior must eventually be treated.

Presently, there are therefore no firm and general guidelines available to designers for use of feedback control as a method for improving the performance of a design. That is not to say that no progress has been made. In fact, sufficient knowledge and experience have been gained that possible use of feedback control indeed merits serious consideration in particular applications.² There is no question that continuing research is merited. One purpose of this chapter is to explain briefly not only the development and current status of the subject but also the limitations presently understood.

A recent paper by Hermann and Hoffmann (2005) summarizes what is likely the most advanced—and well-documented—experience with practical application of a system for active control of oscillations in a combustor. The control system used is a development based on research carried out first at the Technische Universität München (Gleis, Vortmeyer and Rau, 1990; Hermann, Gleis and Vortmeyer 1996; Hantschk, Hermann and Vortmeyer 1996; and Seume *et al.* 1997). Control of oscillations in a Siemens 267 MW gas turbine was achieved for extended periods under practical conditions; the system is not now used owing to other improvements in the machine. The example is discussed further in Section 9.4.

¹We prefer the terms feedback control or ‘active feedback control of combustion’ to descriptors such as ‘active control of combustion’ or ‘active combustion control’, both of which are conveniently abbreviated to ACC. Feedback is an important aspect of the subject, and if it is absent we will refer simply to ‘control’ or ‘open-loop control’. Inclusion of the adjective ‘active’ in ‘active feedback control’ implies that there is a source of energy in the feedback path.

²A much more optimistic view is held by Professor Zinn (2005), clearly put forward in his recent review, “Smart Combustors—Just Around the Corner.”

It is important to understand that the subject of this chapter differs in fundamental ways from the older and better known field of ‘anti-sound’ or ‘anti-noise’, a term implying destructive interference. Covered first by a U.S. patent issued to Lueg (1936), following the German patent filed in 1933, active noise control, or cancellation, eventually grew into a successful business owing to the developments of miniature electronics. A well-known consumers’ product is the Bose headset costing approximately one-thousand dollars for the finest version available to private pilots in 2006 and a few hundred dollars for the type suitable for less demanding use. The principle of operation is based on active cancellation of unwanted background noise; it’s a remarkably effective device guaranteed to be a pleasant surprise when experienced for the first time. Ffowes-Williams (1984), for example, has given an informative early review of anti-sound; much has happened in the past two decades but we will consider the subject no further.

Active control of combustion is not a matter of destructive interference in a sound field. In contrast to active noise control, the process produces successful results by favorable disruption of the sources generating the sound. This distinction was not always obvious or convincing in early works relying on secondary sources of sound for control (e.g., see the apparatus used by Dines 1983, sketched in Figure 9.6). However, it seems that subsequent work has established beyond doubt that all works on active feedback control of combustion involve modifications of the primary sources as well as additional secondary sources. This aspect of the general problem is probably the least well understood of all, while being crucial to success.

To place the ideas in a familiar context, we may interpret the intent of feedback control with the help of Figure 9.1, an extended form of Figures 1.1 and 8.3. In connection with the latter we have seen that passive control can be used to affect favorably either the dynamics of the combustor (mainly the values of the resonant frequencies and their attenuation) or the combustor dynamics (e.g. by changing the composition of the propellant or by modifying the injector of liquid reactants). Similarly, feedback control may change the combustor dynamics or, more significantly, the combustion dynamics, the processes responsible for providing energy to unstable motions. However, unlike the case for passive control, we can conceive that feedback control provides a more flexible means for modifying the system’s behavior. That additional capability is contained in the control blocks labeled C_f in the forward path and C_{fb} in the feedback path in Figure 9.1, representing control not necessarily associated with the behavior of the combustor or of combustion dynamics.

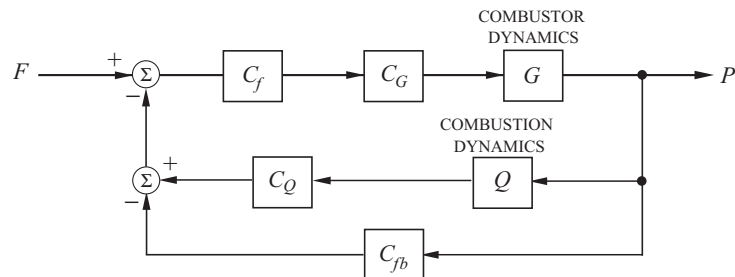


FIGURE 9.1. Block diagram for a system containing passive (C_G and C_Q) and feedback (C_f and C_{fb}) control.

The scalar transfer function P/F for the system is³

$$\frac{P}{F} = \frac{G(C_G C_f)}{1 + G(C_G C_f)(C_Q Q + C_{fb})} \quad (9.1)$$

³Although the use of block diagrams can be helpful in analysis of nonlinear systems, Figure 9.1 and the following manipulations are restricted to a linear system, here having single-input and single-output, a SISO system.

We can combine $C_G C_f = H$ to represent the transfer function of the passively controlled combustor; we let $C_Q Q + C_{fb} = G_{fb}$ represent passive and feedback control of the combustion dynamics. These definitions lead to the form emphasizing control in the forward (GH) and feedback (G_{fb}) paths:

$$\frac{P}{F} = \frac{GH}{1 + GHG_{fb}} \quad (9.2)$$

The appearance of P/F is simplified further by defining $G_f = GH$ and the last formula becomes

$$\frac{P}{F} = \frac{G_f}{1 + G_f G_{fb}} \quad (9.3)$$

This form, the simplest possible, shows that the block diagram in Figure 9.2 is quite general⁴ for the basic linear behavior of combustion systems we are concerned with here, but G_f and G_{fb} must be interpreted appropriately. It is therefore adequate for carrying out analysis that we need. The expanded form (9.1) is useful for maintaining clarity in modeling the system.

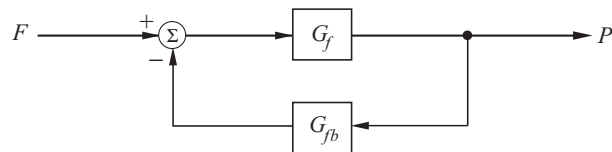


FIGURE 9.2. General block diagram of a combustion system with passive and active control.

One purpose of this chapter is to make clear the connections between the possible physical systems we are concerned with here, and the known methods and principles of feedback control. It is important, however, to remember that Figure 9.1 and the related powerful methods of analysis which have been developed, almost always imply, or explicitly require, non-flowing systems. Whether that happens to be a crucial factor in a particular instance should always be checked.

Figure 9.3 is a generic form of block diagram showing essentially the content of Figure 9.1, but including external disturbances ('noise') and with some labels commonly found in texts of control theory (e.g., Franklin *et al.* 2002). Other forms are possible, differing only in detail (e.g. placement of sensors) but the ideas are the same. The block labeled 'estimator' is often called 'observer', the term used in the original works; see Franklin *et al.*, Chapter 7 for a good summary.

All of the material covered so far in this book has been concerned with the part of Figure 9.3 labeled 'system', including passive control. In this chapter we will be dealing with problems associated with the outer feedback loop containing the 'controller'; and, to some extent with actuators and sensors which, with the system, form the 'plant'. The blocks labeled 'combustor dynamics' and 'combustion dynamics' may here contain forms of passive control. Note that the diagram in Figure 9.3 contains that in Figure 9.2, G_f standing for the dynamics of the plant, and G_{fb} for the controller.

Displays like Figures 9.1 to 9.3 are very useful as convenient summaries; and as helpful aids to guiding analysis, understanding and just thinking about the problems. Methods based on them have evolved in the context of classical control theory; have been developed further in modern control theory; and have occasionally been applied in the main subject of this chapter. It's a seductive strategy that should be followed with caution, for at least two reasons which may render the methods seriously imperfect or, in the extreme, useless: the systems considered in this chapter involve flow of the working fluid; and their behavior is intrinsically nonlinear. We shall return later to limitations of the methods at present, but only

⁴Note, however, that external disturbances are not accounted for in Figure 9.1; see Figure 9.3.

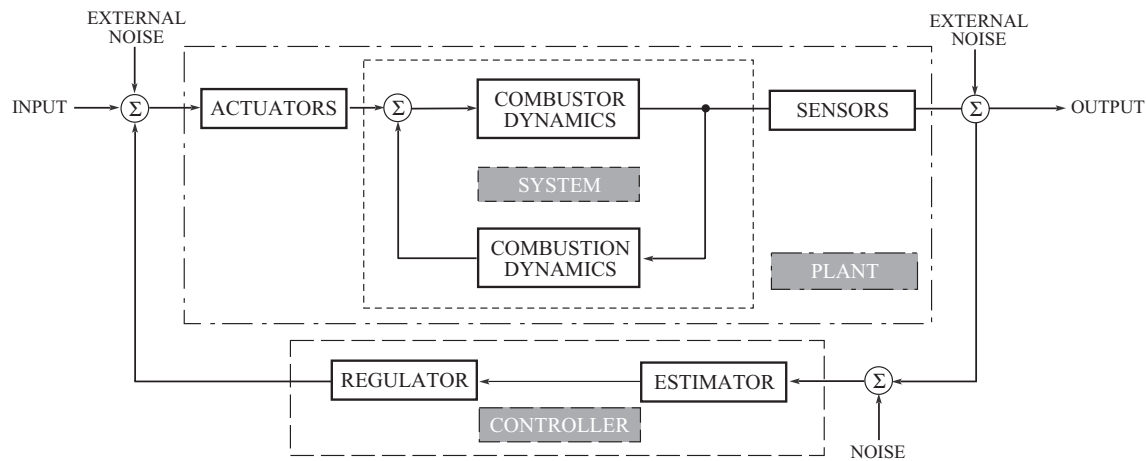


FIGURE 9.3. A general block diagram for classical and modern control.⁵ (Adapted from a diagram due to Professor R.C. Murray, private communication.)

in commentary. The field is generally very promising, but still requires careful and extensive development. A recent compilation of review articles edited by Lieuwen and Yang (2005) emphasizes the point.

At present there appear to be two principal types of applications of feedback control of dynamics to combustion systems: control of oscillations in gas turbine combustors operating near the lean limit of combustion; and suppression of combustion instabilities arising in thrust augmentors operated at low flight Mach numbers and high altitude, or higher Mach numbers and low altitude (see Figure 2.52). In both cases, understanding of the unsteady motions occurring in the absence of control is largely semi-empirical (emphasis placed on both parts of the term!). Consequently, treating practical problems is unavoidably tedious and expensive. The situation is improving slowly.

As a practical matter, lean blowout (LBO) sets a limit on the operation of a gas turbine. Unexpected disturbances may cause a combustor to execute a transient carrying operation beyond the LBO limit. Safety margins are set based on experience, but are occasionally violated in practice. Active control is attractive as a possible means of avoiding LBO in operating systems.

There is only one reported example of application of feedback control to a full-scale thrust augmentor (Moran, Steele and Dowling 2000). Because of the requirement for low emission of NO_x , gas turbine combustors are commonly designed to operate with lean premixed pre-vaporized (LPP) reactants, as explained in Section 2.2. An alternative strategy of design, identified as “rich-quench-lean” (RQL) is currently used by one manufacturer, Pratt and Whitney, Inc. (Sabnis 2005), and possibly also by Rolls-Royce, Ltd. Most of our limited discussion here will therefore be devoted to experience with LPP systems, which have inevitably exhibited problems with combustion instabilities at sufficiently lean fuel/air ratios.

Note in the RTO report:

In order to make this document available for printing, and limited distribution to the most interested community as early as possible, Chapter 9 was not completed, May 2006. The last section, 9.5, intended to cover recent progress in applications of feedback control, has therefore been cut short and forms an abrupt ending to be greatly expanded in its final version.

⁵‘Classical control’ is based on methods (mainly involving the frequency response of a system, Bode plots and the root locus) which grew from the use of transforms, principally the Laplace transform. The methods are generally applicable only to linear systems. ‘Modern control’ is based on representing systems and their evolution in state space. Methods have been developed for analyzing nonlinear as well as linear behavior.

9.1. The Idea of Feedback Control First Applied to Combustion Systems

The proposal by Tsien (1952) for using feedback control of combustion in a liquid rocket was based on modulating the capacitance of the supply line of a liquid rocket. Figure 9.4, is Figure 4 of the original paper, redrawn for inclusion here. With the actuation, the amplitude and phase of energy released in the chamber might be controlled to combat the common problem of pulsations of pressure at low frequencies ('chugging').

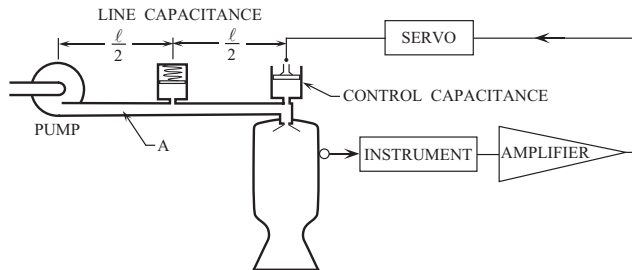


FIGURE 9.4. Schematic of the first proposal for active feedback control of the dynamics in a combustion system (Tsien 1952).

Following the reasoning given in Section 1.6.1, we write a model equation for the pressure fluctuation including a feedback process proportional to the pressure with a time delay, and an external input $u(t)$:

$$\frac{d^2p'}{dt^2} + 2\alpha \frac{dp'}{dt} + \omega_0^2 p' = \beta p'(t - \tau) + u(t) \quad (9.4)$$

The Laplace transform of (9.4) with zero initial conditions leads to

$$P(s) = \frac{\beta e^{-s\tau} G(s)}{1 - \beta e^{-s\tau} G(s)} U(s) \quad (9.5)$$

where $P(s)$, $U(s)$ are the transforms of $p'(t)$ and $u'(t)$, and the transfer function for the chamber is

$$G(s) = \frac{1}{s^2 + 2\alpha s + \omega_0^2} \quad (9.6)$$

Equation (9.5) can be interpreted with the block diagram given in Figure 9.5.

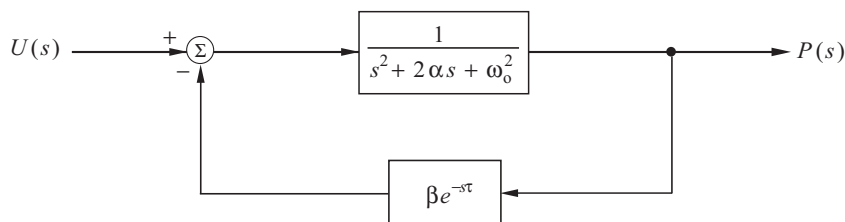


FIGURE 9.5. Block diagram for the system shown in Figure 9.4.

Successful control in this case rests on being able to adjust the parameter β and the delay τ within the frequency range of the dynamics so the roots of the denominator of (9.5) lie in the left half s-plane. The roots are found as the solutions to

$$s^2 + 2\alpha s + (\omega_0^2 + e^{-\tau s}) = 0 \quad (9.7)$$

When $\tau = 0$, there are of course only two roots, both lying in the left half plane if $\alpha > 0$, representing stable normal modes. However, for $\tau \neq 0$, there are infinitely many roots and the system is said to be 'infinite-dimensional'.

Tsien's discussion of the problem was much more involved than the preceding summary, relying heavily on Crocco's formulation of a time lag existing between the moments of injection and combustion of an element of propellant. The procedure was described in Section 2.3.2. The oscillations are taken to have sufficiently low frequency that the pressure is uniform (cf. the L^* instability treated in Section 6.2) and consequently is governed by a linear first order equation in time, which Tsien showed to be

$$\bar{\rho}V \frac{dp'}{dt} + \bar{m}p' = \bar{p}m'(t - \tau) + n[m'(t) - m'(t - \tau)] \quad (9.8)$$

where $\bar{\rho}V$ is the total mass in the chamber. The constant n is the same n appearing in Crocco's $n - \tau$ representation discussed in Section 2.3.2. Hence, the last two terms on the right hand side arise from the combustion processes while $\bar{p}m'(t - \tau)$ is due to the injection process; it is absent if the rate of injection is assumed constant.

When the Laplace transform of (9.8) is taken, the exponential $e^{-s\tau}$ appears in two places. That's the source of a difficulty when the inverse transform is taken to determine the time histories of the pressure and mass flux m' . Tsien solved the difficulty by using a little trick due to Satche (1949) in comments on a paper by Ansoff (1949). See the references for explanations. Software now available allows one to obtain results without taking special measures to treat the exponentials.

The complete feedback problem represented in Figure 9.4 requires a second equation for the dynamics of the loop containing the servo. With the additional features, the calculations are more tedious but the same basic method produces the results required. Tsien showed, with a combination of the Nyquist criterion and Satche's method for handling the exponential, that the combustion chamber could be stabilized for any value of the time lag appearing in (9.8).

Marble (1955) and Marble and Cox (1953) extended Tsien's analysis to a bipropellant rocket (oxidizer and fuel). Although the computations are considerably more complicated, the character of the analysis required does not change. Crocco and Cheng (1956, Chapter 2) gave a thorough coverage of the works referenced, with careful attention to computational details and results. There was, in the mid-1950s, considerable optimism that feedback control might offer the solution to a nagging problem. When Tsien made his proposal, some practical difficulties caused realization to be impossible. Without the aid of electronic computers, investigation of the behavior of the roots of the governing characteristic equation as the time lag was varied became very tedious. With the availability of digital computers and many versions of the necessary software, the early methods are now obsolete.

More significantly, inadequate instrumentation and hardware in the early 1950s apparently blocked experimental application of Tsien's proposal. So far as the author is aware, no successful tests were accomplished although the idea was tried in laboratory tests at Aerojet Corporation. The only residual of the program seems to be the paper by Lee *et al.* (1953), an analysis of feedback control applied to a liquid rocket.

9.2. Early Laboratory Demonstrations

The idea of applying active feedback control to combustion systems was resurrected successfully at Cambridge University thirty years later. Dines (1983) demonstrated control of a flame-driven Rijke tube shown in Figure 9.6(a), using a speaker as an actuator to inject pressure waves. The speaker was placed in a feedback loop allowing controllable gain and phase. Dines used a light sensor to monitor the light emission from CH radicals as a measure of heat release. That information was processed as the basis for adjusting the gain and phase of the speaker. Subsequently Heckl (1985) used the output of a microphone sensing pressure fluctuations in a much-improved apparatus, Figure 9.6(b), and showed that the amplitude of the instability could be reduced over a broad frequency range. That result demonstrated that control of the

combustion instability is not explained by the principle of 'anti-sound', which requires a well-defined phase relation. Eventually the injected field had a significant effect on the heat transferred from the flame to the oscillations.

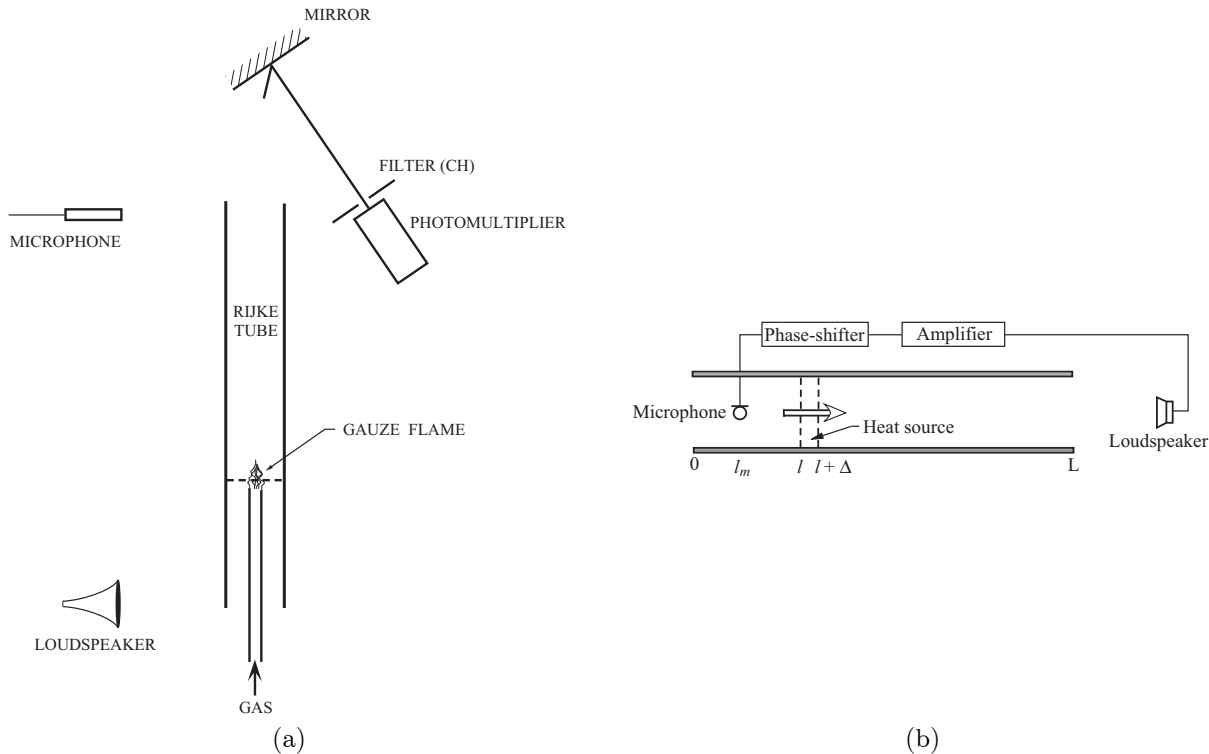


FIGURE 9.6. Feedback control of a Rijke tube by injection of acoustic waves. (a) Emitted radiation as the sensed variable (Dines 1983); (b) pressure as the sensed variable with air forced by a blower through the horizontal tube (Heckl 1985, 1986).

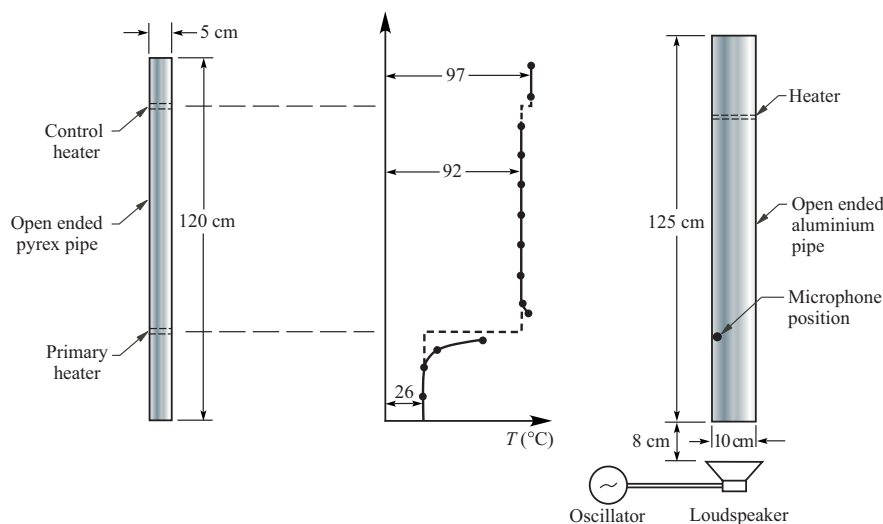


FIGURE 9.7. An early example of control based on Rayleigh's Criterion (Sreenivasan *et al.* 1985).

In her second work on the subject, Heckl (1988, 1990) showed convincingly that for her apparatus, and the conditions of her experiments, the dominant nonlinear effects limiting the amplitude of the oscillations were associated with flow in the vicinities of the ends of the tube; and with the energy transfer rate when the acoustic velocity is of the same order as the mean flow speed. This seems to have been the first identification of the dominant nonlinear processes in a simple controlled combustion tube. As experiences already discussed show, the result cannot be generalized. In any case, the experimental work by Dines and Heckl served, with the ideas of Ffowes-Williams, to form the basis for the first patent in the field, granted to Ffowes-Williams, Dines and Heckl (1986).

At about the same time, Sreenivasan, Raghu and Chu (1985) used secondary heaters in the upper half of a Rijke tube as actuators, perhaps the first example of control clearly based on Rayleigh's Criterion. Figure 9.7 shows the apparatus they used. The idea had been at least discussed for many years and likely tried informally; some earlier results were reported by Collyer and Ayers (1972) but not in the context of control. If the fluctuation ϕ' of the equivalence ratio has the proper phase and spacial distribution, then the contribution $\int \hat{\phi}^{(i)} \psi_n dV$ in the formula for the growth constant can be made negative, so disturbances are attenuated. In the Rijke tube, the control heater need not be oscillated by external means.

With the source is placed in the upper half of the tube, the fluctuating heat addition arises from interactions with the velocity and, as implied in Section 2.7, necessarily has the phase lying in the range to attenuate the waves. That is, the heat source in fact extracts energy from the field, on the average. Similar results were reported in the same paper by Sreenivasan *et al.* with the secondary heaters installed in an organ pipe and a "whistler-nozzle." The experiments were interesting and useful demonstrations but, if only because true external control was not exercised, application to propulsion systems seems a doubtful enterprise.

Following the demonstrations at Cambridge, three groups in Europe launched research programs having the eventual purpose of applying active control to full-scale systems, a goal which would require roughly a decade. At Cambridge, Rolls-Royce supported work directed to control an instability in an afterburner; modest success with full-scale tests was eventually reported by Moran, Steele and Dowling (2000) noted here in Section 9.5. Work carried out at the Technische Universität München was eventually used as the basis for the first demonstration of control of an instability in a large stationary gas turbine (see Hermann *et al.* 2000 and Section 9.4).

Research at École Centrale in Paris seems to have been motivated in the first instance more by understanding the problem than by rapidly sought applications. Initially, experiments were done in collaboration with the Munich group (Lang, Poinsot and Candel 1987; Poinsot *et al.* 1989), using a premixed propane/air burner in a duct. An acoustic speaker was used as an actuator. Ten years later, problems with the Ariane 5 (see Section 2.2.9) suggested the work reported by Mettenleiter (2000) and Mettenleiter and Candel (2000). The method, which is described later, has not been used in a full-scale solid propellant rocket.

A series of works carried out at Cambridge in the late 1980s included most significantly the first use of a modulated fuel supply to exercise control of a combustion instability. The program is distinguished by its orderly development, and results which served as catalysts for research in several other laboratories. Dowling and Bloxsidge (1984) began work with calculations of the stability of one-dimensional unsteady flow in a duct containing an approximately two-dimensional or cylindrically symmetrical flame held on a 'gutter' in a uniform duct as shown in Figure 9.8. In agreement with experimental conditions set in a rig at Rolls-Royce, Derby, they assumed the flow to be choked at the inlet to the duct, and exhausting to atmospheric pressure. The flow field was approximated as one-dimensional except that the orientation of the flame was accounted for, as shown in Figure 9.8. Fluctuations in the axial flow speed cause the flame to move to and fro. Following Dowling and Bloxsidge, suppose that the flame remains anchored at the lip of the gutter so that during the unsteady motions, the reacting sheet rotates about the lip, causing its area to change when the flow speed

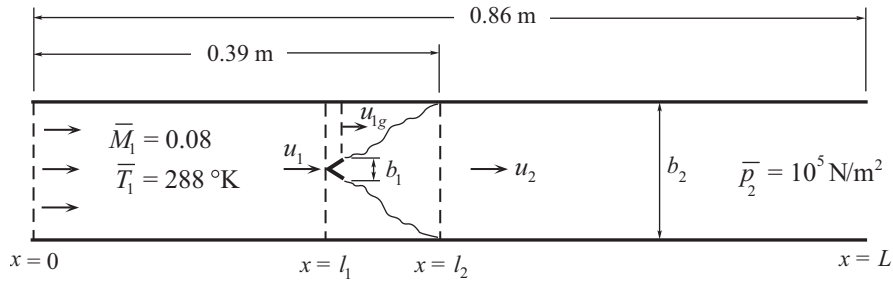


FIGURE 9.8. The geometry of the rig at Rolls-Royce, Derby, with one set of flow conditions (Dowling and Bloxsidge 1984).

does so. This motion is represented by the relation

$$\frac{b_2 - b_1}{\sin \theta} \frac{d\theta}{dt} = (u_{1g} \sin \theta)' \quad (9.9)$$

where $(b_2 - b_1)/\sin \theta$ is the length of the flame, and u_{1g} is the speed at the lip (Figure 9.8). For small harmonic motions, this formula gives the connection between the complex amplitude of the rotations and the fluctuation of axial speed⁶

$$\hat{\theta} = -\frac{\sin \bar{\theta}}{\bar{u}_{1g} \cos \bar{\theta} - i\omega \frac{(b_2 - b_1)}{\sin \theta}} \hat{u}_{1g} \quad (9.10)$$

For a two-dimensional or cylindrically symmetric flame, Dowling and Bloxsidge found the change of area \hat{S}_f due to an increment $\hat{\theta}$ in angle to be

$$\frac{\hat{S}_f}{\bar{S}_f} = -\frac{\cos \bar{\theta}}{\sin \bar{\theta}} \hat{\theta} = \frac{1}{1 - i\omega(b_2 - b_1)/\bar{u}_{1g} \sin \bar{\theta} \cos \bar{\theta}} \frac{\hat{u}_1}{\bar{u}_1} \quad (9.11)$$

Heat is released by the flame at the rate $\rho_1 u_f S_f \Delta H$, where u_f is the flame speed and ΔH is the enthalpy change in combustion. Then the fluctuation in the total heat release rate for the flame is

$$\frac{\hat{Q}}{\bar{Q}} = -\frac{\hat{\rho}_1}{\bar{\rho}_1} + \frac{1}{1 - i\omega(b_2 - b_1)/\bar{u}_{1g} \sin \bar{\theta} \cos \bar{\theta}} \frac{\hat{u}_1}{\bar{u}_1} \quad (9.12)$$

In this model of the problem, \hat{Q}/\bar{Q} represents a possible mechanism for an instability. The result (9.12) with the linearized equations of motion; the equation of state for a perfect gas; and the boundary conditions that the flow is choked at the entrance and open to the atmosphere at the exit (see Figure 9.7), define a soluble problem. Dowling and Bloxsidge found that the flow should be unstable over a broad range of equivalence ratio, with fairly reasonable agreement between their calculated results and observations at Rolls-Royce. This basic model of the instability was developed in subsequent works.

Reports of the completed work were published by Langhorne (1988) covering the details of experiments; and by Bloxsidge, Dowling and Langhorne (1988) discussing their theoretical results for interpreting the experimental results. Both papers were concerned with the apparatus sketched in Figure 9.9(a). The work is particularly distinguished by the collaboration of experiment and theory. That is perhaps an obvious strategy to encourage, but it seems that too often experiments have been carried out without useful efforts at applying or working out theoretical ideas. Without at least an approximate ‘theoretical’ framework it is difficult to discern the extent to which experimental results may be general or useful (or, perhaps, even correct).

⁶Because the Cambridge group uses $e^{i\omega t}$ where here we use $e^{-i\omega t}$, the sign of ω here is everywhere different from that in the original paper.

Because the results reported contain more detail than is appropriately covered here, we restrict our discussion to three items: frequencies of oscillation; amplitudes of limit cycles; and mode shapes. The observed limit cycles referred to here are of course not the ideal forms having constant amplitudes, but are motions having dynamical properties approximately constant for some finite time. Because the experiments used blow-down apparatus, tests were limited to lengths of about twenty minutes. The fuel was ethylene (C_2H_4) injected through a manifold upstream of the choked nozzle. Measurements of the equivalence ratio confirmed that mixing was essentially complete upstream of the flame holder; combustion was ignited downstream of the gutter. In a typical test, after a flame was established, steady incoming flow was maintained with Mach number usually 0.08, with a few results obtained at $\bar{M} = 0.15$. Later tests reported by Macquisten and Dowling (1993) were carried out with Mach numbers between 0.15–0.27.

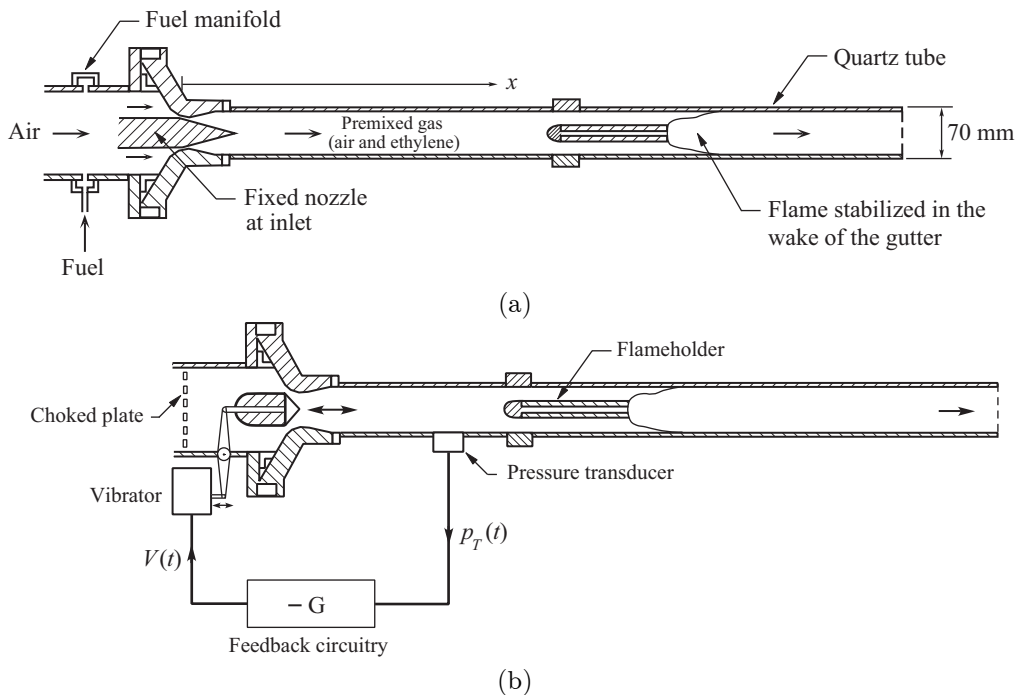


FIGURE 9.9. Cambridge apparatus. (a) Fixed nozzle for studies of longitudinal instabilities (Langhorne 1988); (b) Variable nozzle for experiments to determine transfer functions and for active control (Bloxsidge *et al.* 1988a, b).

Oscillations were excited and assumed to be driven mainly by interactions between acoustic waves and the combustion processes; no consideration was given to entropy waves or to possible influences of vorticity. Hence, the primary variables to be determined by measurements are the unsteady pressure; and heat release, the mechanism for the unstable waves. The pressure was measured using accurate commercial transducers and a high-quality microphone (Brüel and Kjaer). The heat release was determined indirectly, from the light emitted by species in the flame. Following previous researchers (Hurle *et al.* 1968 may have been the first), Langhorne used emission from C_2 radicals, assuming that the rate of heat addition is proportional to the intensity of radiation. The method is potentially subject to substantial errors from several causes; a discussion of the problems was not offered by the authors, and is outside the present discussion. Langhorne took care with peripheral experiments to try to minimize the errors.

An example of the distributions of the magnitude and phase for the pressure are shown in Figure 9.10(a). Data and two computations of the unsteady pressure fields are taken from Figure 4 of Langhorne (1988).

The transfer function for the unsteady heat release; and the steady heat release all inferred for the same test, are shown in Part (b) of the figure.

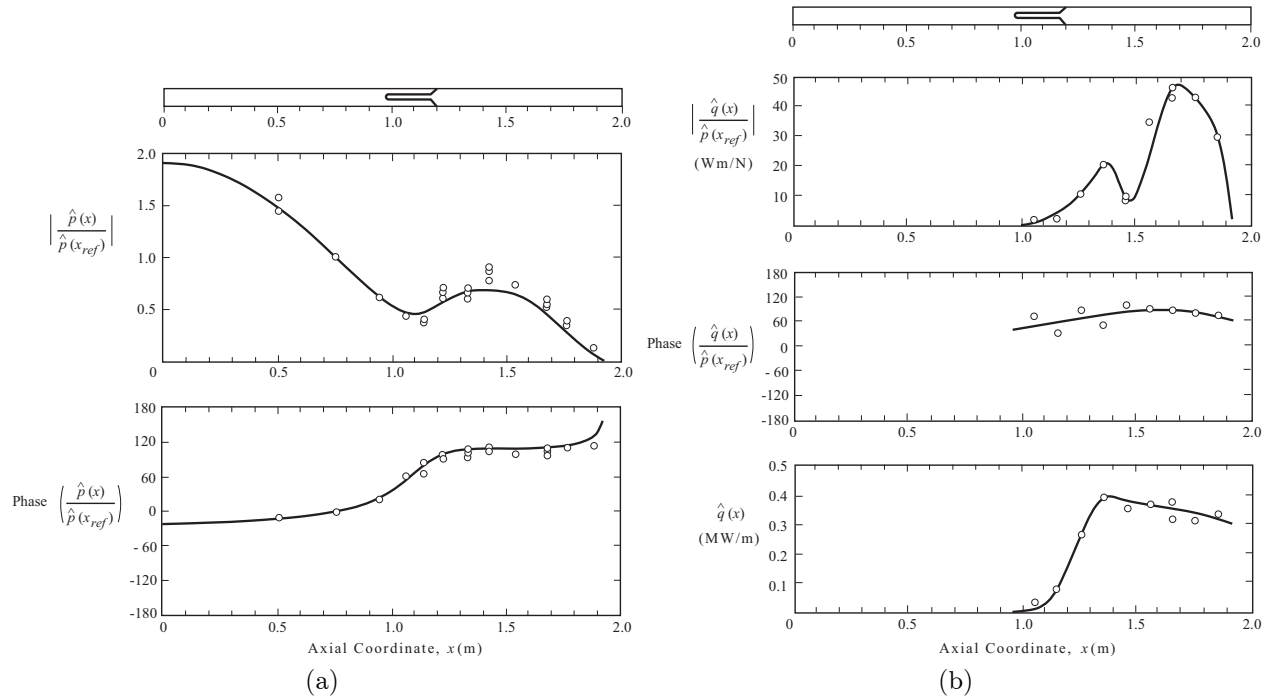


FIGURE 9.10. Magnitude and phase of the pressure distribution (a) and the transfer function for heat release (b) for one configuration of the test apparatus shown in Figure 9.9(a). The solid lines are spline fits to the data. Adapted from Figure 4 of Langhorne (1988).

Two different sorts of unsteady behavior were described by Langhorne, called *convecting* and *concurrent*, identified according to the dependence of the unsteady C_2 emission on space and time. In the first case, the phase of C_2 radiation (hence, by assumption, the heat addition) varies linearly with respect to that of the pressure. For the second case, the phase difference is small and approximately constant. Concurrent behavior then provides, according to Rayleigh's Criterion (Section 6.6), the most favorable conditions for supporting unstable motions.

Apparently, for many test conditions a flame extends from the flameholder, or 'gutter', as shown in Figure 9.8, until it strikes the lateral walls. Initially when the flow is unsteady, convecting behavior dominates, but if 'established buzz' occurred (large amplitude pressure oscillations) Langhorne found concurrent behavior downstream of some axial position upstream of the anticipated intersection of the flame with the walls. Then "...the flame alternately fills the duct then contracts, leaving only a kernel of flame on the gutter." That sort of behavior was evidently always (?) observed for equivalence ratios greater than about 0.65, with accompanying strong oscillations. The paper contains further observations not covered here. Unfortunately there are no pictures of the flow, although some were taken.

In Part 2 of the work, a one-dimensional 'theory' was worked out to give mainly the frequency and mode shape of the instability. For all cases considered, the mean heat release was assumed to have the same piecewise linear distribution with constants adjusted for different conditions. The authors correctly recognized that the most important part of the unsteady problem is the heat release provided by the unsteady flame. Their discussion of their procedure for developing the modes of an unsteady flame and the accompanying

unsteady heat release occupies nearly one-third of Bloxsidge *et al.* (1988). The experimental basis was established by measurements using the apparatus shown in Figure 9.9(b) without the feedback shown (i.e., $G = 0$). The flame anchored at the gutter was exposed to small, approximately sinusoidal perturbations produced by the oscillating nozzle. Measurements of the light emission gave an approximation to the phase between the heat release and the velocity at the lip of the gutter similar to that given above,

$$\frac{\hat{q}(x)}{\bar{q}(x)} = \frac{1}{iSt} \left(1 - \frac{e^{i\beta St}}{iSt} \right) \frac{\bar{u}_G}{\hat{u}_G} e^{-i\omega\tau(x)} \quad (9.13)$$

where $St = 2\pi\omega r_G/\bar{u}_G$ is a Strouhal number defined with r_G the radius of the gutter; \bar{u}_G is the local flow speed; and $\tau(x)$ is a time delay, the time for a disturbance to pass from the gutter at x_G to position x , $\tau = (x - x_G)/\bar{u}_G$. For the conditions of the experiments, the author found that the second term in parentheses is the larger of the two and approximately

$$\frac{\hat{q}(x)}{\bar{q}(x)} = \frac{\hat{\eta}_G}{2\pi r_G} e^{-i\omega\tau(x)} \quad (9.14)$$

The displacement of a fluid particle is $\hat{\eta}_G$ at the lip of the gutter. Boundary conditions for choked flow at the entrance ($x = 0$) and subsonic exhaust flow ($x = L$) complete the formulation. Figure 9.10 shows one example of six cases computed by Bloxsidge *et al.* (1988). The results of a simplified version of the problem were also discussed by Dowling (1988). Because the treatment is linear, the actual values of the amplitude could not be computed, but generally fairly good agreement between calculated values of the frequency and observations was found (7% difference, about 6 Hz). Also, the authors report good results for changes with inlet Mach number; equivalence ratio; and geometry, the length of the chamber and location of the flameholder.

Probably the weakest part of the entire analysis is the description of the unsteady heat addition. Although the model seems a simple, realistic basis for the calculations, the intermittent character of the unsteady burning, suggestive of vortex shedding, is not captured in the analysis. Apparent similarity between experimental results and calculations shown, for example by plots of \hat{q}/\bar{p} such as that in Figure 9.10, is not consistent with the behavior cited by Langhorne in the quotation above. As we have discussed several times with examples in Chapters 2 and 6, vortices, or identifiable regions of concentrated vorticity shed at flameholders of various configurations, are common phenomena arising in combustion instabilities. The general problem has not been satisfactorily solved.

Following the early experiments on control of oscillations in Rijke tubes by Dines (1983) and Heckl (1985, 1986), the initial results on feedback control at Cambridge were reported by Bloxsidge *et al.* (1988) and Langhorne *et al.* (1989). They first used the device shown in Figure 9.9(b) showing that control of the oscillations was exercised by operating the movable nozzle in a feedback path. Figure 9.11(a) shows the effect of control on the oscillations in the duct, and Figure 9.11(b) is the spectrum of the unsteady pressure, all measured upstream of the flameholder. The authors conclude that their method of control worked by increasing the flux of acoustic energy loss at the downstream end of the duct. Their analysis is incomplete, having nothing to say, for example, about the substantial reduction of the second harmonic clearly evident in Figure 9.11(b). This may be simply due to a decrease in the consequences of nonlinear coupling causing flow of energy from the fundamental to the second harmonic, but the matter is not addressed in the paper. The overall performance of the system was, however, quite promising, the peak of the spectrum being reduced by 20 dB (or 12 dB according to a second paper by Bloxsidge *et al.* 1987); and the total acoustic energy in the range 0–800 Hz was lower by 10–11%. One is left wondering why the reduction of amplitude is this large—or this small.

Although appearing in print earlier, the 1987 paper by Bloxsidge *et al.* contains some analysis and design of the control system which is not included in their 1988 paper. Evidently motivated in part by consultation with a colleague expert in control theory, the authors use a method of ‘loop shaping’ to improve the control system by inserting elements (e.g. a Butterworth filter as well as a phase shifter and two additional filters)

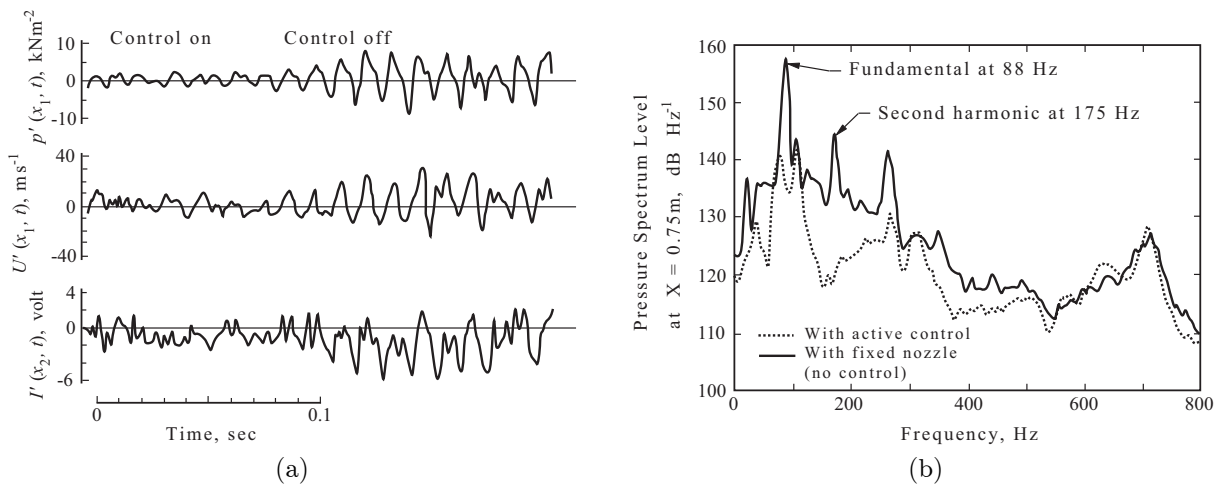


FIGURE 9.11. Unsteady motions in the test rig shown in Figure 9.9(a). (a) Pressure, velocity and light emission between the inlet nozzle and flameholder; (b) spectrum of the pressure (Bloxsidge, Dowling, Hooper and Langhorne 1988).

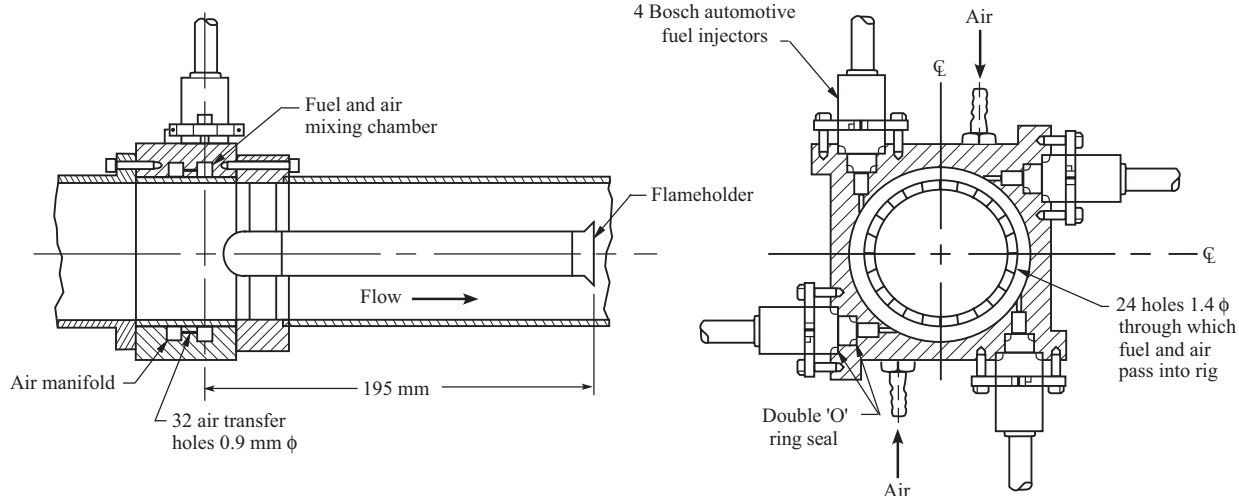


FIGURE 9.12. The device for mixing secondary fuel and air at the upstream end of the flameholder shown in Figure 9.9 (Langhorne *et al.* 1989).

in the feedback loop. The discussion of the design process is the first application of modern feedback control design to a combustor, quite detailed, and helpful in understanding the current work as well as later works by others. It is out of place to cover the subject here; the inclusion of a bit of control theory serves to emphasize the point that attempts to use active control for improving the performance of combustion systems must pay attention to both the principles of control and to the physical behavior of combustion processes. It is in respect to the second that much of the reported work seems often to fall short.

In their second work on active control, Langhorne, Dowling and Hooper (1990) reported the first use of secondary fuel injection to reduce a combustion instability. Again they used the apparatus shown in Figure 9.9(a), but the device sketched in Figure 9.12 was installed at the upstream end of the flameholder. Automotive fuel injectors, essentially solenoid valves, pulsed the inflow of fuel. In operation, then, the flame

is supplied by the primary premixed stream, plus a non-uniform supply of pulsed fuel/air mixture. The secondary air flowed steadily; only the secondary fuel was pulsed. Because the control supply of flow entered through twenty-four radial holes (see Figure 9.12), mixing in transverse planes was likely quite good. Control was exerted by varying the voltage operating the solenoid valves, thereby changing the fuel flow only. In the paper, the discussion of the test results draws virtually not at all on the picture of the flow developed in the works described above, but is based principally on some ideas of linear control theory. For the most part, the analysis used is that worked out in the 1987 paper by Bloxsidge *et al.*, although there are some differences in detail.

Langhorne *et al.* found that with the addition of fuel at a rate equal to 3% of the steady flow, the peak of the pressure spectrum was lower by 12 dB. The acoustic energy in the range 0–400 Hz was reduced by 18% when oscillations were controlled. That (fractional) amount of fuel flow is too large for many practical applications. Later systems have been shown to be less demanding in their requirements.

Soon after the early Cambridge work on control of combustion instabilities, the group at École Centrale in Paris began a modest collaborative program of research with a group at Technische Universität München. Both groups had experience for some years with oscillations in laboratory combustors; the new feature was the application of control. A postdoctoral researcher from Munich (W. Lang) was the live connection between the two institutions, participating in tests performed at École Centrale. Two experimental devices were used, shown in Figures 9.13 and 9.14 (Lang *et al.* 1987; Poinsot *et al.* 1987).

The simpler apparatus, Figure 9.13, was a vertical tube containing a flame burning premixed gases at the midpoint. An approximate analysis of this burner has been given in Section 2.7. It is not truly a Rijke tube because its operation does not require that the flow be induced by buoyancy. At an equivalence ratio of 0.8, and flow rate of 0.23 l/s, the system oscillated at 630 Hz, with an amplitude of 220 Pa, i.e., 2.2×10^{-3} atmospheres. This was the second acoustic mode, approximately three-quarters of a wavelength contained in the tube closed at the bottom and open at the top. The main purpose of the tests was to demonstrate application of feedback control using a speaker as actuator and a microphone as sensor, both items contained in the single feedback path shown in Figure 9.13(b). Various combinations of the locations of the actuator and sensor were reported, including cases when both were on the same side of the flame vertically, location D, but placed on opposite sides of the tube. Satisfactory suppression of the instability could be obtained in all cases treated, the noise level being reduced to 1/2 its original value in the best case.

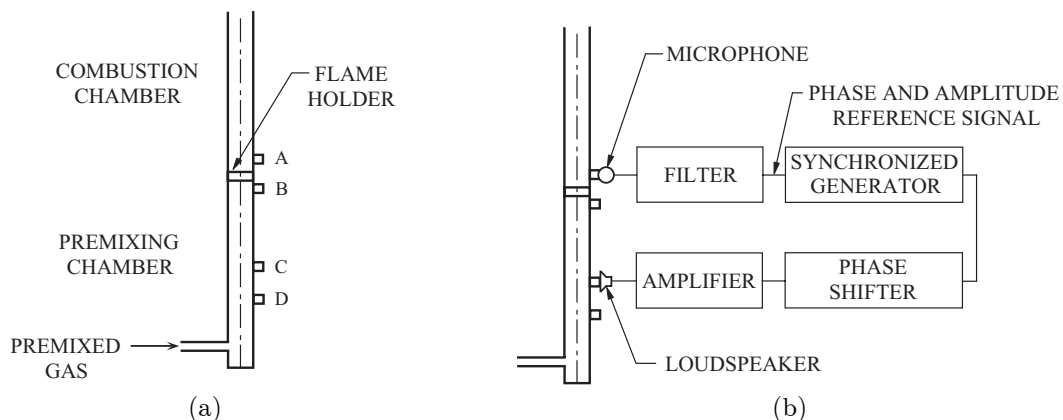


FIGURE 9.13. Apparatus used in the first tests of feedback control of combustion at École Centrale and the Technische Universität München. (a) Tubular burner exhibiting oscillations; (b) the configuration with provision for feedback control (Lang *et al.* 1987; Poinsot *et al.* 1987, 1989).

Although the authors suggest at the beginning of this paper that their experiments demonstrate ‘anti-sound’, they (correctly) later note that the control “system suppresses the noise source by directly controlling the sound emission by the flame.” The point is that, unlike noise control by the use of anti-sound, (Ffowes-Williams 1984), the process demonstrated in this work, as in the Cambridge tests, involves active modification of the processes in noise production, and the coupling between the motions of the flame and the acoustic field. It’s an important fundamental point distinguishing combustion systems from most electro-mechanical systems which have been the usual subjects of control. Application of control in the present case is necessarily accompanied by changes in the properties of the system, properties which contain both the causes and corrections of the problem (the instability).

At essentially the same time, tests at École Centrale were carried out with the apparatus shown in Figure 9.14. The duct burner, Figure 9.14(a), was used to demonstrate feedback control in a configuration somewhat closer to those of practical systems, and under somewhat more realistic conditions. Results were obtained for turbulent flows, and reactants not premixed. The combustor, downstream of the injector, had quartz windows in the lateral walls, was thirty centimeters long and had cross section 10 cm × 5 cm. Tests were performed with an airflow rate of 24 g/s, and equivalence ratio of 0.4; the combustor then operated at 250 kW, which should be compared with the 1 kW burner in Figure 9.13(a).

The control system used speakers shown in Figure 9.14(a); apparently the instrumentation was identical with that indicated in Figure 9.13(b). Figure 9.14(b) gives a clear picture of the effectiveness of (even) simple actuation. At 230 Hz the peak in the microphone signal was reduced by 24 dB. As implied in the Cambridge reports, but shown explicitly in the work at École Centrale, the flames responsible for the instability were noticeably affected by the actions of the oscillations. Figure 9.14(c) shows schleiren photographs of the region containing the processes of injection, mixing and combustion. Control of the system was accompanied by streamwise stretching of the two-dimensional mixing layers formed by the injected gas jets. Evidently the apparent periodic ‘pinching-off’ process was interrupted by the action of control, as suggested by comparison of the pictures (i) and (ii), part (c) of the figure. Part (c) is a striking example of one property distinguishing control of combustion systems, that the action of control itself changes the system being controlled. That characteristic is fundamental and quite likely lies behind many of the difficulties in this field, blocking success with practical systems. Although the two situations are unrelated, note the suggestive similarities between the flows shown in Figure 9.14(c) and in Figure 7.37 for a rearward facing step.

Some further discussion and additional tests of details of the work were included—e.g. use of the control to aid study of the initiation and growth of the instability—but to a large extent the problem remains open. It seems that the setting chosen for these tests still offers a good possibility for studying fundamental behavior not yet well understood.

Soon after the results at Cambridge and École Centrale became known, a small program of feedback control was begun at the General Electric Corporate Research and Development Laboratory, initially with two closely connected efforts reported by Goodman and Houpt (1991) and by Gulati and Mani (1992). The apparatus was essentially the same for the two works, sketched in Figure 9.15(a). Each demonstration used the combustor having length $a = 0.5$ m and cross section 5 cm × 5 cm, and a perforated plate as a flameholder. Flow rates of premixed air and methane varied from 200–500 ml/s, giving velocities 8–20 cm/s and equivalence ratio from the lean limit ($\phi = 0.6$) to ($\phi = 1.4$). For the lengths used, the frequencies of observed oscillations were mainly below 10,000 Hz.

Figure 9.15(b) shows two examples of the spectra measured when (i) there was no flame (but flow); and (ii) when there was a flame controlled and uncontrolled. The flow rates were 220 ml/s ($\phi = 0.8$) and 330 ml/s ($\phi = 1.0$). A dominant peak appeared in all cases. It was identified by the authors as the second longitudinal mode of pressure, having an antinode at upstream end (approximately closed by the speaker); and two nodes, one upstream of the flame and one at the open exhaust. As comparison of (i) and (ii) in Figure 9.21(b)

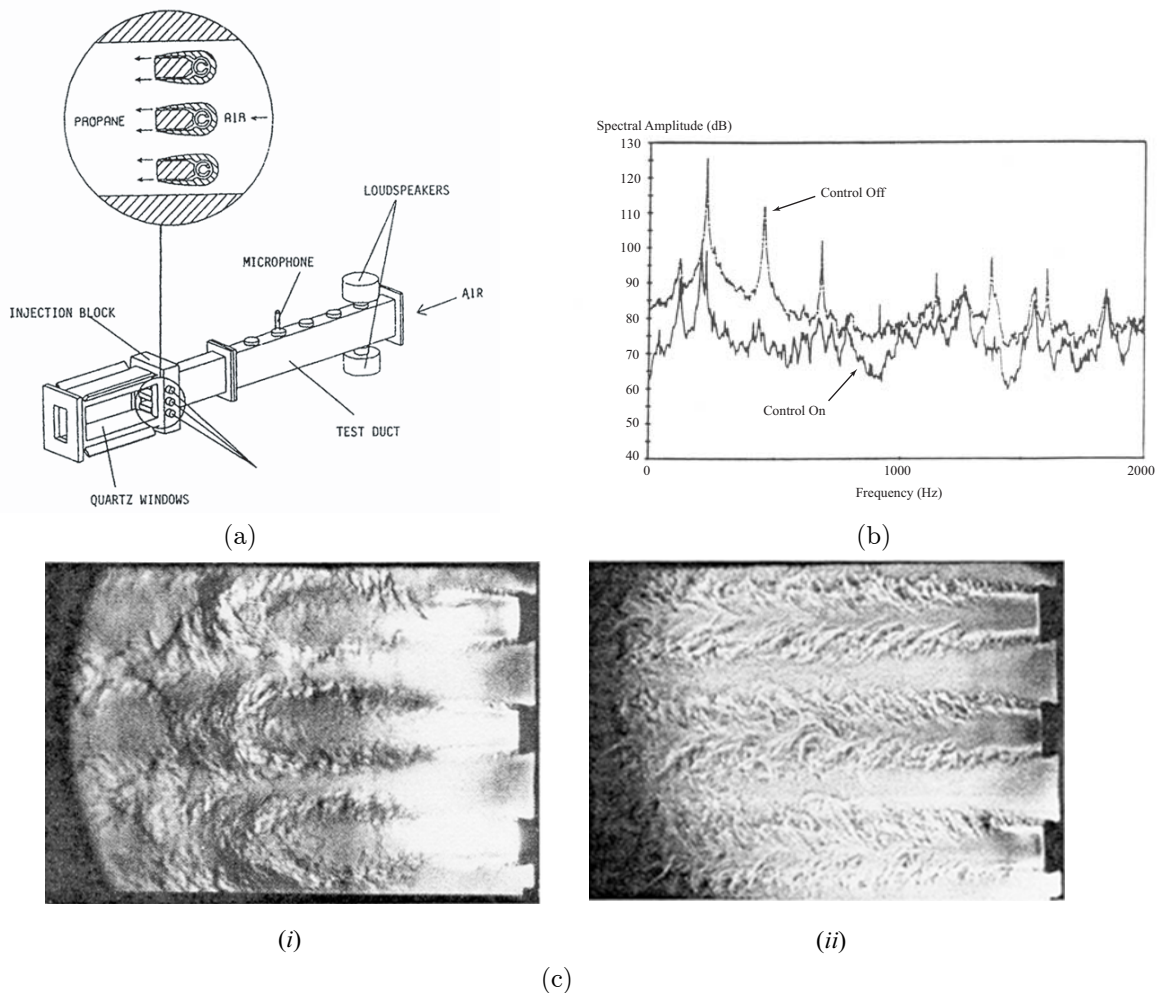


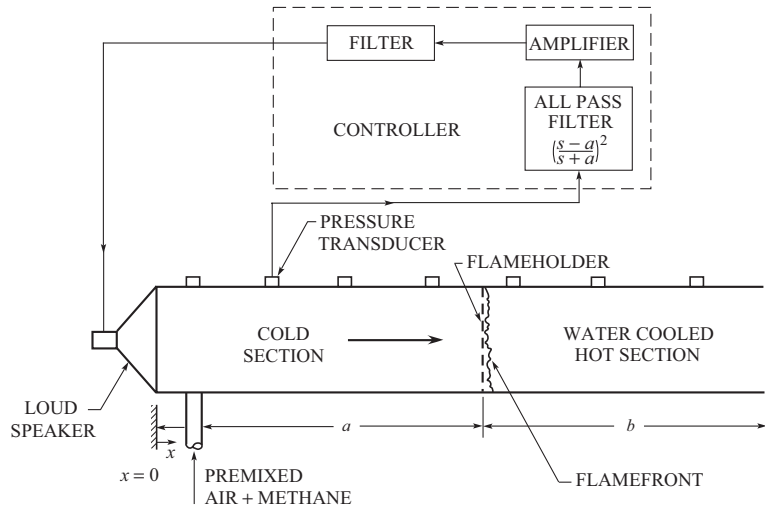
FIGURE 9.14. Feedback control at École Centrale (a) apparatus with a 250 kW combustor; (b) effects of control on the light emission; (c) schlieren photographs of the combustion region (i) without and (ii) with control (Poinsot *et al.*, 1987, 1988, 1989).

shows, modes having higher frequencies were favored by higher flow speeds. Unfortunately, the controller became less effective as the flow speed increased. The controller acted by adjusting the amplitude of waves injected by the speaker, and their phase relative to the measured wave. As the flow speed increased, the usable ranges of amplitude and phase of the control signal became less. At equivalence ratios greater than 0.8 and flow speeds greater than 330 ml/s the control system would not suppress oscillations. Because the speaker (the actuator) was not affected by the flow, the authors concluded that reduced performance of the control system was likely caused by unfavorable characteristics of the controller.

To improve the performance of their system, Gulati and Mani modified the design of their controller by appealing to ideas of 'loop-shaping', following the first application of this approach to a combustion system by Bloxsidge *et al.* (1987, 1988). The general idea (see, e.g., Doyle, Francis and Tannenbaum 1992, McFarlane and Glover 1992) is that the performance of a feedback system depends on the transfer function of the 'open loop', for example $G_f G_{fb}$ in Figure 9.2. Thus, to understand the behavior of the *closed-loop* system, for which the transfer function is $G_f G_{fb} / (1 + G_f G_{fb})$, we really need to know and work with the much simpler function $G_f G_{fb}$ for the *open-loop*.

The basis for doing so was established in 1932 by Nyquist in his wonderful paper “Regeneration Theory,” ‘regeneration’ being a synonym for feedback. Annex G here is a discussion of Nyquist’s ‘criterion’, the relation (G.10),

$$Z = N + P \quad (9.15)$$



(a)

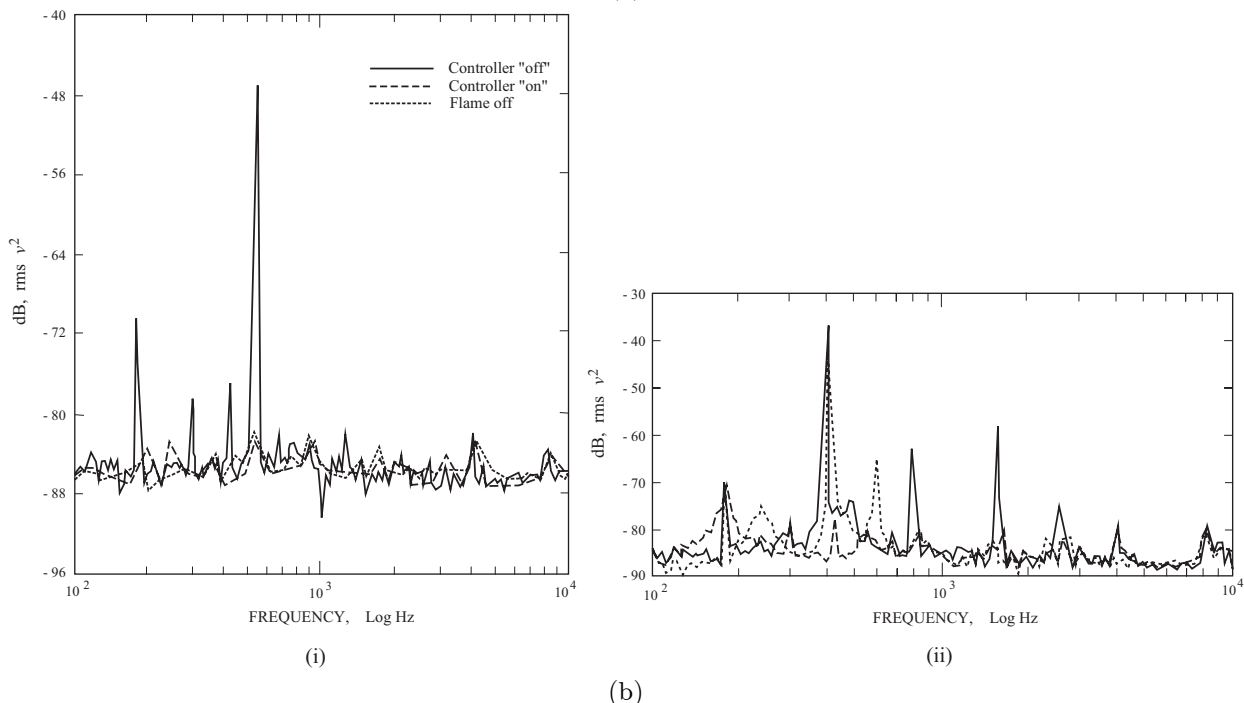


FIGURE 9.15. GE demonstration of feedback control, results for the first type of controller; (a) sketch of apparatus and instrumentation; (b) measured power spectra for (i) flow only, and (ii) with a flame (Gulati and Mani 1992).

where Z is the number of zeros of the transfer function for the *closed-loop* system in the right half s -plane; P is the number of poles of the transfer function for the *open-loop* system; and N is the number of *counter-clockwise* encirclements of the point -1 by the polar plot of the *open-loop* transfer function.

$$N = -P \geq 0 \quad (9.16)$$

Examples, and much theoretical work with Nyquist's Criterion, make use of explicit forms for the loop transfer function, labelled HG in Annex G. In contrast to the choice by Bloxsidge *et al.* (1987) and Langhorne *et al.* (1990) to use simple approximations for HG , Gulati and Mani constructed HG from measurements on their system. Based on the results, they changed the components in the controller as required. The measurements include the dynamics of the flame, but must be performed under conditions when oscillations due to instabilities are suppressed. Figure 9.16 shows an example of a Nyquist diagram obtained from the measurements. Results discussed in the reference led to inclusion of a notch filter to eliminate a peak in the spectrum, and a lead compensator to correct for an additional phase shift. That approach gives wider gain and phase margins (see the discussion in Annex G and Figure G.8).

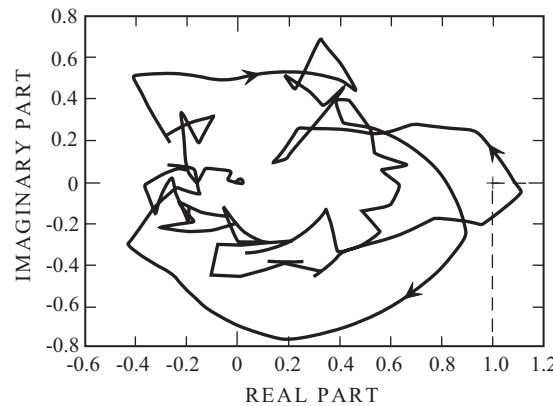


FIGURE 9.16. A Nyquist diagram recorded by Gulati and Mani (1992) for their combustor with their first controller. Because of their choice of conventions, encirclements of $+1$ rather than -1 are counted (cf equation 9.15); only half of the symmetric diagram is shown.

Using essentially the same apparatus, Houpt and Goodman (1991) also applied principles of control theory to improve the design and performance of a controller indicated by the dashed box in Figure 9.15(a). Like Gulati and Mani, they measured open-loop dynamics and Nyquist plots for several variants of the system. The emphasis of the brief work is on difficulties arising with control of a distributed system approximated as a lumped-parameter system, no attention being directed to the consequences of possible changes in the hardware or characteristics of the combustion processes. Thus the work is directed to adaption of methods well-known for control of electro-mechanical systems to systems involving flow and combustion. The results are much less important than the tack taken.

In a little noticed short paper, Tierno and Doyle (1991) reported an interesting demonstration of applying system identification as the basis for controlling the oscillations in an electrically-driven Rijke tube. A speaker was used as an actuator and a small FET microphone was the sensor, both devices placed near the intake to the tube. The open-loop transfer function $H(s)$ for the combined system of amplifier, speaker, Rijke tube and microphone was measured for sufficiently high flow rate giving stable operation, and represented by a collection of second order systems:

$$\frac{Y(s)}{D(s)} = H(s) = \sum_{n=1}^M \frac{b_n c_n}{s^2 + 2\delta_n \omega_n + \omega^2} \quad (9.17)$$

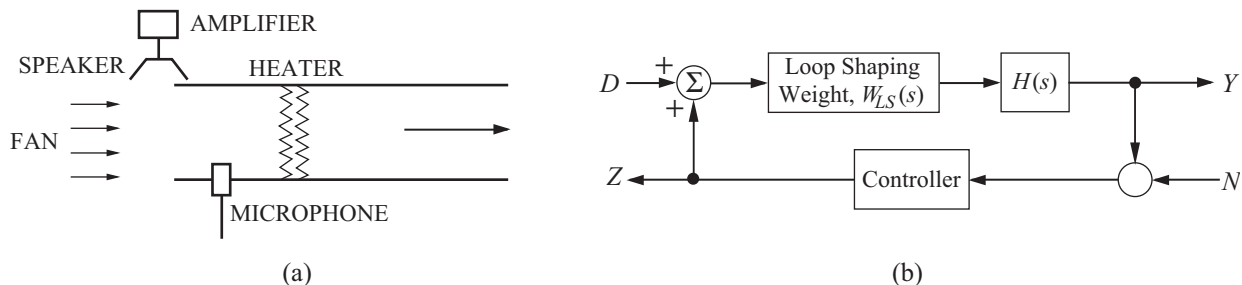


FIGURE 9.17. Schematic of a Rijke tube apparatus (a) and the block diagram (b) for loop shaping design (Tierno and Doyle 1992).

Because control is exercised under conditions when the system is unstable—so $H(s)$ is not exactly given by the function on the right side of (9.17)—the control system must have certain amount of ‘robustness.’ Except in the range of frequencies 200–400 Hz, equation 9.17 is quite a good representation for $100 < f < 2000$ Hz, a range containing about ten modes.

With the objective of reducing the quality factor (center frequency divided by the 3 dB bandwidth of the spectrum) of the two lowest modes, the authors follow a procedure for designing a controller based on ‘loop-shaping’ (McFarlane and Glover 1989, 1992). Figure 9.17(b) shows the configuration for the loop-shaping design procedure. The loop-shaping weight W_{LS} is defined by the shape $L(s)$ required to meet the performance specification, which in this case if $|L| \gg 1$, where

$$L(s) = W_{LS}(s)H(s) \quad (9.18)$$

with the chosen weight

$$W_{LS}(s) = \frac{7}{(s + 1500)(s + 3000)^2} \quad (9.19)$$

Design of the controller, Figure 9.17(b), involves calculations which we will not cover here, and are only referred to by Tierno and Doyle.

The main result is successful reduction, by the closed loop control, of the resonances exhibited by the open loop system. Figure 9.18 shows an example for unspecified flow rate and heater power. The system did not sustain limit cycles at the reduced levels reached where closed loop control was applied.

This is an interesting demonstration introducing the use of a ‘loop shaping H_∞ ’ technique similar to that used in the GE work (Horupt and Goodman, 1991; Gulati and Main, 1992). A significant difference is the use of an electric heater to drive the instability. Thus the dynamics of the heat source are quite different. No investigation of the differences between the two cases has been published.

Application of feedback control to combustion systems requires merging two historically distinct fields of study to form a third new field. Historically, virtually no single person has simultaneously had experience, knowledge, and depth of understanding in both originating fields. As a result, emphasis in particular works has tended to lie on one side of the other. As a practical matter, it has been a natural tendency that a combustion group (in a university or in a commercial organization) would invite people with background in controls to participate, or advise, in a research project. The interesting—and instructive—aspect of the work at General Electric is the very substantial influence exerted by the controls people. Unfortunately, the program was abandoned, leaving still unanswered many questions raised by the limited tests, and incomplete interpretations of the behavior observed. Similarly, the demonstration reported by Tierno and Doyle did not lead to further work elaborating their only study.

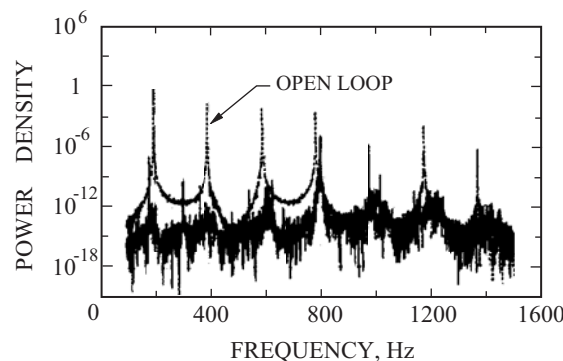


FIGURE 9.18. Open and closed loop power spectra for the Rijke tube shown in Figure 9.17(a) (Tierno and Doyle 1992).

9.3. Modal Control for Combustion Systems

It is probably not an exaggeration to claim that the experimental work with elementary situations in the 1980's had exposed the general character of most of the basic problems to be overcome before control of combustion systems could be regarded as successfully achieved. Before we review progress to date, it is helpful to summarize the general basis for our subsequent remarks.

Given that at a sufficiently high level practically all control systems fit the picture shown in Figure 9.1, and further that the principles of linear control are well-known and their applications highly developed, it is a reasonable question: What is special about the problem of controlling the dynamics of a combustion system? Perhaps the best simple answer is that combustion systems bring together at least five defining characteristics each of which individually already may be difficult to treat in control of other kinds of systems:

- internal instabilities
- substantial time lags
- intrinsic nonlinearities
- substantial internal noise
- the action of control changes the properties of the system

The fact that the system is unstable—the origin, after all, of the problems discussed here—is not unusual, nor is the presence of time lags. Control of nonlinear systems has successfully been treated in special cases and it seems that much is known about controlling some kinds of nonlinear behavior in other types of physical systems. Presently the significance of noise in respect to controlling combustion systems is not understood; the matter merits consideration since often in combustion chambers the levels of noise are not negligibly small compared with those of the instabilities. When a combustion system is controlled, significant changes in the defining characteristics, such as the distribution of average energy release may occur. In fact those changes may account for elimination of an instability. That sort of behavior is quite different from the usual situation in a mechanical system whose defining properties such as masses, are not normally affected by the action of control.

All five of the items listed above raise issues of modeling, analysis and, ultimately, experimental work. In the context of control, that situation justifies the principal thrust of this book. The general framework based on spatial averaging is attractive for at least two important reasons:

- (i) the process of averaging tends to reduce the consequences of errors in details of modeling;

- (ii) there is a wonderful match between the methods of feedback control in state space on the one hand; and the theory of combustor dynamics based on spatial averaging and expansion in acoustic modes on the other.

In the literature of control theory this merging of control theory and the behavior of a continuous system is often called ‘control of a distributed parameter system.’ Note, however, that label normally implies representation—i.e. a mathematical model—of the system based on partial differential equations.

The main subject of this chapter is perhaps more appropriately identified by the standard term *modal control*, using a representation of the system based on ordinary differential equations describing the amplitudes and relative phases of the modes. Modal control has been developed mainly in the field of structures, nonflowing systems generally, which can be represented as ‘lumped parameter’ systems by working with Lagrange’s equations. Figure 9.19 shows one way of summarizing the scheme we have discussed in the preceding eight chapters. Matters of control arise in the bottom line of blocks. Our remarks here are limited to linear control, which encompasses both classical and modern control. It is essential to understand the well-established principles of classical control. However, for several reasons it is often preferable to treat control of combustion systems within modern control theory, using representations in state space.

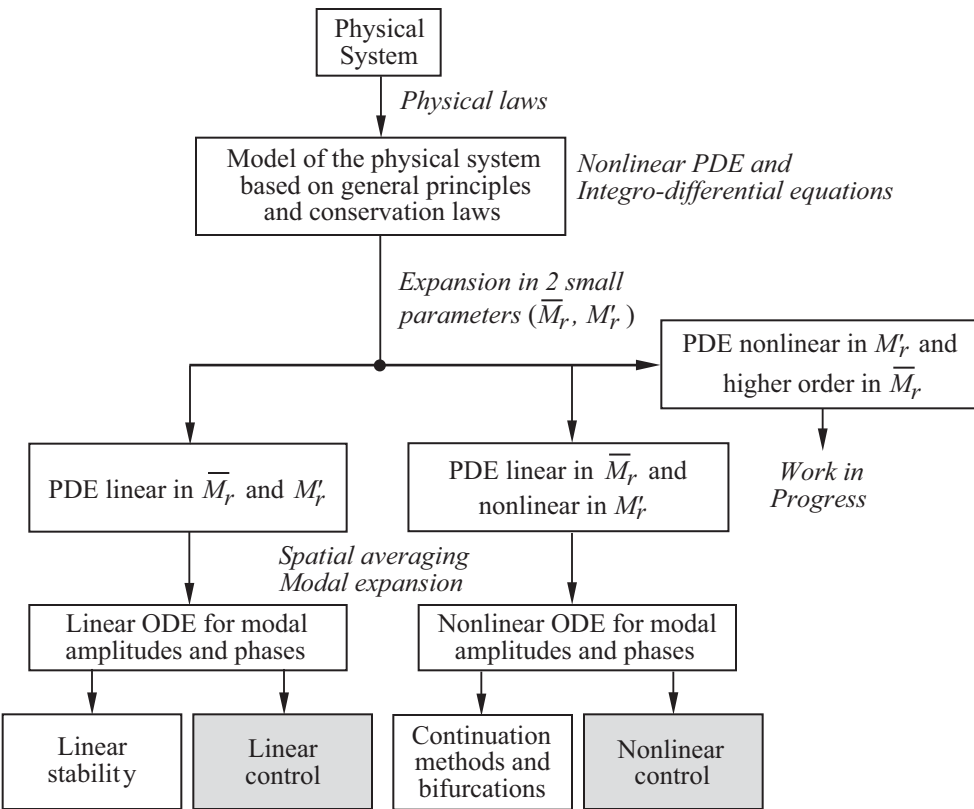


FIGURE 9.19. The general scheme according to the procedures followed here for connecting the physical system (a combustor), physical modeling, mathematical modeling, dynamics and control.

It happens that the formulation based on spatial averaging becomes a state space representation by simple redefinition of symbols. Hence the entire apparatus of modern control theory becomes immediately applicable. The group at Penn State, for example, seems to have been first to take advantage of that

attractive feature (Fung, 1991), as described in Section 9.3.1. Many subsequent works by other groups are related in some respects or other.

The basic idea is quite straightforward, following from the form of the equations (3.53) and their boundary conditions (3.55) governing the evolution of arbitrary unsteady motions in a combustor:

$$\nabla^2 p' - \frac{1}{\bar{a}^2} \frac{\partial^2 p'}{\partial t^2} = h + h_c \quad (9.20)$$

$$\hat{\mathbf{n}} \cdot \nabla p' = -f - f_c \quad (9.21)$$

The functions h_c and f_c represent the actions of control. The splitting on the right-hand sides of (9.20) and (9.21) is legitimate for linear problems because any means of control (passive or active) can work only because it affects the mass, momentum and energy of the system; additivity follows from the assumption of linearity. In principle, h_c and f_c can be computed with the same formulas defining h and f discussed in Section 3.4. The formalism of spatial averaging worked out in Chapters 3 and 4 can be applied without change to (9.20) and (9.21), giving the extended oscillator equations corresponding to (4.36), written here for the n^{th} mode,

$$\ddot{\eta}_n + \omega_n^2 \eta_n = F_n + F_n^{(c)} \quad (9.22)$$

where $F_n^{(c)}$ is the ‘force’ of control acting on the n^{th} oscillator, (i.e. the n^{th} mode). The set of equations (9.22) forms the mathematical model used in application of the principles of control. We emphasize once again that the most difficult part of applications consists in modeling the physical processes⁷ contained in F_n and $F_n^{(c)}$.

As a simple example of the general procedure, suppose that the combustor is given and that its internal processes are well-characterized. Thus the mean flow field, and the steady distribution of chemical reactions and energy release are known. Hence we may assume that the basis functions ψ_n and the normal frequencies can be computed and are known. Hidden in F_n are quantities that must be modeled. In particular, the most important is the fluctuation of energy release, \dot{Q}' , associated with the chemical reactivity of the flow. Its contribution to F_n has already been introduced in the simple example of the Rijke tube discussed in Section 2.2. The term representing energy addition is

$$F_N^Q = \frac{\gamma - 1}{\bar{p}} \frac{1}{\int \psi_n^2 dV} \int \psi_n \frac{\partial \dot{Q}'}{\partial t} dV \quad (9.23)$$

in which influences of the mean flow have been ignored. In reality \dot{Q}' depends on local fluctuations of pressure, temperature, velocity and species concentrations. It therefore cannot be determined from elementary considerations of chemistry and chemical kinetics alone.

A term similar to (9.23) arises in $F_n^{(c)}$ so on the right-hand side of (9.22) we have the combination

$$F_n^Q + F_n^{Q(c)} = \frac{\gamma - 1}{\bar{p}} \frac{1}{\int \psi_n^2 dV} \int \psi_n \left[\frac{\partial \dot{Q}'}{\partial t} + \frac{\partial \dot{Q}'_c}{\partial t} \right] dV \quad (9.24)$$

where \dot{Q}'_c is the local fluctuation of heat release rate ascribed to the controlled actuation. If $\frac{\partial}{\partial t}(\dot{Q}' + \dot{Q}'_c)$ vanishes, then there is no effect of heat in energy release in the excitation and maintenance of unsteady motions. This seems a simple if not almost obvious result. It seems to be the most elementary formal expression within the analysis developed here, of what is likely the most effective practical means of actively controlling the dynamics of gas turbine combustors, modulation of the fuel supply.

⁷The formulation here is very general and of course is valid for non-reacting flows. Hence, at least in principle, these equations with noise sources included (Section 7.9) are applicable as well to active control of sound or noise (Nelson and Elliott, 1992; Peake and Crighton, 2000).

The basic idea is that if the fuel supply is so modulated, or if a secondary fuel supply is injected in the chamber, and the modulation as effected according to the appropriate control law, then the fluctuation of energy release rate \dot{Q}'_c due to its action might, under ideal conditions, exactly compensate the amount \dot{Q}' due to fluctuations due to other causes. ‘Other causes’ might include coupling between the mean flow (e.g. vortex shedding) and acoustic modes, and destabilization of flame stabilization processes near the lean blowout limit. This kind of control can be interpreted in terms of Rayleigh’s original criterion, Section 6.6: If $\dot{Q}'_c = -\dot{Q}'$ and only this process is accounted for, then $\nabla \xi_n$, equation (6.67), vanishes. Hence, control by modulation of the fuel supply is frequently referred to as a strategy “according to Rayleigh’s Criterion” or similar words. For example, the idea is expressed often in the works published by the group at Georgia Tech (e.g., Butts *et al.* 2003, Conrad *et al.* 2004, Zinn 2005). A fundamental difficulty, apparent in Figure 9.14(c), are the unpredictable significant effect that the action of control has on the dynamical properties of the combustion and flow processes. Evidently the meanings and interpretation of \dot{Q}' and \dot{Q}'_c are not clearly defined.

9.3.1. State Feedback Control Based on Spatial Averaging. A group at Pennsylvania State University first worked out some results for feedback control using the representation in normal modes. In his Ph.D. thesis Fung (1991) has covered most of the results reported by Fung, Yang, and Sinha (1991), Fung and Yang (1991), and Yang, Sinha, and Fung, (1992). Their analyses are based on the formulation covered in earlier chapters here, leading to the governing equation (9.20) with the boundary condition (9.21). In terms of the general contributions \mathcal{P}_c in the equation (D.1)d for pressure and \mathcal{F}_c in the momentum equation ((D.1)b, the source terms representing the actions of control are formed from the last two terms of (D.4)a and the last term of (D.4)b:

$$h_c = \nabla \cdot \mathcal{F}'_c - \frac{1}{\bar{a}^2} \frac{\partial \mathcal{P}'_c}{\partial t} \quad (9.25)$$

$$f_c = -\hat{n} \cdot \mathcal{F}'_c \quad (9.26)$$

The procedure for spatial averaging worked out earlier with the approximations introduced for combustion with flow, gives the set of coupled equations for the normal modes,

$$\frac{d^2 \eta_n}{dt^2} + \omega_n^2 \eta_n = F_n \quad (9.27)$$

and

$$\begin{aligned} F_n = & - \sum_{i=1}^{\infty} [D_{ni} \dot{\eta}_i + E_{ni} \eta_i] - \sum_{i=1}^{\infty} \sum_{j=1}^{\infty} [A_{nij} \dot{\eta}_i \dot{\eta}_j + B_{nij} \eta_i \eta_j] \\ & + \sum_{i=1}^{\infty} [\xi_{ni}^{(\ell)} v \dot{\eta}_i + \xi_{ni}(t) n_i] + \Xi_c(t) + U_n(t) \end{aligned} \quad (9.28)$$

As defined in Chapter 4, the coefficients D_{ni}, E_{ni} can be calculated if the mean flow and the mode shapes or eigenfunctions ϕ_n are known. In general, they may be constructed from information given or assumed for the linear processes in question. The coefficients A_{nij}, B_{nij} depend only on the mode shapes and are well-defined. They arise from nonlinear acoustical interactions which are independent of the mean flow. Sources of noise are represented by $\xi_{ni}^{(\ell)} v \dot{\eta}_i$, $\xi_{ni} \eta_i$ and $\Xi(t)$. At the present state of theory and experiment, one has little choice but informed modeling as the basis for specifying representations of noise. The limited results obtained to date suggest that relatively straightforward and simple models of noise will suffice for obtaining useful results. See Sections 7.9 and 7.10. Additional processes may be included in (9.28) but attention must be paid to the ordering procedure explained in Chapter 4.

The last term in (9.28) represents the control input,

$$U_n(t) = -\frac{\bar{a}^2}{\bar{p} E_n^2} \left[\int \psi_n h_c dV + \oint \psi_n f_c dS \right] \quad (9.29)$$

In terms of \mathcal{F}'_c and \mathcal{P}'_c introduced with (9.25) and (9.26), we have

$$U_n(t) = \frac{\bar{a}^2}{\bar{p}E_n^2} \int [\mathcal{F}'_c \cdot \nabla \psi_n + \frac{1}{\bar{a}^2} \frac{\partial \mathcal{P}'_c}{\partial t} \psi_n] dV \quad (9.30)$$

Formulation for problems of control is completed, within the present scheme, by specifying \mathcal{F}'_c and \mathcal{P}'_c . Whether one continues with a description set in terms of the variables defined in physical space ($\mathbf{x}, d\mathbf{x}/dt, p, \dots$) or transforms to a description grounded in state space as described shortly, the basic problem is specifying the control input, which means determining explicit forms for \mathcal{F}'_c and \mathcal{P}'_c . That is the most difficult part of the entire field of controlling combustion systems, rendered especially challenging because, as implied by the last item of the list at the beginning of this section, \mathcal{F}'_c and \mathcal{P}'_c are dependent upon the action of control in ways which are unknown; see, for example, Figure 9.14(c).

Transformation to a description in state space is straightforward. Following Fung (1991), define the state variables x_n as the amplitudes x_n of the modes. Assume that the first N modes are controllable and that the system is defined to include the first K modes, $K > N$. Then the state vector is taken to be composed of the controllable, x_N and residual, x_R , parts,

$$\mathbf{x} = [x_n, x_r]^t \quad (9.31)$$

where superscript $[\]^t$ represents the transpose, and

$$\mathbf{x}_N = [\eta_1, \dots, \eta_N; \dot{\eta}_1, \dots, \dot{\eta}_N]^t \quad (9.32a)$$

$$\mathbf{x}_R = [\eta_{N+1}, \dots, \eta_K; \dot{\eta}_{N+1}, \dots, \dot{\eta}_K]^t \quad (9.32b)$$

For combustion systems, which in principle have an infinite number and in practice exhibit a large number of excited modes (cf. Figure 9.14(b) for example), limitations of control systems must cause both N and K to be non-zero. In other words, there will always be N controlled modes and $K-N$ modes that are not controlled, the residual modes.⁸ If the nonlinear part of (9.28) is dropped, then the set (9.27) is linear and well-known methods developed for control of electro-mechanical systems are applicable. Fung (1991); Fung, Yang, and Sinha (1991) reported their results based on methods explained by Franklin *et al.* (2002); Franklin and Powell (1980); and Ogata (1987, 1990).

To illustrate the transformation to a description in state space, we assume that only three modes are active and that the system is linear ($A_{nij} = B_{nij} = 0$ in F_N). Then the state vector is

$$\mathbf{x} = [n_1, n_2, n_3; \dot{n}_1, \dot{n}_2, \dot{n}_3]^T \quad (9.33)$$

We do not include uncontrolled (residual) modes. The first order equations for the components of the state vector are formed by inspection, using the definitions of the \dot{x}_i and the equations for

$$\dot{x}_1 = \dot{\eta}_1 = x_4 \quad (9.34)$$

$$\dot{x}_2 = \dot{\eta}_2 = x_5 \quad (9.35)$$

$$\dot{x}_3 = \dot{\eta}_3 = x_6 \quad (9.36)$$

$$\begin{aligned} \dot{x}_4 = -\omega_1^2 x_1 + [D_{11}x_4 + E_{11}x_1] + [D_{12}x_5 + E_{12}x_2] + [D_{13}x_6 + E_{11}x_3] \\ + [\xi_{11}^\nu x_4 + \xi_{11}x_1] + [\xi_{12}^2 x_5 + \xi_{12}x_2] + [\xi_{13}^\nu x_6 + \xi_{13}x_3] + \Xi_1(t) + v_1(t) \end{aligned} \quad (9.37)$$

$$\begin{aligned} \dot{x}_5 = -\omega_1^2 x_2 + [D_{21}x_4 + E_{21}x_1] + [D_{22}x_5 + E_{22}x_2] + [D_{23}x_6 + E_{23}x_3] \\ + [\xi_{21}^\nu x_4 + \xi_{21}x_1] + [\xi_{22}^2 x_5 + \xi_{22}x_2] + [\xi_{23}^\nu x_6 + \xi_{23}x_3] + \Xi_3(t) + v_2(t) \end{aligned} \quad (9.38)$$

$$\begin{aligned} \dot{x}_6 = -\omega_1^2 x_3 + [D_{31}x_4 + E_{31}x_1] + [D_{32}x_5 + E_{32}x_2] + [D_{33}x_6 + E_{33}x_3] \\ + [\xi_{31}^\nu x_4 + \xi_{31}x_1] + [\xi_{32}^2 x_5 + \xi_{32}x_2] + [\xi_{33}^\nu x_6 + \xi_{33}x_3] + \Xi_3(t) + v_2(t) \end{aligned} \quad (9.39)$$

⁸Although the representation in terms of acoustic modes means strictly that $K \rightarrow \infty$, we assume for this discussion that K is finite.

Stochastic sources represented by $\Xi_n(t)$ and the various terms containing ξ_{ij}^ν and ξ_{ij} are not accounted for in the traditional formulations of modern control theory so we split them apart and write

$$\dot{\mathbf{x}} = \mathbf{A}\mathbf{x} + \boldsymbol{\xi}\mathbf{x} + \boldsymbol{\Xi}(t) + \mathbf{u}(t) \quad (9.40)$$

$$\mathbf{A} = \begin{bmatrix} 0 & 0 & 0 & 1 & 0 & 0 \\ 0 & 0 & 0 & 0 & 1 & 0 \\ 0 & 0 & 0 & 0 & 0 & 1 \\ -\omega_1^2 + E_{11} & E_{12} & E_{13} & D_{11} & D_{21} & D_{31} \\ E_{21} & -\omega_1^2 + E_{22} & E_{23} & D_{21} & D_{22} & D_{23} \\ E_{31} & E_{32} & -\omega_1^2 + E_{33} & D_{31} & D_{32} & D_{33} \end{bmatrix} \quad (9.41)$$

$$\boldsymbol{\xi} = \begin{bmatrix} 0 & 0 & 0 & 0 & 0 & 0 \\ 0 & 0 & 0 & 0 & 0 & 0 \\ 0 & 0 & 0 & 0 & 0 & 0 \\ \xi_{11} & \xi_{12} & \xi_{13} & \xi_{11}^\nu & \xi_{12}^\nu & \xi_{13}^\nu \\ \xi_{21} & \xi_{22} & \xi_{23} & \xi_{21}^\nu & \xi_{22}^\nu & \xi_{23}^\nu \\ \xi_{31} & \xi_{32} & \xi_{33} & \xi_{31}^\nu & \xi_{32}^\nu & \xi_{33}^\nu \end{bmatrix} \quad (9.42)$$

$$\boldsymbol{\Xi}(t) = \begin{bmatrix} 0 \\ 0 \\ 0 \\ \Xi_1(t) \\ \Xi_2(t) \\ \Xi_3(t) \end{bmatrix} \quad ; \quad \mathbf{u}(t) = \begin{bmatrix} 0 \\ 0 \\ 0 \\ u_1(t) \\ u_2(t) \\ u_3(t) \end{bmatrix} \quad (9.43)a,b$$

Much of the theory of linear systems in state space is formulated in terms of the 'ABCD' matrices defined so the systems are described by the equations⁹

$$\dot{\mathbf{x}} = \mathbf{A}\mathbf{x} + \mathbf{B}\mathbf{u} \quad (9.44)$$

$$\mathbf{y} = \mathbf{C}\mathbf{x} + \mathbf{D}\mathbf{u} \quad (9.45)$$

where \mathbf{y} is the matrix of the outputs of the system. For a 'single-input single-output' (SISO) system, both \mathbf{u} and \mathbf{y} are scalars, so \mathbf{B} is a column matrix, \mathbf{C} is a row matrix and \mathbf{D} is a scalar. In general the matrices have the following forms for systems having N degrees of freedom, giving $n = 2N$ state equations, p inputs and q outputs:

$$n \begin{bmatrix} A \end{bmatrix} \quad n \begin{bmatrix} B \end{bmatrix} \quad q \begin{bmatrix} C \end{bmatrix} \quad q \begin{bmatrix} D \end{bmatrix} \quad (9.46)$$

Equations ((9.43)a,b) and (9.44) apply if stochastic processes are not accounted for and $\mathbf{u}(t)$ is appropriately defined.

⁹Franklin *et al.* (2002) distinguish between 'ABCD' matrices used for the 'model canonical form' of the governing equations and then 'FGHJ' matrices for describing a system in general. The non-uniqueness of the state-space formulation causes technical difficulties but is not a fundamental matter and we will not elaborate here.

Most early experimental results for combustors have been accomplished for SISO systems; see Figures 9.4, 9.8(a), 9.14, and 9.15. In such cases, $q = p = 1$ and \mathbf{u} becomes u , a scalar. This special but very important case is treated at length by Franklin *et al.* (2002).

Although we will not need the result, for completeness we sketch the derivation of a basic result showing the connection between the transfer function for a linear system and the description in terms of the matrices \mathbf{ABCD} . Take the Laplace transform of the state equation (9.44) to find

$$s\mathbf{X}(s) - \mathbf{x}(0) = \mathbf{AX}(s) + \mathbf{BU}(s). \quad (9.47)$$

Solve for $\mathbf{X}(s)$ to find

$$\mathbf{X}s = (s\mathbf{I} - \mathbf{A})^{-1}\mathbf{BU}(s) + (s\mathbf{I} - \mathbf{A})^{-1}\mathbf{x}(0) \quad (9.48)$$

where \mathbf{I} is the identity matrix having off-diagonal elements zero and diagonal elements 1.

The transform of the output, equation (9.45), is

$$\mathbf{Y}(s) = \mathbf{CX}(s) + \mathbf{DU}(s) \quad (9.49)$$

and substitution of (9.47) gives

$$\mathbf{Y}(s) = \mathbf{G}(s)\mathbf{U}(s) + \mathbf{C}(s\mathbf{I} - \mathbf{A})^{-1}\mathbf{x}(0) \quad (9.50)$$

where the transfer function, or better, the transfer matrix, is

$$\mathbf{G}(s) = \mathbf{C}(s\mathbf{I} - \mathbf{A})^{-1}\mathbf{B} + \mathbf{D} = \frac{\mathbf{C}\text{Adj}(s\mathbf{I} - \mathbf{A})\mathbf{B}}{\det(s\mathbf{I} - \mathbf{A})} + \mathbf{D} \quad (9.51)$$

For a single-input single-output system, (9.51) can be put in the simpler scalar form

$$G(s) = \frac{\det \begin{bmatrix} \mathbf{A} - s\mathbf{I} & \mathbf{B} \\ \mathbf{C} & \mathbf{D} \end{bmatrix}}{\det[\mathbf{A} - s\mathbf{I}]} \quad (9.52)$$

The results (9.50), (9.51), and (9.52) are the basis, in principle, for calculating the behavior of a linear system.

9.3.2. Application to Combustion Systems. The results just quoted have wide applications discussed particularly in tests already referred to. In the Penn State work, special results for combustion systems were obtained by assigning the source functions $U_n(t)$ forms which follow from use of representations of physical behavior established previously. Thus, the assumption of M ‘point actuators’ implies the form for the source function in the wave equation for pressure

$$h_c(\mathbf{r}, t) = \sum_{i=1}^M \delta(\mathbf{r} - \mathbf{r}_i)u_i(t) \quad (9.53)$$

and the first integral in (9.29) gives

$$U_n(t) = \frac{\bar{a}^2}{\bar{p}E_n^2} \sum_{i=1}^M u_i(t)\psi_n(\mathbf{r}_i) \quad (9.54)$$

For these calculations we assume that there is no actuation in the surface of the chamber so $f_c = 0$.

The additional assumption of J point sensors exhibiting no direct dependence on actuation processes allows (9.45) to take the form

$$y_j(t) = c_j p'(\mathbf{r}_j, t) \quad (9.55)$$

where the c_j are real numbers determined in principle by the sensors. With the usual form of the pressure field,

$$y_j(t) = c_j \bar{p} \sum_{s=1}^J \eta_s(t) \psi_s(\mathbf{r}_s) \quad (9.56)$$

What remains to complete specification of the general problems is definition of the control law, the rule governing the time-dependent action of the actuators. That is, $\mathbf{u}(t)$, which is to say the $u_i(t)$ must be set explicitly. Put another way, the feedback law is required. The most common choice, originated by Collander *et al.* (1936) is ‘PID control,’ proportional-integral-derivative control, illustrated by the simplified diagram shown in Figure 9.20 for time-dependent behavior. In the case shown, a single state variable $x(t)$ has a specified (desired or reference) state $r(t)$ and output $y(t)$.

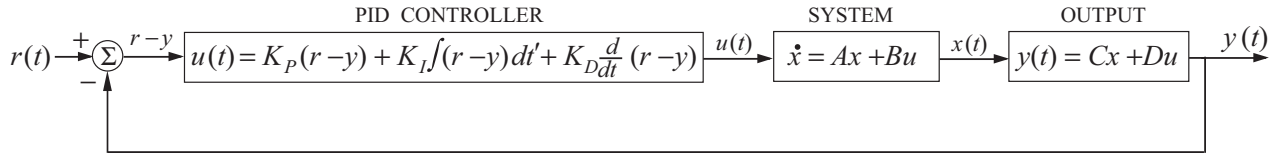


FIGURE 9.20. A simple block diagram for proportional-integral-derivative (PID).

Properties and behavior of linear feedback control are usually treated as functions of frequency (‘in the frequency domain’), leading to the appropriate block diagram corresponding to Figure 9.20. Shelves of texts treat the various effects and uses of PID control, and consequences of varying the three main control variables, K_P , K_I , and K_D .

Yang *et al.* (1992) first chose to follow a path common in modern control theory, assuming ‘state feedback’ control, that is, setting the control linear in the state variables

$$\mathbf{u}(t) = -K \hat{\mathbf{x}}_N \quad (9.57)$$

where $\hat{\mathbf{x}}_N$ is an approximation to the true state vector, an approximation at least because in practice only a finite number of modes can be controlled. The result is often referred to as an ‘estimation’ quantified by an ‘estimator’ introduced in the system.

This situation introduces the idea of an observer first discussed by Luenberger in his Ph.D. thesis, later summarized in Luenberger (1971). The use of an observer and estimator is well-developed in control theory (see Franklin *et al.* 2002 for a good discussion) and we will not cover the subject here. Put most simply, the observer acquires approximate (measured) information about the state of the system, which the estimator then uses to construct the approximation to the state, $\hat{\mathbf{x}}_N$, used by the controller according to (9.57) for example. With this formal basis, Yang *et al.* follow known procedures and then work out examples showing application of state feedback. It is not surprising that the results demonstrate success; no connections with the behavior physical systems are given. At that time (late 1980s, early 1990s) testing had barely begun.

In a subsequent (not according to date of publication, but essentially contemporaneous) paper, Fung *et al.* (1991) worked out some results based on assuming distributed actuators, suggested by their Figure 1 redrawn as Figure 9.22. Their analysis differs from that worked out by Yang *et al.* (1992) (submitted earlier but published later) mainly in the representation of actuators, and the type of control they assumed. Rather than pursue formalism based on state feedback which offers few hints of practical realization, the authors suppose instead that control involves injection of secondary fuel burning according to the $n-\tau$ model of Crocco and Cheng (1956) explained here in Section 2.3.2. Eventually this approach applied to n actuators

leads to the representation of $h_c(\vec{r}, t)$

$$h_c(\mathbf{r}, t) = - \sum_{i=1}^M u_i(t) \delta(\mathbf{r} - \mathbf{r}_i) \quad (9.58)$$

with

$$u_i(t) = R(\mathbf{r}_i t - \tau_i) \Delta V(\mathbf{r}_i) \frac{R \Delta H_c}{a^2 C_v} \frac{\partial m_i(t - \tau_i)}{\partial t} \quad (9.59)$$

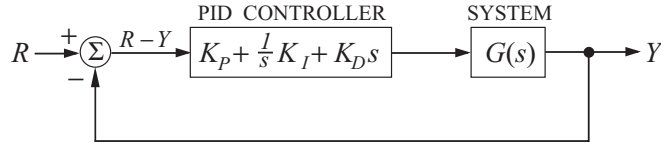


FIGURE 9.21. Block diagram for PID control applied to a linear system; the transfer function $G(s)$ is given by equation (9.52)

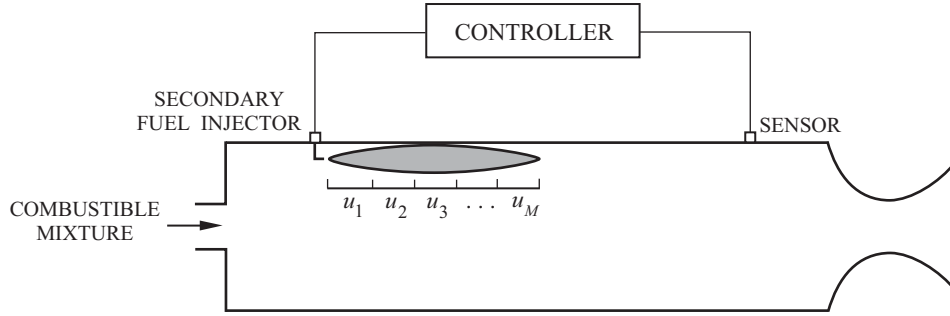


FIGURE 9.22. Simplified sketch of the system analyzed by Fung, Sinha, and Yang (1991).

Equation (9.58) relates the control source in the wave equation to the time-dependence of point actuators whose effects (i.e., wave generation) are assumed to be exerted with time lags, each actuator characterized by a different lag or delay. The model is completed by specifying the way in which the mass sources $m_i(t)$ vary in time. Yang *et al.* chose a proportional/integral (PI) controller, each mass source (actuator) varying according to the rule

$$m_i(t) = K_1 \int_{t_0}^t e(t' - \tau_c) dt' + K_2 e(t - \tau_c) \quad (9.60)$$

where τ_c is the ‘time delay in the feedback loop’ on $e(t) = r(t) - y(t)$ is the error, the difference between the desired response, $r(t)$ -pressure fluctuation—of the system, specified to be zero; and the actual pressure $p(t)$, here set equal to $y(t)$ to conform with standard usage in control theory. Substitution of (9.60) in (9.59) leads to

$$u_i(t) = K_{Pi} e(t - \tau_c) + K_{Di} \dot{e}(t - \tau_c) \quad (9.61)$$

The source term in the wave equation for the amplitudes $\eta_n(t)$ may then be put in the form with $r(t) = 0$ so $e(t) = -y(t) \equiv -p'(t) \sim \eta(t)$:

$$u(t) = - \sum_{i=1}^M \sum_{j=1}^N [K_{Pni} \eta_j(t - \tau_i - \tau_c) + K_{Dni} \dot{\eta}_j(t - \tau_i - \tau_c)] \quad (9.62)$$

where the details of K_{Pni} and K_{Dni} are easily found but are unimportant here. What matters is that the assumptions regarding physical behavior have, in the manner summarized, led to a formulation which can

be used for solving specific problems. How realistically the actual source terms in an operating combustor are represented by a form like (9.62) is a totally different and crucial question.

Probably the principal value of the three papers by Fung and coworkers is their explicit and clear use of examples within the general formulation covered here in Chapters 3 and 4 to study well-known problems in linear control theory. Results obtained depend on assumptions built into construction of the terms representing the controller(s). At the time, the work was done (late 1980s) and given the state of the state of the field, the choices made were reasonable, and the results make sense within that context. However, the use of time lag models is no longer defensible for representation of realistic behavior. To achieve meaningful theoretical results requires much deeper models.

The work just described was extended into the areas of modern control by Hong *et al.* (2000, 2002), works which primarily adapt formalisms worked out by others but do not get at the truly fundamental problems presented by combustion systems. Haddad *et al.* (1996) cover similar ground, with somewhat different emphasis. Their discussion is also a useful introduction to adaptation of some of the ideas taken from modern control theory.

9.4. An Example of Practical Application of Feedback Control

Virtually all progress in applications of feedback control to combustion systems has been achieved without benefit of special theoretical results. General ideas have been useful for interpretation of experiments and to aid broad planning of tests, but the ability to produce quantitative predictions routinely is missing. In short, there is no proper theory of the subjects encompassed by the title of this chapter. Highly developed theory of course exists for feedback, and for systems built on the idea of feedback, but relatively little has been accomplished to accommodate the theory and actual physical behavior of combustion systems. It is helpful at this point to summarize a particularly interesting example illustrating how far, nevertheless, practical application has been accomplished in one case.

So far as the author is aware, there has been only one example of the application of feedback to control the dynamics over an extended period of time in operational gas turbines. The case was mentioned at the beginning of this chapter, a Siemens gas turbine used for power generation. Two other programs have produced documentation of brief experiences with full-scale combustors (Westinghouse; Pratt and Whitney), and a third (Rolls-Royce) describes limited tests with an augmentor designed many years ago. It seems that presently there is little industrial activity in pursuing fundamental development of feedback systems for controlling the dynamics of combustors. Probably a major reason is that the emissions requirements have been met without resorting to control of oscillations and lean burning conditions. The possible gains suggested by experiments performed to date apparently do not justify the added expense and complications. Passive control in the general sense still wins.

Studies of oscillating flames and acoustics at the Technische Universität München began in the 1970s with thesis work by Schimmer (1974), reported by Schimmer and Vortmeyer (1977). Apparatus was designed and constructed to produce flat flames, found when the flow speeds of the propane/air mixture was less than or equal to the laminar flame speed. Figure 9.23(a) is a sketch of the apparatus, a matrix burner specially constructed to give flat flames stabilized near the base. Figure 9.23(b) is a stability diagram in the plane equivalence ratio versus period of oscillation obtained when the flow speed just upstream of the flame is less than or equal to the adiabatic flame speed. Greater flow speeds give wrinkled flames,¹⁰ perhaps indicating incipient turbulence. The abscissa is the inverse of the frequency, $T = 1/f$, which is changed by varying the length L of the tube; if end corrections are ignored, $T \sim L/\bar{a} \sim L$, where \bar{a} is the mean speed of sound.

¹⁰The velocity of flow can be varied and need not be equal to the unique adiabatic flame speed because of the upstream heat losses both to the matrix structure and to the surrounding provisions for cooling.

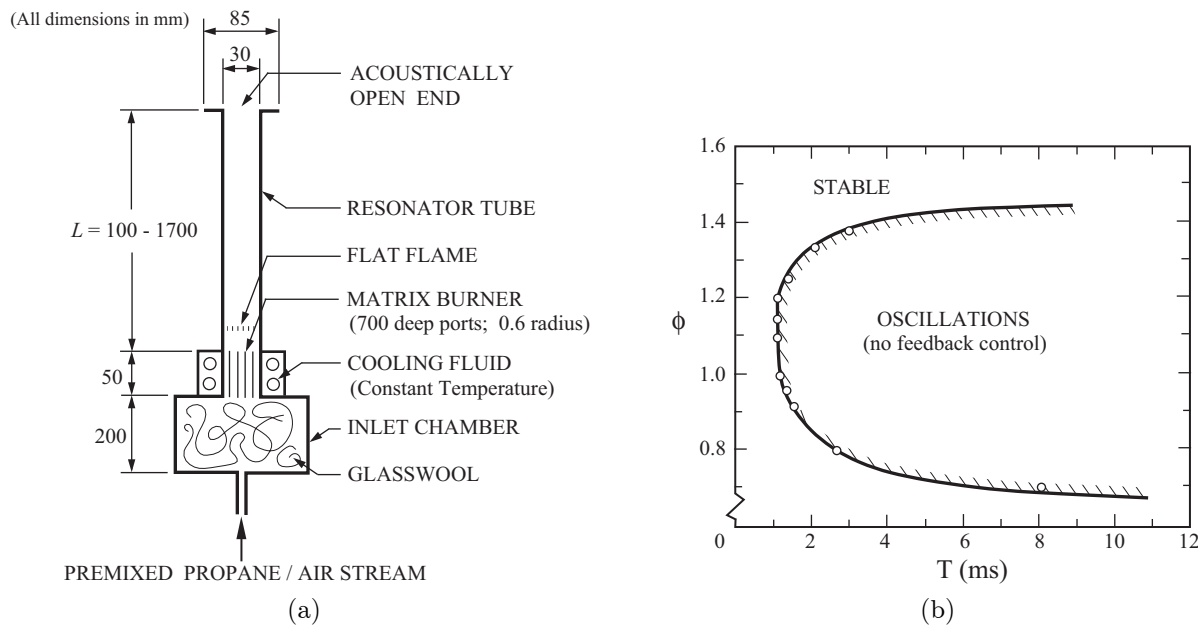


FIGURE 9.23. The apparatus (a) and stability diagram (b) for the results with no feedback control reported by Schimmer and Vortmeyer (1977).

Because only flat flames extending nearly to the inner surface of the tube were tested, it is a good approximation to treat the system as one-dimensional for analyzing the acoustics. The unsteady flow is then represented in piecewise fashion by sums of appropriate travelling waves matched at the flame to give a standing wave system; cf. the ideas and analyses introduced in Sections 2.7.3 and 5.7. Schimmer and Vortmeyer interpreted the behavior of the acoustical system in terms of the analogy with electrical waves: pressure voltage and current \sim velocity, all quantities carrying harmonically in time. It's an interesting discussion, but oversimplifies the actual physical behavior. For example, the treatment would be greatly improved if the ideas developed by Chu (1953) were taken into account. The experimental situation developed in Schimmer's thesis offers a wonderful opportunity to do so.

Joos (1984), and Joos and Vortmeyer (1986) reported later results using apparatus closely resembling Schimmer's. A significant difference is measurement of OH^- radiation, and the assumption that the intensity of the radiation, based on the work by Lenz (1980), is a "direct measure of the momentary reaction," an assumption which has never been thoroughly investigated. As in the early investigation by Schimmer, the behavior of the flame and the acoustics in the tube is interpreted with the help of appeal to electrical waves. The principal improvements are the measurements of radiation—and consequent inferences of energy release—and considerations of simultaneous oscillations having unequal frequencies. As in the case of Schimmer's work, the experiments could be fruitfully repeated with improved forms of the same apparatus, and with the much superior instrumentation now available.

Investigations of possible use of feedback control at the Technische Universität München were first reported in a note by Gleis and Vortmeyer (1989); more easily accessible is the short paper by Gleis, Vortmeyer and Rau (1990) given at an AGARD meeting. These works used apparatus similar to that sketched in Figure 9.13 for the initial tests at École Centrale, Paris, which were the result of a collaboration between École Centrale and Technische Universität München. Because combustion took place in a jet, vortex shedding was found to be a contributing mechanism under some conditions when pressure oscillations were driven.

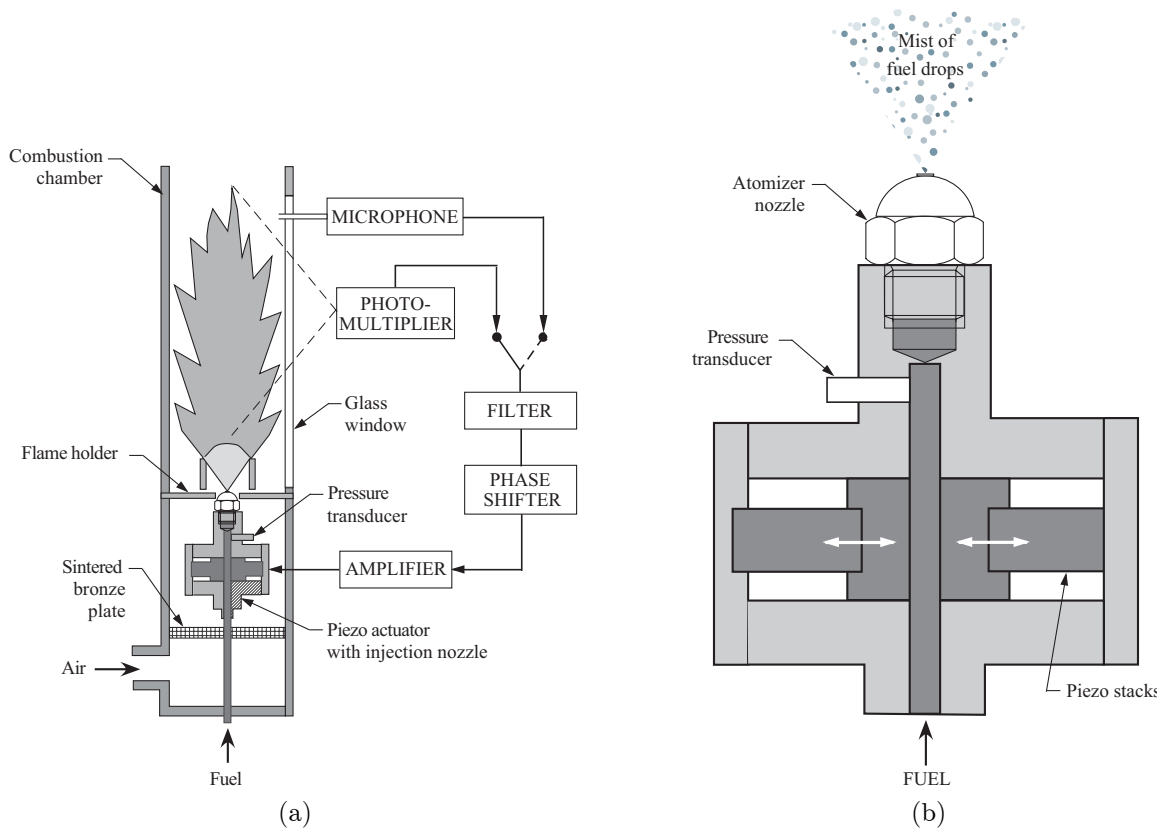


FIGURE 9.24. Feedback control at Technische Universität München. (a) apparatus; (b) the piezo actuator (Hermann, Gleis and Vortmeyer 1996).

A step towards practical application of feedback control was taken with demonstration tests by Gulati and Bigalow (1990) who used a servo valve to modulate their supply of liquid fuel. They found only a small (4 dB) reduction of sound pressure level at 130 Hz, but theirs were the first tests of control with a liquid system. Five years later, Hermann, Gleis and Vortmeyer (1996) reported the first success over a practical frequency range (200–600 Hz) with a piezo actuator that was operable to “several thousand Hz.” They demonstrated the effectiveness of their device with the apparatus sketched in Figure 9.24(a); the piezo actuator is shown, much simplified, in Figure 9.24(b). Note that the entire fuel flow is modulated by the actuator.

A typical test result is reproduced in Figure 9.25; the unsteady pressure served as input to the controller; similar results were obtained when the radiation for OH^- was used. Self-excited oscillations having dominant frequency 360 Hz were found to have peak pressure approximately 140 dB when the equivalence ratio was 0.95. The control system caused the peak to be reduced by about 40 dB, i.e., the oscillatory pressure became roughly one-quarter its original value (see equation 5.75).

A telling disadvantage of piezo actuators is their relatively short lifetime, far shorter than desirable for practical application to control systems in power generation equipment. It was therefore a necessary and significant advance when Hantschk, Hermann and Vortmeyer (1996) reported successful use of a ‘direct-drive valve’ (DDV) developed by MOOG-Germany (Teutsch 1990). The test apparatus had the familiar form, differing only in details from that in Figure 9.26. An important aspect of the equipment is the frequency response of the fuel supply system and the significance of achieving a favorable match with the fuel nozzle and the combustion chamber.

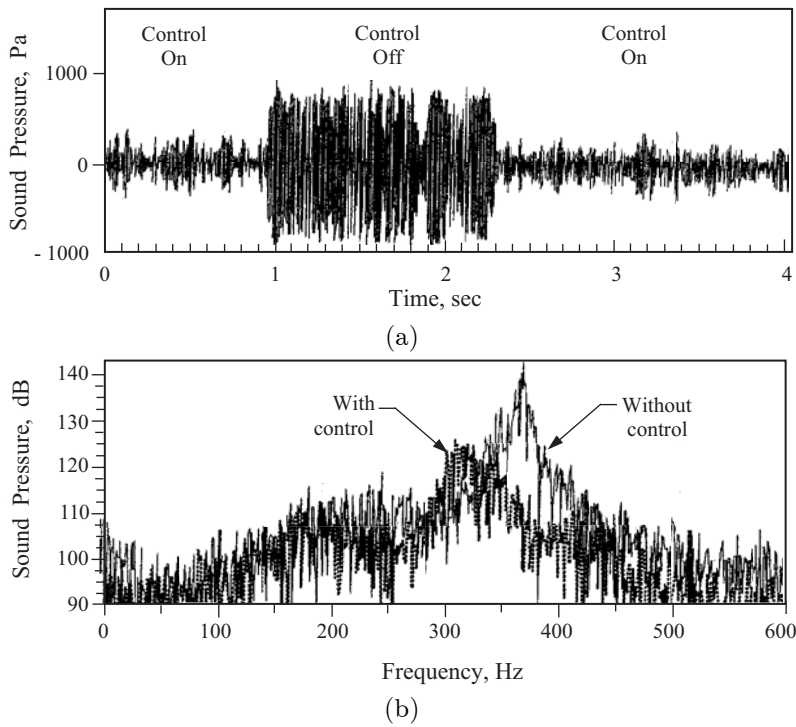


FIGURE 9.25. Test results found with the apparatus shown in Figure 9.24, Figure 14 of Hermann, Gleis and Vortmeyer (1996).

The principle variable is the distance l from the DDV to the fuel nozzle in the chamber. Part of the development process involved changing l to maximize the amplitude of fluctuations in flow rate when the direct-drive valve was operated in the frequency range covering the instability in the chamber. Details of using the DDV and perfecting the system are given in the reference. As a result, the authors learned the importance of matching the dynamical properties of the DDV and fuel supply on the one hand with the fuel nozzle and combustor on the other.

Successful control of oscillations in a liquid-fueled laboratory device independently came at a time when Siemens AG encountered serious troubles with a prototype machine, the Model V84.31 gas turbine, intended to drive a unit generating 170 MW electric power. The experience gained at Technische Universität München was an important part of the background for constructing and installing a feedback control system which, at that time, by contemporary standards in the field, constituted a large step forward. Not only had feedback control been used only on laboratory scale devices,¹¹ characterized by combustion powers less than 1 MW, but there was no experience with axisymmetric combustors, in this case a ring configuration. Further, in the Siemens machine, troublesome oscillations occurred when the operating point of the gas turbine was changing, as during start-up, and large adjustments of power level.

Tests with the V84.31 gas turbine fitted with a control system developed by Hermann *et al.* (see Seume *et al.* 1998) could reduce the amplitudes of combustion-driven oscillations by 86%. Subsequent re-design of the combustor eliminated the instabilities and the control system was removed. However, rejoicing with the success of passive control came to an end with tests of the later model gas turbine, V94.3A, intended for use in a 270 MW electric power generation unit. The problems and their solution with a feedback control

¹¹As reported in the open literature. For some time (at least, roughly, since 1994 or so) rumors persisted that Rolls-Royce had successfully tested feedback control of combustion instabilities in a thrust augmentor. The first publicly available paper (Moran *et al.* 2000) was given at an RTO meeting. No documentation has appeared publicly since that time.

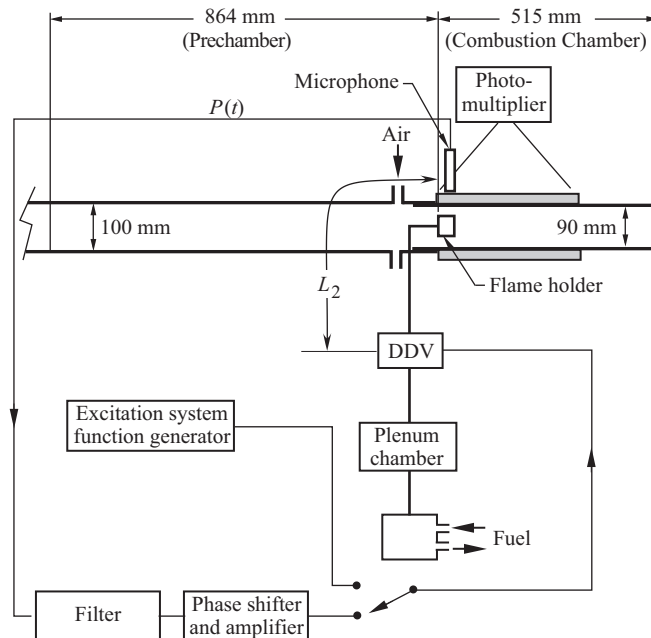


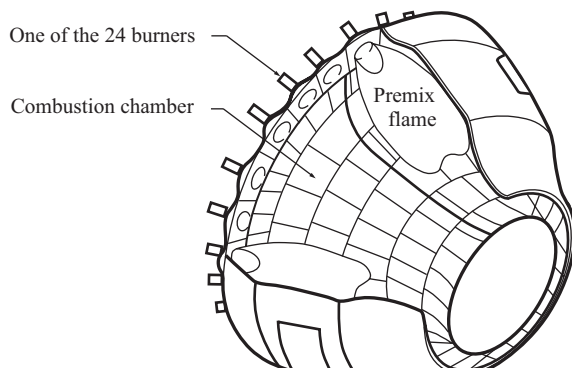
FIGURE 9.26. Test apparatus and feedback control with a simple liquid fuel nozzle and the direct drive valve (DDV) (Hantschk, Hermann and Vortmeyer 1996).

system are well documented in the papers by Hermann, Orthmann, and Hoffmann (1999) and by Hermann and Hoffmann (2005).

The combustors in the Siemens Vx4.3A series of machines are annular, having the shape sketched in Figure 9.27(a); a suggestion of their size is given by the photograph reproduced in Figure 9.27(b). There are 24 burners, each fed by a nozzle like that sketched in Figure 9.28; either liquid or gaseous fuels may be used, but the small diffusion pilot burner always uses gaseous fuel, and generates “approximately 10% of the thermal power.” Only the flow through the pilot burner is modulated by the controller. “Detached research showed that the main premix flame of the Siemens hybrid burner, controlled by much smaller pilot-diffusion flames comprising no more than approximately 10% of the entire mass flow, will respond very precisely to fluctuations in conversion rates of those pilot flames” (Hermann and Hoffmann 2005).

The basic idea of the control system was that modulating flow through the pilot burners only would perturb the combustion processes sufficiently to effect the desired control. With 24 burners the control system seem to present a problem of becoming excessively complicated if some reasonable simplification could not be achieved. As examples of combustion instabilities have already shown, it’s usually the lowest modes that are unstable. If also standing, not travelling, waves are found, the situation really is much simpler to treat. For the Siemens Vx3.4 combustor, for example, the first, second, and fourth standing azimuthal modes tended to be dominant. If only the second harmonic needed to be controlled, one sensor and one controller would suffice to provide the input signals for the necessary four direct-drive valves (Figure 9.29).

Hermann, Othmann and Hoffmann (1999) describe details of the system based on twelve control loops, six signal processors, each having two input signals and four output signals. Thus there are $6 \times 4 = 24$ outputs, one for each direct drive valve. When used, the system was used to control two modes (frequencies); more frequencies could be handled with more elaborate signal processing.



(a)



(b)

FIGURE 9.27. A sketch (a) of a combustor used in the Vx4.3A series Siemens gas turbines, (b) an illustration of the size of the combustor (courtesy of Siemens AG, and Dr. J. Hermann).

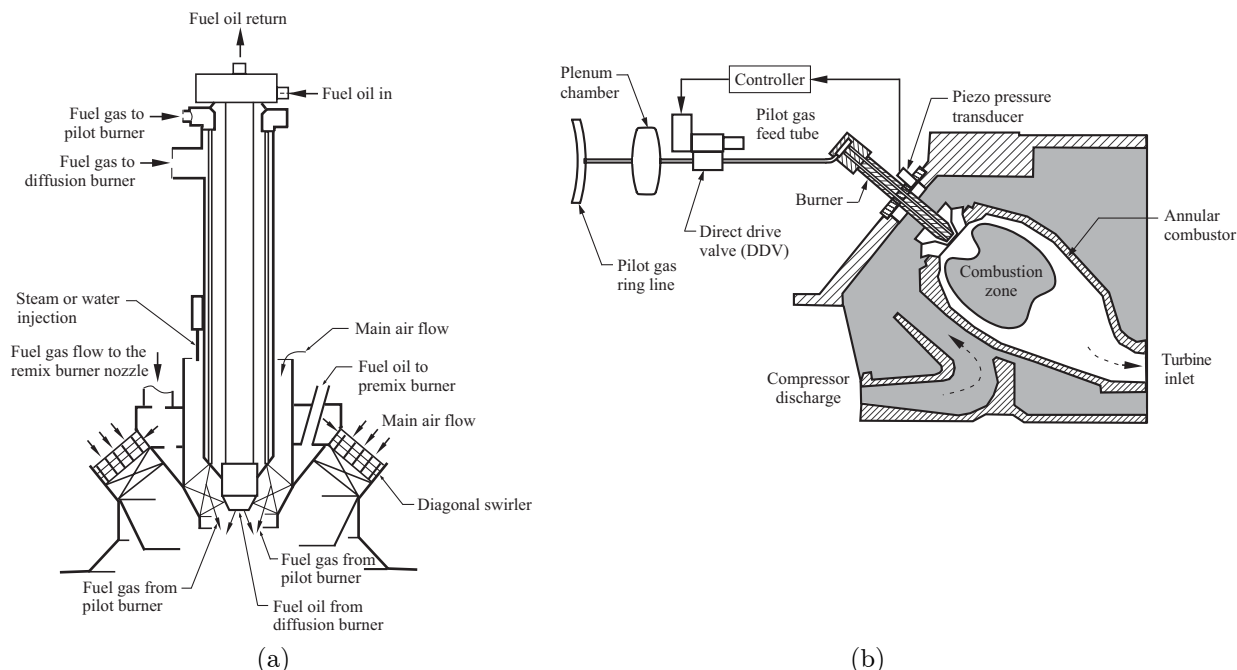


FIGURE 9.28. Simplified sketches (a) of the Siemens Hybrid Burner; (b) installation of the controller in the supply for the pilot burner (adapted from Berenbrink and Hoffmann 2000 and Hermann and Hoffmann 2005).

Much more information is contained in the papers cited; three important points should be noted. First, the feedback control systems were used successfully on fourteen commercially operated V94.3A machines, over a period of three years. Two systems accumulated more than 18,000 hours of operation; there were no failures of controls.

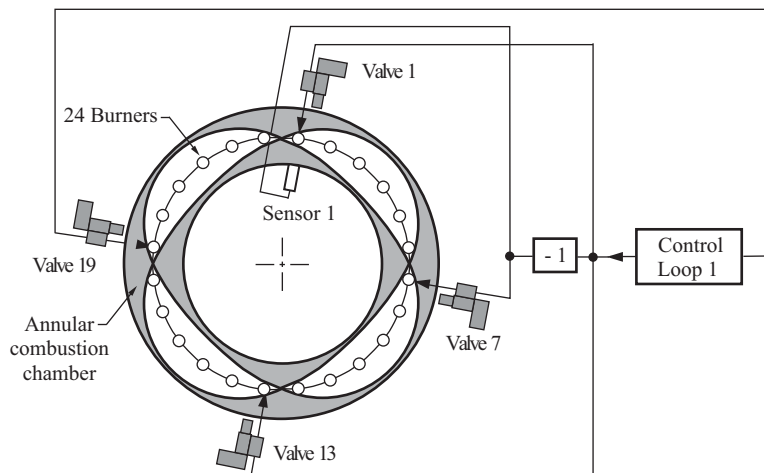


FIGURE 9.29. Minimum number of four actuators, one sensor and one controller to control a standing second azimuthal mode (Hermann and Hoffmann 2005).

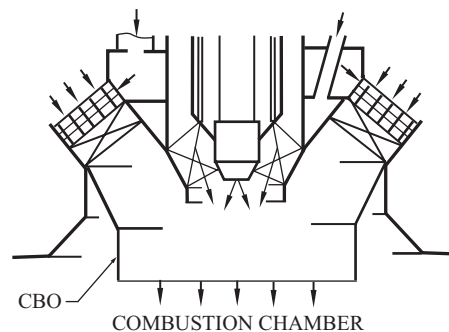


FIGURE 9.30. Addition of the cylindrical burner outlet (CBO) to the Siemens Hybrid Burner (Berenbrink and Hoffmann 2000).

Second, two changes in the geometry of the combustor allowed Siemens to cease using the feedback control systems (Berenbrink and Hoffmann 2000). A cylindrical extension (cylindrical burner outlet, CBO) was added to the combustor, as sketched in Figure 9.30. This change of geometry modified the flow field so as to change the “phase/time lag of the heat release response to pressure fluctuations” (Berenbrink and Hoffmann). In this case, “the length of the cylinder was chosen to increase the time lag from the injection port to the flame front by approximately a quarter of an acoustic period.” The clear azimuthal symmetry of the original combustor was also broken by misaligning the centerlines of a few of the burner nozzles. Berenbrink and Hoffmann offer the useful observation that “This clearly shows the benefit of circumferential asymmetries for the suppression of combustion oscillations in multiburner arrangements.” They evidently do not have longitudinal modes in mind.

Finally, no analysis or quantitative theory accompanied the last modifications of the hardware. The final form of the burners (Figure 9.30), and the modified orientation of their center-lines, rested on further reasoning supported partly by good intuition, but likely required trial and error interactions with testing. Interpretation with a time lag is helpful, but should not be mistaken for a theory and the over-simplification may be misleading. The idea that intentionally misaligning the burner destroyed azimuthal symmetry is surely correct. Working out the details requires elaborate three-dimensional calculations accessible, in some

approximation, to currently available resources. It seems that the Siemens practical experience has suggested analysis and computations having potentially important implications both for development of theory and for details of design. Perhaps most importantly, the clear success due partly to three-dimensional behavior should be an indication of the limitations of, for example, heavy reliance on single-nozzle tests as a sole guide to combustor development.

9.5. Briefly on Progress in Practical Feedback Control of Combustor Dynamics

Discussions in the preceding four sections have summarized the first works on feedback control of combustor dynamics (Sections 9.1 and 9.2); and have described a practical case demonstrating the possibility for actual realization (Section 9.4). Beginning in the early 1990s, literature dealing with the subject grew rapidly, although, as we have already noted, interest and research efforts have slowed considerably in the recent past. Space and time limitations here do not permit including details of developments beyond those covered to this point. We must be satisfied with only a few remarks. The material covered so far should provide a reasonable introduction and basis for appreciating subsequent works.

Almost all of the research related to feedback control of combustors has been motivated by possible applications to gas turbine combustors, and within that domain combustion instabilities have been the main concern. The report of an AGARD Workshop prepared by Schadow *et al.* (1997) is an excellent overall summary of the state of the field at that time. It provides the best general assessment of the outstanding problems in 1996, as understood by those interested mainly in applications to propulsion systems. Combustion instabilities in augmentors and gas turbines were understandably the main object of attention, but other reasons for pursuing the subject—e.g., controlling emissions and blow-out limits—were discussed.

At about the same time, in the mid- to late-1990s, the Department of Energy (DoE), as part of its Advanced Gas Turbine Systems Research (AGTSR) program, included feedback control of combustion dynamics¹² of gas turbines primarily for generating electric power. More recently, the US Department of Defense and NASA have, at least in principle, included feedback control of combustion dynamics in long-range programs for advances in gas turbines to be used for propulsion. Our concern in this book lies with matters at a lower level, encompassing in a general way the research that must be accomplished before the wonders of automatic control of combustors will be accomplished satisfactorily in all respects.

The recent volume, *Combustion Instabilities in Gas Turbine Engines: Operational Experience, Fundamental Mechanisms and Modeling*, edited by Liewen and Yang (2005), is a useful collection of lengthy papers summarizing several important aspects of the field, from basic behavior to experiences with combustion dynamics in installed commercial gas turbines. Zinn (2005) has offered a good (though understandably slanted towards Georgia Tech accomplishments) introduction and review of control applied to combustor dynamics, including also considerations of control applied to lean blow-out (LBO) and pattern factors.

In fact, the greater part of published works are identified with a relatively small number of organizations in Europe and the U.S. Research has tended to be strongly biased by the (virtually) immediate needs for practical results. Unfortunately, therefore, possible fundamental developments have often not been produced. Practically all of the research has been experimental, for the most part serving to demonstrate the success (complete or partial) of proposed methods.

While it is true that the essential elements of all activities devoted to control of combustion systems are captured by the general block diagram in Figure 9.3, the details, emphasis, and points of view may differ greatly as specific applications are worked out. At one extreme is the sanguine view that the system to be

¹²The title of the subject has sometimes been shortened to ACC, active control of combustion; or AIC, active instability control; or ACS, active control systems, all of which imply inclusion of open-loop as well as closed-loop control.

controlled requires minimal characterization and may successfully be treated as a ‘black box.’ The process of control consists then in determining—i.e., measuring with sensors—the time-varying status of the system; processing that information with a controller, in the feedback path, Figure 9.3; and using the results to cause operation of actuators which, if effective, will alter favorably an unwanted dynamical state of the system.

Even the most devoted followers of the ‘black box’ view of control recognize that at least a certain minimal understanding of how the system works is necessary. For example, the choice and operation of actuators, such as those shown in Figures 9.24, 9.26, and 9.28, clearly rests on some understanding of the connection between operation of the mechanical device and the response of the combustion processes. Moreover, deeper understanding of certain internal processes in this case allowed the feedback control system to be discarded and replaced by permanent passive modification of the system, Figure 9.30 (Berenbrink and Hoffman 2000).

The program of research on feedback control at Georgia Tech advanced significantly in the late 90s with development of a rapidly acting ‘real-time observer’ (Neumeier and Zinn, 1994, 1998); Neumeier, Markopoulos and Zinn 1997) and a responsive actuator to operating on the fuel supply (Neumeier, Nabi, Arbel, Vatzberger and Zinn 1997). Viewed broadly, the Georgia Tech approach is approximately the same as that taken by Siemens. However, perhaps because they were controlling instabilities in a lower frequency range, Hermann and co-workers do not make a special point of their ‘observer’ or ‘estimator.’ The Georgia Tech device has operated successfully for extended periods of time and under conditions when the waveforms of the unstable motion has not been so simple.

A significant difference in practical application is Siemens’ use of a MIMO (multi-input-multi-output) system. Because of the attention they gave to the three-dimensional character of the instability, that feature in a certain sense led to the eventual elimination of dynamical control, supplanted by successful use of passive control (Figure 9.30). The problem was somewhat simpler in this case as the instability contained only two well-defined frequencies.

Perhaps the most extensive industrial program concerned with instabilities has been that led by Mongia at General Electric. Mongia *et al.* 2003, 2005 have given the most recent summaries of the work which has progressed over more than a decade (e.g., see Joshi *et al.* 1994, 1995 for remarks on earlier work). The work at General Electric has produced a large number of research reports, many of which are included here in the list of references. To achieve the required low emissions levels, GE has followed the common strategy based on lean premixed combustion which, in the case of liquid fuels, is often identified as ‘lean prevaporized premixed’ (LPP) combustion. It is the presence of the lean combustion, as explained in Section 2.6, that tends to lead to problems with combustion instabilities—and motivated, for example, the recent collection edited by Lieuwen and Yang (2005).

Because the characteristics and geometries of the combustors are not readily available, only qualitative observations can be offered here, based on incomplete information. The recent articles by Mongia *et al.* (2003, 2005) summarize well the history and current status of the GE ‘land and marine’ (LM) series of engines, the LM6000, LM2500, and LM1200. Instabilities have been treated largely by passive measures, including installation of ‘damper tubes;’ scheduled (both spatially and temporally) operation of the fuel nozzles; and small adjustments to the distribution of injected fuel. Apparently ‘active control’ is integrated in the control system with ‘ABAL’ (acoustics and blowout avoidance logic). All measures are evidently standard on all engines. Much less information is currently available for flight qualified machines.

A contrasting approach to reducing emissions is based on combustor design called generically ‘rich-quench-lean’ (RQL). The idea is not recent, dating at least to the 1970s. Fuel-rich burning takes place near the dome of the combustor, followed by a region of rapid quenching by injected air, leading then to further combustion under lean conditions. Sabnis (2005) has described the use of RQL by Pratt and Whitney in the TALON (technology for advanced low NO_x) series of combustors. Mongia (2004) has presented some

charts comparing several contemporary combustors, including the TALON II. At this time (June 2006) the performance and emissions characteristics of the two types of combustors are similar. It seems that projections by the manufacturers also do not differ greatly.

In his recent presentation, Sabinis (2005) has given an informative introduction to the basis for the success of the Pratt and Whitney TALON series of combustors. Consistent with earlier comments regarding RQL combustors, passive control devices are not required, and Sabinis makes no mention of special demands placed on the control system by combustion dynamics. The cost of these savings relative to a lean premixed system is learning how to use, in a rather detailed fashion, the chemical and mixing dynamics of the system. That process requires, at minimum, careful tailoring of the spatial distribution of the injected fuel, and axial history of flow velocity.

A particularly important aspect of that tailoring is the severe restriction on generation of unburnt hydrocarbons and soot, generally regarded as a virtually unavoidable consequence of rich combustion. In the TALON design, smoke formed in the region of rich combustion is consumed downstream as combustion continues under lean conditions. As a result, the Pratt and Whitney combustor design meets current requirements of reduced emissions and is being developed to satisfy future restrictions.

Most simply put, the two types of combustor design may be characterized qualitatively as 1) lean premixed, or rapidly mixed, combustion tending to be unstable in some sense, the possible presence of combustion instabilities being a major problem in practical machines; 2) initially (i.e., at the front end) fuel rich combustion followed by rapid quenching and mixing leading to lean combustion which produces acceptably low levels of smoke and gaseous pollutants (NO_x , CO, UHC). In return for the much reduced tendency for instabilities, the RQL combustor presents particular problems of design in the flow system in order to realize the favorable consequences of mixing and chemical dynamics. A reasonable question is: Why are there obvious difficulties in LPP combustors with combustion instabilities which seem practically absent in RQL combustors?

There seems to be no generally recognized answers to the question, despite many discussions of possible mechanisms of instabilities. For example, more than fifty years ago, fluctuations of the fuel/oxidizer ratio were recognized as a source of disturbances in a solid propellant rocket. If one assumes that a change in fuel/oxidizer (or fuel/air, f/a, in the present context) translates to a change in reaction rate and hence rate of heat release, this becomes practically a generic cause of instabilities and difficult to accept as a distinction between LPP and RQL designs. To show a distinction, one would probably need to show that $\delta(f/a) \neq 0$ produces consequences more significant as f/a tends to zero in a LPP combustor.

Perhaps one should explicitly look rather to the reason(s) for loss of stability in an LPP system. As the lean limit of combustion is approached, stability of the combustion field in the upstream (inlet) region tends to vanish. That is, the processes anchoring the flame zone to the inlet region of the combustor—i.e. the fuel nozzles—become weaker. Hence the ‘base(s)’ of the flame(s) becomes increasingly sensitive to disturbances, eventually entering a condition allowing oscillatory motion coupled to the main flow in the combustor. The RQL system will not undergo such a transition because the anchoring region of the combustion zone is always operating under fuel-rich conditions.

The bulk of published works on feedback and open-loop control of combustors has been at the research level. Since the field began in the mid-1980s, there have been notable shifts of emphasis. Early positive results justified the optimistic view of long-term possibilities. Beginning in the early 1990s some results and methods known from the analysis of systems were introduced with works at the General Electric Research Laboratory (Gulati and Mani 1992; Goodman and Haupt 1992); Caltech (Tierno and Doyle 1992) and École Centrale (Billoud *et al.* 1992). The last work was the first on use of adaptive control which has not generated wide interest. The latest works seem to be the thesis by Evesque (2000) and immediate developments (Evesque

et al. 2003, 2004). Mettenleiter (2000) has carried out the most thorough examination of application of adaptive control to solid propellant rockets (Mettenleiter and Candel 2000, Mettenleiter *et al.* 2000). Those works were evidently motivated by the oscillations in the Ariane 5 motor (Sections 2.2.9 and 6.15) but have not led to practical application.

Beginning in the mid-1990s (Annaswamy and Ghoniem 1995) a group at MIT initiated a research program based on the modal decomposition of the acoustic field developed here (Chapters Three and Four). They assume longitudinal oscillations and develop a flame model (Fleifil *et al.* 1996) extending earlier works explained for example, by Williams (1985). With that model of a combustor, the MIT group has carried out a number of works drawing on experiences with control theory developed for applications in electrical engineering.

Research at the United Technologies Research Center has gone far to join the fields of control and combustion; and to pursue possible applications, taking advantage of their connections to Pratt and Whitney. An example is the recent article by Cohen and Banaszuk (2005). The work is one example of several from UTRC involving use of control theory to interpret results of combustion tests, always with a view to improving the behavior of actual combustors.

Since their initial works on active control referenced above, the group at Georgia Tech has supported probably the largest university research effort in the field. The program seems to be directed eventually to practical applications based on stationary gas turbines (Zinn 2005), but for the most part is devoted to applied research.

Space and time do not allow proper coverage of results accomplished to date. The general problem of joining the fields of combustion and control at both the research and practical levels remains highly attractive. The boundaries of both theoretical and experimental progress seem still to be far away.

CHAPTER 10

References

Some entries in this list were used as general background in preparation of the text but are not explicitly cited. This collection therefore serves partly as a compilation of relevant literature without promise of completeness.

Aaron, K.M. (1985) "Edgetones and Acoustic Resonances in a Duct," Ph.D. Thesis, Aeronautics, California Institute of Technology.

Aaron, K.M. and Culick, F.E.C. (1985) "Coupled Vortex Shedding and Acoustic Resonances in a Duct," *22nd JANNAF Combustion Meeting*.

Abouseif, G.E., Keklak, J.A. and Toong, T.Y. (1984) "Ramjet Rumble: The Low-Frequency Instability Mechanism in Coaxial Dump Combustors," *Comb. Sci. and Tech.*, Vol. 36, pp. 83–108.

Acker, T.L. and Mitchell, C.E. (1994) "Combustion Zone—Acoustic Cavity Interactions in Rocket Combustors," *J. Prop. and Power*, Vol. 10, No. 2, pp. 235–243.

AGARD (1958) *Combustion and Propulsion*, Third AGARD Colloquium, Pergamon Press, London.

Agarkov, A.F., Denisov, K.P., Dranovsky, M.L., Zavorokhin, I.A., Ivanov, V.N., Pikalov, V.P. and Shibanov, A.A. (1993) "Injector Flame Stabilization Effects on Combustion Instability," *1st International Symposium on Liquid Rocket Combustion Instabilities*, Pennsylvania State University, AIAA Progress Series, Vol. 169.

Akiba, R. and Tanno, M. (1959) "Low Frequency Instability in Solid Propellant Rocket Motors," *Proceedings of the 1st Symposium (International) on Rockets and Astronautics*, Tokyo, pp. 74–82.

Altman, D., Carter, J.M., Penner, S.S. and Summerfield, M. (1960) *Liquid Propellant Rockets*, Princeton University Press, Princeton, NJ.

Altseimer, J.H. (1952) "Photographic Techniques Applied to Combustion Studies — Two Dimensional Transparent Thrust Chamber," *ARS J.*, Vol. 22, No. 1, March–April, pp. 86–91.

American Astronautical Society (1993) *History of Rocketry and Astronautics*, AAS History Series, Vol. 7–14 (IAA History Symposia, Vol 1–8).

Ananthkrishnan, N. and Culick, F.E.C. (2004) "Dynamics of Nonlinear Acoustic Waves in Combustion Chambers: Multimodal Instability Phenomena," *Proceedings of the Tenth Asian Congress of Fluid Mechanics*, Peradeniya, Sri Lanka.

REFERENCES

- Ananthkrishnan, N., Deo, S. and Culick, F.E.C. (2005) "Reduced-Order Modeling and Dynamics of Nonlinear Acoustic Waves in a Combustion Chamber," *Comb. Sci. and Tech.*, Vol. 177, No. 2, pp. 221-248.
- Ananthkrishnan, N., Sudershan, S., Sudhakar, K. and Verma, A. (2000) "Large Amplitude Limit Cycles in Resonantly Coupled Oscillators," *J. Sound and Vib.*, Vol. 231, No. 5, pp. 1377-1382.
- Ananthkrishnan, N., Sudhakar, K., Sudershan, S. and Agarwal, A. (1998) "Application of Secondary Bifurcations to Large Amplitude Limit Cycles in Mechanical Systems," *J. Sound and Vib.*, Vol. 215, No. 1, pp. 183-188.
- Anderson, F.A., Strehlow, R.A. and Strand, L.D. (1963) "Low Pressure Rocket Extinction," *AIAA J.*, Vol. 1, No. 11, pp. 2669-2671.
- Anderson, J.M. (1971) "Structural Damping of Acoustic Oscillations in Solid Propellant Rocket Motors," *CPIA No. 220*, Vol. 1, pp. 321-343.
- Anderson, T.J., Sowa, W.A. and Morford, S.A. (1998) "Dynamics Flame Structure in a Low NO_x Premix Combustor," *ASME Paper 98-GT-568*.
- Andreev, N.N. (1954) "Concerning Certain Second-Order Quantities in Acoustics," *J. Physics (USSR)*, Vol. 2, pp. 305-313.
- Andrepon, W.C. and Felix, R.M. (1994) "The History of Large Solid Rocket Motor Development in the United States," *30th AIAA/ASME/SAE/ASEE Joint Propulsion Conference*, Paper AIAA-94-3057.
- Andrepon, W.C. and Schoner, R.J. (1972) "The T-Burner Test Method for Determining the Combustion Response of Solid Propellants," *AIAA/SAE 8th Joint Propulsion Specialist Conference*, AIAA-72-1053.
- Andrepon, W.C. and Siuru, Jr., W.D. (1975) "Prediction of Instability in Solid Rocket Motors—A Status Report," *11th AIAA/ASME/SAE Joint Propulsion Conference*, AIAA-75-1198.
- Andronov, A.A. and Khaikin, S.E. (1949) *Theory of Oscillators*, Princeton University Press, Princeton, N.J.
- Andronov, A.A., Vitt, A.A. and Khaikin, S.E. (1987) *Theory of Oscillators*, Dover Publications, first published in 1966, Pergamon Press.
- Angelus, T.A. (1960) "Unstable Burning Phenomenon in Double-Base Propellants," *Progress in Astronautics and Rocketry*, Academic Press, Inc., NY, pp. 527-559.
- Anil Kumar, K.R. and Lakshmisha, K.N. (2000) "Nonlinear Intrinsic Instability of Solid Propellant Combustion Including Gas-Phase Thermal Inertia," *Comb. Sci. and Tech.*, Vol. 158, pp. 135-166.
- Anil Kumar, K.R. and Lakshmisha, K.N. (2002) "Dynamic Combustion of Solid Propellants: Effects of Unsteady Condensed Phase Degradation Layer," *J. Prop. and Power*, Vol. 15, No. 2, pp. 312-321.
- Ankarsward, B. (1972) "The Missile Liquid Rocket Propulsion Unit VR35 and Some of Its Development Problems," *AIAA/SAE 8th Joint Propulsion Specialist Conference*, AIAA-72-1102.

- Anonymous, (1978) *Pocket Ramjet Reader*, United Technologies Corporation, Sunnyvale, CA.
- Ansoff, H.I. (1951) "Stability of Flow in a Rocket Motor," *J. Appl. Mech.*, Vol. 73, pp. 114–116.
- Anthoine, J. (2000) "Experimental and Numerical Study of Aeroacoustic Phenomena in Large Solid Propellant Boosters," von Karman Institute for Fluid Dynamics, Thesis for the degree of Docteur en Sciences Appliquées, Bruxelles, Belgium.
- Aoki, I. and Kubota, N. (1994) "History of Solid Propellant Development in Japan," *30th AIAA/ASME/SAE/ASEE Joint Propulsion Conference*, AIAA-94-3059.
- Archer, D.H. and Sattler, S. (1998) "Premixed Fuel-Air Flame Transfer Functions: Dynamic Response of Flame Surface and Burning Rate to Flow, Flame Root and Burning Velocity Fluctuations," (prepared paper, unpublished).
- Ar'kov, O.F., Voitsekhovskii, B.V., Mitrofanov, V.V. and Topchiyan, M.E. (1970) "On the Spinning-Detonation-Like Properties of High Frequency Tangential Oscillations in Combustion Chambers of Liquid Fuel Rocket Engines," *J. App. Mech. and Tech. Phys.*, V. 11, pp. 159–161.
- Artamov, K.I. (1963) "Stability of Liquid Fuel Rocket Engine Operation," *AIAA J.*, Vol. 1, No. 1, pp. 263–266 (translated from *Isvestia Akademii Nauk*).
- Artamanov, K.I. (1963) "Stability of Liquid Fuel Rocket Engine Operation," *AIAA J.*, Vol. 1, No. 1, pp. 263–266.
- Avalon, G. Ugurtas, B., Grisch, F. and Bresson, A. (2000) "Numerical Computations and Visualization Tests of the Flow Inside a Cold Gas Simulation with Characterization of a Parietal Vortex Shedding," *36th AIAA/ASME/SAE/ASEE Joint Propulsion Conference*, AIAA-2000-3387.
- Avalon, G. Casalis, G. and Griffond, J. (1998) "Flow Instabilities and Acoustic Resonance of Channels with Wall Injection," *34th AIAA/ASME/SAE/ASEE Joint Propulsion Conference*, AIAA-98-3218.
- Awad, E. (1983) "Nonlinear Acoustic Instabilities in Combustion Chambers," Ph.D. Thesis, Mechanical Engineering, California Institute of Technology.
- Awad, E. and Culick, F.E.C. (1984) "Influence of the Phase Shifts on Triggering of Pressure Oscillations in Combustion Chambers," *19th AIAA/ASME/SAE/ASEE Joint Propulsion Meeting*.
- Awad, E. and Culick, F.E.C. (1986) "On the Existence and Stability of Limit Cycles for Longitudinal Acoustic Modes in a Combustion Chamber," *Comb. Sci. and Tech.*, Vol. 46, pp. 195–222.
- Baade, P.K. (1978) "Design Criteria and Models for Preventing Combustion Oscillations," *Proc. ASHRAE Symp. on Combustion-Driven Oscillations*, Atlanta, GA.
- Bachelor, G.K. (1967) *An Introduction to Fluid Dynamics*, Cambridge University Press.

REFERENCES

- Baer, M.R. and Mitchell, C.E. (1977) "Theoretical Evaluation of Rigid Baffles in Suppression of Combustion Instability," *AIAA J.*, Vol. 15, No. 2, pp. 212–217.
- Baer, M.R., Mitchell, C.E. and Espander, W.R. (1974) "Stability of Partially Lined Combustors with Distributed Combustion," *AIAA J.*, Vol. 12, No. 4, pp. 475–480.
- Bailey, J.J. (1957) "A Type of Flame-Excited Oscillation in a Tube," *J. Appl. Mech.*, Vol. 24, pp. 333–339.
- Bairamov, F.D. (1975) "Technical Stability of Systems with Distributed and Lumped Parameters," *Soviet Aeronautics*, V. 18, pp. 13–17.
- Bairanov, F.D. (1978) "On Stability of Operation of Liquid Rocket Engine (LRE) with Turbopump Assembly (TPA)," *Soviet Aeronautics*, Vol. 21, pp. 10–15.
- Balas, M.J. (1978) "Feedback Control of Flexible Systems," *IEEE Transactions on Automatic Control*, Vol. AC-23, No. 4, pp. 673–679.
- Balas, M.J. (1982) "Trends in Large Space Structure : Fondest Hopes, Wildest Dreams," *IEEE Transactions on Automatic Control*, Vol. AC-27, No. 3, pp. 522–535.
- Barrére, M. (1976) "Analysis of Rocket Engine Transient Regimes," *XXVII Congress, International Astronautical Federation*, Paper IAF-76-160.
- Barrére, M. and Bernard, J.J. (1956) "Influences of the Injector Pressure Drop on Low Frequency Instability in Liquid Propellant Rockets," *Sixth (International) Symposium on Combustion*, Reinhold Publishing Corp., N.Y.
- Barrére, M. and Bernard, J.J. (1962) "Combustion Instability of Solid Propellant with Time Delay Distribution," *Ninth (International) Symposium on Combustion*, William and Wilkins, pp. 886–894.
- Barrére, M., Nadaud, L. and Lhuillier, J.N. (1974) "Survey of ONERA and SNPE Work on Combustion Instability in Solid Propellant Rockets," *J. Spacecraft and Rockets*, Vol. 11, pp. 33–40.
- Barrére, M. and Williams, F.A. (1968) "Comparison of Combustion Instabilities Found in Various Types of Combustion Chambers," *Twelfth (International) Symposium on Combustion*, The Combustion Institute.
- Barron, J.T., Van Moorhem, W.K. and Majdalani, J. (2000) "A Novel Investigation of the Oscillatory Field Over a Transpiring Surface," *J. Sound and Vib.*, Vol. 235, No. 2, pp. 281–297.
- Bastress, E.K., Harris, G.H. and Miller, I. (1967) *Statistical Derivation of Design Criteria for Liquid Rocket Combustion Instability*, NASA CR-72370.
- Baum, J.D. (1980) "Experimental Determination of the Admittances of Solid Propellants by the Admittance Tube Technique," Ph.D. Thesis, School of Aerospace Engineering, Georgia Institute of Technology.
- Baum, J.D. (1988) "Investigation of Flow Turning Phenomenon: Effect of Upstream and Downstream Propagation," *26th AIAA Aerospace Sciences Meeting*, AIAA-88-0544.

- Baum, J.D., Daniel, B.R. and Zinn, B.T. (1981) "Determination of Solid Propellant Admittance by the Impedance Tube Method," *AIAA J.*, Vol. 19, No. 2, pp. 214–220.
- Baum, J.D. and Levine, J.N. (1982) "Numerical Techniques for Solving Nonlinear Instability Problems in Solid Rocket Motors," *AIAA J.*, Vol. 20, No. 7, pp. 955–961.
- Baum, J.D. and Levine, J.N. (1986) "Modeling of Nonlinear Longitudinal Instability in Solid Rocket Motors," *Acta Astronautica*, Vol. 13, Nos. 6–7, pp. 339–348.
- Baum, J.D. and Levine, J.N. (1987) "Numerical Investigation of Acoustic Refraction," *AIAA J.*, Vol. 15, No. 12, pp. 1577–1586.
- Baum, J.D., Levine, J.N., Chew, J.S.B. and Lovine, R.L. (1984) "Pulsed Instability in Rocket Motors: A Comparison Between Predictions and Experiments," *22nd AIAA Aerospace Sciences Meeting*, AIAA-84-0290.
- Baum, J.D., Levine, J.N. and Lovine, R.L. (1984) "Pulse-Triggered Instability in Solid Rocket Motors," *AIAA J.*, Vol. 22, No. 10, pp. 1413–1419.
- Baum, J.D., Levine, J.N. and Lovine, R.L. (1988) "Pulsed Instability in Rocket Motors: A Comparison Between Predictions and Experiments," *J. Prop. and Power*, Vol. 4, No. 4, pp. 308–316.
- Baum, J.D., Lovine, R.L. and Levine, J.N. (1983) "Pulsing Techniques for Solid-Propellant Rocket Motors: Modeling and Cold-Flow Testing," *Journal of Spacecraft and Rockets*, Vol. 20, No. 2, pp. 150–157.
- Bazarov, V.G. (1979) *Fluid Injector Dynamics*, Mashinostroenie Publishing, Moscow, Russia.
- Bazarov, V.G. (1995) "Dynamics of Liquid Rocket Injectors," *Proceedings of the 2nd International Symposium on Liquid Rocket Propulsion*, ONERA, Châtillon, France.
- Bazarov, V.G. (1998) "Nonlinear Interactions in Liquid Rocket Engine Injectors," *34th AIAA/ASME/SAE/ASEE Joint Propulsion Conference*, Paper AIAA-98-4039.
- Bazarov, V.G. (2000) "Peculiarities of Liquid Atomization by Means of Porous Swirl Injector," *8th Int. Conf. on Liq. Atom. and Spray Systems*.
- Bazarov, V.G. and Yang, V. (1998) "Liquid Rocket Engine Injector Dynamics," *J. Prop. and Power*, Vol. 14, No. 5, pp. 797–806.
- Bazarov, V., Yang, V. and Puri, P. (2004) "Design and Dynamics of Jet and Swirl Injectors," Chapter 2, *Liquid Rocket Thrust Chambers: Aspects of Modeling, Analysis, and Design*, AIAA Progress in Astronautics and Aeronautics, Vol. 200, pp. 19–103.
- Beck, W.H. and Jolley, W.H. (1986) "Harmonic Analysis of Piston and Pyrotechnic Pulsers for T-Burners," *J. Prop. and Power*, Vol. 4, No. 3, pp. 283–285.
- Becker, R. and Günther, R. (1970) "The Transfer Function of Premixed Turbulent Jet Flames," *Thirteenth (International) Symposium on Combustion, Proc. of the Comb. Inst.*, Vol. 13, pp. 517–526.

REFERENCES

- Beckstead, M.W. (1967) "Low Frequency Instability: A Comparison of Theory and Experiment," Paper 67-13, *The Combustion Institute*.
- Beckstead, M.W. (1980) "Model for Double-Base Combustion," *AIAA J.*, Vol. 18, No. 8, pp. 980-985.
- Beckstead, M.W. (1987)a "Nonlinear Mechanisms of Solid Propellant Combustion Instability," *24th JANNAF Combustion Meeting*, CPIA No. 476, Vol. I, pp. 27-40.
- Beckstead, M.W. (1987)b "Evidence for Distributed Combustion in Solid Propellants," *24th JANNAF Combustion Meeting*, CPIA No. 476, Vol. I, pp. 1-12.
- Beckstead, M.W. (1991) "A Review of Soviet Combustion and Combustion Instability Work on Solid Propellants," *28th JANNAF Combustion Meeting*.
- Beckstead, M.W. (2000) "Unsteady Combustion," *36th AIAA/ASME/SAE/ASEE Joint Propulsion Conference*, AIAA-2000-3176.
- Beckstead, M.W. and Boggs, T.L. (1967) "The Effect of Oxidizer Particle Size on Non-Acoustic Instability," *Fourth ICRPG Combustion Conference*, Stanford Research Institute.
- Beckstead, M.W., Braithwaite, P.C. and Gordon, D.L. (1985) "Measurements of Distributed Combustion," *66th AGARD Specialists' Meeting of the Propulsion and Energetics Panel*, AGARD CP 391.
- Beckstead, M.W. and Brooks, K.P. (1990) "A Model for Distributed Combustion in Solid Propellants," *27th JANNAF Combustion Meeting*, CPIA No. 557, Vol. II, pp. 237-258.
- Beckstead, M.W. and Butcher, A.G. (1974) "The Velocity-Coupled T-Burner," *12th AIAA Aerospace Sciences Meeting*, AIAA-74-200.
- Beckstead, M.W. and Culick, F.E.C. (1971) "A Comparison of Analysis and Experiment for Solid Propellant Combustion Instability," *AIAA J.*, Vol. 9, No. 1, pp. 147-154.
- Beckstead, M.W., Derr, R.L. and Price, C.F. (1972) "A Model of Composite Solid Propellant Combustion Based on Multiple Flames," *AIAA J.*, Vol. 8, pp. 2200-2207.
- Beckstead, M.W. and Erikson, W.W. (1996) "Solid Monopropellant Oscillatory Combustion Instabilities," *Proceedings of the 2nd International Conference on Combustion Conversion and Environmental Problems of Energetic Materials*, St. Petersburg, Russia.
- Beckstead, M.W. and Jensen, R.C. (1972) "Nonlinear Interpretation of Linear T-Burner Data," *9th JANNAF Combustion Meeting*, CPIA No. 231, Vol. I.
- Beckstead, M.W., Krashin, M., Butcher, A.G. and Pilcher, D.L. (1974) "Acoustic Stability Characterization of the Trident I (C-4) Motors," *11th JANNAF Combustion Meeting*, CPIA No. 261, Vol. I, pp. 535-566.
- Beckstead, M.W., Mathes, H.B., Price, E.W. and Culick, F.E.C. (1968) "Combustion Instability of Solid Propellants," *Twelfth (International) Symposium on Combustion*, pp. 203-211.

- Beckstead, M.W., Meridith, K.V. and Blomshield, F.S. (2000) "Examples of Unsteady Combustion in Non-Metalized Propellants," *36th AIAA/ASME/SAE/ASEE Joint Prop. Conf.*, AIAA-2000-3696.
- Beckstead, M.W. and Price, E.W. (1967) "Nonacoustic Combustion Instability," *AIAA J.*, Vol. 5, No. 11, pp. 1989–1996.
- Beckstead, M.W., Richards, R.S. and Brewster, B.S. (1987) "Distributed Combustion Effects of Particle Damping," *AIAA J.*, Vol. 22, No. 3, pp. 383–387.
- Beckstead, M.W., Ryan, N.W. and Baer, A.D. (1966) "Non-Acoustic Instability of Composite Propellant Combustion," *AIAA J.*, Vol. 4, No. 9, pp. 1622–1628.
- Beddini, R.A. (1998) "The Role of Turbulence Interactions in Combustion Instability," *34th AIAA/ASME/SAE/ASEE Joint Propulsion Conference*, AIAA-98-3703.
- Beddini, R.A. (1986) "Injection-Induced Flows in Porous-Walled Ducts," *AIAA J.*, Vol. 24, No. 11, pp. 1766–1773.
- Beddini, R.A. and Lee, Y. (1998) "The Threshold Condition of Propellant Velocity Response and Its Relation to Local Turbulence Transition," *35th JANNAF Combustion Meeting*.
- Beddini, R.A. and Roberts, T.A. (1992) "Response of Propellant Combustion to a Turbulent Acoustic Boundary Layer," *J. Prop. and Power*, Vol. 8, pp. 290–296.
- Bell, W.A., Daniel, B.R. and Zinn, B.T. (1973) "Experimental and Theoretical Determination of the Admittance of Nozzles Subjected to Axial Instabilities," *J. Sound and Vib.*, Vol. 30, No. 2, pp. 179–190.
- Bell, W.A. and Zinn, B.T. (1973) "The Prediction of Three-Dimensional Liquid-Propellant Rocket Nozzle Admittances," NASA-CR-121129.
- Bell, W.A. (1972) "Experimental Determination of Three-Dimensional Liquid Rocket Nozzle Admittances," Ph.D. Thesis, School of Aerospace Engineering, Georgia Institute of Technology.
- Bellucci, V., Rohr, P., Paschereit, C.O. and Magni, F. (2004) "On the Use of Helmholtz Resonators for Damping Acoustic Pulsations in Industrial Gas Turbines," *ASME J. Eng. Gas Turb. and Power*, Vol. 126, pp. 271–275.
- Beltran, M.P., Wright, R.O. and Breen, B.P. (1966) "Combustion Stability Limits Calculated Utilizing a Nonlinear Model," Dynamic Science Report No. SN-70-F, Final Report in Contract NAS 7-366.
- Bénoit, A., Collin, G. and Mestie, A. (1974) "Etude de la stabilité la combustion dans un foyer à flux giratoire," *La Recherche Aérospatiale*, No. 1 (Janvier–Février), pp. 37–48.
- Bergman, G.H. and Jessen, E.C. (1971) "Evaluation of Conventional Rocket Motor Instrumentation for Analysis of Oscillatory Combustion," *AIAA/SAE 7th Propulsion Joint Specialist Conference*, AIAA-71-755.

REFERENCES

- Berl, W.G., editor (1963) *Scientific Papers, 1960–1963*, Technical Panel on Solid Propellant Instability of Combustion, The Johns Hopkins University Applied Physics Laboratory.
- Berman, A.S. (1953) “Laminar Flow in Channels with Porous Walls,” *J. Appl. Phys.*, Vol. 24, pp. 1232–1235.
- Berman, K. and Cheng, S.H. (1953) “Combustion Studies in Rocket Motors,” *ARS J.*, Vol. 23, No. 2, March–April, pp. 89–96.
- Berman, K. and Logan, S.E. (1952) “Combustion Studies with a Rocket Motor Having a Full-Length Observation Window,” *ARS J.*, Vol. 22, No. 2, pp. 78–85.
- Berman, K. and Scharres, E.H. (1953) “Photographic Techniques in Jet Propulsion Studies,” *ARS J.*, Vol. 23, No. 3, May–June, pp. 170–173.
- Bernier, D., Lacer, F. and Candel, S.M. (2004) “Instability Mechanisms in a Premixed Prevaporized Combustor,” *J. Prop. and Power*, Vol. 20, No. 4, pp. 648–656.
- Betchov, R. (1958) “Nonlinear Oscillations of a Column of Gas,” *Phys. of Fluids*, Vol. 1, No. 3, pp. 205–212.
- Bhatia, R. and Sirignano, W.A. (1991) “One-Dimensional Analysis of Liquid-Fueled Combustion Instability,” *J. Prop. and Power*, Vol. 7, No. 6, pp. 953–961.
- Bird, J.F., McClure, F.T. and Hart, R.W. (1963) “Acoustic Instability in the Transverse Modes of Solid Propellants,” *XIIth International Astronautical Congress Proceedings*, Academic Press, New York, pp. 459–473.
- Bird, J.F., et al., (1960) “Effect of Solid Propellant Compressibility on Combustion Instability,” *J. Chem. Phys.*, Vol. 32, pp. 1423–1429.
- Biron, D., Hébrard, P., Pauzin, S. and Laverdant, A. (1986) “Etude du couplage acoustique – instabilités aérodynamiques sur une maquette de statoréacteur,” *IUTAM Symposium Aero et Hydro-acoustique*, École Centrale de Lyon, 1986, Proceedings edited by Springer-Verlag.
- Biron, D., Hébrard, P., Pauzin, S. and Laverdant, A. (1986) “Couplage acoustique – structures cohérentes: une approche expérimentale et théorique sur une configuration de base,” *7^{eme} Journées d’Etudes sur la Propagation Acoustique (JESPA)*, Lyon.
- Bisio, G. and Rubatto, G. (1999) “Sondhauss and Rijke Oscillations—Thermodynamic Analysis, Possible Applications and Analogies,” *Energy*, Vol. 24, pp. 117–131.
- Blackman, A.W. (1960) “Effect of Nonlinear Losses on the Design of Absorbers for Combustion Instabilities,” *ARS J.*, Vol. 30, No. 11, pp. 1022–1028.
- Blackshear, P.L. (1952) “Driving Standing Waves by Heat Addition,” *Fourth (International) Symposium on Combustion*, pp. 553–566.
- Blackshear, P.L. and Rayle, W.D. (1957) “Oscillations in Combustors,” Chapter VIII, NACA TR 1300.

- Blackshear, P.L., Rayle, W.D. and Tower, L.K. (1953) "Experimental Determination of Gas Motion Accompanying Screeching Combustion in a 6 in. Simulated Afterburner," NACA-RM 53128.
- Blokhintsev, D.I. (1956) "Acoustics of a Nonhomogeneous Moving Medium," NACA TM 1399, translation of *Akustika Neodnorodnoi Dvizhushcheisya Sredy*, Ogiz, Gosudarstvennoe Izdatel'stvo, Tekhniko-Teoreticheskoi Literatury, Moskva (1946), Leningrad.
- Blomshield, F.S. (2001) "Historical Perspective of Combustion Instability in Motors: Case Studies," *37th AIAA/ASME/SAE/ASEE Joint Propulsion Conference*, AIAA-2001-3875.
- Blomshield, F.S. (2000)a "Pulsed Motor Firings," Naval Warfare Center Weapons Division, China Labs, CA, NAWCWPNS TP 8444.
- Blomshield, F.S. (2000)b "Pulsed Motor Firings," Chapter 3.7 of *Solid Propellant Chemistry, Combustion, and Motor Interior Ballistics*, of AIAA *Progress in Astronautics and Aeronautics*, Vol. 185.
- Blomshield, F.S. (2000)c "Summary of Multi-Disciplinary University Research Initiative in Solid Propellant Combustion Instability," *36th AIAA/ASME/SAE/ASEE Joint Propulsion Conference*, AIAA-2000-3172.
- Blomshield, F.S. and Beckstead, M.W. (1999) "Combustion Instability Additive Investigation," *35th AIAA/ASME/SAE/ASEE Joint Propulsion Conference*, AIAA-99-2226.
- Blomshield, F.S. and Beckstead, M.W. (1992) "Nonlinear Characteristics of Solid Propellant Combustion Instability," *29th JANNAF Combustion Meeting*, CPIA No. 593, pp. 197–207.
- Blomshield, F.S., Crump, J.E. Mathes, H.B. and Stalnaker, R.A. (1997) "Stability Testing of Full-Scale Tactical Motors," *J. Prop. and Power*, Vol. 13, No. 3, pp. 349–355.
- Blomshield, F.S., Crump, J.E. Mathes, H.B. and Beckstead, M.W. (1991) "Stability Testing and Pulsing of Full-Scale Tactical Motors," Naval Warfare Center Weapons Division, China Labs, CA, *27th AIAA/ASME/SAE/ASEE Joint Propulsion Conference*, AIAA-91-1954.
- Blomshield, F.S., Mathes, H.B., Crump, J.E., Beiter, C.A. and Beckstead, M.W. (1997) "Nonlinear Stability Testing of Full-Scale Tactical Motors," *J. Prop. and Power*, Vol. 13, No. 3, pp. 356–366.
- Blomshield, F.S. and Mathes, H.B. (1993) "Pressure Oscillations in Post-Challenger Space Shuttle Redesigned Solid Rocket Motors," *J. Prop. and Power*, Vol. 9, No. 2, pp. 219–221.
- Blonbou, R. and Laverdant, A. (2000) "Control of Combustion Instabilities on a Rijke Tube by a Neural Network," RTO AVT Symposium on *Active Control Technology for Enhanced Performance Operational Capabilities of Military Aircraft, Land Vehicles and Sea Vehicles*, Braunschweig, Germany, paper PSP21.
- Bloxsidge, G.J., Dowling, A.P. and Langhorne, P.J. (1988) "Reheat Buzz: An Acoustically Coupled Combustion Instability, Part 2. Theory," *J. of Fluid Mech.*, Vol. 193, pp. 445–473.
- Bodén, J. and Åbom, M. (1995) "Modelling of Fluid Machines as Sources of Sound in Duct and Pipe Systems," *Acta Acustica*, pp. 549–560.

REFERENCES

- Bogar, T.J., Sajben, M. and Krontil, J.C. (1983) "Characteristic Frequencies of Transonic Diffuser Flow Oscillations," *AIAA J.*, Vol. 21, No. 9, pp. 1232–1240.
- Bogar, T.J., Sajben, M. and Krontil, J.C. (1983) "Response of a Supersonic Inlet to Downstream Perturbations," *19th AIAA/SAE/ASME Joint Propulsion Conference*, AIAA-83-2017.
- Bogar, T.J. and Sajben, M. (1986) "Response of Transonic Diffuser Flows to Abrupt Increases of Back Pressure: Wall-Pressure Measurements," *23rd JANNAF Combustion Meeting*.
- Boggs, T.L. and Zinn, B.J. (Eds.) (1978) *Experimental Diagnostics in Combustion of Solids*, of AIAA *Progress in Astronautics and Rocketry*, Vol. 63.
- Bogoliubov, N.N. and Mitropolskii, Y.A. (1961) *Asymptotic Methods in the Theory of Nonlinear Oscillations*, Gordon and Breach, Science Publishers, N.Y.
- Bollay, W. (1951) "Aerodynamic Stability and Automatic Control," *J. Aero. Sci.* Vol. 18, No. 9, pp. 569–640.
- Bonnell, J.M., Marshall, R.L. and Rieche, G.T. (1971) "Combustion Instability in Turbojet and Turbofan Augmentors," *AIAA/SAE 7th Propulsion Joint Specialist Conference*, AIAA-71-698.
- Bourehla, A. and Baillot, F. (1998) "Appearance and Stability of a Laminar Conical Premixed Flame Subjected to an Acoustic Perturbation," *Comb. and Flame*, Vol. 114, No. 3, pp. 303–318.
- Boys, S.F. and Schofield, A. (1942) "Studies Accessory to the Development of Classified Rockets," Woolwich Arsenal, England.
- Boys, S.F. and Schofield, A. (1943) "Investigations of Secondary Peaks," Propulsion Establishment, Report 1943/5, Abesporth, England, UK.
- Bracco, F.V. (1975) "Standing Acoustic Waves in a Confined Non-Uniform Gas," *J. Sound and Vib.*, Vol. 41, No. 3, pp. 301–309.
- Braithwaite, P.C., Beckstead, M.W. and Raun, R.L. (1984) "Measurements of Distributed Combustion," *21st JANNAF Combustion Meeting*, CPIA No. 412, Vol. I, pp. 177–186.
- Brewster, M.Q. (2000) "Solid Propellant Combustion Response: Quasi-Steady (QSHOD) Theory Development and Validation," of AIAA *Progress in Astronautics and Aeronautics*, Vol. 185, Washington, DC, pp. 607–637.
- Brewster, M.Q., Zebrowski, M.A., Schroeder, T.B. and Son, S.F. (1995) "Unsteady Combustion Modeling of Energetic Solids," *31st AIAA/ASME/SAE/ASEE Joint Propulsion Conference*, AIAA-95-2859.
- Brewster, M.Q. and Son, S.F. (1995) "Quasi-Steady Combustion Modeling of Homogeneous Solid Propellants," *Comb. and Flame*, Vol. 103, pp. 11–26.

- Briffa, F.E.J. and Furrey, R.A.E. (1967) "Reduction of Audible Flame Noise by the Application of Ultrasonics," *Nature*, Vol. 214, pp. 75–76.
- Brookes, S.J., Cant, R.S., Dupere, I.D.J. and Dowling, A.P. (2000) "Computational Modeling of Self-Excited Combustion Instabilities," ASME Paper 2000-GT-0104, *ASME J. Eng. Gas Turbines Power*, Vol. 123, pp. 322–326.
- Brooks, K.P. and Beckstead, M.W. (1995) "The Dynamics of Aluminum Combustion," *J. Prop. and Power*, Vol. 11, No. 4, pp. 769–780.
- Brown, G.L. and Roshko, A. (1974) "On Density Effects and Large Structure in Turbulent Mixing Layers," *J. of Fluid Mech.*, Vol. 64, pp. 775–816.
- Brown, R.S. (1995) "Combustion Stability of Interceptor Rocket Motors: A Practical Approach to Managing Instability Problems," CPIA Publication CPTR 95-57.
- Brown, R.S. (1986) "Blowdown Pulser Design Criteria for Solid Propellant Rockets," *J. Prop. and Power*, Vol. 2, No. 2, pp. 110–116.
- Brown, R.S. *et al.* (1983) "Ramjet Combustor Instability Investigation," Final Report for Period 1 October 1981 - 31 March 1983, AFWAL-TR-83-2056, Vol. II.
- Brown, R.S., Blackner, A.M., Willoughby, P.G. and Dunlap, R. (1986) "Coupling Between Acoustic Velocity Oscillations and Solid Propellant Combustion," AIAA-86-0531, and *J. Prop. and Power*, Vol 2, No. 5, pp. 428–437.
- Brown, R.S., Culick, F.E.C. and Zinn, B.T. (1978) "Experimental Methods for Combustion Admittance Measurements," pp. 191–220 of Boggs and Zinn (1978).
- Brown, R.S., Dunlap, R., Young, S.W. and Waugh, R.C. (1981) "Vortex Shedding as a Source of Acoustic Energy in Segmented Solid Rockets," *J. Spacecraft and Rockets*, Vol. 18, No. 4, pp. 312–319.
- Brown, R.S., Dunlap, R., Young, S.W. and Waugh, R.C. (1985) "Periodic Vortex Shedding in Simulated Coaxial Dump Combustors," *J. Prop. and Power*, Vol. 1, pp. 413–415.
- Brown, R.S., Erickson, J.E. and Babcock, W.R. (1974) "Combustion Response Function Measurements by the Rotating Valve Method," *AIAA J.* Vol. 12, No. 11, pp. 1502–1510.
- Brown, R.S. and Muzzy, R.J. (1970) "Linear and Nonlinear Pressure Coupled Combustion Instability of Solid Propellants," *AIAA J.*, Vol. 8, No. 8, pp. 1492–1500.
- Brown, R.S., Muzzy, R.J. and Steinle, M.E. (1967) "Effect of Surface Reactions on Acoustic Response of Solid Propellants," *AIAA J.*, Vol. 5, No. 9, p. 1718.
- Brown, R.S., Waugh, R.C. and Kelly, V.L. (1982) "Rotating Valve for Velocity-Coupled Combustion Response Measurements," *J. Spacecraft*, Vol. 19, No. 5, pp. 437–444.

REFERENCES

- Brownlee, W.G. (1964) "Nonlinear Axial Combustion Instability in Solid Propellant Rocket Motors," *AIAA J.*, Vol. 2, No. 2, pp. 275–284.
- Brownlee, W.G. (1959) "An Experimental Investigation of Unstable Combustion in Solid Propellant Rocket Motors," Ph.D. Thesis, Jet Propulsion Center, Aeronautics, California Institute of Technology.
- Brownlee, W.G. and Kimbell, G.H. (1966) "Shock Propagation in Solid-Propellant Rocket Combustors," *AIAA J.*, Vol. 4, No. 6, pp. 1132–1134.
- Brownlee, W.G. and Marble, F.E. (1960) "An Experimental Investigation of Unstable Combustion in Solid Propellant Rocket Motors," in *Progress in Astronautics and Rocketry: Solid Propellant Rocket Research*, Vol. 1, M. Summerfield, ed., Academic Press, New York, pp. 455–494.
- Buckmaster, J., Jackson, T.L. Massa, L. and Ulrich, M. (2003) "Response of a Burning Heterogeneous Propellant to Small Pressure Disturbances," (to be published).
- Burnley, V.S. (1996) "Nonlinear Combustion Instabilities and Stochastic Sources," Ph.D. Thesis, California Institute of Technology.
- Burnley, V.S. and Culick, F.E.C. (2000)a "Influence of Random Excitations on Acoustic Instabilities in Combustion Chambers," *AIAA J.*, Vol. 38, No. 8, pp. 1403–1410.
- Burnley, V.S. and Culick, F.E.C. (2000)b "Comment on 'Triggering of Longitudinal Instabilities in Rocket Motors: Nonlinear Combustion Response,'" *J. Prop. and Power*, Vol. 16, No. 1, pp. 164–165.
- Burnley, V.S. and Culick, F.E.C. (1997) "Comment on 'Triggering of Longitudinal Combustion Instabilities in Rocket Motors: Nonlinear Combustion Response,'" *J. Prop. and Power*, Vol. 16, No. 1, 164–165; "Reply by the Authors to V.S. Burnley and F.E.C. Culick," J.M. Wicker and V. Yang, *J. Prop. and Power*, Vol. 16, No. 1, pp. 165–166.
- Burnley, V.S. and Culick, F.E.C. (1996) "Some Dynamics of Acoustics Oscillations with Nonlinear Combustion and Noise," Proceedings, Fourth International Conference on Special Topics in Combustion, *Challenges in Propellants and Combustion 100 Years After Nobel*, Stockholm, Sweden.
- Burstein, S.A., Chinitz, W. and Schechter, H.S. (1972) "A Nonlinear Model of Combustion Instability in Liquid Propellant Rocket Engines," *AIAA/SAE 8th Propulsion Joint Specialist Conference*, AIAA-72-1146.
- Byrne, R.W. (1981) "A Note on Longitudinal Pressure Oscillations in Ramjet Combustors," *18th JANNAF Combustion Meeting*.
- Byrne, R.W. (1983) "Longitudinal Pressure Oscillations in Ramjet Combustors," *AIAA/SAE/ASME 19th Joint Propulsion Conference*, Seattle, Washington, AIAA-83-2018.
- Callender, A., Hartree, D.R. and Porter, A. (1938) "Time Lag in a Control System," *Trans. Roy. Soc. London*, Vol. A235, pp. 415–444.

- Campbell, I.C., Bray, K.N.C. and Moss, J.B. (1983) "Combustion Oscillation in a Ducted Premixed Flame," *Inst. Mech. Engineers, Int. Conf. on Comb. in Eng.*, Oxford, pp. 85–94.
- Campos-Delgado, D.V., Scheuermans, B.B.H., Zhou, K.M., Paschereit, C.O., Gallestey, E.A. and Poncet, A. (2003) "Thermoacoustic Instabilities: Modeling and Control," *IEEE Trans. on Cont. Syst. Tech.*, Vol. 11, pp. 429–447.
- Campos-Delgado, D.V., Zhou, K., Allgood, D. and Acharya, S. (2003) "Active Control of Combustion Instabilities Using Model-Based Controllers," *Comb. Sci. and Tech.*, Vol. 175, pp. 27–53.
- Candel, S., Durox, D., Ducruix, S. and Thibault, D. (1998) "Dynamics of Flames Interacting with Pressure Waves," Paper 98-1, Plenary Lecture of the Western States Section of Combustion Institute, UC Berkeley.
- Candel, S., Durox, D. and Schuller, T. (2004) "Flame Interactions as a Source of Noise and Combustion Instabilities," AIAA/CEAS Aeroacoustics Conference, AIAA-2004-2928.
- Cantrell, R.H. and Hart, R.W. (1964) "Interaction Between Sound and Flow in Acoustic Cavities: Mass, Momentum and Energy Considerations," *J. Acoust. Soc. of Amer.*, Vol. 36, No. 4, pp. 697–706.
- Cantrell, R.H., Hart, R.W. and McClure, F.T. (1964) "Linear Acoustic Gains and Losses in Solid Propellant Rocket Motors," *AIAA J.*, Vol. 2, No. 6, pp. 1100–1105.
- Cantrell, R.H., McClure, F.T. and Hart, R.W. (1965) "Effects of Thermal Radiation on the Acoustic Response Function of Solid Propellants," *AIAA J.*, Vol. 3, No. 3, pp. 418–426.
- Capener, E.L., Dickinson, L.A. and Kier, R.J. (1967) "Driving Processes in Finite-Amplitude Axial Mode Instability in Solid Propellant Rockets," *AIAA J.* Vol. 5, No. 6, pp. 938–945.
- Cardiff, E.H., Pinkham, J.D. and Micci, M.M. (1999) "Magnetic Flowmeter Measurement of the Pressure-Coupled Response of a Plateau Solid Propellant," *J. Prop. and Power*, Vol. 15, No. 6, pp. 844–848.
- Cargill, A.M. (1982) "Low Frequency Sound Radiation and Generation Due to the Interaction of Unsteady Flow with a Jet Pipe," *J. Fluid Mech.*, Vol. 121, pp. 59–105.
- Carrier, G.F. (1955) "The Mechanics of the Rijke Tube," *J. App. Mech.*, Vol. XII, No. 4, pp. 383–395.
- Casalis, G., Avalon, G. and Pineau, J.-P. (1998) "Spatial Instability of Planar Channel Flow with Fluid Injection Through Porous Walls," *Phys. Fluids*, Vol. 10, pp. 2558–68.
- Caughey, T.K. (1963) "Equivalent Linearization Techniques," *J. Acoust. Soc. Amer.*, V. 35, No. 11, pp. 1706–1711.
- Cauty, F. (1999) "Solid Propellant Combustion Response Function from Direct Measurement Methods: ON-ERA Experience," *J. Prop. and Power*, Vol. 15, No. 6, pp. 837–843.
- Caveny, L.H., Collins, K.L. and Cheng, S.W. (1981) "Direct Measurement of Acoustic Admittance Using Laser Doppler Velocimetry," *AIAA J.* Vol. 19, No. 7, pp. 913–918.

REFERENCES

- Chamberlain, J. (1983) "Combustion Instability in Turbine Engine Afterburners and Ramjets," ONR/AFOSR Workshop.
- Chapman, S. and Cowling, T.G. (1939) *The Mathematical Theory of Non-Uniform Gases*, Cambridge University Press.
- Chedevergne, F. and Casalis, G. (2005) "Thrust Oscillations in Reduced Scale Solid Rocket Motors Part II: A New Theoretical Approach," *41st AIAA/ASME/SAE/ASEE Joint Propulsion Conference*, AIAA-2005-4000.
- Chen, C.P., Sajben, M. and Kroutil, J.C. (1979) "Shock-Wave Oscillations in a Transonic Diffuser Flow," *AIAA J.*, Vol. 17, No. 10, pp. 1079–1083.
- Cheng, S.-I. (1954)a "High Frequency Combustion Instability in Solid Propellant Rockets," *Jet Propulsion*, Vol. 24, Part I, pp. 27–32; Part II, pp. 102–109.
- Cheng, S.-I. (1954)b "Unconditional Stability of Low Frequency Oscillations in Liquid Propellant Rockets," *Jet Propulsion*, Vol. 24, pp. 310–319.
- Cheng, S.-I. (1959) "Combustion Instability in Solid Rockets Using Propellants with Suspended Metallic Powders," *1st Symposium (International) on Rockets and Astronautics*, Tokyo, pp. 62–70.
- Cheng, S.-I. (1960) "Combustion Instability in Solid Rockets Using Propellants with Reactive Additives," in *ARS Progress in Astronautics and Rocketry: Solid Propellant Rocket Research*, Vol. 1, edited by M. Summerfield, Academic Press, pp. 393–422.
- Cheng, S.-I. (1962) "Unstable Combustion in Solid Propellant Rocket Motors," *Ninth (International) Symposium in Combustion*, Williams and Wilkins, Baltimore, Maryland, pp. 81–90.
- Cherne, J.M. (1967) "Mechanical Design of the Lunar Module Descent Engine," XVIII International Astronautical Congress, IAF.
- Chester, W. (1964) "Resonant Oscillations in Closed Tubes," *J. Fluid Mech.*, Vol. 18, pp. 44–64.
- Chester, W. (1981) "Resonant Oscillations of a Gas in an Open-Ended Tube," *Proc. Roy. Soc. Lond.*, Vol. A337, pp. 449–667.
- Cho, J.H. and Lieuwen, T.C. (2003) "Modeling the Response of Premixed Flames to Mixture Ratio Perturbations," *ASME Turbo Expo 2003*, Paper GT2003-38089.
- Chu, B.-T. (1953) "On the Generation of Pressure Waves at a Plane Flame," *Fourth Int. Symp. on Comb.*, pp. 603–612.
- Chu, B.-T. (1956)a "Energy Transfer to Small Disturbances in a Viscous Compressible Heat Conductive Medium," Department of Aeronautics, Johns Hopkins University, Air Force Office of Scientific Research, Contract AF 18(600)–1121.

- Chu, B.-T. (1956)b "Stability of Systems Containing a Heat Source—The Rayleigh Criterion," NACA RM 56D27.
- Chu, B.-T. (1963) "Analysis of a Self-Sustained Thermally Driven Nonlinear Vibration," *Physics of Fluids*, Vol. 6, No. 11, pp. 1638–1644.
- Chu, B.-T. (1964) "On the Energy Transfer to Small Disturbances in Fluid Flow," (Pt. 2) *Acta Mechanica*, Vol. 1, pp. 215–234.
- Chu, B.-T. and Kovasznay, L.S.G. (1957) "Non-linear Interactions in a Viscous Heat-Conducting Compressible Gas," *J. Fluid Mech.*, Vol. 3, No. 5, pp. 494–512.
- Chu, B.-T. and Ying, S.J. (1963) "Thermally Driven Nonlinear Oscillations in a Pipe with Travelling Shock Waves," *The Physics of Fluids*, Vol. 6, No. 11, pp. 1625–1639.
- Clapp, C.J. (1967) "Full Scale Turbofan Duct Burner Test Program," NASA CR-54637.
- Clark, W.H. (1982)a "Experimental Investigation of Pressure Oscillations in a Side Dump Ramjet Combustor," *J. of Spacecraft and Rockets*, Vol. 19, No. 1, pp. 47–53.
- Clark, W.H. (1982)b "Geometric Scale Effects on a Side Dump Liquid Fuel Ramjet," *19th JANNAF Combustion Meeting*.
- Clark, W.H. and Humphrey, J.W. (1986) "Identification of Longitudinal Acoustic Modes Associated with Pressure Oscillations in Ramjets," *AIAA J. Propulsion*, Vol. 2, No. 3, pp. 199–205.
- Clavin, P. (1985) "Dynamic Behavior of Premixed Flame Fronts in Laminar and Turbulent Flows," *Prog. Energy Comb. Sci.*, Vol. 11, pp. 1–59.
- Clavin, P. (1991) "Sounds and Flames," *NATO-AST Series*, Vol. 276, pp. 223–232.
- Clavin, P., Kim, J.S. and Williams, F.A. (1994) "Turbulence Induced Noise Effects on High-Frequency Combustion Instabilities," *Comb. Sci. and Tech.*, Vol. 96.
- Clavin, P. and Lazmi, D. (1992) "Theoretical Analysis of Oscillatory Burning of Homogeneous Solid Propellant Including Non-Steady Gas Effects," *Comb. Sci. and Tech.*, Vol. 83, pp. 1–32.
- Clavin, P., Pelcé, P. and Longting, He (1990) "One-Dimensional Vibrating Instability of Planar Flames Propagating in Tubes," *J. Fluid Mech.*, Vol. 216, pp. 299–322.
- Clayton, R.M., Rogero, R.S. and Sotter, J.G. (1968) "An Experimental Description of Destructive Liquid Rocket Resonant Combustion," *AIAA J.*, Vol. 6, No. 7, pp. 1252–1259.
- Cline, M.C., Micklow, G.J., Yang, S.L. and Nguyen, N.L. (1992) "Numerical Analysis of the Flow Fields in a RQL Gas Turbine Combustor," *AIAA/SAE/ASME/ASEE 28th Joint Propulsion Conference*, Paper AIAA 92-3308.

REFERENCES

- Coats, C.M. (1996) "Coherent Structures in Combustion," *Prog. in Energy and Comb. Sci.*, Vol. 22, pp. 427–509.
- Coates, R.L., Cohen, N.S. and Harvill, L.P. (1967) "An Interpretation of L* Combustion Instability in Terms of Acoustic Instability Theory," *AIAA J.*, Vol. 5, No. 5, pp. 1097–2004.
- Coates, R.L. and Horton, M.D. (1968) "Design Considerations for Combustion Stability," *ICRPG/AIAA 3rd Solid Propulsion Conference*, AIAA-68-532.
- Coates, R.L., Horton, M.D. and Ryan, N.W. (1964) "T-Burner Method of Determining the Acoustic Admittance of Burning Propellants," *AIAA J.*, Vol. 2, No. 6, pp. 1019–1122.
- Cohen, J.M. and Anderson, T. (1996) "Experimental Investigation of Near-Blowout Instabilities in a Lean Premixed Combustor," AIAA-96-0819.
- Cohen, J.M., Wake, B.E. and Choi, D. (2003) "Investigation of Instabilities in a Lean, Premixed Step Combustor," *J. Prop. and Power*, Vol. 19, No. 1, pp. 81–88.
- Cohen, N.S. and Strand, L. (1985) "Effects of AP Particle Size on Combustion Response to Crossflow," *AIAA J.*, Vol. 23, pp. 776–780.
- Cohen, N.S. and Strand, L.D. (1985) "Combustion Response to Compositional Fluctuations," *AIAA J.*, Vol. 23, No. 5, pp. 760–767.
- Cohen, N.S., Shusser, M., Culick, F.E.C. and Beddini, R.A. (1999) "Combustion Modeling of AP Composite Propellants for Stability Analysis," *36th JANNAF Combustion Meeting*.
- Cohen, N.S., Taylor, D.E., Small, K.R., Epstein, R.H. and Churchill, H.L. (1972) "Design of a Smokeless Solid Rocket Motor Emphasizing Combustion Stability," *CPIA No. 27*, Vol. 2, pp. 205–220.
- Cole, J.D. (1968) *Perturbation Methods in Applied Mathematics* Blaisdell Publishing Company, Waltham, MA.
- Cole, J.D. and Roshko, A. (1954) "Heat Transfer from Wires at Reynolds Numbers in the Oseen Range," *Proc. of the Heat Transfer and Fluid Mech. Institute*, University of California, Berkeley.
- Collyer, A.A. and Ayres, D.J. (1972) "The Generation of Sound in a Rijke Tube Using Two Heating Coils," *J. Phys. D: Appl. Phys.*, Vol. 5, pp. L73–L75.
- Combs, L.P., Oberg, C.L., Coulter, T.A. and Evers, W.H., Jr. (1974) "Liquid Rocket Engine Combustion Stabilization Devices," *NASA SP-8113*.
- Condon, J.A. (1979) "A Model for the Velocity Coupled Response of Composite Propellants," *16th JANNAF Combustion Conference*, Monterey, CA.
- Correa, S.M. (1998) "Power Generation and Aero-Propulsion Gas Turbines: From Combustion Science to Combustion Technology," *27th (International) Symposium on Combustion*, The Combustion Institute, pp.

1793–1807.

Cozzi, F., DeLuca, L.T. and Novozhilov, B.V. (1999) “Linear Stability and Pressure-Driven Response Function of Solid Propellants with Phase Transition,” *J. Prop. and Power*, Vol. 15, No. 6, pp. 806–875.

Cremer, L. (1971) “The Second Annual Fairy Lecture: The Treatment of Fans as Black Boxes,” *J. Sound and Vib.*, Vol. 16, pp. 1–15.

Crocco, L. (1952) “Aspects of Combustion Instability in Liquid Propellant Rockets,” *ARS J.* Part I, Vol. 21, No. 6, pp. 163–178, 1951, Part II, Vol. 22., No. 1, pp. 7–16.

Crocco, L. (1953) “Supercritical Gas Discharge with High Frequency Oscillations,” *Aerotechnica*, Vol. 33, pp. 46–53.

Crocco, L. (1956) “Considerations on the Problem of Scaling Rocket Motors,” *AGARD Selected Combustion Problems*, Vol. 2, Butterworths Scientific Publications, London, pp. 457–468.

Crocco, L. (1958) “Comments on the Zucrow-Osborn Paper on Combustion Oscillations,” *Jet Propulsion*, Vol. 28, No. 12, p. 843.

Crocco, L. (1958) “One-Dimensional Treatment of Steady Gas Dynamics,” Section B of *Fundamentals of Gas Dynamics*, (Ed. H.W. Emmons) Princeton University Press.

Crocco, L. (1964) “Theoretical Studies on Liquid- Propellant Rocket Instability, *Tenth (International) Symposium on Combustion*, The Combustion Institute, pp. 1101–1128.

Crocco, L. (1966) “The Relevance of a Characteristic Time in Combustion Instability,” *2nd ICRPG Combustion Conference*.

Crocco, L. (1968) “Research on Combustion Instabilities in Liquid Propellant Rockets,” *Twelfth (International) Symposium on Combustion*, The Combustion Institute, pp. 85–99.

Crocco, L. and Cheng, S.-I. (1952) “High-Frequency Instability in Rocket Motors with Concentrated Combustion,” *8th International Congress of Applied Mechanics*, Istanbul, Turkey; also *ARS J.*, Vol. 23 (1953), pp. 301–313.

Crocco, L. and Cheng, S.-I. (1953) “High-Frequency Combustion Instability in Rockets with Concentrated Combustion,” *ARS J.*, Vol. 23, pp. 301–312.

Crocco, L. and Cheng, S.-I. (1956) *Theory of Combustion Instability in Liquid Propellant Rocket Motors*, AGARDograph No. 8, Butterworths Scientific Publications, London.

Crocco, L. and Grey, J. (1956) “Combustion Instability in Liquid Propellant Rocket Motors,” *Proc. Gas Dyn. Symp. on Aerothermochemistry*, Northwestern University.

Crocco, L. and Grey, J. (1958) “Measurement of High-Frequency Limits of Stability in a Liquid Bipropellant Rocket Motor,” *L'Aerotechnica*, Vol. 38, pp. 135–144.

REFERENCES

- Crocco, L. and Mitchell, C.E. (1969) "Nonlinear Periodic Oscillations in Rocket Motors with Distributed Combustion," *Comb. Sci. and Tech.*, Vol. 1, pp. 147-169.
- Crocco, L. and Sirignano, W.A. (1966) "Effects of the Transverse Velocity Component on the Nonlinear Behavior of Short Nozzles," *AIAA J.*, Vol. 4, No. 8, pp. 1428-1430.
- Crocco, L. and Sirignano, W.A. (1967) "Behavior of Supercritical Nozzles Under Three-Dimensional Oscillatory Conditions," AGARDograph 117.
- Crocco, L., Grey, J. and Harrje, D.T. (1960) "Theory of Liquid Propellant Rocket Combustion Instability and Its Experimental Verification," *ARS J.*, Vol. 30, No. 2, pp. 159-168.
- Crocco, L., Grey, J. and Harrje, D.T. (1958) "On the Importance of the Sensitive Time Lag in Longitudinal High-Frequency Combustion Instability," *Jet Propulsion*, Vol. 28, No. 12, pp. 841-849.
- Crocco, L., Grey, J. and Matthews, G.B. (1954) "Preliminary Measurement of the Combustion Time Lag in a Monopropellant Rocket Motor," *Fifth (International) Symposium on Combustion*, Reinhold, pp. 164-170.
- Crocco, L., Harrje, D.T., Lee, D.H., Strahle, W.C., Sirignano, W.A., Bredfeldt, H.R. and Seebaugh, W.R. (1967) "Nonlinear Aspects of Combustion Instability in Liquid Propellant Rocket Motors," Princeton University Aeronautical Engineering Report 5530.
- Crocco, L., Harrje, D.T. and Reardon, F.H. (1962) "Transverse Combustion Instability in Liquid Propellant Rocket Motors," *ARS J.*, Vol. 32, No. 3, pp. 366-373.
- Crocco, L., Harrje, D.T., Sirignano, W.A., *et al.* (1967) "Nonlinear Aspects of Combustion Instability in Liquid Propellant Rocket Motors," NASA CR 72270.
- Crocco, L., Harrje, D.T., Sirignano, W.A. *et al.* (1968) "Nonlinear Aspects of Combustion Instability in Liquid Propellant Rocket Motors," NASA CR 72426.
- Crocco, L., Monti, R. and Grey, J. (1961) "Verification of Nozzle Admittance Theory by Exact Measurement of the Admittance Parameter," *ARS J.*, Vol. 31, No. 6, pp. 771-775.
- Cronemyr, P.J.M., Hulme, C.J. and Troger, C. (1998) "Coupled Acoustic-Structure Analysis of an Annular DLE Combustor," *Int. Gas Turb. and Aeroeng. Congress*.
- Crow, S.C. and Champagne, F.H. (1971) "Orderly Structure in Jet Turbulence," *J. of Fluid Mech.*, Vol. 48, pp. 547-591.
- Crump, J.E. and Price, E.W. (1961) "Effect of Acoustic Environment on the Burning Rate of Double-Base Propellants," *ARS J.*, Vol. 31, pp. 1026-1029.
- Crump, J.E. and Price, E.W. (1964) "Effect of Acoustic Environment on the Burning Rate of Solid Propellants," *AIAA J.*, Vol. 2, pp. 1274-1278.

Crump, J., Mathes, H.B., Clark, W.H. and Beckstead, M.W. (1987) "Motor Test Data Comparisons With Laboratory Data and Test Predictions," (Private Communication).

Crump, J.E., Schadow, K.C., Blomshield, F.S. and Bicker, C.J. (1981) "Combustion Instability in a Research Dump Combustor: Pressure Oscillations," *18th JANNAF Combustion Meeting*.

Crump, J.E., Schadow, K.C., Yang, V. and Culick, F.E.C. (1986) "Longitudinal Combustion Instabilities in Ramjet Engines: Identification of Acoustic Modes," *J. Prop. and Power*, Vol. 2, No. 2, p. 105.

Culick, F.E.C. (1961) "High Frequency Pressure Oscillations in Liquid Rockets," Sc.D. Thesis, M.I.T. Department of Aeronautics and Astronautics.

Culick, F.E.C. (1963) "High Frequency Oscillations in Liquid Rockets," *AIAA J.*, Vol. 1, No. 5, pp. 1097–1104.

Culick, F.E.C. (1966)a "Acoustic Oscillations in Solid Propellant Rockets," *Astronautica Acta*, Vol. 12, No. 2, pp. 113–126.

Culick, F.E.C. (1966)b "Rotational Axisymmetric Mean Flow and Damping of Acoustic Waves in a Solid Propellant Rocket," *AIAA J.*, Vol. 4, No. 8, pp. 1442–1444.

Culick, F.E.C. (1967) "Calculation of the Admittance Function for a Burning Surface," *Astronautica Acta*, Vol. 13, No. 3, pp. 221–238.

Culick, F.E.C. (1968)a "Some Nonacoustic Instabilities in Rocket Chambers are Acoustic," *AIAA J.*, Vol. 6, No. 12, pp. 1421–1422.

Culick, F.E.C. (1968)b "A Review of Calculations for Unsteady Burning of a Solid Propellant," *AIAA J.*, Vol. 6, No. 12, pp. 2241–2255.

Culick, F.E.C. (1969)a "An Elementary Calculation of the Combustion of Solid Propellants," *Astronautica Acta*, Vol. 14, pp. 171–181.

Culick, F.E.C. (1969)b "Some Problems in the Unsteady Burning of Solid Propellants," Naval Weapons Center Report NWC TP 4668.

Culick, F.E.C. (1969)c "Remarks on Extinguishment and the Response Function for a Burning Propellant," *AIAA J.*, Vol. 7, No. 7, pp. 1403–1404.

Culick, F.E.C. (1969)d "T-Burner Manual," *Chemical Propulsion Information Agency*, CPIA No. 191, Laurel, MD.

Culick, F.E.C. (1970) "Stability of Longitudinal Oscillations with Pressure and Velocity Coupling in a Solid Propellant Rocket Motor," *Comb. Sci. and Tech.*, Vol. 2, pp. 179–201.

Culick, F.E.C. (1971)a "Nonlinear Growth and Limiting Amplitude of Acoustic Oscillations in Combustion Chambers," *Comb. Sci. and Tech.*, Vol. 3, No. 1, pp. 1–16.

REFERENCES

- Culick, F.E.C. (1971)b "Research on Combustion Instability and Application to Solid Propellant Rocket Motors," *AIAA/SAE 7th Propulsion Joint Specialist Conference*, AIAA-71-753.
- Culick, F.E.C. (1972) "Interactions Between the Flow Field, Combustion and Wave Motions in Rocket Motors," Naval Weapons Center Report NWC TP 5349.
- Culick, F.E.C. (1973)a "The Stability of One-Dimensional Motions in a Rocket Motor," *Comb. Sci. and Tech.*, Vol. 7, pp. 165-175.
- Culick, F.E.C. (1973)b "Nonlinear Behavior of Acoustic Waves in Combustion Chambers," *10th JANNAF Combustion Meeting*, Vol. 3, pp. 714-757.
- Culick, F.E.C., Ed. (1974) "T-Burner Testing of Metallized Solid Propellants," Air Force Rocket Propulsion Laboratory, Report AFRPL TR-74-28; also CPIA No. 275.
- Culick, F.E.C. (1975) "Stability of Three-Dimensional Motions in a Combustion Chamber," *Comb. Sci. and Tech.*, Vol. 10, pp. 109-124.
- Culick, F.E.C. (1976) "Nonlinear Behavior of Acoustic Waves in Combustion Chambers," Parts I and II, *Acta Astronautica*, Vol. 3, pp. 714-757.
- Culick, F.E.C. (1977) "Remarks on Entropy Production in the One-Dimensional Approximation to Unsteady Flow in Combustion Chambers," *Comb. Sci. and Tech.*, Vol. 15, pp. 95-97.
- Culick, F.E.C. (1979)a "Some Problems of Nonlinear Waves in Solid Propellant Rocket Motors," *53rd AGARD Specialists' Meeting of the Propulsion and Energetics Panel*, AGARD Conference Proceedings No. 259.
- Culick, F.E.C. (1979)b "Some Recent Results for Nonlinear Wave Motions in Solid Propellant Rockets," *AIAA/SAE/ASME 15th Joint Propulsion Conference*, AIAA-79-1208.
- Culick, F.E.C. (1980) Report of the JANNAF Workshop on Pressure Oscillations in Ramjets," *17th JANNAF Combustion Meeting*.
- Culick, F.E.C. (1981) "Combustion Instability in Solid Rocket Motors, Vol. II: A Guide for Motor Designers," CPIA No. 290.
- Culick, F.E.C. (1987)a "A Note on Rayleigh's Criterion," *Comb. Sci. and Tech.*, Vol. 56, pp. 159-166.
- Culick, F.E.C. (1987)b "Report of the JANNAF Workshop on Mechanisms of Instabilities in Ramjet Engines," *24th JANNAF Combustion Conference*.
- Culick, F.E.C. (1988) "Combustion Instabilities in Liquid-Fueled Propulsion System—An Overview," *AGARD 72B Specialists' Meeting of the Propulsion and Energetics Panel*, AGARD CP 450.
- Culick, F.E.C. (1989) "Technical Evaluation Report," *AGARD 72B Specialists' Meeting of the Propulsion and Energetics Panel*, AGARD CP 450.

- Culick, F.E.C. (1992) "Combustion Instabilities and Rayleigh's Criterion," in *Modern Research Topics in Aerospace Propulsion (In Honor of Corrado Cacci)*, edited by G. Angelino, L. DeLuca and W.A. Sirignano, Springer Verlag, New York, pp. 135–151.
- Culick, F.E.C. (1994) "Some Recent Results for Nonlinear Acoustics in Combustion Chambers," *AIAA J.* Vol. 32, No. 1, pp. 146–169.
- Culick, F.E.C. (1995) "Some Basic Problems and Control of Combustion Instabilities," *Colloque CNES/ONERA/CNRS sur les Ecoulements Propulsifs dans les Systèmes de Transport Spatial*, Bordeaux.
- Culick, F.E.C. (1996) "On the Roles of Approximate Methods of Analysis and Numerical Simulations for Investigation of Combustion Instabilities in Solid Propellant Rockets," *Second International Conference on Combustion Conversion and Environmental Problems of Energetic Materials*, St. Petersburg.
- Culick, F.E.C. (1997) "A Note on Ordering Perturbations and the Insignificance of Linear Coupling in Combustion Instabilities," *Comb. Sci. and Tech.*, Vol. 126, pp. 359–379.
- Culick, F.E.C. (1999) "Combustor Dynamics: Fundamentals, Acoustics and Control," a course of lectures given at the United Technologies Research Center, October 1998–June 1999, accessible on the website www.culick.caltech.edu.
- Culick, F.E.C. (2000) "Combustion Instabilities: Mating Dance of Chemical, Combustion, and Combustor Dynamics," (Revised 10 October 2000) *36th AIAA/ASME/SAE/ASEE Joint Propulsion Conference*, AIAA-2000-3178.
- Culick, F.E.C. (2001)a "Dynamics of Combustion Systems: Fundamentals, Acoustics and Control," two lectures in the Short Course *Active Control of Engine Dynamics*, von Karman Institute for Fluid Dynamics.
- Culick, F.E.C. (2001)b "A Short Course of Lectures on Combustion Dynamics: Fundamentals, Acoustics and Control," Short Course given at NASA Glenn Research Center, 9–13 September, accessible on the website www.culick.caltech.edu.
- Culick, F.E.C., Editor (2002)a "Final Report: Caltech Multidisciplinary University Research Initiative (MURI)," California Institute of Technology, Jet Propulsion Center, 30 April 2002.
- Culick, F.E.C. (2002)b "Combustion Instabilities in Rocket Motors," two lectures in the Short Course *Internal Aerodynamics in Solid Rocket Propulsion*, von Karman Institute for Fluid Dynamics.
- Culick, F.E.C. (2002)c "Combustion Instabilities in Liquid Rocket Engines: Fundamentals and Control," short course given at ONERA, Paris, France, 28–29 October, accessible at www.culick.caltech.edu.
- Culick, F.E.C., Burnley, V.S. and Swenson, G. (1995) "Pulsed Instabilities in Solid Propellant Rockets," *J. Prop. and Power*, Vol. 11, No. 4, pp. 657–665.
- Culick, F.E.C. and Dehority, G.L. (1969) "An Elementary Calculation for the Burning Rate of Composite Solid Propellants," *Comb. Sci. and Tech.*, Vol. 1, pp. 193–204.

REFERENCES

- Culick, F.E.C., Derr, R.L. and Price, C.F. (1972) "Linear Analysis of One-Dimensional Oscillations in a Variable-Area T-Burner," *9th JANNAF Combustion Meeting*.
- Culick, F.E.C., Heitor, M.V. and Whitelaw, J.H. (Editors) (1996) *Unsteady Combustion*, Kluwer Academic Publishers, Dordrecht.
- Culick, F.E.C., Isella, G. and Seywert, C. (1998) "Influences of Combustion Dynamics in Linear and Nonlinear Unsteady Motions in Solid Propellant Rockets," *34th AIAA/ASME/SAE/ASEE Joint Propulsion Conference*, AIAA-98-3704.
- Culick, F.E.C. and Levine, J.N. (1974) "Comparison of Exact and Approximate Analyses of Nonlinear Combustion Instability," *12th AIAA Aerospace Sciences Meeting*, AIAA-74-201.
- Culick, F.E.C. and Magiawala, K.R. (1979) "Excitation of Acoustic Modes in a Chamber by Vortex Sheding," *J. Sound and Vib.*, Vol. 64, No. 3, pp. 455-457.
- Culick, F.E.C., Paparizos, L., Sterling, J. and Burnley, V.S. (1992) "Combustion Noise and Combustion Instabilities in Propulsion Systems," *AGARD Conference on Combat Aircraft Noise*, AGARD CP 512.
- Culick, F.E.C. and Perry, E.H. (1969) "T-Burner Data and Combustion Instability in Solid Propellant Rockets," *AIAA J.*, Vol. 7, No. 6, pp. 1204-1205.
- Culick, F.E.C. and Roe, T.-S. (1996) "Applications of Various Methods of Analysis of Combustion Instabilities in Solid Propellant Rockets," *32nd JANNAF Combustion Meeting*.
- Culick, F.E.C. and Rogers, T. (1980) "Modeling Pressure Oscillations in Ramjets," *16th AIAA/SAE/ASME Joint Propulsion Meeting*, AIAA-80-1192.
- Culick, F.E.C. and Rogers, T. (1983) "The Response of Normal Shocks in Diffusers," *AIAA J.*, Vol. 21, No. 10, pp. 1382-1390.
- Culick, F.E.C. and Schadow, K.G. (1988) "Pressure Oscillations in Ramjets," CPIA No. 535.
- Culick, F.E.C. and Yang, V. (1995) "Overview of Combustion Instabilities in Liquid-Propellant Rocket Engines," *First (International) Symposium on Liquid Rocket Engine Combustion Instability*, The Pennsylvania State University, *AIAA Progress Series*, Vol. 169.
- Culick, F.E.C. and Yang, V. (1992) "Prediction of the Stability of Unsteady Motions in Solid Propellant Rocket Motors," Chapter 18 in *Nonsteady Burning and Combustion Instability of Solid Propellants*, of *AIAA Progress in Astronautics and Rocketry*, Vol. 143, Washington, DC.
- Cullom, R.R. and Johnsen, R.L. (1979) "Operating Condition and Geometry Effects on Low Frequency Afterburner Combustion Instability in a Turbofan at Altitude," NASA TP-1475.
- Cumpsty, N.A. (1979) "Jet Engine Combustion Noise: Pressure, Entropy and Vorticity Perturbations Produced by Unsteady Combustion or Heat Addition," *J. Sound and Vib.*, Vol. 66, No. 4, pp. 527-544.

- Cumpsty, N.A. and Marble, F.E. (1977) "Core Noise from Gas Turbine Exhausts," *J. Sound and Vib.*, Vol. 54, No. 2, pp. 297–309.
- Curran, E.T. (1979) "An Investigation of Flame Stability in a Coaxial Dump Combustor," Ph.D. Dissertation, Air Force Institute of Technology, Report AFIT/AE/DS79-1.
- Darling, D., Radhakrishnan, K. and Oyediran, A. (1997) "Combustion Noise at Elevated Pressures in a Liquid-Fueled Premixed Combustor," NASA TM 107481 (paper ASME-97-GT-308, *ASME Turbo Expo 1997*).
- Davenas, A. (Ed.) (1993) *Solid Rocket Propulsion Technology*, Pergamon Press, New York.
- Davis, D.L. (1981) "Coaxial Dump Combustors Combustion Instabilities, Part I — Parametric Test Data," Aero Propulsion Laboratory Air Force Wright Aeronautical Laboratories, Wright Patterson AFB, Ohio, Interim Report.
- Davis, J.A. and Strahle, W.C. (1988) "Acoustic Vortical Interaction in a Complex Turbulent Flow," *26th AIAA Aerospace Sciences Meeting*, AIAA-88-0595.
- Dawson, M.C., Andrepong, W.C., Luther, D.R. and Flandro, G.F. (1981) "Elimination of Flow Induced Instabilities in Solid Rocket Motors by Aerodynamic Contouring of Internal Grain Geometries," *18th JANNAF Propulsion Conference*, CPIA No. 340, Vol. V, pp. 257–269.
- Dehority, G.L. and Kraeutle, K.J. (1976) "Procedure for the Calculation of Particulate Damping of Acoustic Oscillations," Naval Weapons Center, Technical Memorandum 2889.
- DeLuca, L. (1990) "A Critical Review of Solid Rocket Propellant Transient Flame Models," *Pure and Applied Chem.*, Vol. 63, p. 825.
- DeLuca, L. (1992) "Theory of Nonsteady Burning and Combustion Stability of Solid Propellants by Flame Models," Chapter 14 in *Nonsteady Burning and Combustion Instability of Solid Propellants*, AIAA *Progress in Astronautics and Rocketry*, Vol. 143, Washington, DC.
- DeLuca, L., DiSilvestro, R. and Cozzi, F. (1995) "Intrinsic Combustion Instability of Solid Energetic Materials," *J. Prop. and Power*, Vol. 11, No. 4, pp. 804–875.
- DeLuca, L. and Galfetti, L. (1991) "Combustion Modeling and Stability of Double-Based Propellants," *Modern Research Topics in Aerospace Propulsion*, Springer-Verlag, New York, pp. 109–134.
- DeLuca, L., Price, E.W. and Summerfield, M. (Editors) (1992) *Nonsteady Burning and Combustion Instability of Solid Propellants* AIAA *Progress in Astronautics and Aeronautics*, Vol. 143, Washington, pp. 519–600.
- Denbigh, K.B. (1961) *The Principles of Chemical Equilibrium*, Cambridge at the University Press.
- Denisov, K.P., Kadishevich, A.S. and Povolotzky, J.D. (1993) "Full-Scale Component and Engine Stability Testing Using Spectral Analysis," of AIAA *Progress in Astronautics and Aeronautics*, Vol. 169.

REFERENCES

- Denisov, Y.N., Shchelkin, K.I. and Troshin, Y.K. (1962) "Some Questions of Analogy Between Combustion in a Thrust Chamber and in a Detonation Wave," *Ninth (International) Symposium on Combustion*, Williams and Wilkins, pp. 1152–1159.
- Dennison, M. R. and Baum, E. (1961) "A Simplified Model of Unstable Burning in Solid Propellants," *American Rocket Society Journal*, Vol. 31, No. 8, pp. 1112–1122.
- Dernovoy, V.S. (1938) "Development of Solid Propellants for Rockets," Moscow Science Institute of Chemistry and Mechanics, TR, Moscow, (in Russian).
- Derr, R.L., Churchill, H.L. and Fleming, R.W. (1974) "Aluminum Behavior in Solid Propellant Combustion," Air Force Rocket Propulsion Laboratory, Report AFRPL-TR-74-13.
- Derr, R.L. and Mathes, H.B. (1974) "Cold Gas Acoustic Tests for Resolving T-Burner Uncertainties," *11th JANNAF Combustion Meeting*.
- Derr, R.L., Mathes, H.B. and Brown, B.G. (1974) "Progress in Resolving T-Burner Uncertainties Using Cold Gas Acoustic Tests: Part 1, Effect of Burner Geometry," CPIA No. 261, Vol. 1, pp. 499–509.
- Derr, R.L., Mathes, H.B. and Crump, J.E. (1979) "Application of Combustion Instability Research to Solid Propellant Rocket Motor Problems," *AGARD Conference Proceedings*, No. 259, Paper No. 23.
- Dickinson, L.A. (1962) "Command Initiation of Finite Wave Axial Combustion Instability in Solid Propellant Rocket Engines," *ARS J.*, Vol. 32, pp. 643–644.
- Dickinson, L.A. and Jackson, F. (1963) "Combustion in Solid Propellant Rocket Engines," *Fifth AGARD Colloquium*, pp. 531–550.
- Diederichsen, J. (1963) "A Singing Flame as a Tool for Evaluation of Damping Agents for Solid Propellant Rocket Motors," *Comb. and Flame*, Vol. 7, No. 1, pp. 29–37.
- Dines, P.J. (1983) "Active Control of Flame Noise," Ph.D. Thesis, Cambridge University.
- Dipprey, D.F. (1972) "Liquid Propellant Rockets," in *Chemistry in Space Research* (R.F. Landel and A. Rembaum, Ed.), American Elsevier Publishing, Inc.
- Dix, D.M. and Smith, G.E. (1971) "Analysis of Combustion Instability in Aircraft Engine Augmentors," *7th AIAA/SAE Propulsion Joint Specialist Conference*, AIAA-71-700.
- Doak, P.E. (1973) "Fundamentals of Aerodynamic Sound Theory and Flow Duct Acoustics," *J. Sound and Vib.* Vol. 28, No. 3, pp. 527–561.
- Docquier, N., Candel, S. (2002) "Combustion Control and Sensors: A Review," *Prog. in Energy Comb. Sci.*, Vol. 28, pp. 107–150.

- Doedel, E.J., Champneys, A.R., Fairgrieve, T.F., Kuznetsov, Y.A., Sandstede, B. and Wang, X. (1997) "AUTO 97: Continuation and Bifurcation Software for Ordinary Differential Equations," Concordia University, Montreal, Canada.
- Doedel, E.J., Keller, H.B. and Kernevez, J.P. (1991)a "Numerical Analysis and Control of Bifurcation Problems, (I) Bifurcation in Finite Dimensions," *International Journal of Bifurcation and Chaos*, Vol. 1, No. 3, pp. 493–520.
- Doedel, E.J., Keller, H.B. and Kernevez, J.P. (1991)b "Numerical Analysis and Control of Bifurcation Problems, (II) Bifurcation in Infinite Dimensions," *International Journal of Bifurcation and Chaos*, Vol. 1, No. 4, pp. 745–772.
- Doedel, E.J. and Kernevez, J.P. (1984) "Software for Continuation Problems in Ordinary Differential Equations with Applications," Applied Mathematics Publication 217–50, Calif. Inst. of Tech., Pasadena, CA.
- Dombrowski, N. and Hooper, P.C. (1964) "A Study of the Sprays Formed by Impinging Jets in Laminar and Turbulant Flows," *J. Fluid Mech.*, Vol. 18, pp. 392–406.
- Dordain, J.J., Lourme, D. and Estoueig, C. (1974) "Etude de l'Effet POGO sur les Lanceurs EUROPA II et DIAMANT B," *Acta Astronautica*, Vol. 1, pp. 1357–1384.
- Dotson, K.W., Baker, R.L. and Bywater, R.J. (1998) "Launch Vehicle Self-Sustained Oscillations from Aeroelastic Coupling. Part II: Analysis," *J. Spacecraft and Rockets*, Vol. 35, No. 3, pp. 374–379.
- Dotson, K.W., Baker, R.L. and Sako, B.H. (1998) "Launch Vehicle Self-Sustained Oscillations from Aeroelastic Coupling. Part I: Theory," *J. Spacecraft and Rockets*, Vol. 35, No. 3, pp. 365–373.
- Dotson, K.W., Koshigoe, S. and Pace, K.K. (1997) "Vortex Shedding in a Large Solid Rocket Without Inhibitors at the Segment Interfaces," *J. Prop. and Power*, Vol. 13, No. 2, pp. 197–206.
- Dotson, K.W., Murdock, J.W. and Kamimoto, D.K. (1999) "Launch Vehicle Dynamic and Control Effects from Solid Rocket Motor Slag Ejection," *J. Prop. and Power*, Vol. 15, No. 3, pp. 468–475.
- Dowling, A.P. (1988) "Reheat Buzz—An Acoustically Coupled Combustion Instability," *AGARD 72B Specialists' Meeting of the Propulsion and Energetics Panel*, AGARD CP 450.
- Dowling, A.P. (1995) "The Calculation of Thermoacoustic Oscillations," *J. Sound and Vib.*, Vol. 180, No. 4, pp. 557–581.
- Dowling, A.P. (1996) "Nonlinear Acoustically-Coupled Combustion Oscillations," *2nd AIAA/CEAS Aeroacoustics Conference*, pp. 1–12, AIAA-96-1749.
- Dowling, A.P. (1997) "Nonlinear Self-Excited Oscillations of a Ducted Flame," *J. Fluid Mechanics*, Vol. 346, pp. 271–290.
- Dowling, A.P. (1999) "A Kinematic Model of a Ducted Flame," *J. Fluid Mech.*, Vol. 394, pp. 51–72.

REFERENCES

- Dowling, A.P. (1999) "Thermoacoustic Instability," *6th International Congress on Sound and Vibration*, pp. 3277–3292.
- Dowling, A.P. and Bloxsidge, G.J. (1984) "Reheat Buzz — An Acoustically Driven Combustion Instability," *AIAA/NASA 9th Aeroacoustics Conference*, AIAA-84-2321.
- Dowling, A.P. and Ffowcs Williams, J.E. (1983) *Sound and Sources of Sound*, Ellis Horwood Publishers, Chichester.
- Dowling, A.P. and Hubbard, S. (2000) "Instability in Lean Premixed Combustors," *Inst. Mech. Eng.*, Vol. 214, Part A, pp. 317–332.
- Dowling, A.P. and Stow, S.R. (2003) "Acoustic Analysis of Gas Turbine Combustion," *J. Prop. and Power*, Vol. 19, No. 5, pp. 722–734.
- Dranovsky, M.L. (2005) *Evaluation of Stability in Liquid Rocket Engine Combustion Chambers*, Culick, F.E.C. and Yang, V. (Editors); to be published.
- Drobyazko, B.S., Pavlovskii, V.P., Makhin, V.A., Kryzhanovskii, N.A. (1975) "On the Possibility of Using Modeling Devices to Study Liquid Propellant Combustion Process Stability," *Izvestiya VVZ Aviatsionnaya Teknika*, V. 18, pp. 78–80.
- Dubinkin, B.N., Natanzon, M.S. and Cham'yan, A.E. (1978) "Two Regimes of Combustion in a Combustion Chamber with a Recirculation Zone," *Phys. of Comb. and Expl.*, Vol. 14, No. 6, pp. 693–700.
- Ducruix, S. (1999) "Dynamique des Interactions Acoustique-Combustion," Ph.D. Thesis, École Centrale Paris.
- Ducruix, S., Schuller, T., Durox, D. and Candel, S. (2003) "Combustion Dynamics and Instabilities: Elementary Coupling and Driving Mechanisms," *J. Prop. and Power*, Vol. 19, No. 5, pp. 722–734.
- Duer, J. and Hessler, R. (1984) "Forced Oscillation Theory and Applications," *20th AIAA/ASME/SAE/ASEE Joint Propulsion Conference*, AIAA-84-1356.
- Dunlap, R., Willoughby, P.G. and Hermsen, R.W. (1974) "Flowfield in the Combustion Chamber of a Solid Propellant Rocket Motor," *AIAA J.*, Vol. 12, No. 10, pp. 1440–1442.
- Dunlap, R. and Brown, R.S. (1981) "Exploratory Experiments on Acoustic Oscillations Driven by Periodic Vortex Shedding," *AIAA J.*, Vol. 19, No. 3, pp. 408–409.
- Dunlap, R. *et al.* (1986) "Internal Flow Field Investigation," Chemical Systems Division, United Technologies Corporation, Report 2805-FR.
- Dunlap, R., Blackner, A.M., Waugh, R.C., Brown, R.S. and Willoughby, P.G. (1990) "Internal Flow Field Studies in a Simulated Cylindrical Port Rocket Chamber," *J. Propulsion*, Vol. 6, No. 6, pp. 690–704.
- Dupays, J. (1996) "Contribution à l'Etude du Rôle de la Phase Condensée dans la Stabilité d'un Propulseur à Propergol Solide pour Lanceur Spatial," Thèse pour le Titre du Docteur de l'Institut National Polytechnique

de Toulouse.

Dupays, J. (2000) "Mass Transfer Effects on Sound Propagation in a Droplet-Gas Mixture," *5th International Symposium on Special Topics in Chemical Propulsion (5-ISICP) Combustion of Energetic Materials*, Stesa, Italy.

Dupays, J. (2002) "Two-Phase Unsteady Flow in Solid Rocket Motors," *Aerospace Science and Technology*, Vol. 6, No. 6, pp. 413–422.

Dupays, J., Fabignon, Y., Villedieu, P., Lavergne, G. and Estivalizes, J.L. (2000) "Some Aspects of Two-Phase Flows in Solid-Propellant Rocket Motors," in *Solid Propellant Chemistry, Combustion, and Motor Interior Ballistics*, of AIAA *Progress in Astronautics and Aeronautics*, Vol. 185, Washington, DC.

Dupays, J., Prévost, M., Tarrin, P. and Vuillot, F. (1996) "Effects of Particulate Phase on Vortex Shedding Driven Oscillations in Solid Rocket Motors," *32nd AIAA/ASME/SAE/ASEE Joint Propulsion Conference*, AIAA-96-3248.

Dupays, J. and Vuillot, F. (1998) "Propagation of an Acoustic Wave in a Two-Phase Reactive Medium," *34th AIAA/ASME/SAE/ASEE Joint Propulsion Conference*, AIAA-98-3696.

Dupays, J. and Vuillot, F. (2001) "Propagation of Acoustic Waves in a Two-Phase Vaporizing Mixture," *J. Prop. and Power*, Vol. 18, No. 1, pp. 222–224.

Dupère, I.D.J. and Dowling, A.P. (2002) "The Absorption of Sound by Helmholtz Resonators With and Without Flow," AIAA Paper 2002-2590.

Dupère, I.D.J. and Dowling, A.P. (2005) "The Use of Helmholtz Resonators in a Practical Combustor," *J. of Eng. for Gas Turb. and Power*, Vol. 127, No. 2, pp. 268–275.

Duroshenko, V.E. and Silverstov, V.M. (1982) "Experimental Investigation of Entropy Waves During Unstable Combustion in the Chamber of a Gas Turbine Engine," *Combustion, Explosion and Shock Waves*, Vol. 18, pp. 20–25.

Durox, D., Baillot, F., Searby, G. and Boyer, L. (1997) "On the Shape of Flames Under Strong Acoustic Forcing: A Mean Flow Controlled by an Oscillating Flow," *Journal of Fluid Mechanics*, Vol. 350, pp. 295–310.

Edelman, R.B., Harsha, P.T. and Schmotolocka, S.N. (1981) "Modeling Techniques for the Analysis of Ramjet Combustion Processes," *AIAA J.*, Vol. 19, No. 5, pp. 601–609.

Edelman, R. (1981) "Spray Combustion in Ramjet Environments," Report of a JANNAF Workshop, CPIA No. 343.

Edwards, N.R., McIntosh, A.C. and Brindley, J. (1996) "The Development of Pressure Induced Instabilities in Premixed Flames," *Comb. Sci. and Tech.*, Vol. 99, pp. 373–386.

REFERENCES

- Ehrich, F.F. (1971) "A Dynamic Model of Gas Turbine Engine Main Combustion Instability," *ASME Gas Turbine Conference and Products Show*, Houston.
- Eisel, J.L. (1964) "The Effect of Acoustic Pressure on the Burning Rate of Solid Rocket Propellants," *Pyrodynamics*, Vol. 1, pp. 61–70.
- Eisel, J.L. and Dehority, G.L. (1966) "A Technique for Investigating Low Frequency Velocity-Coupled Combustion Instability," CPIA No. 105, Vol. 1, pp. 703–712.
- Eisel, J.L., Horton, M.D., Price, E.W. and Rice, D.W. (1964) "Preferred Frequency Oscillatory Combustion of Solid Propellants," *AIAA J.*, Vol. 2, No. 7, pp. 1319–1323.
- Eldredge, J.D. and Dowling, A.P. (2003) "The Absorption of Axial Acoustic Waves by a Perforated Liner with Bias Flow," *J. Fluid Mech.*, Vol. 485, pp. 307–335.
- Elias, I. and Gordon, R. (1952) "Longitudinal Vibrations of Gas at Ambient Pressure in a Rocket Thrust Chamber," *ARS J.*, Vol. 2., No. 5, September–October, pp. 263–268.
- Ellis, H., Odgars, I., Stosik, A.J., Van de Verg, N. and Wick, R.S. (1952) "Experimental Investigation of Combustion Instability in Rocket Motors," *Fourth (International) Symposium on Combustion*, Williams and Wilkins Co., pp. 880–885.
- Elverum, G.W., Jr., Staudhammer, P., Miller, J., Hoffman, A. and Rockow, R. (1967) "The Decent Engine for the Lunar Module," *AIAA 3rd Propulsion Joint Specialist Conference*, AIAA-67-521.
- Emmons, H.W. (1958) "Flow Discontinuities Associated with Combustion," Chapter 2 of Section G in *Fundamentals of Gas Dynamics*, Vol. III of *High Speed Aerodynamics and Jet Propulsion*, H.W. Emmons, Editor, Princeton University Press.
- Engler, J.F. and Nachbar, W. (1964) "Experiments with a Solid-Propellant Acoustic Oscillator," *AIAA J.* Vol. 2, No. 7, pp. 1279–1284.
- Entezam, B., Van Moorhem, W.K. and Majdalani, J. (2002) "Two-Dimensional Numerical Verification of the Unsteady Thermoacoustic Field Inside a Rijke-Type Pulse Combustor," *Numerical Heat Transfer, Part A*, Vol. 41, pp. 245–265.
- Epstein, P.S. and Carhart, P.R. (1953) "The Absorption of Sound in Suspensions and Emulsions. I. Water Fog in Air," *J. Acoust. Soc. of Amer.*, Vol. 25, pp. 553–565.
- Epstein, A.H., Ffowcs Williams, J.E. and Greitzer, E.M. (1986): "Active Suppression of Compression Instabilities," *AIAA 10th Aeroacoustics Conference*, AIAA-86-1994.
- Ernst, R.C. (1976) "A Combustion Model for Low Frequency Instability in Turbofan Augmentors," *AIAA/SAE 12th Propulsion Conference*, AIAA-76-680.
- Evesque, S. (2000) "Adaptive Control of Combustion Oscillations," PhD Thesis, Cambridge University, UK.

- Evesque, S. and Polifke, W. (2002) "Low Order Acoustic Modeling for Annular Combustors: Validation and Inclusion of Modal Coupling," ASME Paper GT-2002-30064.
- Fabignon, Y., Dupays, J., Avalon, G., Vuillot, F., Lupoglazoff, N., Casalis, G. and Prévost, M. (2003) "Instabilities and Pressure Oscillations in Solid Rocket Motors," *Aerosp. Sci. and Tech.*, Vol. 7, pp. 191–200.
- Fang, J.J. (1984) "Application of Combustion Time-Lag Theory to Combustion Stability Analysis of Liquid and Gaseous Propellant Rocket Engines," *22nd AIAA Aerospace Sciences Meeting*, AIAA-84-0510.
- Fang, J.J. (1987) "Combustion Instability Model Study," Phase I Report (September 1986–October 1987) Contract NAS 8-36274, NASA Marshall Space Flight Center.
- Fang, J.J. and Jones, Y.T. (1984) "Comparison of Analytical Modeling Results with O₂/H₂ Combustion Stability Data," *21st JANNAF Combustion Meeting*.
- Fang, J.J. and Jones, Y.T. (1987) "Development of a Generic Combustion Stability Code for Liquid Propellant Rocket Engines," *24th JANNAF Combustion Meeting*.
- Fannin, C.A., Baumann, W.T., Saunders, W.R., Richards, G.A. and Straub, D.L. (2000) "Thermoacoustic Stability Analysis for Multi-Port Fuel Injection in a Lean Premixed Combustor," AIAA Paper 2000-0711.
- Feiler, C.E. and Heidmann, M.F. (1967) "Dynamic Response of Gaseous-Hydrogen Flow System and its Application to High Frequency Combustion Instability," NASA TN D-4040.
- Feldman, K.T., Jr. (1968) "Review of the Literature on Rijke Thermoacoustic Phenomena," *J. Sound and Vib.*, Vol. 7, No. 1, pp. 83–89.
- Fenn, J.B., Forney, H.B. and Garmon, R.C. (1950) "Burners for Supersonic Ram-Jets — Instability in a Two-Inch Ram-Jet Burner," *Engineering and Process Development*, Vol. 43, No. 7, pp. 1663–1672.
- Féralle, T., Casalis, G. and Dupays, J. (2002) "Particle Effects on Solid-Propellant Motors Flow Stability," *38th AIAA/ASME/SAE/ASEE Joint Propulsion Conference*, AIAA-2002-3144.
- Ferris, H.G., Corcoran, W.H., Sage, B.H. and Wimpress, R.N. (1945) "Classified Studies Carried Out in the Development of Solid Rockets," California Institute of Technology (unavailable).
- Ffowcs Williams, J.E. (1982) "Sound Sources in Aerodynamics—Fact and Fiction," *AIAA J.*, Vol. 20, No. 3, pp. 307–315.
- Ffowcs Williams, J.E. (1984): "Anti-Sound," *Proc. Roy. Soc. London*, A395, pp. 63–88.
- Ffowcs Williams, J.E. (1986): "The Aerodynamic Potential of Anti-Sound," ICAS-86-0.1.
- Filimonov, V.I. (1968) "Investigation of Instability of Combustion of Liquid-Propellant Rocket Motors," *Soviet Applied Mechanics*, Vol. 4, No. 9, pp. 80–81.

REFERENCES

- Filimonov, V.I. (1968) "Investigation of Instability of Combustion of Liquid-Propellant Rocket Motors," *Soviet Applied Mechanics*, Vol. 4, No. 9, pp. 80–81.
- Finlinson, J.C., Nelson, M.A. and Beckstead, M.W. (1987) "Characterization of a Modified Rijke Burner for Distributed Combustion," *24th JANNAF Combustion Meeting*, CPIA No. 476, Vol. I, pp. 13–26.
- Flanagan, S.N., Flandro, G.A. and Thomas, H.D. (1995) "A New Approach to Velocity Coupling," *31st AIAA/ASME/SAE/ASEE Joint Propulsion Conference*, AIAA-95-2734.
- Flandro, G.A. (1964) "Roll Torque and Normal Force Generation in Acoustically Unstable Rocket Motors," *AIAA J.*, Vol. 2, No. 7, pp. 1303–1306.
- Flandro, G.A. (1967) "Rotating Flows in Acoustically Unstable Rocket Motors," Ph.D. Thesis, Jet Propulsion Center, California Institute of Technology.
- Flandro, G.A. (1974) "Solid Propellant Acoustic Admittance Corrections," *J. Sound and Vib.*, Vol. 36, No. 3, pp. 297–312.
- Flandro, G.A. (1983) "A Nonlinear Time-Dependent Theory of Combustion of a Solid Propellant with Velocity Coupling," *19th AIAA/SAE/ASME Joint Propulsion Conference*, AIAA-83-1269.
- Flandro, G.A. (1985) "Energy Balance Analysis of Nonlinear Combustion Instability," *J. Prop. and Power*, Vol. 1, No. 3, pp. 210–221.
- Flandro, G.A. (1986) "Vortex Driving Mechanism in Oscillatory Rocket Flows," *J. Prop. and Power*, Vol. 2, No. 3, pp. 206–214.
- Flandro, G.A. (1995)a "Effects of Vorticity on Rocket Combustion Stability," *J. Prop. and Power*, Vol. 11, No. 4, pp. 607–625.
- Flandro, G.A. (1995)b "On Flow Turning," *31st AIAA/ASME/SAE/ASEE Joint Propulsion Conference*, AIAA-95-2730.
- Flandro, G.A., Cai, W., Yang, V. (2000) "Turbulent Transport in Rocket Motor Unsteady Flowfield," *AIAA Progress in Astronautics and Rocketry*, Vol. 185, pp. 837–858.
- Flandro, G.A. *et al.* (1982) "Elimination of Flow Induced Instabilities in Solid Rocket Motors by the Aerodynamics Contouring of Internal Grain Geometries," Air Force Rocket Propulsion Laboratory, AFRPL-82-058.
- Flandro, G.A. and Finlayson, P.A. (1984) "Nonlinear Interactions Between Vortices and Acoustic Waves in a Combustion Chamber," *21st JANNAF Combustion Meeting Proceedings*, pp. 71–81.
- Flandro, G.A., Fischbach, S.R., Majdalani, J. and French, J.C. (2004) "Nonlinear Rocket Motor Stability Prediction: Limit Amplitude, Triggering, and Mean Pressure Shift," *40th AIAA/ASME/SAE/ASEE Joint Propulsion Conference*, AIAA-2004-4054.
- Flandro, G.A., Isaacson, L.K., Boys, D.L. and Lin, P.T. (1972) "The Influence of Mean Flow on Rocket Motor Combustion Instability," AFRPL TR-72-103, Vol. 3, Contract No. F04611-71-C-0047, University of

Utah.

Flandro, G.A. and Jacobs, H.R. (1975) "Vortex Generated Sound in Cavities," in *Aeroacoustics: Jet and Combustion Noise* of AIAA *Progress in Astronautics and Aeronautics*, Vol. 37, pp. 521–533.

Flandro, G.A. and Majdalani, J. (2003) "Aeroacoustic Instability in Rockets," *AIAA J.*, Vol. 44, No. 3, pp. 485–497.

Flandro, G.A., Majdalani, J. and French, J.C. (2004) "Incorporation of Nonlinear Capabilities in the Standard Stability Prediction Program," *40th AIAA/ASME/SAE/ASEE Joint Propulsion Conference*, AIAA-2004-4182.

Fleifil, M., Annaswamy, A.M., Ghoniem, Z.A. and Ghoniem, A.F. (1996) "Response of a Laminar Premixed Flame to Flow Oscillations: A Kinematic Model and Thermoacoustic Instability Results," *Comb. and Flame*, Vol. 106, pp. 487–510.

Foner, S.N., Hudson, R.L. and Hall, B.N. (1964) "Admittance Measurements of Solid Propellants by an Acoustic Oscillator Technique," *AIAA J.*, Vol. 2, No. 6, pp. 1123–1129.

Fontaine, R.J., Levine, R.S. and Combs, L.P. (1968) "Secondary Non Destructive Instability in Medium Size Liquid Fuel Rocket Engines," Chapter 3, *AGARD Conference Proceedings, Advances in Tactical Rocket Propulsion*.

Fowler, J.R. and Rosenthal (1971) "Missile Environment for Solid Propellant Oscillatory Burning," *7th AIAA/SAE Propulsion Joint Specialist Conference*, AIAA-71-756.

Fox, J.L. (1951) "Preliminary Investigation of Helmholtz Resonators for Damping Pressure Fluctuations in 3.6 Inch Ram Jet at Mach Number 1.90," NACA RM E51CO5.

French, J.C. (2003) "Nonlinear Combustion Stability Prediction of SRMs Using SPP/SSP," *39th AIAA/ASME/SAE/ASEE Joint Propulsion Conference*, AIAA-2003-4668.

French, J.C. and Flandro, G.A. (2003) "Linked Solid Rocket Motor Combustion Stability and Internal Ballistics Analysis," *41st AIAA/ASME/SAE/ASEE Joint Propulsion Conference*, AIAA-2005-3998.

French, J.C. and Flandro, G.A. (2003) "Nonlinear Combustion Stability Prediction with SPP/SSP," *39th JANNAF Combustion Meeting*.

French, J.C., Flandro, G.A. and Majdalani, J. (2004) "Improvements to the Linear Stability Prediction Program (SSP)," *40th AIAA/ASME/SAE/ASEE Joint Propulsion Conference*, AIAA-2004-4181.

Friedlander, M.M., Smith, T.J.B. and Powell, A. (1964) "Experiments on the Rijke Tube Phenomenon," *J. Acoust. Soc. of Amer.*, Vol. 36, pp. 1737–1738.

Friedly, J.C. and Petersen, E.E. (1966) "Influence of Combustion Parameters on Instability in Solid Propellant Motors," *AIAA J.*, Vol. 4, Pt. I: "Development of Model and Linear Analysis," pp. 1604–1609; Pt. II: "Nonlinear Analysis," pp. 1932–1937.

REFERENCES

- Ganichev, A.I. (1984) "Influence of Liquid Rocket Engine Hot Wall Compliance on Low-Frequency Instability," *Soviet Aeronautics*, Vol. 27, pp. 24–28.
- Garrison, G.D. (1972) "Investigation of Damping Methods for Low Frequency Augmentor Instability," *AIAA/SAE 8th Joint Propulsion Specialist Conference*, AIAA Paper 72-1207.
- Garrison, G.D., Russell, P.L. and Stettler (1972) "Investigation of Damping Methods for Augmentor Combustion Instability," Air Force Aero Propulsion Laboratory, Report AFAPL TR-72-84.
- Geckler, R.D. (1954)a "The Mechanism of Combustion of Solid Propellants", in *Selected Combustion Problems: Fundamentals and Aeronautical Applications*, AGARD, Butterworths Scientific Publications, London, pp. 289–339.
- Geckler, R.D. (1954)b "Unsolved Problems in Solid Propellant Combustion," *Fifth (International) Symposium on Combustion*, Reinhold, pp. 29–40.
- Geisler, R.L. (1977) "Summary Report on 1977 JANNAF Aluminum Combustion Workshop," *14th JANNAF Combustion Meeting*, CPIA No. 292, Vol. I.
- Gelb, A. and Vander Velde, W.E. (1968) *Multiple-Input Describing Functions and Nonlinear System Design*, McGraw-Hill Book Co., N.Y.
- Glick, R.L. and Renie, J.P. (1984) "On the Nonsteady Flowfield in Solid Rocket Motors," *20th AIAA/SAE/ASME Joint Propulsion Conference*, AIAA-84-1475.
- Goldstein, M.E. (1976) *Aeroacoustics*, McGraw-Hill Book Company, New York.
- Grad, H. (1949) "Resonance Burning in Rocket Motors," *Communications in Pure and Applied Mathematics*, Vol. 2, pp. 79–102.
- Graham, D. and McRuer, D. (1961) *Analysis of Nonlinear Control Systems*, John Wiley & Sons, Inc., New York.
- Greatrix, D.R. (2005) "Numerical Modeling Considerations for Transient Burning of Solid Propellants," *41st AIAA/ASME/SAE/ASEE Joint Propulsion Conference*, AIAA-2005-4005.
- Green, L., Jr. (1954) "Unstable Burning of Solid Propellants," *Jet Prop.*, Vol. 24, No. 4, pp. 252–253.
- Green, L., Jr. (1956) "Observations on the Irregular Reaction of Solid Propellant Charges," *Jet Prop.*, Vol. 26, No. , pp. 656–659.
- Green, L., Jr. (1958) "Some Properties of a Simplified Model of Solid Propellant Burning," *Jet Prop.* Vol. 28, No. 6, pp. 386–392.
- Green, L. (1958) "Some Effects of Change Configuration in Solid Propellant Combustion," *Jet Prop.* Vol. 28, No. 7, pp. 483–485.

Green, L., Jr. and Nachbar, W. (1958) "A Comment on Combustion Instability in Solid Propellant Rocket Motors," *Jet Prop.*, Vol. 28, No. 9, p. 769.

Green, W.D. (1990) "Triggering of Longitudinal Combustion Instabilities in Rocket Motors," M.S. Thesis, Dept. of Aerospace Engineering, Pennsylvania State University, University Park, PA.

Grenda, J.M., Venkateswaran, S. and Merkle, C.L. (1995) "Application of Computational Fluid Dynamics Techniques to Engine Instability Studies," Chapter 19 in *Liquid Rocket Engine Combustion Instability*, Vol. 169 of AIAA *Progress in Astronautics and Aeronautics*, pp. 503–525.

Grenleski, S.E., Kiersey, J.L., Stevens, C.E. and Dale, L.A. (1977) "Effect of Fuel Injector-Flameholder Configuration on Pressure Distributions in ASAR-ER Combustor," *14th JANNAF Combustion Meeting*, Vol. 3, pp. 49–67.

Grifford, J. and Casalis, G. (2001) "On the Nonparallel Stability of the Injection Induced Two-Dimensional Taylor Flow," *Phys. Fl.* Vol. 13, pp. 1635–44.

Gunder, D.F. and Friant, D.R. (1950) "Stability of Flow in a Rocket Motor," *J. App. Mech.*, Vol. 17, No. 3, pp. 327–333.

Gusachenko, L.K., Zarko, V.E. and Rychkov, A.D. (1999) "Effect of Melting on Dynamic Combustion Behavior of Energetic Materials," *J. Prop. and Power*, Vol. 15, No. 6, pp. 876–882.

Gutmark, E., Ho, C.-M. (1983) "Preferred Modes and the Spreading Rates of Jets," *Phys. Fl.*, Vol. 26, No. 10, pp. 2932–2938.

Gutmark, E., Parr, T.P., Hanson-Parr, D.M. and Schadow, K.C. (1987) "Azimuthal Structure of an Annular Diffusion Flame," *Western States Section of the Combustion Institute*, Spring Meeting, Paper 87–27.

Gutmark, E., Parr, T.P., Hanson-Parr, D.M. and Schadow, K.C. (1989) "On the Role of Large and Small-Scale Structures in Combustion Control," *Comb. Sci. and Tech.*, Vol. 66, pp. 107–126.

Gutmark, E., Parr, T.P., Hansen-Parr, D.M. and Schadow, K.C. (1990) "Stabilization of a Premixed Flame by Shear Flow Excitation," *Comb. Sci. and Tech.*, Vol. 73, pp. 521–535.

Gutmark, E., Parr, T.P., Parr, D.M. and Schadow, K.C. (1986) "Visualization of Vortex Dynamics in Flame Combustion," *Bulletin of the American Physical Society*, Vol. 31, No. 10, p. 1681.

Gutmark, E., Parr, T.P., Parr, D.M. and Schadow, K.C. (1989) "Planar Imaging of Vortex Dynamics in Flames," *Trans. ASME*, Vol. 111, pp. 148–155.

Gutmark, E., Schadow, K.C., Sivasegaram, S. and Whitelaw, S.H. (1991) "Interaction Between Fluid-Dynamic and Acoustic Instabilities in Combusting Flame Within Ducts," *Comb. Sci. and Tech.*, Vol. 79, pp. 161–166.

Gysling, D.L., Copeland, G.S., McCormick, D.C. and Proscia, W.M. (1998) "Combustion System Damping Augmentation with Helmholtz Resonators," ASME Paper 98-GT-268.

REFERENCES

- Habiballah, M., Lourme, D. and Pit, F. (1988) "A Comprehensive Model for Combustion Stability Studies Applied to the Ariane Viking Engine," *26th AIAA Aerospace Sciences Meeting*, Reno, AIAA-88-0086.
- Habiballah, M., Lourme, D. and Pit, F. (1991) "PHEDRE - Numerical Model for Combustion Stability Studies Applied to the Ariane Viking Engine," *J. Propulsion*, Vol. 7, No. 3, pp. 322–329.
- Habiballah, M., Maraffa, L. and Monin, H. (1985) "Numerical Simulation of High Frequencies Instabilities in a Liquid Propellant Engine Through a Combustion Pressure Coupling," *10th International Colloquium on Dynamics of Explosions and Reactive Systems*, Berkeley.
- Habiballah, M. and Monin, H. (1984) "Two-dimensional Model for the Two Phase Flow Simulation in a Viking Rocket Engine Combustion Chamber," *9th International Conference on Numerical Methods in Fluid Dynamics*, SACLAY.
- Habiballah, M., Popp, M. and Yang, V. (Editors) (1995) *Liquid Rocket Combustion Devices*, Second International Symposium on Liquid Rocket Propulsion, ONERA, Châtillon.
- Hackett, R.M. (1985) "Analytical Model of Pulsing of Solid Propellant Rocket Motors," *J. Spacecraft and Rockets*, Vol. 22, No. 10, pp. 201–210.
- Hadwig, S. (1971) "Combustion Instability: System Analysis," *J. Inst. Fuel*, Vol. 44, pp. 550–558.
- Hall, P.H. (1978) "Generic Ordnance Ramjet Engine - GORJE Tests of the Inlet Combustor," Naval Weapons Center, China Lake, NWC TP-6068.
- Hall, P.H. (1980) "Response of Supercritical Inlets to Downstream Pressure Fluctuations," *AIAA/SAE/ASME 16th Joint Propulsion Conference*, AIAA-80-1118.
- Hanson, R.K., Vandsburger, V., Allen, M.G. and McManus, K. (1986) "Effects of Fuel Spray Characteristics and Vaporization on Energy Release Rates and Flow Field Structure in a Dump Combustor," *23rd JANNAF Combustion Meeting*.
- Hardesty, D.R. (1970) "Unsteady Combustion in Gaseous Propellant Rocket Motors," Princeton University Department of Aerospace and Mechanical Sciences, Report T-965, Ph.D. Thesis, Dept. of Aerospace Sciences, Princeton University.
- Harp, J.L., Jr., Velie, W.W. and Bryan, L. (1954) "Investigation of Combustion Screech and a Method of its Control," NACA-RM-E53L24b.
- Harris, P.G. (1994) "Experimental Evaluation of One-Dimensional Design Technology for Linear Combustion Instability," *30th AIAA/ASME/SAE/ASEE Joint Propulsion Conference*, AIAA-94-3191.
- Harris, P.G. and DeChamplain, A. (2000) "Transverse Pressure Waves in Solid Propellant Rocket Motors: Pulse-Triggered Unstable Mode," Chapter 3.8 *Solid Propellant Chemistry, Combustion, and Motor Interior Ballistics*, Vol. 185 of *AIAA Progress in Astronautics and Aeronautics*, Washington, DC.
- Harrje, D.J. and Reardon, F.H. (Ed.) (1972) *Liquid Propellant Rocket Instability*, NASA SP-194.

- Harsha, P.T. and Edelman, R.B. (1982) "Assessment of Modular Ramjet Combustor Model," *J. Spacecraft and Rockets*, Vol. 19, No. 5, pp. 430–436.
- Hart, R.W., Bird, J.F, Cantrell, R.H. and McClure, F.T. (1964) "Nonlinear Effects in Instability of Solid Propellant Rocket Motors," *AIAA J.*, Vol. 2, No. 7, pp. 1270–1273.
- Hart, R.W. and Cantrell, R.H. (1963) "Amplification and Attenuation of Sound by Burning Propellants," *AIAA J.*, Vol. 1, No. 2, pp. 398–404.
- Hart, R.W., Farrell, R.A. and Cantrell, R.H. (1966) "Theoretical Study of a Solid Propellant Having a Heterogeneous Surface Reaction. I-Acoustic Response, Low and Intermediate Frequencies," *Comb. and Flame*, Vol. 10, pp. 367–380.
- Hart, R.W. and McClure, F.T., (1959) "Combustion Instability: Acoustic Interaction with a Burning Surface," *J. Chem. Phys.*, Vol. 30, pp. 1501–1414.
- Hart, R.W. and McClure, F.T., (1964) "Theory of Acoustic Instability in Solid-Propellant Rocket Combustion," in *Tenth (International) Symposium on Combustion*, pp. 1047–1065.
- Harten, A. and Zwas, G. (1972) "Self-Adjusting Hybrid Schemes for Shock Computations," *J. of Computational Physics*, Vol. 9, pp. 568–583.
- Harten, A. (1977) "The Artificial Compression Method for Computation of Shocks and Contact Discontinuities: III. Self-Adjusting Hybrid Schemes," Report prepared for the Air Force Office of Scientific Research, AFOSR TR-77-0659.
- Haymes, W.G. (1969) "Combustion Oscillations in a Dual Thrust Rocket Motor—A Status Report," CPIA No. 192, Vol. II, pp.101–114.
- Heckl, M.A. (1985) "Heat Sources in Acoustic Resonators," Ph.D. Thesis, Cambridge University.
- Heckl, M.A. (1990) "Nonlinear Acoustic Effects in the Rijke Tube," *Acustica*, Vol. 72, pp. 63–71.
- Hefner, R.J. (1966) "Review of Combustion Stability Development with Storable Propellants," *J. Spacecraft*, Vol. 3, No. 7, pp. 1046–1051.
- Hegde, U.G., Reuter, D. and Zinn, B.T. (1990) "Frequency Control in Unstable and Pulse Combustors," *23rd Symposium (International) on Combustion*.
- Hegde, U.G., Reuter, D. and Zinn, B.T. (1988)a "Sound Generation by Ducted Flames," *AIAA J.*, Vol. 26, No. 5, pp. 532–537.
- Hegde, U.G., Reuter, D. and Zinn, B.T. (1988)b "Combustion Instability Mechanisms in Ramjets," *26th AIAA Aerospace Sciences Meeting*, AIAA-88-0150.
- Hegde, U.G., Reuter, D., Daniel, B.R. and Zinn, B.T. (1987) "Flame Driving of Longitudinal Instabilities in Dump Type Ramjet Combustors," *Comb. Sci. and Tech.*, Vol. 55, pp. 125–138.

REFERENCES

- Hegde, U.G., Reuter, D., Zinn, B.T. and Daniel, B.R. (1987) "Fluid Mechanically Coupled Combustion-Instabilities in Ramjet Combustors," *25th AIAA Aerospace Sciences Meeting*, Reno, Nevada, AIAA-87-0216.
- Hegde, U.G., Chen, F. and Zinn, B.T. (1986) "Investigation of the Acoustic Boundary Layer in Porous-Walled Ducts with Flow," *AIAA J.*, Vol. 24, No. 9, pp. 1474-1482.
- Hegde, U.G. and Strahle, W.C. (1985) "Sound Generation by Turbulence in Simulated Rocket Cavities," *AIAA J.*, Vol. 23, No. 1, pp. 71-72.
- Heidmann, M.F. and Humphrey, J.C. (1952) "Fluctuations in a Spray Formed by Two Impinging Jets," *ARS J.*, Vol. xx, No. 3, May-June, pp. 127-138.
- Heidmann, M.F. and Feiler, C.E. (1966) "Evaluation of Tangential Velocity Effects on Spinning Transverse Combustion Instability," NASA TN D-3406.
- Heidmann, M.F. and Wieber, P.R. (1966)a "Analysis of n-Heptane Vaporization in Unstable Combustor With Traveling Transverse Oscillations," NASA TN D-3424.
- Heidmann, M.F. and Wieber, P.R. (1966)b "Analysis of Frequency Response Characteristics of Propellant Vaproization," NASA TN D-3749.
- Heising, R., Lubarsky, E., Neumeier, M., Neumeier, Y. and Zinn, B.T. (2000) "Periodic Liquid Fuel Sprays Combustion Processes and Their Damping of Combustion Instabilities," *39th Aerospace Sciences Meeting*, Paper AIAA-2000-1024.
- Heitor, M.V., Taylor, A.M.K.P. and Whitelaw, J.W. (1984) "Influence of Confinement in Combustion Instabilities of Premixed Flames Stabilized on Axisymmetric Baffles," *Comb. and Flame*, Vol. 57, pp. 109-121.
- Henderson, M.C. and Donnelly, G.J. (1962) "Acoustic Resonance Tube for High Pressures and Low f/p^* ," *J. Acoust. Soc. of Amer.*, Vol. 34, No. 6, pp. 779-784.
- Henderson, B.E. and Lewis, J.S. (1988) "Characteristics of Combustion Driven Pressure Oscillations in Advanced Turbo-Fan Engines with Afterburner," *AGARD 72B Specialists' Meeting of the Propulsion and Energetics Panel*, AGARD CP 450.
- Hendricks, G.J. (1986) "Two Mechanisms of Vorticity Generation in Combusting Flow Fields," Ph.D. Thesis, California Institute of Technology.
- Hersh, A.S. and Walker, B. (1979) "Effect of Grazing Flow in the Acoustical Impedance of Helmholtz Resonators Consisting of Single and Clustered Orifices," NASA Report CR 3177.
- Hessler, R. (1979) "Studies of Motor Instability Problems," *16th JANNAF Combustion Sub-Committee Meeting*.
- Hessler, R. (1980) "Prediction of Finite Pressure Oscillations in Stable Rocket Motors," *17th JANNAF Combustion Sub-Committee Meeting*.

Hessler, R. (1982) "Forced Oscillation Predictions," *19th JANNAF Combustion Sub-Committee Meeting*.

Hessler, R. and Glick, R. (1998) "Application of Maximum Entropy Method to Passively Extract Motor Stability Information," Workshop *Measurement of Thermophysical and Ballistic Properties of Energetic Material*, Politecnico di Milano, Milan, Italy.

Higgens, B. (1802) "On the Sound Produced by a Current of Hydrogen Gas Passing Through a Tube," *Nicholson's J.*, Vol. 1 (New Series), pp. 129–132.

Hildebrand, F.B. (1952) *Methods of Applied Mathematics*, Prentice-Hall, New York.

Hirschfelder, J.O., Curtiss, C.F. and Bird, R.B. (1954) *Molecular Theory of Gases and Liquids*, Wiley and Sons, New York.

Ho, C.M. and Huang, L.S. (1982) "Subharmonics and Vortex Merging in Mixing Layers," *J. of Fluid Mech.*, Vol. 119, p. 443.

Ho, C.M. and Huerre, P. (1984) "Perturbed Free Shear Layers," *Annual Review of Fluid Mechanics*, Vol. 16, p. 365–424.

Hobson, D.E., Fackrell, J.E. and Hewitt, G. (2000) "Combustion Instabilities in Industrial Gas Turbines—Measurements on Operating Plant and Thermoacoustic Modeling," *J. of Eng. for Gas Turb. and Power*, Vol. 122, No. 3, pp. 420–428.

Hoehn, F.W. (1972) "Experimental Evaluation of a 600 LBF Spacecraft Rocket Engine," *AIAA/SAE 8th Propulsion Joint Specialist Conference*, AIAA-72-1129.

Hoffman, R.J., Wright, R.O. and Breen, B.P. (1968) "Combustion Instability Prediction Using a Bipropellant Vaproization Model," NASA CR-920.

Hoffmann, S., Weber, G., Judith, H., Hermann, J. and Orthmann, A. (1998) "Application of Active Combustion Control to Siemens Heavy Duty Gas Turbines," RTO AVT Symposium on *Gas Turbine Engine Combustion, Emissions and Alternate Fuels*, Lisbon, Portugal.

Hong, Z.-C. and Ko, T.-H. (1988) "A Numerical Study on the Three-Dimensional Vortex Motion in a Side-Inlet Dump Cumbustor," *AIAA/ASME/SAE/ASEE 24th Joint Propulsion Specialist Meeting*, AIAA-88-3009.

Horton, M.D. (1960) "Acoustic Admittance of a Burning Solid Surface," *ARS J.*, Vol. 32, pp. 644–646.

Horton, M.D. (1961) "Oscillatory Burning of Solid Rocket Propellants," Ph.D. Thesis, Dept. of Chemical Engineering, University of Utah.

Horton, M.D. (1961) "One-Dimensional Solid Propellant Oscillatory Burner," *ARS J.*, Vol. 31, pp. 1596–1597.

REFERENCES

- Horton, M.D. Eisel, J.L. and Price, E.W. (1963) "Low Frequency Acoustic Oscillatory Combustion," *it AIAA J.*, Vol. 1, No. 11, pp. 2652–2654.
- Horton, M.D. and Price, E.W. (1962) "Dynamic Characteristics of Solid Propellant Combustion," *Ninth (International) Symposium on Combustion*, Academic Press, New York, pp. 303–310.
- Horton, M.D. and Rice, D.W. (1964) "The Effect of Compositional Variables Upon Oscillatory Combustion of Solid Rocket Propellants," *Comb. and Flame*, Vol. 8, pp. 21–28.
- Howe, M.S. (1979) "Attenuation of Sound in a Low Mach Number Nozzle Flow," *J. Fluid Mech.*, Vol. 91, pp. 209–229.
- Howe, M.S. (1998) *Acoustics of Fluid-Structure Interactions*, Cambridge University Press, UK.
- Hsieh, T., Wardlaw, A.B., Jr. and Coakley, T. (1984) "Numerical Simulation of a Ramjet Inlet Flowfield in Response to Large Amplitude Combustion Pressure Oscillations," *AIAA/ASME/SAE 20th Propulsion Joint Specialist Conference*, AIAA-84-1363.
- Hsieh, T. (1986) "Downstream Boundary Effects on the Frequency of Self-Excited Oscillations in Transonic Diffuser Flow," *23rd JANNAF Combustion Meeting*.
- Hsieh, T. and Coakley, T.J. (1987) "Downstream Boundary Effects on the Frequency of Self-Excited Oscillations in Transonic Diffuser Flows," *25th AIAA Aerospace Sciences Meeting*, AIAA-87-0161.
- Hsieh, K. C., Yang, V. and Tseng, I. S. (1988) "Navier-Stokes Calculations of Solid-Propellant Rocket Motor Internal Flowfields," *AIAA/ ASME/SAE/ASEE 24th Joint Propulsion Conference*, AIAA-88-3181.
- Huang, I-T. and Micci, M.M. (1991) "Unsteady Gas Phase Analysis of Homogeneous Solid Propellant Combustion," *Comb. Sci. and Tech.*, Vol. 75, pp. 73–88.
- Huang, Y. and Yang, V. (2004) "Effect of Swirl on Combustion Dynamics in a Lean-Premixed Swirl-Stabilized Combustor," *Proc. of the Combustion Institute*, Vol. 30, pp. 1771–1778.
- Hubbard, S. and Dowling, A.P. (1998) "Acoustic Instabilities in Premix Burners," *4th AIAA/CEAS Aeroacoustics Conference*, Toulouse, AIAA-98-2272.
- Huggett, C. Bartley, C.E. and Mills, M.M. (1960) *Solid Propellant Rockets*, Princeton University Press, Princeton, NJ.
- Hughes, I.J. and Dowling, A.P. (1990) "The Absorption of Sound by Perforated Linings," *J. Fluid Mech.*, Vol. 218, pp. 299–335.
- Hughes, P.M. and Smith, D.L. (1979) "Nonlinear Combustion Instability in Solid Propellant Rocket Motors — Influence of Geometry and Propellant Formulations," *53rd AGARD Specialists Meeting of the Propulsion and Energetics Panel, AGARD Conference Proceedings*, No. 259.
- Hulka, J. and Huff, J.J. (1995) "Instability Phenomena in Liquid Oxygen/Hydrogen Propellant Rocket Engines," Chapter 2 in *Liquid Rocket Engine Combustion Instability*, of AIAA *Progress in Astronautics and*

Aeronautics, Vol. 169, Washington, DC.

Humphrey, J.W. III (1987) "Linear and Nonlinear Acoustics with Nonuniform Entropy in Combustion Chambers," Ph.D. Thesis, Mechanical Engineering, California Institute of Technology.

Humphrey, J.W. and Culick, F.E.C. (1986) "Linear Coupling of Acoustics and Entropy and Acoustic Stability in Ramjet Combustion Chambers Containing a Plane Flame," *23rd JANNAF Combustion Meeting*.

Humphrey, J.W. and Culick, F.E.C. (1987)a "Linear and Nonlinear Stability of Acoustics with Nonuniform Entropy in Chambers with Mean Flow," *AIAA 19th Fluid Dynamics, Plasma Dynamics and Laser Conference*, AIAA-87-1417.

Humphrey, J.W. and Culick, F.E.C. (1987)b "Acoustic Energy Interactions in Ramjet Combustion Chambers," *23rd AIAA/SAE/ASME/ASEE Joint Propulsion Meeting*, AIAA-87-1872.

Humphrey, J.W. and Culick, F.E.C. (1987)c "Pressure Oscillations and Acoustic-Entropy Interactions in Ramjet Combustion Chambers," *23rd AIAA/SAE/ASME/ASEE Joint Propulsion Meeting*, AIAA-87-1872.

Hurle, I.R., Price, R.B., Sugden, T.M. and Thomas, A. (1968) "Sound Emission from Open Turbulent Premixed Flames," *Proc. Roy. Soc. of London*, A303, pp. 409–507.

Ibiricu, M.W. and Williams, F.A. (1975) "Influence of Externally Applied Thermal Radiation on the Burning Rates of Homogeneous Solid Propellants," *Comb. and Flame*, Vol. 24, pp. 185–198.

Iljukhin, V.S., Levichek, M.I., Margolin, A.D. and Pokhil, P.F. (1970) "Investigation of Propellant Combustion Acoustic Instability with Methods of High Speed Film Recording," *Vibrational Combustion in Model Installations*, edited by A.D. Margolin, Kazan Univ., Kazan Russia, pp. 81–90.

Im, H.G. and Chen, J.H. (2000) "Effects of Flow Transients of the Burning Velocity of Laminar Hydrogen/Air Premixed Flames," *Proc. of the Comb. Inst.*, Vol. 28, pp. 1833–1840.

Ingard, U. and Ising, H. (1967) "Acoustic Nonlinearity of an Orifice," *J. Acoust. Soc. of Amer.*, Vol. 42, No. 1, pp. 6–17.

Ingard, U. and Labate, S. (1950) "Acoustic Circulation Effects and the Nonlinear Impedance of Orifices," *J. Acoust. Soc. of Amer.*, Vol. 22, No. 2, pp. 211–218.

Ingard, U. (1953) "On the Theory and Design of Acoustic Resonators," *J. Acoust. Soc. of Amer.*, Vol. 25, No. 6, pp. 1037–1061.

Ioos, G. and Joseph, D. (1980) *Elementary Stability and Bifurcation Theory*, Springer-Verlag, New York.

Isella, G. (2001) "Modeling and Simulation of Combustion Chamber and Propellant Dynamics and Issues in Active Control of Combustion Instabilities," Ph.D. Thesis, California Institute of Technology.

Isella, G. and Culick, F.E.C. (2000) "Modeling the Combustion Response Function with Surface and Gas Phase Dynamics," *38th AIAA Aerospace Sciences Meeting*, AIAA-2000-0310.

REFERENCES

- Istratov, A.G. and Librovich, V.B. (1964) "On the Stability of Propellant Combustion," *Zh. Prikl. Mekh. I Tekh. Fiz.*, No. 5, pp. 38–43.
- Ivanov, S.M. and Tsukanov, N.A. (2000) "Estimate of the Dynamic Characteristics of Unsteady Combustion of a Solid Propellant in a Semi-Closed Volume from Measurements of Variable Pressure," *Comb., Expl. and Sh. Waves*, Vol. 38, No. 1, pp. 71–80.
- Ivanov, S.M. and Tsukanov, N.A. (2002) "Estimate of the Dynamic Characteristics of Unsteady Combustion of a Solid Propellant in a Semi-Closed Volume from Measurements of Variable Pressure," *Comb. Expl. and Shock Waves*, Vol. 38, pp. 71–80.
- Iwan, W.D. (1973) "A Generalization of the Concept of Equivalent Linearization," *Int. J. Non-Linear Mech.*, Vol. 8, pp. 279–287.
- Iwan, W.D. (1974) "Application of Nonlinear Analysis Techniques," ASME Symposium, Volume AMD8, pp. 135–161.
- Jackson, T.L. and Buckmaster, J. (2002) "Heterogeneous Propellant Combustion," *AIAA J.*, Vol. 40, No. 6, pp. 1122–1130.
- Jahnke, C. and Culick, F.E.C. (1994) "Application of Dynamical Systems Theory to Nonlinear Combustion Instabilities," *J. Prop. and Power*, Vol. 10, No. 4, pp. 508–517.
- Jahnke, E. and Emde, F. (1938) *Tables of Functions With Formulas and Curves*, G.E. Stechert, New York.
- Janardan, A., Daniel, B.R., Bell, W.A. and Zinn, B.T. (1979) "Measurements of Reactive Gaseous Rokets' Admittances," *Comb. Sci. and Tech.*, Vol. 20, pp. 185–193.
- Janus, M.C. and Richards, G.A. (1996) "Results of a Model for Premixed Combustion Oscillations," *Proceedings of the 1996 AFRC International Symposium*, American Forest Resource Council.
- Jaqua, V.W. and Ferrenberg, A.J. (1989) "The Art of Injector Design," *Threshold*, No. 4, published by Rockwell International Corporation.
- Jeffreys, H. and Jeffreys, B.S. (1946) *Methods of Mathematical Physics*, Cambridge University Press, UK.
- Jensen, R.C. (1971) "A Mathematical Model for the Amplitude of Acoustic Pressure Oscillation in Solid Rocket Motors," *8th JANNAF Combustion Meeting*, CPIA No. 220, Vol. I.
- Jensen, R.C. and Beckstead, M.B. (1972) "Nonlinear Analysis of Combustion Instability Data," *10th JANNAF Combustion Meeting*, CPIA No. 231, Vol. II, pp. 163–177.
- Jensen, R.J., Dodson, H. and Trueblood, B. (1988) "Oxygen/Methane Combustion Stability Investigation," *Advanced Earth-to-Orbit Technology Conference*, Huntsville, AL (May 1988).
- Johnson, C.E., Neumeier, Y., Neumeier, M., Zinn, B.T., Darling, D.D. and Sattinger, S.S. (2001) "Demonstration of Active Control of Combustion Instabilities on a Full-Scale Gas Turbine Combustor," *ASME Turbo*

Expo 2001, Paper 2001-GT-0519.

Johnson, R.G., McIntosh, A.C. and Brindley, J. (1994) "Nonlinear Oscillations of Premixed Flames Caused by Sharp Pressure Changes," *Comb. Sci. and Tech.*, Vol. 99.

Jones, A.T. (1945) "Singing Flames," *J. Acoust. Soc. of Amer.*, Vol. 16, No. 4, pp. 254–266.

Jones, H. (1977) "The Mechanics of Vibrating Flames in Tubes," *Proceedings of the Royal Society of London Series A*, Vol. 353, pp. 459–473.

Joos, F. and Vortmeyer, D. (1986) "Self-Excited Oscillations in Combustion Chambers with Premixed Flames and Several Frequencies," *Comb. and Flame*, Vol. 65, pp. 253–262.

Jou, W.-H. and Menon, S. (1986) "Numerical Simulation of the Vortex Acoustic Wave Interaction in a Dump Combustor," *24th AIAA Aerospace Sciences Meeting*, Reno, Nevada, AIAA-86-0002.

Jou, W.-H. and Menon, S. (1990) "Modes of Oscillation in a Nonreacting Ramjet Combustor Flow," *J. Prop. and Power*, Vol. 6, No. 5, pp. 535–543.

Kahn, P.B. (1990) *Mathematical Methods for Scientists and Engineers. Linear and Nonlinear Systems*, John Wiley & Sons, New York.

Kailasanath, K., Gardner, J.H., Boris, J.P. and Oran, E.S. (1985) "Acoustic-Vortex Interactions in an Idealized Ramjet Combustor," *22nd JANNAF Combustion Meeting*.

Kailasanath, K., Gardner, J.H., Oran, E.S. and Boris, J.P. (1986) "Numerical Simulation of Combustion Oscillation in Compact Ramjets," *Proceedings of the 1986 JANNAF Propulsion Meeting*.

Kailasanath, K., Gardner, J., Boris, J. and Oran, E (1986) "Numerical Simulations of the Flowfield in a Central-Dump Ramjet Combustor. I. Tests of the Model and Effects of Forcing," Naval Research Laboratory, Washington, D.C., NRL Memorandum Report.

Kailasanath, K., Gardner, J.H., Boris, J.P. and Oran, E.S. (1987)a "Numerical Simulations of Acoustic-Vortex Interactions in a Central-Dump Combustor," *J. Propulsion*, Vol. 3, No. 6, pp. 525–533.

Kailasanath, K., Gardner, J.H., Boris, J.P. and Oran, E.S. (1987)b "Acoustic-Vortex Interactions and Low Frequency Oscillations in Axisymmetric Combustors," *25th AIAA Aerospace Sciences Meeting*, AIAA-87-0165.

Kailasanath, K., Gardner, J.H., Boris, J.P. and Oran, E.S. (1989) "Acoustic-Vortex Interactions and Low-Frequency Oscillations in Axisymmetric Combustors," *J. Prop.*, Vol. 5, pp. 165–171.

Karagozian, A.R. and Manda, V.S. (1990) "Flame Structure and Fuel Consumption in the Field of a Vortex Pair," *Comb. Sci. and Tech.*, Vol. 49, pp. 185–200.

Karagozian, A.R. and Marble, F.E. (1986) "Study of a Diffusion Flame in a Stretched Vortex," *Comb. Sci. and Tech.*, Vol. 45, pp. 65–84.

REFERENCES

- Karthik, B., Kumar, B.M. and Sujith R.I. (2000) "Exact Solutions to One-dimensional Acoustic Fields with Temperature Gradient and Mean Flow," *Acoust. Soc. Am.*, Vol. 108, No. 1, pp. 38–43.
- Kaskan, W.E. and Noreen, A.E. (1955) "High Frequency Oscillations of a Flame Held by a Bluff Body," *ASME Transactions*, Vol. 77, pp. 885–895.
- Katsuki, M. and Whitelaw, J.H. (1986) "The Influence of Duct Geometry on Unsteady Premixed Flames," *Comb. and Flame*, V. 63, pp. 87–94.
- Katto, Y. and Sajiki, A. (1977) "Onset of Oscillation of Gas Column in a Tube Due to the Existence of Heat Conduction Field," *Bulletin of the JSME*, Vol. 20, No. 147, pp. 1161–1168.
- Keller, J.J., Vaneveld, L., Korschelt, D., Hubbard, G.L., Ghoniem, A.F., Daily, J.W. and Oppenheim, A.K. (1982) "Mechanisms of Instabilities in Turbulent Combustion Leading to Flashback," *AIAA J.*, Vol. 20, No. 2, pp. 254–262.
- Keller, J.J. and Daily, J.W. (1985) "The Effects of Highly Exothermic Chemical Reaction on a Two-Dimensional Mixing Layer," *AIAA J.*, Vol. 23, No. 12, pp. 1937–1945.
- Keller, J.J. (1995) "Thermoacoustic Oscillations in Combustion Chambers of Gas Turbines," *AIAA J.*, Vol. 33, No. 12, pp. 2280–2287.
- Kendrick, D.W. (1995) "An Experimental and Numerical Investigation into Reacting Vortex Structure Associated with Unstable Combustion," Ph.D. Thesis, Jet Propulsion Center, Mechanical Engineering, California Institute of Technology.
- Kendrick, D.W., Anderson, T.J., Sowa, W.A. and Snyder, T.W. (1999) "Acoustic Sensitivities of Lean-Premixed Fuel Injectors in a Single Nozzle Rig," *J. Eng. for Gas Turb. and Power*, Vol. 121, No. 3, pp. 429–436.
- Kenworthy, M.J., Bahr, D.W., Mungur, P., Burrus, D.L. and Mehta, J.M. (1988) "Dynamic Instability Characteristics of Aircraft Turbine Engine Combustors," *AGARD 72B Specialists' Meeting of the Propulsion and Energetics Panel*, AGARD CP 450.
- Kenworthy, M.J., Woltmann, I.E. and Corley, R.C. (1974) "Augmentor Combustion Stability Investigation," Air Force Aero Propulsion Laboratory, Report AFAPL-TR-74-61.
- Kevorkian, G. and Cole, J. (1996) *Multiple Scale and Singular Perturbation Methods*, Springer, New York.
- Kidin, N., Librovich, V., Roberts, J. and Vuillermoz, M. (1984) "On Sound Sources in Turbulent Combustion," Vol. 95 of *AIAA Progress in Astronautics and Aeronautics*, pp. 343–355.
- Kim, J.S. (1995) "Effects of Turbulence on Linear Acoustic Instability: Spatial Inhomogeneity," Chapter 16 in *Liquid Rocket Engine Combustion Instability*, of *AIAA Progress in Astronautics and Aeronautics*, Washington, DC.

- Kim, S.I. (1989) "Nonlinear Combustion Instabilities in Combustion Chambers," Ph.D. Thesis, Mechanical Engineering, Pennsylvania State University, University Park, PA.
- King, M.K. (1979) "Erosive Burning of Composite Solid Propellants: Experimental and Modeling Studies," *J. Spacecraft and Rockets*, Vol. 16, No. 3, pp. 154–162.
- King, M.K. (1980) "Composite Propellant Modeling," AIAA-80-1124.
- Kochevets, S., Buckmaster, J. and Jackson, T.L. (2000) "Random Propellant Packs and the Flames They Support," AIAA-2000-3461.
- Kolesnikov, K.S. (1972) *Longitudinal Vibrations of Rockets with Liquid Fuel Engines*, Foreign Technology Division, Wright Patterson Air Force Base, FTD-HC-23-1198-72.
- Kooker, D. E. (1974) "Numerical Solution of Axial-Mode Instability Problems in Solid Propellant Rocket Motors," Ballistic Research Laboratory Contract Report No. 141.
- Kooker, D.E. and Zinn, B.T. (1973)a "Triggering Axial Mode Instabilities in Solid Rockets and T-Burners," AIAA-73-1298.
- Kooker, D.E. and Zinn, B.T. (1973)b "Numerical Solution of Axial Instabilities in Solid Propellant Rocket Motors," *10th JANNAF Combustion Meeting*.
- Kopasakis, G. (2003) "High-Frequency Instability Suppression Controls in a Liquid-Fueled Combustor," *39th AIAA/ASME/SAE/ASEE Joint Propulsion Conference and Exhibit*, AIAA-2003-1458.
- Korman, H. F. and Micheli, P. L. (1971) "Nonlinear Particulate Damping of Acoustic Oscillations," *8th JANNAF Combustion Conference*.
- Kotake, S. (1975) "On Combustion Noise Related to Chemical Reactions," *J. Sound and Vib.*, Vol. 43, No. 3, pp. 399–410.
- Kovasznay, L.S.G. (1953) "Turbulence in Supersonic Flow," *J. Aero. Sci.*, Vol. 20, pp. 657–682.
- Kraeutle, K.J. (1977) "Particle Size Analysis of Aluminized Propellants," Preprint AIAA-77-978.
- Kraeutle, K.J., Derr, R.L. Mathes, H.B. and Dehority, G.L. (1976) "Combustion Instability Studies Using Metallized Solid Propellants: Additional Evidence for the Validity of Particle Damping Theory," *13th JANNAF Combustion Meeting*, CPIA No. 281, Vol. II, pp. 155–166.
- Kraeutle, K.J., Mathes, H.B. and Derr, R.L. (1979) "The Role of Particulate Damping in the Control of Combustion Instability by Aluminum Combustion," *AGARD Conference Proceedings*, No. 259, pp. 15.1–15.14.
- Krebs, W., Bethke, S., Lepers, J., Flohr, P., Prade, B., Johson, C. and Sattinger, S. (2005) "Thermoacoustic Design Tools and Passive Control: Siemens Power Generation Approaches," *Progress in Astronautics and*

REFERENCES

- Aeronautics*, Vol. 210, Chapter 5 of *Combustion Instabilities in Gas Turbine Engines: Operational Experience, Fundamental Mechanisms, and Modeling*, (T.C. Lieuwen and V. Yang, Editors).
- Krebs, W., Flohr, P., Prade, B. and Hoffmann, S. (2003) "Thermoacoustic Stability Chart for High Intense Gas Turbine Combustion Systems," *Comb. Sci. Tech.*, Vol. 174, pp. 99–128.
- Krieg, H.C., Jr. (1962) "Tangential Mode of Combustion Instability," *ARS Progress in Astronautics and Rocketry: Detonation and Two-Phase Flow*, Vol. 6, Edited by S.S. Penner and F.A. Williams, Academic Press, New York.
- Krier, H. and Hafenrichter, T.J. Editors (2002) "Technical Report: Pressure-Coupled Response Function Measurements by Various Techniques for MURI Propellants," Department of Mechanical Engineering, University of Illinois at Urbana-Champaign, Report UILU-ENG-2002-4003.
- Krier, H., Tien, J., Sirignano, W.A. and Summerfield, M. (1968) "Nonsteady Burning Phenomenon of Solid Propellants: Theory and Experiment," *AIAA J.*, Vol. 6, No. 2, pp. 278–285.
- Krüger, U., Hüren, J., Hoffmann, S., Krebs, W., Flohr, P. and Bohn, D. (2001) "Prediction and Measurement of Thermoacoustic Improvements in Gas Turbines with Annular Combustion Systems," *J. of Eng. for Gas Turb. and Power*, Vol. 123, pp. 557–566.
- Kruse, R.B. and Glick, R.L. (1979) "Velocity-Coupled Instability in Prototype RS MK36 Motors," *16th JANNAF Combustion Conference*, Monterey, CA.
- Kruse, R.B., Glick, R.L. and Cohen N.S. (1979) "Stability Aspects of Prototype RS MK 36 Motors," CPIA No. 297, Vol. 2, pp. 43–53.
- Krylov, N. and Bogoliubov, N.N. (1947) *Introduction to Nonlinear Mechanics*, Princeton University Press.
- Kubota, N. (2002) "Propellants and Explosives: Thermochemical Aspects of Combustion," Wiley–VCH GmbH, Weinheim, Germany.
- Kuentzmann, P. and Laverdant, A. (1984) "Experimental Determination of the Response of a Solid Propellant to High Frequency Pressure Oscillations," *La Recherche Aerospatiale*, No. 1, pp. 39–55.
- Kuentzmann, P. and Nadaud, L. (1975) "Réponse des Propergols Solides aux Oscillations de Pression et de Vitesse," *Comb. Sci. and Tech.*, Vol. 11, pp. 119–139.
- Kumar, B.M. and Sujith, R.I. (1998) "Exact Solution for One-dimensional Acoustic Fields in Ducts with Polynomial Mean Temperature Profiles," *J. Vib. and Acoustics*, Vol. 120, No. 4, pp. 965–969.
- Kumar, R.N. (1973) "Condensed Phase Details in the Time-Independent Combustion of AP/Composite Propellants," *Comb. Sci. and Tech.*, Vol. 8, No. 2, pp. 133–148.
- Kumar, R.N. and Culick, F.E.C. (1977) "Role of Condensed Phase Details in the Oscillatory Combustion of Composite Propellants," *Comb. Sci. and Tech.*, Vol. 15, No. 2, pp. 179–199.

Kuo, K.K., Gore, J.P. and Summerfield, M. (1984) "Transient Burning of Solid Propellants," *Fundamentals of Solid-Propellant Combustion*, of AIAA *Progress in Astronautics and Aeronautics*, Vol. 90, edited by K.K. Kuo and M. Summerfield, New York, pp. 599–659.

Kuznetsov, A.A., Margolin, A.D., Pokhil, P.F. and Svetlichnyi, B. (1970) "Interaction of Gaseous and Condensed Phases of Vibration Powder Burning," *Vibrational Combustion in Model Installations*, edited by A.D. Margolin, Kazan Univ., Kazan, Russia, pp. 90–100.

Kwon, Y.-P. and Lee, B.-H. (1985) "Stability of the Rijke Thermoacoustic Oscillation," *J. Acoust. Soc. of Amer.*, Vol. 78, No. 4, pp. 1414–1420.

Kychakoff, G., Howe, R.D., Hanson, R.K. and McDaniel, J.C. (1982) "Quantitative Visualization of Combustion Species in a Plane," *Applied Optics*, Vol. 21, pp. 3225–3227.

Landau, L.D. and Lifschitz, E.M. (1959) *Fluid Mechanics*, Addison-Wesley Publishing Co.

Landsbaum, E., Kuby, W.C. and Spaid, F.W. (1960) "Experimental Investigations of Unstable Burning in Solid Propellant Rocket Motors," in *Progress in Astronautics and Rocketry: Solid Propellant Rocket Research*, Vol. 1, M. Summerfield, ed., Academic Press, New York, pp. 495–525.

Lang, W., Poinsot, T. and Candel, S. (1987): "Active Control of Combustion Instability," *Comb. and Flame*, Vol. 70, pp. 281–289.

Langhorne, P.J. (1988) "Reheat Buzz: An Acoustically Coupled Combustion Instability. Part 1. Experiment." *J. of Fluid Mech.*, Vol. 193, pp. 417–443.

Laudien, E., Pongratz, R., Pierro, R. and Preelik, D. (1995) "Experimental Procedure Aiding the Design of Acoustic Cavities," Chapter 14 in *Liquid Rocket Engine Instability*, of AIAA *Progress in Astronautics and Aeronautics*, Vol. 169, V. Yang and W. Anderson (Editors).

Laverdant, A.M., Poinsot, T. and Candel, S.M. (1986) "Influence of the Mean Temperature Field on the Acoustic Mode Structure in a Dump Combustor," *AIAA/SAE/ASME 21st Joint Propulsion Conference*, Monterey, CA, also in *J. Prop. and Power*, Vol. 2, July–August.

Laverdant, A.M. and Candel, S.M. (1987)a "A Numerical Analysis of a Diffusion Flame Vortex Interaction," *SIAM Conference on Numerical Combustion*, San Francisco, CA.

Laverdant, A.M. and Candel, S.M. (1987)b "Computation of Diffusion and Premixed Flames Rolled up in Vortex Structures," *23rd AIAA/SAE/ASME/ASEE Joint Propulsion Conference*, San Diego, CA.

Laverdant, A.M. and Candel, S.M. (1989) "Computation of Diffusion and Premixed Flames Rolled up in Vortex Structures," *J. Propulsion*, Vol. 5, No. 2, pp. 134–143.

Laverdant, A.M. and Candel, S.M. (1988) "A Numerical Analysis of a Diffusion Flame-Vortex Interaction," *Comb. Sci. and Tech.*.

REFERENCES

- Lavrentjev, J. and Åbom, M. (1996) "Characterization of Fluid Machines as Acoustic Multiport Sources," *J. Sound and Vib.*, Vol. 197, pp. 1–16.
- Lawn, C.J. (1982) "Criteria for Acoustic Pressure Oscillations to be Driven by a Diffusion Flame," *Nineteenth (International) Symposium on Combustion*, The Combustion Institute, pp. 237–244.
- Lax, P.D. and Wendroff, B. (1960) "System of Conservation Laws," *Comm. on Pure and App. Math.*, Vol. 13, pp. 217–237.
- Lazmi and Clavin (1992) "Theoretical Analysis of Oscillatory Burning of Homogeneous Solid Propellant Including Non-Steady Gas Effects," *Comb. Sci. and Tech.*, Vol. 83, pp. 1–32.
- Lebedinsky, E. and Mosolov, S. (2000) "Experimental Method of Effectiveness Estimation of Different Damped Measures for Oscillations in LRE Combustion Chambers and Gas Generators," *Proc. Fourth Int'l Symp. on Liquid Space Prop.*, Heilbronn, Germany.
- LeBreton, P., Guéry, J.-F., Vuillot, F. and Prévost, M. (1999) "Recent Advances in the Prediction of SRM Thrust Oscillations," *Premier Colloque Européen sur la Technologie des Lanceurs-Vibrations des Lanceurs*, Toulouse, France.
- Leconte, J. (1858) "On the Influence of Musical Sounds on the Flame of a Jet of Coal-Gas," *Phil. Mag.*, S.4, Vol. 15, pp. 235–239.
- Lecourt, R., Fouceud, R. and Keuntzmann, P. (1986) "Experimental Study of the Acoustical Sensitivity of Liquid Fuel Rocket Motors Injectors," *La Recherche Aerospatiale* (English edition), pp. 11–22.
- Lecourt, R. and Foucaud, R. (1987) "Experiments on Stability of Liquid Propellant Rocket Motors," *AIAA/SAE/ASME/ASEE 23rd Joint Propulsion Conference*, San Diego, California, AIAA-87-1772.
- Ledder, G. and Kapila, A.K. (1991) "The Response of Premixed Flames to Pressure Perturbations," *Comb. Sci. and Tech.*, Vol. 76, pp. 21–44.
- Lee, D.S. and Anderson, T.J. (1999) "Measurements of Fuel/Air—Acoustic Coupling in Lean Premixed Combustion Systems," *37th AIAA Aerospace Sciences Meeting*, AIAA-99-0450.
- Lee, J.G., Kim, K. and Santavicca, D.A. (2000) "Measurement of Equivalence Ratio Fluctuation and Its Effect on Heat Release During Unstable Combustion," *Proc. of the Comb. Inst.*, Vol. 28, pp. 415–421.
- Lee, S.-T., Seo, S., Broda, J.C., Pal, S. and Santoro, R.J. (2000) "An Experimental Estimation of Mean Reaction Rate and Flame Structure During Combustion Instability in a Lean Premixed Gas Turbine Combustor," *Proc. of the Comb. Inst.*, Vol. 28, pp. 775–782.
- Lee, Y.C., Gore, M.R. and Ross, C.C. (1953) "Stability and Control of Liquid Propellant Rocket Systems," *ARS J.*, Vol. 23, pp. 75–81.
- Legendre, D. (1986) "Internal Acoustics in Turbomachinery," *Rech Aerosp.*, 1986–3, pp. 75–79.

LeHalley, P. (1994) "Etude Théorique et Experimentale des Instabilités de Combustion et de leur Contrôle dans un Brûleur Luminaire Prémélangé," Ph.D. Thesis, École Centrale Paris.

Leipunskii, O.I. (1945) "The Physical Bases of the Internal Ballistics of Rocket Motors," D.Sc. Thesis, Institute of Chemical Physics, USSR Academy of Sciences, Moscow.

Lengellé G. (1975) "A Model Describing the Erosive Combustion and Velocity Response of Composite Propellants," *AIAA J.*, Vol. 13, No. 3, pp. 315–322.

Lengellé, G., Kuentzmann, P. and Rendolet, C. (1974) "Response of a Solid Propellant to Pressure Oscillations," AIAA-74-1209.

Lenoir, J.M. and Robillard, G. (1953) "A Mathematical Model to Predict the Effects of Erosive Burning in Solid Propellant Rockets," *Sixth Symposium (International) on Combustion*, Reinhold Publishing Corp., pp. 663–667.

Levine, H. and Schwinger, J. (1948) "On the Radiation of Sound From an Unflanged Circular Pipe," *Phys. Revs.*, Vol. 73, pp. 383–406.

Levine, R.S. (1958) "Development Problems in Large Liquid Rocket Engines," in AGARD (1958) *Combustion and Propulsion*.

Levine, R.S. (1964) "Experimental Status of High Frequency Liquid Rocket Combustion Instability," *Tenth (International) Symposium on Combustion*, The Combustion Institute, pp. 1083–1099.

Levine, J.N. and Andrepon, W.C. (1979) "Measurement Methods of Transient Combustion Response Characteristics of Solid Propellant—An Assessment," *AIAA/SAE/ASME 15th Joint Propulsion Conference*, AIAA-79-1200.

Levine, J.N. and Baum, J.D. (1982) "Modeling of Nonlinear Combustion Instability in Solid Propellant Rocket Motors," *Nineteenth (International) Symposium on Combustion*, The Combustion Institute, Pittsburgh, PA.

Levine, J.N. and Baum, J.D. (1983) "A Numerical Study of Nonlinear Instability Phenomena in Solid Rocket Motors," *AIAA J.*, Vol. 212, No. 4, pp. 557–564.

Levine, J.N., Baum, J.D. and Lamine, R.L. (1984) "Pulse-Triggered Instability in Solid Rocket Motors," *AIAA J.*, Vol. 22, No. 10, pp. 1413–1419.

Levine, J.N. and Baum, J.D. (1988) "Pulsed Instability in Rocket Motors: A Comparison Between Predictions and Experiments," *J. Prop. and Power*, Vol. 4, No. 4, pp. 308–316.

Levine, J.N. and Culick, F.E.C. (1972) "Numerical Analysis of Nonlinear Longitudinal Combustion Instability in Metalized Solid-Propellant Rocket Motors, Vol. 1 Analysis and Results," Ultrasystems, Inc., Report prepared for the Air Force Rocket Propulsion Laboratory, AFRPL TR-72-88.

REFERENCES

- Levine, J.N. and Culick, F.E.C. (1974) "Nonlinear Analysis of Solid Rocket Combustion Instability," Ultra-systems, Inc., Report prepared for the Air Force Rocket Propulsion Laboratory, AFRPL TR-74-45.
- Levine, J.N., Fuchs, M.D. and Park, T.W. (1988) "Particle Damping of Nonlinear Longitudinal-Mode Oscillations," *AIAA/ASME/SAE/ASEE 24th Joint Propulsion Conference* AIAA-88-2943.
- Lewis Laboratory Staff (1954) "Summary of Preliminary Investigations into the Characteristics of Combustion Screech in Ducted Burners," NACA TR 1384.
- Lewis, B. and von Elbe, G. (1961) "Combustion, Flames and Explosions of Gases," Academic Press, Inc., NY.
- Lewis, G.D. and Garrison, G.D. (1971) "The Role of Acoustic Absorbers in Preventing Combustion Instability," *AIAA/SAE 7th Propulsion Joint Specialist Conference*, AIAA-71-699.
- Lewis, J.S. (1967) "The Effect of Local Fuel Concentration on Reheat Jet Pipe Vibrations," *Proceedings of the International Symposium on Combustion in Advanced Gas Turbine Systems*, Cranfield.
- Li, Y.T. (1953) "Dynamic Pressure Measuring Systems for Jet Propulsion Research," *ARS J.*, Vol. 23, No. 3, May–June, pp. 124–127; 145.
- Liang, P.-Y., Fisher, S. and Chang, Y.M. (1986) "Comprehensive Modeling of a Liquid Rocket Combustion Chamber," *J. Propulsion*, Vol. 2, No. 2, pp. 97–104.
- Liang, P.-Y., Fisher, S. and Chang, Y.M. (1987) "Numerical Analysis of SSME Preburner Injector Atomization and Combustion Processes," *J. Propulsion*, Vol. 3, No. 6, pp. 508–513.
- Liang, P.-Y. and Schumann, M.D. (1987) "A Numerical Investigation of the Flame-Holding Mechanism Downstream of a Coaxial Injection Element," *24th JANNAF Combustion Meeting*.
- Liang, P.-Y., Charakhani, A. and Jensen, R. (1987) "A Finite Difference Analysis of Wave Damping and Acoustic Cavities," *24th JANNAF Combustion Meeting*.
- Lieuwen, T. (2002) "Experimental Investigation of Limit Cycle Oscillations in an Unstable Gas Turbine Combustor," *J. Prop. and Power*, Vol. 18, No. 1, pp. 61–67.
- Lieuwen, T. (2003) "Analytical Modeling of Combustion-Acoustic Wave Interactions: A Review," *J. Prop. and Power*, Vol. 11, No. 22, pp. 222–444.
- Lieuwen, T. (2003) "Modeling Premixed Combustion-Acoustic Wave Interactions: A Review," *J. Prop. and Power*, Vol. 19, No. 5, pp. 765–781.
- Lieuwen, T. (2003) "Statistical Characteristics of Pressure Oscillations in a Premixed Combustor," *J. Sound and Vib.*, Vol. 260, pp. 3–17.
- Lieuwen, T. and Neumeier, Y. (2002) "Nonlinear Pressure-Heat Release Transfer Function Measurements in a Premixed Combustor," *29th Symposium (International) on Combustion*, The Combustion Institute, pp. 99–105.

- Lieuwen, T. (2001) "Phase Drift Characteristics of Self Excited, Combustion Driven Oscillations," *J. Sound and Vib.*, Vol. 242, No. 5, pp. 893-905.
- Lieuwen, T., Torres, H., Johnson, C and Zinn, B.T. (2001) "A Mechanism of Combustion Instability in Lean Premixed Gas Turbine Combustors," *Trans. of the ASME, J. of Eng. for Gas Turb. and Power*, Vol. 123, pp. 182–189.
- Lieuwen, T. and Zinn, B.T. (2000) "On the Experimental Determination of Combustion Process Driving in an Unstable Combustor," *Comb. Sci. and Tech.*, Vol. 157, pp. 111–127.
- Lieuwen, T., Neumeier, Y. and Zinn, B.T. (1998) "The Role of Unmixedness and Chemical Kinetics in Driving Combustion Instabilities in Lean Premixed Combustors," *Comb. Sci. and Tech.*, Vol. 135, pp. 193–211.
- Lieuwen, T. and Zinn, B.T. (1998) "The Role of Equivalence Ratio Oscillations in Driving Combustion Instabilities in Low NO_x Gas Turbines," *Twenty-Seventh (International) Symposium on Combustion*, The Combustion Institute, Vol. 27, pp. 1809–1816.
- Lighthill, M.J. (1949) "A Technique for Rendering Approximate Solutions to Physical Problems Uniformly Valid," *Phil. Mag.*, Vol. 40, pp. 1179–1201.
- Lin, C.C. (1954) "On a Perturbation Theory Based on the Method of Characteristics," *J. Math. Phys.*, Vol. 33, pp. 117–134.
- Liou, T.-M. and Wu, S.-M. (1988) "Flow Field in a Dual-Inlet Side-Dump Combustor," *J. Prop. and Power*, Vol. 4, No. 1, pp. 53–60.
- Liou, T.-M., Hwang, Y.-H. and Hung, Y.-H. (1988) "Computational Study of Flow Field in Side Inlet Ramjet Combustors," *AIAA/ASME/SAE/ASEE 24th Joint Propulsion Specialist Meeting*, AIAA-88-3010.
- Lord Rayleigh (1878) "The Explanation of Certain Acoustic Phenomena," *Royal Institution Proceedings*, Vol. VIII, pp. 536–542.
- Lord Rayleigh (1945) *Theory of Sound*, Vol. 2, Dover, New York, Section 322g, pp. 232–234.
- Lord Rayleigh (1945) *The Theory of Sound*, Dover Publications, New York.
- Lores, E.M. and Zinn, B.T. (1972) "The Prediction of Nonlinear Longitudinal Combustion Instability in Liquid Propellant Rockets," NASA CR 12094.
- Lores, E.M. and Zinn, B.T. (1973) "Nonlinear Longitudinal Combustion Instability in Rocket Motors," *Comb. Sci. and Tech.*, Vol. 7, pp. 245–256.
- Lourme, D. and Schmitt, D. (1983) "Les moyens nécessaires à l'étude fondamentale des instabilités de combustion d'une moteur biliquide," IAF Paper No. 82-364, 33rd IAF Congress, Paris, 1982, and *Astronautica Acta*, Vol. 10, No. 12, pp. 761–775.

REFERENCES

- Lourme, D., Schmitt, D. and Brault, F. (1984) "Experimental Characterization of the Spray Originating from an Impinging-Jet Injector in a Liquid Rocket Engine," *Acta Astronautica*, Vol. 11, pp. 469–482.
- Lourme, D., Schmitt, D. and Brault, F. (1985) "Experimental Characterization of a Spray Formed by Two Impinging Jets in Liquid Rocket Injector," *3rd International Conference on Liquid Atomization and Spray Systems (ICLASS)*, London.
- Lourme, D. (1986) "Like-on-like Injector Spray Characterization for the Ariane Viking Engine," *AIAA/SAE/ASME 22nd Joint Propulsion Conference*, Huntsville, Alabama, AIAA-86-1444.
- Louwers, J. and Gadiot, G.M.H.J.L. (1999) "Model for Nonlinear Transient Burning of Hydrazine Nitroformate," *J. Prop. and Power*, Vol. 15, No. 6, pp. 778–782.
- Lovett, J.A. and Uzmanski, K.T. (2002) "Prediction of Combustion Dynamics in a Staged Premixed Combustor," ASME Paper GT-2002-30646.
- Lovine, R.L., Dudley, D.P. and Waugh, R.C. (1976) "Standardized Stability Prediction Method for Solid Rocket Motors," Vol. I, II and III. Aerojet Solid Propulsion Company, Rocket Propulsion Laboratory, AFRPL TR-76-32.
- Lovine, R.L., Baum, J.D. and Levine, J.N. (1985) "Ejecta Pulsing of Subscale Solid Propellant Rocket Motors," *AIAA J.*, Vol. 23, No. 3, pp. 416–423.
- Lupoglazoff, N. and Vuillot, F. (1992) "Numerical Simulations of Vortex Shedding Phenomenon in 2D Test Case Solid Rocket Motors," *30th AIAA Aerospace Sciences Meeting*, AIAA-92-0776.
- Lupoglazoff, N. and Vuillot, F. (1996) "Parietal Vortex Shedding as a Cause of Instability for Long Solid Propellant Motors—Numerical Simulations and Comparisons with Firing Tests," *34th AIAA Aerospace Sciences Meeting*, AIAA-96-0761.
- Lupoglazoff, N. and Vuillot, F. (1998) "Numerical Simulation of Parietal Vortex-Shedding Phenomenon in a Cold Flow Set-Up," *34th AIAA Aerospace Sciences Meeting*, AIAA-98-3220.
- Lupoglazoff, N. and Vuillot, F. (1999) "Simulations of Solid Propellant Rocket Motors' Instability Including Propellant Combustion Response," *6th International Congress on Sound and Vibration*, Lyngby, Denmark.
- Lupoglazoff, N., Vuillot, F., Dupays, J. and Fabignon, Y. (2002) "Numerical Simulations of the Unsteady Flow Inside Segmented Solid-Propellant Motors With Burning Aluminum Particles," *40th AIAA Aerospace Sciences Meeting*, AIAA-2002-0784.
- Lupoglazoff, N., Vuillot, F., Dupays, J. and Fabignon, Y. (2002) "Numerical Simulations of the Unsteady Flow Inside Ariane 5 P230 SRM Booster With Burning Aluminum Particles," *2nd European Conf. on Launcher Technology*, Paper 87.
- Ma, Y., Van Moorhem, W.K. and Shorthill, R.M. (1990) "An Innovative Method of Investigating the Role of Turbulence in the Velocity Coupling Phenomenon," *Transactions of the ASME, J. Vibration and Acoustics*, Vo. 112, pp. 550–555.

- Ma, Y., Van Moorhem, W.K. and Shorthill, R.M. (1991) "Experimental Investigation of Velocity Coupling in Combustion Instability," *J. Prop. and Power*, Vol. 7, No. 5, pp. 692–699.
- MacDonald, N. (1993) "Choices in the Harmonic Balance Technique," *J. Phys. A: Math. Gen.*, V. 26, pp. 6367–6377.
- Mach, K.D. (1971) "Systems Aspects of Augmentor Combustion Instability," AIAA/SAE 7th Propulsion Joint Specialist Conference, AIAA-71-697.
- Macquisten, M.A. and Dowling, A.P. (1993) "Combustion Oscillations in a Twin-stream Afterburner," *J. Sound and Vib.*, Vol. 188, No. 4, pp. 545–560.
- Macquisten, M.A. and Dowling, A.P. (1993) "Low-Frequency Combustion Oscillations in a Model Afterburner," *Comb. and Flame*, Vol. 94, pp. 253–264.
- Madarame, H. (1981) "Thermally Induced Acoustic Oscillations in a Pipe," *Bulletin of the JSME*, Vol. 24, No. 195, pp. 1626–1633.
- Magiawala, K. and Culick, F.E.C. (1979) "Measurements of Energy Exchange Between Acoustic Fields and Non-Uniform Steady Fields," *J. of Vibration and Sound*, Vol. 75, pp. 503–517.
- Majdalani, J. (1999) "Vortical and Acoustic Mode Coupling Inside a Two-Dimensional Cavity with Transpiring Walls," *J. Acoust. Soc. of Amer.*, Vol. 106, No. 1, pp. 46–56.
- Majdalani, J. (2005) "The Taylor-Culick Profile with Uniform Headwall Injection," 41st AIAA/ASME/SAE/ASEE Joint Propulsion Conference, AIAA-2005-4534.
- Majdalani, J. and Flandro, G.A. (2002) "The Oscillatory Pipe Flow with Arbitrary Wall Injection," *Proc. Roy. Soc., Series A*, Vol. 458, pp. 1621–1651.
- Majdalani, J. and Roh, T.-S. (2000) "The Oscillatory Channel Flow with Large Wall Injection," *Proc. Roy. Soc., Series A*, Vol. 456, pp. 1625–1657.
- Majdalani, J., Flandro, G.A. and Roh, T.-S. (2000) "Convergence of Two Flowfield Models Predicting a Destabilizing Agent in Rocket Combustion," *J. Prop. and Power*, Vol. 16, pp. 492–497.
- Majdalani, J. and Van Moorhem, W.K. (1997) "Multiple-Scales Solution to the Acoustic Boundary Layer in Solid Rocket Motors," *J. Prop. and Power*, Vol. 13, No. 2, pp. 186–193.
- Majdalani, J. and Van Moorhem, W.K. (1998) "Improved Time-Dependent Flowfield Solution for Solid Rocket Motors," *AIAA J.* Vol. 36, No. 2, pp. 241–248.
- Male, T., Kerslake, W.P. and Tischler, A.O. (1954) "Photographic Study of Rotary Screaming and Other Oscillations in a Rocket Engine," NACA RM E54A29.
- Malhotra, S. (2004) "On Combustion Instability in Solid Rocket Motors," Ph.D. Thesis, Jet Propulsion Center, Aeronautics, California Institute of Technology.

REFERENCES

- Malina, F.J. (1940) "Characteristics of the Rocket Motor Unit Based on the Theory of Perfect Gases," *J. of the Franklin Institute*, Vol. 230, No. 4, October, pp. 433–454.
- Maling, G.C., Jr. (1963) "Simplified Analysis of the Rijke Tube Phenomenon," *J. Acoust. Soc. of Amer.*, pp. 1058–1060.
- Marble, F.E. and Cox, D.W., Jr. (1953) "Servo-Stabilization of Low-Frequency Oscillations in a Liquid Bipropellant Rocket Motor," *ARS J.*, pp. 63–81.
- Marble, F.E. (1955) "Servo-Stabilization of Low-Frequency Oscillations in Liquid Propellant Rocket Motors," *ZAMP*, Vol. VI/1, pp. 1–35.
- Marble, F.E. (1963) "Dynamics of a Gas Containing Small Solid Particles." In *Combustion and Propulsion*, 5th AGARD Colloquium, Pergamon Press, pp. 175–213.
- Marble, F.E. (1969) "Some Gasdynamic Problems in the Flow of Condensing Vapors," *Astronautica Acta*, Vol. 14, pp. 585–614.
- Marble, F.E. (1970) "The Dynamics of Dusty Gases," *Annual Reviews of Fluid Mechanics*, Vol. 2, pp. 397–446.
- Marble, F.E. (1973) "Acoustic Disturbance From Gas Non-Uniformities Connecting Through a Nozzle," *Symposium on Transportation Noise*, Stanford University, Vol. 1.
- Marble, F.E. (1985) "Growth of a Diffusion Flame in the Field of a Vortex," *Recent Advances in the Aerospace Sciences* (C. Casci, Ed.), pp. 395–413.
- Marble, F.E. and Candel, S.M. (1978) "An Analytical Study of the Non-Steady Behavior of Large Combustors," *Seventeenth (International) Symposium on Combustion*, pp. 761–769.
- Marble, F.E. and Wooten, D.C. (1970) "Sound Attenuation in a Condensing Vapor," *Physics of Fluids*, Vol. 13, pp. 2657–2664.
- Marchenko, U.N. and Timoshenko, V.I. (1970) "Investigation of the Thermal Generation of Sound in a Rijke Tube," *Soviet Physics-Acoustics*, Vol. 16, No. 2, pp. 274–275.
- Margolin, A.D. (1961) "Combustion Instability," Ph.D. Dissertation, Institute of Chemical Physics, USSR Academy of Sciences, Kazan Univ., Kazan, Russia.
- Margolin, A.D., Svetlichnyi, I.B. and Pokhil, P.F. (1970) "Effect of Pressure and Sample Geometry on Acoustic Instability of Powder Burning in Semi-confined Volume," *Vibrational Combustion in Model Installations*, edited by A.D. Margolin, Kazan Univ., Kazan, Russia, pp. 100–117.
- Margolin, A.D., Svetlichnyi, I.B. and Pokhil, P.F. (1970) "Nonlinear Self-Excitation of Vibrational Burning," *Vibrational Combustion in Model Installations*, edited by A.D. Margolin, Kazan Univ., Kazan, Russia, pp. 117–135.

- Margolin, A.D., Svetlichnyi, I.B., Pokhil, P.F. and Tsyrul'nikov, A.C. (1970) "Acoustic Conductivity Recording of Burning Powder Surface," *Journal of Applied Mechanics and Technical Physics*, No. 1, pp. 149–153.
- Margolin, A.D. (1999) "Early Investigations of Solid-Propellant Combustion Instability in Russia," *J. Propulsion*, Vol. 15, No. 6, pp. 922–925.
- Markham, J.J. (1952) "Second-Order Acoustic Fields: Energy Relations," *Phys. Rev.*, Vol. 86, No. 5, pp. 712–714.
- Markham, J.J. (1953) "Second-Order Acoustic Fields: Relations Between Energy and Intensity," *Phys. Rev.*, Vol. 89, No. 5, pp. 972–977.
- Markstein, G.H. (1951)a "Experimental and Theoretical Studies of Flame-Front Stability," *J. Aero. Sci.*, Vol. 18, No. 3, pp. 199–209.
- Markstein, G.H. (1951)b "Interaction of Flow Pulsations and Flame Propagation," *J. Aero. Sci.*, Vol. 18, No. 6, pp. 428–429.
- Markstein, G.H. (1964) *Nonsteady Flame Propagation*, The MacMillan Company, New York.
- Marone, I.Y. and Tarakanovskii, A.A. (1967) "Investigation of Sound Generation in a Rijke Tube," *Soviet Physics-Acoustics*, Vol. 13, No. 2, pp. 261–263.
- Marone, I.Y. and Tarakanovskii, A.A. (1967) "Investigation of Sound Generation in a Rijke Tube," *Soviet Physics-Acoustics*, Vol. 13, No. 2, pp. 302–304.
- Marxman, G.A. and Wooldridge, C.E. (1968) "Effects of Surface Reactions on the Solid Propellant Response Function," *AIAA J.*, Vol. 6, No. 3, pp. 468–471.
- Marxman, G.A. and Wooldridge, C.E. (1971) "Finite-Amplitude Axial Instability in Solid-Rocket Combustion," *12th (International) Symposium on Combustion*, pp. 115-127.
- Maslen, S.H. and Moore, F.K. (1956) "On Strong Transverse Waves Without Shocks in a Circular Cylinder," *J. Aero Sci.*, Vol. 23, pp. 583–593.
- Mason, D.R., Folkman, S.L. and Behring, M.A. (1979) "Thrust Oscillations of the Space Shuttle Solid Rocket Booster Motor During Static Tests," AIAA-79-1138.
- Mathes, H.B. (1992) "Applications of Combustion-Stability Technology to Solid-Propellant Rocket Motors," in *Nonsteady Burning and Combustion Stability of Solid Propellants*, of AIAA *Progress in Astronautics and Aeronautics*, Vol. 143, pp. 781–804.
- Mathes, H.B. (1980) "Assessment of Chamber Pressure Oscillations in the Shuttle Solid Rocket Booster Motors," AIAA-80-1091.
- Mathes, H.B. and Price, E.W. (1975) "Methods for Determining Characteristics of Acoustic Waves in Rocket Motors," *J. of Spacecraft and Rockets*, Vol. 12, No. 1, pp. 39–43.

REFERENCES

- Mathes, H.B., Price, E.W., Summerfield, M. and Krier, H. (1968) "Entropy Waves Produced in Oscillatory Combustion of Solid Propellants," *Third ICRPG/AIAA Solid Propulsion Conference*, Atlantic City, NJ.
- Matsui, Y. (1981) "An Experimental Study in Pyro-Acoustic Amplification of Premixed Laminar Flames," *Comb. and Flame*, Vol. 43, pp. 199–209.
- Matthews, J. and Walker, R.L. (1964) *Mathematical Methods of Physics*, W.A. Benjamin, New York.
- Matveev, K.I. (2004) "Vortex-Acoustic Instability in Chambers with Mean Flow and Heat Release," *Technical Acoustics*, Vol. 14, pp. 1–15.
- Matveev, K.I. and Culick, F.E.C. (2002)a "Experimental and Mathematical Modeling of Thermoacoustic Instabilities in a Rijke Tube," *40th AIAA Aerospace Sciences Meeting and Exhibit*, Reno, NV, USA, AIAA-2002-1013.
- Matveev, K.I. and Culick, F.E.C. (2002)b "A Model for Combustion Instability due to Vortex Shedding in Rocket Motors," *9th International Congress on Sound and Vibration*, Orlando, FL, USA.
- Matveev, K.I. and Culick, F.E.C. (2002)c "On the Nonlinear Characteristics of a Rijke Tube," *9th International Congress on Sound and Vibration*, Orlando, FL, USA.
- Matveev, K.I. and Culick, F.E.C. (2003)a "A Model for Combustion Instability Involving Vortex Shedding," *Comb. Sci. and Tech.*, Vol. 175, No. 6, pp. 1059–1083.
- Matveev, K.I. and Culick, F.E.C. (2003)b "Limit-Cycle Properties of a Rijke Tube," *Technical Acoustics*, Vol. 12, pp. 1–13.
- Matveev, K.I. and Culick, F.E.C. (2003)c "A Study of the Transition to Instability in a Rijke Tube with Axial Temperature Gradient," *J. Sound and Vib.*, Vol. 264, No. 3, pp. 689–706.
- Mayhue, R.J. (1962) "NASA Scout ST-1 Flight Test Results and Analyses," NASA TN D-1240, pp. 37–38; pp. 69–71.
- McClure, F.T., Bird, J.F. and Hart, R.W. (1960) "The Influence of Erosive Burning on Acoustic Instability in Solid Propellant Rocket Motors," *Progress in Astronautics and Rocketry*, Vol. I, Solid Propellant Rocket Research, Academic Press, pp. 425–451.
- McClure, F.T., Bird, J.F. and Hart, R.W. (1962) "Erosion Mechanisms for Nonlinear Instability in the Axial Modes of Solid Propellant Rocket Motors," *J. Amer. Acoust. Soc.*, Vol. 32, pp. 374–385.
- McClure, F.T., Bird, J.F. and Hart, R.W. (1962) "Erosion Mechanism for Nonlinear Stability in Axial Modes of Solid Propellant Rocket Motors," *ARS J.*, Vol. 32, pp. 374–378.
- McClure, F.T., Hart, R.W. and Bird, J.F. (1960)a "Solid Propellant Rocket Motors as Acoustic Oscillators," in *Solid Propellant Rocket Research, of Progress in Astronautics and Rocketry*, Vol. 1, M. Summerfield, ed., Academic Press, New York, pp. 561–602.

- McClure, F.T., Hart, R.W. and Bird, J.F. (1960)b "Acoustic Resonance in Solid Propellant Rockets," *Jr. Appl. Phys.*, Vol. 31, pp. 884–896.
- McFarlane, D.C. and Glover, K. (1992) "A Loop Shaping Design Procedure Using H_∞ Synthesis," *IEEE Trans. on Auto. Cont.*, Vol. 37, No. 6, pp. 759–769.
- McIntosh, A.C. (1986) "The Effect of Upstream Acoustic Forcing and Feedback on the Stability and Resonance Behavior of Anchored Flames," *Comb. Sci. and Tech.*, Vol. 49, pp. 143–167.
- McIntosh, A.C. (1987) "Combustion-Acoustic Interaction of a Flat Flame Burner System Enclosed Within an Open Tube," *Comb. Sci. and Tech.*, Vol. 54, pp. 217–236.
- McIntosh, A.C. (1990) "On Flame Resonance in Tubes," *Comb. Sci. and Tech.*, Vol. 69, pp. 147–152.
- McManus, K. and Lieuwen, T. (2002) "That Elusive Hum," *Mech. Eng. Power*, June.
- Menon, S. and Jou, W.-H. (1988) "Simulations of Self-Sustained Oscillatory Non-Reacting Flows in a Ramjet Combustor," Submitted to Physics of Fluids; based on AIAA-87-1421, *AIAA 19th Fluid Dynamics, Plasma Dynamics and Lasers Conference* (1987).
- Menon, S. and Jou, W.-H. (1991) "Large Eddy Simulations of Combustion Instability in a Ramjet Combustor," *Comb. Sci. and Tech.*, Vol. 75, pp. 53–72.
- Meridith, K.V., Beckstead, M.W. and Waroquet, C. (2001) "CFD Analysis of the T-Burner," *37th AIAA/ASME/SAE/ASEE Joint Prop. Conf.*, AIAA-2001-3430.
- Merk, H.J. (1956)a "An Analysis of Unstable Combustion of Premixed Gases," *6th (International) Symposium on Combustion*, pp. 500–512.
- Merk, H.J. (1956)b "Analysis of Heat-Driven Oscillations," *Appl. Sci. Res.*, Vol. A7, pp. 175–191.
- Merk, H.J. (1957)a "Analysis of Heat-Driven Oscillations of Gas Flows I. General Considerations," *Appl. Sci. Res.*, Vol. A6, pp. 317–335.
- Merk, H.J. (1957)b "Analysis of Heat-Driven Oscillations of Gas Flows II. On the Mechanisms of the Rijke Tube Phenomenon," *Appl. Sci. Res.*, Vol. A6, pp. 402–420.
- Merkli, P. and Thomann, H. (1975) "Transition to Turbulence in Oscillating Pipe Flow," *J. Fl. Mech.*, Vo. 68, Part 3, pp. 567–576.
- Micci, M.M. (1986) "Workshop Report: Methods for Measuring Solid Propellant Combustion Responses," CPIA No. 457, pp. 51–57.
- Micci, M.M., Caveny, L.H. and Sirignano, W.A. (1979) "Linear Analysis of Forced Longitudinal Waves in Rocket Motor Chambers," *AIAA J.*, Vol. 19, No. 2, pp. 198–204.

REFERENCES

- Micci, M.M. and Caveny, L.H. (1980) "MHD Measurement of Acoustic Velocities in Rocket Motor Chambers," *AIAA J.*, Vol. 20, No. 4, pp. 516–521.
- Michalke, A. (1965) "On Spatially Growing Disturbances in an Inviscid Shear Layer," *J. Fluid Mech.*, Vol. 25, Pt. 4, pp. 683–704.
- Micheli, P.L. and Schmidt, W.G. (1977) "Behavior of Aluminum in Solid Rocket Motors," Air Force Rocket Propulsion Laboratory, Report AFRPL-TR-77-29.
- Mickelson, W.R. and Baldwin, L.V. (1957) "Aerodynamic Mixing in a High-Intensity Standing-Wave Sound Field," *J. Acoust. Soc. of Amer.*, Vol. 29, No. 1, pp. 46–49.
- Mihlfeith, C.M., Baer, A.D. and Ryan, N.W. (1972) "Propellant Combustion Instability as Measured by Combustion Recoil," *AIAA J.* Vol. 10, No. 10, pp. 1280–1285.
- Mikolowsky, W.T. (1968) "Three-Dimensional Combustion Instability in Liquid-Propellant Rocket Engines: Parametric Study," *AIAA Student Journal*, Vol. 7, pp. 179–184.
- Minorsky, N. (1947) "Introduction to Non-Linear Mechanics," J.W. Edwards, Ann Arbor, MI.
- Minorsky, N. (1942) "Self-Excited Oscillations in Dynamical Systems Possessing Retarded Actions," *Transactions ASME, J. App. Mech.*, pp. A65–A71.
- Minorsky, N. (1962) *Nonlinear Oscillations*, Van Nostrand, N.Y.
- Mitchell, C.E. (1967) "Axial Mode Shock Wave Combustion Instability in Liquid Propellant Rocket Engines," Ph.D. Thesis, Department of Aerospace and Mechanical Sciences, Princeton University; published as NASA CR 72259.
- Mitchell, C.E. (1969) "Stability Limits for a Liquid Rocket Engine Using a Droplet Vaporization Model," *AIAA 5th Propulsion Joint Specialist Conference*, AIAA-69-483.
- Mitchell, C.E. (1970) "The Effect of Entropy Waves on High Frequency Pressure Oscillations in Liquid Rocket Motors," *Comb. Sci. and Tech.*, Vol. 1, pp. 269–274.
- Mitchell, C.E. (1972) "Stability of Combustors With Partial Length Acoustic Liners," *Comb. Sci. and Tech.*, Vol. 6, pp. 61–70.
- Mitchell, C.E. (1984) "An Integral Closed Loop Combustion Stability Model — Status and Review," *21st JANNAF Combustion Meeting*.
- Mitchell, C.E. (1985) "Improvement of and Integral Stability Model," *22nd JANNAF Combustion Meeting*.
- Mitchell, C.E. (1993) "Preventing and Suppressing Combustion Instabilities: Passive and Active Means," in *Combustion Instability in Liquid Rocket Engines* (Ed. H.F.R. Schoyer) European Space Agency Report esa WPP-062.

- Mitchell, C.E. and Baer, M.R. (1975) "Stability Predictions for Combustors with Acoustic Absorbers and Continuous Combustion Distributions," *AIAA J.*, Vol. 13, No. 8, pp. 1107–1109.
- Mitchell, C.E., Crocco, L. and Sirignano, W.A. (1969) "Nonlinear Longitudinal Instability in Rocket Motors with Concentrated Combustion," *Comb. Sci. and Tech.*, Vol. 1, pp. 35–64.
- Mitchell, C.E., Dodd, F.E. (1987) "Two Dimensional Acoustic Cavity Models," *24th JANNAF Combustion Meeting*.
- Mitchell, C.E., Dodd, F.E., Hudson, T.J. and Howell, D.J. (1986) "Acoustic Cavity Model Development," *23rd JANNAF Combustion Meeting*.
- Mitchell, C.E. and Eekert, K. (1979) "A Simplified Computer Program for the Prediction of the Linear Stability Behavior of Liquid Propellant Combustors," NASA CR 3169.
- Mitchell, C.E., Howell, D.J., Dodd, F.E. and Acker, T.L. (1987) "User's Manual for the Multidimensional Baffle Model Computer Programs," Mechanical Engineering Preort, Colorado State University.
- Mitchell, C.E., Howell, D.J. and Fang, J.J. (1987) "An Improved Predictive Model for Injector Face Baffles," *24th JANNAF Combustion Meeting*.
- Mitchell, C.E. and Jotiban, Y. (1976) "Wave Distortion Effects on Vaporization Limited Combustion Stability," *13th JANNAF Combustion Meeting*.
- Mitchell, J.P. (1965) "Advanced Throttling Concept Study," Pratt and Whitney, Report AFRPL TR-65-98.
- Mohanraj, R. and Zinn, B.T. (1998) "Numerical Study of Active Control Systems for Combustion Instabilities," *36th AIAA Aerospace Sciences Meeting*, AIAA-98-0356.
- Molavi, K. and Sirignano, W.A. (1988) "Computational Analysis of Acoustic Instabilities in Dump Combustor Configuration," *AIAA/ASME/SAE/ASEE 24th Joint Propulsion Specialist Meeting*, AIAA-88-2856.
- Mongia, R.K., Dibble, R.W. and Lovett, J. (1998) "Measurement of Air-Fuel Ratio Fluctuations Caused by Combustor Driven Oscillations," ASME Paper 98-GT-304.
- Mongia, H.C., Gore, J.P., Grinstein, F.F., Gutmark, E.J., Jeng, S.-M., McDonnel, V.G., Menon, S., Samuelson, G.S., Santavicca, D. and Santoro, R.G. (2001) "Combustion Research Needs for Helping Development of Next Generation Advanced Combustors," *37th AIAA/ASME/SAE/ASEE Joint Propulsion Conference*, AIAA-2001-3853.
- Mongia, H.C., Held, T.J., Hsiao, G.C. and Pandalai, R.P. (2005) "Incorporation of Combustion Instability Issues into Design Process: GE Aeroderivative and Aero Engines Experience," *Progress in Astronautics and Aeronautics*, Vol. 210, Chapter 3 of *Combustion Instabilities in Gas Turbine Engines: Operational Experience, Fundamental Mechanisms, and Modeling*, (T.C. Lieuwen and V. Yang, Editors).
- Mongia, H.C., Held, T.J., Hsiao, G.C. and Pandalai, R.P. (2003) "Challenges and Progress in Controlling Dynamics in Gas Turbine Compressors," *J. Prop. and Power*, Vol. 19, No. 5, pp. 822–829.

REFERENCES

- Mongia, R.K., Tomita, E., Hsu, F.K., Talbot, L. and Dibble, R.W. (1996) "Use of an Optical Probe for Time-Resolved *In situ* Measurement of Local Air-to-Fuel Ratio and Extent of Fuel Mixing with Applications to Low NOx Emissions in Premixed Gas Turbines," *Proc. of the Comb. Inst.*, Vol. 26, pp. 2749–2755.
- Mongia, R.K., Torres, J., Dibble, R., Lee, D., Anderson, T. and Sowa, W. (1999) "Fast Response Extraction Probe for Measurement of Air-Fuel Ratio Fluctuations in lean Premixed Combustors," ASME Paper 99-GT-277.
- Moore, F.K. and Maslen, S.H. (1954) "Transverse Oscillations in a Cylindrical Combustion Chamber," NACA-TN-3152.
- Moreau, R., Candel, S.M., Piquemal, J.P. and Borghi, R. (1981) "Phénomènes d'instabilité dans un foyer turbulent," *First International Specialists' Meeting of the Combustion Institute*, Bordeaux.
- Morfouace, V. and Tissier, P.Y. (1995) "Two-Phase Flow Analysis of Instabilities Driven by Vortex-Shedding in Solid Rocket Motors," *31st AIAA/ASME/ASEE Joint Propulsion Conference and Exhibit*, AIAA-95-2733.
- Morphy, C.L. (1971) "Acoustic Energy in Non-Uniform Flows," *J. Sound and Vib.*, Vol. 14, No. 2, pp. 159–170.
- Morris, E.P. (1965) "A Pulse Technique for the Evaluation of Combustion Instability in Solid Propellant Rockets," *Can. Aero. and Space J.*, Vol. 11, pp. 329–333.
- Morse, P.M. (1936) *Vibration and Sound*, McGraw-Hill Book Co., New York.
- Morse, P.M. and Feshbach, H. (1953) *Methods of Theoretical Physics, Part I*, and *Methods of Theoretical Physics, Part II*, McGraw-Hill Book Co., New York.
- Morse, P. and Ingard, K.U. (1968) *Theoretical Acoustics*, McGraw-Hill Book Co., New York.
- Mugridge, B.D. (1980) "Combustion Driven Oscillations," *J. Sound and Vib.*, Vol. 70, pp. 437–452.
- Munjal, M.L. (1987) *Acoustics of Ducts and Mufflers with Application to Exhaust and Ventilation System Design*, Wiley, New York.
- Murray-Lasso, M.A. (1966) "The Model Analysis and Synthesis of Linear Distributed Control Systems," Sc.D. Dissertation, Massachusetts Institute of Technology.
- Muss, J.A. and Peiper, J.L. (1987) "Performance and Stability Characterization of LOX/Hydrocarbon Injectors," *1987 JANNAF Propulsion Conference*.
- Muss, J.A. and Peiper, J.L. (1988) "Performance and Stability Characterization of LOX/Hydrocarbon Injectors," *AIAA/SAE/ASME/ASEE 24th Joint Propulsion Specialist Conference*.
- Nachbar, W. and Green, L., Jr. (1959) "Analysis of a Simplified Model of Solid Propellant Resonant Burning," *J. Aerospace Sci.*, Vol. 26, No. 8, pp. 518–526.

- Nachbar, W. and Green, L., Jr. (1960) "Closure," *ARS J.*, Vol. 30, No. 6, pp. 576–577.
- Nagel, R.T., Denham, J.W. and Papothanasian, A.G. (1983) "Supersonic Jet Screech Tone Cancellation," *AIAA J.*, Vol. 21, No. 11, pp. 1541–1545.
- Nair, S. and Lieuwen, T. (2005) "Acoustic Detection of Blowout in Premixed Flames," *J. Prop. and Power*, Vol. 21, No. 1, pp. 32–39.
- Nair, S., Murugunandam, T., Olsen, R., Meyer, A., Seitzman, J., Zinn, B.T., Lieuwen, T., Held, T. and Mongia, H. (2004) "Lean Blowout Detection in a Single Nozzle, Swirl Cup Combustor," *42nd AIAA Aerospace Sciences Meeting*, Paper AIAA-2004-0138.
- Najon, H.N. and Ghoniem, A.F. (1993) "Modeling Pulsating Combustion due to Flow-Flame Interactions in Vortex Stabilized Pre-Mixed Flames," *Comb. Sci. and Tech.*, Vol. 94, pp. 259–278.
- Narendra, K. and Annaswamy, A. (1989) *Stable Adaptive Systems*, Prentice-Hall International.
- NASA Design Criteria Office (1974) "Liquid Rocket Engine Combustion Stabilization Devices," NASA SP-8113.
- Natanzon, M.S. (1999) *Unsteady Combustion in Liquid Rocket Engines*, Electronic translation from the Russian edition (1984) with a revised Chapter 8 on Bifurcations; translation editor F.E.C. Culick.
- Natanzon, M.S. and Menshikova, O.M. (1992) "Bifurcation of Steady Combustion Regimes and Their Influence on the Onset of High-Frequency Oscillations in Combustion Chambers," *Physics of Combustion and Explosion*, Vol. 23, No. 4, pp. 10–18.
- Natanzon, M.S., Lapina, Z.S. and Merkerlov, I.V. (1985) "Combustion Stability in a Combustion Chamber," *Doklady, AN USSR, Series Power Engineering and Transport*, No. 4, pp. 137–146.
- Naudascher, E. and Rockwell, D. (Ed.) (1980) *Practical Experiences with Flow-Induced Vibrations*, Springer-Verlag, Berlin.
- Naudascher, E. and Rockwell, D. (1994) *Flow-Induced Vibrations*, A.A. Balkema, Rotterdam.
- Nayfeh, A.H. and Mook, D.T. (1979) *Nonlinear Oscillations*, Wiley, N.Y.
- Nelson, P.A. and Elliott, S.J. (1992) *Active Control of Sound*, Academic Press, New York.
- Nestlerode, J.A. and Oberg, C.L. (1969) "Combustion Instability in an Annular Engine," *6th ICRPG Combustion Conference*.
- Neumann, E.-G. (1974) "An Impedance Condition for Avoiding Acoustic Oscillations Generated by Flames," *Acustica*, Vol. 30, pp. 229–235.

REFERENCES

- Neuringer, J.L. and Hudson, G.E. (1952) "An Investigation of Sound Vibrations in a Tube Containing a Heat Source," *J. Acoust. Soc. of Amer.*, Vol. 24, pp. 667-674.
- Nguyen, T.V. and Muss, J.A. (1987) "Modification of the Agosta-Hammer Vaporization Response Model for the Prediction of High Frequency Combustion Stability," *24th JANNAF Combustion Meeting*.
- Nguyen, T.V. (1988) "An Improved High-Frequency Combustion Stability Model," *AIAA/ASME/SAE/ASEE 24th Joint Propulsion Conference*, AIAA-88-2853.
- Nicholls, J.A. and Cullen, R.E. (1965) "Gaseous Detonation Studies in an Annular Rocket Motor Chamber," *First ICRPG Combustion Instability Conference*, CPIA No. 68, p. 165-184.
- Nicholson, H.M. and Radcliffe, A. (1953) "Pressure Fluctuations in a Jet Engine," *British J. App. Phys.*, Vol. 4, pp. 359-364.
- Nickerson, G. R., Culick, F.E.C. and Dang, L.G. (1983) "Standard Stability Prediction Method for Solid Rocket Motors: Axial Mode Computer Program, User's Manual," Software and Engineering Associates, Inc. Report prepared for the Air Force Rocket Propulsion Laboratory, AFRPL TR-83-017.
- Nickerson, G. and Nguyen, T.K. (1984)a "A Computer Program for Modeling Steady-State Combustion in a Rocket Engine Thrust Chamber," Software and Engineering Associates, Inc.
- Nickerson, G. and Nguyen, T.K. (1984)b "A Computer Program for Prediction of Combustion Instability Using a Nonlinear Bipropellant Vaporization Model," Software and Engineering Associates, Inc.
- Nicoli, C. and Pelcé, P. (1989) "One-Dimensional Model for the Rijke Tube," *J. Fluid Mech.*, Vol. 202, pp. 83-96.
- Niculescu, S. and Annaswamy, A. (2000) "A Simple Adaptive Controller for Positive Real Systems with Time Delay," *Proceedings of the American Control Conference*, Chicago, IL.
- Niculescu, S., Verriest, E., Dugard, L. and Dion, J.M. (1997) "Stability and Robust Stability of Timedelay Systems: A Guided Tour," chapter in *Stability and Control of Time-Delay Systems*, (Ed. L. Dugard and E. Verriest), Lecture Notes in Control and Information Sciences (LNCIS), Springer-Verlag, London.
- Nomoto, H. and Culick, F.E.C. (1982) "An Experimental Investigation of Pure Tone Generation by Vortex Shedding in a Duct," *J. Sound and Vib.*, Vol. 84, No. 2, pp. 247-252.
- Norton, O.P. (1983) "The Effects of a Vortex Field on Flames with Finite Kinetics," Ph.D. Thesis, California Institute of Technology.
- Nosseir, N.S. and Behar, S. (1986) "Characteristics of Jet Impingement in a Side-Dump Combustor," *AIAA J.*, Vol. 24, No. 11, pp. 1752-1757.
- Novick, A.S., Troth, D.L. and Notardonato, J. (1982) "Multifuel Evaluation of Risk/Quench/Lean Combustor," NASA TM-82986.

- Novikov, S.S. and Ryazantzev, Yu.S. (1964) "On the Stability of Propellant Combustion," *Zh. Prikl. Mekh. i Tekh. Fiz.*, No. 1, pp. 57–61.
- Novozhilov, B.V. (1965)a "Condition of Stability of Steady-State Propellant Burning," *Zh. Prikl. Mekh. i Tekh. Fiz.*, No. 4, pp. 157–169 .
- Novozhilov, B.V. (1965)b "Propellant Burning at Harmonically Varying Pressure," *Zh. Prikl. Mekh. i Tekh. Fiz.*, No. 6, p. 141–144.
- Novozhilov, B.V. (1965)c "Burning of a Powder Under Harmonically Varying Pressures," *J. Appl. Mech. and Tech. Phys.*, Vol. 6, No. 6, pp. 141–144.
- Novozhilov, B.V. (1965)d "Stability Criterion for Steady-State Burning of Powders," *J. Appl. Mech. and Tech. Phys.*, Vol. 6, No. 4, pp. 157–160.
- Novozhilov, B.V. (1966) "Nonlinear Oscillations of Propellant Burning Rate," *Zh. Prikl. Mekh. i Tekh. Fiz.*, No. 5, pp. 31–41.
- Novozhilov, B.V. (1967) "Nonsteady Propellant Burning of Propellants Having a Variable Surface Temperature," *Zhurnal Prikladnoi Mekhaniki i Tekhnicheskoi Fiziki*, No. 1, pp. 54–77.
- Novozhilov, B.V. (1968) "Theory of Nonstationary Combustion of Homogeneous Propellants," *Explosion, Combustion, and Shock Waves*, Vol. 4, No. 4, pp. 276–282.
- Novozhilov, B.V. (1970) "Equation for Nonsteady Propellant Burning Rate," *Zh. Prikl. Mekh. i Tekh. Fiz.*, No. 4, p. 73–78.
- Novozhilov, B.V. (1973) "Nonstationary Combustion of Solid Rocket Fuels," Nauka, Moscow (Translation AFSC FTD-MD-24-317-74).
- Novozhilov, B.V. (1992) "Second Harmonic Nonlinear Resonance in Propellant Combustion," *Twenty-Fourth (International) Symposium on Combustion*, The Combustion Institute, pp. 1939–1945.
- Novozhilov, B.V. (1992) "Theory of Nonsteady Burning and Combustion Stability of Solid Propellants by the Zeldovich-Novozhilov Methods," *Nonsteady Burning and Combustion Stability of Solid-Propellant*, Vol. 143 of *AIAA Progress in Astronautics and Aeronautics*, L. DeLuca, E.W. Price and M. Summerfield (Editors), Washington, DC, pp. 601–641.
- Novozhilov, B.V. (1993) "Acoustic Admittance of the Surface of Burning Condensed Matter," *Sov. J. Chem. Physics*, Vol. 10, No. 11, pp. 2363–2384.
- Novozhilov, B.V., Kohno, M., Maruizumi, H., Shimada, T. (1996) "Solid Propellant Burning Rate Response Function of Higher Order," The Institute of Space and Astronautical Science, Report No. 661, Kanagawa, Japan.
- Oberg, C.L. (1968) "Combustion Instability: The Relationship Between Acoustical Nonacoustic Instability," *AIAA J.*, Vol. 6, No. 2, pp. 265–271.

REFERENCES

- Oberg, C.L. (1969) "Final Report — Lunar Module Ascent Engine Acoustic Cavity Study," Rocketdyne Division, North American Rockwell, Report R-7935.
- Oberg, C.L. (1971) "Combustion Stabilization with Acoustic Cavities," *J. Spacecraft*, Vol. 8, No. 12, pp. 1220–1225.
- Oberg, C.L., Haymes, W.G. and Wong, T.L. (1971) "Solid Propellant Combustion Instability Supression Devices," CPIA No. 220, Vol. 1, pp. 229–252.
- Oberg, C.L., Kesselring, R.C. and Warner, C. 111 (1974) "Analysis of Combustion Instability in Liquid Propellant Engines With or Without Acoustic Cavities," Rocketdyne Division, Rockwell International, Report R-9353.
- Oberg, C.L. and Kukula, N.M. (1969) "Acoustic Liners for Large Engines," Rocketdyne Report No. K-7792.
- Oberg, C.L. and Kukula, N.M. (1971) "Analysis of the F-1 Acoustic Liner," *J. Spacecraft*, Vol. 8, No. 12, pp. 1138–1143.
- Oberg, C.L., Wong, T.L. and Ford, W.M. (1972) "Evaluation of Acoustic Cavities for Combustion Stabilization," AIAA/SAE 8th Joint Propulsion Specialist Conference, AIAA-72-1147.
- Oefelein, J. and Yang, V. (1993) "Comprehensive Review of Liquid Propellant Combustion Instabilities in F-1 Engines," *J. Prop. and Power*, Vol. 9, No. 5, pp. 657–677.
- Oppenheim, A.K. and Laderman, A.J. (1965) "Role of Detonation in Combustion Instability," *First ICRPG Combustion Instability Conference*, CPIA No. 68, Vol. 1, pp. 275–297.
- Oran, E.S. and Gardner, J.H. (1985) "Chemical-Acoustic Interactions in Combustion Systems," *Prog. Energy Combust. Sci.*, Vol. 11, pp. 253–276.
- Ortega, R. and Lozano, R. (1988) "Globally Stable Adaptive Controller for System with Delay," *Int. J. Control*, Vol. 47, 17–23.
- Padmanhan, M.S. and Zinn, B.T. (1979) "Applicability of the Method of Averaging in Solid Rocket Stability," *Comb. Sci. and Tech.*, Vol. 20 (5-6), pp. 179–184.
- Pankiewitz, C. and Sattelmayer, T. (2002) "Time Domain Simulation of Combustion Instabilities in Annular Combustors," ASME Turbo Expo '02, GT-2002-30063.
- Paparizos, L. and Culick, F. E. C. (1989) "The Two-Mode Approximation to Nonlinear Acoustics in Combustion Chambers. I. Exact Solution for Second Order Acoustics," *Combustion Science and Technology*, Vol. 65, No. 1–3, pp. 39–65.
- Paparizos, L. and Culick, F. E. C. (1989) "The Two-Mode Approximation to Nonlinear Acoustics in Combustion Chambers. II: Influence of Third-Order Acoustics and Mean Flow in Triggering," (unpublished).

- Paschereit, C.O. and Gutmark, E. (2002) "Passive Combustion Control Applied to Premix Burners," *40th AIAA Aerospace Sciences Meeting*, AIAA-2002-1007.
- Parker, J. Sawyer, R.F. and Ganji, A.R. (1979) "Measurement of Vortex Frequencies in a Lean, Premixed Prevaporized Combustor," *Comb. Sci. and Tech.*, Vol. 20, pp. 235–241.
- Paxson, D. (2000) "A Sectored-One-Dimensional Model for Simulating Combustion Instabilities in Premix Combustors," *38th Aerospace Sciences Meeting & Exhibit*, AIAA Paper 2000-0313, NASA TM-1999-209771.
- Pelce, P. and Rochwerger, D. (1992) "Vibratory Instability of Cellular Flames Propagating in Tubes," *Journal of Fluid Mechanics*, Vol. 239, pp. 293–307.
- Perracchio, A.A. and Proscia, W.M. (1999) "Nonlinear Heat-Release/Acoustic Model for Thermo-Acoustic Instability in Lean Premixed Combustors," *ASME J. Eng. Gas Turb. Power*, Vol. 121, No. 3, pp. 415–421.
- Perring, W.G.A. (1946) "A Critical Review of German Long-Range Rocket Development," *J. Roy. Aero. Soc.*, pp. 483–525.
- Perry, E.H. (1970) "Investigations of the T-Burner and Its Role in Combustion Instability Studies," Ph.D. Thesis, Jet Propulsion Center, California Institute of Technology.
- Perry, E.H. and Culick, F.E.C. (1974) "Measurement of Wall Heat Transfer in the Presence of Large-Amplitude Combustion-Driven Oscillations," *Comb. Sci. and Tech.*, Vol. 9, pp. 49–53.
- Peters, N. (1986) "Laminar Flamelet Concepts in Turbulent Combustion," *Proc. of the Comb. Inst.*, Vol. 21, pp. 1232–1250.
- Philippart, K.D. (1987) "Stability Characteristics and Analysis of Liquid Oxygen/Methane Injectors," *24th JANNAF Combustion Meeting*.
- Philippart, K.D. and Moser, M.D. (1988) "Stability Analysis of Liquid Oxygen/Methane Injectors Using Currently Available Analytical Tools," *24th AIAA/ASME/SAE/ASEE Joint Propulsion Conference*, AIAA-88-2851.
- Phillipe, A. and Tchepedjian, P. (1984) "Prediction of Longitudinal Combustion Instabilities in Axisymmetrical Propellant Grains," *20th AIAA/ASME/SAE/ASEE Joint Propulsion Conference*, AIAA-84-1358.
- Phillips, B., Hannum, N.P. and Russell, L.M. (1969) "On the Design of Acoustic Liners for Rocket Engines: Helmholtz Resonators Evaluated with a Rocket Combustor," NASA TN D-5171.
- Phillips, B. and Morgan, C.J. (1967) "Mechanical Absorption of Acoustic Oscillations in Simulated Rocket Combustion Chambers," NASA TND-3792.
- Pieper, J.L. and Fang, J.J. (1986) "Combustion Characterization Methodology for LOX/Hydrocarbon Engines," 1986 JANNAF Propulsion Conference.
- Pierce, A.D. (1981) *Acoustics*, McGraw-Hill Book Company, New York.

REFERENCES

- Poinsot, T. and Candel, S.M. (1988) "A Nonlinear Model for Ducted Flame Combustion Instabilities," *Comb. Sci. and Tech.*, Vol. 61, pp. 121–153.
- Poinsot, T., Husseini, K., LeChatelier, C., Candel, S.M. and Esposito, E. (1986) "An Experimental Analysis of Noise Sources in a Dump Combustor," *Dynamics of Reacting Systems, Part I: Flames and Configurations*, Vol. 105 of *AIAA Progress in Astronautics and Aeronautics*, pp. 333–345.
- Poinsot, T., LeChatelier, C., Candel, S.M. and Esposito, F. (1986) "Experimental Determination of the Reflection of Coefficient of a Premixed Flame in a Duct," *J. Sound Vib.*, Vol. 107, No. 2, pp. 265–278.
- Poinsot, T., Trouvé, A.C., Veynante, D.P., Candel, S.M. and Esposito, E.J. (1987) "Vortex Driven Acoustically Coupled Combustion Instabilities," *J. Fluid Mech.*, Vol. 177, pp. 265–292.
- Poinsot, T. and Veynante, D. (2001) *Theoretical and Numerical Combustion*, R.T. Edwards, Inc.
- Poinsot, T., Yip, B., Veynante, T., Trouvé, A., Samaniego, J.M. and Candel, S. (1992) "Active Control: An Investigation Method for Combustion Instabilities," *J. Phys. III France*, Vol. 2, pp. 1331–1357.
- Polifke, W., Fischer, A. and Sattelmayer, T. (2003) "Instability of a Premix Burner with Non-Monotonic Pressure Drop Characteristics."
- Poncia, G. (1998) "A Study on Thermoacoustic Instability Phenomena in Combustion Chambers for Active Control," Doctors Thesis, Dipartimento di Elettronica e Informazione Politecnico di Milano.
- Powell, A. (1964) "Theory of Vortex Sound," *J. Acoust. Soc. of Amer.*, Vol. 36, No. 1, pp. 177–195.
- Powell, E.A. (1970) "Nonlinear Combustion Instability in Liquid Propellant Rocket Engines," Ph.D. Thesis, School of Aerospace Engineering, Georgia Institute of Technology.
- Powell, E.A. and Zinn, B.T. (1971) "A Single Mode Approximation in the Solution of Nonlinear Combustion Instability Problems," *Comb. Sci. and Tech.*, Vol. 3, No. 3, pp. 121–132.
- Powell, E.A. and Zinn, B.T. (1974) "Theoretical Investigation of Nonlinear Three-Dimensional Instabilities in Liquid Rockets with Real Nozzles," *Acta Astronautica*, Vol. 1, pp. 1051–1073.
- Prakash, S. and Sirignano, W.A. (1980) "Theory of Convective Droplet Vaporization with Unsteady Heat Transfer in the Circulating Liquid Phase," *Int. J. of Heat and Mass Transfer*, Vol. 23, pp. 253–268.
- Press, W.A., Flannery, B.P., Teukolsky, S.A. and Vetterling, W.T. (1989) *Numerical Recipes—The Art of Scientific Computing*, Cambridge University Press.
- Prévost, M., Godon, J.C. and Innegrave, O. (2005) "Thrust Oscillations in Reduced Scale Solid Rocket Motors Part I: Experimental Investigations," *41st AIAA/ASME/SAE/ASEE Joint Propulsion Conference*, AIAA-2005-4003.
- Prévost, M., Vuillot F. and Trainau, J.C. (1996) "Vortex-shedding driven oscillations in subscale motors for the Ariane 5 MPS solid rocket motors," *AIAA-96-3247, 32nd AIAA Joint Propulsion Conference*, July 1–3,

Orlando, FL.

Price, E.W. (1953) "Theory of Steady Flow with Mass Addition," *ARS J.*, Vol. 23, No. 4, July–August, pp. 237–241.

Price, E.W. (1958) "Combustion Instability in Solid-Propellant Rocket Motors," *IX Annual Congress of the IAF, Astronautica Acta*, Vol. 5, pp. 63–72.

Price, E.W. (1959) "Review of the Combustion Instability Characteristics of Solid Propellants," *AGARD Conference Proceeding, Advances in Tactical Rocket Propulsion*, pp. 139–194.

Price, E.W. (1960) "Review of Experimental Research on Combustion Instability of Solid Propellants," in *Solid Propellant Rocket Research, of Progress in Astronautics and Rocketry*, Vol. 1, M. Summerfield, ed., Academic Press, New York, pp. 561–602.

Price, E.W. (1960) "Combustion Instability in Solid Propellant Rocket Motors," *ARS J.*, Vol. 30, pp. 574–576; Closure by W. Nachbar and L. Green, Jr., *ARS J.*, Vol. 30, pp. 576–577.

Price, E.W. (1961) "Review of Combustion Instability in Solid Propellant Rockets," *Bulletin of the 17th JANAF-ARPA NASA Solid Propellant Group*, Vol. I, pp. 165–193.

Price, E.W. (1964)a "Axial Mode, Intermediate Frequency Combustion Instability in Solid Propellant Rocket Motors," *12th AIAA Aerospace Sciences Meeting*, AIAA-64-146.

Price, E.W. (1964)b "Experimental Solid Rocket Combustion Instability," *Tenth (International) Symposium on Combustion*, The Combustion Institute, Pittsburgh, PA, pp. 1067–1082.

Price, E.W. (1967) "Solid Propellant Combustion: State of Knowledge 1967," American Institute of Chemical Engineers, *62nd National Meeting*, Salt Lake City, Utah, Paper No. 3b.

Price, E.W. (1968)a "Recent Advances in Solid Propellant Combustion Instability," *Twelfth (International) Symposium on Combustion*, The Combustion Institute, Pittsburgh, PA, pp. 101–113.

Price, E.W. (1968)b "Review of the Combustion Instability Characteristics of Solid Propellants," *Proceedings of the 25th Meeting of the AGARD Combustion and Propulsion Panel*, pp. 139–194.

Price, E.W. (1969) "Relevance of Combustion Models for Perturbation Combustion of Solid Propellants," *AIAA J.*, Vol. 7, No. 1, pp. 153–154.

Price, E.W. (1971) "Comments on 'Role of Aluminum in Suppressing Instability in Solid Propellant Rocket Motors,'" *AIAA J.*, Vol. 9, No. 5, pp. 987–990.

Price, E.W. (1979) "Velocity Coupling in Oscillatory Combustion of Solid Propellants," *AIAA J.* Vol. 17, No. 7, pp. 799–800.

Price, E.W. (1984) "Combustion of Metallized Propellants," in *Fundamentals of Solid Propellant Combustion*, Vol. 90, AIAA *Progress in Astronautics and Aeronautics*, pp. 479–513.

REFERENCES

- Price, E.W. (1992) "Solid Rocket Combustion Instability — An American Historical Account," Chapter 1 in *Nonsteady Burning and Combustion Stability of Solid Propellants*, DeLuca, Price and Summerfield (Editors), Vol. 143, AIAA *Progress in Astronautics and Aeronautics*, pp. 1–16.
- Price, E.W. (1993) "The History of Combustion Instability," paper presented at *AIAA/ASME/SAE 29th Joint Propulsion Conference*, Monterey CA.
- Price, E.W. and Culick, F.E.C. (1968) *Combustion of Solid Rocket Propellants*, AIAA Professional Study Series, Atlantic City, N.J., June 2–3.
- Price, E.W. and Dehority, G.L. (1967) "Velocity Coupled Axial Mode Combustion Instability in Solid Propellant Rocket Motors," *ICRPG/AIAA 2nd Solid Propulsion Conference*, Anaheim, CA, pp. 213–227.
- Price, E.W. and Flandro, G.A. (1991) *Combustion Instability in Solid Propellant Rockets*, (monograph in preparation).
- Price, E.W., Kraeutle, K.J., Prentice, J.L., Boggs, T.L., Crump, J.E. and Zurn, D.E. (1982) "Behavior of Aluminum in Solid Propellant Combustion," Naval Weapons Center Report NWC TP 6120.
- Price, E.W., Mathes, H.B., Crump, J.E. and McGill, M.R. (1961) "Experimental Research in Combustion Instability of Solid Propellants," *Comb. and Flame*, Vol. 5, pp. 149–162.
- Price, E.W., Siegman, R.K. Sambamurthi, J.K. and Park, C.J. (1982) "Behavior of Aluminum in Solid Propellant Combustion," Scientific Report, Georgia Institute of Technology.
- Price, E.W. and Sofferis, J.W. (1958) "Combustion Instability in Solid Propellant Rocket Motors," *Jet Propulsion*, Vol. 28, pp. 190–192.
- Priem, R.J. and Heidmann, M.F. (1960) "Propellant Vaporization as a Design Criterion for Rocket-Engine Combustion Chambers," NASA Technical Report R-67.
- Priem, R.J. and Guentert, D.C. (1962) "Combustion Instability Limits Determined by a Nonlinear Theory and a One-Dimensional Model," NASA TN D-1409.
- Priem, R.J. and Rice, E.J. (1968) "Combustion Instability with Finite Mach Number Flow and Acoustic Liners," NASA TMX 52412.
- Priem, R.J. and Breisacher, K.J. (1988) "Combustion Instability Coupling with Feed System Acoustics," Earth-to-Orbit Technology Conference, Huntsville, AL (May, 1988).
- Pun, W. (2001) "Measurements of Thermo-Acoustic Coupling," Ph.D. Thesis, California Institute of Technology.
- Pun, W., Palm, S.L. and Culick, F.E.C. (2003) "Combustion Dynamics of an Acoustically Forced Flame," *Comb. Sci. and Tech.*, Vol. 175, pp. 499–521.

- Putnam, A.A. (1976) "Combustion Roar of Seven Industrial Burners," *J. of the Inst. of Fuel*, Vol. 49, pp. 135–138.
- Putnam, A.A. (1964) "General Considerations of Autonomous Combustion Oscillations," Chapter F of *Non-Steady Flame Propagation*, G.F. Markstem (Ed.), The MacMillan Co., New York.
- Putnam, A.A. (1971) *Combustion Driven Oscillations in Industry*, American Elsevier.
- Putnam, A.A., Belles, F.E. and Kentfield, J.A.C. (1986) "Pulse Combustion," *Prog. Energy Combust. Sci.*, Vol. 12, pp. 43–79.
- Putnam, A.A. and Dennis, W.R. (1952) "Organ Pipe Oscillations is a Flame-Filled Tube," *Fourth (International) Symposium on Combustion*, The Williams and Wilkins Company, pp. 566–575.
- Putnam, A.A. and Dennis, W.R. (1953) "A Study of Burner Oscillations of the Organ-Pipe Type," *Transactions of the ASME*, Vol. 73, pp. 15–26.
- Putnam, A.A. and Faulkner, L. (1982) "An Overview of Combustion Noise," *J. Energy*, Vol. 7, pp. 458–469.
- Quinn, T.J., Colclough, A.R. and Chandler, T.R.D. (1976) "A New Determination of the Gas Constant by an Acoustical Method," *Phil. Trans.*, Vol. 283, pp. 367–420.
- Ramechandra, M.K. and Strahle, W.C. (1983) "Acoustic Signature from Flames as a Combustion Diagnostic Tool," *AIAA J.*, Vol. 21, pp. 1107–1114.
- Rangal, R. H. and Sirignano, W. A. (1989) "An Evaluation of the Point-Source Approximation in Spray Calculations," *Numerical Heat Transfer*, Part A, Vol. 16, pp. 57–57.
- Rankine, W.J.M. (1870) "On the Thermodynamic Theory of Waves of Finite Longitudinal Disturbance," *Phil. Trans.*, Vol. clx, pp. 277–286.
- Rannie, W.D. (1962) "A Perturbation Analysis of One-Dimensional Heterogeneous Flow in Rocket Nozzles," in *Progress in Astronautics and Rocketry*, Vol. 6: *Detonation and Two Phase Flow*, Academic Press, NY.
- Ranz, W.E. and Marshall, W.R., Jr. (1952) "Evaporation From Drops, Part I," *Chem. Eng. Prog.*, Vol. 48, No. 3, pp. 141–146.
- Raun, R.L. and Beckstead, M.W. (1993) "A Numerical Model for Temperature Gradient Effects on Rijke Burner Oscillations," *Comb. and Flame*, Vol. 94, Nos. 1/2, pp. 1–29.
- Raun, R.L., Beckstead, M.W., Finlinson, J.C. and Brooks, K.P. (1993) "A Review of Rijke Tubes, Rijke Burners and Related Devices," *Prog. in Comb. Energy and Science*, Vol. 19, No. 4, pp. 313–364.
- Rauschenbakh, B.V. (1963) *Vibrational Combustion*, Air Force Systems Command, Foreign Technology Division, Report FTD- TT-62-942.

REFERENCES

- Lord Rayleigh (1878) "The Explanation of Certain Acoustic Phenomena," *Royal Institution Proceedings*, Vol. VIII, pp. 536–542.
- Lord Rayleigh (1945) *The Theory of Sound*, Dover Publications, New York.
- Reardon, F.H. (1961) *An Investigation of Transverse Mode Combustion Instability in Liquid Propellant Rocket Motors*, Princeton University Aeronautical Engineering Report No. 550.
- Reardon, F.H. (1973) "Guidelines for Combustion Stability Specifications and Verification Procedures," J.P.J.A. Publication 247; NASA CR 136745.
- Reardon, F.H. (1981) "Analysis of Very Low Frequency Oscillations in a Ramjet Combustor by Use of a Sensitive Time Lag Model," *18th JANNAF Combustion Meeting*.
- Reardon, F.H. (1983) "The Sensitive Time Lag Model Applied to Very Low Frequency Oscillations in Side-Dump Liquid-Fueled Ramjet Engines," *20th JANNAF Combustion Meeting*.
- Reardon, F.H. (1984) "Modeling of Very Low Frequency Oscillations in Side-Dump Liquid Fueled Ramjet Engines," California State University, report prepared for Universal Energy Systems, Dayton, OH.
- Reardon, F.H. (1985) "An Examination of Some Possible Mechanisms of Combustion Instability in Liquid-Fueled Ramjets," *22nd JANNAF Combustion Meeting*.
- Reardon, F.H. (1988) "Very Low Frequency Oscillations in Liquid-Fueled Ramjets," *AGARD 72B Specialists' Meeting of the Propulsion and Energetics Panel*, "Combustion Instabilities in Liquid-Fueled Propulsion Systems."
- Reardon, F.H., Crocco, L. and Harrje, D.T. (1964) "Velocity Effects in Transverse Mode Liquid Propellant Rocket Combustion Instability," *AIAA J.*, Vol. 2, pp. 1631–1641.
- Reardon, F.H., McBride, J.M. and Smith, A.J., Jr. (1966) "Effect of Injection Distribution on Combustion Stability," *AIAA J.*, Vol. 4, No. 3, pp. 506–512.
- Reichel, R.H., Hague, D.S., Jones, R.T. and Glatt, C.R. (1973) "Program User's Manual for Optimizing the Design of a Liquid or Gaseous Propellant Rocket Engine with the Automated Combustor Design Code AUTOCOM," NASA CR-2293.
- Reichel, R.H., Hague, D.S., Jones, R.T. and Glatt, C.R. (1974) "System Oriented Design Optimization for Liquid Propellant Rocket Engines," *Raumfahrtforschung*, Vol. 1/1974, pp. 16–24.
- Renard, P.H., Thèvenin, D. Rolon, J.C. and Candel, S. (2000) "Dynamics of Flame/Vortex Interactions," *Prog. Energy and Comb. Sci.*, Vol. 26, No. 3, pp. 225–282.
- Renard, P.H., Rolon, J.C., Thèvenin, D., and Candel, S. (1999) "Investigation of Heat Release, Extinction and Time Evolution of the Flame Surface for a Nonpremixed Flame Interacting with a Vortex," *Comb. and Flame*, Vol. 117, No. 1, pp. 189–205.

- Renie, J.P. and Osborne, J.R. (1981) "Pressure and Velocity-Coupled Response of Composite Solid Propellants Based Upon a Small Perturbation Analysis," *17th AIAA/ASME/SAE/ASEE Joint Propulsion Conference*, AIAA-81-1556.
- Reuter, D.M., Daniel, B.R., Jagoda, J. and Zinn, B.T. (1986) "Periodic Mixing and Combustion Processes in Gas Fired Pulsating Combustors," *Comb. and Flame*, Vol. 65, pp. 281–290.
- Reuter, D.M., Hegde, D.E. and Zinn, B.T. (1988) "Flowfield Measurements in an Unstable Ramjet Burner," *AIAA/ASME/SAE/ASEE 24th Joint Propulsion Conference*, AIAA-88-2855.
- Reynst, F.H. (1961) *Pulsating Combustion*, (M.W. Thring, Editor), Pergamon Press, New York.
- Richards, G.A., Gemmen, R.S. and Yip, M.J. (1997) "A Test Device for Premixed Gas Turbine Combustion Oscillations," *J. of Eng. for Gas Turb. and Power*, Vol. 119, pp. 776–782.
- Richards, G.A. and Janus, M.C. (1998) "Characterization of Oscillations During Premix Gas Turbine Combustion," *ASME J. Eng. Gas Turb. and Power*, Vol. 120, pp. 294–302.
- Richards, G.A., Janus, M.C. and Robey, E.H. (1999) "Control of Flame Oscillations with Equivalence Ratio Modulation," *J. Prop. and Power*, Vol. 15, No. 2, pp. 232–240.
- Richards, G.A., Straub, D.L. and Robey, E.H. (2003) "Passive Control of Combustion Dynamics in Stationary Gas Turbines," *J. Prop. and Power*, Vol. 19, No. 5, pp. 795–810.
- Richardson, E.G. (1922) "The Theory of the Singing Flame," *Proc. Phys. Soc. London*, Vol. 35, pp. 47–55.
- Riemann, B. (1858) "Über die Fortpflanzung ebener Luftwellen von endlicher Schwingungsweite," *Gott. Abh.*, viii, pp. 43–62.
- Rijke, P.L. (1859) "Notice of a New Method of Causing a Vibration of the Air Contained in a Tube Open at Both Ends," *Phil. Mag.*, Vol. XVII, pp. 419–422. (Translation of the original paper in *Annalen des Physik*, 107, pp. 339–343.)
- Roberts, A.K. (1962) "Development of the 9KS11000 Black Brant III Rocket Engines," *Can. Aero. and Space J.*, Vol. 8, pp. 137–143.
- Roberts, A.K. and Brownlee, W.G. (1970) "Nonlinear Longitudinal Combustion Instability: Influence of Propellant Composition," *AIAA J.* Vol. 9, No. 1, pp. 140–147.
- Rocker, M. (2002) "A Brief Review of LOX/Kerosene Combustion Instability in American and Russian Combustion Devices in Application to the Second-Generation Reusable Launch Vehicle," (Unpublished Briefing)
- Rockwell, D. (1982) "Oscillations of Impinging Shear Layers," *20th AIAA Aerospace Sciences Meeting*, AIAA-82-0047.
- Rockwell, D. and Naudascher, E. (1979) "Self-Sustained Oscillations of Impinging Free Shear Layers," *Ann. Rev. Fluid Mech.*, Vol. 11, pp. 67–94.

REFERENCES

- Rogers, D.E. (1954) "An Experimental Investigation of High Frequency Combustion Instability in a Fuel-Air Combustor," Thesis for the degree of Aeronautical Engineer, California Institute of Technology.
- Rogers, D.E. and Marble, F.E. (1956) "A Mechanism for High Frequency Oscillations in Ramjet Combustors and Afterburners," *Jet Propulsion*, Vol. 26, pp. 456–462.
- Rogers, T. (1980)a "Ramjet Inlet/Combustor Pulsations Study," Naval Weapons Center, China Lake, NWC Report TP-6053.
- Rogers, T. (1980)b "Ramjet Inlet/Combustor Pulsations Test and Analysis," Naval Weapons Center, China Lake, NWC Report TP-6155.
- Roginskii, O.G. (1961) "Oscillatory Combustion," *Soviet Physics-Acoustics*, Vol. 7, No. 2, pp. 107–122.
- Roh, T.-S. (1995) "Numerical Simulation of Combustion Instabilities of Double-Base Homogeneous Propellants in Rocket Motors," Thesis in M.E., The Pennsylvania State University.
- Roh, T.-S., Apte, S. and Yang, V. (2000) "Combustion Dynamics of Homogeneous Solid Propellants in a Rocket Motor with Acoustic Excitations," Chapter 25 in *Solid Propellant Chemistry, Combustion and Motor Interior Ballistics*, of AIAA *Progress in Astronautics and Aeronautics*, Vol. 185.
- Roh, T.-S., Tseng, I.-S. and Yang, V. (1995) "Effects of Acoustic Oscillations in Flame Dynamics of Homogeneous Propellants in Rocket Motors," *J. Prop. and Power*, Vol. 11, No. 4, pp. 640–650.
- Ross, C.C. and Datner, P.P. (1954) "Combustion Instability in Liquid Propellant Rocket Motors — A Survey," *Selected Combustion Problems*, Butterworths Scientific Publications, London, pp. 352–401.
- Rossiter (1966) "Wind-Tunnel Experiments on the Flow Over Rectangular Cavities at Subsonic and Transonic Speeds," Aeronautical Research Council, R&M No. 3438.
- Rott, N. (1980) "Thermoacoustics," in *Advances in Applied Mechanics*, Vol. 20, pp. 135–175.
- Rott, N. (1979) "Recent Research on Thermoacoustic Oscillations," *J. Acoust. Soc. of Amer.*, Vol. 65, p. 541.
- Rott, N. (1969) "Damped and Thermally Driven Acoustic Oscillations in Wide and Narrow Tubes," *Z. Angew. Math. Phys.*, Vol. 20, p. 230-243.
- Rubin, S. (1966) "Longitudinal Instability of Liquid Rockets Due to Propulsion Feedback (POGO)," *AIAA J. Spacecraft*, Vol. 3, No. 8, pp. 1188–1195.
- Rubin, S., Wagner, R.G. and Payne, J.G. (1973) "POGO Suppression on Space Shuttle — Early Studies," NASA CR-2210.
- Rudnick, I. (1953) "On the Attenuation of a Repeated Sawtooth Shock Wave," *J. Acoust. Soc. of Amer.*, Vol. 25, pp. 1012–1013.

- Rupe, J.H. (1967) "An Experimental Correlation of the Nonreactive Properties of Injection Schemes and Combustion Effects in a Liquid Propellant Rocket Engine. Part V. On the Influence of Vanes on Combustion and Combustion Instability," Caltech Jet Propulsion Laboratory Report TR 32-255.
- Russell, P.L., Brant, G., Ernst, R. and Underwood, F.N., Jr. (1978) "Low-Frequency Augmentor Instability Study," *AIAA/SAE 14th Joint Propulsion Conference*, AIAA-78-996.
- Ryan, N.W. and Coates, R.L. (1964) "Acoustic Instability: Influence of and on the Solid Phase," *AIAA J.*, Vol. 2, No. 6, pp. 1130–1134.
- Sabersky, R.H. (1954) "Effect of Wave Propagation in Feed Lines on Low Frequency Rocket Instability," *Jet Propulsion*, Vol. 24, pp. 172–174.
- Sabnis, J.S. (2005) "Emissions and Noise: Next Frontier for Aircraft Engine Technologies," *AIAA/AAAF Aircraft Noise and Emissions Reduction Symposium*.
- Sabnis, J.S. (2003) "Numerical Simulation of Distributed Combustion in Solid Rocket Motors with Metalized Propellant," *J. Prop. and Power*, Vol. 19, No. 1, pp. 48–55.
- Sabnis, J.S., deLong, F.G. and Gibeling, H.J. (1992) "Calculation of Particle Trajectories in Solid-Rocket Motors with Arbitrary Acceleration," *J. Prop. and Power*, Vol. 8, No. 5, pp. 961–967.
- Sabnis, J.S., Gibeling, H.J. and McDonald, H. (1985) "Calculation of Solid Propellant Rocket Motor Internal Flowfield Using an Implicit Navier-Stokes Procedure," AIAA Fluid Mechanics and Plasma Conference, AIAA-85-1625.
- Sabnis, J.S., Gibeling, H.J. and McDonald, H. (1989) "Navier-Stokes Analysis of Solid Propellant Rocket Motor Internal Flows," *J. Prop. and Power*, Vol. 5, No. 6, pp. 657–664.
- Sabnis, J.S., Madabhushil R., Gibeling, H.J. and McDonald, H. (1989) "On the Use of $k - \epsilon$ Turbulence for Computation of Solid Rocket Internal Flows," *37th AIAA Aerospace Sciences Meeting*, AIAA-89-2558.
- Saito, T. (1965) "Vibrations of Air Columns Excited by Heat Supply," *Bulletin of the JSME*, Vol. 8, No. 32, pp. 651–659.
- Sajben, M., Bogar, T.J. and Krontil, J.C. (1984) "Forced Oscillation Experiments in Super Critical Diffuser Flows," *AIAA J.*, Vol. 22, No. 4, pp. 465–474.
- Saluri, R.J., Wanhainen, J.P. and Hannum, N.P. (1968) "Effect of Thrust per Element in Combustion Stability Characteristics of Hydrogen-Oxygen Rocket Engines," NASA TN D 4851.
- Samaniego, J.M. and Mantel, R.S. (1999) "Fundamental Mechanisms in Premixed Turbulent Flame Propagation via Flame-Vortex Interactions Part I Experiment; Part II Numerical Simulation," *Comb. and Flame*, Vol. 118, pp. 537–582.
- Samaniego, J.M., Yip, B., Poinsot, T. and Candel, S.M. (1993) "Low-Frequency COmbustion Instability Mechanisms in a Side-Dump Combustor," *Comb. and Flame*, Vol. 94, pp. 363–380.

REFERENCES

- Sanaf Kumar, V.R., Raghunandan, B.N., Setoguchi, T. and Raghunathan, S. (2005) "Diagnostic Investigation of Instabilities and Pressure Oscillations in High-Performance Solid Rockets," *41st AIAA/ASME/SAE/ASEE Joint Propulsion Conference*, AIAA-2005-3999.
- Sankar, S.V., Jagoda, J.I., Daniel, B.R. and Zinn, B.T. (1987) "Flame Driving of Axial Acoustic Waves: Comparison of Theoretical Predictions and Experimental Observations," *35th AIAA Aerospace Sciences Meeting*, AIAA-87-0219.
- Satche, M. (1949) discussion of "Stability of Linear Oscillating Systems With Constant Time Lag," by H.I. Ansoff, *J. App. Mech.*, Vol. 16 (Dec. 1949), pp. 419–420.
- Scala, S.M. (1957) "Transverse Wave and Entropy Wave Combustion Instability in Liquid Propellant Rockets," Ph.D. Thesis, Aeronautical Engineering, Princeton University.
- Scarinci, T. (2005) "Combustion Instability and its Passive Control: Rolls-Royce Aeroderivative Engine Experience," *Progress in Astronautics and Aeronautics*, Vol. 210, Chapter 4 of *Combustion Instabilities in Gas Turbine Engines: Operational Experience, Fundamental Mechanisms, and Modeling*, (T.C. Lieuwen and V. Yang, Editors).
- Scarinci, T. and Halpin, J.L. (2000) "Industrial Trent Combustor—Combustion Noise Characteristics," *J. of Eng. for Gas Turb. and Power*, Vol. 122, No. 2, pp. 280–286.
- Schadow, K.C. (2001) "Combustion Dynamics: Passive Combustion Control," a lecture in the Short Course *Active Control of Engine Dynamics*, von Karman Institute for Fluid Dynamics.
- Schadow, K.C., Crump, J.E. and Blomshield, F.S. (1981) "Combustion Instability in a Research Dump Combustor: Inlet Shock Oscillations," *18th JANNAF Combustion Meeting*.
- Schadow, K.C., Crump, J.E. and Blomshield, F.S. (1983) "Effect of Dump Plane Design on Pressure Oscillations in a Sudden Expansion Ramjet Combustor," *20th JANNAF Propulsion Meeting*.
- Schadow, K.C., Crump, J.E., Mahan, V.A., Nabity, J.A., Wilson, K.J. and Gutmark, E. (1985) "Large-Scale Coherent Structures as Drivers of Ramjet Combustion Instabilities," *22nd JANNAF Propulsion Meeting*.
- Schadow, K.C. and Gutmark, E. (1992) "Combustion Instability Related to Vortex Shedding in Dump Combustors and Their Passive Control," *Prog. Energy Comb. Sci.*, Vol. 18, pp. 117–132.
- Schadow, K.C., Gutmark, E., Parr, T.P., Parr, D.M. and Wilson, K.J. (1986) "Passive Shear Control to Minimize Ramjet Combustion Instabilities," *23rd JANNAF Propulsion Meeting*.
- Schadow, K.C., Gutmark, E., Parr, D.M. and Mahan, V.A. (1987a) "Effect of Shear-Flow Dynamics in Combustion Processes," *Proceedings of the Eighth International Symposium on Airbreathing Engines*.
- Schadow, K.C., Gutmark, E., Parr, T.P., Parr, D.M., Wilson, K.J. and Crump, J.H. (1989) "Large-Scale Coherent Structures as Drivers of Combustion Instability," (first appeared as AIAA-87-1326), *Comb. Sci. and Tech.*, Vol. 64, 167-186.

- Schadow, K.C., Gutmark, E. and Wilson, K.J. (1992) "Active Combustion Control in a Coaxial Dump Combustor," *Comb. Sci. and Tech.*, Vol. 81, pp. 285–300.
- Schadow, K.C., Gutmark, E., Wilson, K.J., Parr, D.M., Mahan, V.A. and Ferrell, G.B. (1987)b "Effect of Shear-Flow Dynamics in Combustion Processes, *Comb. Sci. and Tech.*, Vol. 54, pp. 103-116.
- Schadow, K.C., Gutmark, E., Wilson, K.J. and Smith, R.A. (1990)a "Multistep Dump Combustor Design to Reduce Combustion Instabilities," (first appeared as AIAA-88-2854), *J. Propulsion*, Vol. 6, No. 4, pp. 407–411.
- Schadow, K.C., Gutmark, E., Wilson, K.J. and Smith, R.A. (1990)b "Noncircular Inlet Duct Cross-Section to Reduce Combustion Instabilities," *Comb. Sci. and Tech.*, Vol. 73, pp. 537–553.
- Schadow, K.C., Wilson, K.J., Crump, J.E., Foster, J.B. and Gutmark, E. (1984)a "Interaction Between Acoustics and Subsonic Ducted Flow with Dump," *22nd AIAA Aerospace Sciences Meeting*, Reno, Nevada, AIAA-84-0530.
- Schadow, K.C., Wilson, K.J. and Lee, M.J. (1984)b "Enhancement of Mixing in Ducted Rockets with Elliptic Gas-Generator Nozzles," *20th AIAA/SAE/ASME Joint Propulsion Conference*, AIAA-84-1260.
- Schadow, K.C., Wilson, K.J. and Gutmark, E. (1987)c "Characterization of Large-Scale Structures in a Forced Ducted Flow with Dump," *AIAA J.*, Vol. 25, No. 9, pp. 1164–1170.
- Schadow, K.C., Yang, V., Culick, F.E.C., Rosfjord, T.J., Sturgess, G. and Zinn, B.T. (1997) "Active Combustion Control for Propulsion Systems," AGARD Report 820.
- Schaeffer, C.W. and Brown, R.S. (1992) "Oscillatory Internal Flow Studies," United Technologies, Chemical Systems Division, Report 2060FR.
- Scherrer, D. (1985)a "Combustion d'une goutte en milieu réactif avec décomposition exothermique préalable du combustible," *Jointées sur la Simulation Numérique des Phenomènes de Combustion*, Sophia-Antipolis, 1985.
- Scherrer, D. (1985)b "Combustion d'une goutte immobile: etude numerique de l'influence des hypothésés conduisant a la 'Loi en D^l,'" *La Recherche Aerospatiale*, 1985, No. 5, pp. 331–322.
- Scherrer, D. (1986) "Effet de la convection sur l'évaporation et la combustion d'une goutte de combustible," *70th AGARD P.E.P. Symposium on Combustion and Fuel in Gas Turbine Engines*.
- Schimmer, H. and Vortmeyer, D. (1977) "Acoustical Oscillation in a Combustion System with a Flat Flame," *Comb. and Flame*, Vol. 28, pp. 17–24.
- Schlichting, H. (1960) *Boundary Layer Theory*, McGraw-Hill Book Co., New York.
- Schlichting, H. (1968) *Boundary Layer Theory*, 6th Edition, McGraw-Hill Book Co., New York.
- Schmitt, D. and Lourme, D. (1982) "A Model of Instability of Liquid Propellant Engine with Radial Injection," IAF Paper No. 81-362, 32nd IAF Congress, Rome, 1981, and *Astronautica Acta*, Vol. 9, No. 6–7, pp.

REFERENCES

445–454.

Schob, W.J., Glassman, I. and Webb, M.J. (1963) “An Experimental Investigation of Heat Transfer and Pressure Effects on Longitudinal Combustion Instability in a Rocket Motor Using Premixed Gaseous Propellants,” Princeton University, Aeronautical Engineering Report 649.

Schoch, A. (1953) “The Concept of Acoustic Energy,” *Acustica*, Vol. 3, pp. 181–184.

Schoyer, H.F.R. (1982) “Helmholtz Resonator Burners: Analysis for Response Function Measurements,” *J. of Spacecraft and Rockets*, Vol. 19, pp. 188–192.

Schoyer, H.F.R. (Ed.) (1993) *Combustion Instability in Liquid Rocket Engines*, European Space Agency, Report ESA WPP-062.

Schoyer, H.F.R. and Kluyverweg, I. (1979) “Low Frequency Oscillatory Combustion: Experiments and Results,” *Solid Rocket Motor Technology*, AGARD CP 259, pp. 25-1–25-16 (see also: Schoyer, H.F.R. (1980) “Results of Experimental Investigations of the L Phenomenon,” *J. of Spacecraft and Rockets*, Vol. 17, pp. 200–207.

Schuermans, B., Polifke, W. and Paschereit, C. (1999) “Modeling Transfer Matrices of Premixed Flames and Comparison with Experimental Results,” *ASME Turbo Expo 1999*, Indianapolis, IN, Paper 99-GT-132.

Schuller, T., Ducruix, S., Durox, D. and Candel, S. (2002) “Modeling Tools for the Prediction of Premixed Flame Transfer Functions,” *Twenty-Ninth (International) Symposium on Combustion*, pp. 107–113.

Schuller, T., Durox, D. and Candel, S. (2002) “Dynamics of and Noise Radiated by a Perturbed Impinging Premixed Jet Flame,” *Comb. and Flame*, Vol. 128, No. 1, pp. 88–110.

Schuller, T., Durox, D. and Candel, S. (2003) “Self-Induced Combustion Oscillations of Laminar Premixed Flames Stabilized on Annular Burners,” *Comb. and Flame*, Vol. 135, No. 4, pp. 525–538.

Schuller, T., Durox, D. and Candel, S. (2003) “A Unified Model for the Prediction of Flame Transfer Functions: Comparison Between Conical and V-flame Dynamics,” *Comb. and Flame*, Vol. 134, No. 1–2, pp. 21–34.

Schultz, R., Green, L., Jr. and Penner, S. (1958) “Studies of the Decomposition Mechanism, Erosive Burning, Sonance and Resonance for Solid Composite Propellants,” *3rd AGARD Colloquium on Combustion and Propulsion*, Pergamon Press, pp. 367–420.

Searby, G. (1992) “Acoustic Instability in Premixed Flames,” *Comb. Sci. and Tech.*, Vol. 81, pp. 221–231.

Searby, G. and Rochwerger, D. (1991) “A Parametric Acoustic Instability in Premixed Flames,” *J. Fluid Mech.*, Vol. 231, pp. 529–543.

Sehgal, R. and Strand, L. (1964) “A Theory of Low-Frequency Combustion Instability in Solid Rocket Motors,” *AIAA J.*, Vol. 2, No. 4, pp. 696–702.

- Seifert, H.S., Mills, M.M. and Summerfield, M. (1947) "The Physics of Rockets," *Am. J. of Physics*, Vol. 15, Jan.–Feb. (pp. 1–21); Mar.–Ap. (pp. 121–140); May–June (pp. 255–272).
- Seume, J., Vortmeyer, N., Krauss, W., Hermann, J., Hantsch, C. and Zangl, P. (1998) "Application of Active Combustion Instability Control to a Heavy Duty Gas Turbine," *J. Eng. Gas Turb. and Power*, Vol. 120, pp. 721–726.
- Seywert, C. (2001) "Combustion Instabilities: Issues in Modeling and Control," Ph.D. Thesis, Jet Propulsion Center, Aeronautics, California Institute of Technology.
- Seywert, C. and Culick, F.E.C. (1998) "Comparison of Different Approaches for the Approximate Analysis of Combustion Instabilities," *34th JANNAF Combustion Meeting*.
- Seywert, C. and Culick, F.E.C. (1999) "Some Influences of Noise on Combustion Instabilities and Combustor Dynamics," *36th JANNAF Combustion Meeting*, Cocoa Beach, FL.
- Shaeffer, C.W., Flandro, G.A. and Brown, R.S. (1987) "Ramjet Combustion Instability Investigation," Final Report for Period July 1985–December 1986, AFWAL-TR-85-2017.
- Shaeffer, C.W. and Brown, R.S. (1992) "Oscillatory Internal Flow Studies," United Technologies, Chemical Systems Division, 2060 FR.
- Shapiro, A. H. (1953) *The Dynamics and Thermodynamics of Compressible Fluid Flow*. Ronald Press Co., New York, Volume 1.
- Shchelkin, K.I. and Troshin, Y.K. (1964) *Gas Dynamics of Combustion*, NASA Technical Translations F-231.
- Shelton, S.V. (1967) "A Technique for Measurement of Solid Propellant Burning Rates During Rapid Pressure Transients," *4th ICRPG Combustion Conference*, CPIA No. 162, Vol. 1, pp. 361–372.
- Shih, W.P., Lee, J. and Santavicca, D. (1996) "Stability and Emissions Characteristics of a Lean Premixed Gas Turbine Combustor," *Twenty-Seventh Symposium (International) on Combustion*, The Combustion Institute, Vol. 26, pp. 2771–2778.
- Shivashankars, B.N., Strahle, W.C. and Handley, J.C. (1975) "Evaluation of Combustion Noise Scaling Laws by an Optical Technique," *AIAA J.*, Vol. 13, pp. 623–627.
- Shuen, J.-S. (1987) "Prediction of the Structure of Fuel Sprays in Cylindrical Combustion Chambers," *J. Propulsion*, Vol. 3, pp. 105–112.
- Shufflebeam, J.H., Kendrick, D.W., Sowa, W.A. and Snyder, T.S. (1999) "Quantifying Fuel/Air Unmixedness in Premixing Nozzles Using an Acetone Fluorescence Technique," ASME Paper 99-GT-399, *J. of Eng. for Gas Turb. and Power*, January 2002, Vol. 124, No. 1, pp. 39–45.
- Shusser, M., Cohen, N.S. and Culick, F.E.C. (2000) "Combustion Response of AP Composite Propellants," *37th JANNAF Combustion Meeting*, submitted to *AIAA J. Prop. and Power*.

REFERENCES

- Shusser, M. and Cohen, N.S. (2001) "Effect of Variable Thermal Properties of the Solid Phase on Composite Solid Propellant Combustion," Caltech Internal Document CI01-04, submitted to *Astronautica Acta*, 2005.
- Shusser, M., Culick, F.E.C. and Cohen, N.S. (2001) "Pressure Exponent of a Composite Solid Propellant," Caltech Internal Document CI01-03, submitted to *AIAA J.*, 2001.
- Shusser, M., Culick, F.E.C. and Cohen, N.S. (2000) "Combustion Response of Ammonium Perchlorate," *AIAA J.*, Vol. 40, No. 4, pp. 722-730.
- Shusser, M. and Culick, F.E.C. (2001) "Analytical Solution for Composite Solid Propellant Response Function," *37th AIAA Joint Propulsion Conference*, Caltech Internal Document CI01-02, submitted to *AIAA J.*, 2001.
- Sirignano, W.A. (1964)a "A Theoretical Study of Nonlinear Combustion Instability: Longitudinal Mode," Ph.D Thesis, Department of Aerospace and Mechanical Sciences, Princeton University, New Jersey.
- Sirignano, W.A. (1964)b "A Theory of Axial-Mode Shock-Wave Oscillations in a Solid Rocket Combustor," *Tenth (International) Symposium on Combustion*, Elsevier.
- Sirignano, W.A. and Crocco, L. (1964) "A Shock Wave Model of Unstable Rocket Combustors," *AIAA J.*, Vol. 2, No. 7, pp. 1285-1296.
- Sirignano, W.A., Crocco, L. and Harrje (1967) "Acoustic Liner Studies," *3rd ICRPG Combustion Conference*.
- Sirignano, W. A. (1986) "The Formulation of Spray Combustion Models: Resolution Compared to Droplet Spacing," *J. of Heat Transfer*, Vol. 108, pp. 633-639.
- Sirignano, W.A., Abranizon, B., Raju, M. and Molavi, K. (1986) "Spray Combustion: A Driving Mechanism for Ramjet Combustion Instability," *23rd JANNAF Combustion Meeting*.
- Sivasegaram, S. Thompson, B.B. and Whitelaw, J.H. (1989) "Acoustic Characterization Relevant to Gas Turbine Augmentors," *J. Prop. and Power*, Vol. 5, No. 1, pp. 109-115.
- Sivasegaram, S. and Whitelaw, J.H. (1987)a "Oscillations in Confined Disk-Stabilized Flames," *Comb. and Flame*, Vol. 68, pp. 121-129.
- Sivasegaram, S. and Whitelaw, J.H. (1987)b "Suppression of Oscillations in Confined Disk Stabilized Flames," *25th AIAA Aerospace Sciences Meeting*, AIAA-87-0434; *J. Propulsion and Power*, Vol. 3, No. 4, pp. 291-295.
- Sivasegaram, S. and Whitelaw, J.H., (1987)c "Oscillations in Axisymmetric Dump Combustors," *Comb. Sci. and Tech.*, Vol 52, pp. 413-426.
- Sivasegaram, S. and Whitelaw, J.H., (1991) "The Influence of Swirl on Oscillations in Ducted Premixed Flames," *Comb. and Flame*, Vol 85, pp. 195-205.

- Smart, A.E., Jones, B. and Jewell, N.T. (1976) "Measurement of Unsteady Parameters in a Rig Designed to Study Reheat Combustion Instabilities," *14th AIAA Aerospace Sciences Meeting*, AIAA-76-1141.
- Smith, A.F. (1960) "A Theory of Oscillatory Burning of Solid Propellants Assuming a Constant Surface Temperature," *ARS Progress in Astronautics and Rocketry: Solid Propellant Rocket Research*, Vol. I, edited by M. Summerfield, Academic Press, pp. 375–391.
- Smith, D.A. (1987) "An Experimental Study of Acoustically Excited, Vortex Driven, Combustion Instability Within a Rearward Facing Step Combustor," Ph.D. Dissertation, Jet Propulsion Center, California Institute of Technology.
- Smith, D.A. and Zukoski, E.E. (1985) "Combustion Instability Sustained by Unsteady Vortex Combustion," *AIAA/SAE/ASME/ASEE 21st Joint Propulsion Conference*, AIAA-85-1248.
- Smith, G.E. and Henderson, R.E. (1971) "Combustion Instability in a Turbofan Mixed-Flow Augmentor," *AIAA/SAE 8th Joint Propulsion Specialist Conference*, AIAA Paper No. 72-1206.
- Smith, L.O., Jr., Partus, F.P. and O'Hara, J.C. (1975) "Analysis of Liquid Rocket Combustion Chamber Turbulence Levels from Diffusion Data," *Comb. and Flame*, Vol. 25, pp. 161–176.
- Smith, O. (1959) "A Controller to Overcome Dead Time," *ISA J.*, Vol. 6, 28–33.
- Smith, R.P. and Sprenger, D.F. (1952) "Combustion Instability in Solid-Propellant Rockets," *Fourth (International) Symposium on Combustion*, The Combustion Institute, pp. 893–906.
- Sneddon, I.N. (1957) *Elements of Partial Differential Equations*, McGraw-Hill, New York.
- Snellink, G. (1973) "Optical Measurements in Premixed Flames to Locate the Noise Sources," *Comb. Int. European Symp.*, Sheffield, pp. 553–558.
- Sondhauss, C. (1850) "Über die Schallschwingungen der Luft in erhitzten Glasrohren und in gedekten Pfeifen von ungleicher Weite," *Ann. der Phy.* (Leipzig) 79,1.
- Sondhauss, C. (1860) "Über die chemische Harmonika, Part I," *Annalen der Physik und Chemie*, Vol. 109, No. 1, pp. 1–43.
- Sondhauss, C. (1860) "Über die chemische Harmonika, Part II," *Annalen der Physik und Chemie*, Vol. 109, No. 3, pp. 426–469.
- Sotter, J.G., Woodward, J.W. and Clayton, R.M. (1969) "Injector Response to Strong High-Frequency Pressure Oscillations," *J. Spacecraft*, Vol. 6, No. 4, pp. 504–506.
- Sotter, J.G. and Flandro, G.A. (1968) "Resonant Combustion in Rockets," *Scientific American*, Vol. 219, No. 12, pp. 95–103.
- Souchier, A., Lemoine, J.C. and Dorville, G. (1982) "Résolution du problème des instabilités sur le moteur Viking," IAF Paper No. 82-363, *33rd IAF Congress*, Paris.

REFERENCES

- Spanos, P.-T.D. (1977) "Linearization Techniques for Non-Linear Dynamical Systems," Ph.D. Dissertation, California Institute of Technology, Division of Engineering and Applied Science.
- Sreenivasan, K.R., Raghu, S. and Chu, B.T. (1985) "The Control of Pressure Oscillations in Combustion and Fluid Dynamical Systems," *AIAA Shear Flow Conference*, AIAA-85-0540.
- Steele, R.C., Cowell, L.H., Cannon, S.M. and Smith, C.E. (2000) "Passive Control of Combustion Instability in Lean Premixed Combustors," *J. of Eng. for Gas Turb. and Power*, Vol. 122, pp. 412–419.
- Sterling, J. (1993) "Nonlinear Analysis and Modelling of Combustion Instabilities in a Laboratory Combustor," *Comb. Sci. and Tech.*, Vol. 89, pp. 167–179.
- Sterling, J. (1987) "Longitudinal Mode Instabilities in Air Breathing Engines," Ph.D. Dissertation, Jet Propulsion Center, California Institute of Technology.
- Sterling, J.D. and Zukoski, E.E. (1991) "Nonlinear Dynamics of Laboratory Combustor Pressure Oscillations," *Comb. Sci. and Tech.*, Vol. 77, pp. 225–238.
- Sterling, J.D. and Zukoski, E.E. (1987) "Longitudinal Mode Combustion Instabilities in a Dump Combustor," *25th AIAA Aerospace Sciences Meeting*, AIAA-87-0220.
- Sternfeld, H.J. (1971) "Leistungsverhalten koaxialer Einspritzsysteme in $L0_2/GH_2$ - Rockettriebwerken," Durssche Luft-und Raumfahrt DLR FB 71-56.
- Stow, S.R. and Dowling, A.P. (2004) "Low Order Modelling of Thermoacoustic Limit Cycles," Proc. *ASME Turbo Expo 2004*, Vienna, Austria.
- Stow, S.R. and Dowling, A.P. (2003) "Modelling of Circumferential Modal Coupling Due to Helmholtz Resonators," ASME Paper GT2003-38168.
- Stow, S.R. and Dowling, A.P. and Hynes, T.P. (2002) "Reflection of Circumferential Modes in a Choked Nozzle," *J. Fl. Mech.*, Vol. 467, pp. 215–239.
- Stow, S.R. and Dowling, A.P. (2001) "Thermoacoustic Oscillations in an Annular Combustor," ASME Paper 2001-GT-0037.
- Strahle, W.C. (1971) "On Combustion Generated Noise," *J. Fluid Mech.*, Vol. 49, pp. 399–414.
- Strahle, W.C. (1978) "Combustion Noise," *Prog. in Energy and Comb. Sci.*, Vol. 4, pp. 157–176.
- Strahle, W.C. (1983) "ONR/AFOSR Workshop on Mechanisms of Instability in Liquid-Fueled Ramjets," CPIA No. 375.
- Strahle, W.C. (1985) "A More Modern Theory of Combustion Noise," in *Recent Advances in the Aerospace Sciences*, Plenum Press, pp. 103–114.

- Strand, L.D. and Brown, R.S. (1992) "Laboratory Test Methods for Combustion Stability Properties of Solid Propellants," in *Nonsteady Burning and Combustion Stability of Solid Propellants*, of AIAA *Progress in Astronautics and Aeronautics*, Vol. 143, pp. 689–718.
- Strand, L.D., Magiawala, K.R., McNamara, R.P. (1980) "Microwave Measurement of the Solid Propellant Pressure-Coupled Response Function," *J. of Spacecraft and Rockets*, Vol. 17, No. 6, pp. 483–488.
- Strand, L.D., Schultz, A.L. and Reedy, G.K. (1974) "Determination of Solid Propellant Transient Regression Rates Using a Microwave Doppler Shift Technique," *J. Spacecraft and Rockets*, Vol. 11, No. 2, pp. 75–83.
- Stratonovich, R.L. (1963) *Topics in the Theory of Random Noise*, translated by R.A. Silverman; Gordon and Breach, Science Publishers, New York.
- Straub, D.L., Casleton, K.H., Lewis, R.E., Sidwell, T.G., Maloney, D.J. and Richards, G.A. (2003) "Assessment of RQL Trapped Vortex Combustor for Stationary Gas Turbines," *ASME Turbo Expo 2003*, Paper GT-2003-38569.
- Strittmater, R., Watermeier, L. and Pfaff, S.P. (1963) "An Experimental Study of the Aluminum Additive Role in Unstable Combustion of Solid Rocket Propellant Surfaces by a Resonant Tube Technique," *Ninth Symposium (International) on Combustion*, Academic Press, pp. 311–315.
- Stromecki, D.J. (1980) "An Assessment of Gas Turbine Engine Augmentor Technology and Needs for the 80's," *AIAA/SAE/ASME 16th Joint Propulsion Conference*, Paper AIAA-80-1200.
- Stull, F.D., Craig, R.R., Streby, G.D. and Vanka, S.P. (1983) "Investigation of a Dual Inlet Side Dump Combustor Using Liquid Fuel Injection," *21st AIAA Aerospace Sciences Meeting*, AIAA-83-0420.
- Stuttaford, P., Martling, V., Green, A. and Lieuwen, T. (2003) "Combustion Noise Measurement System for Low Emissions Combustor Performance Optimization and Health Monitoring," ASME Paper GT2003-38255.
- Subbaiah, M.V. (1983) "Non-Steady Flame Spreading in Two-Dimensional Ducts," *AIAA J.*, Vol. 21, No. 5, pp. 1557–1524.
- Subrahmanyam, P.B., Sujith, R.I. and Lieuwen, T. (2001) "A Family of Exact Transient Solutions for Acoustic Wave Propagation in Inhomogeneous, Non-uniform Area Ducts," *J. Sound and Vib.*, Vol. 240, No. 4, pp. 705–715.
- Sujith, R.I. (2001) "Exact Solutions for Modeling Sound Propagation Through a Combustion Zone," *J. Acoust. Soc. Am.*, Vol. 110, No. 4, pp. 1839–1844.
- Sujith, R.I., Waldherr, G.A. and Zinn, B. (1995) "An Exact Solution for One-dimensional Acoustic Fields in Ducts with an Axial Temperature Gradient," *Sound and Vib.*, Vol. 184, No. 3, pp. 389–402.
- Summerfield, M. (1951) "A Theory of Unstable Propulsion in Liquid Propellant Rocket Systems," *ARS J.*, Vol. 21, No. 5, pp. 108–114.
- Summerfield, M., Caveny, L.H., Battista, R.A., Kubota, N., Gostintsev, Yu.A. and Isoda, H. (1971) "Theory of Dynamic Extinguishment of Solid Propellants with Special Reference to Nonsteady Heat Feedback Law,"

REFERENCES

J. of Spacecraft and Rockets, Vol. 8, No. 3, pp. 251–258.

Sutton, R.D., Hines, W.S. and Combs, L.P. (1972) “Development and Application of a Comprehensive Analysis of Liquid-Rocket Combustion,” *AIAA J.*, Vol. 10, No. 2, pp. 194–203.

Svetlichnyi, I.B., Margolin, A.D. and Pokhil, P.F. (1970) “Helmholtz Resonator Applied for Investigation of Condensed Systems Vibrational Combustion,” *Vibrational Combustion in Model Installations*, edited by A.D. Margolin, Kazan Univ., Kazan, Russia, pp. 72–81.

Swenson, G.D. (2000) “Numerical Simulations of Combustion Instabilities in Gas Turbine Combustors, with Applications,” Ph.D. Thesis, California Institute of Technology.

Swenson, G.D., Burnley, V.S. and Culick, F.E.C. (1995) “Pulsed Instabilities in Solid-Propellant Rockets,” *AIAA J. Prop. and Power*, Vol. 11, No. 4, pp. 657–665.

Swithenbank, J. and Sotter, G. (1963) “Vortices in Solid Propellant Rocket Motors,” *AIAA J.*, Vol. 1, No. 7, pp. 1682–1684.

Swithenbank, J. and Sotter, G. (1964) “Vortex Generation in Solid Propellant Rockets,” *AIAA J.*, Vol. 2, No. 7, pp. 1297–1302.

Szuch, J.R. (1969) “Application of a Double Dead-Time Model Describing Chugging to Liquid Propellant Rocket Engines Having Multielement Injectors,” NASA TN D-5303.

Szuch, J.R. and Wenzel, L.M. (1968)a “Experimental Verification of a Double Dead-Time Model Describing Chugging in Liquid Bipropellant Rocket Engines,” NASA TN D-5303.

Szuch, J.R. and Wenzel, L.M. (1968)b “Double Dead-Time Model for Combustion Stability Analysis in Liquid Bipropellant Rocket Engines,” NASA TN D-4564.

Tacina, R., Mao, C.-P. and Way, C. (2004) “Experimental Investigation of a Multiple Fuel Injector Module with Discrete Jet Swirlers for Low Emission Combustors,” *42nd AIAA Aerospace Sciences Meeting*, AIAA-2004-0135.

Tang, P.K. and Sirignano, W.A. (1973) “The Theory of a Generalized Helmholtz Resonator,” *J. Sound and Vib.*, Vol. 26, No. 2, pp. 247–262.

Taylor, G.I. (1956) “Fluid Flow in Regions Bounded by Porous Surfaces,” *Proc. Roy. Soc. Lond.* Vol. A234, pp. 456–475.

Temkin, S. (1981) *Elements of Acoustics*, John Wiley & Sons, New York.

Temkin, S. and Dobbins, R. A. (1966)a “Attenuation and Dispersion of Sound by Particulate Relaxation Processes,” *J. of the Acoustical Society of America*, Vol. 40, No. 2, pp. 317–324.

Temkin, S. and Dobbins, R. A. (1966)b “Measurements of Attenuation and Dispersion of Sound by Aerosols,” *Ibid.*, Vol. 40, No. 5, pp. 1016–1024.

- Tennekes, H. and Lumley, J.L. (1972) *A First Course in Turbulence*, MIT Press.
- T'ien, J.S. (1972) "Oscillatory Burning of Solid Propellants Including Gas Phase Time Lag," *Comb. Sci. and Tech.*, Vol. 5, No. 2, pp. 47–54.
- T'ien, J.S. (1984) "Transient Burning of Solid Propellants," Chapter 14 of *AIAA Progress in Astronautics and Aeronautics*, Vol. 90, Washington, DC.
- Tierno, J.E. and Doyle, J.C. (1992) "Multi Mode Active Stabilization of a Rijke Tube," *ASME Winter Meeting*, Vol. DSC-Vol. 38.
- Tijedman, H. (1975) "On the Propagation of Sound in Cylindrical Tubes," *J. Sound and Vib.*, Vol. 39, No. 1, pp. 1–33.
- Tong, A.Y. and Sirignano, W.A. (1986)a "Multicomponent Droplet Vaporization in a High Temperature Gas," *Comb. and Flame*, Vol. 66, pp. 221–235.
- Tong, A.Y. and Sirignano, W.A. (1986)b "Multicomponent Transient Droplet Vaporization: Integral Equation Formulation and Approximate Solution," *Numerical Heat Transfer*, Vol. 10, pp. 253–278.
- Tong, A.Y. and Sirignano, W.A. (1987) "Vaporization Response of Fuel Droplet in Oscillatory Field," *ASME National Heat Transfer Conference*, Paper No. 87-HT-58.
- Tonon, T.S., Tang, P.K., Sirignano, W.A. and Harrje, D.T. (1971) "Acoustic Liner Design from a Fluid Mechanics Approach," *AIAA/SAE 7th Propulsion Joint Specialist Conference*, AIAA-71-757.
- Torres, H., Lieuwen, T., Johnson, C., Daniel, B.R. and Zinn, B.T. (1999) "Experimental Investigation of Combustion Instabilities in a Gas Turbine Combustor Simulator," *37th AIAA Aerospace Sciences Meeting*, AIAA-99-0712.
- Trainea, J.C., Prévost, M., Vuillot, F., LeBreton, P., Cuny, A., Preioni, N. and Bee, R. (1997) "A Subscale Test Program to Assess the Vortex-Shedding Driven Instabilities in Segmented Solid Rocket Motors," *33rd AIAA/ASME/SAE/ASEE Joint Propulsion Conference*, AIAA-97-3247.
- Trouvé, A., Candel, S.M. and Daily, J.W. (1988) "Linear Stability of the Inlet Jet in a Ramjet Dump Combustor," *26th AIAA Aerospace Sciences Meeting*, AIAA-88-0149.
- Trubridge, G.F.P. and Badham, H. (1963) "Experimental Studies of Unstable Combustion in Solid Propellant Rockets," *Combustion and Propulsion, Fifth AGARD Colloquium*, pp. 497–530.
- Truesdell, C. and Toupin, R. (1960) "The Classical Field Theories," *Handbuch der Physik*, Vol. III/1, Springer-Verlag, Berlin.
- Truman, J.C. (1955): Comments in the Discussion appended to Kaskan and Noreen (1955).
- Truman, J.C. and Newton, R.T. (1955) "Why Do High-Thrust Engines Screech?," *Aviation Age*, May, pp. 136–143.

REFERENCES

- Tseng, I.S. and Yang, V. (1991) *Numerical Simulation of Velocity-Coupled Combustion Response of Solid Rocket Propellants*, Pennsylvania State University, Department of Mechanical Engineering, Report to Air Force Philips Laboratory.
- Tseng, I.S. and Yang, V. (1994) "Combustion of a Double-Base Homogeneous Propellant in a Rocket Motor," *Comb. and Flame*, Vol. 96, pp. 325–342.
- Tsien, H.S. (1951) "Influence of Flame Front on the Flow Field," *J. Appl. Mech.* (June), pp. 188–194.
- Tsien, H.S. (1952) "The Transfer Functions of Rocket Nozzles," *ARS J.*, Vol. 22, pp. 139–143.
- Ugurtas, B., Avalon, G., Lupuglazoff, N. and Vuillot, F. (1999) "Numerical Computations of Hydrodynamics Inside Channels with Wall Injection," *35th AIAA/ASME/SAE/ASEE Joint Propulsion Conference*, AIAA-99-2505.
- Ugurtas, B., Avalon, G., Lupuglazoff, N., Vuillot, F. and Casalis, G. (2000) "Stability and Acoustic Resonance of Internal Flows Generated by Side Injection," in *Solid Propellant Chemistry, Combustion, and Motor Interior Ballistics*, of *AIAA Progress in Astronautics and Aeronautics*, Vol. 185, Washington, DC.
- Underwood, F.N., Rusnak, J.P., Ernst, P.C., Petrino, E.A., Russell, P.L. and Murphy, P., Jr. (1977) "Low Frequency Combustion Instability in Augmentors," *AGARD CP 229, High Temperature Problems in Gas Turbine Engines*.
- Usow, K.H., Meyer, C.L. and Schulze, F.W. (1953) "Experimental Investigation of Screeching Combustion in Full-Scale Afterburner," NACA RM-E53101.
- Utvik, D.H., Ford, H.J. and Blackman, A.W. (1966) "Evaluation of Absorption Liners for Suppression of Combustion Instability in Rocket Engines," *J. Spacecraft*, Vol. 3, No. 7, pp. 1039–1045.
- Vaezi, V. and Aldredge R.C. (2000) "Influences of Acoustic Instabilities on Turbulent-Flame Propagation," *Exp. in Therm. and Fl. Sci.*, Vol. 20, No. 3, pp. 162–169.
- Valentine, R.S. (1972) "Liquid Rocket Performance, Stability, and Compatibility," *J. Spacecraft*, Vol. 9, No. 5, pp. 295–307.
- Van Dyke, M. (1975) *Perturbation Methods in Fluid Mechanics*, The Parabolic Press, Stanford, CA.
- Van Dyke, M. (1982) *An Album of Fluid Motion*, The Parabolic Press, Stanford, CA.
- Van Moorhem, W. K. (1982) "Flow-Turning in Solid-Propellant Rocket Combustion Stability Analysis," *AIAA J.*, Vol. 20, No. 10, pp. 1420–1425.
- Vanka, S.P., Stull, F.D. and Craig, R.R. (1983) "Analytical Characterization of Flow Fields in Side Inlet Dump Combustors," *AIAA/SAE/ASME 19th Joint Propulsion Conference*, AIAA-83-1399.
- Vanka, S.P., Craig, R.R. and Stull, F.S. (1985) "Mixing, Chemical Reaction and Flow Field Development in Ducted Rockets," *AIAA/SAE/ASME/ASEE 21st Joint Propulsion Conference*, AIAA-85-1271.

Vanka, S.P., Krazinski, J.L. and Nejad, A.S. (1988) "An Efficient Computational Tool for Ramjet Combustor Research," *26th AIAA Aerospace Sciences Meeting*, AIAA-88-0060.

Vantoch, P.V. (1965) "Combustion Instability in Solid-Propellant Rockets," *Foreign Science Bulletin*, Vol. 1, No. 9, pp. 1-29.

Varapaev, V.N. and Yagodkin, V.I. (1969) "Flow Stability in a Channel with Porous Walls," *Fluid Dynamics*, Vol. 4, No. 5, pp. 60-62.

Venkataraman, K.K. (2000) "An Investigation of the Instability Mechanism in Lean Premixed Dump Combustors," Ph.D. Thesis, The Pennsylvania State University.

Venkataraman, K.K., Preston, L.H., Simons, D.W., Lee, B.J., Lee, J.G. and Santavicca, D.A. (1999) "Mechanism of Combustion Instability in a Lean Premixed Dump Combustor," *J. Prop. and Power*, Vol. 15, No. 6, pp. 909-918.

Vincent, D.W., Phillips, B. and Wanhainen, S.P. (1968) "Experimental Investigation of Acoustic Liners to Suppress Screech in Storable Propellant Rocket Motors, NASA TN-D-4442.

Vingert, L., Gicquel, P., Lourme, D. and Ménoret (1995) "Coaxial Injector Atomization," Chapter 6 in *Liquid Rocket Engine Combustion Instability*, of AIAA *Progress in Astronautics and Aeronautics*, Vol. 169, Washington, DC.

von Kármán, T. and Malina, F.J. (1940) "Characteristics of the Ideal Solid Propellant Rocket," Caltech Jet Propulsion Laboratory Report No. 1-4.

von Kármán, T. (1956) "The Present Status of the Theory of Laminar Flame Propagation," *Sixth (International) Symposium on Combustion*, Reinhold, p. 1011.

von Kármán, T., Emmons, H.W. and Tankin, R.S. (1958) "Gas Dynamics of Combustion and Detonation," Section G of *Fundamentals of Gas Dynamics*, Vol. III of *High Speed Aerodynamics and Jet Propulsion*, Princeton Univ. Press.

Vuillot, F. (1991) "Numerical Computation of Acoustic Boundary Layers in Large Solid Propellant Space Booster," *29th AIAA Aerospace Sciences Meeting*, AIAA-91-0206.

Vuillot, F. (1995) "Vortex Shedding Phenomena in Solid Rocket Motors," *J. Prop. and Power*, Vol. 11, No. 4, pp. 626-639.

Vuillot, F. and Avalon, G. (1991) "Acoustic Boundary Layers in Solid Propellant Rocket Motors Using Navier-Stokes Equations," *J. Prop. and Power*, Vol. 7, No. 2, pp. 231-239.

Vuillot, F. and Casalis, G. (2002) "Motor Flow Instabilities-Part 1 and Part 2," Notes in *Internal Aerodynamics in Solid Rocket Propulsion*, RTO/VKI Short Course, von Karman Institute.

Vuillot, F. and Kuentzmann, P. (1986) "Flow Turning and Admittance Correction: An Experimental Expansion," *J. Prop. and Power*, Vol. 2, No. 4, pp. 345-353.

REFERENCES

- Vuillot, F., Trainau, J.C., Prévost, M. and Lupoglazoff, N. (1993) "Experimental Validation of Stability Assessment Methods for Segmented Rocket Motors," *AIAA/SAE/ASME/ASEE 29th Joint Propulsion Conference*, AIAA-93-1883.
- Waesche, R.H.W. (1999) "Mechanisms and Methods of Suppression of Combustion Instability by Metallic Additives," *J. Prop. and Power*, Vol. 15, No.6, pp. 919–922.
- Waesche, R.H.W., Wenograd, J. and Summerfield, M. (1961) "Research on Solid Propellant Combustion Instability," Aeronautical Engineering Report, 564b, Princeton University.
- Waesche, R.H.W., Wenograd, J. and Summerfield, M. (1961) "Entropy Wave Observations in Oscillatory Combustion of Solid Propellants: A Progress Report," AIAA-64-154.
- Waesche, R.H.W. and Summerfield, M. (1961) "Solid Propellant Combustion Instability: Oscillatory Burning of Solid Rocket Propellants," Aerospace and Mechanical Sciences Report, 751, Princeton University.
- Wake, B.E., Choi, D. and Hendricks, G.J. (1996) "Numerical Investigation of Pre-Mixed Step-Combustor Instabilities," AIAA Paper 96-0816.
- Ward, M.J., Son, S.F. and Brewster, M.Q. (1998) *Comb. and Flame*, Vol. 114, pp. 556–568.
- Watermeier, L.A. (1961) "Experimental Study of Combustion Instability in Solid Propellant Rockets," *ARS J.*, Vol. , pp. 564–566.
- Watermeier, L.A., Aungst, W.P. and Pfaff, S.P. (1963) "An Experimental Study of the Aluminum Additive Role in Unstable Combustion of Solid Rocket Propellants," *Ninth Symposium (International) on Combustion*, Academic Press, pp. 316–327.
- Waugh, R.C., Brown, R.S., Hood, T.S., Flandro, G.A., Oates, G.C. and Reardon, F.H. (1983) "Ramjet Combustor Instability Investigation: Vol. I. Literature Survey and Preliminary Design Study; Vol. II: Ramjet Combustor Instability Investigation: Cold-Flow Studies, Hot-Flow Studies, and Design Guidelines," Final Report for Period 1 October 1981 – 31 March 1983, AFWAL TR-83-2056.
- Waugh, R.C. and Brown, R.S. (1983) "A Literature Survey of Combustion Instability," CPIA No. 375.
- Waugh, R.C. and Brown, R.S. (1984) "Ramjet Combustor Instability Comparison of Data and Analysis," *21st JANNAF Combustion Meeting*.
- Webber, W.T. (1972) "Calculation of Low Frequency Unsteady Behavior of Liquid Rockets from Droplet Combustion Parameters," *J. Spacecraft*, Vol. 9, No. 4, pp. 231–237.
- Webber, W.T. and Hoffman, R.J. (1972) "A Mechanistic Model for Analysis of Pulse-Mode Engine Operation," *8th AIAA/SAE Joint Propulsion Specialist Conference*, AIAA-72-1184.
- Westerwelt, P.J. (1950) "The Mean Pressure and Velocity in a Plane Acoustic Wave in a Gas," *J. Acoust. Soc. of Amer.*, Vol. 22, No. 3, pp. 319–327.

- White, F.M. (1979) *Fluid Mechanics*, McGraw-Hill Book Co., New York.
- Whitham, G.B. (1974) *Linear and Nonlinear Waves*, Wiley, New York.
- Wicker, J.M., Greene, W.D., Kim, S.-I. and Yang, V. (1996) "Triggering of Longitudinal Combustion Instabilities in Rocket Motors: Nonlinear Combustion Response," *J. Prop. and Power*, Vol. 12, No. 6, pp. 1148–1158.
- Wicker, J.M. and Yang, V. (2000) "Reply by the Authors to V.S. Burnley and F.E.C. Culick," *J. Prop. and Power*, Vol. 16, No. 1, pp. 165–166.
- Wicker, J.M., Yoon, M.W. and Yang, V. (1995) "Linear and Nonlinear Pressure Oscillations in Baffled Combustion Chambers," *J. Sound and Vib.*, Vol. 184, No. 1, pp. 141–171.
- Wickliff, J.L. and Geyer, M.S. (1982) "On the Flow Reversal Condition in Combustion Instability," *18th AIAA/SAE/ASME Joint Propulsion Conference*, AIAA-82-1221.
- Williams, F.A. (1985) *Combustion Theory* (Second Edition), The Benjamin/Cummings Publishing Co., Inc., Menlo Park, CA.
- Williams, F.A. (1962) "Response of a Burning Solid to Small Amplitude Pressure Oscillations," *J. of Applied Physics*, Vol. 33, p. 3153.
- Wilson, J.R. and Micci, M.M. (1987) "Direct Measurement of High Frequency, Solid Propellant, Pressure-Coupled Admittances," *J. Prop. and Power*, Vol. 3, No. 4, pp. 296–307.
- Wimpress, R.N. (1950) *Internal Ballistics of Solid-Fuel Rockets*, McGraw-Hill Book Company, New York.
- Wong, K., Peddieson, J., Jr. and Ventrice, M. (1980) "Analysis of Combustion Instability in Liquid Fuel Rocket Motors," NASA CR-159733.
- Wood, W.A. (1962) "Oscillatory Burning of Solid Composite Propellants," *Ninth (International) Symposium on Combustion*, Academic Press, pp. 335–344.
- Woodward-Waesche, R.H. (1965) "Oscillatory Burning of Solid Rocket Propellants," Ph.D. Thesis, Princeton University.
- Wooten, D.C. (1966) "The Attenuation and Dispersion Sound in a Condensing Medium," Part I of Ph.D. Thesis, California Institute of Technology.
- Wu, J.Z. and Wu, J.M. (1996) "Vortex Dynamics on Boundaries," *Advances in Applied Mechanics*, Vol. 37, pp. 119–275.
- Wuerker, R.F. and Briones, R.A. (1978) "Application of Holography to the Combustion Characterization of Solid Rocket Propellants," TRW, Inc., Report AFRPL TR-77-90.

REFERENCES

- Jing, Xiaodong and Sun, Xiaodong (1999) "Experimental Investigations of Perforated Liners with Bias Flow," *J. Acoust. Soc. of Amer.*, Vol. 106, No. 5, pp. 2436–2441.
- Yachter, M. (1951) discussion of "Stability of Flow in a Rocket Motor," by Grenden, D.E. and Firant, D.R (1950) in *J. Appl. Mech.*, Vol. 18, No. 1, pp. 1114–116.
- Yang, V. and Anderson, W. (Editors) (1995) *Liquid Rocket Engine Combustion Instability*, Vol. 169 of AIAA *Progress in Astronautics and Aeronautics*, Washington, DC.
- Yang, V., Brill, T.B. and Ren, W.-Z. (Editors) (2000) *Solid Propellant Chemistry, Combustion, and Motor Ballistics*, Vol. 185 of AIAA *Progress in Astronautics and Aeronautics*, Washington, DC.
- Yang, V. and Culick, F.E.C. (1983) "Linear Theory of Pressure Oscillations in Liquid-Fueled Ramjet Engines," *21st AIAA Aerospace Sciences Meeting*, AIAA-83-0574.
- Yang, V. (1984) "Pressure Oscillations in Liquid-Fueled Ramjet Engines," Ph.D. Thesis, California Institute of Technology.
- Yang, V. and Culick, F.E.C. (1984) "Analysis of Low Frequency Oscillations in a Laboratory Ramjet Combustor," *Comb. Sci. and Tech.*, Vol. 45, pp. 1–25.
- Yang, V. and Culick, F.E.C. (1985) "Analysis of Unsteady Inviscid Diffuser Flow with a Shock Wave," *J. Prop. and Power*, Vol. 1, No. 3, pp. 222–228.
- Yang, V. and Culick, F.E.C. (1986)a "Nonlinear Analysis of Pressure Oscillations in Ramjet Engines," *24th AIAA Aerospace Sciences Meeting*, AIAA-86-0001.
- Yang, V. and Culick, F.E.C. (1986)b "Stochastic Excitation of Acoustic Waves in a Combustion Chamber," *23rd JANNAF Combustion Meeting*.
- Yang, V. and Culick, F.E.C. (1990) "On the Existence and Stability of Limit Cycles for Transverse Acoustic Oscillations in a Cylindrical Combustion Chamber, I. Standing Modes," *Comb. Sci. and Tech.*, Vol. 72, No. 1, pp. 37–65.
- Yang, V., Kim, S.-I. and Culick, F.E.C. (1987) "Third-Order Nonlinear Acoustic Instabilities in Combustion Chambers, Part I: Longitudinal Modes," *AIAA/SAE/ASME/ASEE 23rd Joint Propulsion Specialist Conference*, AIAA-87-1873.
- Yang, V., Kim, S.-I. and Culick, F.E.C. (1988) "Third-Order Nonlinear Acoustic Instabilities in Combustion Chambers, Part II: Transverse Modes, Part II: Transverse Modes," *26th AIAA Aerospace Sciences Meeting*, AIAA-88-0152.
- Yang, V., Kim, S.-I. and Culick, F.E.C. (1990) "Triggering of Longitudinal Pressure Oscillations in Combustion Chambers, I. Nonlinear Gas Dynamics," *Comb. Sci. and Tech.*, Vol. 75, No. 5, pp. 183–214.
- Yang, V., Hsieh, K. C. and Tseng, I. S. (1988) "Velocity-Coupled Flow Oscillations in a Simulated Solid-Propellant Rocket Environment," *26th AIAA Aerospace Sciences Meeting*, AIAA-88-0543.

- Yip, M.J., Straub, D.L., Richards, G.A. and Rogers, W.A. (1998) "A Cold-Flow Experimental and Numerical Study of Fuel Injector Nozzle and Combustor Chamber Dynamics with Swirl and Non-Swirl Flows," *Proc. of the 1998 Int. Joint Power Gen. Conf.*, Vol. 1, pp. 267-274.
- Yodzis, C.W. (1968) "Engines for Manned Spacecraft, *AIAA 4th Propulsion Joint Specialist Conference*, AIAA-68-567.
- Yount, R.A. and Angelus, T.A. (1964) "Chuffing and Nonacoustic Instability Phenomena in Solid Propellant Rockets," *AIAA J.*, Vol. 2, No. 7, pp. 1307-1313.
- Yu, K.H., Lee, S., Trouvé, A., Stewart, H. and Daily, J.W. (1987)a "Vortex-Nozzle Interactions in Ramjet Combustors," *AIAA/SAE/ASME/ASEE 23rd Joint Propulsion Conference*, AIAA-87-1871.
- Yu, K.H., Trouvé, A. and Daily, J.W. (1987)b "Low Frequency Pressure Oscillations in a Model Ramjet Combustor," *24th JANNAF Combustion Meeting*; published in *J. Fl. Mech.*, Vol. 232 (1991), pp. 47-72.
- Yu, K.H. and Schadow, K.C. (1997) "Role of Large Coherent Structures in Turbulent Compressible Mixing," *Exp. Therm. and Fl. Sci.*, Vol. 14, pp. 75-84.
- Yuan, S.W. and Finkelstein, A.B. (1956) "Laminar Pipe Flow with Injection and Suction Through a Porous Wall," *Trans. ASME, J. Appl. Mech.*, Vol. 78, pp. 719-724.
- Zarko, V. (1998) "Development of 2-mm Band Microwave Meter for Measurement of Solid Propellant Burning Rate," Institute of Chemical Kinetics and Combustion, Novosibirsk, Russia, (For information, contact Prof. M.W. Beckstead, Brigham Young University, Provo, Utah, 84602-4100).
- Zebrowski, M.A. and Brewster, M.Q. (1996) "Theory of Unsteady Combustion of Solids: Investigation of Quasi-Steady Assumption," *J. Prop. and Power*, Vol. 12, No. 3, pp. 564-573.
- Zel'dovich, Ya. B. (1942) "On the Theory of Combustion of Powders and Explosives," *Zh. Eksperim i Teoret. Fiziki*, Vol. 12, pp. 498-524.
- Zel'dovich, Ya. B. (1963) "Propellant Combustion Instability in a Semiconfined Volume," *J. Appl. Mech. and Tech. Phys.*, No. 1, pp. 67-76.
- Zel'dovich, Ya. B., Barenblatt, G.I., Librovich, V.B. and Mikhviladze, G.M. (1985) *The Mathematical Theory of Combustion and Explosions*, Translated from the Russian by D.H. McNeill, Consultants Bureau (Plenum Press), New York.
- Zel'dovich, Ya. B., Leipunskii, O.I. and Librovich, V.B. (1975) *Theory of Nonsteady Propellant Burning*, Nauka, Moscow.
- Zetterström, K.-A. and Sjöblom, B. (1985) "An Experimental Study of Side Dump Ramjet Combustors," *International Symposium on Airbreathing Engines*, Paper 85-7024.
- Zhao, Q., Staub, P.L., Kassoy, D.R. and Kirkhoprū, K. (2000) "Acoustically Generated Vorticity in Internal Flow," *J. Fluid Mech.*, Vol. 413, pp. 247-285.

REFERENCES

- Zhu, M., Dowling, A.P. and Bray, K.N.C. (2001) "Self-excited Oscillations in Combustors with Spray Atomisers," *J. of Eng. for Gas Turb. and Power*, Vol. 123, No. 4, pp. 779–786.
- Zikikout, S., Candel, S., Poinsot, T., Trouvé, A. and Esposito, E. (1986) "High-Frequency Combustion Oscillations Produced by Mode Selective Acoustic Excitation," *Twenty-First (International) Symposium on Combustion*, The Combustion Institute, pp. 1427–1434.
- Zink, J.W. and Delsasso, L.P. (1958) "Attenuation and Dispersion of Sound by Solid Particles Suspended in a Gas," *J. Acoust. Soc. of Amer.*, Vol. 30, No. 8, pp. 765–771.
- Zinn, B.T. (1966) "A Theoretical Study of Nonlinear Transverse Combustion Instability in Liquid Propellant Rocket Motors," Ph.D. Thesis, Princeton University.
- Zinn, B.T. (1968) "A Theoretical Study of Nonlinear Combustion Instability in Liquid Propellant Rocket Engines," *AIAA J.*, Vol. 6, No. 10, pp. 1966–1972.
- Zinn, B.T. (1970) "A Theoretical Study of Nonlinear Damping by Helmholtz Resonators," *J. Sound and Vib.*, Vol. 13, No. 3, pp. 347–356.
- Zinn, B.T. (1972) "Longitudinal Mode Acoustic Losses in Short Nozzles," *J. Sound and Vib.*, Vol. 22, No. 1, pp. 93–105.
- Zinn, B.T. (1986) "Pulsating Combustion," Chapter 5 in *Advanced Combustion Methods*, Academic Press.
- Zinn, B.T. and Crocco, L. (1968) "The Nozzle Boundary Condition in the Nonlinear Rocket Instability Problem," *Astronautica Acta*, Vol. 13, pp. 489–496.
- Zinn, B.T. and Lieuwen, T.C. (2005) "Combustion Instabilities: Basic Concepts," to be published in *AIAA Progress in Astronautics and Aeronautics*, Vol. 210, (T.C. Lieuwen and V. Yang, Editors).
- Zinn, B.T. and Lores, M.E. (1972) "Application of the Galerkin Method in the Solution of Nonlinear and Axial Combustion Instability Problems in Liquid Rockets," *Comb. Sci. and Tech.*, Vol. 4, No. 6, pp. 269.
- Zinn, B.T. and Neumeier, Y. (1997) "An Overview of Active Control of Combustion Instabilities," *35th AIAA Aerospace Sciences Meeting*, AIAA-97-0461.
- Zinn, B.T. and Powell, E.A. (1968) "Application of the Galerkin Method in the Solution of Combustion Instability Problems," *Proceedings, XIX Congress*, International Astronautical Federation.
- Zinn, B.T. and Powell, E.A. (1970) "Application of the Galerkin Method in the Solution of Combustion Instability Problems," *Proceedings of the 19th International Astronautical Congress*, Vol. 3, pp. 59–73.
- Zinn, B.T. and Powell, E.A. (1970) "Nonlinear Combustion Instability in Liquid-Propellant Rocket Engines," *Thirteenth (International) Symposium on Combustion*, The Combustion Institute, Vol. 13, pp. 491–503.
- Zinn, B.T. and Savell, C.T. (1968) "A Theoretical Study of Three-Dimensional Combustion Instability in Liquid-Propellant Rocket Engines," *Twelfth (International) Symposium on Combustion*, The Combustion

Institute, pp. 139–147.

Zinn, B.T., Bell, W.A., Daniel, B.R. and Smith, A.J., Jr. (1973) “Experimental Determination of Three-Dimensional Liquid Rocket Nozzle Admittances,” *AIAA J.*, Vol. 11, No. 3, pp. 267–272.

Zsak, T. (1993) “An Investigation of the Reacting Vortex Structures Associated in Combustion,” Ph.D. Thesis, Mechanical Engineering, California Institute of Technology, Pasadena, CA.

Zukoski, E.E. and Marble, F.E. (1955) “Experiments Concerning the Mechanism of Flame Stabilization in the Wakes of Bluff Bodies,” *Proceedings of the Symposium on Gas Dynamics*, Northwestern University.

Zukoski, E.E. and Auerbach, J.M. (1976) “Experiments Concerning the Response of Super sonic Nozzles to Fluctuating Inlet Conditions,” *Transactions of the ASME, Journal of Engineering for Power*, pp. 61–64.

Zukoski, E.E. (1985) “Afterburners,” Chapter 2 of *Aerothermodynamics of Aircraft Engine Components*, G.C. Oates (Ed.), AIAA Education Series.

REFERENCES

REFERENCES ON FEEDBACK CONTROL OF COMBUSTION SYSTEMS

Alstom (formerly ABB)

Bellucci, V., Paschereit, C.O., Flohr, P. and Magni, F. (2001) "On the Use of Helmholtz Resonators for Damping Acoustic Pulsations in Industrial Gas Turbines," ASME Paper GT-2001-0039.

Bellucci, V., Paschereit, C.O., Flohr, P. and Schuermans, B. (2001) "Thermoacoustic Simulation of Lean Premixed Flames Using an Enhanced Time-Lag Model," *31st AIAA Fluid Dynamics Conference*.

Paschereit, C.O. and Gutmark, E. (2002) "Passive Combustion Control Applied to Premix Burners," *40th AIAA Aerospace Sciences Meeting*, AIAA-2002-1007.

Paschereit, C.O. and Gutmark, E. (2002) "Proportional Control of Combustion Instabilities in a Simulated Gas-Turbine Combustor," *J. Prop. and Power*, Vol. 18, No. 6, pp. 1298-1304.

Paschereit, C.O., Gutmark, E. and Schuermans, B. (2001) "Performance Enhancement of Gas Turbine Combustor by Active Control of Fuel Injection and Mixing Process: Theory and Practice," RTO Meeting, *Active Control Technology for Enhanced Performance of Operational Capabilities of Military Aircraft, Land Vehicles and Sea Vehicles*, AGARD Report RTO-MP-051.

Paschereit, C.O., Gutmark, E. and Weisentsein, W. (2002) "Excitation of Thermoacoustic Instabilities by Interaction of Acoustics and Unstable Swirling Flow," *AIAA J.*, Vol. 38, No. 6, pp. 1025-1034.

Paschereit, C.O., Gutmark, E. and Weisenstein, W. (2000) "Excitation of Thermoacoustic Instabilities by the Interaction of Acoustics and Unstable Swirling Flow," *AIAA J.*, Vol. 38, No. 6, pp. 1025-1034.

Paschereit, C.O., Gutmark, E. and Weisenstein, W. (1999) "Control of Combustion Driven Oscillations by Equivalence Ratio Modulations," *American Society of Mechanical Engineers, ASME Turbo Expo 1999*, Paper 99-GT-118.

Paschereit, C.O., Gutmark, E. and Weisenstein, W. (1999) "Control of Thermoacoustic Instabilities in a Premixed Combustor by Fuel Modulation," *37th AIAA Aerospace Sciences Meeting*, AIAA-99-0711.

Paschereit, C.O., Weisenstein, W. and Gutmark, E. (1999) "Suppression of Acoustically Excited Combustion Instability in Gas-Turbines," *5th AIAA/CEAS Aeroacoustics Conference*, AIAA-99-1846.

Paschereit, C.O., Gutmark, E. and Weisenstein, W. (1998) "Acoustic Control of Combustion Instabilities and Emissions in an Gas-Turbine Combustor," *Proc. 1998 IEEE Int. Conf. on Control Applications*.

Paschereit, C.O., Gutmark, E. and Weisenstein, W. (1998) "Control of Thermoacoustic Instabilities and Emissions in an Industrial-Type Gas-Turbine Combustor," *Twenty-Seventh Symposium (International) on Combustion*, The Combustion Institute, pp. 1817-1824.

Paschereit, C.O., Gutmark, E. and Weisenstein, W. (1998) "Flow-acoustic Interactions as a Driving Mechanism for Thermoacoustic Instabilities," *4th AIAA/CEAS Aeroacoustics Conference*, Toulouse, France.

Paschereit, C.O., Weisenstein, W. and Gutmark, E. (1998) "Role of Coherent Structures in Acoustic Combustion Control," *29th AIAA Fluid Dynamics Conference*, AIAA-98-2433.

Paschereit, C.O., Gutmark, E. and Weisenstein, W. (1998) "Structure and Control of Thermoacoustic Instabilities in a Gas-Turbine Combustor," *Comb. Sci. and Tech.*, Vol. 138, pp. 213–232.

Paschereit, C.O., Gutmark, E. and Weisenstein, W. (1998) "Suppression of Combustion Instabilities by Acoustic Control of Shear Layer Properties," *Advances in Turbulence*, edited by U. Frisch, Kluwer Academic Press, pp. 293–296.

Paschereit, C.O., Gutmark, E. and Weisenstein, W. (1979) "Coherent Structures in Swirling Flows and Their Role in Acoustic Combustion Control," *Phys. of Fl.*, Vol. 11, No. 9, pp. 2667–2678.

Paschereit, C.O., Polifke, W., Schuermans, B. and Mattson, W. (2002) "Measurement of Transfer Matrices and Source Terms of Premixed Flames, *J. of Eng. for Gas Turb. and Power*, Vol. 124, No. 2, pp. 239–247.

Paschereit, C.O., Schuermans, B., Polifke, W. and Mattson, O. (1999) "Measurement of Transfer Matrices and Source Terms of Premixed Flames," *ASME Turbo Expo 1999*, Indianapolis, IN.

Polifke, W., Poncet, A., Paschereit, C.O. and Döbbeling, K. (2001) "Reconstruction of Acoustic Transfer Matrices by Instationary Computational Fluid Dynamics," *J. Sound and Vib.*, Vol. 245, No. 3, pp. 483–510.

Polifke, W., Paschereit, C.O. and Sattelmayer, T. (1997) "A Universally Applicable Stability Criterion for Complex Thermo-Acoustic Systems," *VDI-Bericht*, pp. 455–460.

Schuermans, B.H., Bellucci, V. and Paschereit, C.O. (2003) "Thermoacoustic Modeling and Control of Multi-Burner Combustion Systems," *ASME Turbo Expo 2003*, Paper GT2003-38688.

Schuermans, B.H., Paschereit, C.O. and Polifke, W. (1999) "Modeling Transfer Matrices of Premixed Flames," *ASME Turbo Expo 1999*, Indianapolis, IN.

Schuermans, B.B.H., Polifke, W., Paschereit, C.O. and van der Linden, J.H. (2000) "Prediction of Acoustic Pressure Spectra in Combustion Systems Using Swirl Stabilized Gas Turbine Burners," *ASME Turbo Expo 2000*, 2000-GT-0105.

CALTECH

Culick, F., Heitor, M.V. and Whitelaw, J.H. (eds.) (1996) *Unsteady Combustion*, Kluwer, Boston.

Isella, G., Seywert, C., Culick, F.E.C. and Zukoski, E.E. (1997) "A Further Note on Active Control of Combustion Instabilities," *Comb. Sci. and Tech.*, Vol. 126, pp. 381–388.

Knoop, E., Culick, F.E.C. and Zukoski, E.E. (1996) "Extension of the Stability of Motions in a Combustion Chamber by Nonlinear Active Control Based on Hysteresis," *Comb. Sci. and Tech.*, Vol. 123, pp. 363–376.

Marble, F.E. and Cox, D.W. (1953) "Servo-Stabilization of Low Frequency Oscillations in a Liquid Bipropellant Rocket Motor," *J. Am. Rocket Soc.*, Vol. 23, pp. 63–74.

REFERENCES

- Marble, F.E. (1955) "Servo-Stabilization of Low Frequency Oscillations in Liquid Propellant Rocket Motors," *ZAMP*, Vol. VI, pp. 1-35.
- Poncia, G. (1998) "A Study of Thermoacoustic Instability Phenomena in Combustion Chambers for Active Control," Ph.D. Dissertation, Dipartimento di Elektronica e Informazione, Politecnico di Milano.
- Seywert, C., Isella, G. and Culick, F.E.C. (2000) "Active Feedback Control of Combustor Dynamics with Time Delay and Noise," *36th AIAA/ASME/SAE/ASEE Joint Propulsion Conference*, AIAA-2000-3124.
- Tsien, H.S. (1952) "Servo-Stabilization of Combustion in Rocket Motors," *ARS J.*, Vol. 22, pp. 256-263.
- Tsien, H.S. (1956) *Engineering Cybernetics*, McGraw-Hill Book Co., New York.

CAMBRIDGE UNIVERSITY

- Bloxside, G.J., Dowling, A.P., Hooper, N. and Langhorne, P.J. (1987) "Active Control of an Acoustically Driven Combustion Instability," *J. Theor. and App. Mech.*, Supplement to Vol. 6, pp. 161-175.
- Bloxside, G.J., Dowling, A.P., Hooper, N. and Langhorne, P.J. (1988) "Active Control of Reheat Buzz," *AIAA J.*, Vol. 26, No. 7, pp. 783-790.
- Cheung, W.S., Sims, G.J.M., Copplestone, R.W., Tilston, J.R., Wilson, C.W., Stow, S.R. and Dowling, A.P. (2003) "Measurement and Analysis of Flame Transfer Function in a Sector Combustor Under High Pressure Conditions," ASME Paper GT-2003-38219.
- Chu, Y.-C., Dowling, A.P. and Glover, K. (1998) "Robust Control of Combustion Oscillations," *Proc. 1998 IEEE Int. Conf. Control App.*, pp. 1165-1169, Trieste, Italy.
- Dowling, A.P. and Bloxside, G.J. (1984) "Reheat Buzz—An Acoustically Driven Instability," *AIAA/NASA 9th Aeroacoustics Conference*, AIAA-84-2321.
- Dowling, A.P. and Hubbard, S. (2000) "Instability in Lean Premixed Combustors," *Proc. Inst. Mech. Eng.*, Vol. 214, Part A, pp. 317-331.
- Dowling, A.P. and Morgans, A.S. (2005) "Feedback Control of Combustion Oscillations," *Ann. Rev. Fluid Mech.*, Vol. 37, pp. 151-182.
- Evesque, S. (2000) "Adaptive Control of Combustion Instabilities," Ph.D. Dissertation, University of Cambridge.
- Evesque, S., Chu, Y., Dowling, A. and Glover, K. (1999) "Feedback Control of a Premixed Ducted Flame," *Proceedings of the ISABE XIV International Symposium*, Florence, Italy, paper IS-7187.
- Evesque, S. and Dowling, A.B. (2001) "LMS Algorithm for Adaptive Control of Combustion Oscillations," *Comb. Sci. and Tech.*, Vol. 164, pp. 65-94.

Evesque, S., Dowling, A.P. and Annaswamy, A. (2003) "Self-Tuning Regulators for Combustion Oscillations," *Proc. Roy. Soc. Lond.*, Series A., Vol. 459 (2035), pp. 1709–1749.

Evesque, S., Park, S., Riley, A.J., Annaswamy, A.M. and Dowling, A.P. (2004) "Adaptive Combustion Instability Control with Saturation: Theory and Validation," *J. Prop. and Power*, Vol. 20, No. 6, pp. 1086–1095.

Heckl, M.A. (1986) "Active Control of the Noise From a Rijke Tube," IUTAM Symposium on Aero and Hydro-Acoustics, Lyon 1985, Springer-Verlag, pp. 211–216.

Heckl, M.A. (1988) "Active Control of the Noise From a Rijke Tube," *J. Sound and Vib.*, Vol. 124, pp. 117–133.

Hubbard, S. and Dowling, A.P. (1998) "Acoustic Instabilities in Premix Burners," AIAA Paper 98-2272.

Langhorne, P.J., Dowling, A.P. and Hooper, N. (1990) "Practical Active Control System for Combustion Oscillations," *Journal of Propulsion*, Vol. 6, No. 3, pp. 324–333.

Moran, A.J., Steele, D. and Dowling, A.P. (2000) "Active Control of Combustion and its Applications," RTO AVT Symposium on *Active Control Technology for Enhanced Performance Operational Capabilities of Military Aircraft, Land Vehicles and Sea Vehicles*, Braunschweig, Germany.

Peake, N. and Crighton, D.G. (2000) "Active Control of Sound," *Ann. Rev. Fluid Mech.*, Vol. 32, pp. 137–164.

Stow, S.R. and Dowling, A.P. (2004) "Low-Order Modeling of Thermoacoustic Limit Cycles," *ASME Turbo Expo 2004—Power for Land, Sea and Air*, Paper GT2004-54245.

Stow, S.R., Dowling, A.P. and Hynes, T.P. (2002) "Reflection of Circumferential Modes in a Choked Nozzle," *J. Fl. Mech.*, Vol. 467, pp. 215–239.

Wang, C.H. and Dowling, A.B. (2003) "Actively Tuned Passive Control of Combustion Instabilities," *Int. Colloq. of Comb. Noise Cont.*, Cranfield University Press.

Zhu, M., Dowling, A.P. and Bray, K.N.C. (2001) "Flame Transfer Calculations for Combustion Oscillations," ASME Paper 2001-GT-0374.

Zhu, M., Dowling, A.P. and Bray, K.N.C. (2001) "Self-excited Oscillations in Combustors with Spray Atomizers," *J. of Eng. for Gas Turb. and Power*, Vol. 123, No. 4, pp. 779–786.

ÉCOLE CENTRALE PARIS

Billoud, G., Galland, M.A., Huynh, C. and Candel, S.M. (1992) "Adaptive Active Control of Combustion Instabilities," *Comb. Sci. and Tech.*, Vol. 81, pp. 257–283.

Candel, S.M. (1992) "Combustion Instabilities Coupled by Pressure Waves and Their Active Control," *Twenty-Fourth (International) Symposium on Combustion*, The Combustion Institute, pp. 1277–1296.

REFERENCES

- Candel, S.M. (2002) "Combustion Dynamics in Control: Progress and Challenges," *29th (International) Symposium on Combustion* pp. 1–28.
- Candel, S.M., Huynh, C. and Poinsot, T. (1996) "Some Modeling Methods of Combustion Instabilities," Chapter 5 of *Unsteady Combustion* (Culick, F.E.C., Heitor, M.V. and Whitelaw, Editors), Kluwer Academic Publishers.
- Docquier N. and Candel, S. (2002) "Combustion Control and Sensors: A Review," *Prog. in Energy and Comb. Sci.*, Vol. 28, pp. 107–150.
- Ducruix, S., Durox, D. and Candel, S.M. (2000) "Theoretical and Experimental Determination of the Transfer Function of a Laminar Pre-Mixed Flame," *Twenty-Eighth (International) Symposium on Combustion*, The Combustion Institute, Vol. 28, pp. 765–773.
- Lang, W., Poinsot, T. and Candel, S.M. (1987) "Active Control of Combustion Instability," *Comb. and Flame*, Vol. 70, pp. 281–289.
- McManus, K.R., Poinsot, T. and Candel, S.M. (1993) "A Review of Active Control of Combustion Instabilities," *Prog. Energy Combust. Sci.*, Vol. 19, pp. 1–29.
- Mettenleiter, M. (2000) "Contrôle Adaptif der Instabilités Aeroacoustiques Application aux Systèmes de Propulsion," Thèse pour l'obtention du Grade de Docteur, Laboratoire E. M2.C, École Centrale, Paris.
- Mettenleiter, M. and Candel, S.M. (2000) "Developments of Adaptive Methods for Active Instability Control," RTO AVT Symposium on *Active Control Technology for Enhanced Performance Operational Capabilities of Military Aircraft, Land Vehicles and Sea Vehicles*, Braunschweig, Germany.
- Mettenleiter, M., Haile, E. and Candel, S.M. (2000) "Adaptive Control of Aeroacoustic Instabilities," *J. Sound and Vib.*, Vol. 230, No. 4, pp. 761–784.
- Mettenleiter, M., Vuillot, F. and Candel, S.M. (2002) "Numerical Simulation of Adaptive Control: Application to Unstable Solid Rocket Motors," *AIAA J.*, Vol. 40, No. 5, pp. 860–868.
- Poinsot, T., Bourienne, F., Candel, S.M., Esposito, E. and Lang, W. (1989) "Suppression of Combustion Instabilities by Active Control," *J. Prop. and Power*, Vol. 5, No. 1, pp. 14–20.
- Poinsot, T., Veynante, D., Bourienne, F., Candel, S.M., Esposito, E. and Surget, J. (1988): "Initiation and Suppression of Combustion Instabilities by Active Control," *22nd Symposium (International) on Combustion*, The Combustion Institute, pp. 1363–1370.
- Poinsot, T., Yip, B., Veynante, T., Trouvé, A., Samaniego, J.M. and Candel, S. (1992) "Active Control: An Investigation Method for Combustion Instabilities," *J. Phys. III France*, Vol. 2, pp. 1331–1357.

GENERAL ELECTRIC

- Gulati, A. and Bigelow, E.C. (1990) "Control of Combustion Instabilities," *UK Patent Application*, GB 2,239,961 A, Application No. 9027565.2.

Gulati, A. and Mani, R. (1992) "Active Control of Unsteady Combustion-Induced Oscillations," *J. Prop. and Power*, Vol. 8, No. 5, pp. 1109–1115.

Held, T.J., Mueller, M.A., Li, S.C. and Mongia, H.C. (2001) "A Data-Driven Model for NOx, CO and UHC Emissions for a Dry Low Emissions Gas Turbine Combustor," *37th AIAA/ASME/SAE/ASEE Joint Propulsion Conference*, AIAA-2001-3425.

Houpt, P.K. and Goodman, G.C. (1991) "Active Feedback Stabilization of Combustion for Gas Turbine Engines," *Proc. of Amer. Control Conf.*, Boston, MA.

Hsiao, G.C., Pandalai, R.P., Hura, H.S. and Mongia, H.C. (1998a) "Combustion Dynamic Modeling for Gas Turbine Engines," *34th AIAA/ASME/SAE/ASEE Joint Propulsion Conference*, AIAA-98-3380.

Hsiao, G.C., Pandalai, R.P., Hura, H.S. and Mongia, H.C. (1998b) "Investigation of Combustion Dynamics of Dry-Low-Emission (DLE) Gas Turbine Engines," *34th AIAA/ASME/SAE/ASEE Joint Propulsion Conference*, AIAA-98-3381.

Joshi, N.D., Mongia, H.C., Leonard, G., Stegmaier, J.W. and Vickers, E.C. (1998) "Dry Low Emissions Combustor Development," *ASME Turbo Expo 1998*, Paper 98-GT-310.

Mongia, H.C. (1998) "Aero-Thermal Design and Analysis of Gas Turbine Combustion Systems: Current Status and Future," *34th AIAA/ASME/SAE/ASEE Joint Propulsion Conference*, AIAA-98-3982.

Mongia, H.C., Gore, J.E., Grinstein, F.F., Gutmark, E.J., Jeng, S.-M., McDonell, V.G., Menon, S., Samuelson, G.S., Santavicca, D. and Santoro, R.J. (2001) "Combustion Research Needs for Helping Development of Next Generation Advanced Combustors," *37th AIAA/ASME/SAE/ASEE Joint Propulsion Conference*, AIAA-2001-3853.

Mongia, H.C., Held, T.J. and Hsiao, G.C. (2005) "Challenges and Progress in Gas Turbine Combustors," *Progress in Astronautics and Aeronautics*, Vol. 210, (T.C. Lieuwen and V. Yang, Editors).

Mongia, C., Held, T., Hsiao, G. and Pandalai, R. (2003) "Challenges and Progress in Controlling Dynamics in Gas Turbine Combustors," *J. Prop. and Power*, Vol. 19, No. 5, pp. 822–829.

Mongia, H.C. (2003) "TAPS: A 4th General Low Emissions propulsion Engine Combustion System," *The AIAA/ICAS Int. Air and Space Symp. (2003)*, AIAA.

Pandalai, R.P. and Mongia, H.C. (1998) "Combustion Instability Characteristics of Industrial Engine Dry Low Emission Combustion Systems," *34th AIAA/ASME/SAE/ASEE Joint Propulsion Conference*, AIAA-98-3379.

GEORGIA INSTITUTE OF TECHNOLOGY

Butts, D., Lubarsky, E., Neumeier, Y., Shcherbik, D., Zinn, B.T., McManus, Y., Fric, T.F. and Srinivasan, S. (2003) "Active Adaptive Control of Combustion Instabilities in a High Pressure Power Turbine Combustor Simulator," *41st AIAA Aerospace Sciences Meeting*, Paper AIAA-2003-1005.

REFERENCES

- Cho, J.H. and Lieuwen, T.C. (2003) "Modeling the Response of Premixed Flames to Mixture Ratio Perturbations," *ASME Turbo Expo 2003*, Paper GT2003-28089.
- Coker, A., Neumeier, Y., Lieuwen, T., Zinn, B.T. and Menon, S. (2003) "Studies of Active Instability Control Effectiveness in a High Pressure, Liquid Fueled Combustor," *41st AIAA Aerospace Sciences Meeting and Exhibit*, AIAA-2003-1009.
- Conrad, T.J., Bibik, A., Shcherbik, D., Lubarsky, E. and Zinn, B.T. (2004) "Control of Instabilities in Liquid Fueled Combustor by Modification of the Reaction Zone Using Smart Fuel Injector," *40th AIAA/ASME/SAE/ASEE Joint Prop. Conf.*, Paper AIAA-2004-4029.
- Haddad, W.M., Leonessa, A., Corrado, J.R. and Kapila, V. (1997) "Robust Reduced-Order Control of Combustion Instabilities," *Proc. IEEE Int. Conf. on Contr. App.*, pp. 253-258.
- Johnson, C.E. (2006) "Adaption Control of Combustion Instabilities Using Real-Time Modes Observation," Georgia Institute of Technology, Ph.D. Dissertation, Mechanical Engineering.
- Johnson, C.E., Neumeier, Y., Lubarsky, E., Lee, J.Y., Neumeier, M. and Zinn, B.T. (2000) "Suppression of Combustion Instabilities in a Liquid Fuel Combustor Using a Fast Adaptive Control Algorithm," *38th Aerospace Sciences Meeting*, Paper AIAA-2000-0476.
- Johnson, C.E., Neumeier, Y., Neumeier, M., Zinn, B.T., Darling, D.D. and Sattinger, S.S. (2001) "Demonstration of Active Control of Combustion Instabilities on a Full-Scale Gas Turbine Combustor," *ASME Turbo Expo 2001*, Paper GT2001-0519.
- Kappei, K., Lee, J.Y., Johnson, C.E., Lubarsky, E., Neumeier, Y. and Zinn, B.T. (2000) "Investigation of Oscillatory Combustion Processes in Actively Controlled Liquid Fuel Combustor," *36th Joint Prop. Conf.*, Paper AIAA-2000-3348.
- Lee, J.-Y., Kushari, A., Lubarsky, E., Zinn, B.T., Rosenberg, S. and Levy, Y. (2002) "Control of Combustion Instabilities and Emissions Using an Internally Mixed Liquid Atomizer with a Vaporizer," *40th Aerospace Sciences Meeting*, Paper AIAA-2002-0617.
- Lieuwen, T. (2002) "Experimental Investigation of Limit Cycle Oscillations in an Unstable Gas Turbine Combustor," *J. Prop. and Power*, Vol. 18, No. 1, pp. 61-67.
- Lieuwen, T., Neumeier, Y. and Zinn, B.T. (1998) "The Role of Unmixedness and Chemical Kinetics in Driving Combustion Instabilities in Lean Premixed Combustors," *Comb. Sci. and Tech.*, Vol. 135, pp. 193-211.
- Lieuwen, T. and Yang, V. (Edition) (2005) *Combustion Instabilities in Gas Turbine Engines*, AIAA Progress in Astronautics and Aeronautics, Vol. 210.
- Lovett, J.A. and Uznanski, K.T. (2002) "Prediction of Combustion Dynamics in a Staged Premixed combustor," ASME Paper GT-2002-30646.
- Lubarsky, E., Shcherbik, D., Bibik, A. and Zinn, B.T. (2003) "Active Control of Combustion Oscillations by Non-Coherent Fuel Modulation," Paper AIAA-2003-3180.

- Lubarsky, E., Shcherbik, D., Bibik, A. and Zinn, B.T. (2004) "Open Loop Control of Severe Combustion Instabilities by Fuel Flow Modulation at Non-Resonant Frequencies," *42nd AIAA Aerospace Sciences Meeting*, AIAA-2004-0634.
- Lubarsky, E., Shcherbik, D. and Zinn, B.T. (2003) "Active Control of Instabilities in High-Pressure Combustor by Non-Coherent Oscillatory Fuel Injection," *39th Joint Propulsion Conference*, Paper AIAA-2003-4519.
- Menon, S. (2004) "CO Emission and Combustion Dynamics Near Lean Blow-Out in Gas Turbine Engines," ASME GT-2004-53290.
- Menon, S. and Yang, V. (1993) "Some Issues Concerning Active Control of Combustion Instability in a Ramjet," *31st Aerospace Sciences Meeting*, AIAA-93-0116.
- Mohanraj, R. and Zinn, B.T. (1998) "Numerical Study of Active Control Systems for Combustion Instabilities," *36th Aerospace Sciences Meeting*, AIAA-98-0356.
- Mongia, C., Held, T., Hsiao, G. and Pandalai, R. (2003) "Challenges and Progress in Controlling Dynamics in Gas Turbine Combustors," *J. Prop. and Power*, Vol. 19, No. 5, pp. 822–829.
- Mongia, H.C., Held, T.J., Hsiao, G.C. and Pandalai, R.P. (2003) "Challenges and Progress in Controlling Dynamics in Gas Turbine Combustors," *Proc. of the Comb. Inst.*, Vol. 19, pp. 822–829.
- Mongia, R.K., Dibble, R.W. and Lovett, J. (1998) "Measurement of Air-Fuel Ratio Fluctuations Caused by Combustor Drives Oscillations," ASME Paper 98-GT-304.
- Munjal, M.L. (1987) *Acoustics of Ducts and Mufflers with Application to Exhaust and Ventilation System Design*, Wiley, New York.
- Muruganandam, T.M., Nair, S., Scarborough, D., Neumeier, Y., Jagoda, J., Lieuwen, T., Seitzman, J. and Zinn, B.T. (2005) "Active Control of Lean Blowout for Turbine Engine Combustors," *J. Prop. and Power*, Vol. 21, No. 5, pp. 807–814.
- Neumeier, Y., Cohen, J., Shcherbik, D., Lubarsky, E. and Zinn, B.T. (2002) "Suppression of Combustion Instabilities in Gaseous Fuel Combustor Using Fast Adaptive Control Algorithm Part 1: Controllability Tests," *38th AIAA/ASME/SAE/ASEE Joint Propulsion Conference*, Paper AIAA-2002-4076.
- Neumeier, Y., Markopoulos, N. and Zinn, B.T. (1997) "A Procedure for Real-Time Mode Decomposition, Observation, and Prediction for Active Control of Combustion Instabilities," *IEEE Int. Conf. on Cont. App.*, pp. 818–823.
- Neumeier, Y., Nabi, A., Arbel, A., Vertzberger, M. and Zinn, B.T. (1997) "Open-Loop Performance of a Fast-Response, Actively Controlled Fuel Injector Actuator," *J. Prop. and Power*, Vol. 13, No. 6, pp. 705–713.
- Neumeier, Y., Zinn, B.T. and Jagoda, J.I. (1993) "Frequency Domain Analysis of the Performance of a Valved Helmholtz Pulse Combustor," *Comb. Sci. and Tech.*, Vol. 94, pp. 295–316.

REFERENCES

- Neumeier, Y. and Zinn, B.T. (1998) "Methods, Apparatus and Systems for Real Time Identification and Control of Modes of Oscillation," United States Patent No. 5,719,791.
- Neumeier, Y. and Zinn, B.T. (1994) "Active Control of Combustion Instabilities Using Real Time Observation of Unstable Combustor Modes," *34th AIAA Aerospace Sciences Meeting*, AIAA-96-0758.
- Neumeier, Y. and Zinn, B.T. (1996) "Experimental Demonstration of Active Control of Combustion Instabilities Using Real Time Modes Observation and Secondary Fuel Injection," *26th Symposium (International) on Combustion*, The Combustion Institute, Vol. 2, pp. 2811–2818.
- Pandalai, R.P. and Mongia, H.C. (1998) "Combustion Instability Characteristics of Industrial Engine Dry Low Emission Combustion Systems," AIAA Paper 98-3379.
- Sattelmayer, T. (2000) "Influence of the Combustor Aerodynamics on Combustion Instabilities from Equivalence Ratio Fluctuations," ASME Paper 2000-GT-0082.
- Sattinger, S.S., Neumeier, Y., Nabi, A., Zinn, B.T., Amos, D.J. and Darling, D.D. (1998) "Sub-Scale Demonstration of the Active Feedback Control of Gas-Turbine Combustion Instabilities," ASME 98-GT-258, *J. of Eng. for Gas Turb. and Power*, Vol. 122, pp. 262-268.
- Shcherbik, D., Lubarsky, E., Zinn, B.T., McManus, K., Fris, T.F. and Srinivasan, S. (2004) "Suppression of Instabilities in Gaseous Fuel Combustor Using Non-Coherent Fuel Injection," *ASME Turbo Expo 2003*, Paper GT2003-38103.
- Stone, C. and Menon, S. (2002) "Active Swirl and Fuel Modulation to Control Combustion Instability in Gas Turbine Engines," *NAVO MSRC Navigator*, Spring 2002, pp. 4-6.
- Stone, C. and Menon, S. (2003) "Open Loop Control of Combustion Instabilities in Model Gas Turbine Combustor," *J. of Turbulence*, Vol. 4, 020.
- Thiruchengode, M., Nair, S., Olsen, R., Neumeier, Y., Myers, A., Seitzman, J., Jagoda, J., Lieuwen, T. and Zinn, B.T. (2004) "Blowout Control in Turbine Engine Combustors," *42nd AIAA Aerospace Sciences Meeting*, Paper AIAA-2004-0637.
- Torres, H., Lieuwen, T.C., Johnson, C., Daniel, B.R. and Zinn, B.T. (1999) "Experimental Investigation of Combustion Instabilities in a Gas Turbine Combustor Simulator," *37th AIAA Aerospace Sciences Meeting*, AIAA-99-0712.
- Zinn, B.T. (2005) "Smart Combustors—Just Around the Corner," *ASME Turbo Expo 2005*, Paper GT2005-69138.
- Zinn, B.T., Lieuwen, T. and Neumeier, Y. (1998) "Combustion Instabilities in Low NO_x Gas Turbines and Their Active Control," *AGARD-AVT Gas Turbine Engine Combustion Symposium*, Lisbon, Portugal, 1998.
- Zinn, B.T. and Neumeier, Y. (1997) "An Overview of Active Control of Combustion Instabilities," *35th Aerospace Sciences Meeting*, AIAA-97-0461.

MASSACHUSETTS INSTITUTE OF TECHNOLOGY

Annaswamy, A.M., El Rifai, O., Fleifil, M., Hathout, J. and Ghoniem, A.F. (1998) "A Model-Based Self-Tuning Controller for Thermoacoustic Instability," *Comb. Sci. and Tech.*, Vol. 185, pp. 213–240.

Annaswamy, A.M., Fleifil, M., Hathout, J. and Ghoniem, A.F. (1997) "Impact of Linear Coupling on the Design of Active Controllers for Thermoacoustic Instability," *Comb. Sci. and Tech.*, Vol. 128, pp. 131–180.

Annaswamy, A.M., Fleifil, M., Rumsey, J.W., Prasanth, R., Hathout, J.P. and Ghoniem, A.F. (2000) "Thermoacoustic Instability: Model-Based Optimal Control Designs and Experimental Validation," *IEEE Trans. on Cont. Syst. Tech.*, Vol. 8, No. 6, pp. 905–918.

Annaswamy, A.M. and Ghoniem, A.F. (1995) "Active Control of Combustion Systems," *IEEE Cont. Syst. Mag.*, Vol. 15, No. 6, pp. 49–63.

Fleifil, M., Annaswamy, A.M., Ghoniem, Z.A. and Ghoniem, A.F. (1996) "Response of a Laminar Premixed Flame to Flow Oscillations: A Kinematic Model and Thermoacoustic Instability Results," *Comb. and Flame*, Vol. 106, No. 4, pp. 487–510.

Fleifil, M., Hathout, J., Annaswamy, A.M. and Ghoneim, A.F. (1998) "The Origin of Secondary Peaks with Active Control of Thermoacoustic Instability," *Comb. and Flame*, Vol. 133, pp. 227–265.

Fleifil, M., Hathout, J., Annaswamy, A.M. and Ghoneim, A.F. (2000) "Reduced Order Modeling of Heat Release Dynamics and Active Control of Time-Delay Instability," *38th AIAA Aerospace Sciences Meeting*, AIAA-2000-0708.

Gould, L.A. and Murray-Lasso, M.A. (1966) "On the Modal Control of Distributed Systems with Distributed Feedback," *IEEE Transactions on Automatic Control*, Vol. AC-11, No. 4, pp. 729–737.

Hathout, J.P., Annaswamy, A.M., Fleifil, M. and Ghoniem, A.F. (1998) "A Model-Based Active Control Design for Thermoacoustic Instability," *Comb. Sci. and Tech.*, Vol. 132, pp. 99–138.

Hathout, J., Fleifil, M., Annaswamy, A.M. and Ghoniem, A.F. (2000) "Managing Heat Release Dynamics for Control of Thermoacoustic Instability Using Pulsed-Fuel Injection," *RTO AVT Symposium on Active Control Technology for Enhanced Performance Operational Capabilities of Military Aircraft, Land Vehicles and Sea Vehicles*, Braunschweig, Germany.

Hathout, J.P., Fleifil, M., Annaswamy, A.M. and Ghoniem, A.F. (2000) "Heat-Release Actuation for Control of Mixture-Inhomogeneity-Driven Combustion Instability," *Twenty-Eighth (International) Symposium on Combustion*, Vol. 28, pp. 721–730.

Hathout, J., Fleifil, M., Rumsey, J., Annaswamy, A.M. and Ghoneim, A.F. (1997) "Model-Based Analysis and Design of Active Control of Thermoacoustic Instability," *Proc. 1997 IEEE Int. Conf. on Cont. App.*, Hartford, CT.

Niculescu, S., Annaswamy, A.M., Hathout, J. and Ghoniem, A.F. (2000) "Control of Time-Delay Induced Instabilities in Combustion Systems," *IEEE CDC Conference*.

REFERENCES

Park, S., Annaswamy, A.M. and Ghoniem, A.F. (2002) "Heat Release Dynamics Modeling of Kinetically Controlled Burning," *Comb. and Flame*, Vol. 128, No. 5, pp. 217–231.

Prasanth, R., Annaswamy, A.M., Hathout, J. and Ghoniem, A.F. (2000) "When Do Open-Loop Strategies for Combustion Control Work?," *36th AIAA/ASME/SAE/ASEE Joint Propulsion Conference*, AIAA-2000-3350.

Rumsey, J., Fleifil, M., Annaswamy, A.M., Hathout, J. and Ghoniem, A.F. (1997) "The Role of Active Control in Suppressing Thermoacoustic Instability," *American Control Conference*, pp. 2697–2702.

Rumsey, J., Fleifil, M., Annaswamy, A.M., Hathout, J. and Ghoniem, A.F. (1998) "Low-Order Nonlinear Models of Thermoacoustic Instabilities and Linear Model-Based Control," *MIT Adaptive Control Laboratory Report*.

MORGANTOWN ENERGY TECHNOLOGY CENTER

Richards, G.A., Straub, D.L. and Robey, E.H. (2003) "Control of Combustion Dynamics Using Fuel System Impedance," ASME Paper GT-2003-38521.

Richards, G.A., Straub, D.L. and Robey, E.H. (2001) "Dynamic Response of a Premix Fuel Injector," ASME Paper 2001-GT-036.

Richards, G.A., Yip, M.J., Robey, E.H., Cowell, L. and Rawlins, D. (1995) "Combustion Oscillation Control by Cyclic Fuel Injection," ASME Paper 95-GT-224.

Richards, G.A., Janus, M. and Robey, E.H. (1999) "Active Control of Flame Oscillations with Equivalence Ratio Modulation," *J. Prop. and Power*, Vol. 15, No. 2, pp. 232–240.

Richards, G.A. and Janus, M.C. (1998) "Characterization of Oscillations During Premix Gas Turbine Combustion," *J. Eng. for Gas Turb. and Power*, Vol. 120, No. 2, pp. 294–302.

Richards, G.A., Gemmen, R.S. and Yip, M.J. (1997) "A Test Device for Premixed Gas Turbine Combustion Oscillations," *J. of Eng. for Gas Turb. and Power*, Vol. 119, pp. 776–782.

Richards, G.A., Morris, G.J., Shaw, D.W., Keely, S.A. and Welter, M.J. (1993) "Thermal Pulse Combustion," *Combustion Science and Technology*, Vol. 94, pp. 75–85.

Straub, D.L., Richards, G.A., Baumann, W.T. and Saunders, W.R. (2001) "Measurement of Dynamics Flame Response in a Lean Premixed Single-Can Combustor," ASME Paper 2001-GT-0038.

Straub, D.L., Richards, G.A., Yip, M.J., Rodgers, W.A. and Robey, E.H. (1998) "Importance of Axial Swirl Vane Location on Combustion Dynamics for Lean Premix Fuel Injectors," *34th AIAA/ASME/SAE/ASEE Joint Propulsion Conference*, AIAA-98-3909.

NAVAL WEAPONS CENTER (NWC)

Acharya, S., Gutmark, E.J., Stephens, J. and Li, J. (2002) "Open-Loop Control of Swirl Stabilized Spray Flames," Chapter 20 of *Combustion Instabilities in Gas Turbines*, Vol 210 of *Progress in Astronautics and Aeronautics*, (T. Lieuwen and V. Yang, Editors), pp. 323–340.

Schadow, K.C., Gutmark, E. and Wilson, K.J. (1992) "Active Combustion Control in a Coaxial Dump Combustor," *Comb. Sci. and Tech.*, Vol. 51, pp. 285–300.

Yu, K.H., Wilson, K.J., Parr, T.P. and Schadow, K.C. (2002) "Liquid-Fueled Active Control for Ramjet Combustors," Chapter 21 of *Combustion Instabilities in Gas Turbines*, Vol 210 of *Progress in Astronautics and Aeronautics*, (T. Lieuwen and V. Yang, Editors), pp. 341–360.

PENNSYLVANIA STATE UNIVERSITY

Broda, J.C., Seo, S., Santoro, R.J., Shirhattikar, G. and Yang, V. (1998) "An Experimental Study of Combustion Dynamics of a Premixed Swirl Injector," *Twenty-Seventh Symposium (International) on Combustion, Proc. of the Comb. Inst.*, Vol. 27, pp. 1849–1856.

Fung, Y.-T. and Yang, V. (1992) "Active Control of Nonlinear Pressure Oscillations in Combustion Chambers," *J. Prop. and Power*, Vol. 8, No. 6, pp. 1282–1289.

Fung, Y.-T., Yang, V. and Sinha, A. (1991) "Active Control of Combustion Instabilities with Distributed Actuators," *Comb. Sci. and Tech.*, Vol. 78, No. 6, pp. 217–245.

Fung, Y.-T. (1991) *Active Control of Linear and Nonlinear Pressure Oscillations in Combustion Chambers*, Ph.D. Thesis, The Pennsylvania State University.

Hong, B.S. (1999) *Robust Control of Combustion Instabilities*, Ph.D. Thesis, The Pennsylvania State University.

Hong, B.-S., Yang, V. and Ray, A. (2000) "Robust Feedback Control of Combustion Instability with Modeling Uncertainty," *Comb. and Flame*, Vol. 120, pp. 91–106.

Hong, B.-S., Yang, V. and Ray, A. (2002) "Wide-Range Robust Control of Combustion Instability," *Comb. and Flame*, Vol. 128, pp. 242–258.

Kim, K., Lee, J.G. and Santavicca, D.A. (2002) "Optimization of the Spatial and Temporal Fuel Distribution for Active Control of Combustion Dynamics in Lean Premixed Combustors," AIAA-2002-4024.

Koshigoe, S., Komatsuzaki, T. and Yang, V. (1999) "Adaptive Control of Combustion Instability with On-Line System Identification," *J. Prop. and Power*, Vol. 15, No. 3, pp. 383–389.

Lee, J.G. and Santavicca, D.A. (2003) "Experimental Diagnostics for the Study of Combustion Instabilities in Lean-Premixed Combustors," *J. Prop. and Power*, Vol. 19, No. 5, pp. 735–749.

REFERENCES

- Lee, J.G., Kim, K. and Santavicca, D.A. (2000) "Measurement of Equivalence Ratio Fluctuation and Its Effect on Heat Release During Unstable Combustion," *Proc. of the Comb. Inst.*, Vol. 28, pp. 415–421.
- Lee, J.G., Kim, K. and Santavicca, D.A. (2002) "A Study of the Role of Equivalence Ratio Fluctuation During Unstable Combustion in a Lean Premixed Combustor," AIAA Paper 2002-4015.
- Lee, J.G., Kim, K. and Santavicca, D.A. (2000) "Effect of Injection Location on the Effectiveness of an Active Control System Using Secondary Fuel Injection," *Proc. of the Comb. Inst.*, Vol. 28, pp. 739–746.
- Lee, S.Y., Seo, S., Broda, J.C., Pal, S. and Santoro, R.J. (2000) "An Experimental Estimation of Mean Reaction Rate and Flame Structure During Combustion Instability in a Lean Premixed Gas Turbine Combustor," *Proc. of the Comb. Inst.*, Pittsburgh, PA, Vol. 28, pp. 775–782.
- Venkataraman, K.K., Preston, L.H., Simons, D.W., Lee, B.J., Lee, J.G. and Santavicca, D.A. (1999) "Mechanism of Combustion Instability in a Lean Premixed Dump Combustor," *J. Prop. and Power*, Vol. 15, No. 6, pp. 909–918.
- Yang, V., Hong, B.-S. and Ray, A. (2002) "Robust Feedback of Combustion Instabilities with Model Uncertainties," Chapter 22 of *Advances in Chemical Propulsion*, (G.D. Roy, Ed.), pp. 361–380.
- Yang, V., Sinha, A. and Fung, Y.-T. (1988): "Linear Theory of Active Control of Pressure Oscillations in Combustion Chambers, *AIAA/ASME/SAE/ASEE 24th Joint Propulsion Conference*, AIAA-88-2944.
- Yang, V., Sinha, A. and Fung, Y.-T. (1992) "State-Feedback Control of Longitudinal Combustion Instabilities," *J. Prop. and Power*, Vol. 8, No. 1, pp. 66–73.
- You, D.N., Huang, Y. and Yang, V. (2005) "A Generalized Model of Acoustic Response of Turbulent Premixed Flame and Its Application to Gas-Turbine Combustion Instability Analysis," *Combustion Science and Technology*, Vol. 177, No. 5-6, pp. 1109–1150.

STANFORD UNIVERSITY

- Franklin, G.F., Powell, J.D. and Emami-Naeini, A. (2002) *Feedback Control of Dynamic Systems* (4th Edition), Prentice Hall Inc., Upper Saddle River, N.J.
- Kemal, A. and Bowman, C.T. (1996) "Real-Time Adaptive Feedback Control of Combustion Instability," *Twenty-Sixth Symposium (International) on Combustion*, The Combustion Institute, pp. 2803–2809.
- McManus, K.R. and Bowman, C.T. (1990) "Effects of Controlling Vortex Dynamics on the Performance of a Dump Combustor," *Twenty-Third Symposium (International) on Combustion*, The Combustion Institute, pp. 1093–1099.
- McManus, K.R., Vandsburger, V. and Bowman, C.T. (1990) "Combustor Performance Enhancement Through Shear Layer Excitation," *Comb. and Flame*, Vol. 82, pp. 75–92.
- Padmanabhan, K.T., Bowman, C.T. and Powell, J.D. (1994) "An Adaptive Optimal Combustion Control Strategy," *Comb. and Flame*, Vol. 100, pp. 101–110.

Padmanabhan, K.T., Bowman, C.T. and Powell, J.D. (1995) "On-Line Combustor Performance Optimization," SPIE Proceedings Vol. 2494, Paper 2494-13, pp. 138–149.

Padmanabhan, K.T., Bowman, C.T. and Powell, J.D. (1996) "On-Line Adaptive Optimal Combustor Control," *IEEE Trans. on Cont. Syst. Tech.*, Vol. 4, No. 3, 217–229.

TECHNISCHE UNIVERSITÄT, MÜNCHEN/SIEMENS

Berenbrink, P. and Hoffmann, S. (2000) "Suppression of Dynamic Combustion Instabilities by Passive and Active Means," *ASME Turbo Expo 2000*, Paper 2000-GT-0079.

Casentini, F., Hermann, J., Vortmeyer, D. and Gleis, S. (1997) "NO and CO Reduction by Pulsating the Air FFlow on a Swirl Spray Burner," *Fourth International Conference on Technologies and Combustion for a Clean Environment*, Lisbon, Portugal.

Gleis, S., Vortmeyer, D. and Rau, W. (1990) "Experimental Investigation on the Transition from Stable to Unstable Combustion by Means of Active Instability Control," *75th Symposium*, PEP Panel, AGARD, *Hypersonic Combined Cycle Propulsion*, CP479.

Gleis, S. and Vortmeyer, D. (1989)b "Die Aktive Instabilitätskontrolle" als Untersuchungsmethode für Selbsterregte Verbrennungsininstabilitäten," VDI Berichte NR. 765, pp. 645–656.

Hantschk, C., Hermann, J. and Vortmeyer, D. (1996) "Active Instability Control with Direct-Drive Servo Valves in Liquid-Fueled Combustion Systems," *26th (International) Symposium on Combustion*, The Combustion Institute, pp. 2835–2841.

Hantschk, C.-C. and Vortmeyer, D. (2002) "Numerical Simulations of Self-Excited Combustion Oscillations in a Non-Premixed Burner," *Comb. Sci. and Tech.*, Vol. 174, pp. 189–204.

Hermann, J., Gleis, S. and Vortmeyer, D. (1996) "Active Instability Control (AIC) of Spray Combustors by Modulation of the Liquid Flow Rate," *Comb. Sci. and Tech.*, Vol. 118, pp. 1–25.

Hermann, J., Orthmann, A., Hoffmann, S. and Berenbrink, P. (2000) "Combination of Active Instability Control and Passive Measures to Prevent Combustion Instabilities in a 260 MW Heavy Duty Gas Turbine," *RTO AVT Symposium on Active Control Technology for Enhanced Performance Operational Capabilities of Military Aircraft, Land Vehicles and Sea Vehicles*, Braunschweig, Germany.

Hermann, J., Zangl, P., Gleis, S. and Vortmeyer, D. (1995) "Untersucheng der Anregungsmechanismen selbsterregter Verbrennungschwingunger an einem Verbrennungssystem für Flüssigkraftstoff," VDI Berichte NR. 1193, pp. 251–260.

Hoffman, S., Weber, G., Judith, J., Hermann, J. and Orthmann, J. (1998) "Application of Active Combustion Instability Control to Siemens Heavy Duty Gas Turbines," *Symposium of the AVT Panel on Gas Turbine Engine Combustion, Emissions and Alternative Fuels*, RTO-MP-AGARD.

Krüger, U., Hüren, J., Hoffmann, S., Krebs, W., Flohr, P. and Bohn, D. (2001) "Prediction and Measurement of Thermoacoustic Improvements in Gas Turbines with Annular Combustion Systems," *J. of Eng. for*

REFERENCES

Gas Turb. and Power, Vol. 123, pp. 557–566.

Krüger, U., Hüren, J., Hoffmann, S., Krebs, W. and Bohn, D. (1999) “Prediction of Thermoacoustic Instabilities with Focus on the Dynamic Flame Behavior for the 3A-Series Gas Turbine of Siemens KWU,” ASME Paper 99-GT-111.

Lang, W. and Vortmeyer, D (1987) “Messung der Scallschnelle in einer Schwingenden Flamme mit einen Laser-Doppler Anemometer,” VDI Berichte NR. 645, pp. 337–349.

Seume, J.R., Vortmeyer, N., Krause, W., Hermann, J., Hantsch, C.-C., Zangl, P., Gleis, S., Vortmeyer, D. and Ortmann, A. (1998) “Application of Active Combustion Instability Control to a Heavy Duty Gas Turbine,” *J. of Eng. for Gas Turb. and Power*, Vol. 120, pp. 721–726.

Schimmer, J. and Vortmeyer, D. (1977) “Acoustical Oscillation in a Combustion System with a Flat Flame,” *Comb. and Flame*, Vol. 28, pp. 17–24.

Schuermans, B., Polifke, W. and Paschereit, C.O. (2000) “Prediction of Acoustic pressure Spectra in Gas Turbines Based on Measured Transfer Matrices,” ASME Turbo Expo '00.

Teutsch, H. (1990) “Elektromagnetischer Linearmotor für direkt betätigte Servoventile,” *Ölhydraulik und Pneumatik*, V. 34, Nr. 11, pp. 754–761.

UNITED TECHNOLOGIES RESEARCH CENTER

Banaszuk, A., Aryiur, K.B., Krstic, M. and Jacobson, C.A. (2004) “An Adaptive Algorithm for Control of Combustion Instability,” *Automatica* Vol. 40, No. 11, pp. 1965–1972.

Banaszuk, A., Hagen, G., Mehta, P.G. and Oppelstrup, J. (2003) “A Linear Model for Control of Thermoacoustic Instabilities on Annular Domain,” *Proceedings of the 42nd IEEE Conference on Decision and Control*, pp. 2346–2351.

Banaszuk, A., Jacobson, C.A., Khibnik, A.I. and Mehta, P.G. (1999) “Linear and Nonlinear Analysis of Controlled Combustion Processes, Part I: Linear Analysis,” *Proceedings of the 1999 IEEE International Conference on Control Applications*, Kohala-Coast, HI.

Banaszuk, A., Jacobson, C.A., Khibnik, A.I. and Mehta, P.G. (1999) “Linear and Nonlinear Analysis of Controlled Combustion Processes, Part II: Nonlinear Analysis,” *Proceedings of the 1999 IEEE International Conference on Control Applications*, Kohala-Coast, HI, pp. 199–212.

Banaszuk, A., Mehta, P.G., Jacobson, C.A. and Khibnik, A.I. (2005) “Limits of Achievable Performance of Controlled Combustion Processes,” submitted to *IEEE Trans. on Cont. Syst. Tech.*

Barooah, P., Anderson, T.J. and Cohen, J.M. (2002) “Active Combustion Instability Control with Spinning Valve Actuator,” *ASME J. of Eng. for Gas Turb. and Power*, Vol. 125, pp. 925–932, ASME Paper GT-2002-30042.

- Cohen, J.M. and Banaszuk, A. (2003) "Factors Affecting the Control of Unstable Combustors," *J. Prop. and Power*, Vol. 19, No. 5, pp. 811–821; also, AIAA *Progress in Astronautics and Aeronautics*, Vol. 210, (T.C. Lieuwen and V. Yang, Editors).
- Cohen, J.M., Banaszuk, A., Hibshman, J.R., Anderson, T.J. and Alholm, H.A. (2005) "Active Control of Combustion Instability in a Liquid-Fueled Sector Combustor," to appear in ASME *J. of Eng. for Gas Turb. and Power*.
- Cohen, J.M. and Proscia, W. (2005) "Characterization and Control of an Aeroengine Combustion Instability," to be published in AIAA *Progress in Astronautics and Aeronautics*, Vol. 210, (T.C. Lieuwen and V. Yang, Editors).
- Cohen, J.M., Rey, N.M., Jacobson, C.A. and Anderson, T.J. (1999) "Active Control of Combustion Instabilities in a Liquid-Fueled Low-NOx Combustor," *J. of Eng. for Gas Turb. and Power*, Vol. 121, No. 2, pp. 281–284.
- Cohen, J.M., Shufflebeam, J.H. and Proscia, W. (2001) "The Effect of Fuel/Air Mixing on Actuation Authority in an Active Combustion Instability Control System," ASME *J. Eng. Gas Turb. and Power*, Vol. 123, pp. 537–542.
- Cohen, J.M., Shufflebeam, J.H. and Proscia, W. (2001) "The Effect of Fuel/Air Mixing on Actuation Authority in an Active Combustion Instability Control System," *J. of Eng. for Gas Turb. and Power*, Vol. 123, No. 3, pp. 537–542.
- Hagen, G. and Banaszuk, A. (2004) "Symmetry-Breaking and Uncertainty Propagation in a Reduced Order Thermo-Acoustic Model," *Proceedings of the 43rd IEEE Conference on Decision and Control*.
- Hibshman, J.R., Cohen, J.M., Banaszuk, A., Anderson, T.J. and Alholm, H.A. (1999) "Active Control of Combustion Instability in a Liquid-Fueled Sector Combustor," *ASME Turbo Expo 1999*, Paper 99-GT-215.
- Kendrick, D.W., Anderson, T.J. and Sowa, W.A. (1998) "Acoustic Sensitivities of Lean-Premixed Fuel Injectors in a Single Nozzle Rig," ASME Paper 98-GT-382.
- Krstic, M. and Banaszuk, A. (2005) "Multivariable Adaptive Control of Instabilities Arising in Jet Engines," to appear in *Control Engineering Practice*.
- Lieuwen, T. and Banaszuk, A. (2005) "Background Noise Effects on Combustor Stability," *J. Prop. and Power*, Vol. 21, No. 1, pp. 25–31.
- Lovett, J.A. and Uzmanski, K.T. (2002) "Prediction of Combustion Dynamics in a Staged Premixed Combustor," ASME, Paper GT-2002-30646.
- Lovett, J.A., Chu, W.-W. and Shah, S.N. (1999), "Modeling of Combustion Chamber Acoustics and Control of Combustion Instabilities in Gas Turbines," *6th International Congress on Sound and Vibration*.
- Mehta, P.G. and Banaszuk, A. (2001) "On the Identification of a Nonlinear Function in a Feedback Loop," *Proceedings of the IEEE Conference on Decision and Control*.

REFERENCES

- Mehta, P.G. and Soteriou, M.C. (2003) "Reduced Order Modeling of Premixed Flame Dynamics in Bluffbody Combustors," submitted to *Comb. and Flame*.
- Mehta, P.G., Soteriou, M.C. and Banaszuk, A. (2004) "Distributed Control-Oriented Modeling of Thermoacoustic Dynamics in a Duct," *American Control Conference*, Vol. 6, pp. 5692–5697.
- Mehta, P.G., Soteriou, M.C. and Banaszuk, A. (2005) "Impact of Exothermicity on Steady and Linearized Response of Premixed Ducted Flame," *Comb. and Flame*, Vol. 141, pp. 392–405.
- Mehta, P.G., Soteriou, M.C., Banaszuk, A. and Mezic, I. (2003) "Fuel Control of a Ducted Bluffbody Flame," *Proceedings of the 42nd IEEE Conference on Decision and Control*, pp. 2340–2345.
- Murray, R.M., Jacobson, C.A., Casas, R., Khibnik, A.I., Johnson, C.R. Jr., Bitmead, R., Peracchio, A.A. and Proscia, W.M. (1998) "System Identification for Limit Cycling System: A Case Study for Combustion Instabilities," *American Control Conference*, pp. 2004–2008.
- Peracchio, A.A. and Proscia, W.M. (1998) "Nonlinear Heat Release/Acoustic Model for Thermo-Acoustic Instability in Lean Premixed Combustors," *ASME Paper 98-GT-269*.
- Tuncer, O., Acharya, S. Banaszuk, A. and Cohen, J. (2003) "Side Air-Jet Modulation for Control of Heat Release and Pattern Factor," *ASME Turbo Expo 2003*, Paper GT2003-38853.

ADDITIONAL REFERENCES ON ACTIVE CONTROL OF COMBUSTION SYSTEMS

- Acharya, S., Murugappan, S., O'Donnell, M. and Gutmark, E.J. (2003) "Characteristics and Control of Combustion Instabilities in a Swirl-Stabilized Spray Combustor," *J. Prop. and Power*, Vol. 19, No. 3, pp. 484–496.
- Bhidayasiri, R., Sivasegaram, S. and Whitelaw, J.H. (2002) "Control of Oscillations in Premixed Gas Turbine Combustors," Chapter 19 of *Combustion Instabilities in Gas Turbines*, Vol 210 of *Progress in Astronautics and Aeronautics*, (T. Lieuwen and V. Yang, Editors), pp. 303–322.
- Bode, H.W. (1945) *Network Analysis and Feedback Amplifier Design*, D. Van Nostrand Company, Inc., N.Y.
- Di Stefano, J.J. III, Stubberud, A.P. and Williams, I.J. (1990) *Feedback and Control Systems*, Schaum's Outline Series, McGraw-Hill, Inc., N.Y.
- Doyle, J.C., Francis, B.A. and Tannenbaum, A.R. (1992) *Feedback Control Theory*, Macmillan Book Publishing Co., N.Y.
- Fannin, C.A., Saunders, W.R., Vaudrey, M.A., Eisenhower, B. and Vandsburger, U. (1999) "Analytical and Practical Consideration for Control of Thermoacoustic Instabilities," *37th AIAA Aerospace Sciences Meeting*, AIAA-99-0718.
- Freudenberg, J.S. and Looze, D.P. (1987) "A Sensitivity Tradeoff for Plants with Time Delay," *IEEE Trans. on Auto. Contr.*, Vol. AC-32, No. 2, pp. 99–104.

- Hayashi, A.K., Yamazaki, Y., Mizuno, T., Ozawa, S., Yamamoto, T., Kagiya, S. and Motagi, T. (2002) "Active Control of Combustion Oscillations for Premixed Combustion Systems," *J. Phys. IV*, Vol. 12, pp. 281–289.
- Hobson, D.E., Fackrell, J.E. and Hewitt, G. (2000) "Combustion Instabilities in Industrial Gas Turbines—Measurements on Operating Plant and Thermoacoustic Modeling," *J. of Eng. for Gas Turb. and Power*, Vol. 122, No. 3, pp. 420–428.
- Ichikawa, K. (1985) "Frequency-Domain Pole Assignment and Exact Model-Matching for Delay Systems," *Int. J. Control*, Vol. 41, No. 4, 1015–1024.
- Kochenburger, R.J. (1950) "A Frequency Response Method for Analyzing and Synthesizing Contactor Servomechanisms," *AIEE Transactions*, Vol. 69, pp. 270–284.
- Kopasakis, G. (2003) "High-Frequency Instability Suppression Controls in a Liquid-Fueled Combustor," *39th AIAA/ASME/SAE/ASEE Joint Propulsion Conference and Exhibit*, AIAA-2003-1458.
- Le, D., DeLaat, J. and Chang, C. (2003) "Control of Thermo-Acoustic Instabilities: The Multi-Scale Extended Kalman Approach," *39th AIAA/ASME/SAE/ASEE Joint Propulsion Conference and Exhibit*, AIAA-2003-4934.
- McManus, K.R., Magill, J.C. and Miller, M.F. (1998) "Combustion Instability Suppression in Liquid-Fueled Combustors," *37th AIAA Aerospace Sciences Meeting*, AIAA-98-0642.
- McManus, K.R., Magill, J.C., Miller, M.F. and Allen, M.G. (1997) "Closed Loop System for Stability Control in Gas Turbine Combustors," AIAA Paper 97-0463.
- Murugappan, S., Acharya, S., Gutmark, E. and Messina, T. (1999) "Characteristics and Control of Combustion Instabilities in a Swirl-Stabilized Spray Combustor," *35th Joint Propulsion Conference and Exhibit*, AIAA-99-2487.
- Nyquist, H. (1932) "Regeneration Theory," *Bell System Technical Journal*, Vol. 16, pp. 126–147.
- Ogata, K. (1990) *Modern Control Engineering*, Prentice Hall, Englewood Cliffs, NJ.
- Rhode, M.A., Rollins, R.W., Markworth, A.J., Edwards, K.D., Nguyen, K., Daw, C.S. and Thomas, J.F. (1995) "Controlling Chaos in a Model of Thermal Pulse Combustion," *Applied Physics*, Vol. 78, No. 4, p. 2224–2232.
- Richards, G. and Straub, D. (2003) "Passive Control of Combustion Dynamics in Stationary Gas Turbines," *J. of Prop. and Power*, Vol. 19, No. 5, pp. 795–810.
- Saunders, W.R., Vaudrey, M.A., Eisenhower, B.A., Vandsburger, U. and Fannin, C.A. (1999) "Perspectives on Linear Compensator Designs for Active Combustion Control," *37th AIAA Aerospace Sciences Meeting*, AIAA-99-0717.

REFERENCES

- Scarinci, T. and Freeman, C. (2000) "The Propagation of a Fuel-Air Ratio Disturbance in a Simple Premixer and its Influence on Pressure Wave Amplification," ASME Paper 2000-GT-0106.
- Scarinci, T., Freeman, C. and Day, I. (2004) "Passive Control of Combustion Instability in a Low Emissions Aeroderivative Gas Turbine," ASME Paper 2004-53767.
- Scarinci, T. and Halpin, J.L. (2000) "Industrial Trent Combustor—Combustion Noise Characteristics," *J. of Eng. for Gas Turb. and Power*, Vol. 122, No. 2, pp. 280–286.
- Schwarzenbach, J. and Gill, K.F. (1978) *System Modeling and Control*, John Wiley & Sons, New York.
- Sivasegaram, S., Tsai, R.F. and Whitelaw, S.H. (1995) "Control of Oscillations by Forced Oscillation of Part of the Fuel Supply," *Comb. Sci. and Tech.*, Vol. 105, pp. 67–83.
- Steele, R.C., Cowell, L.H., Cannon, S.M. and Smith, C.E. (2000) "Passive Control of Combustion Instability in Lean Premixed Combustors," *J. of Eng. for Gas Turb. and Power*, Vol. 122, pp. 412–419.
- Truxal, J.G. (1955) *Automatic Feedback Control System Synthesis*, McGraw-Hill Book Company, Inc., N.Y.
- Yu, K.H., Pang, B. and Hsu, O. (2001) "Implementing Active Combustion Control in Propulsion Systems," *37th AIAA/ASME/SAE/ASEE Joint Propulsion Conference*, AIAA-2001-3849.
- Ziada, S. and Gref, H. (1998) "Feedback Control of Combustion Oscillations," *J. Fl. and Struct.*, Vol. 14, pp. 491–507.

REFERENCES ON ADAPTIVE CONTROL

- Anthoine, J., Mettenleiter, M., Repellin, O., Buchlin, J.-M. and Candel, S. M. (2000) "Influence of Adaptive Control on Vortex Driven Instabilities in a Scaled Model of Solid Propellant Motors," *J. Sound and Vib.*, Vol. 262, No. 5, pp. 1009-1046.
- Åstöm, K.J. (1983) "Theory and Applications of Adaptive Control—A Survey," *Automatica*, Vol. 19, No. 5, pp. 471–486.
- Åstöm, K.J. and Wittenmark, B. (1995) *Adaptive Control*, Addison-Wesley Publishing Company, Inc., Reading, MA.
- Banaszuk, A., Aryiur, K.B., Krstic, M. and Jacobsen, C.A. (2004) "An Adaptive Algorithm for Control of Combustion Instability," *Automatica*, Vol. 40, No. 11, pp. 1965–1972.
- Billoud, G., Galland, M.A., Huynh, C. and Candel, S.M. (1992) "Adaptive Active Control of Combustion instabilities," *Comb. Sci. and Tech.*, Vol. 81, pp. 257–283.
- Evesque, S., Park S., Riley, A.J., Annaswamy, A.M. and Dowling, A.P. (2004) "Adaptive Combustion Instability Control with Saturation: Theory and Validation," *J. Prop. and Power*, Vol. 20, No. 6, pp. 1086–1095.

Kopasakis, G. and DeLaat, J. (2002) "Adaptive Instability Suppression Controls in a Liquid-Fueled Combustor," *38th AIAA/ASME/SAE/ASEE Joint Propulsion Conference and Exhibit*, AIAA-2002-4075, NASA TM-2002-21805.

Mettenleiter, M. and Candel, S. (2000) "Developments of Adaptive Methods for Active Instability Control," RTO AVT Symposium on *Active Control Technology for Enhanced Performance Operational Capabilities of Military Aircraft, Land Vehicles and Sea Vehicles*, Braunschweig, Germany.

Mettenleiter, M., Halie, E. and Candel, S.M. (2000) "Adaptive Control of Aeroacoustic Instabilities," *J. Sound and Vib.*, Vol. 230, No. 4, pp. 761-784.

Mettenleiter, M. (2000) "Contrôle Adaptif der Instabilités Aeroacoustiques Application aux Systèmes de Propulsion," Thèse pour l'obtention du Grade de Docteur, Laboratoire E. M2.C, École Centrale, Paris.

Stone, C. and Menon, S. (2002) "Adaptive Swirl Control of Combustion Instability in Gas Turbine Combustors," *Proc. of the Comb. Inst.*, Vol. 29, pp. 155-160.

Riley, A.J., Park, S., Dowling, A.P., Evesque, S. and Annaswamy, A.J. (2003) "Adaptive Closed-Loop Control of an Atmospheric Gaseous Lean-Premixed Combustor," *ASME Turbo Expo 2003*, Paper GT2003-38418.

Widrow, B. and Stearns, S.D. (1985) *Adaptive Signal Processing*, Prentice-Hall, New York.

REFERENCES



ANNEX A

Equations of Motion

Combustion systems commonly contain condensed phases: liquid fuel or oxidizer and combustion products including soot and condensed metal oxides. Hence the equations of motion must account for two or three phases and at least one species in each. For investigating the dynamics of combustors, it is entirely adequate to represent each phase as its mass average over all member species. It is unnecessary to distinguish liquid and solid material and we assume a single species in the condensed phase, denoted by subscript $(\)_l$. For some applications it is appropriate to extend the representation slightly to accommodate distributions of particle sizes, not included in this annex. There is some advantage to treating the gas phase as a multi-component reacting mixture. As the primitive conservation equations we therefore begin with the following set:

A.1. General Equations of Motion

Conservation of Species, Gas Phase¹

$$\frac{\partial \rho_{gi}}{\partial t} + \nabla \cdot (\rho_{gi} \mathbf{u}_{gi}) = w_{gi} + w_{gi}^{(l)} + w_{gei} \quad (\text{A.1})$$

Global Conservation of Mass, Gas Phase

$$\frac{\partial \rho_g}{\partial t} + \nabla \cdot (\rho_g \mathbf{u}_g) = w_g^{(l)} + w_{eg} \quad (\text{A.2})$$

Global Conservation of Mass, Condensed Phase²

$$\frac{\partial \rho_l}{\partial t} + \nabla \cdot (\rho_l \mathbf{u}_l) = -w_g^{(l)} + w_{el} \quad (\text{A.3})$$

Global Conservation of Momentum

¹Superscript $(\)^{(l)}$ on $w_{gi}^{(l)}$ means that the source material is liquid. Thus $w_{gi}^{(l)}$ is the rate at which species i of the gas phase is produced from the liquid phase. The dimensions of $w_{gi}^{(l)}$ are mass per unit volume of space, per unit time.

²Note that ρ_l represents the mass of condensed material per unit volume of chamber, *not* the density of the material itself. Subscript $(\)_l$ denotes ‘liquid’; at the temperature prevailing in combustion chambers, most condensed materials are liquid.

$$\frac{\partial}{\partial t} \left(\sum^i \rho_{gi} \mathbf{u}_{gi} + \rho_l \mathbf{u}_l \right) + \nabla \cdot \left(\sum \rho_{gi} \mathbf{u}_{gi} \mathbf{u}_{gi} + \rho_l \mathbf{u}_l \right) + \nabla p = \nabla \cdot \vec{\tau}_v + \mathbf{m}_{eg} + \mathbf{m}_{el} \quad (A.4)$$

Global Conservation of Energy

$$\frac{\partial}{\partial t} \left(\sum \rho_{gi} e_{goi} + \rho_l e_{ol} \right) + \nabla \cdot \left(\sum \rho_{gi} \mathbf{u}_{gi} e_{goi} + \rho_l \mathbf{u}_l e_{ol} \right) + \nabla \cdot \left(\sum p_i \mathbf{u}_{gi} \right) = \nabla \cdot \left(\vec{\tau}_v \cdot \mathbf{u}_g \right) - \nabla \cdot \mathbf{q} + Q_e \quad (A.5)$$

Equation of State, Gas Phase

$$p = \rho_g R_g T_g \quad (A.6)$$

For simplification, the above equations already contain some terms involving mass averaging over the species comprising the gas phase, namely the viscous tensor $\vec{\tau}_v$; the vector \mathbf{q} representing heat conduction; and the equation, of state (A.6). For more complete derivations of the equations for multicomponent mixtures, see for example Chapman and Cowling (1939); Hirschfelder, Curtis and Bird (1954); Toupin and Truesdell (1960); and Williams (1985). Superscript (l) means that the liquid or condensed phase is the source and subscript (e) denotes an external source. Thus $w_g^{(l)}$ represents the rate at which gas is generated from liquid, and w_{ge} stands for the rate at which gas is generated by an external source. It follows from repeated use of the Gibbs-Dalton law for mixtures of perfect gases that p is the sum of partial pressures; ρ_g is the sum of the densities; and R is the mass average of the individual gas species, so for the gas phase we have

$$p = \sum p_i$$

$$\rho_g = \sum \rho_{gi} \quad (A.7) \text{ a,b,c}$$

$$R_g = \frac{1}{\rho_g} \sum \rho_{gi} R_i$$

Subscript (i) identifies the i^{th} gaseous species; and in all cases except T_g , $()_g$ means a mass average over all gas species as, for example,

$$\mathbf{u}_g = \frac{1}{\rho_g} \sum \rho_{gi} \mathbf{u}_{gi} = \sum Y_{gi} \mathbf{u}_{gi} \quad (A.8)$$

where $Y_{gi} = \rho_{gi}/\rho_g$ is the mass concentration of the i^{th} species.

A.2. Mass, Momentum and Energy Transfer by Diffusion

The chief reasons for writing equations (A.1)–(A.5) explicitly with sums over species is to show the way in which diffusion of species arises; and to introduce the formula for the energy released by chemical reactions written in the conventional fashion. When definite problems are addressed, some approximations will be made to eliminate explicit dependence on diffusion velocities, but here we retain diffusion explicitly. Let \mathbf{V}_i denote the diffusion velocity of the i^{th} species with the definition

$$\mathbf{u}_{gi} = \mathbf{u}_g + \mathbf{V}_i \quad (\text{A.9})$$

Multiply by ρ_{gi} and sum:

$$\sum \rho_{gi} \mathbf{u}_{gi} = \left(\sum \rho_{gi} \right) \mathbf{u}_g + \sum \rho_{gi} \mathbf{V}_i$$

Thus with (A.7)b and (A.8), this relation becomes

$$\sum \rho_{gi} \mathbf{V}_i = 0 \quad (\text{A.10})$$

With $\rho_{gi} = \rho_g Y_{gi}$ and $\mathbf{u}_{gi} = \mathbf{u}_g + \mathbf{V}_i$, and substitution of equation (A.2) for global conservation of mass, the species equation (A.1) becomes

$$\rho_g \frac{\partial Y_{gi}}{\partial t} + \rho_g \mathbf{u}_g \cdot \nabla Y_{gi} = -\nabla \cdot (\rho_g \mathbf{V}_i Y_{gi}) + w_{gi} + w_{gi}^{(l)} + w_{gei} \quad (\text{A.11})$$

In the momentum equation, $\sum \rho_{gi} \mathbf{u}_{gi} = \rho_g \mathbf{u}_g$ and with (A.10),

$$\sum \rho_{gi} \mathbf{u}_{gi} \mathbf{u}_{gi} = \sum \rho_{gi} (\mathbf{u}_g + \mathbf{V}_i) (\mathbf{u}_g + \mathbf{V}_i) = \sum \rho_{gi} (\mathbf{u}_g \mathbf{u}_g + \mathbf{V}_i \mathbf{u}_{gi} + \mathbf{u}_{gi} \mathbf{V}_i + \mathbf{V}_i \mathbf{V}_i)$$

Hence (A.4) is

$$\begin{aligned} \frac{\partial}{\partial t} (\rho_g \mathbf{u}_g + \rho_l \mathbf{u}_l) + \nabla \cdot (\rho_g \mathbf{u}_g + \rho_l \mathbf{u}_l) + \nabla p &= \nabla \cdot \vec{\tau}_v + \mathbf{m}_{eg} + \mathbf{m}_{el} \\ &\quad - \sum \{ \nabla \cdot (\rho_{gi} \mathbf{V}_i \mathbf{u}_{gi} + \rho_{gi} \mathbf{u}_{gi} \mathbf{V}_i) + \nabla \cdot (\rho_{gi} \mathbf{V}_i \mathbf{V}_i) \} \end{aligned} \quad (\text{A.12})$$

Diffusion in a multicomponent mixture generally involves coupling among all species, accounted for by introducing a matrix of diffusion coefficients and Fick's law relating the diffusion velocities to the gradients of species concentrations. That representation introduces unnecessary complications in the present context. We use the common approximation that the diffusion velocity of every species is proportional to the concentration gradient of that species only, and obeys Fick's law of diffusion in a binary mixture,

$$\rho_{gi} \mathbf{V}_i = -\rho_g \mathcal{D} \nabla Y_{gi} \quad (\text{A.13})$$

where \mathcal{D} is the binary diffusion coefficient assumed to have the same value for all species.

ANNEX A – EQUATIONS OF MOTION

Even with the simple law (A.13), the momentum equation (A.12) is formally coupled nonlinearly to the species concentrations and to the total velocities \mathbf{u}_{gi} of the species. Let \mathbf{m}_D denote the terms involving diffusion,

$$\mathbf{m}_D = - \sum \{ \nabla \cdot (\rho_{gi} \mathbf{V}_i \mathbf{u}_{gi} + \rho_{gi} \mathbf{u}_{gi} \mathbf{V}_i) + \nabla \cdot (\rho_{gi} \mathbf{V}_i \mathbf{V}_i) \} \quad (\text{A.14})$$

and the global momentum equation is

$$\frac{\partial}{\partial t} (\rho_g \mathbf{u}_g + \rho_l \mathbf{u}_l) + \nabla \cdot (\rho_g \mathbf{u}_g \mathbf{u}_g + \rho_l \mathbf{u}_l \mathbf{u}_l) + \nabla p = \nabla \cdot \vec{\tau}_v + \mathbf{m}_e + \mathbf{m}_D \quad (\text{A.15})$$

where

$$\mathbf{m}_e = \mathbf{m}_{eg} + \mathbf{m}_{el} \quad (\text{A.16})$$

is the total momentum addition from external sources.

The viscous stress tensor $\vec{\tau}_v$ has a complicated form for a multicomponent mixture (Hirschfelder, Curtis and Bird, 1954). When necessary we will use a simple approximation. Unless shock waves are present, viscous effects internal to the flow field are negligible for combustion instabilities; they cannot be ignored at the boundaries.

Similar rearrangements of the energy equation (A.5) will lead to a form corresponding to (A.15). Substitute (A.8) in the first term of (A.5) and expand to give

$$\sum \rho_{gi} e_{goi} = \sum \rho_{gi} \left(e_{gi} + \frac{(\mathbf{u}_g + \mathbf{V}_i)^2}{2} \right) = \rho_g e_{og} + \sum \rho_{gi} \frac{\mathbf{V}_i^2}{2} \quad (\text{A.17})$$

where (A.10) has been applied and the mass averaged stagnation energy is

$$\rho_g e_{og} = \sum \rho_{gi} e_{goi} \quad (\text{A.18})$$

The term representing the total rate of work done by the partial pressures is

$$\sum p_i \mathbf{u}_{gi} = \sum p_i (\mathbf{u}_g + \mathbf{V}_i) = p \mathbf{u}_g + \sum p_i \mathbf{V}_i \quad (\text{A.19})$$

and the net effect of convection of energy by the motions of the individual species can be written in the form:

$$\begin{aligned}
 \sum \rho_{gi} \mathbf{u}_{gi} e_{goi} &= \sum \rho_{gi} \mathbf{u}_g \left(e_{gi} + \frac{\mathbf{u}_{gi}^2}{2} \right) + \sum \rho_{gi} \mathbf{V}_i e_{goi} \\
 &= \rho_g \mathbf{u}_g e_{og} + \mathbf{u}_g \sum \frac{1}{2} \rho_{gi} (\mathbf{u}_g + \mathbf{V}_i)^2 + \sum \rho_{gi} \mathbf{V}_i e_{goi} \\
 &= \rho_g \mathbf{u}_g e_{og} + \mathbf{u}_g \sum \rho_{gi} \mathbf{u}_g \cdot \mathbf{V}_i + \mathbf{u}_g \sum \frac{1}{2} \rho_{gi} \mathbf{V}_i^2 + \sum \rho_{gi} \mathbf{V}_i e_{goi} \\
 &= \rho_g \mathbf{u}_g e_{og} + \mathbf{u}_g \sum \frac{1}{2} \rho_{gi} \mathbf{V}_i^2 + \sum \rho_{gi} \mathbf{V}_i e_{goi}
 \end{aligned} \tag{A.20}$$

Substitution of (A.17), (A.19) and (A.20) in (A.5) leads to

$$\begin{aligned}
 & \frac{\partial}{\partial t} (\rho_g e_{og}) + \nabla \cdot (\rho_g \mathbf{u}_g e_{og}) + \frac{\partial}{\partial t} (\rho_l e_{ol}) + \nabla \cdot (\rho_l \mathbf{u}_l e_{ol}) + \nabla \cdot (p \mathbf{u}_g) + \\
 & + \left[\frac{\partial}{\partial t} \left(\sum \frac{1}{2} \rho_{gi} \mathbf{V}_i^2 \right) + \nabla \cdot \left\{ \mathbf{u}_g \sum \frac{1}{2} \rho_{gi} \mathbf{V}_i^2 + \sum (\rho_{gi} \mathbf{V}_i e_{goi} + p_i \mathbf{V}_i) \right\} \right] = \\
 & = \nabla \cdot (\overleftrightarrow{\tau}_v \cdot \mathbf{u}_g) - \nabla \cdot \mathbf{q} + Q_e
 \end{aligned} \tag{A.21}$$

Let χ_D denote all terms depending explicitly on the diffusion velocities;

$$-\chi_D = \frac{\partial}{\partial t} \left(\sum \frac{1}{2} \rho_{gi} \mathbf{V}_i^2 \right) + \nabla \cdot \left\{ \mathbf{u}_g \sum \frac{1}{2} \rho_{gi} \mathbf{V}_i^2 + \sum (\rho_{gi} \mathbf{V}_i e_{goi} + p_i \mathbf{V}_i) \right\} \tag{A.22}$$

and the energy equation is

$$\begin{aligned}
 & \frac{\partial}{\partial t} (\rho_g e_{og}) + \nabla \cdot (\rho_g \mathbf{u}_g e_{og}) + \frac{\partial}{\partial t} (\rho_l e_{ol}) + \nabla \cdot (\rho_l \mathbf{u}_l e_{ol}) + \nabla \cdot (p \mathbf{u}_g) = \nabla \cdot (\overleftrightarrow{\tau}_v \cdot \mathbf{u}_g) - \nabla \cdot \mathbf{q} \\
 & + Q_e + \chi_D
 \end{aligned} \tag{A.23}$$

A.3. Construction of the Single Fluid Model

The discussion so far has been concerned with a medium consisting of two phases: the condensed phase denoted by subscript ()_l and the gas phase, identified by subscript ()_g comprising many species. For a broad range of conditions in practical propulsion systems, the volume fraction occupied by the condensed phase is small compared with that for the gas phase, although the mass fraction may be large. For example, if the propellant contains 19% aluminum, the combustion products in a solid rocket will contain about 38% by mass of condensed aluminum oxide. In liquid fueled combustors (gas turbines, afterburners and liquid rockets) limited regions may contain large volumetric fractions of liquid, but generally the volume occupied by the gaseous species is the greater part.

ANNEX A – EQUATIONS OF MOTION

Under these conditions it is a valid approximation to use a ‘single-fluid model’ of the medium, a representation in which the density is the sum of the densities (mass per unit volume) of gas and condensed phase, $\rho = \rho_g + \rho_l$; the compressibility and pressure are those of the gas phase only; and the thermodynamic properties are mass averages of the gas and liquid phases. The chief immediate consequence is that the speed of sound for the single fluid correctly takes into account the primary individual effects of the gas and liquid phases: The sound speed is reduced by the presence of condensed material. Furthermore, the flow of the medium is dominated by the gas phase, with perturbations of its motion arising from interactions between the gas and condensed phases. We therefore seek a system of equations in which the density is the sum

$$\rho = \rho_g + \rho_l . \quad (\text{A.24})$$

Eventually the primary dependent variables for investigating the dynamics of a combustor will be ρ and the pressure, density and temperature of the gas.³

A.3.1. Equation for the Density. To find an equation for the density, add (A.2) and (A.3):

$$\frac{\partial \rho}{\partial t} + \nabla \cdot (\rho_g \mathbf{u}_g + \rho_l \mathbf{u}_l) = w_e \quad (\text{A.25})$$

where $\rho = \rho_g + \rho_l$ and the external source of mass is

$$w_e = w_{eg} + w_{el} \quad (\text{A.26})$$

Add $\nabla \cdot (\rho_l \mathbf{u}_g)$ to both sides of (A.25) and rearrange to give the desired equation,

$$\frac{\partial \rho}{\partial t} + \nabla \cdot \rho \mathbf{u} = \mathcal{W} \quad (\text{A.27})$$

where we have set $\mathbf{u} := \mathbf{u}_g$ and the source is

$$\mathcal{W} = w_e - \nabla \cdot (\rho_l \delta \mathbf{u}) \quad (\text{A.28})$$

The ‘slip velocity’ is

$$\delta \mathbf{u}_l = \mathbf{u}_l - \mathbf{u}_g \quad (\text{A.29})$$

³The basic idea of constructing a single-phase model seems to have originated in early work in two-phase flow, e.g. Rannie (1962) and Marble (1963, 1970)

A.3.2. Equation for Momentum. The momentum equation for the single-fluid model may be found by expanding the left-hand side of (A.15) and substituting equations (A.2) and (A.3); rearrangement gives

$$\rho_g \left[\frac{\partial \mathbf{u}_g}{\partial t} + \mathbf{u}_g \cdot \nabla \mathbf{u}_g \right] + \nabla p = \nabla \cdot \vec{\tau}_v + \mathbf{m}_e + \mathbf{m}_D - \boldsymbol{\sigma}_e + \delta \mathbf{u}_l w_g^{(l)} + \mathbf{F}_l \quad (\text{A.30})$$

where

$$\boldsymbol{\sigma}_e = \mathbf{u}_g w_{eg} + \mathbf{u}_l w_{el} \quad (\text{A.31})$$

$$\mathbf{F}_l = -\rho_l \left[\frac{\partial \mathbf{u}_l}{\partial t} + \mathbf{u}_l \cdot \nabla \mathbf{u}_l \right] \quad (\text{A.32})$$

Now add $\rho_l \left[\frac{\partial \mathbf{u}_g}{\partial t} + \mathbf{u}_g \cdot \nabla \mathbf{u}_g \right]$ to both sides of (A.30) and combine terms on the right-hand side to give

$$\rho \left[\frac{\partial \mathbf{u}}{\partial t} + \mathbf{u} \cdot \nabla \mathbf{u} \right] + \nabla p = \mathcal{F} \quad (\text{A.33})$$

where

$$\mathcal{F} = \nabla \cdot \vec{\tau}_v + \mathbf{m}_e + \mathbf{m}_D - \boldsymbol{\sigma}_e - \delta \mathbf{u}_l w_g^{(l)} - \rho_l \frac{D \delta u_l}{Dt} \quad (\text{A.34})$$

$$\mathbf{u} := \mathbf{u}_g \quad (\text{A.35})$$

and \mathbf{u} has been written for \mathbf{u}_g .

A.3.3. Equation for Energy. The energy equation must be handled somewhat differently in order to introduce the conventional definition of the heat of reaction and the mass-averaged thermodynamic properties. Denbigh (1961) provides good accessible discussions of these matters; it's a good reference for basic chemical thermodynamics. First replace the energy e_{og} by the enthalpy $h_{og} = e_{og} - p/\rho_g$ in (A.21) and use equation (A.2) to find

$$\rho_g \left[\frac{\partial h_{og}}{\partial t} + \mathbf{u}_g \cdot \nabla h_{og} \right] - \rho_g \left[\frac{\partial}{\partial t} \left(\frac{p}{\rho_g} \right) + \mathbf{u}_g \cdot \nabla \left(\frac{p}{\rho_g} \right) + \nabla \cdot (p \mathbf{u}_g) \right] = H \quad (\text{A.36})$$

where H stands temporarily for the remaining terms,

$$H = \nabla \cdot (\vec{\tau}_v \cdot \mathbf{u}_g) - \nabla \cdot \mathbf{q} - (e_{og} w_g + e_{ol} w_l) - \rho_l \left[\frac{\partial e_{ol}}{\partial t} + \mathbf{u}_l \cdot \nabla e_{ol} \right] + Q_e + \chi_D$$

ANNEX A – EQUATIONS OF MOTION

The enthalpy of the mixture is

$$h_g = \frac{1}{\rho_g} \sum \rho_{gi} h_i = \sum Y_{gi} h_i \quad (\text{A.37})$$

with

$$h_i = h_i^{(r)} + \int_{T_r}^T c_{\rho i} dT' = h_i^{(r)} + h_i^{(T)} \quad (\text{A.38})$$

and $h_i^{(r)}$ is the enthalpy of the i^{th} species at the reference temperature T_r ; $h_i^{(T)}$ is sometimes called the ‘thermal enthalpy’. Because the $h_i^{(r)}$ are constants here,

$$\begin{aligned} \frac{\partial h_{og}}{\partial t} + \mathbf{u}_g \cdot \nabla h_{og} &= \left[\frac{\partial h_g}{\partial t} + \mathbf{u}_g \cdot \nabla h_g \right] + \left[\frac{\partial}{\partial t} \left(\frac{u_g^2}{2} \right) + \mathbf{u}_g \cdot \nabla \left(\frac{u_g^2}{2} \right) \right] \\ &= \sum Y_{gi} \left[\frac{\partial h_i^{(T)}}{\partial t} + \mathbf{u}_g \cdot \nabla h_i^{(T)} \right] + \left[\frac{\partial}{\partial t} \left(\frac{u_g^2}{2} \right) + \mathbf{u}_g \cdot \nabla \left(\frac{u_g^2}{2} \right) \right] \\ &\quad + \frac{1}{\rho_g} \sum \left(h_i^{(r)} + h_i^{(T)} \right) \left[-\nabla \cdot (\rho_g \mathbf{V}_i Y_{gi}) + w_{gi} + w_{gi}^{(l)} + w_{gei} \right] \end{aligned} \quad (\text{A.39})$$

after (A.11) has been substituted in the last summation. The sum $\sum (h_i^{(r)} + h_i^{(T)}) w_{gi}$ is related to the heat of reaction at the local temperature and pressure. The precise connection is not important here and for simplicity we will define the heat of reaction Q and reaction rate w by

$$-Qw = \sum (h_i^{(r)} + h_i^{(T)}) (w_{gi} + w_{gi}^{(l)} + w_{gei}) \quad (\text{A.40})$$

Substitution in (A.37) and defining

$$h_0^{(T)} = h^{(T)} + \frac{\mathbf{u}_g^2}{2} \quad (\text{A.41})$$

we have

$$\rho_g \left[\frac{\partial h_{og}}{\partial t} + \mathbf{u}_g \cdot \nabla h_{og} \right] = \rho_g \left[\frac{\partial h_{og}^{(T)}}{\partial t} + \mathbf{u}_g \cdot \nabla h_{og}^{(T)} \right] - Qw - \sum h_i \nabla \cdot (\rho_g \mathbf{V}_i Y_{gi}) \quad (\text{A.42})$$

Consistent with the definition (A.38), the thermal internal energy is $e^{(T)} = h^{(T)} + p/\rho_g$ and

$$e_{og}^{(T)} = e^{(T)} + \frac{1}{2} \mathbf{u}_g^2 \quad (\text{A.43})$$

Substitution of (A.42) and (A.43) in (A.36) and use of (A.3) leads to the new form of the energy equation

$$\begin{aligned} \rho_g \left[\frac{\partial e_{og}^{(T)}}{\partial t} + \mathbf{u}_g \cdot \nabla e_{og}^{(T)} \right] + \rho_l \left[\frac{\partial e_l}{\partial t} + \mathbf{u}_g \cdot \nabla e_l \right] + \nabla \cdot (p \mathbf{u}_g) &= \nabla \cdot (\vec{\tau}_v \cdot \mathbf{u}_g) - \nabla \cdot \mathbf{q} + Qw + Q_e \\ &\quad - (e_{og} w_g + e_{ol} w_l) + \chi_D + \sum h_i \nabla \cdot (\rho_g \mathbf{V}_i Y_{gi}) \end{aligned} \quad (\text{A.44})$$

where $w_l = w_{el} - w_g^{(l)}$.

Now remove the kinetic energies of the gas and liquid phases from this equation by subtracting the scalar products of \mathbf{u}_g with (A.31) and \mathbf{u}_l with (A.33). to give

$$\begin{aligned} \rho_g C_v \left[\frac{\partial T_g}{\partial t} + \mathbf{u}_g \cdot \nabla T_g \right] + \rho_l C_l \left[\frac{\partial T_l}{\partial t} + \mathbf{u}_l \cdot \nabla T_l \right] + p \nabla \cdot \mathbf{u}_g = \\ = \nabla \cdot (\vec{\tau}_v \cdot \mathbf{u}_g) - \nabla \cdot \mathbf{q} + Qw + Q_e - (e_{og} w_g + e_{ol} w_l) + \chi_D + \sum h_i \nabla \cdot (\rho_g \mathbf{V}_i Y_{gi}) \\ - \mathbf{u} \cdot \mathbf{F} + \mathbf{u}_l \cdot \mathbf{F}_l \end{aligned} \quad (\text{A.45})$$

where the specific heats are defined by

$$\begin{aligned} de_g^{(T)} &= C_v dT_g \\ de_l &= C_l dT_l \end{aligned} \quad (\text{A.46}) \text{ a,b}$$

Rearrangement of (A.45) in a manner similar to that used for rewriting the momentum equation in the form (A.34) produces the result

$$\rho \mathbf{C}_v \left[\frac{\partial T}{\partial t} + \mathbf{u} \cdot \nabla T \right] + p \nabla \cdot \mathbf{u} = \mathcal{Q} \quad (\text{A.47})$$

where the symbol T_g has been replaced by T^4 and

$$\begin{aligned} \mathcal{Q} &= \vec{\tau}_v \cdot \nabla \cdot \mathbf{u} - \nabla \cdot \mathbf{q} + Qw + Q_e - (e_{og} w_g + e_{ol} w_l) + \chi_D + \sum h_i \nabla \cdot (\rho_g \mathbf{V}_i Y_{gi}) \\ &\quad - \mathbf{u} \cdot (\mathbf{m}_e + \mathbf{m}_D - \boldsymbol{\sigma}_e) + (\mathbf{u} \cdot \boldsymbol{\delta} \mathbf{u}) w_g^{(l)} + \delta Q_l + \delta \mathbf{u} \cdot \mathbf{F}_l - \mathbf{u} \cdot (\mathbf{F} - \mathbf{F}_l) \end{aligned} \quad (\text{A.48})$$

$$\delta Q_l = -\rho_l \mathbf{C}_l \left[\frac{\partial \delta T}{\partial t} + \mathbf{u}_l \cdot \nabla \delta T + \delta \mathbf{u}_l \cdot \nabla T \right] \quad (\text{A.49})$$

with the definitions

$$\delta T = T_l - T \quad ; \quad \mathbf{m} = \mathbf{m}_e + \mathbf{m}_D \quad (\text{A.50})$$

$$\mathbf{C}_v = \frac{\rho_g C_v + \rho_l C_l}{\rho_g + \rho_l} = \frac{C_v + C_m C_l}{1 + C_m} \quad (\text{A.51})$$

The mass fraction $C_m = \rho_l / \rho_g$ is often called the *particle loading* because it has commonly appeared in problems involving flows of gases containing small solid or liquid particles.

⁴Thus, in contrast with the density (equation A.25), the temperatures of the gaseous and condensed phases are not formally combined and the temperature of the condensed phase must be calculated separately.

A.3.4. Equation for the Pressure. Let R_g denote the gas constant for the mixture and add T times (A.27) to \mathbf{C}_v^{-1} times (A.47) to find

$$\frac{\partial}{\partial t}(\rho T) + \mathbf{u} \cdot \nabla(\rho T) + \left(\rho T + \frac{p}{\mathbf{C}_v} \right) \nabla \cdot \mathbf{u} = T\mathcal{W} - T\nabla \cdot (\rho_l \delta \mathbf{u}) + \frac{1}{\mathbf{C}_v} \mathcal{Q} \quad (\text{A.52})$$

The two-phase mixture behaves as a perfect gas having density $\rho_g + \rho_l$ and mass averaged properties if we assume that the mixture of gases only obeys the Gibbs-Dalton law, (A.6):

$$p = R_g \rho_g T \quad (\text{A.53})$$

where R_g is the mass-averaged gas constant. Now multiply and divide the right side by $\rho_g + \rho_l = \rho$ and set $T_g = T$ to give

$$p = \mathbf{R} \rho T \quad (\text{A.54})$$

where

$$\mathbf{R} = \frac{R_g}{1 + C_m} \quad (\text{A.55})$$

With (A.51), the last implies that the specific heat at constant volume and $\gamma = \mathbf{C}_p/\mathbf{C}_v$ for the two-phase mixture are:

$$\begin{aligned} \mathbf{C}_v &= \frac{C_v + C_m C_l}{1 + C_m} \\ \gamma &= \frac{C_p + C_m C_l}{C_v + C_m C_l} \end{aligned} \quad (\text{A.56}) \text{ a,b}$$

For several reasons clarified in the main text, the theory of combustion instabilities discussed in this book is based on the wave equation for the pressure derived in Chapter 3. The first order equation for the pressure is derived by adding T times equation (A.27) to \mathbf{C}_v^{-1} times (A.48):

$$\frac{\partial}{\partial t}(\rho T) + \mathbf{u} \cdot \nabla(\rho T) + \left(\frac{p}{\mathbf{C}_v} + \rho T \right) \nabla \cdot \mathbf{u} = T [\mathcal{W} - \nabla \cdot (\rho_l \delta \mathbf{u}_l)] + \frac{1}{\mathbf{C}_v} \mathcal{Q}$$

Hence with (A.55) we find

$$\frac{\partial p}{\partial t} + \gamma p \nabla \cdot \mathbf{u} + \mathbf{u} \cdot \nabla p = \mathcal{P} \quad (\text{A.57})$$

where

$$\mathcal{P} = \frac{\mathbf{R}}{\mathbf{C}_v} \mathcal{Q} + \mathbf{R} T [\mathcal{W} - \nabla \cdot (\rho_l \delta \mathbf{u}_l)] \quad (\text{A.58})$$

A.4. Muster of Equations

The set of equations forming the basis for all of the theory and analysis we discuss in this book is:

$$\frac{D\rho}{Dt} = -\rho \nabla \cdot \mathbf{u} + \mathcal{W} \quad (\text{A.59})$$

$$\rho \frac{D\mathbf{u}}{Dt} = -\nabla p + \mathbf{F} \quad (\text{A.60})$$

$$\rho \mathbf{C}_v \frac{DT}{Dt} = -p \nabla \cdot \mathbf{u} + \mathcal{Q} \quad (\text{A.61})$$

$$\frac{Dp}{Dt} = -\gamma p \nabla \cdot \mathbf{u} + \mathcal{P} \quad (\text{A.62})$$

$$\frac{Ds}{Dt} = \frac{1}{T} \mathcal{S} \quad (\text{A.63})$$

$$p = \mathbf{R} \rho T \quad (\text{A.64})$$

where $\frac{D}{Dt} = \frac{\partial}{\partial t} + \mathbf{u} \cdot \nabla$ is the connective operator based on the mass-averaged velocity \mathbf{u} of the gases.

For completeness we have also included the equation (A.63) for the entropy, obtained in familiar fashion by applying the combined First and Second Laws of Thermodynamics to an element of fluid. That is, the relation $de = Tds - pdv$ can be written

$$\begin{aligned} \frac{Ds}{Dt} &= \frac{1}{T} \left(\frac{De}{Dt} + p \frac{Dv}{Dt} \right) \\ &= \frac{1}{T} \left(\mathbf{C}_v \frac{DT}{Dt} + p \frac{Dv}{Dt} \right) \end{aligned} \quad (\text{A.65})$$

Substitution of (A.59) and (A.61) gives (A.63) with the source

$$\mathcal{S} = \mathcal{Q} - \frac{p}{\rho^2} \mathcal{W} \quad (\text{A.66})$$

It is important to realize that this formulation contains all relevant physical processes, including those representing the actions of external influences associated, for example, with active control of combustor dynamics.

The source functions in (A.59)–(A.63) are

$$\mathcal{W} = w_e - \nabla \cdot (\rho_l \delta \mathbf{u}_l) \quad (\text{A.67})$$

$$\mathbf{F} = \nabla \cdot \vec{\tau}_v + \mathbf{m}_e + \mathbf{m}_D - \boldsymbol{\sigma}_e - \delta \mathbf{u}_l w_g^{(l)} - \rho_l \frac{D \delta u_l}{Dt} \quad (\text{A.68})$$

$$\begin{aligned} \mathcal{Q} &= \vec{\tau}_v \cdot \nabla \cdot \mathbf{u} - \nabla \cdot \mathbf{q} + Qw + Q_e - (e_{og} w_g + e_{ol} w_l) + \chi_D + \sum h_i \nabla \cdot (\rho_g \mathbf{V}_i Y_{gi}) \\ &\quad - \mathbf{u} \cdot (\mathbf{m}_e + \mathbf{m}_D - \boldsymbol{\sigma}_e) + (\mathbf{u} \cdot \delta \mathbf{u}_l) w_g^{(l)} + \delta Q_l + \delta \mathbf{u}_l \cdot \mathbf{F}_l - \mathbf{u} \cdot (\mathbf{F} - \mathbf{F}_l) \end{aligned} \quad (\text{A.69})$$

$$\mathcal{P} = \frac{\mathbf{R}}{\mathbf{C}_v} \mathcal{Q} + \mathbf{R}T [\mathcal{W} - \nabla \cdot (\rho_l \delta \mathbf{u}_l)] \quad (\text{A.70})$$

$$\mathcal{S} = \mathcal{Q} - \frac{p}{\rho^2} \mathcal{W} \quad (\text{A.71})$$

Recall that Q and w are defined together as the heat (and enthalpy) supplied per unit volume by chemical reactions, equation (A.40). Also, we have set $u_g := u$ and $T_g := T$.

A.5. Expansions in Mean and Fluctuating Variables

Following the steps suggested in Section 3.3 to produce equations (3.22)–(3.27) will give the expressions for the brackets defined there to simplify the appearance of the equations. As an intermediate step it is helpful to introduce the definitions:

$$\{\rho\}^1 = \frac{\bar{D}\rho'}{Dt} + \bar{\rho}\nabla \cdot \mathbf{M}' + \rho'\nabla \cdot \bar{\mathbf{M}} + \mathbf{M}' \cdot \nabla \bar{\rho} - \mathbf{W}'_1 \quad (\text{A.72})$$

$$\{\rho\}^2 = \mathbf{M}' \cdot \nabla \rho' + \rho'\nabla \cdot \mathbf{M}' - \mathbf{W}'_2 \quad (\text{A.73})$$

$$\{M\}^1 = \bar{\rho} \frac{\bar{D}\bar{\mathbf{M}}}{Dt} + \bar{\rho}\mathbf{M}' \cdot \nabla \mathbf{M}' + \nabla p' + \rho' \frac{\bar{D}\bar{\mathbf{M}}}{Dt} - \mathbf{F}'_1 \quad (\text{A.74})$$

$$\{M\}^2 = \rho' \frac{\bar{D}\mathbf{M}'}{Dt} + \rho'\mathbf{M}' \cdot \nabla \bar{\mathbf{M}} + \bar{\rho}\mathbf{M}' \cdot \nabla \mathbf{M}' - \mathbf{F}'_2 \quad (\text{A.75})$$

$$\{M\}^3 = \rho'\mathbf{M}' \cdot \nabla \mathbf{M}' - \mathbf{F}'_3 \quad (\text{A.76})$$

$$\{T\}^1 = \bar{\rho}\mathbf{C}_v \frac{\bar{D}T'}{Dt} + \bar{\rho}\mathbf{C}_v \mathbf{M}' \cdot \nabla \mathbf{M}' + \nabla \bar{T} + \bar{p}\nabla \mathbf{M}' + \rho' \mathbf{C}_v \frac{\bar{D}\bar{T}}{Dt} - \mathcal{Q}'_1 \quad (\text{A.77})$$

$$\{T\}^2 = \rho' \mathbf{C}_v \frac{\bar{D}T'}{Dt} + \rho' \mathbf{C}_v \mathbf{M}' \cdot \nabla \bar{T} + \bar{\rho}\mathbf{C}_v \mathbf{M}' \cdot \nabla T' - \mathcal{Q}'_2 \quad (\text{A.78})$$

$$\{T\}^3 = \rho' \mathbf{C}_v \mathbf{M}' \cdot \nabla T' - \mathcal{Q}'_3 \quad (\text{A.79})$$

$$\{p\}^1 = \frac{\bar{D}p'}{Dt} + \gamma \bar{\rho}\nabla \cdot \mathbf{M}' + \gamma p'\nabla \cdot \bar{\mathbf{M}} - \mathcal{P}'_1 \quad (\text{A.80})$$

$$\{p\}^2 = \mathbf{M}' \cdot \nabla p' + \gamma p'\nabla \cdot \mathbf{M}' - \mathcal{P}'_2 \quad (\text{A.81})$$

$$\{s\}^1 = \bar{\rho}\bar{T} \frac{\bar{D}s'}{Dt} + (\rho'\bar{T} + \bar{\rho}T') \frac{\bar{D}\bar{s}}{Dt} + \bar{\rho}\bar{T}\mathbf{M}' \cdot \nabla \bar{s} - \mathcal{S}'_1 \quad (\text{A.82})$$

$$\{s\}^2 = (\rho' \bar{T} + \bar{\rho} T') \frac{\bar{D}\bar{s}}{Dt} + \bar{\rho} \bar{T} \mathbf{M}' \cdot \nabla s' + \rho' T' \bar{\mathbf{M}} \cdot \nabla s' + (\rho' \bar{T} + \bar{\rho} T') \mathbf{M}' \cdot \nabla \bar{s} - \mathcal{S}'_2 \quad (\text{A.83})$$

$$\{s\}^3 = \rho' T' \frac{\bar{D}s'}{Dt} + \rho' T' \bar{\mathbf{M}} \cdot \nabla s' + \rho' T' \mathbf{M}' \cdot \nabla \bar{s} - \mathcal{S}'_3 \quad (\text{A.84})$$

$$\{s\}^4 = \rho' T' \mathbf{M}' \cdot \nabla s' - \mathcal{S}'_4 \quad (\text{A.85})$$

where $\bar{D}/Dt = \partial/\partial t + \bar{\mathbf{M}} \cdot \nabla$ as defined in Chapter 3, equation (3.21), is the dimensionless convective operator based on the steady mass-averaged velocity. Superscript $\{ \ }^n$ and subscript $(\)_n$ always mean here that the indicated quantities are to be written to order n in the fluctuations of the flow variables.

The fluctuations of the source functions $\mathcal{W}, \dots, \mathcal{S}$ will be formed as required for particular applications and cannot be written until literal models are constructed.

A.6. Definitions of the Ordering Brackets

The brackets introduced in equations (3.22)–(3.27) are obtained by rearrangement of the sums of brackets defined in Section A.5:

$$\{\rho\}^1 + \{\rho\}^2 = \{[\rho]\}_1 + \{\rho\}_2 - \mathcal{W}' \quad (\text{A.86})$$

$$\{\mathbf{M}\}^1 + \{\mathbf{M}\}^2 + \{\mathbf{M}\}^3 = \{[\mathbf{M}]\}_1 + \{\mathbf{M}\}_2 + \{[\mathbf{M}]\}_2 + \{\mathbf{M}\}_3 - \mathcal{F}' \quad (\text{A.87})$$

$$\{T\}^1 + \{T\}^2 + \{T\}^3 = \{[T]\}_1 + \{T\}_2 + \{[T]\}_2 + \{T\}_3 - \mathcal{Q}' \quad (\text{A.88})$$

$$\{p\}^1 + \{p\}^2 = \{[p]\}_1 + \{p\}_2 - \mathcal{P}' \quad (\text{A.89})$$

$$\{s\}^1 + \{s\}^2 + \{s\}^3 + \{s\}^4 = \{[s]\}_1 + \{s\}_2 + \{[s]\}_2 + \{s\}_3 + \{s\}_4 - \mathcal{S}' \quad (\text{A.90})$$

By identifying corresponding terms in these relations, we find⁵

⁵As in Chapter 3, bold symbols \mathbf{R} , \mathbf{C}_v and $\boldsymbol{\gamma}$ are replaced here by the usual forms R , C_v , γ , but the symbols continue to represent mass-averaged properties.

ANNEX A – EQUATIONS OF MOTION

$$\{[\rho]\}_1 = \bar{\mathbf{M}} \cdot \nabla \rho' + \mathbf{M}' \cdot \nabla \bar{\rho} + \rho' \nabla \cdot \bar{\mathbf{M}}$$

$$\{\rho\}_2 = \mathbf{M}' \cdot \nabla \rho' + \rho' \nabla \cdot \mathbf{M}'$$

$$\{[M]\}_1 = \bar{\rho} (\bar{\mathbf{M}} \cdot \nabla \mathbf{M}' + \mathbf{M}' \cdot \nabla \bar{\mathbf{M}}) + \rho' \frac{\bar{D} \bar{\mathbf{M}}}{Dt}$$

$$\{M\}_2 = \rho' \frac{\partial \mathbf{M}'}{\partial t} + \rho' (\bar{\mathbf{M}} \cdot \nabla \mathbf{M}' + \mathbf{M}' \cdot \nabla \bar{\mathbf{M}}) + \bar{\rho} \mathbf{M}' \cdot \nabla \mathbf{M}'$$

$$\{[M]\}_2 = \rho' (\bar{\mathbf{M}} \cdot \nabla \mathbf{M}' + \mathbf{M}' \cdot \nabla \bar{\mathbf{M}})$$

$$\{M\}_3 = \rho' \mathbf{M}' \cdot \nabla \mathbf{M}'$$

$$\{[p]\}_1 = \bar{\mathbf{M}} \cdot \nabla p' + \gamma p' \nabla \cdot \bar{\mathbf{M}} + \mathbf{M}' \cdot \nabla \bar{p}$$

$$\{p\}_2 = \mathbf{M}' \cdot \nabla p' + \gamma p' \nabla \cdot \mathbf{M}'$$

$$\{[T]\}_1 = \bar{\rho} C_v (\bar{\mathbf{M}} \cdot \nabla T' + \mathbf{M}' \cdot \nabla \bar{T}) + C_v \rho' \frac{\bar{D} \bar{T}}{Dt} + p' \nabla \cdot \bar{\mathbf{M}}$$

$$\{T\}_2 = \rho' C_v \frac{\partial T'}{\partial t} + \bar{\rho} C_v \mathbf{M}' \cdot \nabla T' + p' \nabla \cdot \mathbf{M}'$$

$$\{[T]\}_2 = \rho' C_v (\bar{\mathbf{M}} \cdot \nabla T' + \mathbf{M}' \cdot \nabla \bar{T})$$

$$\{T\}_3 = \rho' C_v \mathbf{M}' \cdot \nabla T'$$

$$\{[s]\}_1 = \bar{\rho} \bar{T} (\bar{\mathbf{M}} \cdot \nabla s' + \mathbf{M}' \cdot \nabla \bar{s})$$

$$\{s\}_2 = (\bar{\rho} T' + \rho' \bar{T}) \frac{\partial s'}{\partial t} + \bar{\rho} \bar{T} \mathbf{M}' \cdot \nabla s' + (\rho' \bar{T} + \bar{\rho} T') + (\mathbf{M}' \cdot \nabla \bar{s}) + \rho' T' \frac{\partial \bar{s}}{\partial t}$$

$$\{[s]\}_2 = (\bar{\rho} T' + \rho' \bar{T}) \bar{\mathbf{M}} \cdot \nabla s'$$

$$\{s\}_3 = \rho' T' \frac{\partial s'}{\partial t} + (\bar{\rho} T' + \rho' \bar{T}) \mathbf{M}' \cdot \nabla s' + \rho' T' (\mathbf{M}' \cdot \nabla \bar{s}) + \bar{\mathbf{M}} \cdot \nabla s'$$

$$\{s\}_4 = \rho' T' \mathbf{M}' \cdot \nabla s'$$

$$\{p - R\rho T\}_1 = p' - R(\rho' \bar{T} + \bar{\rho} T')$$

$$\{p - R\rho T\}_2 = -R\rho' T'$$

The subscript $\{ \}_n$ on the curly brackets means that the contained quantities are written to order n in the fluctuations of flow variables. Similarly, the square brackets indicate that the terms are of first order in the Mach number of the mean flow. Higher order square brackets are not required, as explained in Section 3.3.1.

ANNEX B

The Equations for One-Dimensional Unsteady Motions

These are many problems for which the flow may be approximated as one-dimensional. Even when the approximation may not seem as accurate as we might like, it is always a good beginning. The desired results are usually obtained without real effort and often are inspiringly close to the truth. An elementary example is computation of the normal modes for a straight tube having discontinuities, Section 5.7.2. Here we are concerned with situations in which influences at the lateral boundary must be accounted for. The formulation of the general problem is then essentially the counterpart of the constitution of the one-dimensional equations for steady flow in ducts thoroughly discussed by Shapiro (1950) and Crocco (1958).

Accounting for changes of area in the one-dimensional approximation is a straightforward matter; following the rules applied to derivations appearing in the three-dimensional equations:

$$\begin{aligned}
 \mathbf{u} \cdot \nabla (\quad) &\rightarrow u \frac{\partial}{\partial x} (\quad) \\
 \nabla \cdot (\quad) &\rightarrow \frac{1}{S_c} \frac{\partial}{\partial x} S_c (\quad) \\
 \nabla^2 (\quad) &\rightarrow \frac{1}{S_c} \frac{\partial}{\partial x} S_c \frac{\partial (\quad)}{\partial x}
 \end{aligned} \tag{B.1}$$

where the axis of the duct lies along the x-direction and $S_c(x)$ is the distribution of the cross-section area.

More interesting are consequences of processes at the lateral boundary, particularly when there is flow through the surface. The most important applications arise in solid propellant rockets when burning propellant forms all or part of the lateral surface. Inflow of mass momentum and energy must be accounted for (Culick 1971, 1973; Culick and Yang 1990). The equations have the same form as the three-dimensional equations derived in Annex A, equations (A.59)–(A.63) but the rule (B.1) has been applied and only the velocity component u along axis of the duct is non-zero:

Conservation of Mass

$$\frac{D\rho}{Dt} = -\rho \frac{1}{S_c} \frac{\partial}{\partial x} (S_c u) + (\mathcal{W}_1 + \mathcal{W}_{1s}) \tag{B.2}$$

Conservation of Momentum

$$\rho \frac{Du}{Dt} = -\frac{\partial p}{\partial x} + (\mathcal{F}_1 + \mathcal{F}_{1s}) \tag{B.3}$$

Conservation of Energy

$$\rho C_v \frac{DT}{Dt} = -p \frac{1}{S_c} \frac{\partial}{\partial x} (S_c u) + (\mathcal{Q}_1 + \mathcal{Q}_{1s}) \tag{B.4}$$

Equation for the Pressure

$$\frac{Dp}{Dt} = -\gamma p \frac{1}{S_c} \frac{\partial}{\partial x} (S_c u) + (\mathcal{P}_1 + \mathcal{P}_{1s}) \quad (\text{B.5})$$

Equation for the Entropy

$$\frac{Ds}{Dt} = \frac{1}{T} (\mathcal{S}_1 + \mathcal{S}_{1s}) \quad (\text{B.6})$$

where

$$\frac{D}{Dt} = \frac{\partial}{\partial t} + u \frac{\partial}{\partial x} \quad (\text{B.7})$$

The source terms \mathcal{W}_1 , \mathcal{F}_1 , \mathcal{Q}_1 , \mathcal{P}_1 and \mathcal{S}_1 are the one-dimensional forms of (A.67)–(A.71) written for the axial component of velocity only and with the rules (B.1) applied:

$$\mathcal{W}_1 = -\frac{1}{S_c} \frac{\partial}{\partial x} (S_c \rho_l \delta u_l) + w_e \quad (\text{B.8})$$

$$\mathcal{F}_1 = \frac{\partial \tau_v}{\partial x} + m_e + m_D - \sigma_e - \delta u_l w_g^{(l)} - \rho_l \frac{D \delta u_l}{Dt} \quad (\text{B.9})$$

$$\begin{aligned} \mathcal{Q}_1 = & \tau_v \frac{\partial u}{\partial x} - \frac{\partial q}{\partial x} + Qw + Q_e - (e_{og} w_g + e_{ol} w_l) \\ & + \chi_0 + \Sigma h_i \frac{\partial}{\partial x} (\rho_g V_i Y_{gi}) - u(m_e + m_D - \sigma_e) \\ & + (u \delta u_l) w_g^{(l)} + \delta Q_l + \delta u_l F_l - u(\mathcal{F}_1 - F_l) \end{aligned} \quad (\text{B.10})$$

$$\mathcal{P}_1 = \frac{R}{C_v} \mathcal{Q}_1 + RT \left[\mathcal{W}_1 - \frac{\partial}{\partial x} (\rho_l \delta u_l) \right] \quad (\text{B.11})$$

$$\mathcal{S}_1 = \mathcal{Q}_1 - \frac{p}{\rho^2} \mathcal{W}_1 \quad (\text{B.12})$$

and F_l is the one-dimensional form of (A.32).

In addition, sources of mass, momentum and energy associated with flow through the lateral boundary are represented by the symbols with subscript ()_s (Culick 1973; Culick and Yang 1990):

$$\mathcal{W}_{1s} = \frac{1}{S_c} \int m_s dq = \frac{1}{S_c} \int [m_{sg} + m_{sl}] dq \quad (\text{B.13})$$

$$\mathcal{F}_{1s} = \frac{1}{S_c} \int [(u_s - u)m_{sg} + (u_{ls} - u_l)m_{sl}] dq \quad (\text{B.14})$$

$$\mathcal{Q}_{1s} = \frac{1}{S_c} \int [(h_{0s} - e_0)m_{sg} + (e_{l0s} - e_{l0})m_{sl}] dq \quad (\text{B.15})$$

$$\mathcal{P}_{1s} = \frac{R}{C_v} \mathcal{Q}_{1s} + RT_s \mathcal{W}_{1s} = \frac{R}{C_v} \frac{1}{S_c} \int [(h_{0s} - e_0)m_{sg} + (e_{l0s} - e_{l0})m_{sl} + C_v T m_{sg}] dq \quad (B.16)$$

$$\mathcal{S}_{1s} = \frac{1}{\rho} \mathcal{Q}_1 - \frac{p}{\rho} \mathcal{W}_{1s} \quad (B.17)$$

A useful form for \mathcal{P}_{1s} is

$$\mathcal{P}_{1s} = \frac{1}{S_c} \int (a^2 + \gamma R \Delta T_s) m_{sg} dq + \frac{R}{C_v} \frac{1}{S_c} \int (e_{l0s} - e_{l0}) m_{sl} dq \quad (B.18)$$

where $\Delta T_s = T_s - T$. Terms containing $u_s^2 m_{sg}$ or $u^2 m_{sg}$ are of higher order and therefore are negligible.

Superscripts $(\)_g$ and $(\)_l$ refer respectively to the gas and liquid phases and subscript $(\)_s$ denotes values at the surface. The mass fluxes at the surface, m_{sg} and m_{sl} are of course computed as values normal to the boundary and are positive for inward flow. Here q stands for the perimeter of the local section normal to the axis.

B.1. Equations for Unsteady One-Dimensional Motions

Forming the equations for the fluctuating motions within the one-dimensional approximation is done in exactly the same way as for the general equations, Annex A. We need only apply the rules (B.1) and add to the inhomogeneous functions h and f the contributions from processes at the boundary. As for the general three-dimensional equations, we defer writing the fluctuations $\mathcal{W}'_1, \mathcal{F}'_1, \dots$ until we consider specific problems.

The procedure introduced in Section 3.3.3 for forming the systems of equations for a hierarchy of problems applies equally to one-dimensional motions. As above, the equations are obtained from the three-dimensional equations by applying the rules (B.1): the results can be constructed when needed. However, the contributions from processes at the lateral boundary are special. Written to first order in the fluctuations and the Mach number of the mean flow, (B.13)–(B.17) become:

$$\mathcal{W}'_{1s} = \frac{1}{S_c} \int m'_s dq \quad (B.19)$$

$$\begin{aligned} \mathcal{F}'_{1s} = & \frac{1}{S_c} \left\{ (\bar{u}_s - \bar{u}) \int m'_{sg} dq + (\bar{u}_{ls} - \bar{u}) \int m'_{sl} dq \right\} \\ & + \frac{1}{S_c} \left\{ (u'_s - u') \int \bar{m}_{sg} dq + (u'_{ls} - u'_l) \int \bar{m}_{sl} dq \right\} \end{aligned} \quad (B.20)$$

$$\begin{aligned} \mathcal{Q}'_{1s} = & \frac{1}{S_c} \left\{ (\bar{h}_{0s} - \bar{e}_0) \int m'_{sg} dq + (\bar{e}_{l0s} - \bar{e}_{l0}) \int m'_{sl} dq + C_v \bar{T} \int m'_{sg} dq \right\} \\ & + \frac{1}{S_c} \left\{ (h'_{0s} - e'_0) \int \bar{m}_{sg} dq + (e'_{l0s} - e'_{l0}) \int \bar{m}_{sl} dq + C_v T' \int \bar{m}_{sg} dq \right\} \end{aligned} \quad (B.21)$$

$$\begin{aligned} \mathcal{P}'_{1s} = & \frac{R}{C_v} \frac{1}{S_c} \left\{ (\bar{h}_{0s} - \bar{e}_0) \int m'_{sg} dq + (\bar{e}_{l0s} - \bar{e}_{l0}) \int m'_{sl} dq + C_v \bar{T} \int m'_{sg} dq \right\} \\ & + \frac{R}{C_v} \frac{1}{S_c} \left\{ (h'_{0s} - e'_0) \int \bar{m}_{sg} dq + (e'_{l0s} - e'_{l0}) \int \bar{m}_{sl} dq + C_v T' \int \bar{m}_{sg} dq \right\} \end{aligned} \quad (B.22)$$

$$S'_{1s} = \frac{1}{p} Q'_{1s} - \frac{p}{\rho} \mathcal{W}'_{1s} \quad (B.23)$$

The procedure for forming the wave equation in the one-dimensional approximation is the same as that week in Chapter 4, with the results valid to second order in small quantities

$$\frac{1}{S_c} \frac{\partial}{\partial x} \left(S_c \frac{\partial p'}{\partial x} \right) - \frac{1}{\bar{a}^2} \frac{\partial^2 p'}{\partial t^2} = h_1 \quad (B.24)$$

$$\frac{\partial p'}{\partial x} = -f_1 \quad (x = 0, L) \quad (B.25)$$

and

$$\begin{aligned} h_1 = & -\bar{\rho} \frac{1}{S_c} \frac{\partial}{\partial x} \left(S_c \frac{\partial \bar{u} u'}{\partial x} \right) + \frac{\bar{u}}{\bar{a}^2} \frac{\partial^2 p'}{\partial t \partial x} + \frac{\bar{\gamma}}{\bar{a}^2} \frac{\partial p'}{\partial t} \frac{1}{S_c} \frac{\partial}{\partial x} (S_c \bar{u}) \\ & - \frac{1}{S_c} \frac{\partial}{\partial x} S_c \left(\bar{\rho} u' \frac{\partial u'}{\partial x} + \rho' \frac{\partial u'}{\partial t} \right) \\ & + \frac{1}{\bar{a}^2} \frac{\partial}{\partial x} \left(u' \frac{\partial p'}{\partial x} \right) + \frac{\bar{\gamma}}{\bar{a}^2} \frac{\partial p'}{\partial t} \frac{1}{S_c} \frac{\partial}{\partial x} (S_c u') \end{aligned} \quad (B.26)$$

$$+ \frac{1}{S_c} \frac{\partial}{\partial x} S_c (\mathcal{F}'_1 + \mathcal{F}'_{1s}) - \frac{1}{\bar{a}^2} \frac{\partial (\mathcal{P}'_1 + \mathcal{P}'_{1s})}{\partial t} \quad (B.27)$$

$$f_1 = \bar{\rho} \frac{\partial u'}{\partial t} + \bar{\rho} \frac{\partial}{\partial x} (\bar{u} u') + \bar{\rho} u' \frac{\partial u'}{\partial x} + \rho' \frac{\partial u'}{\partial t} - (\mathcal{F}'_1 + \mathcal{F}'_{1s})$$

The normal modes for one-dimensional motions are found as the solutions to

$$\frac{1}{S_c} \frac{d}{dx} \left(S_c \frac{d\psi_l}{dx} \right) + k_l^2 \psi_l = 0 \quad (B.28)$$

$$\frac{d\psi_l}{dx} = 0 \quad (z = 0, L) \quad (B.29)$$

and the basic expansions for the acoustic field are

$$p'(x, t) = \bar{p} \sum_{j=1}^M \eta_j(t) \psi_j(x) \quad (B.30)$$

$$u'(x, t) = \sum_{j=1}^M \frac{\dot{\eta}_j(t)}{\bar{\gamma} k_j^2} \frac{d\psi_j(x)}{dx} \quad (B.31)$$

Orthogonality of the normal modes is expressed as

$$\int_0^L \psi_j \psi_l S_c dx = E_l^2 \delta_{jl} \quad (B.32)$$

$$E_l^2 = \int_0^L \psi_l^2 S_c dx \quad (B.33)$$

With a procedure similar to that leading to equation (4.36), we find the equations for the amplitudes:

$$\frac{d^2 \eta_l}{dt^2} + \omega_l^2 \eta_l = F_l \quad (B.34)$$

$$F_l = -\frac{\bar{a}^2}{\bar{\rho} E_l^2} \left\{ \int_0^L h_1 \psi_l S_c dx + [f_1 \psi_l S_c]_0^L \right\} \quad (B.35)$$

Note that F_l here is not the one-dimensional form of the force found from (A.32). The current context will distinguish the two symbols.

Development of the principal basic results for stability treated with the approximation of one-dimensional motions is covered in Section 6.9.



ANNEX C

The Acoustic Boundary Layer

Consider an impermeable rigid wall exposed to a flow of gas oscillating parallel to the surface but having no average motion. The gas is viscous and heat conducting. At the surface, the velocity is zero and the temperature is maintained constant. Far from the surface all flow properties oscillate sinusoidally and the motion is isentropic. The values of the velocity and temperature vary from their fixed values at the surface to their sinusoidal values far from the surface through a two-dimensional boundary layer. For the following analysis we assume that there is no communication parallel to the surface. That is, we assume that flow within the boundary layer at any position x depends only on the conditions imposed locally by the external flow. This assumption is valid because the flow is oscillating with no mean velocity. Figure C.1 is a sketch of the flow.

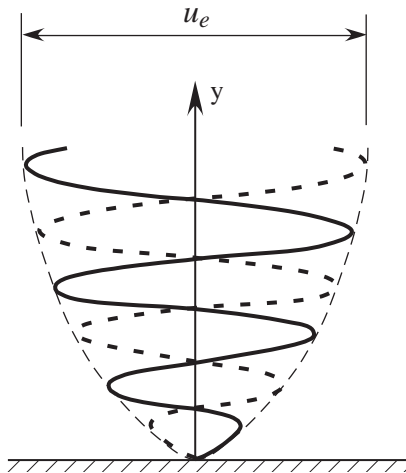


FIGURE C.1. Sketch of the flow in an acoustic boundary layer showing the velocity field at two instants separated by one-half period.

We assume that the oscillations are sustained by some external actions far from the region under consideration. Moreover, for small viscosity—high Reynolds number based on the amplitude of the velocity outside the boundary layer, and the ‘thickness’ of the layer, found as part of the solution—the boundary layer is thin. We may assume this to be the case, and check the assumption later. Then according to the principles of boundary layer theory, we take the pressure constant in the direction normal to the surface.

ANNEX C – THE ACOUSTIC BOUNDARY LAYER

The linearized mass, momentum and energy equations, (5.7)–(5.9) written for incompressible flow with viscous stresses and heat combustion included, are

$$\begin{aligned} \frac{\partial \rho'}{\partial t} + \bar{\rho} \nabla \cdot \mathbf{u}' &= 0 \\ \bar{\rho} \frac{\partial \mathbf{u}'}{\partial t} + \nabla p' &= \nabla \cdot \boldsymbol{\tau}'_v \\ \bar{\rho} \frac{\partial e'}{\partial t} + \bar{\rho} \nabla \cdot \mathbf{u}' &= -\nabla \cdot \mathbf{q}' \end{aligned} \quad (\text{C.1})\text{a,b,c}$$

It is convenient for this problem to replace the energy by the enthalpy, $h = e + p/\rho$, so

$$\frac{\partial e}{\partial t} = \frac{\partial h}{\partial t} - \frac{1}{\rho} \frac{\partial p}{\partial t} + \frac{p}{\rho^2} \frac{\partial \rho}{\partial t}$$

For incompressible flow, ρ' is zero and (C.1)a gives $\nabla \cdot \mathbf{u}' = 0$. By definition, $dh = C_p dT$, and the energy equation (C.1)c becomes

$$\bar{\rho} C_p \frac{\partial T'}{\partial t} = \frac{\partial p'}{\partial t} - \nabla \cdot \mathbf{q}' \quad (\text{C.2})$$

Under the conditions supposed here, the contributions from viscous and heat conduction are (see, e.g., Schlichting 1960):

$$\nabla \cdot \boldsymbol{\tau}'_v = \mu \frac{\partial^2 u'}{\partial y^2} \quad ; \quad \nabla \cdot \mathbf{q}' = -\lambda_c \frac{\partial^2 T'}{\partial y^2} \quad (\text{C.3})$$

Hence the momentum and energy equations for this problem are¹

$$\begin{aligned} \bar{\rho} \frac{\partial u'}{\partial t} &= \mu \frac{\partial^2 u'}{\partial y^2} + \bar{\rho} \frac{\partial u'_e}{\partial t} \\ \bar{\rho} C_p \frac{\partial T'}{\partial t} &= \lambda_c \frac{\partial^2 T'}{\partial y^2} + \frac{\partial p'_e}{\partial t} \end{aligned} \quad (\text{C.4})\text{a,b}$$

It is an important feature of this formulation that the coordinate x along the surface appears only parametrically in $u'_e(x; t)$ and $p'_e(x; t)$. Later we discuss application and interpretation of this feature.

We assume sinusoidal time dependence and write

$$u' = \hat{u} e^{-i\omega t} \quad ; \quad u'_e = \hat{u}_e e^{-i\omega t} \quad ; \quad p'_e = \hat{p}_e e^{-i\omega t}$$

Equations (C.4)a,b become

$$\begin{aligned} \frac{d^2 \hat{u}}{dy^2} + i \frac{2}{\delta^2} \hat{u} &= +i \frac{2}{\delta^2} \hat{u}_e \\ \frac{d^2}{dy^2} \left(\frac{\hat{T}}{\hat{T}_e} \right) + i \frac{2Pr}{\delta^2} \left(\frac{\hat{T}}{\hat{T}_e} \right) \hat{u} &= +i \frac{2Pr}{\delta^2} \frac{\gamma - 1}{\gamma} \left(\frac{\hat{p}}{\hat{p}_e} \right) \end{aligned} \quad (\text{C.5})\text{a,b}$$

where the characteristic thickness of the boundary layer is

$$\delta = \sqrt{\frac{2\nu}{\omega}} \quad (\text{C.6})$$

¹We have replaced the pressure gradient in the momentum equation by the rate of change of acoustic momentum. That follows because the pressure doesn't change through this layer and therefore obeys the acoustic momentum equation for the external flow.

and $\nu = \mu/\bar{\rho}$ is the kinematic viscosity and $Pr = C_p\mu/\lambda_c$ is the Prandtl number. The solutions to the boundary layer equations can be written as sums of homogeneous and particular solutions

$$\begin{aligned}\hat{u} &= \hat{u}_h + \hat{u}_e \\ \hat{T} &= \hat{T}_h + \frac{\gamma - 1}{\gamma} \left(\frac{\bar{T}_e}{\bar{p}_e} \right) \hat{p}_e\end{aligned}\quad (\text{C.7a,b})$$

and \hat{u}_h, \hat{T}_h satisfy

$$\begin{aligned}\frac{d^2 \hat{u}_h}{dy^2} + i \frac{2}{\delta^2} \hat{u} &= 0 \\ \frac{d^2 \hat{T}_h}{dy^2} + i \frac{2Pr}{\delta^2} \hat{T}_h &= 0\end{aligned}\quad (\text{C.8a,b})$$

The solutions (C.7a,b) must satisfy the boundary conditions

$$\begin{aligned}y \rightarrow \infty : \quad \hat{u} &= \hat{u}_e \quad , \quad \hat{T} = \hat{T}_e \\ y = 0 : \quad \hat{u} &= 0 \quad ; \quad \hat{T} = 0\end{aligned}\quad (\text{C.9})$$

Homogeneous solutions to (C.8a,b) are

$$\hat{u}_h = c_1 e^{-\lambda y} \quad ; \quad \hat{T}_h = c_2 e^{-\sqrt{Pr}y} \quad (\text{C.10a,b})$$

with λ satisfying the equation

$$\lambda^2 - i \frac{2}{\delta^2} = 0 \quad (\text{C.11})$$

Hence $\lambda = \sqrt{2i}\frac{1}{\delta}$,

$$\lambda = \frac{1}{\delta}(1 - i) \quad (\text{C.12})$$

The value of λ having positive real part is chosen so $\hat{u}_h \rightarrow 0$ as $y \rightarrow \infty$; replacing (C.10a,b) in (C.7a,b), we have

$$\begin{aligned}\hat{u} &= c_1 e^{-\lambda y} + \hat{u}_e \\ \hat{T} &= c_2 e^{-\sqrt{Pr}y} + \frac{\gamma - 1}{\gamma} \left(\frac{\bar{T}_e}{\bar{p}_e} \right) \hat{p}_e\end{aligned}\quad (\text{C.13a,b})$$

To satisfy the boundary conditions at the surface, c_1 and c_2 are assigned the values

$$c_1 = -\hat{u}_e \quad ; \quad c_2 = -\frac{\gamma - 1}{\gamma} \left(\frac{\bar{T}_e}{\bar{p}_e} \right)$$

Hence the solutions for the distributions of velocity and temperature within the boundary layer are

$$\begin{aligned}\hat{u} &= \hat{u}_e [1 - e^{-\lambda y}] \\ \hat{T} &= \hat{T}_e [1 - e^{-\lambda \sqrt{Pr}y}]\end{aligned}\quad (\text{C.14a,b})$$

where we have assumed isentropic motion in the external flow:

$$\frac{\hat{T}_e}{\bar{T}_e} = \frac{\gamma - 1}{\gamma} \frac{\hat{p}_e}{\bar{p}_e} \quad \text{and} \quad \hat{u}_e = \frac{-i}{\bar{\rho}\omega} \frac{dp_e}{dx}$$

Although we have assumed the flow to be incompressible in the above analysis, the boundary layer is usually referred to as the ‘acoustic boundary layer’. The flow near the surface is dominated by inertial and viscous forces so compressible effects are ignored. However, the result can (and usually is) used with a compressible, i.e. acoustic, field external to the boundary layer.

ANNEX C – THE ACOUSTIC BOUNDARY LAYER

Mechanical energy of motion is dissipated within the acoustic boundary layer, causing acoustic waves incident on a wall to be attenuated. That process is analyzed in Section 5.9. For the calculations we need a formula for the rate of dissipation of energy within the acoustic boundary layer. The general form is (A.63) with the sources given by (A.66) and the definitions (A.67) and (A.69) for \mathcal{W} and \mathcal{Q} :

$$\frac{Ds}{Dt} = \frac{\partial s}{\partial t} + \mathbf{u} \cdot \nabla \mathbf{u} = \frac{1}{T} \left[\mathcal{Q} - \frac{p}{\rho^2} \mathcal{W} \right] \quad (\text{C.15})$$

For the conditions here, the only terms surviving in \mathcal{Q} and \mathcal{W} are those due to viscous stresses and heat conduction; then $\mathcal{W} = 0$ and

$$\mathcal{Q} = \boldsymbol{\tau}_v \cdot \nabla \cdot \mathbf{u} - \nabla \cdot \mathbf{q}$$

For the one-dimensional flow in the acoustic layer,

$$\begin{aligned} \boldsymbol{\tau}_v \cdot \nabla \cdot \mathbf{u} &= \mu \left(\frac{\partial u}{\partial y} \right)^2 \\ -\nabla \cdot \mathbf{q} &= \frac{\partial}{\partial y} \left(\lambda_c \frac{\partial T}{\partial y} \right) \end{aligned} \quad (\text{C.16a,b})$$

and

$$\frac{1}{T} \mathcal{Q} = \frac{\mu}{T} \left(\frac{\partial u}{\partial y} \right)^2 + \frac{1}{T} \frac{\partial}{\partial y} \left(\lambda_c \frac{\partial T}{\partial y} \right)$$

The last term can be rewritten and for this flow (C.15) becomes

$$\frac{\partial s}{\partial t} = \left[\frac{\mu}{T} \left(\frac{\partial u}{\partial y} \right)^2 + \frac{\lambda_c}{T^2} \left(\frac{\partial}{\partial y} \right)^2 \right] + \frac{\partial}{\partial y} \left(\frac{\lambda_c}{T} \frac{\partial T}{\partial y} \right) \quad (\text{C.17})$$

To understand this result, consider an element of the flow extending between the planes y_1 and y_2 and having unit area. The right hand side of (C.17) represents the rate of entropy production per unit volume associated with this element. There are two contributions which can be interpreted with the following calculation. First integrate (C.17) over the volume of the element; for one dimensional flow, only the integral over y remains:

$$\int_{y_1}^{y_2} \frac{\partial s}{\partial t} dy = \int_{y_1}^{y_2} \left[\frac{\mu}{T} \left(\frac{\partial u}{\partial y} \right)^2 + \frac{\lambda_c}{T^2} \left(\frac{\partial T}{\partial y} \right)^2 \right] dy + \left[\frac{\lambda_c}{T^2} \frac{\partial T}{\partial y} \right]_{y_1}^{y_2} \quad (\text{C.18})$$

This result represents the total entropy production associated with the volume element. The bracketted terms under the integral must be interpreted as the entropy production per unit volume arising from dissipation of energy. The first term is due to action of viscous stresses and the second is due to conduction of heat.

The last term in (C.18) is the net entropy production due to conduction of heat through the two faces of the element at $y = y_1, y_2$. This part of the entropy production must be assigned to the environment of the element, for the following reason. Now apply (C.18) to the acoustic boundary layer with $y_1 = 0$ at the wall, and $y_2 \rightarrow \infty$ so the entire layer is included in the integration. Then $\partial T / \partial y = 0$ in y_2 and (C.18) is

$$\int_0^\infty \frac{\partial s}{\partial t} dy = \int_0^\infty \left[\frac{\mu}{T} \left(\frac{\partial u}{\partial y} \right)^2 + \frac{\lambda_c}{T^2} \left(\frac{\partial T}{\partial y} \right)^2 \right] dy - \left(\frac{\lambda_c}{T^2} \frac{\partial T}{\partial y} \right)_{y=0}$$

Suppose that the temperature increases with y . Then heat is transferred from the element to the wall, causing a loss of entropy of the element and an increase of entropy of the wall. That heat flow is non-zero because of the temperature rise due to energy dissipation within the element. Therefore, if we are concerned

only with the consequences of processes within the element, we may drop this term. Hence the formula for the rate of entropy production per unit volume within the element is

$$\frac{\partial s}{\partial t} = \frac{\mu}{T} \left(\frac{\partial u}{\partial y} \right)^2 + \frac{\lambda_c}{T^2} \left(\frac{\partial T}{\partial y} \right)^2 \quad (\text{C.19})$$

ANNEX C – THE ACOUSTIC BOUNDARY LAYER



ANNEX D

Accounting for Waves of Vorticity and Entropy

In Chapters 3 and 4, the equations of motion have been written in dimensionless variables, mainly as the basis for the two-parameter expansion. It is often preferable to use dimensionless variable, for example, in modeling some of the physical processes treated in special problems. In this annex, the main results of Chapter 3 are reproduced, and extended to show explicitly the formal consequences of including unsteady vorticity and entropy in the method of spatial averaging developed in Chapter 4.

The basis for the calculations in the set of equations¹ (A.59)–(A.64)

$$\begin{aligned}
 \frac{D\rho}{Dt} &= -\rho\nabla \cdot \mathbf{u} + \mathcal{W} \\
 \rho \frac{D\mathbf{u}}{Dt} &= -\nabla p + \mathcal{F} \\
 \rho C_v \frac{DT}{Dt} &= -p\nabla \cdot \mathbf{u} + \mathcal{Q} \\
 \frac{Dp}{Dt} &= -\gamma p \nabla \cdot \mathbf{u} + \mathcal{P} \\
 \frac{Ds}{Dt} &= \frac{1}{T} \mathcal{S} \\
 p &= \rho RT
 \end{aligned} \tag{D.1)a-f}$$

Following the procedure explained in Chapter 3, expansion of (D.1)a-f to third order in the fluctuations. Problem III defined in Section 3.3.3 leads to the equations governing the unsteady field. To simplify the

¹Here bold symbols for the mass-averaged fluid properties \mathbf{R} , \mathbf{C}_p , \mathbf{C}_v and $\boldsymbol{\gamma}$ are replaced by R , C_p , C_v and γ

ANNEX D – ACCOUNTING FOR WAVES OF VORTICITY AND ENTROPY

results we assume that the average values $\bar{\rho}$, \bar{p} , \bar{T} are constant and uniform to give:

$$\begin{aligned}
 \frac{\partial \rho'}{\partial t} + \bar{\rho} \nabla \cdot \mathbf{u}' &= -[\bar{\mathbf{u}} \cdot \nabla \rho' + \mathbf{u}' \cdot \nabla \bar{\rho} + \rho' \nabla \cdot \bar{\mathbf{u}}] - [\mathbf{u}' \cdot \nabla \rho' + \rho' \nabla \cdot \mathbf{u}'] + \mathcal{W}' \\
 \bar{\rho} \frac{\partial \mathbf{u}'}{\partial t} + \nabla p' &= -[\bar{\rho}(\bar{\mathbf{u}} \cdot \nabla \mathbf{u}' + \mathbf{u}' \cdot \nabla \bar{\mathbf{u}})] - \left[\bar{\rho} \mathbf{u}' \cdot \nabla \mathbf{u}' + \rho' \frac{\partial \mathbf{u}'}{\partial t} \right] - [\rho' \mathbf{u}' \cdot \nabla \mathbf{u}'] + \mathcal{F}' \\
 \bar{\rho} C_v \frac{\partial T'}{\partial t} + \bar{p} \nabla \cdot \mathbf{u}' &= -[\bar{\rho} C_v (\bar{\mathbf{u}} \cdot \nabla T' + \mathbf{u}' \cdot \nabla \bar{T}) + p' \nabla \cdot \bar{\mathbf{u}}] - \left[\rho' C_v \frac{\partial T'}{\partial t} + \bar{\rho} C_v \mathbf{u}' \cdot \nabla T' + p' \nabla \cdot \mathbf{u}' \right] \\
 &\quad - [\rho' C_v \mathbf{u}' \cdot \nabla T'] + \mathcal{Q}' \\
 \frac{\partial p'}{\partial t} + \gamma \bar{p} \nabla \cdot \mathbf{u}' &= -[\bar{\mathbf{u}} \cdot \nabla p' + \gamma p' \nabla \cdot \bar{\mathbf{u}}] - [\mathbf{u}' \cdot \nabla p' + \gamma p' \nabla \cdot \mathbf{u}'] + \mathcal{P}' \\
 \bar{\rho} \bar{T} \frac{\partial s'}{\partial t} &= -[\bar{\rho} T' (\bar{\mathbf{u}} \cdot \nabla s' + \mathbf{u}' \cdot \nabla \bar{s})] - \left[(\bar{\rho} T' + \rho' \bar{T}) \frac{\partial s'}{\partial t} + \bar{\rho} \bar{T} \mathbf{u}' \cdot \nabla s' \right] \\
 &\quad - [\rho' T' \frac{\partial s'}{\partial t} + (\bar{\rho} \bar{T} + \rho' \bar{T}) \mathbf{M}' \cdot \nabla s'] + \mathcal{S}' \\
 p' &= [R(\rho' \bar{T} + \bar{\rho} T')] + [R \rho' T'] \\
 \end{aligned} \tag{D.2a-f}$$

Combination of (D.2)b and (D.2)d gives the nonlinear wave equation for the pressure fluctuations and its boundary condition

$$\begin{aligned}
 \nabla^2 p' - \frac{1}{\bar{a}^2} \frac{\partial^2 p'}{\partial t^2} &= h \\
 \hat{n} \cdot \nabla p' &= -f
 \end{aligned} \tag{D.3a,b}$$

with

$$\begin{aligned}
 h &= -\bar{\rho} \nabla \cdot \{[\mathbf{u}]\}_1 + \{\mathbf{u}\}_2 + \{\mathbf{u}\}_3 + \frac{1}{\bar{a}^2} \frac{\partial}{\partial t} \{[p]\}_1 + \{p\}_2 + \{p\}_3 + \nabla \cdot \mathcal{F}' - \frac{1}{\bar{a}^2} \frac{\partial p'}{\partial t} \\
 f &= -\bar{\rho} \frac{\partial \mathbf{u}'}{\partial t} \cdot \hat{\mathbf{n}} + \bar{\rho} \hat{\mathbf{n}} \cdot \{[\mathbf{u}]\}_1 + \{\mathbf{u}\}_2 + \{\mathbf{u}\}_3 - \mathcal{F}' \cdot \hat{\mathbf{n}}
 \end{aligned} \tag{D.4a,b}$$

The brackets are defined similarly to those in Annex A.6:

$$\{[\mathbf{u}]\}_1 = \bar{\rho}(\bar{\mathbf{u}} \cdot \nabla \mathbf{u}' + \mathbf{u}' \cdot \nabla \bar{\mathbf{u}}) \quad \{[p]\}_1 = \bar{\mathbf{u}} \cdot \nabla p' + \gamma p' \nabla \cdot \bar{\mathbf{u}}$$

$$\begin{aligned}
 \{\mathbf{u}\}_2 &= \rho' \frac{\partial \mathbf{u}'}{\partial t} + \bar{\rho} \mathbf{u}' \cdot \nabla \mathbf{u}' \\
 &\quad + \rho'(\bar{\mathbf{u}} \cdot \nabla \mathbf{u}' + \mathbf{u}' \cdot \nabla \bar{\mathbf{u}}) \quad \{p\}_2 = \mathbf{u}' \cdot \nabla p' + \gamma p' \nabla \cdot \mathbf{u}' \\
 \{\mathbf{u}\}_3 &= \rho' \mathbf{u}' \cdot \nabla \mathbf{u}' \quad \{p\}_3 = p' \nabla \cdot \mathbf{u}' + \gamma p' \mathbf{u}' \cdot \nabla \mathbf{u}' + \rho' \mathbf{u}' \cdot \nabla p' + \bar{\rho} \mathbf{u}' \cdot \nabla \bar{p}
 \end{aligned} \tag{D.5a-e}$$

A system of oscillator equations is formed as in Chapter 4. Expand the pressure fluctuation in normal modes:

$$p'(\mathbf{r}, t) = \bar{p} \sum_{m=0}^M \eta_m(t) \psi_m(\mathbf{r}) \quad (\text{D.6})$$

Spatial averaging leads to the result (4.36) with n replacing N ,

$$\ddot{\eta}_n + \omega_n^2 \eta_n = F_n \quad (\text{D.7})$$

and

$$F_n = -\frac{\bar{a}^2}{\bar{p}E_n^2} \left\{ \int h\psi_n dV + \oint f\psi_n dS \right\} \quad (\text{D.8})$$

With some use of familiar vector identities, for h and f given by (D.6)a,b, F_n can eventually be written

$$\begin{aligned} -\frac{\bar{p}E_n^2}{\bar{a}^2} F_n = & \bar{\rho}I_1 + \frac{1}{\bar{a}^2} I_2 + \bar{\rho}I_3 + \frac{1}{\bar{a}^2} I_4 + \bar{\rho}I_5 + \oint \bar{\rho} \frac{\partial \mathbf{u}}{\partial t} \cdot \hat{\mathbf{n}} dS \\ & - \int \mathbf{F}' \cdot \nabla \psi_n dV + \frac{1}{\bar{a}^2} \int \frac{\partial \mathcal{P}'}{\partial t} \psi_n dV \end{aligned} \quad (\text{D.9})$$

where

$$I_1 = \int (\bar{\mathbf{u}} \cdot \nabla \mathbf{u}' + \mathbf{u}' \cdot \nabla \bar{\mathbf{u}}) \cdot \nabla \psi_n dV$$

$$I_2 = \frac{\partial}{\partial t} \int (\gamma p' \nabla \cdot \bar{\mathbf{u}} + \bar{\mathbf{u}} \cdot \nabla p') \psi_n dV$$

$$I_3 = \int (\mathbf{u}' \cdot \nabla \mathbf{u}' + \frac{\rho'}{\bar{\rho}} \frac{\partial \mathbf{u}'}{\partial t}) \cdot \nabla \psi_n dV \quad (\text{D.10)a-e}$$

$$I_4 = \frac{\partial}{\partial t} \int (\gamma p' \nabla \cdot \mathbf{u}' + \mathbf{u}' \cdot \nabla p') \psi_n dV$$

$$I_5 = \int \frac{\rho'}{\bar{\rho}} (\mathbf{u}' \cdot \nabla \mathbf{u}') \cdot \nabla \psi_n dV$$

It is important that both the steady and unsteady velocity fields have *not* been assumed to be irrotational. Note also that in (D.9) there is only one surface term, involving the acceleration $\frac{\partial \mathbf{u}'}{\partial t}$. However, for irrotational acoustic motions some of the integrands combine to form a divergence which by Gauss' theorem leads to a surface integral representing convection of mechanical energy throughout the surface.

These results establish the formal basis for investigating influences of vorticity and entropy waves on an acoustic field in a chamber. We emphasize again that the expansion (D.6) of the pressure field is only the zeroth order approximation. The oscillator equations govern the time-evolution of the amplitudes of the chosen basis functions, the mode shapes, but the spatial distributions to higher order require further computations, as explained in Section 4.6. The dependent variables in h and f are not to this point restricted. Hence in particular, following the idea discussed in Section 4.1 that generally a disturbance in a compressible flowing medium may be synthesized of three modes of propagation, we write the variables as sums of three

parts labeled $(\)_a$ for acoustic, $(\)_\Omega$ for vorticity, $(\)_s$ for entropy; the second column of Table D.1 shows the defining properties of the contributions from the three modes in their zeroth approximation.

TABLE D.1. Definition of Splitting a Disturbance in the Three Modes of Propagation (Chu and Kovasznay, 1958).

	Splitting Variables	Basic Properties
Pressure	$p' = p'_a + p'_\Omega + p'_s$	$p'_a \neq 0$; $\Omega'_\Omega = \Omega'_s = 0$
Vorticity	$\Omega' = \Omega'_\Omega + \Omega'_s + \Omega'_a$	$\Omega'_\Omega \neq 0$; $\Omega'_s = \Omega'_a = 0$
Entropy	$s' = s'_s + s'_a + s'_\Omega$	$s'_s \neq 0$; $s'_a = s'_\Omega = 0$

The zeroth approximations (small amplitude; no mean flow) to the flow variables in the three modes are given in Table D.2.

TABLE D.2. Zeroth Approximation for the Flow Variables in the Three Modes.

	Pressure	Velocity
Acoustic Mode	$p'_a = \bar{p} \sum_{m=1}^M \eta_m(t) \psi_m(\mathbf{r})$	$\mathbf{u}'_a = \sum_{m=1}^M \frac{\dot{\eta}_m}{\gamma k_m^2} \nabla \psi_m$
Vorticity Mode	$p'_\Omega = 0$	$\nabla \times \mathbf{u}'_\Omega = 0$; $\nabla \cdot \mathbf{u}'_\Omega = 0$
Entropy Mode	$p'_s = 0$	$\nabla \times \mathbf{u}'_s = 0$; $\nabla \cdot \mathbf{u}'_s = \frac{1}{c_p} \frac{\partial s'}{\partial t}$

Thus the total velocity fluctuation **to zeroth order** is

$$\mathbf{u}'(\mathbf{r}; t) = \mathbf{u}'_a + \mathbf{u}'_\Omega + \mathbf{u}'_s \quad (D.11)$$

The density fluctuation contains a contribution from the entropy fluctuation (related to the temperature); from the formula for the entropy of a perfect gas,

$$s - s_0 = c_p \log \frac{(p/p_0)^{1/\gamma}}{(\rho/\rho_0)} \quad (D.12)$$

We find, to second order in the pressure fluctuations,

$$\frac{\rho'}{\bar{\rho}} = \left[\frac{1}{\gamma} \frac{p'}{\bar{p}} - \frac{s'}{c_p} \right] - \frac{\gamma - 1}{2\gamma^2} \left(\frac{p'}{\bar{p}} \right)^2 \quad (D.13)$$

The next step is substitution of (D.11) in the integrals (D.10)a-e and rearrangement to give the formulas for the first and second order contributions:

$$\begin{aligned} I_1 &= I_1^a + I_1^\Omega + I_1^s \\ I_2 &= I_2^a \\ I_3 &\rightarrow I_3^{ij} \\ I_4 &= I_4^{aa} \end{aligned} \quad (D.14)a-d$$

The elements I_3^{ij} forming $I_3 = \sum_{j=1}^3 \sum_{i=1}^3 I_3^{ij}$ are

$$\begin{aligned}
 I_3^{aa} &= \int \left(\mathbf{u}'_a \cdot \nabla \mathbf{u}'_a + \frac{\rho'_a}{\bar{\rho}} \frac{\partial \mathbf{u}'_a}{\partial t} \right) \cdot \nabla \psi_n dV ; \quad I_3^{a\Omega} = \int (\mathbf{u}'_a \cdot \nabla \mathbf{u}'_\Omega) \cdot \nabla \psi_n dV ; \\
 I_3^{as} &= \int \left(\mathbf{u}'_a \cdot \nabla \mathbf{u}'_s + \frac{\rho'_a}{\bar{\rho}} \frac{\partial \mathbf{u}'_s}{\partial t} \right) \cdot \nabla \psi_n dV \\
 I_3^{\Omega a} &= \int (\mathbf{u}'_\Omega \cdot \nabla \mathbf{u}'_a) \cdot \nabla \psi_n dV ; \quad I_3^{\Omega\Omega} = \int (\mathbf{u}'_\Omega \cdot \nabla \mathbf{u}'_\Omega) \cdot \nabla \psi_n dV ; \\
 I_3^{\Omega s} &= \int (\mathbf{u}'_\Omega \cdot \nabla \mathbf{u}'_s) \cdot \nabla \psi_n dV \\
 I_3^{sa} &= \int \left(\mathbf{u}'_s \cdot \nabla \mathbf{u}'_a + \frac{\rho'_s}{\bar{\rho}} \frac{\partial \mathbf{u}'_a}{\partial t} \right) \cdot \nabla \psi_n dV ; \quad I_3^{s\Omega} = \int (\mathbf{u}'_s \cdot \nabla \mathbf{u}'_\Omega) \cdot \nabla \psi_n dV ; \\
 I_3^{ss} &= \int \left(\mathbf{u}'_s \cdot \nabla \mathbf{u}'_s + \frac{\rho'_s}{\bar{\rho}} \frac{\partial \mathbf{u}'_s}{\partial t} \right) \cdot \nabla \psi_n dV
 \end{aligned} \tag{D.15}$$

Equation (D.13) gives the two parts of the density fluctuation:

$$\begin{aligned}
 \frac{\rho'_a}{\bar{\rho}} &= \frac{1}{\gamma} \frac{p'}{\bar{p}} \\
 \frac{\rho'_s}{\bar{\rho}} &= -\frac{s'}{c_p}
 \end{aligned} \tag{D.16}a,b$$

The remaining integrals in (D.14)a-d are defined as

$$\begin{aligned}
 I_1^a &= \int [\nabla(\bar{\mathbf{u}} \cdot \mathbf{u}'_a) - \mathbf{u}'_a \times (\nabla \times \bar{\mathbf{u}})] \cdot \nabla \psi_n dV \\
 I_1^\Omega &= \int [\nabla(\bar{\mathbf{u}} \cdot \mathbf{u}'_\Omega) - \mathbf{u}'_\Omega \times (\nabla \times \bar{\mathbf{u}}) - \bar{\mathbf{u}} \times \Omega'] \cdot \nabla \psi_n dV \\
 I_1^s &= \int [\nabla(\bar{\mathbf{u}} \cdot \mathbf{u}'_s) - \mathbf{u}'_s \times (\nabla \times \bar{\mathbf{u}}) - \bar{\mathbf{u}} \times (\nabla \times \mathbf{u}'_s)] \cdot \nabla \psi_n dV
 \end{aligned} \tag{D.17}a,b$$

and

$$\begin{aligned}
 I_2 = I_2^{aa} &= \frac{\partial}{\partial t} \int (\gamma p'_a \nabla \cdot \bar{\mathbf{u}} + \bar{\mathbf{u}} \cdot \nabla p'_a) \psi_n dV \\
 I_4 = I_4^{aa} &= \frac{\partial}{\partial t} \int (\gamma p'_a \nabla \cdot \mathbf{u}'_a + \mathbf{u}'_a \cdot \nabla p'_a) \psi_n dV
 \end{aligned} \tag{D.18}a,b$$

Because the integrals I_i are additive in (D.9), we can set down the parts which involve only acoustic, vorticity or entropy fluctuations, and the interactions; it is more physically appealing to write F_n , equation (D.9), as the sum:

$$\begin{aligned}
 -\frac{\bar{p}E_n^2}{\bar{a}^2} F_n &= I_{aa} + I_{\Omega\Omega} + I_{ss} + I_{a\Omega} + I_{as} + I_{\Omega s} \\
 &\quad - \int \mathbf{F}' \cdot \nabla \psi_n dV + \frac{1}{\bar{a}^2} \int \frac{\partial \mathcal{P}'}{\partial t} \psi_n dV
 \end{aligned} \tag{D.19}$$

with the definition

$$I_{aa} = \bar{\rho} k_n^2 \int \bar{\mathbf{u}} \cdot \mathbf{u}'_a \psi_n dV - \bar{\rho} \int (\mathbf{u}'_a \times \nabla \times \bar{\mathbf{u}}) \cdot \nabla \psi_n dV + \frac{1}{\bar{a}^2} \frac{\partial}{\partial t} \int (\gamma p'_a \nabla \cdot \bar{\mathbf{u}} + \bar{\mathbf{u}} \cdot \nabla \mathbf{u}'_a) \psi_n dV \\ + \bar{\rho} I_3^{aa} + \frac{1}{\bar{a}^2} I_4^{aa} + \bar{\rho} \oint \frac{\partial \mathbf{u}'}{\partial t} \cdot \hat{\mathbf{n}} \psi_n dV \quad (D.20)$$

Substitution of the acoustic approximations to the acoustic pressure and velocity (see Table D.2) leads eventually to the simpler formula for I_{aa} :

$$I_{aa} = \bar{\rho} \oint \left[\frac{\partial \mathbf{u}'}{\partial t} \cdot \hat{\mathbf{n}} + \frac{1}{\gamma} (\bar{\mathbf{u}} \cdot \hat{\mathbf{n}}) \eta_n \psi_n \right] \psi_n dS + \bar{\rho} \sum_{j=1}^M' \frac{\dot{\eta}_j}{\gamma} \left(\frac{k_n^2}{k_j^2} + 1 \right) \int (\bar{\mathbf{u}} \cdot \nabla \psi_j) \psi_n dV \\ - \bar{\rho} \int (\mathbf{u}'_a \times \nabla \times \bar{\mathbf{u}}) \cdot \nabla \psi_n dV + \bar{\rho} I_3^{aa} + \frac{1}{\bar{a}^2} I_4^{aa} \quad (D.21)$$

Note that the surface integral contains the entire velocity fluctuation, $\mathbf{u}' = \mathbf{u}'_a + \mathbf{u}'_\Omega + \mathbf{u}'_s$.

Without modeling the relevant physical processes, the remaining integrals in (D.19) cannot be simplified further than their primitive definition written as the sums appearing in (D.9), the individual contributions being given in (D.15) and (D.17):

$$I_{\Omega\Omega} = \bar{\rho} \{ I_1^\Omega + I_3^{\Omega\Omega} \} \\ = \bar{\rho} \left\{ \int [\nabla(\bar{\mathbf{u}} \cdot \mathbf{u}'_\Omega) - \mathbf{u}'_\Omega \times (\nabla \times \bar{\mathbf{u}}) - \bar{\mathbf{u}} \times \Omega'] \cdot \nabla \psi_n dV + \int (\mathbf{u}'_\Omega \cdot \nabla \mathbf{u}'_\Omega) \cdot \nabla \psi_n dV \right\} \\ I_{ss} = \bar{\rho} \{ I_1^s + I_3^{ss} \} \\ = \bar{\rho} \left\{ \int [\nabla(\bar{\mathbf{u}} \cdot \mathbf{u}'_s) - \mathbf{u}'_s \times (\nabla \times \bar{\mathbf{u}}) - \bar{\mathbf{u}} \times (\nabla \times \mathbf{u}'_s)] \cdot \nabla \psi_n dV + \int \left[(\mathbf{u}'_s \cdot \nabla \mathbf{u}'_s) + \frac{\rho'_s}{\bar{\rho}} \frac{\partial \mathbf{u}'_s}{\partial t} \right] \cdot \nabla \psi_n dV \right\} \\ I_{a\Omega} = \bar{\rho} \{ I_3^{a\Omega} + I_3^{\Omega a} \} \\ = \bar{\rho} \int [\mathbf{u}'_a \cdot \nabla \mathbf{u}'_\Omega + \mathbf{u}'_\Omega \cdot \nabla \mathbf{u}'_a] \cdot \nabla \psi_n dV \\ I_{as} = \bar{\rho} \{ I_3^{as} + I_3^{sa} \} \\ = \bar{\rho} \int \left[\mathbf{u}'_a \cdot \nabla \mathbf{u}'_s + \mathbf{u}'_s \cdot \nabla \mathbf{u}'_a + \frac{\rho'_a}{\bar{\rho}} \frac{\partial \mathbf{u}'_s}{\partial t} + \frac{\rho'_s}{\bar{\rho}} \frac{\partial \mathbf{u}'_a}{\partial t} \right] \cdot \nabla \psi_n dV \\ I_{s\Omega} = \bar{\rho} \{ I_3^{s\Omega} + I_3^{\Omega s} \} \\ = \bar{\rho} \int [\mathbf{u}'_s \cdot \nabla \mathbf{u}'_\Omega + \mathbf{u}'_\Omega \cdot \nabla \mathbf{u}'_s] \cdot \nabla \psi_n dV \quad (D.22)a-e$$

ANNEX E

Accommodating Discontinuities in the Method of Spatial Averaging

Especially in problem arising from unsteady behavior in gas turbine combustors and augmentors or after-burners, representing the combustion field with one or more flame sheets is a common strategy; see, for example Marble and Candel (1978), Cumpsty (1979), Dowling and Bloxsidge (1984), and Dowling (1996). Modeling with discontinuities requires a little care: not only are distributions of physical quantities affected—in obvious ways—particularly the density, temperature, velocity, and energy release fields, but there is also a contribution arising with the formulation of the averaged equations. Figure E.1 illustrates several possibilities. We shall examine only the simplest case of a flame front normal to a one-dimensional flow, shown in Figure E.1(c).

Chu (1953) was first to examine in detail the transient behavior of a flame treated as a discontinuity. His analysis was based on equations derived by Tsien (1951) and Emmons (1958). In general, when subject to a disturbance, the flame speed, and therefore the position of the flame, changes. Those perturbations must be taken into account to obtain completely correct results (cf. the analysis in Section 2.1) but we will ignore them here in favor of emphasizing certain aspects of the formalism. Our purpose is modest, to show that spatial discontinuities must be treated carefully to account for all contributions, some of which arise specially in the process of spatial averaging.

We can most clearly see the problem in the simplest situation of one-dimensional flow sketched in Figure E.2. For this calculation only we suppose that the velocity and pressure fluctuations are non-zero, but we ignore all other contributions, notably density changes. The inhomogeneous equation for the pressure is

$$\begin{aligned} \frac{\partial^2 p'}{\partial x^2} - \frac{1}{\bar{a}^2} \frac{\partial^2 p'}{\partial t^2} &= h_1 \\ \frac{\partial p'}{\partial x} &= -f_1 \quad (x = x_1, x_0, x_2) \end{aligned} \quad (\text{E.1a,b})$$

with

$$\begin{aligned} h_1 &= \frac{1}{\bar{a}^2} \frac{\partial m}{\partial t} - \frac{\partial \mathcal{M}}{\partial x} \\ f_1 &= \bar{\rho} \frac{\partial u'}{\partial t} + \mathcal{M} \end{aligned} \quad (\text{E.2a,b})$$

and

$$\begin{aligned} \mathcal{M} &= \bar{\rho} \left(\bar{u} \frac{\partial u'}{\partial x} + u' \frac{du'}{dx} \right) = \bar{\rho} \frac{\partial}{\partial x} (\bar{u}' u') \\ m &= \gamma p' \frac{d\bar{u}}{dx} + \bar{u} \frac{\partial p'}{\partial x} \end{aligned} \quad (\text{E.3a,b})$$

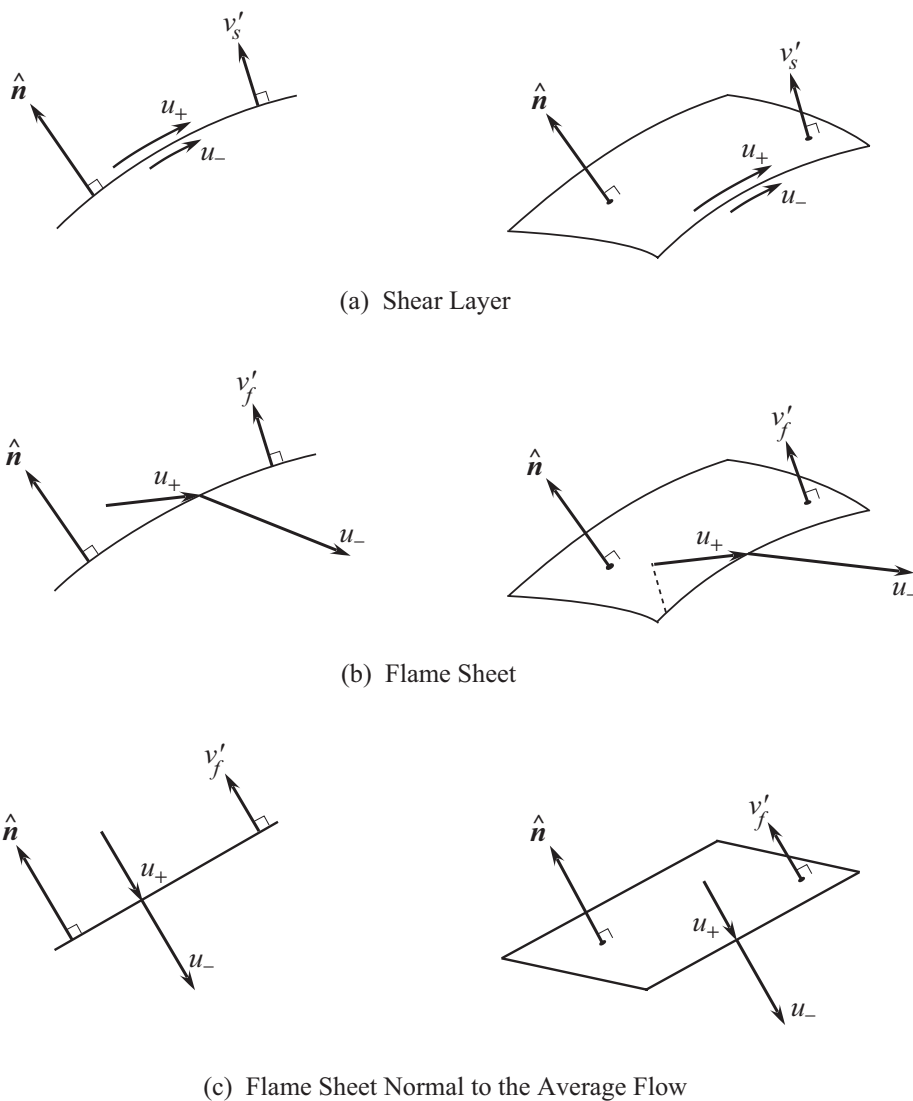


FIGURE E.1. Three examples of discontinuities in a flow field.

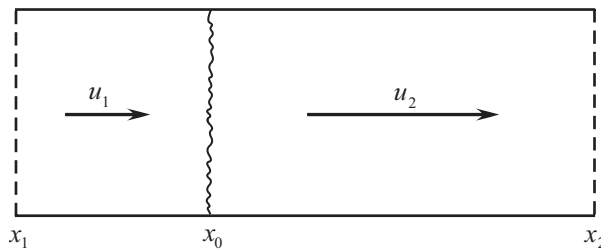


FIGURE E.2. A discontinuity in a one-dimensional flow.

We assume the familiar separable forms for the pressure and velocity perturbations,

$$p' = \bar{\rho} \eta_\ell \psi_\ell ; \quad u' = \frac{\dot{\eta}_\ell}{\gamma k_\ell^2} \frac{d\psi_\ell}{dx} \quad (E.4)$$

Following the procedure worked out in Chapter 3 and applied in Section 6.7 to one-dimensional flows, we find the equation for η_ℓ ,

$$\frac{d^2 \eta_\ell}{dt^2} + \omega_\ell^2 \eta_\ell = -\frac{\bar{a}^2 S_c}{\bar{p} E_\ell^2} \left\{ \int_{x_1}^{x_2} h_1 \psi_\ell dx + [\psi_\ell f_1]_{x_1}^{x_2} + [\psi_\ell f_1]_{x_0-}^{x_0+} \right\} \quad (E.5)$$

The last term containing the jump in $\psi_\ell f_1$ at the discontinuity is, at this stage, the only obvious evidence of a discontinuity in the flow. In three dimensions, a corresponding arises at a surface where the function f is discontinuous. For f_1 given by (E.2)a,b,

$$[\psi_\ell f_1]_{x_0-}^{x_0+} = \left[\psi_\ell \bar{\rho} \left(\frac{\partial u'}{\partial t} + \frac{\partial}{\partial x} (\bar{u} u') \right) \right]_{x_0-}^{x_0+} = \bar{\rho} \psi_{\ell 0} \left[\bar{u} \frac{\partial u'}{\partial x} \right]_{x_0-}^{x_0+} = \bar{\rho} \psi_{\ell 0} \frac{\partial u'_0}{\partial x} \Delta \bar{u} \quad (E.6)$$

$$\Delta u_0 = \bar{u}(x_{0+}) - \bar{u}(x_{0-}) \quad (E.7)$$

The weighted integral of h_1 has three parts:

$$\int_{x_1}^{x_2} \psi_\ell h_1 dx = -\bar{\rho} \int_{x_1}^{x_2} \psi_\ell \frac{\partial^2}{\partial x^2} (\bar{u} u') dx + \frac{1}{\bar{a}^2} \frac{\partial}{\partial t} \int_{x_1}^{x_2} \psi_\ell \left(\gamma p' \frac{d\bar{u}}{dx} + \bar{u} \frac{\partial p'}{\partial x} \right) dx \quad (E.8)$$

Each of the three pieces has special contributions at the discontinuity: Integration of the first term by parts gives

$$-\bar{\rho} \int_{x_1}^{x_2} \psi_\ell \frac{\partial^2}{\partial x^2} (\bar{u} u') dx = -\bar{\rho} \psi_{\ell 0} \left[\frac{\partial}{\partial x} (\bar{u} u') \right]_{x_0-}^{x_0+} - \bar{\rho} \left[\psi_\ell \frac{\partial}{\partial x} (\bar{u} u') \right]_{x_1}^{x_2} + \bar{\rho} \int_{x_1}^{x_2} \frac{d\psi_\ell}{dx} \frac{\partial}{\partial x} (\bar{u} u') dx \quad (E.9)$$

The last term can be simplified for the step change assumed for the mean velocity,

$$\bar{\rho} \int_{x_1}^{x_2} \frac{d\psi_\ell}{dx} \frac{\partial}{\partial x} (\bar{u} u') dx \approx \bar{\rho} \frac{d\psi_{\ell 0}}{dx} u'(0) \Delta \bar{u} - \frac{1}{\bar{a}^2} \frac{\partial}{\partial t} \int_{x_1}^{x_2} \bar{u} \frac{d\psi_\ell}{dx} p' dx \quad (E.10)$$

With similar calculations, the last two integrals in (E.8) become

$$\frac{1}{\bar{a}^2} \frac{\partial}{\partial t} \int_{x_1}^{x_2} \psi_\ell \bar{u} \frac{\partial p'}{\partial x} dx \approx \frac{\bar{p}}{2\bar{a}^2} \left[(\bar{u}_2 \psi_\ell^2(x_2) - \bar{u}_1 \psi_\ell^2(x_1)) + \psi_{\ell 0}^2 \Delta \bar{u} \right] \dot{\eta}_\ell \quad (E.11)$$

$$\frac{\gamma}{\bar{a}^2} \frac{\partial}{\partial t} \int_{x_1}^{x_2} \psi_\ell p' \frac{d\bar{u}}{dx} dx \approx \frac{\gamma \bar{p}}{\bar{a}^2} \psi_{\ell 0}^2 \Delta \bar{u} \dot{\eta}_\ell \quad (E.12)$$

Substitution of (E.9)–(E.12) in (E.8) gives

$$\begin{aligned} \int_{x_1}^{x_2} \psi_\ell h_1 dx = & -\bar{\rho} \psi_{\ell 0} \left[\frac{\partial}{\partial x} (\bar{u} u') \right]_{x_0-}^{x_0+} - \bar{\rho} \left[\psi_\ell \frac{\partial}{\partial x} (\bar{u} u') \right]_{x_1}^{x_2} + \bar{\rho} \frac{d\psi_{\ell 0}}{dx} u'(0) \Delta \bar{u} - \frac{1}{\bar{a}^2} \frac{\partial}{\partial t} \int_{x_1}^{x_2} \bar{u} \frac{d\psi_\ell}{dx} p' dx \\ & + \frac{\bar{p}}{2\bar{a}^2} \left[(\bar{u}_2 \psi_\ell^2(x_2) - \bar{u}_1 \psi_\ell^2(x_1)) + \psi_{\ell 0}^2 \Delta \bar{u} \right] + \frac{\gamma \bar{p}}{\bar{a}^2} \psi_{\ell 0}^2 \Delta \bar{u} \dot{\eta}_\ell \end{aligned} \quad (E.13)$$

ANNEX E – ACCOMMODATING DISCONTINUITIES IN THE METHOD OF SPATIAL AVERAGING

Finally, inserting (E.13) in (E.5) and using (E.2)a,b to evaluate the terms containing f_1 , gives the equation for η_ℓ :

$$\ddot{\eta}_\ell + \omega_\ell^2 \eta_\ell = -\frac{\bar{a}^2 S_c}{\bar{\rho} E_\ell^2} \left\{ \bar{\rho} \left(\psi_{\ell 0} \frac{\partial u'_0}{\partial x} + \frac{d\psi_{\ell 0}}{dx} u'_0 \right) + \dot{\eta}_\ell \left(\gamma + \frac{1}{2} \right) \frac{\bar{p}}{2\bar{a}^2} \psi_{\ell 0}^2 \right\} \Delta \bar{u} + \dots \quad (\text{E.14})$$

Only the terms arising at the discontinuity are shown. Note that because u'_0 , the velocity fluctuation at the discontinuity, is proportional to $\dot{\eta}_\ell$, all such terms contribute to damping.

The calculations leading to (E.14) have been carried out only as an artificial example to suggest what may happen in the analysis when a discontinuity is present in the flow. It should be clear that the result, equation (E.14), is at best incomplete. Even proper ‘jump’ conditions across the flame have not been used; correct conditions would, for example, set the value of $\Delta \bar{u}$ in (E.14). One purpose of the analysis carried out here has been to emphasize that in addition to jump conditions, or some sort of comparable formal statement, special care is required carrying out integrals. The steps leading from (E.9) to (E.13) make the point.

ANNEX F

Basis Functions Satisfying Homogeneous Boundary Conditions

The purpose of this annex is to clarify an important point that has been misunderstood by several critics of the methods followed in this book. It's a difficulty whose source is readily identified but a bit of effort is required to resolve the matter. The issue is perhaps best captured by the general question:

How is a true solution satisfying inhomogeneous boundary conditions represented accurately by an expansion in basis functions satisfying homogeneous boundary conditions?

In the problems treated in this book, we are concerned often with the unsteady pressure field governed by the inhomogeneous wave equation (3.53) with the inhomogeneous boundary condition (3.55),

$$\nabla^2 p' - \frac{1}{\bar{a}^2} \frac{\partial^2 p'}{\partial t^2} = h \quad (F.1)$$

$$\hat{n} \cdot \nabla p' = -f \quad (F.2)$$

The approximate method of solution has been based on expansion of the unsteady pressure and velocity fields expressed in the basis functions ψ_n taken as normal modes satisfying the problem

$$\nabla^2 \psi_n + k_n^2 \psi_n = 0 \quad (F.3)$$

$$\hat{n} \cdot \nabla \psi_n = 0 \quad (F.4)$$

Then the pressure and velocity fields are approximated by the classical forms with amplitudes $\eta_n(t)$ to be determined:

$$\tilde{p}'(\mathbf{r}, t) = \bar{p} \sum_{n=1}^N \eta_n(t) \psi_n(\mathbf{r}) \quad (F.5)$$

$$\tilde{\mathbf{u}}'(\mathbf{r}, t) = \sum_{n=1}^N \frac{\dot{\eta}_n(t)}{\gamma k_n^2} \nabla \psi_n(\mathbf{r}) \quad (F.6)$$

where N may become infinite; see Section 4.3.

With the representation (F.5), spatially averaging the difference between the actual problem. (F.1), (F.2), and the normal mode problem (F.3), (F.4), gives the equations (4.36) for the amplitudes $\eta_n(t)$:

$$\frac{d^2 \eta_n}{dt^2} + \omega_n^2 \eta_n = -\frac{\bar{a}^2}{\bar{p}} \frac{1}{E_n^2} \left\{ \int h \psi_n dV + \iint f \psi_n dS \right\} \quad (F.7)$$

For reasons explained in Section 4.6, we require in this book *only* the classical formulas for the pressure and velocity because we compute all quantities—notably the amplitudes η_n and, if necessary, the pressure—to first order in the expansion parameter \bar{M}_r , a measure of the mean flow Mach number. That is, with only a modest (but tedious) extension of the apparatus we have covered, we could calculate p' and \mathbf{u}' to first

order,

$$p'(\mathbf{r}, t) = \bar{p} \sum_{n=0}^N \eta_n(t) \psi_n(\mathbf{r}) [1 + \bar{M}_r \mathcal{P}(r, t)] \quad (\text{F.8})$$

$$\mathbf{u}'(\mathbf{r}, t) = \sum_{n=0}^N \frac{\dot{\eta}_n(t)}{\gamma k_n^2} [\nabla \psi_n(\mathbf{r}) + \bar{M}_r \mathbf{U}(r, t)] \quad (\text{F.9})$$

We will avoid the calculations necessary to prove that the approximate solution, the expansions (F.5) and (F.6) really do solve the problem (F.1), (F.2) to the order required. To carry through the ‘proof’ would require finding \mathcal{P} and \mathbf{U} which the developments in the main text have shown are not needed for useful results. Therefore we make the point with a much simpler model problem.

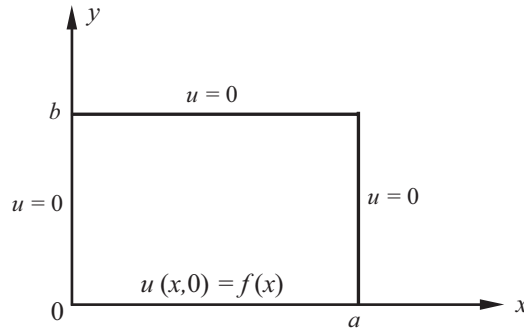


FIGURE F.1. The problem defined for determining $p(x, y)$.

The example was apparently first worked out by Friedman (1956, pp. 269–272). I learned the lesson, as well as useful explanation, from Professor D.S. Cohen, who clarified the problem in class notes. The following is an extended and paraphrased version of those notes as well as including what I learned from private conversations.

We consider the two-dimensional steady problem of finding $u(x, y)$ satisfying Laplace’s equation with non-zero boundary condition only on the x -axis where $u(x, 0) = f(x)$. Solution is found in the rectangle $0 < x < a$, $0 < y < b$, Figure F.1. Symbolically we have

$$\frac{\partial^2 p}{\partial x^2} + \frac{\partial^2 p}{\partial y^2} = 0 \quad \begin{cases} 0 < x < a \\ 0 < y < b \end{cases} \quad (\text{F.10})$$

$$\begin{cases} p(x, 0) = f(x) \\ p(x, b) = 0 \end{cases} \quad \left. \right\} \quad 0 \leq x \leq a \quad (\text{F.11})$$

$$\begin{cases} p(0, y) = 0 \\ p(a, y) = 0 \end{cases} \quad \left. \right\} \quad 0 \leq y \leq b \quad (\text{F.12})$$

Corresponding to the zeroth order form (F.5) for the pressure field, we assume the solution to (F.10) which seemingly cannot satisfy the boundary condition (F.11),

$$p(x, y) = \sum_{n=1}^{\infty} c_n(x) \sin \frac{n\pi y}{b} \quad (\text{F.13})$$

so

$$c_n(x) = \frac{2}{b} \int_0^b p(x, y) \sin \frac{n\pi y}{b} dy \quad (F.14)$$

The series (F.13) may be regarded as an expansion in the eigenfunctions $\sin \frac{n\pi y}{b}$ corresponding to ψ_n in (F.5). Spatial averaging of the governing equation (F.10) over y , weighted by the basic function, gives

$$\frac{2}{b} \int_0^b \frac{\partial^2 p}{\partial x^2} \sin \frac{n\pi y}{b} dy + \frac{2}{b} \int_0^b \frac{\partial^2 p}{\partial y^2} \sin \frac{n\pi y}{b} dy = 0$$

Then substitution of the assumed form (F.13) and integration of the second term by parts leads to

$$\frac{d^2 c_n}{dx^2} + \frac{2}{b} \left\{ \left[\frac{\partial p}{\partial y} (x, y) \sin \frac{n\pi y}{b} \right]_{y=0}^{y=b} - \frac{2n\pi}{b^2} \int_0^b \frac{\partial p}{\partial y} \cos \frac{n\pi y}{b} dy \right\} = 0$$

The second term is zero and integration of the third term gives

$$\frac{d^2 c_n}{dx^2} - \frac{2n\pi}{b^2} \left[p(x, y) \cos \frac{n\pi y}{b} \right]_{y=0}^{y=b} + \frac{2}{b} \left(\frac{n\pi}{b} \right)^2 \int_0^b p(x, y) \sin \frac{n\pi y}{b} dy = 0$$

After substitution of the boundary condition on $y = 0$ in the first term, and the definition (F.14) in the last, the equation for $c_n(x)$ is

$$\frac{d^2 c_n}{dx^2} - \left(\frac{n\pi}{b} \right)^2 c_n = -\frac{2n\pi}{b^2} f(x) \quad (F.15)$$

with the end conditions

$$c_n(0) = c_n(a) = 0 \quad (F.16)$$

Solution for $c_n(x)$ is conveniently constructed using a one-dimensional Green's function. Hildebrand (1952, pp. 388ff) has given a particularly clear discussion of the calculation which, with only minor changes, is directly applicable here. The Green's function $G(x|\xi)$ satisfies the same differential equation as $c_n(x)$ does except that the inhomogeneous right-hand side is non-zero at a single point ξ which lies in the range $a < \xi < b$,

$$\frac{d^2 G(x|\xi)}{dx^2} - \kappa^2 G(x|\xi) = \delta(x - \xi) \quad (F.17)$$

where $\kappa = n\pi/b$ and $\delta(x - \xi)$ has the property,

$$\int_{x < \xi}^{x > \xi} \delta(x - \xi) d\xi = 1 \quad (F.18)$$

Without additional justification, we require G to have the four properties:

- (i) G is composed of two parts, f and g , which because of the defining property (F.17) satisfy the same homogeneous equation:

$$\begin{aligned} \frac{d^2 g}{dx^2} - \kappa^2 g &= 0 & (0 \leq x < \xi) \\ \frac{d^2 h}{dx^2} - \kappa^2 h &= 0 & (\xi < x \leq a) \end{aligned}$$

and

$$G = \begin{cases} g(x) & 0 \leq x < \xi \\ h(x) & \xi < x \leq a \end{cases} \quad (\text{F.19})$$

(ii) G satisfies the prescribed homogeneous boundary conditions (F.16),

$$G(0|\xi) = G(a|\xi) = 0 \quad (\text{F.20})$$

which imply

$$g(0) = 0, \quad h(a) = 0 \quad (\text{F.21})$$

(iii) G is continuous at $x = \xi$,

$$g(\xi) = h(\xi) \quad (\text{F.22})$$

(iv) the derivative of G has discontinuity equal to -1 at the point $x = \xi$:

$$\frac{dh}{dx} - \frac{dg}{dx} = -1 \quad (x = \xi)$$

Conditions (i) and (ii) are satisfied by the functions

$$\begin{aligned} g(x) &= A \sinh \kappa x \\ h(x) &= B \sinh \kappa(a - x) \end{aligned} \quad (\text{F.23a,b})$$

Conditions (iii) and (iv) then become

$$A \sinh \kappa \xi - B \sinh \kappa(a - \xi) = 0 \quad (\text{F.24})$$

$$A \cosh \kappa \xi + B \cosh \kappa(a - \xi) = \frac{1}{\kappa} \quad (\text{F.25})$$

The constants A and B are therefore

$$\begin{aligned} A &= \frac{1}{\Delta} \begin{vmatrix} 0 & -\sinh \kappa(a - \xi) \\ \frac{1}{\kappa} & +\cosh \kappa(a - \xi) \end{vmatrix} = \frac{1}{\kappa \Delta} \sinh \kappa(a - \xi) \\ B &= \frac{1}{\Delta} \begin{vmatrix} \sinh \kappa \xi & 0 \\ \cosh \kappa \xi & \frac{1}{\kappa} \end{vmatrix} = \frac{1}{\kappa \Delta} \sinh \kappa \xi \end{aligned} \quad (\text{F.26a,b})$$

where

$$\Delta = \sinh \kappa \xi \cosh \kappa(a - \xi) + \cosh \kappa \xi \sinh \kappa(a - \xi) = \sinh \kappa a \quad (\text{F.27})$$

Thus $A = \sinh \kappa(a - \xi)/\kappa \sinh \kappa a$, $B = \sinh \kappa \xi/\kappa \sinh \kappa a$ and the Green's function for this problem follows from (F.19):

$$G(x|\xi) = \begin{cases} \frac{\sinh \kappa x \sinh \kappa(a - \xi)}{\kappa \sinh \kappa a} = \frac{\sinh \frac{n\pi x}{b} \sinh \frac{n\pi}{b}(a - \xi)}{\frac{n\pi}{b} \sinh n\pi \frac{a}{b}} & 0 \leq x \leq \xi \\ \frac{\sinh \kappa \xi \sinh \kappa(a - x)}{\kappa \sinh \kappa a} = \frac{\sinh \frac{n\pi \xi}{b} \sinh \frac{n\pi}{b}(a - x)}{\frac{n\pi}{b} \sinh n\pi \frac{a}{b}} & \xi \leq x \leq a \end{cases} \quad (\text{F.28})$$

Solution for $c_n(x)$ is found in familiar fashion by combining (F.15) and (F.17). Multiply (F.17) by $c_n(x)$, (F.15) by $G(x|\xi)$, subtract the results and integrate over the range of the solution:

$$\begin{aligned} \int_0^a \left[c_n(x) \frac{d^2 G(x|\xi)}{dx^2} - G(x|\xi) \frac{d^2 c_n}{dx^2} \right] dx - \int_0^a \left[\kappa^2 c_n(x) G(x|\xi) - \left(\frac{n\pi}{b} \right)^2 G(x|\xi) c_n(x) \right] dx \\ = \int_0^a \left[c_n(x) \delta(x - \xi) + \frac{2n\pi}{b^2} f(x) G(x|\xi) \right] dx \end{aligned} \quad (\text{F.29})$$

The first term is integrated by parts with the boundary conditions (F.16) and (F.20) applied:

$$\int_0^a \left[c_n(x) \frac{d^2 G(x|\xi)}{dx^2} - G(x|\xi) \frac{d^2 c_n(x)}{dx^2} \right] dx = \left[c_n \frac{dG}{dx} - G \frac{dc_n}{dx} \right]_0^a - \int_0^a \left[\frac{dc_n}{dx} \frac{dG}{dx} - \frac{dG}{dx} \frac{dc_n}{dx} \right] dx = 0$$

Because $\kappa = n\pi/b$, the integrand of the second integral in (F.29) is zero, giving

$$\int_0^a c_n(x) \delta(x - \xi) dx = -\frac{2n\pi}{b^2} \int_0^a f(x) G(x|\xi) dx$$

With the property (F.18),

$$c_n(\xi) = -\frac{2n\pi}{b^2} \int_0^a f(x) G(x|\xi) dx$$

Interchange x and ξ , and use the symmetry property which can be confirmed with (F.27)¹, $G(x|\xi) = G(\xi|x)$, the solution $c_n(x)$ is

$$c_n(x) = -\frac{2n\pi}{b^2} \int_0^a f(\xi) G(x|\xi) d\xi \quad (\text{F.30})$$

Thus with (F.28) we have

$$\begin{aligned} c_n(x) &= -\frac{2n\pi}{b^2} \int_0^x f(\xi) [G(x|\xi)]_{0 \leq \xi \leq x} d\xi - \frac{2n\pi}{b^2} \int_x^a f(\xi) [G(x|\xi)]_{x \leq \xi \leq a} d\xi \\ &= -\frac{2}{b} \frac{\sinh \frac{n\pi}{b}(a-x)}{\sinh n\pi \frac{a}{b}} \int_0^x f(\xi) \sinh \frac{n\pi \xi}{b} d\xi - \frac{2}{b} \frac{\sinh \frac{n\pi x}{b}}{\sinh n\pi \frac{a}{b}} \int_x^a f(\xi) \sinh \frac{n\pi}{b}(a-\xi) d\xi \end{aligned} \quad (\text{F.31})$$

Substitution into (F.13) gives the solution for $p(x, y)$ in terms of its boundary values $p(x, 0) = f(x)$ on the side of the rectangular region on the x -axis:

$$p(x, y) = -\frac{2}{b} \sum_{n=1}^{\infty} \frac{\sin \frac{n\pi y}{b}}{\sin \frac{n\pi a}{b}} \left\{ \sinh \frac{n\pi}{b}(a-x) \int_0^x f(\xi) \sinh \frac{n\pi \xi}{b} d\xi + \sinh \frac{n\pi x}{b} \int_x^a f(\xi) \sinh \frac{n\pi}{b}(a-\xi) d\xi \right\} \quad (\text{F.32})$$

This result gives $p(x, 0) = 0$ on the side of the rectangle on the x -axis—where we have already specified, and presumably satisfied, the condition $p(x, 0) = f(x)$. We therefore have the paradoxical situation quite analogous to that prevailing for the acoustic field treated with the method described in Chapter 4: The solution (F.32) has been constructed to satisfy the boundary condition (F.11) on $y = 0$, but because $\sin \frac{n\pi y}{b}$ is zero on $y = 0$, the specified boundary condition is obviously not satisfied.

Owing to the relative simplicity of the formulas arising in this problem, we can resolve the apparent paradox explicitly and quite easily. The key to doing so is to show that (F.32) is *not* a continuous function of y as $y \rightarrow 0$, expressed by the statements

- (i) $p(x, 0) = 0$, which follows immediately from (F.32); but
- (ii) $\lim_{y \rightarrow 0} p(x, y) = f(x)$, the required boundary condition (F.11)

¹Because the differential operator defined by (F.15) is self-adjoint, the associated Green's is symmetric (Morse and Feshbach 1948, for example).

Another way of stating this result is: “the limit of the sum is not equal to the sum of the limits” $\int \sum \neq \sum \int$.

We already know by inspection that $\sum \int = 0$ for (F.32), the result following because $\sin \frac{n\pi y}{b} = 0$ for $y = 0$ in all terms of the finite sum, and then letting the sum become infinite. So we have only to show that statement (ii) follows from the solution (F.32). Write (F.32) in the form (F.13),

$$p(x, y) = \sum_{n=1}^{\infty} c_n(x) \sin \frac{n\pi y}{b}$$

where $c_n(x)$ is given by (F.31). Integrate by parts, the two terms in $c_n(x)$,

$$\int_0^x f(\xi) \sinh \frac{n\pi \xi}{b} d\xi = \frac{b}{n\pi} \left[f(\xi) \cosh \frac{n\pi \xi}{b} \right]_0^x - \frac{b}{n\pi} \int_0^x \frac{df}{d\xi} \cosh \frac{n\pi \xi}{b} d\xi$$

$$\int_x^a f(\xi) \sinh \frac{n\pi}{b} (a - \xi) d\xi = -\frac{b}{n\pi} \left[f(\xi) \cosh \frac{n\pi}{b} (a - \xi) \right]_x^a - \frac{b}{n\pi} \int_x^a \frac{df}{d\xi} \cosh \frac{n\pi}{b} (a - \xi) d\xi$$

The result of substituting into the formula (F.30) can be put in the form

$$c_n(x) = -\frac{2}{n\pi} f(x) + C_n(x) \quad (\text{F.33})$$

where

$$C_n(x) = \frac{2}{n\pi} \frac{1}{\sinh \frac{n\pi a}{b}} \left\{ \left[f(a) \sinh \frac{n\pi x}{b} - f(0) \sinh \frac{n\pi}{b} (a - x) \right] + \left[\int_0^x \frac{df}{d\xi} \cosh \frac{n\pi \xi}{b} d\xi - \int_x^a \frac{df}{d\xi} \cosh \frac{n\pi}{b} (a - \xi) d\xi \right] \right\} \quad (\text{F.34})$$

We take advantage of a result used by Friedman (1956, p. 271) and assumed here without proof. For the Fourier series

$$S = \sum_{n=1}^{\infty} A_n \sin ny,$$

suppose that for n large,

$$A_n = \frac{a_1}{n} + \frac{a_2(n)}{n^2}$$

where a_1 is constant and $a_2(n)$ is bounded. If $a_1 \neq 0$,

$$S = a_1 \sum_{n=1}^{\infty} \frac{\sin ny}{n} + \sum_{n=1}^{\infty} \frac{a_2(n)}{n^2} \sin ny$$

The second sum tends to zero as $y \rightarrow 0$ and the first sum is $a_1(\pi - y)/2$ for $0 < y < \pi$. Hence, for $y \rightarrow 0$,

$$S = \sum_{n=1}^{\infty} A_n \sin n\pi \xrightarrow{y \rightarrow 0} a_1 \frac{\pi - y}{2} + \sum_{n=1}^{\infty} \frac{a_2(n)}{n^2} y \xrightarrow{y=0} a_1 \frac{\pi}{2} \quad (\text{F.35})$$

Therefore, $p(x, y)$ given by (F.13) with $c_n(x)$ expressed as (F.33) is

$$p(x, y) = \frac{2}{\pi} f(x) \sum_{n=1}^{\infty} \frac{\sin ny}{n} + \sum_{n=1}^{\infty} C_n(x) \sin ny$$

For $y \rightarrow 0$,

$$p(x, y \rightarrow 0) = \frac{2}{\pi} f(x) \left(\frac{\pi - y}{2} \right) + \sum_{n=1}^{\infty} C_n(x) \sin ny$$

which for $y = 0$ becomes

$$p(x, 0) = f(x) \quad (\text{F.36})$$

This then demonstrates that with sufficient care, the representation (F.13) which apparently cannot satisfy the boundary condition $p \neq 0$ on $y = 0$, in fact *does* if the infinite series is properly summed.

We have not, and will not here, prove the corresponding property for our case summarized by equations (F.1)–(F.7), but throughout this book, whenever necessary, we assume its truth.



ANNEX G

Nyquist Criterion

Nyquist (1932) established the result which bears his name during his work on problems relating to the development of the US telephone system. It is a wonderful yet simple general result, a relation among the poles and zeros of a complex function, established by applying Cauchy's residue theorem. In Section G.5 we repeat a standard proof to clarify what is implied by use of the criterion in applications to control theory. We treat only linear single-input-single-output (SISO) systems in detail; at the end of this annex we make a few remarks on multi-input-multi-output (MIMO) systems.

There are many books devoted to feedback control, but surprisingly few contain proofs of Nyquist's Criterion. That's a pity because with a little effort one gains a great deal of understanding. Besides Bode's book (1945) volumes that I have found helpful include Franklin *et al.* (2002), McFarlane and Glover (1992), Ogata (1990), and DiStefano *et al.* (1990). For five years I shared with several faculty, a first course in feedback control of dynamical systems. That experience was enormously helpful to me.

In practice, the system or plant dynamics, written in terms of the Laplace transfer variable s and represented by its transfer function $G(s)$, are known. To meet performance specifications (such as steady-state error for a step input), a controller is required, having dynamics $H(s)$. Hence the open-loop transfer function $H(s)G(s)$ is known, practically always in factored form, so the open-loop performance and stability are readily determined.¹

Performance specifications are often such that they cannot be met with open-loop operation. Feedback is then added, the performance specifications are placed on the closed-loop system, and we must be concerned with stability of the system shown in Figure G.1, for which the transfer function is

$$\frac{P}{F} = \frac{H(s)G(s)}{1 + H(s)G(s)}$$

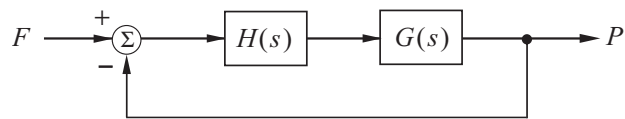


FIGURE G.1. The system $G(s)$ with controller $H(s)$ and negative unity feedback.

Stability now is determined by the zeros of $1 + HG$ and we are usually faced with two problems in the analysis and design of a feedback system:

- (1) given $H(s)G(s)$, find the roots of $1 + H(s)G(s)$;
- (2) for the given transfer function $G(s)$ of the plant, find the transfer function $H(s)$ of a controller required to meet the desired closed-loop performance.

¹Unlike the convention followed in the remainder of this book, we assume in this annex that the time dependence for steady waves is $e^{+i\omega}$, instead of $e^{-i\omega}$, to be consistent with standard usage in control theory. Also, the complex variable, $s = \sigma + i\omega$, which originates as the Laplace transform variable in control theory, takes the part of $z = x + iy$.

The actual performance depends on the zeros of $1 + HG$, which cannot be determined until $H(s)$ is known. Hence there is clearly a design problem which can be solved only if methods of analysis are available, the matter we now address. The design process involves some sort of ‘cut-and-try’ or interactive process, at each stage of which the methods of analysis are applied to check the actual performance and stability.

G.1. The Criterion Stated Without Proof

The closed-loop transfer function will often have the form of 1 plus a rational polynomial,

$$1 + HG = 1 + K \frac{\prod_{j=1}^i (s - z_j)}{s^\ell \prod_{j=1}^i (s - p_j)},$$

where we allow for a pole of order ℓ at the origin in HG . Stability of the *open-loop* system depends on the *poles* of HG , but the stability of the *closed-loop* system depends on the *zeros* of $1 + HG$. Hence it is possible that the closed-loop system may be stable even if the open-loop system is unstable, one of the advantages of feedback.

For practical purposes, it is usually difficult to factor $1 + HG$, so closed-loop stability is not easily found. The Nyquist Criterion allows one to determine *without* factoring $1 + HG$, whether or not the closed-loop system is stable, and, if it is unstable, the number of unstable poles (i.e., zeros of $1 + HG$ in the right-half of the s -plane). This remarkable result is based on a polar plot of the open-loop transfer function, proceeding in the following steps:

- (i) locate the *poles* of $H(s)G(s)$ on the imaginary axis in the s -plane, including the origin;
- (ii) construct the Nyquist *path* in the s -plane (Figure G.2), traversing the imaginary axis *excluding* the poles of HG , and closed by a semi-circle in the right-half s -plane. Poles and zeros of HG within the path are not excluded. Hence the interior of the closed figure lies to the *right* of the path;²

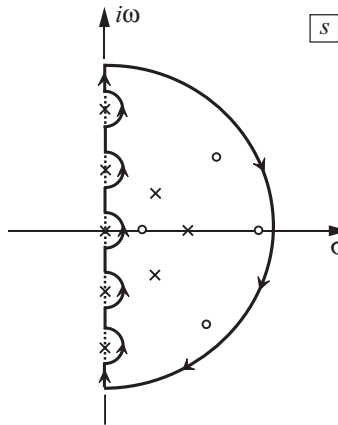


FIGURE G.2. Definition of the Nyquist path excluding poles of HG on the imaginary axis. Examples of poles and zeros within the path are not excluded.

²This is probably the most common definition of the Nyquist path, excluding poles on $Re(s) = 0$. Alternatively, poles on the imaginary axis can be explicitly included by closing the semi-circles to the left of those poles. The details of the following argument would change, and the statement of Nyquist’s Criterion would be different, but the substance of the result would remain.

- (iii) construct the Nyquist contour or polar plot, i.e. the mapping, of the Nyquist path by the open-loop transfer function $H(s)G(s)$;
- (iv) count the number N of encirclements of the point -1 by the polar plot ($N > 0$ if -1 lies inside the contour and $N < 0$ if -1 lies outside, i.e. the contour makes counter-clockwise encirclements of -1);
- (v) let \mathcal{P} be the number of poles of HG in the right-half s -plane (right-half s -plane [RHP] means $Re(s) > 0$); $\mathcal{P} > 0$ if the open-loop system is unstable; $\mathcal{P} = 0$ if the open-loop system is stable, so all poles are in the left-half s -plane, or if HG has poles on the imaginary axis. Thus \mathcal{P} is either zero or a positive integer.
- (vi) then the *Nyquist Criterion* is:

- (1) if $N > 0$, the number Z of zeros of $1 + HG$ in the *right-half* s -plane is

$$Z = N + \mathcal{P} \quad (G.1)$$

- (2) the closed-loop system is *stable* if and only if the number of *counter-clockwise* encirclements equals the number of poles in the right-half s -plane:

$$N = -\mathcal{P} \leq 0 \quad (G.2)$$

Note that the Nyquist Criterion gives information about the *absolute* stability of the closed-loop system but provides no measure of *relative* stability—i.e., how stable or unstable it is. However, we will see in Section G.7 that the Nyquist polar plot provides a clear basis for defining measures of relative stability.

G.2. Some General Properties of Polar Plots

In the present context we view a polar plot as a mapping—in the cases which we deal with a conformal transformation—of a contour in the s -plane to the image figure in the G -plane by $G(s)$. If the contour avoids poles of G , the mapping is conformal and angles are preserved. In particular, a right angle in the s -plane of the contour in the s -plane is mapped to the corresponding right angle in the G -plane.

The polar plot of $G(s) + g$, where $g = g_r + ig_i$, is a complex number, is the polar plot of $G(s)$ with origin shifted to $-g$. This property follows by direct calculation,

$$G + g = (G_r + g_r) + i(G_i + g_i)$$

which can be interpreted with a sketch of a simple example. See Figure G.8 for a case when $g = g_r = 1$.

For a time-invariant linear system the polar plot of $G(s)$ antisymmetric about the real axis for $s = i\omega$,

$$ImG(-i\omega) = -ImG(i\omega) \quad (G.3)$$

To show this, suppose that $G(s)$ is a rational polynomial with a pole of order ℓ at the origin,

$$G(s) = \frac{K \prod(s - z_i)}{s^\ell \prod(s - p_j)} = \frac{K}{s^\ell} \frac{s^{n_N} + a_{N-1}s^{n_N-1} + \dots}{s^{n_D} + a_{n_D-1}s^{n_D-1} + \dots}$$

in which the coefficient in the polynomials, as well as the constant K , are real. On the imaginary axis of s ,

$$G(i\omega) = \frac{K}{(i\omega)^\ell} \frac{\dots (i\omega - z_n)(i\omega - z_n^*) \dots}{\dots (i\omega - p_n)(i\omega - p_n^*) \dots}$$

and the complex conjugate is

$$G^*(i\omega) = G(-i\omega) = G_r - iG_i = \frac{K}{(-i\omega)^\ell} \frac{\cdots (-i\omega - z_n^*)(-i\omega - z_n) \cdots}{\cdots (-i\omega - p_n^*)(-i\omega - p_n) \cdots}$$

Consider the pair of factors shown in the numerators of G and G^* ,

$$\begin{aligned} G : \quad (i\omega - z_n)(i\omega - z_n^*) &= (|z_n|^2 - \omega^2) - i(2\omega z_n^r) \\ G^* : \quad (-i\omega - z_n^*)(-i\omega - z_n) &= (|z_n|^2 - \omega^2) + i(2\omega z_n^r) \end{aligned}$$

These are typical factors so we conclude that $G(-i\omega)$ has imaginary part having the same numerical value, but opposite sign compared with that of $G(i\omega)$ if we ignore the pole of order ℓ at the origin, i.e. take $\ell = 0$. In this case, $G(i\omega)$ is antisymmetric about the real axis, as asserted by (G.1).

When $\ell = 1, 2, 3, \dots$, G has the additional multiplying factor $\frac{1}{s}, \frac{1}{s^2}, \frac{1}{s^3}, \dots$ or $\frac{1}{i\omega}, \frac{1}{(i\omega)^2}, \frac{1}{(i\omega)^3}, \dots$, that is $\frac{1}{i\omega}, -\frac{1}{\omega^2}, -\frac{1}{i\omega^3}, \dots$. Thus G^* contains the corresponding factors $-\frac{1}{i\omega}, -\frac{1}{\omega^2}, \frac{1}{i\omega^3}, \dots$. Hence, when ℓ is even, the pole has no effect on the above argument and (G.1) still holds. But when ℓ is odd, the polar plot of G is symmetric about the real axis and the values of $G(-i\omega)$ overlay those of $G(i\omega)$.

G.3. Construction of Nyquist Contours (Polar Plots)

The Nyquist contour, or polar plot, is the mapping of the Nyquist path, Figure G.2, to the HG plane. Poles on the path are avoided by indenting the path, as shown in Figure G.3, with a small semi-circle of radius ρ ($\rho \rightarrow 0$ eventually); the path is closed by the large semi-circle of radius R ($R \rightarrow \infty$ eventually). The indentations on the imaginary s -axis exclude poles representing undamped motions, for example, oscillations of constant amplitude.

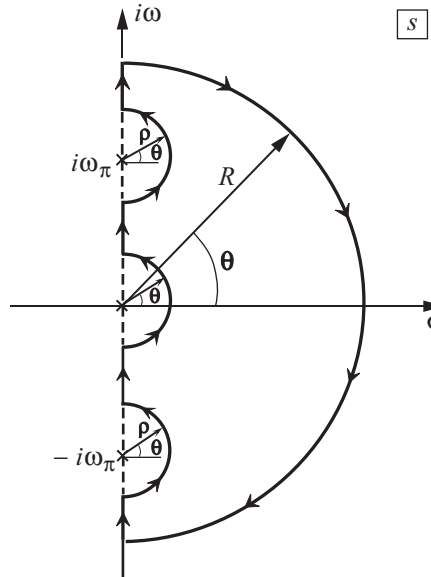


FIGURE G.3. Indentations around poles on the imaginary axis. Poles and zeros within the contour are suppressed.

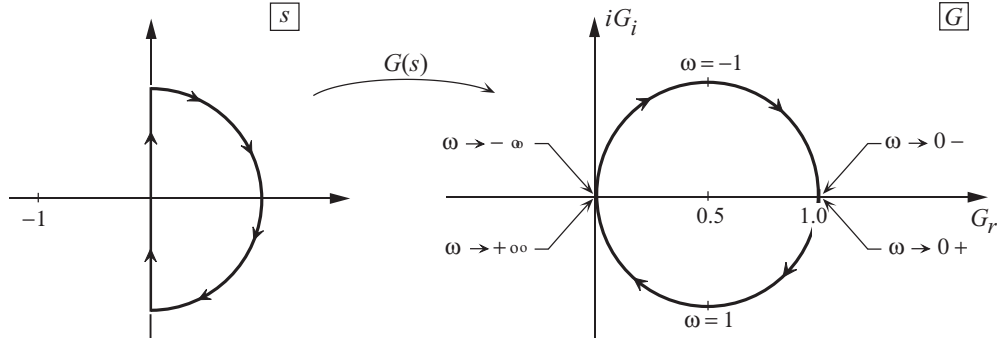
As an aid to constructing the mapping, note that on the various portions of the Nyquist path, s assumes the following values:

- (i) on the positive imaginary axis: $s = i\omega$
- (ii) on an indentation around a pole on the positive imaginary axis: $s = i\omega_p = \rho e^{i\theta} \quad -\frac{\pi}{2} \leq \theta \leq \frac{\pi}{2}$
- (iii) on the large semi-circle: $s = Re^{i\theta} \quad \frac{\pi}{2} \leq \theta \leq -\frac{\pi}{2}$
- (iv) on an indentation around a pole on the negative imaginary axis: $s = i\omega_p + \rho e^{i\theta} \quad -\frac{\pi}{2} \leq \theta \leq \frac{\pi}{2}$
- (v) on the indentation around the origin: $s = \rho e^{i\theta} \quad -\frac{\pi}{2} \leq \theta \leq \frac{\pi}{2}$

For simplicity in the following examples we set $H = 1$.³

(a) $G(s) = \frac{1}{s+1}$

There are no poles on the Nyquist path and the polar plot is sketched below.



(b) $G(s) = \frac{1}{s(s+1)}$

This is example (a) plus a simple pole at the origin. The path in the s -plane must be indented to avoid the pole. On this indentation we set $s = \rho e^{i\theta}$ and G is

$$G = \frac{1}{\rho e^{i\theta} (1 + \rho e^{i\theta})} \xrightarrow{\rho \rightarrow 0} \frac{1}{\rho} e^{-i\theta} \left(-\frac{\pi}{2} \leq \theta \leq \frac{\pi}{2} \right) \implies \left(\frac{\pi}{2} \geq \phi \geq -\frac{\pi}{2} \right)$$

Hence $|G| \rightarrow \infty$ as the radius of the semi-circle shrinks, and the polar angle changes from $-\left(-\frac{\pi}{2}\right) = \frac{\pi}{2}$ to $-\frac{\pi}{2}$, traversing a large semi-circle in the counter-clockwise direction, as sketched below. (Points $A \rightarrow A'$, $B \rightarrow B'$, and $C \rightarrow C'$.)

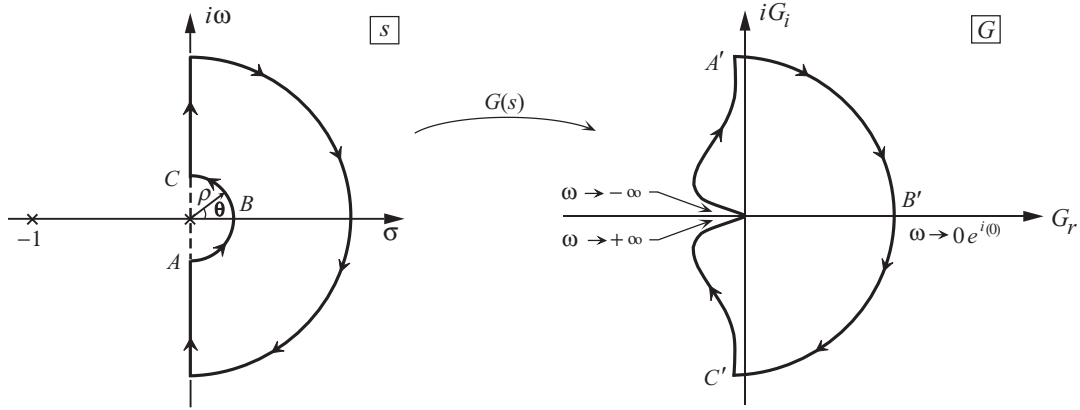
On the large semi-circle of the path, $s = Re^{i\theta}$ and

$$G = \frac{1}{Re^{i\theta} (1 + Re^{i\theta})} \xrightarrow{R \rightarrow \infty} \frac{1}{R^2} e^{-i2\theta} \left(\frac{\pi}{2} \geq \theta \geq -\frac{\pi}{2} \right) \implies (-\pi \leq \phi \leq \pi)$$

³For the examples here and in Section G.6, I have relied heavily on DiStefano, Stubberud and Williams (1990), Franklin *et al.* (2002) and Ogata (1990).

ANNEX G – NYQUIST CRITERION

For $\theta \rightarrow \frac{\pi}{2}$ ($\omega \rightarrow \infty$ on the positive imaginary axis), $G \rightarrow \frac{1}{R^2}e^{-i\pi}$; and for $\theta \rightarrow -\frac{\pi}{2}$ ($\omega \rightarrow -\infty$ on the negative imaginary axis), $G \rightarrow \frac{1}{R^2}e^{i\pi}$. Hence we find the mapping of the Nyquist path to the Nyquist polar plot shown below.



Compare this result with the figure for example (a). The pole at the origin causes the Nyquist contour to approach the origin along the negative real axis instead of tangent to the imaginary axis, and a portion of the contour therefore lies in the left half-plane.

$$(c) G(s) = \frac{1}{s^2(s+1)}$$

Now we have a third-order pole at the origin, which will have a significant effect on the Nyquist contour at infinity. The path in the s -plane is the same as in example (b). For s on the indentation at the origin,

$$G = \frac{1}{\rho^3 e^{i3\theta}} \frac{1}{(1 + \rho e^{i\theta})} \sim \frac{1}{\rho^3} e^{-i3\theta} \quad \left(-\frac{\pi}{2} \leq \theta \leq \frac{\pi}{2} \right)$$

Thus as θ increases from $-\frac{\pi}{2}$ through zero to $+\frac{\pi}{2}$, $\arg G$ decreases from $+\frac{3\pi}{2}$ to $-\frac{3\pi}{2}$. However, care is required to get the proper behavior. A clue is found by computing the total change of $\arg G$ for the change in θ , $\Delta\theta = \pi$:

$$\Delta(\arg G) = -3\Delta\theta = -3\pi$$

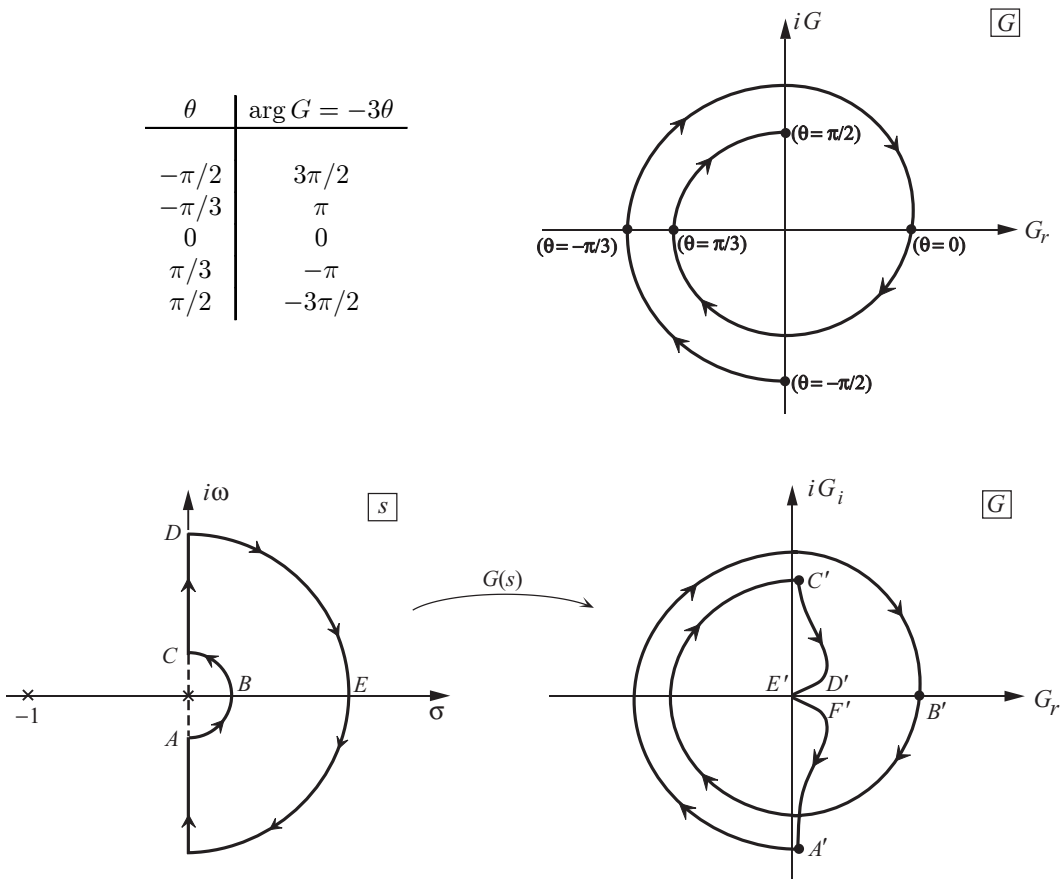
Hence the contour makes an encirclement of the origin, a result that is clarified further by constructing the following table for $\arg G$ as a function of θ , plotted in the adjacent sketch.

The question now is—how does the contour close? For s on the large semi-circle, we have

$$G \sim \frac{1}{R^4} e^{-i4\theta} \quad \left(\frac{\pi}{2} \geq \theta \geq -\frac{\pi}{2} \right)$$

so $\arg G$ changes from -2π for $\omega \rightarrow \infty$ on the positive imaginary axis, to $+2\pi$ for $\omega \rightarrow -\infty$ on the negative imaginary axis. Hence the contour comes into the origin tangent to the positive real axis, in the first quadrant ($\arg G = -2\pi$) for $\omega \rightarrow -\infty$ and in the fourth quadrant for $\omega \rightarrow \infty$.

The Nyquist plot has the form shown in the figure, again with a few corresponding points indicated in the s - and G -planes. The dashed line is completely the image of the portion of the Nyquist path near the origin! Note especially that while the path in the s -plane is traversed once, the image polar plot encircles the origin twice in the G -plane. This is an example of



the importance of the behavior of $G(s)$ for $s \rightarrow 0$. In view of the final value theorem, this reflects the behavior that we can expect in the time domain for large times. So it may not be surprising that encirclements by the contours should be closely related to stability, one aspect of the long-time behavior of a system. In fact, stability is the only characteristic of long-time behavior that is independent of the forcing function or input—and nothing we are doing here is related to the input. These remarks suggest that we should be more precise with our definition of encirclement.

G.4. Definition of Encirclement

A closed contour in the HG plane is said to make N_0 *positive* encirclements of the origin if a line drawn from the origin to a point on the contour rotates *clockwise* through $2\pi N_0$ radians as the point traverses the contour. It is essential that the definition of positive be maintained, as we shall see with the proof of Nyquist's criterion, and emphasized in Figure G.4. The reason for this definition of positive follows from the chosen direction for positive traversal of the Nyquist contour in the s -plane.

As a practical matter, two points should be noted. First, polar plots for the systems we are concerned with are symmetrical about the real axis. That is particularly to be kept in mind when drawing or viewing contours making several encirclements of the origin—it is a matter of convenience in drawing that the portions far from the origin seem not to satisfy that symmetry, as is the case for example (c).

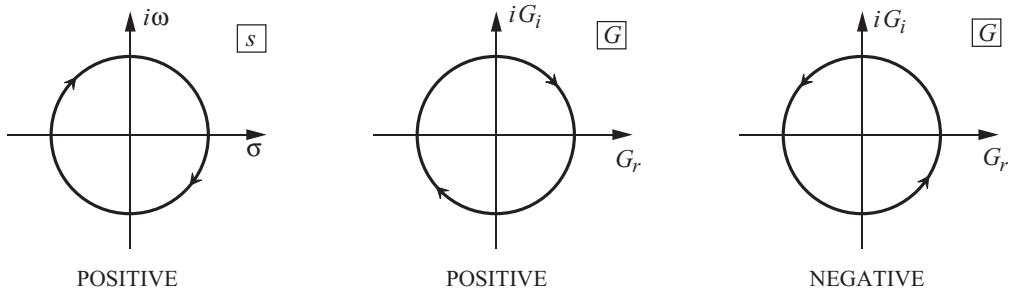


FIGURE G.4. Definitions of positive and negative encirclements.

Second, an operational hint, another way of determining the number of encirclements of the origin by a contour is to draw a line from the origin to infinity and count the *net* number of crossings of that line by the contour, taking into account the definition of ‘positive’ (hence of ‘negative’) given above.

G.5. Proof of Nyquist’s Criterion

G.5.1. Principle of the Argument. We first establish an important relation among the numbers of poles and zeros of a function by applying Cauchy’s residue theorem.⁴ Consider a simple closed contour \mathcal{C} in the s -plane and a function $f(s)$ analytic within \mathcal{C} except for isolated poles, none of which are on \mathcal{C} . Moreover, we assume that $f(s)$ may have zeros in the region enclosed by \mathcal{C} but does not vanish on \mathcal{C} . Now apply Cauchy’s residue theorem to the function f'/f :

$$\frac{1}{2\pi i} \oint_{\mathcal{C}} \frac{f'}{f} ds = \sum \text{Residues of } \frac{f'}{f}$$

The residues of f'/f are the coefficients of $1/(s - s_k)$ in the Laurent-series expansion. In this case, residues are associated with both poles and zeros of f . First, near a zero of order m_i of f , we can approximate $f(s)$ with the form

$$f(s) = (s - z_i)^{m_i} g(s)$$

where $g(s)$ is non-zero and analytic at $s = z_i$. Then

$$\frac{f'}{f} = \frac{m_i}{s - z_i} + \frac{g'}{g}$$

and the residue is m_i at $s = z_i$.

Similarly, near a pole of order n_j ,

$$f(s) = \frac{h}{(s - p_j)^{n_j}}$$

where h is the analytic near p_j ; the logarithmic derivative is

$$\frac{f'}{f} = \frac{-n_j}{s - p_j} + \frac{h'}{h}$$

so the residue is $-n_j$. Hence by the residue theorem we find

$$\frac{1}{2\pi i} \oint_{\mathcal{C}} \frac{f'}{f} ds = \sum m_i - \sum n_j \quad (G.4)$$

⁴We assume for this discussion sufficient knowledge of functions of a complex variable, at the level of a well-educated undergraduate. See, e.g., the Caltech undergraduate course ACM 95.

This result is true independently of the direction in which the contour is traversed: there is no ambiguity of sign.

If we regard each multiple pole (zero) as equivalent to $n_j(m_i)$ simple poles (zeros) we can write

$$\frac{1}{2\pi i} \oint_{\mathcal{C}} \frac{f'}{f} ds = \mathcal{Z} - \mathcal{P} \quad (\text{G.5})$$

where \mathcal{Z} and \mathcal{P} are the numbers of zeros and poles respectively within \mathcal{C} .

Now carry out the integral explicitly:

$$\begin{aligned} \frac{1}{2\pi i} \oint_{\mathcal{C}} \frac{f'}{f} ds &= \frac{1}{2\pi i} [\log f]_{\mathcal{C}} \\ &= \frac{1}{2\pi i} [\log |f|]_{\mathcal{C}} + \frac{1}{2\pi} [\arg |f|]_{\mathcal{C}} \end{aligned}$$

The change of a quantity in one passage around the path \mathcal{C} in the s -plane is denoted by the brackets. Hence the first term vanishes, because $|f|$ returns to its initial value, and the second term is the increment in the argument of f , $\Delta_c(\arg f)$. When the value of s traverses the closed path once in the s -plane, the values of $f(s)$ will also trace a closed contour in the f -plane, which may be simple, or may intersect itself. If the contour in the f -plane encircles the origin once, then the argument of f changes by 2π ; for N_0 encirclements of the origin, the change of argument is $2\pi N_0$. Figure G.5 illustrates two possibilities ($N_0 = 0$ and $N_0 = -2$).

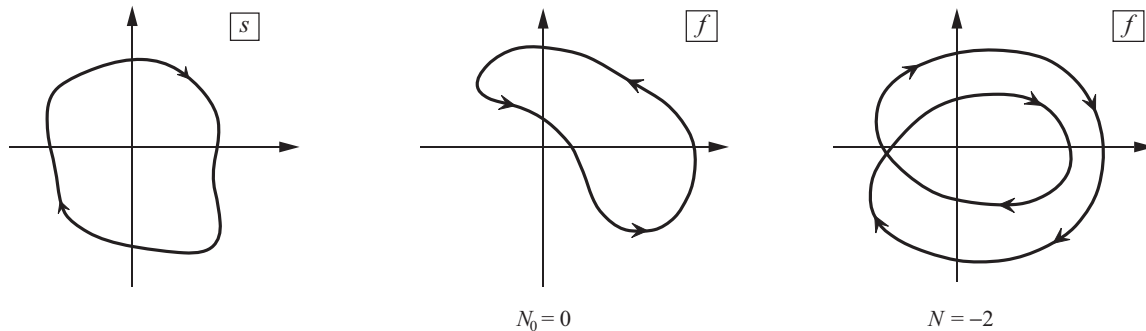


FIGURE G.5. Illustrating no encirclement ($N_0 = 0$) and two negative encirclements ($N_0 = -2$) by $f(s)$ when s executes a closed contour encircling the origin.

Therefore, the value of the integral may be written generally

$$\frac{1}{2\pi i} \oint_{\mathcal{C}} \frac{f'}{f} ds = \frac{1}{2\pi} \Delta_c(\arg f) = N_0 \quad (\text{G.6})$$

Equating the right-hand sides of (G.5) and (G.6), we have the *principle of the argument*:

$$N_0 = \mathcal{Z} - \mathcal{P} \quad (\text{G.7})$$

We emphasize that the result is *independent of the direction in which the path \mathcal{C} is traversed* in the s -plane, but the direction (i.e., the definition of “inside” the path) must be consistently maintained in the f -plane. Figure G.6 shows examples of the point, two cases of clockwise and counter-clockwise traversal of the path in the s -plane each giving rise to two of the many possible cases in the f -plane. Which case arises depends of course on the function f . The shading denotes the interior of a path: the interior of a path in the s -plane maps to the interior of a contour in the f -plane because the mapping is conformal, preserving both the magnitude and sense of angles locally.

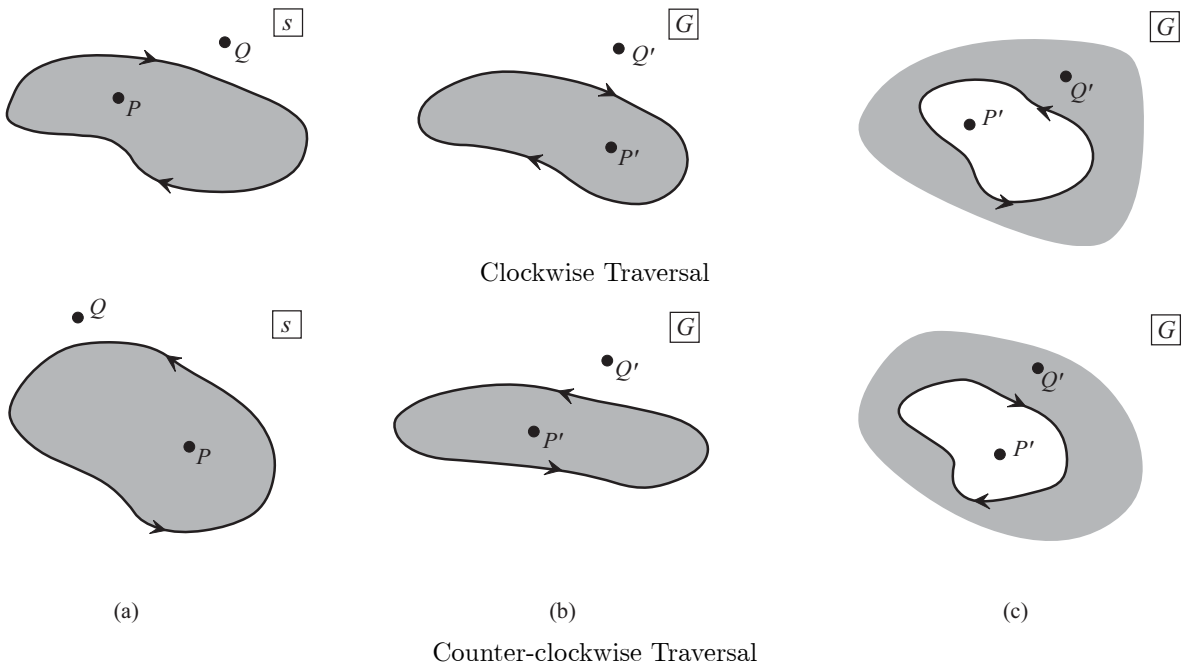


FIGURE G.6. Examples showing consistent maintenance of the definition of ‘interior’ of a path under mapping from the s -plane to the G -plane.

The definition of positive sense of a path is defined in the s -plane. Either case in Figure G.6 is valid: if the path is traversed in the clockwise sense, the interior is to the right, and if in the counter-clockwise sense the interior is to the left. The chosen definition is maintained in the G -plane, so the ‘interior’ regions are mapped as shown. Then an encirclement of a point in the G -plane is positive if that point belongs to the image of the interior of the path in the s -plane and negative if the point belongs to the image of the exterior. If the point lies outside the path in the G -plane, then the net phase change is zero for a vector drawn from the point to a point executing the path. By definition, the encirclement is then zero.

G.5.2. Proof of Nyquist’s Criterion. Returning to the demonstration of Nyquist’s criterion, we set $f = HG$, the forward-path transfer function. Equation (G.7) has then established that the number of encirclements of the origin by the Nyquist contour in the HG -plane is equal to the number of zeros of HG minus the number of poles of HG in the right half-plane. Because we chose to execute the Nyquist path in the clockwise direction in the s -plane, a positive encirclement in the HG -plane is also defined as a 2π increase of $\arg HG$ in the clockwise sense. Figure G.7 illustrates the result.

What we really want to determine is the number of zeros of $1 + HG$ in the right half-plane, a small extension of the reasoning leading to equation (G.7) and achieved in the following steps.

- (i) Let $f(s) = 1 + HG$. Then the origin for the mapping $1 + HG$ in the HG -plane is at $HG = -1$. (Figure G.8 shows the process.)
- (ii) Let N be the number of encirclements of -1 by the *mapping* of the Nyquist path by $HG(s)$.
- (iii) Then according to equation (G.7), $N = \mathcal{Z} - \mathcal{P}$, where \mathcal{Z} , \mathcal{P} are the numbers of zeros and poles of $1 + HG$ enclosed by the Nyquist path in the s -plane (i.e., in the right-half s -plane).

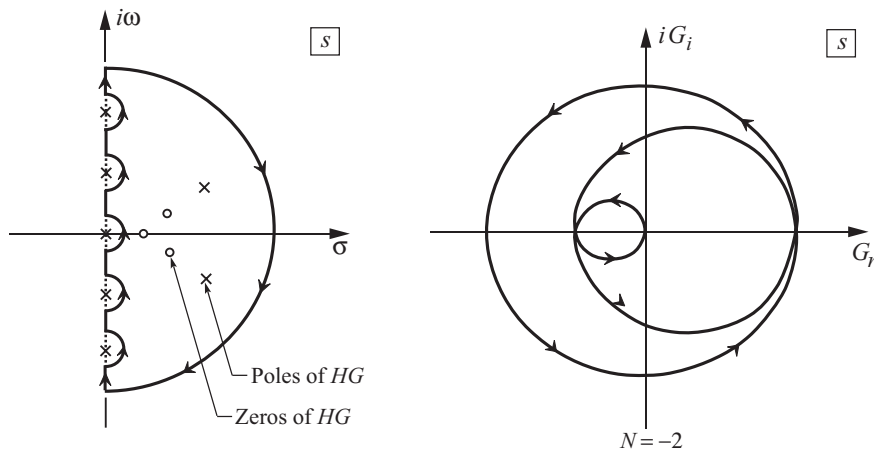


FIGURE G.7. An example showing two negative encirclements of the origin by the path obtained by mapping the Nyquist contour.

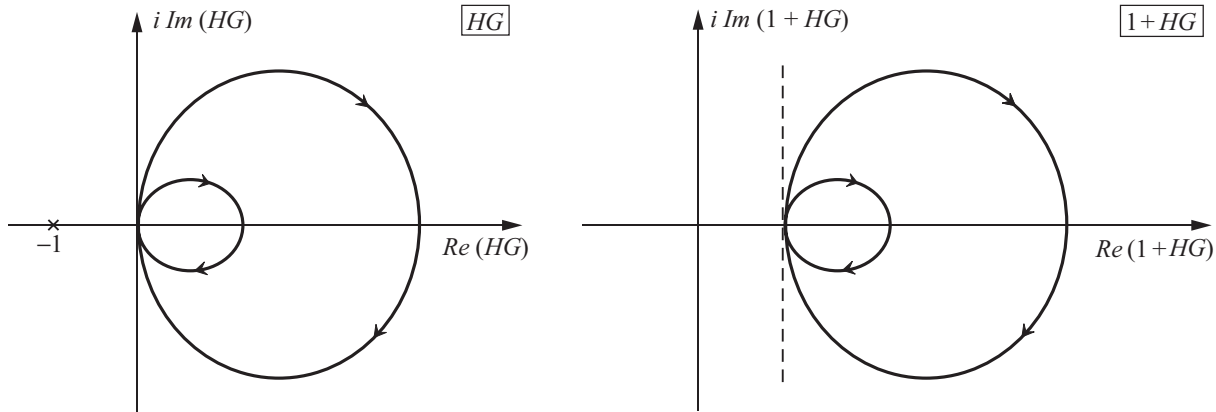


FIGURE G.8. Mappings of the Nyquist contour in the HG and $1 + HG$ planes.

- (iv) The poles of $1 + HG$ are the same as the poles of HG . Hence the number of zeros Z of HG in the right-half s -plane is

$$Z = N + \mathcal{P} \quad (G.8)$$

Z : number of zeros of $1 + HG$ in the right-half s -plane, i.e. the number of unstable roots of the closed-loop system

N : number of encirclements of -1 by the mapping of HG of the Nyquist path

\mathcal{P} : number of poles of HG (hence of $1 + HG$) in the right-half s -plane

Thus we have shown how to determine the number of zeros of the *closed-loop* transfer function in the right half-plane from a polar plot of the *open-loop* transfer function applied to the Nyquist contour.

Note that if the closed loop is stable, there are no zeros of $1 + HG$ in the right half-plane, $Z = 0$, and

$$N = -\mathcal{P} \geq 0 \quad (G.9)$$

ANNEX G – NYQUIST CRITERION

which is zero or negative because by definition \mathcal{P} is 0 or a positive number. Conversely, if $N = -\mathcal{P}$, then $\mathcal{Z} = 0$ and the closed-loop system is stable. Hence (G.9) is the necessary and sufficient condition that the closed-loop system be stable, where ‘stable’ means that the transient motions are bounded for large times (i.e., neutral stability is included). For N to be negative the point -1 is encircled negatively by the Nyquist path and hence by definition lies outside the path (see Figure G.6 and accompanying remarks). An equivalent statement is: if the mapping of the right-half s -plane under $1 + HG(s)$ does not include the point -1 , then the system is stable.

If $\mathcal{P} = 0$ (no poles of HG in the right half-plane), then the system is stable if and only if $N = 0$, for then $\mathcal{Z} = 0$.

If $N > 0$, then the point -1 lies inside the Nyquist contour and there must be at least one zero of $1 + HG$ in the right-half s -plane. Figure G.9 illustrates positive and negative encirclements of -1 .

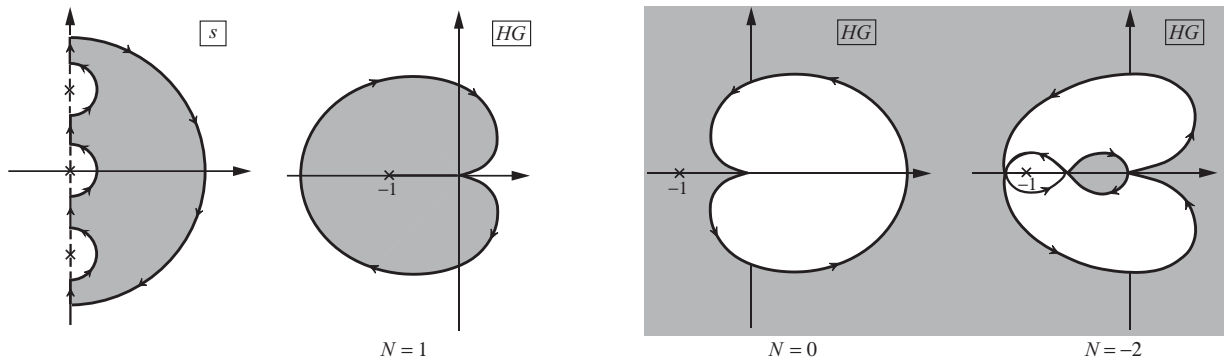


FIGURE G.9. Examples of positive and negative encirclements of -1 by mappings of the Nyquist contour.

As a final remark, we note that the portion of the Nyquist path for $s \rightarrow \infty$ must map to the origin in the HG -plane. Otherwise, the initial value theorem gives for the response near $t = 0$

$$F(t = 0+) = \lim_{s \rightarrow \infty} s H G P(s)$$

and for an impulse of amplitude A , $P(s \rightarrow \infty) = A$, so

$$F(t = 0+) = \lim_{s \rightarrow \infty} s H G A$$

Thus the initial response becomes infinitely large even for infinitesimally small impulses, unless $HG \sim 1/s^{1+\delta}$, where $\delta \geq 0$. Hence for any practically realizable system, the open-loop transfer function must have the behavior

$$H G \sim \frac{1}{s^n} \quad (s \rightarrow \infty, n \geq 1) \quad (G.10)$$

Thus $HG \rightarrow 0$ for $s \rightarrow \infty$ and the Nyquist polar plot approaches the origin for $\omega \rightarrow +\infty$ and leaves the origin for ω decreasing from $-\infty$.

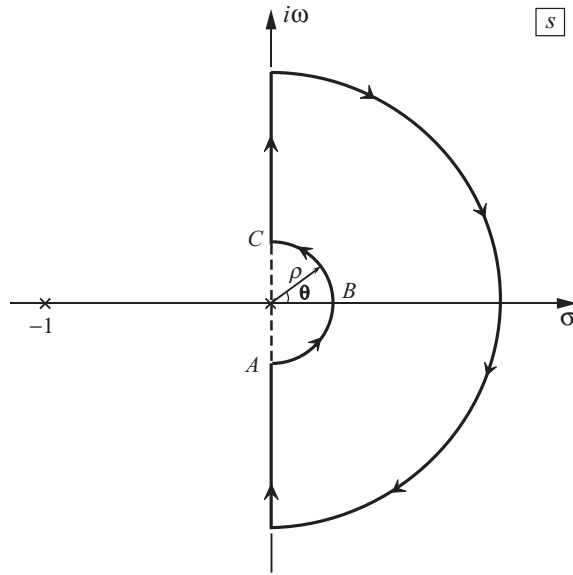
It follows that the character of the Nyquist polar plot (the mapping of the Nyquist path by HG) depends heavily on the portion of the Nyquist path on the imaginary axis. But note that it is not only the array of poles of HG on the axis that matters, for we are really using the mapping of the Nyquist path by the function $HG(s)$ so all poles and zeros matter. The behavior required by equation (G.10) is an example.

G.6. Examples of Nyquist's Criterion

The procedure for applying Nyquist's criterion is straightforward, although the details may cause minor difficulties. According to our discussion in the preceding sections, there are two preliminary tasks: (1) construct the Nyquist plot as the mapping of the Nyquist contour; and (2) count the number N of encirclements of the -1 point. If N is equal to the number \mathcal{P} of poles of the open-loop transfer function in the right half-plane and the encirclements are in the sense opposite to the traversal of the Nyquist contour, then the closed-loop system is stable. Otherwise the closed-loop system is unstable, having $N + \mathcal{P}$ poles in the right half-plane.

$$(a) HG = \frac{K}{s(s+1)} \quad (K > 0)$$

The Nyquist polar plot sketched in example (b), Section G.3, is repeated here. The plot does



not encircle the point -1 , so $N = 0$; there are no open-loop poles in the right half-plane, $\mathcal{P} = 0$, and we have $N = \mathcal{P} = 0 = \mathcal{Z}$: the closed-loop system is stable for all K . This result is easily confirmed from the closed-loop transfer function:

$$\frac{F}{P} = \frac{HG}{1 + HG} = \frac{\frac{K}{s(s+1)}}{1 + \frac{K}{s(s+1)}} = \frac{K}{s^2 + s + K}$$

The roots of the denominator always have negative real parts if $K > 0$.

$$\begin{aligned} s_{1,2} &= -\frac{1}{2} \pm \frac{1}{2}\sqrt{1-4K} \quad (K \leq \frac{1}{2}) \\ &= -\frac{1}{2} \pm i\frac{1}{2}\sqrt{4K-1} \quad (K \geq \frac{1}{2}) \end{aligned}$$

If K is negative, the plot actually closes in the left half-plane, always enclosing the point -1 ; the direction of traversal is clockwise, and $N = 1$. Because $\mathcal{P} = 0$, we then find correctly that $\mathcal{Z} = 1$.

$$(b) HG = \frac{K}{s^3(s+1)} \quad (K > 0)$$

ANNEX G – NYQUIST CRITERION

The Nyquist polar plot is sketched in example (c), Section G.3. The plot encircles -1 twice in the positive direction, $N = 2$. There are no poles of HG in the right half-plane and the closed-loop system is unstable with $Z = N + P = 2$ zeros in the right half-plane. The denominator of the closed-loop transfer function is $s^4 + s^3 + K$, not easily factored, so we cannot confirm the result directly.

$$(c) HG = \frac{K}{s(s+p_1)(s+p_2)} \quad (K > 0; p_1, p_2 > 0)$$

This transfer function may represent use of an integrator with a second-order system having two real stable poles. Now we need to construct the Nyquist plot, sketched in Figure G.10.

We have assumed p_1 and p_2 positive. This assumption sets the position of the asymptote in the left half-plane. To see this, write HG for $\omega \rightarrow 0$ as

$$\begin{aligned} \frac{1}{K} HG &= \frac{1}{i\omega(i\omega + p_1)(i\omega + p_2)} \\ &= -\frac{i}{\omega} \frac{(p_1 - i\omega)(p_2 - i\omega)}{\omega(p_1^2 + \omega^2)(p_2^2 + \omega^2)} \\ &= -\frac{i}{\omega} \frac{(p_1 p_2 - \omega^2) - i\omega(p_1 + p_2)}{(p_1^2 + \omega^2)(p_2^2 + \omega^2)} \end{aligned}$$

Now let $\omega \rightarrow 0$ to find

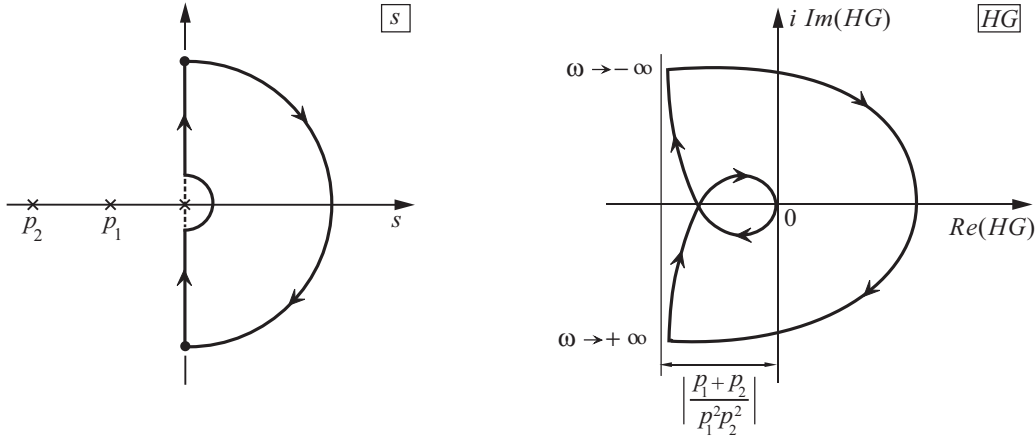


FIGURE G.10. Forming the Nyquist plot for $HG = \frac{K}{s(s+p_1)(s+p_2)}$.

$$\frac{1}{K} HG \rightarrow -\frac{(p_1 + p_2)}{p_1^2 p_2^2} - i \frac{1}{\omega} \frac{1}{p_1 p_2}$$

which shows the asymptote.

Whether or not the plot encircles -1 depends on where the point A is. We can find A by using the condition that at A , the phase of HG , as ω is increasing from 0^+ , is $-\pi$. Then from the definition of HG , we have

$$\frac{1}{K} \arg HG \equiv -\frac{\pi}{K} = -\frac{\pi}{2} - \tan^{-1} \frac{\omega_A}{p_1} - \tan^{-1} \frac{\omega_A}{p_2} \quad (G.11)$$

where ω_A is the frequency at A . Given p_1 , p_2 and K , we solve this equation for ω_A . Then calculate $|HG(\omega_A)|$ to find the position of A ; if $|HG(\omega_A)| > 1$, then the plot makes one positive

encirclement of -1 . Hence $\mathcal{Z} = 1 + \mathcal{P} = 1$, because we assume that both poles lie in the left half-plane ($p_1, p_2 > 0$ so the values of s_1, s_2 are negative at the poles). Hence the imaginary part is

$$\Im \{HG\} = -\frac{K(p_1 p_2 - \omega^2)}{\omega(p_1^2 + \omega^2)(p_2^2 + \omega^2)} \quad (G.12)$$

which vanishes when $\omega = \omega_A = \sqrt{p_1 p_2}$. The magnitude of the real part is then

$$\begin{aligned} |HG| &= K \left| \frac{-(p_1 + p_2)}{(p_1^2 + \omega^2)(p_2^2 + \omega^2)} \right|_{\omega_A} \\ &= K \frac{(p_1 + p_2)}{p_1^2 + p_2^2 + (p_1^2 + p_2^2)(p_1 + p_2) + p_1^2 + p_2^2} \\ &= K \frac{p_1 p_2}{(p_1^2 + 2p_1 p_2 + p_2^2)} \\ &= K \frac{(p_1 + p_2)}{(p_1 p_2)(p_1 + p_2)^2} \\ &= \frac{K}{p_1 p_2 (p_1 + p_2)} \end{aligned}$$

Hence the system is unstable if

$$\frac{K}{p_1 p_2 (p_1 + p_2)} > 1$$

or

$$K > p_1 p_2 (p_1 + p_2) \quad (G.13)$$

G.7. Relative Stability; Gain and Phase Margins

A great advantage of the Nyquist method is that it suggests a quantitative assessment of *relative stability*—i.e., how far is the closed-loop system from being unstable. This result appears in practice as a restriction on the magnitude of the gain arising from the compensator or controller represented by H . We have already seen in example (c) of the preceding section how increasing the gain can cause the Nyquist plot to expand and enclose the -1 point, indicating that the system has become unstable.

To reiterate the point, consider the control system in which a plant having two stable poles at -1 is subject to integral control, $H = K/s$, Figure G.11. The Nyquist plot is the same as Figure G.10, but now with $p_1 = p_2 = 1$, and is re-drawn in Figure G.12. We have already shown, with equation (G.13), that the plot encircles the point -1 if $K > 2$. To make quantitative statements about how close the system is to being unstable (i.e., in this case when $K < 2$), consider the portion of the plot for positive ω and $K < 2$.

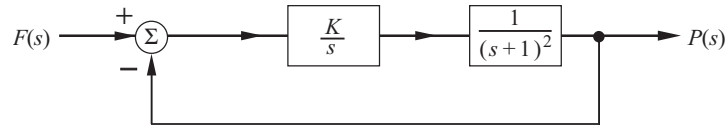


FIGURE G.11. A stable second order system with an integrator.

The *gain margin* is defined as a measure of the change of gain necessary to cause point A to reach -1 . A common ‘general’ definition is

$$GM = \frac{1}{|HG|_\pi} \quad (G.14)$$

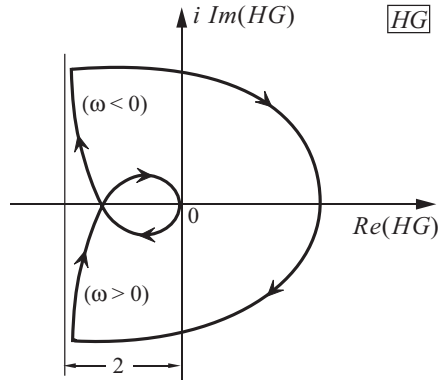


FIGURE G.12. The Nyquist plot for the system shown in Figure G.11.

where $|HG|_\pi$ is the magnitude of HG when $\arg HG = \pi$. The meaning is clear if we set $H = Kh$, where h is now independent of gain, and rewrite (G.14) as

$$(GM)K|hG|_\pi = 1$$

Hence GM is the multiplier of the gain required to make $|HG|_\pi = 1$, so the contour passes through the point -1 (i.e., when $\arg(HG) = \pi$).

Another measure of relative stability is the *phase margin* defined as the difference between π and the phase of HG where $|HG| = 1$; hence for the case drawn here (note that $\arg HG$ is *negative*)

$$PM = \arg HG(i\omega_1) + \pi \quad (G.15)$$

where ω_1 is the frequency at which $|HG| = 1$, the condition denoted $|HG|_\pi = 1$.

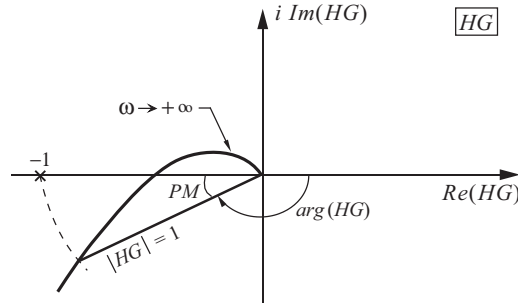


FIGURE G.13. The Nyquist plot for ‘any’ HG near $|HG|_\pi$, i.e., the magnitude of HG when the phase or \arg of HG is π .

For the example $HG = K/s(s + 1)^2$ giving Figure G.11, when $s = i\omega$,

$$HG = \frac{K}{\omega(1 + \omega^2)} e^{-i(\frac{\pi}{2} + 2 \tan^{-1} \omega)} \quad (G.16)$$

The contour crosses the axis when $\arg(HG) = -\pi$;

$$-\left(\frac{\pi}{2} + 2 \tan^{-1} \omega\right) = -\pi$$

or

$$2 \tan^{-1} \omega = \frac{\pi}{2}$$

Hence $\tan^{-1} \omega = \pi/4$, or $\omega = 1$. If we set $\arg(HG) = -\pi$, we find $\omega = -1$, a result also immediately evident from the symmetry of the contour about the real axis.

When $\omega = 1$,

$$|HG|_\pi = \frac{K}{\omega(1 + \omega^2)} \Big|_{\omega=1} = \frac{K}{2}$$

Hence from the definition (G.14) we have

$$GM = \frac{2}{K}$$

which is less than unity, and the system is unstable if $K > 2$, the value given by equation (G.13) for $p_1 = p_2 = 1$. That is, if $K > 2$, then $|HG|_\pi = K/2$ is greater than 1 and the contour encloses 1.

It is more difficult to determine the phase margin from the Nyquist plot, for we require the value of ω satisfying the transcendental equation

$$|HG| = 1 = \frac{K}{\omega(1 + \omega^2)} \quad (G.17)$$

Here, ω is the solution to

$$\omega^3 + \omega - K = 0, \quad (G.18)$$

and this is a *simple* example!

Consequently, while the ideas and definitions of the gain and phase margins are suggested by the Nyquist plot, their values are more easily found from Bode plots. To see how the procedure works we continue with the example given in Figure G.11,

$$HG(i\omega) = \frac{K}{i\omega} \frac{1}{(1 + i\omega)^2}$$

The Bode plot is the graphical representation of the magnitude and phase of HG for $\omega > 0$:

$$20 \log_{10} |HG| = 20 \log_{10} K - 20 \log_{10} \omega - 20 \log_{10}(1 + \omega^2)$$

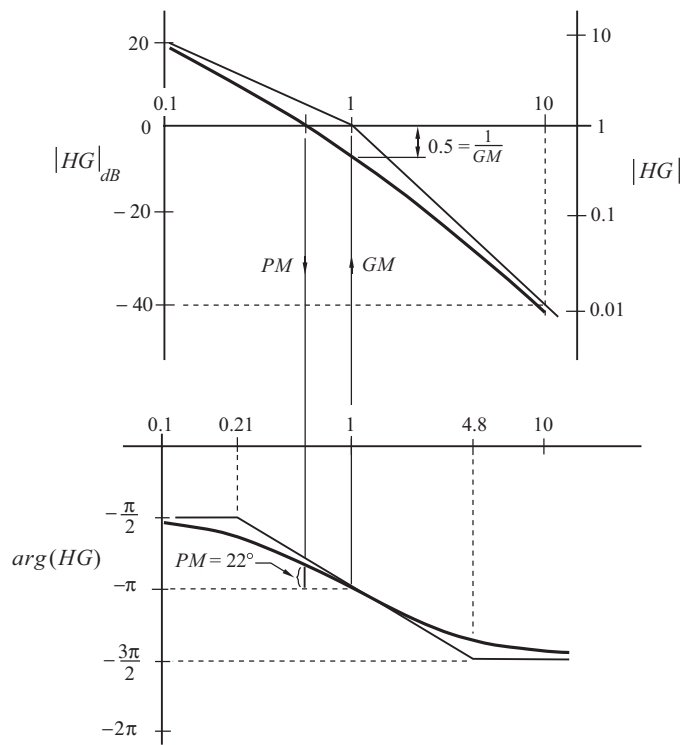
$$\arg HG = -\left(\frac{\pi}{2} + 2 \tan^{-1} \omega\right)$$

These are sketched in Figure G.14; the magnitude is drawn for $K = 1$.

To compute the gain margin, find the value of $|HG|$ for $\arg HG = -\pi$, giving $|HG|_\pi = 0.5$. Hence from equation (G.14), $GM = 1/|HG|_\pi = 2$, which is here the gain margin for $K = 1$. Similarly, to compute the phase margin, find the value of $\arg HG$ at which $|HG| = 1$, giving the value here $PM = 22^\circ$. It should be evident that Bode plots prepared with readily available computer programs can be used to find the gain and phase margins.

The definitions of phase margin and gain margin seemed quite natural for the simple example, Figure G.11, treated here. One should wonder whether more complicated systems will have Nyquist polar plots having such a character that the same ideas can be applied. The answer—perhaps surprisingly—is yes. Although the entire Nyquist plot may be very complicated indeed, nevertheless, in the vicinity of the point -1 , both the Nyquist plot and the Bode plots commonly behave much like this example.

ANNEX G – NYQUIST CRITERION


 FIGURE G.14. The Bode plot for the system shown in Figure G.11, $K = 1$.

ANNEX H

Some Alternative Methods of Approximately Analyzing Nonlinear Behavior

Time-dependent nonlinear behavior has long been an object of intensive research in several other fields, notably electrical and earthquake engineering. Some of the results obtained in this book, or cited, originated in quite different contexts. Probably the main distinguishing feature of the applications motivating much of the present work is the emphasis on the transient growth of a small amplitude motion into a limit cycle executed by a (largely) isolated physical system. Particularly for combustion instabilities in solid propellant rockets, much effort has been devoted to improving the precision of the results; and to broadening applicability of those results to complicated internal configurations. The purpose of this brief annex is solely to call attention to other methods which may be attractive for particular applications. No derivations or results are given and the citations are intended only to provide an entry into the literature. They are neither the most recent nor are they necessarily the most representative works.

Probably the practical methods most commonly encountered are known by the names *harmonic linearization*; *harmonic balance*; *equivalent linearization*; *quasi-linearization*; and *describing function analysis*. Perhaps the best, through brief, treatment for methods useful in the subject of this book is the discussion Natanzon (1999) gives in his Chapter Five. This is a particularly interesting brief coverage of some of the Russian work which evidently was developed for application to liquid rockets, significantly well in advance of comparable analyses in the West. The approaches rest ultimately on the influential work by Krylov and Bogoliubov (1943), Bogoliubov and Mitropolsky (1961) and Andronov, Vitt, and Khaikin (1966). A strong influence, particularly in the earlier works, is the behavior of electronic devices and the properties of radio waves. Attention to continuous systems and the associated systems of nonlinear partial differential equations was therefore not often a leading concern.

Many approximate methods for analyzing nonlinear behavior have developed from the assumption that the motions of the system at hand are dominated by oscillation at a single frequency. That is the essential basis for the first four of the methods listed at the beginning of the preceding paragraph. For example, Natanzon opens his survey with a development of *harmonic linearization*, partly a misnomer because it leads to a nonlinear governing equation which is then ‘linearized’. Simplification of the nonlinear behavior is achieved partly by initially treating steady oscillations occurring in limit cycles. Slow variations are handled in a manner similar to that explained by Krylov and Bogoliubov. Natanzon then discusses ‘hard excitation’ of oscillations, i.e., pulsed nonlinear instabilities, with a simple combination of analytical results and graphical interpretation. It is important to note that, because by assumption motion at one frequency suppresses other frequencies, there is no possibility of treating such phenomena as, for example, energy transfer between modes. However, consequences of nonlinear behavior means the assumed single harmonic can be treated in a heuristic fashion. Natanzon (his Section 5.2) does so using a form of the $n-\tau$ model of combustion. It is an interesting peek at a piece of early Russian work on nonlinear combustion instabilities. See also MacDonald (1993) for a variation of the technique called the *harmonic balance method*.

Methods of *equivalent linearization* have been very popular in earthquake engineering (e.g., Caughey, 1963; Iwan 1973, 1978) but apparently originated in mechanics (Minorsky 1947; Bogoliubov and Mitropolski

1961). As the term ‘equivalent linearization’ suggests, the idea is to replace a nonlinear problem—typically involving the motion of an oscillator—by a linear form. Much of the theory which has been developed is directed to minimizing the error incurred in the process. Caughey (1963), for example, has discussed the method applied to nonlinear oscillators subject to random forces. Iwan (1978) has given a useful discussion of the connections between the methods of equivalent linearization and harmonic balance.

Especially in the field of automatic control—with or without feedback—the method based on *describing functions* has long been favored. It is also the method most easily learned, appearing at length in several texts, e.g., Truxal (1955); Graham and McRuer (1961); and Ogata (1970); and the quite thorough treatment of Gelb and Vander Velde (1968). The quickest way to obtain an extended introduction is to search on the web. You should not expect to find applications to combustion systems. But because the point of view developed in this book emphasizes the central role of oscillations, the discussions in the references will often expand one’s understanding and perhaps suggest novel calculations.

Ogata (p. 652) defines the *describing function* as “the complex ratio of the fundamental harmonic component of the output to the input.” Hence the describing function is an extension to nonlinear systems of the definition of the transfer function for linear systems. The earliest description of the method was by Kochenburger (1950) based on his MIT Ph.D. thesis. Truxal (1955) has briefly summarized background and has given a good introduction to the method. For the most extended treatment, see Gelb and Vander Velde (1968). One should keep these early references in context, for the field of dynamical systems, both theory and analysis, has of course advanced enormously in recent decades. Modern computing machinery has often had far-reaching qualitative as well as quantitative consequences, but the importance of approximate methods remains.

REPORT DOCUMENTATION PAGE																											
1. Recipient's Reference	2. Originator's References	3. Further Reference	4. Security Classification of Document																								
	RTO-AG-AVT-039 AC/323(AVT-039)TP/103	ISBNs 92-837-0059-7 978-92-837-0059-3	UNCLASSIFIED/ UNLIMITED																								
5. Originator	Research and Technology Organisation North Atlantic Treaty Organisation BP 25, F-92201 Neuilly-sur-Seine Cedex, France																										
6. Title	Unsteady Motions in Combustion Chambers for Propulsion Systems																										
7. Presented at/Sponsored by	This AGARDograph was approved by the Propulsion and Energetics Panel (PEP) of NATO's Advisory Group for Aerospace Research and Development (AGARD); subsequently it has been sponsored by the Applied Vehicle Technology Panel (AVT) of NATO's Research and Technology Organisation (RTO).																										
8. Author(s)/Editor(s)	9. Date Multiple December 2006																										
10. Author's/Editor's Address	11. Pages Multiple 664																										
12. Distribution Statement	There are no restrictions on the distribution of this document. Information about the availability of this and other RTO unclassified publications is given on the back cover.																										
13. Keywords/Descriptors	<table style="width: 100%; border-collapse: collapse;"> <tr> <td style="width: 25%;">Air vehicles</td> <td style="width: 25%;">Decision aids</td> <td style="width: 25%;">Methodology</td> <td style="width: 25%;">Simulation</td> </tr> <tr> <td>Computer architecture</td> <td>Design</td> <td>Military vehicles</td> <td>Software development</td> </tr> <tr> <td>Computer programs</td> <td>Integrated systems</td> <td>Models</td> <td>Standards</td> </tr> <tr> <td>Computerized simulation</td> <td>Interoperability</td> <td>Requirements</td> <td>Systems analysis</td> </tr> <tr> <td>Control theory</td> <td>Land vehicles</td> <td>Sea vehicles</td> <td>Systems engineering</td> </tr> <tr> <td>Cost effectiveness</td> <td>M&S (Modelling and Simulation)</td> <td></td> <td></td> </tr> </table>			Air vehicles	Decision aids	Methodology	Simulation	Computer architecture	Design	Military vehicles	Software development	Computer programs	Integrated systems	Models	Standards	Computerized simulation	Interoperability	Requirements	Systems analysis	Control theory	Land vehicles	Sea vehicles	Systems engineering	Cost effectiveness	M&S (Modelling and Simulation)		
Air vehicles	Decision aids	Methodology	Simulation																								
Computer architecture	Design	Military vehicles	Software development																								
Computer programs	Integrated systems	Models	Standards																								
Computerized simulation	Interoperability	Requirements	Systems analysis																								
Control theory	Land vehicles	Sea vehicles	Systems engineering																								
Cost effectiveness	M&S (Modelling and Simulation)																										
14. Abstract	<p>This book has several purposes, including a broad historical summary of combustion instabilities in propulsion systems; a concise compilation of the main mechanisms for instabilities in liquid and solid fueled rockets, ramjets, thrust augmentors and gas turbines; development of a theoretical framework for investigating unsteady motions in combustion systems; and accessible surveys of the basic material required to understand the subject. Emphasis is placed throughout the book on observed behavior. For well-understood reasons, the best, and in many respects most useful quantitative data, have been obtained for solid propellant rockets. Hence that type of device occupies a special position in the subject. The book comprises nine chapters and eight annexes. Material in the annexes is not essential for reading and broadly understanding the main part of the book, but is likely interesting for those choosing to do research on the subject. The nine chapters divide into three parts. Chapter 1 covers basic behavior observed in operational systems, and includes brief historical summaries as well as qualitative interpretations of observed behavior. Chapter 2 contains lengthy descriptions of a few mechanisms, especially for some of the behavior known from observations of solid propellant rockets. The second part of the book comprises Chapters 3 and 4 which summarize the development of the method of spatial averaging and construction of the systems of equations used for analytical studies in the subject; and Chapter 5, a survey of those parts of classical acoustics required to understand unsteady motions in combustors. Applications of the formal structure to problems arising in laboratory and full-scale devices are covered in the last four chapters. Chapter 6 treats linear behavior, including linear stability with examples; and Chapter 7 covers some aspects of nonlinear behavior based on the theory developed in the earlier part of the book. Practical methods of treating combustion instabilities are the subjects of the last two chapters. Chapter 8 describes various methods of passive control and how they fit in the general understanding of combustion instabilities. The last chapter is largely descriptive, a brief summary of some of the accomplishments of active control. It's an interesting and potentially very important subject which has fallen short of many optimistic expectations. There are presently no known practical applications. Successful advancement likely will rest on better understanding of fundamental behavior.</p>																										





BP 25
F-92201 NEUILLY-SUR-SEINE CEDEX • FRANCE
Télécopie 0(1)55.61.22.99 • E-mail mailbox@rta.nato.int



DIFFUSION DES PUBLICATIONS
RTO NON CLASSIFIES

Les publications de l'AGARD et de la RTO peuvent parfois être obtenues auprès des centres nationaux de distribution indiqués ci-dessous. Si vous souhaitez recevoir toutes les publications de la RTO, ou simplement celles qui concernent certains Panels, vous pouvez demander d'être inclus soit à titre personnel, soit au nom de votre organisation, sur la liste d'envoi.

Les publications de la RTO et de l'AGARD sont également en vente auprès des agences de vente indiquées ci-dessous.

Les demandes de documents RTO ou AGARD doivent comporter la dénomination « RTO » ou « AGARD » selon le cas, suivi du numéro de série. Des informations analogues, telles que le titre et la date de publication sont souhaitables.

Si vous souhaitez recevoir une notification électronique de la disponibilité des rapports de la RTO au fur et à mesure de leur publication, vous pouvez consulter notre site Web (www.rta.nato.int) et vous abonner à ce service.

CENTRES DE DIFFUSION NATIONAUX

ALLEMAGNE

Streitkräfteamt / Abteilung III
Fachinformationszentrum der
Bundeswehr (FIZBw)
Gorch-Fock-Straße 7, D-53229 Bonn

BELGIQUE

Etat-Major de la Défense
Département d'Etat-Major Stratégie
ACOS-STRAT – Coord. RTO
Quartier Reine Elisabeth
Rue d'Evêre, B-1140 Bruxelles

CANADA

DSIGRD2
Bibliothécaire des ressources du savoir
R et D pour la défense Canada
Ministère de la Défense nationale
305, rue Rideau, 9^e étage
Ottawa, Ontario K1A 0K2

DANEMARK

Danish Defence Research Establishment
Ryvangs Allé 1, P.O. Box 2715
DK-2100 Copenhagen Ø

ESPAGNE

SDG TECEN / DGAM
C/ Arturo Soria 289
Madrid 28033

ETATS-UNIS

NASA Center for AeroSpace
Information (CASI)
Parkway Center, 7121 Standard Drive
Hanover, MD 21076-1320

FRANCE

O.N.E.R.A. (ISP)
29, Avenue de la Division Leclerc
BP 72, 92322 Châtillon Cedex

**NASA Center for AeroSpace
Information (CASI)**

Parkway Center, 7121 Standard Drive
Hanover, MD 21076-1320
ETATS-UNIS

GRECE (Correspondant)

Defence Industry & Research
General Directorate
Research Directorate
Fakinos Base Camp, S.T.G. 1020
Holargos, Athens

HONGRIE

Department for Scientific Analysis
Institute of Military Technology
Ministry of Defence
P O Box 26
H-1525 Budapest

ISLANDE

Director of Aviation
c/o Flugrad
Reykjavik

ITALIE

Centro di Documentazione
Tecnico-Scientifica della Difesa
Via XX Settembre 123
00187 Roma

LUXEMBOURG

Voir Belgique

NORVEGE

Norwegian Defence Research Establishment
Attn: Biblioteket
P.O. Box 25
NO-2007 Kjeller

PAYS-BAS

Royal Netherlands Military
Academy Library
P.O. Box 90.002
4800 PA Breda

POLOGNE

Armament Policy Department
218 Niepodleglosci Av.
00-911 Warsaw

PORUGAL

Estado Maior da Força Aérea
SDFA – Centro de Documentação
Alfragide
P-2720 Amadora

REPUBLIQUE TCHEQUE

LOM PRAHA s. p.
o. z. VTÚLaPVO
Mladoboleslavská 944
PO Box 18
197 21 Praha 9

ROUMANIE

Romanian National Distribution Centre
Armaments Department
9-11, Drumul Taberei Street
Sector 6, 77305, Bucharest

ROYAUME-UNI

Dstl Knowledge Services
Information Centre
Building 247
Dstl Porton Down
Salisbury
Wiltshire SP4 0JQ

TURQUIE

Milli Savunma Bakanlığı (MSB)
ARGE ve Teknoloji Dairesi Başkanlığı
06650 Bakanlıklar – Ankara

AGENCES DE VENTE

**The British Library Document
Supply Centre**

Boston Spa, Wetherby
West Yorkshire LS23 7BQ
ROYAUME-UNI

**Canada Institute for Scientific and
Technical Information (CISTI)**

National Research Council
Acquisitions, Montreal Road, Building M-55
Ottawa K1A 0S2, CANADA

Les demandes de documents RTO ou AGARD doivent comporter la dénomination « RTO » ou « AGARD » selon le cas, suivi du numéro de série (par exemple AGARD-AG-315). Des informations analogues, telles que le titre et la date de publication sont souhaitables. Des références bibliographiques complètes ainsi que des résumés des publications RTO et AGARD figurent dans les journaux suivants :

Scientific and Technical Aerospace Reports (STAR)

STAR peut être consulté en ligne au localisateur de ressources uniformes (URL) suivant:

<http://www.sti.nasa.gov/Pubs/star/Star.html>

STAR est édité par CASI dans le cadre du programme NASA d'information scientifique et technique (STI)
STI Program Office, MS 157A
NASA Langley Research Center
Hampton, Virginia 23681-0001
ETATS-UNIS

Government Reports Announcements & Index (GRA&I)

publié par le National Technical Information Service
Springfield
Virginia 2216
ETATS-UNIS
(accessible également en mode interactif dans la base de données bibliographiques en ligne du NTIS, et sur CD-ROM)



BP 25

F-92201 NEUILLY-SUR-SEINE CEDEX • FRANCE
Télécopie 0(1)55.61.22.99 • E-mail mailbox@rtt.nato.int



DISTRIBUTION OF UNCLASSIFIED RTO PUBLICATIONS

AGARD & RTO publications are sometimes available from the National Distribution Centres listed below. If you wish to receive all RTO reports, or just those relating to one or more specific RTO Panels, they may be willing to include you (or your Organisation) in their distribution.

RTO and AGARD reports may also be purchased from the Sales Agencies listed below.

Requests for RTO or AGARD documents should include the word 'RTO' or 'AGARD', as appropriate, followed by the serial number. Collateral information such as title and publication date is desirable.

If you wish to receive electronic notification of RTO reports as they are published, please visit our website (www.rta.nato.int) from where you can register for this service.

NATIONAL DISTRIBUTION CENTRES

BELGIUM

Etat-Major de la Défense
Département d'Etat-Major Stratégie
ACOS-STRAT – Coord. RTO
Quartier Reine Elisabeth
Rue d'Evêre
B-1140 Bruxelles

CANADA

DRDKIM2
Knowledge Resources Librarian
Defence R&D Canada
Department of National Defence
305 Rideau Street, 9th Floor
Ottawa, Ontario K1A 0K2

CZECH REPUBLIC

LOM PRAHA s. p.
o. z. VTÚLaPVO
Mladoboleslavská 944
PO Box 18
197 21 Praha 9

DENMARK

Danish Defence Research
Establishment
Ryvangs Allé 1
P.O. Box 2715
DK-2100 Copenhagen Ø

FRANCE

O.N.E.R.A. (ISP)
29, Avenue de la Division Leclerc
BP 72
92322 Châtillon Cedex

GERMANY

Streitkräfteamt / Abteilung III
Fachinformationszentrum der
Bundeswehr (FIZBw)
Gorch-Fock-Straße 7
D-53229 Bonn

NASA Center for AeroSpace Information (CASI)

Parkway Center
7121 Standard Drive
Hanover, MD 21076-1320
UNITED STATES

GREECE (Point of Contact)

Defence Industry & Research
General Directorate
Research Directorate
Fakinos Base Camp
S.T.G. 1020
Holargos, Athens

HUNGARY

Department for Scientific Analysis
Institute of Military Technology
Ministry of Defence
P O Box 26
H-1525 Budapest

ICELAND

Director of Aviation
c/o Flugrad, Reykjavik

ITALY

Centro di Documentazione
Tecnico-Scientifica della Difesa
Via XX Settembre 123
00187 Roma

LUXEMBOURG

See Belgium

NETHERLANDS

Royal Netherlands Military
Academy Library
P.O. Box 90.002
4800 PA Breda

NORWAY

Norwegian Defence Research
Establishment
Attn: Biblioteket
P.O. Box 25
NO-2007 Kjeller

SALES AGENCIES

The British Library Document Supply Centre

Boston Spa, Wetherby
West Yorkshire LS23 7BQ
UNITED KINGDOM

POLAND

Armament Policy Department
218 Niepodleglosci Av.
00-911 Warsaw

PORTUGAL

Estado Maior da Força Aérea
SDFA – Centro de Documentação
Alfragide
P-2720 Amadora

ROMANIA

Romanian National Distribution Centre
Armaments Department
9-11, Drumul Taberei Street
Sector 6, 77305, Bucharest

SPAIN

SDG TECEN / DGAM
C/ Arturo Soria 289
Madrid 28033

TURKEY

Milli Savunma Bakanlığı (MSB)
ARGE ve Teknoloji Dairesi Başkanlığı
06650 Bakanlıklar – Ankara

UNITED KINGDOM

Dstl Knowledge Services
Information Centre
Building 247
Dstl Porton Down
Salisbury, Wiltshire SP4 0JQ

UNITED STATES

NASA Center for AeroSpace
Information (CASI)
Parkway Center
7121 Standard Drive
Hanover, MD 21076-1320

Canada Institute for Scientific and Technical Information (CISTI)

National Research Council
Acquisitions
Montreal Road, Building M-55
Ottawa K1A 0S2, CANADA

Requests for RTO or AGARD documents should include the word 'RTO' or 'AGARD', as appropriate, followed by the serial number (for example AGARD-AG-315). Collateral information such as title and publication date is desirable. Full bibliographical references and abstracts of RTO and AGARD publications are given in the following journals:

Scientific and Technical Aerospace Reports (STAR)

STAR is available on-line at the following uniform
resource locator:

<http://www.sti.nasa.gov/Pubs/star/Star.html>

STAR is published by CASI for the NASA Scientific
and Technical Information (STI) Program
STI Program Office, MS 157A
NASA Langley Research Center
Hampton, Virginia 23681-0001
UNITED STATES

Government Reports Announcements & Index (GRA&I)

published by the National Technical Information Service
Springfield
Virginia 2216
UNITED STATES
(also available online in the NTIS Bibliographic
Database or on CD-ROM)